Petros Nihoyannopoulos
Joseph Kisslo
Editors

Echocardiography

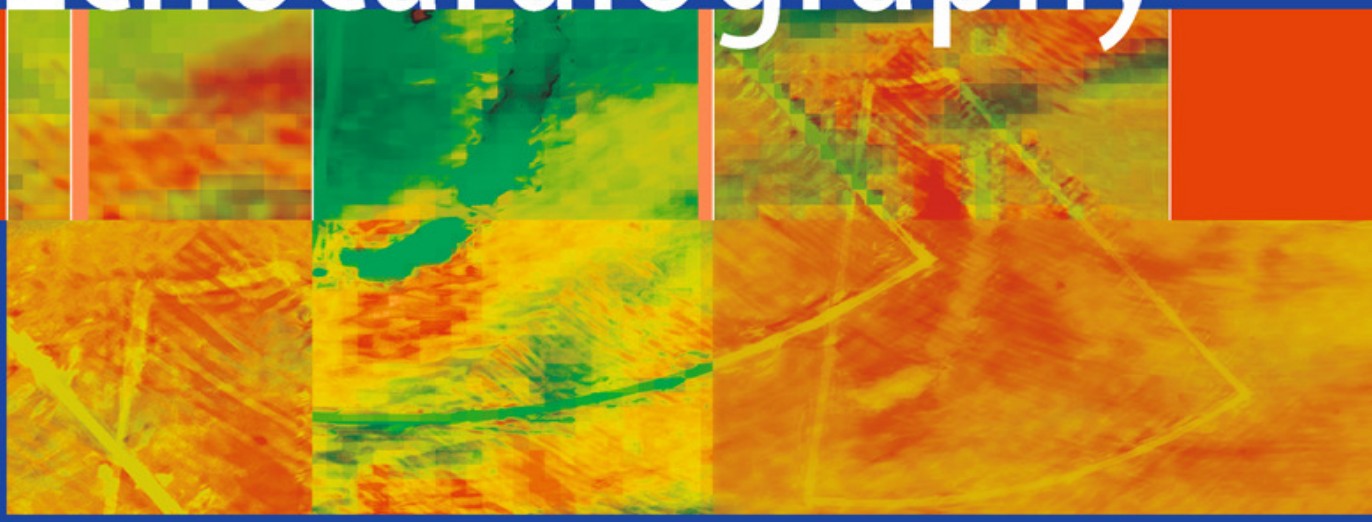

Springer

Echocardiography

Petros Nihoyannopoulos • Joseph Kisslo
Editors

Echocardiography

Springer

Editors
Petros Nihoyannopoulos, MD, FRCP
Imperial College London
National Heart and Lung Institute
Hammersmith Hospital
London
UK

Joseph Kisslo, MD
Division of Cardiovascular Medicine
Duke University Medical Center
Durham, NC
USA

ISBN 978-1-84882-292-4 e-ISBN 978-1-84882-293-1
DOI 10.1007/978-1-84882-293-1
Springer Dordrecht Heidelberg London New York

British Library Cataloguing in Publication Data
A catalogue record for this book is available from the British Library

Library of Congress Control Number: 2009927906

Printed on acid-free paper

Springer is part of Springer Science+Business Media (www.springer.com)

Preface

Echocardiography has expanded greatly over recent years to earn its place as a subspecialty in cardiology in its own right. From the original single M-mode modality of 50 years ago, it has evolved into a complex "multimodality" method for evaluating and quantifying cardiovascular lesions. In addition, the entire spectrum of hemodynamic assessment of the heart can now be performed noninvasively using echocardiography alone. Transesophageal echocardiography has added to the clarity of imaging and proved to be extremely helpful in valve surgery. Lately, three-dimensional echocardiography has added a new dimension and helped the understanding of cardiac anatomy and pathology in real time. Finally, deformation imaging and assessment of myocardial perfusion complete the global assessment of the heart by echocardiography by looking at the various contraction and perfusion patterns in patients with coronary artery disease at rest and during stress.

Echocardiography highlights the clinical utility of these evolving modalities that are now crucial to the renaissance of echocardiography. This book provides a thorough clinical review of the most revealing and adaptable echocardiographic methods of imaging a patient. The editors and their world-class group of contributors have created an essential reference for all who use echocardiography in the practice.

London, UK — Petros Nihoyannopoulos
Durham, NC — Joseph Kisslo

Contents

Contributors

David B. Adams, RCS, RDCS
Department of Cardiology, Echo Lab, Duke University Medical Center, Durham, NC, USA

Ahmed A. Alsaileek, MD
Department of Cardiac Science, King Abdulaziz Medical City, Riyadh, Kingdom of Saudi Arabia

Christopher H. Cabell, MD, MHS
Duke University Medical Center, Durham, NC, USA

John B. Chambers, MD, FRCP, FESC, FACC
Cardiothoracic Centre, St. Thomas Hospital, London, UK

Ronan Curtin, MB, BCh, BAO, MSc, MRCPI
Department of Cardiovascular Medicine, The Cleveland Clinic, Cleveland, OH, USA

Stefano De Castro
Department of Cardiovascular, Respiratory and Morphological Sciences, University of Rome Rome, Italy

Meeney Dhir, MD, FACC, FASE
Sonterra Cardiovascular Institute PA, San Antonio, TX, USA

Kate M. English, MB, ChB, MRCP, PhD
Yorkshire Heart Centre, Leeds General Infirmary, Leeds, UK

Emily Forsberg, BSRT, RDCS-AE, PE
Department of Non-Invasive Cardiology, Park Nicollet Methodist Hospital, St. Louis Park, MN, USA

Michael A. Gatzoulis, MD, PhD, FACC, FESC
Department for Pulmonary Hypertension, Royal Brompton Hospital and the National Heart & Lung Institute, Imperial College, London, UK

Bernhard Gerber, MD, PhD, FESC
Division of Cardiology, Université Catholique de Louvain, Brussels, Belgium

J. Simon R. Gibbs, MA, MD, MB, BChir, FRCP
National Heart and Lung Institute, Imperial College, London, UK

John L. Gibbs, FRCP
Yorkshire Heart Centre, Leeds General Infirmary, Leeds, UK

Donald D. Glower, MD
Duke University Medical Center, Durham, NC, USA

Paramjit Jeetley, MBChB, MRCP (UK)
Department of cardiology, Bristol Royal Infirmary, Bristol, Avon, UK

James J. Jollis, MD
Duke University Medical Center, Durham, NC, USA

Otto Kamp, MD, PhD
Department of Cardiology, VU University Medical Center, Amsterdam, The Netherlands

Bijoy K. Khandheria, MBBS, MD, FACC, FESC, FASE
Cardiovascular Division, Mayo Clinic Arizona, Scottsdale, AZ, USA

Diala Khraiche
The Heart Hospital, London, UK

Joseph Kisslo, MD
Division of Cardiovascular Medicine, Duke University Medical Center, Durham, NC, USA

Allan L. Klein, MD, FRCP, FACC, FAHA, FASE
Department of Cardiovascular Medicine, The Cleveland Clinic, Cleveland, OH, USA

Graham J. Leech, MA
Department of Cardiovascular Science, St. George's Hospital Medical School, London, UK

Wei Li, MD, PhD
Department of Echocardiography and Adult Congenital Heart Disease, Royal Brompton and Harefield NHS Trust, London, UK

Burkhard G. Mackenson, MD
Duke University Medical Center, Durham, NC, USA

Thomas Marwick, MBBS, PhD
University of Queensland, School of Medicine, Princess Alexandra Hospital, Brisbane, QLD, Australia

Gerald R. Marx, MD
Department of Cardiology, Boston Children's Hospital, Boston, MA, USA

Jacques A. Melin, MD, PhD
Division of Cardiology, Université Catholique de Louvain, Brussels, Belgium

Mark J. Monaghan, MSc, PhD
Department of Cardiology, King's College Hospital, London, UK

Daniel Monakier, MD
Toronto General Hospital, Toronto, ON, Canada

Patrick J. Nash, MD, BCh, BAO, FRCPI
Department of Cardiology, Galway University Hospital, Galway, Ireland

Petros Nihoyannopoulos, MD, FRCP, FACC, FESC
Imperial College London, National Heart and Lung Institute, Hammersmith Hospital, London, UK

Jae K. Oh, MD
Department of Cardiology, Mayo Clinic, Rochester, MN, USA

Natesa G. Pandian, MD
Division of Cardiology, Tufts-New England Medical Center, Boston, MA, USA

George A. Pantely, MD
Department of Cardiovascular Medicine, Oregon Health & Science University, Portland, OR, USA

Agnès Pasquet, MD, PhD
Division of Cardiology, Université Catholique de Louvain, Brussels, Belgium

Ayan R. Patel, MD
Division of Cardiology, Tufts-New England Medical Center, Boston, MA, USA

Denis E. Pellerin, MD, PhD
The Heart Hospital, London, UK

Harry Rakowski, MD, FRCPC, FACC, FASE
Toronto General Hospital, Toronto, ON, Canada

J. Daniel Rivera, CVT
Duke University Medical Center, Durham, NC, USA

J.R.T.C. Roelandt, MD, PhD
Department of Cardiology, Erasmus MC, Rotterdam, The Netherlands

Robert M. Savage, MD, FACC
Departments of Cardiothoracic Anesthesia, and Cardiovascular Medicine, The Cleveland Clinic Foundation, Cleveland, OH, USA

Marcy L. Schwartz, MD
Department of Cardiology, Cleveland Clinic, Cleveland, OH, USA

Partho P. Sengupta, MBBS, MD, DM
Cardiovascular Division, Mayo Clinic Arizona, Scottsdale, AZ, USA

Roxy Senior, MD, DM, FRCP, FESC, FACC
Department of Cardiology, Northwick Park Hospital, Harrow, Middlesex, UK

Frank E. Silvestry, MD, FASE
Cardiovascular Division, Department of Medicine, Radnor, PA, USA

Larry J. Sinak, MD
Department of Cardiology, Mayo Clinic, Rochester, MN, USA

William Smith, MD
Division of Cardiovascular Medicine, Duke University Medical Center, Durham, NC, USA

Alexander Stefanidis, MD, FACC, FASE
Section of Cardiovascular Imaging, Department of Cardiovascular Medicine, General Hospital of Nikaias, Piraeus, Greece

William J. Stewart, MD
Department of Cardiovascular Disease, The Cleveland Clinic, Cleveland, OH, USA

Jamil A. Tajik, MD, FACC
Mayo Graduate School of Medicine, Mayo Clinic, Rochester, MN, USA

Teresa S.M. Tsang, MD
Division of Cardiovascular Diseases, Department of Medicine, Mayo Clinic, Rochester, MN, USA

Jean-Louis J. Vanoverschelde, MD, PhD
Department of Cardiology, Cliniques Universitaires St-Luc, Brussels, Belgium

Cees A. Visser†, MD, PhD
Department of Cardiology, VU University Medical Center, Amsterdam, The Netherlands

Eleni C. Vourvouri, MD, PhD, FESC
Thoraxcentre, Erasmus MC, Rotterdam, The Netherlands

William A. Zoghbi, MD
Department of Cardiology, The Methodist DeBakey Heart Center, The Methodist Hospital, Houston, TX, USA

Section 1
How Things Work

Chapter 1
Physical Principles and the Basic Exam

Graham Leech

Introduction

The modern cardiac ultrasound scanner is a very sophisticated piece of equipment. It provides the ability to generate moving images of the heart, together with quantitative data on blood flow and tissue motion. The output is displayed in real time, either as two-dimensional (2-D) tomographic ("slice") images or, more recently, rendered three-dimensional (3-D) "volume" images from which individual sectional planes can be extracted. Although much of the pioneering development in echocardiography was carried out by researchers in academic institutions and small, innovative companies, the cost of developing, manufacturing and supporting the products is now such that the machines are now produced by almost exclusively by multinational electronics corporations.

Most of us drive a car without understanding the intricacies of an automatic gearbox or fuel injection, and we use computers without any need to know how the digital data within them are routed, and computations made millions of times each second. Furthermore, much of the information on the construction of ultrasound transducers and the image processing algorithms employed in the scan converters are closely guarded commercial secrets. Nevertheless, almost every textbook and training course in echocardiography (this volume being no exception) begins with a discussion on "Physics." The positive view is that some knowledge of the principles of ultrasound imaging is fundamental to understanding clinical applications, but there is no doubt that many students regard it as a "necessary evil," to be endured and then forgotten once they have moved on to the clinical applications. Conscious of these facts, the aim of this chapter will be restricted to three areas:

(a) Basic understanding of how images and flow velocity data are obtained
(b) The major user control functions in the machines and how they affect image quality
(c) How limitations both of fundamental physics and current technology can result in image distortion and artifact that not infrequently result in serious misdiagnoses

Basic Concepts

Echocardiography employs high-frequency sound (pressure) waves to generate images of the heart and to study blood flow within the cardiac chambers and blood vessels. It is closely analogous to radar and the reader familiar with the way in which information from radar or a marine depth-sounder is gathered and displayed will recognize many similarities in the two techniques. Because there are fundamental differences in the physical principles underlying imaging of the heart's structure and studying blood flow, these will be considered separately, whereas in practice images and blood flow data are usually displayed and recorded superimposed or concurrently.

Pressure waves are generated by a vibrating object, and are transmitted through a solid, liquid, or gaseous medium as pressure fluctuations – waves of alternating compression and rarefaction. The velocity at which a medium propagates waves is primarily determined by its density, being higher in a solid, whose molecules are close together, than in a liquid or a gas.

G. Leech
Department of Cardiovascular Science,
St. George's Hospital Medical School, London, UK
e-mail: graham@cardiac.demon.co.uk

P. Nihoyannopoulos and J. Kisslo (eds.), *Echocardiography*,
DOI: 10.1007/978-1-84882-293-1_1,

Pressure waves travel in air at approximately 300 $m.s^{-1}$, and in soft body tissues the average value is about 1,540 $m.s^{-1}$. There is a fundamental relationship between propagation velocity, the frequency (pitch) of the waves and their wavelength (the distance between two successive maxima or minima in the train of pressure cycles).

This states that:

propagation velocity = frequency × wavelength

Thus, in soft body tissues, at a frequency of 1,000 Hz (=Hertz or cycles per second), the wavelength is 1.54 m. Commonsense dictates that this is too great to image the heart, which is only about 15 cm across and which contains structures less than 1 mm thick. To achieve a wavelength of 1 mm, the frequency has to be 1,540,000 Hz or 1.54 MHz. Such high frequencies cannot be detected by the human ear, which responds only to frequencies from about 30 to 15,000 Hz, and since the word "sound" implies a sensation generated in the brain, the term, "Ultrasound" is used to describe them.

Pressure waves and light waves share many properties. When a beam of light passes from one medium to another, part of the energy is reflected and the path of the transmitted portion is deviated by refraction. In the same way, when pressure waves encounter an interface between two different body tissues, blood and muscle for example, some of the incident energy is reflected. Another characteristic shared by light and pressure waves is diffraction, whereby the waves "bend" around the edge of an obstacle. The degree to which this is apparent depends on the relative sizes of the wavelength and the obstacle. Thus sound waves, whose wavelength in air is of the order of 1 m, appear to bend around a given obstacle much more than light waves, having a wavelength of 0.000001 m. Ultrasound used for medical imaging typically has a wavelength of the order of 0.001 m (1 mm), half-way between that of sound and light. Ultrasound can therefore be thought of as being similar to a rather poorly focused flashlight; it can be formed into a beam and aimed at regions of the heart of interest, but is far from an infinitely fine "laser" probe. The ultrasound beam comprises a central main beam, which diverges with increasing distance from the transducer, surrounded by a number of smaller, secondary beams called "side lobes." These arise from the physics of wave propagation, and from the fact that the ultrasound transducer comprises a number of individual crystal elements.

Ultrasound waves are usually generated and detected by ceramic crystals, which exhibit strong piezoelectric properties. This means that they change their shape when an electric potential is applied to them and, conversely, they generate an electric charge when mechanically deformed. Because they convert electric energy into mechanical, and vice versa, they are called transducers. The material that has been used almost exclusively for imaging transducers is Lead Zirconate Titanate. This normally is in the form of a polycrystalline ceramic material and is "polarized" by applying an electric field to align the electrical axes of the microscopic crystals. The alignment is, however, not perfect but a new process has been introduced recently, which allows production of large, single crystals, which have a single polarization axis, and this promises to improve transducer performance significantly. An echocardiographic transducer comprises one or more such crystals, mounted on an absorbent backing. When electric impulses are applied to the crystal, it vibrates at a frequency determined by its mechanical dimensions, in the same way that a bell vibrates when struck by a hammer. Transducers used for echocardiography typically generate frequencies in the range 1.5–7 MHz. The same crystal is used to detect returning echoes from ultrasonic waves it has generated.

Imaging of Cardiac Structures

The Ultrasound Beam

Images of cardiac structures are formed by transmitting a stream of very brief "pulses" of ultrasonic waves into the thorax. Each pulse comprises only a few waves and lasts 1–2 microseconds (ms). As a pulse travels through the chest wall, the pericardium, and the heart, it crosses a succession of interfaces between different types of tissue: blood, muscle, fat, etc. At each interface, a proportion of the incident energy is reflected, the remainder being transmitted into deeper tissue layers. Provided that the interfaces are extensive compared to the ultrasound wavelength, the reflections are specular (mirror-like) with the angle of reflection equal to the angle of incidence with respect to a normal to the interface. Only if the incident angle is 90° will the reflected waves re-trace the incident path and return to the transducer as an echo.

This is not always easy to achieve in practice and limits the quality of echo signals from many cardiac structures, though the fact that body tissue interfaces are not totally smooth allows return of some echoes even if the interface is not perpendicular to the ultrasound beam. The transmitted portion of the ultrasound pulse may then encounter additional interfaces and further echoes return to the transducer.

The time delay between transmission of an ultrasound pulse and arrival of an echo back at the transducer (round-trip-time) is given by

Time delay = 2 × interface distance/propagation velocity

Thus, if the propagation velocity is known and the time delay can be measured, the distance of each echo-generating interface from the transducer can be determined. It is important to note that the machine actually measures *time delay* and derives the *distance* from an assumed value for the propagation velocity in soft tissues. If, however, the ultrasound passes through an object having different transmission characteristics from soft tissue, e.g., a silicone ball valve prosthesis, the time delay of returning echoes will change and the derived distance measurements will be false.

The total time for all echoes to return depends on the distance of the furthest structure of interest. This may be up to 24 cm, for which the round trip time in soft tissue is approximately 300 ms. Only then can a second ultrasound pulse be transmitted, but even so it is possible to send more than 3,000 pulses each second. This stream of brief ultrasound pulses emanating from the transducer is referred to as an "ultrasound beam." The first echoes to return and strike the piezoelectric crystal arise from structures closest to the transducer, followed in succession by those from more distant interfaces. The minute electrical signals thus generated are amplified and processed to form a visual display showing the relative distances of the reflecting structures from the transducer, with the signal intensities providing some information about the nature of the interfaces.

The 2-D Sector Image

In order to generate 2-D tomographic (slice) images of the heart, the ultrasound beam has to be scanned across a section of the heart. The limited access to the heart afforded by spaces between the ribs and lungs dictates that cardiac scanners are of the sector scan type. The transducer is positioned on the chest manually and held steady, but the ultrasound beam it generates sweeps rapidly to and fro across a sector of an arc, creating a fan-shaped scan in the same way that a lighthouse beam sweeps across the sea, illuminating objects in its path. In order to avoid blurring of the image by the heart's motion, at least 25 images per second are required. The maximum attainable image frame rate is primarily the result of a trade-off between the required image depth, which limits the number of pulses transmitted per second, and the sector angle and image line density, but other factors such as the display mode and imaging processing power of the machine are now involved. Image frame rate shown on the display screen may be as high as 150 s^{-1} or as low as 6 s^{-1}. It can be improved by reducing image depth and/or narrowing the scan angle.

Almost all commercial echo machines use "phased array" technology to scan the ultrasound beam. Using sophisticated equipment derived from that used to cut silicon for manufacturing electronic "chips," a single piezoelectric crystal is sliced into as many as 256 very thin strips, each connected individually to the electric pulse generator, which activates them in a very rapid and very precisely controlled sequence, as shown in Fig. 1.1. The wavelets from each crystal element merge to form a compound ultrasound wave. By varying the electrical activation sequence, the direction of the compound wave can be changed and a series of pulses generated to form a sector scan configuration. For a sector angle of 90° and working depth of 15 cm, each image comprises about 200 scan lines and takes about 40 ms.

Immediately after each pulse is transmitted, echoes start to return. The minute electrical signals they generate as they strike the transducer and deform its crystal elements are first amplified, then demodulated, which removes the ultrasound-frequency waves leaving just their envelope. The echo signals resulting from a single ultrasound pulse now comprise a sequence of electronic "blips" representing the intensities of the echo reflections it generated (Fig. 1.2). To facilitate further processing these are "digitized" – converted into a series of numbers, whose values represent the echo amplitudes at discrete intervals – and allocated to a digital memory store.

The basic image data comprise a series of radial scan lines like spokes of a wheel which are relatively

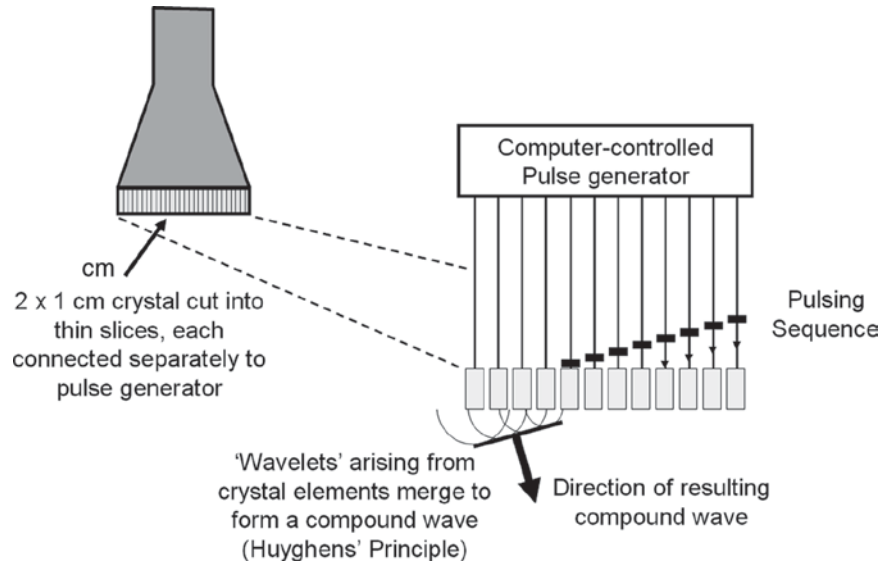

Fig. 1.1 How the ultrasound beam direction is controlled by pulsing the crystal elements in sequence

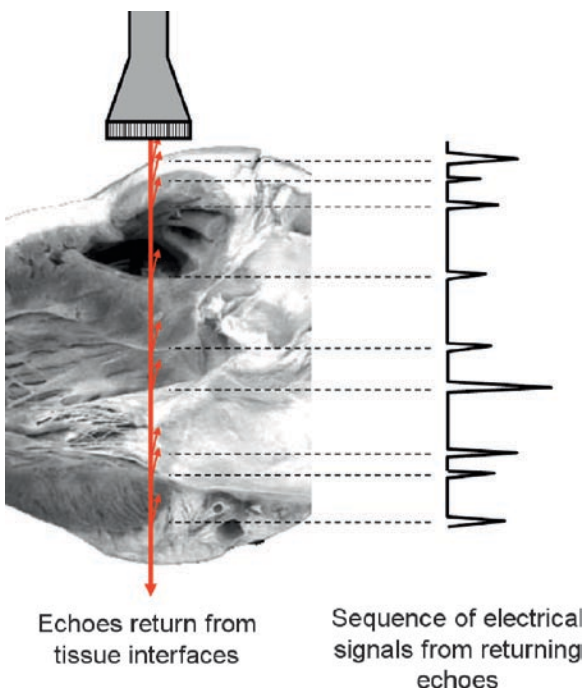

Fig. 1.2 Echoes returning from tissue interfaces are converted into electrical impulses

close together near to the transducer, but deeper into the thorax there are significant gaps between them (Fig. 1.3). In the earliest 2-D scanners of the 1970s, this line structure was evident (Fig. 1.4), but nowadays it is masked by assigning image values to the "empty" memory cells based on averages of surrounding cells. The averaging process employs proprietary algorithms which account in large part for the differences in image texture that are characteristic of the various brands of machine. From this stage onward, the image is represented by a matrix of numbers, enabling the power of the digital computer to be harnessed to process them further and form the visual display on the monitor screen.

M-Mode

In the earliest echo machines, the ultrasound beam was fixed, with the only steering provided by the operator's hand. The beam thus only interrogated structures along a single axis, a so-called "ice-pick" or "needle biopsy" view, with tissue interfaces represented as dots on the display screen. In order to show motion patterns, a linear sweep is added resulting in a graphic display as shown in Fig. 1.5. Though harder for the non-specialist to understand and considered by some to be "old fashioned," the M-mode display still offers important benefits: it shows data from several cardiac cycles on a single image; it provides temporal continuity making it easier, for example, to identify a structure such as the endocardium from background clutter; and it has far greater temporal resolution (1,000 lines.s^{-1} compared to 25 for a 2-D image), making it superior for accurate

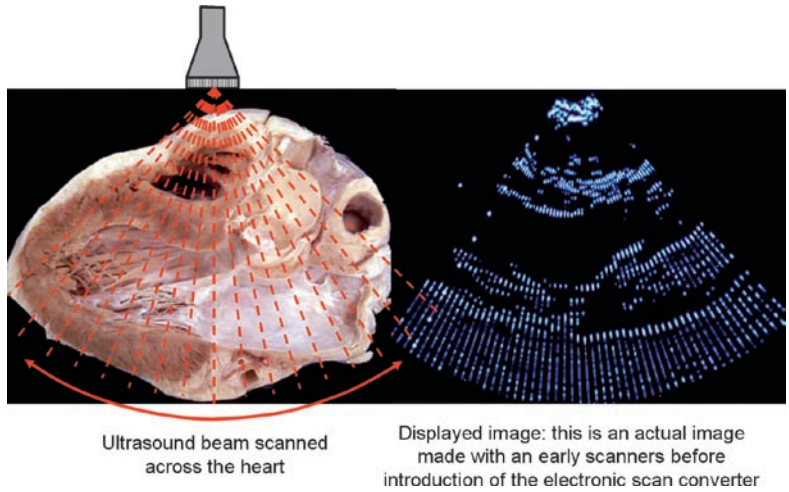

Fig. 1.3 The ultrasound beam is scanned rapidly to and fro across the heart and the echo signals are converted into an electronically generated image

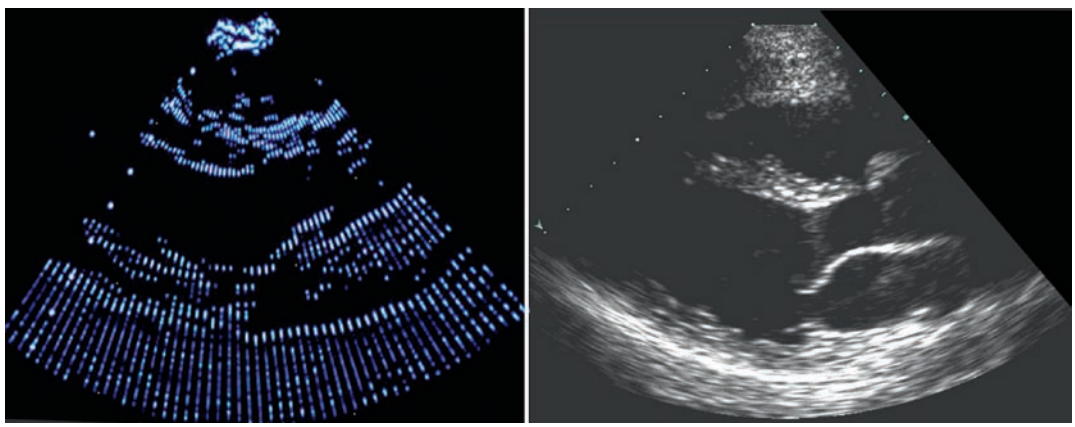

Fig. 1.4 (*Left*) Ultrasound image made in 1977 prior to introduction of scan converters and (*right*) from a modern machine. The scan converter interpolates the spaces between the actual scan lines and creates a more esthetically pleasing image, but does not add new information

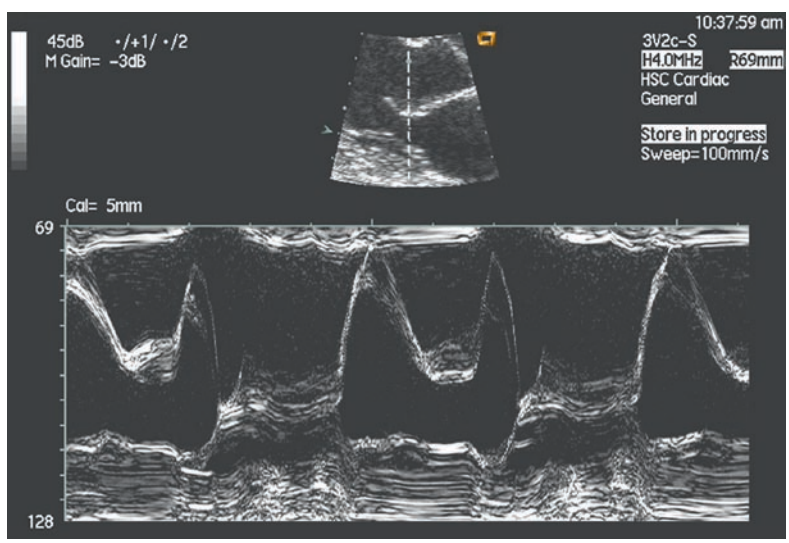

Fig. 1.5 "M-mode" display of the motion pattern of the mitral valve. The beam direction is indicated on the small image icon at the top of the display

timing and resolution of rapid movements such as a vibrating valve prosthesis.

Attenuation, Reflection and Depth Compensation

Attenuation: Ultrasound can travel great distances in water, but soft body tissues are "spongy" and nonhomogeneous, resulting in attenuation of the ultrasound waves. The degree of attenuation depends greatly on the frequency. At 2.5 MHz, approximately half of the amplitude is lost for every 4 cm of path length, rising to half per 2 cm at 5 MHz and half in only 1 cm at 7.5 MHz. This is a cumulative effect, so at 5 MHz the wave amplitude reaching a structure 16-cm distant is only 1/256 (½ × ½ × ½ × ½ × ½ × ½ × ½ × ½) of that transmitted.

Reflection: The proportion reflected at a tissue interface depends mainly on the difference in density of the tissues. Where there is a large difference, such as an interface with air or bone, most of the incident energy is reflected, creating an intense echo but leaving little to penetrate further to deeper structures. It is for this reason that the operator has to manipulate the transducer to avoid ribs and lungs, and that a contact gel is used to eliminate any air between the transducer and the chest wall. In contrast, there is relatively little difference in the densities of blood, muscle and fat, so echoes from interfaces between them are very small – something like 0.1% of the incident amplitude. The echoes are then further attenuated as they return to the transducer, with the result that the amount reaching the transducer is very small indeed. In the case illustrated, approximately (1/256) × (1/1,000) × (1/256) or just 1/65,000,000 of the transmitted amplitude!

Depth compensation: Not only is this a very small signal to detect, but the amplification level required would be vastly greater than that needed for the same interface at a range of 4 cm, for which the returning signal would be approximately (1/4) × (1/1,000) × (1/4) or 1/16,000. To overcome this problem, the machine incorporates Depth Compensation or Time-Gain Compensation (TGC). This automatically increases the amplification during the time echoes from a particular pulse return, so that the last to arrive are amplified much more than the first. Most of this compensation is built into the machine, but the user can fine-tune it by means of a bank of slider controls that adjust the amplification at selected depths.

Attenuation artifacts: the intensity of an echo is determined by the product of the ultrasound beam intensity and the structure of the reflecting object. Thus, if the beam is scanning an essentially homogeneous region such as a blood-filled chamber, we would expect the image to appear homogeneous. However, if the beam itself is not homogeneous (typically there is a "hot spot" around the focal zone), then the image in this region will be more intense and generate an artifact that might be interpreted as a mass within the chamber. Such artifacts are usually in the center of the image sector, a few centimeters from the transducer.

The reflection and attenuation characteristics of various media can be used to help in their identification. Referring to Fig. 1.6, with optimized Depth Compensation a soft-tissue structure having slightly different density from its surroundings would be represented as in panel (a). However, within a liquid-filled cystic lesion attenuation is much lower, so the beam beyond it is more intense than in the surrounding tissues, generating a bright "comet tail" as in panel (b). Conversely, an interface with air, such as may be encountered in a cardiac chamber post cardiopulmonary bypass, reflects almost all the incident energy, generating a very bright proximal boundary, and the high attenuation of air strongly attenuates any remaining transmitted beam casting a dark shadow (c).

Reverberation and Multiple Reflection Artifacts

Reverberations: The presence of structures having transmission and attenuation characteristics greatly different from soft tissue is also the cause of reverberation and multiple reflection artifacts, one of the most common sources of misinterpretation of images. Referring to Fig. 1.7, an ultrasound beam crossing a structure normally generates two echoes – one from each interface. However, the echo returning from the further interface has to cross the nearer interface, so part of it is again reflected. This secondary reflection then meets the distant interface a second time, where further reflection occurs, and so on. Under normal circumstances this effect is not seen because soft-tissue

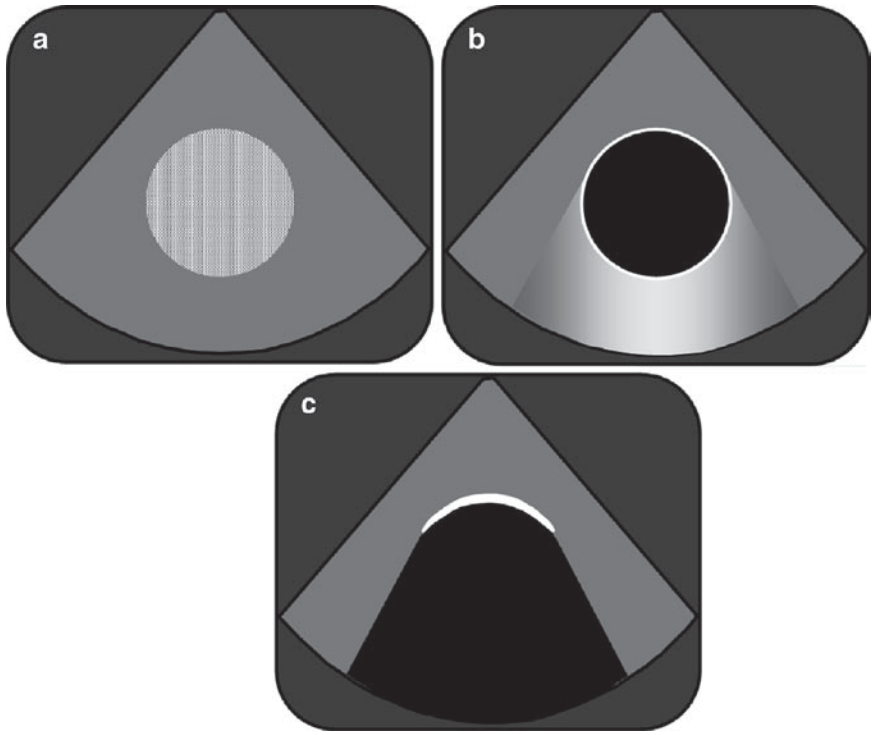

Fig. 1.6 Schematic representation of ultrasound images of (**a**) a soft-tissue mass, (**b**) a liquid-filled cyst, and (**c**) air

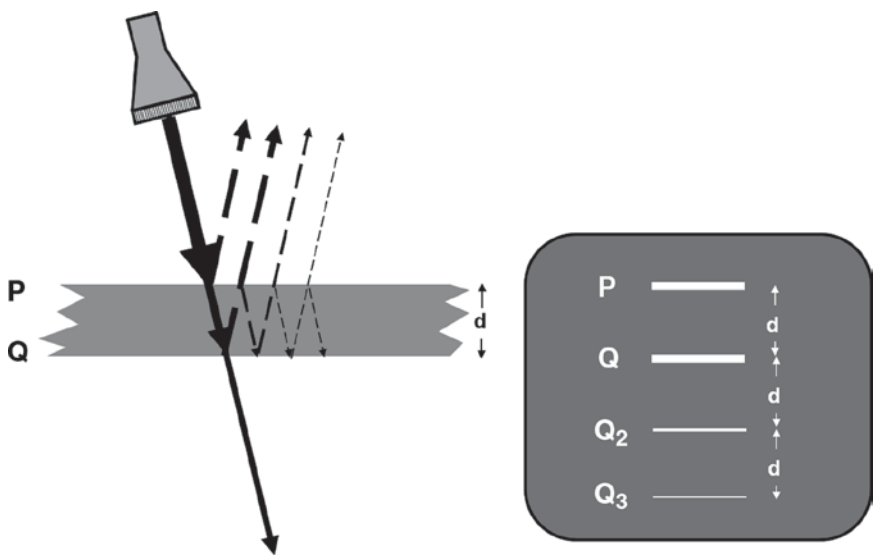

Fig. 1.7 Multiple reflection artifact: If an object generates intense echoes, higher-order reflections are still strong enough to register on the display

reflections are so weak. Thus, if the original echo is 0.1% of the incident wave, the secondary echo has undergone two further reflections and is only (0.1 × 0.1 × 0.1%) and too small to register. If, however, the object is a very strong reflector such as a calcified or prosthetic valve with each reflection, say, 10% of the

incident wave then the secondary or higher-order reverberation echoes are strong enough to be detected and are shown as multiple images of the object (Fig. 1.8).

Reflection artifacts: Another consequence of a high-intensity echo is that it can bounce off the transducer face, or a strongly reflecting structure like the pericardium, and back again to the object, creating a secondary "ghost" image (Fig. 1.9). The clue to their recognition is that they are always exactly twice as far away from the transducer as a high-intensity echo, and if the primary structure moves a certain distance, the image generated by multiple reflections moves twice as far.

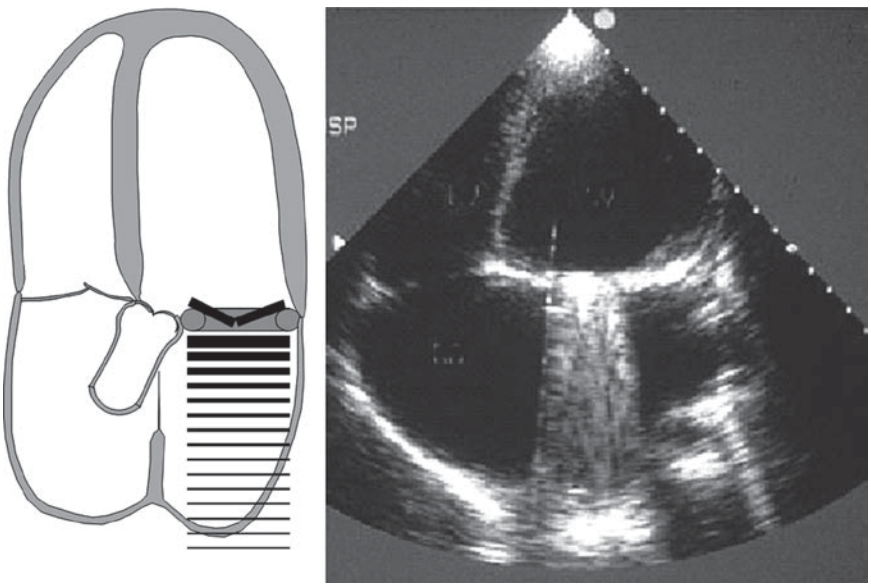

Fig. 1.8 (*Left*) Diagram and (*right*) ultrasound image of a bileaflet prosthetic mitral valve showing multiple reflections from the strongly reflecting hemidiscs. Note how the scan converter has tried to "fill in" the spaces between the echoes

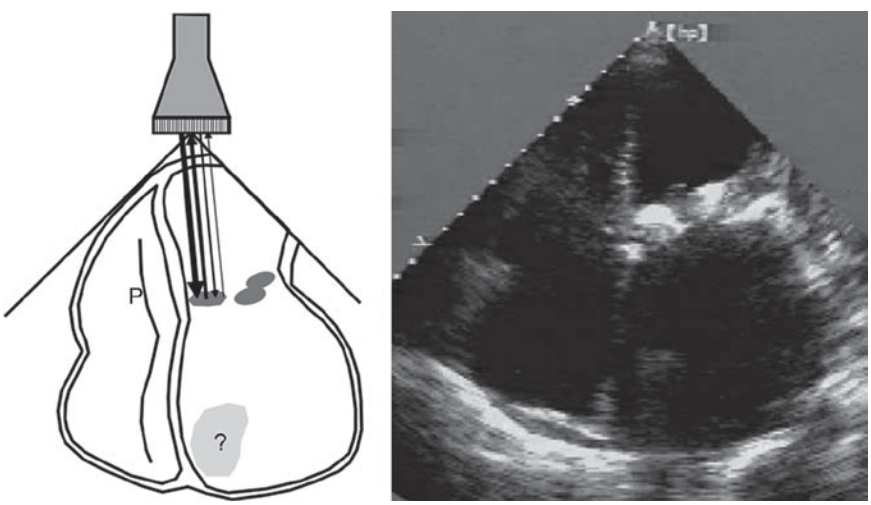

Fig. 1.9 Artifact mimicking a mass in the left atrium resulting from very strong echoes from the calcified mitral valve bouncing off the transducer face

Gray Scale

The intensity of an echo depends on the nature of the tissue interface. As shown earlier, there is a wide range of echo intensities, with a calcified structure generating an echo many thousands of times more intense than a boundary between, say, blood and newly formed thrombus. However, the display system can only represent a fraction of this range (though it may be hard to believe, the difference in light intensity between "black" ink printed on "white" paper is only a factor of 30 or so). Furthermore, the number of gray levels provided in a typical scan converter image memory is only 64. The result is an image with all intense echoes are shown as "white," all weak echoes as "black," and almost no gray tones. This can to some extent be overcome by compressing the intensity scale to create a softer image, but at the expense of loss of boundary definition (Figs. 1.10 and 1.11).

Resolution of Ultrasound Images

The quality of all images is affected by processing imperfections and random "noise." This is quantified by measuring the resolution, which states how close together two objects can be without their images blurring into one. Resolution in an ultrasound image is

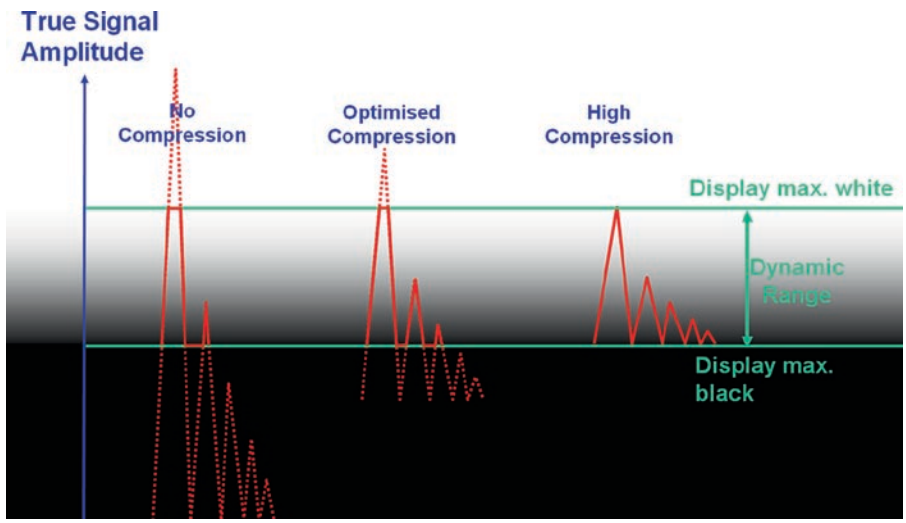

Fig. 1.10 Compression: compressing the echo signal amplitudes helps overcome the very limited dynamic range of the display

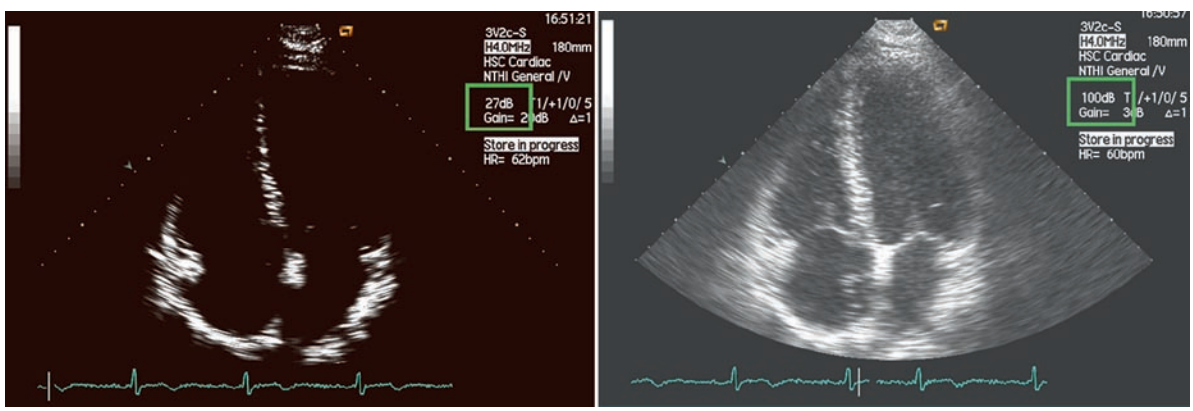

Fig. 1.11 Echo images with (*left*) low gray scale compression (27 dB) giving a harsh "black & white" image and (*right*) high compression (100 dB) resulting in an overly "soft" image

limited by inability to generate infinitely brief pulses and spreading of the beam by diffraction. It is measured along the direction of the beam ("axial" or "range" resolution) and at right angles to the beam direction ("lateral" resolution). The latter is further divided into "azimuthal" resolution, in the plane of the scan, and "elevation" resolution, above and below the scan plane. In a particular imaging system, each of these is different.

Axial resolution: This is determined by the pulse duration. Since each pulse comprises a short burst of waves lasting about 2 ms, with the propagation velocity 1,500 $m.s^{-1}$, this means that the length of the pulse is about 3 mm. If it encounters an object thinner than this, the front of the wave train comes to the second interface before its tail has crossed the first interface, so the two merge into one echo. Axial resolution can be improved by (a) employing a higher ultrasound frequency, for which the pulse duration is corresponding shorter, and (b) reducing "ringing" by lowering the transmitted power (Mechanical Index).

Lateral resolution is primarily determined by the ultrasound beam width. As shown in Fig. 1.12, if two objects are the same distance from the transducer but sufficiently close together that both are illuminated by the beam (or its side-lobes), then their echoes return simultaneously and cannot be resolved. With the image generated by scanning the beam across the image plane, this means that an object is detected over a range of beam directions, resulting in lateral "smearing" on the display, or multiple representations of a small object such as a pacemaker wire. Lateral resolution is the chief factor limiting the quality of all ultrasound images and is worse than axial resolution, typically by a factor of 10. It can be improved by making the ultrasound beam narrower by focusing it, both in transmit and receive modes. A plastic lens fitted on the face of the transducer focuses the beam both in the azimuthal and the elevation planes, in the same way that a glass lens focuses light, though less effectively. Transducers can be constructed with short-, medium-, or long-focus lenses. In addition, the pulsing sequence in a phased array transducer can be modified to provide additional variable focusing as shown in Fig. 1.13. In most machines, this improves focusing only in the azimuthal plane, but some of the more sophisticated machines have matrix arrays, in which the crystal elements are sliced in two directions, providing the ability for focusing also in the elevation plane. Even so, the beam illuminates unwanted objects, but it is possible also to filter some of these selectively using dynamic receive focusing. As shown diagrammatically in Fig. 1.14, echoes from a particular object do not arrive at all the crystal elements in the transducer simultaneously, but the electrical impulses they generate can be selectively delayed so that those from a particular distance and/or direction reinforce each other, while those from other sources do not. This is analogous to tracking a fast-moving airplane by altering the focus of binoculars as its distance changes.

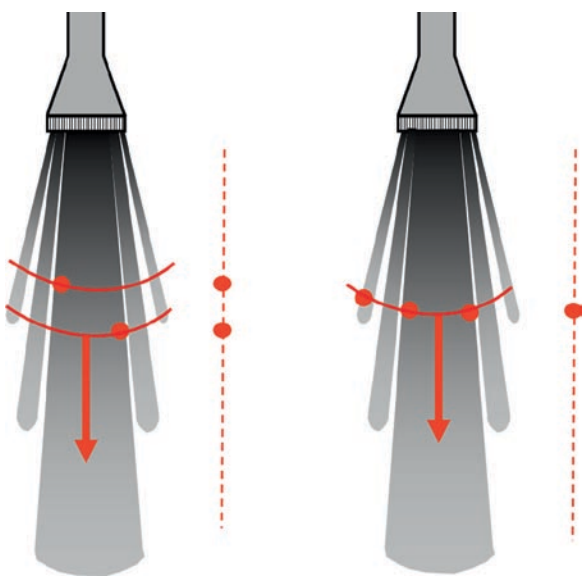

Fig. 1.12 Lateral resolution: (*left*) the ultrasound beam detects only the time taken for echoes to return to the transducer, so only their axial separation is registered. (*Right*) If more than one object is illuminated by the beam at the same range, the echo signals cannot be resolved

Minimizing False Diagnoses from Image

- Always use minimum power consistent with obtaining an image
- Beware of "objects" that
  - Are twice as far from the transducer as intense reflectors
  - Lie on an arc centered at the transducer and including an intense reflection
  - Are in the center of the scan sector and a few centimeters from the transducer

If in doubt, see if they are still present when transducer position and image plane are altered

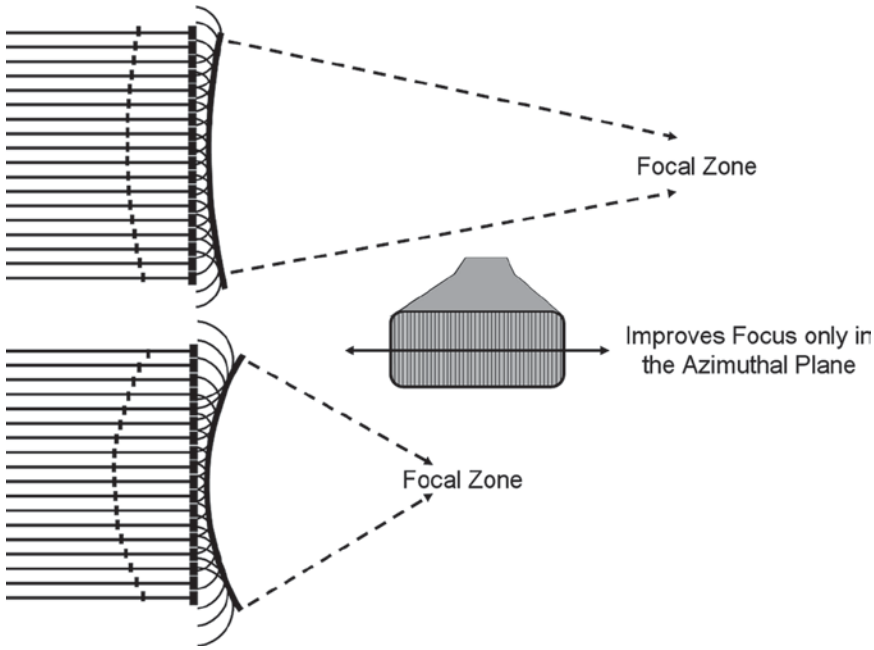

Fig. 1.13 Modification of the electronic pulsing sequence generates a curved wavefront allowing focus in the Azimuthal plane to be adjusted by the operator

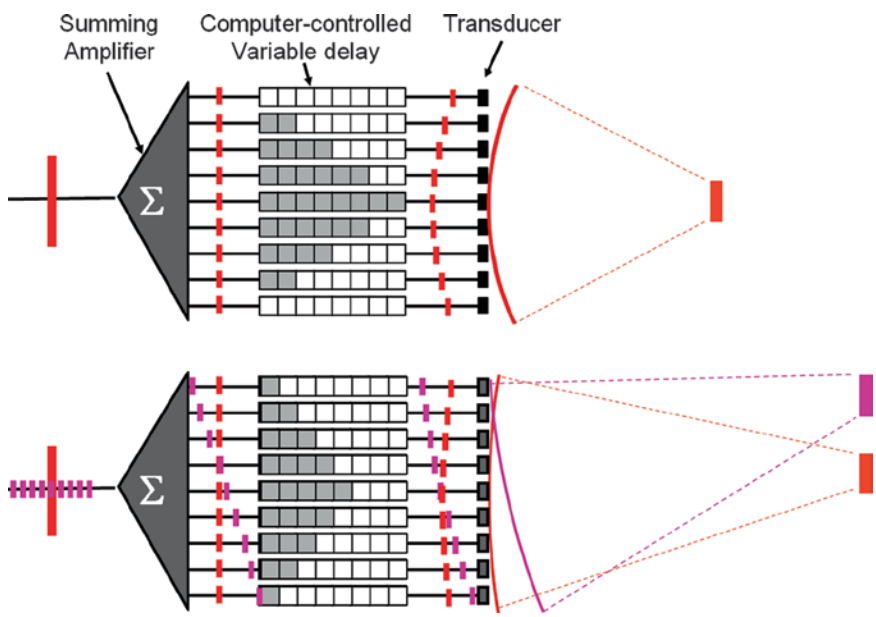

Fig. 1.14 Dynamic receive focusing: as echoes from more distant objects arrive, the delay is changed to keep them in focus, at the same time dispersing off-axis echoes

Parallel Processing

The discussion so far has been based on the formation of images by detecting time echo signals take to return to the transducer and their intensities. Although the transducer contains a number of crystal elements, they act in unison. Image quality is constrained by the scan line density and the beam width. This is not, however,

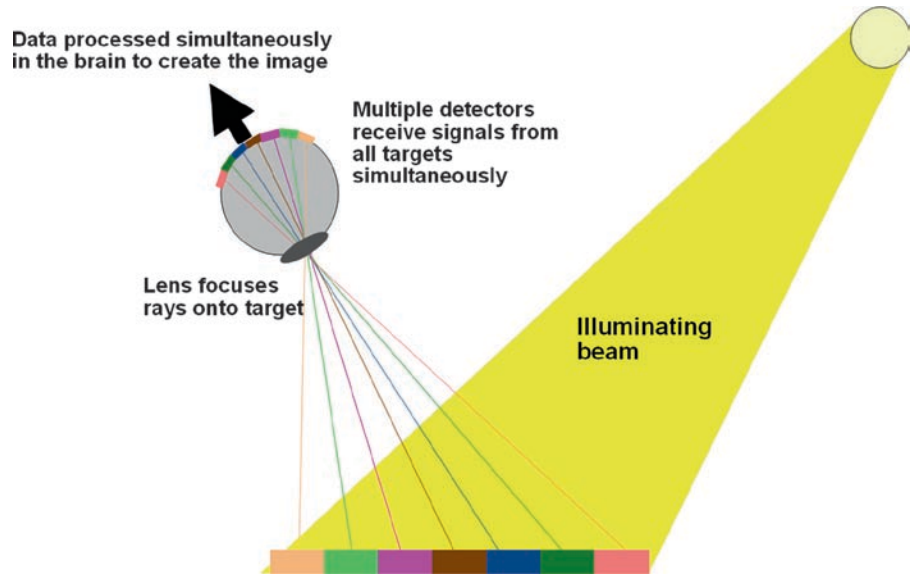

Fig. 1.15 In the eye, a lens focuses reflected light onto an array of detectors, signals from which are processed simultaneously ("parallel processing") by the brain to create the image

the way in which the human eye forms an image (Fig. 1.15). Instead of the eye scanning across the field of view, the scene is flooded with light and image data from it focused onto the millions of individual receptors that comprise the retina. Impulses from these are fed simultaneously to the brain, which processes them to form an image of the complete scene. Why cannot an ultrasound system function similarly? In theory it can, but there are some major practical limitations. The first is that, because of the difference in wavelength, an ultrasound lens would have to be several meters in diameter to be as effective as an optical lens. Secondly, we cannot make transducers with a large number of separate detectors. Thirdly, processing the image data from many detectors simultaneously ("parallel processing") requires more computing power.

However, increased computing power does already allow imaging systems to operate with two parallel processing paths (Fig. 1.16), and this will undoubtedly increase to four or more in time. Even to have two separate detectors provides an enormous benefit because, as with two ears, it provides a directional capability equivalent to a "stereo" music system. A relatively wide ultrasound beam illuminates an area of the heart. An echo from an object in the center of the beam axis arrives simultaneously at the two detector channels, but those from off-axis objects reach one detector channel before the other. The resulting phase delay allows the computer to assign them to corresponding memory cells. As the beam direction changes, objects previously on the central beam axis are still detected, but their echoes are now out of phase, and can be assigned to the correct memory location, where they add to those from the previous pulse. Several major advantages follow:

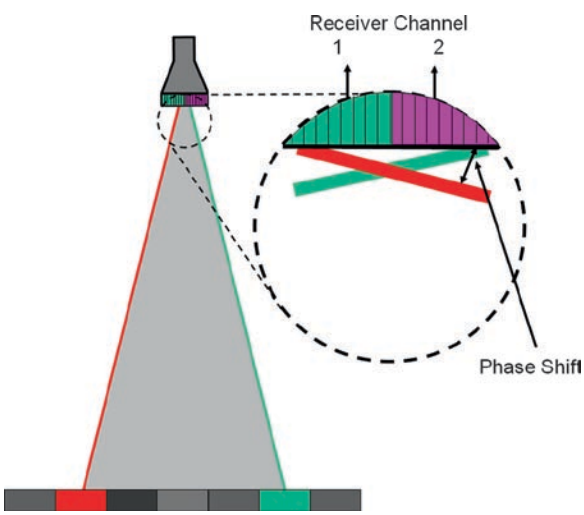

Fig. 1.16 Parallel processing: with two receiver channels, the machine can detect from which part of the illuminated region a particular echo arises

1. It is no longer necessary to a very narrow transmitted beam and to have as many transmitted pulses per image, so the frame rate can be increased.
2. By detecting both amplitude and phase data, the total amount of information is doubled.
3. The image data in each memory cell are built up over several pulses, thus improving sensitivity and reducing noise and allowing higher imaging frequencies to be used with consequent improvement in resolution.

Harmonic Imaging

Fourier's Theorem is a powerful mathematical tool for analyzing waves. It states that any repetitive wave, of whatever shape, can be constructed by adding together a number of regular sine waves of varying frequencies and amplitudes. The basic building block for a particular complex wave is a sine wave having the same frequency and termed the "fundamental." The detail that gives the complex wave its shape is provided by adding to the fundamental further sine waves having frequencies that are exact multiples of that of the fundamental. These are called harmonics (the second harmonic has twice the frequency of the fundamental, the third harmonic three times, and so on). To form a complex wave perfectly, theory requires an infinite number of harmonics, but their contributions become smaller as the frequency increases, and in practice a fundamental plus ten harmonics provides an adequate representation of the complex wave (Fig. 1.17). The reason why a violin and a trumpet playing the same note sound different is that, though they generate the same fundamental frequency, their harmonic contents are different.

A pure sine wave contains no harmonics, but if its shape is distorted it means that harmonics have been added. This is what happens as an ultrasound pulse travels through the body and it is a consequence of the fact that body tissues, unlike a liquid or solid, are "spongy" and can be compressed relatively easily. As shown in Fig. 1.18, as the positive pressure region of the wave passes through the tissue, it compresses it and the negative part of the wave vice versa. The density of the compressed tissue increases, so the positive pressure part of the wave travels faster and conversely the negative pressure part travels more slowly. The fact that the wave shape changes as it progresses through the body means that it has acquired a harmonic component, which application of Fourier analysis shows is

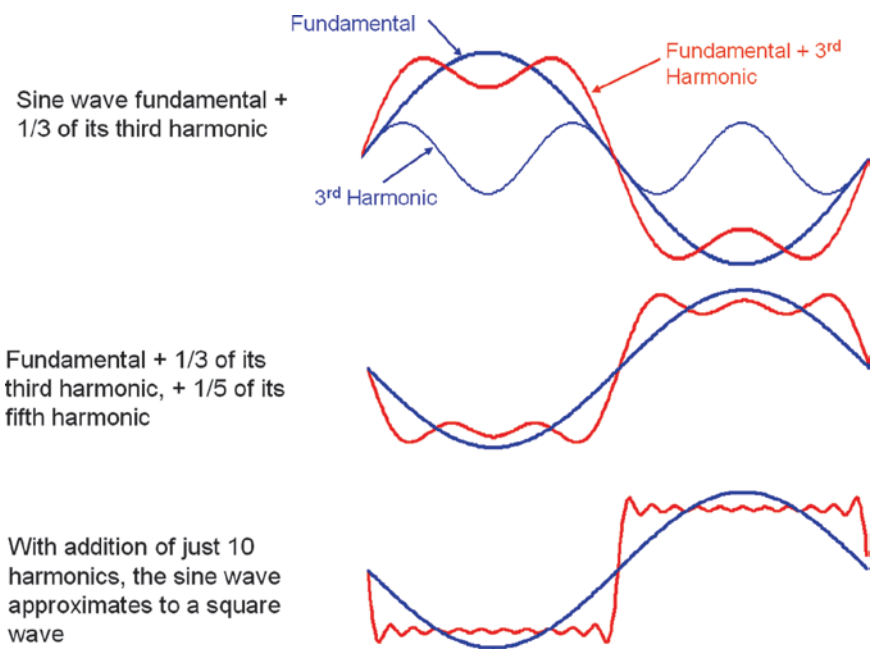

Fig. 1.17 Fourier analysis: the principle by which a complex wave can be created by addition of sine waves or broken down into its sine-wave components

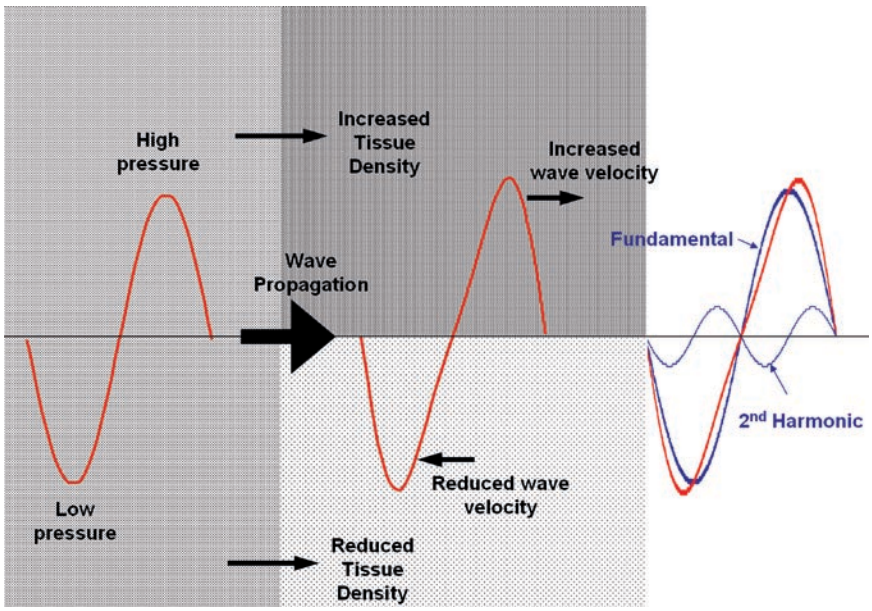

Fig. 1.18 Distortion of a wave as it travels through a compressible medium gives it a significant second-harmonic content

mainly second harmonic, with a smaller proportion of fourth harmonic, and so on.

Thus, when a ultrasound pulse of say, 2 MHz, is transmitted into the body, the echoes that return are not pure 2-MHz sine waves, but include some of its second harmonic (4 MHz), and a little of its fourth harmonic (8 MHz). By selectively filtering out the 2-MHz fundamental, it is possible to form the image from the 4-MHz second harmonic component. This arises mainly from the most intense central part of the beam and, because the wave distortion increases as the transmitted wave travels through the body, there is relatively little harmonic component from proximal structures, and most arises from deeper areas. Harmonic imaging thus provides the following benefits:

1. It combines the penetration power of a transmitted low fundamental frequency with the improved image resolution of the harmonic and twice the frequency.
2. The harmonic image is preferentially derived from deeper structures and reduces artifacts from proximal objects such as ribs.
3. The harmonic image away from the central beam axis is relatively weak and thus not so susceptible to off-axis artifacts.

The improvement in image quality obtained from second harmonic imaging is such that it should be mandatory for all new machine procurement, and machines without it should be regarded as obsolete.

There is just one problem associated with harmonic imaging. Because the image is now formed from echoes of a single frequency, some "texture" is lost and structures such as valve leaflets may appear artificially thick. Thus, if the quality of the fundamental frequency image is very good, using the second harmonic mode will offer little benefit and it is best not to use it, but in most patients the improvement in image quality greatly outweighs this minor disadvantage, and in any case manufacturers are likely soon to offer "broad-band" harmonic imaging which will remove the problem.

Transesophageal Imaging

2-D imaging from a phased array transducer positioned in the esophagus has been commercially available since the late 1980s. The transducer (Fig. 1.19) is similar in construction to a gastroscope, but in place of the fiber-optic bundle used for light imaging, a miniature ultrasound transducer is mounted at its tip. This currently has 64 elements (compared with 128 or 256 for transthoracic transducers), but because there is no attenuation from the chest wall, it operates at higher frequencies (up to 7.5 MHz) and produces excellent image quality. Since limited manipulation is possible within the esophagus, the complete transducer array can be rotated by a small electric motor controlled by

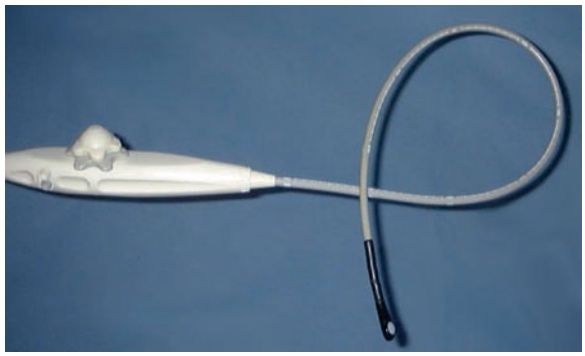

Fig. 1.19 Transesophageal transducer

the operator to provide image planes that correspond to the orthogonal axes of the heart despite the fact that these are not naturally aligned with the axis of the esophagus. As mentioned in the section "Is Ultrasound Safe?", special precautions have to be taken to prevent accidental harm to the patient through heating of the transducer. The potential for it to apply 300 volts electrical impulses to the back of the heart also requires it to be checked regularly to ensure integrity of the electrical insulation.

Real-Time 3-D Imaging

If, as well as scanning the ultrasound beam across a linear section of the heart, the entire image plane is scanned up and down, with the echo data fed into a 3-D memory array, it is possible to generate a complete "data set" of the heart's structures rapidly enough to form real-time 3-D images. To achieve this has required overcoming several daunting technological challenges. The first is the construction of the transducer. Instead of cutting a crystal into slices, with wires attached to their edges, the crystal now has to be cut into a matrix of minute squares, each only 2–3 times the width of a human hair, and a wire attached to each one (Fig. 1.20). Even when this is done, the total number of wires is such as to make the connecting cable too unwieldy for clinical use, so the "front-end" beam forming and image processing has to be controlled by electronics built into the transducer, without making it too large or heavy for the operator to hold.

The second problem is to process the enormous amount of data in real time. In the earliest machines real-time imaging has been possible only in parasternal views (where the smaller depth allows higher pulse rates), and even so has involved significant compromises of frame rate and image depth, with a lot of inter-beam smoothing and interpolation. Currently, the image quality is not as good as that of 2-D images, but with ever-increasing computer power it is only a matter of time before this is overcome.

The final problem is that of displaying the data on 2-D video screens. This is done by computer-generated texturing and shadowing to emphasize closer structures and create the impression of a 3-D solid which can be rotated and tilted by a trackball, and from which individual 2-D sections can be extracted (Fig. 1.21). The clinical possibilities for real-time 3-D imaging are enormous, particularly in congenital heart disease, and are only just beginning to be explored.

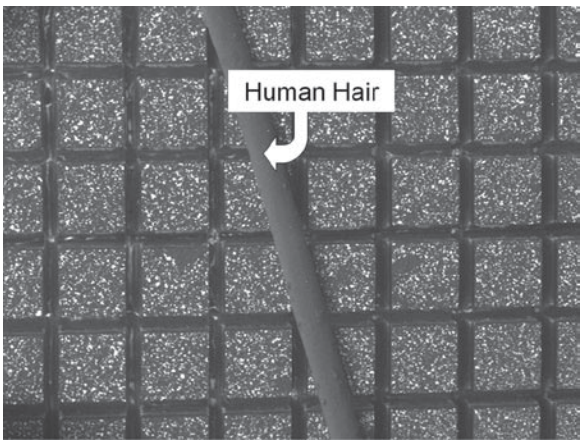

Fig. 1.20 Photomicrograph of the matrix array in a real-time 3-D imaging transducer

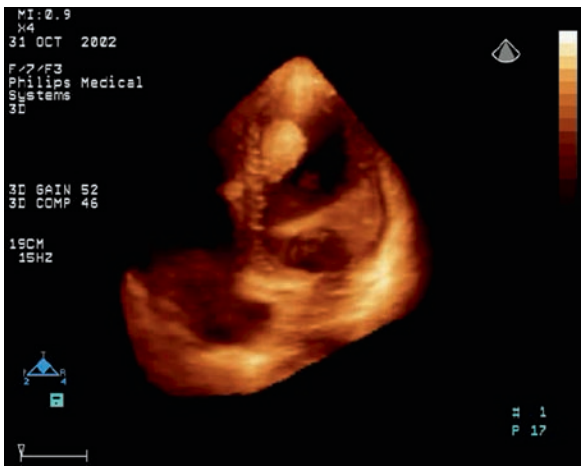

Fig. 1.21 Textured 3-D image showing masses attached to both the left and right sides of the interventricular septum

Doppler Echocardiography

Doppler Principles

The specular ultrasound echoes used for imaging the heart are derived from relatively extensive tissue interfaces. When the ultrasound beam encounters much smaller structures, it interacts with them in a completely different way, and instead of being reflected along a defined path, it is scattered equally in all directions just as the circular ripples formed when a small stone is thrown into a pond. The consequence is that most of the incident energy is dissipated, but a small amount returns along the incident path and can be detected, though the resulting signals are much weaker than the specular image echoes. Red blood cells are ideal scatterers; although the echo from a single cell is negligible, signals from millions of them added together can be detected and, if the blood is moving, the frequency of the backscattered echoes is modified by the Doppler effect.

The Doppler effect was first described in 1843 by Christian Doppler, an Austrian mathematician and scientist. He studied the light spectra of double stars and hypothesized that the shifts he observed in the hydrogen spectral lines arose from rotation of the stars about each other. If a star is moving toward the earth the spectral lines are shifted toward blue, and if its distance is increasing, the shift is toward red. Doppler's theory was confirmed by Buys Ballot in a classical experiment with two trumpeters, one on a moving train and the other on the station. Both played the same note, but observers heard the pitch of the note from the passing train change as it first approached then receded. As the wave source moves toward the observer, the waves are compressed, decreasing the wavelength and increasing the pitch, and as the source moves away from the observer, the apparent wavelength increases and pitch lowers.

Thus, if an ultrasound beam encounters a stream of moving blood, returning backscattered echoes have a slightly different frequency from that of the transmitted beam, the difference being known as the Doppler shift or Doppler frequency. The Doppler equation (Fig. 1.22) shows how this can be used to calculate the blood flow velocity. For a velocity of 1 $m.s^{-1}$ and ultrasound frequency 2.5 MHz the Doppler shift is about 3.3 kHz, only 0.1%, but readily detected and directly proportional to the blood velocity. Note, however, that, application of the Doppler equation requires that that the angle between the beam axis and blood flow direction either must be known or must be so small that its cosine is effectively unity. Also, the Doppler shift for a given blood velocity is related to the ultrasound frequency, so is twice as large for the same blood velocity at 5 MHz as for 2.5 MHz.

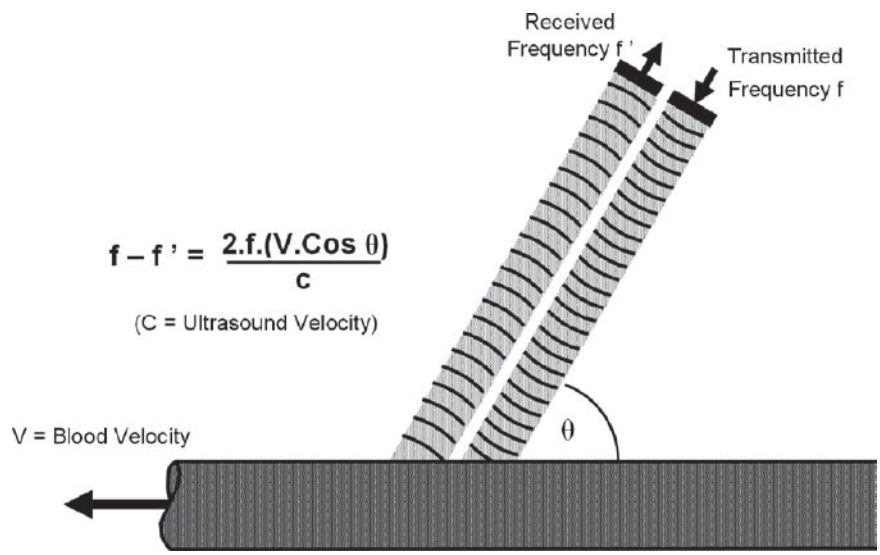

Fig. 1.22 The Doppler equation, relating flow velocity to the ultrasound "Doppler Shift"

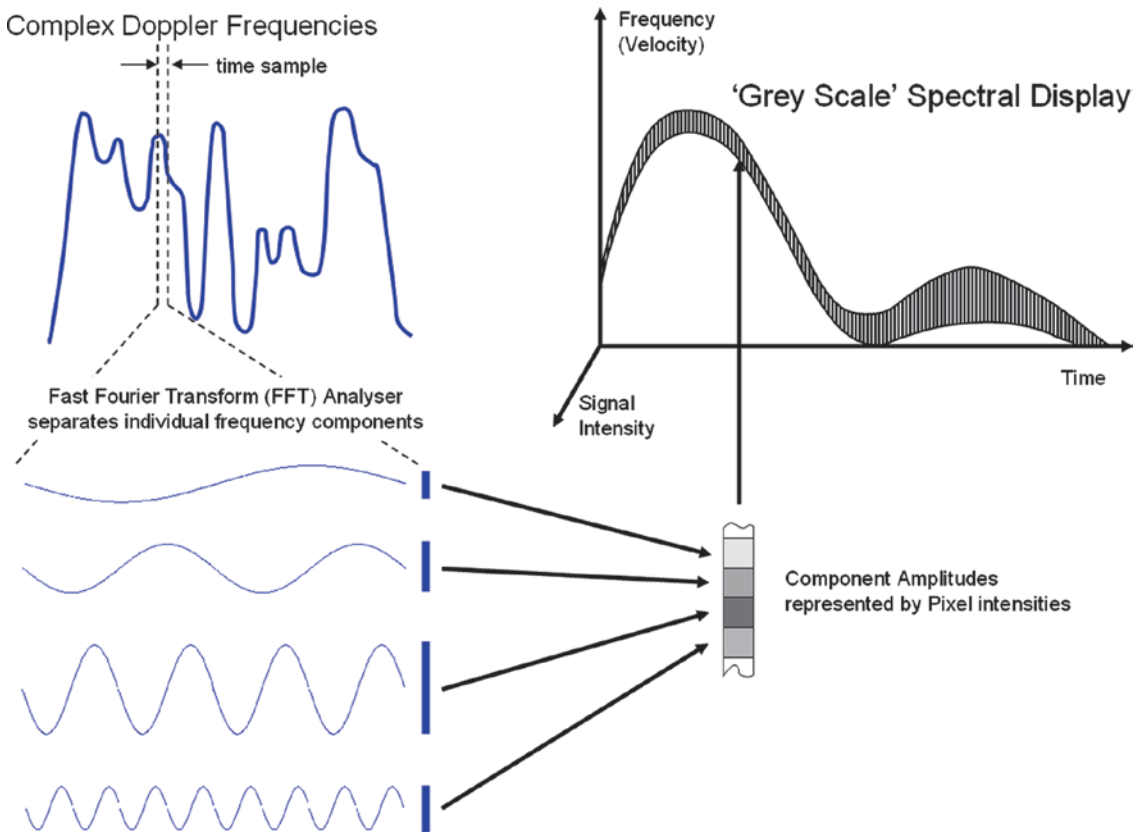

Fig. 1.23 Breaking down a complex waveform into its sine-wave components to generate a spectral Doppler display

In practice, blood in an artery does not all flow at the same velocity, due to friction at the walls. Furthermore, with pulsatile flow the velocity is constantly changing, resulting in complex flow patterns. The interrogating ultrasound beam does not therefore return just one Doppler shift, but a spectrum of frequencies, like the orchestra tuning up before a performance. The complex mix of Doppler shifts is analyzed and the resulting velocity data used to generate a Spectral Doppler Display (Fig. 1.23). This shows the range of velocities detected at each point in the cardiac cycle, with flow toward the transducer shown above the baseline and flow away from the transducer below it. The density of the image shows the amplitude of the signal at each Doppler shift, which depends on the number of scatterers, and thus the proportion of blood flow at that velocity. A line tracing the outer edge of the spectrum shows the peak velocity and a line through the center of the band approximates to the mean velocity (Fig. 1.24).

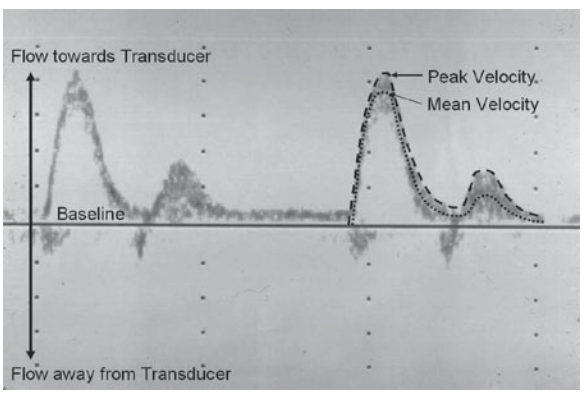

Fig. 1.24 Spectral Doppler display of flow in a carotid artery

Continuous-Wave Spectral Doppler

Instead of the brief pulses used for imaging, Continuous Wave (CW) Doppler requires transmission of a

continuous train of sinusoidal ultrasound waves and simultaneous reception of the returning backscattered echoes. This is achieved either by using a special dedicated transducer (commonly referred to as a "pencil probe") containing two separate crystals, or by assigning the crystal elements in the imaging transducer to two groups, one for transmission and the other to detect the echoes. CW Doppler provides quantitative data on blood velocities of any magnitude, enabling flow volumes and pressure gradients to be calculated.

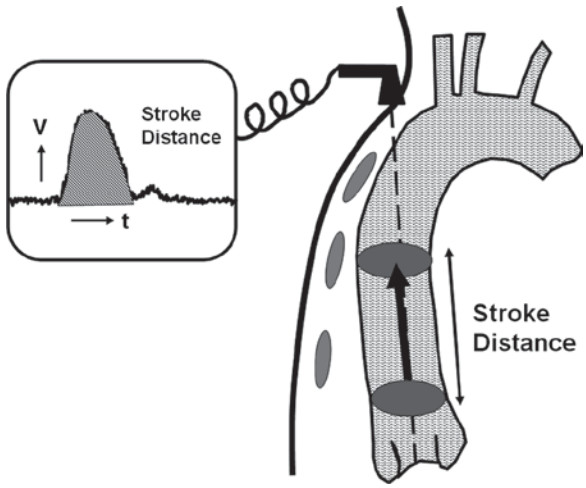

Fig. 1.25 The "Stroke Distance" is calculated by measuring the systolic area of the spectral flow display and corresponds to the distance blood travels along a vessel during one cardiac cycle

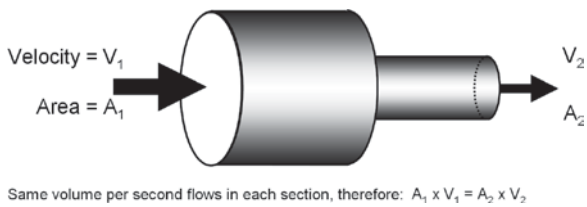

Fig. 1.26 The Continuity equation

Volumetric Flow

For steady-state flow, the volume of liquid flowing through a pipe in a given time is the product of the cross-sectional area of the pipe, the mean velocity, and the time interval (A × V × T). If flow is pulsatile, as in Fig. 1.25, the product of (velocity × time) is replaced by the velocity-time integral $\int_0^T V.\mathrm{d}T$. This is represented by the shaded area under the spectral display and has the dimension of distance (velocity × time = distance). It is called the "Stroke Distance" and in physiological terms it is the measure of the distance that an element of the fluid travels during one pumping cycle.

The Continuity Equation and Flow Through a Restricting Orifice

Referring to Fig. 1.26, if a fluid, which is not compressible, flows along a rigid-walled pipe, the amount entering one end of the pipe must be the same as that leaving the other end. If the diameter of the pipe changes, this still holds true, so a reduction in cross-sectional area is compensated for by an increase in mean velocity. This principle, known as the Continuity Equation, can be expressed as $A_1 \times V_1 = A_2 \times V_2$. Provided three of the terms in the equation are known, the fourth can be derived. This is used, for example, to determine the valve orifice area in aortic stenosis. The orifice is too small and irregular to be measured directly, but if the area of the outflow tract upstream is measured, together with the up-stream and trans-valvar velocities, then the valve area can be calculated.

Liquid only flows along a pipe if there is a pressure difference between its ends. For a fixed pipe diameter and steady-state flow, only a small pressure gradient is required to overcome frictional losses, but when the pipe becomes narrower, its velocity increases and the additional kinetic (motion) energy it thus acquires requires a higher pressure gradient.

Neglecting the frictional and turbulence losses, the relationship between pressure and velocity is:

$$P_1 - P_2 = 1 / 2\rho(\mathrm{V}_2^2 - \mathrm{V}_1^2)$$

where V_1, P_1 and V_2, P_2 are the up-stream and down-stream velocities and pressures, and r is the density of the liquid. This is simply a statement of the Newtonian principle of Conservation of Energy applied to fluids and was first derived by Daniel Bernoulli in the mid-eighteenth century.

Figure 1.27 shows the application of Bernoulli's equation to the pressure-velocity relationships in mitral valve stenosis. In this example and most clinical cases of obstructed blood flow (valve stenoses, aortic coarctation, restrictive VSD, etc.), the upstream velocity is small compared to the downstream velocity, and the

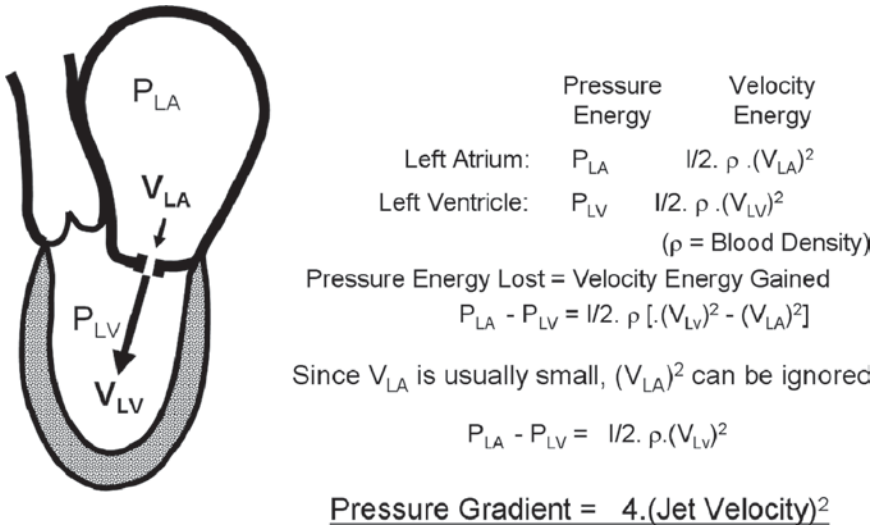

Fig. 1.27 Application of Bernoulli's equation to left heart pressure-velocity relationships in Mitral Stenosis

difference is further magnified when the values are squared, making it admissible to omit this term. In this case, the equation becomes:

$$P_1 - P_2 = 1/2\ \rho\ (V_2^2 - V_1^2)$$

and, when pressure is measured in mmHg, velocity in $m.s^{-1}$, reduces to

$$P_1 - P_2 = 4\ V_2^2$$

This simple, easily memorised relationship, first introduced into clinical cardiology by Dr Liv Hatle and colleagues in 1978, and has largely superseded invasive pressure measurements for evaluation of cardiac lesions.

Successful application of CW Doppler to measure pressure gradients requires some appreciation of its limitations, the greatest of which is the requirement to align the ultrasound beam with the direction of blood flow. Application of the Doppler equation requires that the angle between the ultrasound beam and the blood flow be known, or for the angle to be sufficiently small that its cosine is effectively unity. In practice this means aligning the beam to within 15° of the flow, for which the cosine is 0.97 and the error in the value of $(velocity)^2$ is <7%. A color-flow image (see later) can be used to guide beam alignment, and in the case of aortic stenosis measurement should be checked by using two conjugate axes (e.g., apical and upper right parasternal).

It is also necessary to align the beam with the center of the jet passing through the restriction. In the case of aortic stenosis this is quite small – just a few millimeters diameter and a few centimeters long. Only in this "inlet jet" is flow laminar, to which the Bernoulli equation is applicable; outside it flow is turbulent and cannot be analyzed. The Doppler shift frequencies are within the audible range and the machines provide an audio output from stereo speakers, one responding to flow toward the transducer and the other to flow away from it. When the beam is properly aligned, the sound has a "hissing" quality, but when it is not, the sound is harsh. Use of the "pencil probe," which is optimized for CW Doppler and does not provide a potentially distracting image, is strongly recommended for recording valve jets.

If the upstream velocity is not small compared to that downstream, then it is not permissible to omit it from the Bernoulli equation. This situation occurs, for example, with congenital pulmonary stenosis where there is frequently a muscular, subvalvar restriction combined with a valve lesion. It also applies to very mild obstruction: a velocity of 2 $m.s^{-1}$ across an aortic valve is not a "pressure gradient" of 16 mmHg if the velocity in the outflow tract is 1.5 $m.s^{-1}$.

One potential disadvantage of CW Doppler is that it provides no information on the distance at which a flow signal is detected, since it employs a continuous stream of waves and cannot detect the round-trip time

of any individual echo. It therefore cannot indicate the distance to any moving blood stream, and if it encounters more than one (e.g., normal ventricular inflow through the mitral valve together with a regurgitant stream from the aortic valve), it superimposes the two. Although this appears to be a major problem, it usually is not the case in clinical practice, since identification of the source of a high-velocity jet is usually apparent from the image and from the flow velocity profile. It was, however, to overcome this limitation that an alternative form of Doppler display called Pulsed Wave (PW) was developed.

Pulsed Wave Doppler

PW Doppler extracts flow velocity information from the echoes generated during imaging. As well as the high-amplitude, specular echoes arising from tissue interfaces, the returning signals contain backscattered echoes from blood. A movable electronic cursor on the 2-D image indicates the location of the "sample volume" from which Doppler signals are extracted, amplified, and analyzed to provide velocity data (Fig. 1.28). It should be noted, however, that whereas the axial extent of the sample volume can be made quite small, its lateral extent, governed by the ultrasound beam width, is usually significantly greater than suggested by the icon on the display. PW Doppler overcomes the lack of depth discrimination of CW, but this benefit is offset by the problem of aliasing.

Aliasing: Although PW Doppler allows spatial localization of the flow signals, it suffers from a fundamental technical limitation that severely restricts its clinical use. This is called "aliasing" and it arises from the fact that there are significant time intervals between the ultrasound pulses. Most people are familiar with aliasing as it affects cinema films. The movie camera takes a sequence of individual pictures and between exposures the camera shutter is closed while the film is advanced. Moving objects are thus seen as a sequence of "snapshots" with time gaps between them. This causes the phenomenon typified in the "Western" where, as the stagecoach with its spoked wheels starts to move, the wheels initially are seen to turn normally but, as its speed increases, they appear to stop moving, or rotate in reverse. The explanation of this is shown in Fig. 1.29. Provided the wheel rotates less than half a turn between images, all is well, but if it turns faster the images are ambiguous.

This is an example of Nyquist's Theorem, a very powerful tool of information theory. It states that for a wave to be reproduced accurately, it has to be sampled at least twice per cycle. Applied to PW Doppler, this means that the highest blood velocity that can be detected without ambiguity is that whose Doppler shift is equal to half the pulse repetition frequency (PRF) of

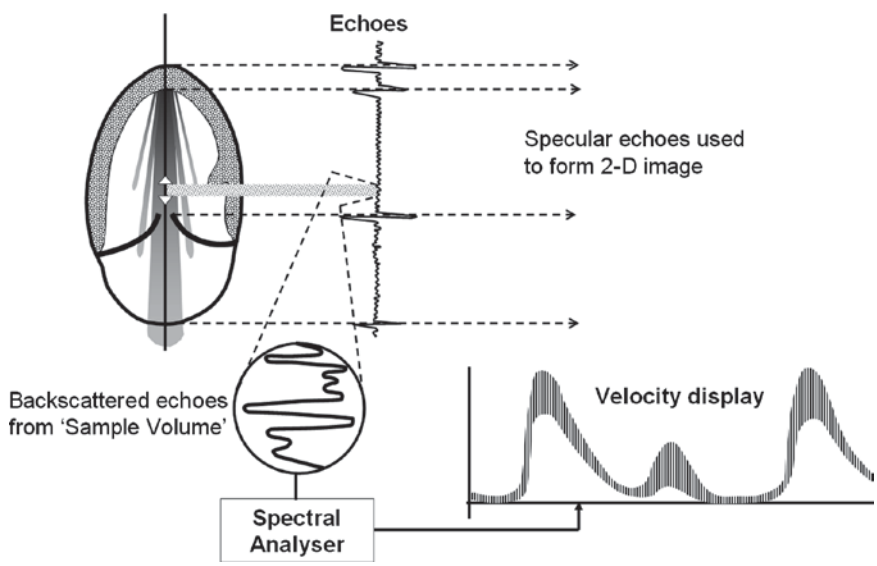

Fig. 1.28 Principle of pulsed wave (PW) Doppler

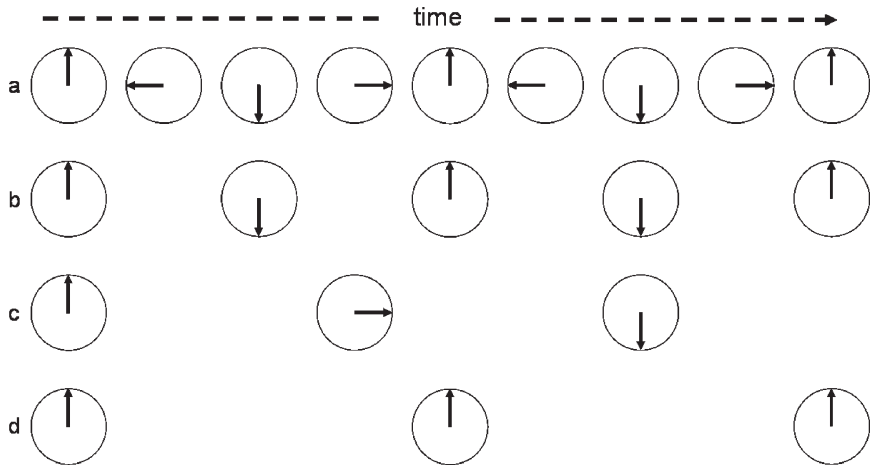

Fig. 1.29 Aliasing: (**a**) the imaging rate is high and the *arrow* is seen to rotate in a counterclockwise direction; (**b**) with only two images per revolution, the direction of rotation is unknown; (**c**) with less than two images per revolution, it appears to rotate in a clockwise direction; (**d**) with only one image per revolution, it appears to be stationary

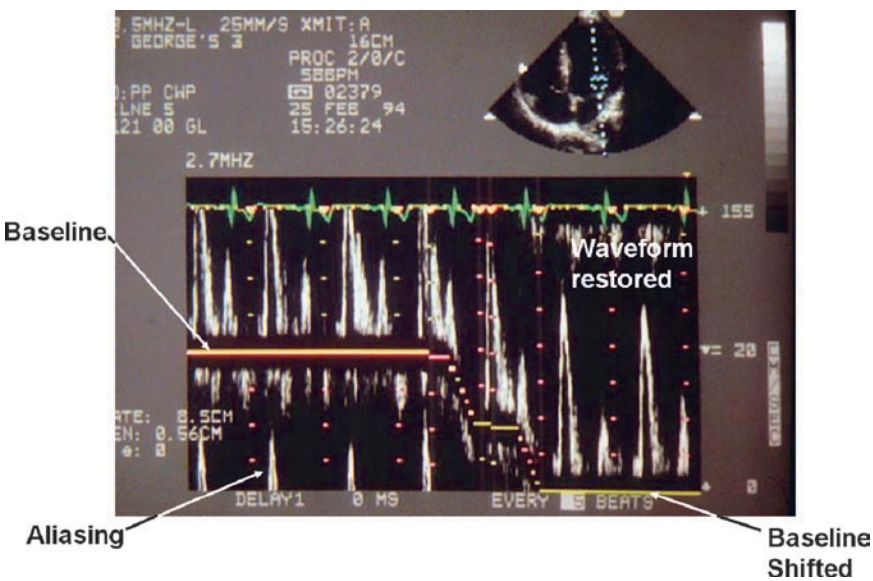

Fig. 1.30 Mild aliasing can be removed by shifting the zero-velocity baseline

the imaging system. This is called the "Nyquist Limit." The PRF is determined by the imaging depth, so as depth increases, the PRF and the Nyquist Limit are correspondingly reduced. This is the basis of the so-called Range-Velocity Product which has constant value for a given ultrasound frequency: doubling the sample depth halves the aliasing velocity and *vice-versa*. Since Doppler shift is also proportional to the ultrasound frequency, aliasing can be reduced, and the Range-Velocity Product increased, by lowering the ultrasound frequency.

The practical effect of aliasing in PW Doppler is illustrated in Fig. 1.30. The tops of the positive velocities that exceed the Nyquist Limit are cut off and displayed as negative velocities, corresponding to the stagecoach wheel turning in reverse. A simple calculation shows that aliasing occurs at quite modest blood velocities: for a working depth of 15 cm, the round-trip

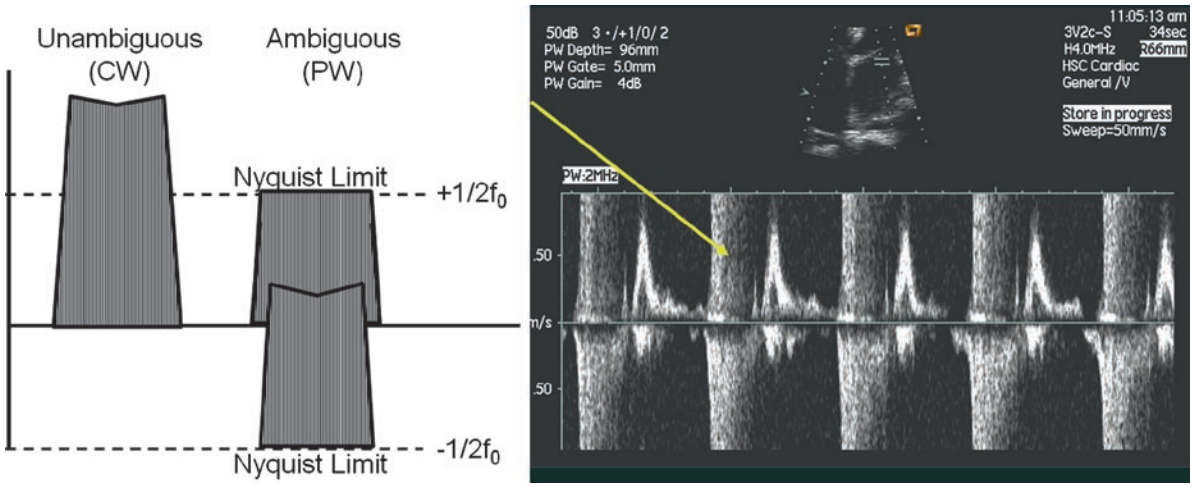

Fig. 1.31 A high-velocity jet caused severe aliasing and the PW spectral display overlaps, resulting in loss of all velocity and direction data

time is approximately 200 ms and the maximum PRF 5,000 s^{-1}. For an ultrasound frequency of 2.5 MHz, the Nyquist Limit is thus 2,500 Hz and aliasing occurs at blood velocities above 0.75 $m.s^{-1}$; and at 5 MHz aliasing begins at only 0.375 $m.s^{-1}$. Provided that the flow is predominantly toward or away from the transducer, the zero velocity baseline can be shifted to favor one direction at the expense of the other, and it is thus possible to increase the aliasing velocity by a factor of up to two. Beyond this nothing can be done, and when high velocities are encountered, the display overlaps and it not possible to tell whether the flow is toward or away from the transducer, let alone measure the velocity (Fig. 1.31).

Clinical applications of PW Doppler: The limitation imposed by aliasing makes PW Doppler generally unsuitable for quantifying obstructive valve lesions and its main clinical applications are to be found where spatial localization is important, and velocities are relatively low (1–2 $m.s^{-1}$ or less). Examples include:

- Flow waveforms across normal mitral and tricuspid valves (e.g., for evaluating diastolic function and respiratory flow variation)
- Flow waveforms in the left- and right-ventricular outflow tracts (e.g., for Continuity Equation calculations and for separating subvalvar from valve lesions)
- Calculating Stroke Volumes in the aorta and pulmonary artery (e.g., for cardiac output and Qp/Qs shunt calculations)
- Pulmonary venous flow waveforms

High PRF PW Doppler

The primary factor determining the aliasing velocity is the PRF, limited by working depth. If, the PRF is doubled, instead of Doppler shift data returning only from a single depth, it will arrive simultaneously from more than one sample volume, leading to ambiguity (Fig. 1.32). However, since the PRF has been doubled, so has the aliasing velocity. This technique, called "High PRF" or "Extended range" Doppler, can lead to confusion as to the origin of Doppler signals, but by judicious placement of the beam so that the additional sample volumes are not in high-velocity areas, this usually can be avoided.

Comparison of spectral Doppler modes

Mode	Velocity data	Depth data
Continuous Wave (CW)	Correct	None
Pulsed Wave (PW)	Limited by aliasing	Correct
High PRF	Aliasing velocity doubled, or quadrupled	May be ambiguous

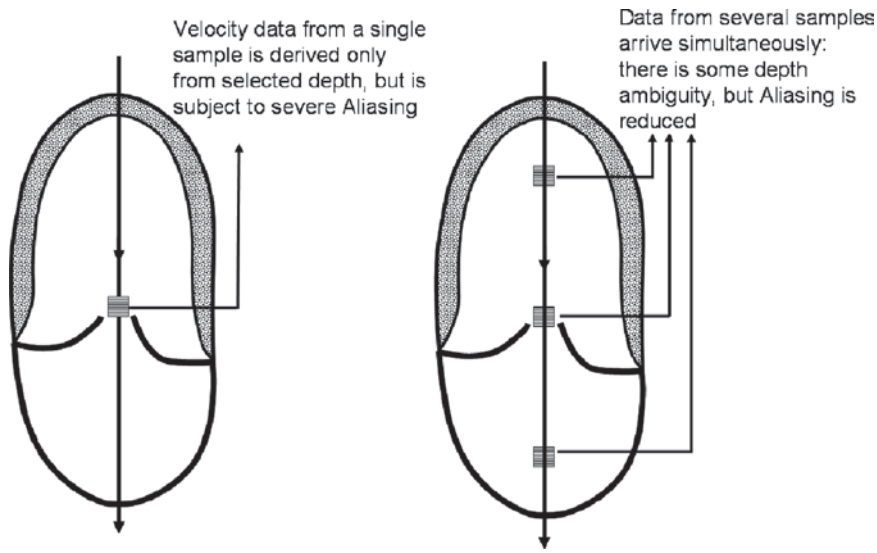

Fig. 1.32 High PRF Doppler reduces aliasing, but introduces some depth ambiguity

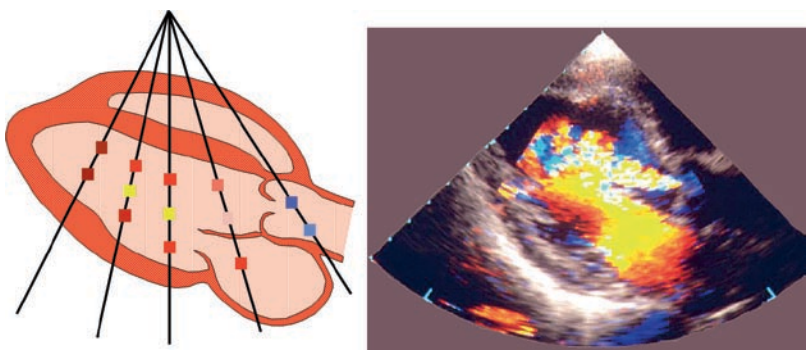

Fig. 1.33 A color flow image is formed by sampling flow velocity at a number of points and indicating mean velocity values by colored pixels superimposed on the 2-D image

Color Flow Imaging

The PW Doppler principle can be extended to detect backscattered echoes, not just from a single "sample volume" but from a matrix of small "pixels" on the 2-D image, or 3-D "voxels" on a real-time 3-D image. To analyze the Doppler shifts in real time imposes burdens on the processing system, and it is not possible to display the full spectral data from numerous sample points simultaneously, but basic velocity information can be provided in the form of a display in which the color of each pixel indicates the local flow direction and the approximate velocity (Fig. 1.33). The color flow data are superimposed on the 2-D or M-mode image. The standard convention is for flow toward the transducer to be shown as red and flow away from the transducer in blue; this is actually opposite to the observation Doppler made when he studied the stars, but it apparently arose when pioneering investigators looked at flow in their own carotid arteries and thought it ought to be colored red!

Advantages of Color Flow Imaging

Since its introduction in the mid-1980s, color Doppler has contributed greatly both to our understanding of blood flow patterns within the heart and great vessels, and also to diagnosis and management of heart disease. Many of these will become apparent in later chapters, but broadly they can be listed as follows:

- It provides a rapid, comprehensive "overview" of blood flow. This enables the echocardiographer rapidly to ascertain the presence of valve and shunt lesions, especially the unexpected, such as finding a persistent arterial duct in a middle-aged patient presenting with "left heart failure."
- It shows the spatial localization and extent of flow jets, for example the site of a VSD, or the path of an eccentric regurgitant jet from degenerative mitral valve disease. This also allows the operator to align the display cursor correctly for measuring the jet velocity with CW Doppler.
- When superimposed on an M-mode, it provides excellent temporal localization, for example to show the point at which a prolapsing mitral valve starts to leak (Fig. 1.34).

Limitations of Color Flow Imaging

While color Doppler has undoubtedly enriched understanding of blood flow within the heart, and is invaluable for detecting valve regurgitation and shunts lesions, it does have severe technical limitations, which must be understood if the images are to be interpreted correctly.

Reduced frame rate: to form a 2-D image and superimpose color Doppler on it requires three or more ultrasound pulses to be transmitted along each image line, with consequent reduction in frame rate and/or line density. With modern parallel-processing systems, this is less important than it used to be, but still requires the operator to minimize sector depth and angle, and restrict the color sector size if acceptable frame rates are to be maintained.

Aliasing: since color Doppler is derived from PW Doppler, it suffers from aliasing, and to an even greater degree, because the effective PRF is reduced. Aliasing in a color image typically occurs at velocities above 0.5 $m.s^{-1}$. It manifests on a color display as color inversion: red turning to blue and vice versa (Fig. 1.35). Thus, for steady flow toward the transducer, a velocity

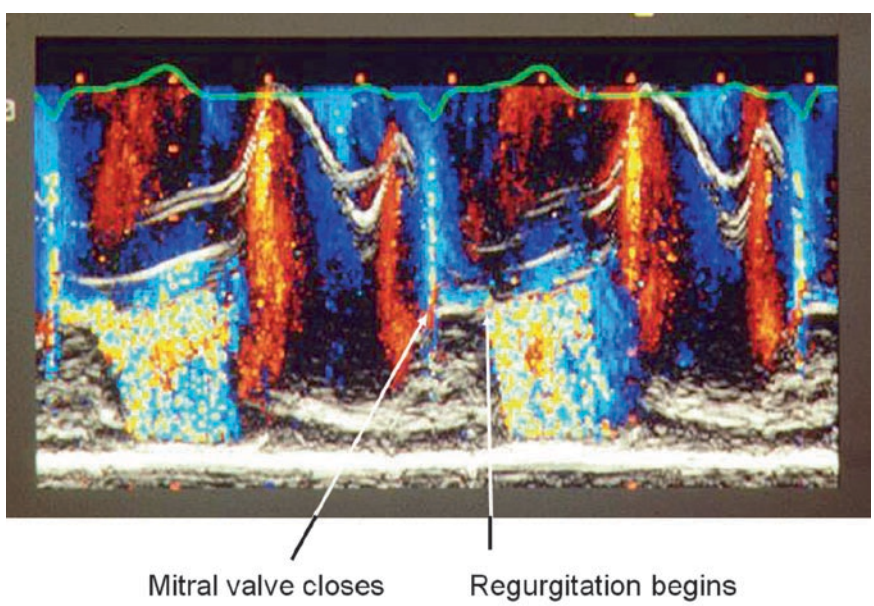

Fig. 1.34 Superimposing color on an M-mode recording relates the timing of valve movements to blood flow

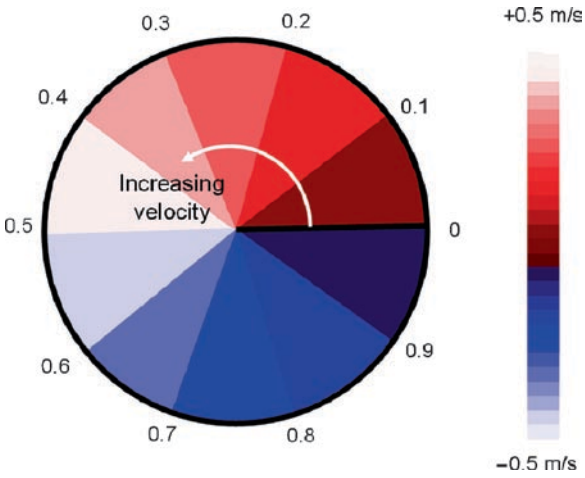

Fig. 1.35 Aliasing in color Doppler. As velocity toward the transducer increases, the display changes from *dark* to *light red*. At the aliasing velocity, it "flips" to *pale blue* and then to *darker blue*. With further velocity increase, this process repeats. Once aliasing has occurred, the observer no longer knows the true velocity

of 0.4 $m.s^{-1}$ is represented by pale red, but as it increases to 0.6 $m.s^{-1}$ it becomes pale blue. At 1.0 $m.s^{-1}$ (twice the aliasing velocity) the color display shows black, at 1.4 $m.s^{-1}$ pale red again, 1.6 $m.s^{-1}$ pale blue, and so on. There is, however, one application where the limitation imposed by aliasing has been turned into a benefit, and this is in the Proximal Isovelocity Surface Area (PISA) method for calculating instantaneous volumetric flow rates, which exploits the fact that as blood accelerates as it approaches a restrictive orifice, the velocity at which the color aliases is precisely known.

Mean velocity, peak velocity and turbulence: A color display can only show velocity at one point and at one time by a single color, and it was therefore sensible that this should represent the mean velocity. Color Doppler does not attempt to show peak velocities. However, when flow is turbulent, there is a wide spectrum of local velocities: high and low, forward and reverse. This is indicated on a CW display as an increased peak velocity and broadening of the spectral band, but since the mean velocity is unchanged, it presented a challenge to color Doppler. The solution was to analyze the time variance of local velocity, and where the same pixel detects greatly different velocities in successive images, to modify the display, for example by showing those pixels in green. This is called variance mapping, but it places further strain on frame rates and aliasing velocity so is seldom used.

Flow angle: Since the Doppler shift is the product of blood velocity and the cosine of the angle between the flow axis and the ultrasound beam, the apparent velocity on a color display is determined both by the true blood velocity and by the angle at which the flow vector is intersected by the scanning beam. Not only does this mean that constant flow velocity is represented by a range of colors, but it can additionally introduce aliasing at higher velocities (Fig. 1.36).

Tissue Doppler Imaging

All moving objects intersected by the ultrasound beam generate Doppler shifts. For study of blood flow, Doppler signals from moving heart structures such as valve leaflets are removed by selective filtering, since they would generate high-amplitude artifacts. The filtering is possible because the characteristics of Doppler signals from blood and tissue are markedly different: blood generally has high velocities, and relatively low signal amplitude since the red cell scatterers are relatively sparse. Conversely, muscle and valve tissue have much slower velocities and higher signal amplitudes as the cells are packed together (Fig. 1.37). The extent to which low velocities are removed can be controlled by the operator; excessive low-velocity attenuation causes a dark band either side of the zero-velocity baseline and is undesirable for recording, say, venous flows.

If, instead of removing low velocities, the high-velocity signals from blood are filtered out and the velocity and amplification scales suitably adjusted, Doppler signals from tissue motions can be recorded, either as PW spectral displays or in color (2-D or M-mode) (Figs. 1.38 and 1.39).

Strain Rate Imaging

The disadvantage of all Doppler is that it only detects motion relative to the transducer. Thus, when viewing the left ventricle from the cardiac apex, longitudinal

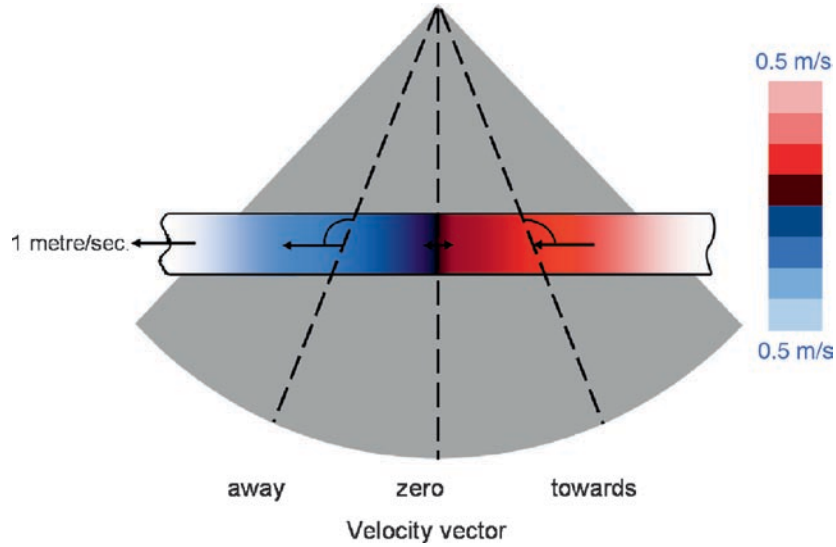

Fig. 1.36 The velocity indicated by a color display is determined both by the true velocity and the angle at which the flow vector intersects the scanning beam

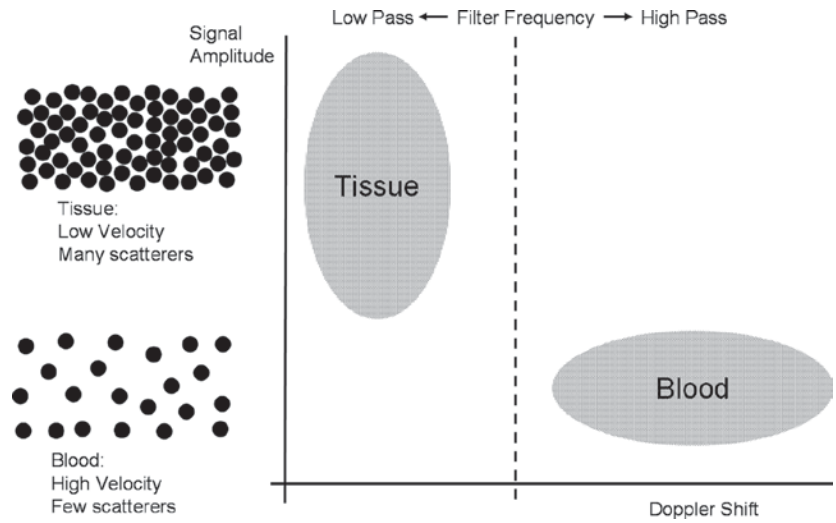

Fig. 1.37 By selectively filtering out high velocities, Doppler signals from tissue are displayed and those from blood are suppressed and vice versa

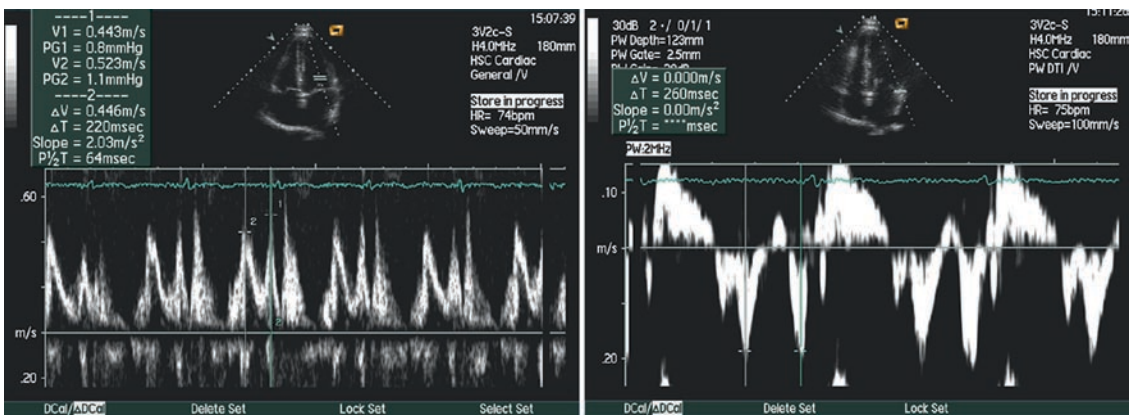

Fig. 1.38 Doppler recordings showing (*left*) blood velocity through the mitral valve and (*right*) the velocity of the valve annulus

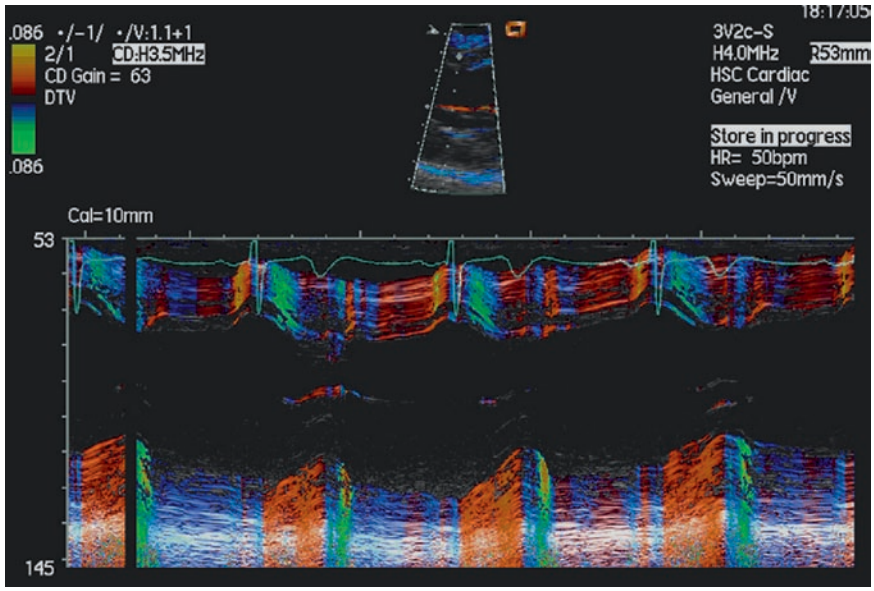

Fig. 1.39 Tissue velocity shown in the form of a color M-mode

motion of the myocardium is recorded, but inward motion of the septum and lateral wall is not. In some systems this can be alleviated by selecting a "center of mass," usually on the long axis approximately one-third of the distance from mitral annulus to apex, and computing velocities relative to this point. However, it is still the case that motion of a particular element of the myocardium is in part the result of its own contractile function and in part the consequence of other elements pushing and pulling it.

The complex arrangement of layers of myocytes means that each element of viable muscle wall changes its shape in all three axes: longitudinal, radial, and circumferential. Strain is the deformation per unit length and is dimensionless; the rate at which the deformation takes place is termed Strain Rate, and longitudinal strain rate can now be derived from Doppler signals in some machines. Since it shows only local deformation, it is independent of extraneous forces.

Second Harmonic Mode Doppler and Contrast Imaging

Second Harmonic imaging was originally developed in order to enhance signals from encapsulated contrast media. These are proprietary products and comprise very small (1–3 mm) microspheres with a hard outer shell containing a gas. At very low ultrasound power levels, these act as normal scatterers, but with slightly greater power (but still lower than normally used for imaging) the pressure waves distort them and they vibrate, emitting energy at the second harmonic frequency. A display based only on the second harmonic Doppler frequency thus selectively comes from the microspheres rather than from tissue or blood. The addition of echo contrast greatly enhances the quality of both images of blood-filled cavities and of Doppler signals, giving a clear velocity profile for even very small jets. At high ultrasound power levels, the microspheres shatter, releasing the contained gas, and generating a brief, but very intense, echo.

Power Mode (Amplitude) Imaging

As stated previously, the Doppler Shift is determined by velocity, but the intensity of the Doppler signal relates to the *number* of scatterers within the ultrasound beam. If there are a lot of scatterers, but they are moving in random directions, the net velocity will be zero, but the amplitude of the Doppler signal remains

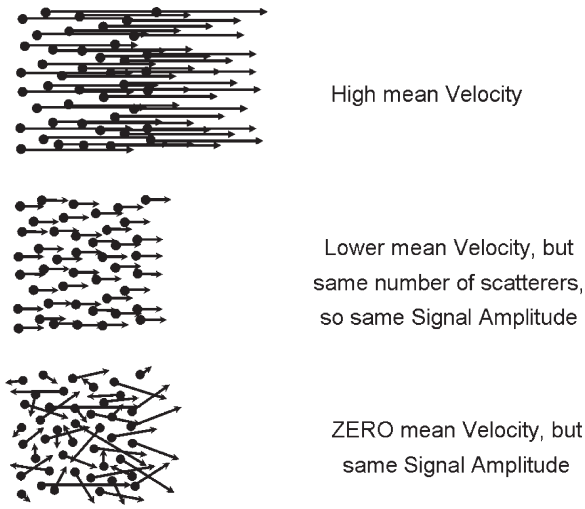

Fig. 1.40 Doppler signal amplitude is determined by the number of scatterers and is independent of their velocities

high (Fig. 1.40). Thus, a display showing the amplitude or power of the Doppler signal shows the *density of scatterers*, regardless of their *velocities*. This type of display is used, often in conjunction with harmonic mode, in contrast studies.

Summary of Doppler modes

Doppler mode	Display
Spectral	Velocity
Continuous Wave (CW)	Blood: high velocities
Pulsed Wave (PW)	Tissue: low velocities
High PRF	Signal amplitude (power) Blood: low amplitude
Color Flow Mapping (2-D and M-mode)	Tissue: high amplitude
Fundamental and harmonic	Strain Rate

Is Ultrasound Safe?

Ultrasound is a form of energy, and at high power levels can be used to coagulate tissues, heat deep muscles, or clean dirty surgical instruments. Potential harmful effects are related to the beam intensity and ultrasound frequency. The energy lost through attenuation as the beam passes through tissues is converted to heat. The peak intensity as the ultrasound pulse passes may be quite high, but in pulsed modes (but not CW), there are large gaps between pulses (pulse duration 2 ms, interval between pulses 200 ms) so the average heating is quite low. The term used to express this is Thermal Index and is the ratio of the actual beam power to that required to raise the temperature of a specific tissue by 1°C. A particular issue arises with transesophageal scanning, where the transducer face is in contact with the esophagus and local heating could, in the event of a fault within the transducer, cause tissue necrosis. For this reason, the probe tip temperature is monitored, and there is an automatic thermal cut-out in the event it becomes too high.

The pressure fluctuations within tissues as the ultrasound waves travel through them can be quite high. The potential for harm is quantified by the Mechanical Index, a parameter derived by dividing the peak negative wave pressure by the square root of the ultrasound frequency. Transthoracic scanning has caused hemorrhagic lesions on the lung surface of monkeys at MI 1.8. For this reason, most commercial cardiac scanners limit the maximum power to MI 1.1.

The fact is that in over almost half a century of use, involving millions of scans in a wide variety of clinical settings (including transvaginal fetal imaging), no case of harm to a patient from diagnostic ultrasound has ever been documented. By any standards the risk-benefit ratio of diagnostic ultrasound is negligibly low, but there is no such thing as zero risk, and to minimize it the user should always employ the "ALARA" principle (As Low As Reasonably Achievable) for machine power levels and patient exposure times.

Conclusions

The modern echo machine derives a great deal of information from echoes generated from the ultrasound beam it transmits into the body. These include specular echoes from which real-time 2-D/3-D images and M-mode traces are formed to study cardiac structures and their motion patterns; and Doppler signals from backscattered from blood and tissues that can be processed to provide spectral displays and color flow maps. Additional processing produces derived data such as strain rate and power mode imaging. It can be likened to a toolkit, all powered by a single source, the ultrasound beam. Each tool has its own particular applications; to use it optimally requires appreciation of its features, strengths, and weaknesses. Together they form a powerful, noninvasive diagnostic armory, which has revolutionized cardiac diagnosis in almost every area of clinical activity from primary care to the operating room.

Chapter 2
Conducting a Cardiac Ultrasound Examination

David Adams and Emily Forsberg

2D Normal Views

Echocardiography is a noninvasive procedure which illustrates the anatomy of the heart, including valves and valve motion, chamber size, wall motion, and thickness. Doppler echocardiography assesses the severity of valvular regurgitation, gradients across stenotic valves or between cardiac chambers, and the detection of intracardiac shunts.

Historical Perspective

Abel L Spallantzani (1729–1799) recognized the existence of Ultrasound. He demonstrated that bats who are blind, navigate by means of echo-reflections using inaudible sounds. He is considered the true "Father of Ultrasound."

Johan C Doppler (1803–1853) worked out the mathematical relationship between the frequency shift of sound and the relative motion of the sound source and the observer for what was later developed as the "Doppler principle." In 1845, CHD Buys Ballot (1817–1890), a Dutch meteorologist, tested the theory of Doppler in an attempt to disprove it!

In 1880, Jacques and Pierre Currie discovered the piezoelectric effect, a phenomenon observed in certain quartz crystals, which were the basis of the early ultrasound systems. P. Langavin (1872–1946) conceived the idea to use a piezoelectric quartz crystal as both transmitter and receiver, which led to the development of the sonar used in World War I.

It was the Austrian KT Dussik who in 1941 first applied ultrasound for medical diagnosis. He outlined the ventricles of the brain using echo transmission, a principle similar to X-ray imaging. He is regarded as the "Father of diagnostic Ultrasound."

It was not until 1950 however that the German WD Keidel first used an echo-transmission technique to perform the first cardiac examination in an attempt to measure cardiac output.

In 1953, I. Edler & CH Hertz in Lund, Sweden, first performed experiments using ultrasound echo-reflection for examining the heart stimulated by their surgeons who wanted a more accurate diagnosis before surgery. They produced the first echocardiogram of the heart in 1953 – "the Ultrasound Cardiogram." Fortuitously, the machine used for detecting faulty metals had the same physical characteristics which were appropriate for the heart!

In 1963, Harvey Feigenbaum in the USA borrowed an unused echoencephalography machine to scan the heart and noted that cardiac images could be recorded. He first described the posterior pericardial effusion. He then substituted the word "cardio" for "encephalo" and gave the name "echocardiography."

In 1968, R. Gramiak and Pravin M. Shah (USA) described contrast echocardiography, an accidental observation, during indocyaine green injections for cardiac output measurements. Later on in 1968 J Somer constructed the first electronic phased-array scanner, and in 1974 J Griffith and W Henry introduced the mechanical sector-scanner.

In 1974, FJ Thurstone and OT von Ram constructed their electronic phased-array scanner, similar to the instrument developed by J Somer.

In 1977 J Holen showed that the Bernoulli equation could be applied to estimate the pressure drop across a

D. Adams (✉) and E. Forsberg
Department of Cardiology, Echo Lab, Duke University Medical Center, Durham, NC, USA
e-mail: david.adams@duke.edu

P. Nihoyannopoulos and J. Kisslo (eds.), *Echocardiography*,
DOI: 10.1007/978-1-84882-293-1_2, © Springer-Verlag London Limited 2009

stenotic orifice from the jet flow velocity. The following year, the Swiss MA Brandestini produced a 128-channel digital multigate Doppler instrument to allow real-time imaging of cardiac structures and blood flow in color.

The American Institute of Ultrasound in Medicine adopted the term echocardiography, which means the use of reflected ultrasound to describe cardiac structures (from the Greek echo = reflection).

Echocardiography has seen a rapid evolution from single crystal M-mode to two-dimensional echocardiography, Doppler, and now color-flow imaging. Clinical use of echocardiography now extends into the operating room, as its utility in both transesophageal (TEE) and intraoperative echocardiography is meeting widespread acceptance among cardiovascular surgeons.

Normal Cardiac Anatomy

A normal heart comprises four cardiac chambers and four cardiac valves. Ultrasonic access to these chambers and valves would be easy if it were not for the fact the heart is normally protected by the rib cage. Additionally, the heart is surrounded by the lungs lying within pleural membranes. The bony structure of the ribs and the air within the lungs provide a formidable obstacle to access the heart using ultrasound. Fortunately there are small acoustic windows beneath the third, fourth, and fifth intercostals spaces for 2 or 3cm to the left of the sternal border. Additional access can be obtained from the subcostal, apical, and suprasternal approach. Some of these approaches are more useful in Doppler echocardiography where it is important to be parallel to blood flow and not so important to be perpendicular to cardiac structures. For imaging purposes where it is important to be perpendicular to structures for the best reflections of the ultrasound, approaches such as the left parasternal are best.

Transthoracic Standard Imaging Planes

The superior ability of two-dimensional echocardiography over M-mode echocardiography for the detection of pathology and its ability to define spatial relationships between the valves and cardiac chambers necessitate the limited discussion of M-mode throughout this book. We will, however, show M-mode recordings for specific disease states when appropriate.

Specific imaging planes to interrogate the heart have been established in order to record all intracardiac structures in a standardized fashion. In this chapter we will cover the basic views of both transthoracic (TTE) and TEE echocardiography.

Left Parasternal Window

Long Axis

- *Long-axis view of the left ventricle.*

Used to evaluate left ventricular (LV) chamber size, performance, septal wall thickness and motion, aortic valve (AV) and aortic root, overriding aorta (Ao), mitral valve (MV), and left atrial (LA) dimensions. Figure 2.1 shows an example of a parasternal long axis in a normal patient during (a) systole and (b) diastole.

The landmarks to look for are the mitral valve in the center of the picture, the aortic root, and the left ventricle.

- *Long-axis view of right ventricular inflow.*

Used to evaluate right atrial (RA) and right ventricular (RV) dimensions, to detect mass lesions, and tricuspid valve (TV) abnormalities. Figure 2.2 shows an example of a parasternal long axis of right ventricular inflow during systole. This view is obtained by rotating the transducer counterclockwise approximately 20° from the long-axis view and angling the beam medial under the sternum.

The landmarks to look for are the tricuspid valve in an oblique projection in the center of the image, dividing the RA at the bottom from the RV on top.

Short Axis

- *Short-axis level of the heart from base to apex.*

Useful for the evaluation of the aortic valve, the mitral valve and left ventricular wall motion, wall thickness, chamber size, and presence of apical masses. The aim here is to produce serial cross-sectional sections of the heart from base to apex so that the entire left ventricular walls and thickening can be evaluated. These views are obtained by rotating the transducer clockwise

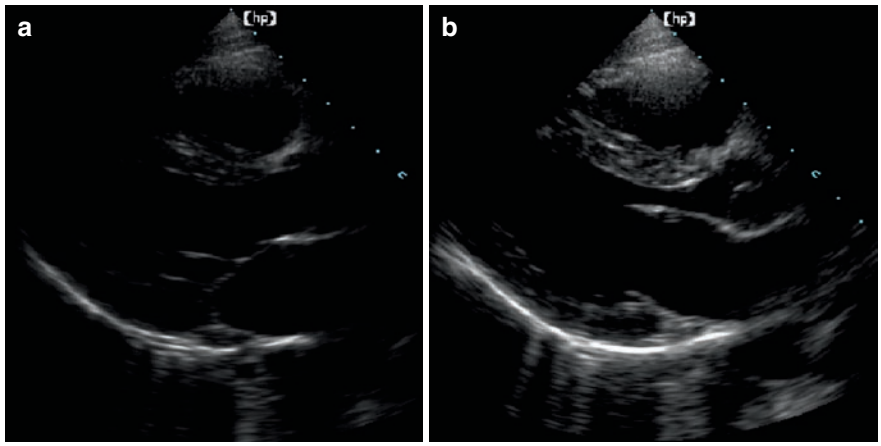

Fig. 2.1 Normal parasternal long-axis view in (**a**) systole and (**b**) diastole

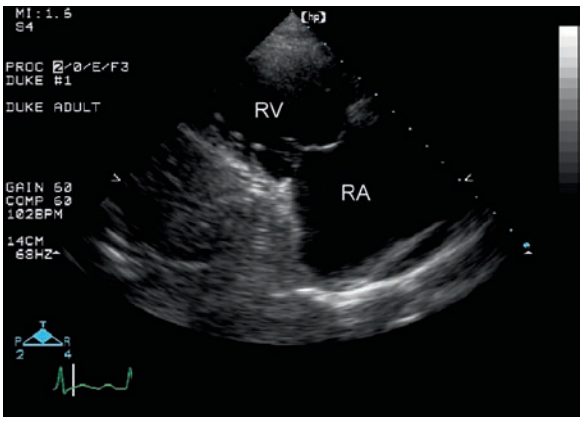

Fig. 2.2 Normal parasternal long axis of right ventricular inflow during systole

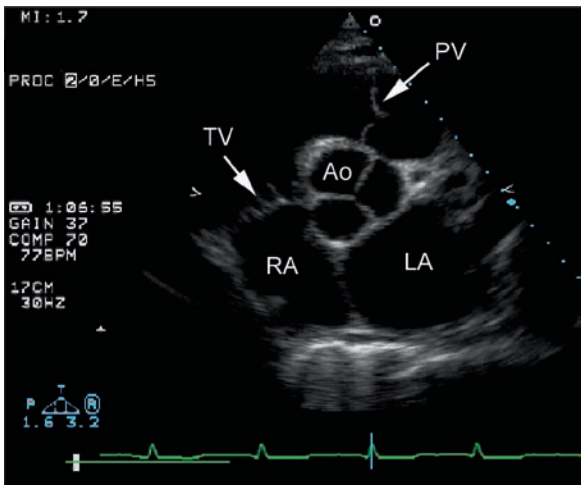

Fig. 2.3 Normal parasternal short axis of the great arteries during diastole

approximately 90° from the long-axis view and then angling the beam from the base of the heart to the apex.

- *Short-axis level of the great arteries (base).*

Figure 2.3 is an example of a parasternal short axis of the great arteries during diastole. This view is used to determine spatial orientation of the great arteries; to see enlargement and drainage of the coronary sinus; to evaluate abnormalities of the aortic, tricuspid, and pulmonic valves; and to determine location of the coronary arteries.

The subpulmonic region may be assessed, whether there is infundibular hypertrophy (tetralogy of Fallot) or RV free wall thinning (arrhythmogenic right ventricle). It is also useful to evaluate right ventricular outflow tract, right atrial size, and to detect intra-atrial masses.

From this projection the presence of an arterial duct can be depicted.

- *Short-axis level of mitral leaflets (LV base).*

Figure 2.4 is an example of a parasternal short axis at the mitral valve level during diastole – useful in evaluating ventricular septum, determining abnormalities of the mitral valve, and estimating the mitral orifice in mitral stenosis. This is a good view to describe both the anterior and the posterior mitral leaflets from the anterolateral to posteromedial commissures.

- *Short-axis level of papillary muscles (mid-LV).*

Figure 2.5 is an example of a parasternal short axis of the left ventricle at the papillary muscle level – useful in

locating and determining the number of papillary muscles in the left ventricle, evaluating interventricular septal motion, determining right and left ventricular chamber dimensions, and detecting intraventricular masses.

It is important that the left ventricle is displayed as a circle implying that the section is truly perpendicular to the left ventricle. In some pathological conditions (RV pressure or volume overload) the septum assumes a noncircular geometry.

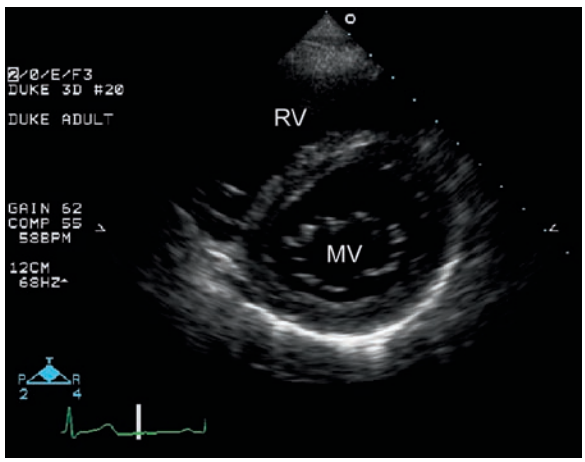

Fig. 2.4 Normal parasternal short axis at the mitral valve level during diastole

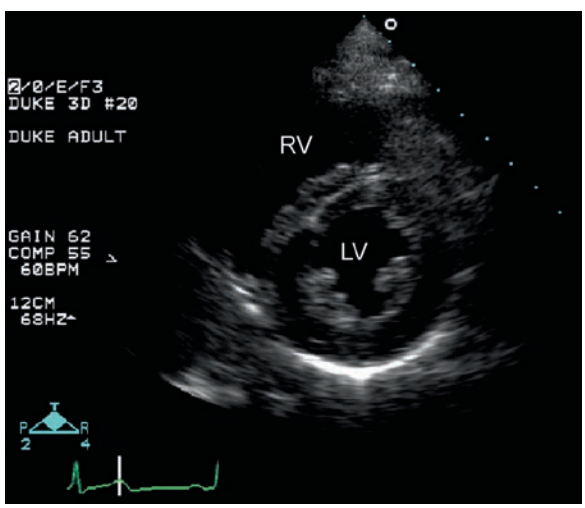

Fig. 2.5 An example of a parasternal short axis of the left ventricle at the papillary muscle level in a normal patient

Apical Window

- *Four-chamber view.*

Figure 2.6 shows an apical view of all four cardiac chambers with the atrial and ventricular septa – used for the detection of intracardiac cardiac masses, evaluation of septal defects, detection of atrial and ventricular septal defects, detection of structural abnormalities of the atrioventricular valves and their tensor apparatus, evaluation of left ventricular function, and imaging left ventricular apex.

Attention should be made to position the ventricular septum in the middle of the sector, although occasionally, this could be shifted more to the left, so that the LV free wall can be better evaluated.

- *Long-axis view.*

Figure 2.7 depicts a normal apical long-axis view – useful for evaluating left ventricular function, imaging the left ventricular apex, detecting left ventricular aneurysms, determining aortic override of the left ventricular septum, and detecting intracardiac masses.

This view complements the parasternal long axis by visualizing the entire subvalvular apparatus of the mitral valve as well as the LV outflow tract.

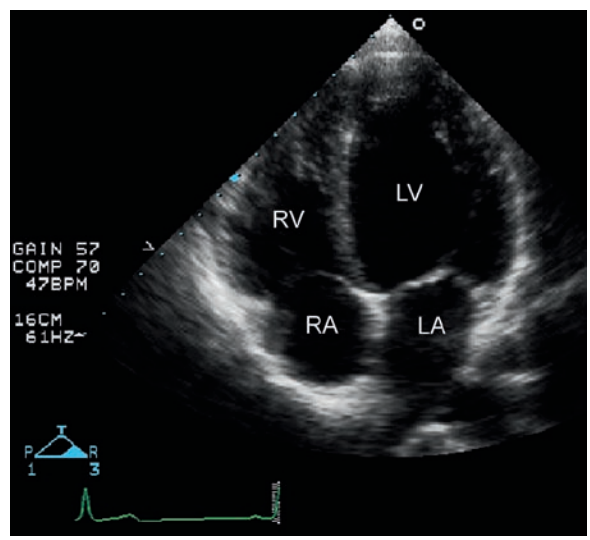

Fig. 2.6 A normal apical four-chamber view of all the cardiac chambers during systole

- *Two-chamber view.*

Figure 2.8 shows a normal apical two-chamber view. This view nicely depicts the anterior and inferior walls of the left ventricle and is commonly used during stress echo examinations – useful in evaluation of left ventricular function, detection of left ventricular aneurysms, and intracardiac masses. The aortic valve is not visualized in this view.

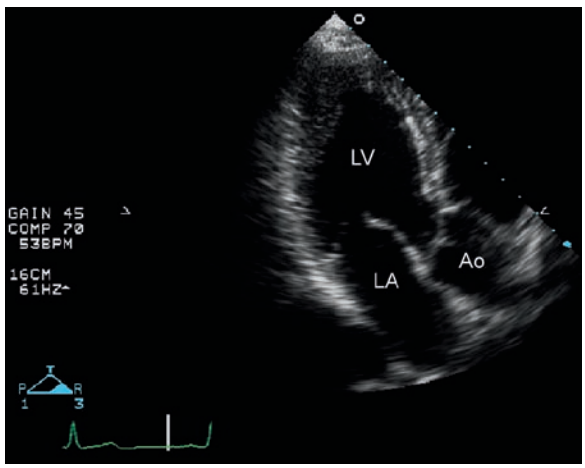

Fig. 2.7 A normal apical long-axis view during diastole

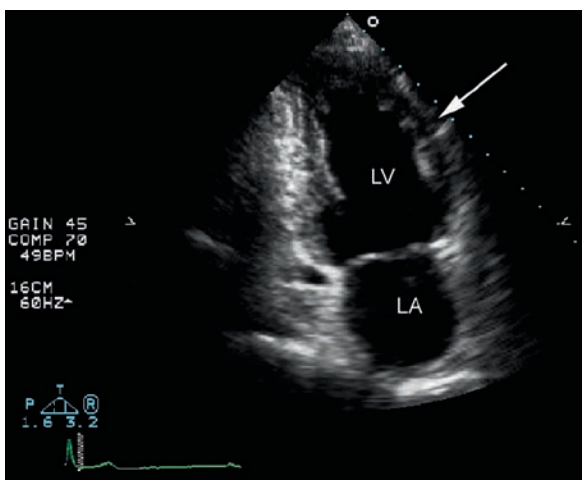

Fig. 2.8 The apical two-chamber view in a normal patient. The anterior wall is marked by the arrow

Subcostal window

- *Four-chamber view.*

Figure 2.9 demonstrates the anatomy seen in a normal subcostal four-chamber view – useful for detection of right and left atrioventricular valve abnormalities, determination of right and left ventricular wall thickness, evaluation of atrial septal motion, and detection of intra-atrial masses.

- *Short-axis left ventricular level.*

Figure 2.10 shows the subcostal short axis at the left ventricular papillary muscle level – useful for evaluation of size and contractility of the right and left ventricles.

- *Long-axis inferior vena cava.*

Figure 2.11 shows the subcostal long axis of the junction of the inferior vena cava (IVC), hepatic vein (HV) and right atrium – used in detecting abnormalities of the IVC, (HV, and right atrium.

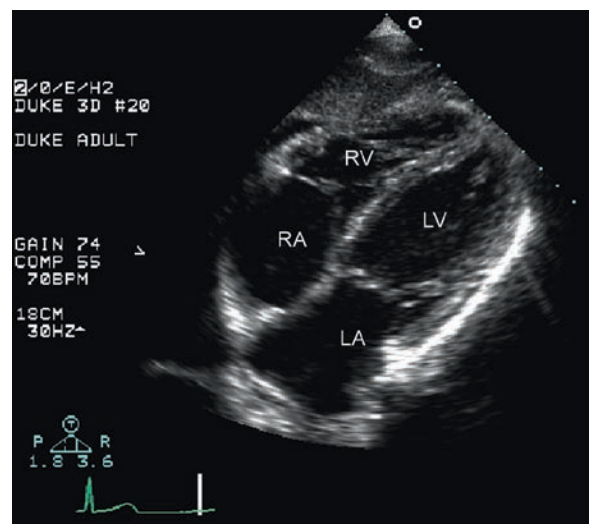

Fig. 2.9 A normal subcostal four-chamber view of all the cardiac chambers during systole

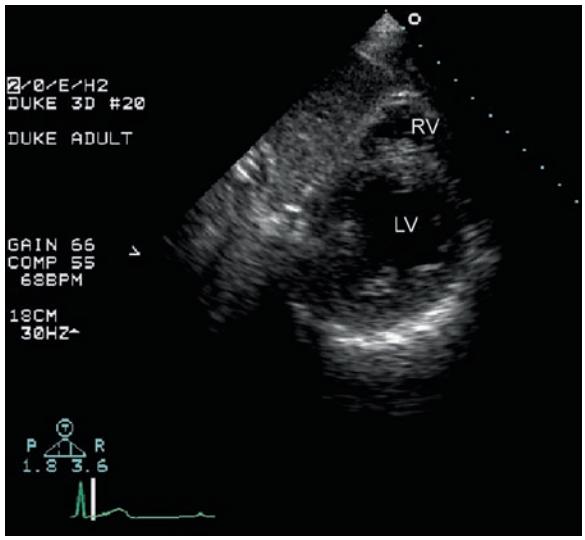

Fig. 2.10 Subcostal short axis of the left ventricle at the papillary muscle level in a normal patient

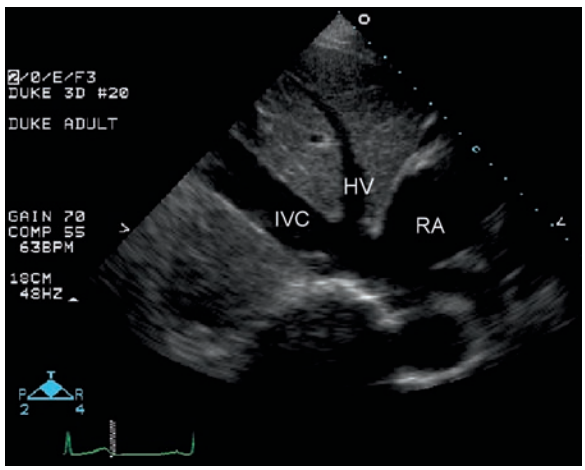

Fig. 2.11 Subcostal view of the junction of the IVC, hepatic vein and RA

Suprasternal Window

- *Long-axis aorta, short-axis right pulmonary artery.*

Figure 2.12 shows a normal suprasternal view of the aortic arch and the right pulmonary artery (RPA) (arrow). – useful in determining the dimensions of the various parts of the aorta, detecting aorta arch abnormalities, determining the size of the (RPA, detecting and localizing possible coarctations of the aorta.

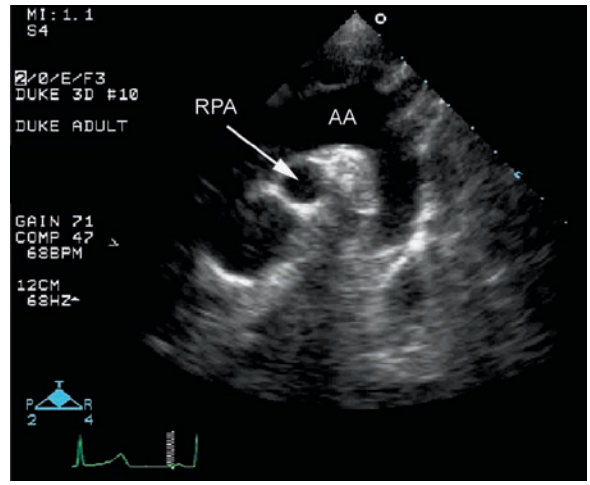

Fig. 2.12 A normal suprasternal view of the aortic arch and the right pulmonary artery (*arrow*)

Transesophageal Standard Imaging Planes

Imaging of the heart from the esophagus was first reported by Dr. Frazin in 1976. At that time there was little directional control over the M-mode transducer once it was swallowed by the patient. Reworking flexible gastroscopes solved the problem of directional control and advances have continued in that. Today TEE probes are smaller, higher frequency, and allow rotation of the 2D beam throughout 180°.

With TEE imaging and the transducer in the esophagus there is little noise and interference from either the bony structures of the rib cage or air in the lungs. In almost every patient the TEE image quality is vastly superior to TTE. While there are unlimited views that can be obtained by transesophageal echo we will concentrate on the basic ones in this chapter.

- *Four-chamber view.*

Figure 2.13 shows four-chamber view of all four cardiac chambers with the atrial and ventricular septa – used for the detection of intracardiac cardiac masses, evaluation of septal defects, detection of atrial and ventricular septal defects, detection of structural abnormalities of the atrioventricular valves and their tensor apparatus, evaluation of left ventricular function.

- *Two-chamber view.*

Figure 2.14 shows a normal apical two-chamber view – useful in evaluation of left ventricular function, detection of left ventricular aneurysms and intracardiac masses. The aortic valve is not visualized in this view.

- *Left atrial appendage view.*

Figure 2.15 shows a normal apical two-chamber view rotated over to visualize the left atrial appendage (LAA) – useful in detection of left atrial thrombi.

- *Short-axis level of the aortic valve (base).*

Figure 2.16 is an example of a TEE short axis at the aortic valve level during systole. This view is used to determine spatial orientation of the great arteries; to see enlargement and drainage of the pulmonary veins; to evaluate abnormalities of the aortic, tricuspid, and pulmonic valves; and to determine location of the coronary arteries.

- *Bicaval view of the right atrium.*

Figure 2.17 is an example of a TEE bicaval view of the right atrium. The left atrium, atrial septum appendage, and inferior (IVC) and superior vena cava (SVC) are visualized. This view also is helpful in documenting sinus venosus defects of the atrial septum.

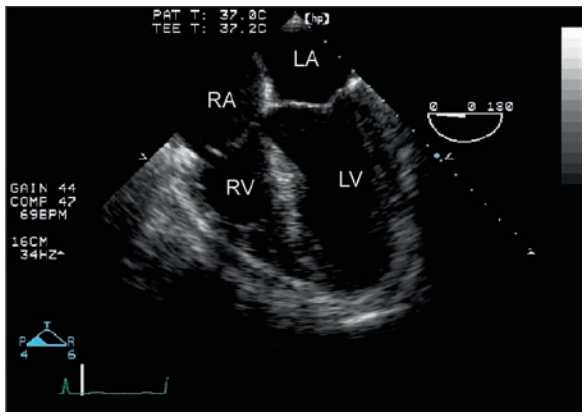

Fig. 2.13 Four-chamber TEE view with the probe in the esophagus the left atrium is the chamber closest to the transducer

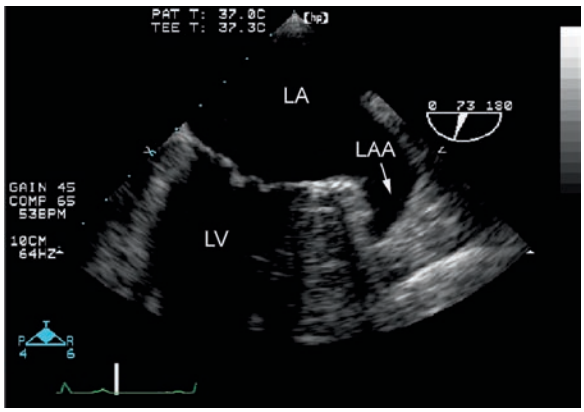

Fig. 2.15 Two-chamber TEE view rotated over to visualize the left atrial appendage (LAA)

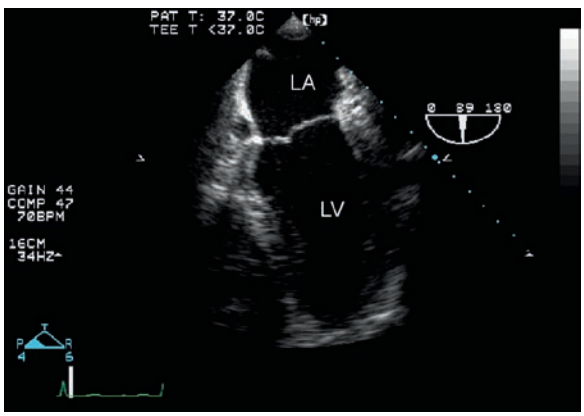

Fig. 2.14 Two-chamber TEE view looking at the left atrium (LA) and left ventricle (LV)

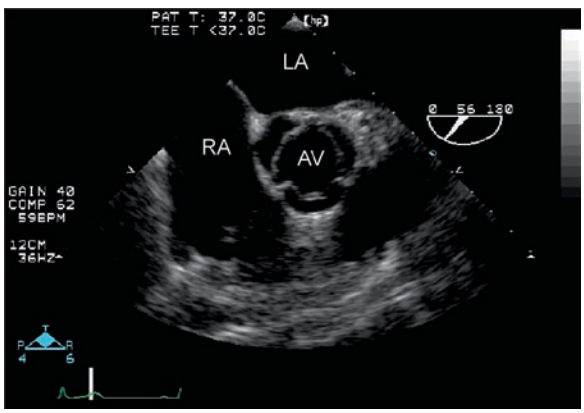

Fig. 2.16 TEE short axis at the aortic valve level during systole

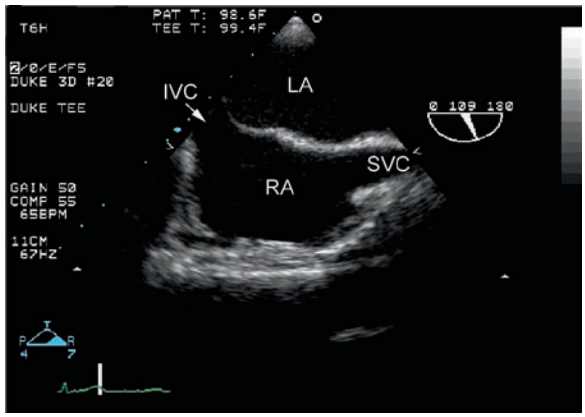

Fig. 2.17 TEE bicaval view of the right atrium. The left atrium, atrial septum appendage, and inferior (IVC) and superior vena cava (SVC) are visualized

Controls Settings

Introduction

It is crucial for those performing an echocardiographic examination to understand how the controls on an ultrasound machine alter the display. Without this knowledge, it is impossible to consistently optimize images. Unskilled manipulations may misrepresent diagnostic information and result in missed diagnoses. Section 2 aims to describe controls found on most ultrasound machines, how they affect the image, and how they are used to optimize the ultrasound image. Table 2.1 describes the most commonly used controls for two-dimensional (2D) imaging.

Preparing the Machine

Preset. After providing power to the machine itself, be sure to define basic parameters for the test by choosing an appropriate *preset*. The preset provides a starting point for such basic machine settings as depth, gain, and process settings. The operator can adjust all the machine's variables from the initially fixed settings as needed. Adjustments to the preset can be permanently saved under a different preset name when desired. Presets are also used to reset the ultrasound machine when the various controls are adjusted incorrectly.

Patient identification and any other relevant information should be entered into the machine. Relevant

Table 2.1 Describes the most commonly used controls and their functions for 2D imaging

2D Variable	Knob(s)	Function
Gain	Gain	Amplifies returning signals before display
TGC/DGC	TGC/DGC toggles	Selectively amplifies returning signals before display (horizontally)
LGC	LGC toggles	Selectively amplifies returning signals before display (vertically)
Compression	Compression	Changes the difference between the highest and the lowest received amplitudes (shades of gray)
Power	Power (dB)	Controls rate at which energy is propagated into an imaged medium
Frequency	Dependent on probe	Determines number of times per second a sound wave completes a cycle
Focal Zone	Focal zone	Alters the placement of the narrowed region that designates an area of improved resolution
Depth	Depth	Selects how shallow or deep an area is imaged
Sector Size	Size, trackball	Narrows or widens the image sector
Zoom	Zoom	Magnifies a particular area of interest within the sector
Freeze	Freeze	Stops or starts live imaging
Measurement	Freeze, caliper, trace, enter, erase	Quantifies features of a 2D image
Harmonics	Harmonics	Uses frequencies created by the tissues, rather than the fundamental frequency, to create an image
Annotation	Annotation	Adds text or picture to image

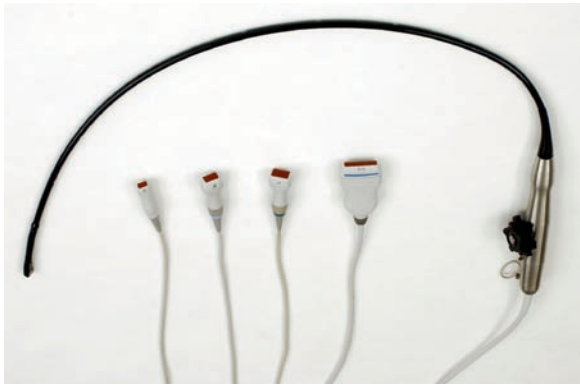

Fig. 2.18 Typical ultrasound probes used in a cardiovascular laboratory. A long TEE probe surrounds an array of cardiac and vascular (far right) transducers

information outside the patient's name and medical record number may include date of birth, sex, videotape number, name of person performing examination, location, or any number of other qualifiers for later reference.

Transducer selection: A transducer must be connected to the machine and selected from other possible transducer options. Figure 2.18 shows typical ultrasound transducers currently in use in cardiovascular laboratories. A transesophageal probe is seen surrounding three-phased array cardiac transducers of varying frequency. The wide probe on the right is a linear-array transducer for vascular studies such as carotid and venous examinations. A high transducer frequency may be selected for most children and pediatric population (better near-field resolution), while for adult patients a lower-frequency transducer will provide penetration (but a loss of resolution).

The four most common modes used during the examinations are two-dimensional gray scale imaging, color Doppler, pulsed-wave Doppler, and continuous-wave Doppler. The usual buttons or markers to enable these modes are: *2D*, *Color*, *PW*, and *CW*. Other scanning modes are often available, although for the sake of simplicity, this chapter will focus on the controls that affect the four primary modes previously listed.

Two-Dimensional Imaging and Basic Image Manipulation

Basic Echo Images: Two-dimensional (2D) gray scale imaging is a type of B-mode imaging (B is for brightness) in which the various amplitudes of returning ultrasound signals are displayed in multiple shades of gray. Higher-amplitude signals are closer to white, while lower-amplitude signals are displayed as closer to black. Many different shades of gray form a representational picture of the patient's cardiac anatomy. The top portion of the sector shows the tissue closest to the transducer.

Gain: Gain is the most important variable to adjust during a study. It is also the one control that is most often misused. Overall gain controls the degree of amplification that returning signals undergo before display. Amplification, or overall gain, is the first postprocessing function performed by the receiver. One of the most common mistakes is to add too much gain to a picture. While this can make the picture brighter and structures more obvious overgaining will destroy image resolution. The appropriate amount of gain for a picture becomes apparent when reflectors and tissue interfaces can be seen, but fluid and blood appear as totally black and echo-free. Myocardium should be adequately dispersed with reflectors, but the muscle should not approach the look of a solid white band. Only the pericardium, certain states of abnormal thickening, calcification, tissue infiltration, or surgically altered valves should be hyperechoic (very bright). The myocardium should be set at a medium shade of gray by the operator. Gain should be incrementally added if the picture is entirely black, or only normally hyperechoic structures can be seen with clarity. Figure 2.19 shows three parasternal long-axis views with varying gain settings. Figure 2.19a demonstrates gain that is set too low, Fig. 2.19b with proper gain setting, and Fig. 2.19c with the gain set too high.

TGC/DGC: The second postprocessing function of the receiver is compensation. It is commonly known as time gain compensation (TGC) or depth gain compensation (DGC). Compensation makes up for energy loss from the sound beam due to attenuation. Attenuation is the loss of intensity and amplitude of the ultrasound beam as it travels deeper into the body. Strong returning signals from the near field (close to the transducer) need to be suppressed, while signals from the far field (deeper depths) require higher amplification.

- TGC/DGC is seen on the machine as a column of toggles that can be slid along a horizontal plane. By sliding a toggle to the right, the operator increases the gain at that given depth. The TGC/DGC is nor-

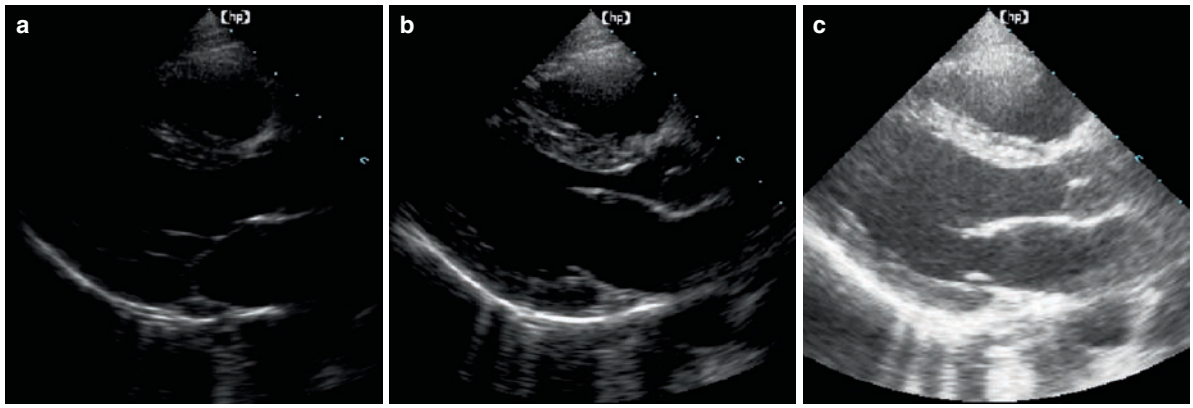

Fig. 2.19 Parasternal long axis with gain that is set too low (**a**), proper gain setting (**b**), and with the gain set too high (**c**)

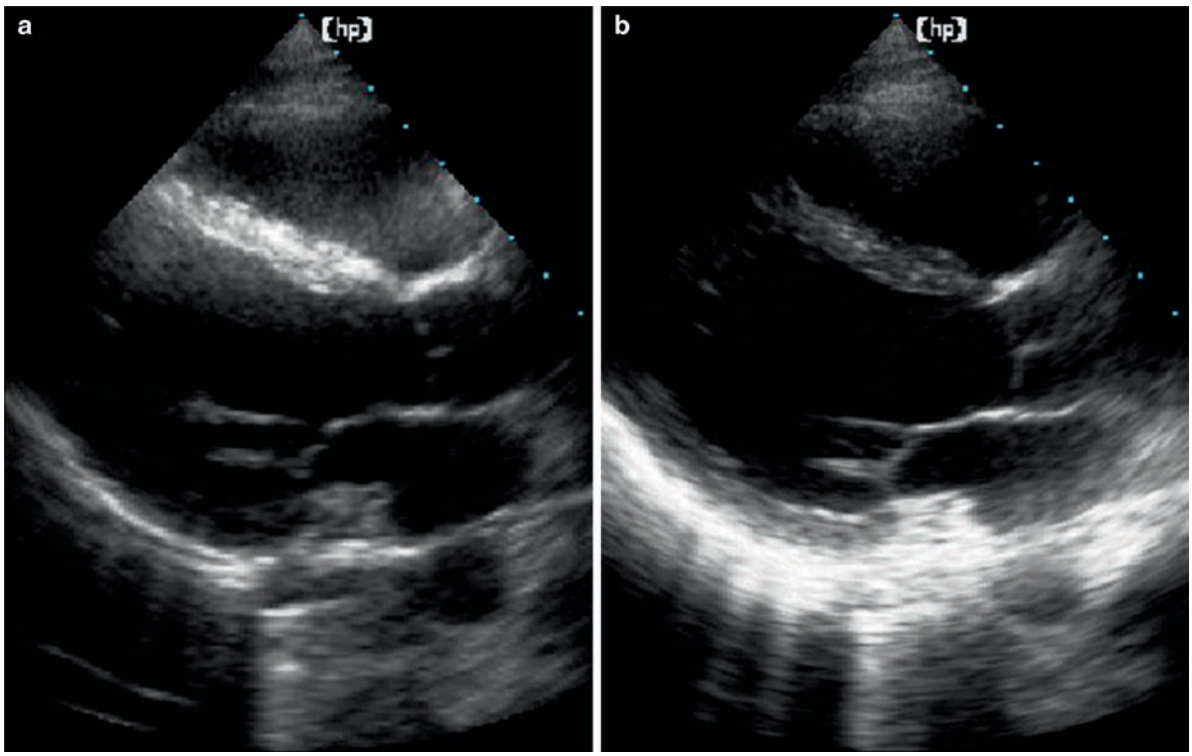

Fig. 2.20 Parasternal long-axis view with the TGCs set incorrectly: 19a has the near-field TGC set too high, so the septum is over-gained and 19b has the far field set too high

mally placed at a diagonal slope of variable steepness. The upper or near-field toggles are often set at a lower degree of compensation, while the lower, far-field toggles are often set at a higher degree of compensation. A pattern of gradual change from one toggle to the next avoids a "striped" look to the ultrasound picture. Figure 2.20 shows a parasternal long-axis view with the TGC's set incorrectly.

LGC: LGC is an acronym for lateral gain compensation and is present on some ultrasound machines. LGCs are toggles similar to TGC/DGCs but act

selectively on the *y*-axis of the picture to change the gain in vertical portions. LGCs are useful to bring out myocardial walls that may be hypoechoic (lacking in brightness) due to technique or positioning.

Compression: Compression or dynamic range is just as important as gain. Compression can decrease or increase the difference between the highest and lowest echo amplitudes received. Compression takes the received amplitudes and fits them into a gray scale range the machines can display. This dynamic range is determined by the degree of compression applied to returning signals. Dynamic range expresses how many shades of gray appear within the image. By increasing the compression, the image displays more shades of gray. Areas of medium amplitudes of gray, such as myocardium, may be better resolved. Decreasing the compression provides a highly contrasted image with strong white-and-black components. While sharply decreasing the compression may improve structure delineation, it will sacrifice low-amplitude targets. Most presets start at roughly midlevel value of compression and gain.

Power: Power can be indirectly assessed by *decibel (dB)* settings, *Mechanical Index* (MI), and *Thermal Index* (TI). Power, expressed in watts (W) or milliwatts (mW), describes the rate at which energy is propagated into the imaged medium. Intensity is a concept that closely relates to power. Intensity is power per unit area (mW/cm^2 or some unit variation). Intensity may not be entirely uniform throughout tissues. Intensity levels more accurately predict risk of bioeffects than power levels. When looking at an image, simply changing the output power from the transducer appears to have a similar effect as changing the overall gain. The power actually functions in a way that is less preferable than overall gain. The difference is that gain settings do not change the amount of energy in tissues. Overall gain works with signals that have already traveled through tissues. *Work with gain variables before ever reaching to change the power*. Recognize the power knob by its unit of measurement. Most machines do not describe the power level in watts or Milliwatts. Instead, they indirectly describe power in terms of *decibels (dB)*.

Because the exact power or intensity levels are not apparent, manufacturers began to put two more variables on the screen to help clinicians to estimate power and intensity levels. The two variables are the *Mechanical Index* (MI) and the *Thermal Index* (TI). Mechanical Index (MI) is intended to convey the likelihood of *cavitation* resulting from the ultrasonic energy during the exam. Cavitation refers to activity of created or pre-existing gas bubbles within the tissues due to ultrasound energy. Thermal index (TI) is the ratio of output power emitted by the transducer to the power needed to raise tissue temperature by 1°C.

Frequency: Frequency is defined as the number of cycles per second. The frequency of most cardiac ultrasound probes is between 2.5 and 7MHz (5–7,000,000 cycles per second). The frequency of the ultrasound probe has a dramatic effect on image quality. Lower transmitted frequencies create very different images than higher frequencies.

- When the wavelength is smaller (higher frequencies), the axial resolution is better.

Resolution is the ability to detect two targets positioned closely to one another. Improved resolution generates a more accurate anatomic rendering. The lower the sound source frequency, the more effective it is in penetrating tissue and not falling subject to attenuation. Unfortunately, low frequencies yield poorer resolution in their resulting images when compared to high-frequency images. When a structure near the chest wall needs to be better resolved, a high-frequency transducer may be preferred.

- While the imaging frequency is dependent on the transducer used, each probe has a *frequency bandwidth*. Some machines have a wide bandwidth and allow an operator to select a part of the bandwidth spectrum to make the images.

Focal zone: The ultrasound beam is not necessarily the same width as it travels into the depths of tissue. Many systems use a technique known as *focusing*. Focusing the ultrasound beam is a process accomplished by mechanical or electronic means. On the other hand, it is possible to influence the way the beam is focused. As the beam proceeds deeper into the tissue, the beam gradually tapers to a narrow region known as the *focal zone*. The central point of the focal zone is the *focal point.* The focal point of a focused ultrasound beam will have the highest intensity (mW/cm^2) of the transmitted ultrasound energy from the transducer. It also produces a higher quality image because it yields better returning signals for the machine to process and display.

Depth: All machines have a control that increases or decreases the overall image depth. Decreasing the depth increases the frame rate by reducing the amount of information that the machine has to process and shortening the time required for the beam to travel to and return from a target of interest. Regardless of frame rate, some cardiac views require a deeper field of view for adequate display.

Sector size: Reducing the width of the sector is another excellent way to increase frame rate and isolate an area of interest. Just as depth will reduce the amount of information needing to be processed so will narrowing the sector.

Zoom: Zooming an area of interest is another good way to remove unwanted information from the sector. Zooming trims from both the x- and the y- axes of the sector. *Zoom* can be selected on the machine and an initial zoom box will appear. Change the zoom parameters using the size and the position buttons along with the trackball, until the area of interest is adequately covered.

Measurements

All echocardiographic images can be measured and quantified. The same buttons that are used for Doppler evaluation are also used for gray scale assessments. Standard buttons are: *freeze*, *caliper*, *trace*, *enter*, and *erase*. Measurements of 2D images can be made either outside or inside the analysis package. If measurements are plugged into the analysis package, the operator will need to select the *analysis* or *measurement package* button and then the proper name for the subsequent measurement. A pair of calipers can tell you exact linear measurements of gray scale images. The first caliper has to be entered onto a point in order to have the second caliper appear. Once the second caliper is set, then the machine calculates the straight linear distance between the two points. Multiple linear caliper measurements can be made. Remove the calipers by using the erase button. To perform planimetry of a valve orifice or measure along the outside borders of a mass, use the *trace*, *trackball*, and *enter* buttons. Once the trace function is selected, set the first given caliper to a starting point and use the trackball to follow the borders of the desired region. Once the border is outlined and the dotted tracing line is returned to the starting point, the outline must be entered before the machine will calculate any area. The operator can backtrack a traced line or completely remove any given trace by pushing the *erase* button (possibly several times to completely eliminate the trace).

Harmonics

Standard transducers transmit and receive frequencies that are the same or within a very close range. The frequency from such a transducer is known as the *fundamental frequency*. As the beam propagates through tissues, it distorts and creates additional frequencies that are multiples of the fundamental frequency. These additional frequencies are the *harmonic frequencies* and are created by the tissues themselves (Chap.1). While the fundamental frequency may undergo a large amount of distortion, the harmonic frequencies do not. In patients with poor sound transmission due to obesity or dense muscle tissue, the harmonic frequencies may make a better image than the fundamental frequency. In fact, when using harmonics the image will likely have poorer resolution than the image created with the fundamental frequency. During contrast studies harmonics will improve image quality whether using agitated saline or one of the new, transpulmonary contrast agents.

Annotation

Annotation can be a label in words or pictures added onto the screen to accompany a corresponding image. Nonstandard views, unusual anatomic variations, or highly edited standard views may need some further explanation. It is also helpful to annotate when a standard view is not available or is of very poor quality. Naming anatomical landmarks, relationship to other anatomic points of reference, body positioning of the patient, or timing of events is often helpful for the interpreting physician. For example, it may be of use to label a heart as pre- or postsurgical event. Be sure to remove any comments after they apply so that later pictures do not become confusing or incorrectly labeled.

Color Doppler

Color Doppler is layered over a 2D image to provide information on blood flow. The 2D images provide a context needed to adequately interpret the color data. All forms of Doppler analysis on the ultrasound machine, including color Doppler, are based on the *Doppler effect*. The Doppler effect is the perceived change in frequency that occurs between a sound source and a sound receiver. When a reflector is stationary and the transducer is stationary, no Doppler shift occurs. The probe crystal samples the constantly moving red blood cells within the cardiac circuit, which create a Doppler shift. The direction of flow is shown on the machine's color map. Many manufacturers provide a red and blue color map, with red moving toward the probe and blue moving away from the probe.

Color Doppler analyzes velocities, direction of flow, and (depending on the color map chosen) areas of turbulence vs. laminar flow. Figure 2.21 shows normal flow in diastole from a pulmonary vein through the mitral valve into the left ventricle.

Quality of color imaging depends on the number of pulses per *color packet*, or packet size, and on the *frame rate* of the overall picture with color. These variables must be carefully balanced due to the fact that more pulses in the color packets result in lower frame rates. Each tiny color packet shows the mean velocity within that particular color packet. The more pulses providing individual pieces of data, the more accurate the received data and the more true the color representation.

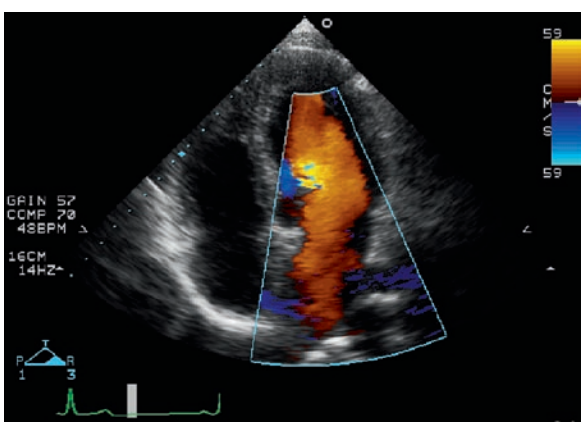

Fig. 2.21 Normal flow by color Doppler in diastole from a pulmonary vein through the mitral valve into the left ventricle

Smoothing determines the degree to which the color packets progressively transition into adjacent color packets. A low smoothing setting will make the individual color packets highly independent of one another and create a speckled impression of color flow. A high degree of smoothing will make the color packets appear as though they blend together to a large degree. The appearance of color filling improves with higher levels of smoothing.

Color Doppler provides data on moving reflectors only. Stationary reflectors detected within each color packet are eliminated from processing. Therefore, only moving reflectors play a role the color display. The machine operator can change many color display properties. A *color invert* option will flip the color map – blue flows toward the probe, red flows away from the probe. The *color map* can also be changed to display flows in an entirely new set of hues or intensities. Some color maps add an element of green or yellow to differentiate between laminar and turbulent flow. The color mode has an adjustable *scale*, as well. The number above and below the color map shows the range of mean velocities that can be displayed, typically in cm/s, without aliasing.

The machine calculates an optimal scale largely based on depth. Lowering the scale number lowers the pulse repetition frequency (PRF) and therefore the Nyquist limit (PRF/2=Nyquist Limit). The lower scale is more sensitive to flow. Raising the scale will reduce sensitivity to flow, raise the pulse repetition frequency and Nyquist limit, and make the color display less likely to alias. The scale should be left alone most of the time – particularly when grading valvular regurgitation.

The frame rate of the image with color Doppler is highly dependent on the machine operator. It is important to know how to raise frame rate without sacrificing diagnostic information. Use the *trackball*, *size*, and *position* controls to change the length, width, and placement of the color box. The length of the color box is of no consequence to the frame rate. However, the overall depth of view does affect the frame rate, so keep the image as shallow as possible in order to have the highest frame rate. Wider color boxes will lower frame rate as more time is required to interrogate a flow in a larger area. The color box should be as narrow as possible

Table 2.2 Describes the most commonly used controls and their functions for adjusting the color Doppler display

Color variable	Knob(s)	Function
Map	Map	Provides key to convert velocities into colors
Scale	Scale	Specifies range of velocities that can be expressed by color and Nyquist Limit
Invert	Invert	Assigns specified color to direction of flow
Sector placement	Position, trackball	Determines placement of color box
Sector size	Size, trackball	Determines size of color box
Gain	Gain	Amplifies color Doppler signal before display
Baseline	Baseline	Shifts the zero baseline of the color scale velocities
Smoothing	Smoothing	Determines degree of separation of color packets

while fully covering the area of interest. If the color appears bright and flashy within the color box, it may help to decrease the *color gain*. Table 2.2 describes the most commonly used controls for adjusting the color Doppler display.

Pulsed-Wave and Continuous-Wave Doppler

- *Pulsed-wave Doppler* samples velocities at a specific point along the beam axis. A gate designates the sampling point and its position within a 2D image. The *trackball* moves the pulse sample gate within the ultrasound image. The disadvantage of pulsed wave lies in its susceptibility to aliasing. This type of Doppler is best for low-velocity flows or mapping a defined area of blood flow. Figure 2.22 shows a pulsed Doppler trace with the sample site in the left ventricular inflow area. Note the systolic flow of mitral regurgitation (arrows) is aliased and an accurate peak velocity unable to be measured, but the mitral inflow velocities can be easily measured.
- *Continuous-wave Doppler* possesses a clear advantage over pulsed wave in its total lack of a Nyquist Limit. This means that the high-velocity flows will not alias. If the scale on the Doppler waveform display is set too low, it may appear to wrap around in the same manner as pulsed-wave Doppler. If this occurs, increase the scale (in cm/s) to the desired velocity range. Continuous-wave Doppler is not depth specific. The machine samples all along the beam axis, sending and receiving Doppler signals constantly. It is of primary importance to have the beam axis at an angle as close as possible to 0 degrees (parallel) with blood flow. On the sector display, position the dotted line designating Doppler beam placement within the area of interest. Figure 2.23 shows a continuous-wave Doppler trace in a patient with aortic insufficiency (AI). The AI jet has a velocity of almost 4m/s, and with continuous-wave Doppler there is no problem with aliasing.
- PW and CW Doppler displays may need to be "cleaned up" before they are acceptable for acquisition. Relevant information should be extracted and refined from the Doppler display. Once Doppler sampling placement is optimal, the resulting Doppler signal can be easily manipulated. Common controls to manipulate the signal include Doppler *sweep speed*, *gain*, *scale*, *baseline*, *compression*, and *reject*.
- *Sweep speed* changes the number and width of Doppler waveforms that can be displayed in a single picture. Increasing the sweep speed effectively zooms on one or a few Doppler waveforms at a time. High sweep speed is optimal for patients in

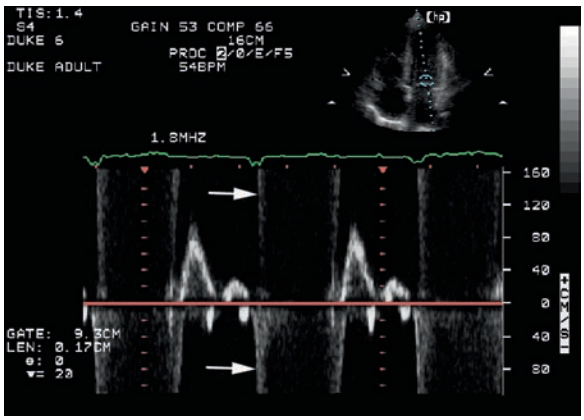

Fig. 2.22 Pulsed Doppler trace with the sample site in the left ventricular inflow area. Note the systolic flow of mitral regurgitation (*arrows*) is aliased

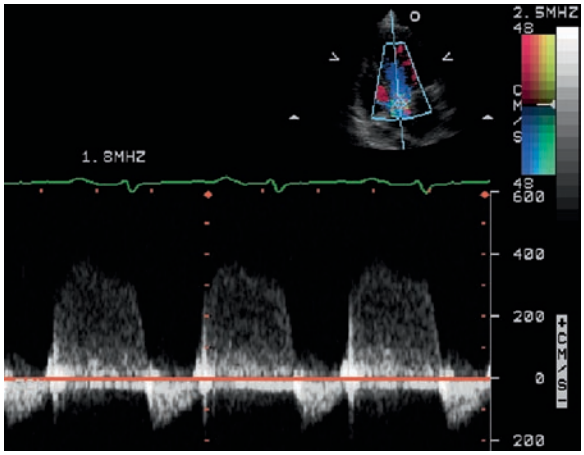

Fig. 2.23 Continuous-wave (CW) Doppler spectral trace in a patient with aortic insufficiency. Note the lack of aliasing with CW Doppler

normal sinus rhythm with multiple uniform Doppler readings over time. Sweep speed should be reduced for patient with significant Doppler variations between cardiac cycles or for arrhythmic patients. Other common indications for very low sweep speed include assessment of tamponade or constriction, where presence or lack of respiratory variation needs to be demonstrated.

- *Gain* amplifies or deamplifies the returning signal from the moving red blood cells. The gain is often preset, but it helps to change gain to compensate for low- or high-density red blood cell movement. The Doppler spectral signal itself should be a midlevel gray, while the Doppler background should be black. If the signal is bright white, turn down the Doppler gain. If it is very faint or totally black but present, turn the Doppler gain up. Increasing the audio volume to hear the Doppler shift may be helpful in optimizing the spectral trace. Audio volume provides critical information when using Pedoff probes, which produce Doppler signals with no 2D image for guidance.
- *The scale setting controls* the highest- and lowest-velocity levels that can be presented on the Doppler display (in cm/s). If the baseline is in the center of the Doppler display y-axis, then the highest velocities that can be potentially detected above and below the baseline (toward and away from the probe) should be the same. If a flow is very high or low velocity, it may at some point be required to alter the Doppler scale.

Table 2.3 Describes the most commonly used controls and their functions for changing PW/CW Doppler variables

PW/CW variable	Knob(s)	Function
Sample placement	Position, trackball	Specifies location of Doppler beam
Scale	Scale	Specifies range of velocities that can be displayed and Nyquist Limit (PW)
Sweep speed	Sweep speed	Changes number of cycles that can be shown on the x-axis of the Doppler display
Gain	Gain	Amplifies PW and CW Doppler signals before display
Baseline	Baseline	Positions the zero baseline of the Doppler display
Compression	Compression	Changes the difference between the highest and the lowest received amplitudes (shades of gray)
Reject	Reject	Eliminates low-velocity signals near zero baseline
Invert	Invert	Determines the presentation of signals as above or below zero baseline regardless of direction of flow
Measurements	Freeze, caliper, trace, enter, erase	Quantifies features of a PW/CW Doppler spectral display

- *The baseline* is a horizontal line showing the zero velocity point over time. Velocities can be shown symmetrically above and below the baseline. The alternative is to eliminate unwanted information by raising or lowering the zero velocity point along the y-axis of the Doppler display to focus attention on flow above or below the baseline. Figure 2.12 demonstrates the baseline shift as the baseline is moved up in order to display the entire spectral trace.
- *Doppler compression* changes the number of shades of gray assigned to the spectral display. Increasing the numerical level of Doppler compression creates a softer, smoother gray Doppler display. A lower numerical level of Doppler compression creates a harsh display with more black/white contrast and fewer shades of gray.

- *Reject* functions to eliminate low-velocity signals, which are usually seen near the baseline. Reject brings the Doppler background to black or close to it. Reject also helps to define the borders of the Doppler signal. When tracing or measuring, be sure that the reject is set at an acceptable level.

Multiple controls play a role in measuring Doppler values. Adding Doppler measurements are often necessary for a complete cardiac assessment. Relevant controls include: *freeze*, *caliper*, *trace*, *enter*, *erase*, and the *trackball*. Caliper measurements of pulsed- and continuous-wave Doppler can be made using the *caliper*, *trackball*, and *enter* controls. Caliper settings give rise to machine calculations of instantaneous velocity values and instantaneous pressure values. Tracing will provide information on peak velocity, peak pressure gradient, and mean pressure gradient. A tracing is made by using the *trace*, *trackball*, and *enter* buttons. Press the *erase* button once or more to remove one or all the Doppler measurements from the image waveforms. Doppler measurements can be recorded inside or outside the machine *analysis* package. The analysis package on any machine is intended to label, identify, and present measurements in an organized manner. Measurements may be named on the display once they are made within the analysis package. Once certain Doppler measurements are accumulated, the machine may be able to calculate further helpful values using previously programmed ultrasound equations. Table 2.3 describes the most commonly used controls for pulsed- and continuous-wave Doppler variables.

Conclusions

It is important to familiarize yourself with the common echocardiographic imaging modes and their controls. Image quality and diagnostic accuracy depend heavily on the knowledge and skill of the clinician operating the ultrasound machine. Awareness of the basic knobology associated with 2D, Color Doppler, PW Doppler, and CW Doppler is absolutely essential for performing a good echocardiographic examination. While even simple display manipulation may seem difficult at first, image optimization becomes second nature with time and experience.

Chapter 3
Principles of Flow Assessment

Ahmed A. Alsaileek and Jamil Tajik

Introduction

Hemodynamic is concerned with the physical and physiological principles governing the movement of blood through the circulatory system. In other words, hemodynamic is the science and art of the relationship among pressure, viscous resistance to flow, and the volume flow rate in the cardiovascular system.

Prior to the application of Doppler echocardiography, hemodynamic assessment was obtained invasively through cardiac catheterization. For most clinical purposes and in daily practice, Doppler echocardiography has replaced cardiac catheterization and becomes the preferred method for hemodynamic assessment. Doppler principle can be applied to calculate flows through different valves, stroke volume, cardiac output, valve areas, regurgitant volumes and shunts. Several animal and clinical studies have validated these methods and have yielded excellent correlations with simultaneously acquired invasive data.[1-5]

The Doppler Principle

The Doppler principle is applied in echocardiography to enable the determination of the blood flow characteristics such as velocity and direction. In principle, the frequency of the sound waves that are reflected by a stationary object is the same as the frequency of the sound waves transmitted by the transducer. On the other hand, the transmitted frequency of sound waves is altered when reflected by a moving object. If the object is moving toward the transducer, the reflected frequency will be slightly higher and if the object is moving away from the transducer the reflected frequency is slightly lower. This phenomenon is called *Doppler Effect*. In cardiovascular imaging, the moving objects are the red blood cells. The echocardiography instruments determine the *frequency (Doppler) shift* (f_D) which is the difference between the transmitted (f_T) and the received frequency (f_R).

$$f_D = f_R - f_T$$

This Doppler shift is affected by speed of sound in the tissue (C = 1,540 m/s), blood flow velocity (V), and the angle (θ) between the ultrasound beam and the blood flow. So the equation can be restated as follows (Doppler equation):

$$f_D = 2 f_T \frac{V \cos\theta}{C}$$

Frequency shift (f_D) is, therefore, directly proportional to the blood flow velocity and the equation may be more practically rewritten this way:

$$V = \frac{f_D C}{2 f_T \cos\theta}$$

(Note that C and f_T are constant and the $\cos\theta$ (when the ultrasound beam is parallel to the flow) is equal to one)

Therefore, with this equation we can easily determine the frequency shift and hence the blood flow velocity. However, this does not determine the direction of blood flow. The direction can be determined by the echo machine by calculating the frequency shift and giving a positive sign for flow toward the transducer and negative sign for that away from the transducer. In the computer screen this is shown in two ways:

A.A. Alsaileek (✉)
Department of Cardiac Science, King Abdulaziz Medical City, Riyadh, Kingdom of Saudi Arabia
e-mail: saileeka@ngha.med.sa

J. Tajik
Mayo Clinic, Scottsdale, AZ, United States

P. Nihoyannopoulos and J. Kisslo (eds.), *Echocardiography*,
DOI: 10.1007/978-1-84882-293-1_3,

- Spectral Doppler analysis, where the time is the horizontal line (baseline), the *Y*-axis determines the velocity of the flow. The spectral envelop, above and below the baseline, determines the flow direction (Fig. 3.1). In this example the envelop is above the baseline which represent a flow toward the transducer.
- Color-flow Doppler analysis where the flow is color coded according to the direction of the flow. The flow toward the transducer is red and the color away from the transducer is blue (Fig. 3.2).

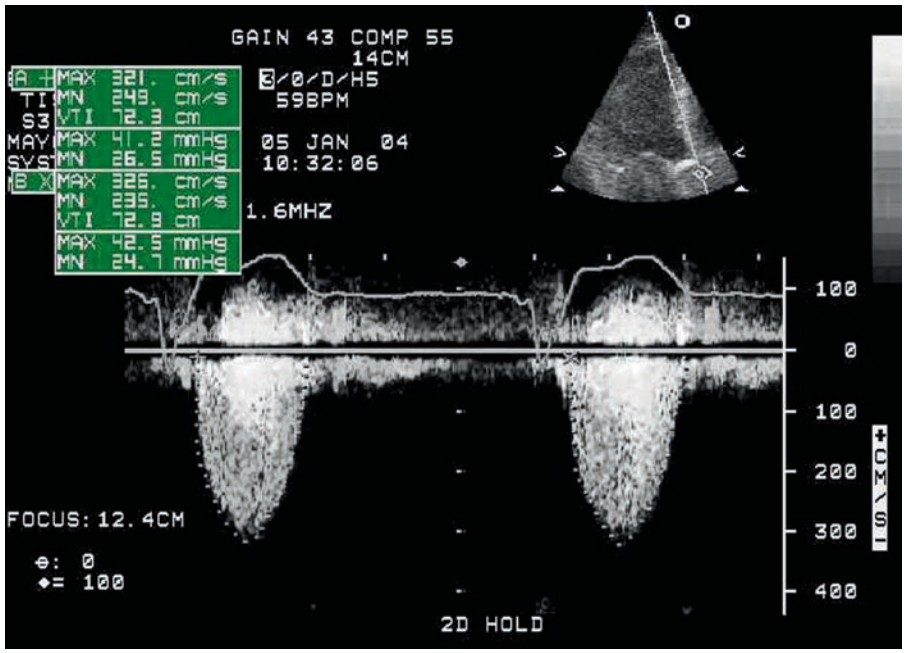

Fig. 3.1 Spectral Doppler analysis, where the time is the horizontal line (baseline), the *Y*-axis determines the velocity of the flow, and the spectral envelop above and below the baseline determines the flow direction. In this example of aortic stenosis, the transducer is at the apex and the stenotic jet velocities are moving away from the transducer and, therefore, are displayed below the baseline

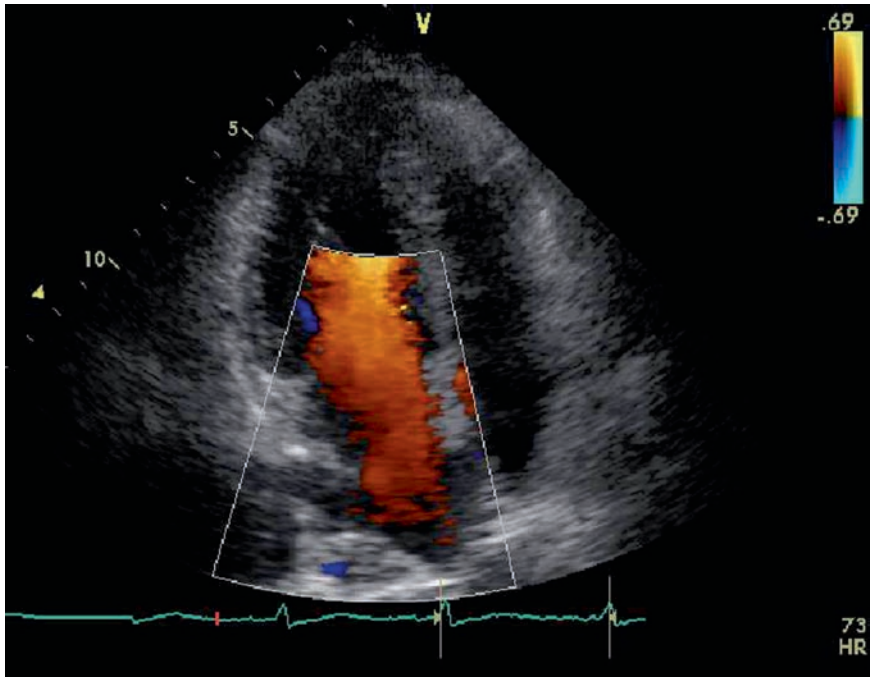

Fig. 3.2 Color Doppler analysis where the flow is color coded according to the direction of the flow. The flow toward the transducer is depicted in shade of *red* and the flow away from the transducer is in shade of *blue*. In this example of the flow across the mitral valve, the transducer is at the apex. The flow is coming toward the transducer, so it is shown as *red*

We will discuss the Doppler assessment of hemodynamics as follows:

- Stroke volume, cardiac output, and cardiac index determination.
- Methodology for calculation of stenotic valve area.
- Principles of calculation of regurgitant volume and effective regurgitant orifice (ERO).
- Determination of transvalvular pressure gradient.
- Estimation of intracardiac pressure and pulmonary artery pressure.

Four equations or principles are commonly used for these purposes:

1. Hydraulic equation of flow.
2. Continuity equation (law of conservation of mass).
3. Proximal isovelocity surface area (PISA) method.
4. Bernoulli equation.

Principle of Flow Assessment

Blood flow (Q) through a tube, vessel, or across a valve can be derived by a simple hydraulic equation as the product of flow velocity (V) and cross-sectional area (A) of the vessel at the site where velocity is measured. The area can be assumed to be circular and calculated as follows:

$$\text{Area} = \pi r^2 \text{ (for circular orifice)} = \pi(D/2)^2 = 3.14\ (D/2)^2 = (3.14/4)D^2 = 0.785\ D^2$$

where D is the diameter of the vessel.

And sometimes the area can be ellipsoid and calculated as follows:

$$\text{Area} = \pi(D_1/2 \times D_2/2)\text{(for ellipsoid orifice)} = 0.785 D_1\ D_2$$

Flow is the product of area and velocity and can be expressed as:

$$Q(\text{cc/s}) = A(\text{cm}^2) \times V(\text{cm/s}) = 0.785\ D^2V$$

$$\text{(for circular orifice)} = 0.785\ D_1D_2V \text{ (for ellipsoid orifice)}$$

This equation assumes a constant flow. However, in pulsatile system (cardiovascular system), flow velocity varies throughout the ejection period and calculation of the volumetric flow is more complex. Therefore, the total flow has to be determined by integrating all individual velocities of the Doppler spectrum over time. In Doppler echocardiography this is known as time velocity integral (TVI), which is determined by measuring the area under the curve of the Doppler spectrum. The area under the curve is a measure of the distance the column of fluid travels (Figs. 3.3 and 3.4).

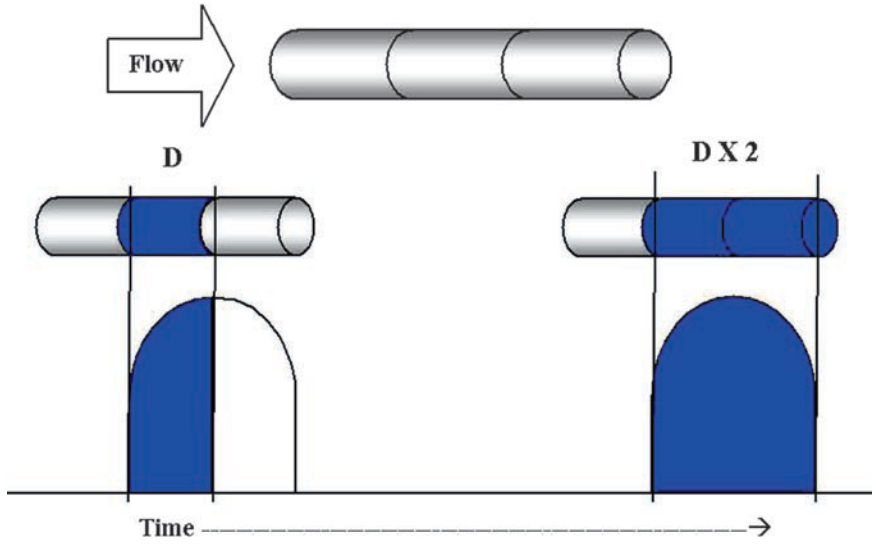

Fig. 3.3 This figure demonstrates the flow in the tube and its representation by spectral method. The relation between the distance (D) and time is also shown. The blood travels longer distance with time. In pulsatile system the flow velocity starts at zero, gradually increases to peak, then again decelerates to zero

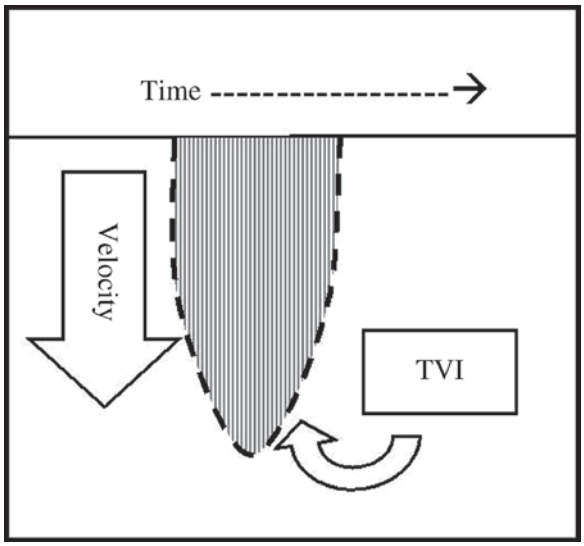

Fig. 3.4 This figure shows schematic illustration of spectral Doppler. The outer border of the spectral Doppler display is traced to determine the TVI

The commercially available echocardiography machines can readily obtain TVI. The modal velocity is derived using the Doppler equation and is dependent on knowing the frequency shift, the velocity of sound in tissue, and the angle between the ultrasound beam and the direction of blood flow. The latter has to be less than 20°; otherwise, significant underestimation of velocity of calculated flow would occur using the assumption of a zero or near-zero intercept between the sound wave and the bloodstream.

The area can be planimetered or calculated utilizing two-dimensional echocardiography to obtain diameter (D) with a circular ($A = 0.785 \times D^2$) or elliptic ($A = 0.785 D_1 D_2$) assumption after the diameter(s) (D) is measured.

Stroke Volume and Cardiac Output

One of the fundamental functions of the heart as a pump is to provide adequate amount of blood flow for the normal function of the human body. In the past, the cardiac output determination required invasive comprehensive and time-consuming methods based upon Fick and indicator dilution principles. Nowadays, stroke volume and cardiac output can be noninvasively and reliably measured by 2D echo/Doppler methodology. The forward stroke volume can be determined by the Doppler method mentioned earlier, which can basically be applied to any of the cardiac valves assuming no significant valvular regurgitation is present. Usually the flow through the aortic valve (or left ventricular outflow tract – LVOT) is calculated because the aortic annulus has the least change in size during the cardiac cycle.[4,6] The aortic annulus diameter is measured in the parasternal long-axis view (Fig. 3.5-lower) and

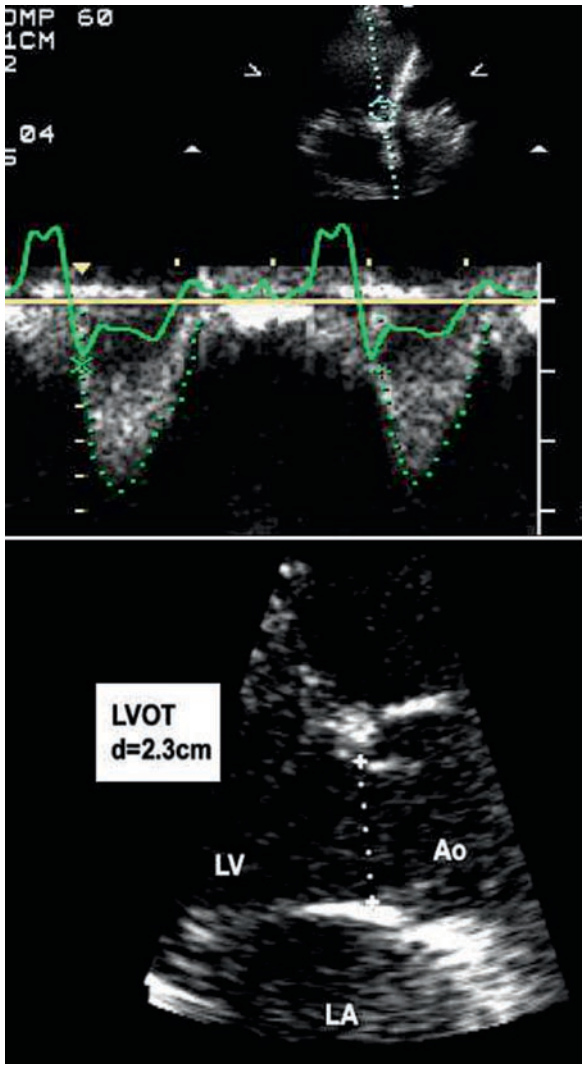

Fig. 3.5 This figure illustrates the Doppler method to determine stroke volume. The diameter of the aortic annulus is usually obtained from parasternal long-axis view (*lower*). In this example aortic annulus diameter is equal to 2.3 cm. The maximum diameter should be recorded. The TVI of the aortic annulus is normally obtained from apical long-axis view and occasionally utilizing 5-chamber view (*upper*). The TVI of LVOT is obtained by tracing the outer border of PW Doppler signal of LVOT. In this example average TVI is equal to 20.0 cm

the maximum diameter is obtained. The velocity at the annulus is obtained utilizing the apical long-axis view and by placing the pulsed-wave (PW) Doppler sample volume at the level of aortic annulus. The closing click of the aortic valve should be recognized to insure good position. This velocity is then planimetered along its outer edge to obtain the TVI (Fig. 3.5-upper). If significant aortic regurgitation is present, the flow through this valve cannot be used to calculate the cardiac output. Errors can be incurred in the area calculation, mostly related to the diameter measurement (the error in area calculation is roughly doubled compared to the error in diameter measurement), but also includes inappropriate geometric assumptions and data acquisition at a different site from where velocity was recorded. Looking at the numbers in the figures (Fig. 3.5) we can calculate the stroke volume as follows:

$$\text{Stroke volume (SV)} = 0.785 \times D^2 \times \text{TVI} = 0.785 \times 2.3^2 \times 20.0 = 83\text{ml}$$

Cardiac output is the product of stroke volume and heart rate (assume the heart rate is 65 beats/min)

$$\text{Cardiac output (CO)} = \text{SV} \times \text{HR} = 86 \times 65 = 5.398\text{ml/min} = 5.4\text{l/min}$$

(by converting the milliliter to liter)

Cardiac index is obtained by dividing the cardiac output by body surface area (BSA)

$$\text{Cardiac index(CI)} = \text{CO/BSA}(1/\text{min}/\text{m}^2)$$

Alternatively, but uncommonly used, cardiac output can be obtained from pulmonic valve or right ventricular outflow tract. In the short axis at the level of aortic valve the ultrasound beam is almost parallel to the blood flow at the level of pulmonic valve or right ventricular outflow tract. The TVI is obtained by pulsed-wave Doppler at the same level where the right ventricular outflow tract area is measured in 2D echocardiography.[7] The cardiac output can be obtained at any valve assuming there is no regurgitation of the valve so the cardiac output is constant for any given cardiac cycle.

Continuity Equation

Continuity equation is based on the principle of conservation of mass. This principle states that, under conditions of cardiovascular stability without any regurgitation or shunt, the net blood volume at any part of circulation must equal the net blood volume at any other part next to it (what comes in must go out) (Fig. 3.6). This situation is true under certain assumptions:

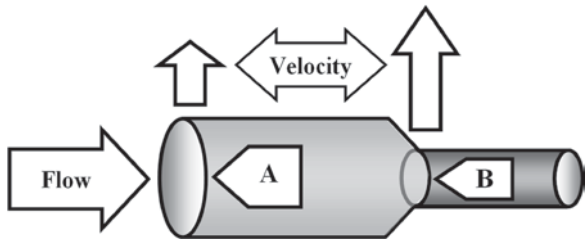

Fig. 3.6 This figure shows two tubes with different diameter in continuity. The continuity equation states that the flow volume at point A is equal to that of point B and mathematically written as follows: (Area *A* × Velocity *A* = Area B × Velocity B). Note that the velocity is higher with smaller area

- The two points are directly connected.
- Blood is neither added nor removed from the system.

In applying the continuity equation to the blood flow in and out of the heart, the mitral valve stroke volume is equal to aortic valve stroke volume provided there is no mitral or aortic regurgitation (Fig. 3.7). In the same way the aortic stroke volume is equal to pulmonic valve stroke volume provided no significant regurgitation is present in any of the valves, and no intracardiac shunt is present. The tricuspid valve stroke is not commonly used in clinical practice because of complex geometry for valve area calculation and because of the presence of tricuspid regurgitation in the majority of normal subjects.

The aortic valve stroke volume is calculated by measuring the aortic annulus diameter in parasternal long-axis view at maximum valve opening in systole. The TVI is obtained utilizing pulsed-wave Doppler sample volume at the level of aortic annulus on the apical long-axis or 5-chamber view. The aortic valve area (AVA) is assumed to be circular and, hence, the area is calculated from the obtained aortic annulus diameter (D_{AA})

$$\text{AVA} = \pi (D_{AA}/2)^2 = 0.785\, D_{AA}^2$$

The stroke volume at the level of aortic valve is then calculated as follows

$$\text{SV}_{AA} = \text{AVA} \times \text{TVI}_{AA}$$

$$\text{SV}_{AA} = 0.785 \times D_{AA}^2 \times \text{TVI}_{AA}$$

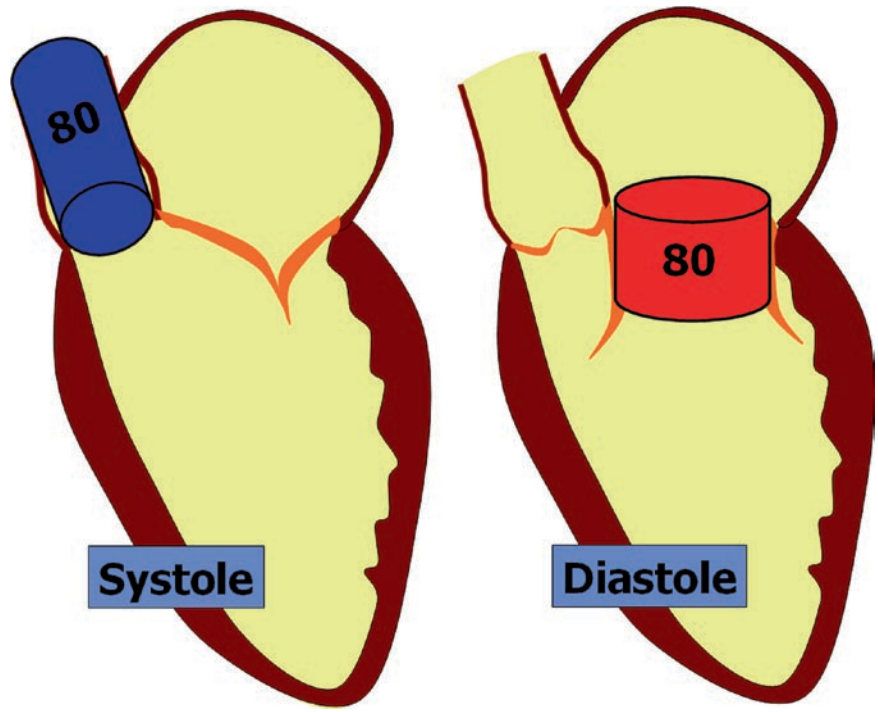

Fig. 3.7 This figure demonstrates the continuity between mitral and aortic valves' stroke volume. The volume of blood that comes in through mitral valve must go out through aortic valve

In calculating the mitral valve stroke volume, the mitral valve area is calculated either by assuming a circular or ellipsoid geometry. For practical purposes, the circular shape is the most often used. The mitral annulus diameter (D_{MA}) is obtained from the apical 4-chamber view at maximum valve opening in diastole. The TVI is obtained from the same view by pulsed-wave Doppler sample volume at the level of the mitral annulus.

$$MVA = 0.785 \times D_{MA}{}^2$$

And therefore:

$$SV_{MA} = MVA \times TVI_{MA}$$

$$SV_{MA} = 0.785 \times D_{MA}{}^2 \times TVI_{MA}$$

Mathematically the continuity equation means that stroke volume through mitral valve is equal to the stroke volume through aortic valve:

$$TVI\ 1 \times Area\ 1\ (mitral) = TVI\ 2 \times Area\ 2\ (aortic)$$

$$0.785 \times D_{MA}{}^2 \times TVI_{MA} = 0.785 \times D_{AA}{}^2 \times TVI_{AA}$$

The concept of continuity is very useful clinically to assess mitral or aortic regurgitant volume (RV), regurgitant fraction, regurgitant orifice, as well as the stenotic mitral or aortic valve area.

Clinical Applications of Continuity Equation

Mitral Regurgitation

In mitral regurgitation (Figs. 3.8 and 3.9), the aortic stroke volume is less than the forward mitral stroke volume because part of the blood contained in the LV at the end of diastole is ejected back to the left atrium through the regurgitant mitral valve.

$$\text{Aortic stroke volume} = \text{mitral stroke volume} - \text{RV (Mitral)}$$

Therefore,

$$\text{Mitral RV} = \text{mitral stroke volume} - \text{Aortic stroke volume} = (0.785 \times D_{MA}{}^2 \times TVI_{MA}) - (0.785 \times D_{AA}{}^2 \times TVI_{AA})$$

Aortic Regurgitation

In aortic regurgitation the aortic stroke volume is more than the mitral stroke volume because the regurgitant volume through aortic valve will be added to the

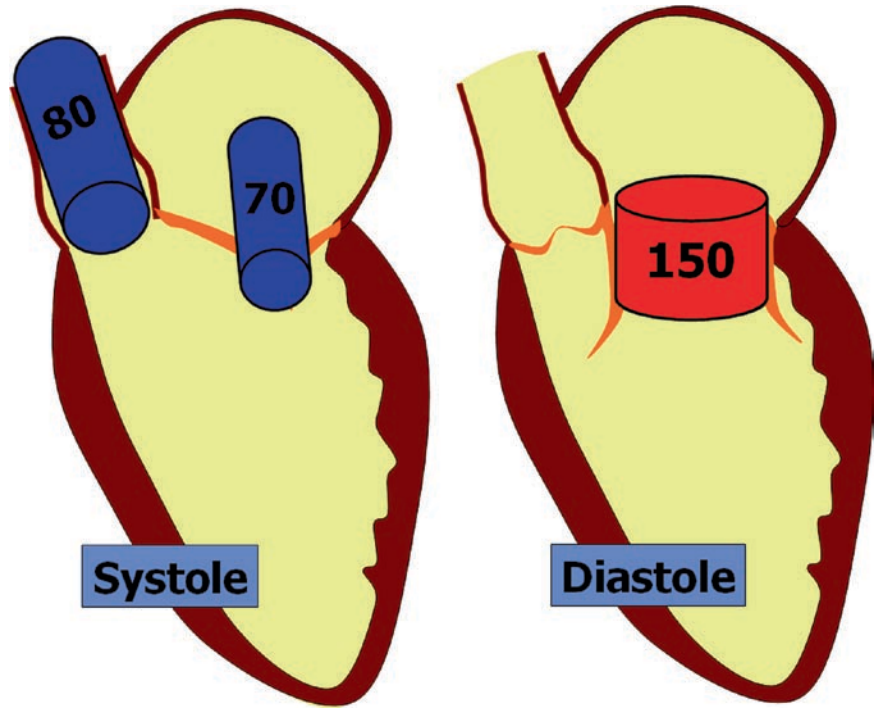

Fig. 3.8 This figure shows schematic illustration of the principle of calculating mitral regurgitant volume based on hydraulic formula. Mitral inflow volume of 150 cc (what goes in) and aortic stroke volume of 80 cc (what goes out) are calculated based on the continuity equation. The difference (150 – 80 = 70 cc) must represent the mitral regurgitation volume

subsequent stroke volume from mitral valve (Figs 3.9 and 3.10). The same methodology described to assess the mitral valve regurgitant volume is used to assess the aortic regurgitant volume. The difference is that the aortic stroke volume will be higher than that of mitral stroke volume (see earlier).

$$\text{Aortic stroke volume} = \text{mitral stroke volume} + \text{RV (Aortic)}$$

Therefore,

$$\text{Aortic RV} = \text{Aortic stroke volume} - \text{mitral stroke volume} = (0.785 \times D_{AA}{}^2 \times \text{TVI}_{AA}) - (0.785 \times D_{MA}{}^2 \times \text{TVI}_{MA})$$

Mitral Stenosis

The mitral valve area in the presence of mitral stenosis can also be estimated using the continuity equation. The stroke volume at mitral valve orifice is equal to the aortic stroke volume (the method to obtain the aortic SV is already discussed). The aortic annulus area multiplied by the aortic TVI is equal to MVA multiplied by the mitral TVI. Mitral valve TVI is obtained by continuous-wave Doppler across the mitral valve from apical 4-chamber or apical long-axis views. The MVA can then be calculated as follows:

$$\text{MVA} \times \text{flow} = \text{AVA} \times \text{flow}$$

$$\text{MVA} \times \text{TVA}_{MA} = 0.785 \times D_{AA}{}^2 \times \text{TVI}_{AA}$$

$$\text{MVA} = 0.785 \times D_{AA}{}^2 \times \text{TVI}_{AA}/\text{TVI}_{MA}$$

The limitation of this method is the presence of more than trivial/mild mitral regurgitation, which may be present in a significant number of patients.[8,9]

Aortic Stenosis

The same principle can be applied to any two orifices connected in series or tube at two different points provided that all the flow goes in one direction. This can be applied to assess the aortic valve area in aortic stenosis (*what comes in must go out*)[10,11] (Fig. 3.11). The volume of blood going through LVOT (proximal) should be equal to that going through a stenotic aortic valve (distal). The LVOT diameter and TVI (TVI_{LVOT}) is determined as discussed previously. One important point to make is to avoid the area of flow acceleration (due to severe aortic stenosis) in the LVOT TVI

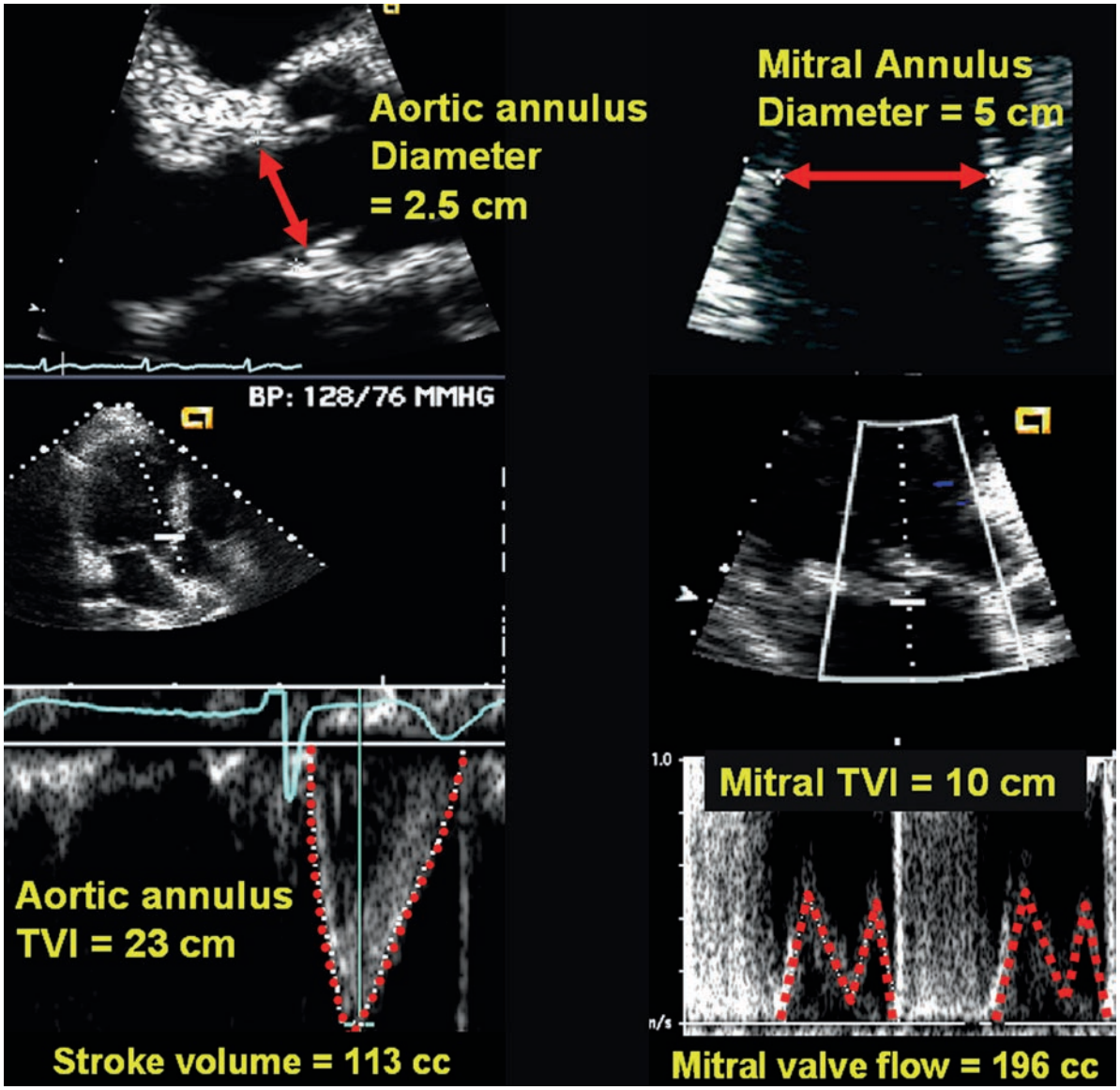

Fig. 3.9 The measurement needed for continuity equation in mitral regurgitation and aortic regurgitation. The mitral inflow volume is calculated from the mitral inflow TVI and mitral annulus diameter ($0.785D_{MA}^{2} \times TVI_{MA}$ = 196 cc). The aortic stroke volume is calculated from the aortic TVI and aortic annulus diameter ($0.785 \times D_{AA}^{2} \times TVI_{AA}$ = 113 cc). The difference (196 – 113 = 83 cc) must be the mitral regurgitation volume

determination by moving the sample volume about 1 cm below the aortic annulus. The aortic TVI (TVI_{AA}) is obtained by CW Doppler across the aortic valve. This should be done from multiple locations (Fig. 3.11) and the highest velocity is used in the calculation. Aortic valve area (AVA) is calculated as:

$$AVA(cm^2) \times TVI_{AA} = (0.785 \times D_{LVOT}^{2} \times TVI_{LVOT})$$

And then,

$$AVA(cm^2) = -(0.785 \times D_{LVOT}^{2} \times TVI_{LVOT})/TVI_{AA}$$

Echocardiographic findings of patients with tricuspid regurgitation generally mirror those found in mitral regurgitation. Therefore, the tricuspid valve stroke volume can be compared to the pulmonic valve stroke

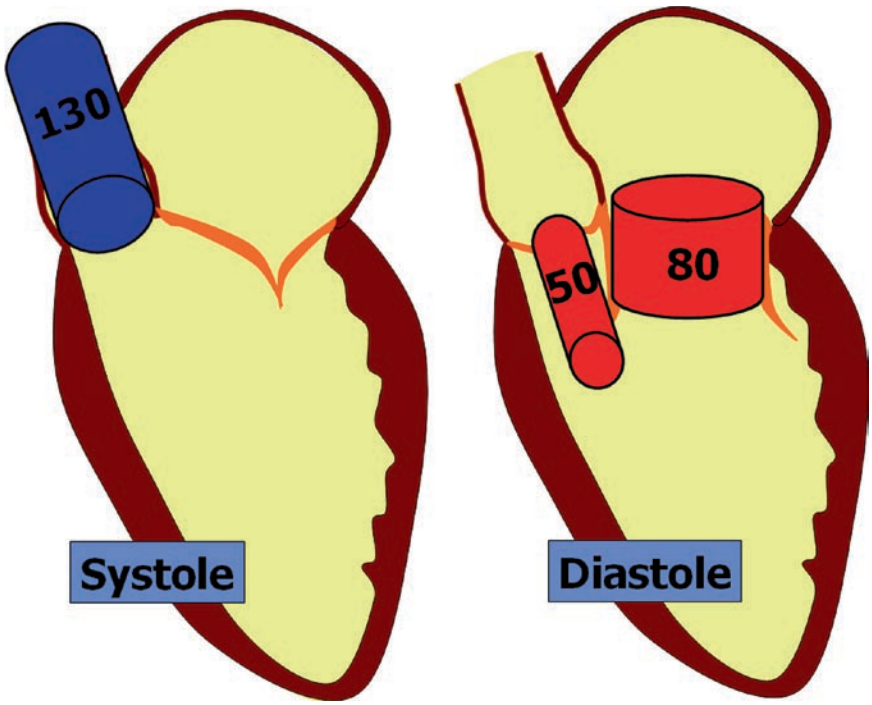

Fig. 3.10 This figure shows schematic illustration of the principle of calculating aortic regurgitant volume based of hydraulic formula. Mitral inflow volume 80 cc (what goes in) and aortic stroke volume 130 cc (what goes out) are calculated based on the continuity equation. The difference (130 − 80 = 50 cc) must represent the aortic regurgitation volume

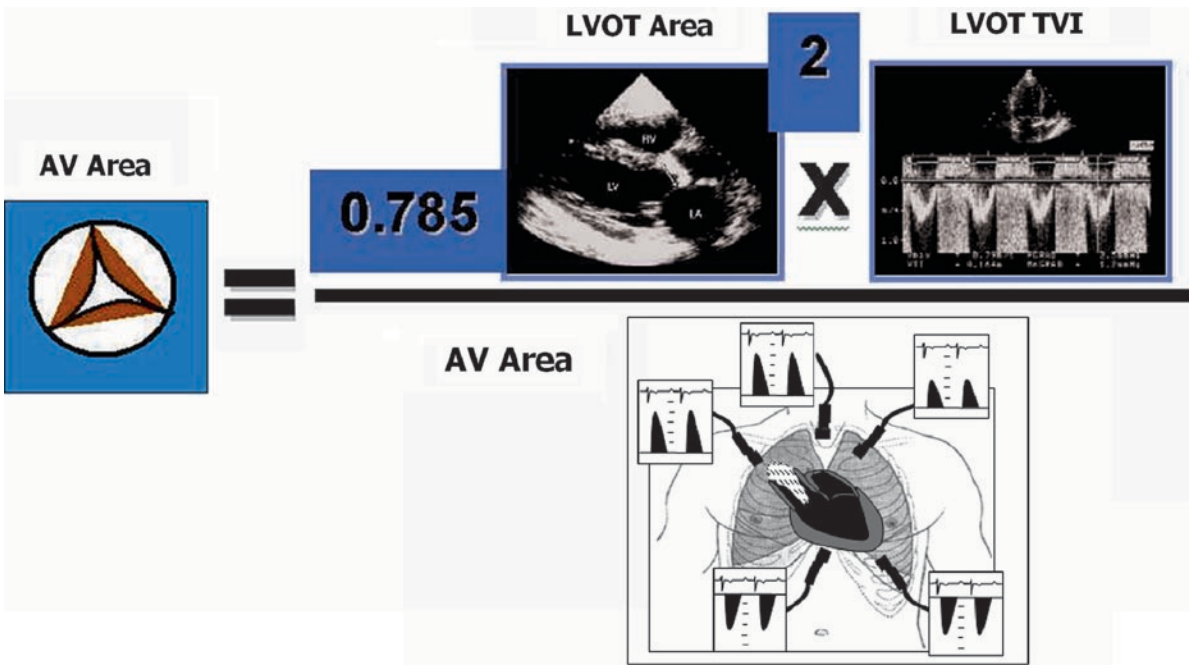

Fig. 3.11 This figure shows the continuity method to assess AS severity. The flow rates at the LVOT and AV are the same. The LVOT flow rate is calculated from the LVOT TVI and diameter (see also Fig. 3.5). The TVI of AV is obtained by tracing the outer border of CW Doppler signal of AV. Then the AVA is calculated as: AVA (cm^2) = $(0.785D_{LVOT}^{\ 2} \times TVI_{LVOT})/TVI_{AA}$

volume and the regurgitant volume can be estimated, but clinically this method is less often used than the PISA method.[12]

Proximal Isovelocity Surface Area method

Proximal Isovelocity Surface Area (PISA) method is based on the law of conservation of flow. The law states the flow rate at two consecutive points is identical. The method uses the advantage of aliasing in color Doppler imaging. In color Doppler the flow is given red or blue color if the direction of flow is toward and away from the transducer, respectively. As the flow approaches a narrowed orifice (stenotic or regurgitant), its velocity increases, in a shape of isovelocity hemispheric shell as blood flow converges from all directions toward the orifice (Fig. 3.12). The flow rate at the surface of the hemispheric shell is equal to the flow rate at the regurgitant orifice (law of conservation of the flow). As the flow converges toward the orifice, it accelerates and aliasing occurs if the velocity exceeds the Nyquist limit. This can be nicely shown using the color Doppler imaging where the color changes from red to blue in a nice hemisphere. If the Nyquist limit is decreased, the aliasing occurs with lower velocity and starts further away from the regurgitant orifice making the hemisphere (PISA) larger. Using this principle, flow rate at the surface of the hemispheric shape can be estimated. The flow rate can be calculated by multiplying the area by velocity (Flow rate = Area × Velocity). The area in case of valve is circular so it is calculated as (πr^2), but in case of hemisphere surface area is calculated as ($2\pi r^2$ or $6.28r^2$), the r is the radius of the hemisphere. The radius of the hemisphere can be measured from the surface to the narrowest area of color flow, which is closely related to the regurgitant or stenotic orifice. The flow rate at the hemisphere (PISA) surface is

$$\text{Flow rate} = AV = 2\pi r^2\, V_{\text{aliasing}} = 6.28r^2\, V_{\text{aliasing}}$$

and according to the law of conservation of flow, flow rate at the regurgitant orifice is equal to flow rate at the surface of the PISA.

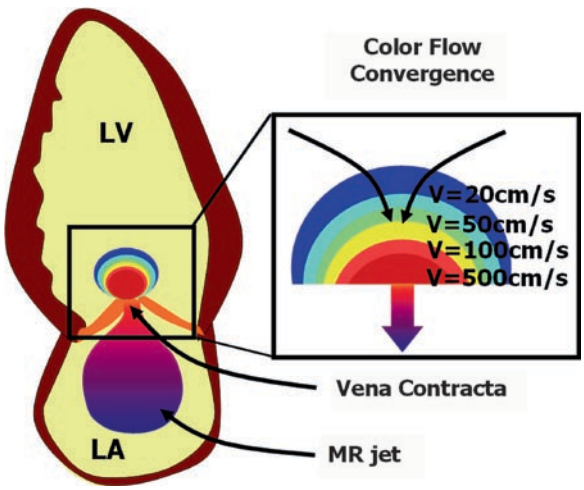

Fig. 3.12 Schematic illustration of the PISA. The flow accelerates as it approaches a narrow orifice forming hemispheric shell. This can be shown on color Doppler (as in case of mitral regurgitation). The flow converges as it approaches the regurgitant mitral valve. The color changes due to high velocity exceeding the Nyquist limit and forming hemispheric shell (PISA)

Clinical Applications of PISA Method

Mitral Regurgitation

In mitral regurgitation, the apical 4-chamber view with color Doppler is commonly used (Figs. 3.12 and 3.13). However, parasternal long-axis view is sometimes used in case of eccentric jet where the PISA is better visualized. The Nyquist limit is shifted downward in the direction of the flow of mitral regurgitation (MR) jet. The velocity of the PISA is measured at mid to late systole (the same time the maximum MR velocity occurs).[13, 14]

$$\text{Area(ERO)} \times V_{\text{max}}\text{MR} = 6.28r^2\, V_{\text{aliasing}}$$

$$\text{Effective regurgitant orifice (ERO)} = 6.28r^2\, V_{\text{aliasing}} / V_{\text{max}}\text{MR}$$

As discussed in the calculation of the stroke volume, flow rate is the product of area and TVI. The same method can be applied to calculate the regurgitant volume (RV). The area here is known (see earlier), which is the ERO of the mitral valve. The TVI is nothing but the TVI of the mitral regurgitation jet. Therefore:

$$\text{Mitral RV} = \text{ERO(PISA)} \times \text{TVI}_{\text{MR}}(\text{CW\ Doppler}) = (6.28r^2\, V_{\text{aliasing}} / V_{\text{max}}\text{MR})\ \text{TVI}_{\text{MR}}$$

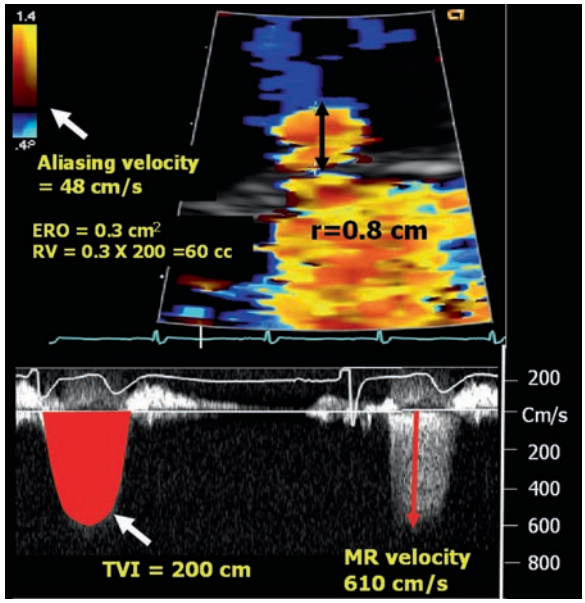

Fig. 3.13 This figure shows the PISA methods to evaluate the severity of mitral regurgitation. The PISA is obtained from the apical 4-chamber view. The baseline is shifted downward toward the regurgitant jet flow (*arrow*). Then the PISA diameter is measured from the surface of the hemisphere to the narrowest area on color Doppler (0.8 cm). The CW Doppler is utilized to measure the mitral regurgitation TVI and peak velocity. The effective regurgitant orifice (ERO) and the regurgitant volume (RV) are calculated as follows: ERO = $6.28r^2V_{aliasing}/V_{max}$MR = $6.28 \times 0.8^2 \times 48/610 = 0.3$ cm^2 and RV = TVI × ERO = 200 × 0.3 = 60 cc

Width of vena contracta is another quantitative method to assess mitral regurgitation. It is defined as the narrowest cross-sectional area of a jet. This can be easily seen, while obtaining the zone of flow convergence, above the mitral valve on the left atrial side (Fig. 3.12). On transthoracic color-flow mapping it has been shown that vena contracta width predicts angiographic severity of mitral regurgitation.[15] Compared to continuity equation, vena contracta of more than 5 mm correlates well with severe mitral regurgitation.[16]

Semiquantitative Doppler methods to evaluate the mitral regurgitation are less sensitive and are considered complementary in mitral regurgitation evaluation.

Color-flow Doppler – The features of severe mitral regurgitation seen on color-flow Doppler imaging arise from the high-energy transfer of a large volume of blood into the left atrium, producing "jets" in the left atrium. Color-flow Doppler remains the easiest and the best method to screen for mitral regurgitation. It also provides semiquantitative assessment of the mitral regurgitation severity. The ratio of the mitral regurgitation jet area to the total left atrial area has been reported to correlate well with MR severity.[17] Severe mitral regurgitation is characterized by large jet (>40%) and extending into the pulmonary veins. However, jets are very sensitive to instrument settings, and the size of a color jet may be misleading such as in an eccentric jet; thus, reliance on these size judgments alone may not be sound practice.[18-20]

Doppler of pulmonary veins – Doppler interrogation of the pulmonary veins has produced insights into hemodynamics. In mitral regurgitation evaluation, pulsed-wave Doppler of the left and right upper pulmonary veins is performed from the apical 4-chamber view. In hemodynamically severe mitral regurgitation, the flow in one or more pulmonary veins show systolic flow reversal. This echo feature is the analog of the V wave seen in the left atrial pressure tracing and on a pulmonary artery wedge pressure tracing.

Continuous-wave Doppler of the mitral regurgitation jet – If the flow signal can be aligned parallel to the beam, in severe mitral regurgitation, the Spectral Doppler of the jet appears uniformly dense throughout its duration and have a well-defined envelop. MR jet velocity does not correlate with the severity.

Other features that are associated with severe mitral regurgitation include dilated or dysfunctional left ventricle, dilated left atrium, elevated pulmonary artery systolic pressure, and the presence of significant tricuspid regurgitation. In severe decompensated mitral regurgitation, the tricuspid regurgitation peak velocity is increased as the result of pulmonary hypertension.

Tricuspid Regurgitation

As with mitral regurgitation, severity of tricuspid regurgitation (TR) can be estimated by effective regurgitant orifice (ERO) by measuring the size of proximal flow convergence zones (PISA).[21]

$$\text{Area(ERO)} \times V_{max}\text{TR} = 6.28r^2\, V_{aliasing}$$

$$\text{ERO(Tricuspid)} = 6.28r^2\, V_{aliasing}/V_{max}\ \text{TR}$$

And even the regurgitant volume (RV) can be calculated

$$\text{RV(Tricuspid)} = \text{Area(ERO)} \times \text{TVI} = (6.28r^2 \; V_{\text{aliasing}}/V_{\text{max}}\text{TR}) \times \text{TVI}_{\text{TR}}$$

Aortic Regurgitation

The severity of aortic regurgitation can be quantitatively assessed utilizing the PISA method.[22] The apical 5-chamber and apical long-axis views are used to visualize the PISA. However, parasternal long-axis view is sometimes used in case of eccentric jet where the PISA is better visualized. The Nyquist limit baseline is shifted toward the flow of the aortic regurgitation jet (Fig. 3.14). The PISA radius is measured at early diastole.[23] Similarly, the maximum aortic regurgitation (AR) velocity is measure in early diastole is measured. The ERO is calculated as follows:

$$\text{Aortic ERO} = \text{PISA flow rate/AR regurgitant velocity} = 6.28r^2 \; (V_{\text{aliasing}}/\text{AR regurgitant velocity})$$

The aortic regurgitant volume is calculated by tracing the aortic regurgitation jet outer surface to measure the aortic regurgitation TVI (TVI_{AR}); therefore:

$$\text{flow volume(RV)} = \text{Area(ERO)} \times \text{TVI} = (6.28r^2 \; V_{\text{aliasing}}/V_{\text{max}}\text{AR}) \times \text{TVI}_{\text{AR}}$$

Vena contracta – It is the narrowest portion of the jet crossing the plane of the valve. It lies immediately next to the area of flow convergence. It can be measured from parasternal long-axis or apical long-axis views. To optimize the visualization, the echo sector should be the narrowest possible and the depth decreased. Vena contracta of equal to or more than 6 mm has been shown to correlate with severe aortic regurgitation. This method was found useful even in eccentric jet.[24-26] Some investigators[27] have used the cross-sectional area of the vena contracta to evaluate aortic regurgitation severity. The approach sounds promising and 3D echo may help to further tune this approach.[24]

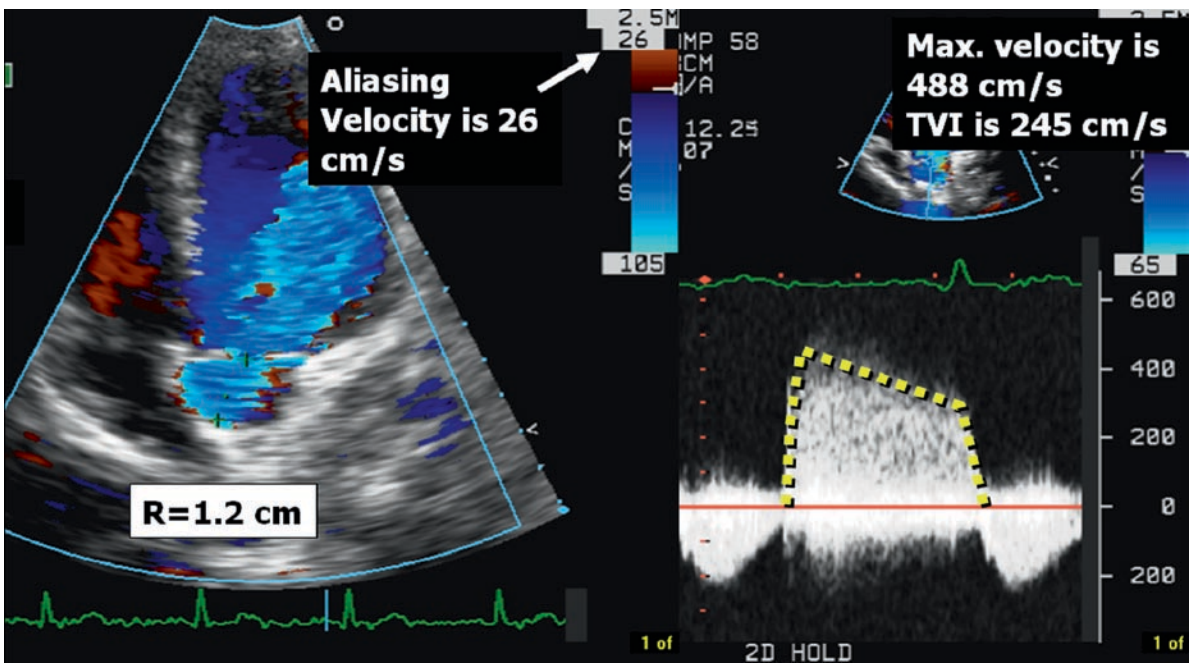

Fig. 3.14 This figure shows the PISA method for calculation of the ERO in case of aortic regurgitation. The PISA is obtained from the apical long-axis or 5-chamber view. The baseline is shifted upward toward the regurgitant jet flow (*arrow*). Then the PISA diameter is measured from the surface of the hemisphere to the narrowest area on color Doppler (1.2 cm). The CW Doppler is utilized to measure the aortic regurgitation TVI and peak velocity. The effective regurgitant orifice (ERO) and the regurgitant volume (RV) are calculated as follows: ERO = $6.28r^2$ $V_{\text{aliasing}}/V_{\text{max}}$ AR = $6.28 \times 1.2^2 \times 24\text{-}488 = 0.5\text{cm}^2$ and RV = TVI × ERO = 245 × 0.5 = 118 cc

There are several Doppler methods to evaluate aortic regurgitation severity, most of which are less accurate and should not be used alone to guide clinical decisions.

Regurgitant Jet size – Similar to most of the valvular lesions, color-flow Doppler is the initial screening method for the aortic regurgitation. With the advent of color Doppler many investigators had attempted to use the regurgitant jet size to quantify aortic regurgitation severity. However, this method has suffered several limitations.[28,29] The jet is frequently eccentric and appears much smaller even in the presence of significant aortic regurgitation, and its spread may be affected by the shape of the ventricular septum. Thus the size of the jet is only used as a screening tool after which other quantitative methods are used.

Jet Height to LVOT Height Ratio – This method depends on using the color Doppler in parasternal long-axis view to record the jet height at the valve orifice and compare it to the LVOT height (Fig. 3.15). This is related to the regurgitant orifice. The higher the ratio, the more severe is the aortic regurgitation. This method also has limitations. Eccentric jet may be difficult to assess. The shape of the regurgitant orifice affects the height of the jet on color Doppler images. Due to 2-Dimensional nature of the color-flow Doppler alignment on 2-Dimentional echo, they may not be perfectly aligned as they may not be in the same plane.[30]

Pressure half-time (PHT) – Aortic regurgitation jet PHT is measured using continuous-wave Doppler spectral display from apical long-axis view. It represents how quickly the aortoventricular pressure gradient equalizes during diastole (Fig. 3.16).[31] The larger the regurgitant orifice, the more quickly the pressure equalizes and the velocity falls. A group of investigators has demonstrated that this sign is useful to judge about severe aortic regurgitation. The PHT of less than 200 ms has been used to indicate severe aortic regurgitation.[32] However, it is important to keep in mind that numerous other factors can impact this, such as systemic vascular resistance and ventricular compliance.[33]

Aortic Diastolic Flow reversal – One of the earliest Doppler techniques to study aortic regurgitation was to examine retrograde diastolic flow reversal in the ascending and descending aorta or arch. Different numbers had been proposed to the measurement of the flow reversal TVI trying to assess severity. In general, flow reversal throughout the entire diastole is consistent with significant aortic regurgitation.[34]

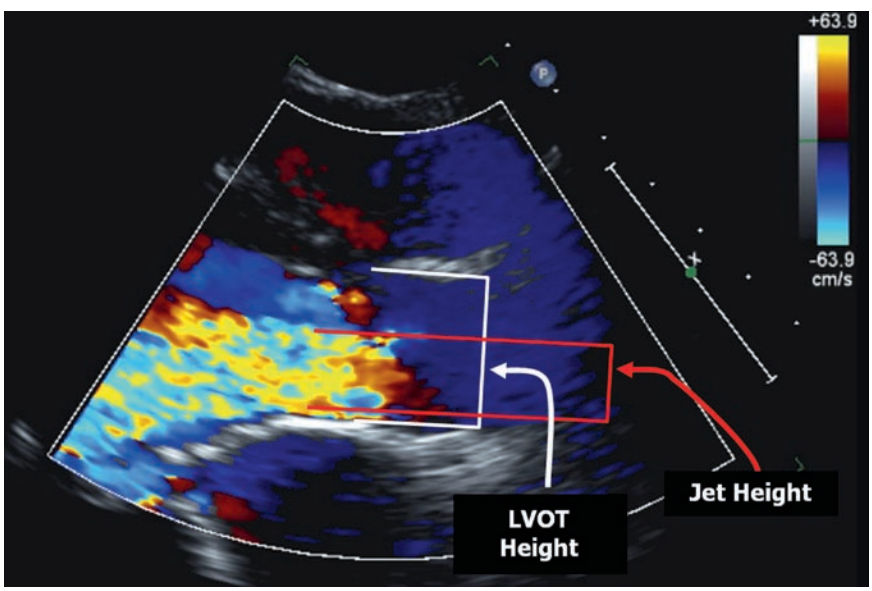

Fig. 3.15 Transthoracic echocardiogram at long-axis view demonstrates color Doppler method of the ratio of jet height to LVOT height to assess the severity of aortic regurgitation

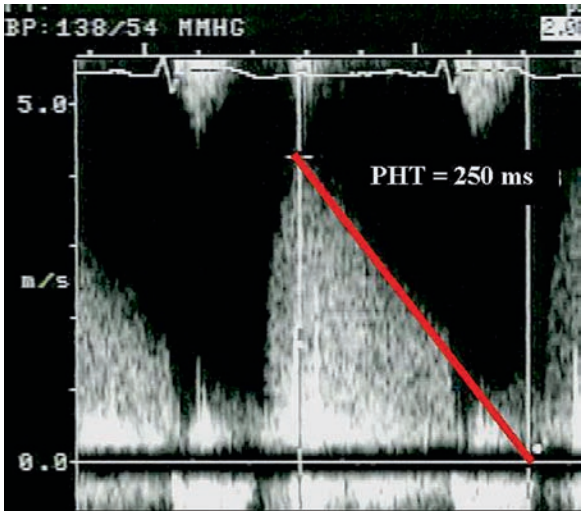

Fig. 3.16 CW spectral Doppler of the aortic regurgitation showing the slope of pressure gradient decays. The pressure-half time is then calculated to assess the severity of aortic regurgitation

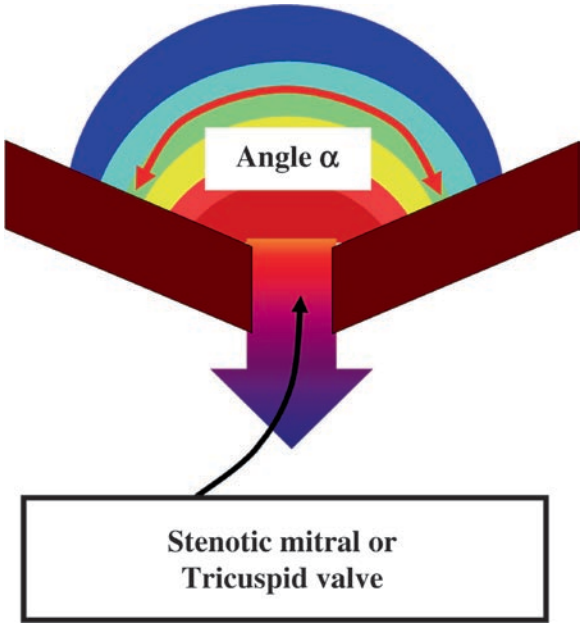

Fig. 3.17 This figure shows the PISA at the mitral or tricuspid valves in case of mitral or tricuspid stenosis. Occasionally, the valve leaflets form an angle while opening during diastole (not flat surface). This angle (α) is less than 180 and needs correction factor (α/180) when using the PISA to calculate stenotic lesion. This makes the method less perfect than for the regurgitant lesions

Mitral Stenosis

The PISA method can also be used to estimate mitral stenosis (MS).[35,36] Because of the stenotic mitral valve, blood flow accelerates at the left atrial side and converges forming nice PISA (Fig. 3.17). With the appropriate setting (moving the Nyquist limit baseline upward the same direction of flow while interrogating the mitral valve from apical views), PISA can be optimized. The flow rate at the PISA surface is equal to the flow rate at the mitral valve orifice. The mitral valve maximum velocity is obtained by continuous Doppler through mitral valve at early diastole. Then the stenotic area (MVA) can be calculated as follows:

$$\text{MVA} = 6.28r^2\ V_{\text{aliasing}}\text{regurgitant maximum velocity}$$

The truly hemispheric shells occurs if surface of the valve is flat with the leaflets apposed at 180°. This PISA method in case of mitral stenosis is not perfect because mitral valve at maximum opening is not flat (less than 180°) (Fig. 3.17). So the angle (alpha = α) has to be corrected for, by dividing this angle by 180°. The estimation of the angle is crude approach and a significant source of error.[35–37] MVA then calculated as:

$$\text{MVA} = 6.28r^2\ (V_{\text{aliasing}}\text{regurgitant maximum velocity})(\alpha/180)$$

The advantage of this approach is that it is not affected by coexisting mitral or aortic regurgitation.[38]

The tricuspid stenosis is not common. The severity can be quantitatively estimated in an identical way as the mitral stensos. Utilizing PISA, the flow at the PISA surface is equal to the flow rate at the tricuspid valve orifice (TVA). Because of complex valve geometry similar to the mitral stenosis, the angle needs to be corrected for (α/180).

$$\text{TVA} = 6.28r^2\ V_{\text{aliasing}}\text{regurgitant maximum velocity} \times (\alpha/180)$$

Again this approach is not perfect and less commonly used than other methods such as mean gradient and pressure half-time.

References

1. Callahan MJ, et al. Validation of instantaneous pressure gradients measured by continuous-wave Doppler in experimentally induced aortic stenosis. *Am J Cardiol*. 1985;56(15):989–993.

2. Currie PJ, et al. Continuous wave Doppler determination of right ventricular pressure: a simultaneous Doppler-catheterization study in 127 patients. *J Am Coll Cardiol.* 1985;6(4):750–756.
3. Burstow DJ, et al. Continuous wave Doppler echocardiographic measurement of prosthetic valve gradients. A simultaneous Doppler-catheter correlative study. *Circulation.* 1989;80(3):504–514.
4. Lewis JF, et al. Pulsed Doppler echocardiographic determination of stroke volume and cardiac output: clinical validation of two new methods using the apical window. *Circulation*. 1984;70(3):425–431.
5. Stewart WJ, et al. Variable effects of changes in flow rate through the aortic, pulmonary and mitral valves on valve area and flow velocity: impact on quantitative Doppler flow calculations. *J Am Coll Cardiol*. 1985;6(3):653–662.
6. Zoghbi WA, Quinones MA. Determination of cardiac output by Doppler echocardiography: a critical appraisal. *Herz*. 1986;11(5):258–68.
7. Maslow A, et al. Pulsed wave Doppler measurement of cardiac output from the right ventricular outflow tract. *Anesth Analg*. 1996;83(3):466–471.
8. Karp K, Teien D, Eriksson P. Doppler echocardiographic assessment of the valve area in patients with atrioventricular valve stenosis by application of the continuity equation. *J Intern Med*. 1989;225(4):261–266.
9. Nakatani S, et al. Value and limitations of Doppler echocardiography in the quantification of stenotic mitral valve area: comparison of the pressure half-time and the continuity equation methods. *Circulation*. 1988;77(1):78–85.
10. Otto CM, et al. Experimental validation of Doppler echocardiographic measurement of volume flow through the stenotic aortic valve. *Circulation*. 1988;78(2):435–441.
11. Skjaerpe T, Hegrenaes L, Hatle L. Noninvasive estimation of valve area in patients with aortic stenosis by Doppler ultrasound and two-dimensional echocardiography. *Circulation*. 1985;72(4):810–818.
12. Miyatake K, et al. Evaluation of tricuspid regurgitation by pulsed Doppler and two-dimensional echocardiography. *Circulation*. 1982;66(4):777–784.
13. Thomas L, et al. Prospective validation of an echocardiographic index for determining the severity of chronic mitral regurgitation. *Am J Cardiol*. 2002;90(6):607–612.
14. Enriquez-Sarano M, et al. Effective mitral regurgitant orifice area: clinical use and pitfalls of the proximal isovelocity surface area method. *J Am Coll Cardiol*. 1995;25(3):703–709.
15. Fehske W, et al. Color-coded Doppler imaging of the vena contracta as a basis for quantification of pure mitral regurgitation. *Am J Cardiol*. 1994;73(4):268–74.
16. Hall SA, et al. Assessment of mitral regurgitation severity by Doppler color flow mapping of the vena contracta [see comment]. *Circulation*. 1997;95(3):636–642.
17. Helmcke F, et al. Color Doppler assessment of mitral regurgitation with orthogonal planes. *Circulation*. 1987;75(1):175–183.
18. Utsunomiya T, et al. Regurgitant volume estimation in patients with mitral regurgitation: initial studies using color Doppler 'proximal isovelocity surface area' method. *Echocardiography*. 1992;9(1):63–70.
19. Stevenson, JG. Two-dimensional color Doppler estimation of the severity of atrioventricular valve regurgitation: important effects of instrument gain setting, pulse repetition frequency, and carrier frequency. *J Am Soc Echocardiogr.* 1989;2(1):1–10.
20. Cape, EG. et al. Adjacent solid boundaries alter the size of regurgitant jets on Doppler color flow maps. *J Am Coll Cardiol.* 1991;17(5):1094–1102.
21. Skjaerpe T, Hatle L. Diagnosis of tricuspid regurgitation. Sensitivity of Doppler ultrasound compared with contrast echocardiography. *Eur Heart J.* 1985;6(5):429–436.
22. Tribouilloy CM, et al. Application of the proximal flow convergence method to calculate the effective regurgitant orifice area in aortic regurgitation. *J Am Coll of Cardiol*. 1998;32(4):1032–1039.
23. Shiota T, et al. Evaluation of aortic regurgitation with digitally determined color Doppler-imaged flow convergence acceleration: a quantitative study in sheep. *J Am Coll of Cardiol*. 1996;27(1):203–210.
24. Quere JP, Tribouilloy C, Enriquez-Sarano M, Vena contracta width measurement: theoretic basis and usefulness in the assessment of valvular regurgitation severity. *Curr Cardiol Rep.* 2003;5(2):110–115.
25. Tribouilloy CM, et al. Assessment of severity of aortic regurgitation using the width of the vena contracta: A clinical color Doppler imaging study. *Circulation*. 2000;102(5):558–564.
26. Willett DL, et al. Assessment of aortic regurgitation by transesophageal color Doppler imaging of the vena contracta: validation against an intraoperative aortic flow probe. *J Am Coll of Cardiol*. 2001;37(5):1450–1455.
27. Nozaki S, et al. New index for grading the severity of aortic regurgitation based on the cross-sectional area of vena contracta measured by color Doppler flow mapping. *Circ J*. 2003;67(3):243–247.
28. Smith MD, et al. Observer variability in the quantitation of Doppler color flow jet areas for mitral and aortic regurgitation. *J Am Coll Cardiol*. 1988;11(3):579–584.
29. Reimold SC, Thomas JD, Lee RT. Relation between Doppler color flow variables and invasively determined jet variables in patients with aortic regurgitation. *J Am Coll Cardiol*. 1992;20(5):1143–1148.
30. Taylor AL, et al. Aortic valve morphology: an important in vitro determinant of proximal regurgitant jet width by Doppler color flow mapping. *J Am Coll Cardiol*. 1990;16(2):405–412.
31. Grayburn PA, et al. Quantitative assessment of the hemodynamic consequences of aortic regurgitation by means of continuous wave Doppler recordings. *J Am Coll Cardiol*. 1987;10(1):135–141.
32. Labovitz AJ, et al. Quantitative evaluation of aortic insufficiency by continuous wave Doppler echocardiography. *J Am Coll Cardiol*. 1986;8(6):1341–1347.
33. Griffin BP, et al. The effects of regurgitant orifice size, chamber compliance, and systemic vascular resistance on aortic regurgitant velocity slope and pressure half-time. *Am Heart J*. 1991;122(4 Pt 1):1049–56.
34. Quinones MA, et al. Assessment of pulsed Doppler echocardiography in detection and quantification of aortic and mitral regurgitation. *Br Heart J*. 1980;44(6):612–620.

35. Rodriguez L, et al. Validation of the proximal flow convergence method. Calculation of orifice area in patients with mitral stenosis [see comment]. *Circulation.* 1993;88(3): 1157–1165.
36. Deng YB, et al. Estimation of mitral valve area in patients with mitral stenosis by the flow convergence region method: selection of aliasing velocity. *J Am Coll Cardiol*. 1994;24(3): 683–689.
37. Rifkin RD, Harper K, Tighe D, Comparison of proximal isovelocity surface area method with pressure half-time and planimetry in evaluation of mitral stenosis. *J Am Coll Cardiol*. 1995;26(2):458–465.
38. Degertekin M, et al. Validation of flow convergence region method in assessing mitral valve area in the course of transthoracic and transesophageal echocardiographic studies. *Am Heart J*. 1998;135(2 Pt 1):207–214.

Chapter 4
Principles of Hemodynamic Assessment

Ahmed A. Alsaileek and A. Jamil Tajik

Doppler echocardiography has become the most practical method for flow and hemodynamic assessment. Flow assessment is discussed earlier in the previous chapter. Both methods are inter-related and Doppler plays a major role in flow and hemodynamic evaluation. In this chapter we will discuss the principles and clinical applications of hemodynamic assessment.

Transvalvular Pressure Gradient

One of the most fundamental applications of Doppler echocardiography is the determination of transvalvular pressure gradient using Bernoulli equation (Fig. 4.1). This theorem states that the pressure drop across a discrete stenosis in the heart or vasculature occurs because of energy loss due to three processes (1) acceleration of blood through the orifice (*convective acceleration*), (2) inertial forces (*flow acceleration*), and (3) resistance to flow at the interfaces between blood and the orifice (*viscous friction*).[1] Therefore, the pressure drop across any orifice can be calculated as the sum of these three variables. As one can realize, the original Bernoulli equation is complex; however, most of its components (flow acceleration and viscous friction) are clinically insignificant and can be ignored. Furthermore, the flow velocity proximal to a fixed orifice (V_1) is usually much lower than the peak velocity through the orifice (V_2) and can also be ignored (Fig. 4.2). Therefore, the simplified form of Bernoulli Equation is commonly used in most clinical situations.

$$P_1 - P_2 \text{ (Pressure reduced} = \Delta P) = 4V^2$$

where V is the maximum instantaneous velocity and 4 is equal to one-half of the blood density.

As seen from the equation, the maximum instantaneous velocity of blood is directly proportional to the peak gradient between the flow proximal and the flow distal to the orifice. The mean gradient can also be estimated as it will be discussed later.

Aortic Stenosis

In addition to continuity equation method to assess aortic stenosis (see previous chapter), the concept of Bernoulli equation is applied to Doppler echocardiography to assess the severity of aortic stenosis. The continuous-wave Doppler provides the peak jet velocity from which the peak and mean gradients are derived. The apical view is the most commonly utilized position to interrogate the aortic valve and to get the ultrasound beam aligned parallel to aortic jet. Occasionally a higher aortic velocity can be obtained from the alternative transducer positions such as right parasternal and suprasternal views (Fig. 4.3). In addition, the use of small footprint nonimaging transducer usually provides a better means of manipulation between ribs and a more parallel position of the ultrasound beam to stenotic jet. This underscores the need for a systematic and meticulous approach for assessment of the severity of aortic stenosis, as the underestimation of the severity is common due to angle-dependent flow

A.A. Alsaileek (✉)
Department of Cardiac Science,
King Abdulaziz Medical City, Riyadh,
Kingdom of Saudi Arabia
e-mail: saileeka@ngha.med.sa

A.J. Tajik
Mayo Clinic, Scottsdale, AZ, United States

P. Nihoyannopoulos and J. Kisslo (eds.), *Echocardiography*,
DOI: 10.1007/978-1-84882-293-1_4,

$$P1 - P2 = \underbrace{\tfrac{1}{2}\rho (V_2^2 - V_1^2)}_{\text{Convective Acceleration}} + \underbrace{\rho \int_1^2 dv/dt \; ds}_{\text{Flow acceleration}} + \underbrace{R(V)}_{\text{Viscous friction}}$$

V1 = velocity of the proximal location.
V2 = velocity of the distal location.
ρ = Mass density of the blood
dt = change in velocity over time period (dt)
ds = the distance over which the pressure decrease
R = viscous resistance in the vessel
V = velocity of the blood flow.

Fig. 4.1 Bernoulli equation. The complete form states that the pressure drop across a discrete stenosis in the heart or vasculature occurs because of energy loss due to three processes (1) acceleration of blood through the orifice (*convective acceleration*), (2) inertial forces (*flow acceleration*), and (3) resistance to flow at the interfaces between blood and the orifice (*viscous friction)*

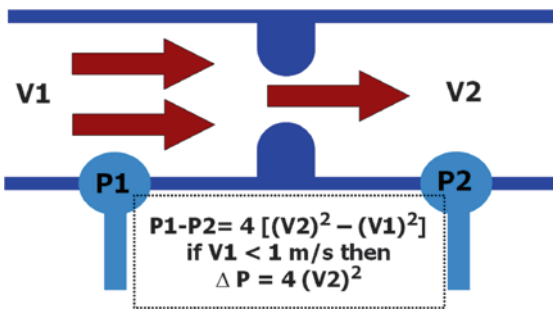

Fig. 4.2 This figure illustrates the simplified Bernoulli equation. Pressure drop across a small orifice can be estimated as four times the square of the peak velocity (if the proximal velocity is less than 1 m/s). V_1 and P_1 = proximal velocity and pressure; V_2 and P_2 = distal velocity and pressure

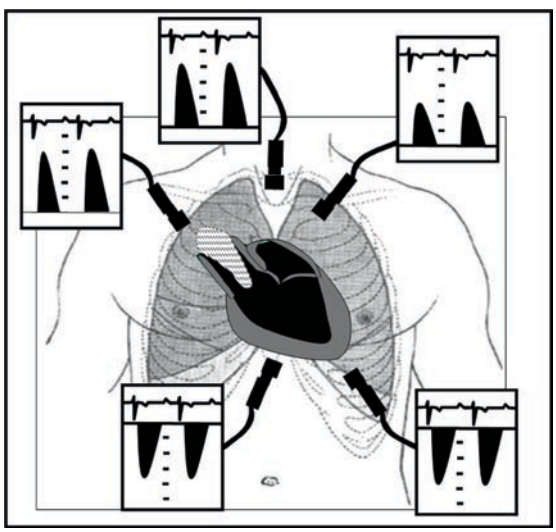

Fig. 4.3 Alternative approaches to assess the blood flow velocity through aortic valve. The maximum velocity should be obtained and recorded

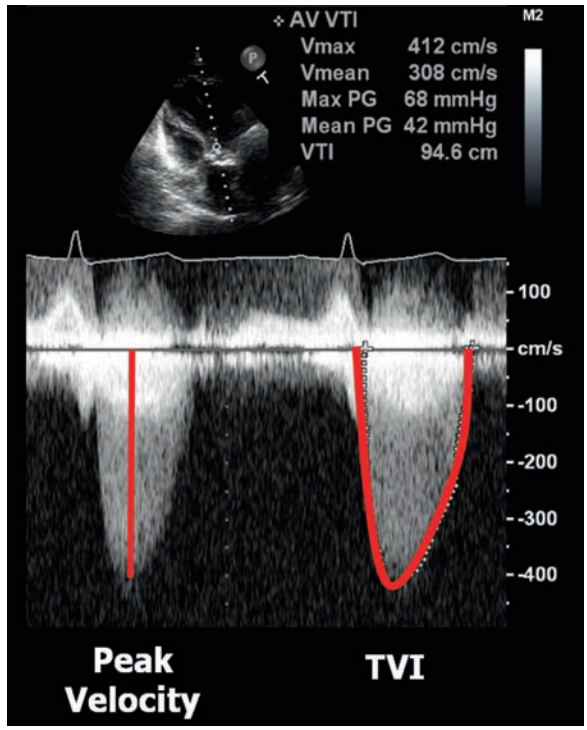

Fig. 4.4 The flow through aortic valve obtained with CW Doppler in the apical 5-chamber or long-axis views. The maximum velocity and the TVI are shown. From TVI the mean gradient can be measured

assessment. The peak instantaneous pressure gradient across aortic valve is obtained utilizing continuous-wave Doppler where the maximum peak velocity is recorded. Then simplified Bernoulli equation is applied to convert the velocity into gradients.

$$\text{Pressure gradient } (\Delta P) = 4V^2$$

where V is the maximum instantaneous velocity across aortic valve.

The maximum instantaneous pressure gradient obtained by Doppler is different from peak-to-peak pressure gradient frequently measured in the catheterization laboratory. The latter is nonphysiologic parameter since the peak left ventricular pressure and peak aortic pressures do not occur simultaneously. The transvalvular mean gradient can also be measured by averaging all the individual velocities (time velocity integral, TVI) over the entire flow period (Fig. 4.4). This can be achieved by tracing the outer border of spectral Doppler envelope from the continuous-wave Doppler interrogation of flow through the aortic valve.[2-4] In patients with normal left ventricular systolic function the mean gradient correlates well with the severity

Table 4.1 Grading aortic stenosis severity in normal cardiac output state

	Mean gradient (mmHg)	Aortic valve area (cm^2)
Mild	<30	>1.5
Moderate	30–40	1.0–1.5
Severe	>40	<1.0

of aortic stenosis and aortic valve area[5] (Table 4.1). However, in patients with impaired left ventricular systolic function there is often a discrepancy between the pressure gradient across the valve and the stenosis severity as defined by valve area. It has long been recognized that an increased transaortic flow rate results in an increased gradient, whereas a decrease in flow rate results in a decreased gradient across the stenotic valve. In this situation, a low transaortic pressure gradient may be caused by mild-to-moderate valve stenosis with a concurrent decline in ventricular contractility. Conversely, a low transaortic pressure gradient may be due to severe aortic stenosis with a low transaortic flow caused by impaired ejection performance. One approach to answer this question is the use of pharmacological agents such as intravenous dobutamine to augment cardiac output. It is the most commonly used approach in clinical settings. It indicates that if valve area increases with an increase in transaortic stroke volume (such as after intravenous dobutamine), the leaflets still are flexible enough to open more fully as more "force" is applied during ventricular ejection, implying only moderate valve stenosis. Conversely, a constant valve area despite an increase in flow (hence the gradient across aortic valve) suggests severe stenosis with stiff leaflets that cannot respond to the increased systolic ejection force.[6] The dobutamine stress hemodynamic data in the setting of low-gradient aortic stenosis have also been shown to have a prognostic value. Surgery seems beneficial for most of the patients with left ventricular contractile reserve. In contrast, the postoperative outcome of patients without reserve is compromised by a high operative mortality.[7,8]

In addition to Doppler findings, aortic stenosis is associated with 2D-echocardiographic features that should be looked for and correlated to hemodynamic data. Severe aortic stenosis, in adults, is often associated with extensive leaflets calcification, marked reduction in leaflet excursion, marked left ventricular hypertrophy, diastolic dysfunction, and even left ventricular systolic dysfunction if left untreated. The amount and severity of valvular calcification is a marker of severity and determinant of the outcome.[9]

Pulmonary Stenosis

The severity of the pulmonic stenosis is approached in the same manner as the aortic stenosis. The pulmonic maximum instantaneous velocity can be obtained from the parasternal short axis at the level of the aortic valve (Fig. 4.5).[10,11] Then the maximum instantaneous gradient is calculated using the simplified Bernoulli equation. The mean gradient can be obtained by tracing the outer border of continuous-wave Doppler spectral envelop. In clinical practice both the maximum gradient and the mean gradient are currently used for therapeutic decisions. Another related Doppler method is to measure the tricuspid regurgitation jet velocity. With increasing pulmonary stenosis severity the right ventricular systolic pressure increases. As discussed earlier tricuspid regurgitation jet velocity can be used to assess right ventricular systolic pressure. So the higher the tricuspid regurgitation velocity, the more severe the pulmonary stenosis. Although Doppler findings are the standard

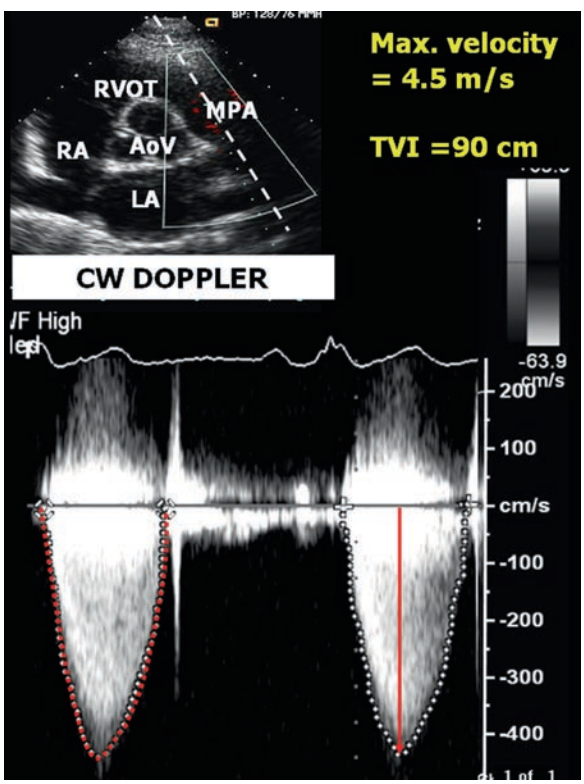

Fig. 4.5 This figure illustrates the Doppler method to assess the severity of pulmonic stenosis. The parasternal short axis at the level of aortic valve is utilized to interrogate the pulmonic valve. The maximum velocity is recorded using CW Doppler through the valve. Then the gradient is calculated by simplified Bernoulli equation

way to use, the 2D-echo features can also help to assess the severity of pulmonary stenosis. Leaflet thickening with restricted opening and right ventricular hypertrophy can often be seen in severe pulmonary stenosis.

Mitral Stenosis

Doppler echocardiography is the gold standard for the determination of the transmitral gradient in patients with native/prosthetic valve stenosis.[12] The mean gradient, rather than the peak, is commonly used to assess mitral stenosis. The apical views are used because the ultrasound beam is most parallel to the flow. Mitral stenosis jet is more complex than the aortic or pulmonic (Fig. 4.6). The direction of flow can be variable and color Doppler guided approach to align the cursor to be parallel to the flow can reduce error in measuring the transmitral gradient. The jet is biphasic with early flow immediately following mitral valve opening and late due to left atrial contraction. The late phase is lost in atrial fibrillation, which is a common association with mitral stenosis. On determining the mean gradient TVI of both early and late flows should be traced. With increasing severity of mitral stenosis or in atrial fibrillation, the gradient persists throughout diastole making it relatively easier to trace the continuous-wave Doppler envelope (Fig. 4.7). Pressure half-time is another concept derived from Bernoulli equation. Pressure half-time is defined, as the time required by the maximum atrioventricular pressure to drop to half of its initial value. With increasing mitral stenosis severity this time becomes progressively longer[13,14] (Fig. 4.8). The slope of the pressure decay is then determined, and the pressure half-time is automatically calculated by most of the currently available echo machines. Moreover the valve area can be estimated

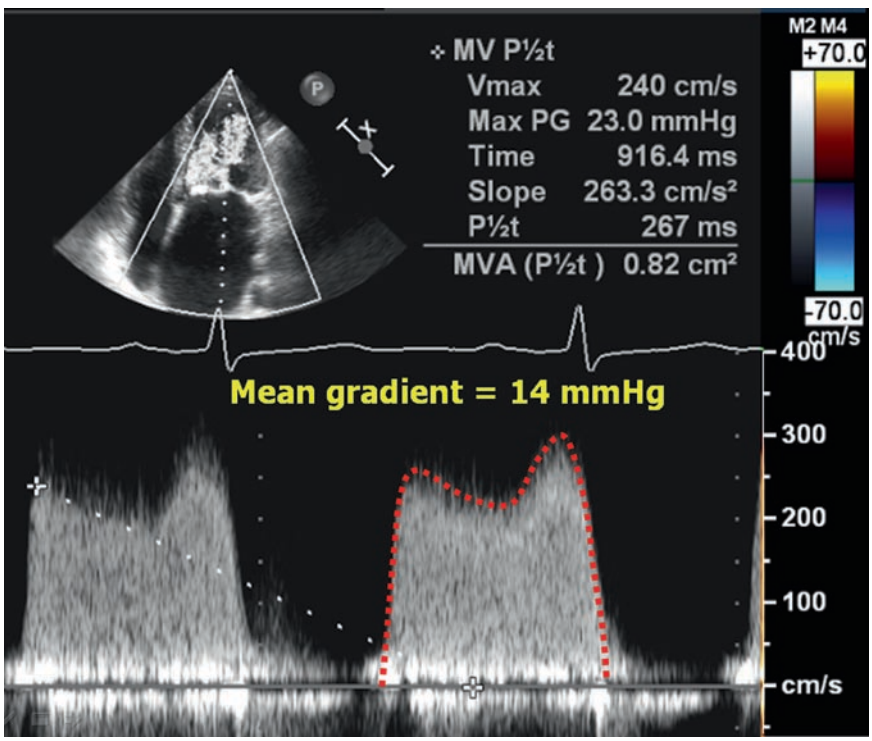

Fig 4.6 This figure illustrates the CW Doppler tracing through mitral valve in mitral stenosis. The flow through mitral valve is biphasic; one is early which is immediately after mitral valve opening and one is late and due to LA contraction. To determine the mean gradient both flows should be traced and recorded

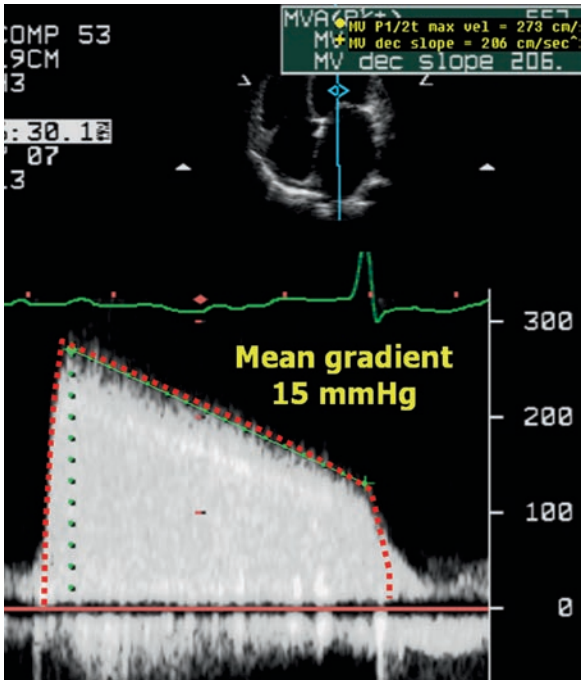

Fig. 4.7 This figure shows the CW Doppler through stenotic mitral valve. The flow is continuous in case of atrial fibrillation due to loss of late flow of atrial contraction. This can also be seen in severe mitral Stenosis

from pressure half-time using Hatle equation [Hatle L. Philadelphia: Lee & Febiger 1982]:

$$\text{MVA (cm}^2\text{)} = 220/\text{PHT}$$

where MVA is mitral valve area and PHT is pressure half-time

Pressure half-time is influenced by other hemodynamic parameters independent of mitral valve area. Hence it is not reliable measure of mitral valve area. In this regard, mitral valve area should routinely be measured utilizing the continuity equation (refer to Chap. 3). Table 4.2 summarizes Echo/Doppler criteria used to grade mitral stenosis severity. Other features of mitral stenosis on the two-dimensional echocardiogram are characteristic since mitral stenosis is almost always caused by rheumatic heart disease; however, none has been shown to be directly related to stenosis severity. One exception is valve area obtained by planimetry from 2D-echo short-axis view at the tip of the mitral valve leaflets. Other 2D-echo features include restricted posterior leaflet, doming anterior leaflet with hockey stick appearance on mitral valve opening, fusion of the commissures, and chordal thickening and foreshortening.

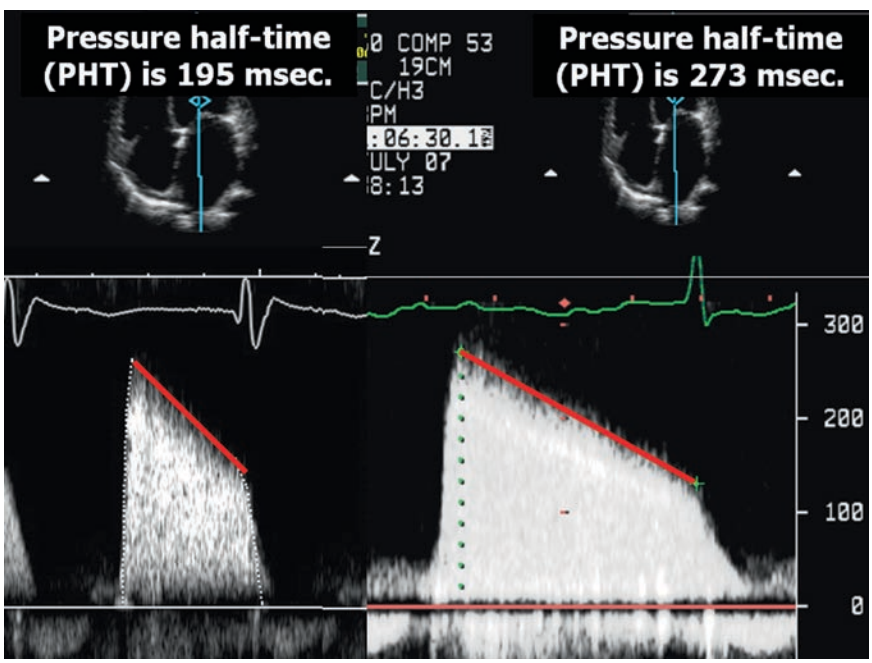

Fig. 4.8 This figure shows the CW Doppler through stenotic mitral valve. The slope of pressure gradient decay is determined. Then the pressure half-time (PHT) can be calculated. With more severe mitral stenosis, the PHT becomes longer

Table 4.2 Grading mitral stenosis severity

	Mean gradient (mmHg)	Mitral valve area (cm^2)
Mild	<6	>1.5
Moderate	6–10	1.1–1.5
Severe	>10	≤1.0

Tricuspid Stenosis

In tricuspid valve stenosis, the same approach as mitral stenosis can be used keeping in mind that the hemodynamic assessment of the tricuspid valve varies with respiration. The mean gradient is the clinically used index to assess tricuspid stenosis severity. The flow through tricuspid valve can be interrogated from different views such as parasternal short axis at the level of aortic valve, right ventricular inflow view, and apical 4-chamber view. The apical view is the most commonly used with the continuous-wave Doppler to obtain the diastolic flow, which is similar to the mitral flow. The mean gradient is obtained by tracing the outer edge of both the early and late flow.

In addition to valvular lesions, the concept of maximum velocity and gradient is widely used for any suspected stenosis such as coarctation of aorta or in the presence of shunt such as ventricular septal defect and patent ductus arteriosus.

Special Considerations with the Use of Simplified Bernoulli Equation

In certain situations, simplified Bernoulli equation may overestimate or underestimate the flow velocity; hence, the other components of the full Bernoulli equation must be taken into consideration.

Increased Flow Acceleration

Greater increase in momentum flow may be required to open the valve as with prosthetic valve. Therefore, flow acceleration may significantly contribute to the derived pressure gradient and may underestimate the pressure gradient.

Increased Viscous Friction

In long tubular obstructions like tunnel subaortic stenosis, diffuse supravalvular aortic stenosis, and diffusely narrowed segment of aortic coarctation, the viscous friction is significantly increased. By ignoring this, simplified Bernoulli equation will underestimate the pressure gradient. One clue in such a situation is that the flow will be continuous during both systole and diastole due to persistent gradient between proximal and distal to the stenosis.

Effect of the Angle

As discussed earlier, the principle of Doppler flow calculation is dependent on the incident angle of interrogation (θ). The maximum accuracy of the flow velocity estimation is obtained when the angle is zero (cosine θ = 1). Remember frequency shift is

$$V = \frac{f_D C}{2 f_T \cos\theta}$$

Angle of less than 20° (cosine 10 = 0.98, cosine 20 = 0.94, and cosine 30 = 0.86) is critical as the extent of error significantly increases beyond this angle (Fig. 4.9).

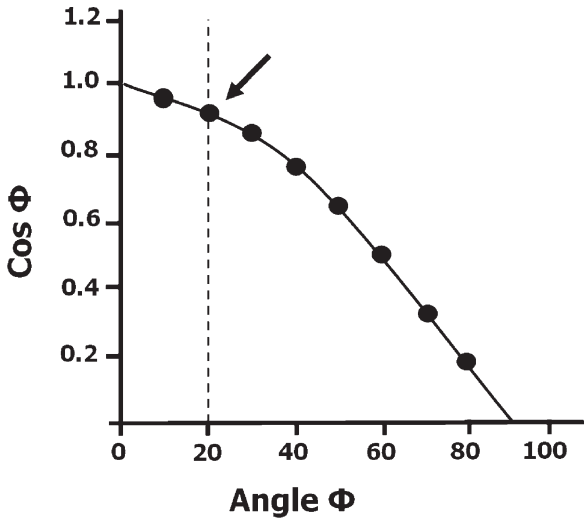

Fig. 4.9 This figure shows the relation between the angle θ and the cos θ. The cos θ quickly approaches zero as the angle exceeds 20° making significant error in Doppler estimation of flow velocity

Increased Proximal Velocity

Proximal velocity is the velocity (V_1) upstream to stenotic orifice. As the V_1 is small, it can be ignored in simplified version of Bernoulli equation. However, in certain situations V_1 can no longer be ignored such as in high cardiac output state (anemia, sepsis, or hyperthyroidism), significant aortic regurgitation and associated subvalvular stenosis.

Alteration of the Blood Viscosity

Anemia (low viscosity) and polycythemia (high viscosity) cause inaccuracy in estimating transvalvular pressure gradient. The normal half of blood viscosity is 4. If this is used in a patient with anemia, where his actual half of blood viscosity is equal to 2, the calculated pressure gradient will be double (overestimated) his actual pressure gradient. Unfortunately, no hemoglobin level can be used to try to correct for because it depends on the baseline hemoglobin level and the extent of cardiovascular compensation to the anemia.

Assessment of Intracardiac Pressures

Left Atrial Pressure

By using the simplified Bernoulli Equation the gradient between any two chambers can be determined. Mitral regurgitation peak velocity is converted to pressure gradient between left atrium and left ventricle (Peak Gradient = $4V^2$). Left atrial pressure then can be estimated[15,16] by the following equation:

$$\text{Transmitral regurgitation gradient} = \text{LV Systolic Pressure} - \text{LA Pressure}$$

In the absence of aortic stenosis (subvalvular, valvular, and supravalvular), left ventricular systolic pressure (LVSP) should be essentially the same as the cuff derived systolic blood pressure (SBP). With advancing age, the systolic blood pressure is augmented by 4–8% due to peripheral wave reflection. Keeping that in mind left atrial pressure (LAP) is determined as:

$$\text{Transmitral regurgitation gradient } [4(V_{MR})^2] = \text{SBP} - \text{LAP}$$

And therefore:

$$\text{LAP} = \text{SBP} - [4(V_{MR})^2]$$

This method provides an approximation of the true left atrial pressure.

Left Ventricular End-Diastolic Pressures

The left ventricular end-diastolic pressure (LVEDP) can be estimated in patients with aortic regurgitation. The aortic regurgitation velocity at the end-diastole (V_{AR-ED}) is converted to gradient using simplified Bernoulli equation: $[4(V_{AR-ED})^2]$. This pressure gradient represents the difference between aortic diastolic blood pressure and the left ventricular end-diastolic pressure. The aortic diastolic pressure should approximately be the same as the cuff-obtained diastolic blood pressure (DBP). Therefore, left ventricular end-diastolic pressure (LVEDP) can be estimated[17-20] as follows (Fig. 4.10):

$$\text{LVEDP} = \text{DBP} - 4(V_{AR-ED})^2$$

Alternatively and more accurately the left ventricular filling pressure (and thus LVEDP) is assessed using the mitral inflow patterns, pulmonary vein flow, and mitral annulus velocities. This has been used for the estimation of filling pressure with great success in the presence and absence of left ventricular systolic dysfunction.[21-23]

Normal transmitral flow is complex and consists of three distinct phases. Early (E-wave) flow which occurs immediately after mitral valve opening and continues till the left atrial to left ventricular pressures are almost equal, followed by a phase of no or minimal flow called diastasis which is then followed by late flow (A-wave) due to left atrial contraction (Fig. 4.11).

The pattern of flow through mitral valve reflects the pressure difference between left atrium and left ventricle. Transmitral flow has been recognized to reflect the atrioventricular interaction during left ventricular filling. With occurrence of diastolic dysfunction, spectrum of filling pressure changes with a predictable pattern of progression has been observed. Initially, left ventricular relaxation is impaired resulting in early flow to be reduced (decreased E-wave velocity) and takes longer time (prolonged E-wave deceleration time) which means less blood has moved from

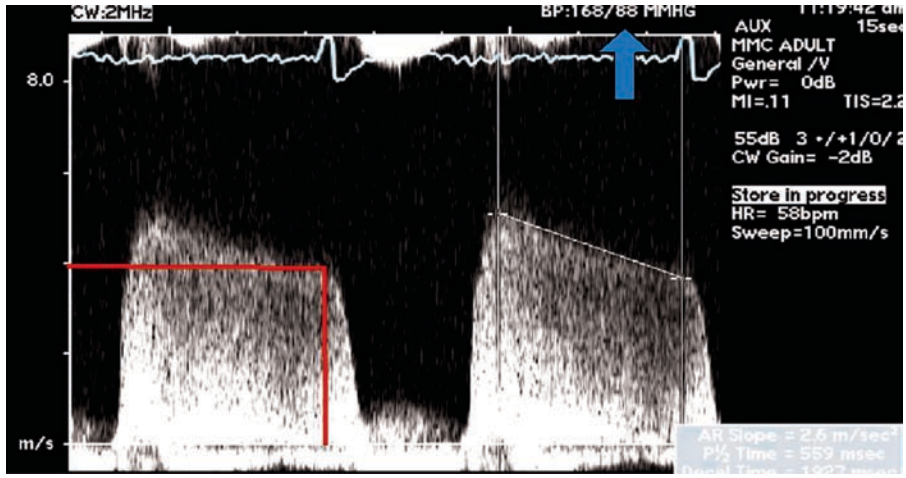

Fig. 4.10 CW Doppler of aortic regurgitation. The end-diastolic pressure gradient between aorta and LV can be measured using the Bernoulli equation. The end-diastolic velocity is 4.0 m/s. Therefore the pressure gradient is $4(V_{AR-ED})^2 = 4 \times (4)^2 = 64$ mmHg. If the diastolic pressure in the aorta is known (approximately the same as the diastolic blood pressure (DBP), left ventricular end-diastolic pressure (LVEDP) can be calculated as: LVEDP = DBP – 4 $(V_{AR-ED})^2$. In the figure (arrow) DBP is 88 mmHg, so the LVEDP is 88 – 64 = 24 mmHg

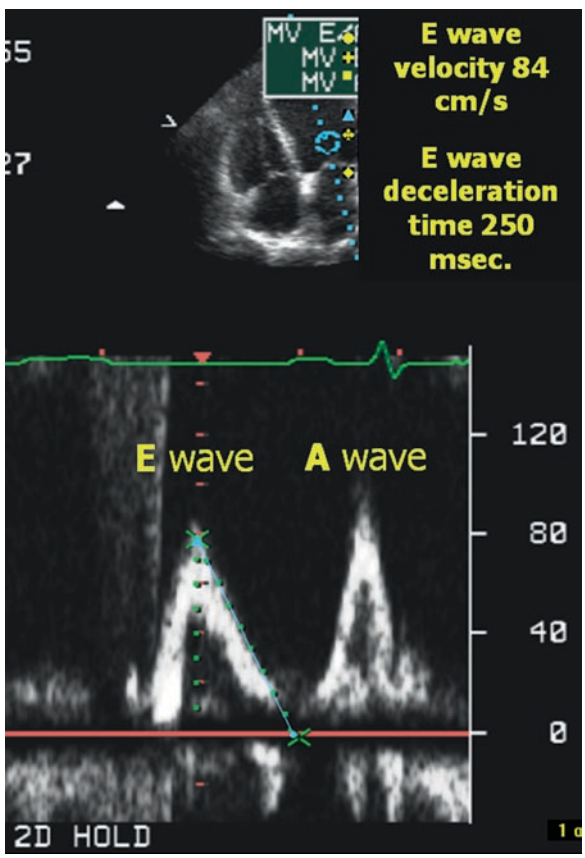

Fig. 4.11 This figure shows the normal flow through mitral valve. The pulsed-wave Doppler is position at the tip of mitral valve leaflets to record the flow from LA to LV. Two phases of flow are identified: early passive flow (E wave) and Late flow due to LA contraction (A wave)

left atrium to left ventricle. This makes more amount of blood available at late diastole, which causes left atrium to stretch. According to the Frank-Starling law, the increased left atrial stretch leads to increased contraction and therefore increased emptying in late diastole, resulting in a high A-wave velocity (Fig. 4.12). Other features, like prolonged isovolumic relaxation time (IVRT), occasionally accompany this abnormal flow pattern. Another transmitral flow pattern is called restrictive physiology pattern where E-wave velocity is high with short E-wave deceleration time and A-wave velocity is low. This is caused by elevated left ventricular filling pressure with greater left atrial to left ventricular pressure gradient early in diastole, which produces fast and short blood flow velocity into left ventricle. There will be a lower forward flow at atrial contraction because of markedly elevated left ventricular pressure (Fig. 4.13). This pattern of flow is associated with severe left ventricular diastolic dysfunction. This pattern can also be due to restrictive and constrictive left ventricular filling. This abnormal flow can be accompanied by short IVRT.

Pulmonary venous flow can also be analyzed to derive the left ventricular filling pressure and can be recorded transthoracically or transesophageally, with a higher feasibility from the transesophageal approach. Also, a higher success rate is encountered in the outpatient setting than in the intensive care unit.[24]

Forward flow into the left atrium from the pulmonary veins occurs in systole and diastole. After atrial contraction, retrograde flow (Ar) into the veins from the left atrium is observed (Fig. 4.14). As left atrial

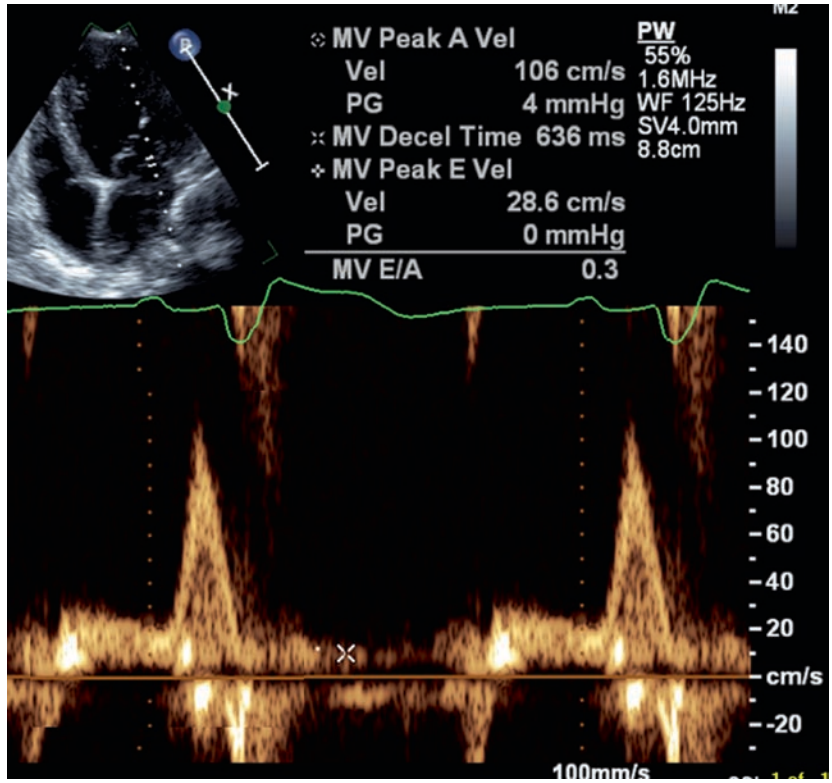

Fig. 4.12 This figure shows transmitral flow pattern in abnormal relaxation. It is characterized by small E wave and larger A wave velocities and long E wave deceleration time

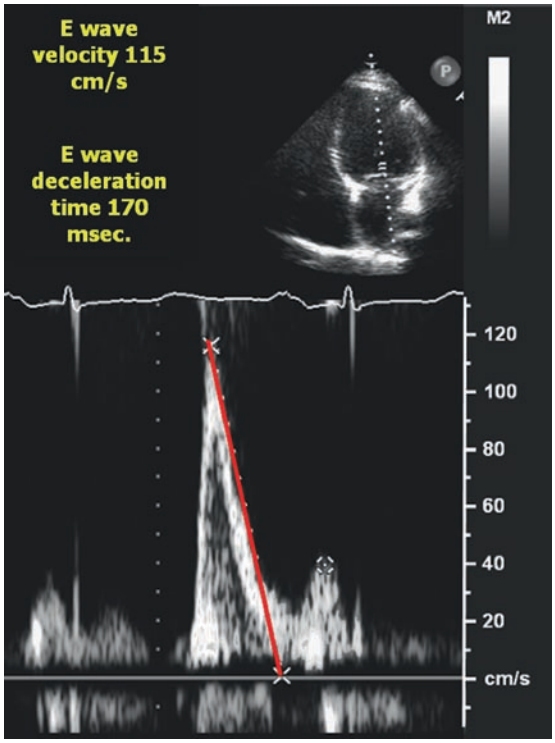

Fig. 4.13 This figure shows mitral flow pattern in restrictive physiology. It is characterized by high E wave velocity, small A wave velocity, and short E wave deceleration time

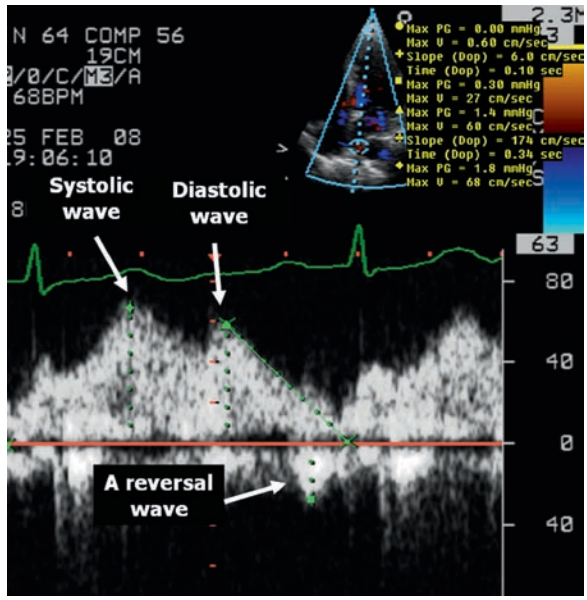

Fig. 4.14 This figure shows the normal flow of the pulmonary vein. The PW Doppler is used in apical 4-chamber view to record two forward waves systolic and diastolic and one backward wave due to atrial contraction

pressure increases, systolic velocity of the pulmonary venous flow (and time velocity integral) is reduced, with a predominance of diastolic flow.[19,25-27] This happens because the left atrium empties in diastole and therefore has a lower pressure in relation to the pulmonary veins at that time. Ar velocity and duration can also provide a reasonable assessment of filling pressures. As filling pressure increases, both the velocity and the duration of Ar increase.[28,29] With a stiff left ventricle, atrial contraction results in an antegrade flow across the mitral valve of short duration and an Ar of longer duration into the pulmonary veins, i.e., a positive Ar wave minus A-wave durations. This parameter was the best predictor (among all other mitral and pulmonary venous flow variables) of elevated left ventricular end-diastolic pressure in patients with normal left ventricular systolic function and in the presence of left ventricular systolic dysfunction.

As discussed earlier the changes in transmitral flow are predictable. With impaired left ventricular relaxation, the E-wave velocity is reduced until left atrial hypertension develops and the E-wave velocity starts to increase again. At one stage these changes are in between abnormal relaxation and restrictive patterns. The resulted flow pattern is exactly similar to normal pattern. This is called pseudonormal pattern but is associated with elevated left ventricular filling pressure. Several methods are used to differentiate this pattern from normal. The use of Valsalva maneuver to decrease the preload shifts the pseudonormal to abnormal relaxation pattern.[30]

Tissue Doppler imaging (TDI) can be combined with transmitral flow to assess left ventricular diastolic function (Fig. 4.15). TDI of the mitral annulus can show the early diastolic annular recoil velocity (E′ wave) and has been shown to be reduced in patients with diastolic dysfunction (Fig. 4.16). With advancing diastolic dysfunction, the E-wave velocity tends to go higher and E′-wave velocity goes lower. Therefore, with increasing filling pressure, E/E′ ratio tends to increase that represents increasing diastolic dysfunction severity. TDI is less flow dependent and can be

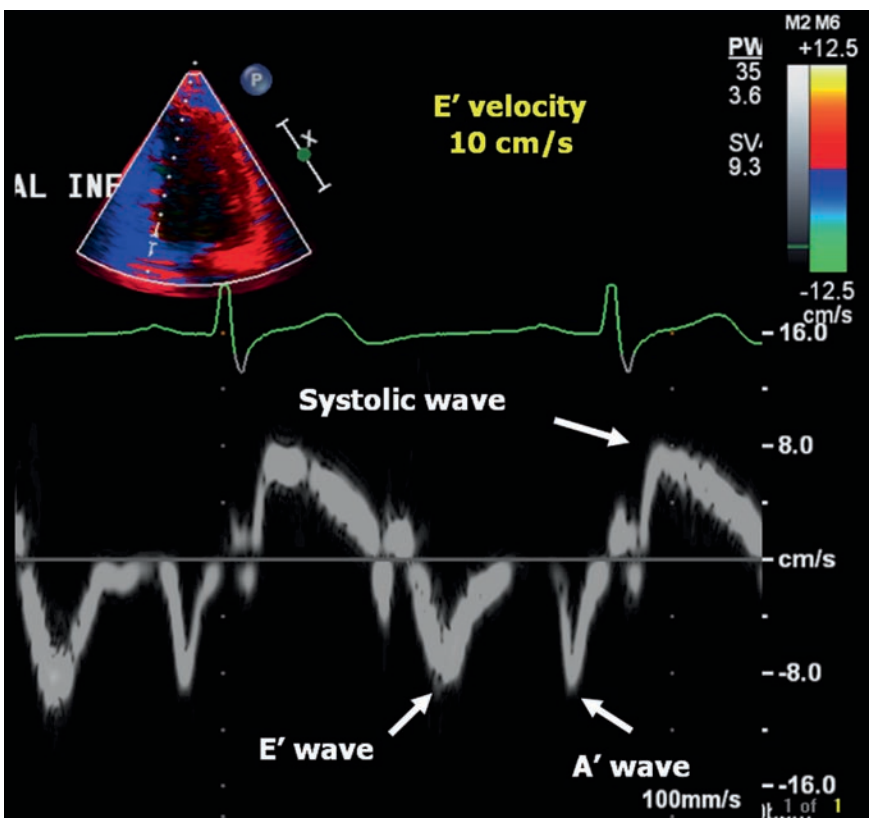

Fig. 4.15 This figure shows a normal Doppler tissue imaging (DTI) of the mitral annulus velocity. Systolic wave, E′ wave and A′ wave are identified

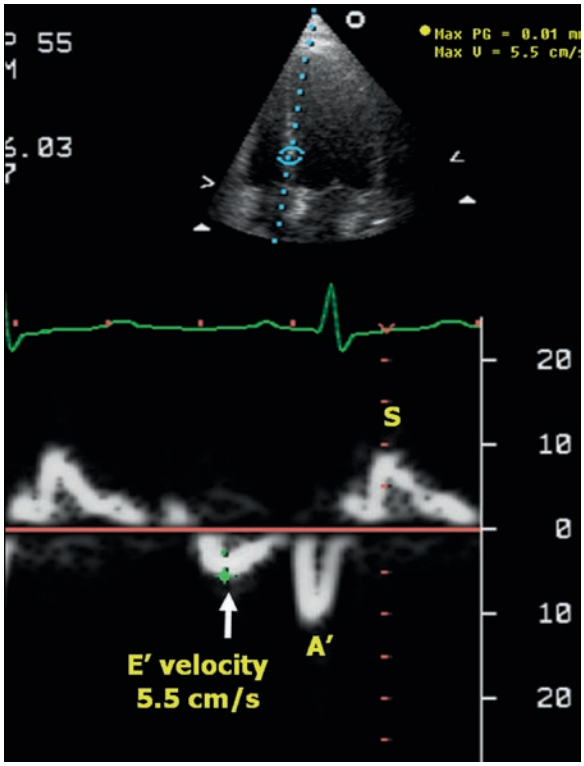

Fig. 4.16 The E′ wave velocity is progressively decreased with increasing diastolic dysfunction severity

applied in case of atrial fibrillation. The E/E′ ratio of more than or equal to 15 is associated with severely elevated left atrial pressure.[23,31] In most of the clinically oriented settings, a combination of transmitral flow pattern, TDI of mitral annulus and pulmonary flow to the left atrium is utilized to assess the left ventricular filing pressure demonstrating changes that correlate with the increasing severity of diastolic dysfunction (fig.4.17).

Several other investigators have used the early flow propagation velocity from left atrium into the left ventricle to determine left ventricular filling pressure (Fig. 4.18). Combined with the mitral flow pattern, it has been demonstrated to provide valuable information about left ventricular filling pressure.[22] With the color M-mode Doppler and the cursor line placed along the central portion of the mitral inflow blood, the first aliasing velocity is obtained and the slope of the first aliasing velocity is determined. Then the rate of flow propagation is determined. With more severe diastolic abnormalities, the flow propagation becomes higher. A flow propagation of more than 50 cm/s is associated with markedly elevated left atrial pressure.

Left atrial volumes can also be used to predict the filling pressure. Patients with elevated filling pressures

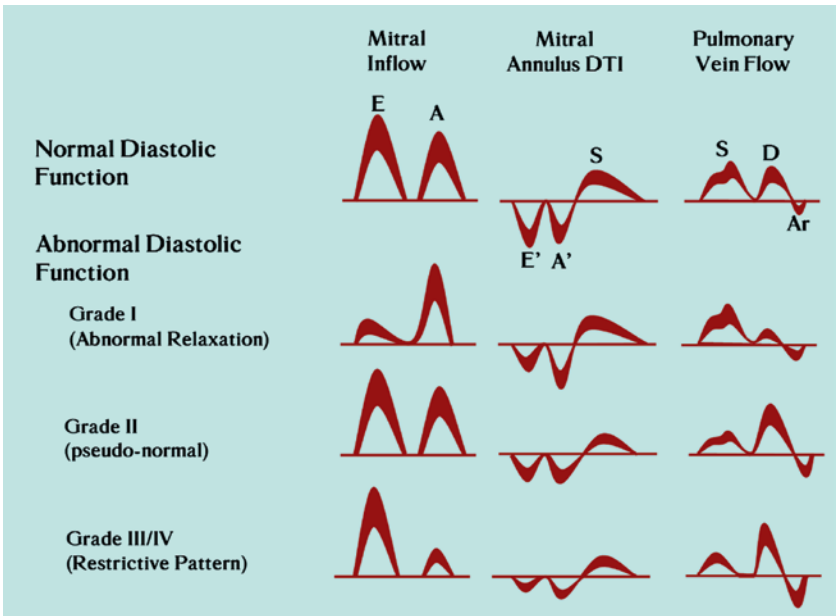

Fig. 4.17 It illustrates stages of diastolic dysfunction as assessed by combining all the information from transmitral flow pattern, TDI of the mitral annulus and pulmonary vein flow to the LA. Grade III can be further defined according to the changes of the mitral flow pattern with maneuver that decreases the preload such as Valsalva. If the flow pattern can be reversed from restrictive pattern to pseudonormal or abnormal relaxation pattern, it is said to be reversible restrictive physiology and termed grade III. If it is not reversible, it is considered grade IV

have larger left atrial volume. It has been shown that left atrial volume indexed to body surface area to be strongly associated with diastolic function grade, independent of left ventricular ejection fraction, age, gender, and cardiovascular risk score. In patients without a history of atrial arrhythmias or valvular heart disease, left atrial volume expressed the severity of diastolic dysfunction and provided an index of cardiovascular risk and disease burden.[32] Left atrial volume is less affected by acute hemodynamic changes and reflects the average effect of chronic or intermittent LV filling pressures elevation.

Right Ventricular Pressure

The tricuspid regurgitation jet velocity is the most commonly used method to assess the right ventricular pressure. Right ventricular systolic pressure is estimated from peak transtricuspid pressure gradient.[33,34] With the transducer at the apex or para-apical position, the continuous-wave Doppler (2D-guided or nonimaging) is used to obtain the peak transtricuspid velocity (Fig. 4.19). In case of weak signal saline contrast enhancement should be performed. Right ventricular systolic pressure (RVSP) is calculated as follows:

$$\text{Peak transtricuspid pressure gradient} = \text{RVSP} - \text{RAP}$$

$$\text{RVSP} = \text{peak transtricuspid pressure gradient} + \text{RAP} = 4(V_{TR})^2 + \text{RAP}.$$

Right atrial pressure (RAP) is estimated by examining the inferior vena cava (IVC) size (normal = 5 mmHg, dilated but compressible during inspiration = 10 mmHg and dilated and noncompressible ≥15 mmHg).[35] Some other investigators have utilized the IVC collapse during inspiration (Fig. 4.20) to estimate the right atrial pressure. If IVC is decreased by 50% or more, the right atrial pressure is less than 10 mmHg.[36]

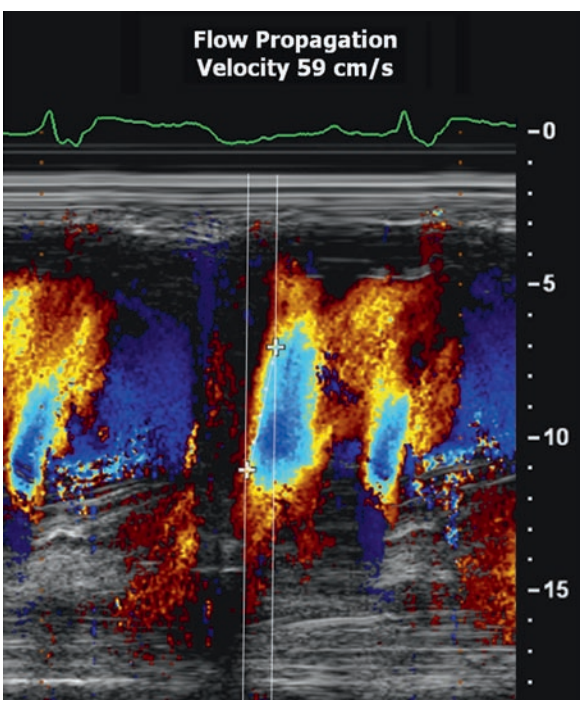

Fig. 4.18 This figure shows rate of the flow propagation utilizing color M-mode imaging. With the cursor line placed along the central portion of the mitral inflow blood, the first aliasing velocity is obtained. Then the slope of the first aliasing velocity is determined. With more severe diastolic abnormalities, the rate of the flow propagation velocity is higher. A velocity of more than 50 cm/s is associated with markedly elevated LA pressure

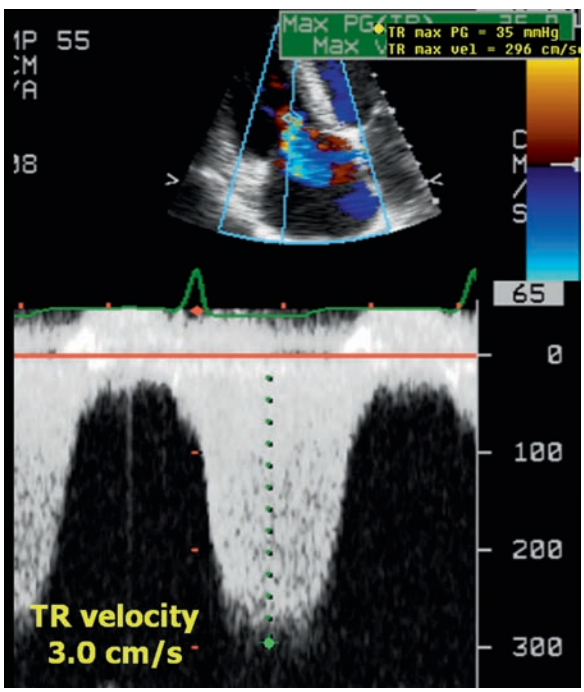

Fig. 4.19 This figure illustrates the CW Doppler interrogation of the tricuspid regurgitation velocity to assess right ventricular systolic pressure (RVSP). With the transducer at the apex, the CW Doppler (2D-guided or nonimaging) is used to obtain the peak tricuspid regurgitation velocity. Using the simplified Bernoulli equation, the velocity is converted to pressure gradient. In this case the transtricuspid gradient is $4 \times (3.0)^2 = 36$ mmHg

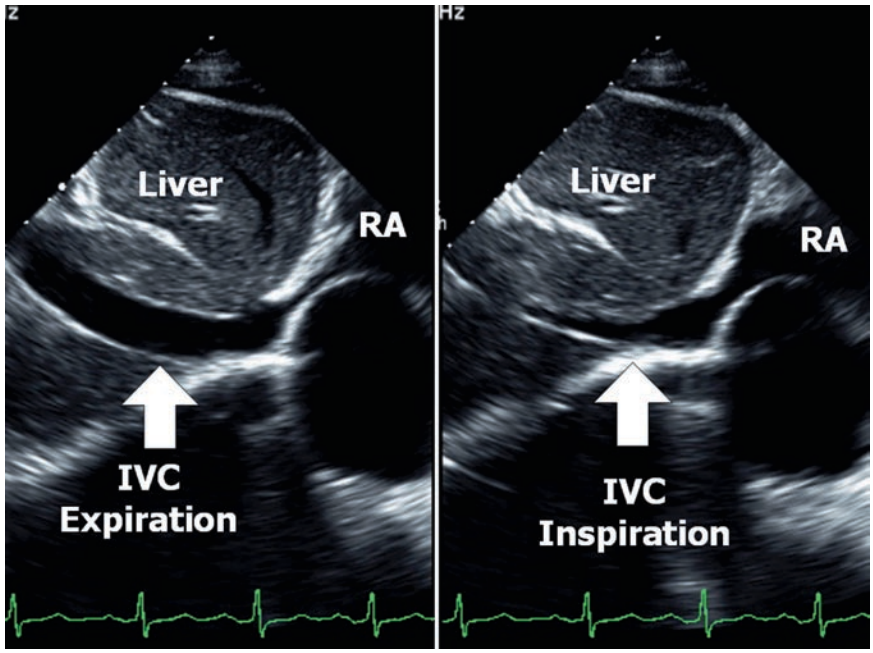

Fig. 4.20 This figure illustrates the inferior vena cava (IVC) from subcostal view. Note the normal respiratory variation of the size of the IVC. With elevated right atrial pressure (RAP), this respiratory variation is lost. If the IVC decreases by less than 50% with inspiration, it suggests elevated RAP

Similar to the mitral valve flow patterns, the tricuspid flow (Fig. 4.21) can be used to estimate the right ventricular filling pressure.[37] The inferior and superior vena cava flow patterns should be interpreted just like the pulmonary vein flow to the left atrium.

In the presence of ventricular septal defect (VSD) the right ventricular pressure can be estimated by obtaining the trans-VSD velocity and thus calculate the maximum systolic gradient between the left and right ventricles.[38] Depending on the VSD type, the best position is selected to obtain the flow most parallel to the ultrasound beam (Fig. 4.22). As discussed earlier the left ventricular systolic pressure (LVSP) is approximately equal to SBP (cuff) in the absence of LVOT obstruction. So the right ventricular systolic pressure (RVSP) is calculated as

$$\text{Trans-VSD pressure gradient} = \text{LVSP} - \text{RVSP} = \text{SBP} - \text{RVSP}$$

Therefore:

$$\text{RVSP} = \text{SBP (cuff)} - \text{trans-VSD pressure gradient} = \text{SBP (cuff)} - \text{VSD } 4V^2$$

Pulmonary Artery Pressures

In the absence of pulmonic stenosis right ventricular systolic pressure is equal to pulmonary artery systolic pressure (PASP). The end-diastolic velocity of the pulmonic regurgitant (PR) jet may be used to estimate the pulmonary artery diastolic pressure.[39] The end-diastolic velocity of the pulmonary regurgitation jet is expressed as $4V^2$ which equals the pressure gradient between the pulmonary artery and the right ventricle at end diastole, i.e., pulmonary artery diastolic pressure minus the right ventricular end-diastolic pressure. The latter pressure is usually close to the right atrial pressure. Accordingly, the pulmonary artery diastolic pressure (PADP) can be calculated as

$$\text{PADP} = 4V^2 \text{ (end-diastolic velocity of PR jet)} + \text{RA pressure}$$

In addition, the mean pulmonary artery pressure (MPAP) can be calculated as: MPAP = $4V^2$ (the peak velocity of the PR)

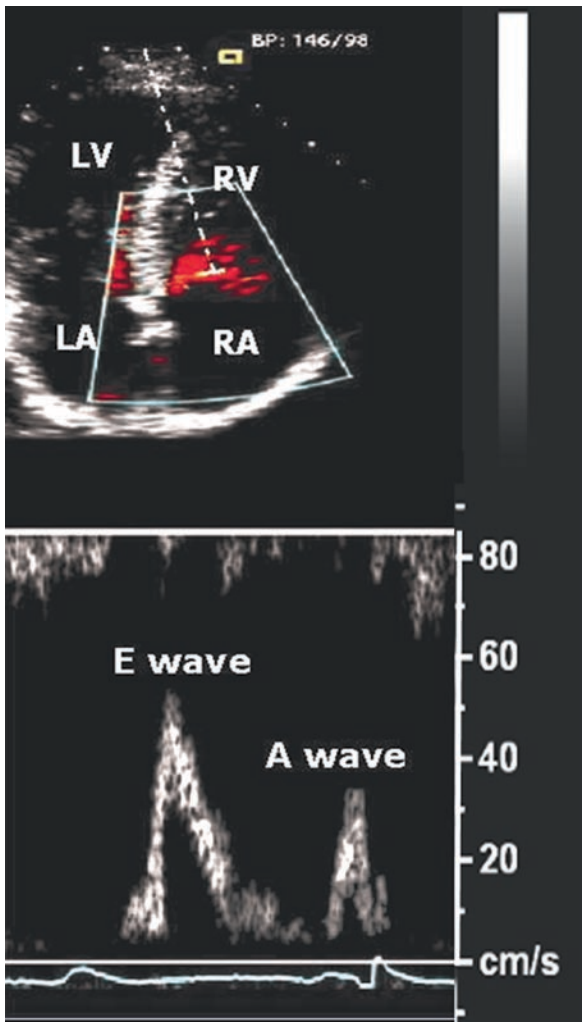

Fig. 4.21 Apical four-chamber view with the PW Doppler sample volume at the tip of tricuspid valve. The transtricuspid flow wave pattern is similar to the transmitral flow. Two distinct waves are identified. E wave due to passive ventricular filling and A wave due to right atrial contraction. Refer to the mitral valve for detailed interpretation

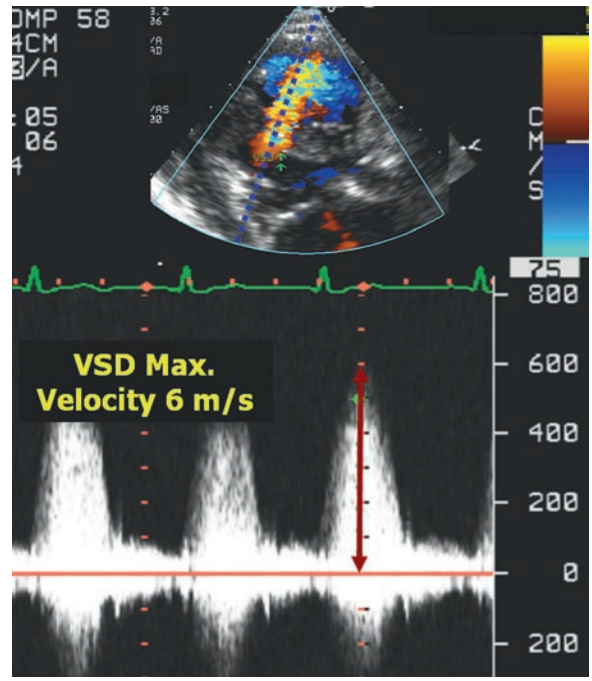

Fig. 4.22 Parasternal long-axis view with color flow is seen through membranous ventricular septal defect (VSD). The maximum velocity, obtained by CW Doppler, is 6 m/s. Note also that flow continues throughout diastole because the left ventricular diastolic pressure is higher than right ventricular diastolic pressure. Applying the concept of Bernoulli equation, the pressure gradient between left and right ventricles is equal to 144 mmHg. If we know that the systolic blood pressure (SBP) by cuff is 110 mmHg (approximately equal to LVSP) then RVSP = trans-VSD pressure gradient – SBP = 144 – 110 = 34 mmHg

Note here that assuming the RV early diastolic pressure is close to zero

In the last two chapters, we discussed in detail the concepts used in assessment of flow and hemodynamics of various cardiovascular function and abnormalities. Both semiquantitative and quantitative methods are discussed with greater emphasis on the quantitative methods. Some of the clinical applications of these methods are presented. However, this is not conclusive as several other clinical uses are not mentioned or not discussed in detail. The purpose is to present the most clinically relevant, the most reliable, and less technically tedious methods available. Which method to use depends on the skill and comfort with that particular method. But it is important to be familiar with strengths and limitations of each method. Finally the art of medicine is to find the diagnostic method that is most useful for your patient, so the quantitative methods should be used as much as possible.

References

1. Holen J, Waag RC, Gramiak R, Violante MR, Roe SA. Doppler ultrasound in orifice flow. In vitro studies of the relationship between pressure difference and fluid velocity. *Ultrasound Med Biol.* 1985;11:261–266.
2. Zoghbi WA, Farmer KL, Soto JG, Nelson JG, Quinones MA. Accurate noninvasive quantification of stenotic aortic valve area by Doppler echocardiography. *Circulation.* 1986;73:452–459.

3. Nishimura RA, Holmes DR, Jr., Reeder GS, et al. Doppler evaluation of results of percutaneous aortic balloon valvuloplasty in calcific aortic stenosis. *Circulation*. 1988;78: 791–799.
4. Otto CM, Pearlman AS, Gardner CL, et al. Experimental validation of Doppler echocardiographic measurement of volume flow through the stenotic aortic valve. *Circulation*. 1988;78:435–441.
5. Casale PN, Palacios IF, Abascal VM, et al. Effects of dobutamine on Gorlin and continuity equation valve areas and valve resistance in valvular aortic stenosis. *Am J Cardiol*. 1992;70:1175–1179.
6. Lin SS, Roger VL, Pascoe R, Seward JB, Pellikka PA. Dobutamine stress Doppler hemodynamics in patients with aortic stenosis: feasibility, safety, and surgical correlations [see comment]. *Am Heart J*. 1998; 136:1010–1016.
7. Monin JL, Quere JP, Monchi M, et al. Low-gradient aortic stenosis: operative risk stratification and predictors for long-term outcome: a multicenter study using dobutamine stress hemodynamics. *Circulation*. 2003;108:319–324.
8. Nishimura RA, Grantham JA, Connolly HM, Schaff HV, Higano ST, Holmes DR, Jr. Low-output, low-gradient aortic stenosis in patients with depressed left ventricular systolic function: the clinical utility of the dobutamine challenge in the catheterization laboratory [see comment]. *Circulation*. 2002;106:809–813.
9. Messika-Zeitoun D, Aubry MC, Detaint D, Bielak LF. Evaluation and clinical implications of aortic valve calcification measured by electron-beam computed tomography. *Circulation*. 2004;110:356–62.
10. Lima CO, Sahn DJ, Valdes-Cruz LM, et al. Noninvasive prediction of transvalvular pressure gradient in patients with pulmonary stenosis by quantitative two-dimensional echocardiographic Doppler studies. *Circulation*. 1983;67: 866–871.
11. Kosturakis D, Allen HD, Goldberg SJ, Sahn DJ, Valdes-Cruz LM. Noninvasive quantification of stenotic semilunar valve areas by Doppler echocardiography. *J Am Coll Cardiol*. 1984;3:1256–1262.
12. Nishimura RA, Rihal CS, Tajik AJ, Holmes DR, Jr. Accurate measurement of the transmitral gradient in patients with mitral stenosis: a simultaneous catheterization and Doppler echocardiographic study. *J Am Coll Cardiol*. 1994;24: 152–158.
13. Libanoff AJ, Rodbard S. Atrioventricular pressure half-time. Measure of mitral valve orifice area. *Circulation*. 1968;38:144–150.
14. Bruce CJ, Nishimura RA. Newer advances in the diagnosis and treatment of mitral stenosis. *Curr Probl Cardiol*. 1998; 23:125–192.
15. Gorcsan J, III, Snow FR, Paulsen W, Nixon JV. Noninvasive estimation of left atrial pressure in patients with congestive heart failure and mitral regurgitation by Doppler echocardiography. *Am Heart J*. 1991;121:858–863.
16. Ge Z, Zhang Y, Fan D, Zhang M, Duran CM. Simultaneous measurement of left atrial pressure by Doppler echocardiography and catheterization. *Int J Cardiol*. 1992;37:243–251.
17. Grayburn PA, Handshoe R, Smith MD, Harrison MR, DeMaria AN. Quantitative assessment of the hemodynamic consequences of aortic regurgitation by means of continuous wave Doppler recordings. *J Am Coll Cardiol*. 1987;10:135–141.
18. Ge ZM, Zhang Y, Fan DS, Zhang M, Fan JX, Zhao YX. Quantification of left-side intracardiac pressures and gradients using mitral and aortic regurgitant velocities by simultaneous left and right catheterization and continuous-wave Doppler echocardiography. *Clin Cardiol*. 1993; 16:863–70.
19. Appleton CP, Galloway JM, Gonzalez MS, Gaballa M, Basnight MA. Estimation of left ventricular filling pressures using two-dimensional and Doppler echocardiography in adult patients with cardiac disease. Additional value of analyzing left atrial size, left atrial ejection fraction and the difference in duration of pulmonary venous and mitral flow velocity at atrial contraction. *J Am Coll Cardiol*. 1993;22: 1972–1982.
20. Nishimura RA, Tajik AJ. Determination of left-sided pressure gradients by utilizing Doppler aortic and mitral regurgitant signals: validation by simultaneous dual catheter and Doppler studies. *J Am Coll Cardiol*. 1988;11:317–321.
21. Mulvagh S, Quinones MA, Kleiman NS, Cheirif J, Zoghbi WA. Estimation of left ventricular end-diastolic pressure from Doppler transmitral flow velocity in cardiac patients independent of systolic performance. *J Am Coll Cardiol*. 1992;20:112–119.
22. Garcia MJ, Ares MA, Asher C, Rodriguez L, Vandervoort P, Thomas JD. An index of early left ventricular filling that combined with pulsed Doppler peak E velocity may estimate capillary wedge pressure. *J Am Coll Cardiol*. 1997;29:448–454.
23. Nagueh SF, Middleton KJ, Kopelen HA, Zoghbi WA, Quinones MA. Doppler tissue imaging: a noninvasive technique for evaluation of left ventricular relaxation and estimation of filling pressures. *J Am Coll Cardiol*. 1997; 30:1527–1533.
24. Nagueh SF, Kopelen HA, Zoghbi WA. Feasibility and accuracy of Doppler echocardiographic estimation of pulmonary artery occlusive pressure in the intensive care unit. *Am J Cardiol*. 1995;75:1256–1262.
25. Kuecherer HF, Muhiudeen IA, Kusumoto FM, et al. Estimation of mean left atrial pressure from transesophageal pulsed Doppler echocardiography of pulmonary venous flow. *Circulation*. 1990; 82:1127–1139.
26. Rossvoll O, Hatle LK. Pulmonary venous flow velocities recorded by transthoracic Doppler ultrasound: relation to left ventricular diastolic pressures [see comment]. *J Am Coll Cardiol*. 1993;21:1687–1696.
27. Pozzoli M, Capomolla S, Pinna G, Cobelli F, Tavazzi L. Doppler echocardiography reliably predicts pulmonary artery wedge pressure in patients with chronic heart failure with and without mitral regurgitation. *J Am Coll Cardiol*. 1996;27:883–893.
28. Nishimura RA, Abel MD, Hatle LK, Tajik AJ. Relation of pulmonary vein to mitral flow velocities by transesophageal Doppler echocardiography. Effect of different loading conditions. *Circulation*. 1990;81:1488–1497.
29. Yamamoto K, Nishimura RA, Chaliki HP, Appleton CP, Holmes DR, Jr., Redfield MM. Determination of left ventricular filling pressure by Doppler echocardiography in patients with coronary artery disease: critical role of left ventricular systolic function. *J Am Coll Cardiol*. 1997;30: 1819–1826.
30. Hurrell DG, Nishimura RA, Ilstrup DM, Appleton CP. Utility of preload alteration in assessment of left ventricular

filling pressure by Doppler echocardiography: a simultaneous catheterization and Doppler echocardiographic study. *J Am Coll Cardiol*. 1997; 30:459–467.
31. Takatsuji H, Mikami T, Urasawa K, et al. A new approach for evaluation of left ventricular diastolic function: spatial and temporal analysis of left ventricular filling flow propagation by color M-mode Doppler echocardiography [see comment]. *J Am Coll Cardiol*. 1996;27:365–371.
32. Tsang TS, Barnes ME, Gersh BJ, Bailey KR, Seward JB. Left atrial volume as a morphophysiologic expression of left ventricular diastolic dysfunction and relation to cardiovascular risk burden. *Am J Cardiol*. 2002;90: 1284–1289.
33. Currie PJ, Seward JB, Chan KL, et al. Continuous wave Doppler determination of right ventricular pressure: a simultaneous Doppler-catheterization study in 127 patients. *J Am Coll Cardiol*. 1985;6:750–756.
34. Yock PG, Popp RL. Noninvasive estimation of right ventricular systolic pressure by Doppler ultrasound in patients with tricuspid regurgitation. *Circulation*. 1984;70:657–662.
35. Simonson JS, Schiller NB. Sonospirometry: a new method for noninvasive estimation of mean right atrial pressure based on two-dimensional echographic measurements of the inferior vena cava during measured inspiration. *Journal Am Coll Cardiol*. 1988;11:557–564.
36. Kircher BJ, Himelman RB, Schiller NB. Noninvasive estimation of right atrial pressure from the inspiratory collapse of the inferior vena cava. *Am J Cardiol*. 1990;66:493–496.
37. Klein AL, Hatle LK, Burstow DJ, et al. Comprehensive Doppler assessment of right ventricular diastolic function in cardiac amyloidosis. *J Am Coll Cardiol*. 1990;15:99–108.
38. Marx GR, Allen HD, Goldberg SJ. Doppler echocardiographic estimation of systolic pulmonary artery pressure in pediatric patients with interventricular communications. *J Am Coll Cardiol*. 1985;6:1132–1137.
39. Masuyama T, Kodama K, Kitabatake A, Sato H, Nanto S, Inoue M. Continuous-wave Doppler echocardiographic detection of pulmonary regurgitation and its application to noninvasive estimation of pulmonary artery pressure. *Circulation*. 1986; 74:484–492.

Chapter 5
Tissue Doppler, Doppler Strain, and Non-Doppler Strain: Tips, Limitations, and Applications

Diala Khraiche and Denis Pellerin

Conventional transthoracic echocardiography remains the most commonly used imaging modality in clinical practice. The improvement of diagnostic tools remains a major goal and considerable technical progress has been made in image quality by utilizing harmonic imaging on conventional echo and with the recent introduction of new imaging techniques.

Assessment of myocardial wall motion is usually performed by visual estimation of 2D images which requires training and remains a subjective and operator-dependent assessment. M-mode technique provides a 1D semiquantitative assessment of a limited number of myocardial segments. Over the years several imaging modalities have been developed for the direct measurement of myocardial wall motion in real time, thus allowing objective assessment of global and regional left and right ventricular function and improving the accuracy and reproducibility of echocardiography studies. The use of Doppler tissue echocardiography has been reported since 1994. Tissue tracking, Doppler strain, and Doppler strain rate imaging were derived from color Doppler tissue echocardiography since 1999. Non-Doppler strain or Speckle tracking was introduced in 2004 to overcome limitations of the Doppler technique and is obtained from processing conventional 2D images. Three-dimensional non-Doppler strain is under development. Although these imaging modalities have been widely available for more than 10 years, they are not routinely used in many echo laboratories due to cumbersome image acquisition and to the expertise required for postprocessing analysis and interpretation. Myocardial tissue parameters cannot be reliably measured after pressing a button on the echo scanner keyboard.

This chapter reviews principles, requirements for image acquisition, postprocessing analysis, clinical applications, and limitations of Tissue Doppler, Doppler strain and strain rate, and non-Doppler tissue velocity and strain.

Doppler Tissue Imaging

Principles and Modalities Have Been Published Previously[1]

Briefly recalled, myocardial motion is characterized by relatively low-velocity and high-amplitude signals (Fig. 5.1). To record wall motion velocity, high pass filters are bypassed with the tissue signal directly entered into the autocorrelator. Doppler tissue echocardiography has three modalities: spectral pulsed-wave Doppler, 2D, and M mode color Doppler. Bidimensional images have good spatial resolution, whereas spectral Doppler and M mode have the best temporal resolution (Fig. 5.2).

Requirements for Image Acquisition when Acquiring Color Tissue Doppler Images

Optimal settings of frame rate, velocity scale, and gain are required. Three cardiac cycles should be stored with breath held at end expiration. Breath holding is required to minimize through plane motion. Image frame rate is increased by decreasing image sector width and changing depth. Optimal frame rate is over

D. Khraiche and D. Pellerin (✉)
The Heart Hospital, London, UK
e-mail: Denis.pellerin@uclh.nhs.uk

P. Nihoyannopoulos and J. Kisslo (eds.), *Echocardiography*,
DOI: 10.1007/978-1-84882-293-1_5, © Springer-Verlag London Limited 2009

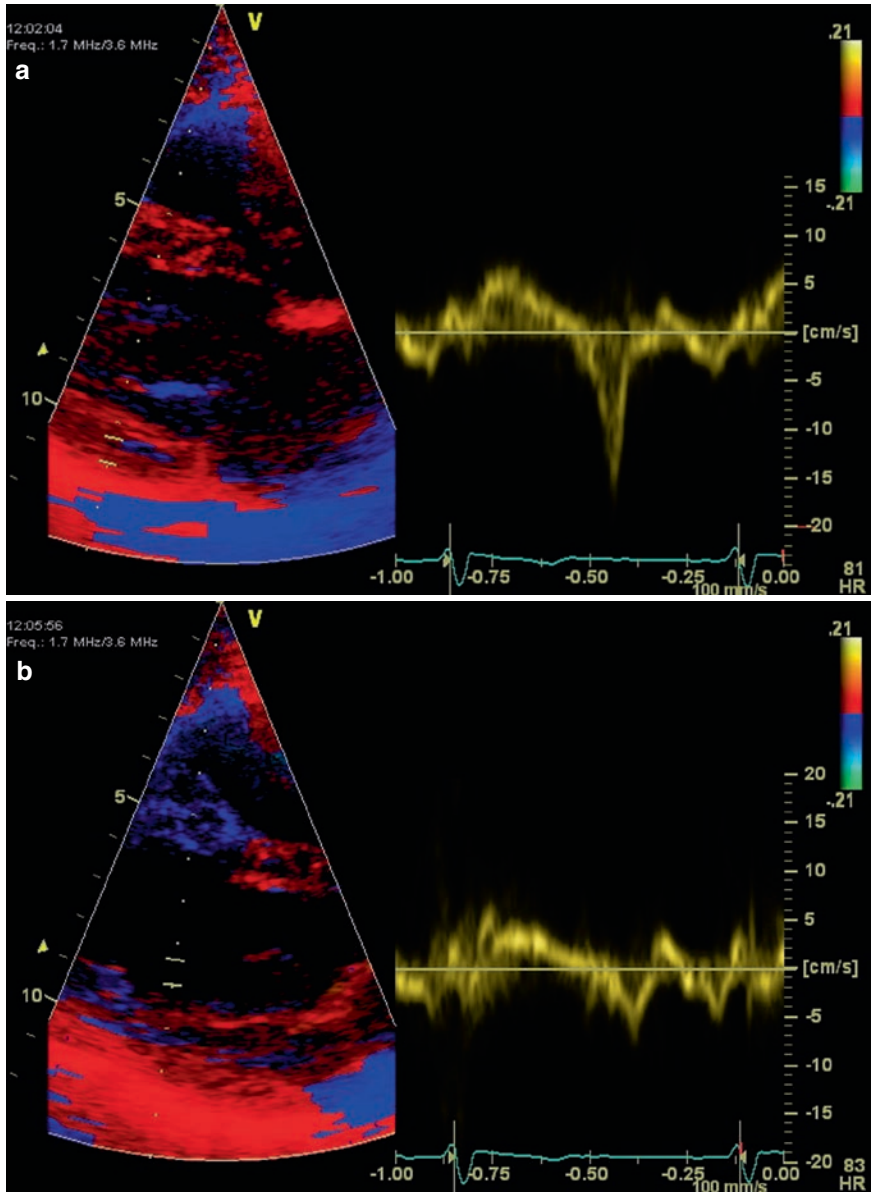

Fig. 5.1 Myocardial motion can be recorded when the sample volume is placed into the posterior wall in parasternal long-axis view (**a**). Myocardial motion is characterized by low-velocity and high-amplitude signals in contrast with conventional flow Doppler signals that are typified by high velocity and low amplitude. Myocardial motion creates Doppler shifts that are approximately 40 dB higher than Doppler signals from blood flow. Due to its high-amplitude signal myocardial motion can also be recorded when the sample volume is placed into the LV cavity (**b**). The spectral Doppler tissue velocity profile is noisier and velocities are lower. Although the sample volume is fixed when the wall is moving, one must pay attention to the position of the sample volume appropriately

150/s. Velocity scale should be modified to avoid aliasing. During stress echocardiography, myocardial velocities increase and velocity scale should also be increased. On the other hand, color velocity scale should be decreased to optimally measure low velocities occurring during pre-ejection and isovolumic relaxation periods at rest.

Postprocessing Analysis

Postprocessing analysis of color images aims to measure velocity data offline after image acquisition. A region of interest (ROI) is manually placed over a myocardial segment, and color pixels within the ROI are converted into myocardial velocities. When analyzing

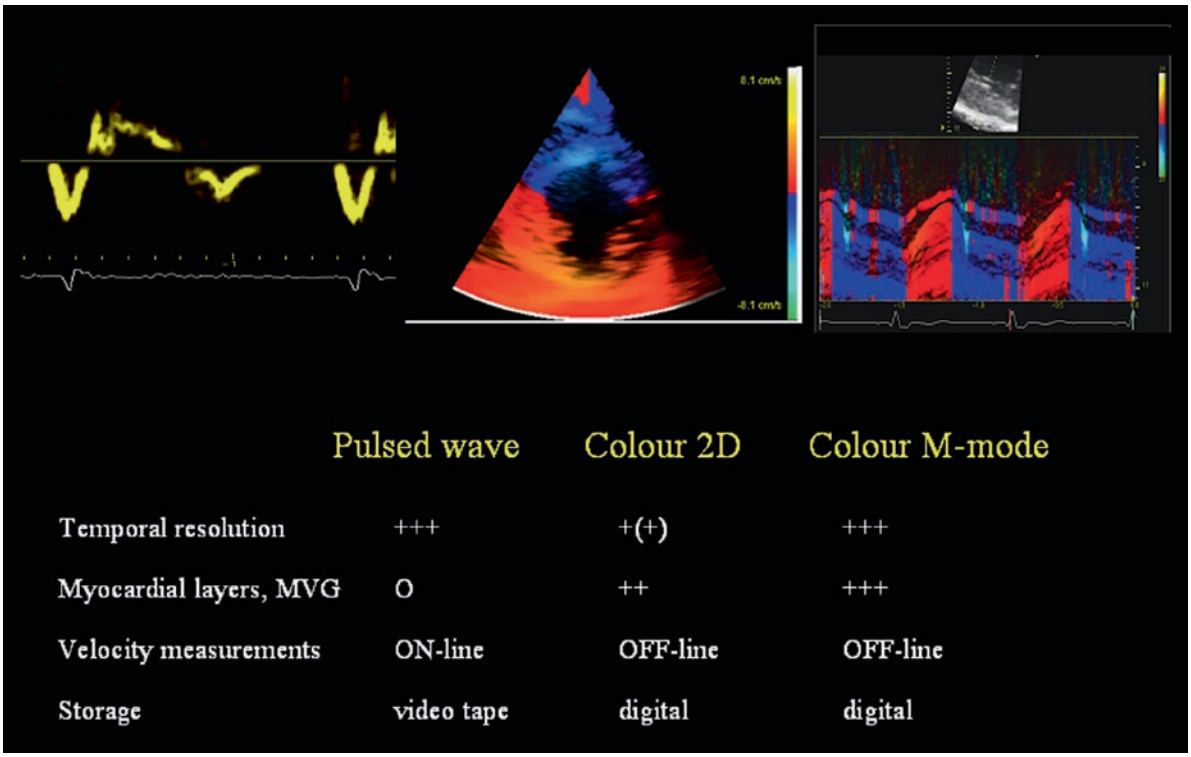

Fig. 5.2 Tissue Doppler echocardiography has three modalities including spectral pulsed-wave Doppler, color 2D, and color M mode which is illustrated here by zoom of the left ventricular posterior wall in the parasternal approach. The characteristics of the three modalities are described

color tissue Doppler 2D cineloops, the software measures myocardial velocities within the ROI on each frame of the cineloop and links the measurements up with lines to create a velocity profile throughout the cardiac cycle. The frame rate determines the number of measurements. If measurements are performed during only one phase of the cardiac cycle, freezing the image at the time of the measurement is useful to make sure that the ROI is positioned within the wall, for example freezing the image during ejection to measure peak ejection velocity (Fig. 5.3). Measurements are made with a sweep speed of 100 mm/s and an average of three measurements is required.

Velocities measured by online spectral pulsed-wave Doppler are 20–25% higher than those measured offline by the postprocessing of high frame rate color 2D cineloops (Fig. 5.4). This should be considered during calculation of the ratio of early diastolic transmitral inflow velocity to early diastolic tissue Doppler velocity of mitral annulus.

Tissue tracking is obtained by time integration of color tissue Doppler 2D cineloops and assesses displacement.

Advantages of Tissue Doppler Echocardiography Over Conventional Echocardiography

Myocardial velocities quantify global and regional left ventricular function independent of endocardial border delineation.

Tissue Doppler echocardiography has been shown to be a more sensitive technique than conventional echo in early detection of cardiomyopathy.

Velocity of each myocardial layer including endocardium, midwall, and epicardium can be measured in animal experiments[2] and in humans.[3] However, no company has made this assessment commercially available and its potential applications have been limited (Fig. 5.5).

Applications

Mitral Annular motion is among indices of global LV systolic performance that are not dependent on endocardial definition and less dependent on loading conditions.

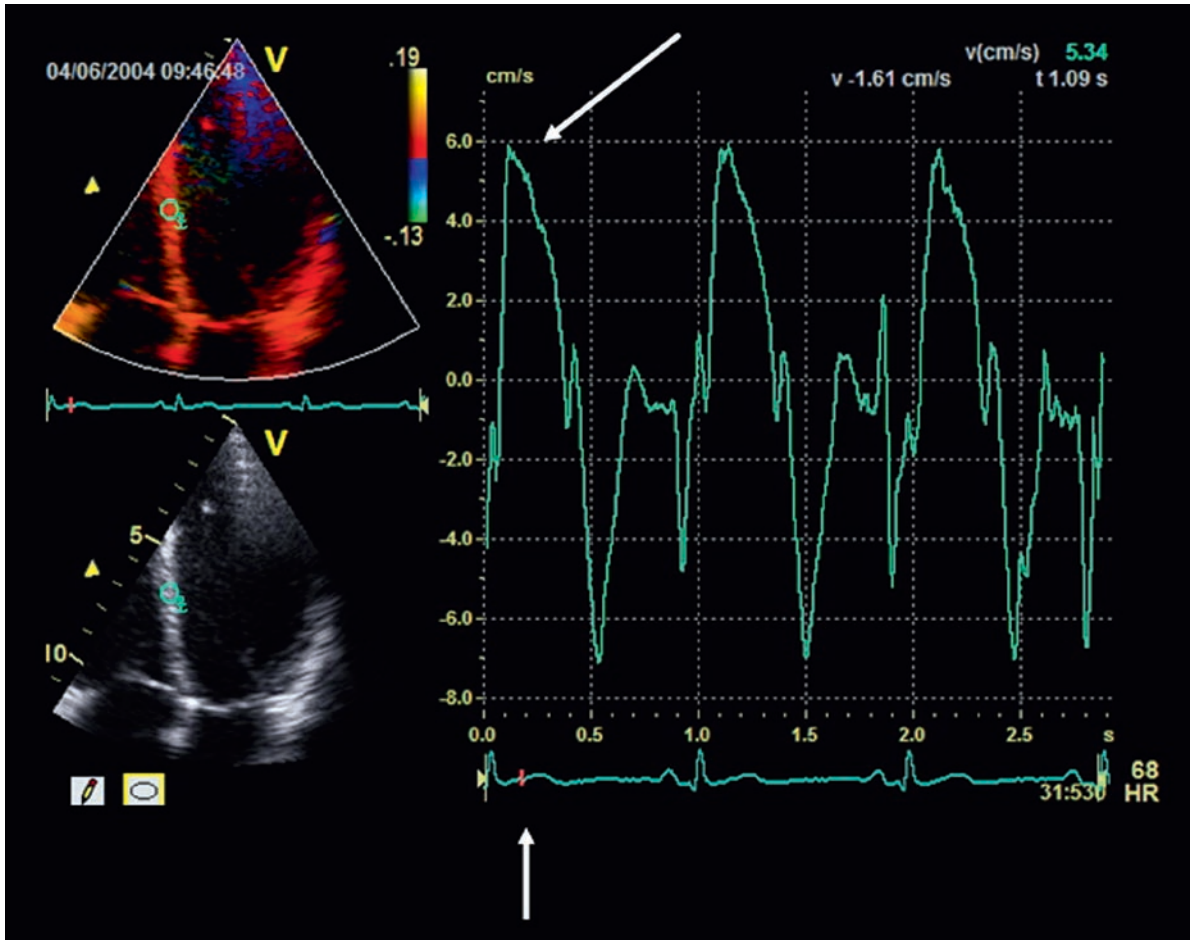

Fig. 5.3 Apical four chamber view recorded with high frame rate and color tissue Doppler imaging. During postprocessing analysis the cineloop is frozen during midejection. Therefore, one can be sure that the ROI is positioned into the septum when the measurement of systolic velocity is made

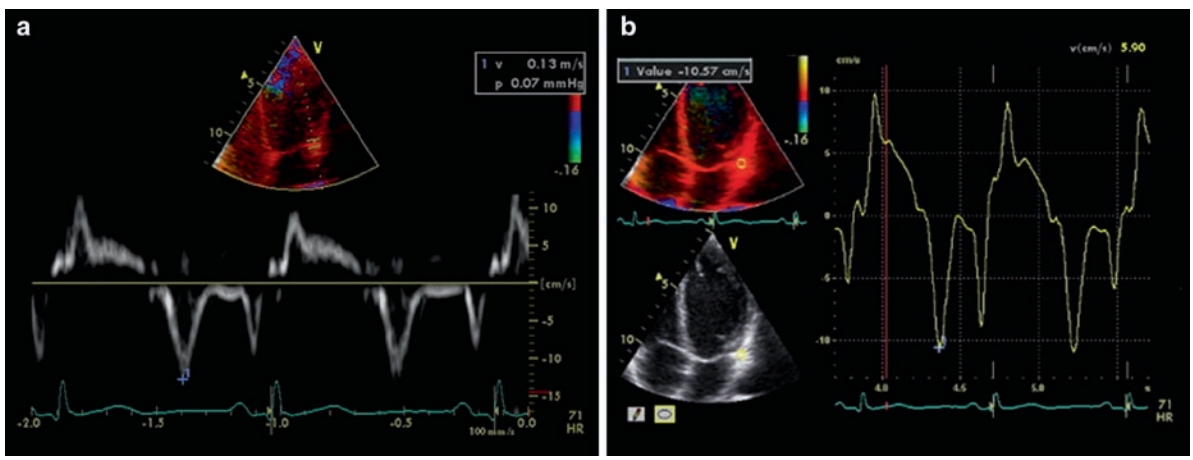

Fig. 5.4 Measurement of lateral mitral annular velocity has been obtained successively in the same patient by online spectral pulsed-wave Doppler (panel A) and by postprocessing of high frame rate color 2D cineloop (panel B). Velocities measured by spectral pulsed-wave Doppler are 20–25% higher than those measured by the postprocessing of color 2D cineloops. This should be considered during calculation of the ratio of early diastolic transmitral inflow velocity to early diastolic tissue Doppler velocity of mitral annulus

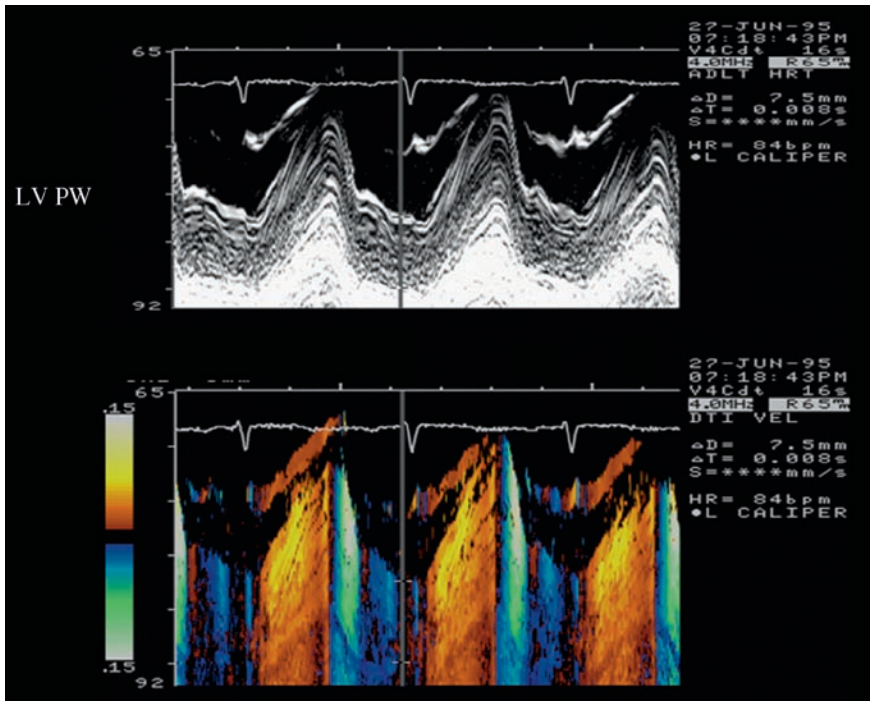

Fig. 5.5 M mode zoom of the left ventricular posterior wall recorded successively with conventional echocardiography and with color Doppler tissue imaging. The additional information obtained with color tissue Doppler includes clear individualization of all the phases of the cardiac cycle, and gradient of velocity across the thickness of the myocardial wall visible during ejection and early diastole. Wall thickness must be measured by calipers on the gray-scale image before calipers are pasted on the color image

Mitral annular velocity can be obtained in 77% of patients using conventional echo and in all patients using pulsed-wave tissue Doppler measurements. Systolic mitral annular velocity determined by pulsed-wave tissue Doppler and averaged over three sites including lateral, septal, and posterior mitral annulus ≤8 cm/s has 94% sensitivity, 93% specificity, and 94% accuracy for the detection of LV ejection fraction <50%. Early diastolic mitral annular velocity (average of three sites) >5.4 cm/s is 88% sensitive and 97% specific for the detection of LV ejection fraction >50%. Tricuspid annular velocity has been used as an index of right ventricular function in patients with heart failure. Systolic annular velocity <11.5 cm/s predicted right ventricular ejection fraction <45% with a sensitivity of 90% and a specificity of 85%.

Assessment of diastolic function and gross estimation of LV filling pressure is currently one of the main applications of the technique.[4] The ratio of mitral inflow early diastolic velocity (*E*) to early diastolic mitral annular velocity (*E′*) correlates with left ventricular filling pressure. Noninvasive hemodynamic assessment of LV filling pressure is not reliable in patients with moderate and severe mitral regurgitation of degenerative origin. The *E*/*E′* ratio is incremental to clinical factors and ejection fraction for the prediction of heart failure events. The number of myocardial segments with altered early to late diastolic strain rate ratio increases with worsening global diastolic function.

Experimental and clinical studies have shown that during acute ischemia, myocardial peak systolic velocity and strain rate were notably reduced or reversed within 5 s after coronary occlusion. Postsystolic shortening or thickening is a sensitive marker of ischemia occurring during the isovolumic relaxation period, often extending into the early filling period. Accurate timing of the aortic valve closure is crucial for recognition of postsystolic shortening. The main limitations of stress echocardiography interpretation are the subjective visual analysis of endocardial motion and wall thickening and the necessity of adequate training. Tissue Doppler echocardiographic criterion to detect stress-induced ischemia is a lack of increase in peak systolic velocity. In patients with severe chronic

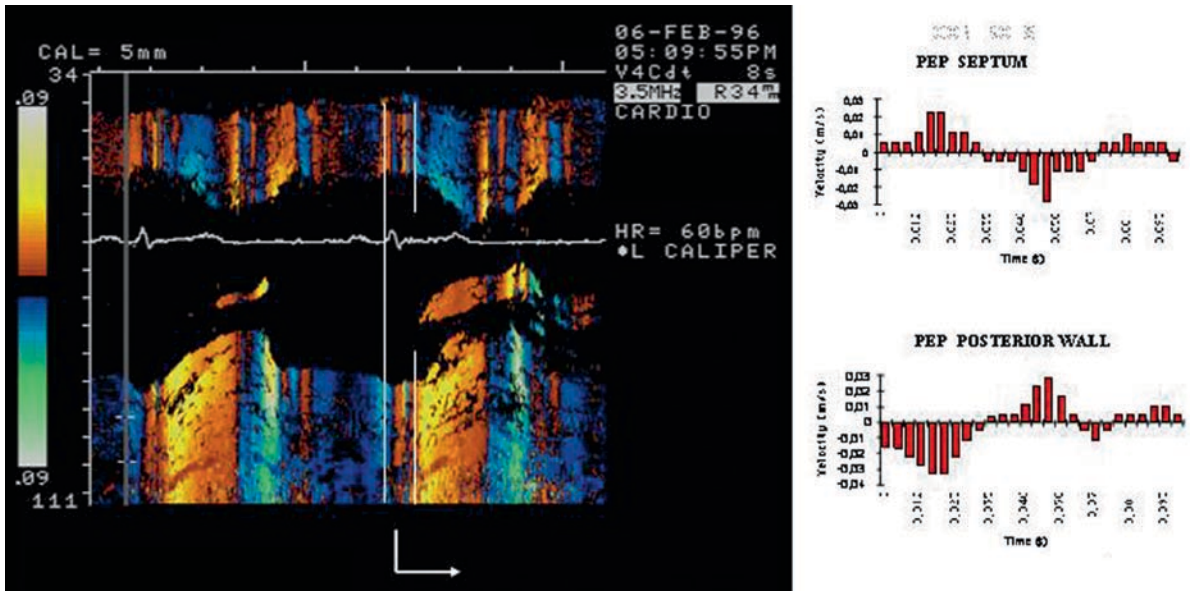

Fig. 5.6 Color M mode Doppler tissue imaging of the left ventricle recorded from a parasternal approach. During the pre-ejection period when mitral and aortic valves are closed, successive color strips are visible in the septum and in the posterior wall corresponding to successive inward and outward wall motions (*left panel*). The conversion of color pixels into velocity shows simultaneous inward motion of both walls toward the left ventricular cavity center (*right panel*).

three-vessel disease and left ventricular dysfunction, Doppler myocardial velocities have been used to distinguish viable from non-viable segments. Tissue Doppler imaging has shown left ventricular wall motion during the pre-ejection period by displaying several color strips within the walls. These color strips represent successive inward and outward wall motions with rapid changes in direction. In both walls, there was a simultaneous inward motion toward the left ventricular cavity center (Fig. 5.6). Pre-ejection inward motion velocity in the posterior wall was shown to correlate linearly with left ventricular systolic function.

Tissue Doppler imaging has been used in patients with dilated cardiomyopathy and severe heart failure (Fig. 5.7). Randomized clinical trials have produced unequivocal support for the use of cardiac resynchronization therapy in patients with refractory heart failure and evidence of LV dyssynchrony on ECG. However, 30% of patients treated by cardiac resynchronization therapy devices do not exhibit left ventricular functional recovery and reverse remodeling. Mechanisms of cardiac resynchronization therapy benefits are incompletely understood, and LV lead positioning is limited by venous anatomy. Mechanical dyssynchrony may be better than electrical dyssynchrony for the selection of potential responders, and several echo parameters have been suggested including intraventricular dyssynchrony combining longitudinal and radial parameters and atrioventricular dyssynchrony parameters. Sensitivity, specificity, and accuracy of these parameters have been high in single center studies, but have suboptimal interinstitutional reproducibility. As a general rule, several parameters must be used and the greater the magnitude of dyssynchrony, the greater the likelihood of positive response to cardiac resynchronization therapy. Echo data are useful in patients with comorbidities or narrow QRS complexes.

Tissue Doppler imaging has been used in patients with hypertrophic cardiomyopathy and detects gene mutation carriers independent of hypertrophy. LVEF ^{3} 68% and $E' < 15$ cm/s showed 100% specificity and 44% sensitivity in detecting gene mutation carriers.[5] Tissue Doppler imaging detected decreased longitudinal velocities in hypertrophic cardiomyopathy patients with apparently normal radial systolic function. In difficult cases, tissue Doppler echocardiography of mitral and tricuspid annuli has been useful for distinguishing

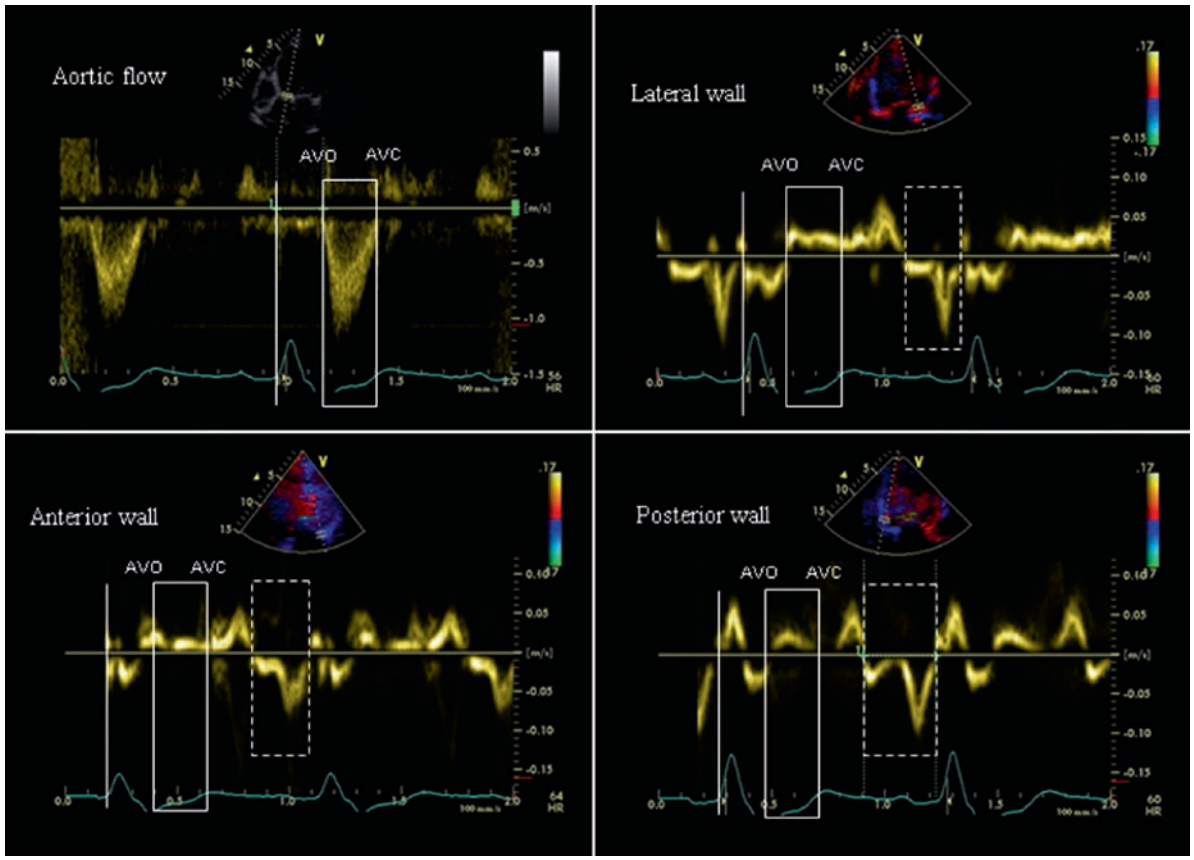

Fig. 5.7 Flow and tissue Doppler recordings in a patient with severe dilated cardiomyopathy. The first panel shows the aortic flow with aortic valve opening and closure. The onset of the Q wave on the ECG is indicated on the Doppler trace. Basal lateral, basal anterior, and basal posterior wall velocity profiles have been recorded with spectral tissue Doppler imaging. The event markers obtained from the aortic flow have been pasted on the velocity profiles since the patient is in regular sinus rhythm. Wall motions are lower during ejection than during pre-ejection and isovolumic relaxation periods suggesting that a lot of energy is used when mitral and aortic valves are closed. *Dotted lines* show mitral valve opening and closure, and therefore, left ventricular filling time in relation to the duration of the cardiac cycle

hypertrophic cardiomyopathy and athlete's heart. Systolic and early diastolic mitral annular velocities <9 cm/s have 87% sensitivity, 97% specificity, and 92% accuracy in the diagnosis of hypertrophic cardiomyopathy versus athlete's heart. Early diastolic tricuspid annular velocity <16 cm/s has 89% sensitivity and 93% specificity in the diagnostic of hypertrophic cardiomyopathy versus athlete's heart. In restrictive cardiomyopathy, mitral annular velocity was reduced, whereas it was within normal range in constrictive pericarditis.[6] Fabry cardiomy opathy is X-linked hypertrophic cardiomyopathy by deficiency of a-galactosidase. Conventional noninvasive tools are unable to provide a preclinical diagnosis allowing prompt institution of enzymatic therapy. Early detection of Fabry cardiomyopathy has been obtained by tissue Doppler imaging before development of left ventricular hypertrophy.

Limitations of Tissue Doppler Echocardiography

This modality is used mainly to quantify longitudinal ventricular function. Tissue Doppler echocardiography is an angle-dependent Doppler technique; therefore, apical segments cannot be analyzed especially in patients with dilated cardiomyopathy who have spherical LV

shape. Tethering by adjacent segments is another limitation of the technique. These limitations also apply to tissue tracking.

Limitations of mitral annular motion include prosthetic mitral valve or prosthetic mitral annulus, mitral annular calcification (Fig. 5.8), and ischemia of the

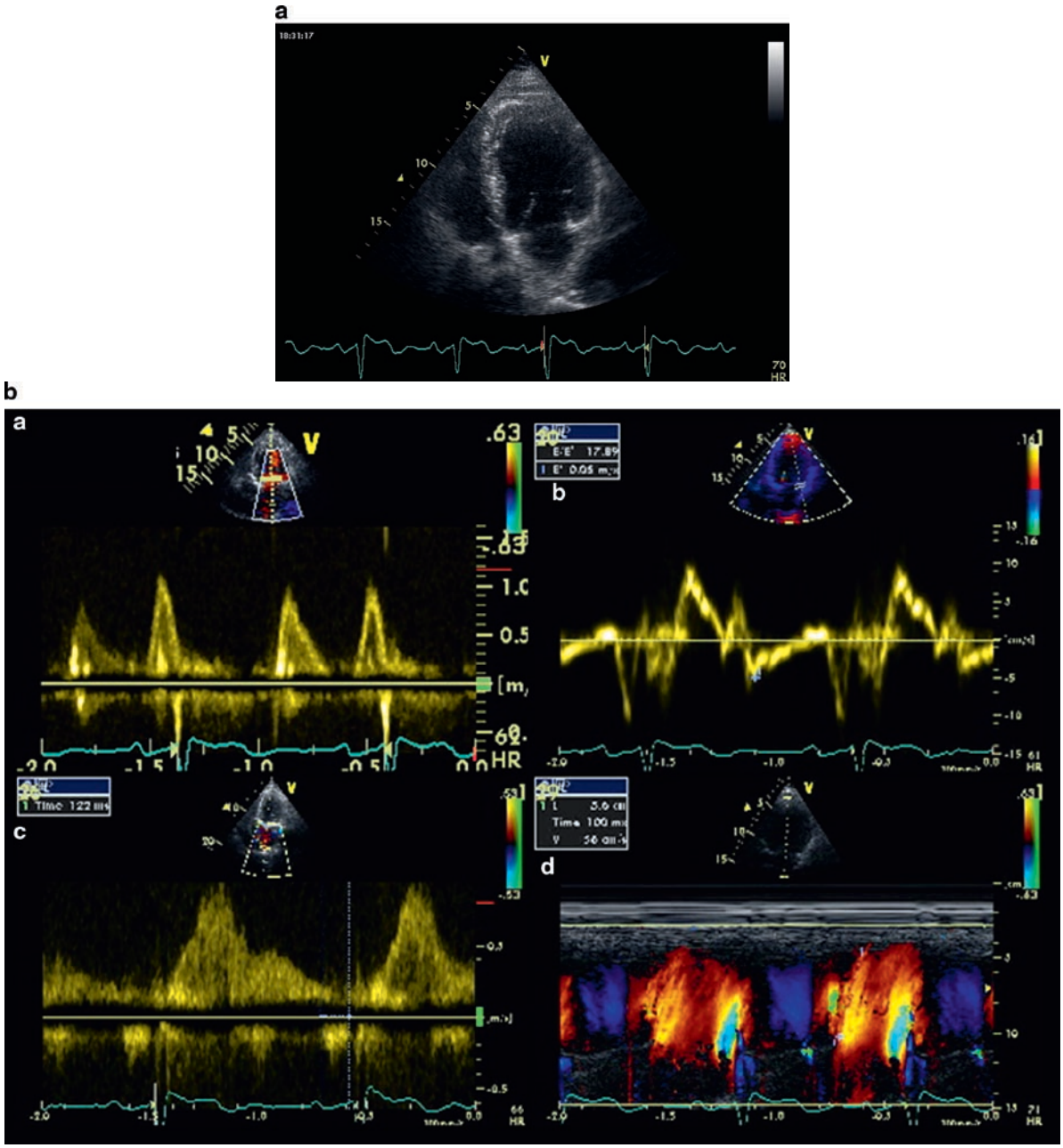

Fig. 5.8 Estimation of left ventricular filling pressure was performed in a 61-year-old subject with normal LVEF. Mitral inflow and tissue Doppler velocity of lateral mitral annulus were recorded first (**a**, **b**). Mitral annular early diastolic velocity (*E′*) was low 0.05 m/s, and septal annular velocity was lower than that of lateral velocity. *E*/*E′* ratio was 17.8. Marked calcification of mitral annulus seen on the apical four chamber view may also be responsible for reduced mitral annular velocity. Therefore, left ventricular flow propagation velocity (**c**) and pulmonary venous flow (**d**) were recorded and showed normal patterns. Derived measurements and calculations were in favor of left ventricular filling pressure being within the normal range

wall above the interrogated annular site which require averaging velocities from multiple sites.

Complex fiber architecture, translation, and rotation of the heart in the chest are common limitations to all cardiac imaging modalities.

Doppler Strain and Strain Rate

Principle and Modalities

The shape of a structure deforms during motion when different elements of the structure move with different velocities. Doppler strain and strain rate are derived from high frame rate 2D color Doppler myocardial imaging cineloops and provide noninvasive quantification of myocardial deformation.[7] These modalities were introduced with the aim of overcoming tethering of abnormal myocardial segments by adjacent normal segments, and distinguishing between segmental thickening and passive motion due to heart translation in the chest. Myocardial strain is the percentage of shortening or lengthening of a myocardial segment. Strain rate is the rate at which the myocardium shortens or lengthens.

Requirements for Image Acquisition

Requirements for Doppler strain and strain rate image acquisition are the same as those for Doppler tissue imaging and should be even more meticulously followed. High frame rate, optimal velocity scale, optimal gain, breath holding at end expiration, and storage of three cardiac cycles are mandatory (Figs. 5.9 and 5.10). Frame rate should be as high as possible taking into account the size of the structure being studied. For the LV, imaging each wall individually with a narrow sector to obtain a frame rate of 200/s or higher is required to study pre-ejection and isovolumic relaxation periods. In addition, recording aortic flow using pulsed-wave flow Doppler to obtain timing of aortic valve opening and closure is useful if the patient is in regular sinus rhythm and if the ECG trace displays high R wave amplitude with reproducible detection of the R wave. Measurements of isovolumic relaxation period and diastolic strain require recording of mitral inflow to obtain timing of mitral valve opening. In normal subjects the posterior wall thickens and expands during ejection in parasternal views (radial deformation), and Doppler strain and strain rate are positive. In apical views (longitudinal deformation) during ejection the base moves toward the apex, the posterior wall as well as the other walls shortens, and Doppler strain and strain rate are negative. However, this technique cannot assess the complex changes of the 3D deformation of the heart, and the main question is whether this assessment is clinically relevant for patient management.

Postprocessing Analysis

Requirements are also the same as those for tissue Doppler echocardiography with the addition of setting the sample distance and using timing of aortic valve opening and closure on the strain profile. Timing of aortic valve closure is crucial to define the end of ejection flow and detect postsystolic myocardial wall motions.

Advantages of Doppler Strain and Strain Rate Over Doppler Tissue Velocity

Doppler strain and strain rate are less affected by translational motion and by the tethering from adjacent segments. Doppler strain is calculated as the spatial gradient between two velocities separated by a short distance (sample distance) within the myocardial wall, whereas tissue Doppler imaging measures wall velocity in the myocardium with reference to the transducer. Systolic strain rate correlates more closely with invasive parameters including peak elastance (E_{max} = slope of end systolic pressure–volume relationships during caval occlusion) than systolic tissue velocity in experiments.[8] Several authors reported that Doppler strain and strain rate were superior to Doppler tissue velocity in the assessment of ischemia, viability, and cardiomyopathy.

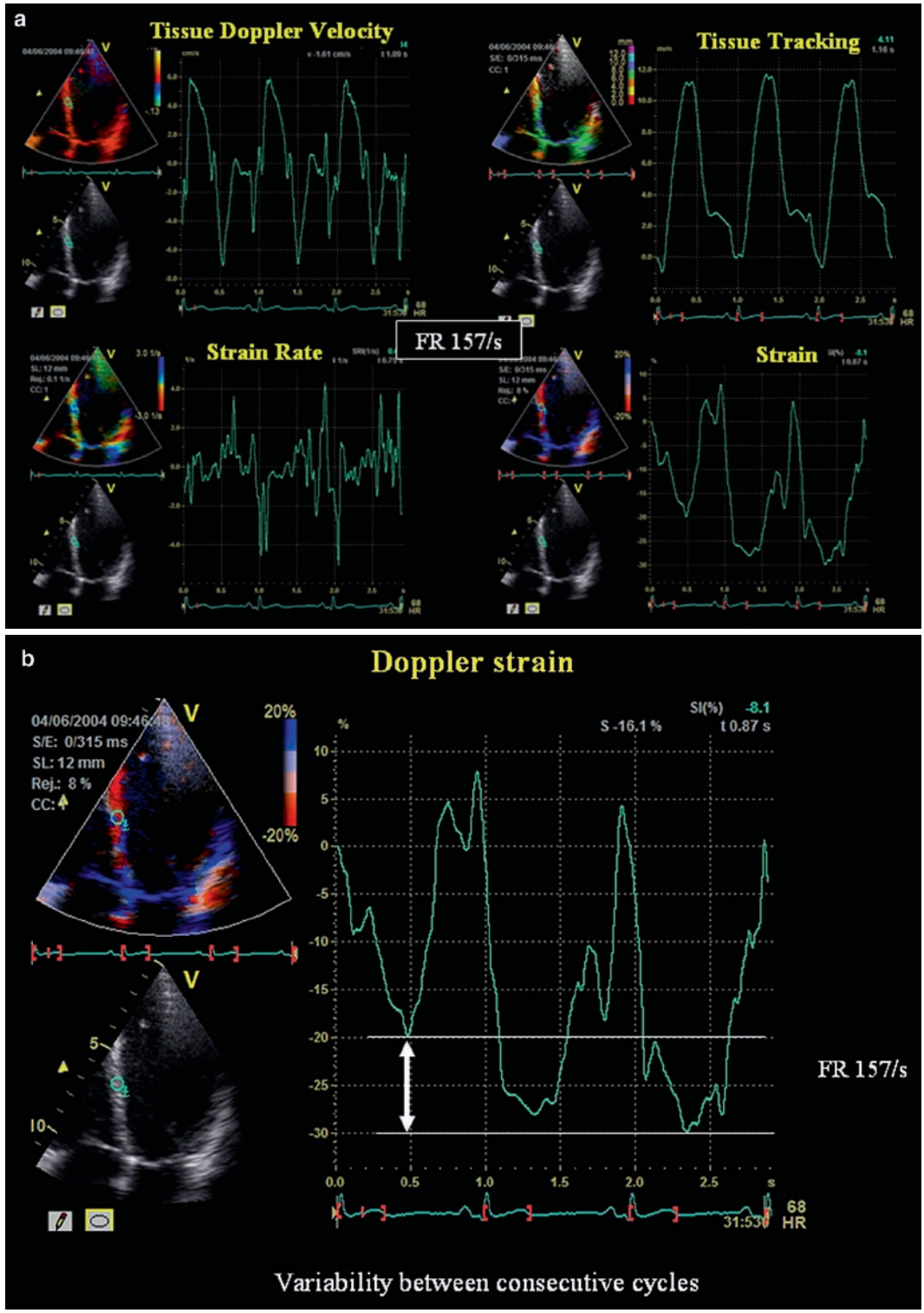

Fig. 5.9 (**a**) Tissue Doppler velocity, tissue tracking, strain rate, and strain curves were obtained in the same patient with the same ROI and a frame rate of 157/s during three cardiac cycles. Velocity and displacement curves showed robust profiles with minor variations between cardiac cycles (**b**). Doppler strain rate and strain curves showed variability between consecutive cycles. This example illustrates the need for very high frame rate obtained with narrower image sector. There is less noise in strain than in strain rate because Doppler strain is obtained through integration of the strain rate signal and integration reduces noise. Doppler strain and strain rate should only be reported when the signal is consistent

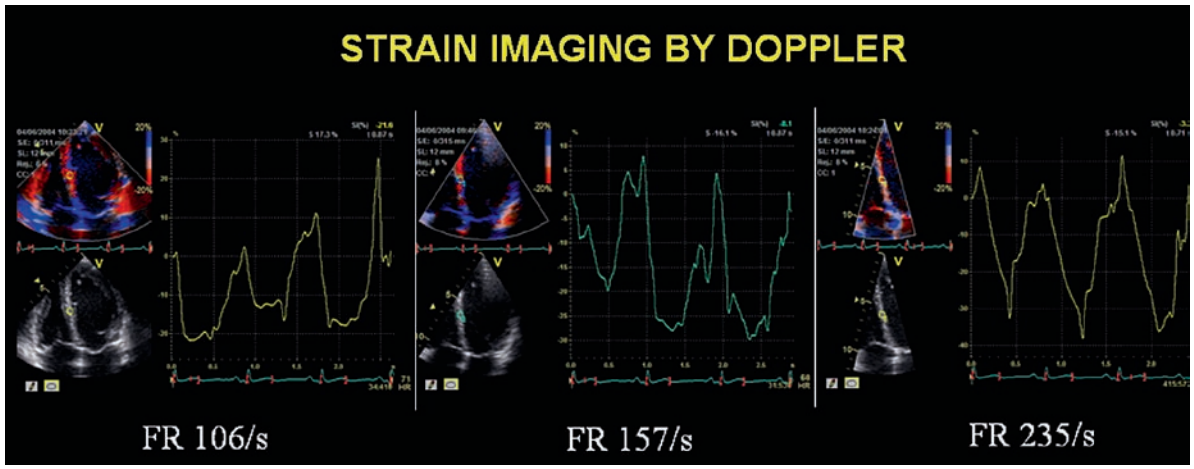

Fig. 5.10 Improvement in cycle-to-cycle variability of midseptum longitudinal peak systolic strain and noise of Doppler strain curves with increasing frame rate in the same patient using the same ROI position and size

Applications

Deformation parameters can identify and quantify regional myocardial ischemia in patients with ischemic heart diseases including chronic myocardial infarction,[9] acute myocardial infarction, and during coronary angioplasty with transient coronary artery occlusion. Prediction of infarct size after primary angioplasty for acute anterior myocardial infarction has also been reported. Strain rate differentiated transmural from nontransmural myocardial infarction which is equivalent to viability assessment at rest. Diastolic deformation parameters differentiated transmural myocardial infarction from stunned myocardium. Experimental and clinical studies using peak strain rate during isovolumic relaxation period were able to distinguish ischemic and nonischemic postsystolic thickening. In patients with severe chronic three-vessel disease and left ventricular dysfunction, myocardial velocity gradient has been used to distinguish viable from nonviable segments[10] (Fig. 5.11). Changes in peak systolic strain rate were superior to changes in peak systolic velocity in the detection of viable segments in patients with depressed left ventricular ejection fraction.

Doppler systolic Strain, strain rate, and isovolumic myocardial acceleration are other indices of global LV systolic performance that are not dependent on endocardial definition and less dependent on loading conditions. Myocardial acceleration during isovolumic contraction has been validated as a sensitive noninvasive method of assessing left and right ventricular performance (Fig. 5.12).

When distinction between hypertrophic cardiomyopathy and physiologic hypertrophy secondary to athletic training is difficult, early diastolic myocardial velocity gradient across the thickness of the posterior wall (equivalent to strain rate) ≤7/s measured in subjects between 18 and 45 years old showed 96% sensitivity and 96% specificity in the diagnosis of hypertrophic cardiomyopathy. There was no similar cut-off value in subjects older than 45 years.[11]

Detection of preclinical abnormalities in patients with cardiomyopathy has also been described. Mean longitudinal strain of eight myocardial segments of −10.6% showed 85% sensibility, 100% specificity, and 91% accuracy in the diagnosis of hypertensive cardiomyopathy versus hypertrophic cardiomyopathy. Paradoxical septal systolic strain rate and strain in midseptum has been described in patients with hypertrophic cardiomyopathy. In patients with Friedrich's ataxia who were homozygous for the GAA expansion in the smaller allele of Friedrich's ataxia gene, systolic and early diastolic radial myocardial velocity gradient was lower than in age-matched control subjects.[12] Myocardial velocity gradient during isovolumic relaxation was positive in restrictive patients and negative in constrictive patients. Primary amyloidosis (cardiac AL) is characterized by an early impairment in systolic function. This abnormality can be detected by systolic strain and strain rate but is not apparent on the systolic velocity profile. In patients with Fabry disease, peak systolic radial strain and strain rate showed improvement in cardiac function 12 months after enzyme replacement therapy.

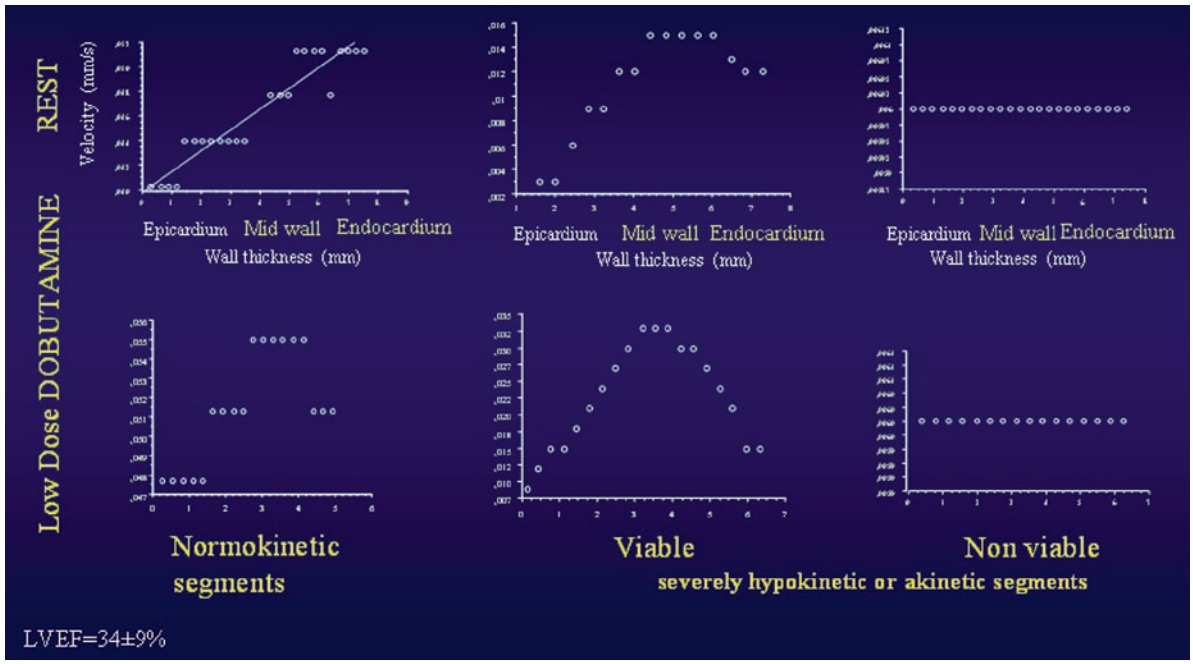

Fig. 5.11 Myocardial velocity gradients distinguished viable from nonviable segments. Velocity gradients were calculated across the thickness of the myocardial wall from endocardium to epicardium using color M mode tissue Doppler images in patients with severe chronic three-vessel disease, coronary artery disease, and LV dysfunction. In viable segments, distribution of velocities did not show the pattern of linearly decreasing velocity from endocardium to epicardium observed in normal segments. The highest velocity was located in the midlayer conferring a bell-shaped pattern to the velocity gradient. In nonviable segments, the distribution of velocity was close to zero or anarchic with small variations in velocities. These results suggest that the contractile properties of diseased but viable myocardium are mainly concentrated in the midlayer. The dramatic ultrastructural changes observed in hibernating myocardium may explain the heterogeneity of the velocity gradient

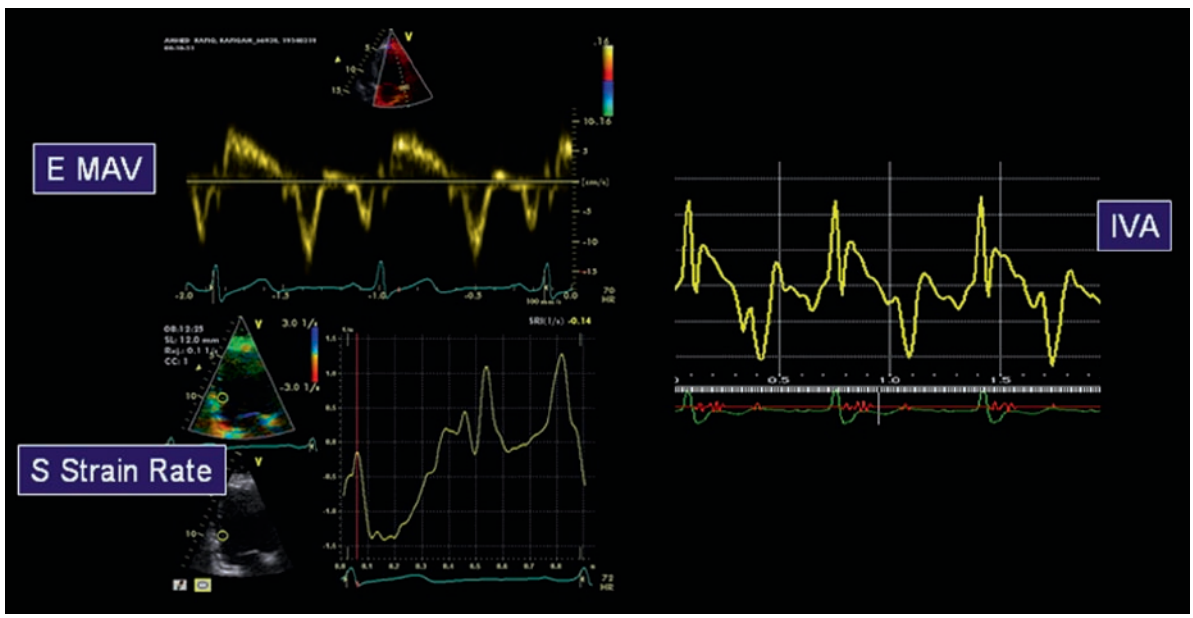

Fig. 5.12 Tissue Doppler imaging and derived modalities have provided indices of global LV systolic function that are not dependent on endocardial delineation and less dependent on loading conditions than conventional indices. These indices are early diastolic mitral annular velocity, systolic strain rate, and isovolumic acceleration during the pre-ejection period

Doppler strain and strain rate are more sensitive than tissue Doppler imaging and conventional echo, and have been shown to detect preclinical abnormalities in systolic function in patients with transplanted heart, diabetes mellitus, under antracycline or epirubicin therapy, aortic coarctation, hypo/hyperthyroidism, acromegaly, GH deficiency, obesity, and rheumatoid arthritis.

Atrial myocardial Doppler strain and strain rate predicted maintenance of sinus rhythm after cardioversion.

Limitations of Doppler Strain and Strain Rate

The main limitation relates to reproducibility including cardiac cycle-to-cycle variability (Fig. 5.9), variability from adjacent and overlapping ROI within the same myocardial segment in controls, and therefore, observer variability. Increasing ROI size, changing sample distance, and very high frame rate above 200/s do not totally solve these issues. There is spatial averaging of calculated strain and strain rate values within the ROI, and a large ROI decreases noise with a reduction in axial resolution. Artifacts related to translational motion, respiration, rib artifact, and ROI close to the border of the image sector must be identified. In theory peak systolic strain rate is the best available parameter for measuring segmental function. Strain rate is more volume independent than strain. Diastolic strain rate might be more specific than systolic strain rate for the diagnosis of ischemia. However, Doppler strain rate curves are noisy and require very high frame rate obtained with the narrowest image sector. Doppler strain is obtained through integration of the strain rate signal and integration reduces noise. Therefore, a very noisy strain rate signal may coexist with a less noisy strain signal of questionable value. Switching the drift compensation function off is a way of assessing the quality of Doppler strain and strain rate data.

As lateral resolution of Doppler strain is influenced by beam width, it is unclear whether reliable resolution exists to separate endocardial from epicardial strain in longitudinal axis. Doppler strain and strain rate are angle-dependent Doppler techniques and are mainly used for the assessment of longitudinal deformation. We must keep in mind that loading variations and myocardial stiffness are important determinants of myocardial deformation. Doppler strain and strain rate should only be reported when the signal is consistent. Careful analysis of normal subjects is crucial before interpreting patient recordings. At the present time, the use of TDI and strain requires specific training before it can be applied to the clinical decision-making process. These limitations may explain why Doppler strain and strain rate have not been included into international guidelines of ischemic heart disease, valvular heart disease, and cardiomyopathy.

Non-Doppler Tissue Velocity and Non-Doppler Strain

Non-Doppler strain, 2D strain, or Speckle tracking echocardiography (STE) is a recent imaging technique that enables an objective assessment of three myocardial deformation components: longitudinal, radial, and circumferential.[13]

Principle

Speckles are unique natural acoustic markers resulting from the interaction of ultrasound energy with tissue and are generated by the reflected ultrasound beam. Their size is 20–40 pixels. The speckle pattern is unique for each myocardial region and is relatively stable throughout the cardiac cycle. Each speckle can be identified and followed accurately over a number of consecutive frames. These markers are tracked by calculating frame-to-frame changes using a sum of absolute difference algorithm. The displacement of this speckled pattern is considered to follow myocardial movement, and a change between speckles represents myocardial deformation (strain). The geometric position of speckles changes from frame to frame with surrounding tissue motion. The geometric shift of each speckle represents local tissue movement. When tracking a defined region of speckles, a software algorithm extracts displacement, velocity, strain, and strain rate. Low image frame rate may not be adequate for strain rate calculations.

Using apical views, longitudinal velocity, longitudinal strain, and longitudinal displacement can be calculated as well as transverse displacement. In short-axis

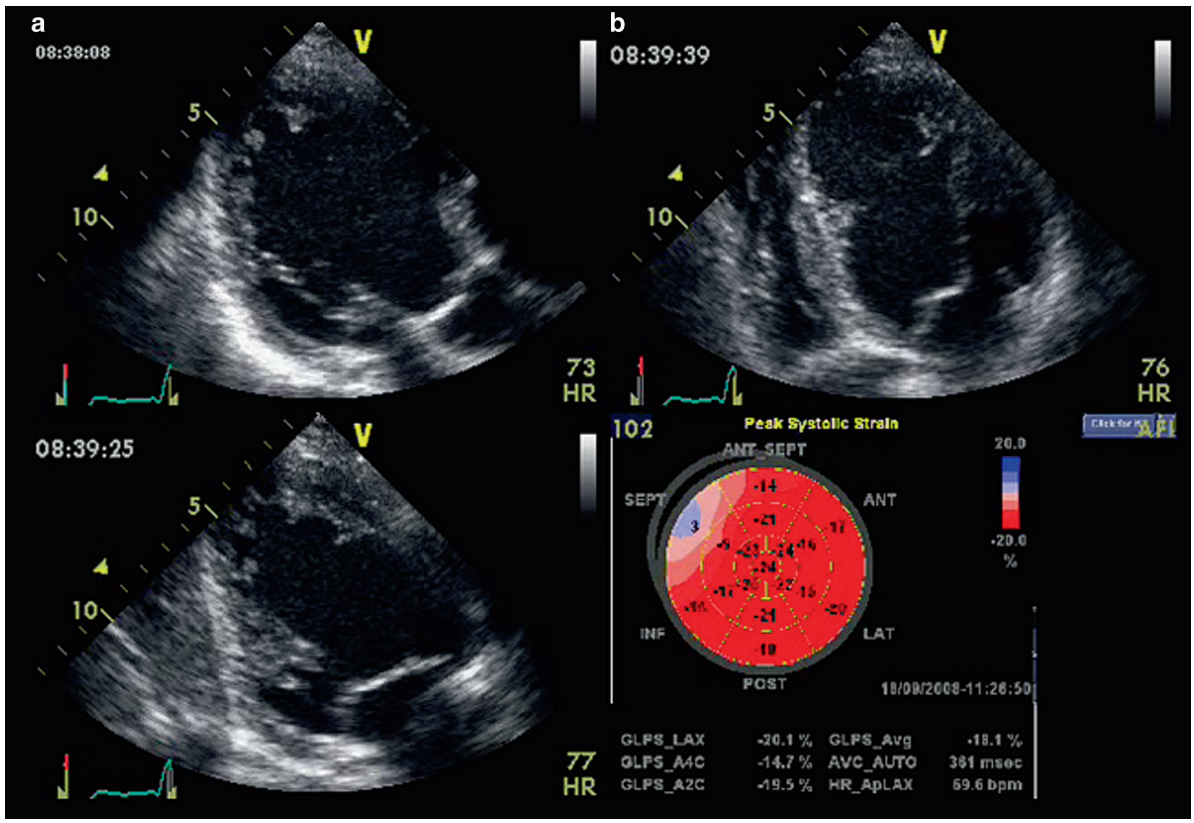

Fig. 5.13 (**a**) Radial non-Doppler peak systolic strain obtained in six myocardial segments from SAX view at mitral valve level in a patient with coronary artery disease. Radial strain is measured at the time of aortic valve closure. (**b**) Radial non-Doppler peak systolic strain obtained from SAX view at the apical level in the same patient. Radial strain is lower at the apex than at the base of the left ventricle

images radial strain (Fig. 5.13), radial displacement, circumferential strain, rotational velocity, and rotational strain can be calculated for all myocardial segments (Figs. 5.14–5.16).

Validation

Using in vivo and in vitro models, STE has been validated as an angle-independent measurement of myocardial strain showing good correlation and agreement with sonomicrometry and MRI tagging.

Requirements for Image Acquisition

Image acquisition for STE only requires storing a cineloop of a full cardiac cycle using conventional gray-scale imaging. Efforts should be made to visualize the endocardial border and obtain the best possible image quality. Frame rate must be between 40 and 90/s and is recommended to be above 70/s. Dual focus should not be used as it markedly decreases frame rate. Image sector width and depth are optimized to include only the region of interest. Optimization of gain and R wave amplitude on ECG trace are also required as well as breath holding. Harmonic imaging is now routinely used.

Postprocessing Analysis

STE analysis begins with the apical three-chamber view where aortic valve closure is visible. Aortic valve closure is automatically detected and could also be determined manually. Subsequently, R wave

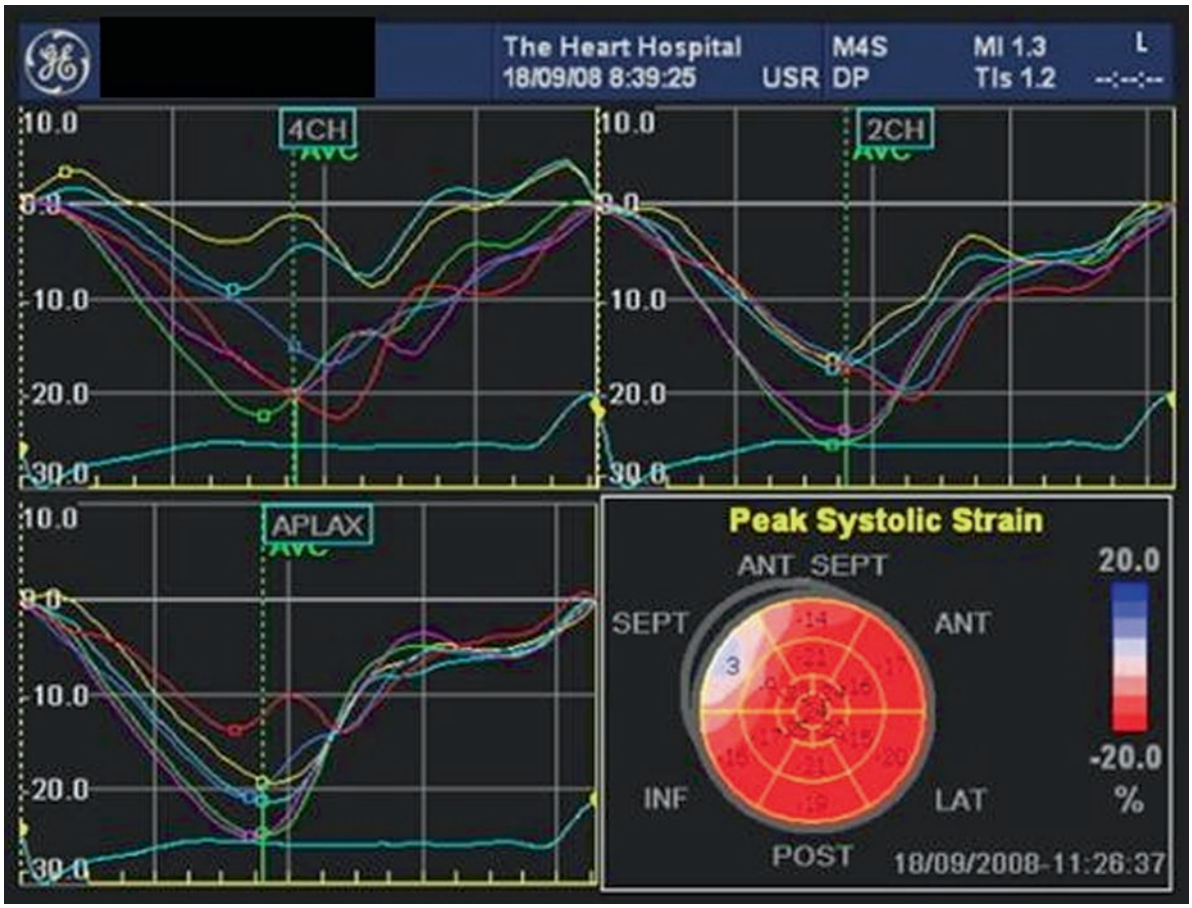

Fig. 5.14 The bull's eye diagram represents longitudinal peak systolic non-Doppler strain measured in all myocardial segments in a 25-year-old professional football player with LBBB. The three apical views recorded with conventional imaging are displayed to compare visual with quantitative assessment of regional wall motion abnormalities

to aortic valve closure time interval is used on the other views. This time interval is also checked against mitral valve opening, which is easily seen in apical views. End-systolic frames are used to trace endocardial border in a click-to-point approach, and the software automatically processes all frames of the loop. Three color-encoded parallel lines are created and should be moving with the myocardial walls. When image quality is suboptimal manual correction of the endocardial line is required to improve wall tracking throughout the cardiac cycle. Segmental wall tracking and analysis cannot be performed when the segment is poorly or not visualized and close to the image sector border. In addition to contour correction wall tracking width can be modified according to wall thickness in patients with dilated or hypertrophic cardiomyopathy.

The image is automatically divided into six segments, and parameters are generated for each segment based on the spatial and temporal shift of the corresponding acoustic markers. Results are shown as traces in specific diagrams successively displaying strain, displacement, and myocardial velocities.

Normal Values

Longitudinal, circumferential, and radial strain have been obtained in normal adults using STE. Normal

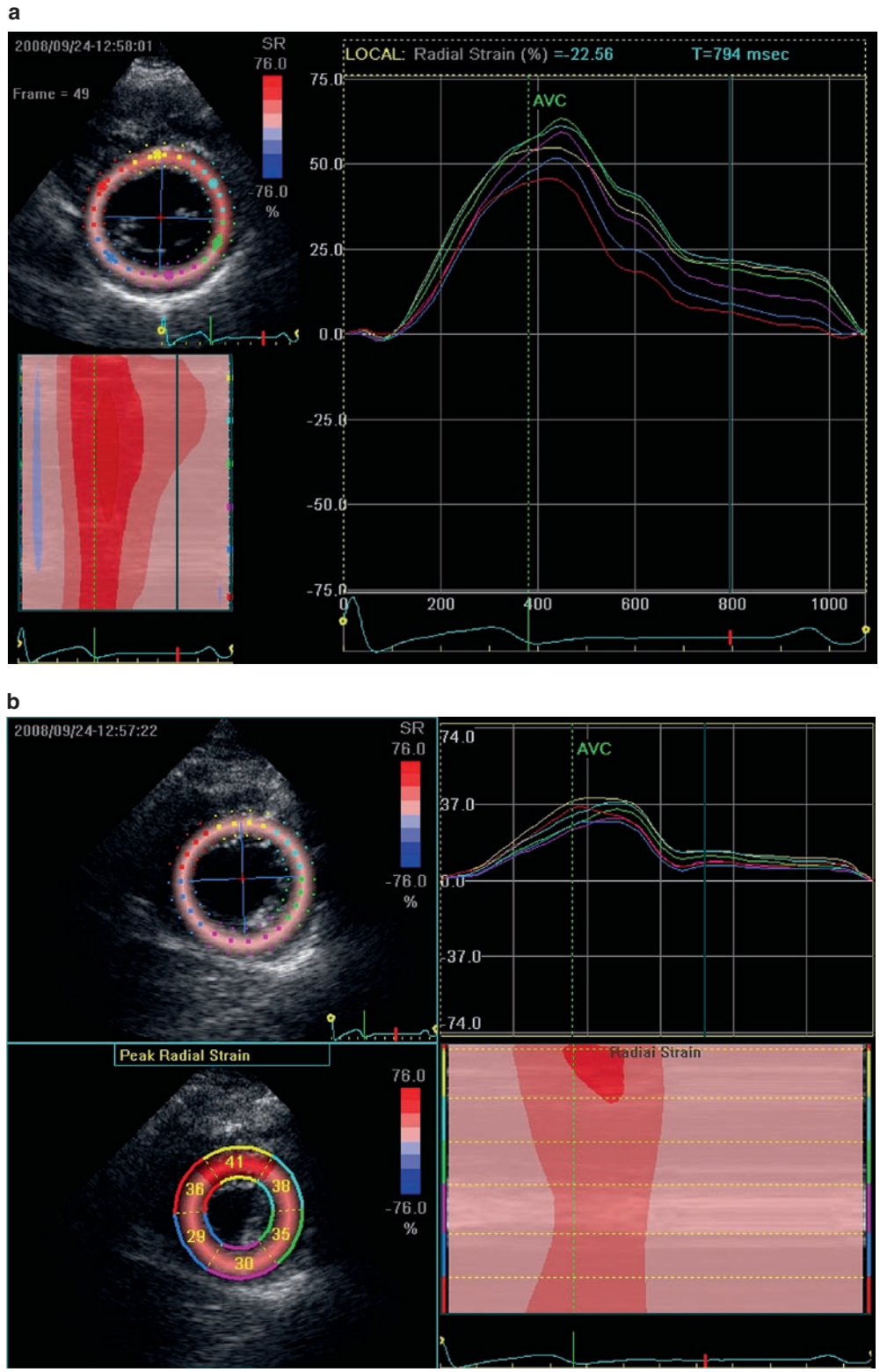

Fig. 5.15 Individual non-Doppler strain curves obtained in myocardial segments of each apical view in the same patient as in Fig. 5.13. Septal strain curves are clearly identified

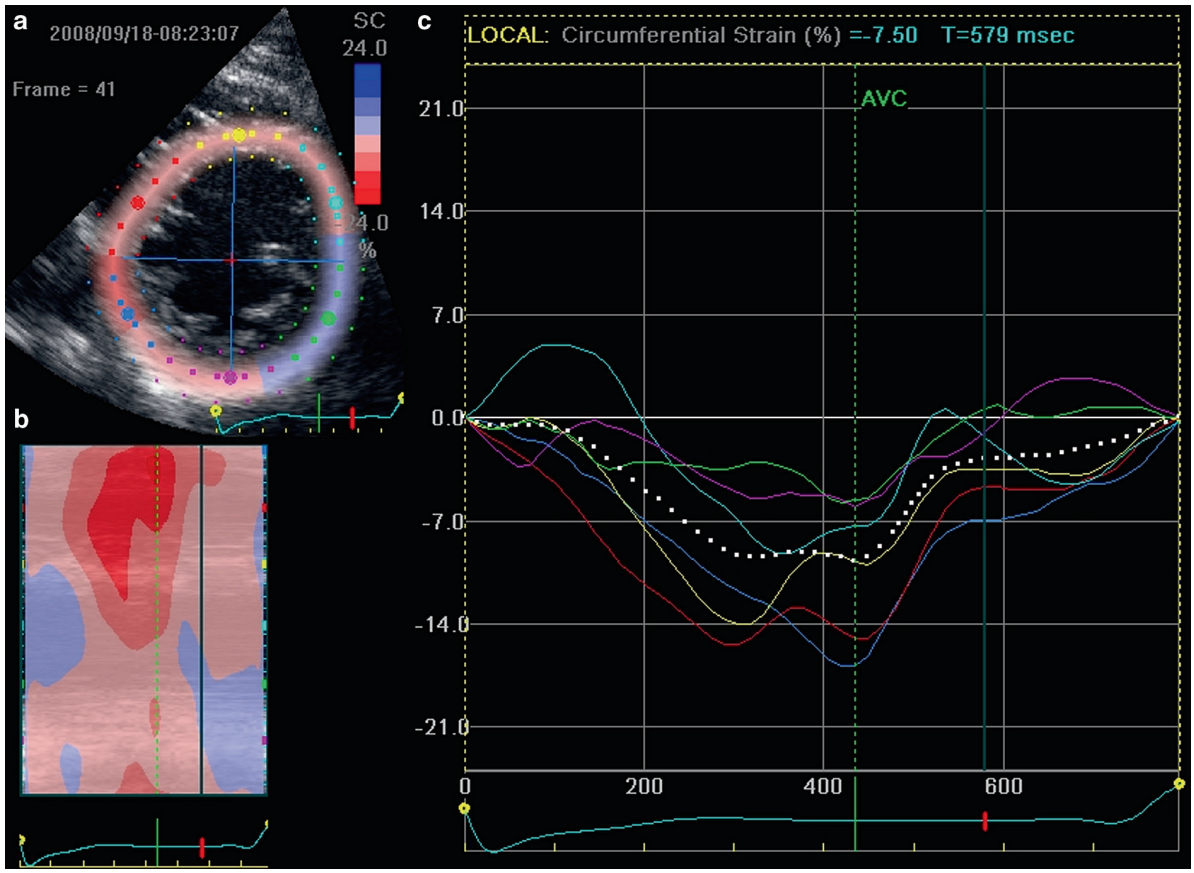

Fig. 5.16 (**a**) Rotation of the base of the left ventricle in 6 myocardial segments throughout the cardiac cycle calculated from the SAX view at mitral valve level. (**b**) Rotation of the left ventricular apex throughout the cardiac cycle in the corresponding segments in the same patient. (**c**) The white line represents the torsion of the left ventricle throughout the cardiac cycle. Amplitude and timing of maximal torsion are visualized and measured

values were 19 ± 4% for longitudinal midseptal strain, 37 ± 17% for radial basal posterior strain, 21 ± 7% for circumferential basal posterior strain, −10.9 ± 3.3 for apical rotation, 4.6 ± 1.3 for basal rotation, and −14.5 ± 3.2 for torsion, respectively.[13-15]

Advantages of STE Over Doppler-Derived Deformation Imaging

Image acquisition is less demanding and all myocardial segments can be interrogated. In contrast to tissue Doppler-derived parameters, STE is an angle-independent technique as the movement of speckles can be followed in any direction. In addition to radial and longitudinal parameters, circumferential parameters, ventricular rotation, and twist can be obtained[13,14] and three components of deformation (longitudinal, radial, and circumferential) are assessed. This is useful in patients without longitudinal motion. STE has better lateral resolution than tissue Doppler echocardiography due to higher density of scan lines on conventional echocardiography. STE also has better reproducibility as it does not require manual positioning of ROI, choice of ROI size, and ROI tracking. This technique generates bull's eye plot of longitudinal global and segmental peak systolic strain (Figs. 5.14 and 5.15). A similar technique uses arrows to display the direction and amplitude of motion at various points

in the heart. Intra- and interobserver variability were found to be lower ranging from 3.6 to 5.3% and 7 to 11.8%, respectively.

As speckle tracking is not dependent on the angle of ultrasound beam or aliasing, experimental studies have tested the feasibility of STE for flow quantification. Preliminary results indicate the ability of speckle tracking to measure laminar flow in a phantom at a beam–vessel angle of 60°.

Applications

Regional LV function can be assessed by frame-by-frame tracking of acoustic markers in 2D echocardiographic images. Left ventricular torsion plays an important role with respect to LV ejection and filling. During the cardiac cycle, there is a systolic twist and an early diastolic untwist of the LV on its long axis because of oppositely directed apical and basal rotations (Fig. 5.16). The magnitude and characteristics of this torsion deformation are a useful tool to assess LV systolic performance. Previously this component of LV contraction was only assessable by MRI tagging, and implementation has therefore been limited by complexity and cost. STE has demonstrated to provide accurate measurement of regional LV rotation and torsion[13,14] with good correlation with sonomicrometry ($r = 0.94$, $P = 0.001$) and MRI ($r = 0.85$, $P = 0.001$).

Global longitudinal non-Doppler strain and strain rate have shown high sensitivity and specificity for the diagnosis of postmyocardial infarction patients.[16] Radial and circumferential non-Doppler strain has shown the ability to describe regional LV function assessed by MRI.

During stress echocardiography evaluation of regional left ventricular abnormalities is subjective, requires expertise, and is at best semiquantitative. A validation of speckle-derived longitudinal, circumferential, and radial strain has been performed during dobutamine stress using an open-chest animal model showing good correlation and agreement between STE and sonomicrometry at rest and during stress. Longitudinal and circumferential strains were abnormal at rest during flow-limiting stenosis and during stress with nonflow-limiting stenosis, whereas radial strain was only abnormal during stress in the setting of flow-limiting stenosis. However, the non-Doppler strain technique does have tracking problems at peak stress in humans which may be related to hyperdynamic LV contractility and excessive annular motion in the base, making this technique challenging in the posterolateral circulation.[17]

Quantification of left ventricular dyssynchrony by echocardiography has emerged as an important potential means to predict improvement of symptoms and positive LV remodeling after cardiac resynchronization therapy in patients with severe chronic heart failure.[18,19] (Several studies suggested that measures of mechanical dyssynchrony by cardiac imaging are superior markers of response to cardiac resynchronization therapy compared with QRS duration.[18,19)] STE radial LV dyssynchrony predicts both immediate and long-term response to cardiac resynchronization therapy.[20] STE detected radial dyssynchrony in a subset of patients with apical dysfunction who showed a favorable response to CRT, although they did not appear to have dyssynchrony by routine longitudinal tissue Doppler assessment. Circumferential STE delay was significantly lower in responders than in nonresponders to CRT and was improved by CRT. In patients with hypertrophic cardiomyopathy non-Doppler strain identified subclinical global systolic dysfunction. There was a good correlation in peak velocity and deformation values but moderate correlation in time intervals between STE and tissue Doppler imaging for the quantification of regional RV function.

Limitations

Poor image quality induces poor wall tracking which may be improved by alterations of endocardial border detection (Fig. 5.17). At present, STE algorithm does not work on contrast images. Non-Doppler strain rate may not be reliable when the frame rate is too low. Assessment of wall thickness is mandatory before image processing. In patients with apical hypertrophic cardiomyopathy increased wall thickness at the apex is often responsible for incorrect wall tracking especially in patients with apparent apical hypokinesia on conventional images (Fig. 5.18). As parameters are averaged over the whole myocardial segment, small regions of myocardial dysfunction may be overlooked. During the early stages of arrhythmogenic right ventricular cardiomyopathy localized right ventricular akinetic

a

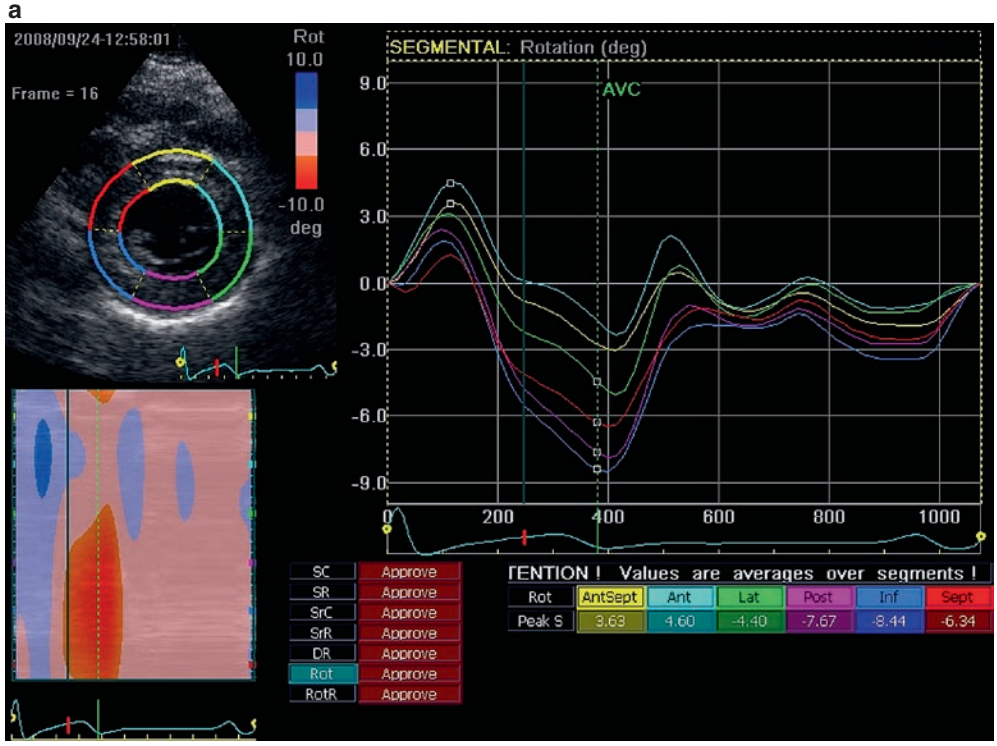

b

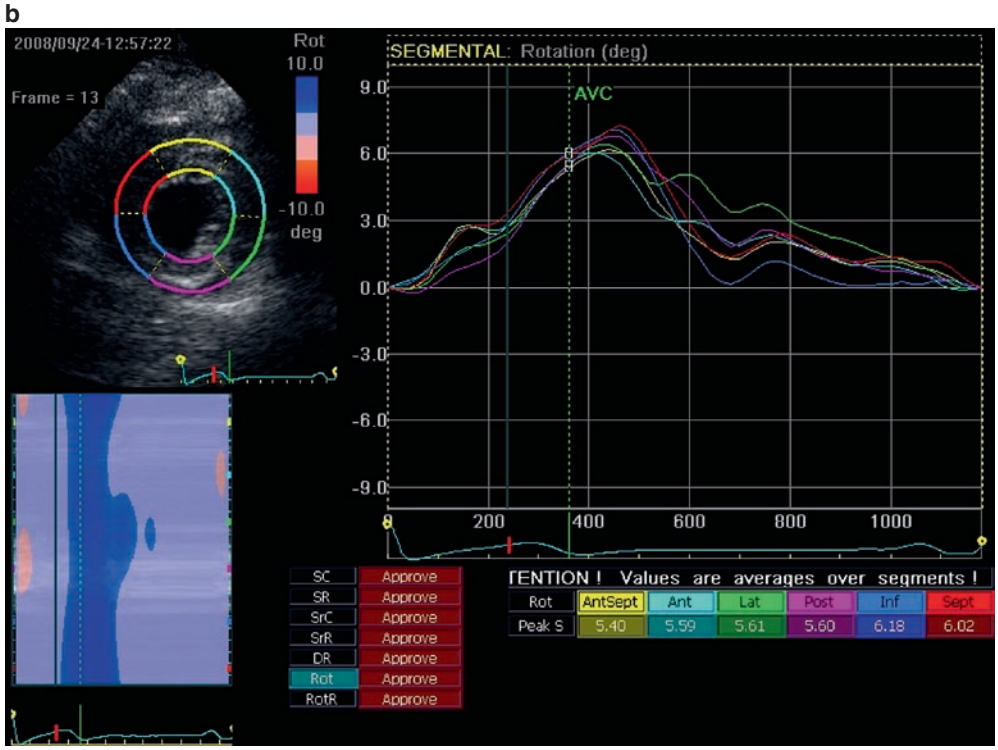

(continued)

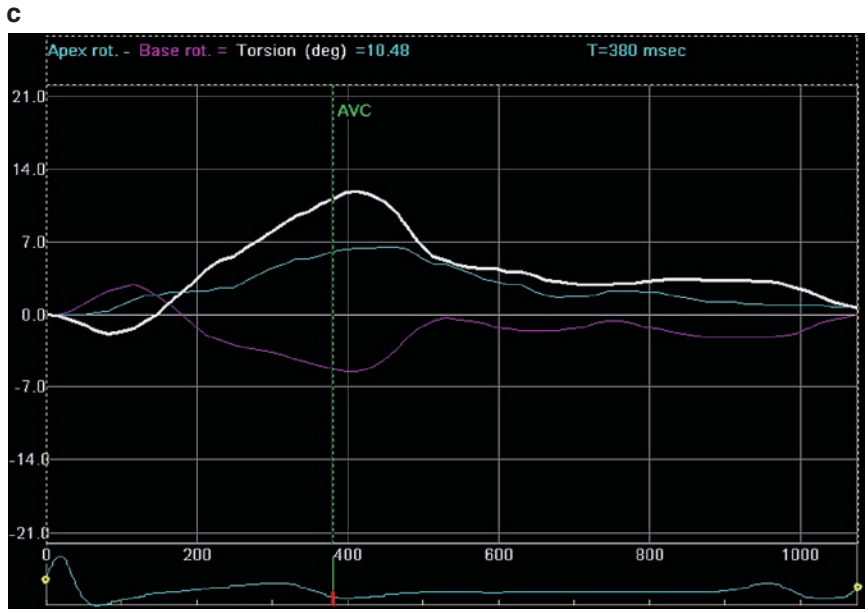

Fig. 5.17 (**a**) Longitudinal non-Doppler strain curves in a patient with suboptimal 2D images showing no segmental abnormalities. (**b**) After contour correction, peak systolic strain was reduced in basal inferior wall and in half of basal infero septum and posterior wall. Wall tracking correction should be performed when wall tracking is not moving with the myocardial walls

areas with diastolic bulging and regional right ventricular hypokinesia may not be detected by STE. Tracking problems at rapid heart rates have been described.[17] Other limitations are related to the out-of-plane motion of speckles, dropouts, and the ability to track speckles with sufficient temporal resolution. Radial strain measurements did not correlate well with sonomicrometry, demonstrated larger variability, and have been measured in fewer locations compared with longitudinal strain. Although speckle-derived strain has been validated in various circumstances this recent technique needs further supporting data to extend its use in clinical practice.

Conclusion

The improvement of diagnostic tools for an optimal assessment of global and regional myocardial performance is a work in progress. These techniques add substantial information on myocardial function compared with conventional echocardiography. Doppler and non-Doppler deformation parameters have provided new indices of global LV systolic performance that are not dependent on endocardial definition and less dependent on loading conditions. These modalities are more sensitive than conventional echo in the detection of early abnormalities in systolic and diastolic function in a large range of cardiac diseases. Tissue Doppler imaging is more sensitive than conventional echocardiography, and strain/strain rate are more sensitive than myocardial velocities. Noninvasive hemodynamic assessment of LV filling pressure is currently one of the main applications of the technique. Myocardial velocity and deformation appear to be of optimal value if image acquisition and analysis are meticulous and the interpretation careful. However, the limitations, the lack of randomized and blinded studies in large populations, and the lack of outcome data may explain why these techniques have not yet been included into international guidelines of ischemic heart disease, valvular heart disease, and cardiomyopathy. Technical progresses may improve reproducibility and wider clinical use.

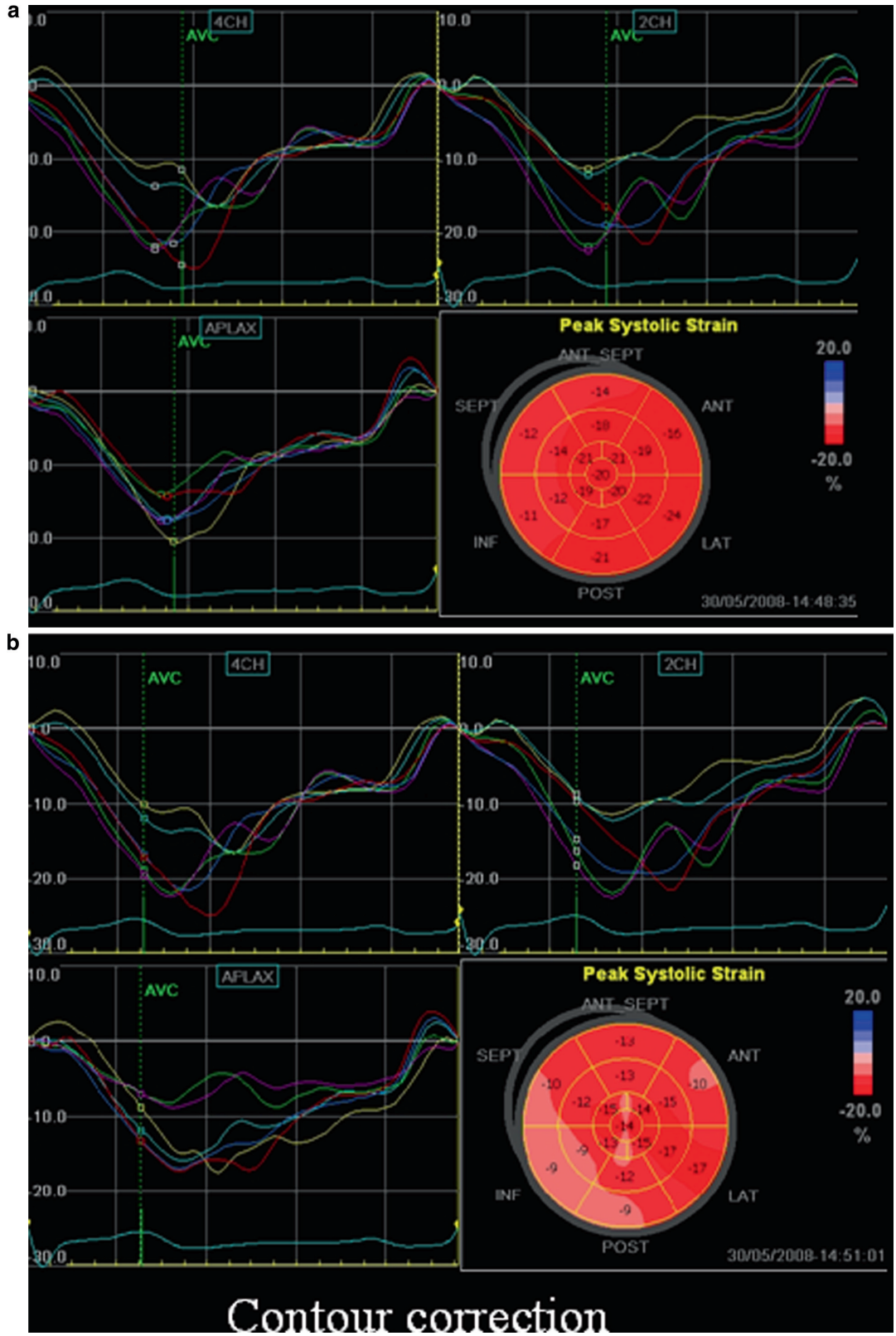

Fig. 5.18 Endocardial border delineation at the apex is challenging as the apex is in the near field of the image sector. (**a**) Longitudinal non-Doppler strain curves in a patient with apical hypertrophic cardiomyopathy showing paradoxical deformation of the apical region. (**b**) After contour correction, peak systolic strain values were highest at the apex

References

1. Sutherland GR, Bijnens B, McDicken WN. Tissue doppler echocardiography: historical perspective and technological considerations. *Echocardiography*. 1999;16:445–453.
2. Derumeaux G, Ovize M, Loufoua J, Pontier G, Andre-Fouet X, Cribier A. Assessment of nonuniformity of transmural myocardial velocities by color-coded tissue Doppler imaging: characterization of normal, ischemic, and stunned myocardium. *Circulation*. 2000;101:1390–1395.
3. Pellerin D, Berdeaux A, Cohen L, Giudicelli JF, Witchitz S, Veyrat C. Comparison of 2 myocardial velocity gradient assessment methods during dobutamine infusion with Doppler myocardial imaging. *J Am Soc Echocardiogr*. 1999;12:22–31.
4. Ommen SR, Nishimura RA, Appleton CP, et al. Clinical utility of Doppler echocardiography and tissue Doppler imaging in the estimation of left ventricular filling pressures: a comparative simultaneous Doppler-catheterization study. *Circulation*. 2000;102:1788–1794.
5. Ho CY, Sweitzer NK, McDonough B, et al. Assessment of diastolic function with Doppler tissue imaging to predict genotype in preclinical hypertrophic cardiomyopathy. *Circulation*. 2002;105:2992–2997.
6. Garcia MJ, Rodriguez L, Ares M, Griffin BP, Thomas JD, Klein AL. Differentiation of constrictive pericarditis from restrictive cardiomyopathy: assessment of left ventricular diastolic velocities in longitudinal axis by Doppler tissue imaging. *J Am Coll Cardiol*. 1996;27:108–114.
7. D'Hooge J, Heimdal A, Jamal F, et al. Regional strain and strain rate measurements by cardiac ultrasound: principles, implementation and limitations. *Eur J Echocardiogr*. 2000;1:154–170.
8. Greenberg NL, Firstenberg MS, Castro PL, et al. Doppler-derived myocardial systolic strain rate is a strong index of left ventricular contractility. *Circulation*. 2002;105:99–105.
9. Voigt JU, Arnold MF, Karlsson M, et al. Assessment of regional longitudinal myocardial strain rate derived from doppler myocardial imaging indexes in normal and infarcted myocardium. *J Am Soc Echocardiogr*. 2000;13:588–598.
10. Larrazet F, Pellerin D, Prigent A, Daou D, Cohen L, Veyrat C. Quantitative analysis of hibernating myocardium by dobutamine tissue Doppler echocardiography. *Am J Cardiol*. 2001;88:418–422.
11. Palka P, Lange A, Fleming AD, et al. Differences in myocardial velocity gradient measured throughout the cardiac cycle in patients with hypertrophic cardiomyopathy, athletes and patients with left ventricular hypertrophy due to hypertension. *J Am Coll Cardiol*. 1997;30:760–768.
12. Dutka DP, Donnelly JE, Palka P, Lange A, Nunez DJ, Nihoyannopoulos P. Echocardiographic characterization of cardiomyopathy in Friedreich's ataxia with tissue Doppler echocardiographically derived myocardial velocity gradients. *Circulation*. 2000;102:1276–1282.
13. Helle-Valle T, Crosby J, Edvardsen T, et al. New noninvasive method for assessment of left ventricular rotation: speckle tracking echocardiography. *Circulation*. 2005;112:3149–3156.
14. Notomi Y, Lysyansky P, Setser RM, et al. Measurement of ventricular torsion by two-dimensional ultrasound speckle tracking imaging. *J Am Coll Cardiol*. 2005;45:2034–2041.
15. Hurlburt HM, Aurigemma GP, Hill JC, et al. Direct ultrasound measurement of longitudinal, circumferential, and radial strain using 2-dimensional strain imaging in normal adults. *Echocardiography*. 2007;24:723–731.
16. Leitman M, Lysyansky P, Sidenko S, et al. Two-dimensional strain-a novel software for real-time quantitative echocardiographic assessment of myocardial function. *J Am Soc Echocardiogr*. 2004;17:1021–1029.
17. Hanekom L, Cho GY, Leano R, Jeffriess L, Marwick TH. Comparison of two-dimensional speckle and tissue Doppler strain measurement during dobutamine stress echocardiography: an angiographic correlation. *Eur Heart J*. 2007;28:1765–1772.
18. Sogaard P, Egeblad H, Kim WY, et al. Tissue Doppler imaging predicts improved systolic performance and reversed left ventricular remodeling during long-term cardiac resynchronization therapy. *J Am Coll Cardiol*. 2002;40:723–730.
19. Yu CM, Chau E, Sanderson JE, et al. Tissue Doppler echocardiographic evidence of reverse remodeling and improved synchronicity by simultaneously delaying regional contraction after biventricular pacing therapy in heart failure. *Circulation*. 2002;105:438–445.
20. Suffoletto MS, Dohi K, Cannesson M, Saba S, Gorcsan J, 3rd. Novel speckle-tracking radial strain from routine black-and-white echocardiographic images to quantify dyssynchrony and predict response to cardiac resynchronization therapy. *Circulation*. 2006;113:960–968.

Chapter 6
Transesophageal Echocardiography: Principles and Application

Partho P. Sengupta and Bijoy K. Khandheria

Transesophageal echocardiography (TEE) involves ultrasound imaging of cardiovascular system from the confines of the gastroesophageal track. This helps reduce signal attenuation and permits the use of higher ultrasound frequencies, thereby providing an enhanced spatial resolution.

TEE for recording continuous-wave Doppler velocities of cardiac flow was first described by Side and Josling in 1971.[1] Subsequently, the first transesophageal M-mode echocardiogram was reported by Frazin et al in 1976,[2] while Hisanaga et al in 1977 illustrated the use of cross-sectional real-time imaging using a scanning device that consisted of a rotating single element in an oil-filled balloon mounted at the tip of the gastroscope.[3] One year after their first report, Hisanaga et al also described a linear mechanical scanner that was suitable for transesophageal echocardiographic studies, but its applications were limited due to rigidity of the mechanical sector scanning device. The initial acceptance of TEE was offset by the logistic difficulties of introducing rigid endoscopes. In 1982, Jacques Souquet produced the first mono- and multiplane electronic phased-array probes. The ensuing technological developments that facilitated the transition of TEE to its present clinical status included the introduction of flexible endoscope, miniaturization and improvements in transducer designs, serial improvement in scanning capabilities from monoplane, biplane to multiplane views (Table 6.1), and the addition of spectral and color Doppler imaging. TEE is currently used in approximately 5–10% of patients being evaluated in the cardiovascular ultrasound imaging and hemodynamic laboratory.

P.P. Sengupta (✉) and B.K. Khandheria
Cardiovascular Division, Mayo Clinic Arizona,
Scottsdale, AZ, USA
e-mail: sengupta.partho@mayo.edu

Patient Preparation and Instrumentation

TEE can be performed as an outpatient or inpatient procedure. Fasting based on conscious sedation guidelines, an intravenous access, careful history to rule out presence of laryngeal or gastroesophageal diseases, and removal of dentures are prerequisites.

- Absolute contraindications to TEE include esophageal stricture, diverticulum, tumor, and recent esophageal or gastric surgery.
- Topical spray, intravenous sedation, a drying agent to minimize oral secretion and use of appropriate lubrication are helpful. Although the risk of bacterial endocarditis is extremely low and routine antibiotic prophylaxis before TEE is not advocated, occasionally, some high-risk patients such as those with prosthetic valves, multivalvular involvement, or those with a past history of infective endocarditis may require antibiotic prophylaxis. However, there is no sufficient scientific evidence that even this is necessary and the practice largely depends on local protocols.
- Before the introduction of the scope into the esophagus, the array is rotated to 0° to place the transducer into a conventional transverse plane. A bite guard is used always unless the patient is edentulous. Placing the imaging surface facing the tongue directs the ultrasound beam toward the anterior chest wall while the transducer is in the esophagus. The tip of the transducer is advanced into the esophagus gently without force and stopped if any resistance is encountered. After moving the transducer into the desired location, the probe is manipulated to orient the imaging planes for obtaining the desired cross-sectional images. The multiplane TEE transducer

P. Nihoyannopoulos and J. Kisslo (eds.), *Echocardiography*,
DOI: 10.1007/978-1-84882-293-1_6, © Springer-Verlag London Limited 2009

Table 6.1 Transesophageal echocardiography cross-sections

Window (depth from incisors)	Cross-section	Multiplane angle range (°)	Structures imaged
Upper esophageal (20–25 cm)	Aortic arch long axis (s)	0	Aortic arch, left brachio v
	Aortic arch short axis (t)	90	Aortic arch, PA, PV, left brachio v
Midesophageal (30–40 cm)	Four chamber (a)	0–20	LV, LA, RV, RA, MV, TV, IAS
	Mitral commissural (g)	60–70	MV, LV, LA
	Two chamber (b)	80–100	LV, LA, LAA, MV, CS
	Long axis (c)	120–160	LV, LA, AV, LVOT, MV, asc aorta
	RV inflow-outflow (m)	60–90	RV, RA, TV, RVOT, PV, PA
	AV short axis (h)	30–60	AV, IAS, coronary ostia, LVOT, PV
	AV long axis (i)	120–160	AV, LVOT, prox asc aorta, right PA
	Bicaval (l)	80–110	RA, SVC, IVC, IAS, LA
	Asc aortic short axis (o)	0–60	Asc aorta, SVC, PA, right PA
	Asc aortic long axis (p)	100–150	Asc aorta, right PA
	Desc aorta short axis (q)	0	Desc thoracic aorta, left pleural space
	Desc aorta long axis (r)	90–110	Desc thoracic aorta, left pleural space
Transgastric (40–45 cm)	Basal short axis (f)	0–20	LV, MV, RV, TV
	Midshort axis (d)	0–20	LV, RV, pap mm
	Two chamber (e)	80–100	LV, MV, chordae, pap mm, CS, LA
	Long axis (j)	90–120	LVOT, AV, MV
	RV inflow (n)	100°–120°	RV, TV, RA, TV chordae, pap mm
Deep transgastric (45–50 cm)	Long axis (k)	0°–20° (anteflexion)	LVOT, AV, asc aorta, arch

Reproduced with permission from the recommendations of American Society of Echocardiography[4]

Brachio v Brachiocephalic vein; *PA* pulmonary artery; *PV* pulmonic valve; *LV* left ventricle; *LA* left atrium; *RV* right ventricle; *RA* right atrium; *MV* mitral valve; *TV* tricuspid valve; *IAS* interatrial septum; *LAA* left atrial appendage; *CS* coronary sinus; *AV* aortic valve; *LVOT* left ventricular outflow tract; *prox* proximal; *RVOT* right ventricular outflow tract; *SVC* superior vena cava; *IVC* inferior vena cava; *RPA* right pulmonary artery; *asc* ascending; *desc* descending; *pap mm* papillary muscles

consists of a single array of crystals that can be electronically and mechanically rotated in an arc of 180° (Figs. 6.1–6.4). Scanning along desired planes is obtained by observing the images develop as the probe is manipulated, rather than by relying on the depth markers on the probe or the angle icon. There are individual variations in the anatomic relationship of the esophagus to the heart; in some patients, the esophagus lies adjacent to the lateral portion of the atrioventricular groove, whereas in others it is positioned directly posterior to the left atrium. This relationship is taken into consideration when developing each desired cross-sectional view.

- Although each of the views represents echocardiographic image in cross-section, moving the probes through the entire extent of a structure permits a rapid 3-D evaluation of cardiac structures. Although the TEE study needs to examine all the regions of the heart and great vessels, examination can be initially targeted for resolving the primary issue for which TEE is being performed. Almost all views obtained by surface echocardiography can be duplicated by TEE.

Left Ventricle

From the midesophagus, LV can be visualized by positioning the transducer posterior to the LA.

0–20°: The four-chamber view is obtained by rotating the multiplane angle from 0 to 10–20°.

80–100°: Midesophageal two-chamber view is developed by rotating the angle by 80–100°. Internal landmarks consist of the left atrial appendage and coronary sinus.

120–160°: For obtaining the long-axis view, the angle is further rotated between 120 and 160°. Here the LV outflow and the ascending aorta can well be visualized.

Transgastric views: The transgastric views of the LV are acquired by advancing the probe into the

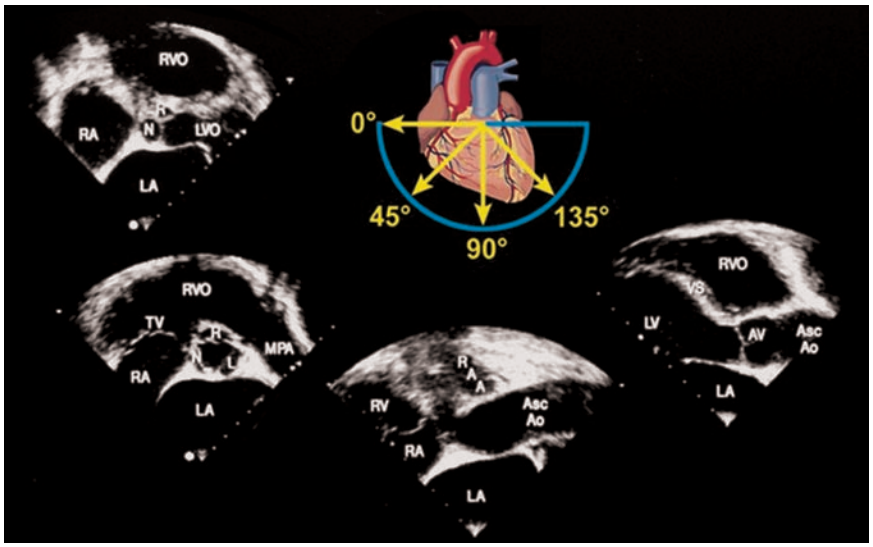

Fig. 6.1 Multiplane transesophageal echocardiographic views (0, 45, 90, and 135°) obtained from midesophagus. (*RA* right atrium; *RAA* right atrial appendage; *TV* tricuspid valve; *RV* right ventricle; *LA* left atrium; *LV* left ventricle; *LVO* left ventricle outflow; *Asc Ao* ascending aorta; *MPA* main pulmonary artery; *R*, *L,* and *N* right, left, and noncoronary aortic sinus). Reproduced with permission from the BMJ Publishing Group. Sengupta PP, Khandheria. Transoesophageal echocardiography. *Heart*. 2005;91(4):541-547

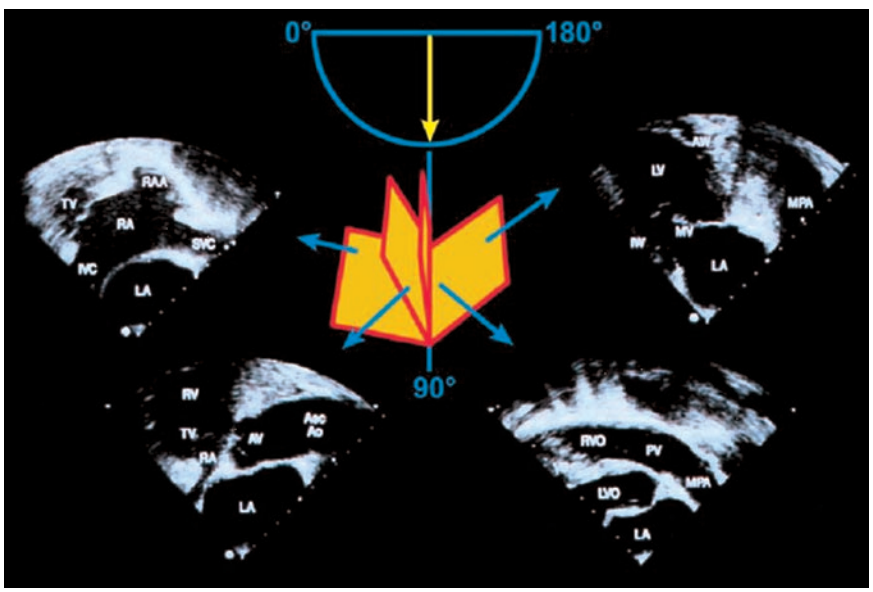

Fig. 6.2 Series of longitudinal views obtained with tip of transducer in midesophagus. The shaft of the scope is rotated to patient's left for obtaining optimal image of the mitral valve (MV) and the left ventricular (LV) inflow views. Sequence of longitudinal views is obtained by progressively rotating the shaft of scope to the patient's right. (*RA* right atrium; *RAA* right atrial appendage; *TV* tricuspid valve; *RV* right ventricle; *LA* left atrium; *LV* left ventricle; *MV* mitral valve; *MPA* main pulmonary artery; *SVC* superior vena cava; *IVC* Inferior vena cava)

stomach and anteflexing the tip. The short-axis view appears at 0°, whereas the long-axis view appears at 90°. The transgastric short-axis view of the LV at the level of midsegment is used for assessing LV chamber size, wall thickness, and chamber functions.

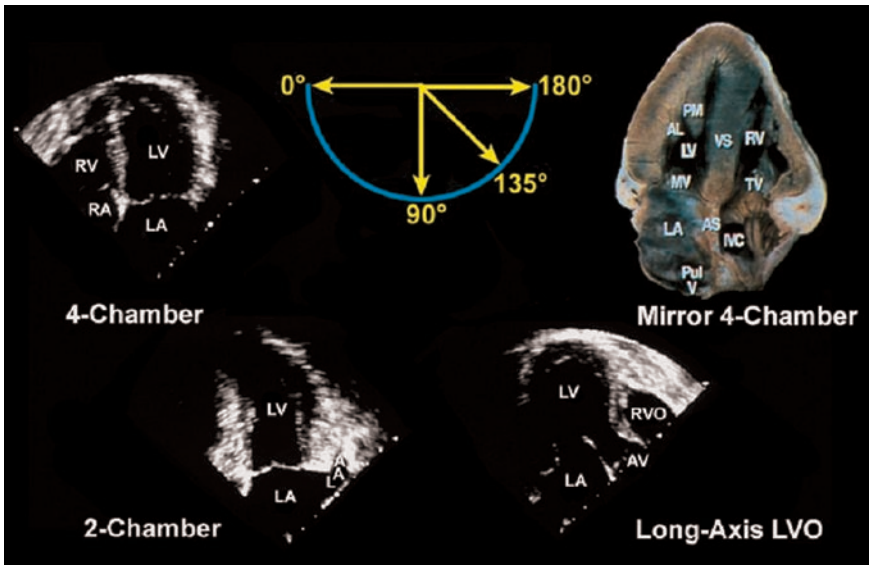

Fig. 6.3 Series of multiplane apical long-axis TEE views obtained by rotating the probe through 0, 90, 135, and 180°. The two-chamber view is comparable to midesophageal two-chamber view but with the transducer retroflexed and cardiac apex displayed upward. Long-axis view is comparable to midesophageal long-axis view of left ventricular outflow but with transducer retroflexed and cardiac apex displayed upward. (*Pul V* pulmonary vein; *VS* ventricular septum; *PM* papillary muscle; *LV* left ventricle; *MV* mitral valve; *TV* tricuspid valve). Reproduced with permission from the BMJ Publishing Group. Sengupta PP, Khandheria. Transoesophageal echocardiography. *Heart*. 2005;91(4):541-547

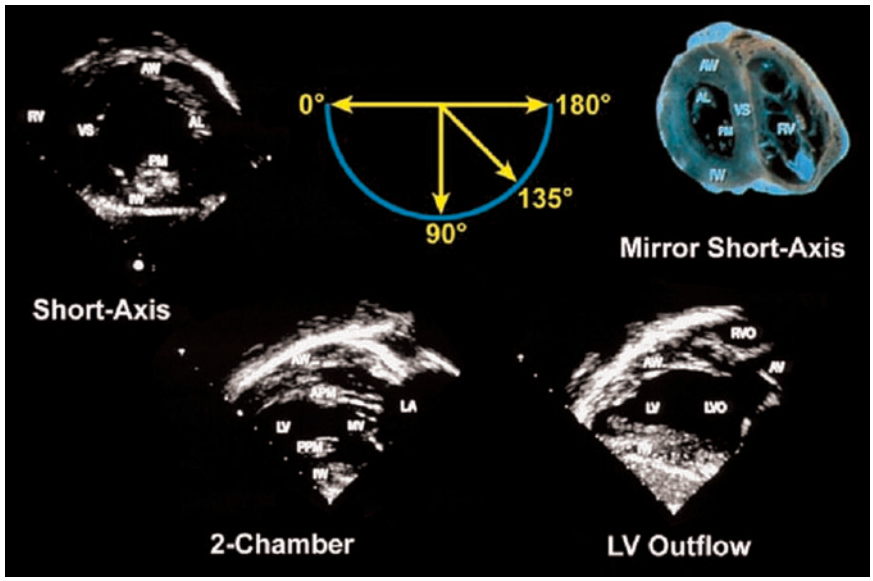

Fig. 6.4 Series of multiplane transgastric views. With tip of transducer in a stable transgastric position, the probe is rotated to obtain an array of short- and long-axis views. (*AW* anterior wall; *IW* inferior wall; *VS* ventricular septum; *AL* anterolateral papillary muscle; *PM* posteromedial papillary muscle; *RVO* right ventricular outflow; *LA* left atrium; *LV* left ventricle; *LVO* left ventricle outflow; *VS* ventricular septum)

Mitral Valve

The mitral valve is examined on TEE by using the four midesophageal and two transgastric views. The transmitral flow velocity profile is examined using spectral pulsed-wave Doppler (PWD) to evaluate LV diastolic function in the midesophageal four chamber or midesophageal long-axis view by placing the sample volume between the tips of the open mitral leaflets.

0–20 degrees: The mitral valve leaflets in this view are visualized along the 4-C chamber view. The posterior mitral leaflet P1 is to the right of the image display, and the anterior mitral leaflet A3 is to the left.

60–70 degrees: Further rotation of the imaging plane aligns it parallel to the line that intersects the two commissures of the mitral valve. Leaflet A2 is seen in the middle, while leaflets P1 and P3 are seen on the right and left sides, respectively.

80–100 degrees: This results in midesophageal two-chamber view in which leaflet P3 is displayed to the left and the leaflet A1 is on the right.

120–160 degrees: This forms the midesophageal long-axis view in which the posterior mitral leaflet P2 is to the left of the display and the anterior leaflet A2 is to the right.

The transgastric basal short-axis view provides a short-axis view of the MV and is generally obtained at a multiplane angle of 0°. The transgastric two-chamber view is useful for examining the chordae tendinae, which lie perpendicular to the ultrasound beam in this view.

Aortic Valve

Midesophagus: Once the aortic valve is viewed during its short axis from the transducer positioned in the midesophagus, the angle is further rotated to approximately 30–60° until a symmetrical image of all three cusps comes into view.

120–130 degrees: The long-axis view is the best for assessing the size of the aortic root by measuring the diameters of the AV annulus, sinuses of Valsalva, sinotubular junction, and proximal ascending aorta.

The transgastric views: Detailed evaluation of the valve anatomy is difficult in these views because the LV outflow tract and the aortic valve are located in the far field. Thus these views are primarily reserved for directing Doppler beam parallel to flow through the aortic valve, which is not possible from the midesophageal window. The transgastric long-axis view is developed by rotating the multiplane angle to 90–120°. For developing the deep transgastric view, the probe is advanced deep into stomach and flexed, turned, rotated, and advanced gradually with trial and error for developing an optimum view.

Left Atrium

Examination of the left atrium (LA) is initiated with the midesophageal four-chamber view. From midesophageal four-chamber view, the multiplane angle is rotated through 90° for obtaining orthogonal view of the LA. In each of the views the entire chamber and its contents can be examined by panning the probe from top to bottom or by turning the probe from side to side. In the four-chamber view, the left atrial appendage (LAA) can be seen to open near the superior and lateral aspect of LA. The left upper pulmonary vein (LUPV) enters the LA just lateral to the LAA.

The left lower pulmonary vein (LLPV) enters the LA just below the LUPV and is then identified by turning the transducer slightly farther to the left and advancing 1–2 cm (Fig. 6.5).

In the four-chamber view, the right upper pulmonary vein (RUPV) is imaged by turning the probe to the right at the level of the LAA. Like the LUPV, the RUPV can be seen entering the LA in an anterior to posterior direction. The right lower pulmonary vein, which enters the LA nearly at a right angle to the Doppler beam, can be identified by turning the probe slightly to right and advancing the probe by 1–2 cm.

90 degrees: The interatrial septum (IAS) is examined at the midesophageal level by moving the probe slightly to the right of midline and advancing and withdrawing the probe through its entire superior-inferior extent. From the midesophageal four-chamber view, the multiplane angle is rotated forward to approximately 90. The LAA is seen as an outpouching of the lateral, superior aspect of the LA. From there, the LUPV is identified by turning the probe slightly farther to the left.

80–110 degrees: The bicaval view is developed from the midesophageal two-chamber view by turning the probe to the right and rotating the multiplane angle forward between 80 and 110° until both the superior vena cava (SVC) and the inferior vena cava (IVC) come into view.

Right Ventricle

The examination of the right ventricle (RV) begins at the midesophageal four-chamber view.

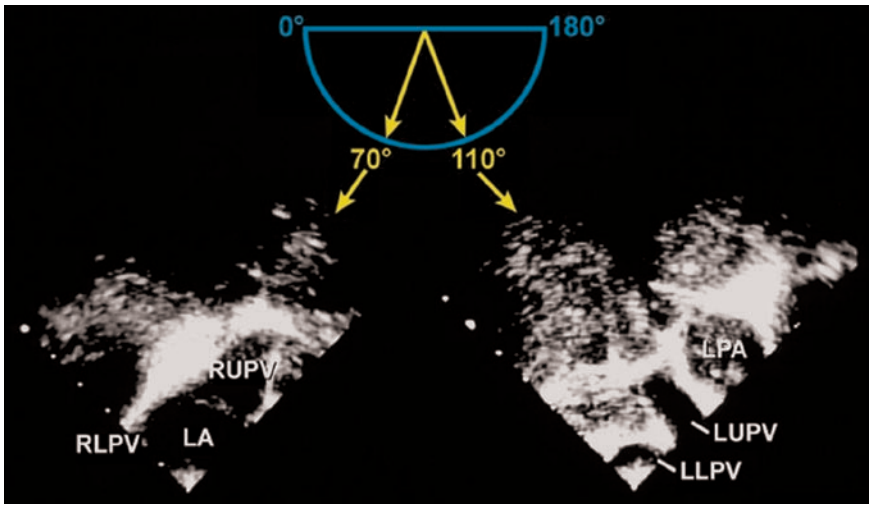

Fig. 6.5 Simultaneous TEE visualization of upper and lower pulmonary veins. For imaging of the right pulmonary veins (*left panel*), the angle is maintained at 70–80° in midesophagus and rotated rightward, whereas for imaging the left pulmonary veins(*right panel*), the angle is rotated at 100–110° and the scope is rotated to left. (*RUPV* right upper pulmonary vein; *RLPV* right lower pulmonary vein; *LUPV* Left upper pulmonary vein; *LLPV* left lower pulmonary vein)

60–90 degrees: The RV inflow-outflow view can be developed by rotating the multiplane angle forward between 60 and 90° keeping the TV visible until the right ventricular outflow track opens up and the pulmonic valve (PV) and the main pulmonary artery (PA) come into view.

The transgastric RV inflow view can be developed further by turning the probe to the right until the RV cavity is located in the center of the display and the multiplane angle is rotated forward between 100 and 120° until the apex of the RV appears in the left side of the display. This cross-section provides good views of the inferior (diaphragmatic) portion of the RV free wall.

Tricuspid Valve

The tricuspid valve can be visualized in the midesophageal four-chamber view.

The multiplane angle can be further rotated to develop the midesophageal RV inflow-outflow view, and these views are repeated with color flow Doppler to detect flow abnormalities of the TV.

The transgastric views of the TV are obtained by advancing the probe into the stomach and developing the transgastric RV inflow view. A short-axis view of the TV can be developed by withdrawing the probe slightly toward the base of the heart until the tricuspid annulus is in the center of the display and rotating the multiplane angle backward to approximately 30°.

Right Atrium

The examination of the RA is initiated from the midesophageal *four-chamber view* followed by the midesophageal *bicaval view* developed by rotating the multiplane angle between *80 and 110°*. This view also provides good images of the right atrial appendage that emanates from the superior, anterior aspect of the RA.

Pulmonary Artery

The midesophageal short-axis view at the level of the aortic valve provides a view of the pulmonary veins and the main pulmonary artery (PA).

0 degrees: The multiplane angle is rotated back toward 0° and the probe is anteflexed or withdrawn slightly to display the bifurcation of the main PA with the right PA at the top of the display coursing off to the patient's right. The left PA arches over the left mainstem bronchus after bifurcating from the main PA and is difficult to visualize with TEE due to the intervening airway.

The midesophageal RV inflow-outflow view displays the pulmonary veins in long axis and is useful for detecting pulmonic regurgitation by color flow Doppler. The main PA and the pulmonary veins can also be seen in the upper esophageal aortic arch short-axis view.

Thoracic Aorta

Midesophageal views can be used for assessing the ascending aorta in its short-axis view by adjusting the angle until the vessel appears circular, usually between 0 and 60°. The probe can be advanced or withdrawn for examining different levels of the aorta.

100–150 degrees: The multiplane angle can be rotated between 100 and 150° to develop the midesophageal ascending aortic long-axis view in which the anterior and the posterior walls of the aorta appear parallel to one another.

Descending aorta: TEE examination of the descending thoracic aorta is accomplished by turning the probe to the left from the midesophageal four-chamber view for displaying the descending aortic short-axis view.

The aortic arch is imaged with the multiplane angle at 0° by withdrawing the probe while maintaining an image of the descending thoracic aorta until the upper esophageal window is reached. The multiplane angle is rotated to 90° to develop the upper esophageal aortic arch short-axis view, and the probe is turned to the right to move the imaging plane proximally through the arch and to the left to move distally.

Clinical Applications

Infective Endocarditis

TEE is superior to transthoracic echocardiography for better delineation of the shape and size of vegetations and for assessing the structural complications such as myocardial abscess, fistulas, mycotic aneurysms, valvular aneurysms or perforations, flail leaflets or prosthetic valve dehiscence.[5] TEE is also more superior than transthoracic echocardiograms TEE has a higher sensitivity (76–100%) and specificity (94%) than transthoracic echocardiography for diagnosing perivalvular extension of infection.[6] The cost effectiveness and incremental utility of TEE when used in conjunction with the clinical information is particularly higher in patients who have an intermediate clinical likelihood of infective endocarditis.[7] A negative TEE in a patient with suspected infective endocarditis virtually rules out an infection of the native valve, except in very early phases of the disease when vegetations may not be detected. When clinical suspicion of infective endocarditis is high and results from TEE are negative, a repeat TEE is warranted within 7–10 days, which may demonstrate previously undetected vegetations or abscess.

Evaluation of Prosthetic Valves

TEE is the procedure of choice for detecting abnormalities of mitral valve prostheses (perivalvular regurgitations, cusp abnormalities in tissue prosthesis, embolic events, patient-prosthesis mismatch, and malfunction of repaired valves and implanted rings) (Fig. 6.3).[8] The aortic valve lies in a plane perpendicular with the esophagus, with a flow that has an asymmetric profile; therefore, assessment of a prosthetic aortic valve by TEE may be more challenging. However TEE is useful in detecting abnormalities of aortic valve prosthesis, particularly those related to periprosthetic tissue. A deep transgastric view is required for assessing the gradient across the prosthesis and for better assessment of prosthetic aortic valve regurgitation.

TEE is also useful in diagnosing prosthetic valve thrombosis and for assessing success of thrombolytic therapy. TEE allows a close examination of the sewing ring and the occluder, thus helping differentiate pannus from a thrombus and for establishing the mechanism of an incomplete occluder opening. TEE is also useful in providing a high-resolution assessment of valves in tricuspid and pulmonic positions.

Cardioembolic Strokes

The likelihood of identifying a potential cardiac source of emboli depends on how thoroughly a patient is evaluated. TEE has a higher accuracy in identifying abnormal lesions in patients with cardioembolic strokes.[9]

These include abnormalities of the left and right atrium and appendages, intra-atrial septum, patent foramen ovale, atrial septal aneurysm, vegetations, spontaneous contrast, left ventricular clots, and various cardiac masses.

The diagnostic yield of TEE for a cardiac source of emboli in a group of patients presenting with unexplained stroke or transient ischemic attacks is high with potential lesions identified in over 50% of the studies. However, one-third of patients who have a cardioembolic stroke also have concomitant cerebral or vascular atherosclerosis, which can confound the diagnosis. Moreover, no absolute clinical or laboratory gold standard exists for diagnosing a potentially cardioembolic lesion; hence, risk stratification schemes have been suggested based upon strength of the association of a given lesion with ischemic strokes.

Atrial Fibrillation

Atrial arrhythmias predispose to emboli formation. A sustained impairment or transient stunning results in poor emptying and enlargement of left atrium and left atrial appendage, leading consequently to stasis and thrombus formation. Transient paroxysms of atrial fibrillation may lead to thrombus formation in the left atrium. Left atrial thrombus may be detected in the presence of sinus rhythm.[10] Conversely, the lack of visualization of appendage thrombi on TEE after stroke does not exclude the appendage as the embolic source. In absence of well-formed thrombi, a dense spontaneous contrast has been shown to be a strong predictor of ischemic strokes. An annual thromboembolic event rate of 12% has been observed in patients with spontaneous echo contrast compared to 3% in patients without it.[11]

In patients with atrial fibrillation, clinical and echocardiographic markers of thromboembolism are helpful for risk stratification and include a history of hypertension, a previous thromboembolic event, and heart failure. Echocardiographic risk factors include left ventricular systolic function, left ventricular hypertrophy, left atrial enlargement, and spontaneous echocardiographic contrast. The absolute risk of stroke in atrial fibrillation shows marked variation with age and coexisting cardiovascular diseases, ranging from 2 to 18% per year depending on the investigated patient population.[12] Short-term anticoagulation combined with TEE before cardioversion has been suggested to be an effective alternative to 3–4 weeks of empiric anticoagulation before cardioversion.[13] Economic analysis of TEE-facilitated acute cardioversion has been shown to result in higher initial treatment costs but a lower subsequent outcome-associated cost, resulting in no significant cost difference between the two strategies.[14]

Aortic Diseases

Transesophageal examination is extremely valuable for managing patients with aortic diseases (aortic dissections, intramural injury, and aortic trauma).[15] In a comparative imaging of multilane TEE with spiral CT and MR imaging, the sensitivity and specificity of TEE for diagnosing aortic dissections has been reported as 98 and 95%, respectively.[16] However care needs to be taken to differentiate reverberation artifacts. Conversely false-negatives may occur when small dissections are located within upper ascending aorta or proximal aortic arch. The reverberation artifacts may be differentiated using M-mode echocardiography. The chief advantage of TEE in imaging aortic dissections is that it provides diagnostic information faster than other modalities and, the only modality which can be used intraoperatively during surgery. TEE has also been found useful in screening patients with suspected aortic trauma and for diagnosing acute aortic intramural hematomas.

There may be an association between large atheromas in the ascending aorta and the aortic arch and an increased risk of cerebral embolic events in patients older than 60 years. Morphologic features such as atheroma protrusion and ulceration have been shown to carry significantly higher risk of embolic events, particularly after cardiopulmonary bypass or following invasive procedures such as cardiac catheterization or intra-aortic balloon placement. Although TEE has been used to assess atheromas and their morphologies, it is not clear whether atheroma thickness is directly related to the mechanism of stroke or represents a marker for other conditions. In a recent study, the association between previous ischemic strokes, transient ischemic episodes, and aortic atherosclerosis was found to be insignificant once age and gender-related

adjustments were made.[17] The overall importance of aortic atherosclerosis in the pathogenesis of cerebrovascular accidents is thus not clear and needs to be correlated with associated risk factors such as hypertension, coagulation, and lipid disorders.

Cardiac Masses

TEE is superior to transthoracic echocardiography in delineating cardiac masses and masses adjacent to the heart, such as in the pulmonary arteries and mediastinum. It is particularly useful for differentiating structural features such as site of attachment, consistency as in cystic vs. solid, and infiltration into surrounding structures, that are useful for differentiating thrombi and benign from malignant neoplasms. TEE is particularly advantageous in detecting masses posterior to mechanical devices or in left atrial appendages. TEE is also useful in detection of thrombi lying in the proximal portion of the pulmonary arteries.[18]

Congenital Heart Diseases and Intracardiac Shunts

Transesophageal echocardiography is superior to routine surface echocardiography for the evaluation of specific cardiac defects, such as certain types of atrial septal defects, anomalous pulmonary venous connections, and complex cardiac malformations. The technique is particularly useful in atrial septal defects. Sinus venosus defects and anomalous pulmonary vein drainage are detected more easily by TEE as compared to transthoracic echocardiography because of the proximity of the transducer to the atrial septum.

TEE is recommended in any patient with an unexplained dilatation of the right side of the heart for ruling out a sinus venosus atrial septal defect and associated pulmonary venous abnormalities.[19]

TEE is also useful for visualizing the margins of an atrial septal defect for defining candidates who may benefit from nonsurgical device closure of the defect.

TEE has been used for detecting shunt flow across foramen ovale in adults. Patent foramen ovale (PFO) and stroke remain a subject of intense investigation with no clear answers. Patent foramen may also be associated with atrial septal aneurysms (Fig. 6.6), and presence of both these lesions has been also been implicated in recurrent embolic strokes.[20] Administration of intravenous contrast is important for defining patency at rest. A right to left shunting of three or more contrast bubbles during normal breathing is diagnostic for presence of a PFO. The sensitivity of an intravenous injection of contrast in detecting a PFO improves threefold if an injection is given through the femoral vein in contrast to antecubetal vein.

Critically Ill Patients

The limited acoustic windows in critically ill patients make TEE an attractive alternative to transthoracic echocardiography. In addition to the usual indications for TEE (suspected endocarditis, source of embolus, and suspected aortic dissection), there are several indications that are unique to critical care patients. These include:

1. Assessment of unexplained hypotension,
2. Suspected massive pulmonary embolism,
3. Unexplained hypoxemia, and
4. Complications of cardiothoracic surgery.

Unlike transthoracic echocardiography, TEE can visualize emboli lodged in the proximal pulmonary arteries. The right pulmonary artery can be observed for most of its course; however, the left pulmonary

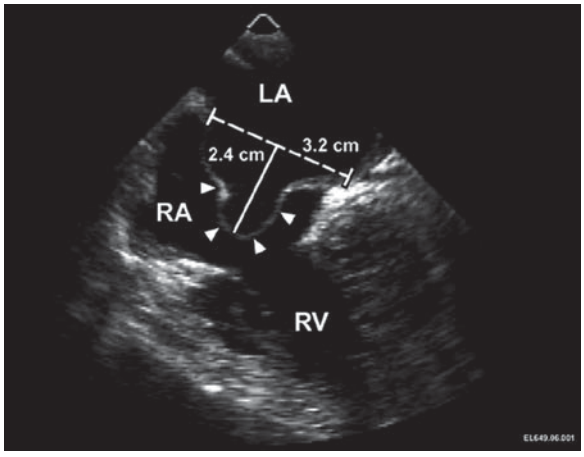

Fig. 6.6 Transesophageal echocardiography for delineating atrial septal aneurysm (*arrows*)

artery rarely can be observed beyond its first two centimeters.

Less common indications for TEE in the critical care unit include continuous hemodynamic monitoring, evaluation of potential transplant donors, and guidance of central-line placement. The recent development of transnasal TEE probes may allow for monitoring in the awake patient. The potential benefits of the transnasal probe include less risk for esophageal trauma in patients with varices or coagulopathies and less need for sedation in those with compromised respiratory or hemodynamic status.

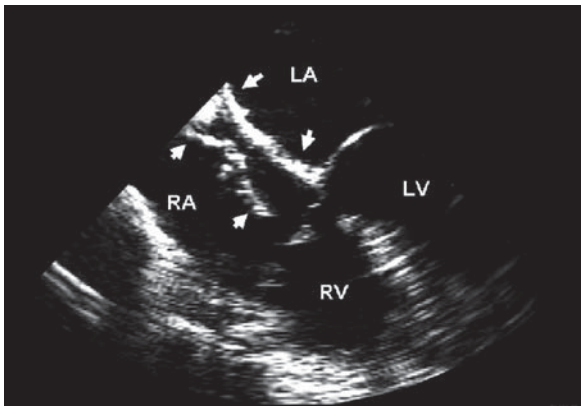

Fig. 6.7 Amplatzer device (*arrows*) positioned across an atrial septal defect

Perioperative and TEE During Procedures

TEE is valuable in the perioperative period and can provide incremental information for either changing the preoperative plan or prompting immediate revision of hemodynamically significant residual defects.

Intraoperative TEE is extremely useful in patients undergoing valve repairs, replacements, and reoperative surgeries. In patients undergoing mitral valve repairs, TEE is extremely useful for the surgeons in making a decision about the choice of the surgical procedure which may include chordal shortening, chordal transfer, artificial chords, posterior leaflet sliding technique, anterior leaflet resection, or placement of annular ring. Routine intraoperative echocardiography has also been found to be cost effective in children undergoing cardiac surgery for congenital heart lesions.[21]

Transeosphageal echocardiography also plays a role in the interventional laboratory for percutaneous interventions such as transcatheter closure of atrial septal defects (Fig. 6.7) and ventricular septal defects. It is used before the procedure for identifying the defect, excluding multiple defects, measuring the adequacy of the rim of the interatrial septum and its distance from the pulmonary vein and the mitral valve and superior vena cava, balloon sizing of the stretched diameter, and for proper placement of the occluder. TEE is also used as an important imaging modality for blade atrial septostomy and closure of baffle fenestrations following total caval pulmonary connection and closure of baffle leak following the Mustard or Senning surgeries.

Other interventional procedures where TEE is useful include balloon mitral valvuloplasty, nonsurgical reduction of ventricular septum in patients with hypertrophic cardiomyopathy, and trans-septal catheterization for placement of catheter during radiofrequency ablation of cardiac arrhythmias.

TEE also plays an important role in patients with heart failure undergoing implantation of left ventricular assist devices for selecting the type of the assist device necessary (right vs. left or biventricular), optimization of device performance, the evaluation of hypoxemia, and the determination of patient's ability to be weaned from the mechanical device.[22] A correct positioning of cannula under TEE guidance optimizes the LV filling, besides intraoperative recognition of right ventricular failure, which can decrease pump flow due to inadequate left-sided filling.

Pitfalls

TEE needs expertise for avoiding potential erroneous diagnosis resulting from misinterpretation of normal and abnormal anatomy (Figs. 6.8–6.10).

- *Air* within the esophagus and stomach, or an air-filled trachea and bronchi intervening between probe and cardiac structures can consistently produce artifacts or interfere with certain tomographic views.
- *Reverberation signals* or ghost shadows are common and result from impedance mismatch resulting in linear artifacts most commonly seen in the upper ascending and mid-descending aorta. Imaging of the upper ascending aorta with the horizontal plane

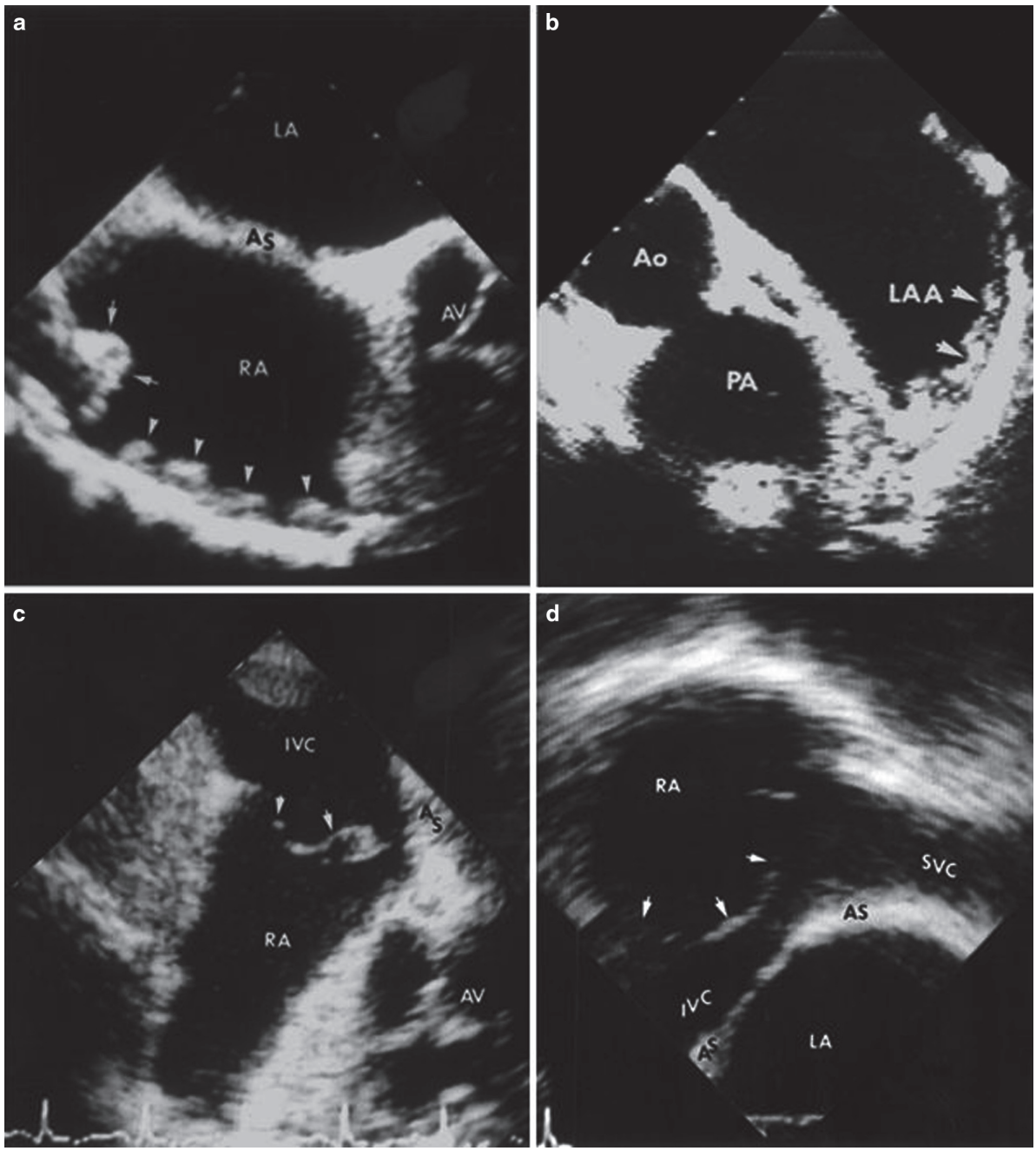

Fig. 6.8 (**a**, **b**) Appearance of pectinate muscle in right and left atrial appendage, respectively, which may be confused as thrombi. (**c**, **d**) Appearance of Eustachian valve in the right atrium which may be interpreted as an abnormal structure

is limited by a blind spot caused by interposed bronchus between the esophagus and upper ascending aorta.

- *Normal anatomy* may be interpreted abnormal. These include muscular trabeculations in the atrial appendage mistaken as mass or thrombus, the terminal portion of the partition between the left atrial appendage and left upper pulmonary vein appearing as a globular mass, fat-laden fossa ovalis or lipomatous hypertrophy of the atrial septum interpreted as

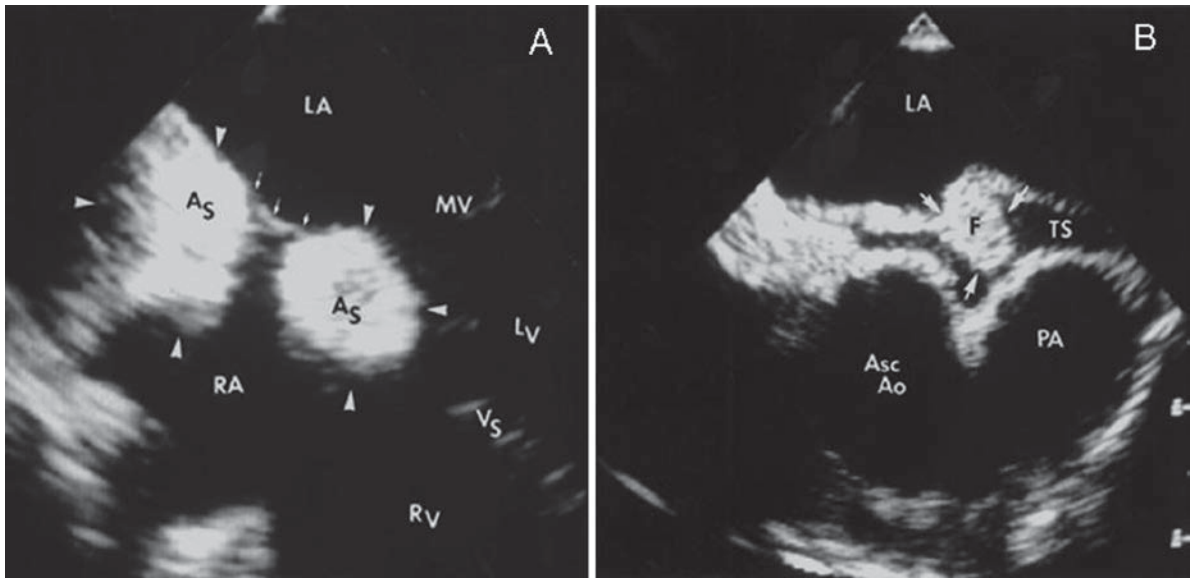

Fig. 6.9 Diagnostic pitfalls during TEE. Lipomatous interatrial septum (*panel A*), the membrane of the fossa ovalis is spared while the remaining septum is thickened resulting in a dumbbell mass like appearance. *Panel B* shows normal appearance of the transverse sinus which appears as an echo-free space

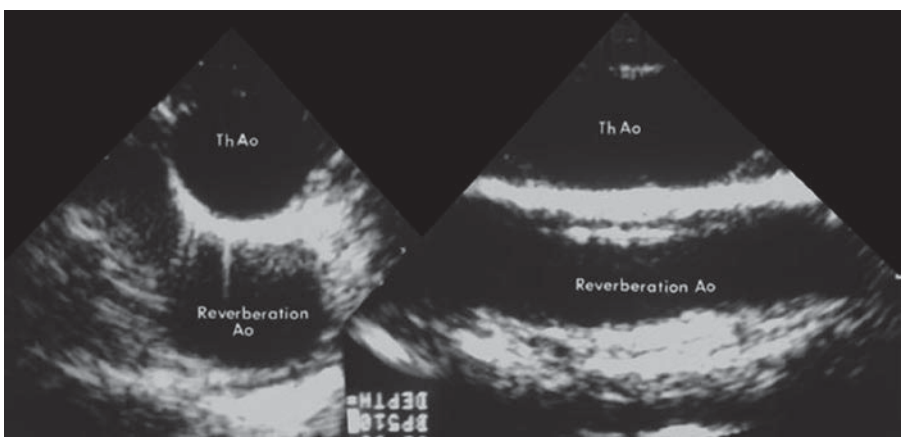

Fig. 6.10 Reverberation artifacts in descending thoracic aorta

a mass, and surgical sutures appearing filamentous or pedunculated and interpreted as mass or vegetations.

- *"Echo-free spaces":* Certain normal structures generate echo-free spaces and may be incorrectly interpreted as cysts or abscesses. These include the transverse and the oblique sinus.
- *Other difficulties* that may be encountered during TEE include the adequate visualization and quantification of aortic valve regurgitation, aortic valve, and pulmonary valve gradient estimation and nonforeshortened visualization of the left ventricular apex.
- Finally, ultrasound transducers generate heat. During prolonged monitoring, the device may be required to be shut down periodically to allow cooling.

Complications

Procedural risks are low in trained hands. However, they need to be explained clearly to the patient. These include transient throat pain, laryngospasm, aspiration, hypotension, hypertension, tachycardia, mucosal

bleeding, esophageal rupture, and rare risk of death. Benzocaine topical spray can cause toxic methemoglobinemia. The treatment is administration of methylene blue in addition to supportive measures. Being semi-invasive, appropriate training requirements are needed and have been laid down by both the American Society of Echocardiography[23] and the British Society of Echocardiography.

Conclusions

Easy applicability, lower costs, portability, and instantaneous availability of test results have made TEE a valuable imaging modality in clinical cardiology. The utility of TEE in visualizing cardiovascular structures and its incremental value over transthoracic echocardiography have been well established. Future miniaturization of the TEE transducer design is likely to improve application in a wider subgroup of patients including premature infants, children, pregnant women, and patients with hemodynamic instability. A smaller probe design would help minimize discomfort from longer monitoring of cardiovascular hemodynamics and therapy.

TEE provides high-quality 2-D images, which therefore provide a basis for 3-D reconstructions. Since the atrial cavities lie close to esophagus, TEE is likely to be useful for 3-D imaging of regurgitation jets, particularly those with eccentric orifices and orientations. Real-time 3-D imaging would also facilitate accurate monitoring of catheter-based techniques, radiofrequency ablations, and for intraoperative monitoring of surgical techniques that require appreciation of complex geometries like the valves and the subvalvular apparatus.

References

1. Side CD, Gosling RG. Non-surgical assessment of cardiac function. *Nature*. 1971;232:335–336.
2. Frazin L, Talano JV, Stephanides L, et al. Esophageal echocardiography. *Circulation*. 1976;54:102–108.
3. Hisanaga KHA, Nagata K, Yoshida S. A new transesophageal real time two dimensional echocardiographic system using a flexible tube and its clinical application. *Proc Jpn Soc Ultrasonics Med*. 1977;32:43–44.
4. Shanewise JS, Cheung AT, Aronson S, Stewart WJ, et al. ASE/SCA guidelines for performing a comprehensive intraoperative multiplanetransesophageal echocardiography examination: recommendations of the American Society of Echocardiography Council for Intraoperative Echocardiography and the Society of Cardiovascular Anesthesiologists Task Force for Certification in Perioperative Transesophageal Echocardiography. *J Am Soc Echocardiogr*. 1999;12:884–900
5. Pearlman AS, Gardin JM, Martin RP, et al. Guidelines for physician training in transesophageal echocardiography: recommendations of the American Society of Echocardiography Committee for Physician Training in Echocardiography. *J Am Soc Echocardiogr*. 1992;5:187–194.
6. Vilacosta I, Graupner C, San Roman JAet al Risk of embolization after institution of antibiotic therapy for infective endocarditis. *J Am Coll Cardiol*. 2002;39:1489–1495.
7. Bayer AS, Bolger AF, Taubert KA, et al. Diagnosis and management of infective endocarditis and its complications. *Circulation*. 1998;98:2936–2948.
8. Heidenreich PA, Masoudi FA, Maini B, et al. Echocardiography in patients with suspected endocarditis: a cost-effectiveness analysis. *Am J Med*. 1999;107:198–208.
9. Khandheria BK, Seward JB, Oh JK, et al. Value and limitations of transesophageal echocardiography in assessment of mitral valve prostheses. *Circulation*. 1991;83:1956–1968.
10. Palazzuoli A, Ricci D, Lenzi C, et al. Transesophageal echocardiography for identifying potential cardiac sources of embolism in patients with stroke. *Neurol Sci*. 2000;21:195–202.
11. Agmon Y, Khandheria BK,Gentile F, et al. Clinical and echocardiographic characteristics of patients with left atrial thrombus and sinus rhythm: experience in 20 643 consecutive transesophageal echocardiographic examinations. *Circulation*. 2002;105:27–31.
12. Leung DY, Black IW, Cranney GB, et al. Prognostic implications of left atrial spontaneous echo contrast in nonvalvular atrial fibrillation. *J Am Coll Cardiol*. 1994;24:755–762.
13. Kamp O, Verhorst PM, Welling RC, et al. Importance of left atrial appendage flow as a predictor of thromboembolic events in patients with atrial fibrillation. *Eur Heart J*. 1999;20:979–985.
14. Klein AL, Grimm RA, Murray RD, et al. Use of transesophageal echocardiography to guide cardioversion in patients with atrial fibrillation. *N Engl J Med*. 2001;344:1411–1420.
15. Klein AL, Murray RD, Becker ER, et al. Economic analysis of a transesophageal echocardiography-guided approach to cardioversion of patients with atrial fibrillation: the ACUTE economic data at eight weeks. *J Am Coll Cardiol*. 2004; 43:1217–1224.
16. Smith MD, Cassidy JM, Souther S, et al. Transesophageal echocardiography in the diagnosis of traumatic rupture of the aorta. *N Engl J Med*. 1995;332:356–362.
17. Keren A, Kim CB, Hu BS, et al. Accuracy of biplane and multiplane transesophageal echocardiography in diagnosis of typical acute aortic dissection and intramural hematoma. *J Am Coll Cardiol*. 1996;28:627–636.
18. Agmon Y, Khandheria BK, Meissner I, et al. Relation of coronary artery disease and cerebrovascular disease with atherosclerosis of the thoracic aorta in the general population. *Am J Cardiol*. 2002;89:262–267.
19. Russo A, De Luca M, Vigna C, et al. Central pulmonary artery lesions in chronic obstructive pulmonary disease: a transesophageal echocardiography study. *Circulation*. 1999;100:1808–1815.
20. Pascoe RD, Oh JK, Warnes CA, et al. Diagnosis of sinus venosus atrial septal defect with transesophageal echocardiography. *Circulation*. 1996;94:1049–1055.

21. Mas JL, Arquizan C, Lamy C, et al. Recurrent cerebrovascular events associated with patent foramen ovale, atrial septal aneurysm, or both. *N Engl J Med*. 2001;345: 1740–1746.
22. Randolph GR, Hagler DJ, Connolly HM, et al. Intraoperative transesophageal echocardiography during surgery for congenital heart defects. *J Thorac Cardiovasc Surg*. 2002;124:1176–1182.
23. Seward JB, Khandheria BK, Freeman WK, et al. Multiplane transesophageal echocardiography: image orientation, examination technique, anatomic correlations, and clinical applications. *Mayo Clin Proc*. 1993;68:523–551.

Section 2
Valvular Heart Disease

Chapter 7
Aortic Valve Disease

A. Aortic Stenosis

Petros Nihoyannopoulos

Introduction

There have been dramatic changes in the incidence of valve disease over the past decade. With the decline of rheumatic fever, the incidence of rheumatic heart disease has been reduced. In contrast, people now live a lot longer than 10–20 years ago, which has led to the increase of degenerative valve disease and in particular aortic stenosis. Valvular aortic stenosis is now the commonest valve lesion seen in adult cardiological practice in the Western world.

Etiology

Can be separated into three categories according to the location of the stenosis, valvular, subvalvular, and supravalvular.

Valvular

- Calcific degenerative aortic stenosis
- Bicuspid aortic valve
- Rheumatic heart disease
- vegetations (infective/sterile)
- Inflammatory disorders (SLE)

P. Nihoyannopoulos
Imperial College London, National Heart and Lung Institute, Hammersmith Hospital, London, UK
e-mail: petros@imperial.ac.uk

Calcific Degenerative Aortic Stenosis

Today, aortic stenosis has become a disease of the elderly, and it is by far the commonest cause of aortic stenosis. The valve is tricuspid and the cusps thickened, fibrotic, and calcified with reduced overall mobility. It is an active process similar to atherosclerosis in the majority of patients. The calcification may extend down to the mitral annulus in the most severe cases (Fig. 7.1).

Aortic sclerosis is probably an early stage of the disease progression and is characterized by focal areas of cusp thickening without affecting the mobility of the cusps and not associated with a significant gradient (>30 mmHg). Clinically, with the exception of a systolic murmur due to the turbulence, the signs of aortic stenosis are absent (slow rising pulse and soft second heart sound).

Calcific aortic stenosis is a progressive disease and the overall rate of hemodynamic progression is predictable with an average annual increase in aortic jet velocity of 0.3 m/s, mean gradient of 7–8 mmHg, and a decrease in valve area of 0.1 cm^2. Echocardiography therefore is pivotal to follow disease progression and predicting clinical outcome.

Bicuspid Aortic Valve

This is the most frequent cause of isolated aortic stenosis in patients under 50 years. It may be separated into two types: the true bicuspid valve, which is associated with two, usually asymmetric aortic sinuses with the larger anterior and the smaller posterior. The valve will open in an oblique fashion seen from short-axis projections (Fig. 7.2). From the parasternal long axis, it will appear doming in systole with the narrowest

P. Nihoyannopoulos and J. Kisslo (eds.), *Echocardiography*,
DOI: 10.1007/978-1-84882-293-1_7,

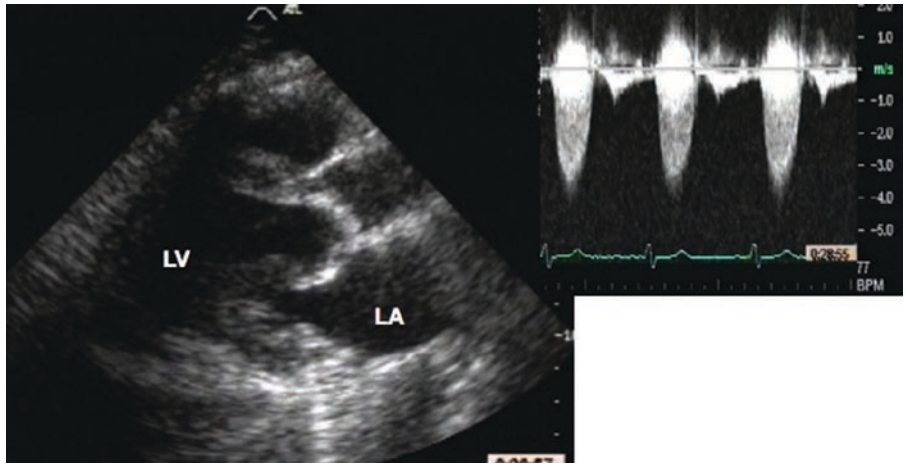

Fig. 7.1 Parasternal long-axis view from a patient with calcific aortic stenosis. Note the extensive calcification of the aortic valve extending up on the aortic root and down the mitral annulus. On the right, continuous-wave Doppler from the same patient demonstrating a significant gradient (mean) of 48 mmHg *LA* left atrium, *LV* left ventricle

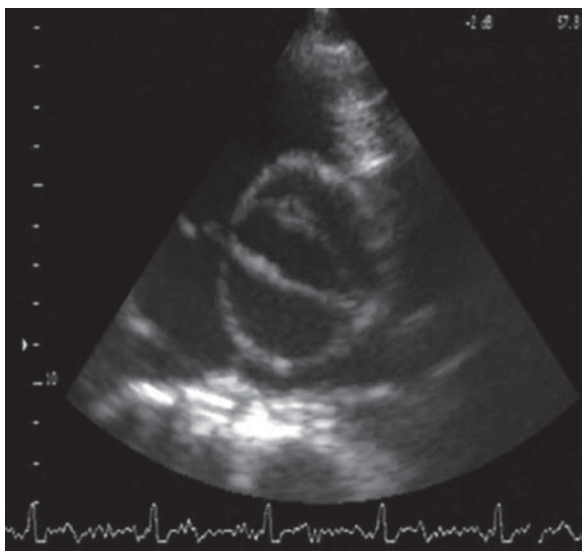

Fig. 7.2 Short-axis projection from a 28-year-old patient with a true bicuspid aortic valve. Notice the two aortic sinuses arranged in an oblique fashion with one anterior (*top*) and one posterior (*bottom*) cusps

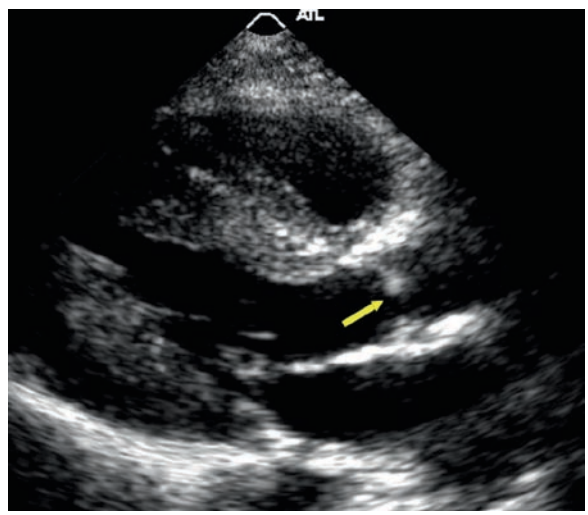

Fig. 7.3 Long-axis projection from another patient with a bicuspid aortic valve. Notice that in systole, the aortic cusps are doming toward the ascending aorta (*arrow*)

orifice area about 1 cm above the cusp insertion (Fig. 7.3). The commonest form is a bicuspid valve associated with a fusion between two cusps or raphe, and it is associated with three aortic sinuses often asymmetrical.

In most instances, there will be a dilation of the ascending aorta beyond the sinotubular junction suggestive of a poststenotic dilatation. It is important to identify whether or not there is such a poststenotic dilatation and how much it is as it is recommended that if the dilation is more than 55 mm, then the surgeon needs to replace the ascending aorta at the same time as the aortic valve. Figure 7.4 is from a patient with a bicuspid aortic valve and a poststenotic dilatation of 55 mm. This patient went on to have an aortic valve replacement together with an interposition graft in the ascending aorta.

Far less common are unicuspid or quadricuspid valves, which probably are the commonest cause of severe aortic stenosis in infancy.

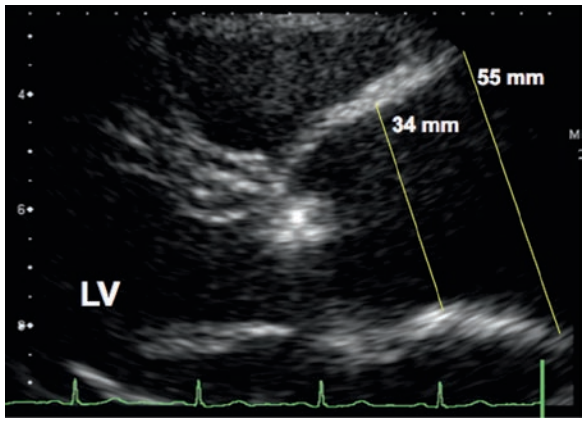

Fig. 7.4 Another patient with a bicuspid aortic valve. Here we can clearly see a poststenotic dilatation of the ascending aorta and some of the basic measurements at the sinotubular junction (34 mm) and the proximal ascending aorta (55 mm) *LV* left ventricle

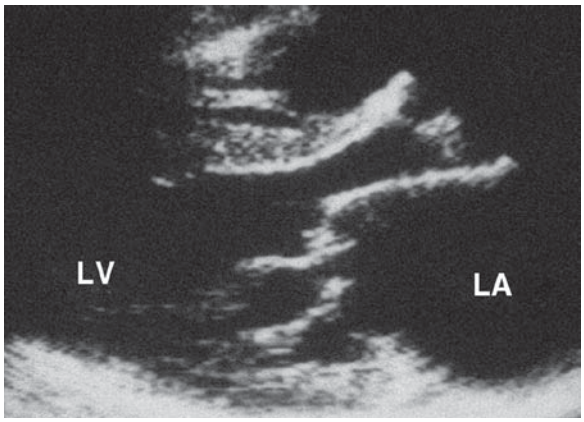

Fig. 7.5 Parasternal long-axis projection from a patient with rheumatic valve disease. Notice that the mitral valve is grossly abnormal (see text) with a dilated LA. In addition, the aortic valve is thickened at the tips with reduced mobility

It is important to remember that congenital abnormalities of the aortic valve may be associated with other cardiac lesions such as coarctation of the aorta so that a careful exploration of the descending aorta may be necessary.

Rheumatic

Rheumatic disease affects predominantly the mitral valve leading to mitral stenosis (Fig. 7.5). Here, the characteristic findings are:

- Diastolic doming or the anterior leaflet
- Fixed posterior leaflet
- Commissural fusion (from short-axis projections)
- Chordal thickening
- Involvement of the aortic valve (thickening)
- Dilated left atrium
- Normal size left ventricle
- Usually atrial fibrillation present

The aortic valve is almost invariably affected to a variable degree. The rheumatic process affects the free edges of the valve cusps, leading to thickened valve cusps and fused commissures (Fig. 7.6). There is often some retraction and shortening of the cusps leading to the inability of the valve to close properly causing some regurgitation. Frequently however the aortic valve morphology is similar to that of calcific degenerative disease except that here the mitral valve is abnormal too.

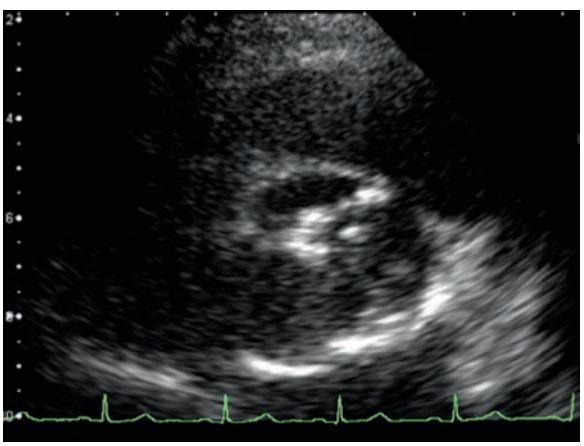

Fig. 7.6 Parasternal short-axis projection from the same patient with rheumatic valve stenosis. Here it shows the classic thickening at the aortic cusp tips of all three cusps with commissural fusion

Disease progression in rheumatic aortic stenosis is slower than that in calcific degenerative disease, and it can take years before becoming severe.

Vegetations

Infective endocarditis can affect the aortic valve with local growth of vegetations (Fig. 7.7). Vegetations are mobile structures, often pedunculated that do not affect the valve mobility. Aortic vegetations with the ensuing aortic regurgitation may contaminate the mitral valve, usually the anterior mitral leaflet, and it is important

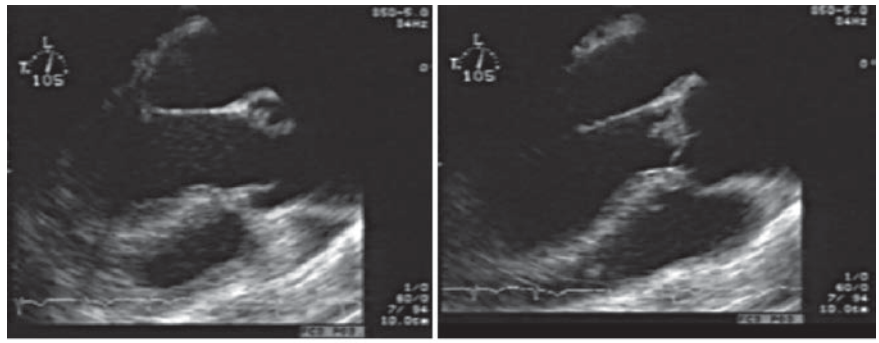

Fig. 7.7 Transesophageal images from a patient with a seemingly normal aortic valve but with clear vegetations of the aortic cusps. The valve itself opened fully and had a normal mobility

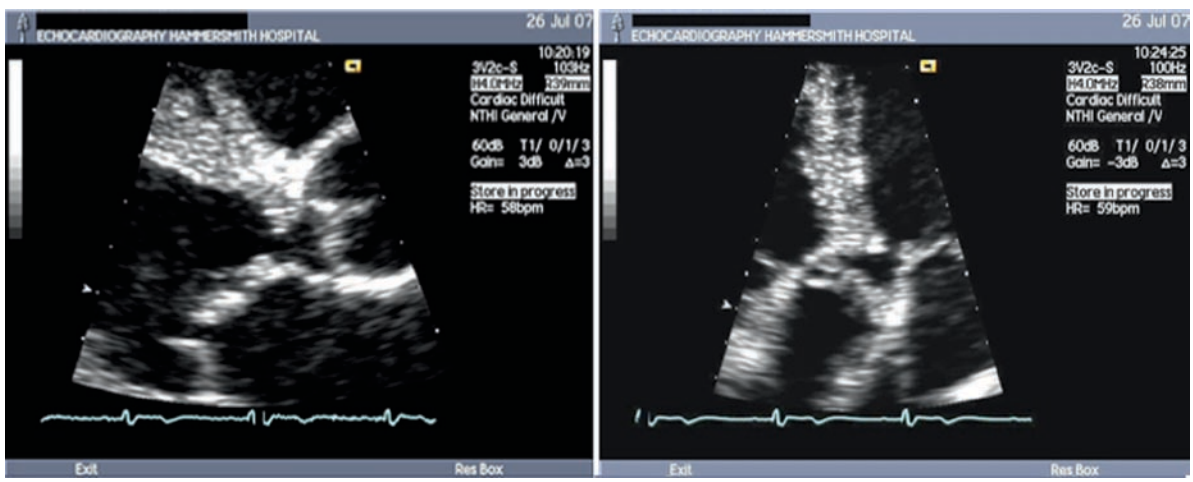

Fig. 7.8 Parasternal long-axis (*left*) and apical 5-chamber view (*right*) from a patient with subaortic stenosis. Notice the shelf-like structure just below the aortic cusps insertion creating a narrowing of the outflow track

therefore always to also look at the mitral valve for possible signs of infection or indeed perforation. Endocarditis will predominantly lead to valve destruction and regurgitation, and it is very rare for the vegetations to become so large and obstructive.

There are however other types of vegetations which are sterile and may be the result of a tumor (marantic endocarditis) or lupus erythematosus.

Subvalvular Aortic Stenosis

Discrete Subaortic Membrane

This is a rare congenital abnormality caused by a fibromuscular ring obstructing the left ventricular outflow track approximately 1 cm below the aortic cusp insertions. From parasternal long-axis projections this is seen as a short notch dipping down from the proximal septum and another notch rising from the root of the anterior mitral leaflet upward (Fig. 7.8). It is associated with turbulent flow in the subaortic area.

Hypertrophic Cardiomyopathy

An autosomal dominant familial disorder causing sudden death in the young. It is characterized by asymmetric left ventricular hypertrophy in about 40% of patients.

There are several phenotypic and genotype variations (see Chap. 20), but it can be associated with

marked hypertrophy of the proximal ventricular septum, which may lead to a functional obstruction to the left ventricular outflow. Here characteristically, the aortic valve is structurally normal and the outflow track velocity high with a characteristic late picking (scimitar) appearance.

Supravalvular Aortic Stenosis

Familial Hypercholesterolemia

Familial hypercholesterolemia (FH) is characterized by dominantly inherited hypercholesterolemia, early appearance of cutaneous and tendon xanthomata, and a predisposition to premature cardiovascular disease. Inheritance of one mutant gene causes heterozygous FH (1:500), while inheritance of two mutant genes gives rise to phenotypic homozygosity (1:1,000,000).

The commonest abnormality is that of a small aortic root and aortic sinuses with highly echogenic walls.[1] Premature coronary artery disease is common in FH, while atheromatous involvement of the aortic valve and root is almost always present in homozygotes.

Lipid infiltration with consequent thickening of the aortic cusps is a unique feature of homozygotes and can affect the valve's mobility (Fig. 7.9a). However, atherosclerotic involvement of the aortic root is an even more common complication, rarely reported in heterozygotes, and leads to ostial stenosis and "supravalvar" aortic stenosis. The characteristic findings are those of a funnel-like narrowing of the aortic root, which is highly echogenic with small but mobile aortic leaflets. The ascending aorta extends to its normal size after several centimeters (Fig. 7.9b).

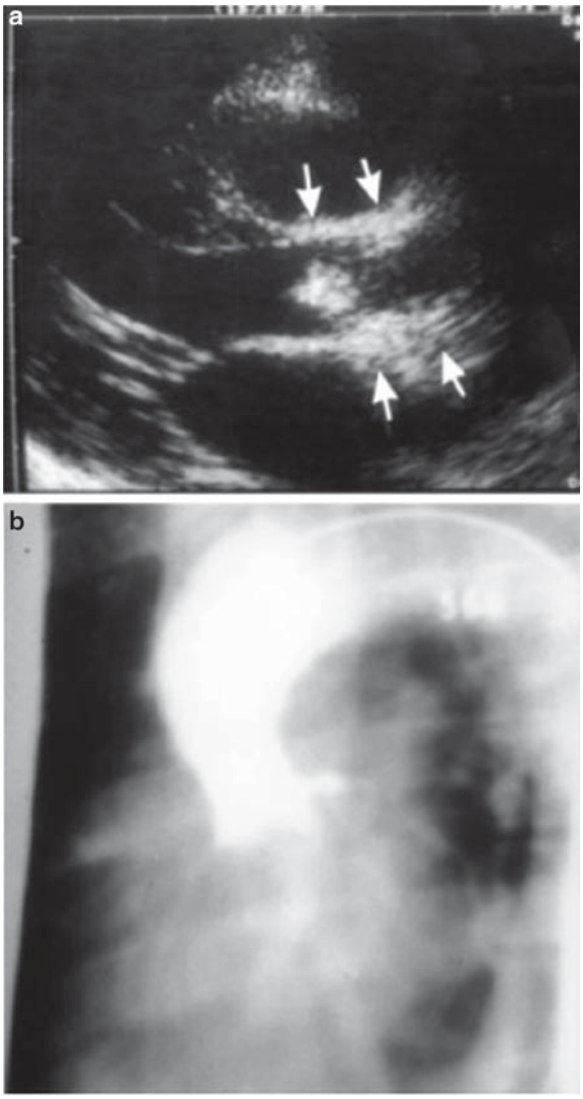

Fig. 7.9 Parasternal long-axis projection (**a**) from a patient with familial hypercholesterolemia. Here the aortic root is narrowed with thickening of the cusps, which maintained a good overall mobility. The ascending aorta is of normal size, thus creating the appearance of a funnel on the aortogram (**b**)

William's Syndrome

This is a rare congenital abnormality caused by a constrictive ridge of fibrous tissue at the level of the sinotubular junction. The condition is most often associated with Williams–Beuren syndrome characterized by an "elfin" facies, mental retardation, low-set ears, strabismus, hypercalcemia, and multiple pulmonary artery stenosis. In its extreme form it is part of the hypoplastic left heart syndrome.

There may be three anatomical variables:

- An hour-glass type with an annular constriction at the sinotubular junction
- A membranous type with a fibromuscular diaphragm
- A hypoplastic type, in which part of the ascending aorta is underdeveloped

The Role of Echocardiography

The role of echocardiography in patients with aortic stenosis is:

- To evaluate the level of stenosis and describe the anatomy
- To evaluate the severity of stenosis
- To assess the left ventricle

Evaluate the Level of Stenosis and Describe the Anatomy

The strength of echocardiography is its spatial resolution and thus the ability to describe the various components of the aortic root, ascending aorta, and valve in great detail. If the valve is normal with freely moving cusps, this excludes aortic stenosis at valve level. The best projections for the anatomic description are the parasternal long- and short-axis views.

A systematic evaluation of the subaortic region, aortic sinuses, the sinotubular junction, and ascending aorta is mandatory. If pathology is strongly suspected yet transthoracic imaging is suboptimal, a transesophageal examination of the aortic root and valve may be necessary.

Very often following a valvular aortic stenosis, particularly of a bicuspid valve, there is a degree of poststenotic dilatation of the ascending aorta, above the sinotubular junction. This is important to notify as when the dilatation exceeds 55 mm, there may be an indication for the surgeons to also replace part of the ascending aorta at the same time as replacing the aortic valve. The poststenotic dilatation of the ascending aorta is almost exclusively seen in congenital aortic valve stenosis, and it is probably due to the eccentric jet impinging on to a soft aortic wall leading to its expansion.

Evaluate Severity of Stenosis

This is performed with a combination of Doppler echocardiography and two-dimensional imaging. Doppler echocardiography is used for the determination of the direction and velocity of a moving blood volume, the estimation of valvular gradients, and the estimation of intracardiac pressures.

Doppler ultrasound measures the difference between the transmitted and returned frequencies. This change in frequency occurs when the ultrasound wave hits the moving blood cells. The faster the blood flow in relationship to the transducer, the greater the change in frequency. Normal blood flow is laminar; the direction and the velocity of red blood cells are approximately the same at one time. When there is disturbance to this blood flow there is disruption to the normal laminar pattern becoming turbulent. Most of the time turbulent blood flow indicates underlying pathology. In aortic stenosis there will be both an increased turbulence and a marked rise in blood flow velocity at the level of stenosis.

Pressure Gradients

Pressure gradients (PG) across a stenotic aortic valve may be measured using the Bernoulli equation:

$$\mathrm{PG\,(mmHg)} = 4\left(V_2^2 - V_1^2\right),$$

where:

– V_1 is the velocity in the LV outflow track, usually measured by Pulsed-wave Doppler at the level where the outflow velocity is aliasing using color Doppler (apical five-chamber projection)
– V_2 the velocity across the aortic valve measured by continuous-wave Doppler

When the proximal (outflow) velocities are below 1 m/s, it is acceptable to ignore this and simply square and multiply by 4 the maximal transaortic velocity.

$$\mathrm{PG\,(mmHg)} = 4V^2.$$

It is important to remember that the maximum instantaneous pressure gradient obtained by Doppler is *different* from peak-to-peak pressure gradient frequently measured in the catheterization laboratory, so that the two are not comparable (Fig. 7.10). The latter is a nonphysiologic parameter since the peak LV pressure and the peak aortic pressures do not occur simultaneously. It is recommended that one should routinely measure the mean transvalvular gradient by tracing the outer border of spectral Doppler envelope from the CW

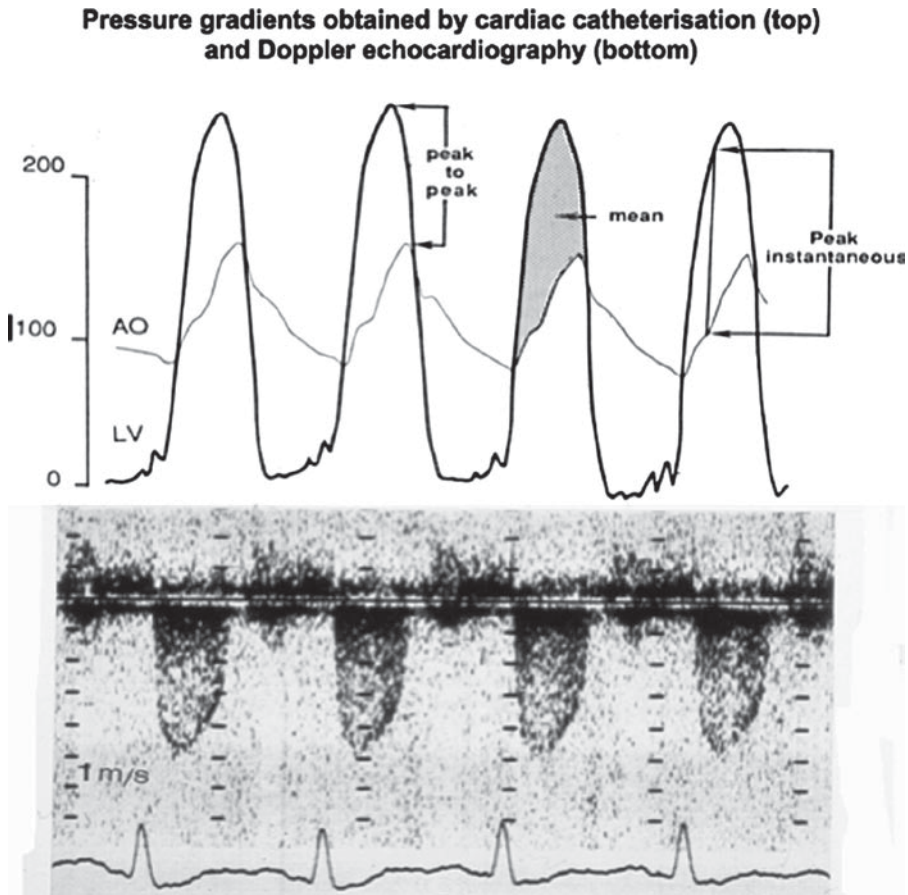

Fig. 7.10 Pressure gradients obtained by cardiac catheterization (*top*) where aortic and left ventricular pressures are obtained simultaneously. The commonest pressure gradient provided here is the peak-to-peak gradient, which is clearly less than the peak instantaneous gradient provided by continuous-wave Doppler (*bottom panel*). The ideal measurement is the mean pressure gradient provided by both cardiac catheterization and Doppler echocardiography (see text)

Doppler interrogation of flow through the aortic valve. If the hemodynamic conditions are similar between the patient studied in the catheter laboratory and the echo laboratory, then those two gradients should be comparable. In patients with normal LV systolic function the mean gradient correlates well with the severity of aortic stenosis and aortic valve area.[2]

Aortic Valve Area

Pressure gradients are largely dependent on left ventricular function. A small hyperdynamic left ventricle will produce high LV outflow velocities, as well as high transaortic velocities translating often to an overestimation of aortic severity. Similarly, an impaired LV function will produce low outflow and transaortic velocities with the potential of underestimating severity of aortic stenosis.

Calculating aortic valve area is taking into consideration the left ventricular contraction, and consequently the LV outflow velocity, which is factored in the continuity equation used to calculate the aortic valve area.

$$\mathrm{AVA\,cm^2} = (\pi R^2 \mathrm{TVI_{LVOT}}) / \mathrm{TVI_{AA}}$$

where AVA is aortic valve area, R the radius of the LV outflow track, $\pi = 3.14$, $\mathrm{TVI_{LVOT}}$ the time velocity interval of the outflow track and $\mathrm{TVI_{AA}}$ is the time velocity interval across the aortic valve

The diameter of the left ventricular outflow is calculated from parasternal long-axis projections just under the insertion of the aortic cusps (Fig. 7.11, left panel).

The flow velocity at the annulus/outflow track is obtained with Pulsed-Wave Doppler from the apical long-axis view and by placing the sample volume at the level of aortic annulus. The closing click of the aortic valve should be recognized (Fig. 7.11, right panel). The product of left ventricular area to the velocity equals left ventricular outflow track flow.

For the transaortic velocities, one should use the Continuous-wave Doppler from several projections to assure that the maximal velocity is obtained. The typical projections are the apical five-chamber, three-chamber, the right parasternal (usually with a stand-alone CW transducer) and suprasternal views. It is also possible to use the maximal velocities instead of the TVI when this is not optimally visualized but in general, for volumetric measurements it is always preferred to use the TVI.

Advantages of Continuity Equation

Coexisting aortic regurgitation does not affect the calculation of the aortic valve area

Coexisting left ventricular dysfunction has little effect on calculating valve area unless the stroke volume is severely reduced.

Problems Using the Continuity Equation

One of the difficulties and consequently source of error in calculating aortic valve area is the measurement of the outflow track diameter. For this, one should obtain a high parasternal long-axis projection centered around the aortic root and ascending aorta with reduced gains so that the subaortic region is perpendicular to the sector. The outflow diameter is then measured at about the level of aortic cusp insertion in systole.

The main problem of this calculation results from the measurement of the outflow diameter, which is hardly reproducible and it varies from individual to individual. In patients with a rather small LV outflow diameter (less than 2 cm) the aortic stenosis severity may be overestimated. Conversely, when the LV outflow is rather large (>3 cm) then the aortic stenosis severity may be underestimated.

The aortic area may vary depending on the patient's body surface area. It is therefore advisable to correct the aortic valve area to body surface area. Table 7.1 shows the range of aortic stenosis severity per aortic valve area.

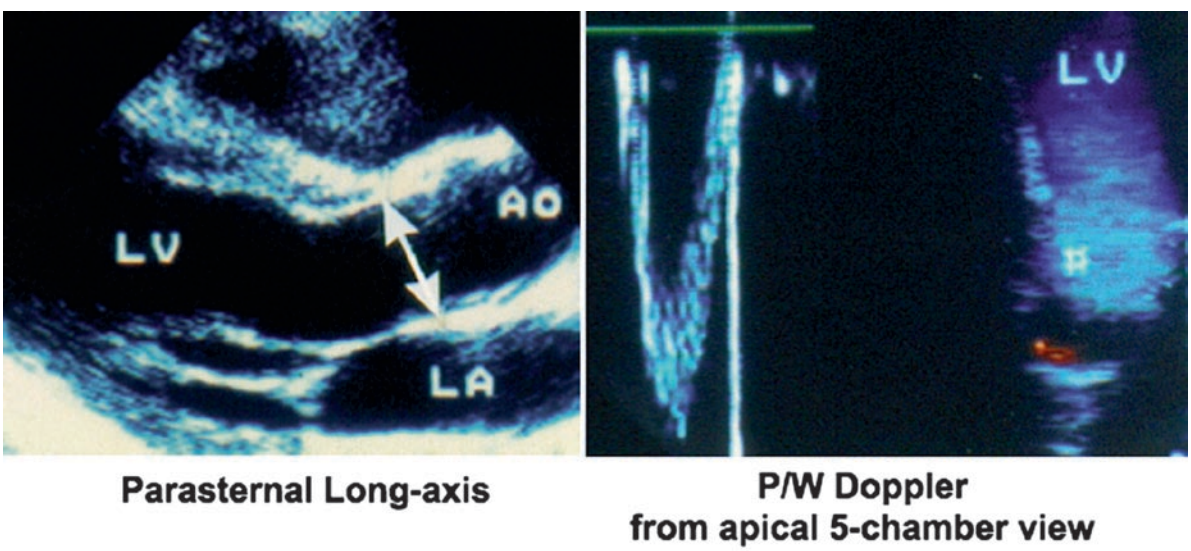

Fig. 7.11 Cross-sectional echocardiographic and Doppler imaging of the heart demonstrating how measurements are performed to assess left ventricular stroke volume (see text). On the left, measurement of the left ventricular outflow and on the right pulsed-wave Doppler with the sample volume positioned at the level of the highest left ventricular outflow track velocity seen on color Doppler

Table 7.1 Definition of severity of aortic stenosis

Degree	ACC/AHA (cm^2)	WG VHD ESC (cm^2/m^2)
Mild	>1.5	>1.0
Moderate	1.0–1.5	0.5–1.0
Severe	<1.0	<0.6

ACC/AHA Guidelines. Bonow, et al. *JACC*. 1998; WG VHD ESC European Guidelines; Lung, et al. *Eur Heart J*. 2002;23:1253–1266

Finally, it is important that the outflow track area and flow measurement using the TVI at the LV outflow be measured at the same level.

Outflow-to-Aortic Velocity Index

This is a simplified way to estimate severity of aortic stenosis by using the basic continuity equation excluding the outflow diameter, which often is a source of error, yet taking into consideration left ventricular contractility.

A ratio of <25% will imply severe aortic stenosis, whereas a ratio of >50% will be normal.

Valve Resistance

Calculations using the Bernoulli equation as well as the continuity equation (to calculate aortic valve area) are flow dependent. Increased flow rate will lead to increased valve area, and a reduced flow rate will lead to reduced valve area. Significant variations of flow rates therefore will introduce a source of error in calculating aortic stenosis severity in low- or high-output states.

To minimize errors in assessing severity of aortic stenosis in these circumstances, it may be possible to calculate the valve resistance, which is relatively a flow-independent measurement and depends on the ratio of mean pressure gradient and mean flow rate calculated as follows:

Resistance (R)

$$(\text{dyne} \times \text{S} \times \text{cm}^{-5}) = \Delta P_{\text{mean}}(\text{mmHg})/Q_{\text{mean}}(\text{ml/ s}) \times 1{,}333(\text{dyne} \times \text{S} \times \text{Cm}^{-5})$$

where:

- Stroke Volume calculated as: $\text{SV(ml)} = \text{VTI}_{\text{LVOT}} \times \text{CSA}_{\text{LVOT}}$
- Mean systolic transvalvular flow rate (Q_{mean}) (ml/s) is obtained by dividing SV (ml) by systolic ejection time (s).
- Peak instantaneous pressure gradients ($\Delta\text{PG}_{\text{peak}}$) were calculated according to the simplified Bernoulli equation:

$$\Delta\text{PG}_{\text{peak}} = 4V^2 \text{ max.}$$

V_{max} is the maximum transvalvular velocity as obtained by CW Doppler

- The mean pressure gradient (ΔP_{mean}) is derived by averaging peak instantaneous pressure gradients over the ejection period. This may be obtained simply by integrating the instantaneous transaortic velocity obtained by CW. Most of equipment software will provide the mean pressure gradient automatically.

Example:

ΔP_{mean} 40 mmHg
SEP (ejection time) systolic ejection period (CW) ms = 344 or 0.344 s
SV (PW) 49 ml
Calculation of Q_{mean} (ml/s) = SV/ET = 49 ml/0.344s = 142 ml/s
R= 40 mmHg/142 ml/s = 0.282 × 1,333 = 375 dyne × S × cm^{-5}.

Potential Advantages

1. It is simple to obtain and, unlike the Gorlin equation, avoids the use of an empirical constant. The constant 1.333 is simply a conversion factor to units of dynes × s × cm^{-5}.
2. It may be less flow dependent than aortic valve area (AVA) calculations.
3. It allows the distinction of mild-to-moderate AS with a functionally small AVA (pseudosevere AS) from truly severe stenosis in the setting of low flow – low gradient AS.[3]

Summary

- While this calculation is useful, it is not used routinely except in those clinical settings where there are concerns regarding cardiac output.
- In low flow – low gradient AS, valve resistance < 120 dyne × S × cm^{-5} appears to identify pseudosevere AS, whereas valve resistance > 180 dyne × s × cm^{-5} implies truly severe AS.

- However, values between 120 and 180 dyne × s × cm^{-5}, which are very common in this setting, are not diagnostic.

Aortic Stenosis and Left Ventricular Dysfunction

In patients with left ventricular dysfunction and reduced cardiac output it is often difficult to assess the true aortic stenosis severity due to the flow dependence of the Bernoulli and continuity equations. Pressure gradients therefore will be low and the aortic valve area may be underestimated. This is a clinically important issue because any aortic valve replacement will carry increased mortality and morbidity in those patients.

Dobutamine stress echocardiography may be useful in evaluating the true aortic stenosis severity by progressively increasing the stroke volume across the stenotic valve with inotropic/chronotropic stimulation of the heart.

Patients with low-gradient aortic stenosis, demonstration of contractile reserve during dobutamine stress echocardiography predicts a low operative risk and a good long-term prognosis after valve surgery, whereas the lack of contractile reserve predicts a high operative mortality.

- With mild to moderate aortic stenosis, augmentation of transaortic flow rate with dobutamine will result in a significant increase (0.2 cm^2) in valve area as the flexible leaflets open to a greater extent. Due to the inotropic stimulation, the outflow velocity will increase disproportionally to the transaortic velocity; thus, the valve area will increase.
- Conversely, with critical aortic stenosis, the valve area will change very little despite increased transaortic flow rate and stroke volume because the cusps are stiff, rigid, and possibly calcified. In such patients, dobutamine infusion will increase outflow and transaortic velocities proportionally so that the ratio of peak aortic velocity and outflow velocity will remain the same.
- The third and worse possibility will be if the left ventricle does not respond to dobutamine stimulation with increased contractility as might occur in the setting of coronary artery disease and extensive myocardial infarction. Here, neither the jet velocity across the aortic valve nor the maximal gradient will increase. These patients will carry a high mortality irrespective of the treatment options.

Clinical Decision Making

Aortic stenosis is a progressive disease irrespective of the underlying cause. The overall rate of progression is with an annual increase in aortic velocity of approximately 0.3 m/s or increase in mean gradient of 8–10 mmHg and a reduction of valve area of 0.1 cm^2.

The management of patients with aortic stenosis will depend upon:

- Severity of aortic stenosis
- Symptoms
- State of the left ventricle
- Associated clinical conditions that may increase the operative risk (comorbidity), i.e., coronary artery disease, general patient's status etc

Most symptomatic patients need to be operated as soon as possible.

Asymptomatic patients will need to be followed up carefully in clinics (every 6 months). The role of echocardiography here is pivotal as any further reduction in valve area, or developing left ventricular dysfunction will need to expedite the patient to surgery.

Stress testing in asymptomatic patients is an important determinant of outcome.

Treadmill exercise may be useful in uncovering functional and hemodynamic impairment that may be clinically silent. Signs such as unexpected hypotension, inadequate blood pressure increase, rhythm disturbances, and signs of ischemia are all of prognostic importance. This however will need to be carefully supervised medically so that early symptoms during exercise may be promptly recognized.

Dobutamine stress may help particularly in patients with impaired left ventricular function (see earlier).

Conclusions

Echocardiography plays a very important role in managing patients with aortic stenosis from diagnosis to monitoring patients with asymptomatic aortic stenosis. Careful quantitation by experts is very important so

that any changes are real rather than falling within the operator's variability of measurements. Patients with ventricular dysfunction and aortic stenosis need some specific consideration as those may be of higher surgical risks. Stress testing is safe as long as it is performed by physicians who know what to look for.

B. Aortic Regurgitation

Introduction

Aortic regurgitation is one of the commonest valvular lesions and has many causes (Table 7.2). While acute aortic regurgitation may be suspected by the patient's symptoms, chronic aortic regurgitation may often passed unnoticed for many years and may be uncovered by an incidental clinical examination of Echocardiographic study. Echocardiography and Doppler are currently the diagnostic methods of choice for the assessment of the severity of aortic regurgitation and remodeling of the cardiac chambers in response to the volume overload state.

Table 7.2 Etiologies of aortic regurgitation

Calcific degenerative disease
Rheumatic
Congenital
Bicuspid, unicuspid, quadricuspid
Aortic cusp prolapse with VSD
Connective tissue disease
Marfan's
Ehlers–Danlos
Osteogenesis imperfecta
Inflammatory aortitis
Ankylosing spondylitis
Rheumatoid arthritis
Reiter's syndrome
Endocarditis
Dissection
Others
Syphilitic aortitis
Aortic root dilatation (hypertension, atheromatous)

Etiology of Aortic Regurgitation (Table 7.2)

There are several conditions that may lead to aortic regurgitation:

- Degenerative
- Rheumatic
- Congenital (bicuspid)
- Endocarditis
- Connective Tissue Disease
- Inflammatory aortitis
- Dissection
- Others

Degenerative Disease

This is by far the commonest etiology and it is related to age degeneration of the aortic valve with cholesterol and fibrous tissue deposition and subsequent calcification. This can lead to a mixed disease, regurgitation, and stenosis of variable predominance. Often encountered in the middle-aged population and the elderly, and usually chronic with little variation from year to year (Fig. 7.12).

Rheumatic

The second commonest etiology typically in association with rheumatic mitral Stenosis. Also usually resulting to mixed disease but often predominantly regurgitant.

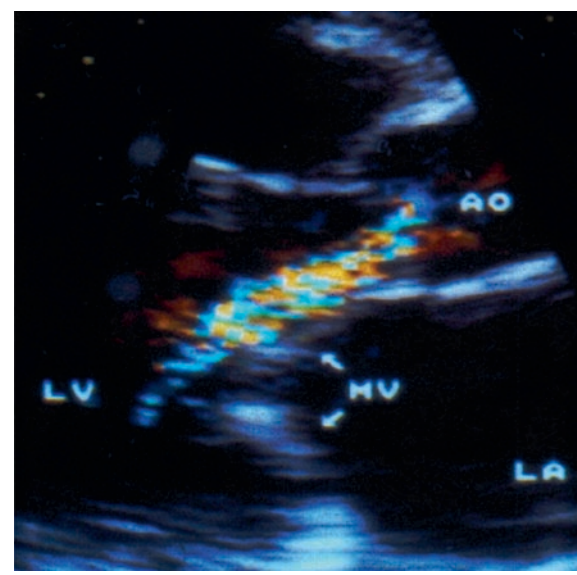

Fig. 7.12 Parasternal long-axis view from a patient with degenerative aortic regurgitation. *Ao* Aorta, *MV* mitral valve, *LA* Left atrium, *LV* Left ventricle

Congenital

The commonest cause here is bicuspid aortic valve. In the young, it is frequently the valve regurgitation that dominates the clinical picture, but occasionally, it may be more stenotic. Other congenital malformations of the aortic valve may be a unicuspid or quadricuspid valve. These malformations however are rare.

An important cause of aortic regurgitation in congenital heart disease is the prolapse of an aortic cusp into a ventricular septal defect just below the valve. While the VSD may be small, the aortic regurgitation may become the dominant lesion often requiring surgical intervention in adolescent or adult life.

Endocarditis

The aortic valve may be the site of infection, particularly if the valve is already abnormal. Depending on the duration of illness and the virulence of the bacteria, there may be a more or less rapid growth of vegetations, the hallmark of endocarditis, but at the same time there may be also direct valve destruction and perforations leading to valvular regurgitation (Fig. 7.13).

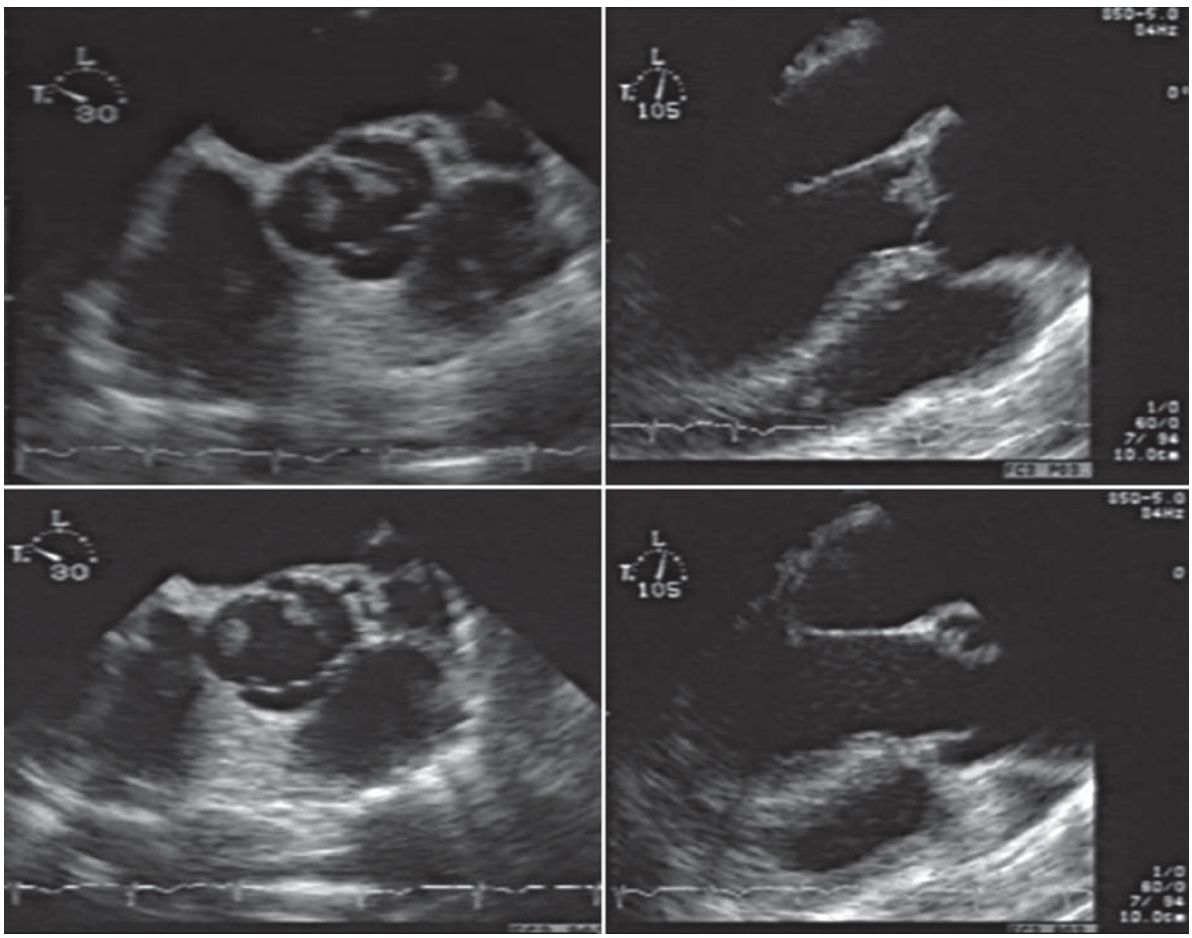

Fig. 7.13 Transesophageal images of the aortic valve in short axis (*left*) and long axis (*right*) demonstrating small vegetations up on the left- and right-coronary cusps during systole. In diastole, the vegetations are seen protruding into the LV outflow track (*top right panel*)

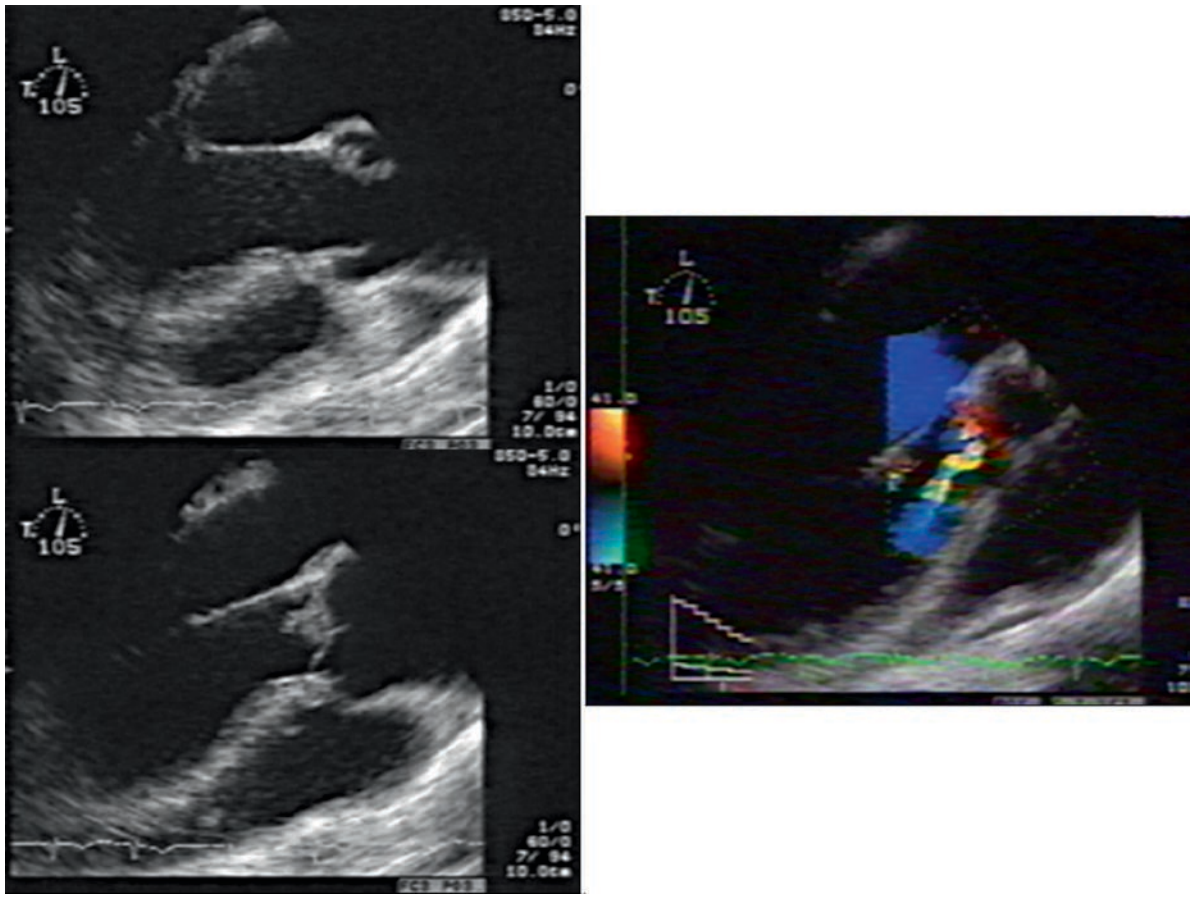

Fig. 7.14 Transesophageal projections from the same patient with infective endocarditis. Notice on the right panel the presence of aortic regurgitation

If infection extends in the perivalvular area upward in the aortic sinuses or downward in the proximal ventricular septum, there may be abscess formation, which may perforate in the surrounding tissues. Figure 7.14 is a transesophageal picture from the same patient demonstrating a typical aortic Regurgitant jet.

Connective Tissue Disease

The following conditions lead to aortic regurgitation secondary to aortic root Dilatation, leaving the aortic cusps largely unaffected. The commonest condition is Marfan's syndrome (Fig. 7.15), which is a disorder of the collagen.

The classical clinical picture is that patients are tall and slim with scoliosis, long thin fingers called

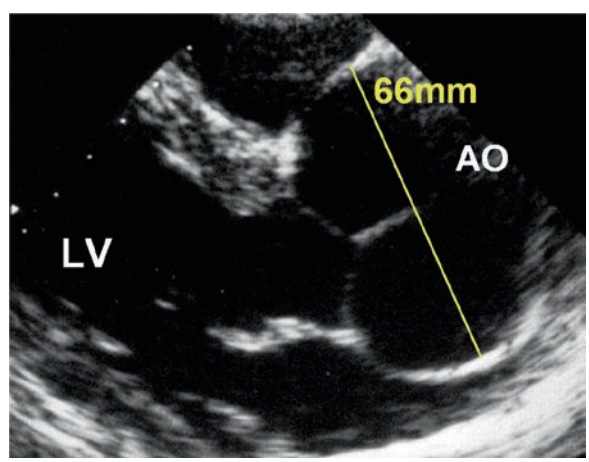

Fig. 7.15 Parasternal long-axis projection from a patient with Marfan's syndrome. Notice the very large aortic root (66 mm) at the level of the aortic sinuses. *Ao* Aortic root, *LV* Left ventricle

arachnodactyly, lax joints, slender "asthenic" built, lens dislocation, high palate, and aortic root dilatation.

Other syndromes that can lead to aortic dilatation are the Ehlers–Danlos syndrome and osteogenesis imperfecta.

Inflammatory Aortitis

These are systemic conditions that affect the aortic wall or even the valve itself, which may appear edematous and inflamed at surgery. Ankylosing spondylitis causes fibrosis that distorts the aortic root and sometimes the valve itself. Similar appearances may be seen in association with rheumatoid arthritis, psoriasis, and Reiter's syndrome.

Aortic Dissection

This is often an acute presentation of a hypertensive patient with chest pain irradiating to the back. ECG changes are nonspecific and chest X-ray shows an enlarged aortic shadow. Echocardiography may show a dilated aortic root, although a normal size root is not infrequent. The hallmark of aortic dissection is the identification of an intimal flap, that is a separation of the aortic wall with the intima "flapping" in the aortic lumen (Fig. 7.16). Aortic dissection may be localized only in the ascending aorta (type A), or extend all the way down to the descending aorta (Type B). Aortic regurgitation may ensue from the protrusion of the aortic intima down to the left ventricular outflow track. Echocardiography is pivotal in the diagnosis, not only of the intimal flap in the proximal aorta but more important for the detection of aortic regurgitation, which will guide the surgical strategy.

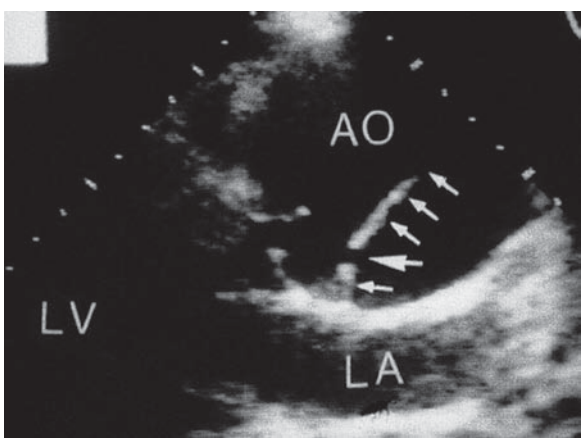

Fig. 7.16 Parasternal long-axis projection from a patient with acute aortic dissection (Type A). Notice the intimal flap (*arrows*) and the lack of apposition of the aortic cusps in diastole. *Ao* Aorta, *LA* Left Atrium, *LV* Left Ventricle

Others

Other rare conditions of the aortic wall can lead to aortic regurgitation secondary to aortic root dilatation. Such conditions are syphilis or aortic aneurysms from chronic systemic hypertension and diffuse atherosclerosis.

Methods of Assessing Aortic Regurgitation

In 2003, the ASE jointly with the ACC Echo committee, the Cardiac Imaging Committee, the American Heart Association and the ESC, working group on echocardiography, developed joint recommendation of the evaluation of the severity of value regurgitation.[4]

Doppler Methods

Color-Flow Doppler

Color-Flow imaging directly shows the regurgitant flow through the aortic valve during diastole. Because the jet direction may be unpredictable, it is important to image the aortic regurgitant jet from several projections so that a three-dimensional evaluation may be obtained. The three most important projections are the parasternal long axis, the apical 5-chamber, and 3-chamber projections.

The regurgitant flow has three components that can be visualized:

- The jet size (area) and direction
- The flow convergence region in the aorta (PISA)
- The vena contracta through the regurgitant orifice

Regurgitant Jet Size

This is simple to do but it has to be assessed from all available projections so that the largest jet area may be

obtained. It is important to remember that the length of the aortic regurgitant jet should not be used as an indicator of severity. It is better to estimate the severity of AR based on jet size in the LV outflow, but this is only as a gross indicator of the degree of AR.

It is important to evaluate the direction of the jet. When the jet is perpendicular against the anterior mitral leaflet or parallel to the ventricular septum, this may lead to an underestimation of the severity of AR. It may also indicate a structural abnormality of the valve (e.g., prolapse, flail, or perforation).

Flow Convergence or PISA

This is less often performed than in mitral regurgitation and its accuracy may not be as good. Transthoracically it is very difficult to quantitate but transesophageally may be easier.

Images are zoomed on the valvular and supravalvular region. The Nyquist limit is adjusted to obtain a rounded and measurable flow convergence zone, and the aliasing radius is measured from the stop frame with the largest observable PISA.

CW Doppler recording of the regurgitant peak velocity and velocity time integral allows calculation of the EROA and regurgitant volume.

The thresholds for severe AR are an EROA ≥0.30 cm^2 and a regurgitant volume ≥60 ml.

Vena Contracta

It is defined as the smallest neck of the flow region at the level of the aortic valve immediately below the flow convergence region and provides an estimate of the EROA.

Imaging of the vena contracta is performed from parasternal long-axis projections with the zoom function centered at the aortic root. To specifically image the vena contracta, it is often necessary to angulate the transducer out of the normal echocardiographic imaging planes such that the area of proximal flow acceleration, the vena contracta, and the downstream expansion of the jet can be distinguished.

The threshold of vena contracta width associated with severe aortic regurgitation is >0.6 cm, while moderate between 0.3 and 0.6 cm.

Pulsed and Continuous-Wave Doppler

Quantitative Flow Methods (See Also Chap. 3)

Quantitation of flow with pulsed Doppler for the assessment of aortic regurgitation is based on comparison of measurement of aortic stroke volume at the LVOT (aortic annulus) with mitral or pulmonic stroke volume.

This method is simple but does require careful measurements and regular practice.

Stroke volume (SV) at the left ventricular outflow track is derived as the product of cross-sectional area (CSA) of the left ventricular outflow at the level of the aortic annulus and the velocity time integral (VTI) of flow at the annulus. So,

$$SV_{LVO} = CSA_{LVO} \times VTI_{LVO}.$$

If the mitral valve is chosen for comparison, which is also the commonest option, then the calculation of the SV across the mitral valve is derived as the product of the mitral annular CSA (assuming a circular geometry) at the level of the mitral annulus (the diameter measured from apical four-chamber views) and the VTI of mitral inflow at the level of the mitral annulus. Thus.

$$SV_{M} = CSA_{M} \times VTI_{M}.$$

Alternatively, the pulmonic stroke volume could be used for comparison with the left ventricular outflow derived as the product of cross sectional area (CSA) of the right ventricular outflow at the level of the pulmonary valve annulus and the velocity time integral (VTI) of flow at the annulus. This method however is not widely used because of the difficulty in measuring the right ventricular outflow diameter. It is used, however, when there is also significant mitral regurgitation, in which case the mitral valve annulus cannot be used for comparison.

In the presence of aortic regurgitation, without any intracardiac shunt, the flow through the aortic valve will be larger than through the other competent valves chosen for comparison (mitral or pulmonic). The difference between the two represents the regurgitant volume (RV):

$$RV(ml) = SV_{LVO} - SV_{M}$$

Regurgitant fraction (%) is then derived as the regurgitant volume divided by Stroke Volume through the left ventricular outflow:

$$RF(\%) = (SV_{LVO} - SV_{M}) / SV_{LVO} \times 100.$$

For mild aortic regurgitation RF is <30%, moderate 30–50%, and severe >50 ml. Effective regurgitant orifice area can be calculated similar to the PISA method as regurgitant volume divided by the velocity time integral of the aortic regurgitant jet velocity (VTI_{AR}) recorded by CW Doppler as:

$$EROA = RV/VTI_{AR}.$$

Total stroke volume (aortic stroke volume) can also be derived from quantitative 2D measurements of LV end-diastolic and end-systolic volumes. This method however may result in a significant underestimate of volumes if optimal endocardial border delineation is not achieved.

A regurgitant volume ≥60 ml and EROA ≥0.30 cm^2 are consistent with severe AR.

Errors

The most common errors encountered in determining these parameters are:

1. Failure to measure the valve annulus properly (error is squared in the formula)
2. Failure to trace the pulsed-wave velocity correctly (brightest signal representing laminar flow)
3. Failure to position the sample volume correctly at the level of the annulus.
4. In the case of significant calcifications of the mitral annulus and valve, quantitation of flow at the mitral site is less accurate and more prone to errors

Aortic Diastolic Flow Reversal

It is normal to observe a brief diastolic flow reversal in the thoracic aorta. The flow reversal is best recorded in the upper descending aorta below the aortic isthmus using a suprasternal view. With increasing aortic regurgitation both the duration and the velocity of the reversal increase. Therefore, a holodiastolic reversal is usually a sign of at least moderate aortic regurgitation and appears to be more specific if recorded from the abdominal aorta.

In severe aortic regurgitation there will be a prominent, holodiastolic flow reversal in the descending aorta.

Signal Density

The density of the CW Doppler spectral display of the AR jet reflects the volume of regurgitation, especially in comparison to the antegrade spectral density Doppler jet density is an imperfect indicator of severity of AR

Diastolic Jet Deceleration

The rate of deceleration of the diastolic regurgitant jet and the derived pressure half-time reflect the rate of equalization of aortic and LV diastolic pressures. With increasing severity of AR, aortic diastolic pressure decreases more rapidly, while left ventricular end-diastolic pressure will be increasing. As a result, the end-diastolic pressure gradient between aorta and LV will be reduced. The rate of such reduction indicates severity of aortic regurgitation. The late diastolic jet velocity is lower and hence pressure half-time is shorter (Fig. 7.17).

Pressure half-time of the aortic regurgitant jet is easily measured if the early peak diastolic velocity is well visualized.

A Pressure half-time ≥500 ms will indicate mild aortic regurgitation, 200–500 moderate, and <200 severe.

One limitation of PHT is that it is also shortened with increasing LV diastolic pressure secondary to left ventricular dysfunction and impaired compliance. The impact of LV dysfunction on the PHT however is much less than the aortic regurgitation itself so that despite this, PHT remains a very valid method of assessing severity of aortic regurgitation. When PHT is >200, it is safe to rule out severe aortic regurgitation.

Assessment of Ventricular Function

Significant aortic regurgitation (moderate and severe) will be accompanied by a characteristic left ventricular remodeling. The LV will become dilated and volume loaded and will be globular in shape. The left ventricle is able to accommodate the large regurgitant volume by dilation and thereby maintain a normal cardiac output until the late stages of the disease. Consequently, patients often tolerate severe aortic regurgitation for many years without developing symptoms. The main concern however is that while the ventricle dilates and the patient remains asymptomatic, irreversible damage to the left ventricle may be occurring that ultimately may impact on mortality and morbidity following valve replacement.

The duration (acute or chronic) and the severity of valvular regurgitation are among the most important

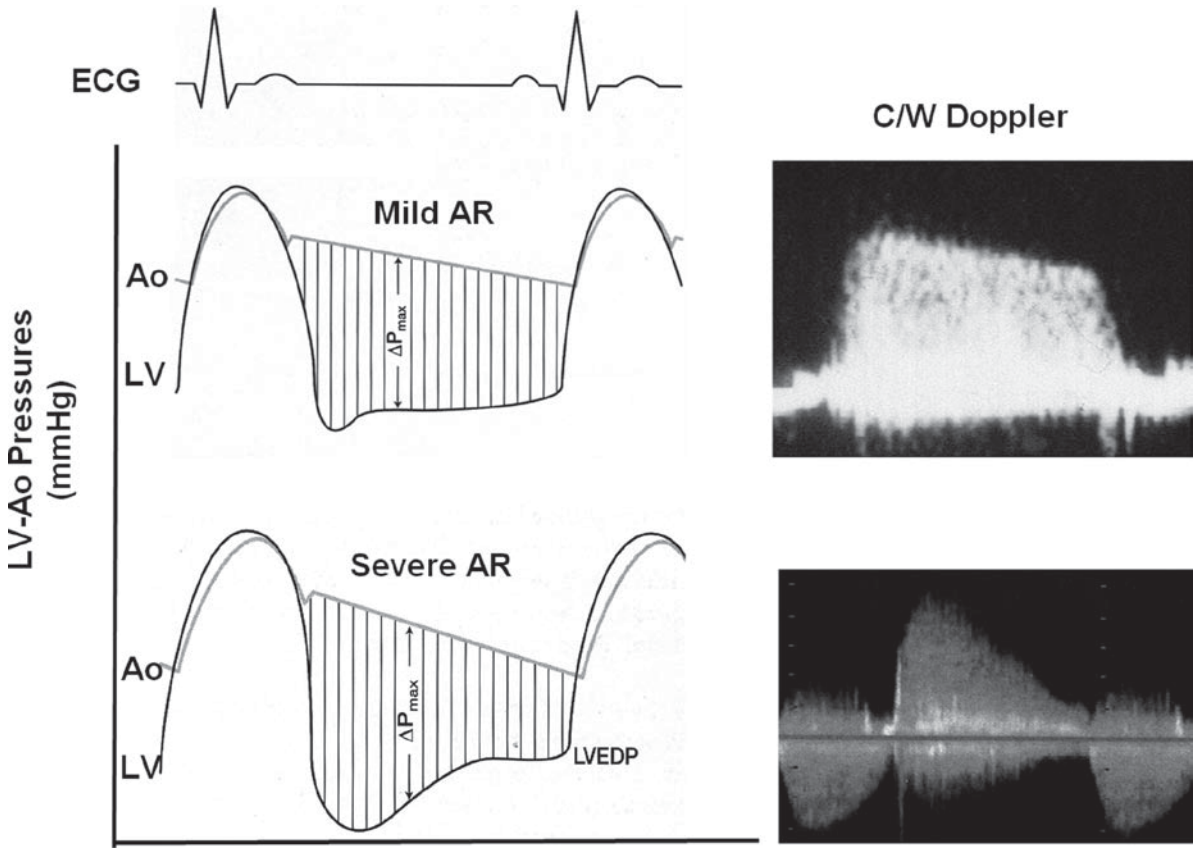

Fig. 7.17 Left-ventricular and aortic pressure tracings in mild (top) and severe (bottom) aortic regurgitation. Note that the late pressure drop is decreasing, with the increasing severity of aortic regurgitation, predominantly because of the increasing left ventricular end diastolic pressure (LVEDP)

determinants of the adaptive changes that occur in the cardiac chambers in response to the regurgitant volume.

Acute aortic regurgitation however will be characterized by normal size left ventricle contracting vigorously. Conditions that lead to such acute changes are acute bacterial endocarditis and aortic dissection. In these conditions, the LV does not result in such remodeling and may be normal in size.

While such cardiac chamber remodeling is not specific for the degree of regurgitation, its absence in the face of chronic regurgitation should imply a milder degree of aortic regurgitation.

Assessing ventricular function is performed with two-dimensional echocardiography.

While assessing ventricular volumes may be useful, simple ventricular dimensions may be more reproducible when it comes to accurate follow-up measurements. What is important in patients follow-up is looking for consistent changes in ventricular size so that a measurement with the least interobserver variability is probably the most reliable.

More recently, Tissue Doppler Imaging may be used to assess more subtle changes in systolic or diastolic function, but longitudinal studies are still scarce.

Acute vs. Chronic Aortic Regurgitation

There are different etiologies for these conditions.

- In chronic aortic regurgitation, the commonest etiologies are bicuspid aortic valve or progressive degenerative aortic degeneration.

The left ventricle is often dilated with a moderate at most diastolic velocity slope and the patient is often asymptomatic.

- In acute aortic regurgitation the etiologies are usually aortic valve endocarditis or aortic dissection. The left ventricle is not dilated but contracting vigorously. Diastolic pressure are rapidly rising,

the diastolic murmur is quieter with a steep diastolic slope on C/W. There may be early mitral closure in severe cases due to the very high end-diastolic LV pressure exceeding that of the left atrial pressure.

The patient is usually sick, tachycardic, and in heart failure with low diastolic blood pressure (<40 mmHg).

Conclusion

If all qualitative parameters indicate that the aortic regurgitation is only mild, there is no need for further quantification. When however the aortic regurgitation is more than mild, then it is desirable to quantitate the severity of aortic regurgitation.

Regurgitant volume and Regurgitant areas have the advantage that they can also be used in chronic moderate aortic regurgitation for follow-up so that any progression of aortic regurgitation severity may be ascertained.

References

1. Rallidis L, Naoumova RP, Thompson GR, Nihoyannopoulos P. Extent and severity of atherosclerotic involvement of the aortic valve and root in familial hypercholesterolaemia. *Heart*. 1998;80:583–590
2. Zoghbi WA, Farmer KL, Soto JG, Nelson JG, Quinones MA. Accurate non invasive quantification of stenotic aortic valve area by Doppler echocardiography *circulation*. 1986;73:452–459
3. Mascherbauer J, Schima H, Rosenhek R, Czerny M, Maurer G, Baumgartner H. Value and limitations of aortic valve resistance with particular consideration of low flow–low gradient aortic stenosis: an in vitro study. *Eur Heart J*. 2004; 25(9):787–793
4. Zoghbi WA, Enriquez-Sarano M, Foster E, et al. Recommen-dations for evaluation of the severity of native valvular regurgitation with two-dimensional and Doppler echocardiography. A report from the American Society of Echocardiography's Nomenclature and Standards Committee and the task force on valvular regurgitation, developed in conjunction with the American College of Cardiology Echocardiography Committee, The Cardiac Imaging Committee, Council on Clinical Cardiology, the American Heart Association, and the European Society of Cardiology Working Group on Echocardiography. *E J Echocardiogr*. 2003;4:237–261

Chapter 8
Mitral Valve Disease

Joseph Kisslo, J. Daniel Rivera, David B. Adams, Burkhard G. Mackenson,
James J. Jollis, and Donald D. Glower

The mitral valve is the most easily recognized moving structure in the heart. Because of its rapid to and fro motion, the mitral valve serves as "home base" for almost all echocardiographic examinations. When the transducer is directed posteriorly from the chest wall toward the heart, the most rapidly moving target will almost invariably be the anterior mitral leaflet. Most echocardiographers, therefore, learn cardiac anatomy and motion based upon relationships of the mitral valve to other structures.

Cardiac Anatomic Relationships

Parasternal Long Axis

Examination of the heart by ultrasound begins with a parasternal long axis. Figure 8.1 shows an anatomic section of the ventricular (LV) long axis from the aortic root (right side) to the left ventricular apex (left side). The right ventricle is seen anteriorly (upward) on the figure as it wraps around the left ventricle. Note that the papillary muscles of the left ventricle emerge from the ventricular free wall (arrow) and give rise to the chordae tendineae of the two mitral valve leaflets.

The longer anterior mitral valve leaflet is easily seen and connects right to the aorta directly with the posterior aortic (Ao) wall and aortic valve. Thus, there is what is called "mitral and aortic continuity" in the left heart. The posterior mitral valve leaflet is seen attached to the mitral annulus along the posterior ventricular free wall. Therefore the posterior mitral leaflet is the mural leaflet. The left atrium (LA) is posterior to the aorta and one of the main pulmonary artery (PA) branches sits posterior to the aorta and just above to the left atrium. Many observers imagine that the left atrial anterior wall and posterior aortic wall are one. That is, however, not true as there is a pericardial sinus, the transverse sinus, that is between the aorta and the left atrium. This transverse sinus will prove to be an important space for surgical approaches to the atrium in the operating room. The circumflex coronary artery and the larger coronary sinus are seen in the posterior atrioventricular groove (not marked).

Selected diastolic and systolic frames from an actual echocardiogram are seen in Fig. 8.2. A large right ventricular trabeculation is seen in the diastolic frame (left panel). In diastole, the aortic valve is in the closed position and the mitral valve is open. The anterior mitral valve leaflet is again noted to be the longest in comparison to the posterior (mural) leaflet and is contiguous with the posterior aortic wall demonstrating mitral-aortic continuity. The right-hand panel shows the same heart in systole with the closed mitral valve and the open aortic valve. The pulmonary artery main branch (PA) is seen above the left atrium and posterior to the aorta, as in the previous figure. In most patients this is the right main stem pulmonary artery branch. Behind the left atrium is the descending aorta (desc Ao). Note that the size of the left atrium (LA) is approximately the diameter of a normal aorta. When looking at an echocardiogram, observers need a quick approximation of sizes, and this is a handy relationship to keep in mind. Of course, if both the aorta and the left atrium are dilated, this approximation estimate can be misleading.

Selected diastolic and systolic frames in Fig. 8.3 show a somewhat thicker left ventricle (LV hypertrophy) with a slightly enlarged left atrium. Again, only a

J. Kisslo (✉) J. D. Rivera, D.B. Adams, B.G. Mackenson,
J.J. Jollis, and D.D. Glower
Duke University Medical Center, Durham, NC, 27710, USA
e-mail: joseph.kisslo@duke.edu

P. Nihoyannopoulos and J. Kisslo (eds.), *Echocardiography*,
DOI: 10.1007/978-1-84882-293-1_8,

portion of the right ventricle is visualized as it wraps around the left. The posterior mitral valve leaflet is attendant to the posterior wall and is easily identified by its attachment only to the wall. The anterior mitral leaflet is again identified by its connection to the posterior wall of the aorta. We emphasize these attachments as they become particularly important for recognition of the two mitral leaflets from the various two- and three-dimensional echocardiographic presentations.

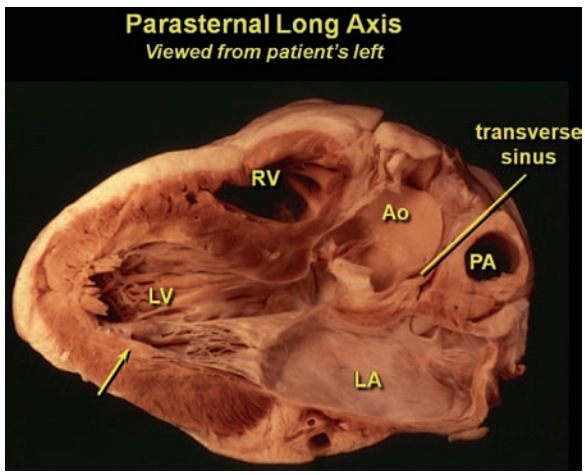

Fig. 8.1 Anatomic section cut along a typical parasternal long axis used in two-dimensional echocardiography. The *arrow* points to the base of the papillary muscles emerging from the left ventricular free wall. *LV* left ventricle; *RV* right ventricle; *LA* left atrium; *Ao* aorta; *PA* main branch of the pulmonary artery. Modified from Kisslo, Leech & Adams. Essentials of Echocardiography

Similar selected frames are seen in Fig. 8.4, this time with a remarkably dilated left atrium that is much bigger than the normal aorta. There is also a dilated left ventricle as well as the atrium in this 50-year-old patient with a severe dilated cardiomyopathy. A portion of the descending aorta (desc Ao) is seen right posterior to the heart. Note in the systolic frame (right panel) the mitral valve leaflets are again identified by their various attachments. The anterior mitral leaflet is attached to the posterior aortic wall, while the posterior mitral leaflet is attached to the ventricular wall itself. Because of this attachment of the anterior mitral leaflet to the aorta, some people call it the "aortic" mitral leaflet. This nomenclature is rarely used, but is wholly descriptive of the attachment. The "mural" leaflet is short, but is easily seen attached to the posterior left ventricular wall at the mitral annulus.

There are numerous small biologic variations in the shape and configuration of cardiac structures, but the relationships pointed out to this point are rather consistent from heart to heart in individuals with normal cardiac relationships. The anatomic section seen in Fig. 8.5

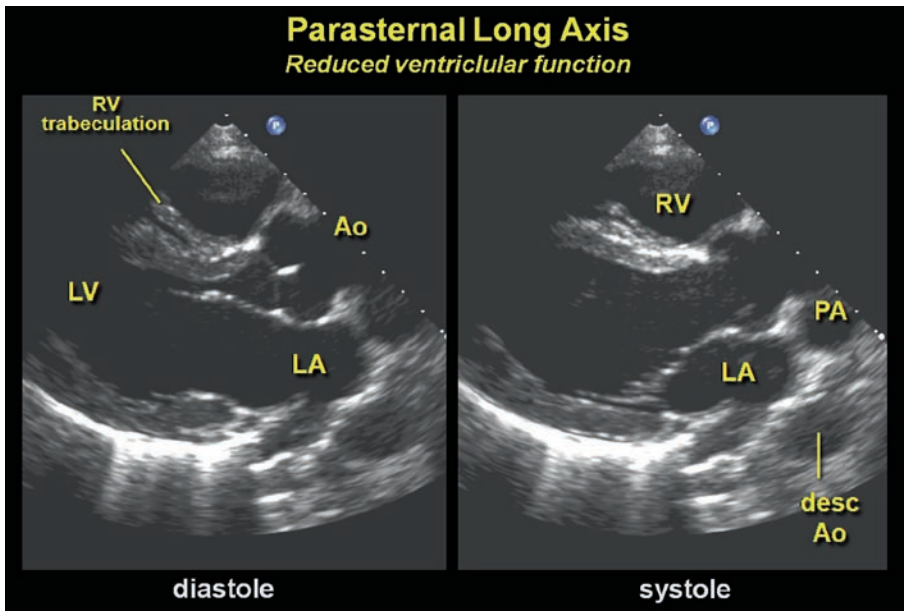

Fig. 8.2 Parasternal long axis from a patient with a normal size left atrium. Note one of the main pulmonary artery branches (PA) on the top of the left atrium (LA). Compare this with Fig. 8.1

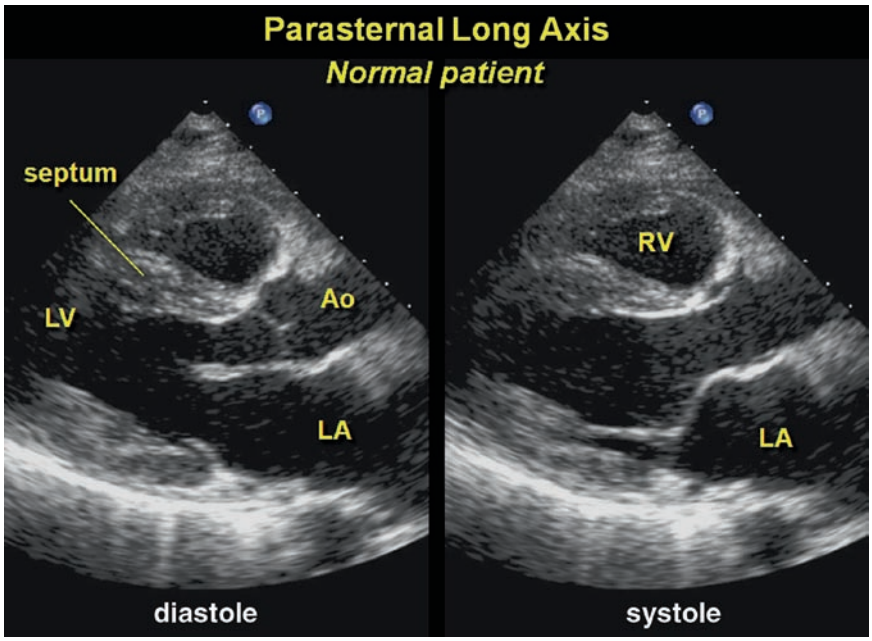

Fig. 8.3 Parasternal two-dimensional echocardiographic images in diastole and systole from a normal patient demonstrating mitral valve echocardiographic anatomy. Note that the anterior mitral leaflet is longer than the posterior mitral leaflet

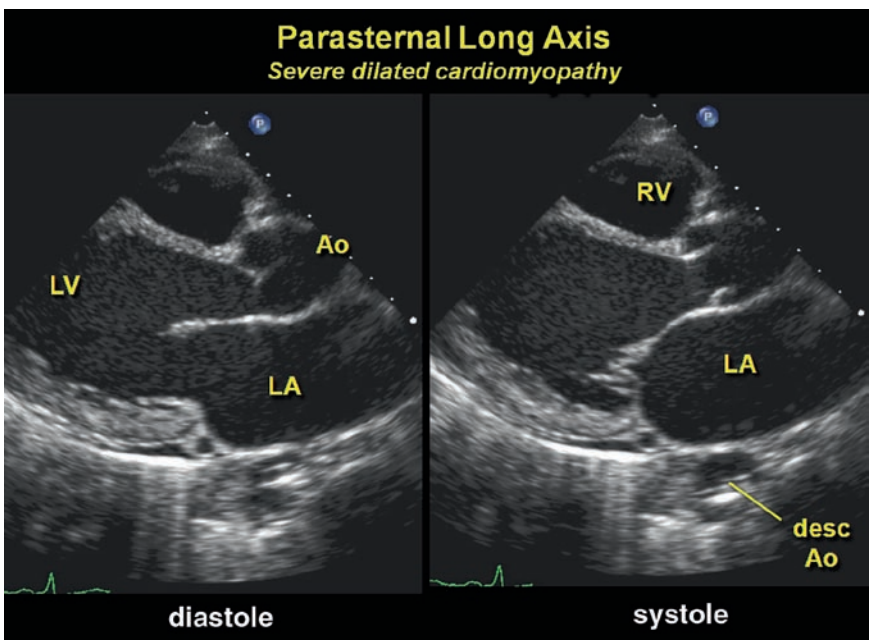

Fig. 8.4 Parasternal two-dimensional echocardiographic images in diastole and systole from a patient with a dilated cardiomyopathy, including a dilated left atrium. Note the mitral-aortic continuity. *desc Ao* descending aorta

shows the long axis of a left ventricle as viewed from the patient's left-hand side from the free wall looking medially. The interior surface of the left ventricular wall is, therefore, the interventricular septum. The face of the intraventricular septum is smooth just underneath the aortic valve, but becomes hypertrabeculated toward the ventricular apex. Again, chordae tendinea can be seen arising from a portion of the papillary muscle on the

inferior side of the ventricle that rests upon the diaphragm. This particular specimen has a uniquely good picture of the coronary sinus as it wraps in the left-sided atrioventricular groove. The transverse sinus of the pericardium is well seen as it separates the aorta and the left atrium. The transverse sinus is rarely differentiated by echocardiography techniques because it is usually collapsed and not filled with fluid. Note that the transverse sinus is not recognizable in Figs. 8.2–8.5.

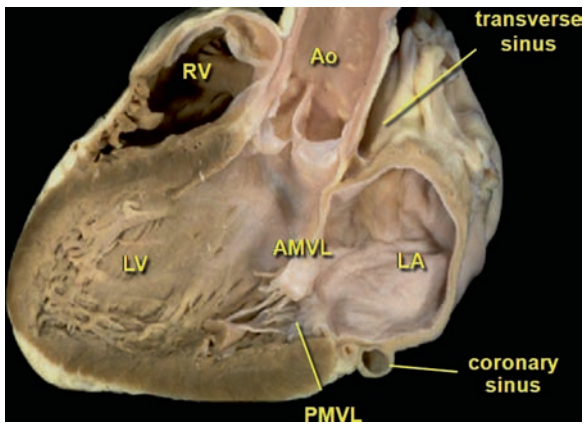

Fig. 8.5 Long-axis cut anatomic cut specimen along the plane of the long axis used for two-dimensional echocardiography. Note the chordae tendineae inserting into the tips of the mitral leaflet tips. A large coronary sinus is easily seen adjacent to a smaller circumflex coronary artery in the posterior atrioventricular groove. *PMVL* posterior mitral valve leaflet. Courtesy of Anderson R.H. Modified from Kisslo J. Thinking in 3D

Three-dimensional echocardiographic sections that appear in Fig. 8.6 show the transverse sinus to be poorly identified. However, one can see the anatomic structures of the face of the interatrial septum inside of the left atrium (LA). The diastolic frame shows the mitral valve structures in the open position and the aortic valve in its closed position.

The right-hand panel of Fig. 8.6 shows the mitral valve in its closed position. A set of primary chordae tendineae (1°) are seen attaching to the tip of the posterior mitral valve leaflet from the tip of the papillary muscle. Secondary (2°) chordae tendinea are seen going to the backside of the anterior mitral leaflet along the left ventricular outflow tract. Such secondary chordae can also be seen from papillary heads to the underside of the posterior mitral leaflet, between the leaflet and ventricular wall. These secondary chordae become very important when severe mitral regurgitation is encountered due to broken mitral chordae and surgical repair is contemplated. If chordae are intact on a leaflet opposite to the leaflet with broken chords, a chordal transfer may be done if appropriate to the repair procedure. In any event, the composite of the mitral valve in long axis contains recognition of the two mitral leaflets, their rough proportions, and details of their attachments.

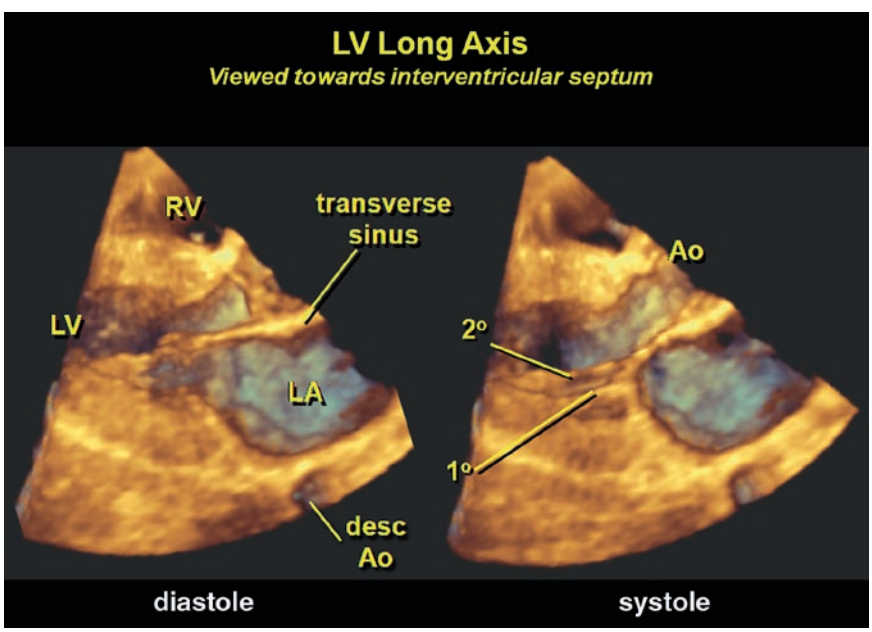

Fig. 8.6 Parasternal long-axis perspective from a three-dimensional echocardiogram viewed from the left ventricular free wall. The descending aorta is seen behind the heart. 1° = primary chordae tendineae, 2° = secondary chordae tendineae

A view from the other side of the left ventricle is seen in Fig. 8.7 where the viewer is looking at the free wall as the interior left ventricular surface. Here, the perspective is that from the intraventricular septum toward the posterior and anterior left ventricular walls. The inferomedial papillary muscle is seen along the inferior aspect of the left ventricle, while the anterolateral papillary is seen in its midventricular position, entirely on the free wall. The various chordae tendinea appear to spring from the tips of the papillary muscles in a vast array and connect to the various mitral leaflet edges as primary chordae tendinea. The attachments of the mitral leaflets are as previously described, the anterior mitral valve leaflet (AMVL) to the posterior aortic wall and aorta and the posterior mitral valve leaflet (PMVL) to the free wall. These attachments will come in handy when trying to differentiate the various leaflets of the mitral valve apparatus in free space.

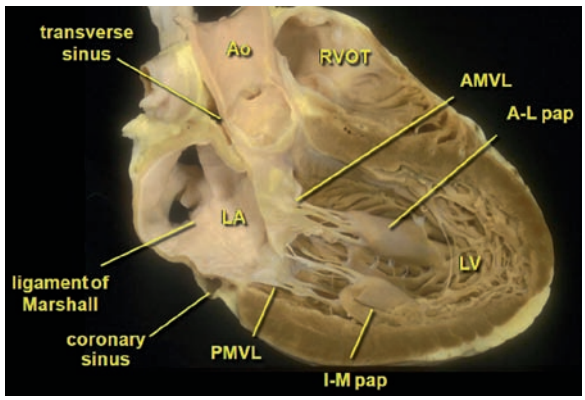

Fig. 8.7 Half of the human left ventricle anatomic specimen cut along the parasternal long axis of the left ventricle. The half shown is opposite to those shown in Figs. 8.1 and Fig. 8.5. Here the LV perspective is viewed from the ventricular septum toward the free wall and includes lateral portions of the left atrium discussed in the text. *AMVL* anterior mitral valve leaflet, *A-L pap* anterolateral papillary, *I-M pap* inferomedial papillary. Courtesy of Ho S.Y. Modified from Kisslo J. Thinking in 3D

Just above the mitral annulus in the left atrium in Fig. 8.7 are other important structures. Two large ostia of the two left pulmonary veins are seen in the superior portions of the left atrial wall. Between two prominent ostia and the mitral valve apparatus is the ligament of Marshall. This ligament is important because it is the site of interest for (RF) ablation for atrial arrhythmias. The left atrial appendage os is then situated between the Ligament of Marshall and the mitral annulus, but is poorly seen in this anatomic specimen.

A similar view, using three-dimensional echo, is seen in Fig. 8.8. The dark shadows of the orifices of the pulmonary veins are seen posteriorly, just behind the ligament of Marshall. Further anterior to the Ligament of Marshall is the os of the left atrial appendage. Other structures such as the aortic valve and mitral valve are easily identified. Note the locations of the papillary muscles within the left ventricle.

Further details of this area within the lateral wall of the left atrium are detailed in Fig. 8.9. Note the left upper pulmonary vein (LUPV) and the relationships of these pulmonary veins to the Ligament of Marshall,

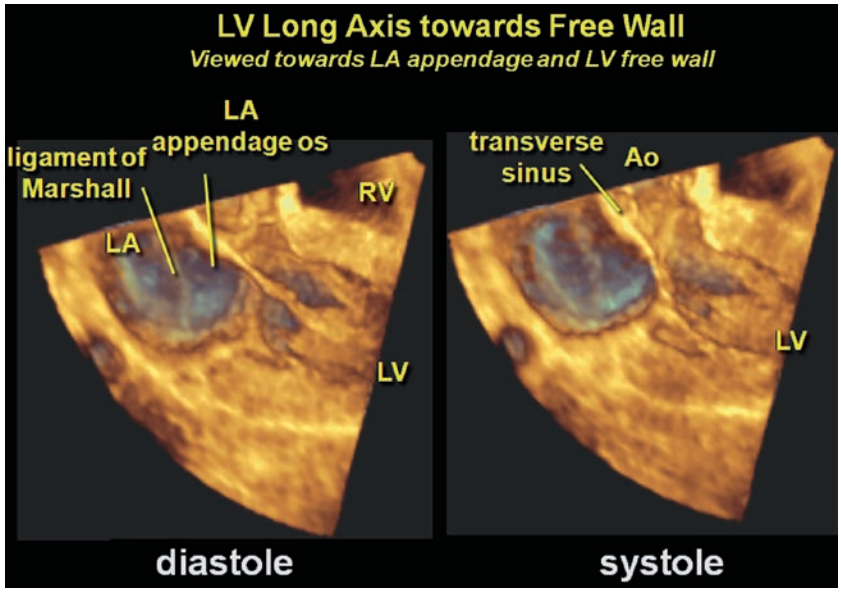

Fig. 8.8 Three-dimensional echocardiogram of the heart from a similar perspective of the cut section seen in the previous figure. Pulmonary atrial veins, ligament of Marshall, and the os of the atrial appendage are seen

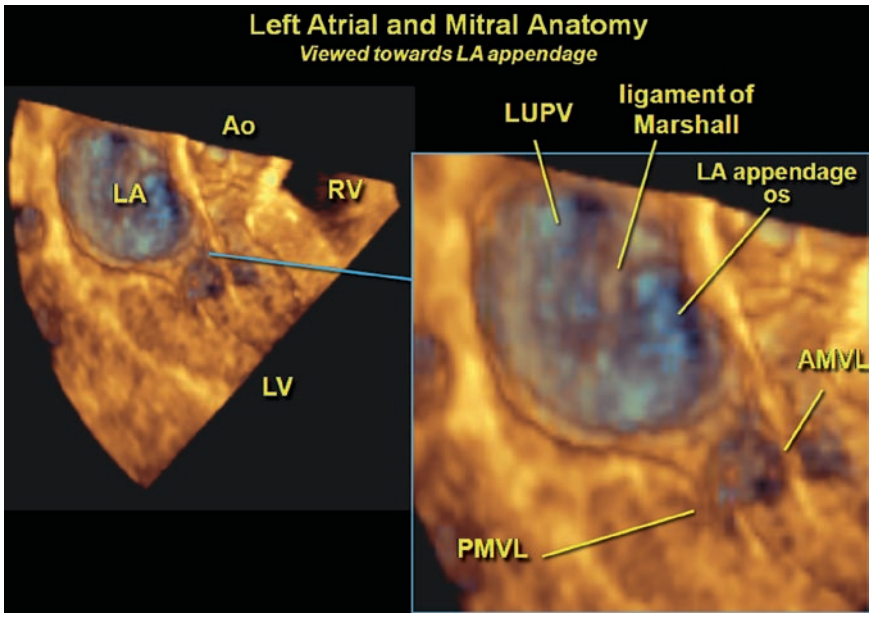

Fig. 8.9 Details of the paired images presented in the previous figure. Detailed images of the left atrial anatomy are possible using three-dimensional echocardiography. *LUPV* left upper pulmonary vein

the os of the left atrial appendage, the mitral annulus, and the mitral leaflets. Real-time, three-dimensional echocardiography clearly shows these relationships that are difficult to appreciate by two-dimensional echocardiography alone. Such relationships are impossible to recognize by M-mode echo as it lacks spatial information in anything beyond depth.

Parasternal Short Axis

With three-dimensional echo, almost any orientation is permissible as it is like holding the heart in one's hand and rotating the heart into any position. Conventional two-dimensional echocardiography views the heart from its apex toward the base. The left-hand panel of Fig. 8.10 shows a cut short-axis section at the level of the mitral valve leaflet tips looking upward toward the cardiac base. The right-hand panel shows a similar section at the level through the papillary muscles. In both panels, the right ventricle is seen to wrap around the left. The interventricular septum is easily identified between the two ventricles. The remaining portions of the left ventricular wall that do not comprise the septum may be referred to as the free wall.

The clinical relationships to learn are those of the papillary muscles and the mitral valve commissures. Note the inferomedial papillary (inferior pap) sits at the junction of the septal and free walls at approximately eight o'clock on the ventricular short axis (right panel). This location at the junction of the septal and free walls is critical to identifying this given papillary. In contrast, the anterolateral papillary (anterior pap) is located only on the ventricular free wall surface, attached only to the free wall. Look back at Fig. 8.7 to see these relationships in the specimen cut along the opposing ventricular long axis.

By comparing the left- and right-hand panels of Fig. 8.10, one can appreciate the location of the inferior mitral commissure to the inferomedial papillary. This commissure is properly called the inferomedial commissure, but this chapter will use "inferior" for short. Likewise, note the location of the anterolateral papillary and its relationship to the anterior commissure. Similarly, we will use the word "anterior" for anterolateral commissure and papillary. Of further critical note is the position of the left atrial appendage tip as it peeks out over the ventricular free wall border in the left panel of Fig. 8.10. It can easily be appreciated how a surgeon could incise the left atrial appendage tip and inserted a finger over the mitral annulus in the left

atrium and into the anterior commissure to perform a mitral commissurotomy for rheumatic mitral stenosis.

These critical relationships are further documented in the series of two-dimensional echocardiograms seen in Figs. 8.11 and Fig. 8.12. In Fig. 8.11 the mitral orifice is seen in the open position in a patient with a dilated cardiomyopathy. The positions of the commissures, identified on this echocardiogram, are obtained from

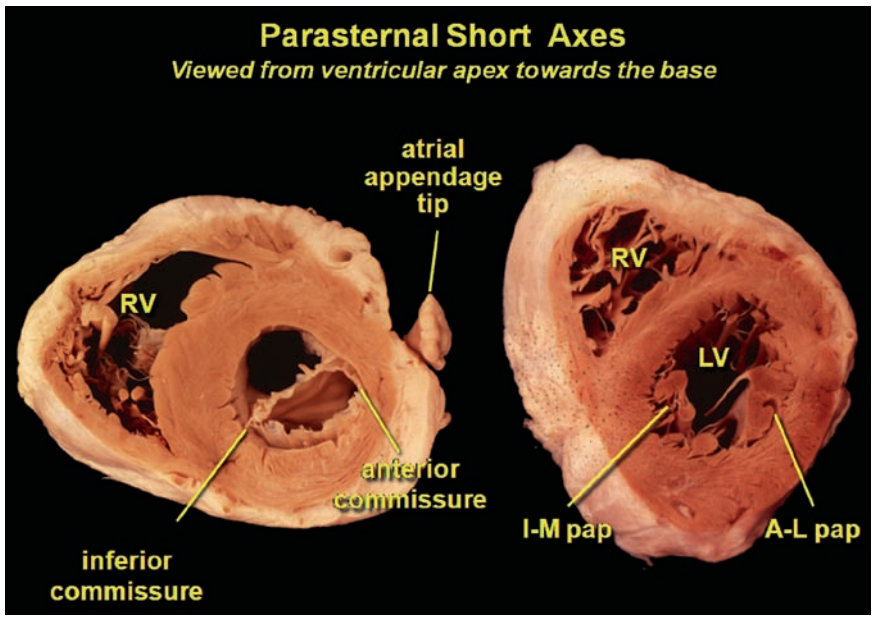

Fig. 8.10 Parasternal short axes obtained from the chest wall in the short-axis view of the mitral leaflet tips and papillary bases seen by two-dimensional echocardiography. Modified from Kisslo, Leech & Adams. Essentials of Echocardiography

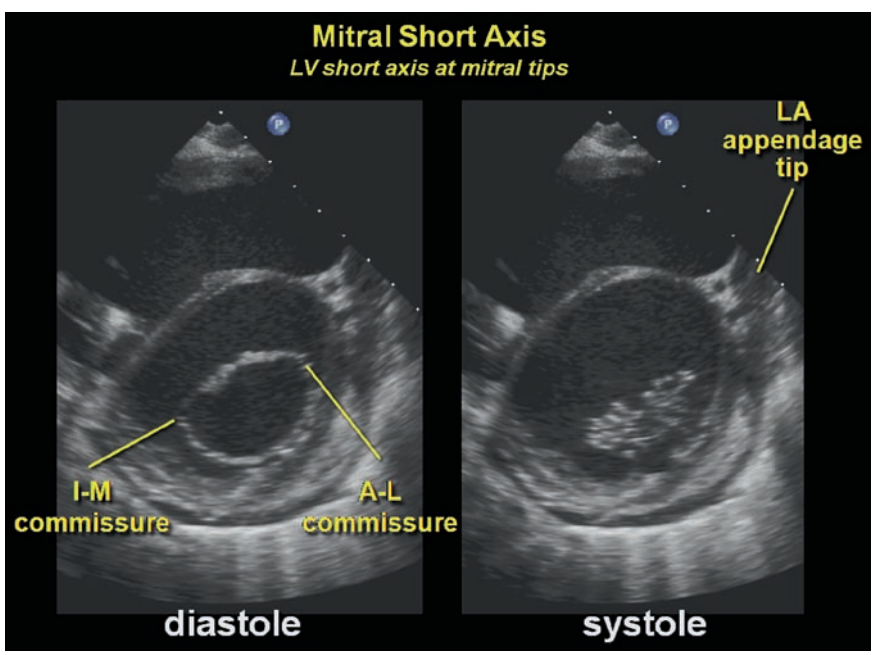

Fig. 8.11 Parasternal short-axis echo view from the chest wall at the level of the papillary tips in a patient with a dilated cardiomyopathy

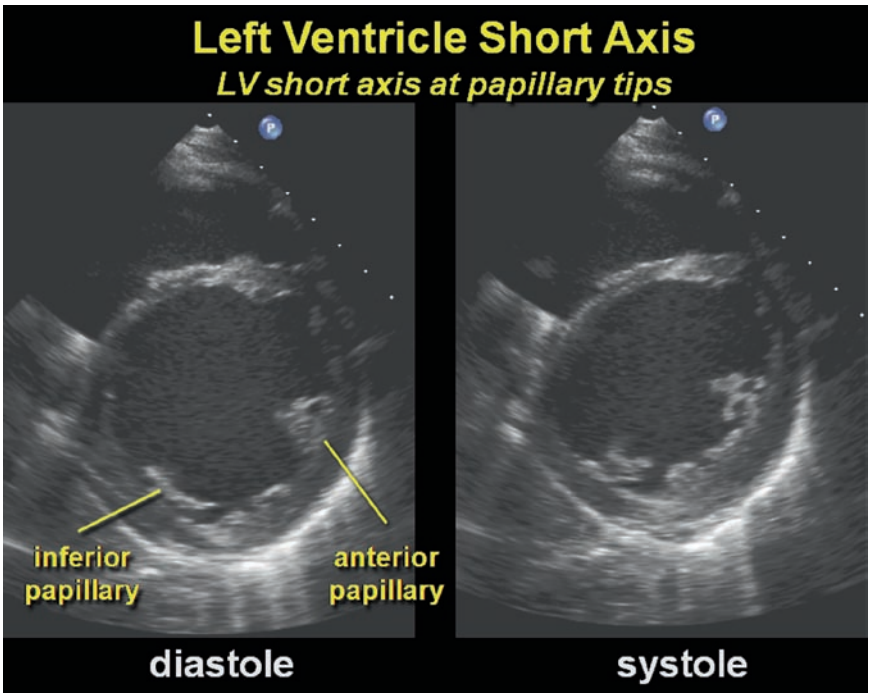

Fig. 8.12 Parasternal short-axis echo view from the chest wall at the level of the papillary bases in a patient with a dilated cardiomyopathy

the chest wall. The mitral valve is seen in the open position in diastole in the left-hand panel and in the closed position in systole in the right-hand panel. The left atrial appendage tip is identified as it peeks over the left ventricular brim. The left atrial appendage tip is not easily identified in most echocardiograms from the chest wall, but can be appreciated in easy to image patients and the operator knows specifically where to point the transducer array.

The locations of the papillary muscles in the mid-ventricular region are seen in Fig. 8.12 when the interrogating plane is angle a bit toward the LV apex from the plane noted in the previous figure. Again, the inferior papillary is adjacent to the junction of the intraventricular septum and the free wall. The anterior papillary sits on the free wall entirely. These are easily identified both in diastole and systole. The size of both papillary heads is roughly symmetric. But sweeping the transducer in the chest wall position from base toward apex, the relationships between papillaries and commissures can be better appreciated.

Apical views

Another critical view for the evaluation of mitral anatomy is the apical four chamber. Traditionally, echocardiography orients this view with the apex of the left ventricle toward the top of the sector arch as visualized in the left-hand panel of the Fig. 8.13. Both ventricles are seen juxtaposed and separated by the intraventricular septum. The interatrial septum is seen between both atria. The arrow points toward yet another septum, the common septum shared by the left ventricle and the right atrium that is called the atrioventricular septum. Thus, there are really three septa to the heart, not just two. Of other note is the fact that the mitral valve apparatus is farther away from the ventricular apex than the tricuspid apparatus. Note the position of these two atrioventricular (AV) valves in this left panel. The chordae tendinea supporting the mitral valve emerge from the papillary muscles attached to the ventricular free wall surfaces. In contradistinction, the tricuspid valve apparatus, nearer to the apex, is supported by chordae tendinea both from the free wall and the interventricular septum. Accordingly, mitral and tricuspid valves can be differentiated by their position in relationship to the cardiac apex and their attachments to ventricular walls.

The other presentation sometime used for the apical four-chamber view is with the cardiac apex in the down position. This, so called, anatomic presentation is much preferred by pediatric cardiologists and other users because one can easily visualize and remember the position of the heart in the intact human. We think

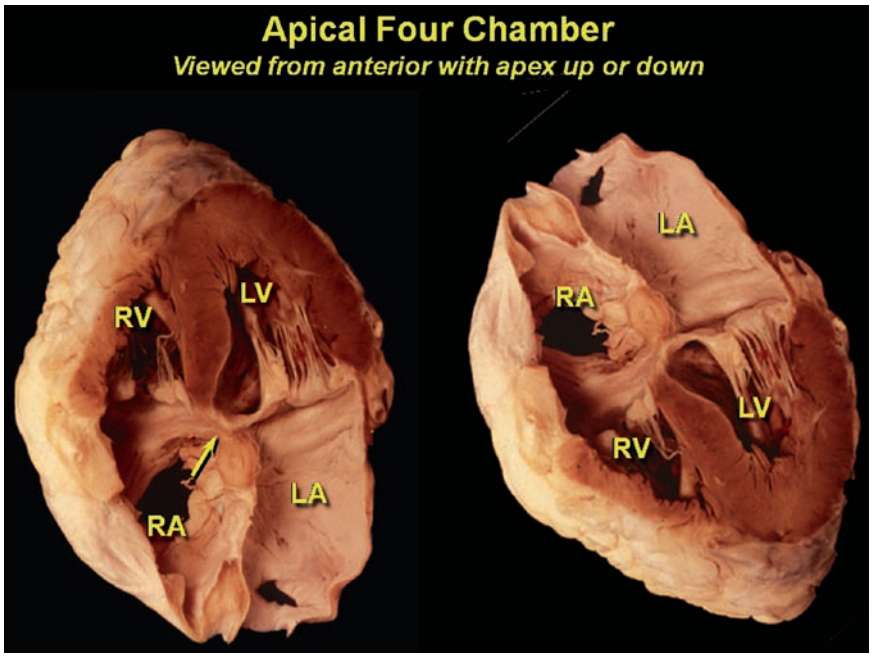

Fig. 8.13 Anatomic cut sections representing the echocardiographic apical four-chamber view. The *arrow* points to the atrioventricular septum. Modified from Kisslo, Leech & Adams: Essentials of Echocardiography

the apex in the down position helps all users of echocardiography to remember anatomic relationships. In addition, it corresponds to presentations of the heart in X-ray, EKG, CT, and other imaging techniques. Of course, relationships between chambers and valves are unaltered no matter what the presentation used for imaging. Users of three-dimensional echocardiography will profit greatly by orienting their apical four-chamber views with the apex down in two-dimensional echocardiography and then creating the three-dimensional images from that point.

An actual echocardiogram of an apical four-chamber view of the left ventricle is seen in Fig. 8.14. Both left and right ventricles (LV and RV) and atria (LA and RA) are identified. The atrioventricular valves are seen to open and close. Again, note that the atrioventricular septum is indicated by the arrow in both the diastolic (left) and systolic (right) still frames. The tricuspid valve is located closest to the ventricular apex, while the mitral valve is the farthest away. An examiner should always note the presence of three septa in the heart. This very short atrioventricular septum is altered in such defects AV canal defects.

A similar view can be obtained with the transducer positioned in the subcostal area and the interrogating array pointed in the same plane, but from a different transducer position. The transducer is then directed superiorly and a similar four-chamber view can be obtained (Fig. 8.15). The arrow points again to the atrioventricular septum,

An actual two-dimensional echocardiogram from a patient with an enlarged left ventricle and a very enlarged left atrium is seen in Fig. 8.16 from the subcostal transducer position. Here the interatrial septum is seen to bulge from the left atrium to the right atrium. The highly reflective targets near the apex of this sector arch are from reflections from the liver tissue. The mitral valve is seen in the closed position. Because the mitral valve apparatus is far away from the transducer the resolution of the details of chordal structures is not as well seen in this view.

One of the more remarkable views of the left ventricle and mitral valve is seen from three-dimensional echocardiography in this so-called, frontal long-axis view (Fig. 8.17). Here, the orientation of the apex is toward the bottom in a more anatomic presentation, with the aorta and the cardiac base oriented toward the top of the figure. Thus, the length of the left ventricle is seen from base to apex while viewing the back of the heart and the papillary muscles relationships to the mitral valve. On both sides are the papillary structures with chordal attachments toward the face of the anterior

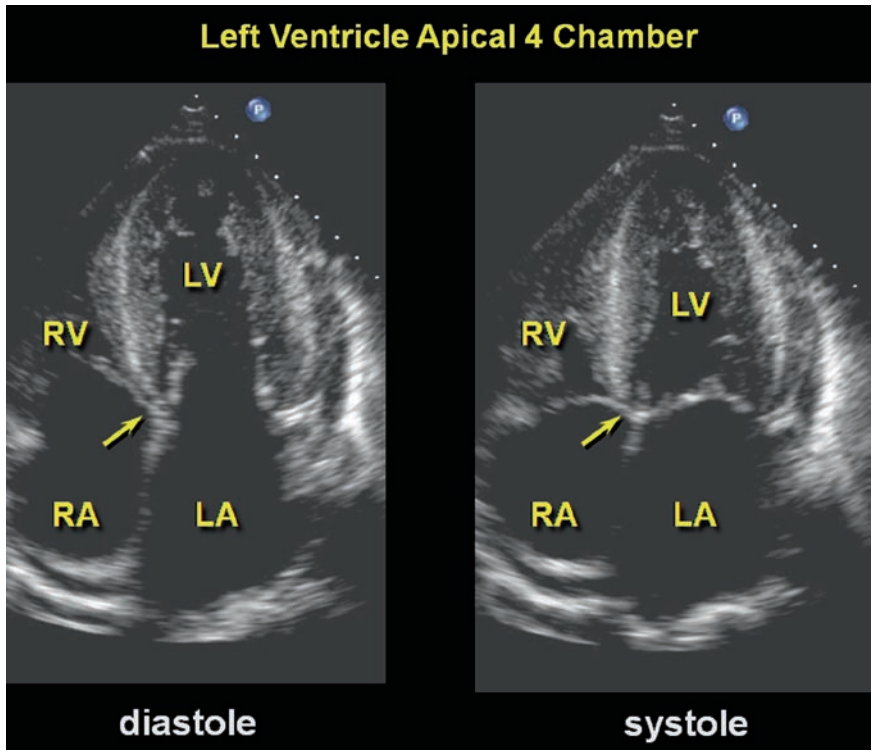

Fig. 8.14 Two-dimensional echocardiographic images in diastole and systole oriented in the apical four-chamber view for comparison. The *arrow* points to the atrioventricular septum

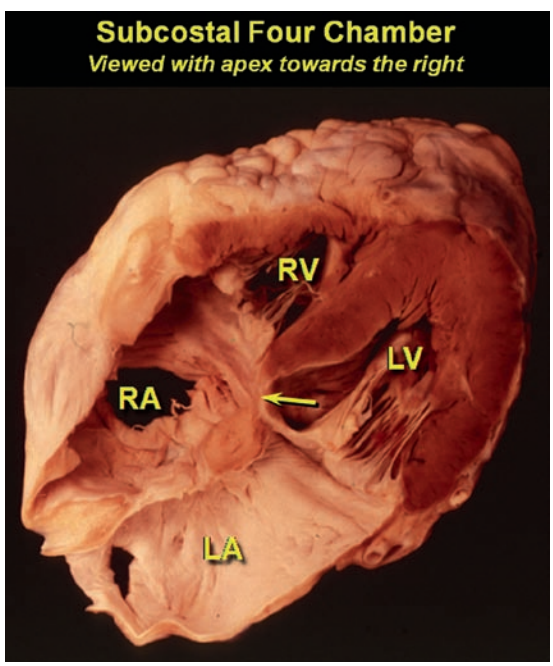

Fig. 8.15 Anatomic cut section along the orientation of the subcostal view from chest wall echocardiography. Modified from Kisslo, Leech & Adams: Essentials of Echocardiography

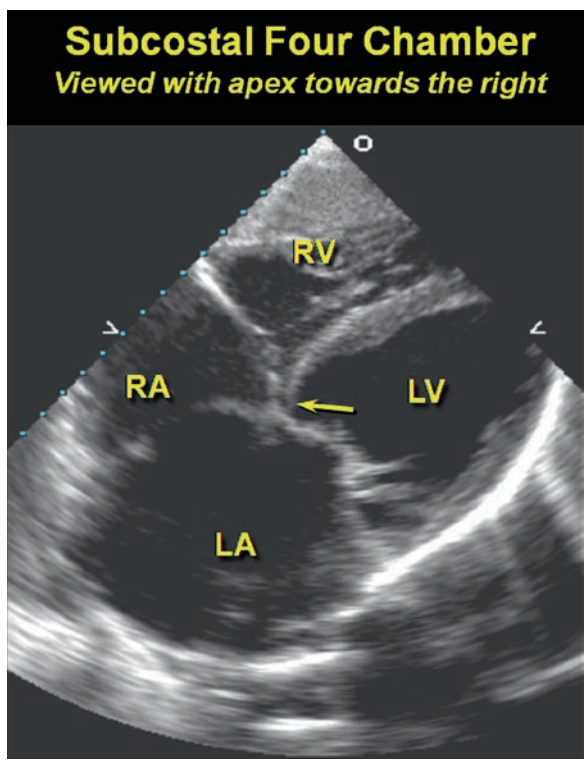

Fig. 8.16 Two-dimensional echocardiogram from the subcostal view. Compare to Fig. 8.15

mitral valve leaflet (AMVL). Here the anterior mitral valve leaflet is seen on *enface* as it moves forward and back toward and away from the viewer when imaged in real time. Remember that the right ventricle is anterior to the left ventricle and curves around the left ventricle. Here, the right ventricle and most of the interventricular septum is cut away, but the right ventricular inlet (RV inlet in the upper left) in the upper left and the right ventricular outlet (RV outlet in the upper right) remain. The actual body of the right ventricle is in the portion that is cut away. Of particular note in this view is that the papillary muscles are in a vertical position and well within the lateral limits for the mitral valve annulus. The papillary to the left is the inferomedial and the papillary to the right is the anterolateral. For best understanding of all these spatial relationships, review all of the anatomic figures from Figs. 8.1–8.17.

The Surgical View

An additional view remains and is termed the surgical view. Until the advent of three-dimensional echo, such a presentation of surfaces that are routinely encountered by surgeons in the operating room was not possible. Using three-dimensional echo, one can record an entire volume of three-dimensional data, and crop the image to view various internal cardiac structures. Three-dimensional images viewed in this chapter are the result of such acquisition techniques and cropping.

One of the best views for the communication of information concerning the mitral valve is this surgical view. When surgeons approach the mitral valve they generally do so from the left atrial approach but cutting into the roof of the atrium in the transverse sinus or some other approach to view directly into the mitral valve orifice. Figure 8.18 shows a section from a porcine heart specimen in a surgical view. The pulmonary artery is seen arising anterior to the aorta and the left atrium is behind the aorta and separated from it by the transverse sinus. Note the location of the left atrial appendage to the left and its relationship to the anterolateral commissure. The inferomedial commissure is seen on the opposite side of the mitral orifice, toward the interatrial septum. Multiple scallops are seen along the posterior mitral valve leaflet.

The observer of this view should be impressed that the anterior mitral valve leaflet comprises approximately 40% of the mitral valve annular structure. The remainder (60%) is taken up by the posterior, or mural, leaflet. Accordingly, the normal anterior mitral leaflet is the longest in length, but the narrowest around the annulus. The opposite is true of the posterior (or mural) mitral leaflet (shortest in length but widest around the annulus).

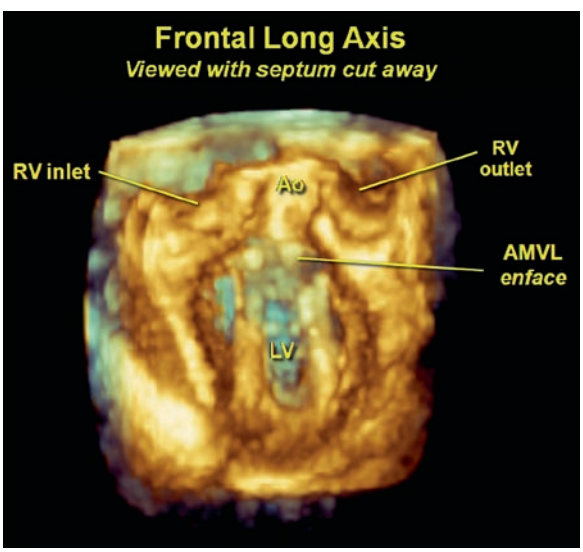

Fig. 8.17 Frontal long axis by three-dimensional echocardiography with the base at the top and left ventricular apex oriented toward the bottom. Using this view, the relation of the papillary muscles to the mitral valve is easily identified

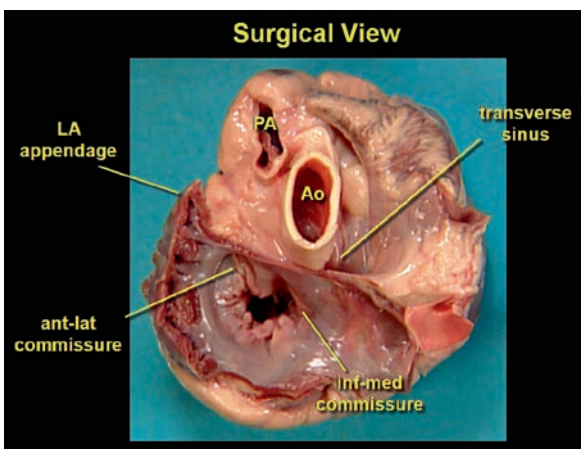

Fig. 8.18 Anatomic specimen of a porcine heart showing the typical surgical approach. The anterior commissure is oriented toward the left atrial appendage. Modified from Kisslo J.: Thinking in 3D

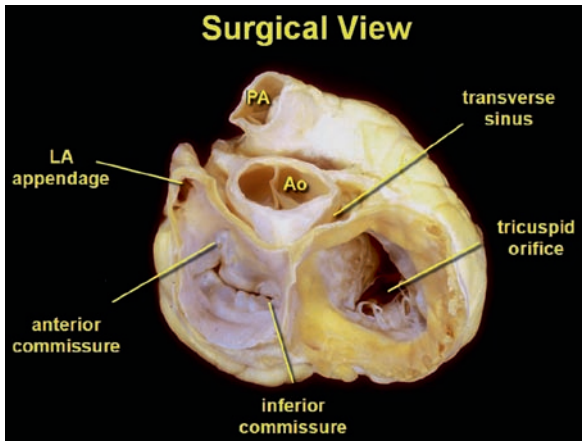

Fig. 8.19 Anatomic human specimen oriented into the surgical view. For details see text. Courtesy of Ho S.Y. Modified from Kisslo J. Thinking in 3D

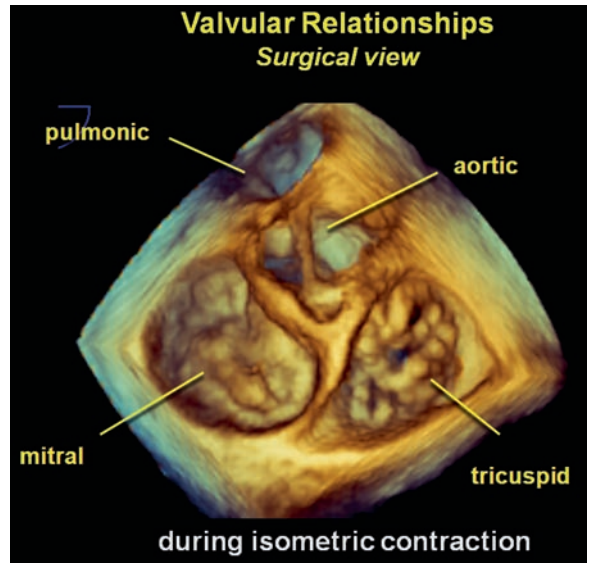

Fig. 8.20 Three-dimensional echocardiographic cut section showing the orientation of the mitral, aortic, and tricuspid valves

This surgeon's view is seen in the human specimen in Fig. 8.19. The pulmonary artery courses from the right to the left, anterior to the aorta (top of the picture). Note the coronary arteries emerging from the aorta at approximately ten (left main) and three (right coronary) o'clock along the aortic circumference. The transverse sinus then separates the aorta from the posterior atrial structures. The left atrium and its appendage are directly behind the aorta.

The most critical relationship is that of the anterior commissure to the atrial appendage. When the atria is opened, one looks for the os of the left atrial appendage, and the commissure just below the os indicates the anterolateral mitral commissure.

In this specimen, structures from the tricuspid orifice are also seen. The two circles of the mitral and tricuspid annuli have the aorta wedged posterior between them. This is a normal relationship in a properly septated atrioventricular valve assembly. In AV Canal defects (atrioventricular septal defects) there is a common mitral-tricuspid orifice, and the aorta is markedly anteriorly displaced.

These remarkable relationships may also be visualized by three-dimensional echocardiography. Figure 8.20 shows such a still frame captured during isometric contraction with the pulmonic, aortic, and mitral and tricuspid valves in the closed positions. The interatrial septum is seen between the two atrioventricular valves. Such a view is not possible by conventional two-dimensional echocardiography.

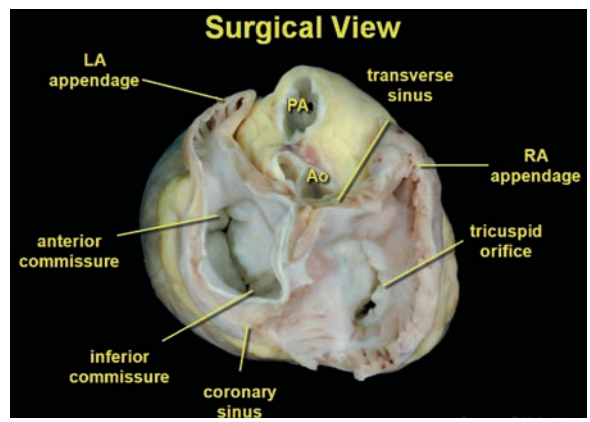

Fig. 8.21 Anatomic human specimen, cut and oriented into the surgical view. Note the anterior commissure orientation toward the left atrial appendage. Courtesy of Anderson R.H. Modified from Kisslo J. Thinking in 3D

Such relationships are further enhanced by studying Fig. 8.21, similar to the previous two previous views. The pulmonary artery and aortic relationships are as previously noted. The transverse sinus is shown to separate the aorta from both the left atrium and right atrium. In addition, both atrial appendages are seen to curl anteriorly around the great vessels. Once again, the anterior commissure points toward the os of the left atrial appendage and the inferior commissure is seen at the opposite side. In addition, the coronary sinus

emerges from the right atrium and circles clockwise around the mitral valve annulus.

This coronary sinus can also be identified by three-dimensional echocardiography. This is demonstrated in Fig. 8.22 where the coronary sinus is easily seen to emerge from the right atrium and circle in the same clockwise pattern around the mitral valve annulus. This is an extraordinary image of the relationship of the coronary sinus to the mitral annulus. While the left atrial appendage itself is not seen in this view, one can see a defect in the annulus where the os is usually located adjacent to the anterior commissure.

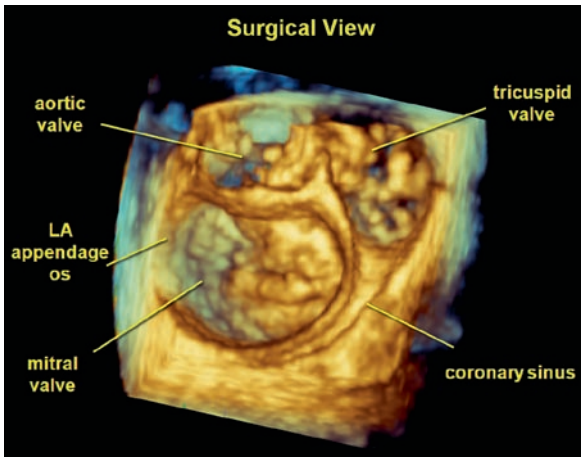

Fig. 8.22 Three-dimensional echocardiographic still frame in systole of the surgical view of the mitral valve. The annulus is cropped to reveal the coronary sinus emerging connecting to the posterior portion of the right atrium. Note how the coronary sinus encircles the mitral annulus

Since a variety of electrophysiology procedures involve the insertion of catheters into the coronary sinus, the identification of this structure is of growing importance. As well, there are a number of forthcoming devices under investigation which may be inserted into the coronary sinus for reconfiguration of the mitral valve annulus in the setting of severe mitral regurgitation. Thus, routine visualization of the coronary sinus will become imperative over time as these techniques demand guidance by echocardiographic approaches.

Further examination of structures above and below the mitral apparatus is seen in Fig. 8.23. Here a long-axis section is shown in the left-hand panel of the left atrium and left ventricle. The ligament of Marshall is identified in this same individual as seen in Figs. 8.8 and Fig. 8.9. Note that there is a slight downward tilting of the left ventricular apex so that this patient is imaged in a more anatomically correct position. The

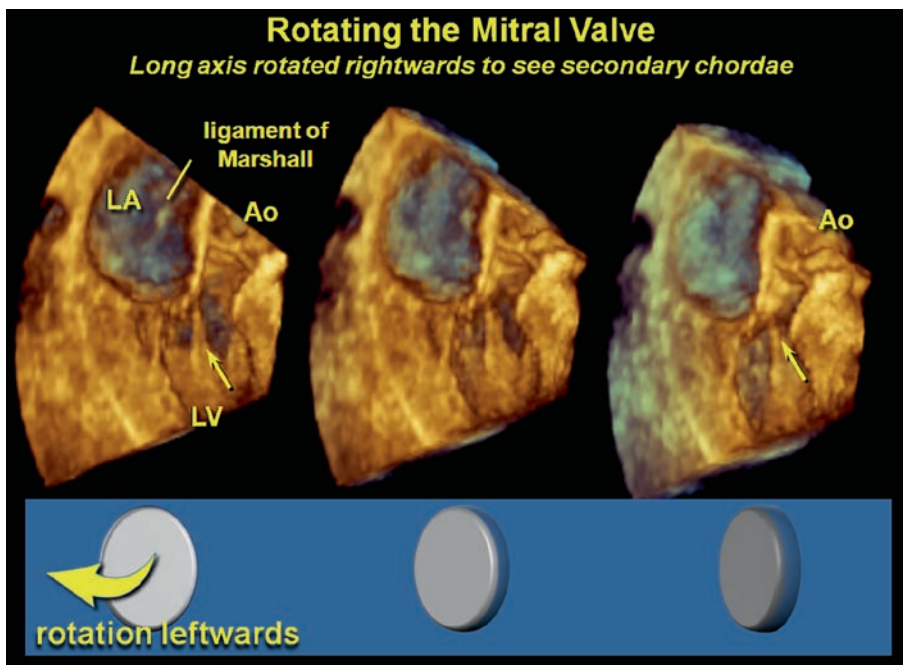

Fig. 8.23 Three-dimensional echocardiographic still frame of the long axis of the left ventricle showing the left atrium, mitral valve, and left ventricle from the septal side toward the LA and LV lateral walls. The *arrow* points toward secondary chordae as the image is rotated

rotation of the left panel clearly shows secondary chordae tendinae to the anterior side of the closed anterior mitral valve leaflet. This section is taken from isometric contraction so that both the aortic and mitral valves are closed. As the heart is progressively tilted toward the left, the back wall of the left atrium is seen and the supporting chordal structures can easily be identified.

Functional Mitral Valve Anatomy

Functional Anatomic Segments

With the advent of mitral valve repair, it became necessary for cardiac surgeons to precisely identify the location of mitral regurgitation. The most popular anatomic descriptive system is the functional classification of Carpentier. This classification recognizes three major regions of the posterior mitral valve leaflet; P_1, P_2, and P_3 as seen in Fig. 8.24 with a schematic diagram in the left panel. This nomenclature system begins at the anterolateral commissure and extends clockwise to the posterior medical commissure. Using the traditional chest wall echo orientation, the numbering would begin (right panel Fig. 8.24) at the right side of the image (left atrial appendage) and circle clockwise. No matter the orientation, or view, one needs to identify the left atrial appendage location in order to properly assign these regions.

Figure 8.25 shows a short axis or mitral apparatus near the midportions of the mitral valve leaflets from the chest wall in a patient with prominent posterior leaflet scallops. This patient has a very large P_2 scallop, and the remaining P_1 and P_3 regions are easily seen. In this individual both commissural areas are also easily identified in this mid-diastolic frame. The orientation is from the standard chest wall short-axis configuration.

Functional Nomenclature in Other Views

The proper orientation for the surgical view may be somewhat confusing at first. The chest wall echo visualizes structures from below (left-hand panel Fig. 8.26) and the surgical view is from above (right-hand panel Fig. 8.26). In these two different orientations, the image seen in the left-hand panel is simply flipped over like turning a playing card from the chest echo orientation to the surgical orientation. To facilitate understanding of this view reversal, one may look at the palm of their

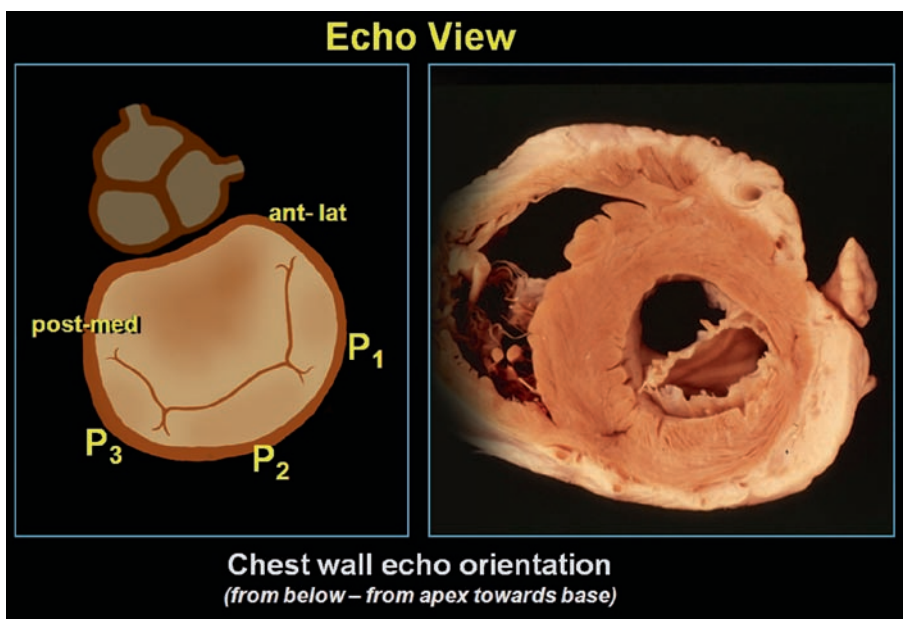

Fig. 8.24 Schematic and anatomic sections demonstrating the posterior mitral leaflet segments from the standard chest wall two-dimensional orientation (from below)

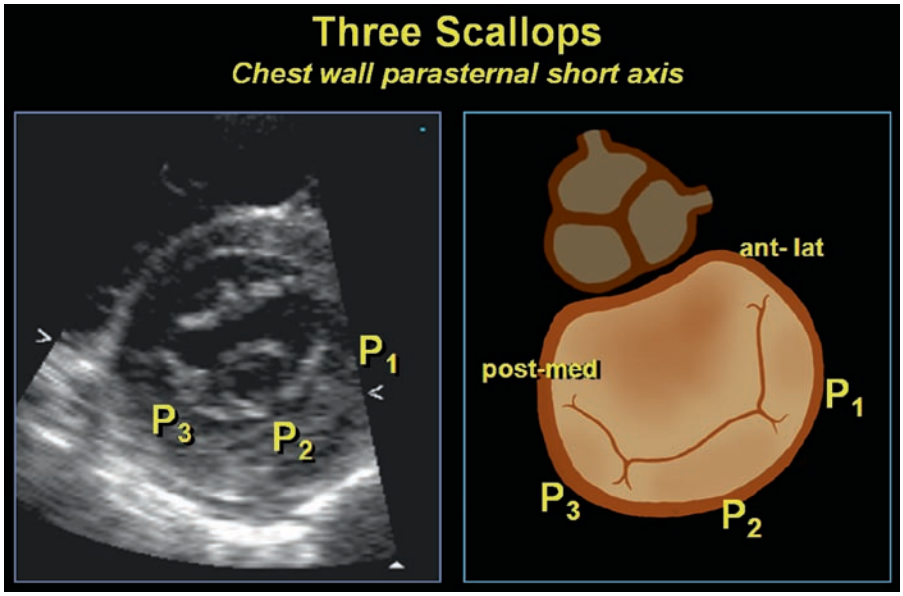

Fig. 8.25 Still frame mid-diastolic short axis of an echocardiogram showing the three scallops of the posterior mitral leaflet and accompanying schematic diagram. The anterior commissure is at the right when oriented from the two-dimensional echo standard from below

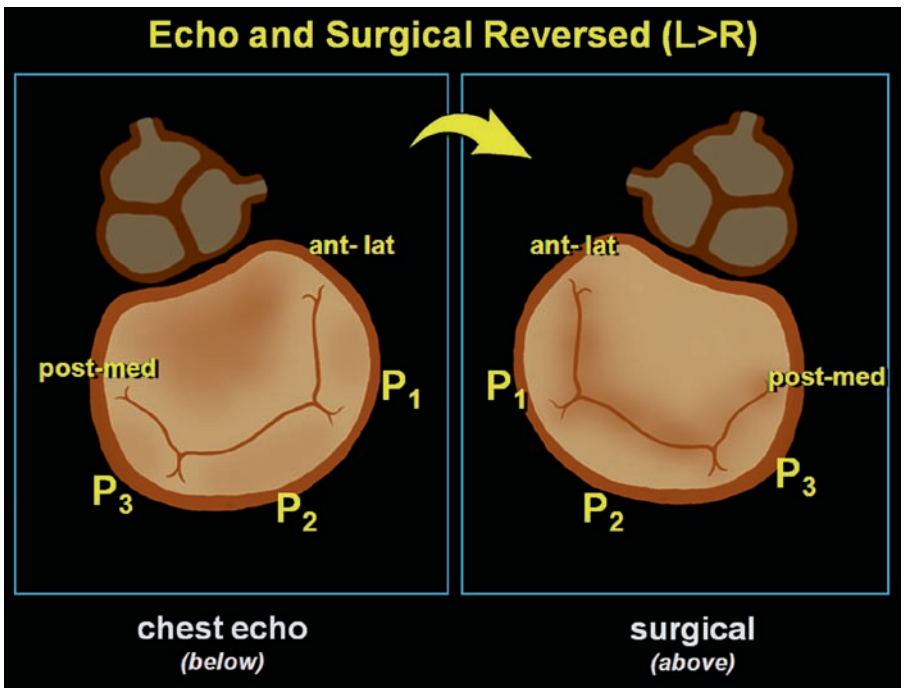

Fig. 8.26 Schematic comparison of the orientations of echocardiographic images from the standard short axis of the mitral valve from the chest wall compared to that visualized by surgeons in the operating room. See text discussion

right hand. This can be imagined as viewing the mitral apparatus from below (with your thumb as the left atrial appendage). Then, simply turn your hand over and look at its backside. Using this orientation, your thumb is at the left, the equivalent of surgical orientation.

Given this turning from one side to the other, the labels identifying the various commissures and posterior valve leaflet scallops are also reversed from one view to the other in Fig. 8.26. Also note the orientation of the aortic valve and the various coronary ostia as views are flipped. Because the views are reversed, the right coronary artery still emerges most anteriorly. The chest wall echo visualizes the ostium of the left coronary artery at approximately three o'clock on the

aortic valve circumference. In the surgical view, surgeons will locate the left coronary artery at approximately nine o'clock on the aortic circumference.

The opposing segments of the anterior mitral valve leaflet are also identified (Fig. 8.27). Since the os of the left atrial appendage is at the upper left of the mitral apparatus in the surgical orientation, the nomenclature begins at the atrial appendage and moves counter clockwise in the surgical presentation. Therefore, the A_1 segment opposes the P_1 segment and so forth.

Figure 8.28 shows an actual three-dimensional echocardiogram presented from the transesophageal

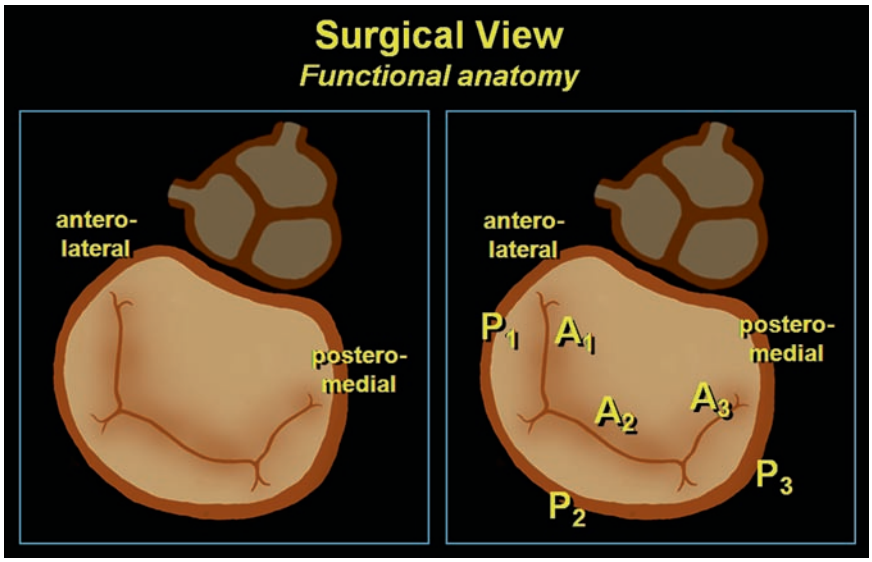

Fig. 8.27 Functional anatomy of the mitral valve presented in the surgical view. The segment numbering starts at the anterolateral commissure

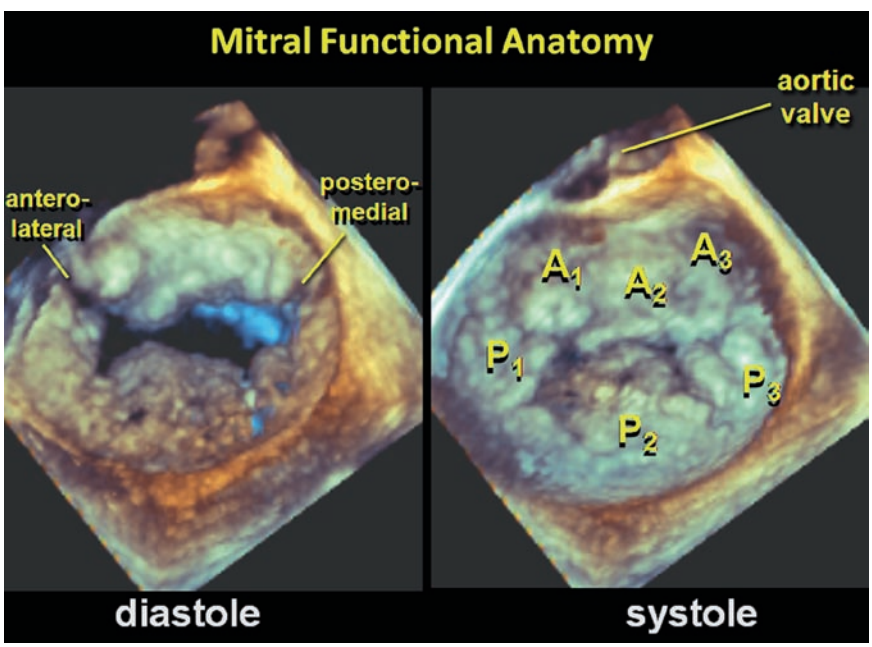

Fig. 8.28 Paired diastolic and systolic three-dimensional views from the surgical view (atrium down toward the ventricle). The various leaflet segments are labeled. The aortic valve is anterior

approach and oriented in the surgical view in a patient with prominent posterior leaflet scallops. Both the anterolateral and posterior-medial commissures are crisply identified in the left-sided diastolic panel. In systole (right-hand panel) the various opposing segments are seen. This patient has a somewhat prominent P_2 segment that makes identification of this scallop most easy in both diastole and systole. In reality, the various mitral valve scallops may comprise several smaller scallops and in normals are much less clearly differentiated. Compare the images seen in Fig. 8.28 with those seen in Figs. 8.18–8.22. Surgeons have little choice in orienting the human mitral valve since standard surgical approaches dictate that valve replacement and/or repair be performed from the atrial perspective. Therefore, it is imperative that echocardiographers learn to reorient their images as to provide surgeons with the appropriate view.

These orientations may be even more complicated when one takes into consideration standard chest wall echo presentations from those seen by standard transesophageal two-dimensional echo orientations (Fig. 8.29). Since the transducer is behind the heart in the transesophageal (TEE) two-dimensional approach, the mitral valve is actually flipped from front to back. The aortic position is, obviously, reversed. Again, the easiest way to identify these structures is to locate both the aorta and the left atrial appendage, and this gives location to the anterolateral commissure and the assignment of all the attendant segments.

As A-mode echo moved into M-mode, then two-dimensional echo emerged and now we are at the advent of three-dimensional echo, there are multiple, confusing orientations that resulted. It is expected that most examiners will orient images anatomically as time moves forward so that images will be consistent from technique to technique. Old image orientations, like old imaging methods, take long to change and even longer to die.

The schematic drawing shown in Fig. 8.30 diagrams the mitral annulus cut at the anterolateral commissure and the mitral leaflets opened to reveal the entire mitral circumference. Doing this reveals the entire array of the various segments to be unfolded in a straight line. Note that since the cut occurred at the anterolateral commissure the P_1 segment is located at the far right in this diagram. It is important to also see that chordal attachments arising from each of the papillary head go to both the leaflets. In this case, the centrally diagramed posteromedial papillary gives chordal structures to

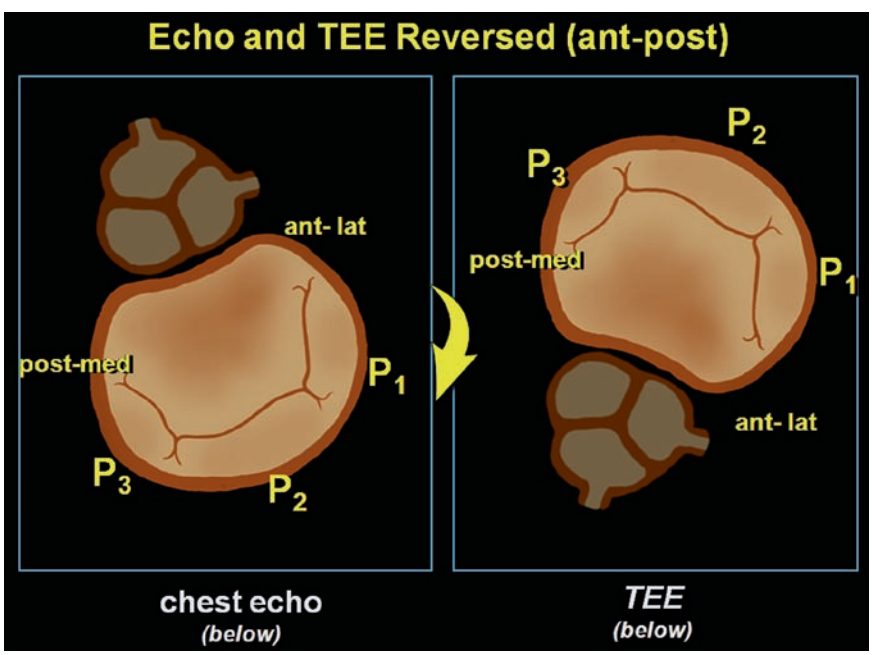

Fig. 8.29 Comparison of schematic diagrams of the orientation of standard chest wall echocardiograms of the mitral valve with those during transesophageal echocardiography

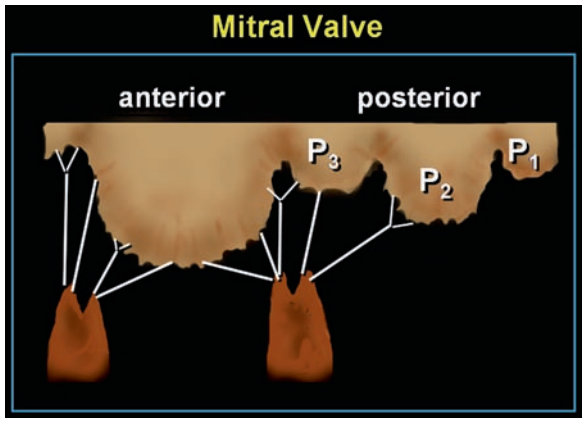

Fig. 8.30 Schematic diagram of the mitral valve, cut at the anterolateral commissure and then laid flat. The anterior leaflet is the longest from top-bottom, but only occupies about 40% of the annulus

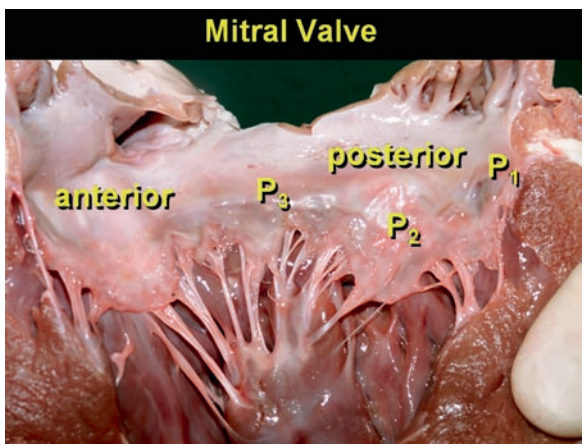

Fig. 8.31 The porcine mitral valve, cut at the anterolateral commissure as in the previous figure. The large papillary muscle at the center is the inferomedial. This demonstrates how each papillary muscle gives rise to chordae tendineae to both leaflets. Modified from Kisslo J. Thinking in 3D

both the anterior and posterior leaflet segments. The same is true for the anteromedial papillary (but not diagrammed).

Such a cut was actually made in a porcine heart and is demonstrated in Fig. 8.31 with the leaflets splayed out along a straight line. Both anterior and posterior mitral leaflets are identified, and chordal structures can be seen to support both the leaflets from any one papillary. In this, a thumb is located in the lower right position. This marks the anterolateral commissure and where the anterior papillary was divided to open the entire array of leaflets, scallops, chordal structures, and papillaries. The inferomedial papillary is located centrally. Note that the delicate attachment of the chordae tendinae is they arise from the papillary heads and then join the tips of the primary chordal insertions in the leaflet tips. Secondary chords are not visualized in this image because they go to the backside of the leaflets.

In summary, it is important to recognize where mitral valve leaflets are attached in order to identify which is the anterior or posterior leaflet. The anterior is attached to the aorta in an otherwise normal individual, while the posterior is attached to the ventricular wall (the "mural" leaflet). Keeping this in mind will always allow an examiner to differentiate these leaflets. As well, the anterior mitral leaflet is the longest in comparison to the posterior leaflet. However, the anterior leaflet takes up only 40% of the mitral valve annulus.

Remember that the left atrial appendage marks the anterolateral commissure, no matter the view or technique. On the ventricular side of the anterolateral commissure is the anterolateral papillary muscle, attached to the free wall of the left ventricle. The posterolateral commissure has the posterolateral papillary just below it in the ventricle. If one looks at the midportion of the anterior mitral leaflet in Figs. 8.18–8.22 as well as the schematic diagrams in Figs. 8.24–8.29, one can appreciate that the midportion of the anterior leaflet is just behind the aorta. Given this anatomic orientation of the aorta to the anterior mitral valve leaflet, one might expect a "cleft" (seen in AV Canal defects) to go directly toward the aorta. As will be seen near the end of this chapter (Fig. 8.139), such a cleft does not go in this direction, because there is a significant rotation of the entire mitral valve apparatus in AV canal defect patients. Rather, such a cleft goes toward the interventricular septum.

Mitral Valve Spatial Movement and Flow Profiles

Cyclical Mitral Valve Movement

The first recognition of mitral valve movement came from the M-mode echocardiogram. Here, a single line of information is directed from the chest wall toward the mitral valve apparatus as seen in Fig. 8.32.

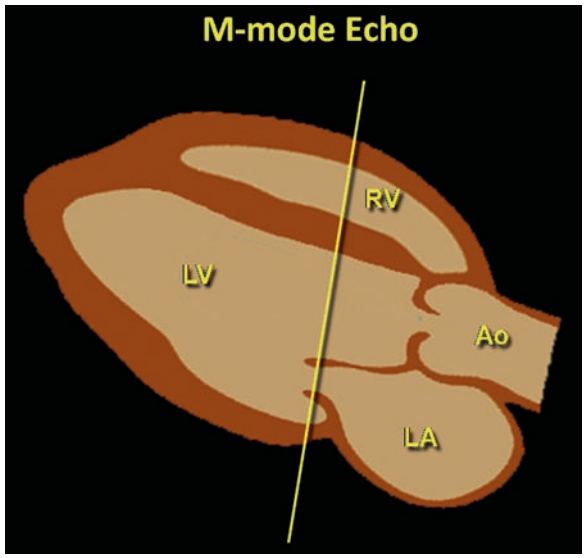

Fig. 8.32 Schematic diagram of the path of a single M-mode beam, directed posteriorly from the chest wall to intercept both leaflets of the mitral valve

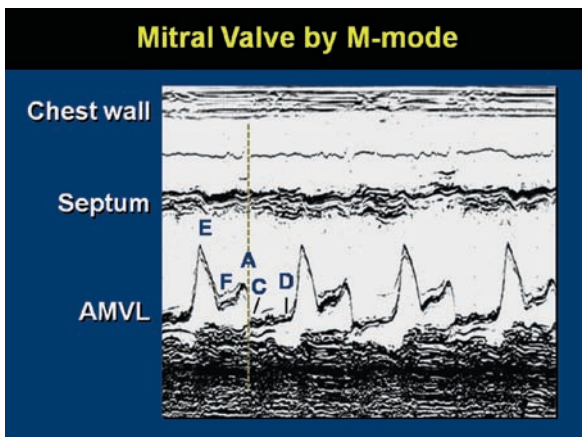

Fig. 8.33 M-mode echocardiogram of the normal mitral valve showing wide excursion of the anterior mitral leaflet (AMVL) in diastole

The diagram of the left ventricle is in the parasternal long-axis orientation with apex at the left and aorta to the right. The chest wall is at the top. Most examiners will easily recognize the rapid to and fro movement of the mitral valve by any examination technique whether it be M-mode, two-dimensional, or three-dimensional echocardiography.

Figure 8.33 shows a typical M-mode echocardiogram of both the anterior and the posterior mitral valve leaflets as they move to and fro between diastole and systole. Because the anterior leaflet is the longest, its motion is the greatest in comparison to the posterior leaflet, which is hardly seen during this examination. In fact, the posterior leaflet appears almost buried on the posterior ventricular wall. The mitral valve first opens and moves anteriorly to its E point, the point of maximum excursion. This corresponds to the rapid inflow of blood during the rapid filling period of diastole. The valve leaflet then drifts posterior to its F point where it lingers during mid-diastole, in the period known as diastasis (where little flow occurs). With atrial contraction, there is a slight anterior movement to the A point. This is followed by systolic closure to the C point following the QRS complex of the EKG (vertical line). At the C point, the anterior and the posterior valve leaflets meet and then drift slightly anterior to the D point during ventricular systole as it is carried with the anteriorly moving left ventricular and aortic supporting structures. Then in diastole, the process repeats itself over and over in a cyclical fashion.

During this cycle, the aorta moves anteriorly in systole and posteriorly in diastole. The mitral annulus itself moves toward the ventricular apex as the left ventricle shortens and contracts.

Given that a patient is in normal sinus rhythm, the patterns of E and A excursions are usually seen in most normal mitral valve leaflet M-mode examinations if the leaflets are pliable and free of intrinsic disease. Of course, best imaging of a mitral valve is obtained when the interrogating sound beam is perpendicular to the mitral valve apparatus itself (a specular orientation). This is generally done from the anterior third through fifth intercostals spaces with the beam directed posterior to encounter the anterior mitral leaflet.

Since the normal mitral valve leaflet is a passive envelope of flow, the mitral valve flow profiles by either pulsed- or continuous-wave Doppler show a marked resemblance to movements detected by M-mode (Fig. 8.34). Note that the E and A points are identified in the M-mode, pulsed-wave, and continuous-wave recordings of mitral valve movement and flow.

The best Doppler recordings are detected from the ventricular apex, parallel to flow. Using this apical approach for Doppler interrogation, a small degree of retrograde flow opposite to the diastolic flow can be seen in systole. Some of this low-velocity flow away from the transducer represents flow out of the left ventricle during mechanical systole that is caught between the leaflets as they close. This is called "backflow."

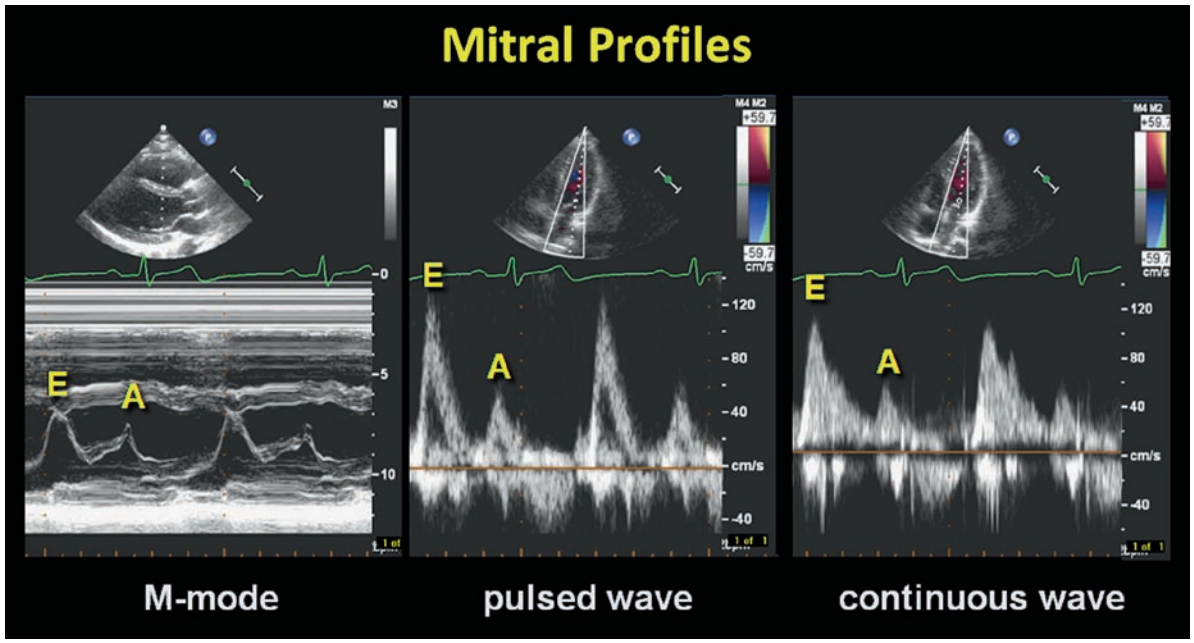

Fig. 8.34 Movement profiles of the mitral valve by M-mode (*left panel*), pulsed-wave Doppler (*middle panel*), and continuous-wave Doppler (*right panel*). All show the greatest degree of movement or flow with passive ventricular filling in the first one-third of diastole

Normal Doppler Mitral Profiles

Cyclical flow through the normal mitral valve orifice is shown in Fig. 8.35 (top panel). Note the relationship of diastolic flow to the EKG. Flow into the left atrium through a pulmonary vein is also shown in the lower panel in this figure. There is filling of the left atrium from the pulmonary vein during the entirety of the cardiac cycle, one being predominantly in diastole (D wave) and the other predominantly in systole (S wave). The general contour of flow through the mitral orifice itself is as previously indicated and forms the E point (occurring with the D point of flow from pulmonary vein D point in diastole). As the mitral valve is *opened*, the atrium serves as a simple conduit of flow from pulmonary vein through the left atrium and into the left ventricle. When the mitral valve is closed, flow continues from the pulmonary vein (S wave) into the left atrium and the atrium functions as a reservoir (S wave lower panel of Fig. 8.35). When pressure rises in the left atrium due to mitral regurgitation or high left ventricular filling pressures, this antegrade flow during systole is frequently suppressed. Most initial students of echocardiography do not realize that flow continues into the heart during the entirety of the cardiac cycle in normal patients. The normal ventricle will fill during diastole, but the normal atrium fills during both diastole *and* systole.

Continuous-wave Doppler interrogation of abnormal mitral flows includes mitral stenosis and mitral regurgitation (Fig. 8.36). Mitral stenosis is a diastolic event (note the EKG in the upper panel) where there is spectral broadening and a slow diastolic descent. Note that the peak velocity in mitral stenosis is between 2.0 and 3.0 m/s. In mitral regurgitation (lower panel) there is a high-velocity flow away from the transducer in systole. This high-velocity flow goes from a very high-pressure chamber (left ventricle) to a low-pressure chamber (left atrium). In this setting of mitral regurgitation there is an increased systolic flow approaching 4–5 m/s retrograde into the left atrium from the left ventricle depending upon the various pressures. In these examples (dashed horizontal lines) the diastolic stenotic flow approaches 2.4 m/s, while the systolic regurgitant flow is slightly over 4 m/s. Note that the scale on the right side shifts from cm/s to m/s between the two interrogations. These continuous-wave Doppler tracings are not from the same patient.

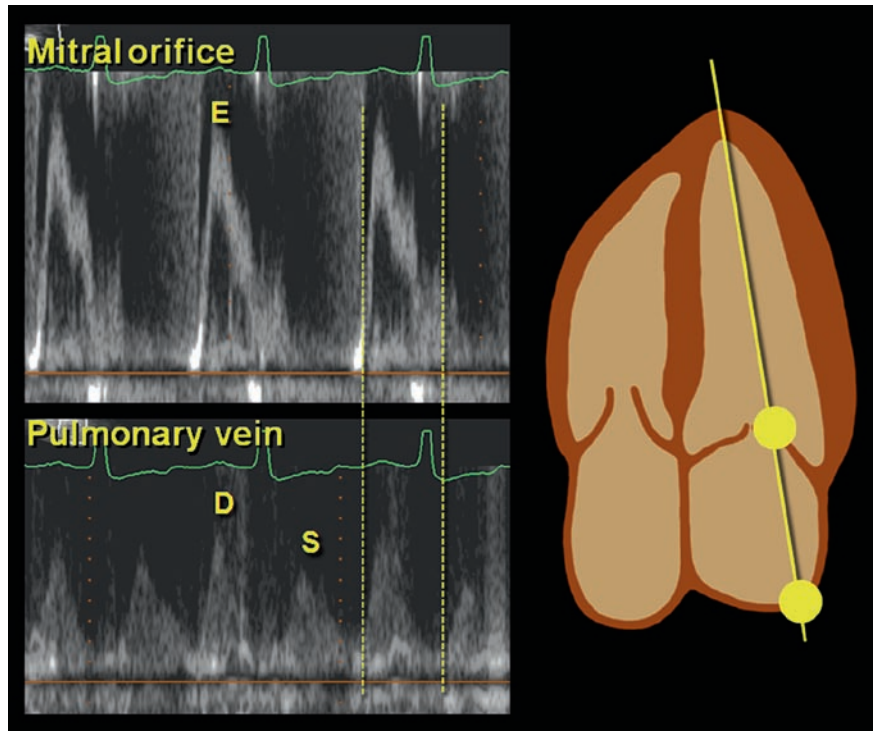

Fig. 8.35 Comparison of pulsed Doppler spectral flow profiles at the level of the mitral orifice (*top panel*) and pulmonary vein (*bottom panel*). Note how the diastolic flow profiles are similar in diastole as the atrium serves as a conduit with flow from lungs through the atrium to the ventricle. In systole, the normal antegrade mitral flow stops but the pulmonary venous flow continues to fill the atrium (now acting as a reservoir)

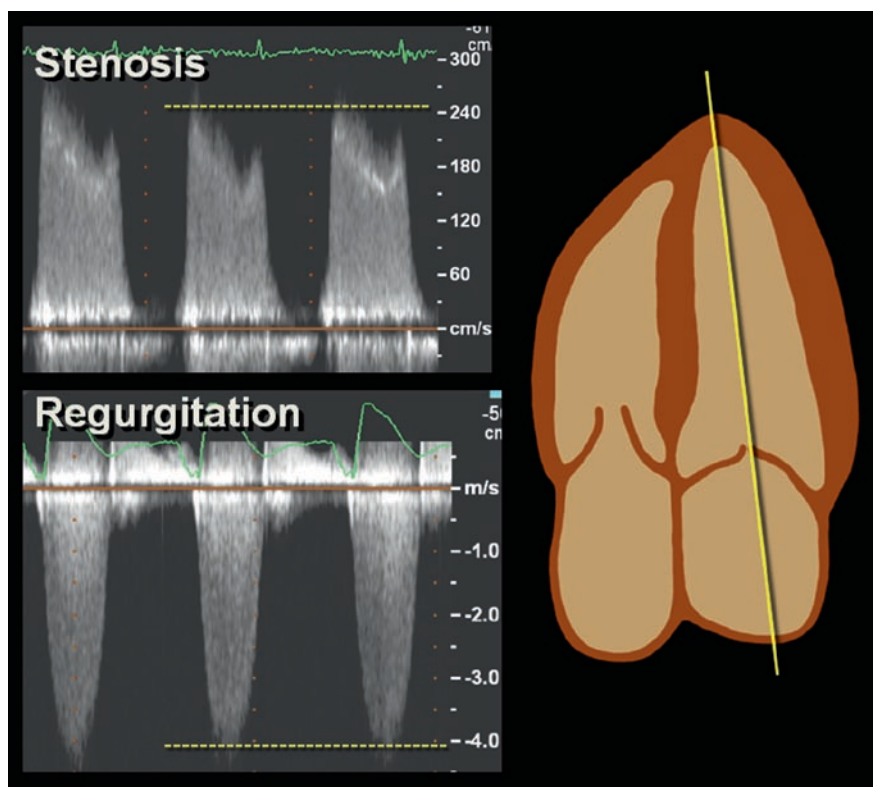

Fig. 8.36 Typical abnormal continuous-wave flow profiles in mitral stenosis (*top panel*) and mitral regurgitation (*bottom panel*)

Comprehensive Evaluation of Mitral Regurgitation

Mitral regurgitant jets have four basic components by color-flow Doppler. Comprehensive evaluation of the mitral valve requires that one examine at all four components of the jet when evaluating color-flow images for mitral regurgitation (Fig. 8.37). As flow converges in the left ventricle in systole just proximal to the regurgitant orifice it forms into a three-dimensional volume of flow convergence. Here, flow begins to accelerate in velocity. It then narrows into the fastest velocity of a regurgitant jet where the flow accelerates through the actual regurgitant orifice itself. Then, as the flow jet emerges from the regurgitant orifice into the left atrium the jet splays out into a large area of turbulence, much like water going over the precipice of the waterfall into the waterfall itself. This third area of turbulence is the first thing a viewer recognizes when viewing a regurgitant jet in the left atrium. The fourth, and last, effect is the downstream effect of suppression or reversal of systolic flow into the left atrium in systole through a pulmonary vein (Fig. 8.38).

Of course, various quantitative indices can be applied to these different areas recognized in the two-dimensional color-flow image. The area of flow convergence can be described in what is known as the PISA (proximal isovelocity surface area) for the derivation of effective regurgitant orifice area (EROA) (Fig. 8.39). As the jet then passes through the area of flow acceleration (the jet orifice) the flow will increase somewhat in velocity (in the vena contracta), and the diameter of this flow acceleration can be measured. The most obvious area is that of the flow disturbance within the left atrium itself. Beginners in echocardiography will be most attracted to this area, but it is the least reliable in the various descriptive indices now described for the severity of mitral regurgitation. Lastly, there is the effect seen downstream from the regurgitation when there is pulmonary venous flow suppression or actual reversal of pulmonary venous inflow during systole. When such suppression or reversal is noted, the regurgitant jet is likely severe.

Of course, as the jet increases in size, one may expect a larger PISA, vena contracta, area of flow

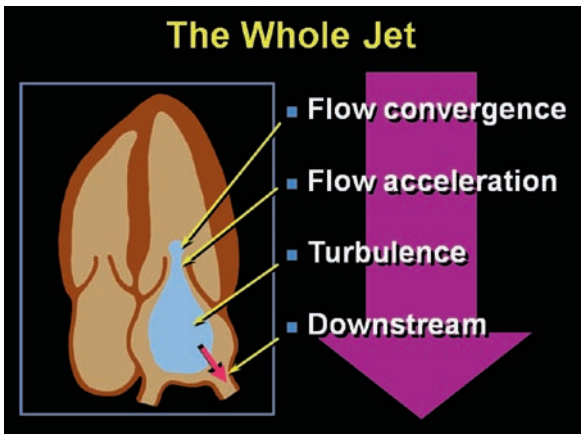

Fig. 8.38 Schematic diagram of the four areas of interest in a comprehensive evaluation of mitral regurgitation by color-flow Doppler

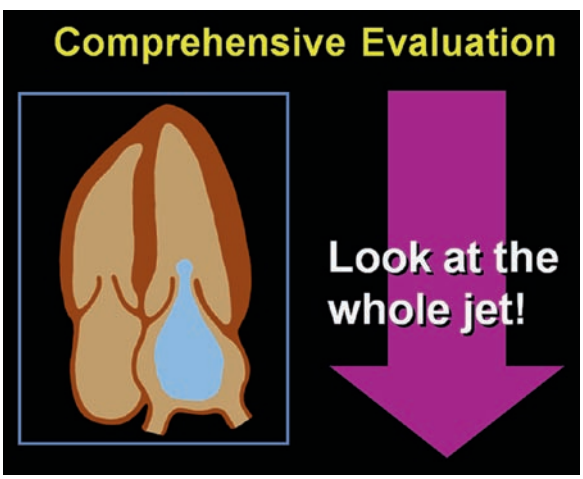

Fig. 8.37 Schematic diagram of the comprehensive color evaluation of mitral regurgitation

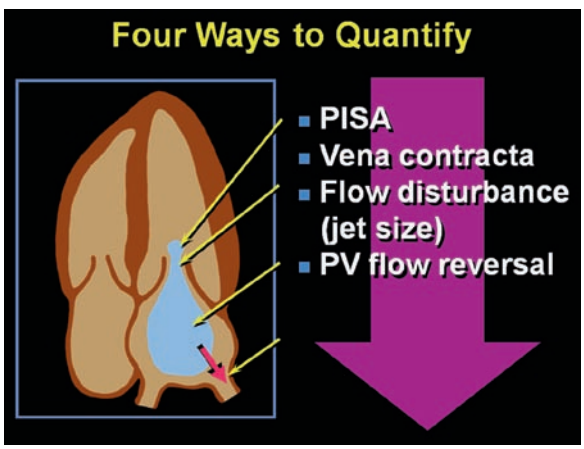

Fig. 8.39 Schematic diagram of the four ways to quantitate the color-flow Doppler of mitral regurgitation

disturbance (jet size) and either a decrease in systolic venous flow or reversal itself (Fig. 8.40). Flow is actually quite organized as it moves into the area of flow acceleration (PISA) and into the vena contracta (flow acceleration). The flow into the atrium is, however, quite disorganized and turbulent at it emerges from the regurgitant orifice. The area of the jet in the left atrium is therefore subject to many factors. One major factor is the size of the atrium. Imagine a jet made up of 50 cc being received in a very large left atrium as opposed to the same volume jet being received in a small left atrium. The dispersal of forces and the size and pressure of the receiving chamber can all, therefore, affect the size of this jet, and thus render it unreliable. Given these observations, however, note the examples of mild and severe mitral regurgitation noted from the chest wall apical four-chamber approach in Fig. 8.41. In each case, note the size of the flow convergence (PISA), flow acceleration (jet diameter at the vena contracta), size of the jet in the left atrium, as well as the presence of flow reversal in the pulmonary vein. The right panel (arrow) shows such actual reversal compatible with severe mitral regurgitation. Always look at all four components of mitral regurgitation when evaluating severity.

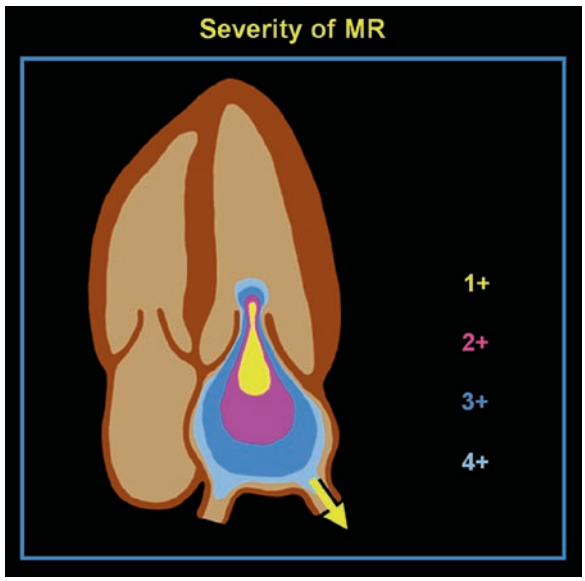

Fig. 8.40 Schematic summary of the degrees of severity of color-flow Doppler in mitral regurgitation. As the severity increases, so do the sizes of all components

As previously mentioned, the size of the jet may be the least reliable quantitative index of these various descriptors. This is in part because the regurgitant flow into the chamber is affected by the constraints induced of the blood that is residual within the left atrium during systole. As well, attenuation of the ultrasound signal may artifactually and significantly reduce the size

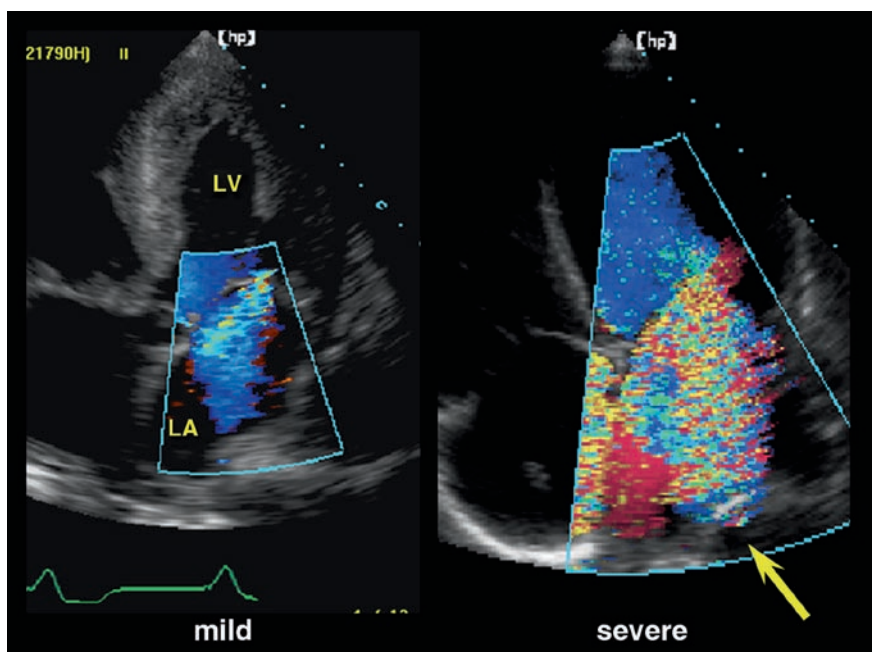

Fig. 8.41 Apical four-chamber views from two different patients, one with mild and the other severe mitral regurgitation

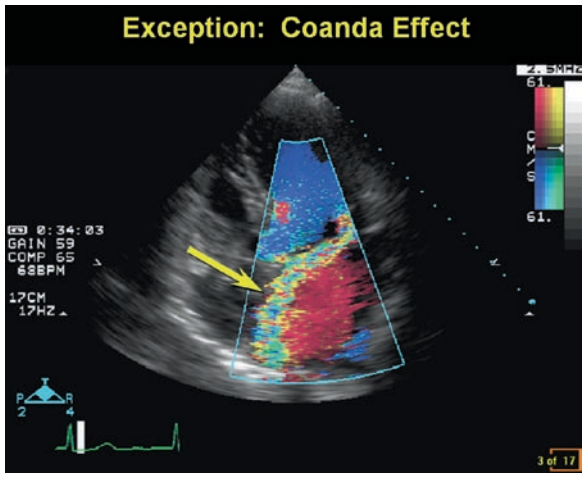

Fig. 8.42 The Coanda effect is present when a regurgitant jet is directed against a wall. Note the large zone of convergence

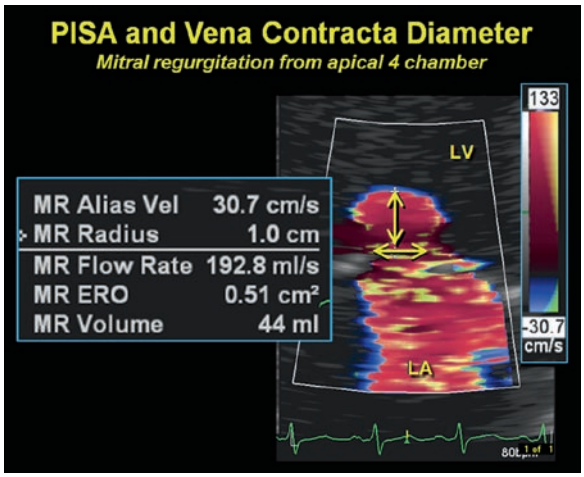

Fig. 8.43 Flow through the zone of convergence (*vertical arrow*) and zone of flow acceleration through the regurgitant orifice (*horizontal arrow*) is generally organized and can be quantified

of the jet. Various individuals have tried to relate the size of the left atrium in relationship to the size of the regurgitant jet, but with little absolute reliability. Jets also have duration and such duration must subjectively, or objectively, be taken into account when assessing regurgitant jet severity.

Another notable example of the unreliability of jet size is the so-called Coanda effect (Fig. 8.42). In this case, the regurgitant jet is directed from the valve orifice directly adjacent the atrial wall where it curls around the left atrium. This is sometimes informally referred to as a "wallhugger" jet and can occur along any of the atrial walls. When this occurs, most subjective analytic schemes increase the severity of mitral regurgitation one grade higher than would be estimated by the size of the jet alone. In the example shown in Fig. 8.42 (arrow) one can appreciate a larger zone of convergence and flow acceleration than would normally be likely from a jet of this modest size. This phenomenon results from rather complex dispersions of kinetic energy and is beyond the scope of discussion in this basic chapter.

Calculations of Jet Severity

It is common in many laboratories to assign values for the calculations of the severity of mitral regurgitation on the basis of PISA and subsequently Effective Regurgitant Orifice Area (EFRO). This is performed by a series of maneuvers described elsewhere in this book. The method is dependent on the assumption that the isovelocity shell revealed by a color baseline shift is a perfectly symmetric hemisphere. The larger the PISA, the larger the regurgitant jet. Calculation of jet diameter through the vena contracta suffers from a similar limitation as it also assumes a symmetric flow acceleration area. Both are demonstrated Fig. 8.43. Larger areas and diameters imply larger jets, but neither is precise measure of mitral regurgitation. Despite all these limitations, one measurement or estimation can be used to verify another, and a comprehensive review can result in a very useful clinical estimate of severity of mitral regurgitation. Values for vena contracta diameter and EFRO are seen in Table 8.1.

Table 8.1 Table of values for estamating severity of mitral regurgitation by Vena Contracta or Effective Regurgitant Orifice Area measurements

	Severity of mitral regurgitation		
	Mild	Moderate	Severe
Vena contracta width (cm)	<0.3	0.3–0.69	≥0.7
EROA (cm2)	<0.20	0.20–0.39	≥0.40

Mitral Timing Relationships

Spectral Doppler indices of the severity of mitral regurgitation also exist. They are dependent on an understanding

of the various pressure relations that exist in left-sided heart contraction and relaxation. Figure 8.44 shows the timing relationships of left-sided pressures in the Aorta (Ao), left ventricle (LV), and the left atrium (LA). As the pressure rises in the left ventricle during mechanical systole, it exceeds that of the left atrium and mitral valve closes. This initiates a period of rising left ventricular pressure with no movement of blood that precedes the opening of the aortic valve. This interval is known as the period of isovolumic contraction. The term "isovolumic," of course, means that there is no volume change prior to aortic valve opening.

As the pressure in the left ventricle exceeds that in the aorta the aortic valve opens, mechanical systole ensues, and blood is ejected until the left ventricular pressure drops below that of the aorta. When aortic pressure drops, the aortic valve shuts. Isovolumic relaxation then ensues as the ventricular pressure falls until mitral valve opening. Diastole then begins. Note the light blue interval areas indicated in Fig. 8.44 of the isovolumic relaxation period at the end of systole and then the isovolumic contraction period at the beginning of systole in the subsequent beat.

Relationships of Spectral Doppler

Of course, both aortic stenosis (AS) and mitral regurgitation (MR) are systolic events. As well, both aortic regurgitation (AR) and mitral stenosis (MS) are diastolic events. Because of the proximity of the aortic to the mitral valve, these various regurgitations and stenoses may be confused for one another. These complex timings in relationship to aortic and mitral stenotic and regurgitant flows are illustrated in Fig. 8.45 where mitral regurgitation and mitral stenosis are illustrated in orange and aortic stenosis and aortic regurgitation are illustrated in green. The various valve left-sided valve openings and closings are indicated with the blue shaded areas denoting isovolumic relaxation and contraction (identified in the previous figure) added. Figures 8.44 and 8.45 should be carefully correlated.

At first, it may appear that the spectral profile of aortic stenosis resembles mitral insufficiency and those of aortic insufficiency resemble mitral stenosis. These various disease profiles may be differentiated by a knowledge of the various timing relationships of left-sided valvular opening and closings. Figure 8.45 shows the relationships between these various normal spectral velocities. The duration of mitral insufficiency is generally longer than that of mitral stenosis, in part, because the time from mitral valve closing to mitral valve opening is longer than from aortic valve opening to closing. Similarly, the aortic closing to aortic opening is longer than from mitral opening to closing.

The problem of recording flow across the mitral and aortic valves simultaneously (Fig. 8.45) results partly

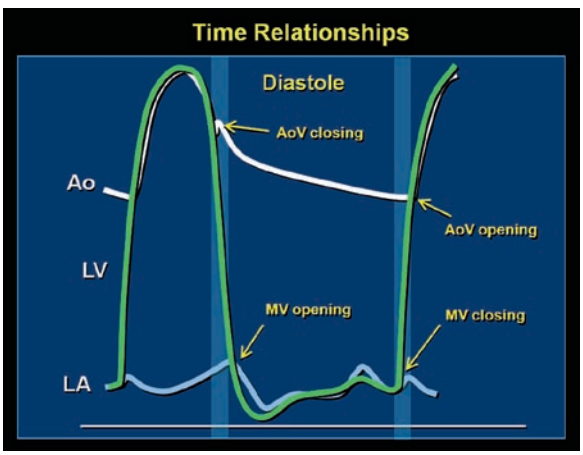

Fig. 8.44 Schematic diagram of the relationship between left atrial, left ventricular, and aortic pressures during the cardiac cycle. The *light blue areas* represent the periods of isovolumic relaxation and isovolumic contraction

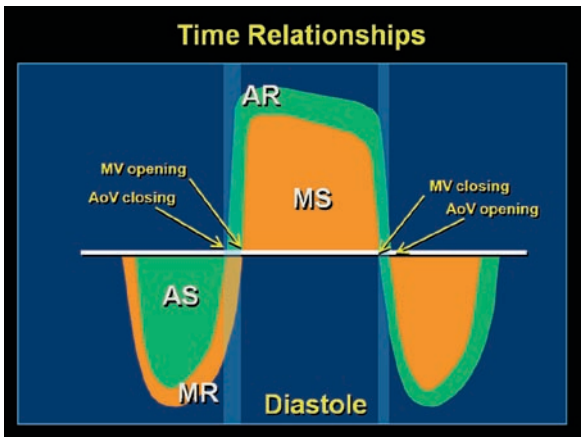

Fig. 8.45 Schematic diagram showing the timing relationships of abnormal flows through the left-sided heart valves. Aortic stenosis and mitral regurgitation are systolic events and may be confused with one another. Aortic regurgitation and mitral stenosis are diastolic events and may also be confused. The *light blue areas* represent the periods of isovolumic relaxation and isovolumic contraction

from the fact that the ultrasound beam width in spectral Doppler is large enough to detect more than one jet at the same time. Failure to appreciate the phenomenon of jet width may lead the unwary beginner to diagnose mitral stenosis, for example, when only aortic regurgitation is present.

Using these principles, spectral aortic and mitral flows may be differentiated using spectral Doppler tracings of mitral flow. Note in Fig. 8.46 that the duration of aortic outflow is quite a bit shorter than the duration of mitral regurgitation in this patient and then compare these observations to Fig. 8.45. While the velocity of mitral regurgitation in this individual is considerably higher than the normal aortic velocity seen in the left panel, aortic flow may be confused with mitral regurgitation in a patient where aortic stenosis and mitral regurgitation coexist. They can be differentiated by their location and duration.

This phenomenon is somewhat better illustrated in Fig. 8.47 where an elevated systolic velocity jet from aortic stenosis is seen in the top panel and coexistent mitral regurgitation is indicated in the bottom panel, also having elevated velocity. In this setting, one could easily confuse the continuous Doppler of aortic stenosis with that of mitral regurgitation or vice versa. The duration of the more severe mitral regurgitation may also be reduced because the mitral regurgitation encroaches into the period of isovolumic relaxation.

Similar problems could exist between aortic regurgitation and mitral stenosis, both diastolic events. The top panel of Fig. 8.48 shows aortic regurgitation and the bottom panel shows the delayed diastolic descent of mitral stenosis. Again, identification of the various isometric periods will help somewhat in differentiating these flows.

Use of Color-Flow Doppler Controls

Mitral regurgitation during systole can be seen by color-flow Doppler in the left atrium in systole using color-flow Doppler (Fig. 8.49). Note that there is an area of color mosaic in the left atrium this patient examined in the parasternal long axis from the chest wall. The patient has a dilated cardiomyopathy, so both the left ventricle and the left atrium are dilated.

One serious problem for color-flow Doppler is the fact that improper use of the color controls can result in the marked increased in jet size (Fig. 8.50). In this

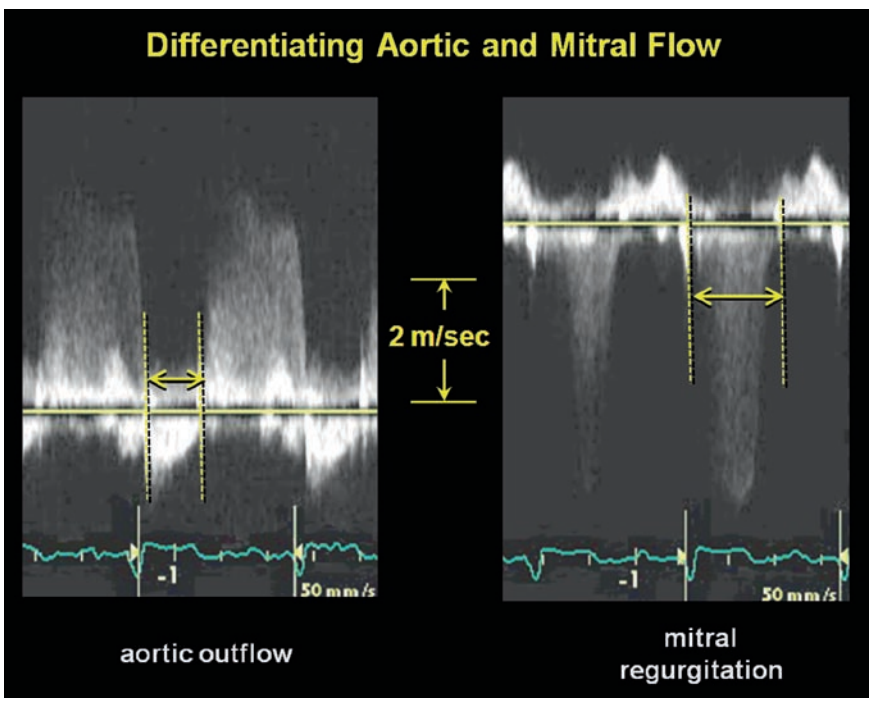

Fig. 8.46 Continuous-wave Doppler recordings through the aortic outflow (*left panel*) and mitral inflow (*right panel*) to differentiate systolic aortic flow from mitral regurgitant flow durations. Mitral flow duration in a normal is longer than aortic flow duration

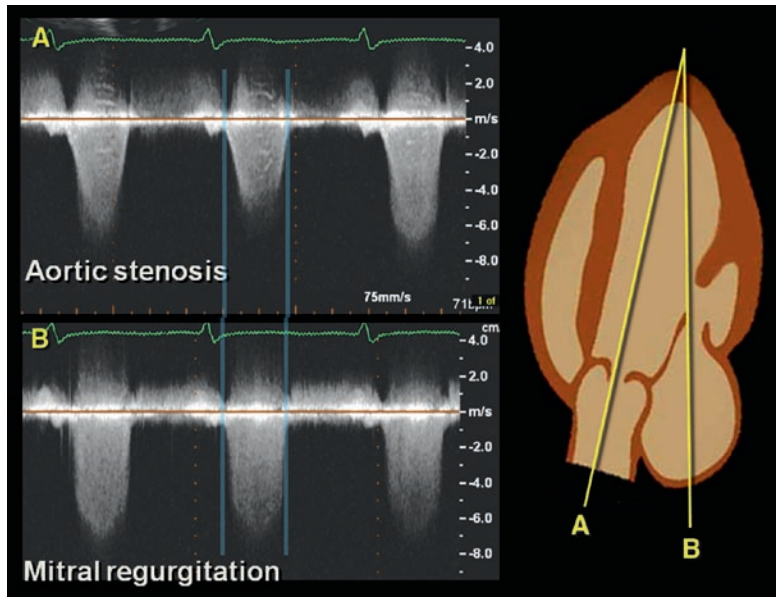

Fig. 8.47 Continuous-wave Doppler recordings from a patient with aortic stenosis (*top panel*) and mitral regurgitation (*bottom panel*). The *light blue areas* represent the periods of isovolumic relaxation and isovolumic contraction

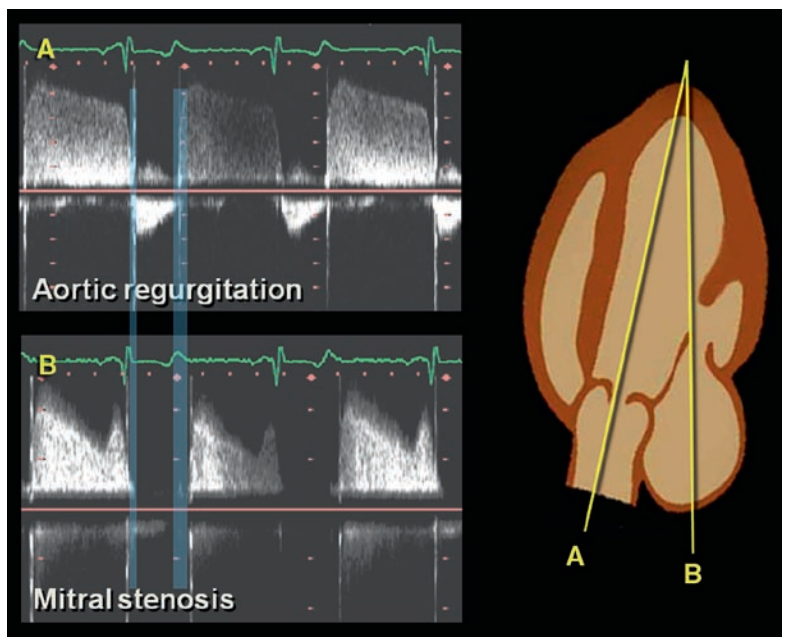

Fig. 8.48 Continuous-wave Doppler recordings from a patient with aortic regurgitation (*top panel*) and mitral stenosis (*bottom panel*). The *light blue areas* represent the periods of isovolumic relaxation and isovolumic contraction

example, a subject with known trivial of mitral regurgitation (left panel) can demonstrate an area of more sizable regurgitation (right panel) when the improper settings are employed. Multiple factors can control this creation of a spuriously sized jet and profoundly affect the estimation of jet severity.

Use of Color Gain

The first, and most obvious, control is that of overall color gain. Figure 8.51 shows a left panel where normal color gain is demonstrated. The right panel shows a remarkable increase in the overall color gain resulting

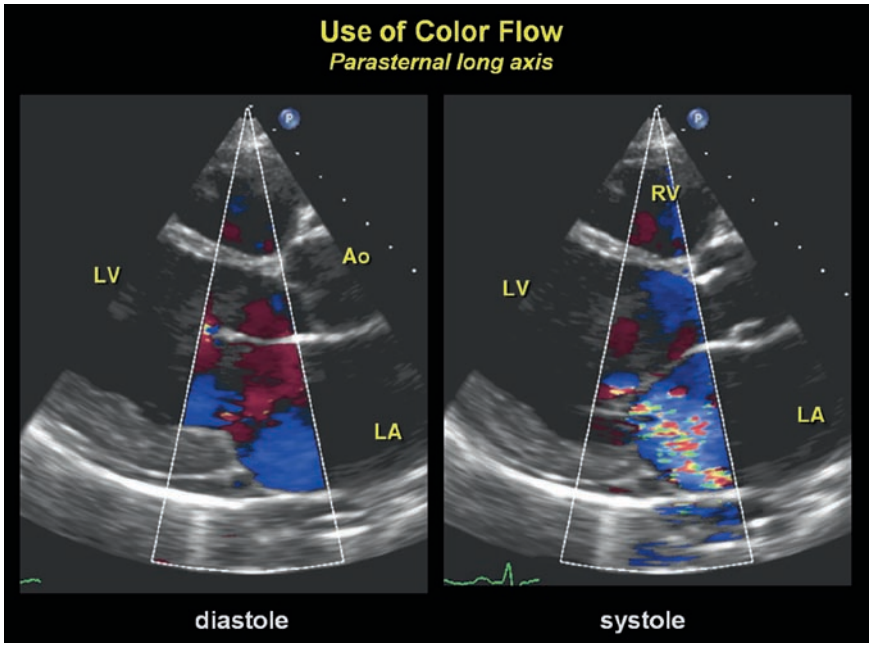

Fig. 8.49 Diastolic and systolic still frames from a parasternal long axis of the left ventricle in mild mitral regurgitation

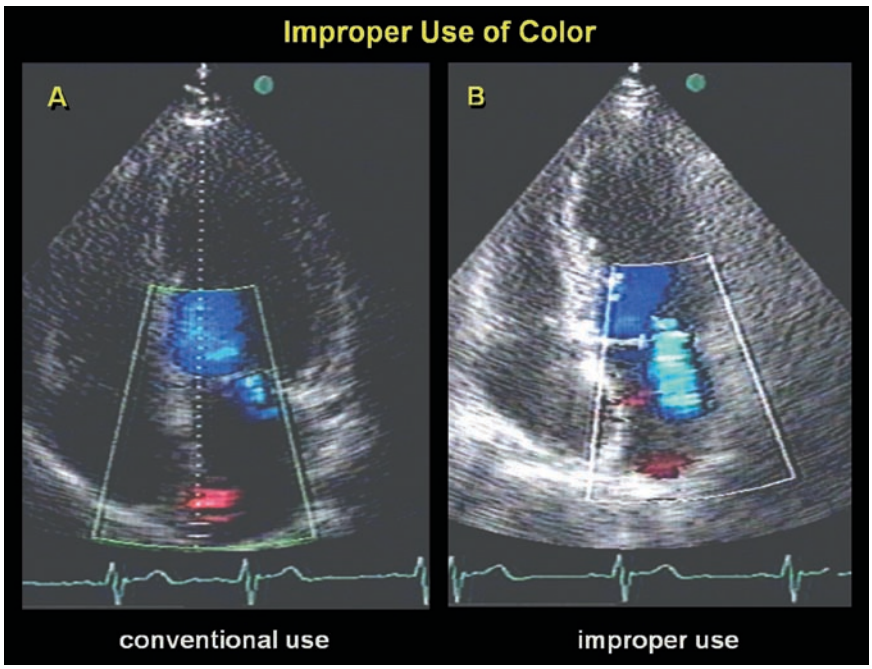

Fig. 8.50 Apical four-chamber views from the same volunteer showing that improper use of the color-flow controls may artifactually increase the size of a regurgitant jet

in a somewhat larger jet when color gain is increased. Both these images were obtained during the isometric contraction period with both the mitral and the aortic valves in the closed positions.

Further evidence of the effect of variable color Doppler gain is noted in Fig. 8.52. Here, there is low color gain in the left panel followed by correct gain in the middle panel, and obvious, excessive color Doppler

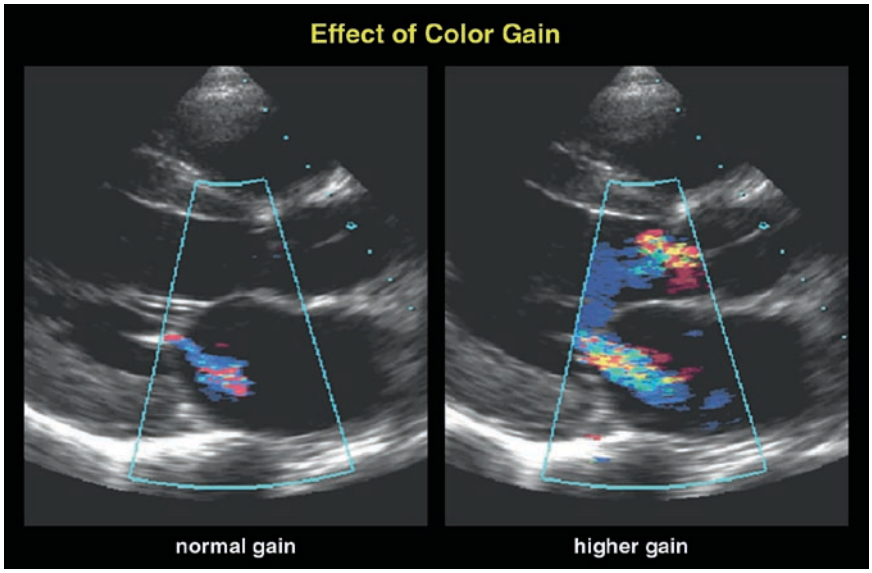

Fig. 8.51 Parasternal long axis from a patient with a centrally directed small degree of mitral regurgitation that increased in size with an increase in color gain

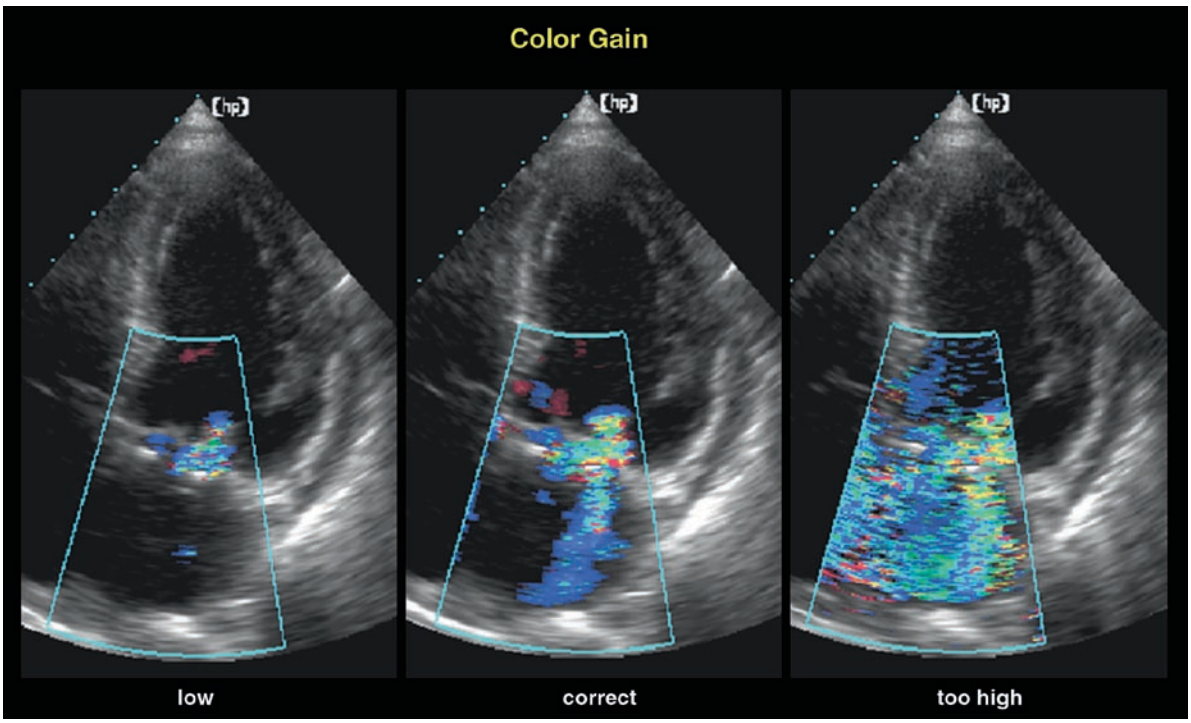

Fig. 8.52 Three panels from the apical four-chamber view in a subject with trivial mitral regurgitation where there is low, correct, and excessively high color gain. The excessive color gain floods the image with sparkling in the low-velocity color

gain in the right panel. Excessive color gain is characterized by the sparkling appearance of a variety of pixels seen in the right color image. The hallmark of correct gain (middle panel) is the detection of some low-velocity flow in the left ventricular outflow tract as well as lower-velocity flows seen surrounding the turbulent jet. The lower-velocity flows surrounding the turbulent jet reflect the movement of red cells already present in the left

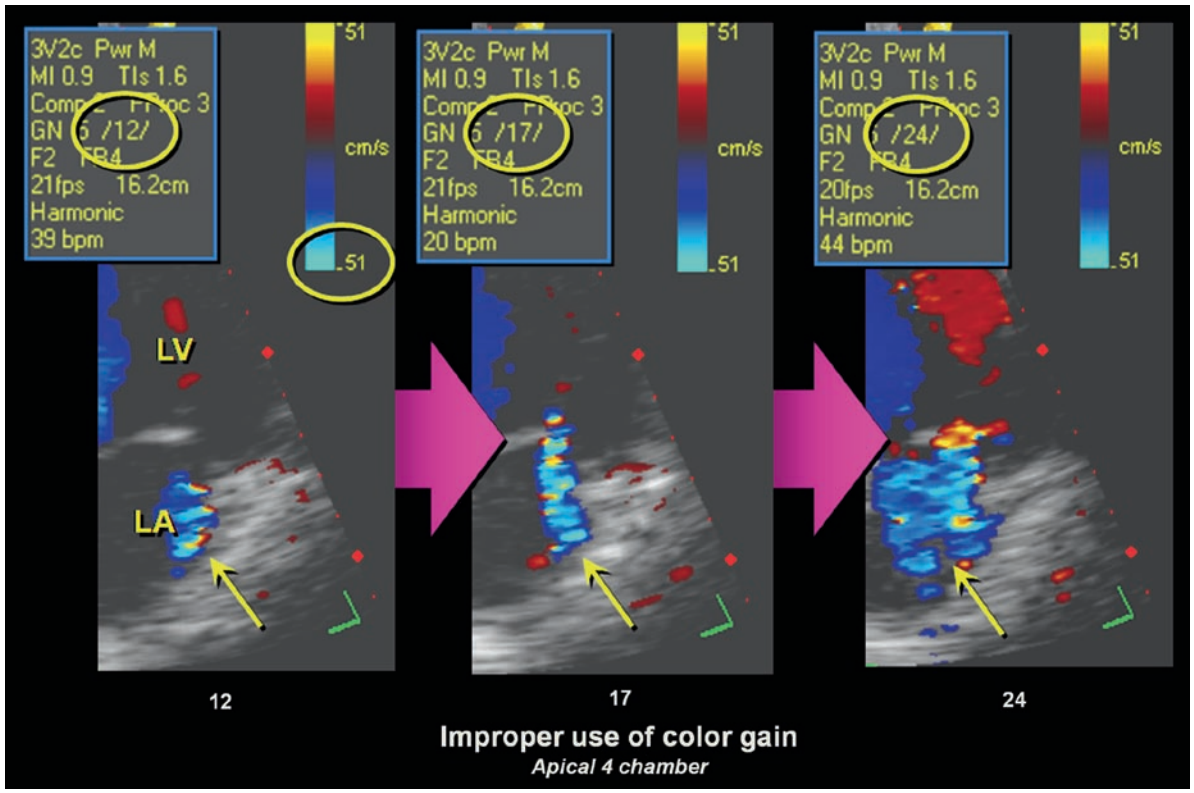

Fig. 8.53 Three panels from a subject with trivial mitral regurgitation from the apical four-chamber view showing artifactual increase in jet size with increase in color-flow gain

atrium that are engaged by the regurgitation. This phenomenon is known as the "entrainment."

These observations of improper use of color gain are not machine manufacturer specific even though various different machines may display color flow somewhat differently. The effect of overall increases in color gain is shown in an alternate manufacturer's device seen in Fig. 8.53. Here the three panels show an obvious increase in the size of the color-flow jet of mitral regurgitation encountered as the color gain is increased from 12 to 24. Numbers displayed on devices for gain are all relative and have no specific meaning except that one gain is higher than another. It should be noted that the individual demonstrated here is the same individual seen in Fig. 8.50. These different machines may display the color noise encountered by remarkably excessive color gain in different ways, but excess color gain will always result in a bigger jet. Figure 8.54 shows evidence of color noise in the apex of the left ventricle in

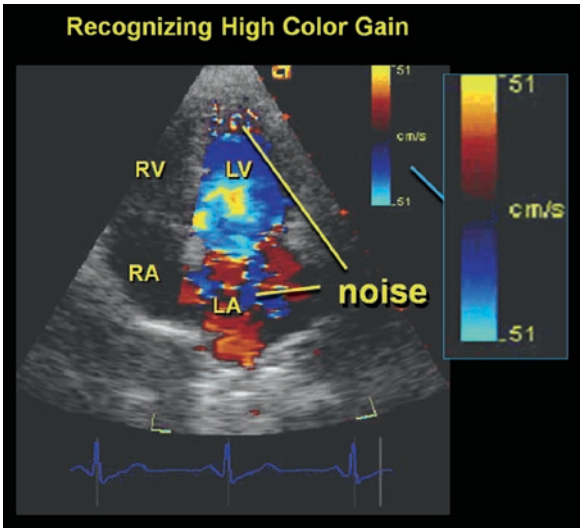

Fig. 8.54 Apical four-chamber view with markedly excessive color gain that renders the color flow unintelligible. Note the excess color gain makes the tissue around the apex sparkle

an apical four-chamber view that renders the color-flow image almost uninterpretable. Note the sparkling of tissue noise at the ventricular apex in this view.

Altered Nyquist (or Scale Factor)

Another major factor that can significantly alter the size of the color jet is Nyquist shift. With lowering of the Nyquist (color scale factor) progressively lower velocities will be displayed with increased brightness, artifactually increasing jet size. Most international standards for the display of color-flow images of mitral regurgitation from the apical four-chamber view recommend scale factor (Nyquist settings) in the 60 cm/s range (0.60 m/s). Figure 8.55 shows a remarkable increase in the size of a color-flow jet from a Nyquist setting of 78 cm/s down to 49 cm/s. All other factors were held the same during this demonstration of this phenomenon in an otherwise normal individual.

Effect of Frame Rate and Persistence

Figure 8.56 shows the effect of decreased frame rate when a moving jet is encountered. The left two panels evidence of a moving jet at 25 frames per second as it moves from frame to frame in time. On the right is the same individual encountered at a slower frame rate where the two jets are "added" into a single frame, obscuring dynamics and artifactually increasing jet size. Obviously, the maximum temporal sampling that is possible will provide a truer depiction of dynamic jet size. One should absolutely avoid widening the color-flow sector arc, thus slowing frame rate and obscuring flow dynamics.

Similarly, color frames obtained over a period of time could potentially be added to one another in any given display using a control called persistence. Figure 8.57 demonstrates the addition of multiple frames in a moving image so that the net effect is to markedly increase jet size. All other factors are held constant, including the Nyquist limit, as indicated in the inset boxes that reflect system settings. Neither two-dimensional echo image nor color persistence should be used in echocardiography. The heart moves much too rapidly to make these controls be of any use in the examination of cardiac structures. Never use persistence any time when examining a heart.

Excess Image Gain

There is also the possibility of decreasing jet size by certain setting factors. This decrease in jet size is demonstrated in Fig. 8.58. Here, excess image gain alone is added to the system settings from the properly obtained image in the left-hand panel. The added image gain encroaches on pixels occupied by color and the color is

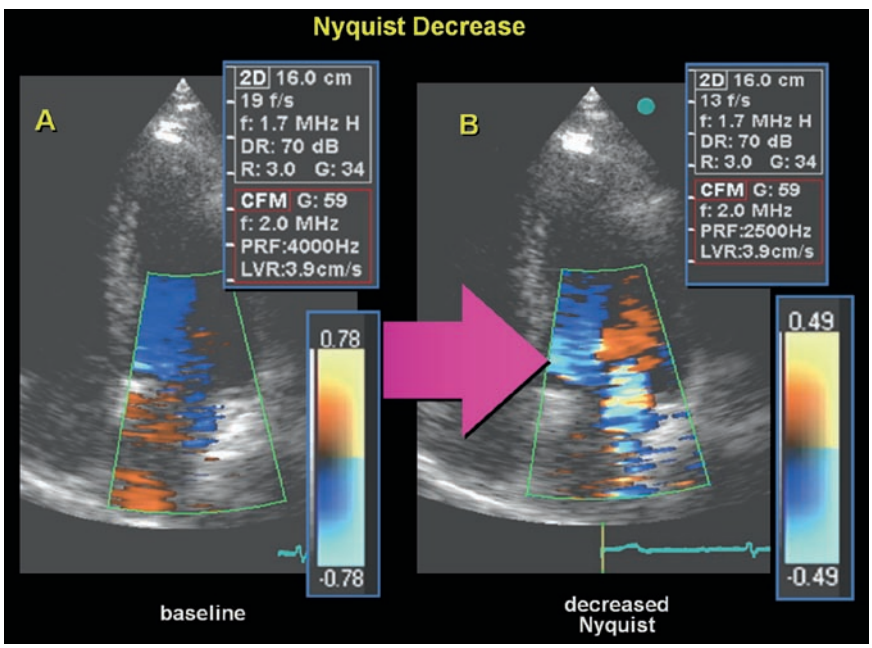

Fig. 8.55 Effect of the decrease in Nyquist limit (scale factor or PRF) as the jet size is markedly increased. For mitral regurgitation, Nyquist limits should be set at about 60 cm/s.

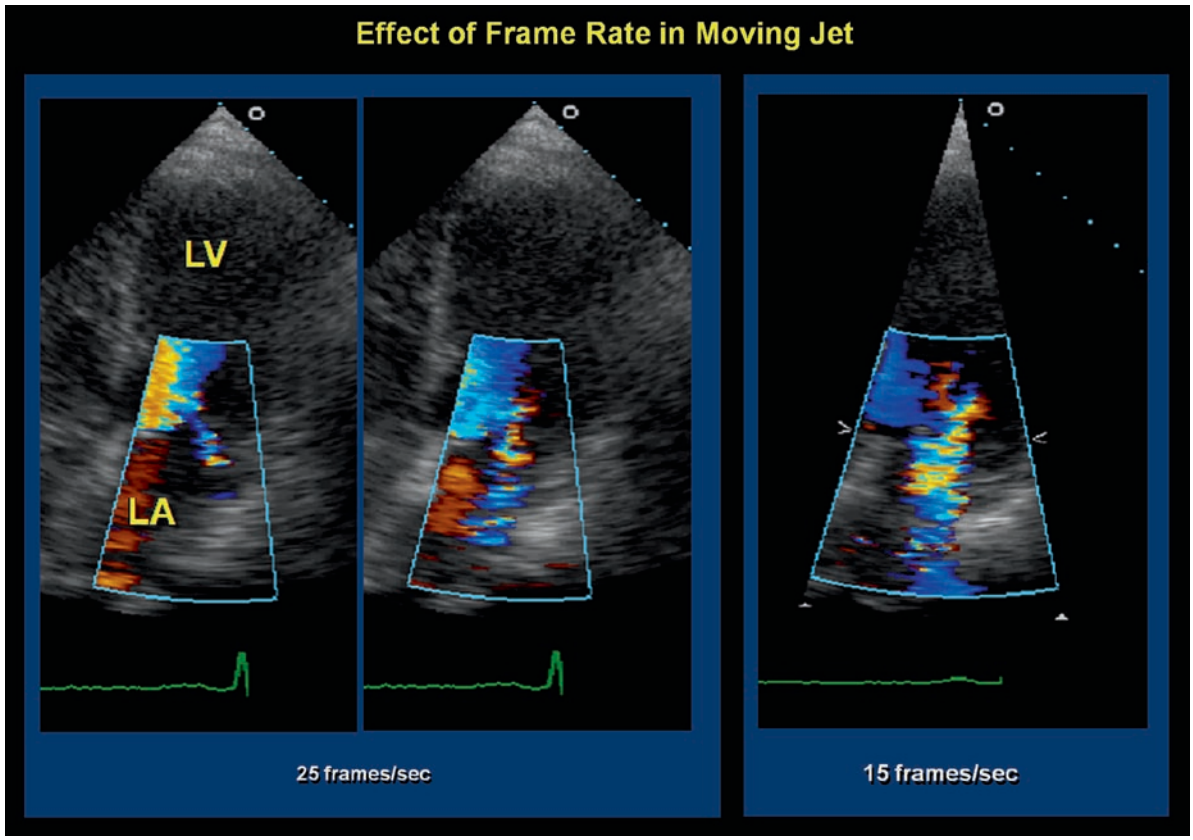

Fig. 8.56 Low frame rates may also increase the size of a mitral regurgitant jet

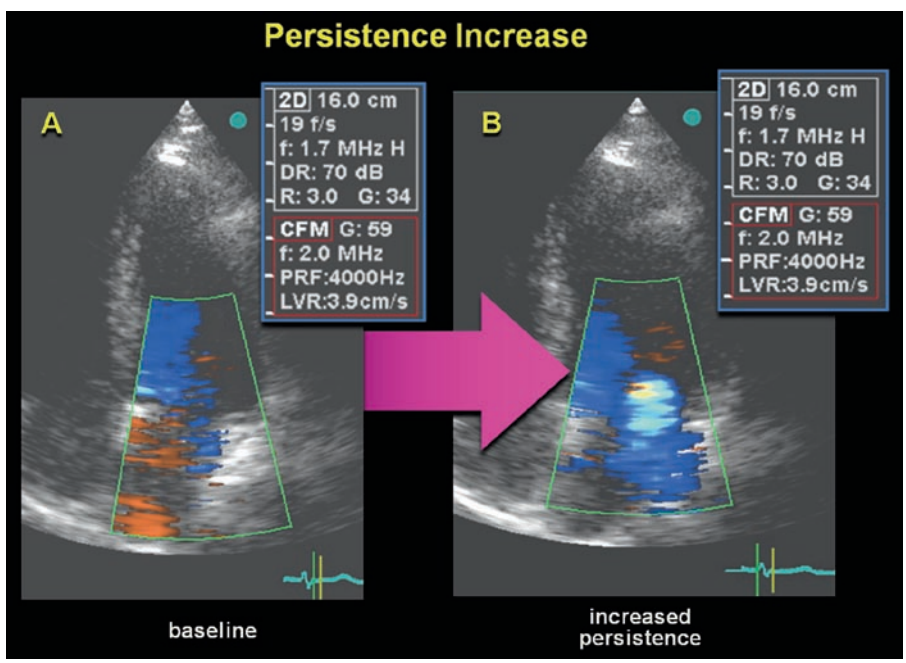

Fig. 8.57 Image persistence may also increase the size of a jet and have no place in echocardiography for examination of the rapidly moving heart

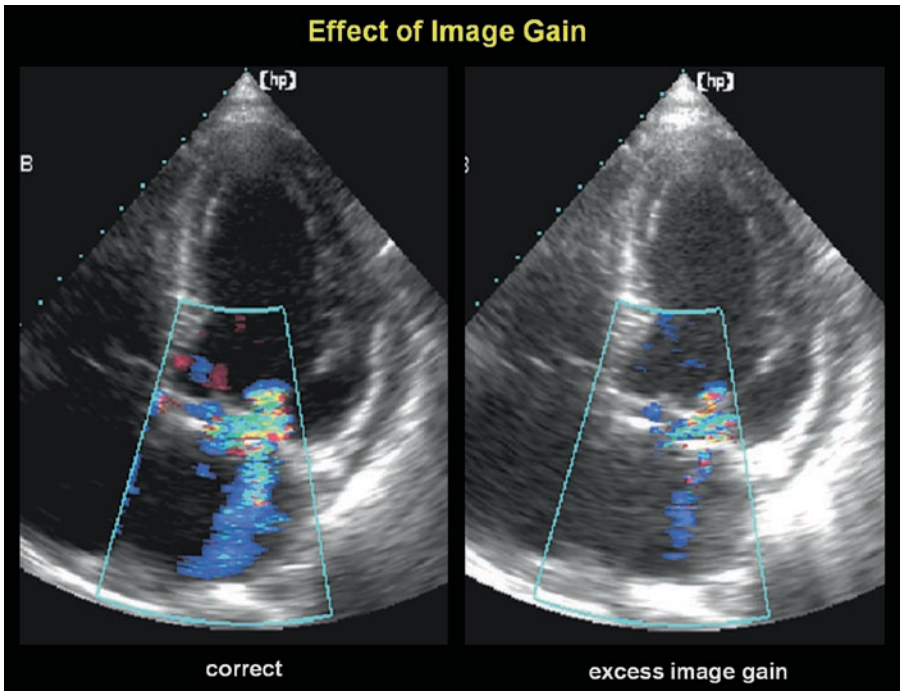

Fig. 8.58 Excess image gain may suppress the color as black-and-white anatomic information competes with color-flow information for display in any given pixel

eliminated as an image display can provide a picture of either black-and-white anatomic information or color-flow information, but not both at the same time. Note the image gain increase on the right has increased low-amplitude image noise into the picture that causes a haze within the cardiac chambers, displacing low-velocity flow, previously detected in the image on the left. Excess image gain, as well as color gain should be avoided in the conduct of any color-flow examination. Beginners with echocardiography will encounter this problem frequently as the use of excess image gain is frequently used to acquire anatomic targets when skill sets for transducer angulation and proper aiming are lacking. This sets up a cycle of increased image gain followed by increased color gain until a terribly distorted image of anatomy and flow is encountered.

System Setting Variability in Jet Size

These and other factors can increase the size of a color-flow jet. Figure 8.59 shows the addition of multiple factors to move a rather negligible jet seen in Panel 1 into a somewhat sizable jet seen in Panel 7. The various steps along the way can be seen to increase the jet size in progressive steps from left to right.

Such manipulated settings can be obtained with any color-flow machine. Figure 8.60 demonstrates such manipulations with an alternate device in the same individual depicted in Fig. 8.59. The major factors that exist in such manipulation are the increase in color gain, together with the decrease in Nyquist settings, but other less obvious factors can be added to distort image reliability of size, and thus, estimation of severity. Both excessive color gain and low Nyquist should always be avoided. Likewise, these manipulations should be recognized by any interpreter of color-flow information.

Jet Duration

The simple size of a jet in a still frame follow image can never be accurately relied upon as an absolute indicator of jet severity by itself. Size and jet duration must be taken together. It is well known that mitral regurgitation is classically described as a holosystolic jet by physical examination. Figure 8.61 shows successive new acoustic frames from the four-chamber chest wall approach in an individual with trivial mitral regurgitation. Note that the jet size remains small throughout the most of systole (solid arrows). Systolic frames are indicated with S and the last frame of the previously diastole and first frame of the next diastole are depicted by D. Figure 8.62 shows an ever-increasing large jet in a patient with more significant mitral regurgitation (solid arrows).

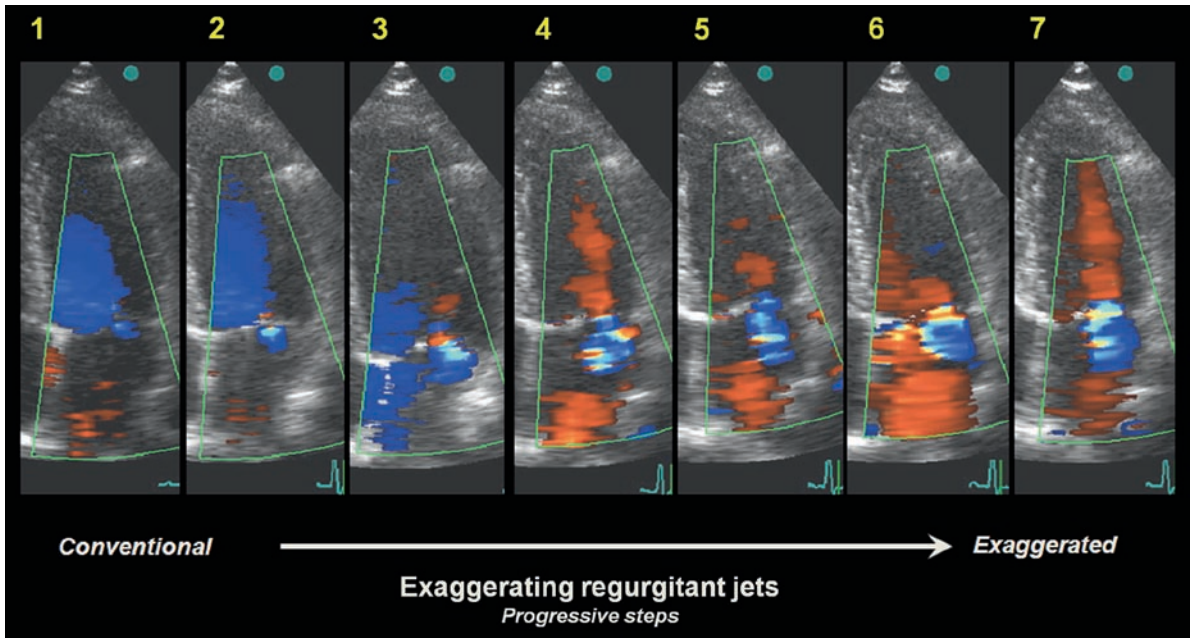

Fig. 8.59 Between *panels 1* and *7*, several color-flow settings are changed to artifactually increase the size of this trivial mitral regurgitant jet

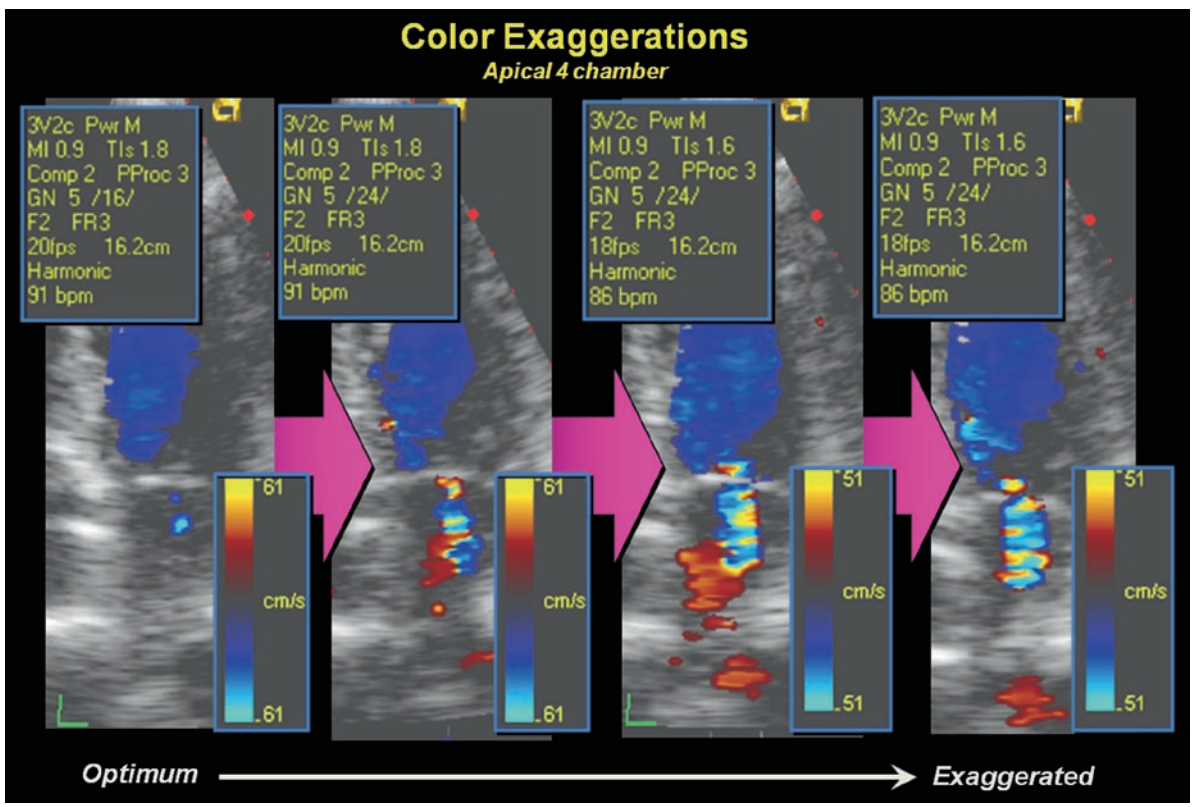

Fig. 8.60 The size of the trivial mitral regurgitant jet is again increased in this image from the apical four-chamber view by use of improper settings. The machine used here is different from that seen in the previous figure. Improper use of color gain and Nyquist are the main problems

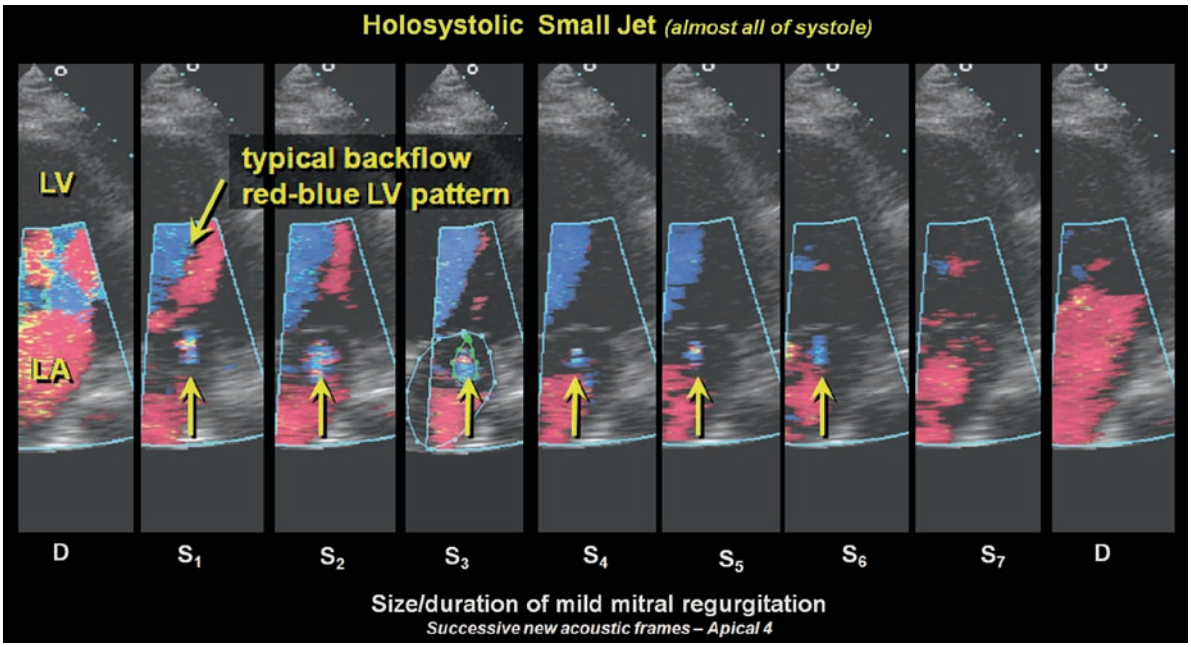

Fig. 8.61 Successive new acoustic frames from a volunteer with mild mitral regurgitation. The last frame of diastole (D) is followed by successive systolic frames and finishes with the first diastolic frame (D) of the next diastolic cycle. The *solid arrow* shows the duration of the minimal mitral regurgitation throughout all but one systolic frame. Jets have duration as well as size

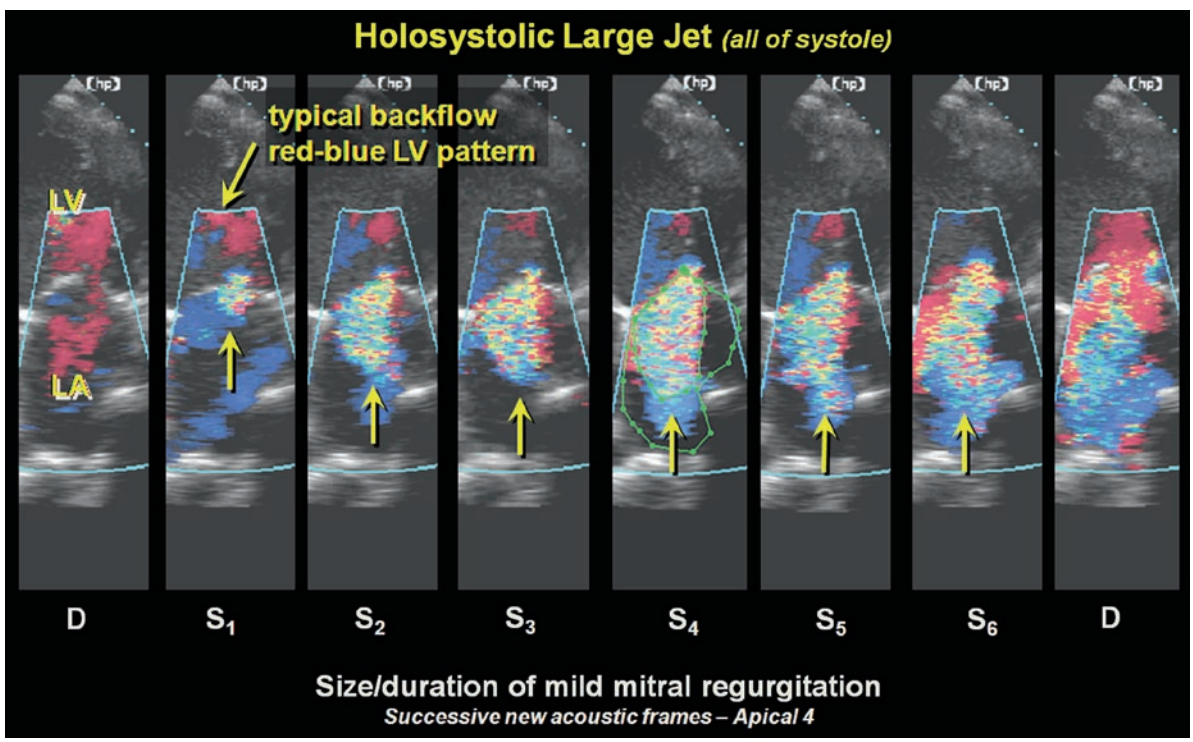

Fig. 8.62 Successive new acoustic frames from a volunteer with severe mitral regurgitation. The *solid arrows* show the jet to grow in size and last throughout systole. All jets have duration as well as size

When the mitral valve shuts in early systole, and before the aortic valve opens, the left ventricle is contracting prior to ventricular ejection (isometric/isovolumic contraction). Some blood is trapped in the closing mitral orifice, and when the leaflets shut there usually is some movement of blood posteriorly into the left atrium that accompanies the closing velocity of the leaflets. This phenomenon is known as "backflow," but may also be termed by the words "closing velocity," "mitral flash," or other such terms. This is found in almost all individuals and is further demonstrated in Fig. 8.63. (dashed arrow). This phenomenon is, therefore, characterized by a frame detected in early systole as well as a quite typical back flow, red–blue pattern of systolic flow within the left ventricle. One would be markedly mistaken if the backflow determined in frame S_2 in Fig. 8.64 was taken as mitral regurgitation. The turbulent flow noted in this acoustic frame is entirely compatible with the backflow phenomenon, and there is no evidence of regurgitation seen is any other systolic frame.

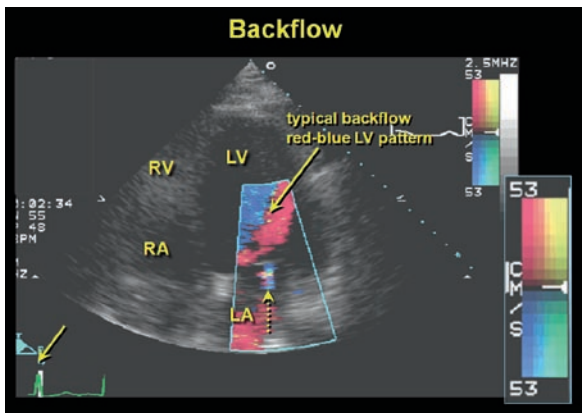

Fig. 8.63 The typical presentation of backflow during the period of isometric contraction. As the mitral leaflets close in early systole, the small degree of blood trapped between the leaflets moves back into the atrium (*dashed arrow*)

Hints from Spectral Doppler

There are other spectral Doppler findings which may assist an examiner in determining the severity of regurgitation. Figure 8.65 shows a continuous-wave spectral Doppler tracing from an individual with mild regurgitation (patient CG, left panel) compared to a patient with more significant regurgitation (patient LR, right panel). The method for determining the severity of mitral regurgitation using spectral Doppler relies on the subtle comparison of diastolic flow (seen above the baseline) to the regurgitant systolic flow seen below the baseline in brightness. Simply expressed, the brightness of any Doppler signal reflects the number of red blood cells moving through a Doppler sample if spectral Doppler gain settings are properly set. The

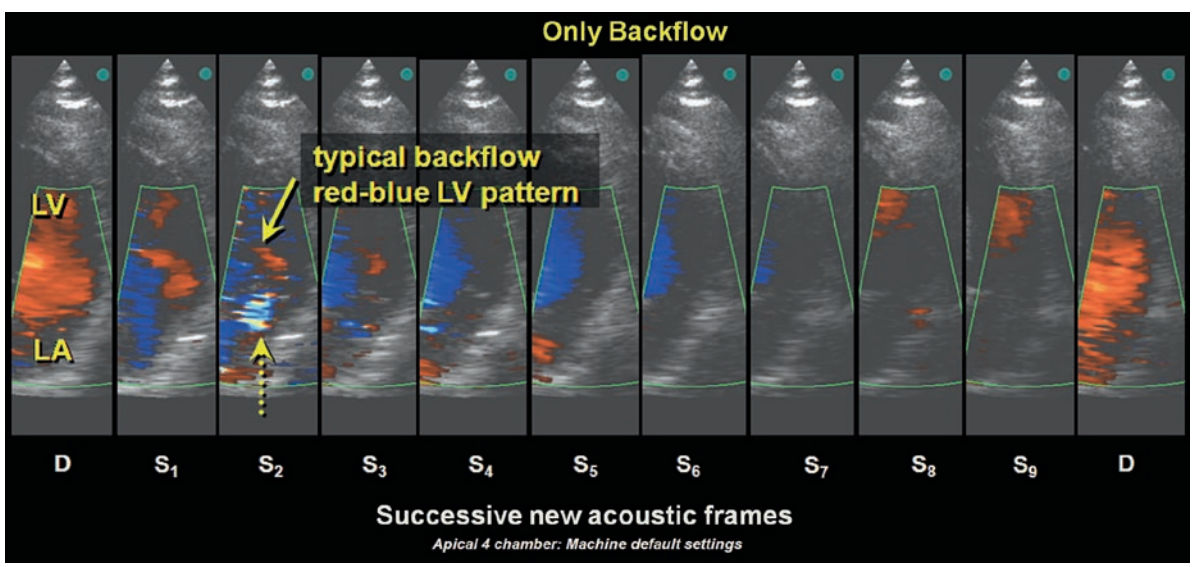

Fig. 8.64 Successive new acoustic frames from a volunteer with only backflow demonstrated during the cardiac cycle. All jets have duration as well as size

left-hand panel of Fig. 8.65 shows a remarkably bright antegrade signal in diastole when compared to the much less bright regurgitant flow signal (dashed arrow). In the right panel, one can compare the antegrade flow through the mitral valve in diastole to the regurgitant flow also represented by the dashed arrow. In this setting the brightness of antegrade flow and retrograde flow is much closer to each other. In both cases, peak velocities of mitral regurgitation are high and do not reflect the volume of regurgitant flow.

The same individuals depicted in Fig. 8.65 are shown in Fig. 8.66 using Doppler color-flow imaging.

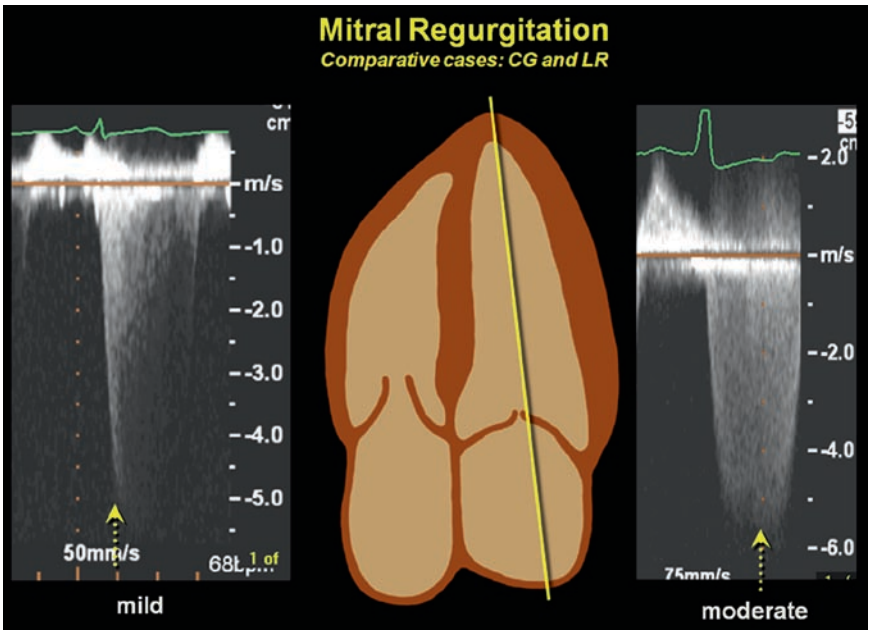

Fig. 8.65 Two contrasting continuous-wave recordings of mild and more severe mitral regurgitation from two different patients. One can also use the intensities of the Doppler recordings to indicate severity of regurgitation. See text

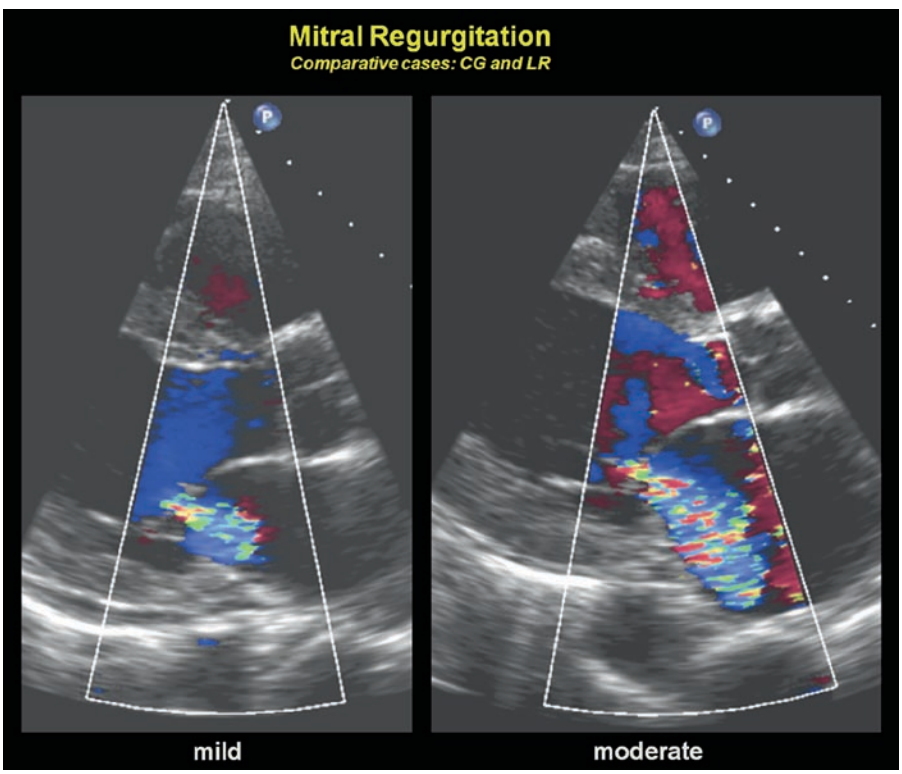

Fig. 8.66 Parasternal long-axis color-flow systolic still frame images from the same patients shown in the previous figure

These findings also reflect the somewhat more significant mitral regurgitation in the patient depicted on the right, in comparison to the patient on the left.

Given all these expressed limitations, it should not be interpreted that Doppler and/or echo methods yield unreliable results. Rather, these methods turn out to be additive as a user of these techniques learns to apply proper control settings and then use the comprehensive characteristics of color flow and spectral Doppler to render a reliable estimate of severity of mitral regurgitation. No single factor should ever be used and jet duration should always be taken into account.

In addition, it is recommended that a beginner always try to avoid the use of hyphenated degrees of mitral regurgitation, such as "mild–moderate" or "moderate–severe." While it is accepted that such borderline degrees may actually occur a simple grading system of none, trivial, mild, moderate, and severe is preferred (or 0, 1+, 2+, 3+, and 4+). When intermediate hyphenated degrees are avoided, the interpreter is forced to check all the factors in arriving at a conclusion. Echocardiography takes discipline to use every tool available to achieve a reliable clinical diagnosis.

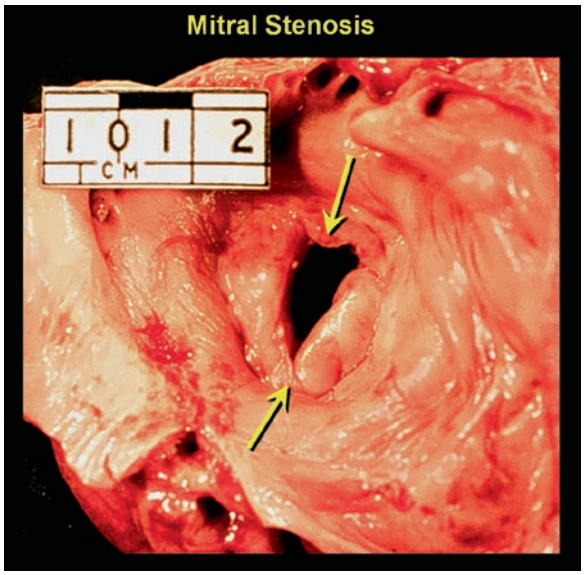

Fig. 8.67 Anatomic pathologic specimen of a rheumatic mitral valve. There is thickening of leaflet tips and commissural fusion (*arrows*). Modified from Kisslo, Leech & Adams. Essentials of Echocardiography

Mitral Stenosis

In examining the disorders that induce abnormal mitral valve flow and function, mitral stenosis first comes into attention. In fact, one of the first applications for the diagnostic use of echocardiography was for the detection and assessment of severity of mitral stenosis. Rheumatic mitral stenosis is manifest by thickening of the mitral valve leaflet tips. Figure 8.67 shows a pathologic specimen of rheumatic mitral stenosis with the irregular orifice that results from this chronic inflammatory process. Not only are the leaflet tips thickened, but the commissures become fused (arrows). Contrast this image viewed from the atrium down toward the mitral valve orifice with other pathologic specimens in Figs. 8.18–8.22.

Also contrast the appearance of a normal M-mode echocardiogram shown in Fig. 8.68 (left panel) with that of mitral stenosis (right panel). The M-mode movement of the tip of a normal mitral valve leaflet shows broad excursion and rapid deceleration during the period of passive ventricular filling from the E to F slope. In mitral stenosis, there is remarkable thickening of the mitral valve leaflet with significant restriction of the E to F slope. During the early days of echocardiography the determination of the rate of E to F slope was used for the estimation of the severity of mitral stenosis. This has long been abandoned and is no longer in common clinical use because it could detect severe mitral stenosis but could not differentiate moderate from mild stenosis. For all clinical purposes, measurement of E–F slope by M-mode has no clinical application.

Most recently, real-time three-dimensional echocardiography has been used to inspect the mitral orifice, either from the chest wall or transesophageal approach. These methods began in this institution, and the first clinical images were introduced from humans in 1993.[1] Figure 8.69 shows a contemporary still frame three-dimensional echocardiographic images in diastole (left panel) and systole (right panel) from an individual with no evidence of rheumatic mitral valve disease using transesophageal echocardiography and displayed in the surgical view. The mitral and tricuspid orifices are clearly visualized. The aorta is positioned as previously described anteriorly between the two atrial–ventricular valve openings. Valve leaflets are easily identified and both A–V orifices open widely.

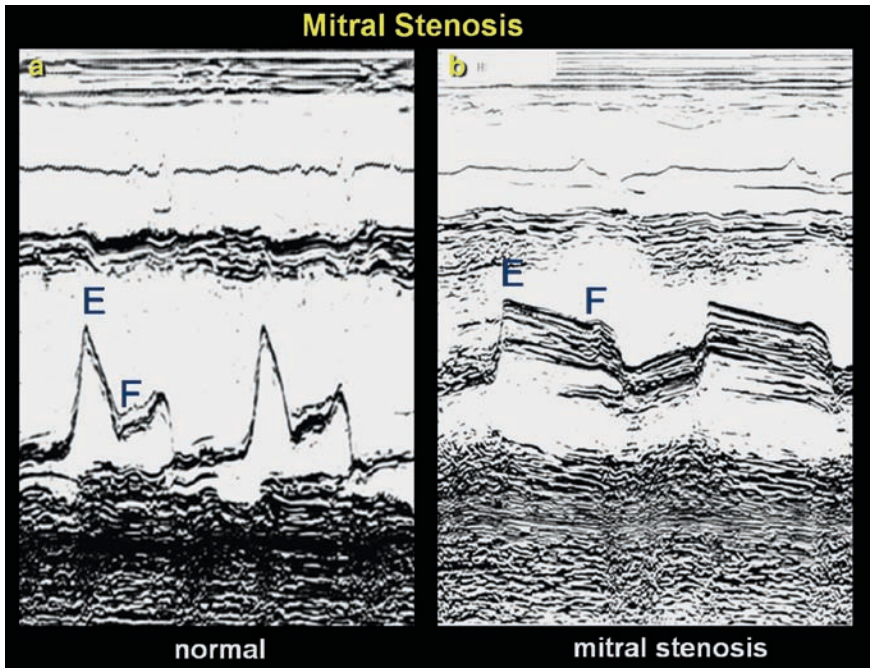

Fig. 8.68 Comparison of M-mode echo recordings from a normal mitral valve and one with mitral stenosis

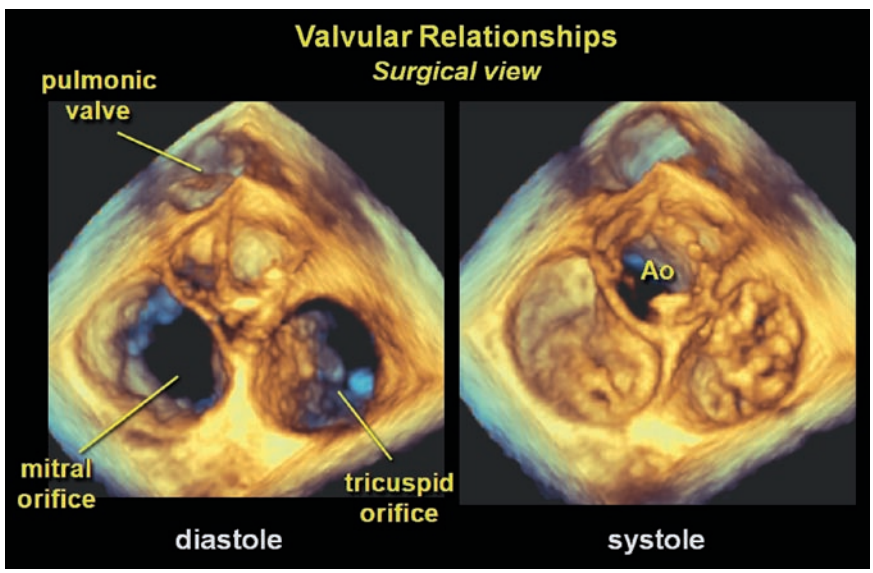

Fig. 8.69 Relationships of the mitral, aortic, and tricuspid valves from the surgical view in a three-dimensional echocardiogram in diastole (*left*) and systole (*right*)

Contrast the findings in Fig. 8.70 (mitral stenosis) with those of 7.69 (no mitral stenosis. In Fig. 8.70 the open mitral orifice in a patient with moderate restriction of diastolic opening is seen from the three-dimensional echocardiographic approach obtained from the chest wall. The mitral valve is viewed from the left ventricular perspective up toward the left atrium in the left panel and shows marked thickening of the leaflet tips together with commissural fusion. In the right panel, the same mitral orifice is visualized from the atrial side

toward the ventricle. The left atrial appendage is clearly seen and is dilated. The commissural fusion is again readily noted.

In severe mitral stenosis, the mitral valve opening is even more severely restricted. The more restricted rheumatic mitral valve orifice is seen Fig. 8.71 from the left ventricular perspective toward the atrium (left panel) and the left atrial side toward the ventricle (right panel). Here there is even more severe leaflet tip thickening and remarkable commissural fusion than noted in the previous figure.

A more troublesome expression of rheumatic mitral valve disease is demonstrated in Fig. 8.72 where both left and right panels are viewed from the left atrium

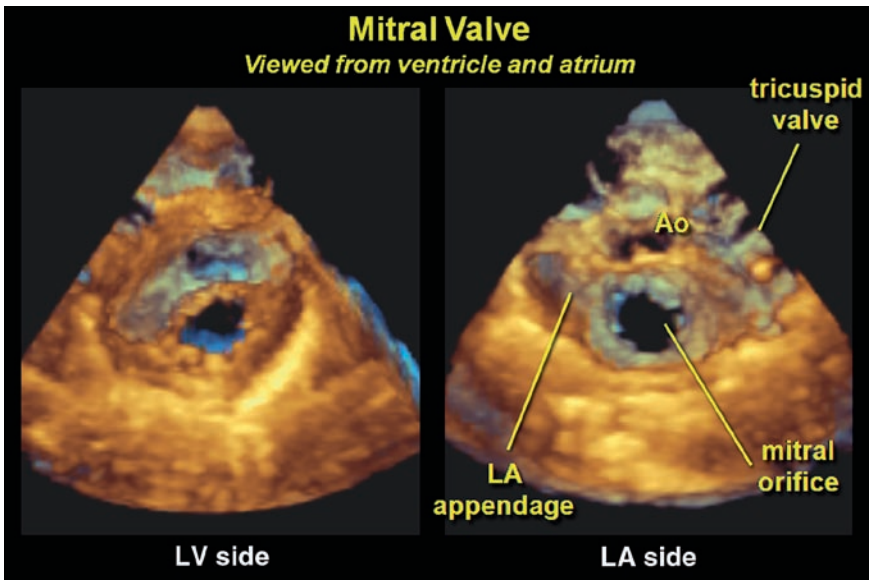

Fig. 8.70 Three-dimensional echocardiographic still frames showing a stenotic mitral valve orifice from the ventricular (*left*) and atrial (*right*) perspectives. There is leaflet tip thickening and commissural fusion

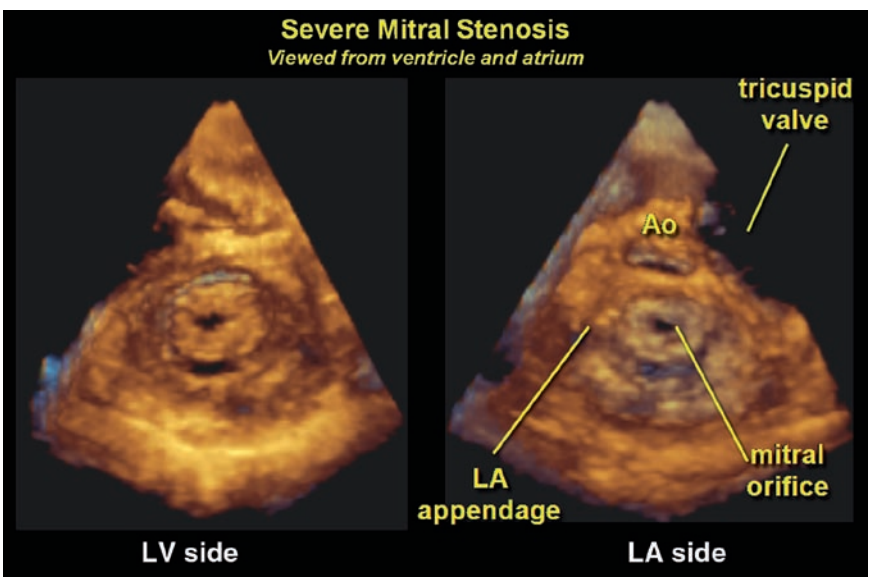

Fig. 8.71 Three-dimensional echocardiographic still frames showing a severely stenotic mitral valve orifice from the ventricular (*left*) and atrial (*right*) perspectives. There is even more leaflet tip thickening and commissural fusion than in the similar views in the previous figure

toward the ventricle. The mitral orifice is severely restricted as seen in previous examples. However, in this patient, there is remarkable thickening of the annulus that can be seen to extend far into the commissures, rendering successful mitral commissurotomy unlikely (arrow). One can also easily appreciate the marked dilation of the left atrial appendage in this patient, together with large trabeculation at the appendage tip which appears to divide the atrial appendage into two. Indeed, this patient underwent mitral valve replacement due to the marked annular and commissural thickening.

Despite the advent of three-dimensional echocardiography, two-dimensional echocardiography still plays a very significant role. The pattern of diastolic movement of the anterior mitral valve leaflet seen in Fig. 8.73 is characteristic of rheumatic mitral stenosis. The leaflet tip is restricted and bends toward the

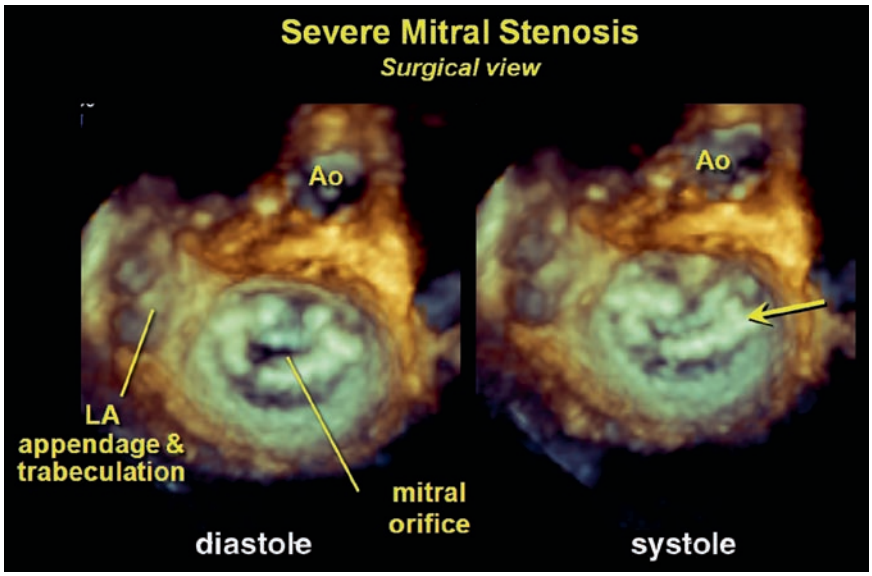

Fig. 8.72 Surgical view of a three-dimensional echocardiogram in mitral stenosis. In this patient, there is marked annular and suprannular thickening and fibrosis (*arrows*)

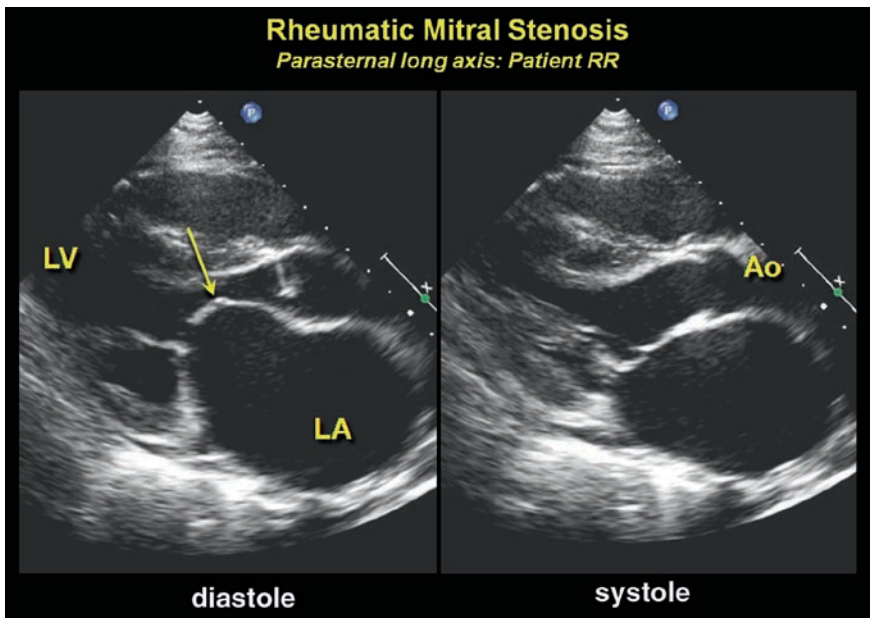

Fig. 8.73 Two-dimensional echocardiographic parasternal long-axis view of rheumatic mitral stenosis showing tethering of the anterior mitral valve leaflet tip. The body of the leaflets remains mobile (*arrow*) in all but the most severe disease. Rheumatic mitral valve disease is a disease of leaflet tips

restricted posterior mitral leaflet in diastole because of leaflet tip attachment and commissural fusion. This pattern results in a very narrow orifice. The body of the anterior mitral leaflet (arrow) is usually, however, frequently spared in this disorder except in its most severe forms. The left atrium is significantly enlarged in both systole and diastole. Note the mitral valve closing patterns in systole. This opening pattern of the mitral valve apparatus in diastole is sometimes referred to as "diastolic doming," as the mitral valve leaflets form a dome-like structure from atrium toward ventricle during ventricular filling. What is most significant is to recognize the attachment of leaflet tips and to recognize that rheumatic involvement of the mitral valve is manifest by disease at the leaflet tips and commissures, frequently sparing the body of anterior mitral valve leaflet.

Because of this leaflet tip restriction, systolic closure is impaired and rheumatic mitral regurgitation can consequently result (Fig. 8.74). Again, the left atrium is seen to be massively dilated in this individual with several mitral stenosis. When mitral stenosis is severe and mitral regurgitation is significant, mitral commissurotomy is not performed either by balloon (at catheterization) or surgically. Rather, the mitral valve is replaced. Open mitral valve repair with this combination of findings has had only variable results.

Doppler patterns of normal and mitral stenosis can also be differentiated. In panel A of Fig. 8.75, the normal antegrade mitral Doppler flow is seen. There is a narrow Doppler spectrum of velocities and a rapid E to F slope with easily recognized preservation of the A wave, following atrial contraction. Panel B shows the typical pattern of mitral valve obstruction with marked delay in the degradation of the E–F slope and significant spectral broadening. Spectral broadening refers to the presence of multiple velocities in the recording at any one point in time.

Planimetry of the Mitral Orifice

Since the mitral orifice may be directly visualized by two-dimensional echocardiography with proper transducer angulation, this is an ideal technique for determining the cross-sectional area of the mitral valve. Figure 8.76 contrasts mitral valve opening during diastole in an individual with no mitral stenosis (left panel) with that in an individual with severe mitral stenosis (right panel). Most echocardiographic systems will provide a method for easy planimetry of these valve orifices.

Figure 8.77 contrasts two patients with mitral stenosis. One is moderate (left panel) and one is severe (right panel).[2] Proper detection of a rheumatic valve orifice by two-dimensional echocardiography requires some operator experience to adjust the plane of examination directly through the leaflet tips. If diagonally

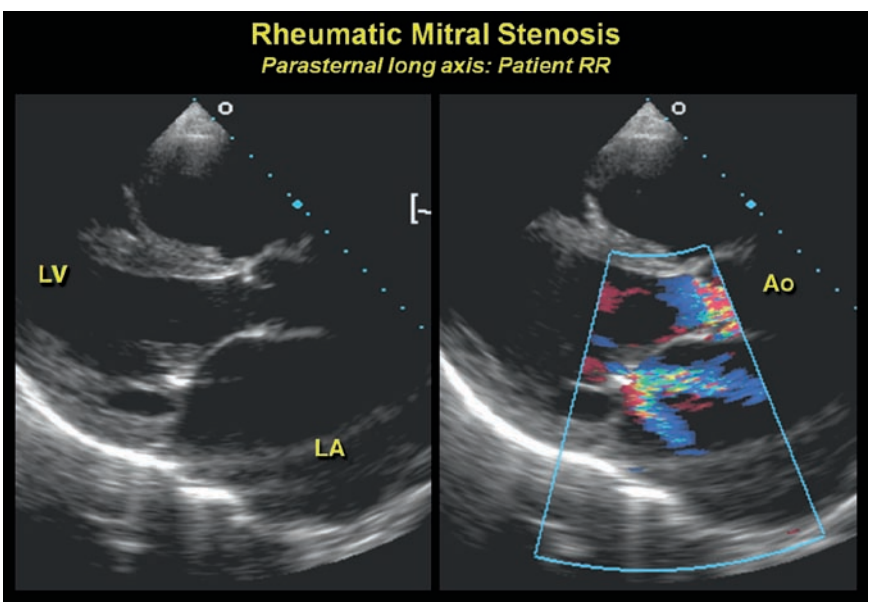

Fig. 8.74 Two-dimensional echocardiographic parasternal long-axis view of rheumatic mitral stenosis. The color-flow image at the *right* shows mitral regurgitation

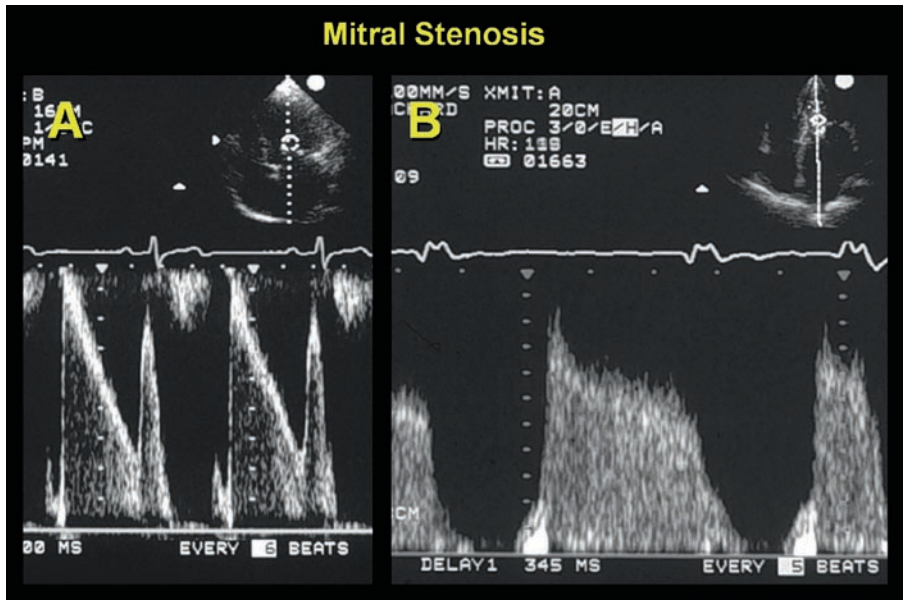

Fig. 8.75 Spectral Doppler recordings from the apex showing normal mitral diastolic flow compared to mitral stenosis. In mitral stenosis there is spectral broadening and a slow diastolic flow decay

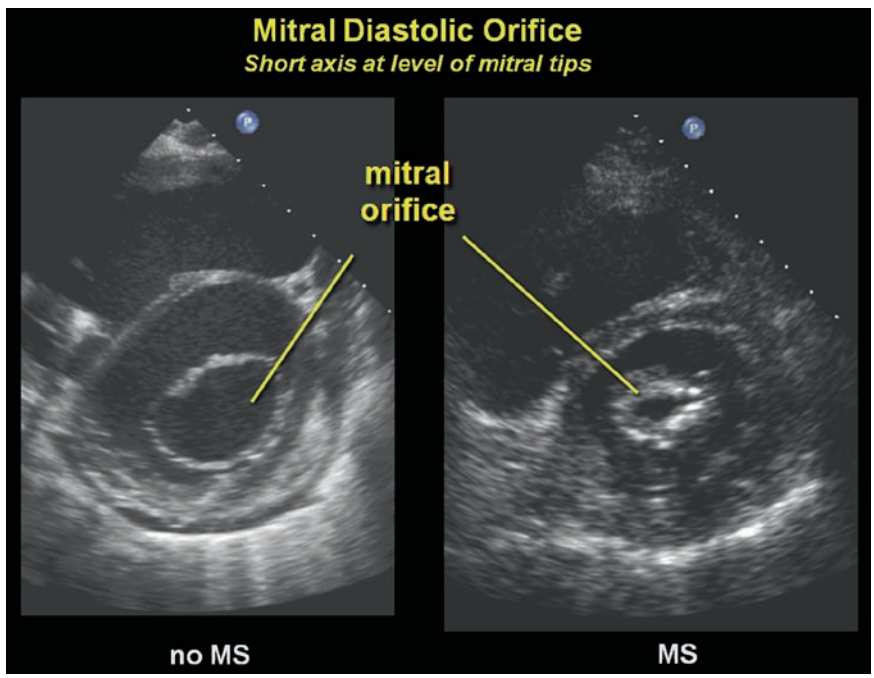

Fig. 8.76 Parasternal two-dimensional short-axis still frames comparing mitral diastolic orifice area in a patient with no mitral stenosis (*left*) to one with a restricted orifice of mitral stenosis (*right*)

oriented through the body of the anterior mitral leaflet to the tip of the posterior leaflet, the orifice will appear artifactually large due to angulation. Proper assessment also requires that the image gain be properly set lest the orifice be depicted as too small by excess image gain.

Using proper technique, it is long been accepted that two-dimensional echocardiography can reliably

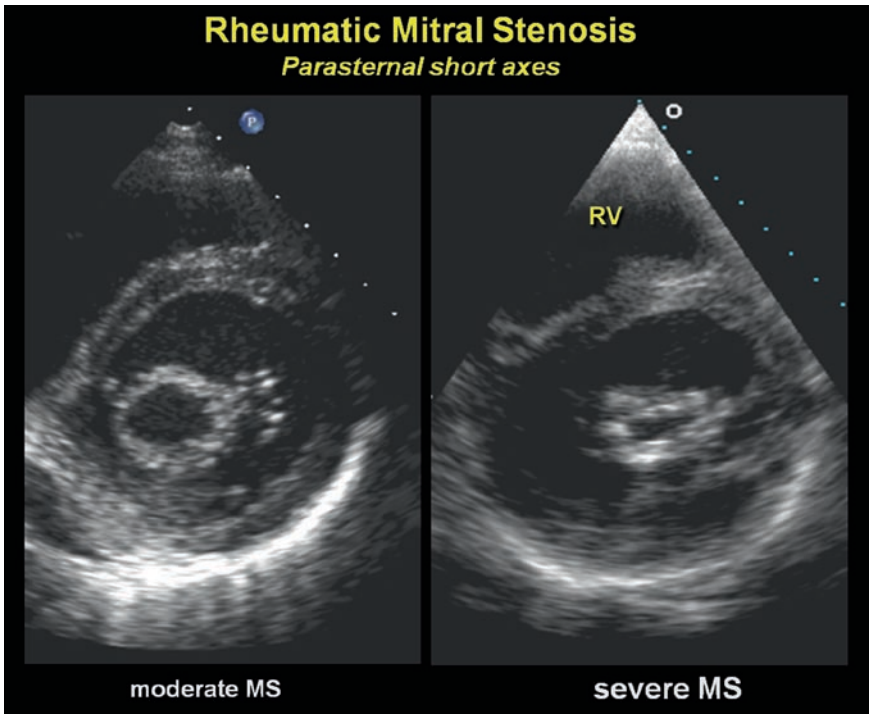

Fig. 8.77 Parasternal two-dimensional diastolic short-axis still frames from a patient with moderate (*left*) mitral stenosis compared to one with severe mitral stenosis (*right*)

demonstrate mitral valve leaflet tip cross-sectional area. Various mitral valve orifices are demonstrated in Fig. 8.78 with comparative echocardiographic and catheterization determined mitral valve orifice area.[2] The correlation of echo and catheterization valve areas is shown in Fig. 8.79 from an early paper where this capability was demonstrated ($r = -0.93$). Of course, consistent methods can be used in any one center that lead to measurement consistencies. Such correlations are generally not as effective following mitral commissurotomy.

Results of such correlations from a multicenter study involving the Balloon Valvuloplasty Registry showed much wider variation when two-dimensional echoes determining valve area and catheterization valve area were compared (Fig. 8.80).[3] While this correlation is less than ideal it does reflect the variations that might occur from institution to institution and as hemodynamic situations may vary between echocardiographic and hemodynamic assessments.

Mean Mitral Gradient by Doppler

Another method for determining severity of mitral stenosis by Doppler is the measurement of mean mitral gradient. When using this method, the Doppler continuous-wave transducer is placed at the ventricular apex and angled through the mitral orifice in diastole. The resulting diastolic flow signal is then traced within the software package of the ultrasound machine to determine the mean mitral gradient according to the method described by Hatle (Fig. 8.81).[4] Figure 8.82 shows the correlations from this approach for determination of mean mitral gradient when measurements are made by Doppler and by hemodynamics simultaneously. The correlations are excellent.

Variations are, however, encountered when measurements are made by multiple institutions and determined nonsimultaneous with catheterization. These variations are seen in Fig. 8.83 from the multicenter study previously mentioned.

Pressure Half-Time Mitral Valve Area

There is another method for determination of mitral valve area using the degradation of the gradient in mitral stenosis by Doppler echocardiography referred to the pressure half-time method. This method is dependent on determining the time interval that it takes for the mitral gradient to drop to half its initial value.

Figure 8.84 shows how the pressure half-time is measured. The starting point is the time of peak velocity

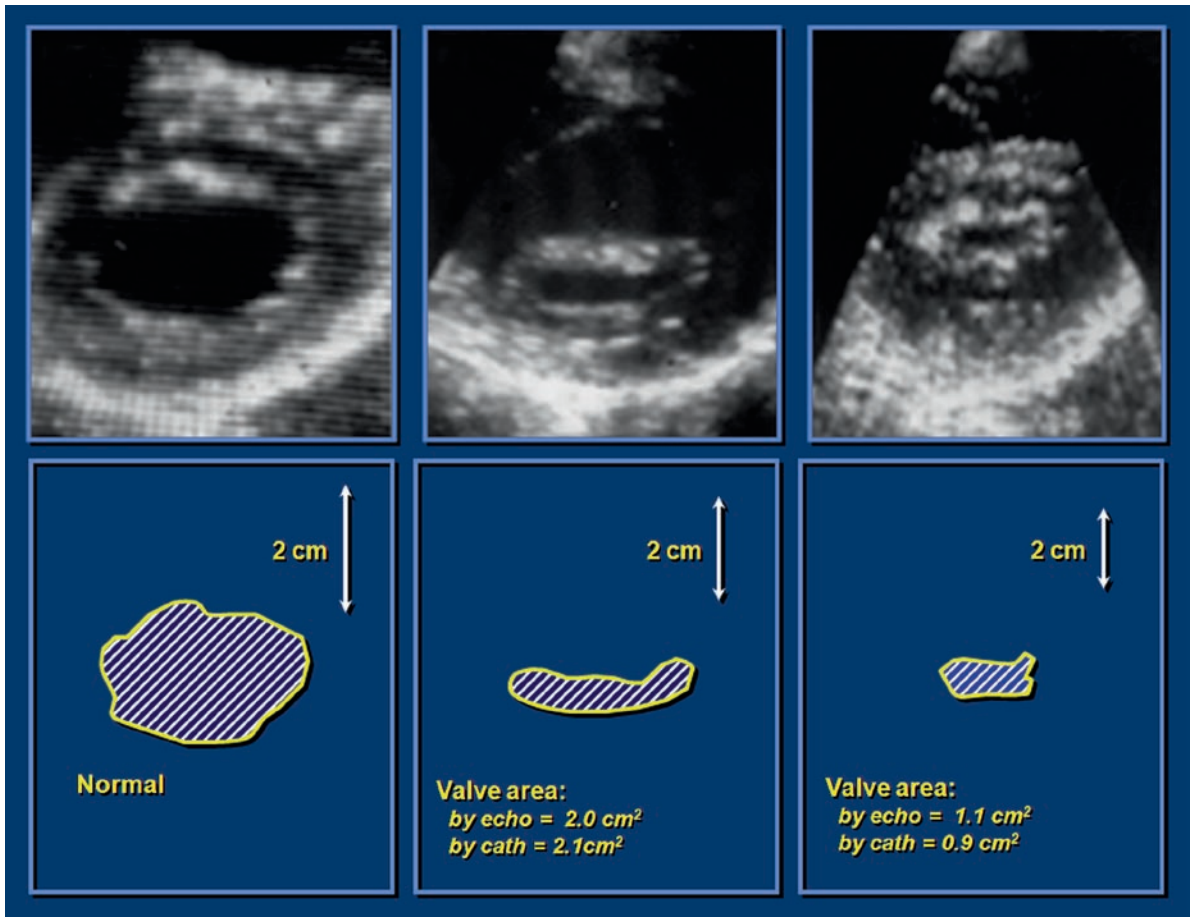

Fig. 8.78 Compared diastolic orifice measurements showing progressively smaller mitral orifice size with more severe mitral stenosis. Redrawn after Nichol et al[2]

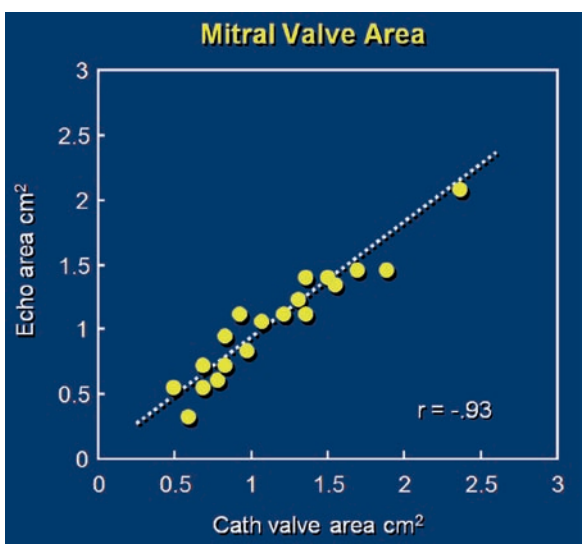

Fig. 8.79 Comparison of echo calculated valve area from catheterization calculated valve area. Redrawn after Nichol et al[2]

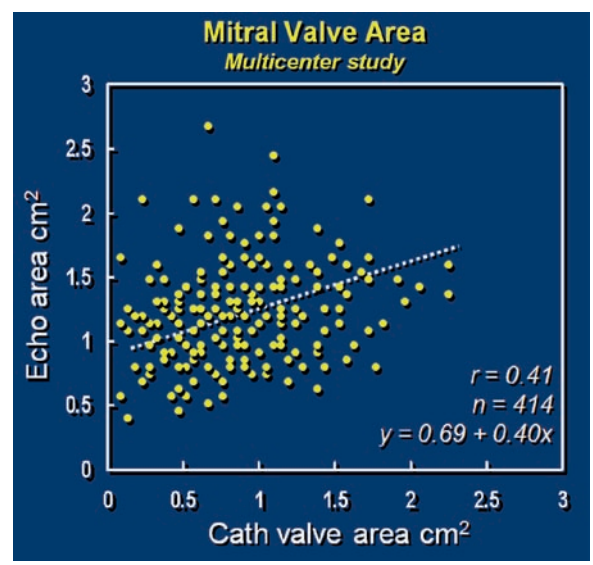

Fig. 8.80 Comparison of echo calculated valve area from catheterization calculated valve area from a large multicenter study. Redrawn after Kisslo[3]

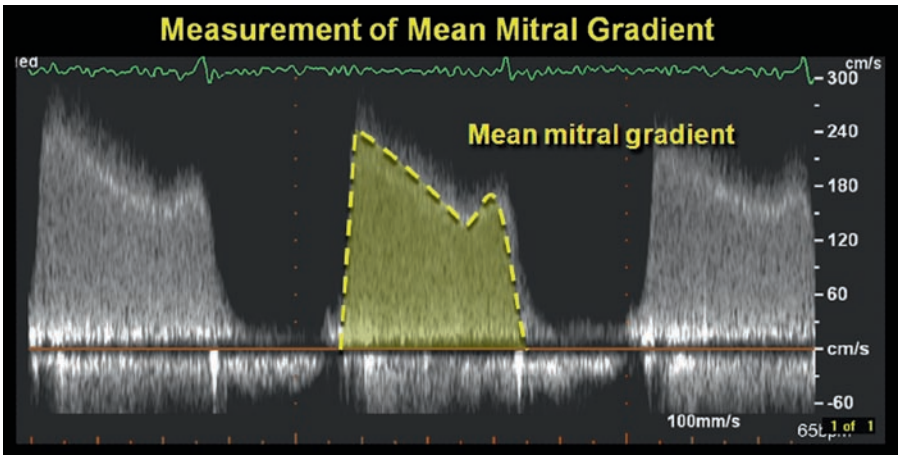

Fig. 8.81 Measurement of mean mitral gradient

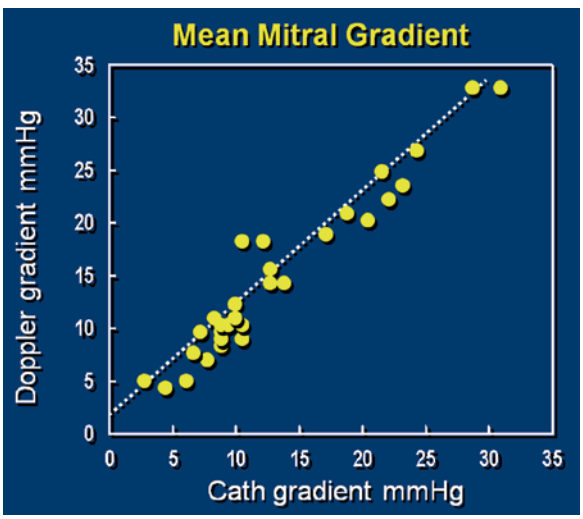

Fig. 8.82 Mean mitral gradient by Doppler compared to simultaneous measurement of mean mitral gradient at catheterization. Redrawn after Hatle and Angelsen[4]

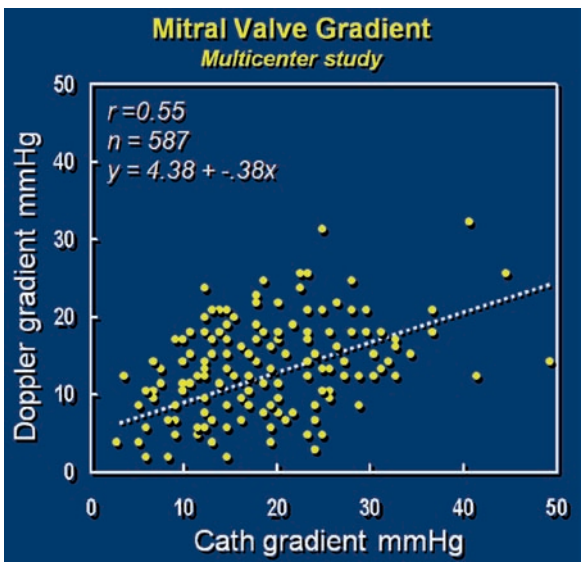

Fig. 8.83 Comparison of Doppler calculated mean mitral gradient to nonsimultaneous catheterization measured mean mitral gradient from a large multicenter study. Redrawn after Kisslo[3]

(Point 1), which in this example is approximately 2.4 m/s. This corresponds to a peak pressure gradient of approximately 24 mmHg by the modified Bernoulli equation. A line along the diastolic descent of the mitral valve spectrum is then drawn (Step 2). The point is then found along this line where the pressure is then dropped to one-half of its initial value (to Point 3). This point is rapidly determined by dividing the initial velocity by the 1.4 (which is the square root of 2). In this case 2.4/1.4 = 1.71 m/s. Thus, when the velocity falls to 1.71 m/s the pressure is at one-half of its initial value seen at Point 1. The pressure half-time is simply the time interval between Point 1 and Point 3, in this case approximately 250 ms (Interval 4).

Subsequently, Hatle and Angelsen[4] found the pressure half-time could be used to estimate mitral valve area from an empirical formula shown in the bottom of Fig. 8.84. In this series of 20 patients, they found a stronger correlation between this Doppler-derived estimate and catheterization-derived mitral valve area (Fig. 8.85). Once again, however, when these quantitative manipulations are applied to larger populations in a multicenter study, these correlations are less exact (Fig. 8.86).

The advantage of all these quantitative approaches is that a clinician is not dependent on any single

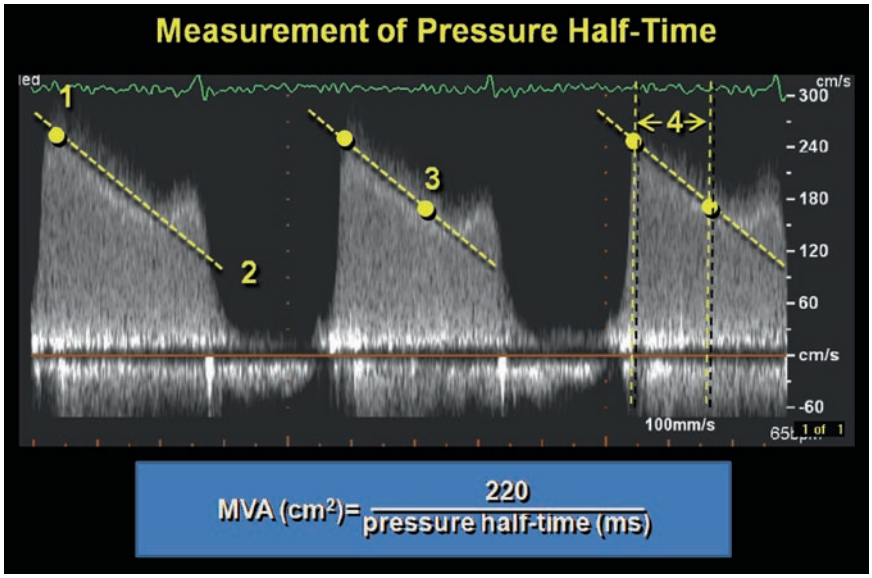

Fig. 8.84 Steps in the calculation of mitral valve area by pressure half-time

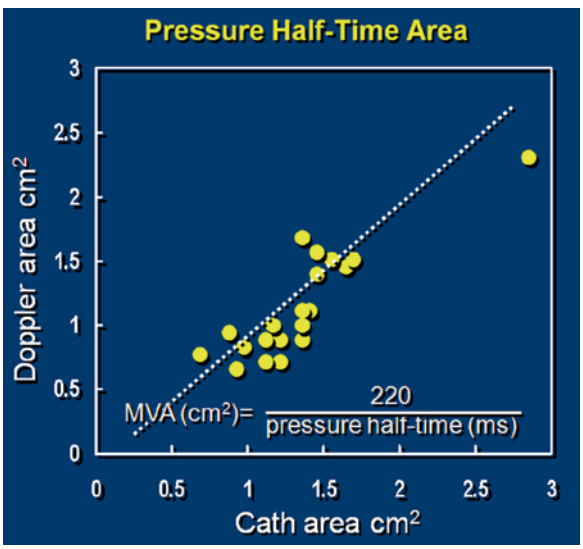

Fig. 8.85 Comparison of mitral valve area calculated from pressure half-time to that calculated at cardiac catheterization. Redrawn after Hatle and Angelsen[4]

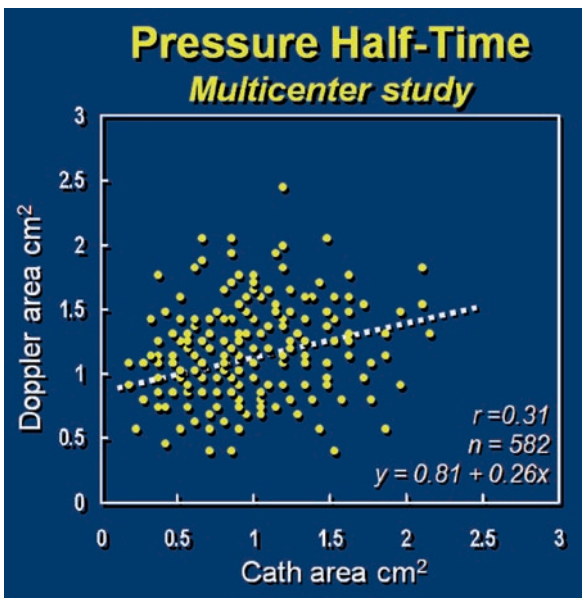

Fig. 8.86 Comparison of mitral valve area calculated from pressure half-time to that calculated at cardiac catheterization from a large multicenter study. Redrawn after Kisslo[3]

measurement for the assessment of the severity of mitral stenosis. Rather, one can implement all methods and then implement a conclusion that is most consistent with the quantitative and subjective findings. In severe mitral stenosis, the left atrium is dilated and right ventricular pressures are elevated (through determination of peak right ventricular systolic pressure from tricuspid regurgitation).

Beginners in echocardiography sometimes think that a single measure can determine the severity of the disorder alone. It is the clinical decision-making process, all factors must be taken into account and then a decision as to severity of stenosis rendered. Observers should take into account other factors such as left atrial size and right ventricular pressure when applying the

terms mild, moderate, or severe to rheumatic mitral stenosis by echocardiography. Measures should correlate to a reasonable degree or the observer has made some error with the measurement that is in conflict with others.

Echocardiography is not alone in this need for proper clinical decision-making processes. A clinician would not apply the diagnosis of diabetes to a single measurement of blood sugar of 140 mg/100 ml. Rather, proper clinical practice is to perform other tests, such as blood sugar determination in a fasting condition and a glucose tolerance testing or other procedure to ensure the reliability of a diagnosis is not dependent on one measurement alone. Echocardiography is no different and still remains the most readily available and best noninvasive or invasive method for determination of the severity of mitral stenosis or insufficiency.

Mitral Prolapse

The combination of echocardiographic imaging methods for determination of mitral valve anatomy together with Doppler assessment of the location and severity of mitral regurgitation is now the principal method for evaluation of mitral degenerative disorders such as mitral valve prolapse. Almost two-third of mitral regurgitation is due to such disorders and these techniques have found immense value in planning surgical procedures as well as evaluating the results of these procedures.

The M-mode echocardiogram in Fig. 8.87 shows the classic appearance of mitral prolapse using this one-dimensional technique. There is a posterior bowing of the mitral valve apparatus in late systole (arrow). Depending on the angulation of a single beam used in M-mode, there are multiple sources for error. In addition, there is no guarantee that the entire mitral valve can be interrogated by a single beam except in the

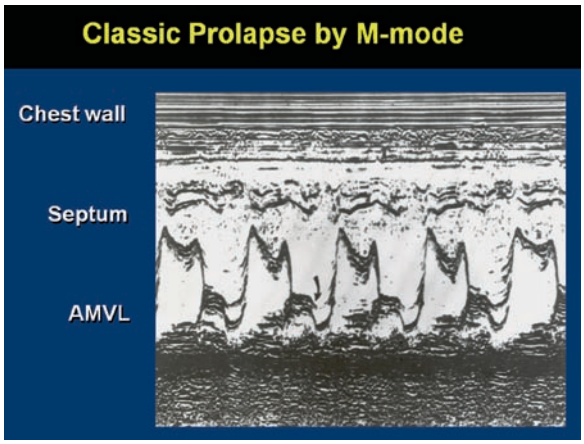

Fig. 8.87 The classic appearance of mitral valve prolapse by M-mode echo. There is a mid-late systolic posterior motion of the mitral valve (*arrow*)

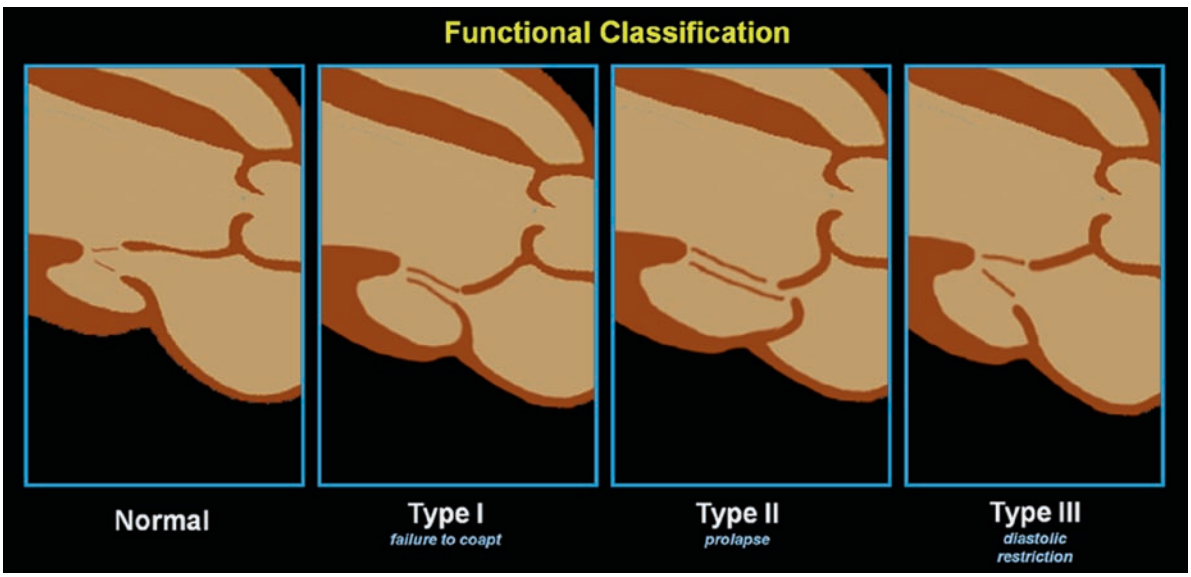

Fig. 8.88 The functional classification of mitral regurgitation. For details, see text

hands of a few experts. Accordingly, the application of M-mode in this disorder lost favor with the advent of two-dimensional echocardiography.

Functional Classification of Mitral Regurgitation

Mitral valve prolapse is included in the currently applied descriptions of the functional classification of the etiology of mitral regurgitation. Because most mitral regurgitation can be surgically managed by valve repair, rather than replaced, this classification is now widely used (Fig. 8.88).

Currently, the functional classification of mitral regurgitation is described as consisting of three basic types. Normal mitral valve coaptation occurs with the tips of the mitral leaflets located well into the left ventricle in systole, far from the mitral valve annulus (Fig. 8.89). This level of coaptation provides adequate surfaces for coaptation of both leaflets to prevent significant regurgitant flow into the atrium in systole.

In Type I mitral regurgitation there the mitral annulus is stretched, usually due to dilatation of the left ventricle as seen with dilated cardiomyopathy. When the annulus dilates, the leaflets are stretched and there is a resultant failure of the leaflets to coapt except at the very leaflet tips, if at all. Accordingly, there is little leaflet surface to impede regurgitation. This Type I will be discussed later in the section on congestive heart failure. Surgical correction of this type of mitral regurgitation involves the placement of a mitral valve ring to bring the leaflet tips down into the left ventricle.

Type II is usually due to abnormalities we commonly describe as mitral valve prolapse where there is a malapposition of leaflet tips. This could occur in the anterior, or posterior mitral valve leaflet tips where coaptation of one or both leaflets approaches the mitral annulus. Given this malapposition, the leaflet tips do not align and mitral regurgitation results. Surgical repair of this type of mitral regurgitation is based upon removal (by quadrilateral resection of a prolapsing P_2 segment) or alignment of prolapsing leaflet tips by chordal transfer, chordal shortening, or other alignment techniques.

Type III mitral regurgitation is due to a specific restriction of a valve leaflet or leaflets. Type IIIa is found in patients with rheumatic mitral stenosis where there is significant diastolic and systolic restriction of

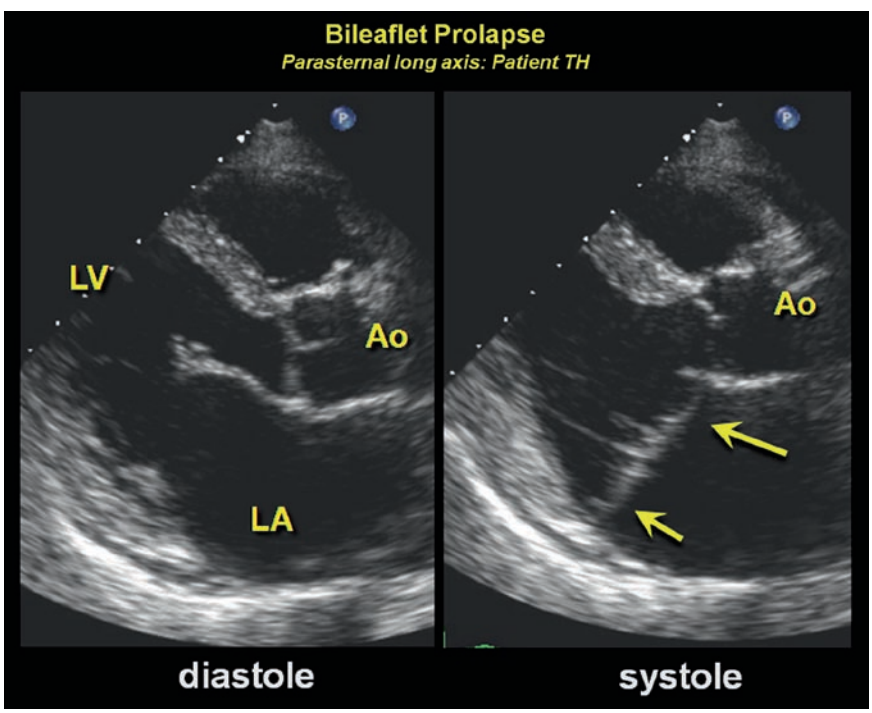

Fig. 8.89 Parasternal long-axis two-dimensional echocardiographic still frames showing marked prolapse of the A_2 and P_2 scallops

the posterior mitral leaflet. Type IIIa uncommonly results in surgical repair. Type IIIb is a bit different and is found in individuals with underlying wall motion abnormalities due to ischemic heart disease. In this setting, there is posterior wall motion abnormalities where there is stretching of the mitral valve apparatus that result in abnormalities of valve movement. Type IIIb is surgically treated by the placement of the smallest mitral ring available to not only approximate the leaflet, but to remodel the proximal ventricle to allow the posterior leaflet chordae to approximate those of the anterior leaflet.

Typical Type II, P_2 Leaflet Prolapse

Figure 8.90 shows a two-dimensional echocardiogram in the parasternal long axis from the chest wall in a 58-year-old patient with Type II valve leaflet motion. Prolapse of both the anterior and the posterior mitral valve leaflets (arrows) is seen as both leaflets billow back into the left atrium in systole. This movement of both leaflets into the atrium in systole is better appreciated in Fig. 8.90 by three-dimensional echocardiography from the transesophageal approach. In this series of systolic still images, the mitral apparatus is viewed from a posterior perspective as both leaflets emerge just over the mitral annulus in systole (left panel). The middle and the right panels show the appearance of these leaflets as the mitral valve annulus is tilted into the more recognizable surgical view. All three panels were obtained during peak systole as both the anterior and the posterior leaflets are billowed upward into the atrium (arrows). The schematic discs below show the tilting of the still frame as the full extent of these leaflets is viewed from the atrium.

Evaluation of leaflet motion can actually be assisted by inspection of color-flow patterns during systole. In the vast majority of instances, the direction of any given regurgitant jet is opposite the leaflet that prolapses. Figure 8.91 shows an apical four-chamber view

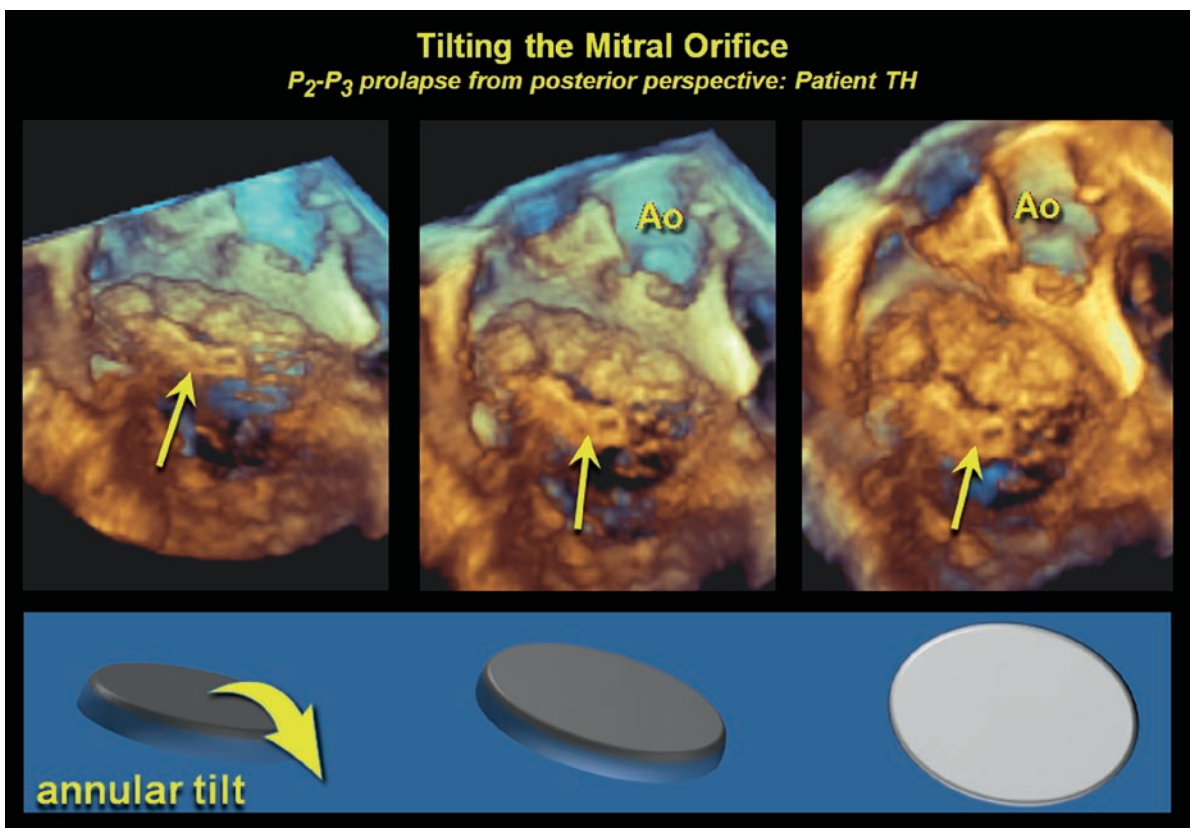

Fig. 8.90 Three-dimensional echo view of the same mitral prolapse seen in the previous figure

in a patient with posterior mitral leaflet prolapse (left panel). The right panel shows the regurgitant jet clearly opposite the prolapse as it is directed toward the atrial septum, then posteriorly into the atrium (arrows). Most mitral regurgitation that comes to surgical repair is anteriorly directed, indicating that most Type II mitral regurgitation is due to posterior leaflet prolapse.

A schematic diagram of P_2 prolapse is shown in Fig. 8.92 from a parasternal long axis (left panel) and the surgical view right panel. Segments A_2 and P_2 are encountered in the two-dimensional echocardiographic long-axis view. From these schematic diagrams, one can appreciate how mitral regurgitation from Type II, P_2 prolapse would therefore be direct anteriorly along the backside of the anterior mitral valve leaflet toward the anterior aspects of the left atrial wall.

Actual three-dimensional echocardiographic images from a systolic frame of significant P_2 leaflet chordal thickening and flail are demonstrated in Fig. 8.93. The massively fibrotic chordal structures can be seen (arrow) to prolapse into the left atrium during systole. The annulus is again tilted as indicated in the discs in the blue bar below. Here, body of the posterior leaflet does not seem to prolapse as much as its thickened tip and remarkable chordal structures.

Contrast the previous three-dimensional figure with that shown in Fig. 8.94. Here there is massive P_2 bulging with obvious chordal flail in this tilting systolic still frame. The annulus is rotated from side to side in the still frame to allow examination of the full extent of the mitral valve prolapse and chordal flail by the three-dimensional echocardiography still frames.

The mitral valve apparatus can also be viewed from below from the left ventricular perspective toward the mitral valve apparatus and into the aortic outflow tract (Fig. 8.95). The upward doming of the P_2 segment can be visualized from this perspective and then revealed further by tilting the heart forward. As the still frame images are tilted anteriorly the gaping orifice of the P_2 segment can be seen (right-hand panel).

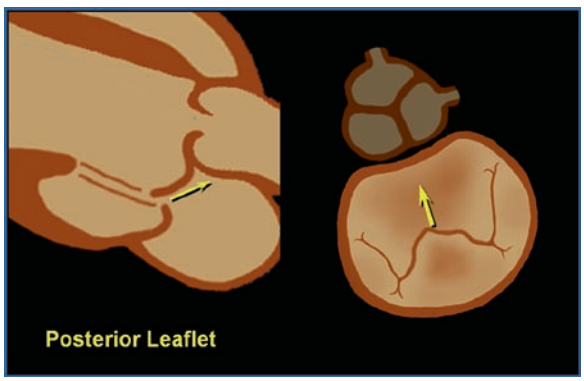

Fig. 8.92 Schematic representation of prolapse of the P_2 segment

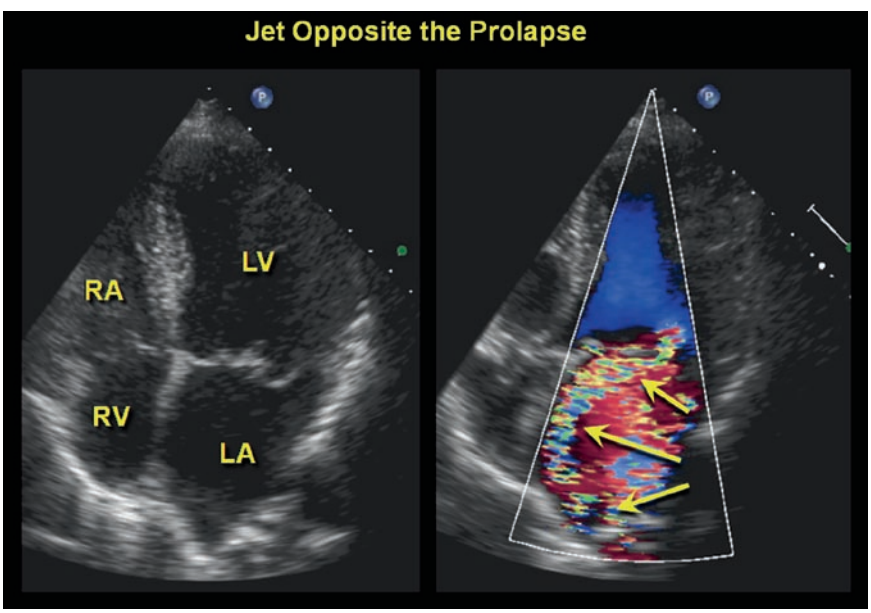

Fig. 8.91 Apical four-chamber view of mitral regurgitation directed against the atrial septum. The jet direction is opposite the prolapsing leaflet

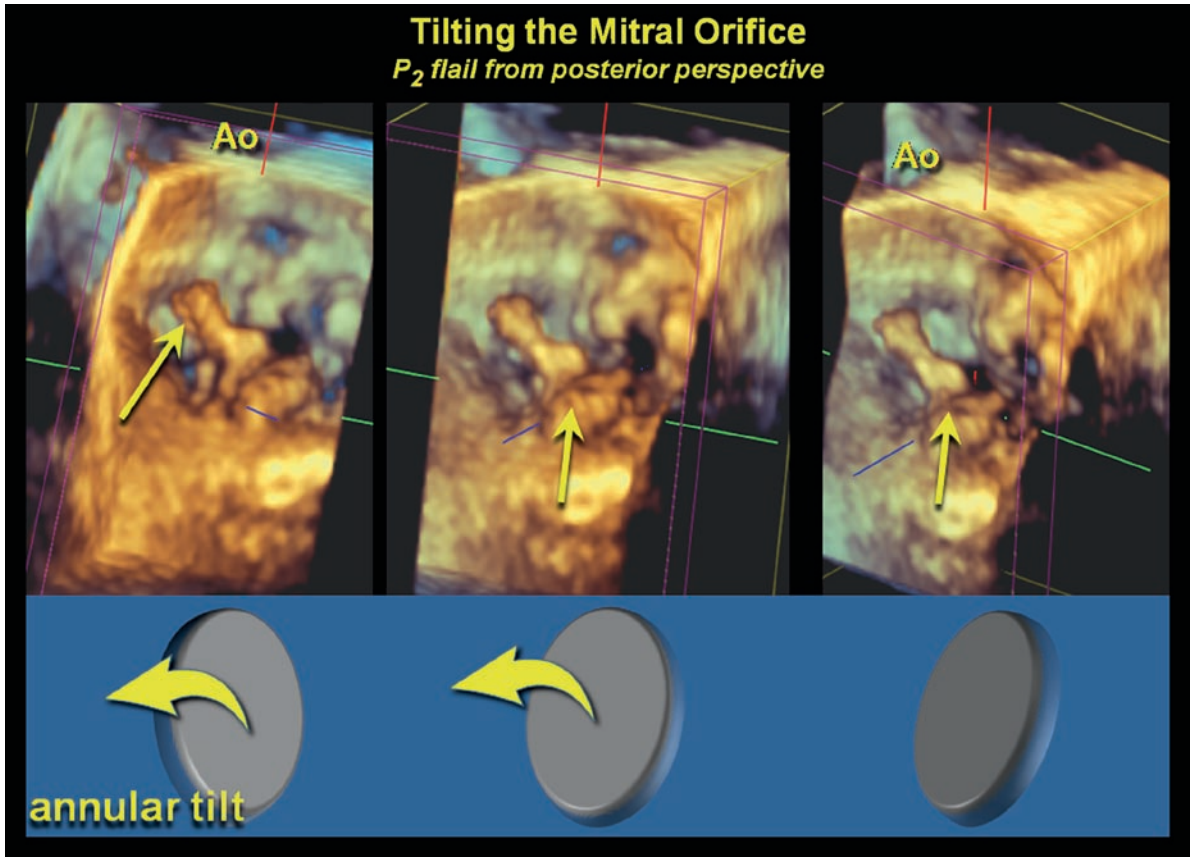

Fig. 8.93 Three-dimensional echo systolic frames from the surgical view in a patient with marked flail of thickened structures from the P_2 segment

An actual surgical photograph of this mitral valve prolapsing segment is shown in Fig. 8.96. The dilated body of the P_2 segment is easily identified as are the broken chordae tendinea. This patient underwent a quadrilateral resection of the P_2 segment and the placement of a ring during mitral valve repair. In a quadrilateral resection, the P_2 segment is excised and the adjacent P_1 and P_3 segments are sutured together and a mitral ring is put into place to stabilize the mitral apparatus. Residual of this approximation of the P_1 and P_3 segments is seen at the arrow in Fig. 8.97.

Figure 8.98 shows an M-mode echocardiogram from another patient with similar P_2 prolapse. The dashed arrow points to the prolapsing segment in the M-mode that markedly resembles the M-mode tracing seen previously in Fig. 8.87. The solid arrow in the two-dimensional parasternal long axis of the inset echocardiogram above shows the P_2 prolapse quite clearly. Two-dimensional echocardiography shows more spatial information than M-mode and is currently the standard for evaluation of mitral prolapse, either from the chest wall or transesophageal approaches.

The transesophageal echocardiogram from this patient also demonstrated the P_2 leaflet prolapse and further indicated that there was flail of the P_2 leaflet tip (Fig. 8.99). There is no need for a diagnostic transesophageal echo in mitral valve prolapse if the chest wall echocardiogram is of superior quality. However, few older patients have such high-quality images, and clinicians must resort to the transesophageal approach for more detailed leaflet analysis.

In this case, the three-dimensional echo from the esophagus revealed even more information as the prolapse was seen to extend from the P_2 segment into the P_3 segment. Figure 8.100 shows the mitral apparatus viewed in three dimensions from the posterior perspective

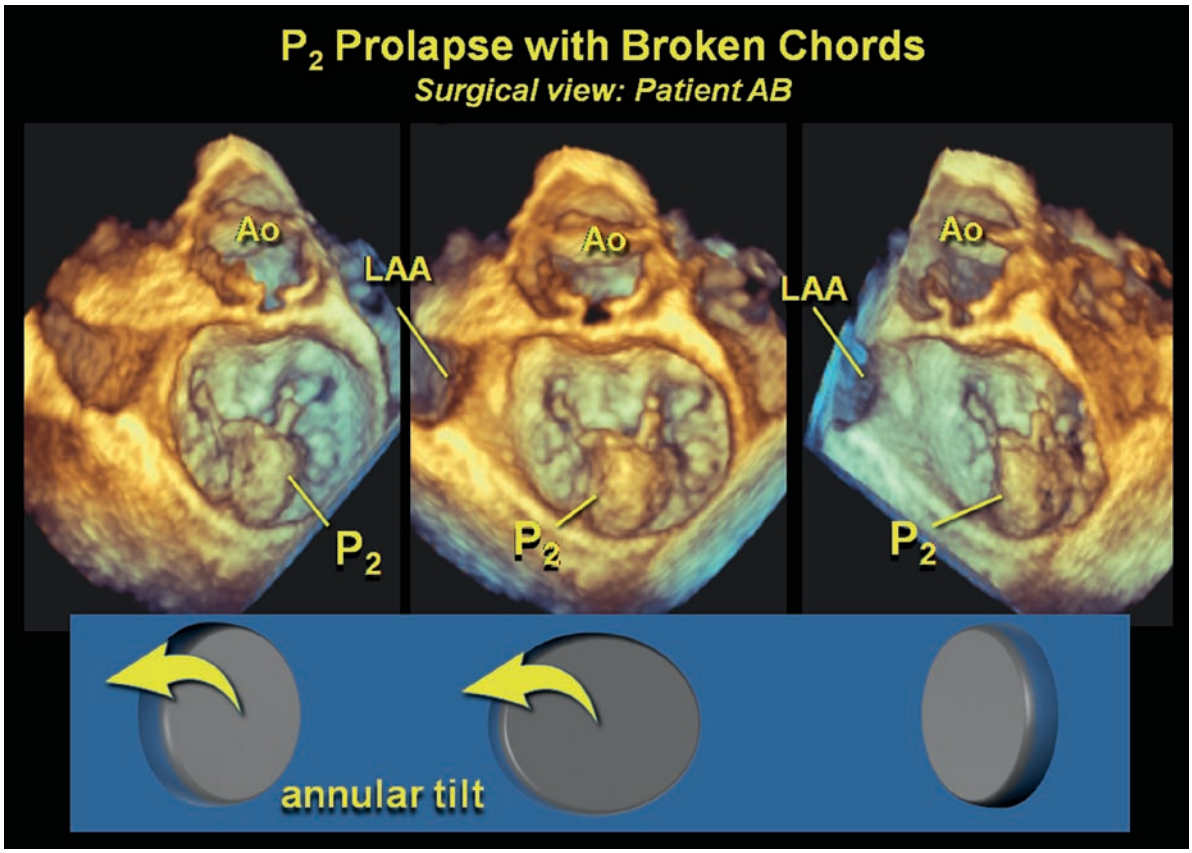

Fig. 8.94 Three-dimensional echo systolic frames from the surgical view in a patient with P_2 prolapse and broken chords to the P_2 segment

and the mitral annulus is rotated into the surgical view. The marked billowing of the P_2 segment with flail of the leaflet tip is easily seen as is billowing of the P_3 segment. A more detailed image set is seen in Fig. 8.101 where these distortions of the P_2–P_3 segments have resulted in failure to coapt between the A_1–P_1 segments, rendering the valve an unlikely candidate for repair.

Repair of the mitral valve was attempted, but failed, and the surgical procedure resulted in the placement of a bileaflet prosthetic valve seen in Fig. 8.102. After weaning from cardiopulmonary bypass, the bileaflet prosthesis is visualized by three-dimensional transesophageal echocardiography in Fig. 8.103. The two prosthetic leaflets are open in diastole (left panel) revealing the three diastolic flow orifices typical of these bileaflet valves. The leaflets are seen in the closed position in the panel on the right.

Typical Type II, A2 Leaflet Prolapse

The anatomic features of prolapse in any mitral valve segment can be visualized by two- or three-dimensional echocardiography. Schematic demonstration of anterior leaflet prolapse of an A_2 segment is shown in Fig. 8.104. When prolapse of this segment is encountered the direction of the mitral regurgitant jet is markedly posterior (Fig. 8.105). In this figure, a massive A_2 prolapse is identified (left panel arrow). The color-flow Doppler frame in the right panel (arrow) shows massive mitral regurgitation opposite the leaflet segment prolapse and directed posteriorly. Occasionally, callus-like patches may be seen on the atrial walls at the impact site of mitral regurgitant jets and are known as McCallum's patches.

The three-dimensional echocardiogram of this patient is seen in Fig. 8.106, where the massively

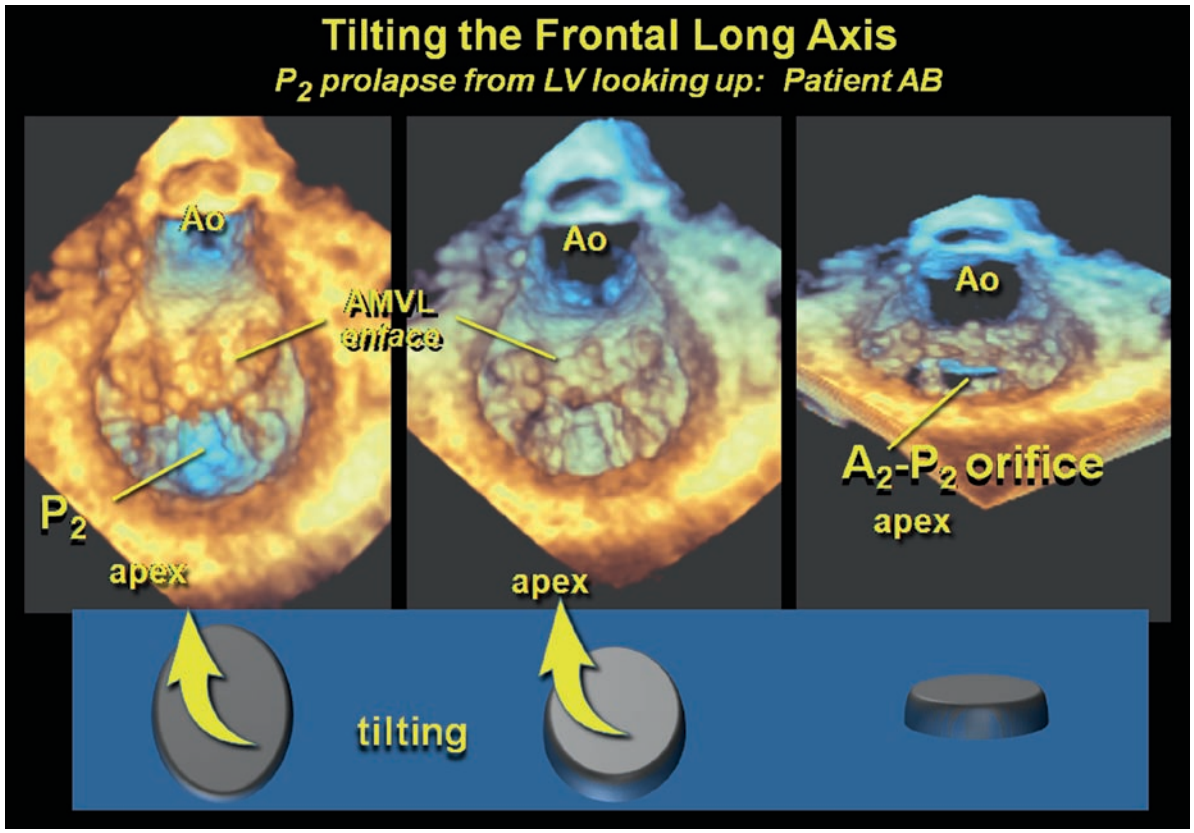

Fig. 8.95 Three-dimensional echo systolic frames of the mitral apparatus viewed from the left ventricle toward the atrium in the same patient with P_2 prolapse as in the previous figure. When tilted downwards, failure of coaptation between A_2 and P_2 is seen

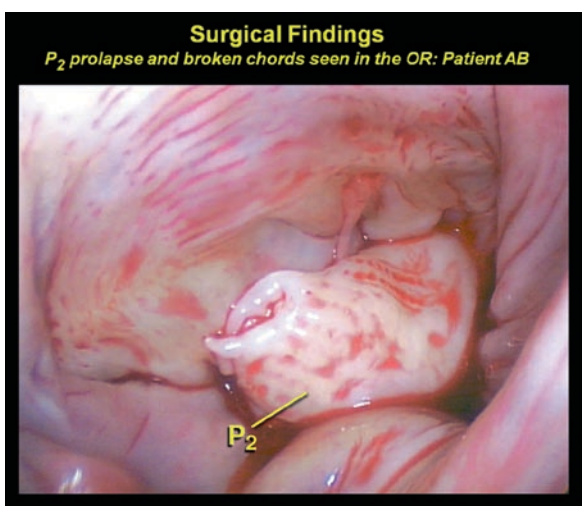

Fig. 8.96 The findings of P_2 mitral prolapse with broken chordae seen at surgery from the same patient seen in the previous two figures

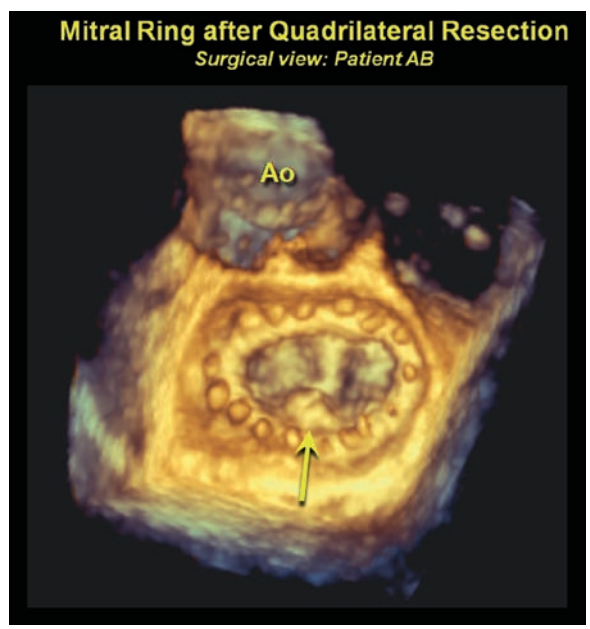

Fig. 8.97 This patient underwent mitral repair with a quadrilateral resection of P_2 and placement of a mitral ring

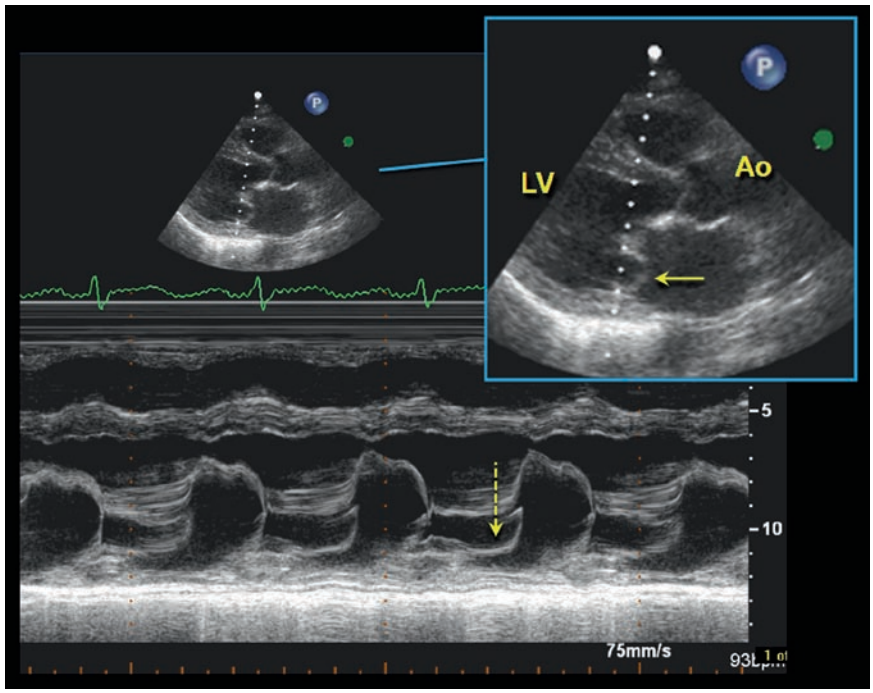

Fig. 8.98 M-mode and two-dimensional echocardiogram showing P_2 prolapse

domed A_2 segment is revealed as it prolapses back into the mitral orifice in this surgical view. The annulus is again rotated side to side in this systolic still frame to allow further examination. In real time, an examiner would perform these rotations as mitral valve apparatus moves with the cardiac cycle to examine the mitral valve in all spatial conditions.

The surgical findings from a patient with a similar problem of A_2 prolapse is demonstrated Fig. 8.107. In this individual, the A_2 prolapse is not as severe as is seen in the patient in the previous Fig. 8.106 but, nevertheless, demonstrates the problem and appearance of this type of prolapse at surgery. This patient underwent successful mitral valve repair that included plastic procedures to the A_2 chordal segments and placement of a mitral valve ring.

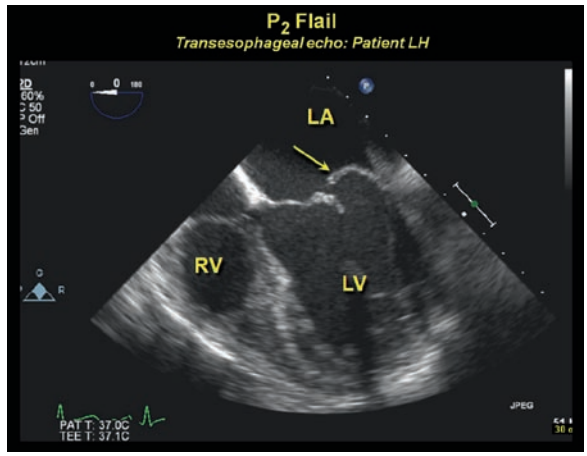

Fig. 8.99 The transesophageal echo showed flail at the tip of the P_2 segment from the patient seen in the previous slide

Visualization of Other Mitral Procedures

Three-dimensional echocardiography can be used for visualization of a variety of prosthetic valves. A mitral bioprosthesis is seen from the left ventricular perspective (looking toward the mitral orifice and left ventricular outflow tract) in Fig. 8.108. The three supporting stents are readily identified, as are the closed valve leaflets in systole. The valve orifice is tilted anteriorly to offer slightly different perspective of the three-dimensional prosthetic valve.

Another surgical technique with growing use is the placement of a surgical stitch between the A_2 and P_2 segments. While this results in a small degree of obstruction

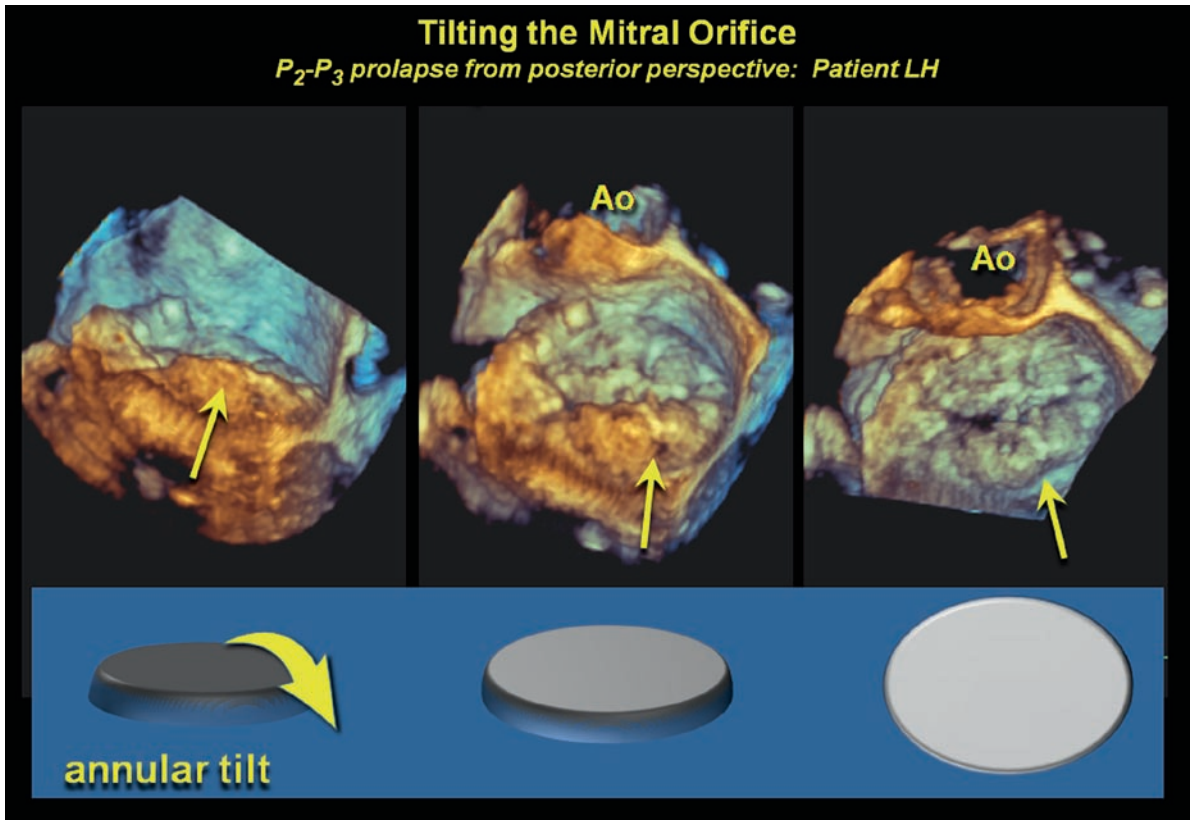

Fig. 8.100 A three-dimensional echocardiogram displayed in the surgeon's view also shows flail extending into the P_3 segment. In addition, there was no coaptation between the P_1 and A_1 segments that confounded surgical repair. This is the same patient seen in the two previous figures

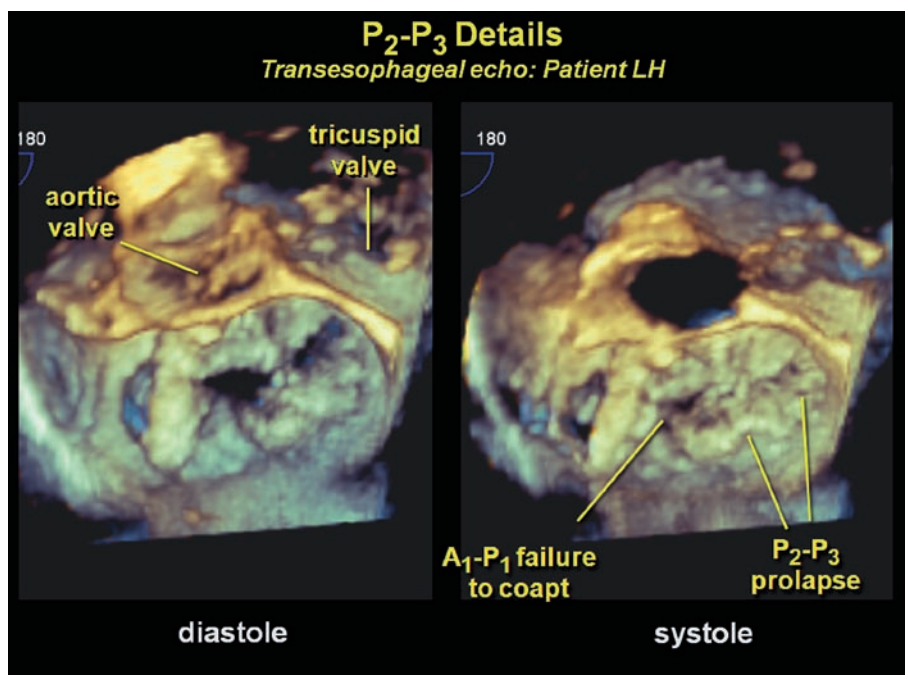

Fig. 8.101 Closer look at the surgeon's view in this patient showing the P_2 and P_1 flail with failure to coapt between the P_1 A_1 segments

at the level of the mitral orifice, there is usually plenty of room to accommodate such a stitch when prolapsing mitral leaflets are encountered. This is commonly called the Alfieri Stitch and can reduce the surgical pump times. Such a stitch is shown in Fig. 8.109 where the two residual mitral orifices are readily demonstrated.

At the time of preparation of this chapter, there is also growing interest and experience in the catheterization-based insertion of mitral valve clips for the repair of A_2–P_2 mitral prolapse and its consequent regurgitation. Figure 8.110 shows the rotation of a mitral valve annulus when such a clip is introduced from the left atrial side (via a catheter across the interatrial septum) and then through the mitral valve orifice. In this figure, the clip is in the open position. The mitral orifice is in the surgical view and is tilted from a slightly posterior perspective directly into the mitral orifice in the right panel.

As the clip is introduced in the heart, the clip is in the closed position as it is advanced toward the mitral

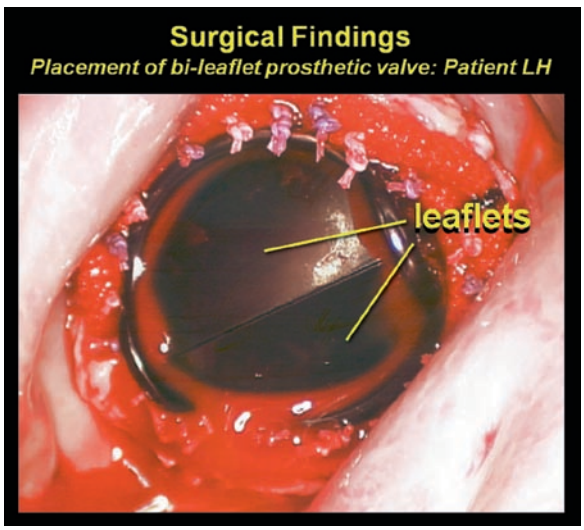

Fig. 8.102 Repair was attempted but failed and the mitral valve was replaced using a bileaflet mechanical prosthesis

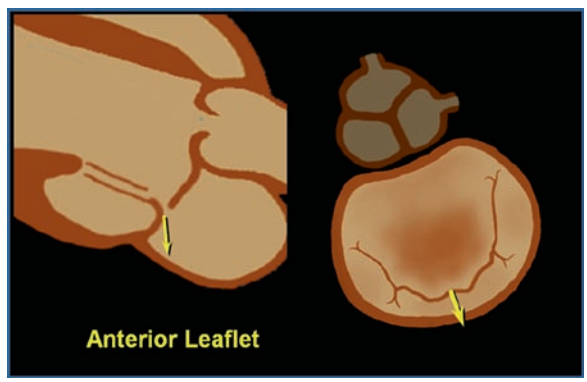

Fig. 8.104 Schematic representation of prolapse of the A_2 segment

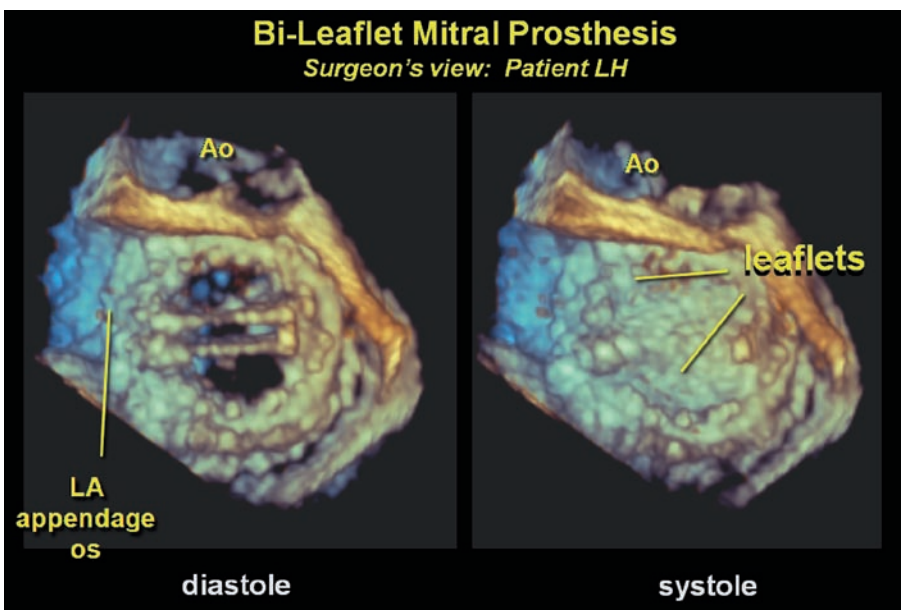

Fig. 8.103 Three-dimensional echo of the mechanical prosthesis seen in the previous figure

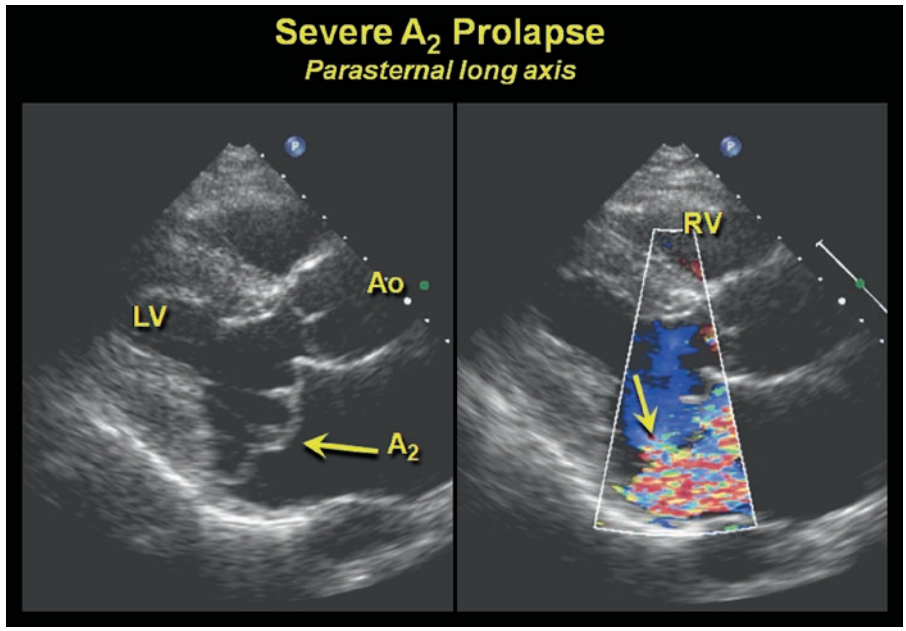

Fig. 8.105 Parasternal long axis of the mitral valve in a patient with huge A_2 segment prolapse (*arrow left panel*). The mitral regurgitation is directed posteriorly (*arrow*, *right panel*)

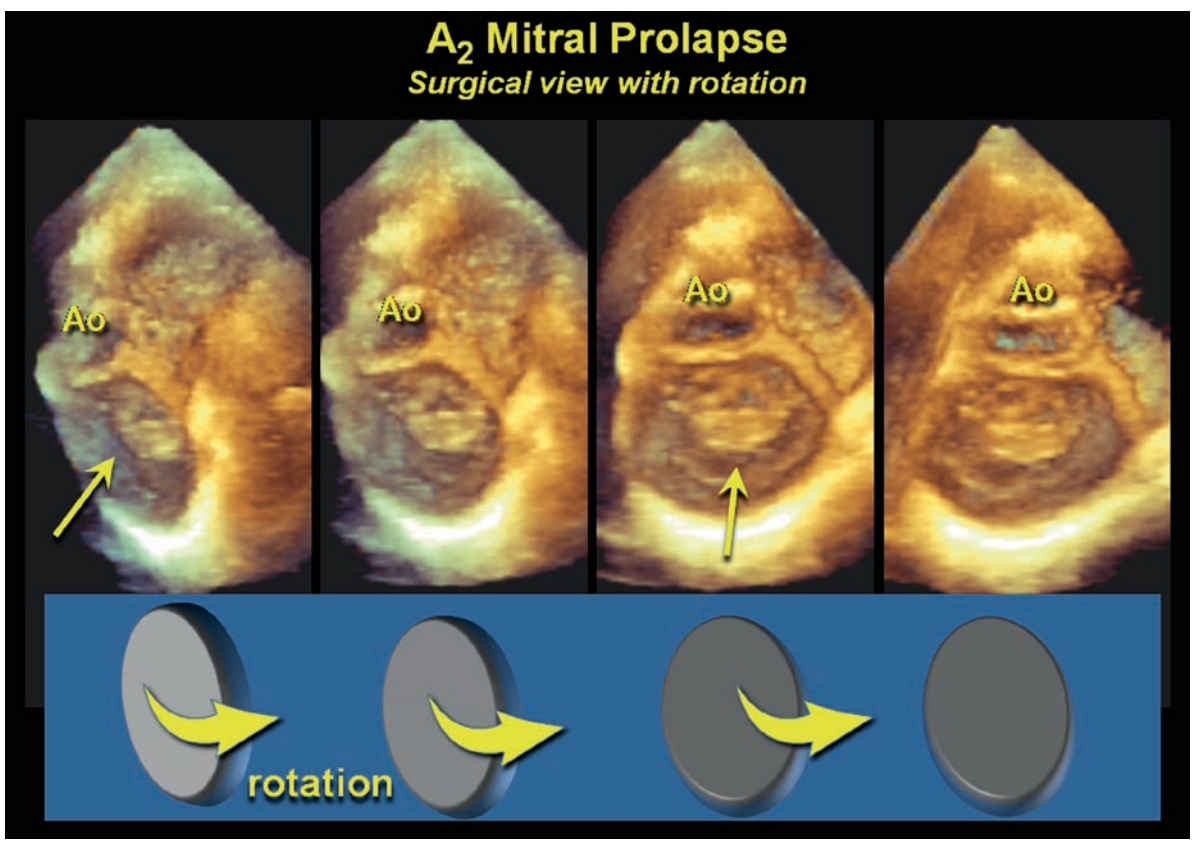

Fig. 8.106 Three-dimensional systolic still frame from the patient seen in the previous figure in the surgical view. There is huge doming of the A_2 segment (*arrow*)

valve orifice and the prolapsing leaflet segments (Fig. 8.111, left panel) and then opened as it approaches the actual orifice (Fig. 8.111, middle panel). The device is then progressively inserted through the mitral valve orifice and then rotated so that the open clip can engage both the A_2 and P_2 segments (Fig. 8.111, right panel). As the open clip is then pulled backward, it can then grasp the A_2 and P_2 segments as it is then closed. The catheter is then disengaged from the stable clip, leaving the mitral orifice with a double opening, markedly resembling the Alfieri stitch.

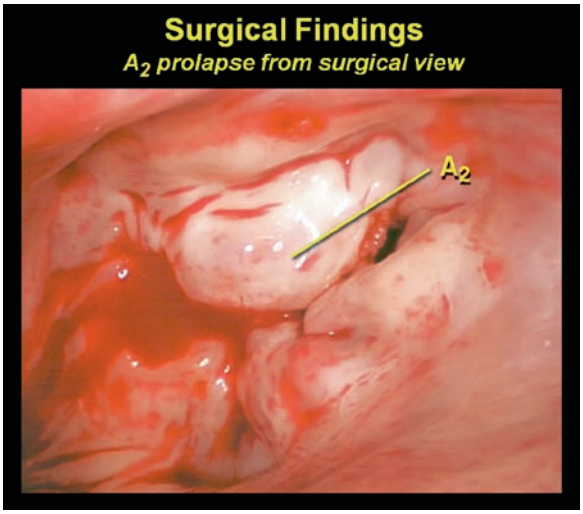

Fig. 8.107 Surgical photograph of the mitral valve from a patient with similar A_2 prolapse

Mitral Regurgitation and Congestive Heart Failure

As any examiner with echocardiography knows, mitral regurgitation is frequently associated with congestive heart failure. This is usually Type I mitral valve regurgitation that results from dilatation of the mitral valve annulus. Figure 8.112 shows parasternal short axis of mitral valve in the closed position in systole, extending from commissure to commissure. When the mitral

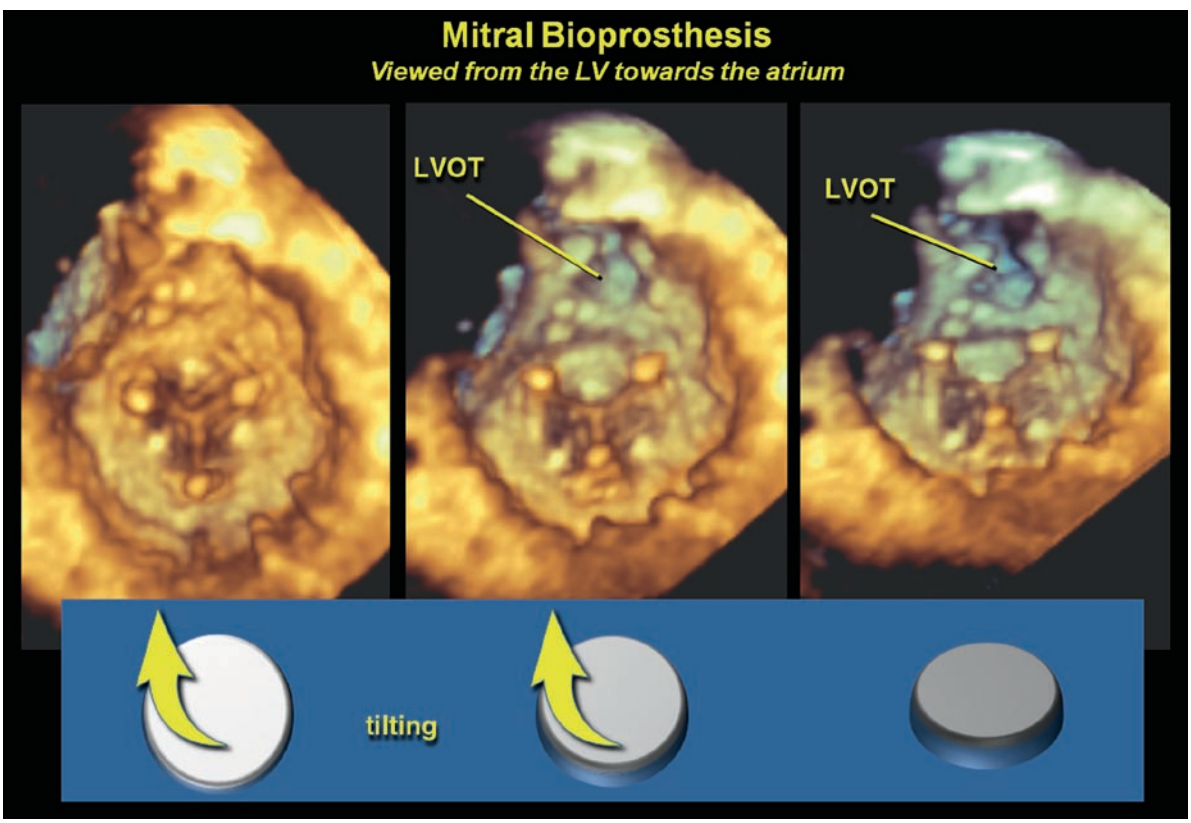

Fig. 8.108 Porcine bioprosthesis depicted in place from the left ventricular perspective, up into the mitral orifice. The stents of the prosthesis are easily recognized

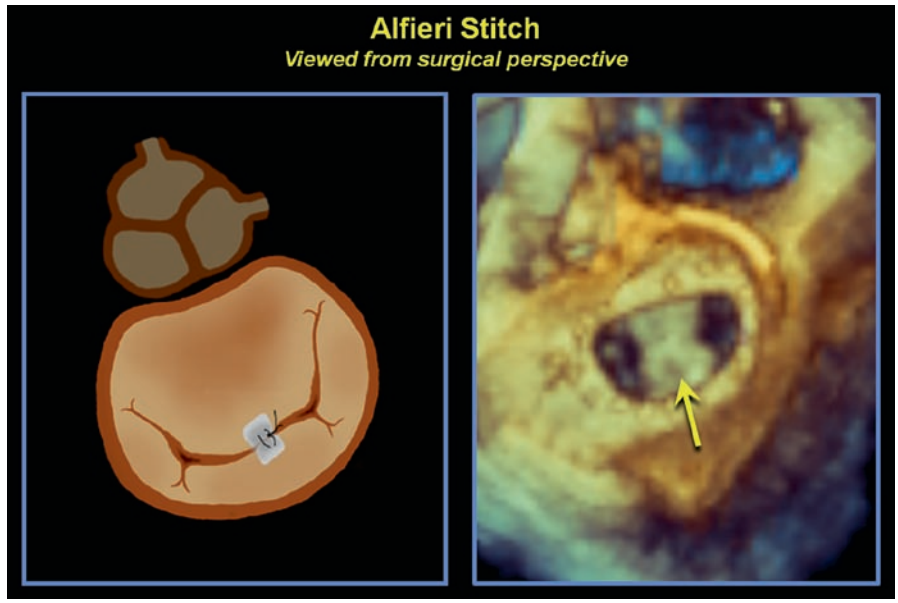

Fig. 8.109 Sometimes it is beneficial for the surgeon to suture the A_2 and P_2 segments, the Alfieri stitch. The characteristic post stitch three-dimensional image is seen on the right and is joined in the center, creating two diastolic orifices. A mitral prosthetic ring is also in place

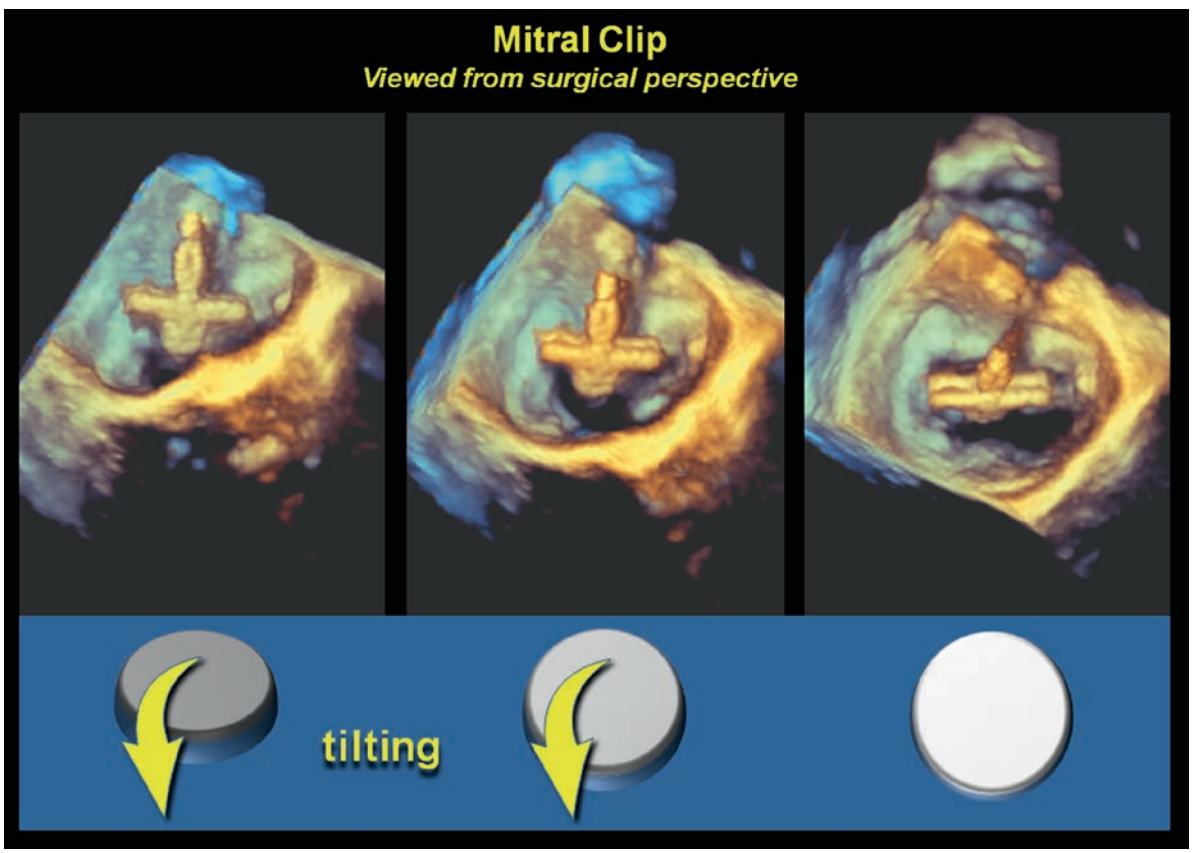

Fig. 8.110 A catheter-based mitral clip is seen above the mitral orifice in a three-dimensional still frame of an open mitral valve in diastole. For details, see text

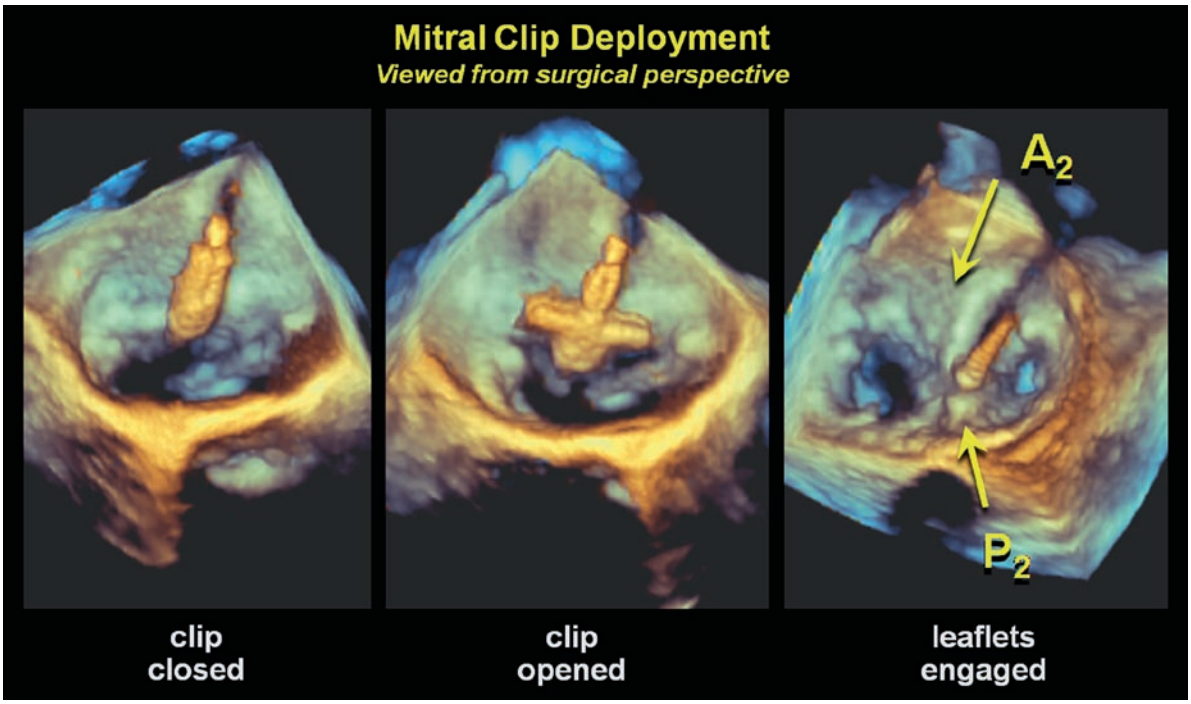

Fig. 8.111 The clip is closed (*left panel*), then opened (*center panel*), then is pushed through the mitral orifice to engage the A_2 and P_2 segments. For details, see text

valve coaptation points are examined in this view with color-flow Doppler, one can appreciate mitral regurgitation along the entire coaptation line (right panel, Fig. 8.112). If surgical intervention is necessary in this disorder, a mitral ring is usually put in place to bring the leaflet tips downward into the left ventricle to allow the leaflets to coapt properly.

The three-dimensional echocardiogram shown in Fig. 8.113 shows the left ventricle in two individuals from the left ventricular frontal long-axis three-dimensional view. The anterior mitral leaflet is seen *enface* and compares the orientation of the papillary muscles in each of these patients. The left panel shows the orientation of the papillary muscles in a patient with mild mitral regurgitation. The papillary muscles are aligned vertically and are within the mitral annulus. Compare the orientation of these papillary muscles to those seen in the right panel from a patient with a dilated cardiomyopathy and more severe mitral regurgitation. In the right panel, the papillary muscles are seen to be laterally displaced and are pointed more medially. Also compare these images to that seen in Fig. 8.17 taken from a normal individual in a similar frontal long-axis view. Thus, mitral valve coaptation is not only a leaflet phenomenon, but is dependent upon the orientation of supporting structures such as the papillary muscles and their relationship to the entire mitral valve apparatus.

Mitral Annular Calcification

Calcification and/or fibrosis of the mitral valve annulus is a common finding in elderly patients. Such a finding is manifest by two-dimensional echocardiography as a bright spot in the posterior mitral valve annulus (MAC = mitral annular calcification). Because of the marked reflectivity of significant calcification and/or fibrosis, sound waves do not usually penetrate such a structure and a shadow can be seen posterior to the abnormal annulus. Such mitral valve annular calcification is usually quite bright and the shadow is the hallmark that this is a calcific structure.

Such mitral valve annular calcification can be much larger, particularly in patients with chronic renal failure. Mitral annular calcification is also seen in patients with hypertrophic cardiomyopathy. A chest wall echocardiogram from a patient with renal failure is seen

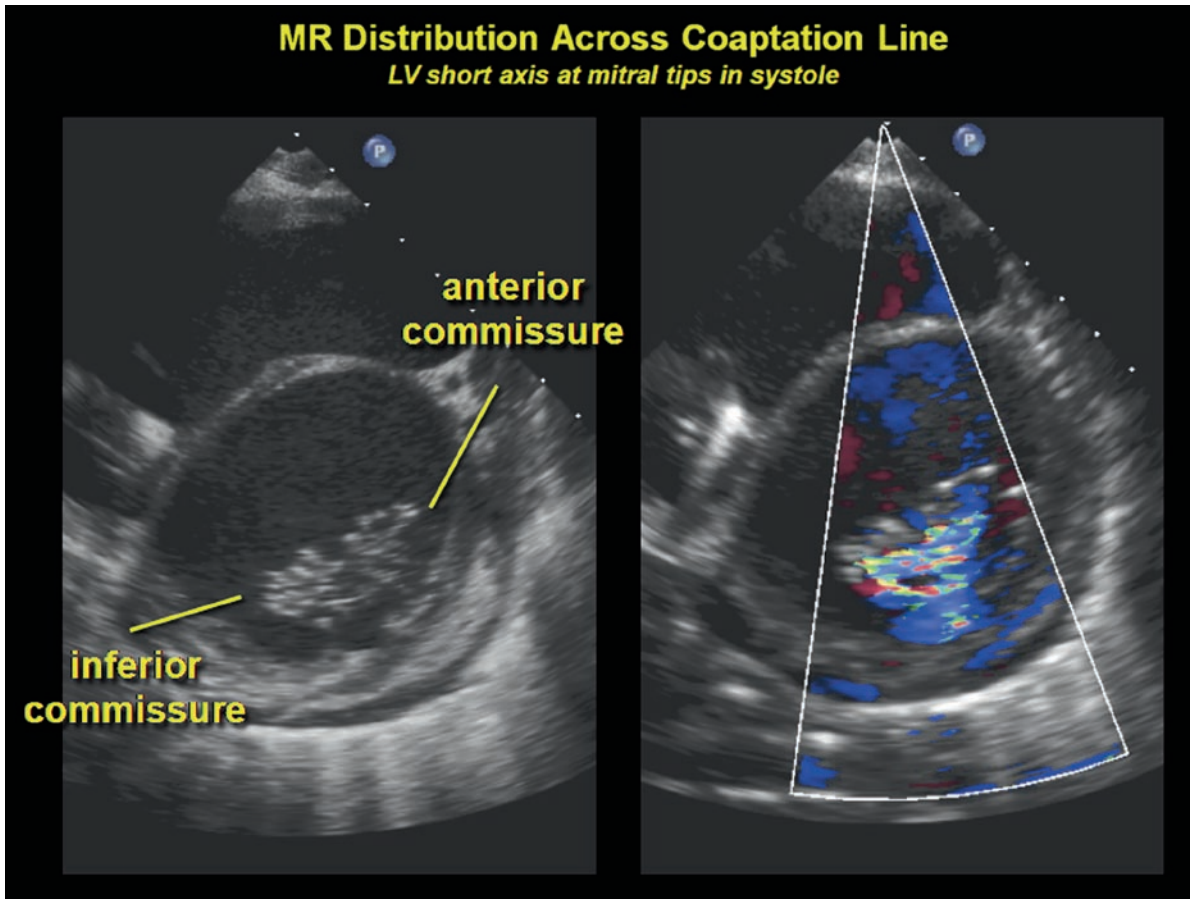

Fig. 8.112 Short-axis parasternal view of a closed mitral orifice in a patient with a dilated cardiomyopathy and mitral regurgitation. Using color flow, the mitral regurgitation can be seen along the entire mitral coaptation line (*right panel*)

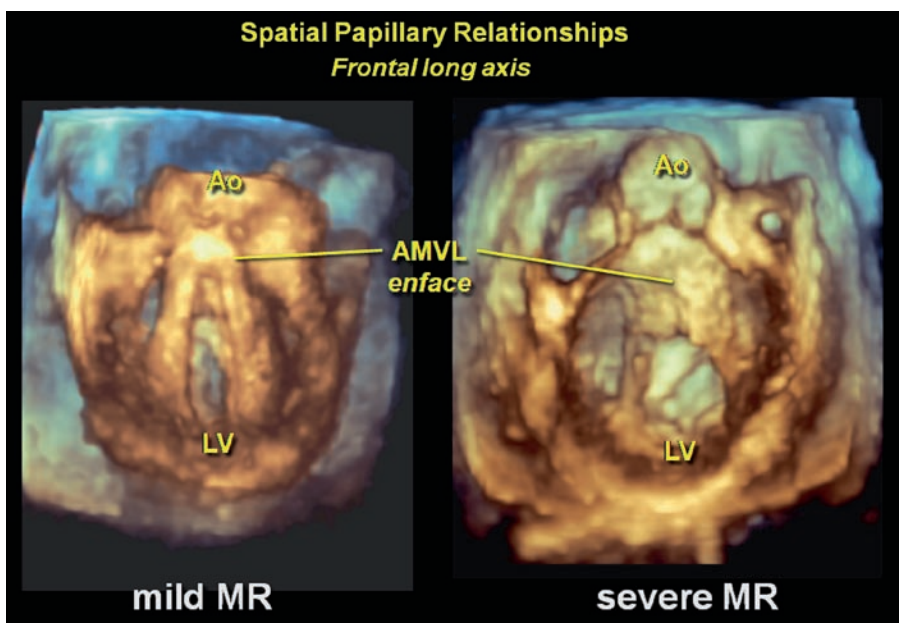

Fig. 8.113 Frontal long axes from base (toward figure *top*) down toward apex (*bottom* of figure) of the left ventricles of two patients. Note the orientation of the papillary muscles vertically in the *left panel* and compare this to the positions of the papillaries in the image in the *right panel* from a patient with dilated cardiomyopathy. For details, see text

in Fig. 8.114 in the parasternal long-axis view. The images are of high quality and the bright target of the annular calcification (MAC) reveals an ultrasonic shadow extending posteriorly from the MAC.

A parasternal long-axis image from an elderly patient demonstrates a large annular calcification from the chest wall parasternal long-axis view in the left panel of Fig. 8.115. The patient also had chronic obstructive lung disease and the quality of the chest wall image is suboptimal. The transesophageal echocardiogram of this patient is seen in the right-hand panel where the annular calcification can be easily differentiated from surrounding mitral structures.

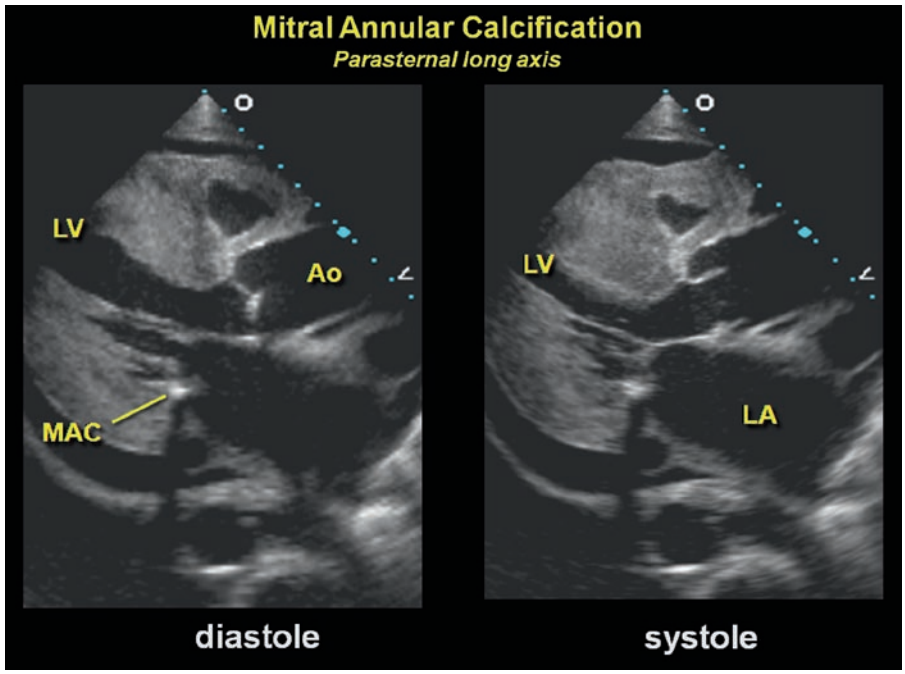

Fig. 8.114 Parasternal long axis from a patient with renal failure and mitral annular calcification (*arrow*). Note the shadowing from the MAC

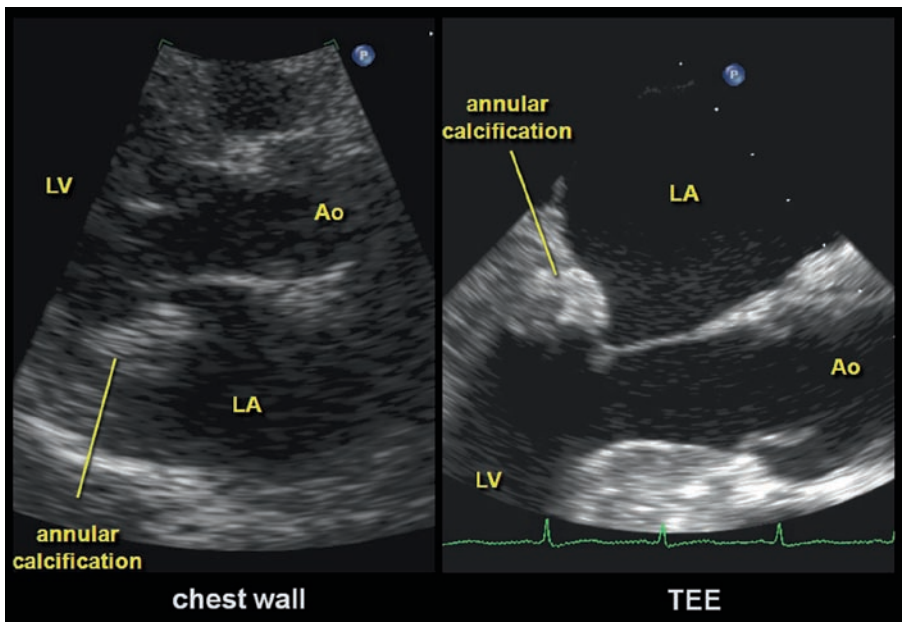

Fig. 8.115 Chest wall and transesophageal echo still frames from a patient with mitral valve calcification

The three-dimensional echocardiogram from the patient seen in the previous figure is demonstrated in Fig. 8.116. The massive annular calcification is seen just posterior to the mitral orifice in the open position in diastole and the closed position in systole. It is necessary to use two-dimensional echocardiography to differentiate this three-dimensional appearance from that of mitral valve prolapse.

Infective Vegetative Endocarditis

The appearance of mitral valve vegetations is dramatic when using any echocardiographic technique. These mass lesions are seen to oscillate rather rapidly and are usually attached to the flow surfaces of cardiac valvular structures. The M-mode echocardiogram in Fig. 8.117 shows the typical rapidly oscillating masses encountered in endocarditis and is seen just anterior to the mitral valve apparatus (arrow). While this oscillation resulted from an aortic valve vegetation that prolapsed into the left ventricular outflow tract during diastole, such oscillations are typical of vegetations from any leaflet. This given lesion resulted in massive aortic regurgitation and preclosure of the mitral valve apparatus (vertical line) prior to the QRS complex of the EKG. Such mitral preclosure is a generally ominous sign in aortic regurgitation as it results from the high late diastolic pressures that prematurely close the mitral valve in late diastole. The role of echocardiography and vegetative endocarditis is discussed fully by Cable elsewhere in this volume.

These oscillating masses can be viewed on the mitral apparatus by two-dimensional echocardiography as shown in Fig. 8.118. Here, a single oscillating mass can be appreciated by two-dimensional echocardiography only in the moving picture. It does, however, result in a posteriorly directed mitral regurgitant jet that is seen in the right-hand panel. This lesion was also attendant to a small number of ruptured chordae tendinea causing mild mitral prolapse of the A_2 segment.

A two-dimensional echocardiogram from another patient with a small oscillating vegetative mass is seen in Fig. 8.119. This lesion was attendant to the P_2 segment and is denoted by the arrow. Immediately after initial detection and blood culture, but in the absence of any untoward hemodynamic complications, the patient suffered a stroke and the follow-up echocardiogram showed disappearance of this vegetative mass (right-hand panel).

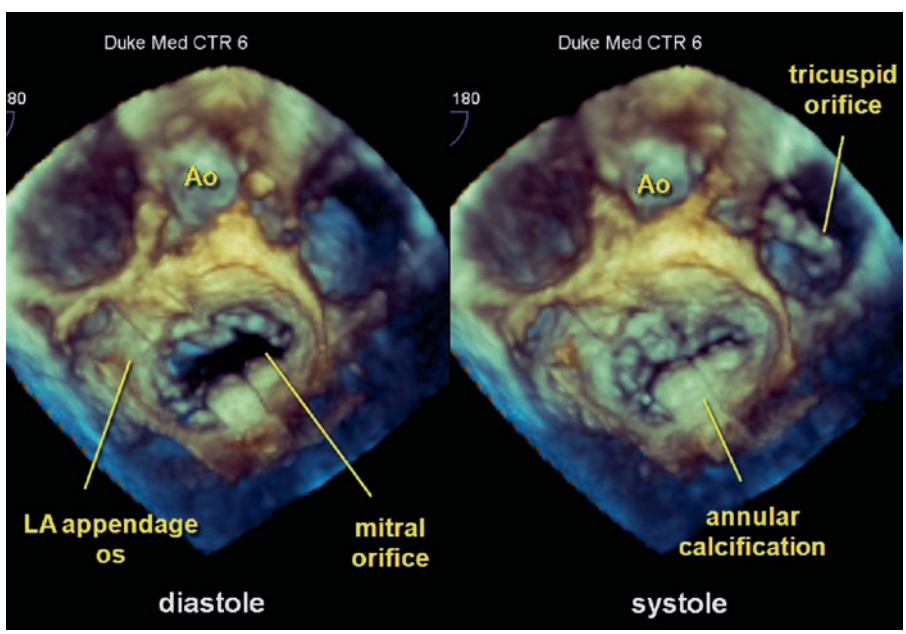

Fig. 8.116 Three-dimensional image of the mitral orifice in the surgeon's view in a patient with mitral annular calcification. Without two-dimensional echo, it is difficult to differentiate mitral annular calcification from prolapse by 3D

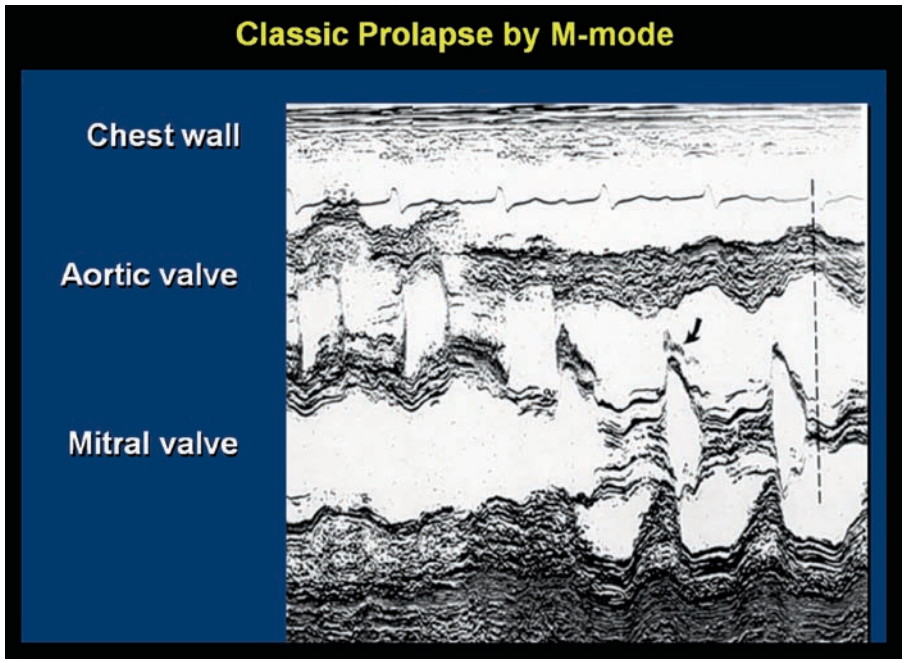

Fig. 8.117 M-mode echocardiogram from a patient with vegetative endocarditis. The rapidly oscillating mass lesion (*arrow*) is seen just anterior to the mitral valve. This vegetation was on the aortic valve and resulted in severe aortic regurgitation, causing premature closure of the mitral apparatus (*dashed line*) because of the high end-diastolic pressures

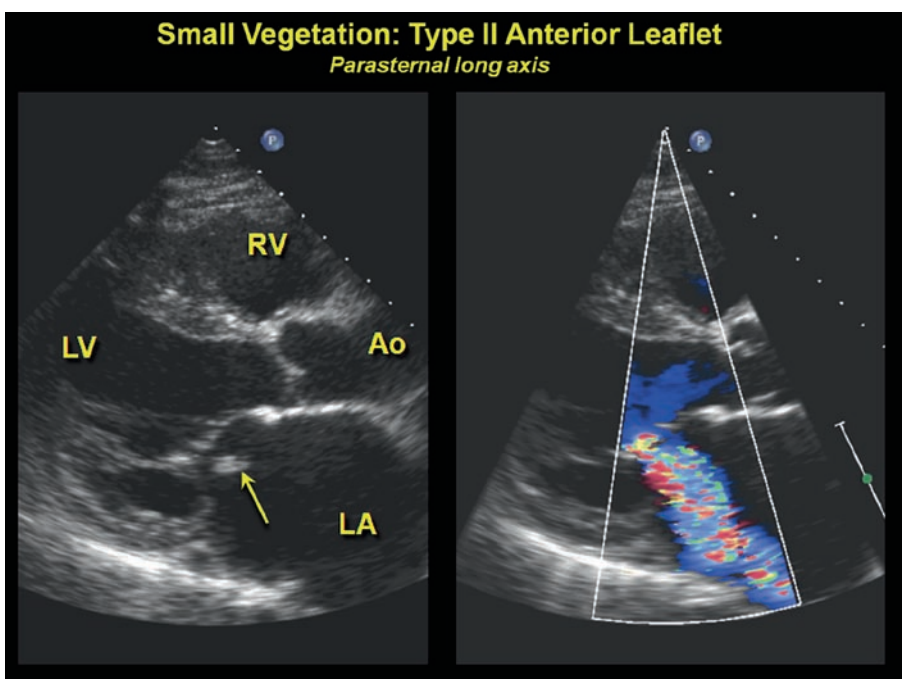

Fig. 8.118 Parasternal long axis from a patient with a small mitral vegetation (*arrow*). This resulted in the mitral insufficiency seen in the color flow in the *right panel*

These lesions may be attendant with all degrees of mitral regurgitation. Figure 8.120 shows mitral regurgitation using three-dimensional echocardiography and color-flow Doppler. There is a perforation of the A_2 segment at its midpoint. The rotation is turned side to side to show the extent of this small perforation.

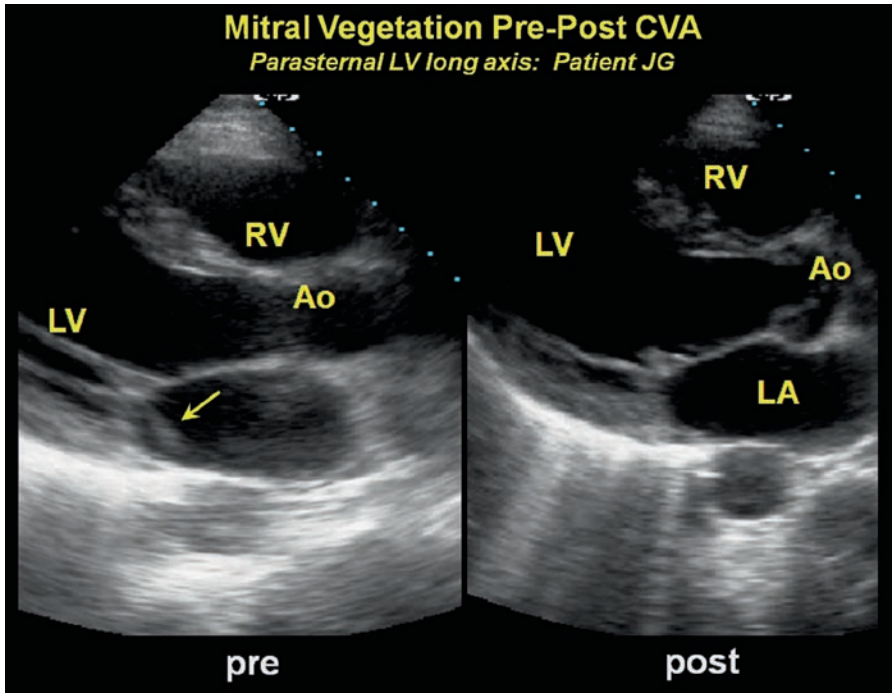

Fig. 8.119 Another small vegetation on the mitral apparatus is seen on the *left panel* (*arrow*). After blood cultures the patient sustained a stroke and the vegetation was no longer seen

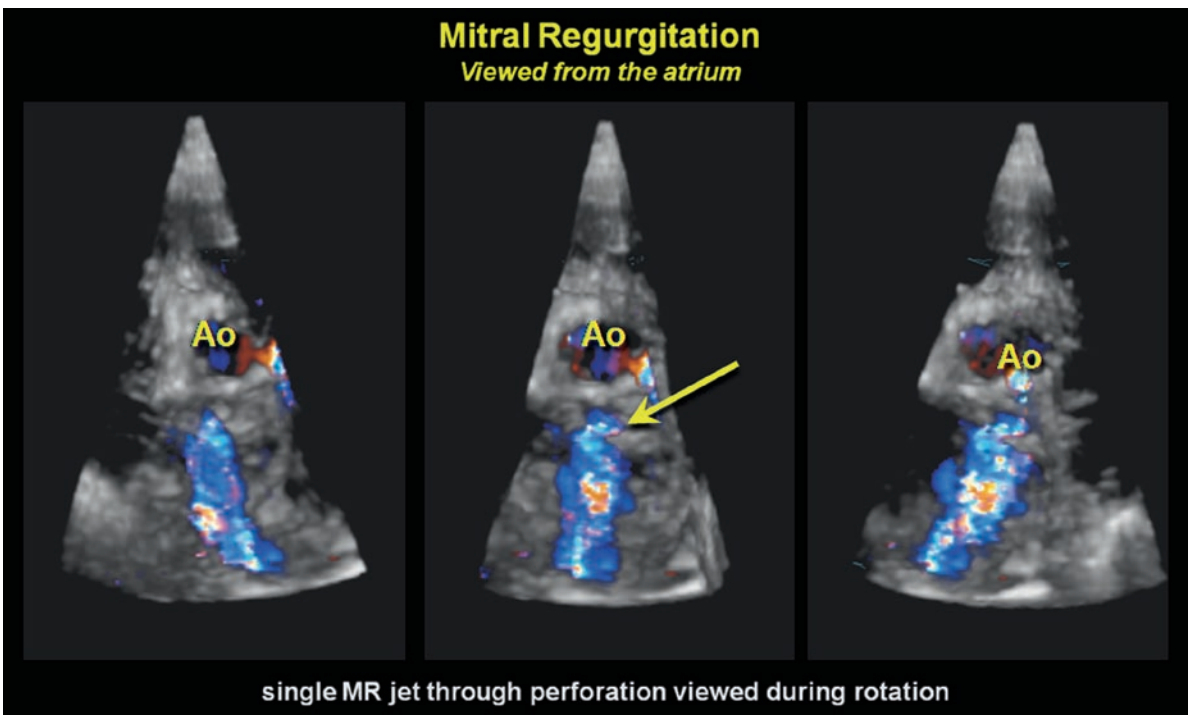

Fig. 8.120 Mitral regurgitation seen in the surgeon's view from the chest wall in a three-dimensional echo. The regurgitation originates through a small perforation in the midportion of the anterior mitral leaflet (*arrow*)

In this patient, the area of perforation was surgically debrided and the anterior mitral valve leaflet was patched. Vegetations come in all varieties and locations along the lines of mitral valvular flow (usually on the atrial side). Occasionally, there may be huge vegetative masses attendant to vegetative endocarditis. Figure 8.121 shows a massive vegetation invading the anterior mitral valve leaflet and extending into the left ventricular outflow tract both in diastole and systole (dashed arrow) in a patient with chronic renal failure, diabetes, and peripheral vascular disease. Another large mass can be seen at the tip of the anterior mitral valve leaflet and extends into the ventricle in diastole and then back into the atrium in systole (solid arrow).

Of interest is this patient's echocardiogram 4 years prior to the onset of the episode of endocarditis showed no evidence of infection and was performed during another episode of infection that did not result in endocarditis. While left ventricular hypertrophy and mild pericardial effusion are identified, no vegetative masses are seen (Fig. 8.122). This vegetation seen 4 years later in Fig. 8.121 was extensive and its invasion of the mitral leaflet dramatic. The overall medical condition of the patient precluded attempts at surgical correction and the patient later died of overwhelming sepsis.

When surgical intervention is entertained, transesophageal and three-dimensional echocardiography are indicated. Figure 8.123 shows a transesophageal echocardiogram from a patient with a large vegetative mass along the posterior mitral valve leaflet. The three-dimensional echocardiogram conducted during mitral valve repair of this same patient is seen with this large mass located primarily on the P_2 segment (Fig. 8.124). The mitral annulus is again rotated from side to side and then tilted. Visualizing the full extent of the mass with three-dimensional echocardiography surgical repair can be readily facilitated, and more and more three-dimensional studies are being conducted for decision making concerning mitral valve repair.

Left Atrial Myxoma

The most dramatic entity seen by echocardiography is the presence of a left atrial myxoma. Here, this benign

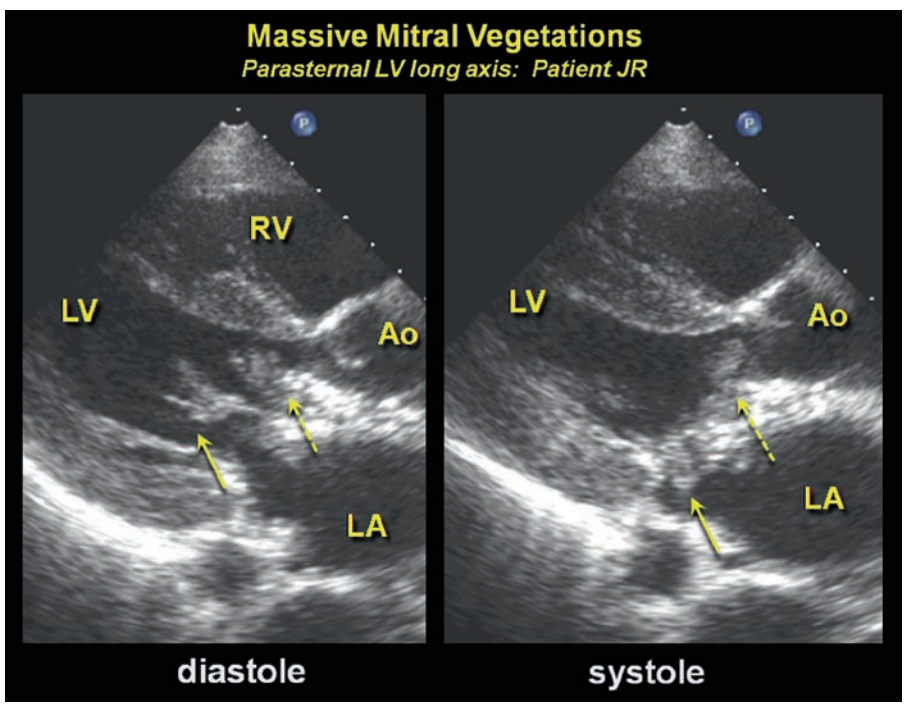

Fig. 8.121 Large vegetative masses invading the anterior mitral leaflet. Portions of the mass partially obstruct the LV outflow tract in systole *(right panel)*, while another part prolapses into the left atrium (*arrow*)

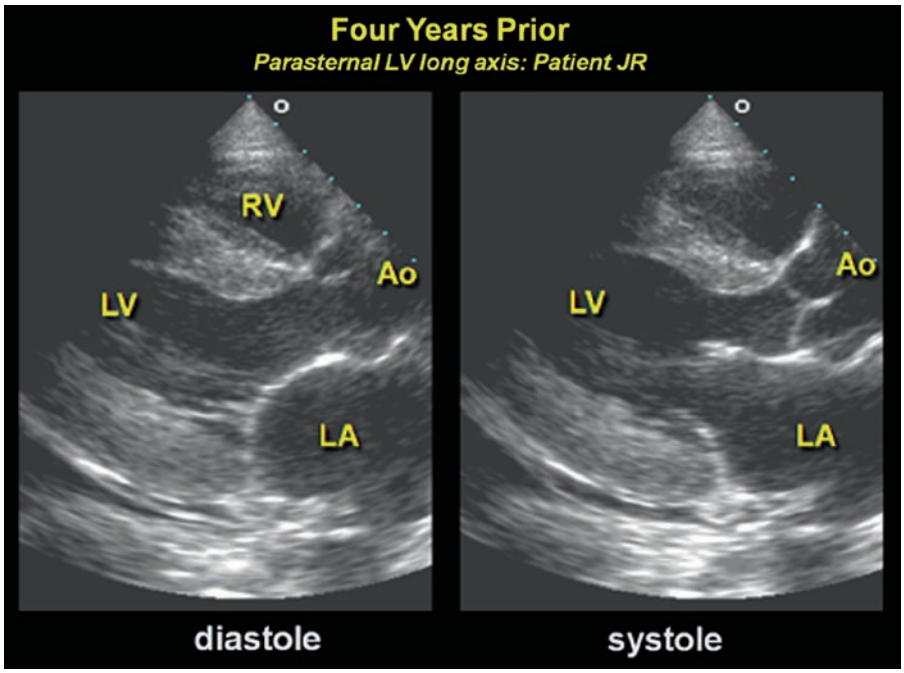

Fig. 8.122 Echocardiogram performed 4 years earlier on the patient seen in Fig. 8.121. No vegetative masses were seen then

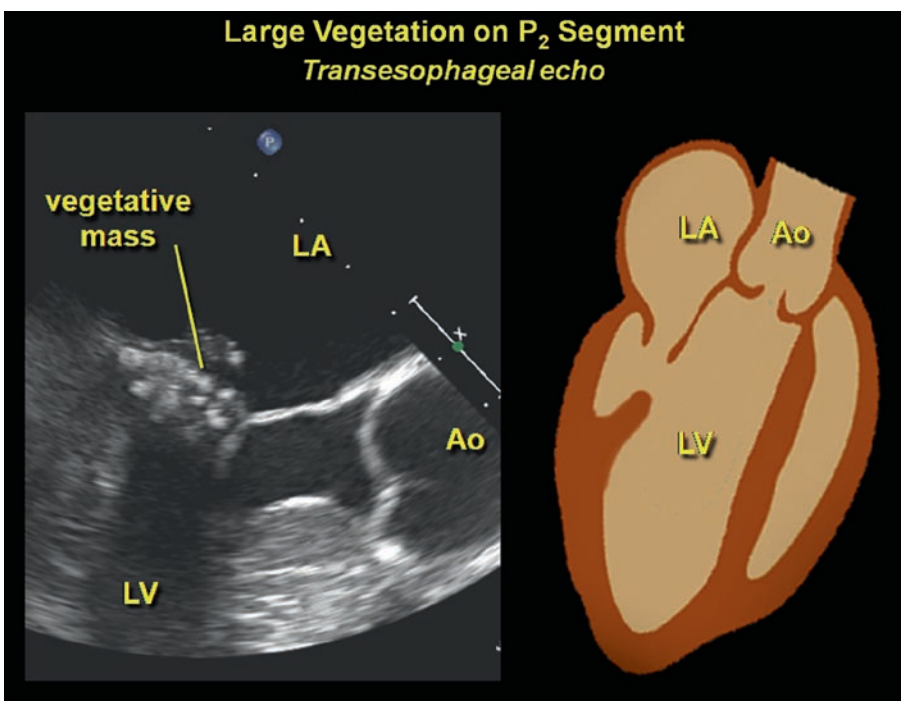

Fig. 8.123 Transesophageal echo with a cluster of vegetations seen along the P_2 segment in a patient with endocarditis

tumor of the left atrium is seen to move through the mitral valve orifice in diastole (Fig. 8.125) with the cardiac cycle. This patient was a 55-year-old female suffering from progressive shortness of breath. Left atrial myxomata are found in predominantly female patients over the age of 50.

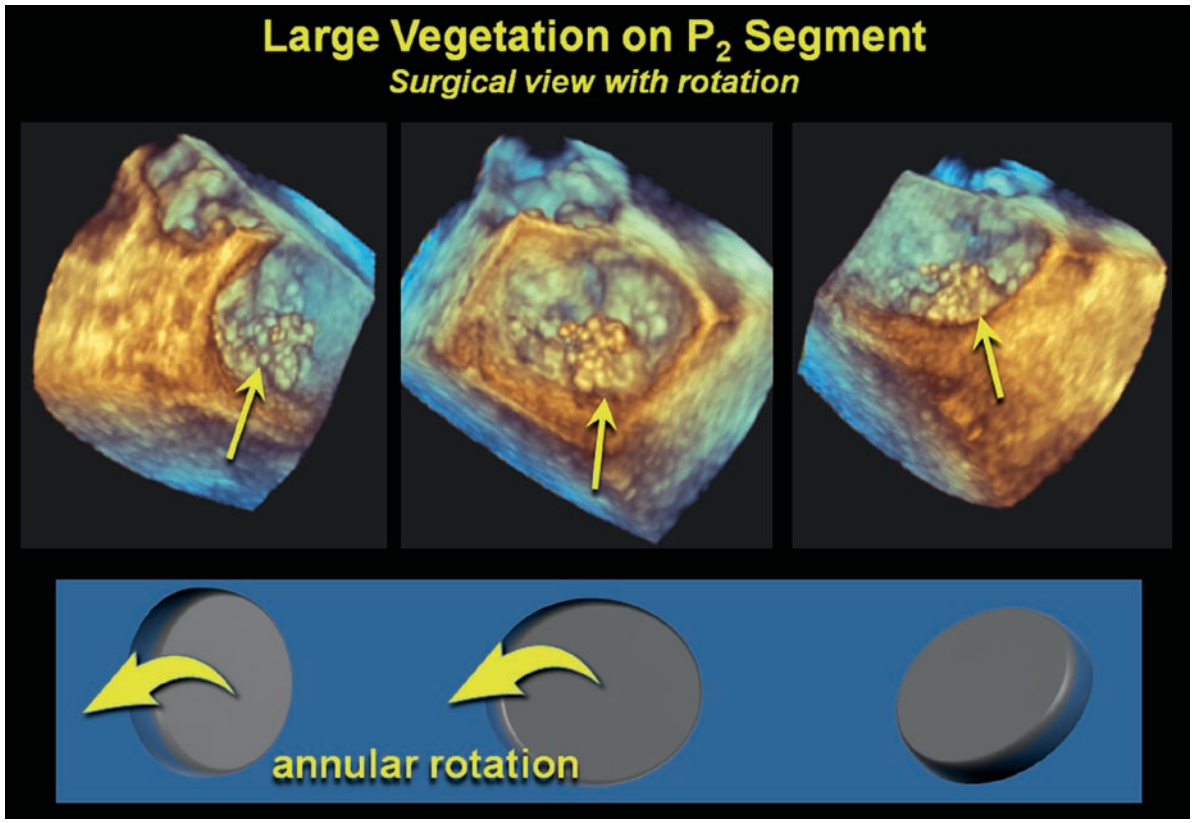

Fig. 8.124 Three-dimensional echo in the surgical view showing the sessile cluster of vegetations residing over the P_2 segment

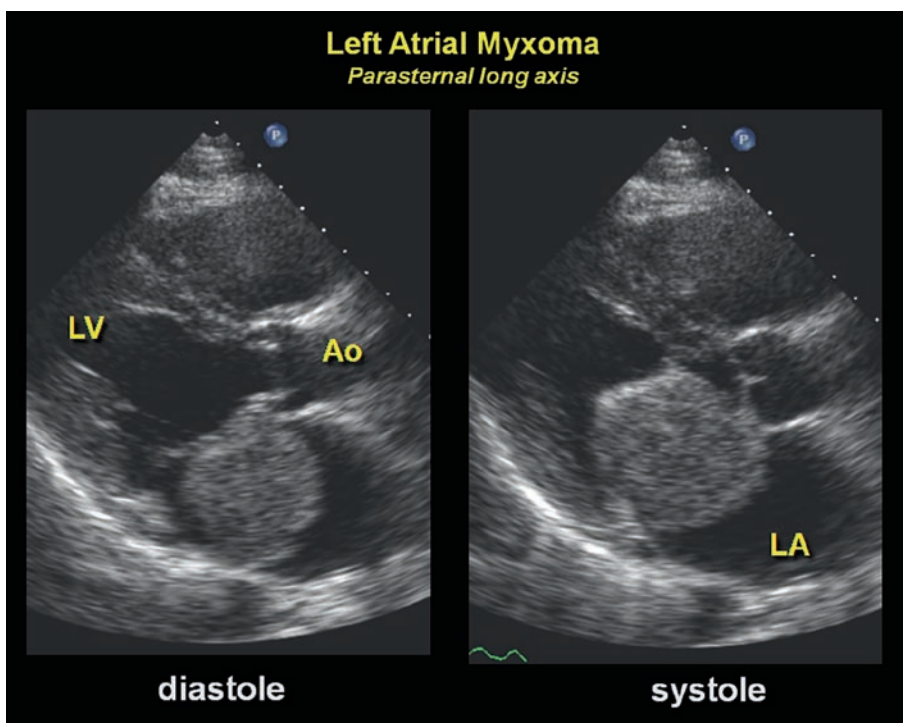

Fig. 8.125 Typical parasternal long axis of a left atrial myxoma, prolapsing into the mitral orifice in diastole

Such tumors are not, however, restricted to older female patients. The parasternal echocardiogram from another patient with a massive left atrial myxoma is seen in Fig. 8.126 and is from a 17-year-old male, also suffering from progressive shortness of breath. The two-dimensional echocardiogram in this picture shows the mitral valve in the open position and the massive tumor prolapsing toward the left ventricle in diastole. The M-mode echocardiogram on the right shows the mitral valve to open in early diastole, rapidly followed by the tumor an instant later (arrow). This movement has been well correlated with the "tumor plop" heard on auscultation in patients with this disorder. Figure 8.127 shows this large tumor in the left atrium in systole (Panel A) and then progressively moving through the mitral valve annulus in diastole (through Panel D). Such movements are incredibly dramatic and this series of still frames is nowhere near as impressive as viewing the tumor movement in real time. The diastolic movements depicted, however, readily demonstrate the physiologic problem encountered in these patients with occlusion of the mitral valve orifice and symptoms of shortness of breath. Note that this tumor is not homogeneous. Panel A shows an area of necrosis within the tumor.

While a large myxoma is responsible for multiple color artifacts seen when using color-flow imaging, the mitral valve should be carefully examined for the presence of mitral regurgitation (right-hand panel, Fig. 8.128). This patient's massive mitral regurgitation was caused by distortion of the mitral valve apparatus due to the tumor and completely disappeared following surgical resection. In fact, attendant mitral regurgitation in patients with atrial myxoma rarely needs surgical repair as the regurgitation usually disappears with tumor removal.

An examiner using echocardiography should not be distracted by the appearance of the tumor itself. One of the most important things that echocardiography can contribute is to determine the location of attachment of these large tumors. It is now well accepted that the point of attachment must be completely surgically excised to eliminate recurrence. Figure 8.129 shows the point of attachment of this tumor to be the midatrial septum. This is the same patient depicted in long axis in Fig. 8.125. Most atrial myxomata will be attached along the atrial septum and the atrial septum is, therefore, removed with the tumor at the time of surgery. The atrial septum is then patched. Wherever the tumor is located, the point of attachment to the heart should never be missed by echocardiography as it can determine the best approach for surgical resection.

A left atrial myxoma may be simulated by mitral prolapse with M-mode echocardiography. One important factor to recognize is that a large P_2 segment of mitral

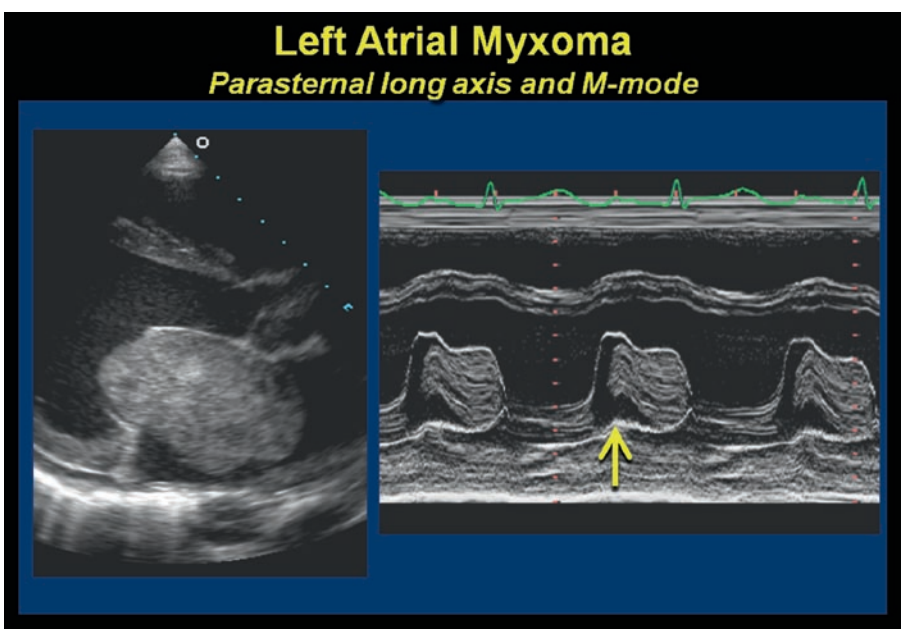

Fig. 8.126 Parasternal long axis of a myxoma in a young male. The M-mode echo shows movement of the tumor mass into the mitral inflow just after mitral valve opening (*arrow*)

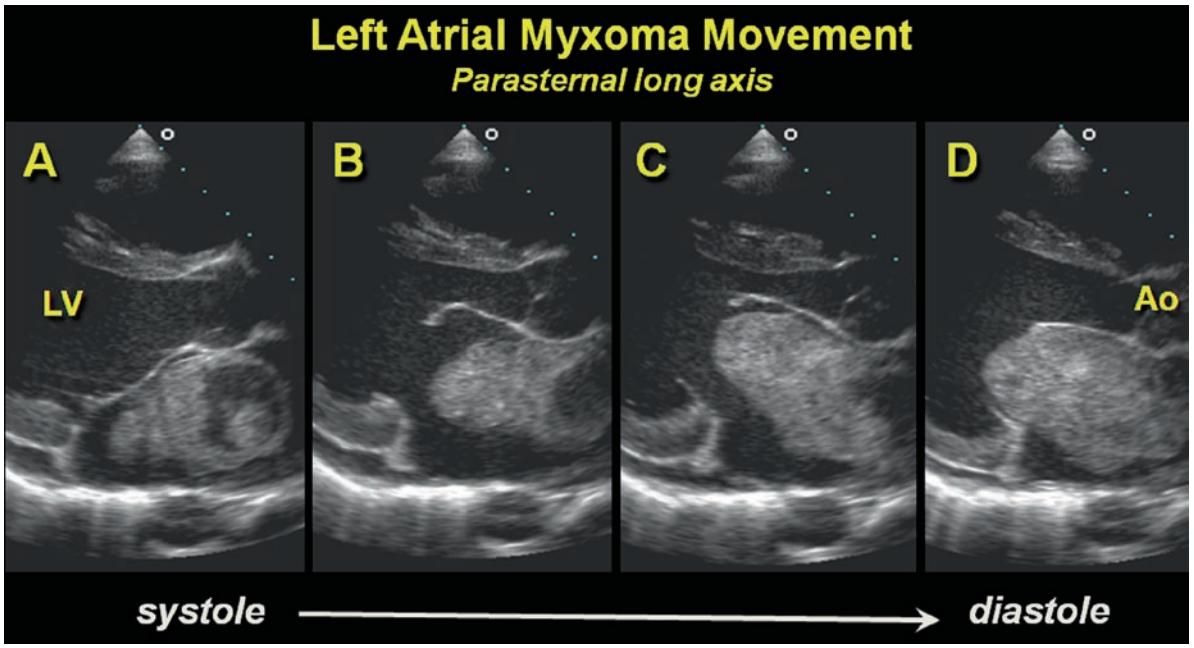

Fig. 8.127 Serial diastolic frames showing prolapse of this massive tumor into the mitral orifice

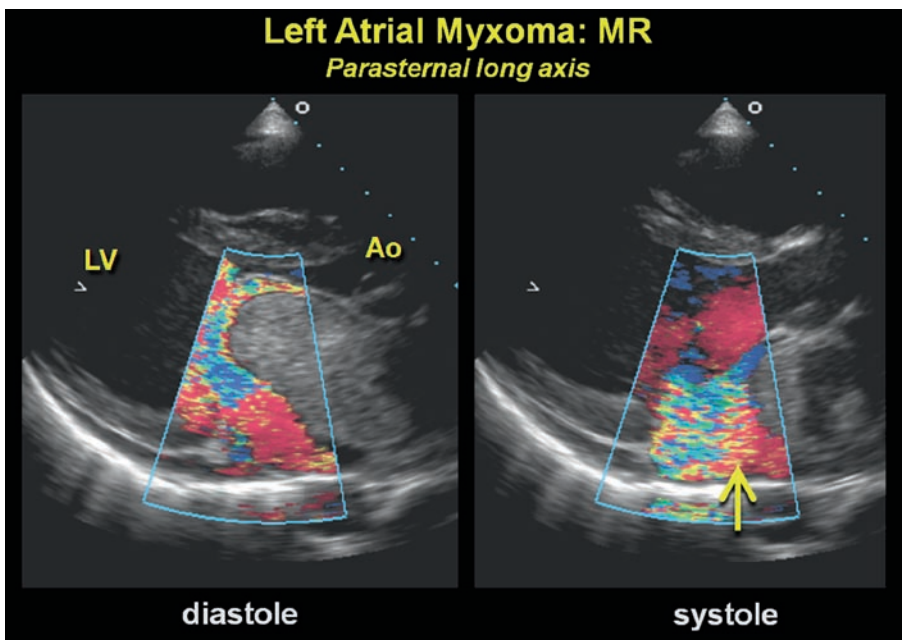

Fig. 8.128 Mitral regurgitation (*right panel*, *arrow*) often results from left atrial myxoma, but frequently resolves after surgical removal

valve prolapse may simulate a left atrial myxoma attached along the posterior left atrial surface. Figure 8.130 shows a normal mitral valve at the leaflet tip by M-mode. When the transducer is angled somewhat more cephalad it encounters the large P_2 segment prolapsing down into the mitral valve orifice. Thus, prolapse is both a systolic and a diastolic phenomenon. Two-dimensional echocardiography can readily differentiate these entities.

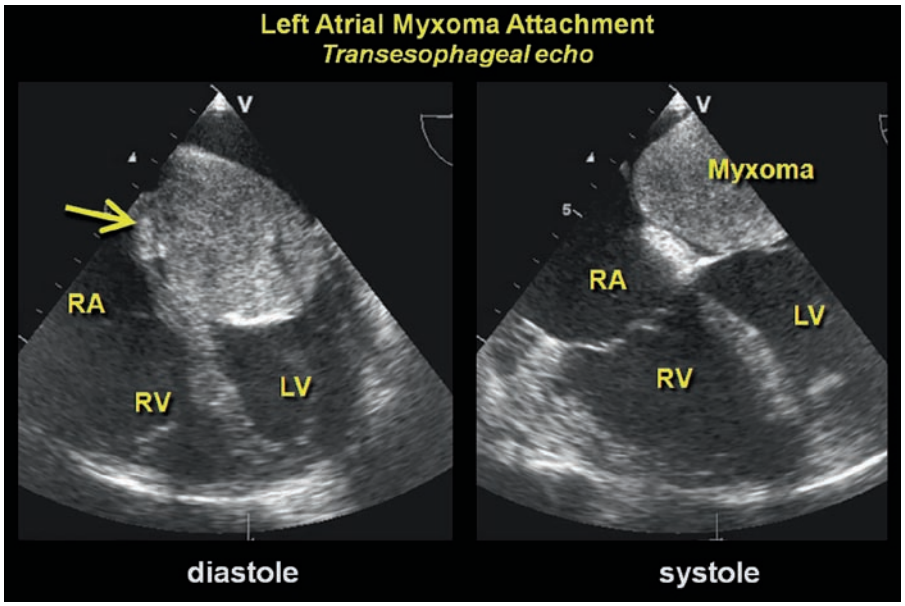

Fig. 8.129 Transesophageal echo showing the point of attachment of a myxoma on the atrial septum in the fossa ovalis. It is important to find the point of attachment to aid in directing the approach for surgical removal of the mass

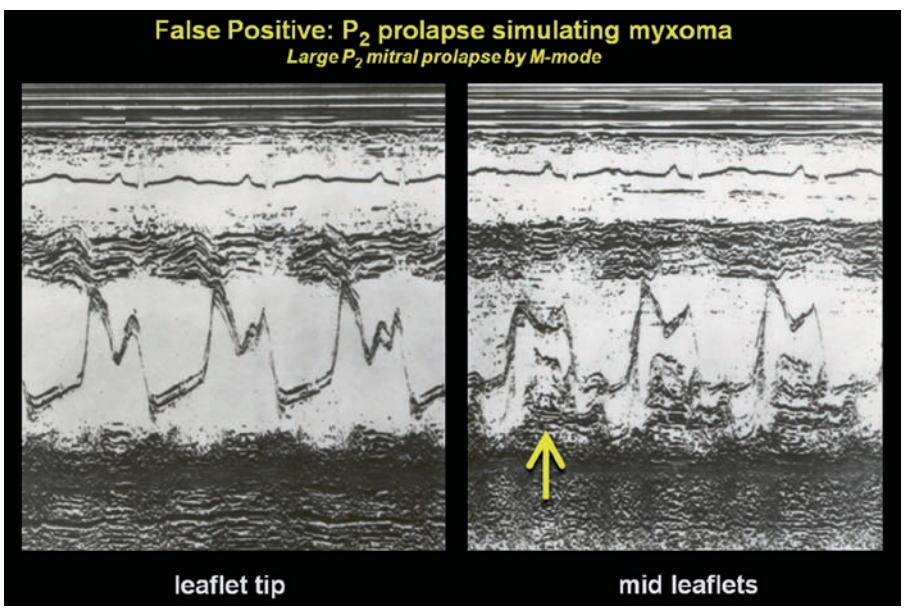

Fig. 8.130 A large P_2 segment prolapsing down into the mitral orifice may simulate left atrial myxoma (*right panel*, *arrow*)

While M-mode echocardiography is hardly ever, if ever, performed as a stand alone procedure over the recent decade, this example serves to help understand spatial movement of cardiac structures.

Figure 8.131 shows a left ventricular, rather than, left atrial myxoma using M-mode echocardiography. The myxoma was located on the septal surface of the left ventricular outflow tract and appeared to represent a massive structure anterior to the moving mitral valve (arrow). While such confusions exist with M-mode echocardiography, two-dimensional echocardiography can readily differentiate the location of these tumors.

Congenital Anomalies of the Mitral Valve

There are multiple congenital anomalies of the mitral valve and only few can be discussed in the context of this chapter. One interesting anomaly is shown in Fig. 8.132, where a congenital double orifice mitral valve is shown. Movement of the mitral apparatus may resemble that of mitral stenosis in this entity with restriction of the valve leaflet tip in the parasternal long axis. In the short-axis view, these patients are sometimes misdiagnosed as having mitral stenosis. If the restriction to flow in diastole is minimum, there may be no symptoms associated with this disorder. However, more commonly, there are symptoms due to mitral valve leaflet obstruction and they are progressive shortness of breath.

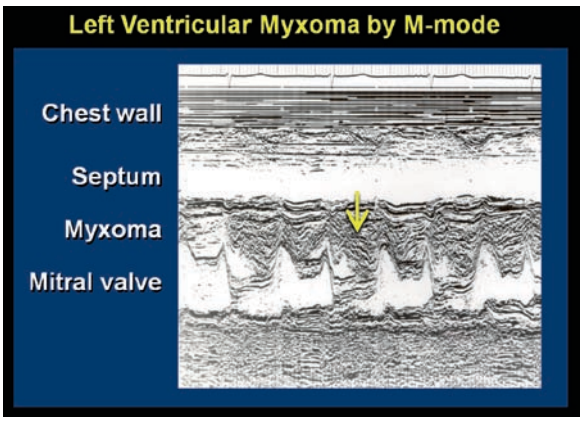

Fig. 8.131 M-mode echocardiogram of a left ventricular myxoma that obliterated the left ventricular outflow tract (*arrow*)

Figure 8.133 shows another patient with such a double orifice of congenital origin. Again, the anterior mitral valve leaflet tip is bowed slightly posteriorly in diastole and the typical double orifice is easily recognized. When the transducer is moved to the apical four-chamber view, the double orifice can again be noted (left-hand panel Fig. 8.134). When color flow is then utilized the double orifice can readily be identified (right-hand panel). Even more rare is the presence of a triple orifice mitral valve. Two-dimensional echocardiogram from the chest wall is identified in such a patient in Fig. 8.135 where a parasternal long axis (left panel) and a short axis (right panel) are shown. Reconstruction of the mitral valve with a triple

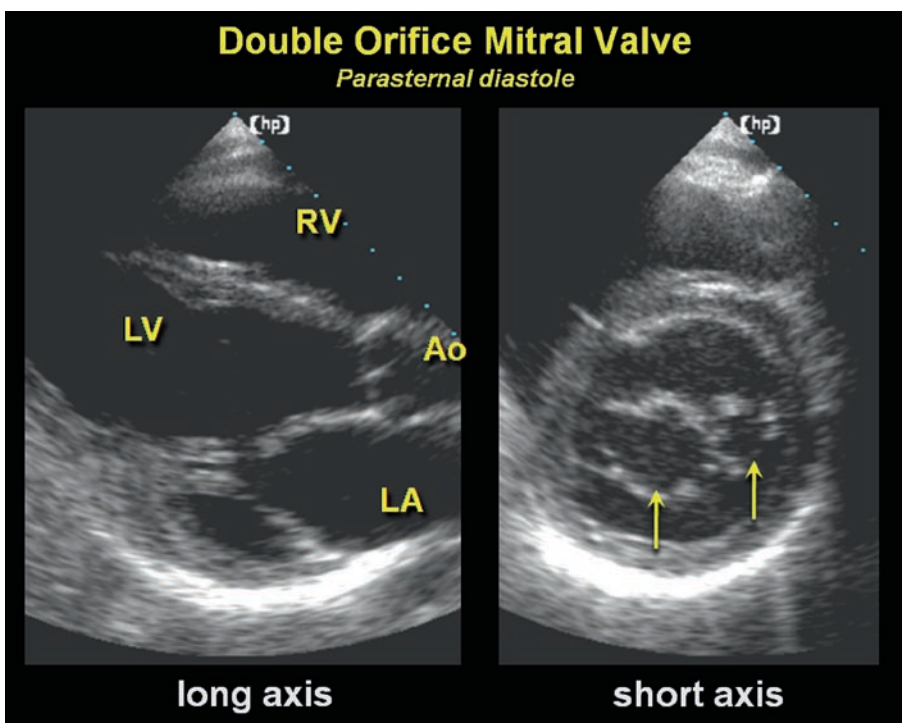

Fig. 8.132 Parasternal long and short axes from a patient with a double orifice mitral valve (*arrows*, *right panel*)

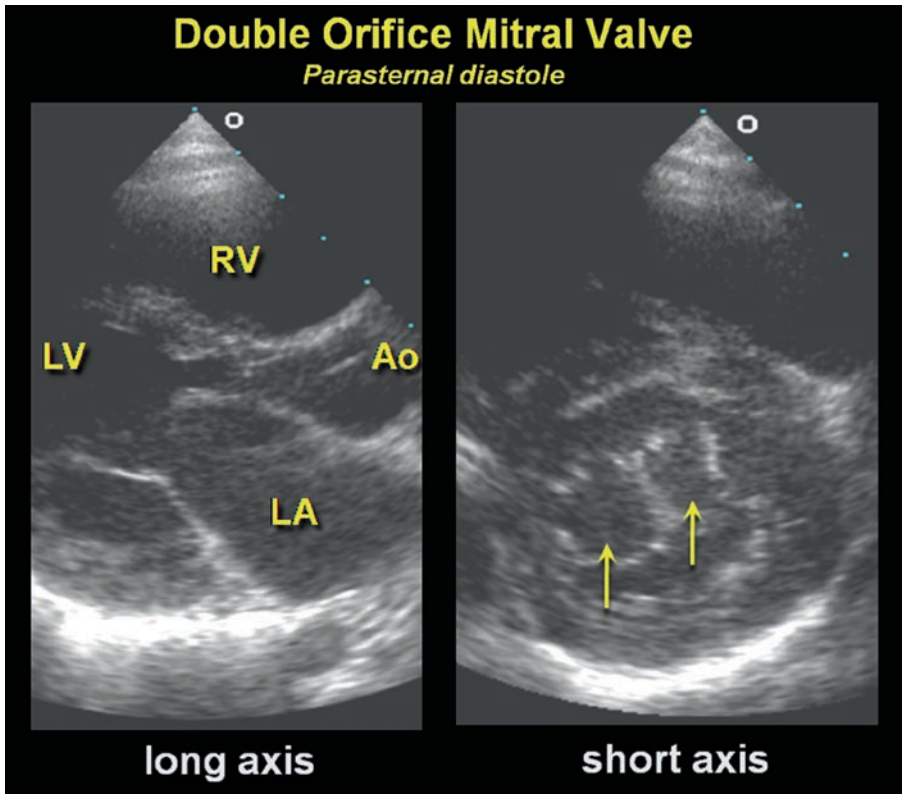

Fig. 8.133 Parasternal long and short axes from yet another patient with a double orifice mitral valve (*arrows*, *right panel*)

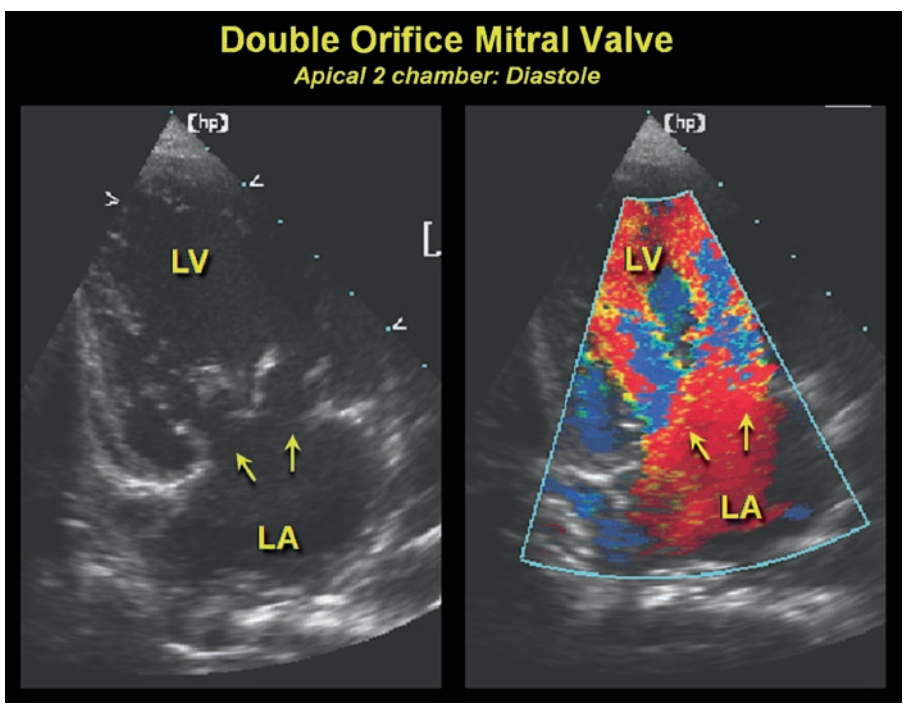

Fig. 8.134 Both orifices of the valve seen in the previous figure can be visualized from the apex. Two LV inlet flow jets can be seen

orifice mitral valve is impossible at the present time, and this patient had to undergo mitral valve replacement consequent to significant symptoms due to mitral restriction.

Figure 8.136 demonstrates an entity where an incorrect diagnosis of mitral valve orifice would be rendered and results from mitral prolapse. The left-hand panel shows a patient with typical P_2 mitral valve prolapse

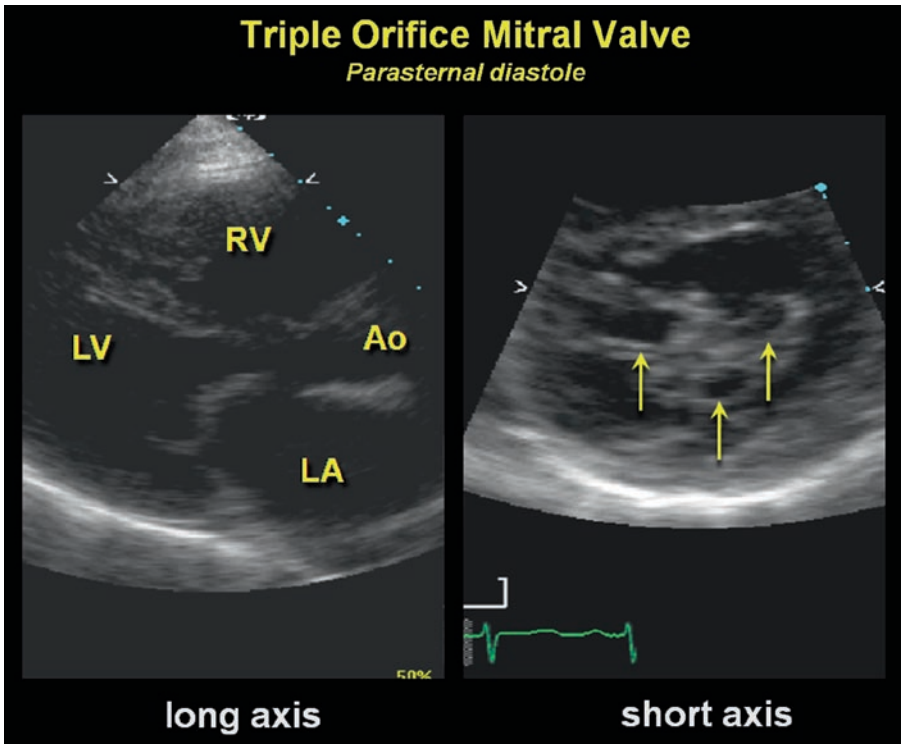

Fig. 8.135 While exceedingly rare, a triple orifice mitral valve can also be detected (*arrows*, *right panel*)

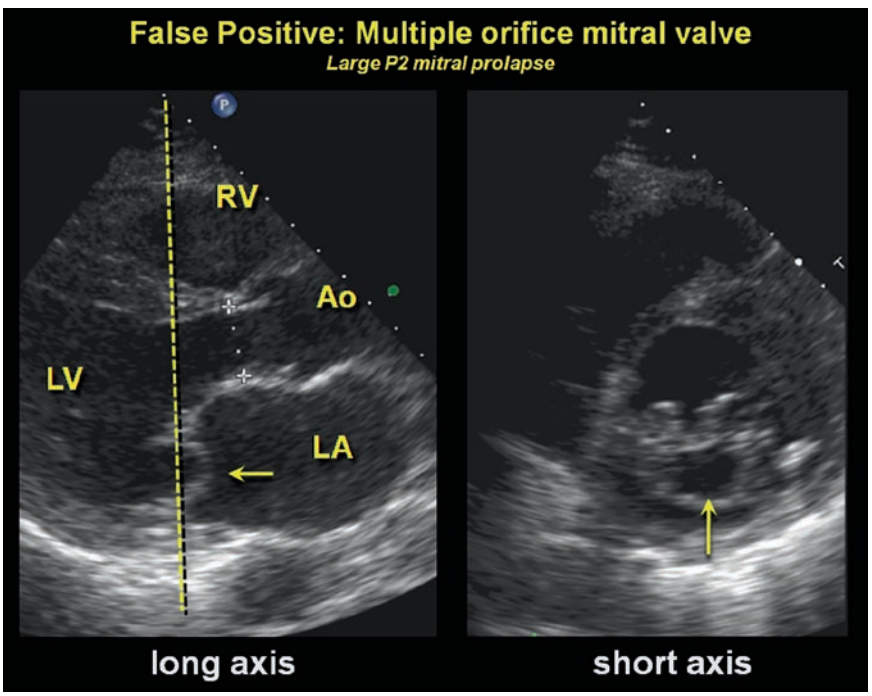

Fig. 8.136 One false positive for a multiple orifice mitral valve is seen where the "dome" of the prolapsing P_2 segment simulates a triple orifice valve in systole (*arrow*, *right panel*)

seen in the parasternal long axis (arrow). The orthogonal short axis (right panel) shows diastolic frame through the body of the large P_2 segment simulating a multiple orifice mitral valve. Obviously, the parasternal long axis in this entity would help differentiate these two entities.

Another false positive for double mitral orifice of the congenital variety is that acquired by patients undergoing the Alfieri stitch procedure. The left-hand panel of Fig. 8.137 from a patient with surgically prove double orifice mitral valve, while the right-hand panel shows a patient after the Alfieri stitch. While the two show a double mitral orifice, one is congenital and the other is obviously surgically acquired. An adequate patient history and physical examination should show evidence of previous surgical intervention and further help differentiate these entities.

Patients with other congenital lesions of the mitral valve may present simulating mitral stenosis. What one such entity is an arcade lesion that is manifest by marked thickening of the posterior leaflet and very poor differentiation of the chordal structures. A patient with this entity is shown in Fig. 8.138. These patients may be easily confused with those of rheumatic mitral stenosis. They are, however, exceedingly rare.

A much more common abnormality of the mitral valve is found in patients with atrioventricular septal defects. In this disorder, there is a huge rotation of the entire mitral apparatus and malformation of the mitral and tricuspid apparatus. There may be a so-called "cleft" of the anterior mitral valve leaflet (Fig. 8.139). With an AV Canal defect, the "cleft" is really due to a trileaflet left-sided AV valve. This "cleft" is typically angled toward the intraventricular septum and may result in attendant mitral regurgitation. Of course, other findings of atrioventricular septal defect (AV canal defect) are usually seen.

One of the more profound anomalies of the mitral valve is that seen in hypoplastic left heart syndrome. Figure 8.140 shows a parasternal long axis from an infant with hypoplastic left heart syndrome with marked dysplasia of the mitral and aortic apparatus and a rather diminutive left ventricle. These patients are, obviously, not encountered in the adult population.

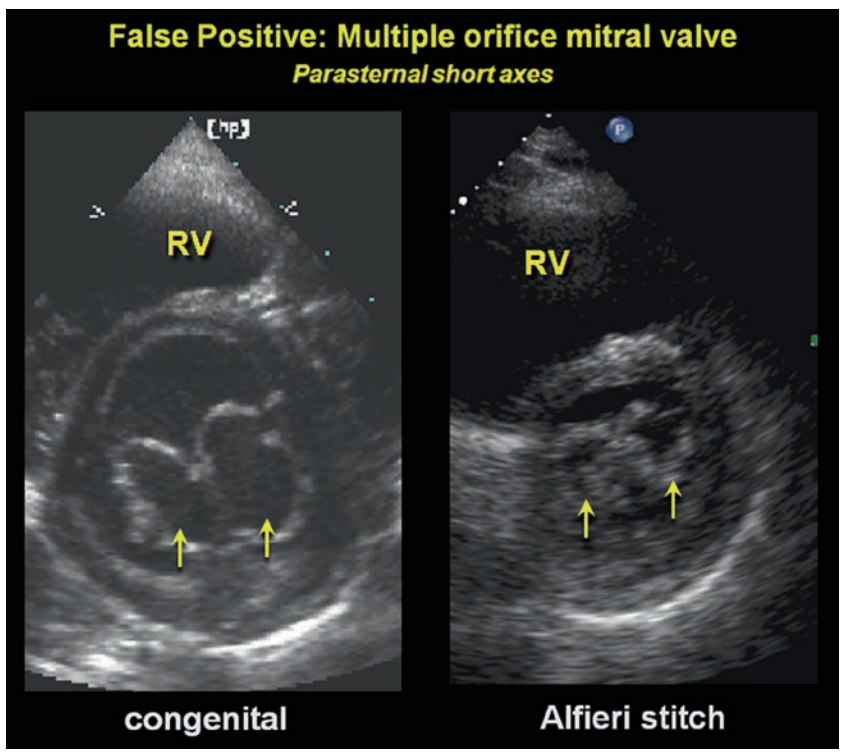

Fig. 8.137 Another false positive for a congenital double orifice mitral valve is in patients with history of Alfieri stitch. An adequate history will obviate this problem

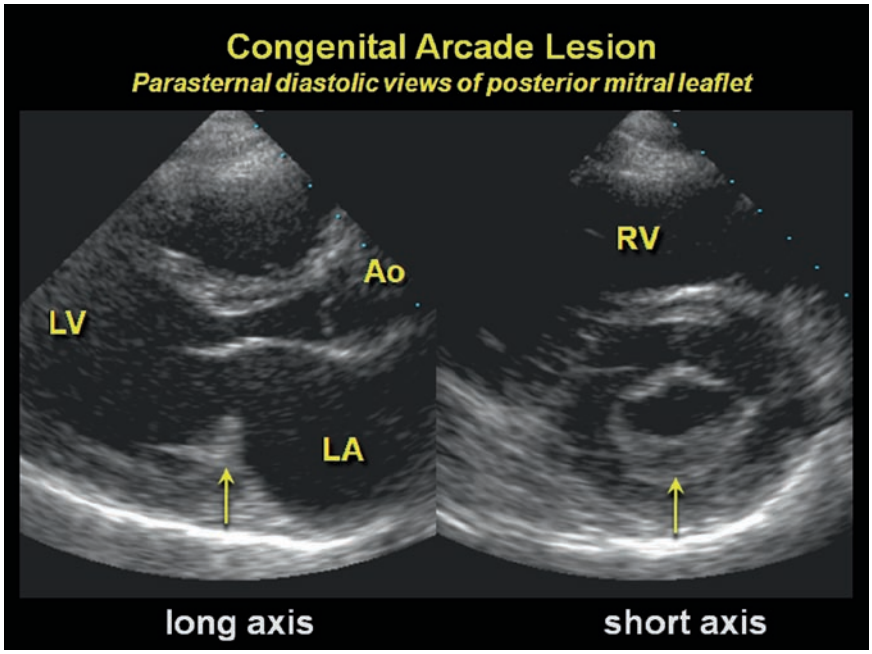

Fig. 8.138 Arcade lesion of the mitral valve in an adult patient. For details, see text

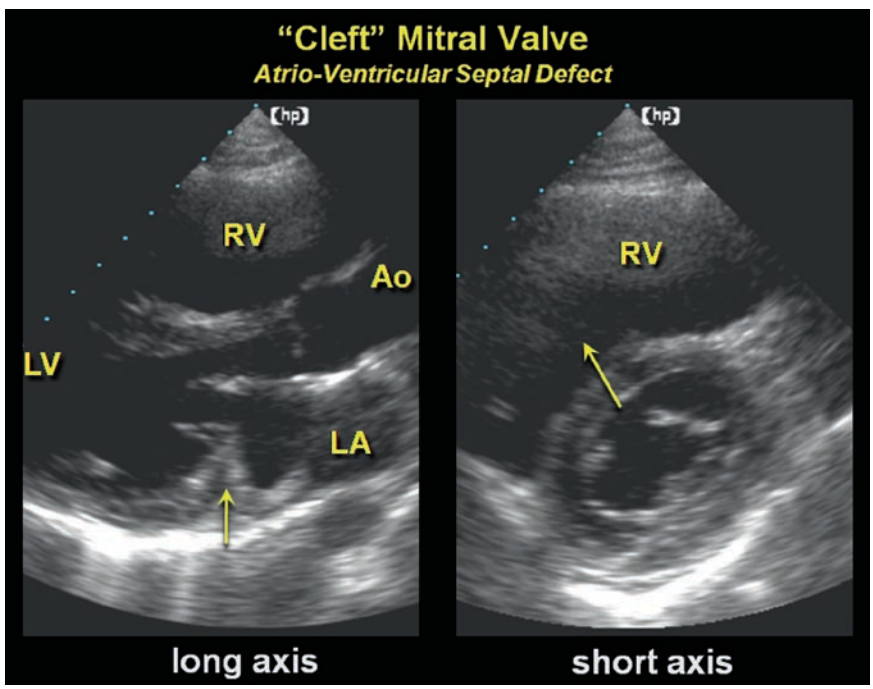

Fig. 8.139 Parasternal long axis from a patient with an AV Canal defect (atrioventricular septal defect) with malalignment of the mitral and aortic valves (*left panel*). The so-called cleft in this disorder seems to be aimed at the interventricular septum (*right panel*, *arrow*)

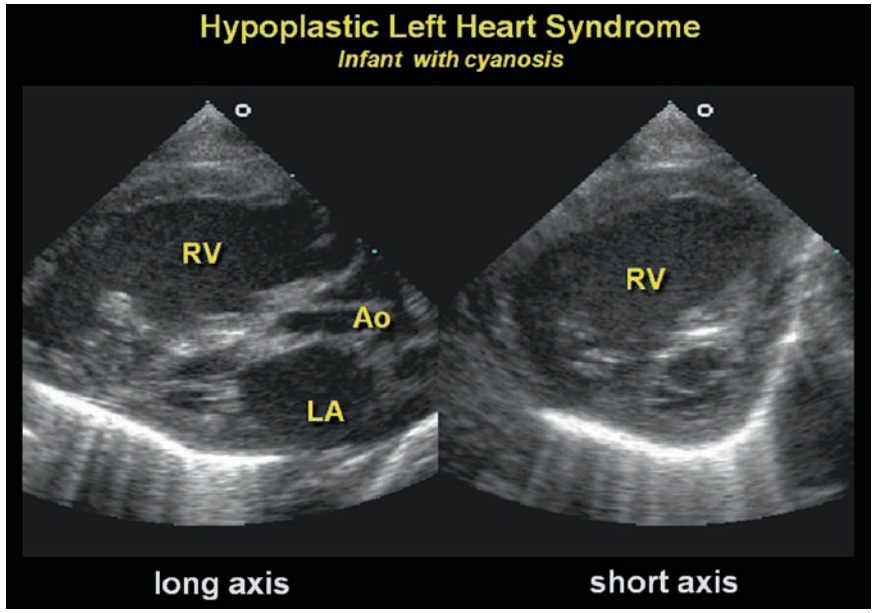

Fig. 8.140 Hypoplastic left heart syndrome in an infant. The mitral and the aortic valves and left ventricle are dysplastic and diminutive

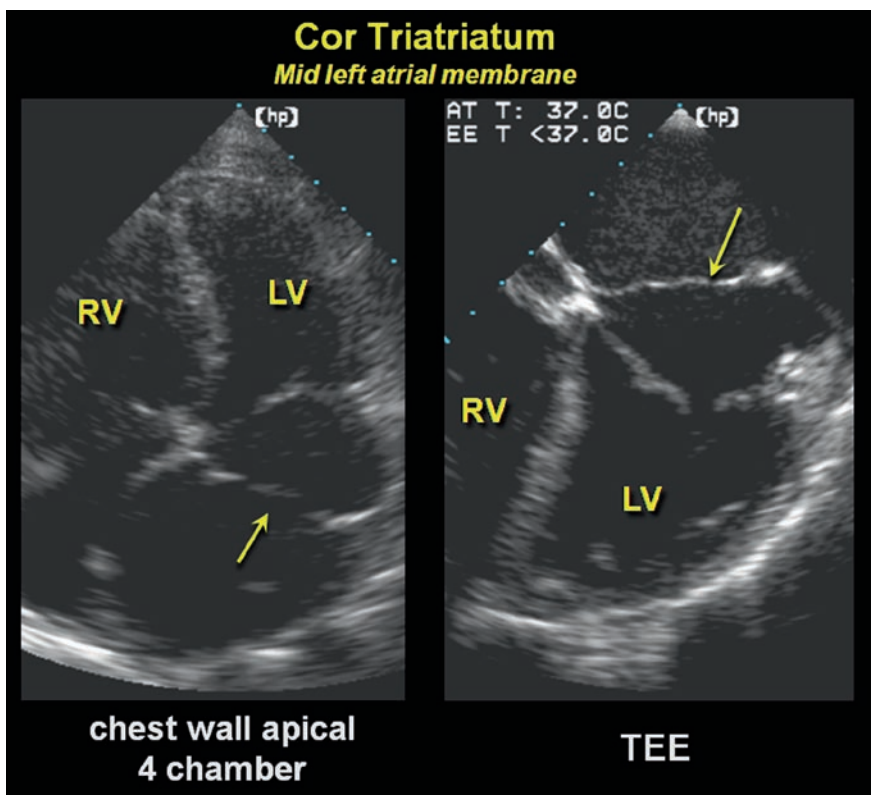

Fig. 8.141 A membrane of cor triatriatum is seen in the apical four-chamber view (*arrow*, *left panel*) and the transesophageal (*right panel*)

Another congenital heart lesion that could present with symptoms of marked mitral valve obstruction is that of cor triatriatum. While the symptoms may be that of mitral stenosis the movements of the mitral valve leaflet are usually quite normal. However, (Fig. 8.141) a membrane is seen across the atrium just superior to the mitral valve annulus. The obstruction is at the level of this membrane. The figure shows such a membrane demonstrated from the apical four chamber in an image obtained from the chest wall or from an attendant transesophageal echocardiogram. Simple surgical removal of this membrane results in a profound alleviation of symptoms.

References

1. Kisslo J, Smith SW, von Ramm OT. Real-time, three-dimensional echocardography: A beginning. In: Chambers J, Monaghan MJ, eds. Echocardiography: *An International Review*. New York: Oxford University Press; 1993:96–101.
2. Nichol PM, Gilbert BW, Kisslo JA. Two-dimensional echocardiographic assessment of mitral stenosis. *Circulation.* 1977;55:120–128.
3. Kisslo J. NHLBI Balloon Valvuloplasty Registry: Doppler-echo evaluation of mitral stenosis pre- and post-balloon valvuloplasty (Abstr). *J Am Coll Cardiol.* 1989;13:114A.
4. Hatle L, Angelsen B. *Doppler Ultrasound in Cardiology*. 2nd ed. Philadelphia: Lea and Febiger; 1985.

Chapter 9
Tricuspid and Pulmonic Valve Disease

Meeney Dhir and William A. Zoghbi

In the adult, the tricuspid and pulmonic valves are in general less affected by disease states compared to left-sided cardiac valves. While right-sided valves are essential in maintaining hemodynamic balance and in dictating long-term prognosis, valvular disease is better tolerated compared to left-sided valves. With the common occurrence of trivial regurgitation in right-sided valves in normal individuals, noninvasive determination of pulmonary pressures using the Bernoulli principle is frequently feasible. In this chapter, we will present an overview of diseases that affect the tricuspid and pulmonic valves, discuss their echocardiographic characteristics and the methodology for evaluating the severity of valvular regurgitation and stenosis.

Tricuspid Valve

The tricuspid valve (TV) is an essential part of the right ventricular (RV) inflow tract and has the largest area of all the valves, estimated at around 6–7 cm^2. It has three leaflets demarcated by commissures: the anterior, posterior, and septal leaflets. Most often there are three papillary muscles that contribute chordae to the leaflets: a large anterior papillary muscle provides chordae to the anterior and posterior leaflets, the posterior papillary muscle to the posterior and septal leaflets, and the conal papillary muscle to the anterior and septal leaflets.

M. Dhir and W.A. Zoghbi (✉)
Baylor College of Medicine, Echocardiography Laboratory,
The Methodist DeBakey Heart and Vascular Center,
6550 Fannin, SM677, Houston, TX, 77030, USA
e-mail: wzoghbi@wzoghbi@tmhs.org

With echocardiography, the tricuspid valve is examined using the parasternal RV inflow, parasternal short-axis, apical four-chamber, and subcostal views. A combination of imaging planes permits visualization of each of the leaflets in at least two orthogonal planes. Within the heavily trabeculated RV, the papillary muscles are usually not prominent, unless involved with hypertrophy.

Tricuspid Regurgitation

A small degree of tricuspid regurgitation (TR) is present in about 70% of normal individuals (Fig. 9.1). Pathologic regurgitation is often due to RV and tricuspid annular dilation secondary to pulmonary hypertension or RV dysfunction. Primary causes of TR include endocarditis, carcinoid heart disease, Ebstein's anomaly, and rheumatic disease (Table 9.1). A detailed discussion of individual conditions and the assessment of TR severity with 2D and Doppler echocardiography follow.

Etiology

Functional

Functional TR occurs with dilatation of the annulus and poor leaflet coaptation. Any condition that results in RV dilation and dysfunction can initiate this cycle. This may be a primary disease of the RV such as cardiomyopathy or infarction. Rarely, unexplained TR and right-sided heart failure is the presenting lesion in a patient with RV dysplasia or Uhl's disease, and is the result of cardiomyopathic changes in the RV. Functional TR may also be secondary to pulmonary hypertension,

P. Nihoyannopoulos and J. Kisslo (eds.), *Echocardiography*,
DOI: 10.1007/978-1-84882-293-1_9,

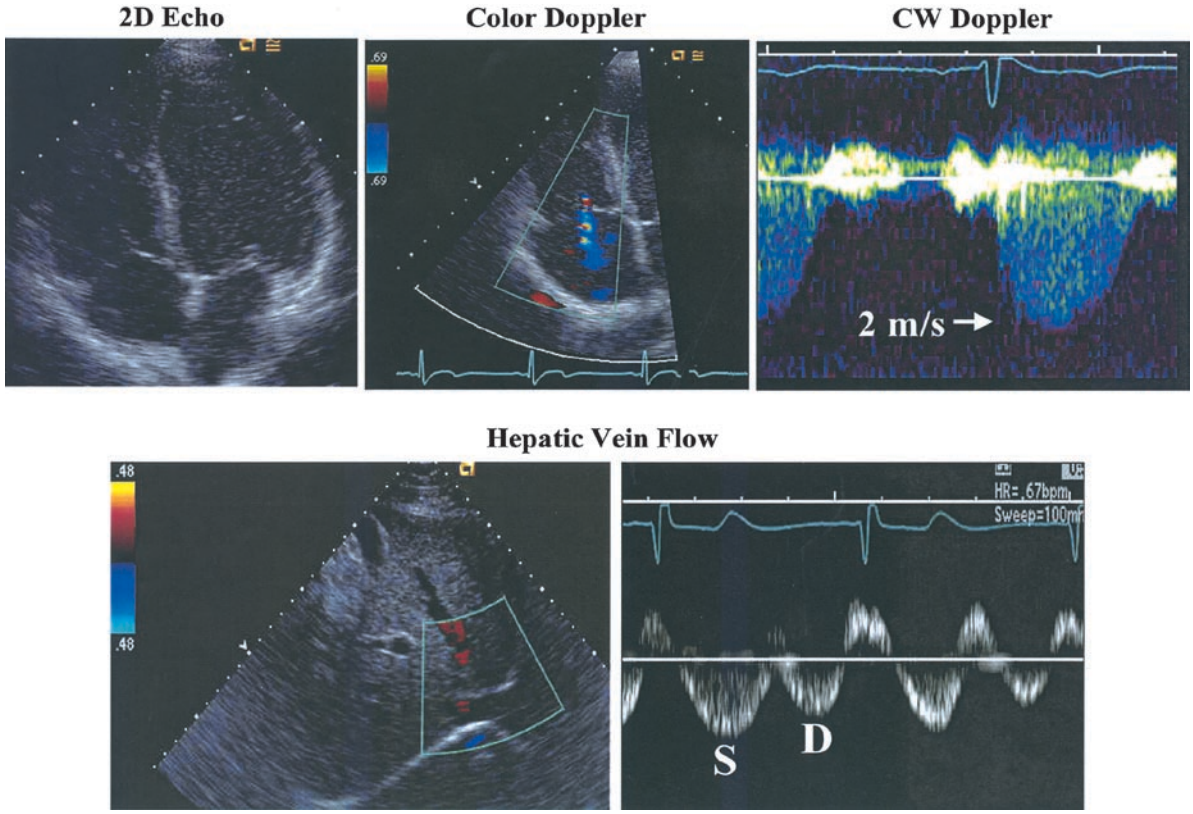

Fig. 9.1 Mild tricuspid regurgitation in an otherwise normal individual. A very thin jet of regurgitation is seen on color Doppler, with a low velocity by continuous-wave Doppler and a round contour to the jet velocity. The hepatic veins and inferior vena cava are of normal size and display a normal hepatic venous flow pattern of systolic dominant flow by pulsed Doppler. *S* systole; *D* diastole

Table 9.1 Etiology of tricuspid regurgitation

Diseases of the tricuspid valve apparatus
- Rheumatic heart disease
- Carcinoid heart disease
- Infective endocarditis
- Trauma
- Right ventricular infarction
- Myxomatous disease
- Right ventricular cardiomyopathy
- Congenital (Ebstein's anomaly)
- Radiation therapy
- Eosinophilic myocarditis

Functional tricuspid regurgitation
- Normal individuals (trivial or mild degree)
- Pulmonary hypertension
  - Primary
  - Secondary
    - Mitral stenosis
    - Congenital heart disease
    - Sleep apnea
    - Collagen vascular disorders
    - Pulmonary parenchymal disease
    - LV dysfunction (diastolic or systolic)
- Diseases of the right ventricle
  - Right ventricular infraction
  - Right ventricular cardiomyopathy
  - Post cardiac transplantation

which in turn may be primary or secondary to left-sided heart disease and/or lung pathology. All these conditions can perpetuate the cycle of "TR begets TR": with progressive RV dilation, the annulus is more stretched, the leaflets tethered, thus worsening the regurgitation. In functional TR, the tricuspid leaflets and chordae themselves appear normal, while there is RV dilatation, with and without hypertrophy with tethering of chordae or poorly aligned papillary muscles. Functional TR is not necessarily only mild, as it can encompass varying degrees of severity.

Infective Endocarditis

Most often infective endocarditis is seen with intravenous drug abuse or indwelling catheters in the central circulation (e.g., hyperalimentation, chemotherapy, or access for hemodialysis). In immunocompromised hosts, endocarditis may be fungal in etiology, with large bulky vegetations seen on echocardiography. In developing countries, TV endocarditis is also associated

with septic abortions. Rarely an infected ventricular septal defect jet may be the culprit. In patients with pacemaker lead infection, there may be incidental involvement of the valve. Most often endocarditis results in TR. Very large vegetations, however, may mimic valvular stenosis. In technically adequate studies, the transthoracic approach is usually sufficient for the detection of the majority of native tricuspid valve vegetations, and for the assessment of the severity of associated TR. Transesophageal echocardiography is reserved for technically difficult cases and where other valvular involvement is suspected.

Ebstein's Anomaly

Ebstein's anomaly is a congenital abnormality characterized by an exaggerated apical displacement of the insertion of the septal and posterior leaflets of the tricuspid valve compared to the septal insertion of the mitral valve (Fig. 9.2). The displacement is usually greater than 11 mm; some investigators normalize this displacement for body surface area (≥8 mm/m^2). This may involve the septal leaflet alone or affects all three leaflets. Additionally, the anterior leaflet is large, "sail-like," and variably attached to the RV free wall, while the septal or posterior leaflet may be hypoplastic or even dysplastic. The basal part of the RV is functionally excluded from the pumping function of the RV, making the right atrium appear enlarged and thus "atrialized." The hemodynamics are made worse by the accompanying TR, which may be of variable degree. Depending on the extent of TV displacement, the remaining functional RV may be of good size or rudimentary. Most patients have an accompanying atrial septal defect or patent foramen ovale. The valve itself may be functionally stenotic but more commonly regurgitant. The RV may progressively dilate due to the volume overload from TR.

Rheumatic Heart Disease and Carcinoid

In rheumatic valvular disease, the tricuspid regurgitation is most often functional, resulting from longstanding pulmonary hypertension from rheumatic mitral stenosis and regurgitation. Primary rheumatic involvement of the TV leaflets occurs in 20–30% of cases, with commissural fusion. This is easily missed, if not specifically sought. Rheumatic tricuspid regurgitation is more common than stenosis, and usually does not occur without concomitant mitral and/or aortic valve involvement.

On the other hand, carcinoid involvement of the TV is seen with carcinoid syndrome that is metastatic to the liver. Although rare, it pathognomonically results in thick, short, stiff, and relatively immobile leaflets that no longer coapt. This results in significant TR and some degree of tricuspid stenosis. The pulmonic valve is also frequently involved. The morphologic characteristics

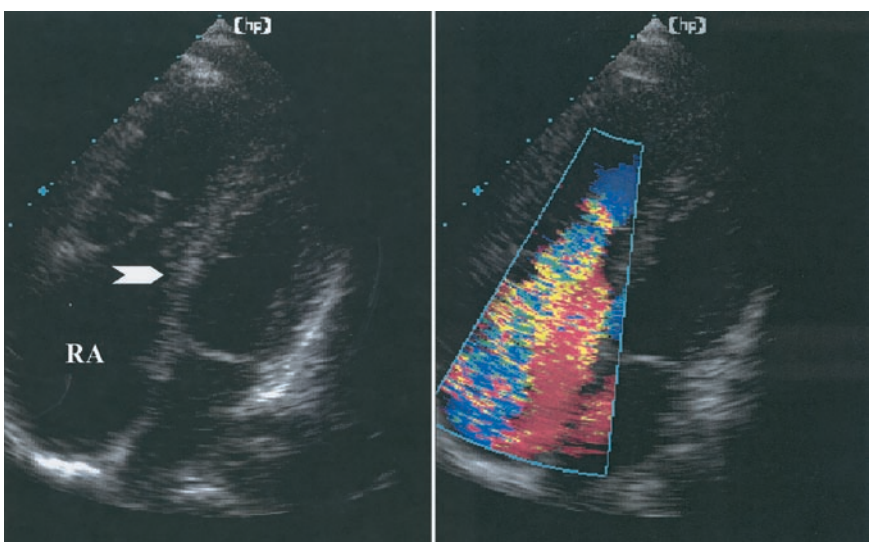

Fig. 9.2 An apical view of a patient with Ebstein's anomaly, showing the apical displacement of the insertion of the septal tricuspid leaflet (*arrow*) compared to the mitral leaflet. An atrialized right ventricle and significant tricuspid regurgitation that starts closer to the apex of the RV is seen by Color Doppler. Courtesy of David B. Adams. *RA* right atrium

of carcinoid valvular involvement can differentiate this entity readily from rheumatic involvement. Carcinoid-like involvement of the TV is also seen in patients on certain drugs like methysergide or ergotamine.

Miscellaneous Etiologies

Iatrogenic TR may occur in cardiac transplant patients after trauma from cardiac biopsies or after the placement of a Swan–Ganz catheter or a pacemaker. After myocardial biopsies, TR may result from damage to the valvular apparatus (papillary muscles, chordae, or leaflets). In this setting, the TR jet is often eccentric. External penetrating *trauma* can also directly injure the TV apparatus including puncture of the leaflets, rupture of the chordae or the papillary muscles. Rarely flail segments may be seen. On the other hand, blunt trauma may result in RV contusion which, if extensive, can lead to RV failure and functional TR.

TV prolapse, like that of the mitral valve, is the result of myxomatous changes with thickening of the spongiosa and weak support from the chordae. Varying degrees of redundancy result in posterior motion of the leaflets past the annular plane into the RA. This entity is seen almost exclusively in the presence of concomitant involvement of the mitral valve. *Loeffler's endocarditis* is usually a combined lesion with tricuspid stenosis (see later), but similar pathology can probably be seen with eosinophilia of other etiologies. Lastly, *Congenital cleft of the anterior leaflet* is usually part of the endocardial cushion defect syndrome. Attachment of the leaflets may also be displaced and tethered.

All entities of TV regurgitation discussed so far dealt with systolic regurgitation. Infrequently, diastolic TV regurgitation, similar to mitral regurgitation, occurs, usually in conditions of elevated right ventricular end diastolic pressure. These are trivial degrees and are detected by Doppler techniques. Diastolic TR without an elevated RV end-diastolic pressure may also be seen with arrhythmias, atrioventricular dissociation, and prolonged atrioventricular conduction delay.

Assessment of TR Severity

Echocardiography remains the preferred method for the assessment of TR. Recently, the American Society of Echocardiography, in collaboration with the American College of Cardiology, American Heart Association, and European Society of Cardiology, put forth recommendations for the evaluation of native valvular regurgitation with 2D- Doppler techniques (see Bibliography). This assessment includes an appraisal of the adaptive remodeling of the cardiac chambers to the volume overload, and a color Doppler and spectral Doppler evaluation of the jet and its effects on hepatic venous flow. While this assessment is limited by the lack of defined quantitative criteria, a semiquantitative evaluation of severity usually suffices.

Two-Dimensional Criteria

Evaluation of the tricuspid valve apparatus with 2D echocardiography is important in determining the etiology of TR. The presence of a flail TV invariably denotes significant TR. Findings like right atrial and RV enlargement often accompany significant chronic TR. Although enlargement of right-sided chambers is not specific for significant chronic regurgitation, its absence suggests milder degree of TR. Paradoxical ventricular septal motion may occur with RV volume overload due to severe TR – flattened septum in diastole returning to normal curvature in systole (Fig. 9.3). However, this sign is not specific for TR since it occurs in severe pulmonic insufficiency, atrial septal defect or conditions of increased RV diastolic pressure. Lastly, dilated or plethoric hepatic veins and inferior vena cava that collapse poorly during inspiration suggest increased RA pressures and significant TR.

Color Doppler

TR is characterized by retrograde flow in systole from the RV into the RA. Most often this is a central jet arising from a defect in the central coaptation of the three leaflets. Less often, this may arise along one of the commissural planes. This flow is best recorded from an apical or low parasternal window, although short-axis recording may also be helpful.

Color Doppler is used to qualitatively assess the severity of TR. It has been shown that evaluation of all the components of a jet is essential in the estimation of severity of the lesion: its flow convergence, vena contracta, and jet area in the receiving chamber (Fig. 9.4). While the size of the jet in the right atrium is helpful in estimating TR severity, it is limited by the fact that the jet size is not a volumetric parameter of regurgitation

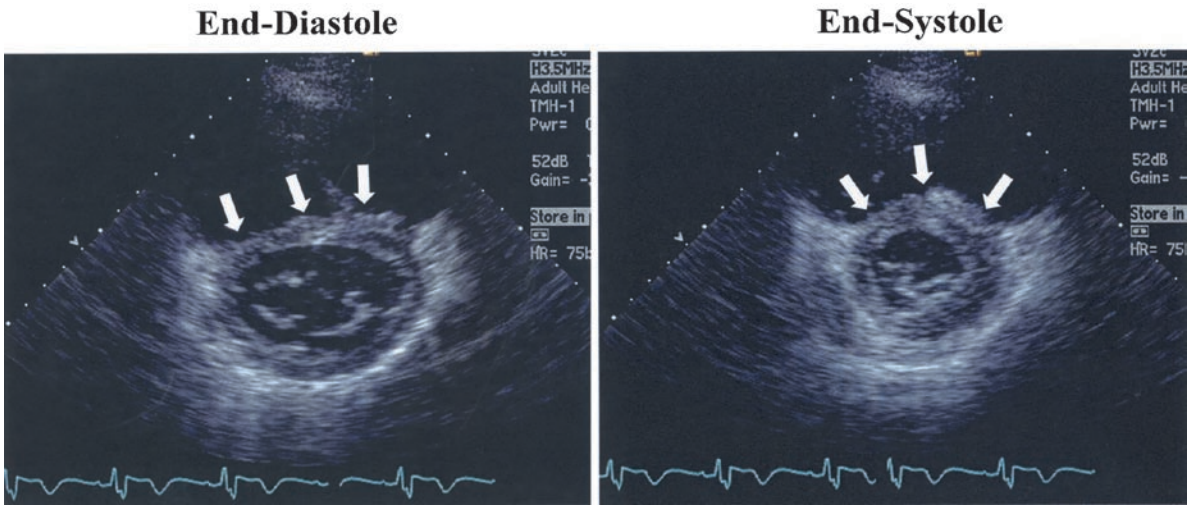

Fig. 9.3 Short-axis view at end-diastole and end-systole in patient with significant tricuspid regurgitation showing typical findings of a paradoxical septal motion seen with RV volume overload (*arrows*): flattening of the septum with deformation of the ventricle (D shape) in diastole, changing to a circular shape in systole

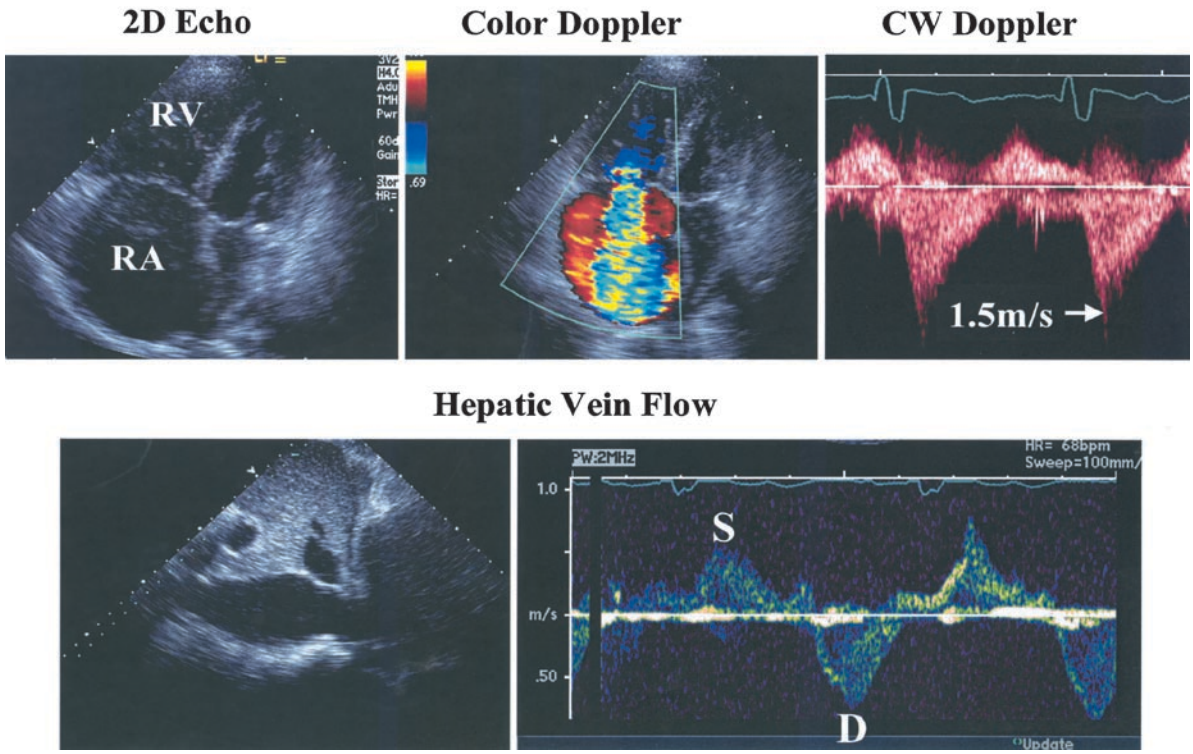

Fig. 9.4 Example of a patient with severe tricuspid regurgitation. The right ventricle and the atrium are severely enlarged and the tricuspid annulus is dilated with poor coaptation of the tricuspid valve. The color jet of TR is central, with a large vena contracta, a prominent flow convergence, and a large area in the right atrium. Continuous-wave Doppler recording shows a low-velocity jet with a triangular shape with early peaking of the velocity consistent with severe TR and near equalization of RV and RA pressures. The inferior vena cava and hepatic veins are plethoric; flow shows systolic reversal, also consistent with severe TR and elevated RA pressures

and is dependent, among other factors, on its driving pressure. Furthermore, eccentric, wall impinging jets appear thin and small by color Doppler, underestimating their severity. On the other hand, for central jets, color flow estimation of jet area in at least two orthogonal planes has had good correlation with the assessment of the severity of TR clinically and angiographically. More recently, the flow convergence or proximal isovelocity surface area (PISA) method of estimating the effective regurgitant orifice area has been validated with TR, just as for mitral regurgitation. Lastly, the jet width at its narrowest portion or vena contracta is a good index of severity. A vena contracta ≥ 0.7 cm is more often associated with severe TR. While the flow convergence and vena contracta methods appear superior to the estimation of TR severity by color jet area, they too are more accurately reflective of the true severity of TR in central jets as opposed to eccentric jets. Moreover, there can be considerable overlap in assessment of mild and moderate lesions. Thus a qualitative assessment of all the components of the TR jet needs to be incorporated, coupled with findings by spectral Doppler (Table 9.2), for a more confident evaluation of TR severity (Figs. 9.1 and 9.4).

Continuous-Wave Doppler

Recording of TR jet velocity by continuous-wave (CW) Doppler provides a useful method for noninvasive measurement of RV or pulmonary artery systolic pressure using the modified Bernoulli equation as: 4 × (peak velocity)^2 + mean RA pressure. It is important to note that the magnitude of the TR jet velocity, similar to other regurgitant lesions, is not related to the volume of regurgitant flow. In fact, massive TR is often associated with a low jet velocity (<2 m/s), as there is near equalization of RV and RA pressures (Fig. 9.4). Conversely, in pulmonary hypertension, the TR jet velocity is very high and may be associated with just mild TR.

The features of the TR jet by CW Doppler that help in evaluating severity of regurgitation are the signal intensity and the contour of the velocity curve (Figs. 9.1 and 9.4). With severe TR, a dense spectral recording is seen along with a triangular, early peaking of the velocity because of a prominent regurgitant pressure wave.

Pulsed Doppler

The severity of TR will affect the early diastolic tricuspid E velocity because of increased flow across the valve. Values above 1.0 m/s are often recorded in patients with severe TR, even without the presence of valve stenosis. Although in theory, tricuspid regurgitant volume can be calculated by subtracting the flow across a nonregurgitant valve from the antegrade flow across the tricuspid valve, this approach is rarely used in TR (in contrast to mitral or aortic regurgitation), partly because of errors in measuring the TV annulus.

Table 9.2 Echocardiographic and Doppler parameters used in grading tricuspid regurgitation severity

Parameter	Mild	Moderate	Severe
Tricuspid valve	Usually normal	Normal or abnormal	Abnormal/flail leaflet/poor coaptation
RV/RA/IVC size	Normal[a]	Normal or dilated	Usually dilated[b]
Jet area – central jets (cm^2)[c]	<5	5–10	>10
VC width (cm)[d]	Not defined	Not defined, but <0.7	>0.7
PISA radius (cm)[e]	<0.5	0.6–0.9	>0.9
Jet density and contour – CW	Soft and parabolic	Dense, variable contour	Dense, triangular with early peaking
Hepatic vein flow[f]	Systolic dominance	Systolic blunting	Systolic reversal

Reproduced with permission from the American Society of Echocardiography

CW Continuous-wave Doppler; *IVC* inferior vena cava; *RA* right atrium; *RV* right ventricle; *VC* vena contracta width

[a]Unless there are other reasons for RA or RV dilation. Normal 2D measurements from the apical four-chamber view: RV mediolateral end-diastolic dimension ≤ 4.3 cm, RV end-diastolic area ≤ 35.5 cm^2, maximal RA mediolateral and superoinferior dimensions ≤ 4.6 and 4.9 cm, respectively, maximal RA volume ≤ 33 ml/m^2

[b]Exception: acute TR

[c]At a Nyquist limit of 50–60 cm/s. Not valid in eccentric jets. Jet area is not recommended as the sole parameter of TR severity due to its dependence on hemodynamic and technical factors

[d]At a Nyquist limit of 50–60 cm/s

[e]Baseline shift with Nyquist limit of 28 cm/s

[f]Other conditions may cause systolic blunting (e.g., atrial fibrillation, elevated RA pressure)

Pulsed-wave Doppler examination of the hepatic veins helps corroborate the semiquantitative assessment of TR severity. With increasing severity of TR, the normally dominant systolic wave is blunted, culminating in systolic flow reversal with severe TR (Fig. 9.4). Hepatic vein flow pattern, however, is also affected by several conditions including abnormalities in RA and RV compliance, respiratory effort, preload, and atrial fibrillation. These factors need to be taken into consideration during interpretation.

Generally, transthoracic echocardiography permits adequate visualization of all the leaflets, allows appropriate interrogation of and alignment with the regurgitant jet, and accurate assessment of the etiology and severity of the lesion. For the most part, transesophageal echocardiography, though possible, is not indicated for assessment of this lesion unless the image quality of the transthoracic study is suboptimal. An integration of the data from the different views and modalities enhances the accuracy of evaluating the etiology and severity of TR.

Tricuspid Stenosis

Tricuspid stenosis is a relatively rare disorder. It is most often a result of rheumatic disease. The leaflets appear thickened and with restricted motion secondary to commissural fusion, leading to a relatively fixed orifice. Diastolic doming of the leaflets is typical of rheumatic involvement. Due to the increased gradient across the valve, the right atrium is enlarged. In severe cases that are still in sinus rhythm, there may be prominent reversal of flow in the inferior vena cava during atrial systole.

Etiology

Rheumatic

Involvement of the TV is almost always in association with rheumatic mitral and aortic involvement, and seldom occurs as an isolated finding. Rheumatic tricuspid stenosis occurs in 10–15% of patients with rheumatic heart disease. Hemodynamically significant tricuspid stenosis is rare. Functionally significant tricuspid regurgitation is present in at least half the cases.

Carcinoid

Carcinoid is the second most common etiology of tricuspid stenosis and is invariably associated with regurgitation, as discussed earlier. The carcinoid plaques are present on both the atrial and the ventricular surfaces of the valve. The thickened and rigid leaflets appear fixed in the open position. Similar findings are seen with drug-related tricuspid stenosis.

Eosinophilic

Eosinophilic myocarditis (both tropical and nontropical or Loeffler's) usually presents as a combined lesion with tricuspid stenosis and regurgitation. There is involvement of the chordae in addition to the valve leaflets. Similar findings are seen with significant eosinophilia from other causes such as parasite infestation, leukemia, or conditions of hypersensitivity.

Metabolic and Others

Metabolic abnormalities such as Fabry's disease, Whipple's disease, and methysergide toxicity can cause endocardial fibrosis and are among the rarer etiologies of tricuspid stenosis. A right atrial mass such as a large tumor, thrombus, TV vegetations, or thrombus in transit from the venous bed can cause RV inflow stenosis and may simulate tricuspid stenosis. Gradients with these conditions, however, are rarely very high.

Assessment of Severity

The sequelae of significant tricuspid stenosis are clinically readily apparent (peripheral edema and limitations in functional class). While clinical evaluation is essential in the management of tricuspid stenosis, 2D and Doppler examination help document the valvular hemodynamics. Indirect parameters of significant tricuspid stenosis include enlarged right atrial size and plethoric vena cava and hepatic veins, with preservation of RV size and function. However, these signs are not specific for tricuspid stenosis. Imaging of the stenotic valve – essential in evaluating its morphology and etiology – is poorly predictive of its severity. Doming of the anterior leaflet and/or significant restriction of

valvular motion is a prerequisite to the presence of a hemodynamically significant lesion. Thickening and restriction of the posterior leaflet can be seen with milder lesions. Direct planimetry of the tricuspid valve area, unlike for the mitral valve, is more difficult to accomplish. This is due to suboptimal cross-sectional alignment of the imaging plane consequent to the position and orientation of the TV. With the advent of real-time 3D echocardiography, determination of valve area may be feasible in the near future.

Similar to other valves, Doppler echocardiography is currently the noninvasive technique of choice to evaluate the hemodynamic severity of tricuspid stenosis (Fig. 9.5). Spectral Doppler detects an increase in velocity across the valve that is proportional to the gradient. As in other valves, the transvalvular gradient can be estimated from the velocities recorded by Doppler using the modified Bernoulli equation (Gradient = $4v^2$). With worsening severity of stenosis, the TV gradient is higher. However, mean gradient is also dependent on heart rate and cardiac output, physiologic variables that have to be taken into consideration when assessing severity of stenosis. Under conditions of normal heart rate and cardiac output, a mean gradient greater than 8–10 mmHg usually denotes severe stenosis.

There are no standards for estimation of tricuspid valve area with the Doppler technique. Using continuous-wave Doppler, a progressive decrease in the deceleration rate of tricuspid inflow is seen with worsening severity of stenosis. Although the concept of pressure half-time method is theoretically valid to assess tricuspid stenosis severity, it is limited by the lack of a validated constant, unlike for the mitral valve. Furthermore, respiratory variation in this parameter is more prominent through the tricuspid valve. Simple application of the mitral constant in the formula (220 ms) has led to varying results. In the rare patient with tricuspid stenosis without regurgitation, it is possible to estimate the stenotic valve area using the continuity equation as: systemic stroke volume divided by the time velocity integral of the stenotic jet. Systemic stroke volume can be determined at the left ventricular outflow or by another method.

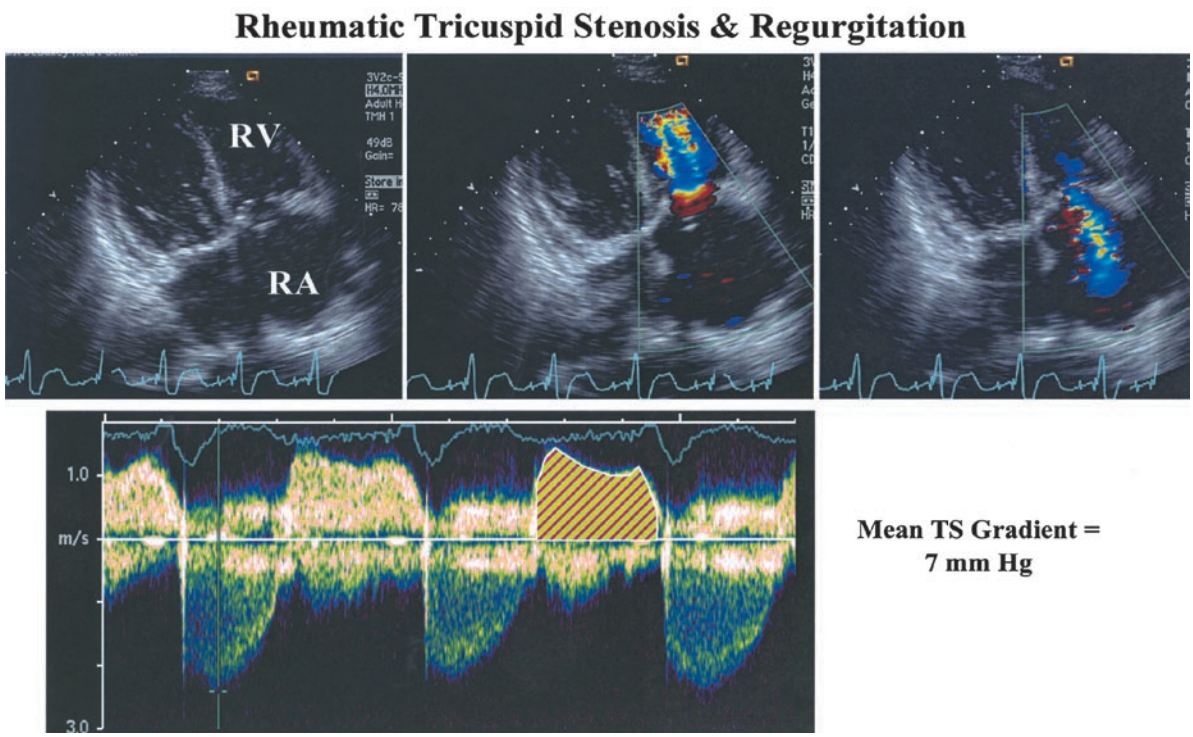

Fig. 9.5 An example of a patient with moderately severe tricuspid stenosis and mild tricuspid regurgitation. The etiology is rheumatic; the patient already had a mitral valve repair. Note the increased diastolic velocities across the tricuspid valve. The mean gradient is 7 mmHg

Pulmonic Valve

The pulmonic valve is a semilunar valve with three cusps (anterior, right posterior, and left posterior) similar to the aortic valve but positioned more superior, leftward, and anterior. Imaging of the pulmonic valve with echocardiography can often be challenging due to interposition of the overlying lungs and the relatively horizontal course of the right ventricular outflow tract. To help imaging, the patient is placed in the left lateral position and imaged during held expiration. Parasternal short-axis view at the aortic valve level and apical or subcostal views of the right ventricular outflow tract are utilized to visualize the valve.

Pulmonic Stenosis

Pulmonic stenosis and right ventricular outflow tract lesions occur in up to 30% of all patients with congenital heart disease. Pulmonic stenosis is invariably congenital in etiology. This is generally classified as supravalvular, subvalvular, or valvular. Supravalvular stenosis involves narrowing of the main pulmonary artery, its bifurcation or distal (peripheral) branches. This may occur in isolation but more commonly keeps the company of valvular pulmonic stenosis and other congenital lesions such as ventricular septal defect, atrial septal defect, patent ductus arteriosus, or tetralogy of Fallot. Subvalvular stenosis may be infundibular or subinfundibular. Invariably it is associated with a ventricular septal defect and seldom occurs as an isolated lesion.

Valvular pulmonic stenosis is congenital in the vast majority and accounts for 10–12% of congenital heart disease in the adult. When acquired, it is the consequence of scarring from trauma, endocarditis, carcinoid, or rheumatic heart disease. This may be accompanied, among other congenital lesions, by a ventricular septal defect or transposition of the great vessels. There is seldom calcification of the valve despite stenosis. There may be evidence of commissural fusion or a bicuspid valve. The leaflets appear thickened and have a systolic bowing motion. The prognosis is benign, with the diagnosis occasionally being missed until adulthood. Patients are generally asymptomatic, but may complain of dyspnea on exertion or easy fatigability, occasionally atypical chest pain or syncope. In severe pulmonic stenosis, right heart failure eventually may occur. If the foramen ovale is patent, there may be intermittent or continuous right to left shunting across it, with attendant cyanosis and clubbing. Pulmonic stenosis may occur as part of genetic syndromes (Noonan, Williams, Trisomy 13, 15 and 18); rarely, this can be the stigmata of congenital Rubella syndrome.

Assessment of Severity

Dilation of the mid and distal part of the main pulmonary artery on a 2D echo examination may be the first hint that leads a sonographer to pursue the diagnosis of pulmonic valve stenosis (Fig. 9.6). In moderate to severe cases, there may be evidence of RV hypertrophy and RV dilation with paradoxical septal motion suggestive of RV pressure overload (septum remains flattened in systole and diastole). In these cases, the RA may also be enlarged. By color Doppler there is evidence of flow acceleration proximal to the valve, just distal to the valve the jet reaches its narrowest point and then appears to expand again. With increasing severity of stenosis, the velocity and the turbulence increase, and the flow is directed more toward the left pulmonary artery. Pulsed-wave Doppler reveals increased systolic velocity that is confirmed by continuous-wave Doppler. The latter permits evaluation of the peak and mean systolic gradients and hence estimate the severity of the stenosis. While interrogation of the jet is quite feasible from the short-axis view, due to the relatively horizontal position of the RV outflow tract, a subcostal approach is also recommended. Longstanding pulmonic stenosis is likely to be associated with significant right ventricular hypertrophy that may manifest as dynamic infundibular obstruction. On Doppler examination, this has the classic dagger-shaped contour with late peaking in systole. If present, differentiation from the fixed obstruction may be difficult and may lead to an overestimation of the true transvalvular gradient, unless two distinct jets, with different characteristics (early and late peaking), are recorded.

The transvalvular gradient, estimated with the modified Bernoulli equation, is an accurate measure of severity. Exception is in reduced flow through the pulmonic valve such as in cases of low output,

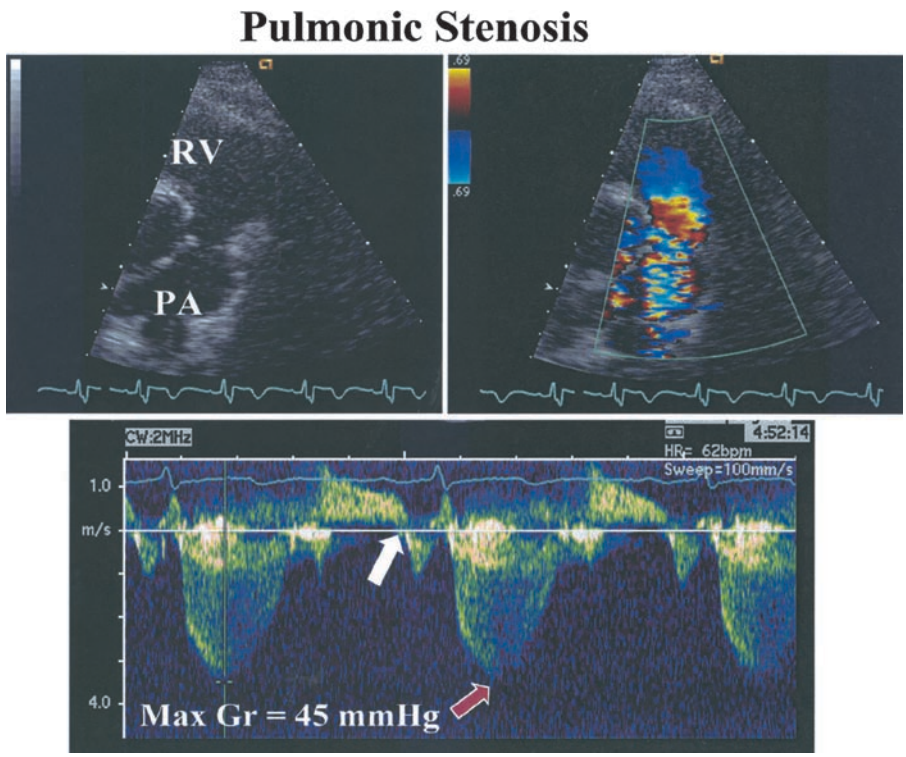

Fig. 9.6 An example of a patient with moderately severe pulmonic stenosis. There is post stenotic dilatation of the main pulmonary artery. Continuous-wave Doppler recording reveals a maximal gradient of 45 mm Hg. Flow also shows premature opening of the pulmonic valve with early termination of pulmonic regurgitation flow (*white arrow*) after atrial contraction (P wave on the ECG)

severe right heart failure, or concomitant severe TR. In these cases, valve area may be estimated using the continuity equation, although this is not well validated. Generally a peak transvalvular gradient under 25 mmHg is considered to be a mild lesion with a less than 5% chance of need for valvulotomy. Moderate lesions have a peak gradient of 25–50 mmHg and a 20% chance of requiring intervention (Fig. 9.6). A maximal gradient greater than 50 mm Hg usually denotes severe pulmonic stenosis. If there is concomitant significant pulmonic regurgitation, maximal gradient may overestimate the severity of stenosis.

Echocardiography has a significant role in timing and identifying candidates for balloon valvulotomy and in the follow-up of patients after the procedure. Indications for a balloon or surgical valvulotomy include symptoms attributable to the stenosis, peak gradient greater than 50 mmHg, intermittent cyanosis, RV systolic pressure greater than 100 mmHg, even without symptoms of RV failure. For gradients between 35 and 50 mmHg, strategies have to be individualized. Patients with markedly thickened leaflets and a small pulmonic annulus are less likely to respond to valvulotomy. After intervention, echocardiography can also assess whether a residual gradient is present and if it is due to infundibular hypertrophy alone. The latter will ultimately regress.

Pulmonic Regurgitation

Minor degrees of pulmonary regurgitation (PR) using Doppler techniques have been reported in close to 75% of individuals with normal pulmonic valves and no other evidence of structural heart disease. PR may also be congenital or acquired (Table 9.3). Congenital lesions are associated with thick and deformed leaflets. On the other hand, acquired PR may be organic or functional. In the adult, acquired PR is most often seen in patients with pulmonary hypertension. PR in this condition, however, is rarely severe. Organic significant

Table 9.3 Etiology of pulmonic regurgitation

Normal Individuals (Trivial or mild degree)
Pulmonary hypertension (primary or secondary)
Diseases of the Pulmonic valve
• After infundibulectomy or valvulotomy for tetralogy of Fallot
• After valvuloplasty or valvulotomy for pulmonic stenosis
• Carcinoid heart disease
• Infective endocarditis
• Trauma
• Idiopathic pulmonary artery dilation
• Rheumatic heart disease

PR is infrequent and is usually seen following pulmonic valvulotomy. Other rare etiologies include endocarditis, carcinoid, rheumatic, myxomatous degeneration, tertiary syphilis, or trauma. Because of the difficulties imaging the pulmonary valve and the low prevalence of severe, life-threatening PR, few validation studies have been conducted to quantitatively evaluate the severity of PR by any modality. Recommendations from the American Society of Echocardiography and other organizations have been recently published for the evaluation of PR and will be hereby reviewed.

Assessment of Severity

Two-dimensional echocardiography is important in the overall evaluation of the etiology and severity of PR. Identification of anatomic abnormalities associated with PR, motion of the valve (doming or prolapse) or structure (hypoplasia or absence of the pulmonary valve) may help define the mechanism of regurgitation and yield clues to its severity. Visualization of the entire pulmonary valve is difficult. However, evaluation of the size and function of the RV in the absence of pulmonary hypertension provides an indirect indicator to the significance of PR and adaptation of the RV to the volume overload.

Color Doppler

Color Doppler flow mapping is the most commonly used method to assess PR. A diastolic jet in the RV outflow tract emanating from the valve and directed toward the RV is diagnostic of PR (Fig. 9.7). Color Doppler can determine the jet size and its spatial orientation. Similar to other regurgitant lesions, several factors affect the size of the jet, including the regurgitant volume and the driving pressure – here namely pulmonary pressure. The PR jet seen in normal pulmonic valves, considered a variation of normal, is usually very small and thin, and originates centrally at the site of leaflet coaptation (Fig. 9.7). Jet length, although one of indicator of severity, is not very reliable (jets < 10 mm in length are trivial, particularly if they are narrow at the origin). Planimetry of jet areas, indexed for body surface area, has been shown to relate to PR severity, but also has a significant degree of variability.

Similar to all regurgitant lesions, the width of the vena contracta is probably a more accurate method to evaluate the severity of PR. Vena contracta measurements however have not been validated for the pulmonic valve, although some investigators have used the method for the serial assessment of pulmonary homografts. In cases of severe PR, the color jet area may be brief and misleading. This is due to early diastolic equalization of diastolic pulmonary artery and RV pressures and almost cessation of regurgitant flow across the pulmonic valve. The large width of the vena contracta and the characteristic findings by spectral Doppler (see later), however, alert the echocardiographer to the severe degree of PR (Fig. 9.7).

Continuous-Wave Doppler

Recording of PR jet velocity can allow the estimation of mean or diastolic pulmonary pressures. There is no clinically accepted method of quantitating PR severity with continuous-wave Doppler. The density of the signal, which relates to the number of regurgitant red cells, provides a qualitative measure of regurgitation. A rapid deceleration rate, while consistent with more severe PR, is influenced by several factors including RV diastolic properties and pressures. In severe PR, a rapid equalization of RV and pulmonary artery pressures can occur before the end of diastole. An intense signal of "to and fro" flow simulating a sine wave can be seen (Fig. 9.7). This finding, however, is not specific for severe PR, as it can be observed in patients with low pulmonary pressure and/or elevated RV diastolic pressure. For differentiating these entities, one has to evaluate the intensity of the PR signal, the color Doppler characteristics of the jet, and pulmonic flow quantitation in the RV outflow tract by pulsed-wave Doppler.

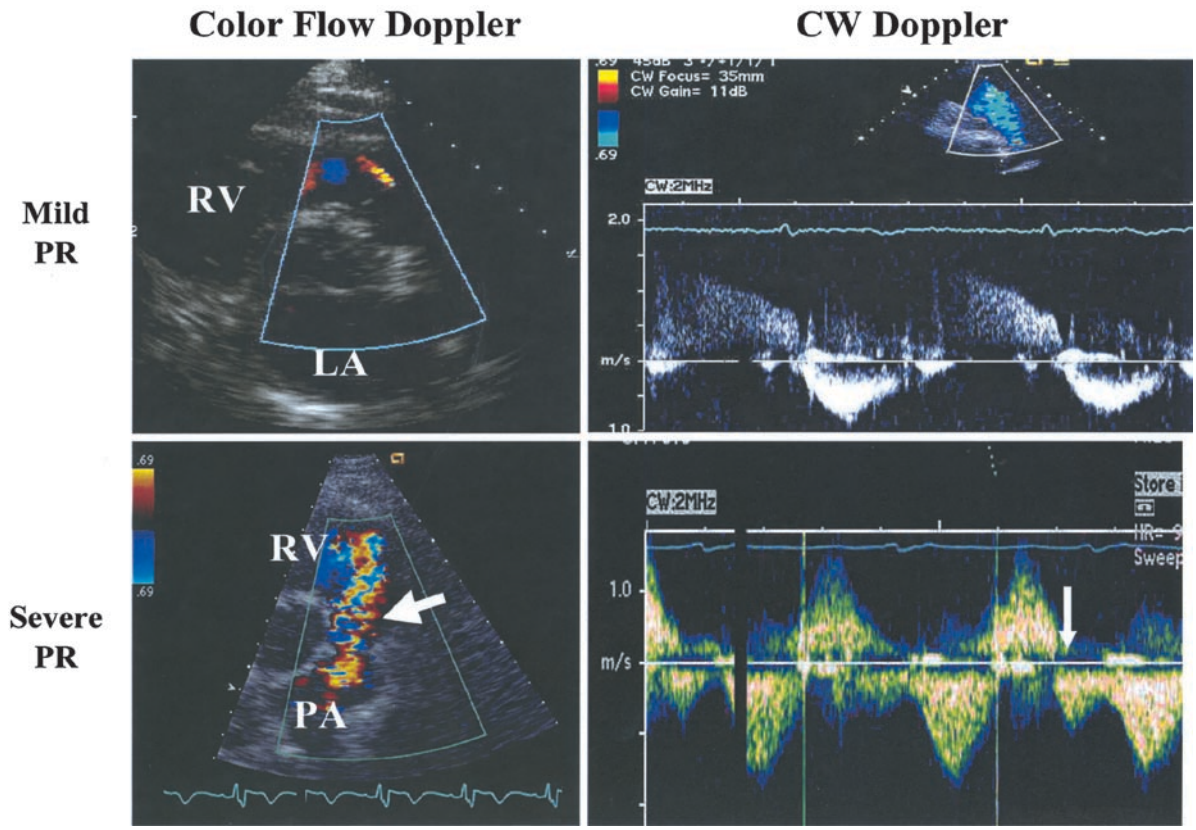

Fig. 9.7 Examples of mild and severe pulmonic regurgitation. In mild PR, a very thin diastolic color jet is seen. The continuous-wave Doppler recording is soft, barely detected. In severe PR, the color jet width at its origin is large (*large arrow*). The spectral recording is intense and shows a steep deceleration in diastole with early termination of diastolic flow (*arrow*). *RV* right ventricle; *LA* left atrium; *PA* pulmonary artery

Pulsed Doppler

Pulsed Doppler evaluation of flow velocity in the RV outflow, just below the pulmonic annulus, and in the pulmonary artery, is useful in evaluating PR severity. In the pulmonary artery, comparison of forward and reverse flows and respective time-velocity integrals by pulsed Doppler have been used to calculate regurgitant volume and regurgitant fraction with variable success. This method, however, is not valid in patients with pulmonic stenosis because of the turbulent flow in the pulmonary artery. On the other hand, stroke volume can be measured in the RV outflow, just below the pulmonic valve, and compared to measurements of stroke volume at other annular sites (aortic, mitral). Stroke volume is derived, as is routinely performed by pulsed Doppler, as cross-sectional area of flow multiplied by the time-velocity integral of flow. Cross-sectional area of the pulmonic annulus is derived from its diameter assuming a circular geometry as: $\pi d^2/4$. The pulmonic annulus may be difficult to measure because of poor visualization and the dynamic size of the RV outflow tract. It is recommended to measure the pulmonic annulus during early ejection (two to three frames after the R wave on the ECG), just below the pulmonic valve. Although not validated for quantitation of PR, flows at the pulmonic annulus can be compared to other sites to derive quantitative parameters of regurgitation (regurgitant volume and fraction). Clinically, this is feasible provided that particular attention is taken to image well the area of the pulmonic annulus and thus minimize errors.

A comprehensive approach to the evaluation of PR severity is suggested (Table 9.4), similar to other valvular regurgitation, as recently recommended by the American Society of Echocardiography and other organizations. Since there are insufficient data on quantitation of PR to recommend a clinically validated quantitative approach, the evaluation is generally qualitative and should include the various parameters discussed earlier. Since the main pulmonary artery is an

Table 9.4 Echocardiographic and Doppler parameters useful in grading pulmonary regurgitation severity

Parameter	Mild	Moderate	Severe
Pulmonic valve	Normal	Normal or abnormal	Abnormal
RV size	Normal[a]	Normal or dilated	Dilated[b]
Jet size by color Doppler[c]	Thin (usually <10 mm in length) with a narrow origin	Intermediate	Usually large, with a wide origin; may be brief in duration
Jet density and deceleration rate – CW[e]	Soft; slow deceleration	Dense; variable deceleration	Dense; steep deceleration, early termination of diastolic flow
Pulmonic systolic flow compared to systemic flow – PW[d]	Slightly increased	Intermediate	Greatly increased

Reproduced with permission from the American Society of Echocardiography

CW Continuous-wave Doppler; *PR* pulmonic regurgitation; *PW* pulsed-wave Doppler; *RA* right atrium; *RF* regurgitant fraction; *RV* right ventricle

[a]Unless there are other reasons for RV enlargement. Normal 2D measurements from the apical four-chamber view: RV mediolateral end-diastolic dimension ≤ 4.3 cm, RV end-diastolic area ≤ 35.5 cm^2

[b]Exception: acute PR

[c]At a Nyquist limit of 50–60 cm/s

[d]Cut-off values for regurgitant volume and fraction are not well validated

[e]Steep deceleration is not specific for severe PR

anterior structure, it is often imaged as well or even better with transthoracic echocardiography compared to the transesophageal approach. Therefore, the role of transesophageal echocardiography is limited in assessing severity of pulmonic regurgitation.

Conclusion

Currently, two-dimensional echocardiography with Doppler is an essential diagnostic tool for the evaluation of patients with diseases of the tricuspid or pulmonic valves. Structural evaluation of the valves, along with imaging of the cardiac chambers, provides the underlying etiology of the valvular disease and cardiac adaptation to the stenotic and /or regurgitant lesion. Transesophageal echocardiography is rarely needed in right-sided valvular heart disease. While quantitative parameters for the evaluation of tricuspid and pulmonic regurgitation are not as widely validated compared to mitral or aortic disease, an integrative approach of 2D imaging, color, and spectral Doppler findings usually suffices for the assessment of the etiology and severity of the valvular disease and for guiding management.

Bibliography

Brickner ME, Hills LD, Lange RA. Congenital heart disease in adults. *N Engl J Med*. 2000;342:256.

DePace NL, Ross J, Iskandrian AS, et al. Tricuspid regurgitation: noninvasive techniques for determining causes and severity. *J Am Coll Cardiol*. 1984;3:1540.

Goldberg SJ, Allen HD. Quantitative assessment by Doppler echocardiography of pulmonary or aortic regurgitation. *Am J Cardiol*. 1985;56:131.

Nagueh SF, Kopelen HA, Zoghbi WA. Relation of mean right atrial pressure to echocardiographic and Doppler parameters of right atrial and right ventricular function. *Circulation*. 1996;93:1160.

Parris TM, Panidis IP, Ross J, et al. Doppler echocardiographic findings in rheumatic tricuspid stenosis. *Am J Cardiol*. 1987;60:1414.

Quinones MA, Otto CM, Stoddard M, et al. Recommendations for quantification of Doppler echocardiography: a report from the Doppler Quantification Task Force of the Nomenclature and Standards Committee of the American Society of Echocardiography. *J Am Soc Echocardiogr*. 2002;15:167.

Shapira Y, Porter A, Wurzel M, et al. Evaluation of tricuspid regurgitation severity: echocardiographic and clinical correlation. *J Am Soc Echocardiogr*. 1998;11:652.

Takao S, Miyatake K, Izumi S, et al. Clinical implications of pulmonary regurgitation in healthy individuals: detection by cross sectional pulsed Doppler echocardiography. *Br Heart J*. 1988;59:542.

Tribouilloy CM, Enriquez-Sarano M, Bailey KR, et al. Quantification of tricuspid regurgitation by measuring the width of the vena contracta with Doppler color flow imaging: a clinical study. *J Am Coll Cardiol*. 2000;36:472.

Waller BF, Howard J, Fess S. Pathology of tricuspid valve stenosis and pure tricuspid regurgitation – part III. *Clin Cardiol*. 1995;18:225.

Yamachika S, Reid CL, Savani D, et al. Usefulness of color Doppler proximal isovelocity surface area method in quantitating valvular regurgitation. *J Am Soc Echocardiogr*. 1997;10:159.

Zoghbi WA, Sarrano ES, Foster E, et al. Recommendations for evaluation of the severity of native valvular regurgitation with two-dimensional and Doppler echocardiography. A report from the American Society of Echocardiography's Nomenclature and Standards Committee and Task Force on Valvular Regurgitation. *J Am Soc Echocardiogr*. 2003;16:777.

Chapter 10
Pulmonary Hypertension Clinical Echocardiography

J. Simon R. Gibbs, Alexander Stefanidis, and Wei Li

Clinical Background

Pulmonary vascular disease is usually progressive and untreated has a poor prognosis. The natural history and course of the disease exhibits wide variation between individuals.

Patients with pulmonary hypertension present at any age with nonspecific symptoms including breathlessness (the most common symptom), syncope, tiredness, angina, and exercise-induced cough and nausea. The correct diagnosis is frequently delayed and bronchial asthma is the most frequent misdiagnosis. A chest radiograph (Fig. 10.1) and ECG (Fig. 10.2) will be abnormal in 80–90% of patients, and echocardiography is the first line of investigation in reaching a diagnosis in a patient where pulmonary hypertension is suspected or who has "unexplained" breathlessness.

Once pulmonary hypertension is confirmed, echocardiography is used in conjunction with other imaging modalities, lung function tests, and cardiac catheterization to determine the etiology, severity, and prognosis. The advent of new therapies for selected patients with pulmonary hypertension has increased the need for accurate diagnosis and serial monitoring of hemodynamics and right ventricular function, which inform the management of these disease-targeted therapies.

The clinician requesting an echocardiogram for the first time will want to know whether pulmonary hypertension is present. If pulmonary hypertension is present they will need to be told the cause (if detectable by echocardiography) and severity of both pulmonary hypertension and right ventricular dysfunction. At follow-up the clinician will want to know whether there is evidence of hemodynamic improvement or deterioration and also about the development of complications. Although other imaging modalities are used in the management of pulmonary hypertension, echocardiography is the most readily available for frequent serial monitoring and managing patients who present with acute hemodynamic decompensation.

J.S.R. Gibbs (✉)
Department of Cardiology, Imperial College London and Hammersmith Hospital, Du Cane Road, London, W12 0HS, UK
e-mail: gibbs@imperial.ac.uk

Pathophysiology

Pulmonary hypertension may occur as a consequence of raised pulmonary vascular resistance or high cardiac output. In the absence of pulmonary vascular disease, pulmonary hypertension will resolve when a high cardiac output returns to normal. Raised pulmonary vascular resistance may occur as a consequence of precapillary pulmonary arterial disease, postcapillary disease (pulmonary venous disease or left heart disease), or a combination. The development and progression of pulmonary hypertension is related to pulmonary vasoconstriction, thrombosis, and inappropriate smooth muscle cell proliferation.

The heart responds to the high resistance by increasing pulmonary arterial pressure to maintain the cardiac output. Since right ventricular function is afterload dependant, this results in right ventricular hypertrophy and dilatation. The change in geometry of the right ventricle and its contractile properties eventually lead to right ventricular failure. There follows a fall in cardiac output and a rise in right atrial pressure. Significant tricuspid regurgitation may develop and this increases the ventricular volume overload thus accelerating the

P. Nihoyannopoulos and J. Kisslo (eds.), *Echocardiography*,
DOI: 10.1007/978-1-84882-293-1_10,

progression of right ventricular failure. The rate of decline in right ventricular function depends on the age of onset of the disease, the rate of increase in pulmonary vascular resistance, the cause of pulmonary hypertension (e.g., scleroderma is associated with worse right ventricular function compared to idiopathic for a given pulmonary arterial pressure), and comorbid factors.

Death occurs as a consequence of right ventricular disease, either suddenly as a consequence of mechanical syncope or arrhythmia, or from progressive right ventricular failure.

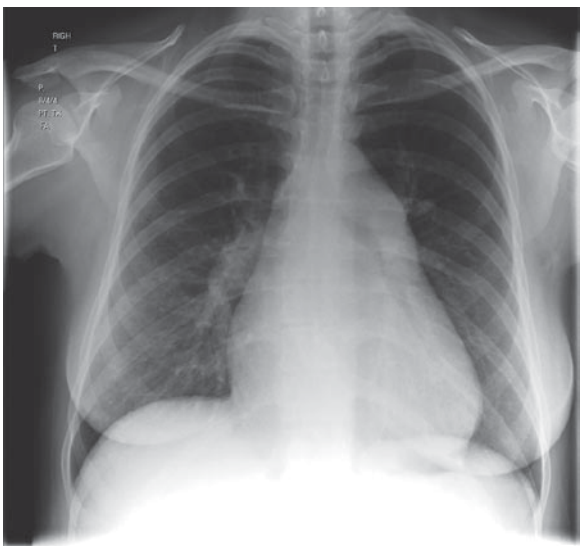

Fig. 10.1 A typical chest radiograph of a patient presenting with idiopathic pulmonary arterial hypertension. There is enlargement of the pulmonary trunk and proximal pulmonary arteries. The heart is enlarged. The lung fields are clear

Clinical Classification

There are numerous causes of pulmonary hypertension and these are shown in Table 10.1. This classification not only groups diseases which cause pulmonary hypertension by similar pathophysiological mechanisms and clinical presentation but also provides a guide to therapy. The term "primary" pulmonary hypertension has been superseded by idiopathic and familial pulmonary arterial hypertension. Familial pulmonary hypertension includes those with a family history as well as patients known to carry a mutation of the bone morphogenetic protein receptor 2 gene.

The importance of reaching an accurate diagnosis is exemplified by patients with pulmonary arterial hypertension who benefit from disease-targeted therapies including prostacyclin analogs, endothelin antagonists,

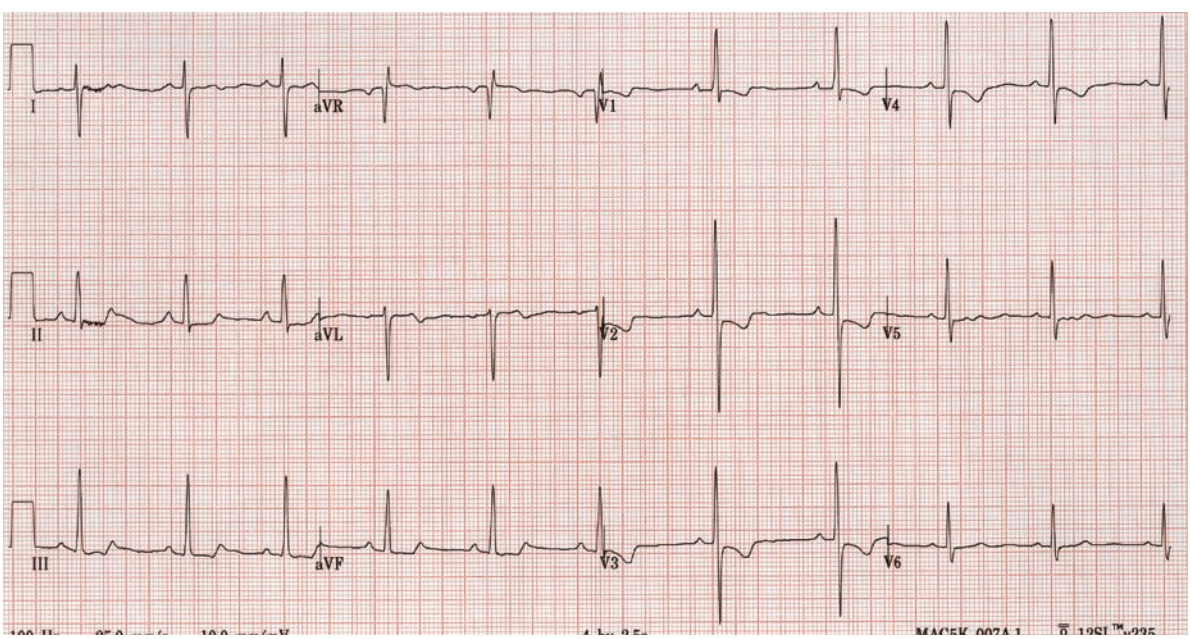

Fig. 10.2 An ECG taken in a patient with idiopathic pulmonary arterial hypertension. Note the signs of right ventricular hypertrophy with a rightward mean frontal QRS axis

Table 10.1 Clinical classification of pulmonary hypertension

1. Pulmonary arterial hypertension (PAH)
   - Idiopathic (IPAH)
   - Familial (FPAH)
   - Associated with (APAH)
     - Collagen vascular disease
     - Congenital systemic to pulmonary shunts
     - Portal hypertension
     - HIV infection
     - Drugs and toxins (e.g., fenfluramine, dexfenfluramine)
     - Other (Thyroid disorders, glycogen storage disease, Gaucher's disease, hereditary hemorrhagic telangiectasia, hemoglobinopathies, myeloproliferative disorders, splenectomy)
   - Associated with significant venous or capillary involvement
     - Pulmonary veno-occlusive disease
     - Pulmonary capillary hemangiomatosis
   - Persistent pulmonary hypertension of the newborn
2. Pulmonary hypertension with left heart disease
   - Left-sided atrial (e.g., cor triatriatum, myxoma) or ventricular disease
   - Left-sided valvular heart disease
3. Pulmonary hypertension associated with lung diseases and/or hypoxemia
   - Chronic obstructive pulmonary disease
   - Interstitial lung disease
   - Sleep disordered breathing
   - Alveolar hypoventilation disorders
   - Chronic exposure to high altitude
   - Developmental abnormalities
4. Pulmonary hypertension due to chronic thrombotic and/or embolic disease
   - Thromboembolic obstruction of proximal pulmonary arteries
   - Thromboembolic obstruction of distal pulmonary arteries
   - Nonthrombotic pulmonary embolism (tumor, parasites, foreign material)
5. Miscellaneous
   - Sarcoidosis, histiocytosis X, lymphangiomatosis, compression of pulmonary vessels (adenopathy, tumor, fibrosing mediastinitis)

and phosphodiesterase inhibitors, whereas in patients with pulmonary venous hypertension these drugs may have a deleterious effect.

Patients with pulmonary arterial hypertension who sustain a fall in mean pulmonary artery pressure ≥10 mm Hg to reach an absolute value ≤40 mm Hg, without a fall in cardiac output when challenged with short-acting pulmonary vasodilators may benefit from calcium channel blockers. Cardiac catheterization is required to detect such patients, and this cannot be reliably achieved using echocardiography.

Patients with proximal chronic thromboembolic pulmonary hypertension should be considered for pulmonary endarterectomy since this operation may be curative for a group of patients with a particularly poor prognosis.

Prognosis

The prognosis of pulmonary hypertension is determined by the etiology, and clinical and hemodynamic severity. For patients with idiopathic pulmonary arterial hypertension 1-year survival has been improved by intravenous epoprostenol (an analog of prostacyclin) from 77% (based on historic controls) to 85–88%, 3-year survival from 41 to 63%, and 5-year survival from 27 to 54–55%. It is expected that this will improve in the near future with newer therapies. The best hemodynamic predictors of prognosis are based on measures of cardiac output and right ventricular failure.

Role of Echocardiography in Pulmonary Hypertension

Screening for Pulmonary Hypertension

Definition of Pulmonary Hypertension

The gold standard definition of pulmonary hypertension is based on the measurement of *mean* pulmonary arterial pressure at cardiac catheterization (Table 10.2). A diagnosis of pulmonary arterial hypertension requires in addition a pulmonary vascular resistance > 3 Wood units with a normal pulmonary capillary wedge pressure.

Table 10.2 Definitions of Pulmonary hypertension

Cardiac catheterization
Pulmonary hypertension is present when the mean pulmonary artery pressure at rest is 25 or 30 mm Hg on exercise
Echocardiographic
Mild pulmonary hypertension is defined by the World Health Organization as a systolic pulmonary artery pressure of 40–50 mmHg, which corresponds to a tricuspid regurgitant velocity on Doppler echocardiography of about 3.0–3.5 m/s

The echocardiographic correlate of pulmonary hypertension is based on tricuspid regurgitation which is used to estimate *systolic* pulmonary arterial pressure. The limitations of using tricuspid regurgitation are discussed later (Tricuspid regurgitation and estimated systolic pulmonary arterial pressure). For these reasons there is no absolute cut-off value for the diagnosis of pulmonary hypertension by echocardiography.

In patients without tricuspid regurgitation, qualitative measurements of pulmonary arterial pressure can be derived from time intervals measured from the

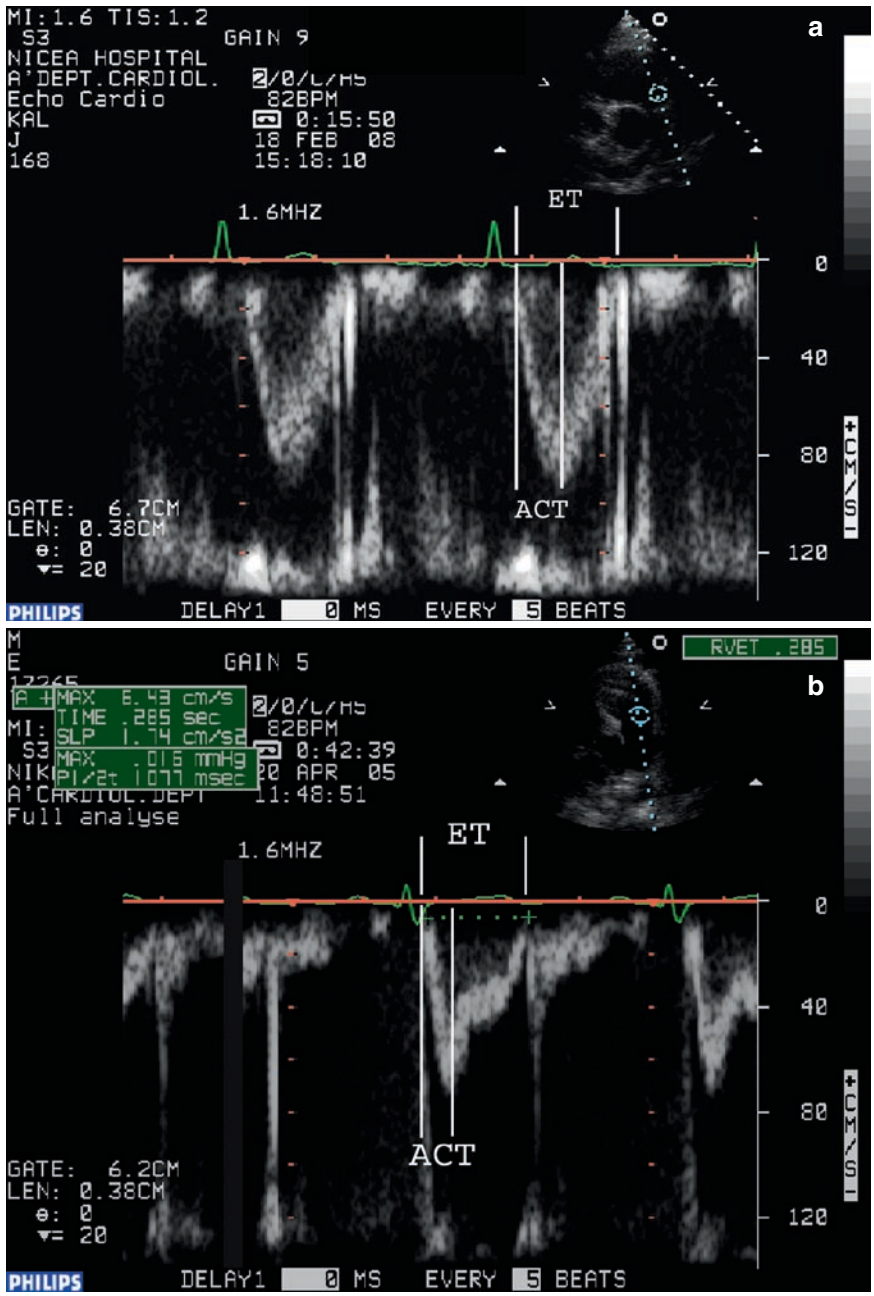

Fig. 10.3 Measurement of pulmonary acceleration time from the pulsed-wave Doppler tracing of pulmonary arterial flow. The shortened acceleration time in pulmonary hypertension is compared to a normal tracing. (**a**) Normal pulmonary Doppler velocity spectrum. (**b**) Pulmonary Doppler velocity spectrum in patient with pulmonary hypertension showing a very short acceleration time (ACT) and short total ejection time (ET) as compared to normal

Doppler flow velocities obtained in the pulmonary trunk. The measurements that have been used include the pre-ejection period, which is the time interval from the onset of electrocardiographic QRS to the onset of pulmonary artery systolic flow; the acceleration time, which is the time between the onset of flow to the peak systolic flow; and ejection time, which is the time interval between the onset to the cessation of flow. Pulmonary flow acceleration time is the most reliable of these and is a marker of increased pulmonary vascular resistance when it is less than one-third of the ejection time (Fig. 10.3). In clinical practice, pulmonary acceleration time is commonly used to demonstrate the raised pulmonary vascular resistance rather than to estimate the pulmonary artery pressure.

While severe pulmonary hypertension is normally a straightforward echocardiographic diagnosis, it is possible to miss mild cases especially when right ventricular function is preserved and the remainder of the echocardiographic examination at rest appears normal. In the presence of pulmonary hypertension right ventricular function may appear normal if the onset of pulmonary hypertension is slow enough to allow the right ventricle to compensate, and/or the pulmonary vascular resistance is less than 3.0 Wood units. For this reason it is important in suspected cases to ensure that the peak tricuspid regurgitant velocity and the pulmonary acceleration time are measured.

Other Signs to Look for

Any diagnosis based on a single measurement by echocardiography may be inaccurate, and the operator should look for other evidence for pulmonary hypertension. Table 10.3 lists the echocardiographic findings which may be elicited in the presence of pulmonary hypertension, and these should be sought to confirm the diagnosis. The main pulmonary artery is enlarged when it is the same diameter as or larger than the aorta (Fig. 10.4). Midsystolic closure of the pulmonary valve is a consequence of a reflected compression wave from the pulmonary circulation and is not present in normal subjects (Fig. 10.5).

Table 10.3 Common echocardiographic signs which may indicate the presence of pulmonary hypertension

Right ventricular hypertrophy
Right ventricular dilatation
Right ventricular dysfunction
Abnormal interventricular septal motion (septum moves with the right ventricle rather than with the left ventricle)
Dilated main pulmonary artery (Fig. 10.4)
Mid or early systolic closure of the pulmonary valve (Fig. 10.5)
Tricuspid regurgitant velocity increased
Dilated inferior vena cava

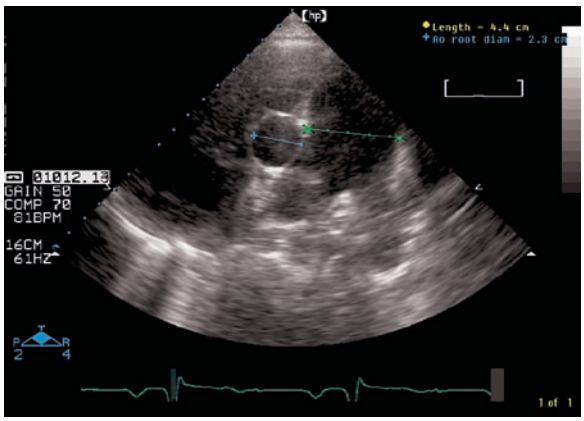

Fig. 10.4 Dilated main pulmonary artery (*red line* delineates diameter) in the left parasternal short-axis view compared to the diameter of the aorta (*blue line*)

Look first at the right ventricle and determine whether it is dilated and/or hypertrophied (Figs. 10.6 and 10.7). Note that dilatation and function of the right ventricle is dependant on the inotropic state and loading conditions. There is a rough inverse relationship between pulmonary artery pressure and systolic right ventricular ejection fraction in pulmonary hypertension.

Right ventricular dysfunction in the absence of measurable pulmonary hypertension may occur at a low cardiac output despite pulmonary vascular disease.

The differential diagnosis of right ventricular hypertrophy and dilatation includes pulmonary stenosis, pulmonary regurgitation, atrial septal defect, severe tricuspid regurgitation, right ventricular myopathy, right ventricular infarction, and infiltrative cardiomyopathy.

Estimation of Pulmonary Vascular Resistance

The measurement of pulmonary vascular resistance in pulmonary hypertension is used to differentiate between high cardiac output states where resistance is normal

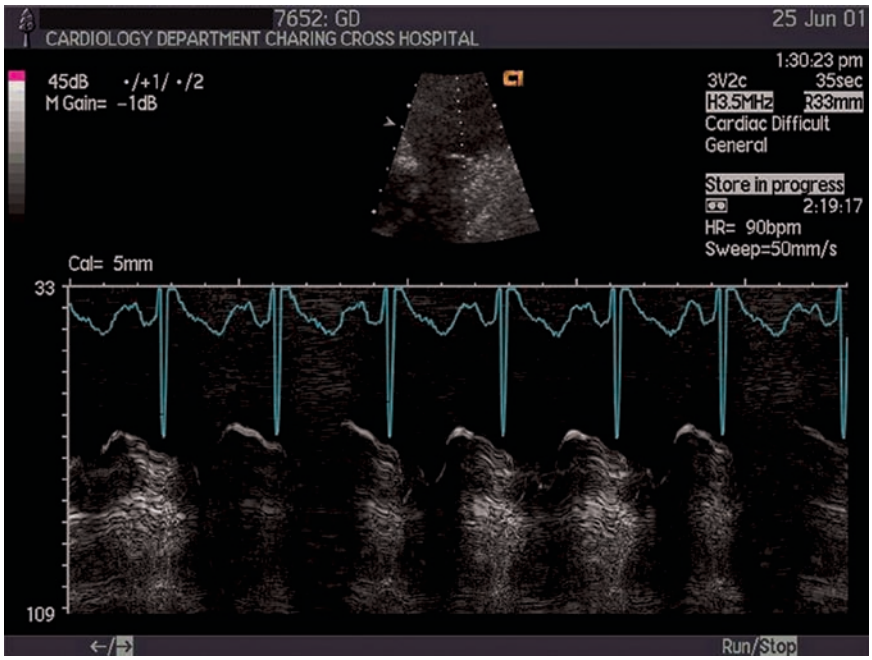

Fig. 10.5 Midsystolic closure of the pulmonary valve shown on M-mode echocardiogram. This is probably caused by a reflected pressure wave from the pulmonary circulation and may also be seen in the pulmonary arterial flow on Doppler

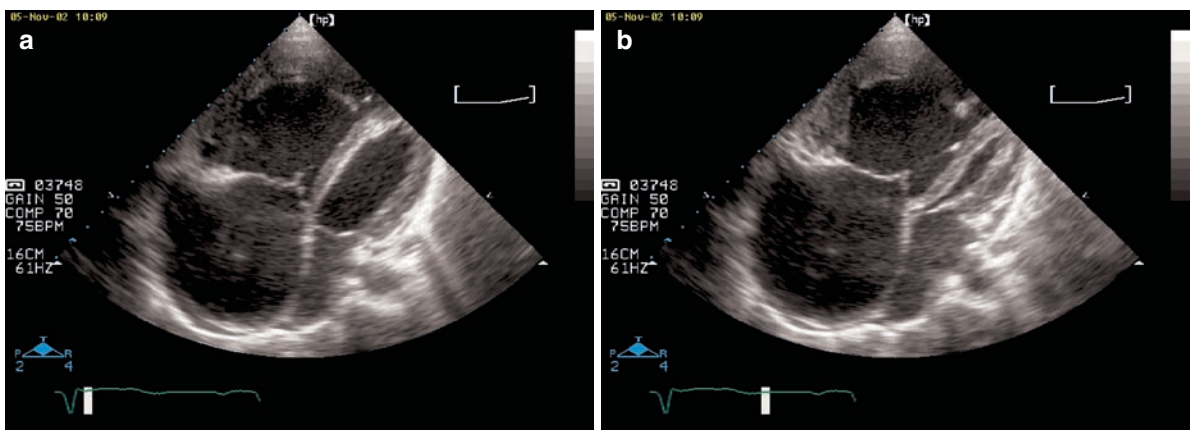

Fig. 10.6 Apical four-chamber view showing right ventricular dilatation in idiopathic pulmonary arterial hypertension in systole (**a**) and diastole (**b**). Note how the left ventricle is compressed by the right side

and pulmonary vascular disease where resistance is elevated. Pulmonary vascular resistance is normally measured at cardiac catheterization by dividing the transpulmonary pressure gradient by transpulmonary flow. Pulmonary vascular resistance can be estimated by echocardiography by taking the ratio of peak tricuspid regurgitant velocity to the right ventricular outflow tract velocity-time integral (TRV/VTI_{RVOT}). It is reported that a value less than 0.2 is likely to have a low pulmonary vascular resistance (<2 Wood units). This formula is valid for heart rates between 60 and 100 bpm.

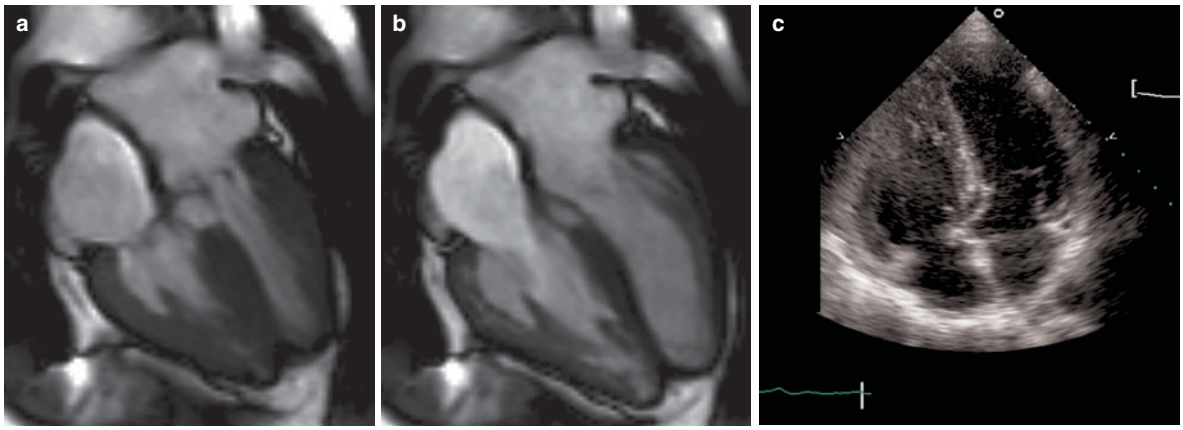

Fig. 10.7 Right ventricular hypertrophy caused by pulmonary hypertension in a patient with previous ostium primum repair. The hypertrophy is seen in a four-chamber view on magnetic resonance imaging in systole (**a**) and diastole (**b**), and echocardiography (**c**) in the same patient

Management of Mild Pulmonary Hypertension Detected by Echocardiography

Where there is doubt about the diagnosis of pulmonary hypertension or mild pulmonary hypertension is detected in asymptomatic individuals it is recommended that the patient be reviewed clinically in approximately 6 months and echocardiography repeated. In patients with symptoms cardiac catheterization is needed to confirm or refute the diagnosis. Patients who are asymptomatic but at high risk of developing pulmonary hypertension (e.g., the presence of risk factors such as family history, scleroderma, appetite suppressant use, portal hypertension, HIV infection, intravenous drug use) should have echocardiography repeated in 6 months. If the presence of mild pulmonary hypertension is confirmed, they should undergo the same evaluation as patients with symptomatic pulmonary hypertension.

Etiology of Pulmonary Hypertension

In conjunction with the history and physical examination, echocardiography should be used to establish presence or absence of congenital heart disease and left heart disease.

Congenital Heart Disease

In congenital heart disease, pulmonary arterial hypertension may be caused by a large left to right shunt, may occur in association with minor congenital heart lesions, and may occur postoperatively in a variety of circumstances. The common lesions which cause pulmonary hypertension are ventricular septal defect, atrioventricular septal defect, patent ductus arteriosus, aortopulmonary window, total or partial anomalous pulmonary venous return, univentricular heart, and large atrial septal defect. Where shunt reversal occurs or the shunt is bidirectional Eisenmenger's syndrome is present.

Some patients with small atrial septal defects (≤2 cm) or small ventricular septal defects (≤1 cm) are found to have pulmonary hypertension without ever having had a large shunt. In such patients another cause of pulmonary hypertension should be sought, and if none is found a diagnosis of idiopathic pulmonary arterial hypertension made.

Pulmonary venous hypertension may occur in congenital heart disease with obstructed left heart inflow.

Left Heart Disease

Left heart disease causes pulmonary hypertension by raising pulmonary venous pressure as a consequence of elevated left atrial pressure. Significant left atrial enlargement with pulmonary hypertension in the presence

of an otherwise apparently normal echocardiogram should prompt a search for left ventricular restriction or atrial septal defect.

If no cause of pulmonary hypertension can be identified on echocardiography other investigations are required to search for a cause. Only after other causes are excluded can a diagnosis of idiopathic pulmonary arterial hypertension be reached.

Other Causes

Lung disease will be detected by lung function tests, arterial blood gases, and high-resolution CT scanning. In most patients with lung disease pulmonary hypertension is of moderate severity, although in a small number it may be out of proportion to the severity of the underlying pulmonary disease.

Chronic thromboembolic pulmonary hypertension is rarely diagnosed by transthoracic echocardiography which cannot see far into the pulmonary circulation. Although proximal thromboembolic disease may be visible on transesophageal echocardiography this is not the optimal imaging modality. Helical CT angiography, nuclear ventilation perfusion scanning, selective pulmonary angiography, and gadolinium magnetic resonance angiography are used as appropriate to confirm the diagnosis and determine the operability of patients (Fig. 10.8). Pulmonary endarterectomy is the treatment of choice in proximal thromboembolic disease and has excellent results in experienced centers. Unoperated this condition has a poor outcome.

Most miscellaneous causes of pulmonary hypertension cannot be diagnosed by echocardiography.

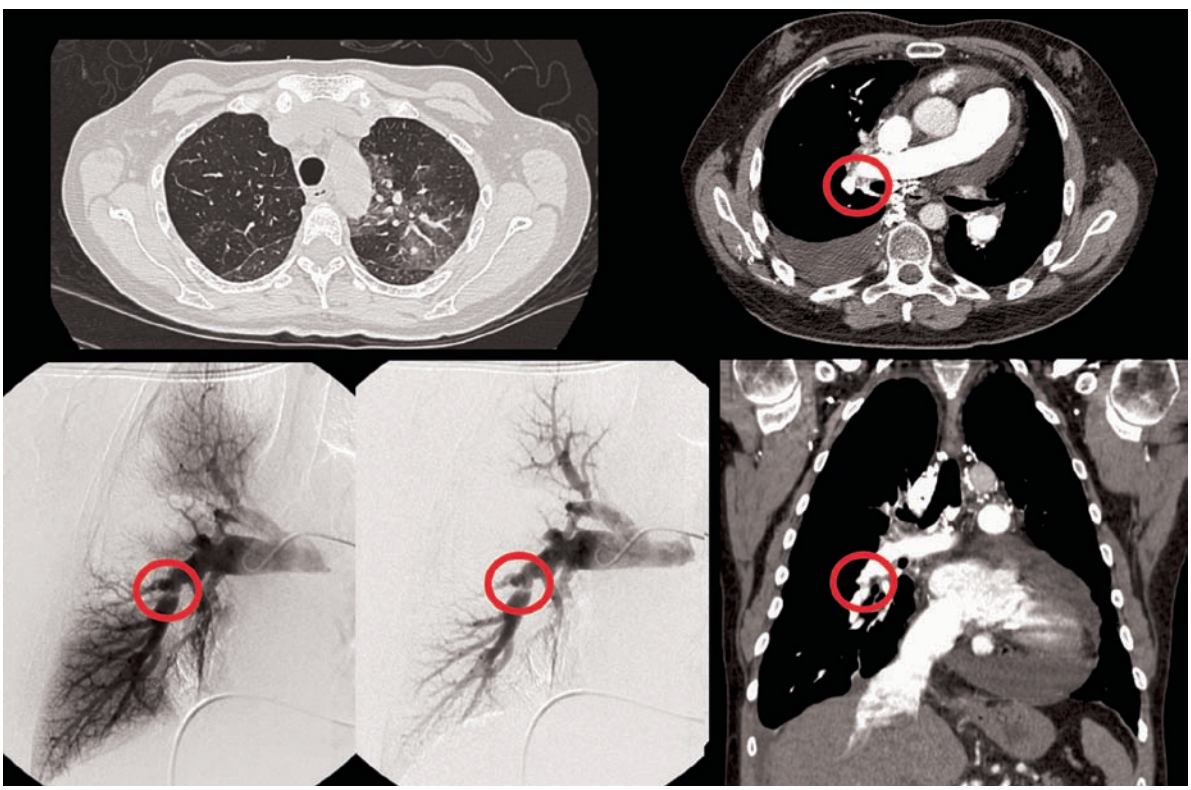

Fig. 10.8 Chronic thromboembolic pulmonary hypertension: high-resolution CT shows a mosaic perfusion pattern, but this is not specific for thromboembolism and may occur in small airways disease (*upper left*); multislice helical CT angiography shows pulmonary arterial webs proximally (*upper right*); CT reconstruction identifies the same web (*down right*); the same lesions are shown on selective pulmonary angiography (*down left*)

Estimation of Severity of Pulmonary Hypertension

Two-Dimensional and M-Mode Echocardiography

Pericardial Effusion

In idiopathic pulmonary arterial hypertension the presence of pericardial effusion is a manifestation of right ventricular failure (Fig. 10.9). It is indicative of a very high right atrial pressure which probably results in impaired lymphatic and venous drainage to the right atrium. The size of the effusion has been shown to be correlated closely with right atrial pressure as well as right atrial size and the severity of tricuspid regurgitation. It is inversely related to cardiac index. Pericardial effusion has been shown in several studies to predict a poor outcome: patients with small or moderate pericardial effusion have been found to have triple the 1-year mortality of patients with trace or no effusion.

The size of the effusion should be assessed in both parasternal long-axis and short-axis views (Table 10.4). Pericardial effusion may also occur in patients with connective tissue disease independent of this mechanism.

Right Atrial Enlargement and Pressure

Right atrial enlargement is associated with elevated right atrial pressure, which itself has been shown to correlate with survival. Right atrial pressure can be estimated semi-quantitatively (Table 10.5) by imaging the inferior vena cava (Fig. 10.10). A qualitative description of atrial size is suitable for diagnostic purposes, but for serial follow-up

Table 10.4 Pericardial effusion score

Echocardiographic findings	Score
Pericardial effusion absent	0
Separation of pericardial layers in systole and diastole	1
Small effusion with separation of pericardial layers in diastole < 1 cm	2
Moderate effusion with separation of pericardial layers in diastole 1–2 cm	3
Large effusion with separation of pericardial layers > 2 cm	4

Table 10.5 Semiquantitative estimation of right atrial

Mean right atrial pressure (mm Hg)	Inferior vena caval diameter (mm)	Inspiratory collapse[a]
0–5	12–23	>50%
5–10	12–23	<50%
10–15	>23	>50%
15–20	>23	<50%

[a]Best tested by asking the patient to breathe in quickly or sniff

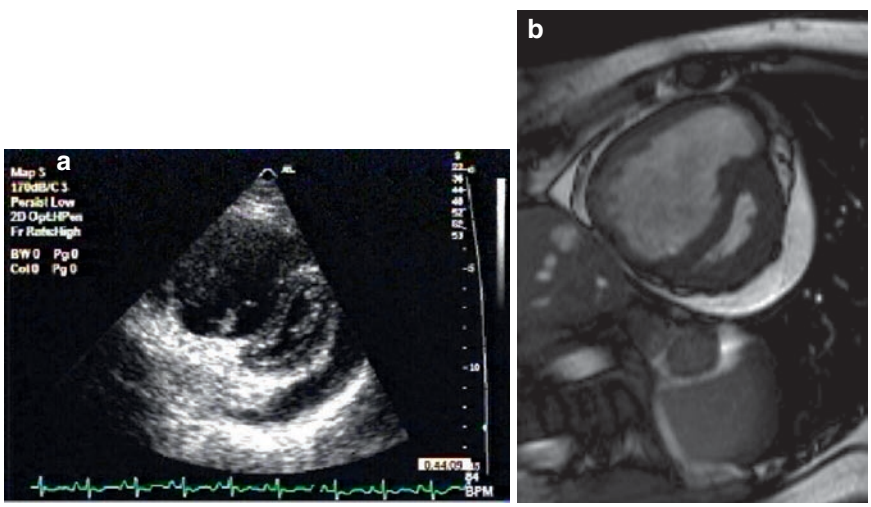

Fig. 10.9 Pericardial effusion in idiopathic pulmonary arterial hypertension shown on short-axis views with echocardiography (**a**) and magnetic resonance imaging (**b**)

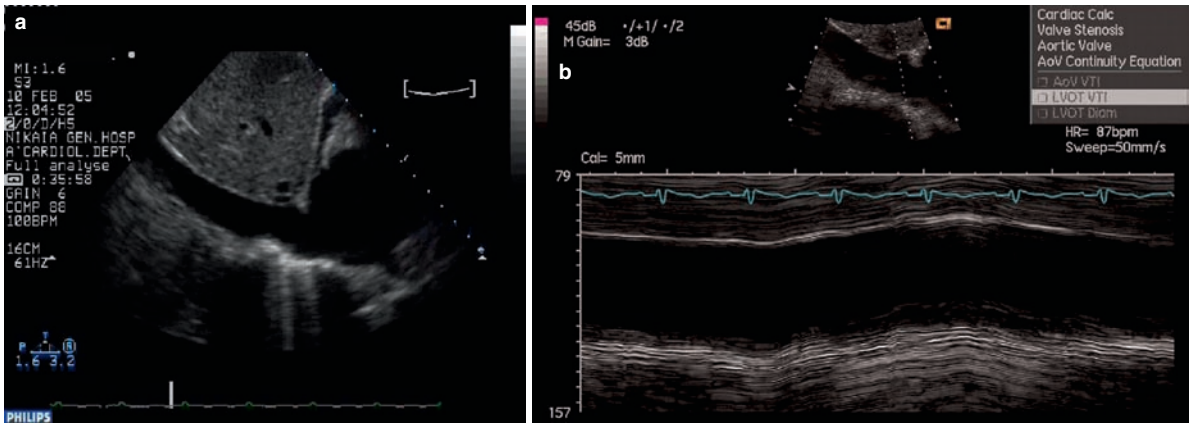

Fig. 10.10 Echocardiographic images of the inferior vena cava which is dilated (**a**) and on M-mode does not alter in diameter with respiration (**b**)

Table 10.6 Useful echocardiographic formulae

Right atrial volume	
Single plane area-length method	Volume = 0.85 A^2/L
Single plane diameter-length method	Volume = $(\pi D^2 L)/6$
Method of discs	Volume = $\pi/4\alpha_i(L/n)$
Pulmonary arterial pressure	
Systolic	4 $(V_{TR})^2$ + RAP
Diastolic	4 $(V_{PR\text{-}ED})^2$ + RAP
Mean	4 $(V_{PR\text{-}PD})^2$ + RAP

atrium; *L* longitudinal dimension of right atrium; *D* transverse dimension of right atrium; α_i, area of disc; *n* number of equal height discs; *RVSP* right ventricular systolic pressure (mmHg); *PASP* pulmonary artery systolic pressure (mmHg); V_{TR} peak tricuspid regurgitation velocity (m/s); *RAP* mean right atrial pressure; *PAEDP* pulmonary artery end diastolic pressure (mmHg); $V_{PR\text{-}ED}$ end-diastolic velocity of pulmonary regurgitation signal; *MPAP* mean pulmonary artery pressure (mmHg); $V_{PR\text{-}PD}$ peak pulmonary regurgitant velocity in early diastole

measurement of right atrial size based on area or volume is helpful (Table 10.6).

Right Ventricular Size and Function

Two-dimensional imaging evaluates the dimensions, shape, and thickness of the right ventricle using several tomographic planes. Useful measurements include the right ventricular end-diastolic diameter, area, and volume.

The end-diastolic diameter of the ventricle is measured at the level of the tricuspid chordae from the parasternal short axis or the four-chamber projection.

The right ventricular end-diastolic (RV-EDA) and end-systolic cavity areas (RV-ESA) are conventionally determined by tracing the endocardial borders in the apical four-chamber view in the plane of the mitral and tricuspid valves.

Automatic endocardial border detection correlates well with the angiographic evaluation of the right ventricle. The use of contrast agents improves accuracy.

The dilated, hypertrophied right ventricle in pulmonary hypertension has distorted and complex geometry making the estimation of ventricular volumes and ejection fraction by two-dimensional echocardiography unreliable. Three-dimensional echocardiography is capable of more accurate estimation of right ventricular volumes although this technique has been shown to be feasible despite limited validation in pulmonary hypertension (Fig. 10.11). Right ventricular volumes are currently most accurately measured by magnetic resonance imaging.

Identification of the severity of right ventricular systolic dysfunction is descriptively important but is subjective.

Interventricular Septal Shift

During cardiac cycle the motion of the interventricular septum reflects the pressure difference between the two ventricles. In volume overload states (e.g., large atrial septal defect) flattening occurs typically only in diastole, since the rising left ventricular pressure

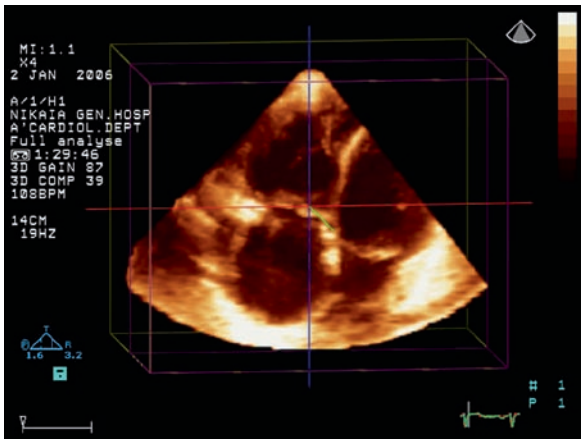

Fig. 10.11 Three-dimensional echocardiogram of the pulmonary hypertensive right ventricle

during systole is higher than the right ventricle. In pressure overload states (e.g., pulmonary hypertension) the right ventricular pressure is generally high enough during the whole of the cardiac cycle, and thus flattening of the septum is present in both systole and diastole. As pulmonary hypertension deteriorates the septal flattening becomes frank deviation into the left ventricle giving it a banana-shaped appearance (Figs. 10.9 and 10.12).

The eccentricity index can be used to measure this septal shift. This is measured in a parasternal short-axis view of the left ventricle at the level of the chordae tendinae. It is the ratio of the minor axis of the left ventricle parallel to the septum divided by the minor axis perpendicular to and bisecting the septum (Fig. 10.13). The index is measured at both end-systole and end-diastole. Over serial measurements these values may not move in parallel. In normal subjects the index is approximately unity, and in pulmonary hypertension becomes >1.0 at both end-systole and end-diastole.

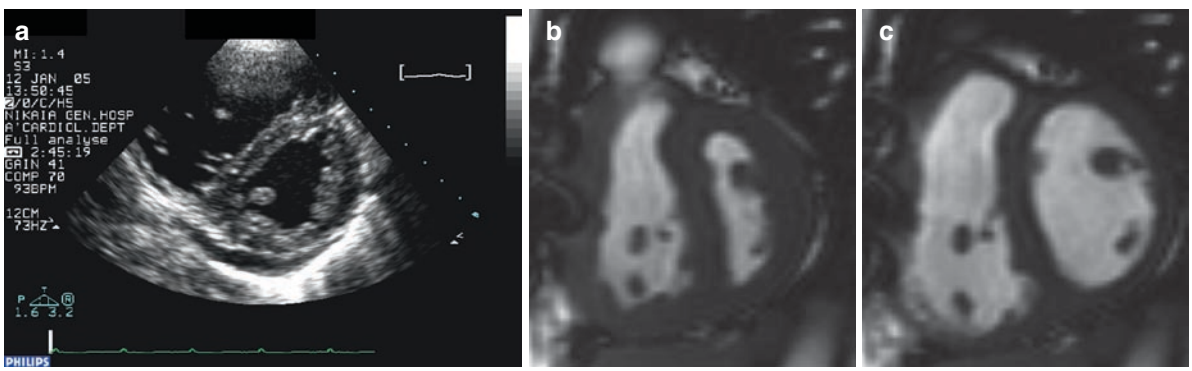

Fig. 10.12 Parasternal short axis of the left ventricle showing deviation of the interventricular septum toward the left ventricle (**a**). Septal motion is also shown in the magnetic resonance images in systole (**b**) and diastole (**c**)

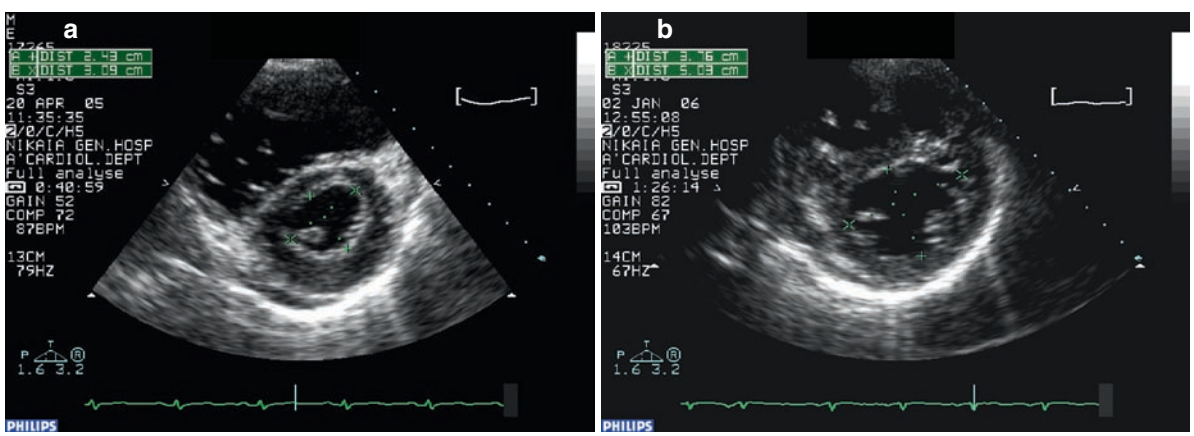

Fig. 10.13 Measurement of the eccentricity index from the parasternal short axis of the left ventricle: in systole (**a**) and in diastole (**b**)

Left Ventricular Size and Function

The consequence of interventricular septal deviation alters left ventricular shape and size. The change in shape is not simply a result of local acute compression but may become the result of long-term remodeling. With increasingly severe pulmonary hypertension the left ventricular cavity size is reduced, and this is further exacerbated by impaired left ventricular filling. An estimate of left ventricular size from dimensions, areas, and volumes is helpful. Left ventricular end-systolic and end-diastolic areas are measured akin to the right ventricle. Left ventricular volume can be measured using three-dimensional echocardiography or by magnetic resonance imaging.

Patent Foramen Ovale

The presence of a patent foramen ovale or a small atrial septal defect predicts a better prognosis. The reason for this may be the ability to decompress high right-sided pressures to the left atrium and increase cardiac output. Selected patients with severe pulmonary hypertension and an intact atrial septum are improved by atrial septostomy which increases cardiac output and reduces right ventricular end-diastolic pressure (Fig. 10.14). In severe pulmonary hypertension a patent foramen ovale is not easily seen on transthoracic echocardiography because of equalization of pressures across it. The presence of a shunt at atrial level can be predicted by Qp and Qs if they are not unity.

Doppler Assessment

Tricuspid Regurgitation Velocity and Calculated Systolic Pulmonary Arterial Pressure

The principal technique for determining pulmonary artery pressure involves the use of the tricuspid regurgitant jet and the Bernoulli equation. Tricuspid regurgitation is readily identified by color-flow Doppler and quantitative measurements can be made (Fig. 10.15). The four-chamber view is used most commonly. The right ventricular systolic pressure is derived from the peak systolic driving pressure between the right ventricle and right atrium. In the absence of pulmonary valve stenosis, it can be assumed that the systolic right ventricular and pulmonary arterial pressure is equal.

Systolic pulmonary arterial pressure is calculated from the peak velocity of tricuspid regurgitation using the modified Bernoulli equation and added to the right atrial pressure (Table 10.6). Proper alignment of the echocardiographic transducer is crucial since malalignment will underestimate the peak velocity. Although right atrial pressure is often assumed to be 5–10 mmHg it is better to estimate the right atrial pressure with echocardiography as described earlier. In reporting the systolic pulmonary arterial pressure it must be stated how right atrial pressure was estimated.

This method tends to underestimate the true pulmonary arterial pressure as pressure rises. This is a consequence of ignoring the valve coefficient, a constant which is omitted from the modified Bernoulli equation.

Underestimation of pressure may also occur when the right ventricular – right atrial pressure gradient is reduced by other mechanisms. This may happen, for example, with the development of restrictive function where right atrial pressure is high and the right ventricle is stiff. Conversely the peak tricuspid regurgitation velocity may remain unchanged when right ventricular pressure and right atrial pressure fall in parallel in association with clinical improvement.

Among 3,790 echocardiographically normal subjects the mean pulmonary arterial systolic pressure was 28.3 mm Hg (95% CI: 18.7, 37.9 mm Hg) using an assumed right atrial pressure of 10 mm Hg. The systolic pressure exceeded 40 mm Hg in a small number of people over 50 years of age or with a body mass index >30 kg/m^2. This means that if a right atrial pressure of 5 mm Hg is assumed, the upper 95% confidence interval equates to a peak tricuspid regurgitant velocity of 2.87 m/s with some older people exceeding 2.98 m/s which is similar to the WHO definition of mild pulmonary hypertension. If higher right atrial pressures are assumed or measured then lower values of peak tricuspid regurgitant velocity will raise the possibility of mild pulmonary hypertension.

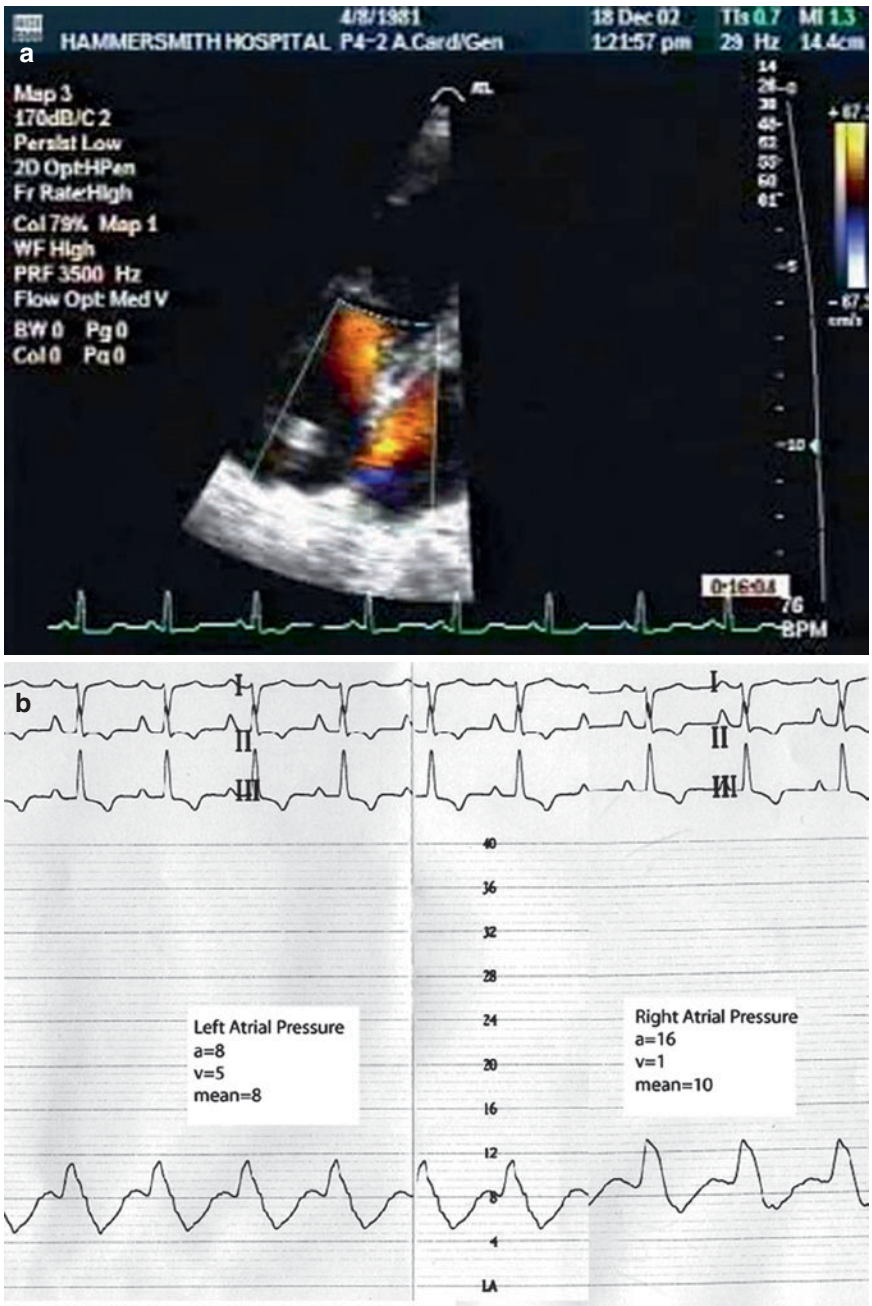

Fig. 10.14 Atrial septostomy in idiopathic pulmonary arterial hypertension: note how flow is directed from right to left atrium (**a**). The patient presented with recurrent syncope and was improved by septostomy. The pressure recording from cardiac catheterization shows a higher pressure in the right than the left atrium (**b**)

Pulmonary Arterial Mean and Diastolic Pressure

The presence of pulmonary regurgitation usually permits the measurement of the end-diastolic gradient between the pulmonary artery and right ventricle from which can be derived the pulmonary arterial diastolic pressure (Table 10.6 and Fig. 10.16).

Mean pulmonary arterial mean pressure can also be estimated and has the advantage that pulmonary hypertension is defined by mean pulmonary arterial pressure

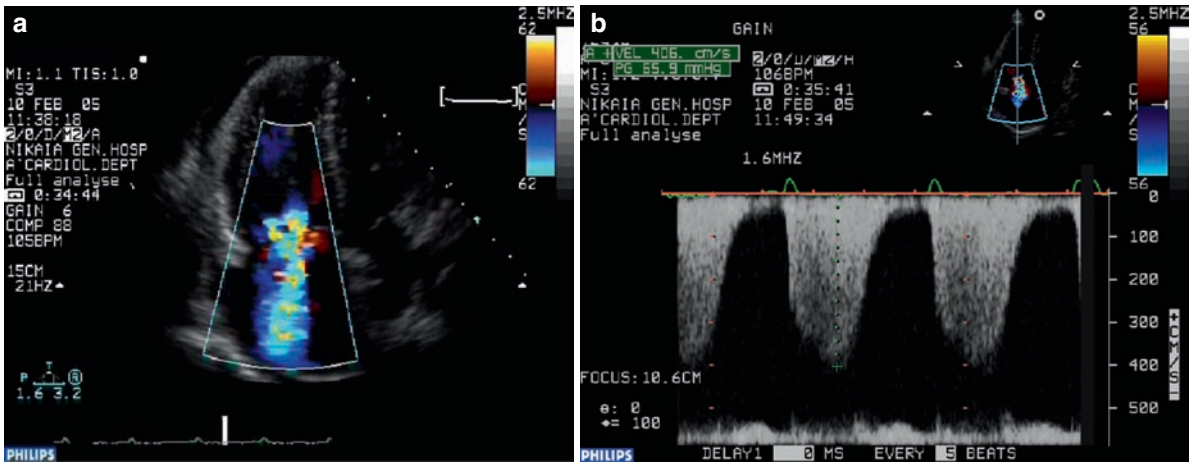

Fig. 10.15 Four-chamber view showing color-flow map of tricuspid regurgitant jet in idiopathic pulmonary arterial hypertension (**a**). The tricuspid regurgitant jet which is used to calculate systolic pulmonary arterial pressure is shown in the same patient (**b**)

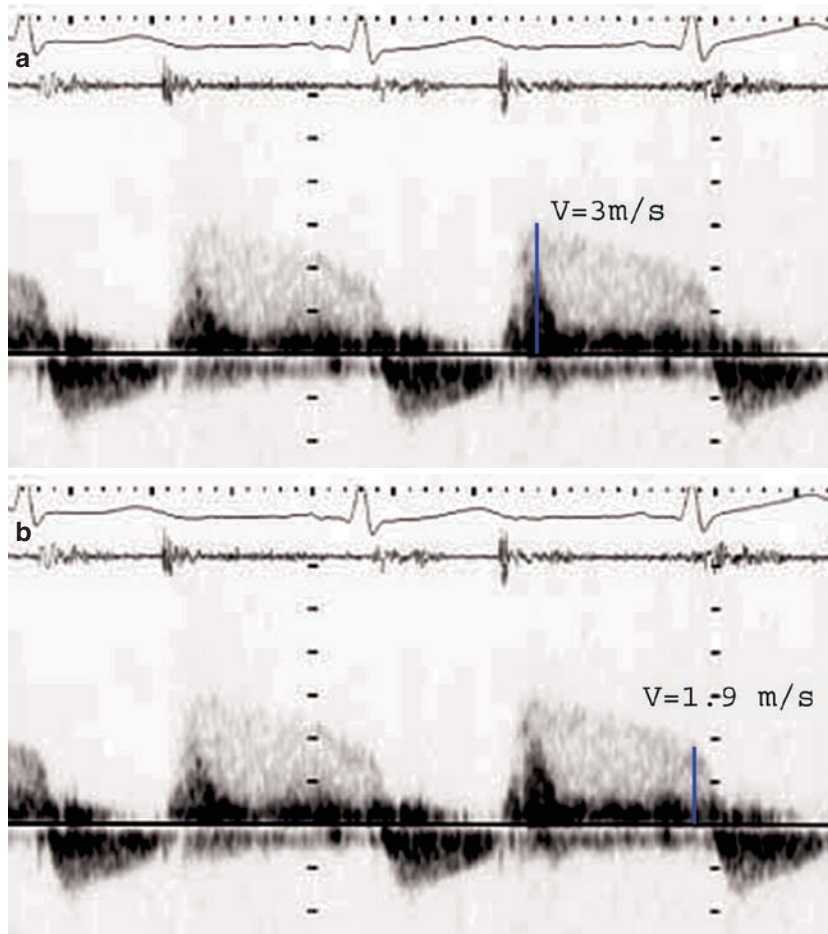

Fig. 10.16 Doppler tracing of pulmonary regurgitation (PR) showing measurement of mean and end-diastolic pulmonary arterial pressures (see also Table 10.6). (**a**) Estimation of the mean pulmonary artery pressure (MPAP) using the pulmonary regurgitant Doppler velocity signal. The early diastolic PR Doppler signal measured approximately 3 m/s. Using the simplified Bernoulli equation, the MPAP is approximately 36 mmHg. (**b**) Estimation of the pulmonary artery end-diastolic pressure (PAEDP) using the pulmonary regurgitant Doppler velocity signal. The end-diastolic PR Doppler signal, recorded from the Q wave of the ECG, measures approximately 1.9 m/s. Using the simplified Bernoulli equation, the end-diastolic pressure difference between the pulmonary artery and the right ventricle equals 14 mmHg. Assuming that the right ventricular end-diastolic pressure equals the right atrial pressure and that the RAP is 10 mmHg, the estimated PAEDP is 24 mmHg

at cardiac catheterization. Although mean pressure can be calculated from the systolic and diastolic pressure it is better measured separately. This can be calculated from the peak pulmonary regurgitant velocity which occurs after pulmonary valve closure in early diastole (Table 10.6 and Fig. 10.16). The correlation with catheter measurements is best when account is taken of right atrial pressure.

Other methods of estimating pulmonary arterial pressure have been reported, such as using right ventricular isovolumic relaxation time. Difficulties are encountered with fast heart rates and, therefore, a short relaxation period. This estimation of pulmonary arterial pressure from the relaxation time assumes a normal right atrial pressure and may not be reliable in pulmonary hypertension with right ventricular failure.

Assessment of Right Ventricular Function

Right Ventricular Doppler Index

The Doppler index of myocardial performance (Tei index or myocardial performance index) has been used for the evaluation of left ventricular function. The ratio of isovolumic contraction time to ejection time has been shown to correlate with +dp/dt, and the ratio of isovolumic relaxation time to ejection time has been shown to correlate with −dp/dt. Thus this Doppler index provides a global assessment of both systolic and diastolic function.

In pulmonary hypertension the right ventricular Doppler index (Fig. 10.17) correlates with symptom severity, improves with current therapies for pulmonary arterial hypertension, correlates with symptomatic improvement, and is prognostic. The normal range is 0.26–0.28. In pulmonary hypertension the index is elevated, falling with clinical improvement.

The right ventricular Doppler index is relatively unaffected by heart rate, right ventricular pressures, or the severity of tricuspid regurgitation. It has good reproducibility and measurements can be made accurately even in the presence of a difficult acoustic window. Its disadvantage is overlapping between the end of tricuspid regurgitation signal and the pulsed signal of the early diastolic filling (E) of the transtricuspid flow that challenges the accurate estimation of the isovolumic relaxation time. Nevertheless this is a robust measurement which is particularly useful for the follow-up of patients.

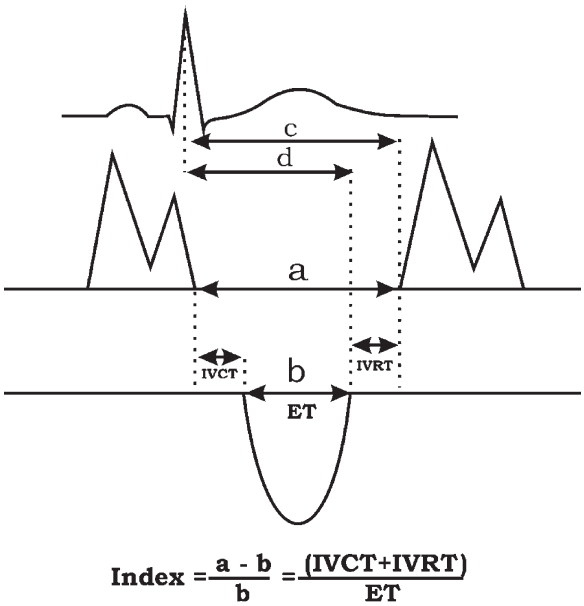

Fig. 10.17 Measurement of the right ventricular Doppler index. The tricuspid inflow velocity pattern is obtained from the apical four-chamber view with the pulsed-wave Doppler sample volume positioned between the tips of the tricuspid leaflets during diastole. The RV outflow velocity curve was recorded from the parasternal short-axis view with the pulsed-wave Doppler sample volume positioned at the pulmonary valve level. Doppler time intervals were measured from inflow and outflow recordings

Right ventricular ejection time, a component of the Doppler index, has been shown to improve on treatment for pulmonary arterial hypertension, on its own.

Tricuspid Regurgitation Severity

Tricuspid regurgitation time is prolonged by increasing right ventricular pressure. Even in the absence of right ventricular free wall dysfunction, the raised transtricuspid pressure difference and slow pressure decline will limit right ventricular filling time (right ventricular diastolic reserve). A short filling time markedly reduces stroke volume and cardiac output especially with a fast heart rate and may lead to syncope. Reduced right ventricular functional reserve can be measured by the ratio of total filling time in relationship to the regurgitation time. Lengthening of tricuspid regurgitation can also be the result of impaired right ventricular function when slow right ventricular relaxation delays tricuspid regurgitation pressure decline, or the consequence of conduction abnormalities.

Although severe tricuspid regurgitation predicts an adverse prognosis its estimation is open to substantial error.

Tissue Doppler Imaging of Right Ventricle

The role of pulsed tissue Doppler imaging is not established. Myocardial velocities recorded from the basal right ventricular wall in pulmonary hypertension show prolongation of isovolumic relaxation which is virtually absent in the normal right ventricle. The early diastolic velocity is reduced by right ventricular hypertrophy. In the presence of severe tricuspid regurgitation in addition to pulmonary hypertension the early diastolic velocity increases and the isovolumic period is reduced by high right atrial pressure (Fig. 10.18). Systolic velocity < 11.5 cm/s can identify the presence of RV dysfunction with a sensitivity and specificity of 90 and 85%, respectively.

Assessment of Left Ventricular Function

Left Ventricular Filling

Left ventricular diastolic dysfunction almost always coexists with significant pulmonary hypertension. The early diastolic distortion of left ventricular geometry associated with prolongation of right ventricular systole into left ventricular diastole results in prolongation of isovolumic relaxation of the left ventricle and reduction in early diastolic filling. This is further exacerbated by severe tricuspid regurgitation which could further diminish early left ventricular filling. This can be assessed using pulsed-wave Doppler signals at the mitral valve with measurement of peak E velocity, E/A ratio, and the time-velocity integral of flow. The severity of left ventricular diastolic dysfunction is related to the severity of pulmonary hypertension in a nonlinear logarithmic association. A fall in E wave velocity, E/A ratio, and time-velocity integral is associated with worsening pulmonary hypertension.

Cardiac Index

The progression of pulmonary hypertension is associated with a falling cardiac output, and this is related to an adverse prognosis. Improvement in cardiac output is expected with successful treatment. The measurement of cardiac output is described in another chapter of this book but without doubt lacks good reproducibility. The accuracy and reproducibility may be improved by three-dimensional echocardiography. The most accurate measurements of cardiac index can be made by magnetic resonance imaging either from stroke volume measurements multiplied by heart rate, or from flow measurements.

Serial Echocardiographic Monitoring

Most patients with pulmonary hypertension require lifelong follow-up. Although drug therapy for pulmonary arterial hypertension or pulmonary thromboendarterectomy for chronic thromboembolic disease may dramatically improve hemodynamics, most patients on drug therapy experience clinical improvement in symptoms and exercise capacity despite little or no qualitative change in the echocardiogram or magnetic resonance scan. While treatments are likely to become more effective with the current interest in this area of medicine, the patients themselves require vigilant follow-up. Patients with pulmonary arterial hypertension on disease-targeted therapies not infrequently require dose changes or substitution and addition of drug therapy in response to clinical deterioration which may occur rapidly.

Along with clinical evaluation and exercise testing, echocardiography plays a key role in the follow-up of patients. Not only can echocardiography be undertaken at routine follow-up appointments but also it is convenient and can provide comprehensive information in the event of acute decompensation. Other cardiac investigations such as cardiac catheterization and magnetic resonance imaging cannot normally be performed frequently.

Bearing in mind the limitations of qualitative descriptions for the serial follow-up of patients, Table 10.7 lists measurements which may be expected to change with treatment. This type of echocardiographic study which is intended to be repeated is quite different in its aim from the initial diagnostic study. In the event of acute deterioration care should be undertaken to perform a comprehensive echocardiographic examination.

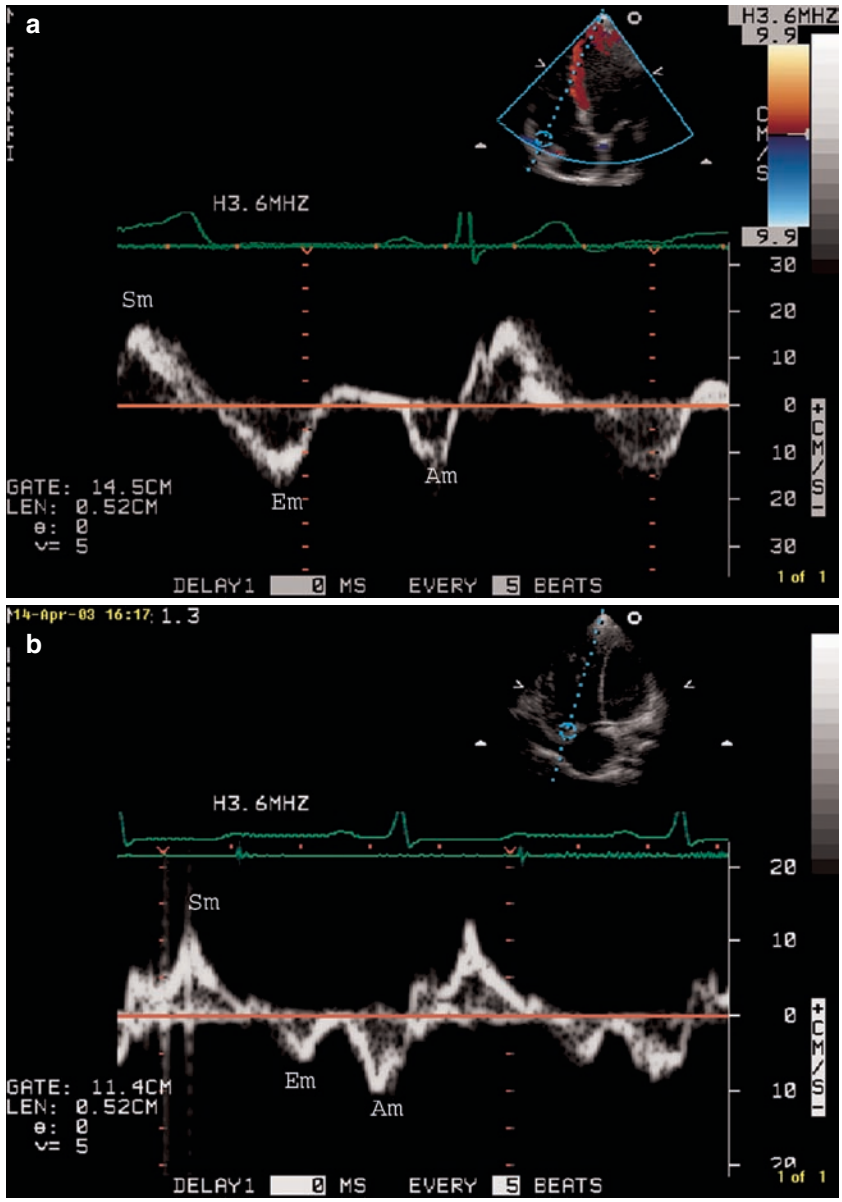

Fig. 10.18 Tissue Doppler imaging of right ventricle in pulmonary hypertension and a normal right ventricle. (**a**) Tissue Doppler recording of right ventricular myocardial velocity in a normal subject. The sample volume positioned at the base of right ventricular free wall. Recording shows systolic positive wave (Sm), early diastolic wave (Em), and atrial wave (Am). (**b**) Tissue Doppler recording of right ventricular myocardial velocity from a patient with pulmonary hypertension. Note significantly reduced early diastolic velocity (Em)

Much clinical attention tends to focus on the estimation of systolic pulmonary arterial pressure. Although clinicians and patients will want to know this, it may not change significantly or may even deviate in an unexpected direction for the reasons given earlier.

Detecting Complications

The development of syncope is a sinister symptom and portends a poor prognosis. In the presence of severe pulmonary hypertension echocardiography

Table 10.7 Suggested echocardiographic measurements for serial follow-up examination of patients with pulmonary hypertension

Pericardial effusion
Right atrium
Area or volume
Assessment of right atrial pressure from IVC diameter and inspiratory collapse
Right ventricular function
Area or volume in systole and diastole
Right ventricular Doppler index
Ejection time
Systolic pulmonary arterial pressure from peak tricuspid regurgitation velocity
Pulmonary regurgitation
Left ventricular function
Area or volume in systole and diastole
Decreased RV:LV diastolic area ratio
Eccentricity index in systole and diastole
Mitral inflow E wave velocity, E/A ratio, and time velocity integral
Stroke volume
Cardiac index

may be able to suggest the mechanism. Shortening of right ventricular filling time as a consequence of prolongation of tricuspid regurgitation or tachycardia may reduce cardiac output and cause syncope (Fig. 10.19). Left ventricular outflow tract obstruction may develop as a consequence of compression by the right ventricle and an enlarged pulmonary artery as illustrated in Fig. 10.20. Note that pulmonary arterial enlargement (usually > 4 cm) may also cause compression of the left main stem coronary artery. The differential diagnosis of syncope includes arrhythmias and pulmonary thrombosis.

The commonest causes of deterioration are intercurrent infection usually of the respiratory tract or intravenous lines for prostacyclin analog infusions, progressive deterioration of hemodynamics, and arrhythmias. Occasionally pulmonary regurgitation becomes severe usually as a conse-

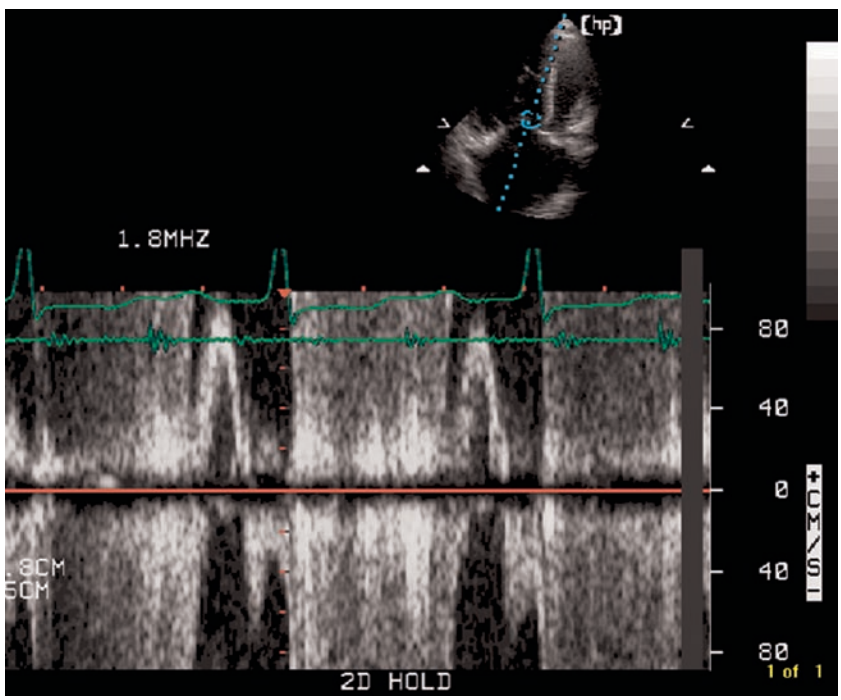

Fig. 10.19 Pulsed-wave (PW) Doppler recording of tricuspid inflow in patient with pulmonary hypertension. Note the inflow mainly occurs during late diastole and the filling time is limited by prolonged early diastolic and also presystolic tricuspid regurgitation

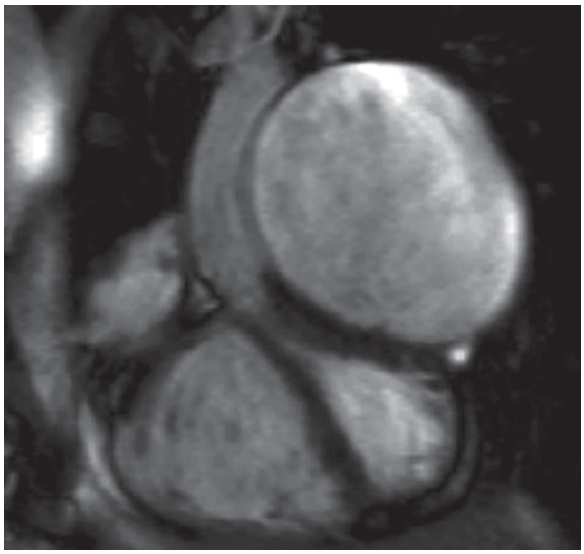

Fig. 10.20 Left ventricular outflow tract compression by the right ventricle and an enlarged pulmonary artery

quence of progressive dilatation of the main pulmonary artery with stretching of the pulmonary valve (Fig. 10.21).

Pulmonary arterial dissection may be fatal and associated with pulmonary arterial rupture, but occasionally it is chronic (Fig. 10.22). Echocardiography is not sensitive for detecting pathology in the main pulmonary artery since it is seen end on in the parasternal short-axis view, and other imaging investigations should be used where this is suspected.

Role of Other Imaging Modalities

The investigation and management of patients with pulmonary hypertension requires the integration of different imaging modalities to image the heart, lungs, and pulmonary circulation. The strengths and

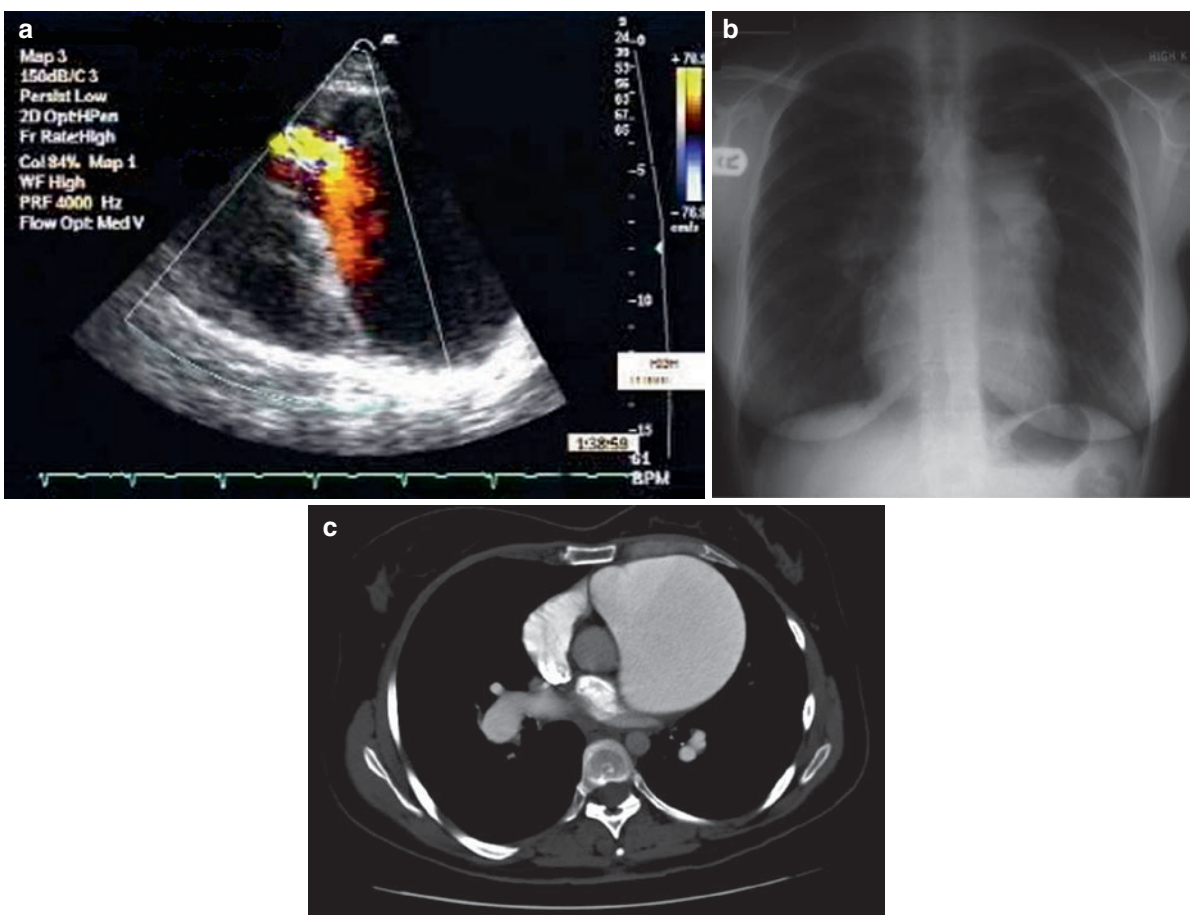

Fig. 10.21 Severe pulmonary arterial dilatation in pulmonary hypertension resulting in severe pulmonary regurgitation (**a**). Chest X-ray (**b**) and CT scan (**c**) show massive pulmonary arterial enlargement which is confirmed on echocardiography. There was malcoaptation of the pulmonary valve as a consequence of stretching of the ring with severe regurgitation illustrated on color-flow mapping

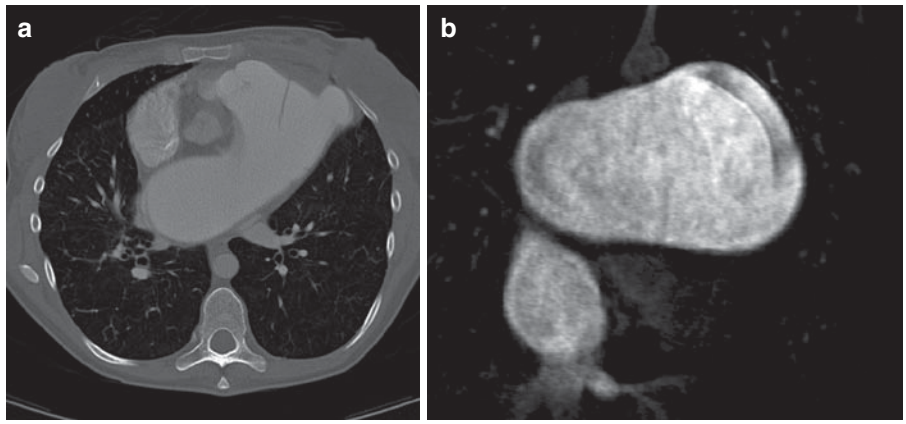

Fig. 10.22 CT (**a**) and magnetic resonance images (**b**) of chronic pulmonary arterial dissection: this could not be seen on the echocardiogram

Table 10.8 Comparison of different imaging modalities and cardiac catheterization in pulmonary hypertension for the assessment of etiology and severity

Investigation	Most suitable for	Unsuitable for
Echocardiography	Congenital heart disease Left heart disease Pulmonary arterial pressure Right atrial pressure Right ventricular function Pericardial effusion	Right ventricular mass Right ventricular volume Vasodilator studies
Cardiac catheterization	Congenital heart disease Left heart disease Pulmonary arterial pressure Right atrial pressure Cardiac index Qp and Qs Vasodilator studies to assess suitability for calcium antagonist therapy	Right ventricular mass Right ventricular volume Pericardial effusion
Magnetic resonance (with gadolinium contrast)	Congenital heart disease Left heart disease Thromboembolic disease Right ventricular mass Right ventricular volume Cardiac index Qp and Qs Pericardial effusion	Pulmonary arterial pressure Right atrial pressure Vasodilator studies
Computerized tomography (high resolution and contrast)	Lung parenchymal disease Thromboembolic disease Mediastinal disease	Hemodynamics
Ventilation perfusion scanning	Thromboembolic disease Right to left shunt	Hemodynamics
Selective pulmonary angiography	Thromboembolic disease	Everything else
Positron emission tomography	Detection of inflammation in pulmonary arteries (vasculitis, tumor)	Hemodynamics

weaknesses of some of these are shown in Table 10.8. These will no doubt change with advancing technology.

Conclusions

Echocardiography plays a central role in screening and detection of pulmonary hypertension. It can evaluate some causes and is best used in association with other imaging investigations and cardiac catheterization. It remains the imaging investigation of choice for investigating sick patients. It has a useful role in guiding therapy during the serial monitoring of patients during follow-up.

Acknowledgments The authors are grateful to the staff of the Cardiac Magnetic Resonance unit at the Royal Brompton Hospital for the magnetic resonance images shown in this chapter.

Bibliography

British Cardiac Society Medical Practice Committee. Recommendations on the management of pulmonary hypertension in clinical practice. *Heart*. 2001;86(Suppl 1):I1–I13.

Galie N, Hinderliter AL, Torbicki A, et al. Effects of the oral endothelin-receptor antagonist bosentan on echocardiographic and Doppler measures in patients with pulmonary arterial hypertension. *J Am Coll Cardiol.* 2003;41:1380–1386.

Rich S. Executive summary from the world symposium on primary pulmonary hypertension 1998. http://www.who.int/ncd/cvd/pph.htm; 1998.

Simonneau G, Galie N, Rubin L, et al. Clinical classification of pulmonary hypertension. *J Am Coll Cardiol.* 2004;43:5S–12S.

Stefanidis A, Koutroulis G, Kollias G, Gibbs JSR, Nihoyannopoulos P. Role of echocardiography in the diagnosis and follow-up of patients with pulmonary arterial and chronic thromboembolic pulmonary hypertension. *Hellenic J Cardiol.* 2004;45:48–56.

Chapter 11
Criteria for Operative Intervention in Valvular Heart Disease Based on Echocardiography

William J. Stewart

Using echocardiography and Doppler echocardiography for deciding on the timing of operative intervention for chronic valvular heart disease entails integrating the anatomy and physiology of the valve lesion with the symptoms and living status of the patient and the expected natural history of the valve lesion (Table 11.1).

This chapter will summarize the clinical practice decisions for each type of chronic valve dysfunction. The current practice is in transition, reflecting multiple trends: improved surgical results, declining perioperative mortality, improved understanding of the natural history of the disorders, and of enhanced imaging capabilities for defining cardiac structure and function.

In this chapter, the issues will be simplified artificially, considering each lesion in isolation and pretending that no other valve lesions are present. In addition, the mechanistic and etiologic factors will be presented as though perfectly clear and isolated, which in many real patients is often not true. Sometimes a patient has valvular disease from two sources, for example, myxomatous mitral valve disease with superimposed ischemic heart disease. In many circumstances, such a separation is artificial. In addition, these discussions will purposefully neglect the settings of acute valvular dysfunction, management of which is different than in chronic valvular lesions, the subject of this chapter. For example, patients with acute valvular regurgitation might have surgical indications based on the process causing their valve dysfunction, such as endocarditis, unstable angina, aortic enlargement, or aortic dissection.

W.J. Stewart
Professor of Medicine, Department of Cardiovascular Medicine, Section of Cardiovascular Imaging, The Cleveland Clinic Foundation, 9500 Euclid Avenue, Desk J1–5, Cleveland, OH, 44195, USA
e-mail: Stewarw@ccf.org

Aortic Stenosis

The most important indication for surgery in aortic stenosis (AS) is the onset of *any* symptoms *that result from* the hemodynamic consequences of aortic stenosis. Because of the importance of symptoms, the echocardiographic patterns in AS superficially seem less important. Most patients present with anginal chest pain or dyspnea, which are more common than the symptoms of syncope or presyncope. The survival curve of patients with aortic stenosis managed without surgery, published in 1968 by Ross and Braunwald (Fig. 11.1), shows the dramatic drop in survival soon after the onset of symptoms.

The phrase *that result from* in the earlier statement is key to the dilemma of deciding on the timing of surgery in AS. The connotation of causality makes a conjectural connection between the patient's symptoms and hemodynamics. To conclude that the symptoms *result from* the stenotic valve, we must see in the echocardiogram a valve gradient and/or valve area that are sufficient in terms of severity. Obviously this depends on many individual factors, especially the patient's activity level, the patient's threshold for symptoms, and their ability to report them.

Most criteria for severe aortic stenosis include a valve gradient above a certain level, usually a mean systolic gradient above 40–50 mm Hg, or a valve area below 0.7–1.0 cm^2 (Table 11.2). Some believe that valve resistance is a less flow-dependent means of assessing AS.

P. Nihoyannopoulos and J. Kisslo (eds.), *Echocardiography*,
DOI: 10.1007/978-1-84882-293-1_11, © Springer-Verlag London Limited 2009

Table 11.1 Components of decisions about valve surgery

Hemodynamics
Echocardiographic imaging
Valve morphology
Ventricular function
Abnormalities of other valves
Doppler echocardiography
Degree of stenosis
Degree of regurgitation
Upstream or downstream effects
Pulmonary artery pressures
Flow reversal in veins, arteries
Cardiac catheterization
Angiography
Invasive measurements of pressure and cardiac output
Magnetic resonance imaging
Computerized tomography
Impact of the valve abnormalities on the patient
History (Symptoms)
Functional studies including stress testing
Understanding the natural history of the patient

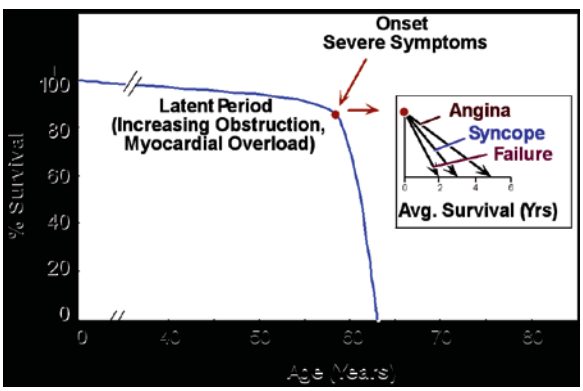

Fig. 11.1 This classical graph tracks the prototypical natural history of aortic stenosis. Despite gradual fibrosis and progressive stenosis, patients remain asymptomatic in a long latency period, until their fifth to seventh decade of life. After the onset of symptoms, there is a sudden and marked reduction in survival, with 50% mortality within 2–3 years. From the *inset*, survival after the onset of heart failure is less than if they present with syncope, which is less than if they present with angina. From Ross J Jr, Braunwald E. Aortic Stenosis. *Circulation.* 1968;38(suppl 5):V-61

Table 11.2 Criteria for characterizing severe aortic stenosis

Mean systolic gradient	> 40–50 mm Hg
Valve area	< 0.7–1.0 cm^2
Dimensionless index	< 0.20–0.25
Valve resistance	> 300 dynes s/cm^5

Gradients in Aortic Stenosis

Determination of valve gradient is one of the strengths of Doppler echocardiography. Attention must be paid to obtaining a clean velocity envelope with the highest possible velocity from the continuous-wave Doppler recordings, using multiple transducer positions. It should be noted that there are multiple types of gradients available, which vary substantially depending on their mode of acquisition.

Doppler echocardiography uses measurements of maximum velocity, to derive peak instantaneous gradient, which correlates well with invasively measured gradients. This utilizes the simplified Bernoulli equation ($4\ V^2$), but assumes that the subaortic velocity is relatively small in comparison with the valvular velocity, and that effects of flow acceleration and viscous friction are negligible. When Doppler-derived gradients are averaged over the systolic interval, this provides a very comparable measurement to catheter-derived gradients, measured with two simultaneous pressure recordings above and below the aortic valve. However, many invasively derived gradients are derived from one catheter that is pulled back from the left ventricle into the aorta, comparing the peak aortic pressure with peak left ventricular pressure. Unfortunately, aortic stenosis often causes an aortic pressure profile with a "tardus and parvus" contour, a delayed timing of the peak aortic pressure. Thus the "peak-to-peak" gradient derived invasively is a very different parameter that substantially underestimates peak instantaneous gradient and misses the mean gradient by a variable amount.

Attention must also be paid to situations where gradients calculated with the simplified Bernoulli equation will over- or under-represent the severity of the valve lesion (Table 11.3). Although native aortic stenosis is less commonly the cause of pressure recovery, it occurs under some circumstances of aortic root size and shape.

Valve Area in Aortic Stenosis

The components of the formula for calculation of AS valve area $[\pi(D/2)^2 \times V_1/V_2]$ include the *subaortic velocity* (V_1, recorded by pulsed-wave Doppler from an apical transducer position), the *valvular velocity* by continuous-wave Doppler (V_2 using the highest velocity obtained of

Table 11.3 Situations where valve gradient misrepresents severity of aortic stenosis

Under-representation
Severe left ventricular dysfunction
Poor recording or poor acoustic access, missing the highest velocity
Over-representation
Pressure recovery
Concomitant subaortic stenosis
High cardiac output
Concomitant aortic regurgitation
Anemia

Table 11.4 Indications for surgery in aortic stenosis

- Symptomatic severe aortic stenosis
- Moderate or severe AS in pt otherwise needing heart surgery
- Asymptomatic pt with severe AS and
  - LV dysfunction
  - Significant MR
  - Ventricular arrhythmias
  - Concomitant coronary disease
  - Critical AVA < 0.5 cm^2, peak instantaneous AVG > 100 mm Hg
  - Suspicion that the AS will progress rapidly, based on
    * Atherosclerotic risk factors
    * Previous Doppler data

any of the 3–5 positions available), and the subaortic diameter (*D*). In calculation of valve area, using the continuity equation, several key factors affect the result. In some patients, the subaortic diameter makes the calculated value unrealistic, either because of being extremely small or large. In others the images from which such a diameter is measured are poor in quality, which makes the valve area less meaningful.

Some feel that other parameters are more applicable to deciding the severity of AS, in certain circumstances. The "dimensionless index" is the ratio of the subaortic velocity (peak, mean, or integral) with the corresponding measurement from the valvular velocity (V_1/V_2). Valve resistance, a more complex calculation derived from the ratio of pressure difference and flow, is a less popular parameter derivable from Doppler echocardiography.

Criteria for Operation for Aortic Stenosis in Asymptomatic Patients

Development of symptoms currently drive most decisions for surgery for aortic stenosis. As the risks of aortic valve replacement become smaller with improvements in surgical technique, it may be appropriate to operate on some asymptomatic patients with severe AS. When aortic stenosis has caused left ventricular dysfunction, atrial or ventricular arrhythmias, mitral regurgitation, or severe left ventricular hypertrophy (Table 11.4), most valve disease experts would recommend valve replacement despite the lack of symptoms. Patients with extremely severe AS, severe valvulor calcification, and those with significant concomitant aortic regurgitation, may also be candidates for surgery when asymptomatic.

Pre-emptive surgery may also be reasonable when aortic stenosis has been demonstrated to be rapidly progressive by serial studies. The average rate of change is a decrease in valve area of about 0.1 cm^2 per year or an increase in gradient of 7 to 10 mm Hg per year. This indication for surgery aligns with the recent under-standing that aortic stenosis involves a process similar to atherosclerosis, involving the aortic valve, that progresses more rapidly in patients with diabetes, hypertension, smoking, dyslipidemia, family history of atherosclerosis, and in the presences of markers of vascular inflammation like ultrasensitive C-reactive protein.

In addition, pre-emptive surgery before symptoms is indicated if the patient has significant coronary artery narrowing. In some asymptomatic patients with severe aortic stenosis, coronary angiography may be reasonable because pre-emptive aortic valve replacement and bypass grafting should be considered if significant silent disease is found. As a corollary, patients with aortic stenosis (and aortic sclerosis) should have aggressive risk factor management, similar to patients with known coronary disease. As percutaneous valve replacement becomes clinically available in the future the threshold for intervention is likely to go down further.

Aortic Regurgitation

In aortic regurgitation (AR), the central portion of the decision on when to operate is also the patient's symptoms, NYHA class II or more, resulting from the valvular dysfunction. But the decision in many patients stems from observation of left ventricular size and function. In some circumstances, it is useful to have the patient undergo a formal exercise study to evaluate their symptoms. This provides a way of following their exercise capacity objectively, and a way to see if symptoms are a significant limitation of their performance.

LV Size and Function in Aortic Regurgitation

With chronic AR, severe regurgitation is often tolerated for many years without symptoms. Because of the left ventricular volume overload that results from AR, combined with the augmented peripheral vasoconstriction, the outcome of this disorder depends, in part, on the degree of chronic LV enlargement (Fig. 11.2). When contractile dysfunction begins to develop, surgery should be recommended, even in the absence of symptoms. In addition systolic dilation above a certain level should be considered a sign of the advent of potentially irreversible myocardial dysfunction, even when ejection fraction is normal.

In any patient with a resting ejection fraction below 55%, or a shortening fraction by M-mode echo of less than 27%, surgery should be considered (Table 11.5). When the combination of eccentric hypertrophy and LV dysfunction has developed so that the left ventricle has an end-systolic diameter of 55 mm, or larger, postoperative survival is significantly decreased. To avoid this, most consider the "fifty-five" rule a sign of having waited too long, so surgical plans are often made when the end-systolic diameter is 50 mm or greater. Looking

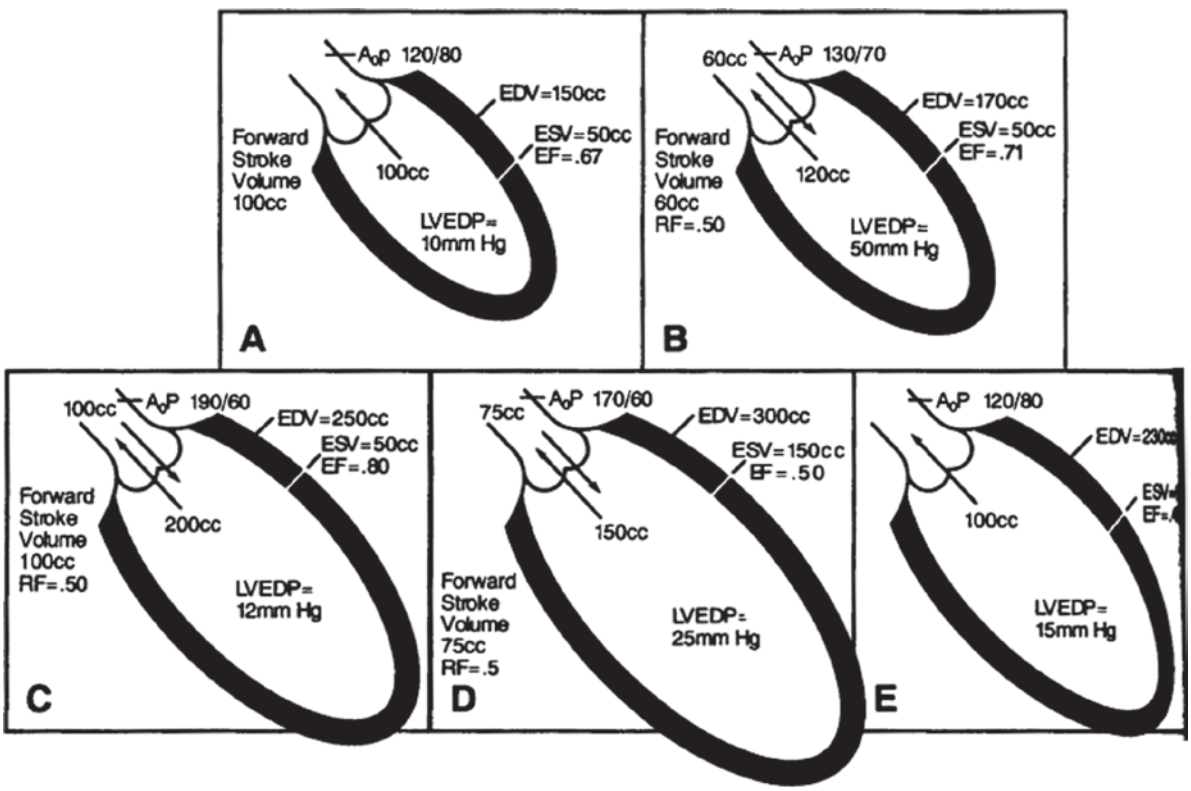

Fig. 11.2 Hemodynamics in various stages of aortic regurgitation. (**a**) Normal hemodynamics with no aortic regurgitation. (**b**) Acute severe decompensated aortic regurgitation produces a large regurgitant volume, requiring a large total stroke volume, but a reduced forward stroke volume. This causes an acute increase in left ventricular filling pressures and severe acute heart failure. (**c**) Chronic compensated severe aortic regurgitation: the left ventricle has dilated markedly, to increase total forward stroke volume back to normal (100 cc), although regurgitant fraction is still 50% and pulse pressure is high, leading to normal left ventricular filling pressures, normal LV end systolic volume (ESV), and a high ejection fraction. (**d**) Chronic decompensated aortic regurgitation. Impaired LV emptying produces an increase in ESV, a reduction in forward stroke volume, and elevation in LV filling pressures, with continued progressive left ventricular dilation, a continued wide pulse pressure, and moderately elevated LVEDP. (**e**) Same patient as "D" immediately after aortic valve replacement. Elimination of aortic regurgitation has left LV dysfunction with a high EDV, though less severe than preop, and milder elevations of LV filling pressures. ESV is also decreased, but to a lesser extent, resulting in an initial decrease in EF to 43%. The forward stroke volume and the blood pressure have returned to normal

Table 11.5 Indications for surgery in severe (4+ or 3–4+) aortic regurgitation

- Symptomatic – NYHA class II or greater
- Asymptomatic, with
  - LV dysfunction
    - EF < 50%
    - Declining EF on exercise testing
  - LV dilation
    - LVESD > 5.0 cm (? 5.5 cm)
    - LVEDD > 7.0 cm (? 7.5 cm)
    - Progressive increase in size

at diastolic diameter, respectively, postoperative survival is significantly decreased with an end-diastolic diameter above 75 mm, so surgical plans are often made when the end-diastolic diameter goes above 70 mm, particularly if they also have an abnormal LV response to exercise (Fig. 11.3). In smaller individuals, particularly women, these criteria should be adjusted for the patient's body surface area.

Additional attention should be paid to the rate of change of LV chamber enlargement and depression of LV function. In patients where systolic dysfunction has just developed, the likelihood of postoperative improvement in ejection fraction is higher. Among patients with severe aortic regurgitation and normal LV systolic function at baseline, about 6% will progress to symptoms and 3% will progress to asymptomatic LV dysfunction each year.

In asymptomatic patients with normal systolic function, it appears that chronic vasodilator therapy with nifedipine, hydralazine, or angiotensin-converting enzyme inhibitors is associated with more favorable long-term outcome, with less transition to surgery or heart failure, though some recent data does not support this practice.

Mitral Stenosis

In mitral stenosis (MS), the threshold for decisions to do surgery is affected by the availability of an excellent nonsurgical alternative, percutaneous balloon valvotomy. Also, the relative lack of effects of MS on the left ventricle makes the size and function of the left ventricle a relatively unimportant factor in the operative decision in this valve lesion (Fig. 11.4).

The threshold that warrants intervention for MS is based on symptoms, but at a some what higher threshold than is the case with aortic stenosis or mitral regurgitation. In addition, what symptom level is the criterion for intervention depends on the degree of rheumatic fibrosis of the mitral valve. Class II symptoms warrant consideration for mitral balloon valvotomy (Fig. 11.5), whereas class III symptoms are the major criterion for intervention when mitral valve surgery is likely (Fig. 11.6).

The criteria for intervention in mitral stenosis, therefore, depends on what intervention will likely be feasible, which can be predicted by the degree of valvular thickening, calcification, restricted leaflet motion, and subvalvular thickening on echocardiography. The "echo score" or "splittability index" is derived from the sum of qualitative assessments on a scale of 1–4 of the echo appearance of these four factors. When the sum is 8 or less, indicating milder rheumatic fibrosis, but the stenosis is severe enough to cause class II symptoms, the patient is eligible to have balloon mitral valvotomy. When patients become unsuitable for balloon treatment, due to persistent left atrial thrombus despite anticoagulation, or if balloon valvotomy is performed but stenosis recurs, then valve repair or valve replacement is a reasonable alternative.

In patients with more valvular fibrosis, calcification, and subvalvular fusion, where the echo score is 9 or greater, we expect that mitral valve surgery will be the outcome if surgery is required. On these patients, we would usually wait longer before intervention, until the patient's symptoms have reached NYHA functional class III. Given the greater risk of mitral prosthetic replacement and the potential long-term complications of a prosthetic mitral valve, there are stricter indications for mitral valve operation than for balloon valvotomy. Repair for such patients entails commissurotomy and debridement of the valve and chordae. Valve replacement, as opposed to repair, is almost always the surgical outcome in patients with a splittability index above 11 who undergo surgery.

Another factor in the decision for intervention for mitral stenosis is the degree of mitral regurgitation (MR), which obviously cannot be improved by balloon valvotomy and may even be worsened. In patients with moderate or more concomitant MR, but a low mitral splittability index, surgical mitral repair with an annuloplasty is preferred by some authors. At surgery, there exists a trade-off between the prospects of repairing the mitral valve, which leaves the patient subject to progressive rheumatic fibrosis in the native valve, versus the life span of the available prosthetic valves, and the associated

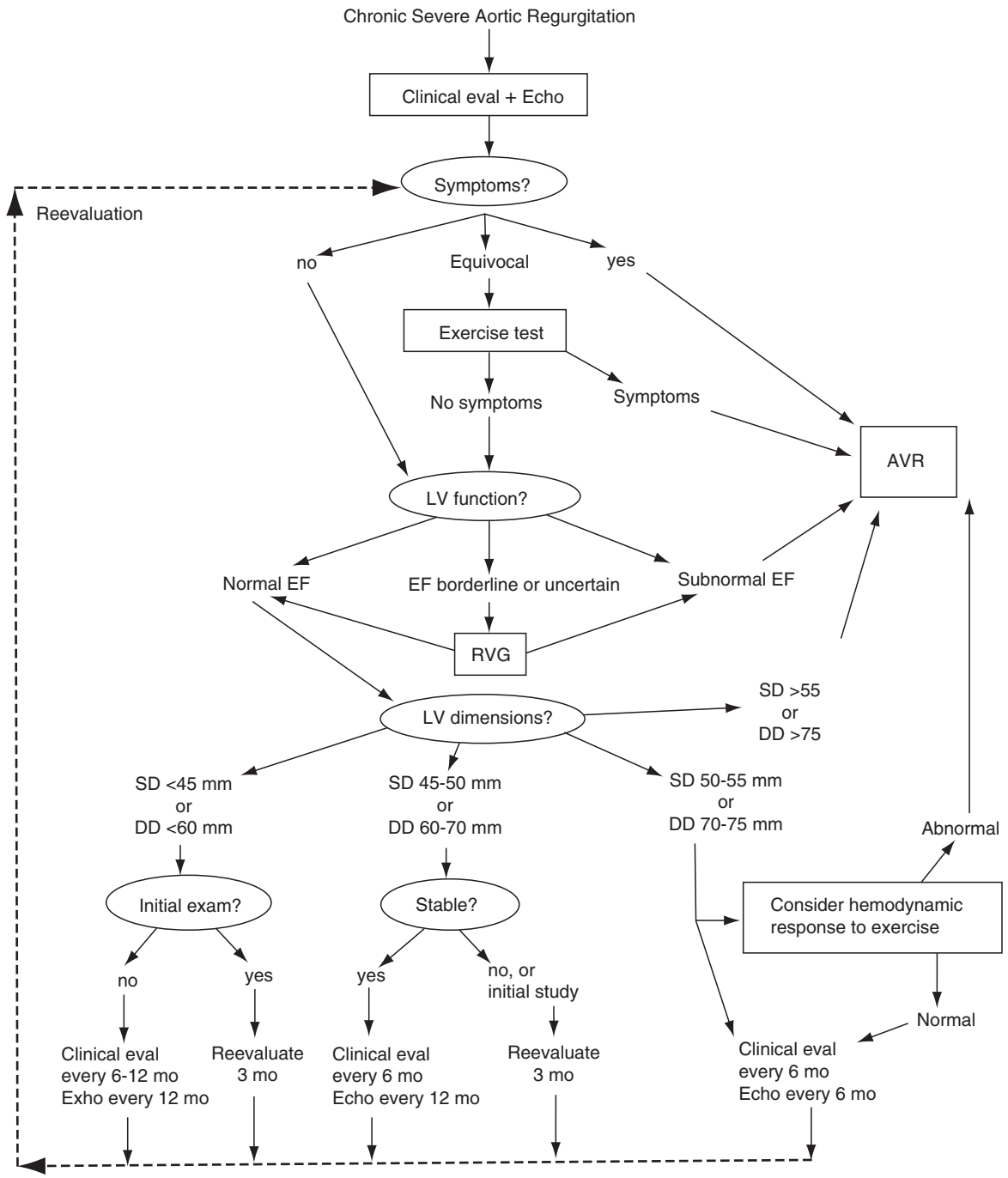

Fig. 11.3 Strategy in chronic severe aortic regurgitation. Management of patients is based on symptoms, exercise testing, left ventricular assessment by echocardiography, and exercise testing. *AVR* aortic valve replacement; *LV* left ventricle; *EF* ejection fraction; *RVG* radionuclide ventriculogram; *SD* systolic diameter; *DD* diastolic diameter; *mo* months; *mm* millimeters. Adapted from Bonow RO, et al. ACC/AHA 2006 guidelines for the management of patients with valvular heart disease: a report of the American College of Cardiology/American Heart Association Task Force on Practice Guidelines. *J Am Coll Cardiol.* 2006;48(3):e1-e148

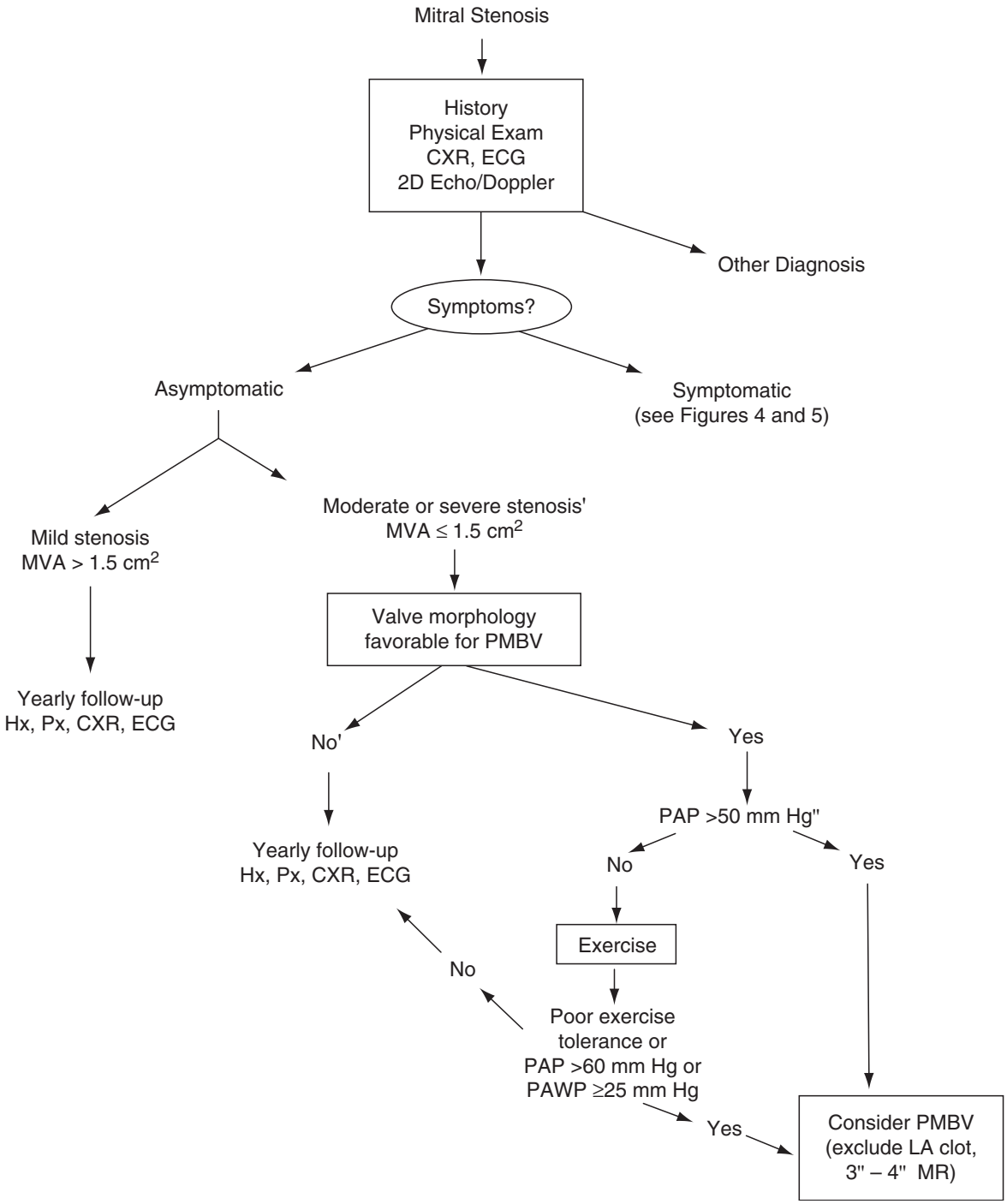

Fig. 11.4 Strategy in of mitral stenosis: Management is based on clinical data, symptoms, and mitral valve area (MVA). Valve morphology is assessed to determine suitability for percutaneous mitral balloon valvotomy (PMBV). *LA* left atrium; *MR* mitral regurgitation; *PAP* pulmonary artery pressure; *PAWP* pulmonary artery wedge pressure; *CXR* chest X-ray; *PX* physical exam; *HX* history; *ECG* electrocardiography. Reproduced from Bonow et al 2006. This figure indicates the decision process in deciding on percutaneous balloon valvotomy for mitral stenosis

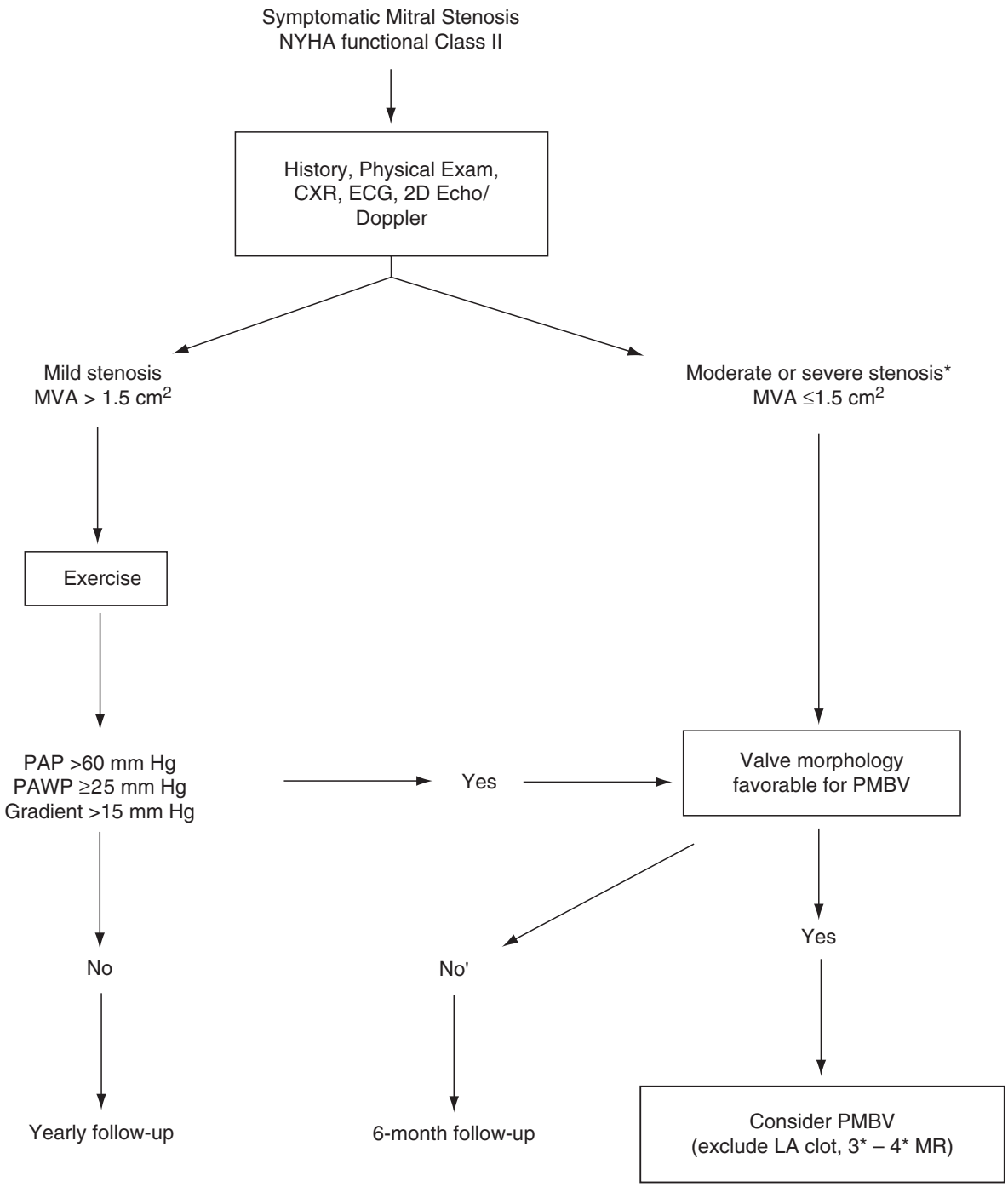

Fig. 11.5 Strategy for patients with class 2 symptoms of mitral stenosis – Management is based on the severity of MS as assessed by echocardiography and Doppler at rest and during exercise testing. When exercise-induced pulmonary artery systolic pressure is greater than 60 mmHg or the mean mitral gradient is greater than 15 mmHg, and the patient has a low splittability index and no left atrial clot, and moderate or less mitral regurgitation, balloon valvotomy is a reasonable choice. Adapted from Figure 4 of Bonow RO et al.

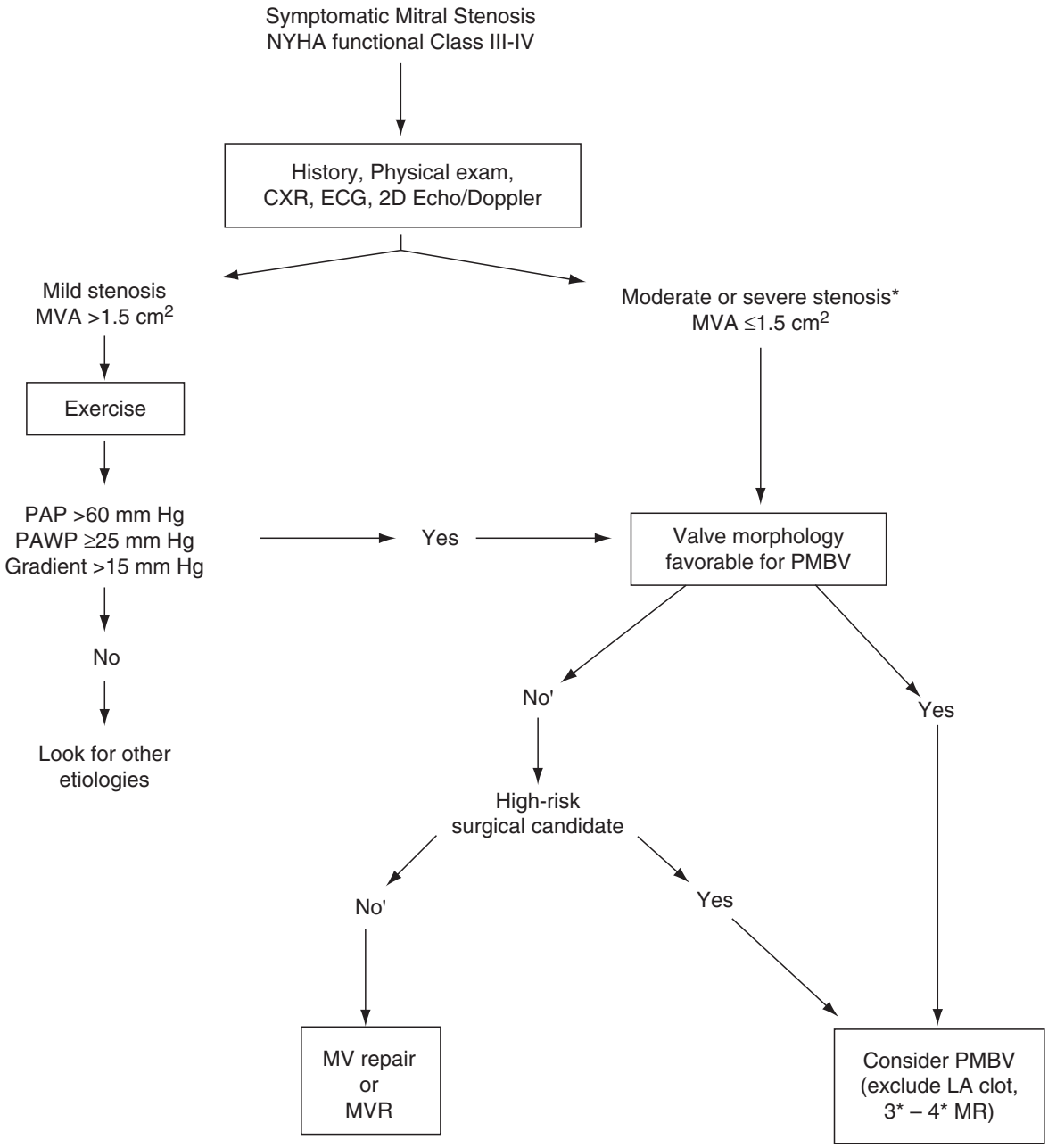

Fig. 11.6 Strategy for patients with mitral stenosis who have more severe NYHA functional class 3–4 symptoms. Management is based on the severity of mitral stenosis by valve area at rest, and mean mitral gradient greater than 15 mmHg at peak exercise, or right ventricular systolic pressure (PAP) greater than 60 mmHg at peak exercise, measured by exercise echocardiography. Patients who are not high risk for surgery, and who do not have valve morphology favorable for balloon valvotomy, are the best surgical candidates. Adapted from Figure 5 of Bonow RO et al.

problems of anticoagulation, prosthetic valve endocarditis, tissue degeneration, and thrombosis.

The onset of atrial fibrillation often heralds the onset of sufficient mitral stenosis to warrant intervention. Although the guidelines for therapy for MS do not include this issue, some would advocate balloon valvotomy or operation on patients who are asymptomatic, if they have recurrent atrial fibrillation, systemic thromboembolism, or moderately severe pulmonary hypertension.

Mitral Regurgitation

In mitral regurgitation (MR), the threshold for mitral operation has moved earlier in recent years, largely due to the increased feasibility and declining operative risk of mitral valvuloplasty and its favorable outcome compared to mitral valve replacement (Fig. 11.7). The threshold is likely to move even earlier with future improvements in surgical methods and with the advent of percutaneous valve repair for mitral regurgitation.

Certainly a patient with ANY symptoms of heart failure *resulting from* the severe MR is a candidate for surgery (Fig. 11.8). Again, the key phrase *resulting from* is clinically difficult to ascertain. The other components of the decision include the presence of atrial fibrillation, whether the valve is easily repairable, and the assessment by imaging of LV function, systolic size of the left ventricle, and pulmonary artery pressure. The resting echocardiogram is used for all these determinations, even the rhythm, if it is not obvious from the EKG. Echo can additionally be used to determine MR severity and mechanism and, using exercise echo, latent myocardial dysfunction.

The echocardiographic determination of the mechanism of mitral regurgitation is used to predict the feasibility of mitral repair. This is done using detail of leaflet motion from echo imaging and information about MR jet direction from the color Doppler study. When there is excessive leaflet motion, the MR jet direction is away from the leaflet with the most pathology, the etiology is usually prolapse or flail, and the feasibility of repair is 90–95%, depending on the complexity of the problem. When there is restricted leaflet motion, the MR jet direction is toward the leaflet with the most pathology, the etiology is usually rheumatic, and the feasibility of repair is 35–63%. When MR exists in the presence of normal leaflets, the jet direction is usually central or slightly posterior, and the mechanism is usually "apical tethering of normal leaflets." The etiology of this "functional" MR is often LV dysfunction from ischemic heart disease or cardiomyopathy, and the feasibility of repair is 80–92%. Less commonly, MR with normal leaflet motion results from a leaflet perforation or congenital cleft. Mitral regurgitation due to myxomatous degeneration, causing leaflet prolapse or flail of the middle scallop of the posterior leaflet, is the most common type of MR, and also the most likely to have successful mitral repair, over 95% in experienced hands.

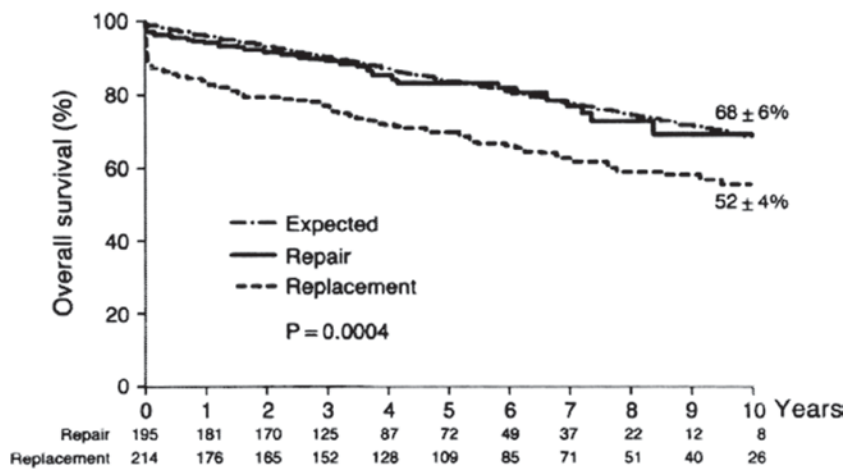

Fig. 11.7 Overall survival after valve surgery for mitral regurgitation, showing a substantial improvement in survival for mitral valve repair compared to replacement. Postoperative survival for patients undergoing valve repair matches the age and sex-matched expected population. Adapted from Sarano M et al.

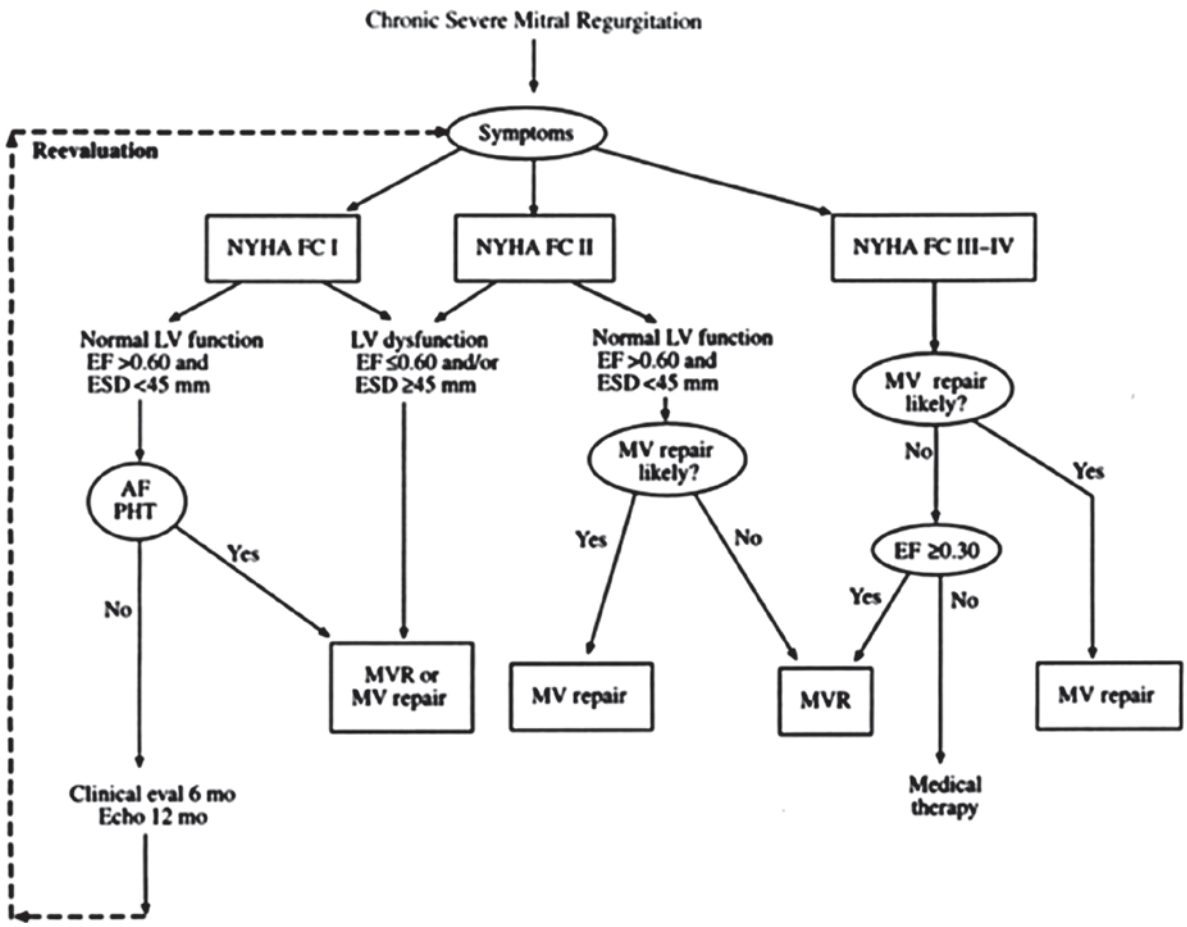

Fig. 11.8 Strategy for chronic severe mitral regurgitation. Management is based on symptoms, resting ejection fraction, echocardiographic left ventricular end systolic diameter (ESD), atrial fibrillation (AF), and pulmonary hypertension (PHT). Note that patients with an ejection fraction of less than 30% in whom symptoms are class 3 or above and repair is unlikely would be managed medically by this set of paradigms, though some exceptions may be made. Adapted from Bonow RO et al.

When repair is highly likely in the hands of the surgeon who will perform the procedure, the threshold for operation is substantially lower than when repair is uncertain or unlikely. In patients where valve repair is uncertain, surgery is more appropriate at a somewhat later phase in the natural history of the disorder.

In deciding on the timing of surgery in patients with MR, it is also important to look for occult LV dysfunction. The myocardial abnormalities are sometimes hidden because the ejection fraction may be normal, due to the increased preload inherent in MR, and the ejection of part of the LV output into the left atrium, which has inherently lower pressure than the aorta. In the presence of severe MR, the truly normal LV should have an elevated, hyperdynamic ejection fraction (Fig. 11.9). Therefore, resting LV ejection fraction is not sensitive to the onset of myocardial dysfunction, especially in presence of altered loading conditions of MR.

An exercise echo may be useful to identify occult LV dysfunction. It also may help determine the patient's symptoms at a significant workload, the presence of inducible atrial fibrillation, the peak exercise blood pressure, the presence of inducible ischemia, and the presence of inducible pulmonary hypertension at rest or with exercise. New findings occurring on a stress echo study that are associated with some consideration for operative intervention in severe MR include: an increase in LV end-systolic volume with exercise, a decrease in LV ejection fraction, an increase in RV volume, inducible ischemia, pulmonary HTN, rest or inducible arrhythmias, or decreased exercise tolerance.

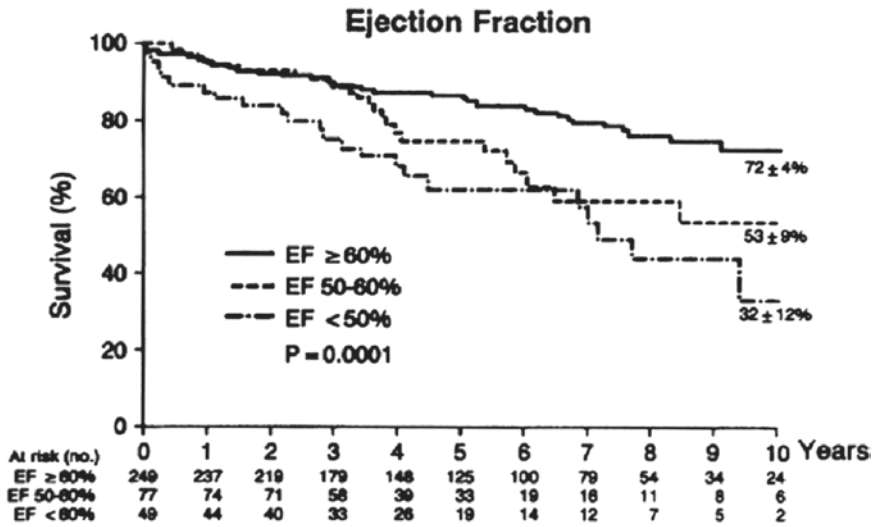

Fig. 11.9 Survival after surgery for mitral regurgitation based on preoperative resting ejection fraction. Ten-year survival for those with a preoperative ejection fraction of 50–60 is lower than those with normal resting preoperative ejection fraction (above 60%) and higher than those with preoperative ejection fraction less than 50%. Adapted from Sarano M et al.

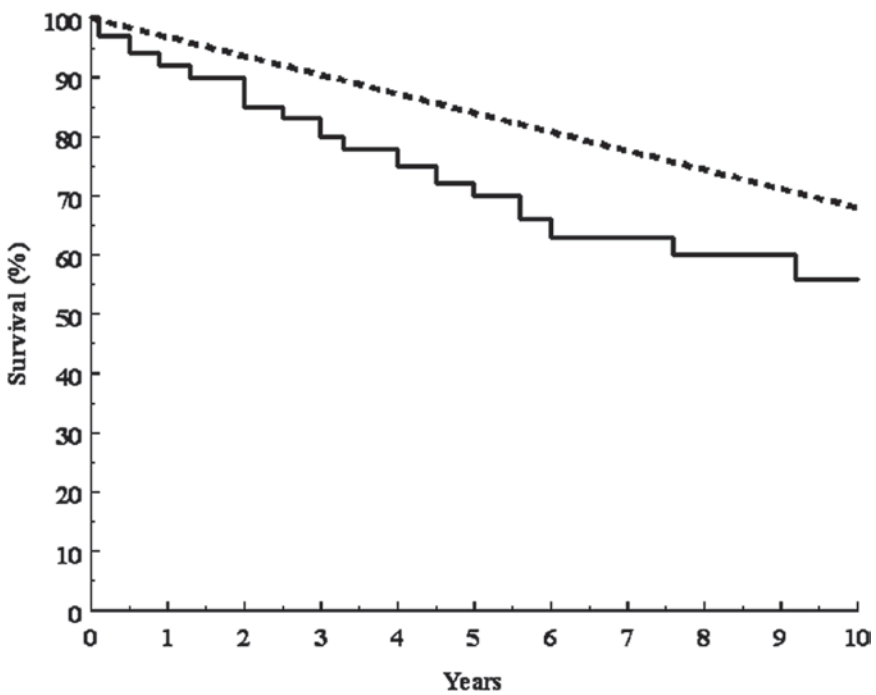

Fig. 11.10 Differential survival based on the presence of flail mitral leaflet, comparing medical therapy (*curved line*) compared to surgical management. Patients with flail who are managed surgically have a higher 10-year survival. Adapted from Ling et al.

Some have advocated operation on patients who are asymptomatic, if they have truly severe mitral regurgitation (by quantitative Doppler echocardiography), if the patient and the surgical plans make valve repair likely, and if the repair can be monitored with intraoperative echo.

One group of investigators has followed patients with mitral flail and noted an increase in mortality with medical compared to surgical management (Fig. 11.10). This has led to the recommendation that patients with flail should undergo surgery even if other surgical indicators are absent, a policy which

Table 11.6 Indications for surgery for mitral reguwrgitation

- Any heart failure symptoms from MR
- Asymptomatic with a repairable valve, severe 4+ MR and
  - Concomitant CAD
  - LV enlargement – LVIDs > 4.5 cm
  - Systolic dysfunction – EF < 55%
  - Pulmonary HTN – RVSP > 55
  - Recurrent atrial fibrillation
  - Exercise echo with "Latent LV dysfunction" (declining EF or increasing ESV from rest to exercise)
  - Flail mitral leaflet ??
  - ROA > 0.6 cm^2 ??

Reprinted from Stewart WJ. Myocardial factor for timing of surgery in asymptomatic patients with mitral regurgitation. Am Heart J. 146(1):5-8. Copyright (2003) with permission from Elsevier

awaits further validation. The finding of mitral flail may be a morphologic marker for *very severe* mitral regurgitation, for example a patient with a regurgitant orifice area much higher than the threshold of 0.40 cm^2, which is the criterion for severe 4+ MR. This may the reason for the observed increase in mortality with medical management in asymptomatic mitral flail managed medically.

If the risk of waiting exceeds the risk of operating on such patients, pre-emptive surgery in asymptomatic patients is appropriate. My own synthesis of the timing of surgery in patients with mitral regurgitation (Table 11.6) incorporates all these features.

Summary

The ultimate decision of "should we operate now?" must be addressed with each patient carefully, looking at the individual characteristics of the patient's signs and symptoms, and comparing those to the expected milestones of the disease in question. Echocardiography give us much invaluable information that is useful in the process. We envision a "golden moment" at which it would be best to intervene surgically on a given patient's valve, that would optimize their survival and quality of life. Unfortunately, these determinations involve the impossible task of trying to predict the future, in diseases that have many and varied outcomes.

Bibliography

Bonow R, et al. ACC/AHA guidelines for valvular heart disease. *J Am Coll Cardiol*. 1998;32:1486.

Cannon JD, Zile MR, Crawford FA, Carabello BA. Aortic valve resistance as an adjunct to the Gorlin formula in assessing the severity of aortic stenosis in symptomatic patients. *J Am Coll Cardiol*. 1992;20(7):1517–1523.

Grigoni et al. J Am Coll Cardiol. Dec, 1999

Klodas E, Enriquez-Sarano M, Tajik AJ, Mullany CJ, Bailey KR, Seward JB. Surgery for aortic regurgitation in women: contrasting indications and outcomes compared with men. *Circulation*. 1996;94:2472–2478.

Ling LH, et al. Clinical outcome of mitral regurgitation due to flail leaflet. *N Engl J Med*. 1996;335:1417–1423.

Otto CM, Lind BK, Kitzman DW, Gersh BJ, Siscovick DS. Association of aortic-valve stenosis with cardiovascular mortality and morbidity in the elderly. *N Engl J Med*. 1999;341:142–147.

Ross J Jr, Braunwald E. Aortic stenosis. *Circulation*. 1968;38:61–67.

Stewart WJ. Myocardial factor for timing of surgery in asymptomatic patients with mitral regurgitation. *Am Heart J*. 2003;146:5–8.

Stewart WJ, Currie PJ, Salcedo EE, Klein AL, Marwick TH, Cosgrove DM. Evaluation of mitral leaflet motion by echocardiography and jet direction by Doppler color flow mapping to determine the mechanism of mitral regurgitation. *J Am Coll Cardiol*. 1992;20:1353–1361.

Wilkins GT, Weyman AE, Abascal VM, Block PC, Palacios IF. Percutaneous balloon dilatation of the mitral valve: an analysis of echocardiographic variables related to outcome and the mechanism of dilatation. *Br Heart J*. 1989;60(4):299–308.

Chapter 12
Clinical Echocardiography Prosthetic Valves

John Chambers

Introduction

The history of heart valve surgery begins in the early twentieth century (Table 12.1) although the first clinical valve implantation was of a Starr–Edwards valve (Fig. 12.1) in 1960. Early assessment of replacement heart valves was by cardiac catheterization and fluoroscopy. Echocardiography is now the gold standard although fluoroscopy remains useful for detecting reduced mechanical leaflet motion in suspected thrombosis.

Classification of Valves

Replacement valves are frequently named both after the surgeon involved with the design and also the manufacturing company (e.g., Bjork–Shiley, Starr–Edwards, Ionescu–Shiley (Table 12.2)). They are usually classified according to type, size, and position. The main types are divided broadly into mechanical and biological.

Mechanical Valves

The proportion of mechanical valves implanted in the West is falling partly as a result of mitral repair becoming more popular. In addition, calcific degenerative aortic valve disease is increasingly common as the population ages and, at surgery, most of these patients will receive a biological valve. The proportion of mechanical valves varies from country to country, but is usually just below 50%. Most of these valves are bileaflet mechanical valves which are the least obstructive design (Fig. 12.2). The various designs differ in the composition and purity of the pyrolytic carbon, in the shape and opening angle of the leaflets, the design of the pivots, size and shape of the housing, and the design of the sewing ring. For example the St Jude Medical valve has a deep housing with pivots contained on flanges which can be imaged echocardiography. The Carbomedics has a shorter housing allowing the leaflet tips to be imaged clearly. The MCRI On-X has a long, flared housing, and this is also obvious at echocardiography.

Biological Valves

Most biological replacement valves are stented xenografts (Fig. 12.3). The stent is a plastic or wire structure covered in fabric with the cusps of the valve placed inside and a sewing ring attached outside. The valve cusps usually consist of pericardium or a porcine aortic valve. The porcine aortic valve may be used in its entirety as in the Carpentier–Edwards valve. However there is a muscle bar at the base of the right coronary cusp which makes it relatively rigid. This cusp may therefore be excised and replaced by a single cusp from another pig or, more frequently, each cusp is taken from up to three different pigs as in the Medtronic Mosaic, or the St Jude Epic, or Carbomedics Synergy. Pericardium is cut using a template and sewn inside the stent posts or occasionally, as in the Carbomedics Mitroflow, to the outside. Usually the pericardium is bovine, but occasionally porcine and, experimentally, from kangaroos.

J. Chambers
Cardiothoracic Department,
St Thomas' Hospital, London, SE1 7EH, UK
e-mail: johnchambers@dial.pipex.com

P. Nihoyannopoulos and J. Kisslo (eds.), *Echocardiography*,
DOI: 10.1007/978-1-84882-293-1_12,

Table 12.1 Sketch history of replacement heart valves

1902	Brunton: cadaver mitral valvotomy
1908	Cushing and Branch: first mitral valvotomy (in a dog)
1914	Tuffier: first digital dilatation of aortic stenosis
1923	Cutler and Levine: first digital dilatation of mitral stenosis
1948	Harken/Bailey/Brock: closed mitral valvotomy
1949	Templeton and Gibbon: mitral reconstruction
1952	Hufnagel: caged ball valve
1953	Gibbon: introduction of bypass machine
1956	Murray: homograft valve for aortic and mitral use
1960	Harken: first caged-ball valve. Starr: first clinical Starr–Edwards valve implanted
1965	Binet: first aortic heterograft
1968	Hancock, Carpentier: first glutaraldehyde and formaldehyde stented heterografts
1969	Bjork: first tilting disk valve
1970	Ionescu: stented bovine pericardial valve
1977	St Jude Medical: first bileaflet mechanical valve
1980	St Jude Medical Toronto stentless valve

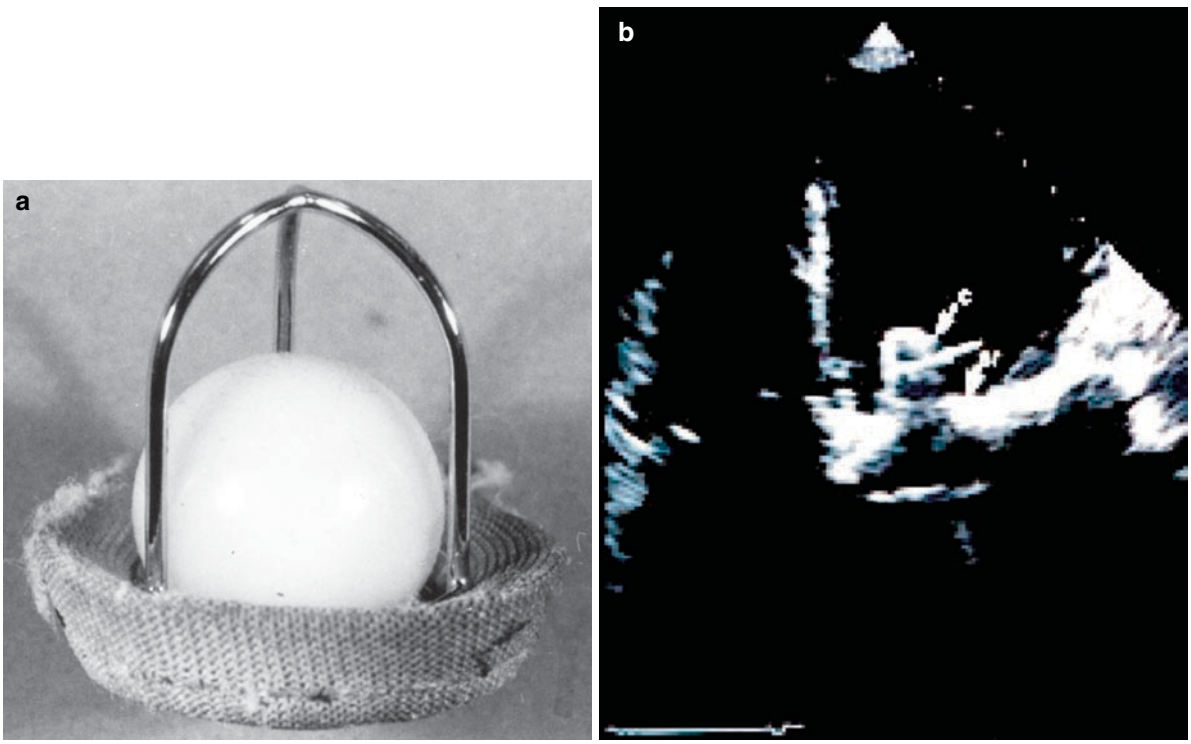

Fig. 12.1 Starr–Edwards valve. An image of an explanted valve is shown with an echocardiogram of a valve in the mitral position. The ball is arrowed. Abbreviations: *c* cage, *sr* sewing ring

A stentless heterograft valve usually consists of a preparation of porcine aorta. The aorta may be relatively long (Medtronic Freestyle) or may be sculpted to fit under the coronary arteries (Edwards Toronto, Cryolife-O'Brien). Some are tricomposite and one is made out of bovine pericardium (Sorin Freedom). The hope is that these valves will be better than stented valves in terms of:

- Hemodynamics because there is no stent to occupy the orifice
- Durability because stresses between the cusp and the stent are thought to be a major cause of valve failure
- Complication rate since the stent may contribute to thrombus formation and possibly endocarditis

Insufficient data exist to determine whether any of these possible advantages is true.

Table 12.2 Designs of replacement heart valve

Biological
Autograft (Ross Operation)
Homograft: Usually aortic, occasionally pulmonary
Stented heterograft, e.g., Hancock (porcine), Mosaic (porcine), Baxter Perimount (pericardial), Carpentier–Edwards (standard and supra-annular porcine), Intact (porcine), Labcor (porcine tricomposite), Biocor (porcine tri-composite), Mitroflow (bovine pericardial)
Stentless heterograft, e.g., Toronto (St Jude Medical), Cryolife-O'Brien, Freestyle (Medtronic), Baxter Prima, Biocor PSB tricomposite, Sorin Pericarbon (pericardial)
Mechanical
Ball-cage, e.g., Starr–Edwards
Single tilting disk, e.g., Bjork–Shiley, Medtronic-Hall, Monostrut, Omniscience, Ultracor
Bileaflet, e.g., St Jude Medical, Carbomedics, MCRI On-X, ATS, Sorin Bicarbon, Edwards Tekna, Edwards Mira

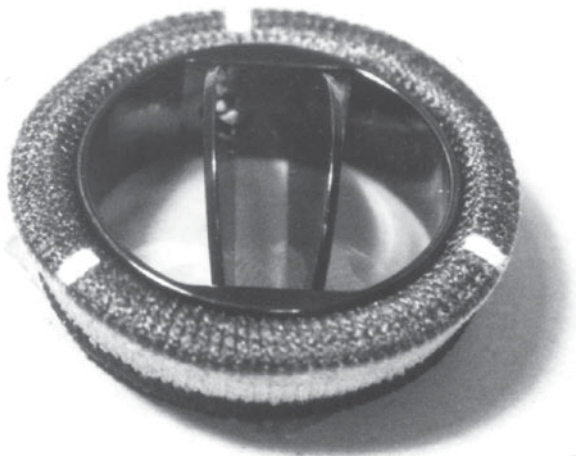

Fig. 12.2 Bileaflet mechanical valve

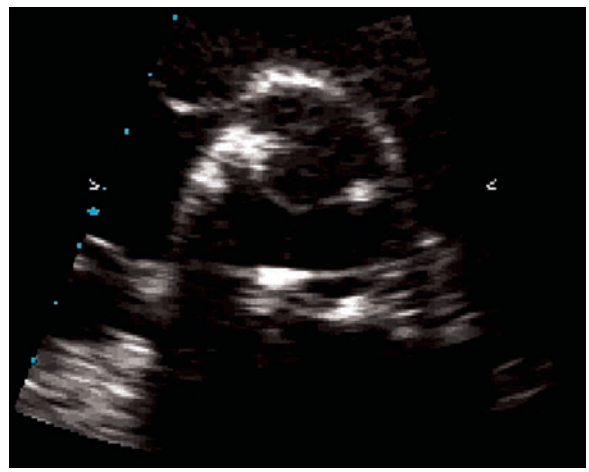

Fig. 12.3 Stented biological valve. A parsternal short-axis transthoracic view. The tips of the three stents can be seen with the edges of the three cusps within

Homograft valves consist of human aortic or occasionally pulmonary valves which are usually cryopreserved and usually left unstented. They have good durability if harvested early after death and do not need anticoagulation. For this reason they may be used as an alternative to a mechanical valve in the young. They may also be used for choice in the presence of endocarditis since they allow wide clearance of infection with replacement of the aortic root and valve and the possibility of using the attached flap of donor mitral leaflet to repair perforations in the base of the recipient's anterior mitral leaflet.

The Ross Procedure consists of substituting the patient's own pulmonary valve for the diseased aortic valve. Usually a homograft is then implanted in the pulmonary position. The rationale for such a complex procedure is that a living valve with good durability is placed in the important aortic side while the replacement valve is placed in the low pressure right side. The procedure has a relatively high early complication rate but good long-term results. There is evidence that the autograft grows which is particularly important for avoiding repeated surgery in children. It may also be relatively resistant of infection.

Position and Sizing

The stent or housing of the replacement valve and its sewing cuff occupy space that could otherwise be used for flow. To increase the area available for flow, some manufacturers reduced the bulk of the sewing ring (e.g., St Jude Medical Regent, Carbomedics reduced cuff, Baxter "Magna"). Another solution was to lift the whole valve into a supra-annular position

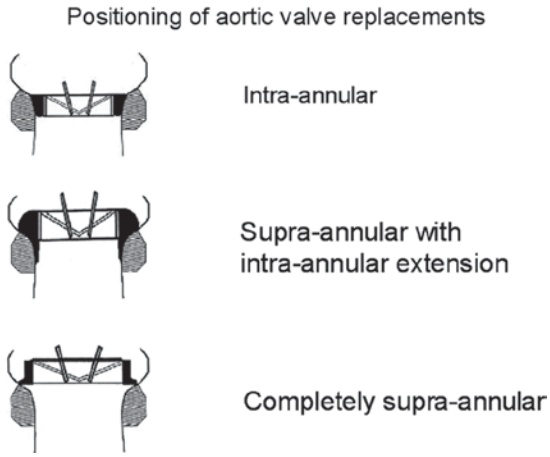

Fig. 12.4 Diagram of the three valve positions relative to the annulus

(e.g., Carpentier–Edwards supra-annular, Sorin Bileaflet mechanical, Carbomedics "Top Hat"). The orifice of a supra-annular valve could theoretically be as large as the patient orifice. However some supra-annular valves are relatively bulky and their size is limited by the diameter of the aortic root or by the position of the right coronary artery. Some valves are intermediate in position since the sewing ring is placed supra-annularly with part of the housing resting within the annulus. The MCRI On-X has a large part of its housing in the annulus, the St Jude EHP a much smaller rim (Fig. 12.4).

Almost every valve is labeled with a size which corresponds approximately to the patient tissue annulus for which it is intended. However sizing conventions vary so that there may be a wide difference between actual and nominal labeled size. The labeled size may vary between about 3 mm smaller and 3 mm larger than the patient tissue annulus diameter. Further variability may be introduced by the suturing technique and the exact positioning of the valve. Some valves are capable of being implanted either intra-annularly or supra-annularly. This is important because hemodynamic function cannot necessarily be compared in valves of the same labeled size. Secondly it is not valid to substitute the labeled size of the valve in place of measurement of the left ventricular outflow tract when applying the continuity equation. Finally the echocardiographic measurement of the left ventricular outflow tract diameter will correspond closely with the tissue annulus diameter measured at surgery, but not necessarily with labeled size so that care must be exercised when using echocardiography to guide sizing of the prosthesis.

Complications

There is no ideal replacement valve and all can have complications:

- Primary failure
- Thrombosis
- Mechanical obstruction by pannus
- Thromboembolism
- Endocarditis
- Dehiscence
- Hemolysis
- Hemorrhage

Primary failure means deterioration of the valve without secondary infection or other cause. It is almost exclusively a problem of the biological valves and occurs more quickly for the mitral than the aortic position. The survival to 10 years is about 70% in the aortic and 60% in the mitral position. Durability is worse in the younger patient (aged under 60 years for the aortic and under 65 years for the mitral position). It may also be affected by blood pressure and cholesterol levels. Leaflet escape has occurred for a small number of types of mechanical valve notably the Bjork–Shiley Convexo-Concave.

Thrombosis is relatively uncommon in biological valves and in mechanical valves in the aortic position. It occurs at a rate of about 0.1–0.2% p.a. in mechanical valve in the mitral position and more frequently in the tricuspid position.

Pannus is overgrowth of endothelium which covers the valve and interferes with the opening of the occluder. It is mainly a problem of mechanical valves. Usually it leads to obstruction, but may occasionally hold a valve open and cause regurgitation. It may also induce secondary thrombosis or thromboembolism.

Thromboembolism is probably related more to patient factors such as age, cardiac rhythm, left ventricular function, and atrial size than to the replacement valve. It occurs at a rate of 1–4% p.a. in mechanical and 1–2% p.a. in biological valves and is more common for valves in the mitral than the aortic position.

Endocarditis occurs in approximately 3% of patients in the first year, then about 0.5–1% per year thereafter. It is similar in frequency in mechanical and biological valves although possibly less common in mechanical valves in the mitral position. The stentless valves (autograft, homograft, and stentless heterografts) are perceived to be relatively resistant to infection although this remains unproved.

Dehiscence is the opening of a gap outside the sewing ring leading to paraprosthetic regurgitation. This may occur at the time of surgery as a result of poor technique or poor tissues as a result of heavy calcification, endocarditis or abnormalities of collagen, e.g., in Marfan Syndrome. It is more likely in valves with relatively thin sewing rings and less likely in valves with bulky sewing rings (e.g., Starr–Edwards). It may occur late as a result of endocarditis, but also on occasions with disintegration of the sewing ring and degeneration of the patient annulus.

Mild hemolysis occurs in almost all mechanical valves, but is usually compensated. The blood lactate dehydrogenase and bilirubin levels are high and the haptoglobin level low, but the hemoglobin level normal. Anemia occasionally occurs in the presence of an aggravating cause such as iron deficiency, but otherwise suggests the presence of a paraprosthetic leak. This is often small and clinically occult. It may only be detected by transesophageal echocardiography.

Bleeding is included as a valve-related complication because warfarin is essential for mechanical valves and so cannot be dissociated from the valve itself. It occurs at a rate of about 2% p.a. in mechanical valves, 1% p.a. for biological mitral valves, and 0.5% p.a. for biological aortic valves.

Criteria for Use

More than 10,000 valves are implanted each year in the UK, and over 100,000 in the USA. Biological valves have the advantage of not needing treatment with warfarin, but the disadvantage of primary failure beginning after about 8 years in the aortic position and 5 years in the mitral position. By contrast mechanical valves effectively have no primary failure, but have the disadvantages of needing treatment with warfarin and therefore being open to the possibility of anticoagulant-related hemorrhage.

In general, patients needing aortic valve replacement are usually given a biological valve if they are aged more than 65 years and a mechanical valve if they are aged below 60 years. In between 60 and 65 years, the choice depends on individual patient factors including their own preference. Exceptions are the younger person unwilling or unable to have warfarin in whom a Ross procedure or homograft are alternatives. In patients not suitable for mitral valve repair, a mechanical valve is usually implanted below the age of 65 years, and a biological valve above the age of 70 years. Individual factors must again be applied in the range 65–70 years. Improvements in life-expectancy mean that many patients with biological valves are beginning to live long enough to require consideration of redo surgery.

Some specific situations are outside these general rules. Some surgeons preferentially use a biological valve in a woman considering childbirth to avoid the need for warfarin. However this necessitates further surgery after a short duration long enough to complete the family. The relative merits of mechanical and biological valves remain unresolved. Recent attempts to combine all events including anticoagulant-related hemorrhage suggest that survival free of redo surgery or adverse events may be similar for both types of valve. The choice of valve is made particularly difficult because durability data on the newer designs including the stentless valves are lacking. It is important to individualize the choice of valve and to involve those patients in that choice if they want to be.

Echocardiography

The echocardiography of replacement heart valves is more demanding than of native valves for the following reasons:

- *Obstruction*. Almost all replacement valves are obstructive compared to normal native valves. The differentiation between normal and pathological obstruction may be difficult.
- *Regurgitation*. Transprosthetic regurgitation is normal for almost all mechanical valves and for many biological valves. This can be mistaken for pathological regurgitation.

- *Normal variability*. The appearance, forward flow, and patterns of regurgitation differ between valve designs. Experience gained from one valve type may lead to confusion if extrapolated to another.
- *Technical difficulties*. Shielding from the ultrasound beam by mechanical parts can obscure vegetations or a regurgitant jet. Blooming or reverberation artifacts can cause overdiagnosis of abnormal masses or of calcification.

Appearance

A replacement valve usually consists of an occluder (tilting disk or cusp) inside a valve housing and attached to a sewing ring (Figs. 12.1 and 12.2). These structures are usually visible on echocardiography and are more obvious in the mitral position. For a valve in the aortic position it may be difficult to image a cage which is usually seen best in an apical long-axis view. There should be no abnormal extrinsic masses attached to the valve although stitches may be seen and thin fibrinous strands are normal. It is normal to see echoes resembling bubbles in the left ventricle in the presence of a replacement mitral valve. These occur with all designs but are most frequent with bileaflet mechanical valves. Their origin is not known. They are probably benign although occasional reports link them to abnormalities of higher cognitive function.

Stentless valves may be surrounded by edema and hematoma. This ultimately resolves over 3–6 months and is associated with a rise in effective orifice area and a fall in transaortic pressure difference. On transesophageal echocardiography, the appearance may be impossible to differentiate from an abscess (Fig. 12.5).

A retained posterior leaflet in the presence of a replacement mitral valve can also look like an abscess since the surgeon may roll the leaflet into a "cigar" before putting a stitch through it and into the sewing ring (Fig. 12.6).

Does the Valve Rock?

This suggests dehiscence and is proved by overlaying color Doppler and demonstrating a paraprosthetic regurgitant jet. Usually rocking in the aortic position implies a large dehiscence, about 30% of the sewing ring.

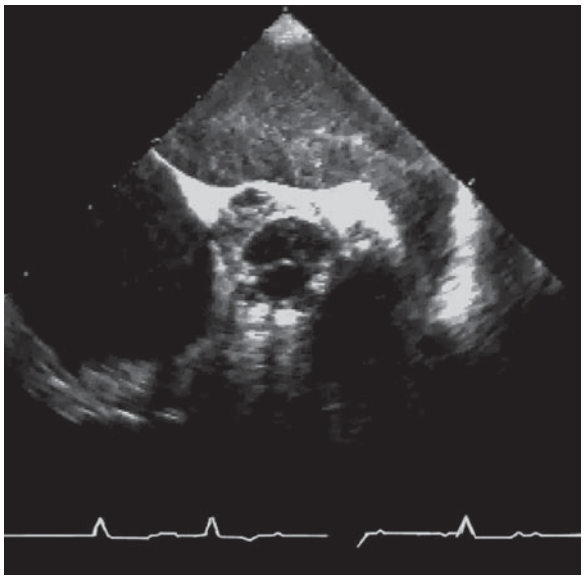

Fig. 12.5 Stentless valve early after implantation. There is edema and hematoma around the valve which is normal, but could be mistaken for an abscess

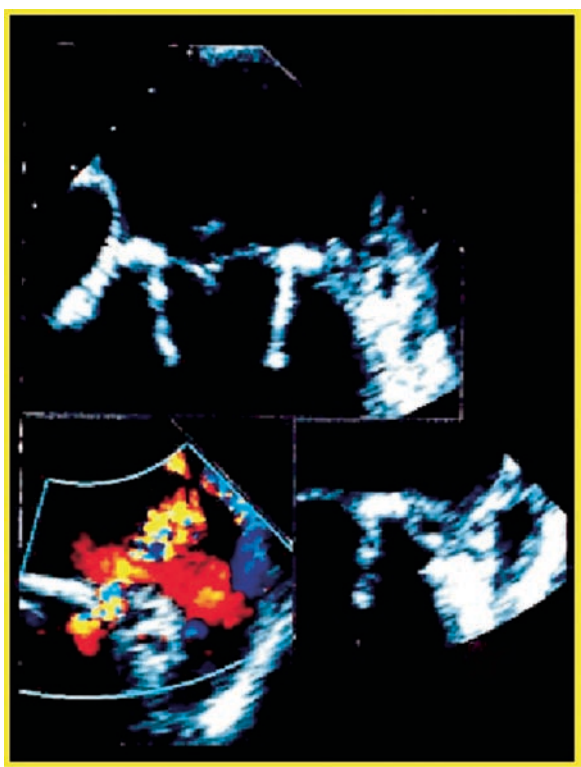

Fig. 12.6 Retained posterior leaflet. There is a rolled appearance to the tissue attached to the lateral part of the sewing ring (*top*) which can be normal. However in this example there is also a dehiscence (*bottom left and right*) as a result of endocarditis

In the mitral position if the surgeon has retained the posterior leaflet there may be rocking without dehiscence

Check the Occluder

If the valve is biological the cusps should be thin (around 1 mm) and fully mobile with no extraneous masses. There should be no movement of any part of the cusp behind the plane of the annulus. If the valve is mechanical, the occluder should open quickly and fully. The color map should fill the whole orifice in all views.

Forward Flow

Measurements should be taken over 1–3 cycles in sinus rhythm but usually five in atrial fibrillation. Measurements needed are:

Aortic position: Peak velocity, derived peak & mean pressure difference and effective online area by the continuity equation.
Mitral position: Peak velocity, mean pressure difference and pressure half-time.
Tricupid position: Peak velocity, mean pressure difference and pressure half-time.

High flow can cause unrepresentatively high peak velocities in replacement aortic valves. It is important to derive the mean pressure difference because it is calculated using the whole waveform and better reflects function than using the peak velocity alone. In a normal valve, the subaortic velocity may not be negligible compared with the transaortic velocity, so the long form of the modified Bernoulli equation should be used. Peak pressure drop across the aortic valve is calculated from the formula:

Peak $\Delta P = 4(v_2^2 - v_1^2)$, where v_1 and v_2 are peak velocities in the subaortic and transaortic signal, respectively. Mean pressure difference cannot be derived from the respective mean velocities. It should ideally be derived from multiple calculations of pressure difference using instantaneous velocities on the pulsed and continuous waveforms. This can be calculated from the online software as aortic mean ΔP – subaortic mean ΔP.

Because of the flow dependency of velocity and pressure difference, effective area by the continuity equation (EOA) should be calculated routinely from the formula:

EOA = CSA × VTI_1/VTI_2, where CSA is left ventricular outflow cross-sectional area in cm^2 calculated from the diameter assuming circular cross-section; VTI_1 is subaortic velocity integral in cm; and VTI_2 is aortic velocity integral in cm. Errors arise if the peak velocity is used in place if the velocity integral. It is not usually appropriate to substitute the labeled size of the replacement valve for the left ventricular outflow tract diameter because, as discussed earlier, this may differ widely from its true size. For serial studies it is reasonable to use the ratio of the velocity integrals since this avoids measuring the left ventricular outflow tract diameter.

For the mitral valve, the subvalve velocity is negligible and in any case cannot be measured. The formula Peak $\Delta P = 4(v^2_2)$ can therefore be used and the mean pressure difference taken from the continuous-wave signal. It is not appropriate to use the Hatle formula to estimate orifice area. This is only valid for moderate or severe stenosis with orifice area <1.5 cm^2. For valve areas above this, the pressure half-time reflects atrial and left ventricular compliance characteristics and loading conditions.

Few tricuspid replacement valves are implanted, but the same methods are applied as for the mitral position. The pressure half-time is even more variable on the right than on the left side of the heart. For a valve in any position, forward flow velocities and derived pressure differences (gradient) cannot be interpreted without knowing the valve type and size. Normal ranges are given in the appendix and criteria for obstruction below in section "Detection of Obstruction."

Regurgitation

Minor regurgitation is normal in virtually all mechanical valves. Early valves had a closing volume as the leaflet closed followed by true regurgitation around the occluder. For the Starr–Edwards, there is a small closing volume and usually little or no true regurgitation. The single tilting disk valves have both types of regurgitation, but the pattern may vary. The Bjork–Shiley valve has a minor and major jet from the two orifices, while the Medtronic-Hall valve has a single large jet through a central hole in the disk (Fig. 12.7).

The bileaflet valves have continuous leakage through the pivotal points where the lugs of the leaflets are held

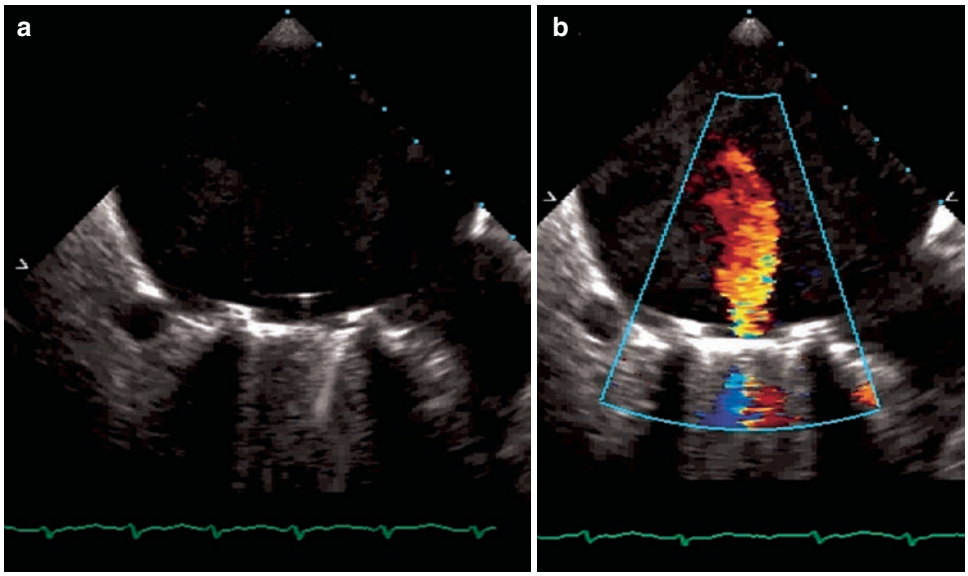

Fig. 12.7 Tilting disk valve in the mitral position. The transesophageal study shows the strut of the Medtronic Hall valve (*left*). There is a hole through the leaflet and a relatively large jet through this is normal (*right*)

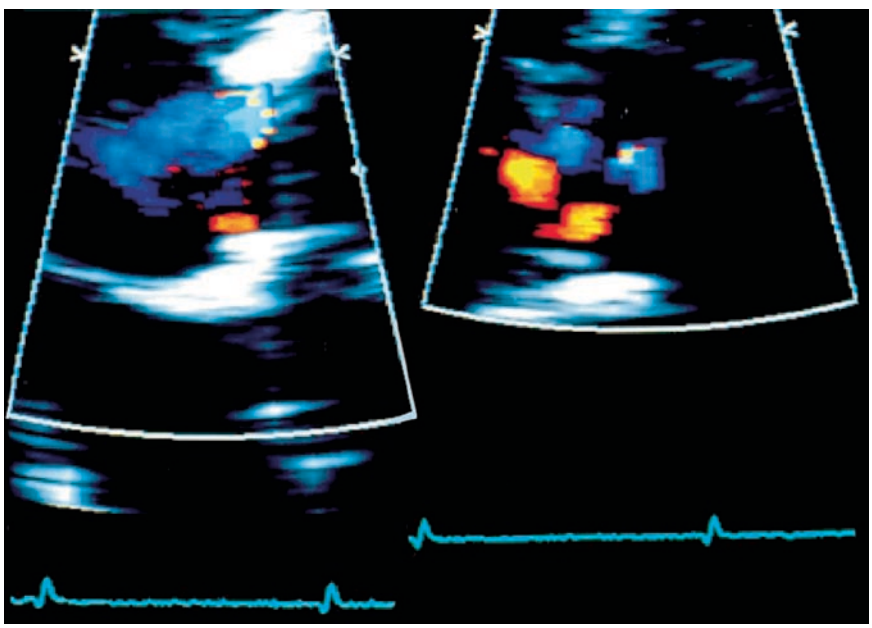

Fig. 12.8 Pivotal washing jets. Parasternal long-axis (*left*) and short-axis (*right*) views showing four jets, two from the upper and two from the lower pivotal point

in the housing (Fig. 12.8). These are thought to prevent the formation of thrombus at sites of stasis and are called "washing jets." The associated regurgitant fraction is directly related to the size of the valve and is also larger at low cardiac outputs. Although the regurgitant fraction is usually no larger than 10–15%, the associated color jets can look large, up to 5 cm long and 1 cm wide. They are usually found in formation, two from each pivotal point giving a characteristic appearance on imaging in a plane just below the valve. Sometimes these single pivotal washing jets divide into two or three separate "plumes," and in some valve designs such as the St Jude Medical there may be a jet around the edge of one or other leaflet. The jets are invariably low in momentum so that they are homogenous in color with aliasing confined to the base of the jet.

Regurgitation through the valve is also increasingly reported in normal biological valves. This is mainly because echocardiography machines are becoming increasingly sensitive. Stentless valves including homografts and autografts are more likely than the stented valves to have minor regurgitant jets, usually at the point of apposition of all three cusps or at one or more commissure. In stented valves, the regurgitation is usually at the point of apposition of the cusps. However the Labcor is a tricomposite valve formed from sewing together three separate porcine noncoronary cusps, and it commonly has trivial regurgitation at the commissures, sometimes at all three.

Detection of Early Failure

The failure mode of biological valves varies with the design, materials, and treatment. Some calcify and become stenotic. However, more tear without calcification as a result of stretching of the tissue, or abrading against the valve housing. The most reliable signs of early failure are:

- Cusp thickness
- New transprosthetic regurgitation

The mean thickness of a cusp on M-mode is 1 mm and a thickness of > 3 mm is taken arbitrarily as a sign of thickening (Fig. 12.9). This is usually a sign, not of overt thickening of the cusp, but of a small tear. This makes a small segment of the cusp turn at an angle to the ultrasound beam and look thicker. It may be associated with prolapse of the cusp and often a jet of regurgitation. About 60% of thickened cusps progress to overt failure requiring redo surgery within two years compared with about 1% of unthickened cusps. Finding a small tear is a warning to follow the patient more carefully and to plan elective surgery. A proportion of biological valves develop sudden catastrophic failure as a result of an early tear or abrasion extending.

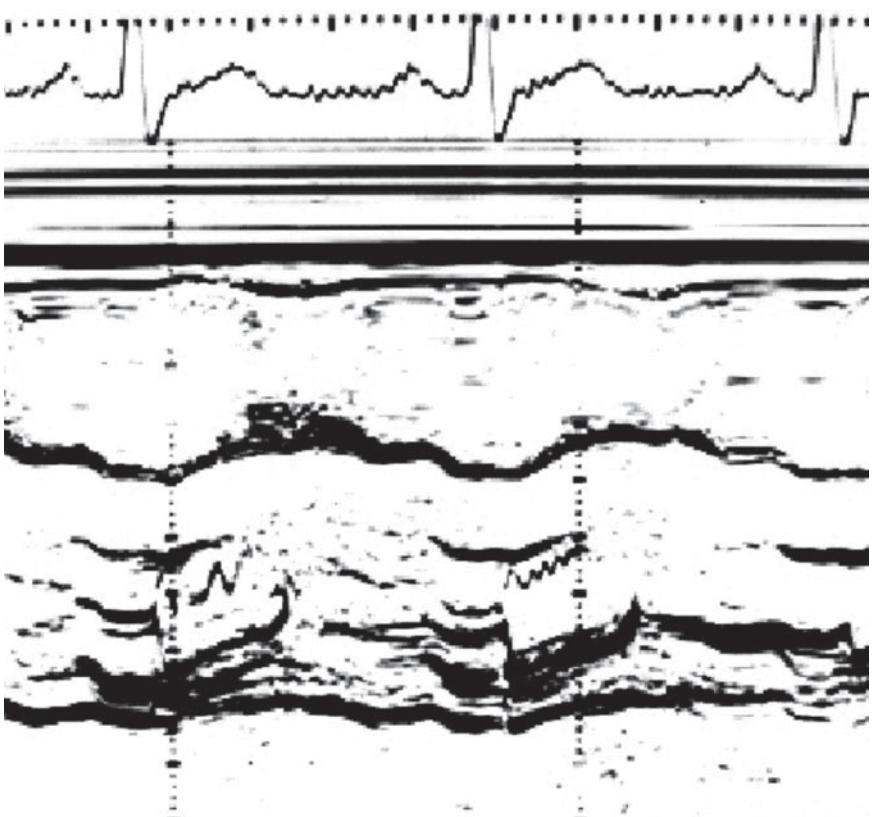

Fig. 12.9 Early failure. The earliest sign in a biological valve is thickening of the cusp usually caused by a small tear

Although apparently precise, the quantitative measures including peak velocity, pressure difference, and effective orifice area have wide normal ranges and also inaccuracies in their application. These are not useful in the detection of early valve failure although they are usually abnormal in overt obstruction.

Detection of Obstruction

Mitral Position

Heavily calcified cusps and reduced occluder motion are the most reliable signs of obstruction particularly for valves in the mitral position since the cusps, disk, or leaflets are usually imaged easily. In a bileaflet mechanical valve, partial obstruction may be obvious when one leaflet clearly moves less than the other. Even if image quality is suboptimal, color mapping can identify obstruction by showing a narrowed, high-velocity inflow jet with "wrap-around" aliasing although transesophageal imaging may sometimes be necessary to confirm this (Fig. 12.10). In a stenotic stented biological valve, the jet can be narrow at the level of the immobile cusps, but can expand rapidly to fill the orifice toward the tips of the stents. It is therefore easy to miss the abnormality. Severe impairment of left ventricular function may also cause reduced valve opening, but this will be associated with a thin, low-velocity inflow signal on color mapping.

The color signal can be unreliable in the presence of severely disturbed flow especially when associated with mobile thrombus or vegetations. These can cause artifacts making the color signal spuriously broad and identified by dark areas mixed with the color.

Quantitative Doppler confirms the diagnosis if the pressure half-time is markedly prolonged usually to >200 ms with an elevated peak velocity usually >2.5 m/s and mean pressure difference >10 mmHg. Indirect signs, including a rising pulmonary artery pressure or a slow-filling left ventricle, may occasionally help.

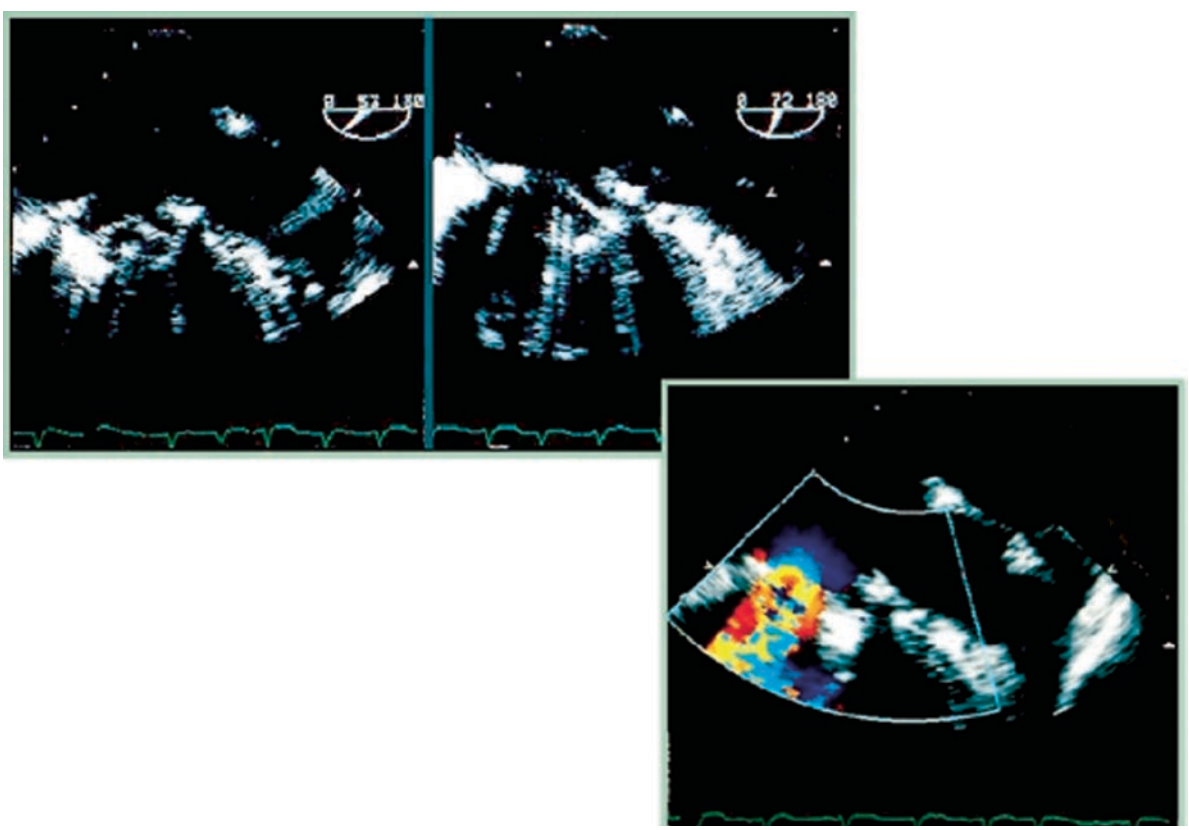

Fig. 12.10 Prosthetic obstruction in a Bileaflet mechanical valve. A TOE showing an apparently normal systolic frame (*top left*) but immobility of the lateral leaflet during diastole (*top right*). On color mapping, flow can only be shown through the medial half of the orifice (*bottom*)

Aortic Position

Apparently high velocities are common in normally functioning size 19 or 21 prostheses in the aortic position, and effective orifice areas considered severely stenotic for a native valve are often normal. Starr–Edwards valves have a particularly high initial velocity caused by the acceleration of flow around the ball as it leaves its housing to enter the cage.

Nowhere is it more important to interpret the echocardiogram in the clinical context. Obstruction is relatively uncommon with mechanical valves in the aortic position and, if the patient is well, it is most likely that the valve is normal. Obstruction is most reliably detected by comparing effective orifice area with the baseline study. Allowing for experimental error, a fall of > 30% is likely to be significant.

Tricuspid Position

These valves are not commonly implanted. Reduced cusp or occluder motion or a narrowed color signal may be helpful. Often the indirect signs are useful since the right atrium and the inferior vena cava can be imaged in most patients even if parasternal and apical views are poor. An engorged, unreactive inferior vena cava with a dilated right atrium and small right ventricle all suggest tricuspid obstruction. A transtricuspid peak velocity >1.5 m/s on mean gradient > 5 mm Hg in the absence of significant tricuspid regurgitation is also suggestive. The pressure half-time is variable and not helpful unless markedly prolonged, >250 ms.

Cause of Obstruction

Although obstruction may often be detected transthoracically, a TOE is necessary to elucidate the underlying cause:

- Thrombus
- Pannus
- Vegetation
- Mechanical
- Primary failure

Thrombus and also vegetations are associated with low density echoes, while pannus is typically highly echogenic. A thrombus is usually larger than pannus and more likely to extend into the left atrium and the appendage (Fig. 12.11). However minor pannus may

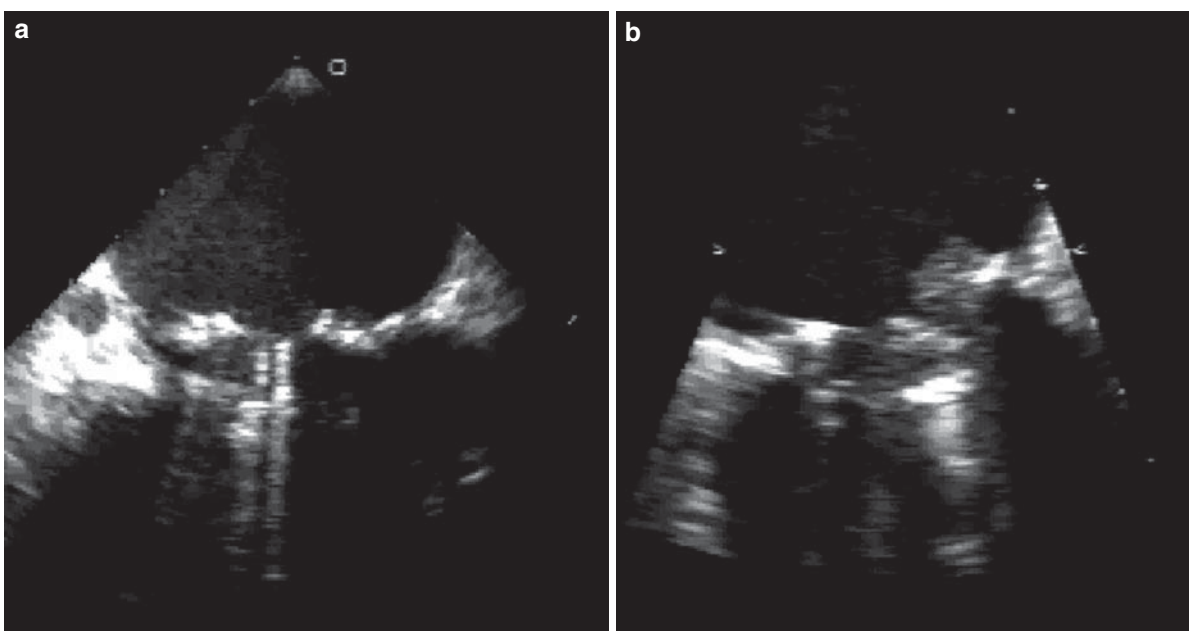

Fig. 12.11 Causes of obstruction. Thrombus is relatively large and of low echo density (*right*). Pannus is more echodense (*left*)

Table 12.3 Classification of prosthetic valve thrombosis

Group 1:	Clinically silent (usually found on routine echocardiography)
Group 2:	Thromboembolic presentation[a] (CVA, TIA, peripheral embolism)
Group 3:	Hemodynamic symptoms and valve obstruction (most common)
Group 4:	Hemodynamic obstruction and systemic embolization

[a]Requires imaging of thrombus on valve to differentiate from thromboembolism

be overlain by thrombus, so conclusive differentiation may not be possible. The clinical history may also be useful. A shorter duration of symptoms and inadequate anticoagulation suggests thrombus rather than pannus. Onset of symptoms less than a month from surgery predicts thrombus as a period of 6 months or more is usually necessary for pannus formation. Guidelines for the management of left-sided valve thrombosis recommend transesophageal echocardiography to visualize abnormal leaflet motion and to image the size and mobility of thrombus in relation to the valve and the left atrium. Patients are then classified into four groups according to the clinical presentation, functional class, and the findings on echocardiography (Table 12.3). Surgery is recommended (a) in groups 3 and 4 if the patients are in NYHA III or IV or (b) in groups 1 and 2 if the thrombus is large and mobile (and the risk of embolization is then high). Thrombolysis is recommended for (a) tricuspid thrombosis, (b) for left-sided thrombosis if surgery is contraindicated, or (c) failure of intravenous heparin in patients in any group with a small clot and/or who are in functional classes I and II.

Regurgitation

Is It Pathological?

The first step is to localize the base of the regurgitation in relation to the sewing ring. This requires a careful and sometimes prolonged study because it may be possible to image only parts of the sewing ring with each cut and the echocardiographer has to build up a 3D image in his or her head. 3D imaging improves localization of regurgitant jets provided that frame rates are adequate.

Many valves have transprosthetic regurgitation as a normal finding or even a design feature (Figs. 12.7 and 12.8). However, in a biological valve, a broad jet, particularly if it is bigger than on previous studies, is a sign of primary failure or endocarditis. Large transprosthetic jets are uncommon in mechanical valves, but can occur if the leaflet is held open by thrombus or a vegetation.

Paraprosthetic leaks have their origin outside the sewing ring (Fig. 12.12) and can usually be detected transthoracically even in the mitral position. Although the mechanical parts of the valve shield the interatrial part of the jet from ultrasound, a significant jet has a neck and an intraventricular portion of flow acceleration (Fig. 12.13). Even these are occasionally invisible for posterior paraprosthetic regurgitation mitral (Fig. 12.14). However, the majority of paraprosthetic leaks occur at the mitral-aortic fibrosa. It may sometimes be difficult to differentiate a paraprosthetic jet from an asymmetric jet through the valve especially those beginning at the base of cusps or at a commissure and TOE is then indicated.

Paraprosthetic leaks are pathological by definition but may not be of clinical significance. Small paraprosthetic leaks are more common in valves with thin sewing rings or patients with poor tissue for example as a result of endocarditis or Marfan syndrome.

Quantification

Broadly, the same methods can be used as for native regurgitation.

However, assessing the height of an aortic jet relative to the left ventricular outflow tract diameter may be difficult if it is eccentric and care must be taken to measure the diameter of the jet perpendicular to its axis. Multiple small normal transprosthetic jets cannot be quantified accurately, but this is not necessary in

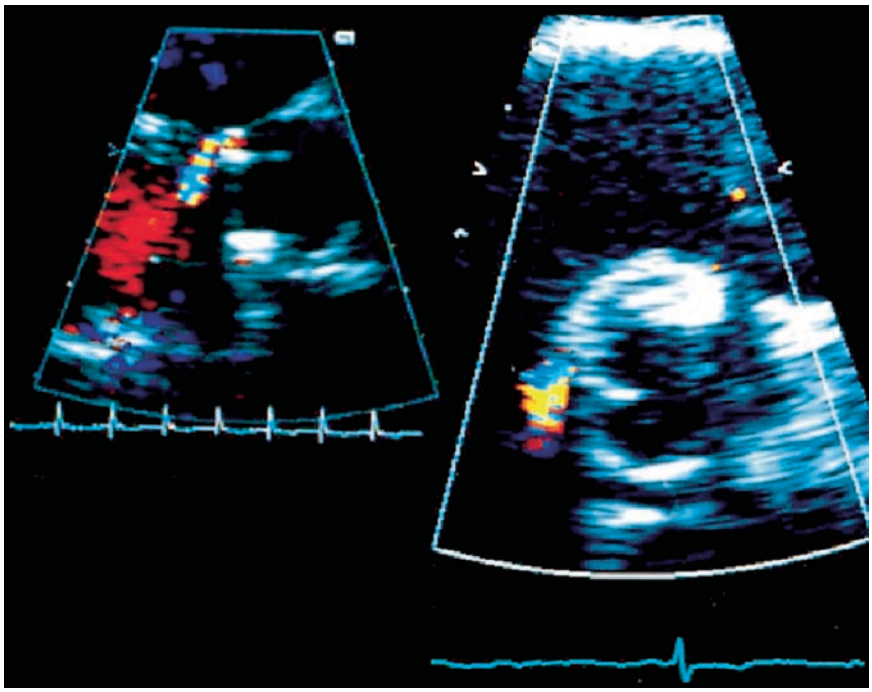

Fig. 12.12 Paraprosthetic aortic regurgitation. Transthoracic parasternal long-axis (*left*) and short-axis (*right*) views are shown

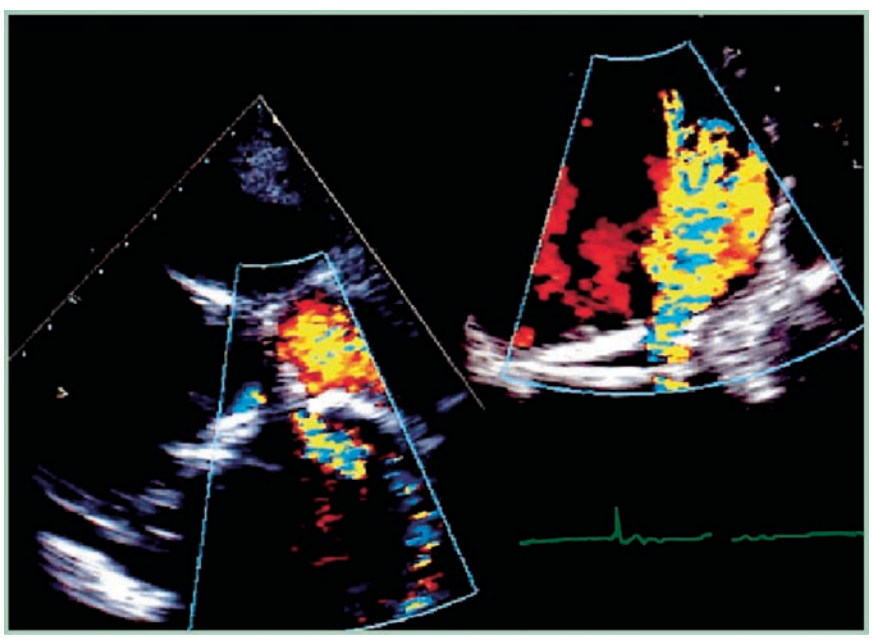

Fig. 12.13 Paraprosthetic mitral regurgitation. Although the interatrial portion of the jet is incompletely seen on transthoracic imaging (*left*) because of shielding, the neck and interventricular flow acceleration are usually visible. The interatrial jet is more easily imaged on TOE (*right*)

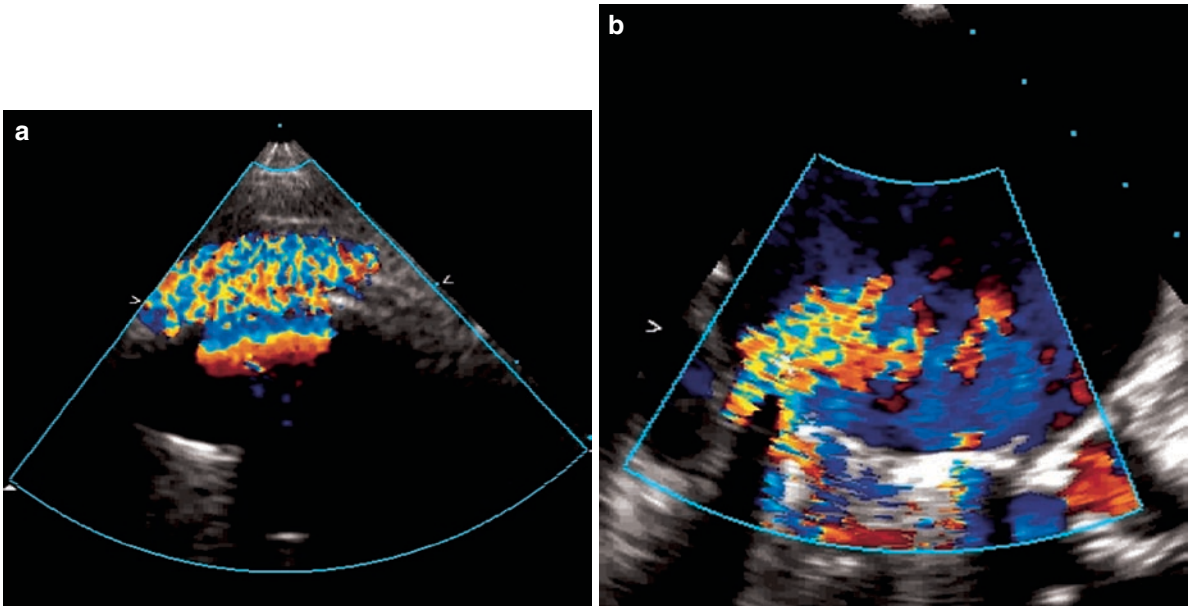

Fig. 12.14 Paraprosthetic mitral regurgitation on transesophageal imaging. The transgastric view (*left*) shows a large inferior dehiscence that was invisible transthoracically because of shielding and reverberation in the posterior part of the sewing ring. Furthermore, the jet was directed toward the center of the valve (*right*) and did not move from the region of flow shielding on transthoracic imaging

clinical practice. For paraprosthetic jets, the proportion of the circumference of the sewing ring occupied by the jet gives an approximate guide to severity: mild (<10%), moderate (10–25%), severe (>25%).

Because of shielding, it may be difficult to quantify a jet in the mitral position. Although TOE is usually necessary, the likelihood of severe regurgitation can be judged by indirect signs predominantly overactivity of the left ventricle or occasionally a rise in pulmonary artery pressure compared with an earlier study. A dense continuous-wave regurgitant signal is another useful transthoracic sign particularly if it depressurizes rapidly. When associated with a low systolic LV and systemic pressure, this signal resembles that obtained from aortic stenosis, an error all the easier to make if the neck of the paraprosthetic jet is at the mitral-aortic fibrosa and the interatrial portion runs parallel with the aorta.

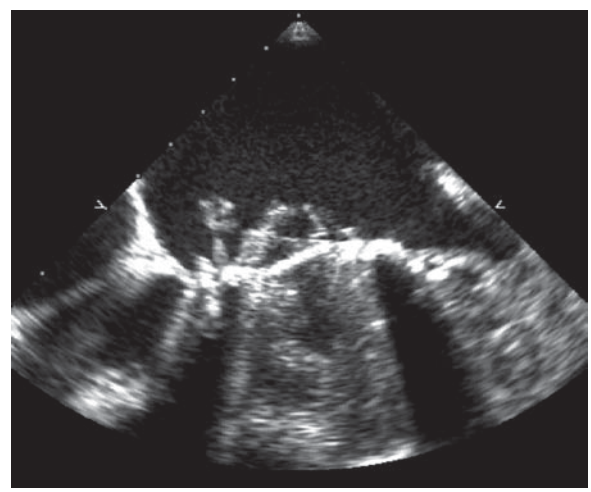

Fig. 12.15 Vegetations on a bileaflet mechanical valve

Endocarditis

Vegetations and local complications (dehiscence, abscess, perforation, fistula) may be obvious even on transthoracic echocardiography especially if the valve is biological. However if the valve is mechanical, vegetations are often difficult to detect transthoracically and TOE is then necessary (Fig. 12.15).

However the echocardiogram must never be interpreted outside the clinical context. It is never possible to differentiate vegetations from a segment of disrupted cusp. Nor is it possible to differentiate generalized

valve thickening as a result of infection from primary failure even on TOE. Similarly, normal swelling and hematoma around a recently implanted stentless valve cannot be differentiated from an abscess (Fig. 12.5).

Timing of Echocardiography

Preoperative

Apart from the obvious task of assessing the index valve disease and left ventricular function, echocardiography has the following roles:

Planning a Ross procedure

It is necessary to check that the pulmonary valve is normal and that the pulmonary and aortic annulis are similar in diameter. Sometimes a Ross procedure is not advisable if the aortic annulus is large, above 27 mm, since this may be associated with progressive dilatation of the autograft. If the aortic root is dilated, the Ross should only be performed as a miniroot rather than by implantation within the aorta.

Planning a Stentless Valve

These valves vary in design but many need to be sized using the sinotubular junction rather than the annulus alone as would be usual with stented valves. If the sinotubular junction is more than 10% larger than the annulus, either a stentless valve cannot be used or an associated aortoplasty must be performed. Sizing by transthoracic echocardiography, usually confirmed by intraoperative TOE, also allows the valve to be washed in advance thus reducing bypass times.

Endocarditis

TOE is often considered essential in native aortic endocarditis since the incidence of complications is high, and these are more accurately detected by the transesophageal route. However this view is controversial and if transthoracic images have been good and the patient is responding adequately to antibiotics, TOE need not be performed. However if the decision for surgery is made, it becomes reasonable to perform a TOE if the finding of an abscess will modify the operation and also to check for involvement of the mitral valve. Some surgeons would choose to perform a Ross procedure or find a homograft under these circumstances, while others would not. This is a matter for individual discussion.

Planning a Homograft

Most valves can be sized at the time of surgery, but a homograft almost always needs to be requested and it is helpful to measure the left ventricular outflow tract diameter to determine whether a large-, medium-, or small-sized homograft should be requested.

Other Valves

The decision whether to operate on other valves is not always easy. Common problems are to decide in the presence of aortic valve disease, whether mitral regurgitation is functional or organic. The decision is usually easy if the valve is morphologically abnormal. Surgery is also likely to be necessary if the regurgitation is severe or the jet is eccentric.

Another frequent problem is the presence of tricuspid regurgitation in the presence of rheumatic mitral valve disease. If the tricuspid regurgitation is moderate or severe especially if the pulmonary artery pressures are normal or only moderately elevated, it is likely that there is organic tricuspid involvement requiring surgery.

If mitral surgery or CABG is to be performed, coexistent aortic valve surgery should be performed if there is moderate or severe stenosis. Usually an EOA <1.0 cm^2 or V_{max} >3.0 m/s are taken as criteria for surgery. In borderline cases, the morphology of the valve is used as a guide. If there is commissural fusion, if the valve is bicuspid or if all three cusps are thickened with reduced mobility the valve is probably more likely to deteriorate quickly. The presence of severe or moderate-to-severe regurgitation, but not usually moderate regurgitation, also suggests the need for coexistent aortic valve replacement.

Right Ventricular Function

Sometimes pulmonary hypertension and right ventricular dysfunction are missed particularly in severe aortic valve disease. This is important because the risk of surgery is higher and the outcome less good.

Perioperative

Intraoperative echocardiography is now routine and is particularly useful:

- To assess a associated mitral valve repair
- In endocarditis to check for an aortic root abscess or involvement of other valves
- To confirm annulus and sinotubular junction diameters when implanting a stentless valve
- To assess competency of a Ross or stentless valve after surgery

In the immediate postoperative period, echocardiography may be needed for assessing left ventricular function, detecting pericardial effusions, and assessing loading conditions. Severe left ventricular hypertrophy usually with outflow obstruction after valve replacement for severe aortic stenosis may cause left ventricular failure and hypotension. These may be treated according to protocol with inotropic agents and diuretics which exacerbate the situation. The diagnosis is made on echocardiography and the treatment is withdrawal of inotropes, the use of drugs to slow the heart and improve LV filling, and the gradual withdrawal of diuretics.

Baseline Study

A study should be performed in the early postoperative period to act as a baseline. Every valve is different and this study acts as a "fingerprint" against which to compare future studies. For example there may be mild paraprosthetic regurgitation. If the patient presents later with fever, the finding of a paraprosthetic jet might be a sign of endocarditis if it is new, but not if it has already been documented. The timing of the baseline study depends on circumstances. Ideally it should be at the first postoperative visit usually after 4–6 weeks when the chest wound has healed, chest wall edema has resolved, and left ventricular function has recovered. However if the patient is being transferred and may not return, it may be best to perform the study before hospital discharge.

Late After Surgery

Routine echocardiography is not necessary if the patient is well and the examination normal. A study is needed if malfunction is suspected based on:

- Symptoms
- Murmur
- Hemolysis
- Fever
- Emboli despite normal INR

For biological valves it may be reasonable to study annually beyond about 5 years after surgery for mitral valves and 8 years for aortic valves because of the known failure rate. The rationale is to detect failure early to allow careful follow-up and planning of elective surgery with acceptable surgical risk. Failing cusps may tear suddenly causing sudden death, shock, or pulmonary edema.

When Is TOE Necessary?

TOE is necessary more frequently than with native valves especially for replacement valves in the mitral position because of the problem of shielding:

- When endocarditis is suspected particularly for mechanical valves. However vegetations and complications may be obvious transthoracically and anterior aortic root abscesses are better seen transthoracically than transesophageally. If the transthoracic study is diagnostic, it is only necessary to have a transesophageal study if surgery is being discussed in order to check the other valves and to look for an abscess. This can be performed perioperatively.
- Despite a normal transthoracic study, if valve dysfunction is suspected from the presence of an abnormal murmur, breathlessness, or hemolysis.

- The grade of mitral regurgitation is uncertain on transthoracic examination.
- Thromboembolism recurs despite adequate anticoagulation since this suggests the presence of vegetation or alternatively of pannus acting as a nidus for thrombus formation.
- Obstruction of a mechanical valve to differentiate thrombosis from the other causes and to decide whether surgery or thrombolysis should be considered.

Conclusions

Echocardiography of replacement heart valves is more demanding than for native valves. There are some key points:

- Quantitative Doppler should always be interpreted in the clinical context; normal ranges vary with design, position, and size.
- Velocities are flow dependent; always calculate effective orifice area for valves in the aortic position.
- Do not use valve size in place of left ventricular outflow tract diameter in calculating the effective orifice area.
- The pressure half-time method for calculating effective orifice area is not valid in normal replacement mitral valves.
- Transvalvar regurgitation is normal in almost all mechanical valves and many biological valves.
- Transthoracic and transesophageal echocardiography are complementary and should not be considered in isolation.

Glossary

Annulus The patient tissue annulus is the orifice left after the surgeon has excised the pathological valve.

Occluder The mechanism closing the orifice to prevent backwash of blood

Paraprosthetic regurgitation A regurgitant jet between the sewing ring of the valve and the patient annulus

Pivotal washing jet Bileaflet mechanical valves have two leaflets with "lugs" that pivot in recesses in the valve housing. Minor regurgitation called pivotal washing jets occurs through these.

Appendix: Normal Ranges for Replacement Heart Valves: Mean (Standard Deviation)

Aortic position

	V_{max} (m/s)	Mean ΔP (mmHg)	EOA (cm^2)
Biological			
Homograft			
22 mm	1.7 (0.3)	5.8 (3.2)	2.0 (0.6)
26 mm	1.4 (0.6)	6.8 (2.9)	2.4 (0.7)
Porcine			
Carpentier–Edwards			
21 mm	2.8 (0.5)		1.2 (0.2)
23 mm	2.8 (0.7)		1.1 (0.2)
25 mm	2.6 (0.6)		1.2 (0.3)
27 mm	2.5 (0.5)		1.3 (0.3)
29 mm	2.4 (0.4)		1.4 (0.1)
Intact			
21 mm	1.0 (0.1)	19.3 (7.4)	1.5 (0.3)
23 mm	1.3 (0.1)	18.8 (6.1)	1.6 (0.3)
25 mm	1.4 (0.2)	18.8 (8.0)	1.9 (0.3)
27 mm		15.0 (3.7)	
Hancock			
23 mm		12.0 (2.0)	
25 mm	2.4 (0.4)	11.0 (2.0)	
27 mm	2.4 (0.4)	10.0 (3.0.)	
Bovine pericardial			
Labcor-Santiago			
19 mm		10.1(3.1)	1.3 (0.1)
21 mm		8.2 (4.5)	1.3 (0.1)
23 mm		7.8 (2.9)	1.8 (0.2)
25 mm		6.8(2.0)	2.1(0.3)
Single tilting disk			
Bjork–Shiley			
21 mm	3.0 (0.9)		1.1 (0.3)
23 mm	2.4 (0.5)	14 (7.0)	1.3 (0.3)
25 mm	2.1 (0.5)	13.0 (5.0)	1.4 (0.4)
27 mm	2.0 (0.3)	10.0 (2.0)	1.6 (0.3)
Medtronic Hall			
21 mm		13.0 (4.0)	1.4 (0.1)
23 mm	2.3 (0.9)		
25 mm	2.1 (0.3)		
Omnicarbon			
21 mm	3.0 (0.3)	20.0 (5.0)	
23 mm	2.7 (0.3)	18.0 (5.0)	
25 mm	2.5 (0.3)	15.0 (4.0)	
27 mm	2.1 (0.2)	12.0 (2.0)	
Bileaflet mechanical			
St Jude			

(continued)

Appendix (continued)

	V_{max} (m/s)	Mean ΔP (mmHg)	EOA (cm^2)
19 mm	3.0 (0.6)	19.4 (7.2)	1.0 (0.3)
21 mm	2.6 (0.3)	14.8 (4.3)	1.3 (0.2)
23 mm	2.5 (0.5)	13.5 (5.9)	1.3 (0.3)
25 mm	2.4 (0.5)	12.2 (5.9)	1.8 (0.4)
27 mm	2.2 (0.5)	11.0 (5.0)	2.4 (0.6)
29 mm	2.0 (0.1)	7.0 (1.0)	2.7 (0.3)
Carbomedics			
19 mm	3.2 (0.4)	19.3 (8.5)	0.9 (0.3)
21 mm	2.5 (0.5)	13.7 (5.5)	1.3 (0.4)
23 mm	2.4 (0.4)	11.0 (4.6)	1.6 (0.4)
25 mm	2.3 (0.3)	9.1 (3.5)	1.8 (0.4)
27 mm	2.1 (0.4)	7.9 (3.4)	2.2 (0.6)
29 mm	1.8 (0.4)	5.6 (3.0)	3.2 (1.6)
Ball and cage			
Caged-ball			
Starr–Edwards			
23 mm	3.4 (0.6)		1.1 (0.2)
24 mm	3.6 (0.5)		1.1 (0.3)
26 mm	3.0 (0.2)		

Mitral position

	V_{max} (m/s)	Mean ΔP (mmHg)	PHT (ms)
Porcine			
Carpentier–Edwards			
27 mm		6.0 (2.0)	95 (12)
29 mm	1.5 (0.3)	4.7 (2.0)	110 (30)
31 mm	1.5 (0.3)	4.5 (2.0)	102 (34)
33 mm	1.4 (0.2)	5.4 (4.0)	94 (26)
Intact			
25 mm		7.8 (2.4)	
27 mm		5.4 (1.5)	
Hancock			
29 mm		2.0 (0.7)	
31 mm		4.9 (1.7)	
33 mm		5.0 (2.0)	
Bovine pericardial			
Labcor-Santiago			
27 mm		2.8 (1.5)	85 (18)
29 mm		3.0 (1.3)	80 (34)
Single tilting disk			
Bjork–Shiley			
25 mm	1.6 (0.3)		
27 mm	1.5 (0.2)	2.7 (0.8)	94 (31)
29mm	1.4 (0.4)	2.0 (0.1)	85 (22)
31 mm	1.5 (0.3)	3.4 (2.2)	81 (20)
33 mm	1.3 (0.6)		75 (25)
Medtronic Hall			
29 mm	1.6 (0.1)		69 (15)
31 mm	1.5 (0.1)		77 (17)
Omnicarbon			
25 mm		6.0 (2.0)	
27 mm		6.0 (2.0)	
29 mm		5.0 (2.0)	
31 mm		6.0 (2.0)	
Bileaflet mechanical			
St Jude			
27 mm	1.6 (0.3)	5.0 (2.0)	
	V_{max} (m/s)	Mean ΔP (mmHg)	PHT (ms)
29 mm	1.6 (0.3)	4.5 (2.4)	81 (9)
31 mm	1.7 (0.4)	5.2 (3.0)	84 (12)
Carbomedics			
25 mm	1.6 (0.2)	4.3 (0.7)	92 (20)
27 mm	1.6 (0.3)	3.7 (1.5)	91 (24)
29 mm	1.8 (0.3)	3.7 (1.3)	79 (11)
31 mm	1.6 (0.4)	3.3 (1.1)	92 (20)
33 mm	1.4 (0.3)	3.4 (1.5)	79 (18)
Edwards-Duromedics			
27 mm	1.9 (0.3)		105 (14)
29 mm	1.8 (0.2)		89 (18)
31 mm	1.7 (0.3)		99 (18)
Caged ball			
Starr–Edwards			
28 mm	1.8 (0.2)		130 (25)
30 mm	1.8 (0.2)		100 (40)
32 mm	1.9 (0.4)		125 (60)

Bibliography

ACC/AHA guidelines for the management of patients with valvular heart disease. A report of the American College of Cardiology/American Heart Association. Task Force on Practice Guidelines (Committee on Management of Patients with Valvular Heart Disease). *JACC*. 1998;32:1486–1588.

Chambers J, Fraser A, Lawford P, Nihoyannopoulos P, Simpson I. Echocardiographic assessment of artificial heart valves: British Society of echocardiography position paper. *British Heart J*. 1994;71 (Suppl 4):6–14.

Grunkemeier GL, Li H-H, Naftel DC, Starr A, Rahimtoola SH. Long-term performance of heart valve prostheses. *Curr Problems Cardiol*. 2000;25:73–156.

Jamieson WRE. Effective current and advanced prostheses for cardiac valvular replacement and reconstructive surgery. Surg Technol Int.

Rahimtoola S. Choice of prosthetic heart valve for adult patients. *JACC*. 2003;41:893–904.

Wang Z, Grainger N, Chambers J. Doppler echocardiography in normally functioning replacement heart valves: a literature review. *J Heart Valve Dis*. 1995;4:591–614.

Rimington H, Chambers J. Echocardiography: A Practical Guide for Reporting. Parthenon Publishing, TN; 1998. ISBN 1-85050-011-7

Chapter 13
The Use of Echocardiography in the Diagnosis and Treatment of Patients with Infective Endocarditis

Christopher H. Cabell and David Adams

Introduction

Since the advent of two-dimensional transthoracic echocardiography (TTE) in the 1970s and high-frequency transesophageal echocardiography (TEE) imaging in the 1980s, echocardiography has become a standard diagnostic tool in patients with suspected infective endocarditis (IE). The first report of the use of echocardiography to detect endocarditis was made by Dillon and colleagues in the 1970s. In the late 1980s, as the technology of TEE imaging became more widely available, Mugge and colleagues described the first experience of the improved diagnostic yield for endocarditis over standard chest wall imaging. Based on these studies, it is now well established that echocardiography is the imaging technology of choice for the diagnosis of IE and that echocardiography can detect cardiac involvement in a significant proportion of patients with clinically occult IE. Because IE is a lethal infection that can be difficult to clinically diagnose, clinicians who care for patients at risk for IE often have a low threshold for employing echocardiography. In fact, because of the role that echocardiography plays in both the diagnosis and in understanding the prognosis of patients with IE, it has been suggested that echocardiography is mandatory in all patients when there is suspicion for IE.

In this chapter we will discuss the imaging considerations in patients with suspected and documented IE, implications on the use of echocardiography, the role of echocardiography in understanding prognosis, how echocardiography can be used to assist in therapeutic decision making, and musings on the future of imaging for diseases such as endocarditis.

C.H. Cabell (✉) and D. Adams
Department of Medicine, Duke University School of Medicine, and the Duke Clinical Research Institute, Durham, NC, USA
e-mail: chris.cabell@duke.edu

Diagnosis of Endocarditis: The Duke Criteria and the Importance of Imaging

Historically, infective endocarditis has been defined as an infection of the endothelial surfaces within the cardiac chambers. In recent years this definition has been expanded to include an infection on any structure within the heart including normal endothelial surfaces (e.g., myocardium and valvular structures), prosthetic heart valves (e.g., mechanical, bioprosthetic, homografts, and autografts), and implanted devices (e.g., pacemakers, implantable cardioverter defibrillators, and ventricular assist devices). As the age of the population in industrialized countries continues to increase, it is likely that the latter categories of prosthetic valves and devices will continue to grow substantially.

To understand the disease process of IE and how echocardiography has become central to making this diagnosis, it is useful to revisit the way in which the diagnosis has been made historically. In 1885 Sir William Osler, as one of the newest members of the Royal College of Physicians, was asked to give the Gulstonian Lectures. In these three lectures Osler provided on overview of infective endocarditis that summarized the current knowledge on the disease at the time. In this era, even before the advent of microbiologic techniques that allowed for routine use of blood cultures, it is not surprising that the actual diagnosis of endocarditis was all too often made at the time of post mortem examination. In fact, Osler is quoted as saying "Few diseases present greater difficulties in the way of diagnosis than malignant endocarditis, difficulties which

P. Nihoyannopoulos and J. Kisslo (eds.), *Echocardiography*,
DOI: 10.1007/978-1-84882-293-1_13, © Springer-Verlag London Limited 2009

Table 13.1 Comparison of diagnostic criteria in 69 cases of pathologically proven infective endocarditis (Adapted from Durack et al[2])

		Beth Isreal criteria			
		Probable	Possible	Rejected	Total (%)
Duke criteria	Definite	32	19	4	55 (80%)
	Possible	3	3	8	14 (20%)
	Reject	0	0	0	0 (0%)
	Total (%)	35 (51%)	22 (32%)	12 (17%)	69 (100%)

in many cases are practically insurmountable. It is no disparagement to the many skilled physicians who have put their cases upon record to say that, in fully one-half the diagnosis was made post mortem." Despite this difficulty, Osler advocated that the diagnosis of IE could be made based on clinical presentation in certain cases of endocarditis. For instance, he stated that "the existence of fever of an irregular type, and the occurrence of embolism, generally suffice to make the diagnosis clear," a situation that is still true to today.

The diagnosis of IE has always hinged upon clinical suspicion derived from association with appropriate signs and symptoms and, most importantly, the demonstration of continuous bacteremia. Surprisingly, it was not until the late 1970s that a strict case definition was developed. Pelletier and Petersdorf developed this definition based on a 30-year experience of caring for patients with IE in Seattle (need to verify). Although this case definition was highly specific for the diagnosis of IE, it lacked sufficient sensitivity.

The next major diagnostic advance came in 1981 when von Reyn and colleagues published an analysis that provided four diagnostic categories in cases of suspected IE (rejected, possible, probable, and definite). These criteria, based upon broader clinical findings than the Pelletier and Petersdorf case definition, improved both the sensitivity and the specificity of the previous case definition, but unfortunately did not incorporate imaging information from the burgeoning field of echocardiography.

In 1994, IE diagnostic criteria were refined further by Durack and colleagues[2] from Duke University Medical Center. These criteria, which have come to be known as the Duke criteria, incorporated echocardiographic evidence of IE for the first time. These criteria had improved test performance characteristics when compared to previous criteria (Table 13.1) and have been validated subsequently by many other studies. Recently, proposed modifications have been published (Table 13.2), but the test performance characteristics of the modified criteria have yet to be fully evaluated by other investigators.

Table 13.2 The modified Duke criteria (Adapted from Li et al[3])

1. Major criteria
   a. Microbiologic

      Typical microorganisms isolated from two separate blood cultures, or microorganism isolated from persistently positive blood cultures, or single positive blood culture for *Coxiella burnetii* (or phase I IgG antibody titer to *C. burnetii* >1:800
   b. Evidence of endocardial involvement

      New valvular regurgitation or positive echocardiogram (intracardiac mass, or periannular abscess, or new dehiscence of prosthetic valve)
2. Minor criteria
   a. Predisposition to infective endocarditis
      i. Previous infective endocarditis
      ii. Injection drug use
      iii. Prosthetic heart valve
      iv. Mitral valve prolapse
      v. Cyanotic congenital heart disease
      vi. Other cardiac lesions creating turbulent flow within the intracardiac chambers
   b. Fever
   c. Vascular phenomena (e.g., embolic event)
   d. Immunologic phenomena (e.g., presence of serologic markers, glomerulonephritis, Osler's nodes, or Roth spots)
   e. Microbiologic findings not meeting major criteria

Echocardiographic Evidence of Infective Endocarditis

Based upon the defined role of imaging in the diagnosis of IE, echocardiography has become the central tenant in evaluating patients that have a clinical presentation that raises the concern for infective endocarditis. On echocardiography there are several findings that provide evidence of infective endocarditis that include: vegetations; evidence of periannular tissue

Table 13.3 Echocardiographic characteristics of infective endocarditis (Adapted from Sachdev et al[4])

Lesion	Description
Vegetation	Irregularly shaped, discrete echogenic mass Adherent to, yet distinct from cardiac surface Oscillation of mass supportive, not mandatory
Abscess	Thickened area or mass within the myocardium or annular region Appearance is nonhomogeneous with both echogenic and echolucent characteristics Evidence of flow within area is supportive, not mandatory
Aneurysm	Echolucent space bounded by thin tissue
Fistulae	Connection between two distinct cardiac blood spaces through nonanatomical channel
Leaflet perforation	Defect in body of myocardial valve leaflet with evidence of flow through defect
Valvular dehiscence	Rocking motion of prosthetic valve with excursion >15° in at least one direction

destruction (abscess); aneurysm; fistula; leaflet perforation; and valvular dehiscence (Table 13.3).

Vegetation

Pathologically, a vegetation is a collection of microorganisms embedded in a meshwork of fibrin and other inflammatory cellular material adherent to an endothelial surface within the heart. White blood cells are uncommon, the absence of which has not fully been explained by experimental work. In part, this may be due to the dense nature of the vegetation tissue which may restrict the migration of white blood cells to the infected area. In addition, the bacteria are frequently embedded in a nongrowing state deep in the vegetation, which may limit the typical host infection response.

With two-dimensional echocardiographic imaging in which the cardiac structures are viewed throughout the cardiac cycle, vegetations are defined as an irregularly shaped, discrete echogenic mass. This mass must be adherent to, yet distinct from the endothelial cardiac surface. Mass oscillation, high-frequency movement independent from that of intrinsic structures, is supportive but not mandatory for the echocardiographic diagnosis of a vegetation.

Vegetations have the consistency of midmyocardium (Fig. 13.1), but may also have areas of both echolucency and echodensity. Vegetations typically occur on the low pressure side of a high-velocity turbulent jet; therefore, with underlying regurgitant valvular disease, vegetations are most often visualized on the atrial aspect of the mitral and tricuspid valves, or on the ventricular aspect of the aortic and pulmonic valves (Fig. 13.2).

Although cardiac valves are the most common site of infection, vegetations may occur in other intracardiac locations. These include nonvalvular surfaces such as atrial or ventricular surfaces, as well as on intracardiac devices such as pacemakers or defibrillators. When a vegetation occurs on a nonvalvular structure it generally appears at a site of endothelial disruption. If this occurs on a myocardial wall, it is common for this to be at a site where a high-velocity jet of blood flow has damaged the endothelial integrity such an uncorrected restrictive VSD or eccentric mitral valve regurgitation jet (Fig. 13.3). In addition to a myocardial wall attachment for a vegetation, other nonvalvular structures include intracardiac devices such as pacemakers or implantable defibrillators (Fig. 13.4). These devices often have nonuniform endotheliazation that allows for

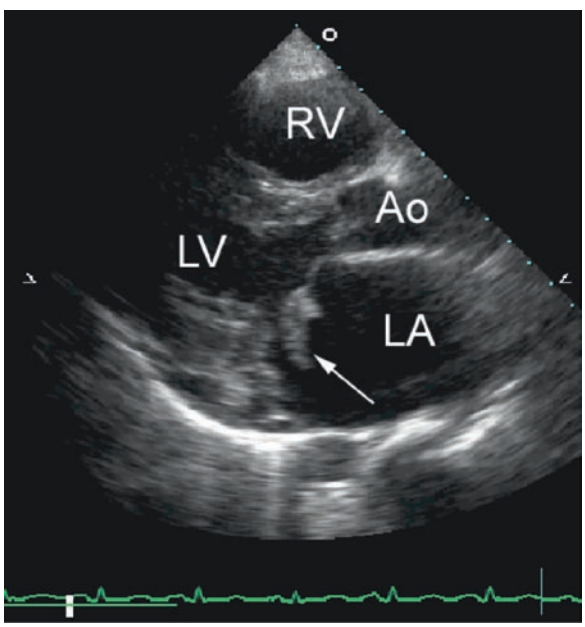

Fig. 13.1 Typical vegetation by transthoracic echocardiography

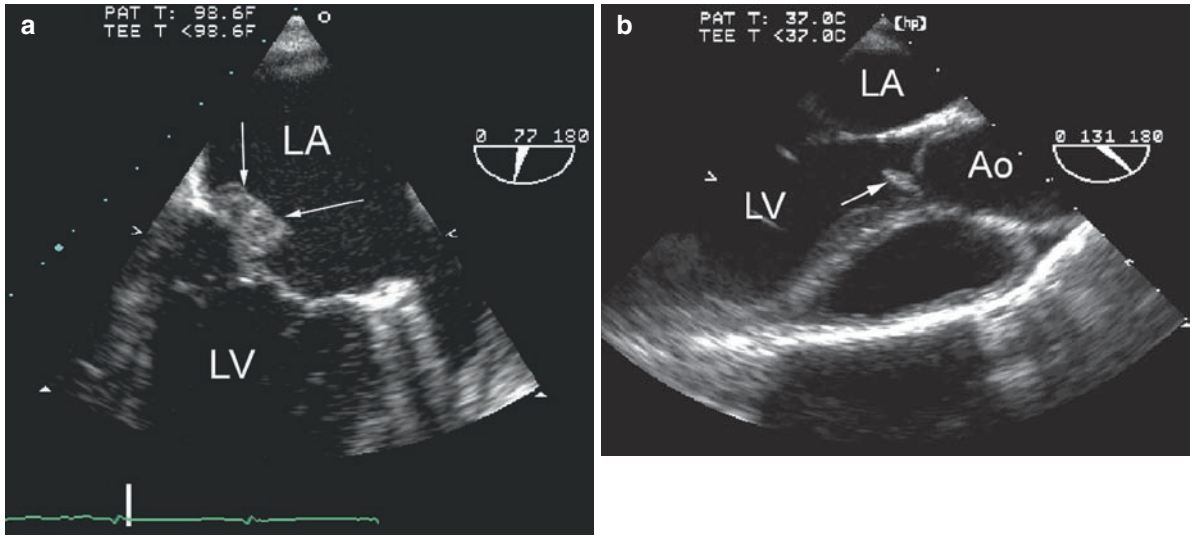

Fig. 13.2 Typical locations of mitral valve and aortic valve vegetations. (**a**) mitral valve vegetation (TEE); (**b**) aortic valve vegetation (TEE)

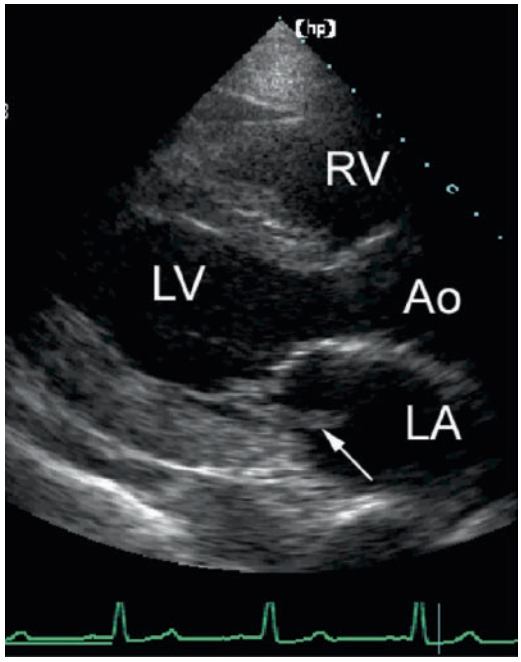

Fig. 13.3 Vegetation located on the myocardial wall

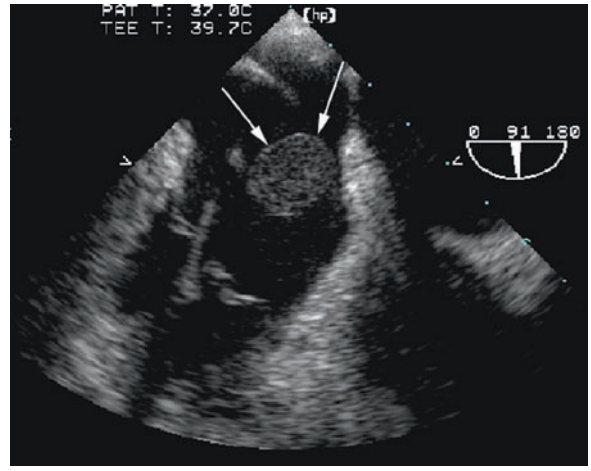

Fig. 13.4 Intracardiac device vegetation

the attachment once bacteria are circulating in the bloodstream.

Not all intracardiac mass lesions represent vegetations from infective endocarditis. For instance, inflammatory disorders such as systemic lupus erythematosus can have associated valvular mass lesions that can be difficult to distinguish from vegetations due to infective endocarditis (Fig. 13.5). Termed Libman-Sacks endocarditis, these inflammatory mass lesions are usually <1 cm in diameter, vary in shape, have irregular borders, and have heterogeneous echodensities. These inflammatory mass lesions are typically broad based and usually do not have independent motion or oscillation characteristics, unlike vegetations due to IE. In addition, Libman-Sacks lesions are typically located on the basilar portion of the aortic and mitral valve leaflets. Again, in contrast to vegetations associated with IE, Libman-Sacks inflammatory lesions are often located on the aortic side of the aortic valve.

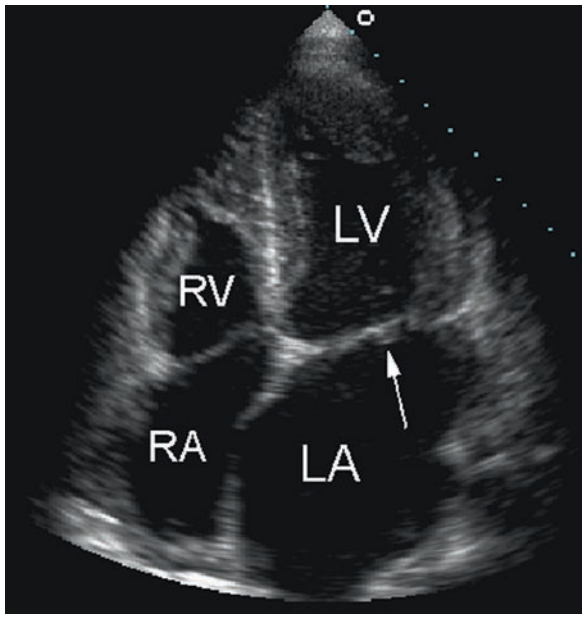

Fig. 13.5 Libman-Sacks endocarditis on the mitral valve

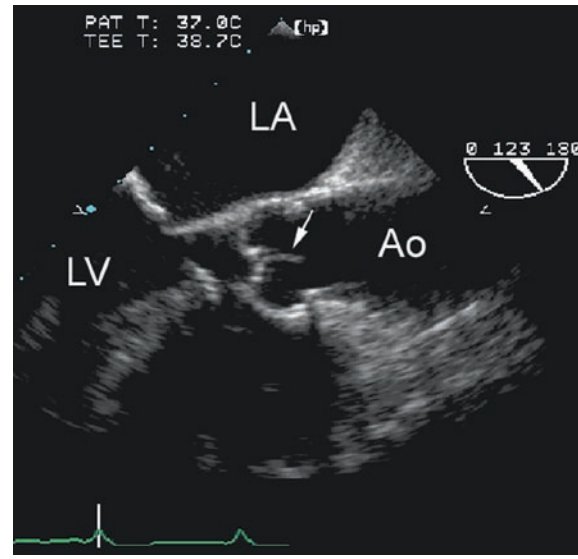

Fig. 13.6 Lambl's excrescence

In addition to Libman-Sacks inflammatory masses, other mass lesions can occur on the valvular structures. For instance, sterile vegetations (termed murantic endocarditis) may also occur in patients with advanced malignancies (e.g., renal cell carcinoma or melanoma). In addition, myxomatous valves, ruptured chordae unrelated to infection, cardiac tumors, and degenerative valvular changes may all involve echocardiographic findings that can be misleading. Moreover, normal variants such as prominent Lambl's excrescences may mimic IE findings (Fig. 13.6).

Lambl's excrescences were first described by Lambl in the 1850s as small filiform processes on the aortic valve. In the 1940s, Margerey studied 250 mitral valves and postulated that the mechanism of formation is intimal damage due to mechanical trauma at the leaflet coaptation. In general, these lesions appear to be wear-and-tear lesions that originate in the endothelium of the contact margins of a valve, commonly the aortic valve. Excision may be necessary in cases of cryptogenic stroke. Although most Lambl's excrescences can be distinguished from vegetations by their small size and filamentous appearance, larger lesions may be more difficult to discern from vegetations due to IE.

Importantly, there are no echocardiographic features of noninfective lesions that can absolutely differentiate them from vegetations due to IE. Therefore, it is always paramount to correlate the echocardiographic findings to the clinical presentation and findings to develop a diagnostic and care plan that is optimized for the individual patient.

Periannular Extension of Infection (Myocardial Abscess Formation)

Periannular extension of infection, or abscess formation, is one of the most serious complications of infective endocarditis. When this occurs, it marks an indication for surgical therapy. On echocardiogram, a myocardial abscess can be defined as a thickened area or mass in the myocardium or annular region with an appearance that is generally nonhomogeneous. If there is evidence of flow within the area then this is considered to be supportive of the diagnosis of abscess formation, but flow within the area is not mandatory for the diagnosis. An echo-free space suggests that complete liquefaction of the myocardium has occurred (Fig. 13.7).

The most important feature of abscess formation is the substantial morbidity and mortality associated with this complication. For instance, the abscess can extend and rupture creating a fistulous tract between two separate blood pools. In addition, if the abscess extends into the septum the conduction system can be affected leading to heart block. In the literature, abscess formation

tends to be more commonly associated with aortic valve IE, particularly those with aortic prosthetic valve IE. Moreover, the mortality rate associated with abscess formation is 1.5–2.0 times higher than similar patients without abscess formation. Although TTE imaging can establish the diagnosis of abscess formation, overall the resolution associated with typical TTE imaging in adults is insufficient for the full characterization of most intracardiac abscess cavities.

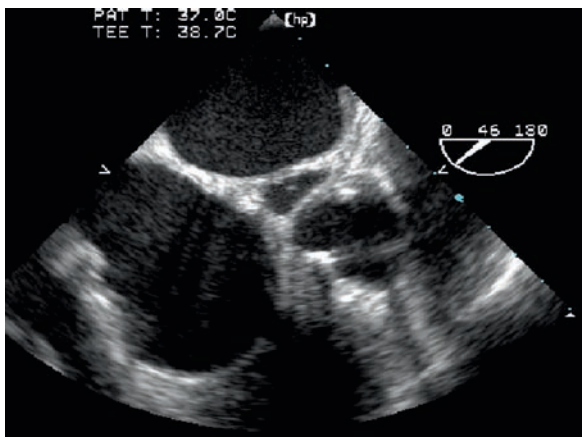

Fig. 13.7 Myocardial abscess with evidence of an echo-free space

Fistula Formation

Spread of infection from valvular structures to the surrounding perivalvular tissue results in periannular complications that may place the patient at increased risk of adverse outcomes including heart failure (HF) and death. This is particularly true with aortic valve IE where aortic abscesses and mycotic pseudoaneurysms involving the sinuses of Valsalva may rupture internally. This leads to the development of aortocavitary or aortopericardial fistulas. Aortocavitary communications create intracardiac shunts, which may result in further clinical deterioration and hemodynamic instability (Fig. 13.8).

Fistula formation due to IE is uncommon; therefore, there are few published series that allow for a broad understanding of this disease process. Recently, a multicenter study from Spain has provided new information related to this complication. In this case series the incidence of fistula formation in patients with IE was 1.6% or 76 fistulas identified in 4,681 episodes of IE. The incidence was higher in selected populations; for instance in patients with prosthetic valve IE the incidence of fistula formation was 3.5%. Not surprisingly, in this series *Staphylococcus aureus* was the most commonly associated microorganism (46%).

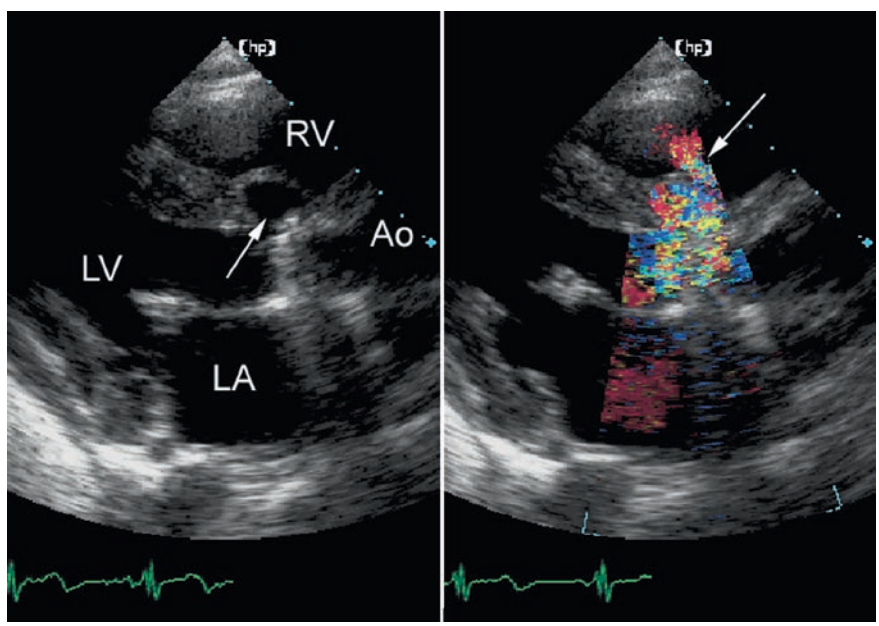

Fig. 13.8 Fistula tract formation due to IE

In addition, despite a high rate of surgery in this population (87%) short-term mortality remained high (41%).

There are few basic tenants that are critical for the diagnosis and management of IE associated fistula tract formation. The first is that suspicion is paramount and if clinical suspicion warrants that TEE imaging is justified early in the clinical course. Second, evidence of fistula tract formation represents an indication for urgent surgery before the infection can cause further tissue destruction and possible hemodynamic compromise. Finally, it is critical for the echocardiographer to provide as much information to the surgical team as possible to help in planning the appropriate surgical approach, particularly to the origin and destination of the fistula tract.

Perforation

Perforation of a valvular leaflet is another lesion that may develop if the infective process is allowed to continue unabated (Fig. 13.9). There is little information available about the timing of perforation formation, but it is generally accepted that this is either associated with a virulent microorganism, such as *S. aureus*, or occurs when the infection process continues for a substantial amount of time without detection. Once a perforation forms, a significant amount of valvular regurgitation may develop. This mechanical complication may then need surgical repair depending on the hemodynamic status of the patient and the amount of regurgitation present.

New Valvular Regurgitation

The endocarditis process can also involve the mechanical function of the valve to cause significant valvular regurgitation. This can occur with or without the presence of a perforated valve leaflet. This mechanical disruption can occur at the valve leaflets secondary to a physical impairment of proper leaflet coaptation or to the vegetative process. In addition, the mechanical disruption can involve the rupture of the chordae tendineae and possibly a flail leaflet. In this instance, significant valvular regurgitation can develop leading to a need for surgical repair.

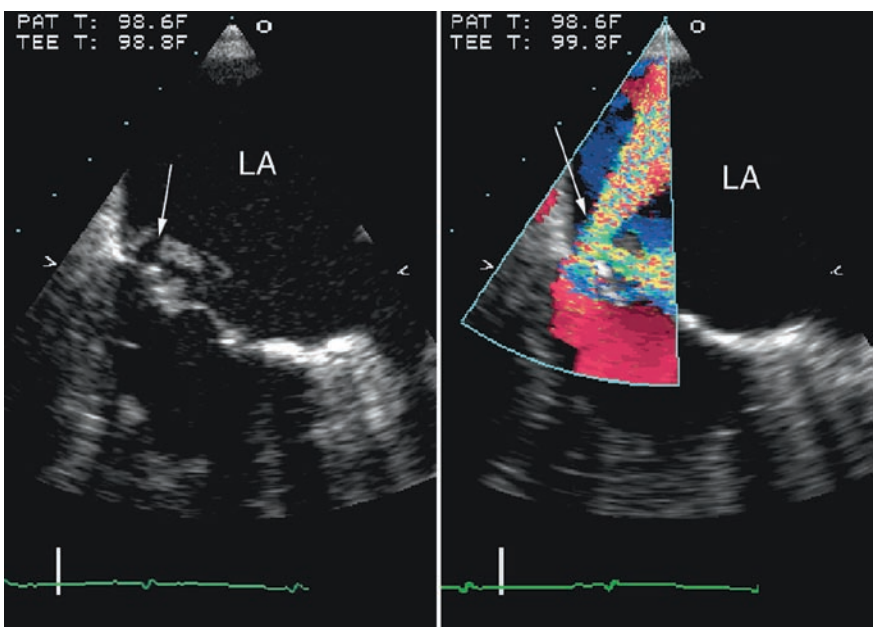

Fig. 13.9 Perforation

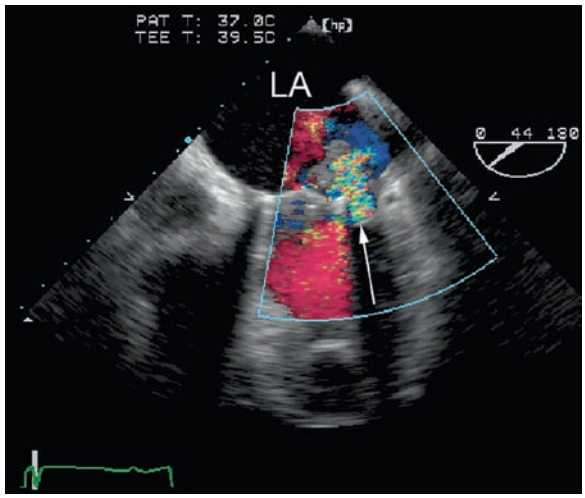

Fig. 13.10 Dehiscence

Dehiscence of Prosthetic Valve

Dehiscence of a prosthetic valve due to IE is a serious complication in patients with prosthetic valves. Dehiscence is generally defined as a rocking motion of the prosthetic valve >15 ° in any one plane (Fig. 13.10). This complication may lead to a gross separation of the prosthetic annulus from the native tissue in the most serious cases. Invariably, prosthetic valve dehiscence is associated with significant perivalvular regurgitation and may be associated with hemodynamic compromise. Dehiscence represents a relative urgent indication for surgical therapy.

The Use and OverUse of Echocardiography to Make the Diagnosis of IE

Use of Echocardiography in Patients Suspected of IE

It is now well established that echocardiography is the imaging technology of choice for the diagnosis of IE and that echocardiography can detect cardiac involvement in a significant proportion of patients with clinically occult IE. Because IE is a lethal infection that can be difficult to diagnose clinically, clinicians who care for patients at risk for IE often have a low threshold for employing echocardiography. In addition, published diagnosis and treatment guidelines advocate the early use of echocardiography to establish the diagnosis of IE. This clinical practice has several implications. While echocardiography can often provide a rapid diagnosis, its optimal use is predicated on the appropriate pretest probability of disease. By contrast, echocardiography is increasingly overused in clinical scenarios with a low (<2–3%) pretest probability of disease, where its diagnostic utility diminishes.

In order to use a diagnostic tool, such as echocardiography, in an effective manner it is important to simultaneously include several clinical features including: an appropriate pretest probability of disease (e.g., >2–3%); an understanding of the diagnostic technology; and a clinical situation in which the diagnostic test results will likely change the management of the patient. Although there are few empiric data to quantitate the pretest probability of disease, there is a general acceptance that certain clinical characteristics increase the pretest probability of disease significantly (Table 13.4). When focusing on the diagnostic technology, the basic characteristics of echocardiography must be kept in mind. For instance, in ~15% of patients the sound transmission from the chest wall may be attenuated by a variety of factors (e.g., obesity, lung hyperinflation) such that there is insufficient resolution to make a firm diagnosis. In these situations, TEE may be indicated as a primary imaging modality.

Overuse of Echocardiography

Recent literature has provided evidence that imaging technologies such as echocardiography can be overused in certain clinical scenarios such as the evaluation of suspected endocarditis. For instance, Kurupuu and

Table 13.4 Characteristics suggestive of endocarditis (Modified from Greaves et al[5])

• Fever
• Organisms grown on blood culture
– Particularly without a known source of infection
• Recent history of injection drug use
• Congenital cardiac structural abnormality
– (e.g., mitral valve prolapse)
• Known rheumatic heart disease
• Presence of prosthetic valve or intracardiac device
• Vasculitic/embolic phenomena

colleagues have shown that 53% of echocardiograms could be avoided without loss of diagnostic accuracy by using a simple algorithm in patients with a low pretest probability of disease. In addition, Greaves and colleagues[5] have shown that the collective absence of five simple clinical criteria indicated a zero probability of a TTE showing evidence of endocarditis. These clinical criteria included: vasculitic/embolic phenomena; presence of central venous access; recent history of injection drug use; presence of prosthetic valve; and positive blood cultures. Collectively, these studies have shown that in patients with very low pretest probability of disease, echocardiography may be avoided without the loss of diagnostic accuracy.

TTE vs. TEE

Both TTE and TEE have an important role in the diagnosis and management of patients with suspected IE. In general, TTE is widely available and can provide rapid important diagnostic information. As discussed earlier, there are clinical situations in which TTE imaging alone does not provide adequate resolution to make a firm diagnosis. TEE imaging is typically performed at a higher frequency (6–7 MHz) compared to TTE (2–4 MHz). This higher frequency allows for greater spatial resolution of nearby structures including the cardiac valves. Under ideal conditions, TTE can reliably identify structures as small as 5 mm in diameter, while TEE can depict structures as small as 1 mm. It is generally accepted that the sensitivity/specificity is superior for TEE compared with TTE (93%/96% vs. 46%/95%).

Cost Effectiveness of Diagnostic Imaging Strategies

While certain clinical scenarios may dictate the type and order of diagnostic strategies, there are recent data that help guide this decision making. For example, there is now evidence for both the evaluation of the general patient suspected of having IE, as well as for the patient with catheter associated *S. aureus* bacteremia.

In the general patient in which there is a suspicion of IE, current guidelines highlight the use of TTE and/or TEE imaging depending on the clinical scenario. Recently, studies have shown that an initial strategy of TEE imaging is most cost effective in the majority of clinical situations. For instance, Heidenreich and colleagues have shown that in suspected endocarditis a diagnostic strategy that focuses on TEE as the initial imaging modality is more cost effective than a staged procedure with TTE and is a dominant strategy over empiric antibiotic therapy alone. In this study, transesophageal imaging was optimal for patients who had a prior probability of endocarditis that is observed commonly in clinical practice (4–60%) with a reduced cost of $18 per person compared with the use of transthoracic echocardiography. In contrast, strategies that reserved the use of TEE for patients who had an inadequate transthoracic study provided similar quality-adjusted life years but cost modestly more per patient.

In a similar study, Rosen and colleagues set out to determine the cost-effectiveness of TEE in establishing the duration of therapy for catheter-associated bacteremia. In this study, three management strategies were compared: (1) empirical treatment with 4 weeks of antibiotics (long course); (2) empirical treatment with 2 weeks of antibiotic therapy (short course); and (3) TEE-guided therapy. In the case of the TEE strategy, a positive TEE dictated long course therapy and a negative TEE dictated short course therapy. The effectiveness of an empiric long course strategy and a TEE-guided strategy were both superior to empiric short course therapy. When costs were taken into account, the TEE-guided strategy was superior to the empiric long course strategy which cost over $1,500,000 per quality-adjusted life year saved.

Echocardiography to Predict Complications and Guide Therapeutic Decision Making

Once the diagnosis of infective endocarditis has been established, the information from the echocardiographic examination can be used to establish the prognosis and guide future decision making. For instance, echocardiographic findings that establish evidence of infection extension into the perivalvular tissue

(e.g., abscess, pseudoaneurysm, and fistula) may indicate a need for urgent surgical consideration. In addition, Doppler data that allow for the assessment of valvular regurgitation and cardiac function can greatly assist the clinician in understanding the current and future hemodynamic status. Finally, there is substantial evidence to support decision making related to the association between vegetation size and risk for thromboembolic complications.

Since the early 1990s multiple studies have shown a strong association between vegetation size and subsequent thromboembolic risk. For instance, Sanfilippo and colleagues[1] found that the risk of embolization was directly related to vegetation size. In fact, for vegetations greater than six mm in size the risk of subsequent embolization was linearly related to an increase in vegetation size (Fig. 13.11). These findings have been verified by several investigators. Tischler and Viatkus conducted a meta-analysis that incorporated 10 studies involving 738 patients with IE. They found that the pooled odds ratio (OR) for risk of embolization was 3 times higher n patients with large vegetations (>10 mm) compared to patients with no detectable or small vegetations (OR: 2.90, 95% CI: 1.95, 4.02).

Importantly, Di Salvo and colleagues have extended these findings by studying both clinically apparent thromboembolic events, as well as clinically silent embolic events diagnosed by standard imaging in all patients. The investigators found that both vegetation size and mobility were predictive of embolic events. Specifically, 70% of the embolic events were in patients with large (>15 mm) vegetations. In addition, vegetation mobility was also related to embolic risk; in the 73 patients with moderate-severe mobility in the vegetation, 45 (62%) had a subsequent embolic event.

One issue in the interpretation of such findings is the high degree of interobserver variability in recording the specific characteristics of vegetations. For instance, Heinle and colleagues observed that there was a high degree of variability in the interpretation of specific vegetation findings. Specifically, they found only 57% agreement in regards to mobility, 36% in shape, and 40% in the site of attachment. Therefore, in the absence of interobserver consistency, these findings must be used with caution to support decision making.

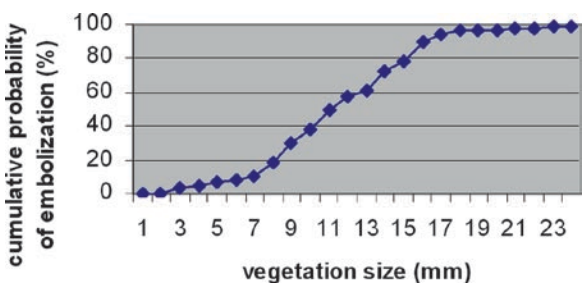

Fig. 13.11 Risk of systemic embolization by size of vegetation. Adapted from Sanfilippo et al[1]

Special Considerations in Patients with IE

Prosthetic Valve IE

Prosthetic valve endocarditis (PVE) is a special case when it comes to choosing an imaging modality. Although we have previously mentioned several aspects in which TEE imaging may be superior to standard TTE imaging, these discussions have presented data on large groups of patients with IE. In specific patient populations, such as those with PVE, characteristics and limitations of the imaging technique are critical. For instance, in aortic valve PVE it is difficult to assess the entire annular circumference with either TTE or TEE alone. In addition, in mitral valve PVE it is likewise difficult to evaluate both the atrial and the ventricular aspects of the annulus with a single technique. Importantly, when there is a prosthesis in both the aortic and the mitral positions there is no single echocardiographic technique that allows for adequate evaluation.

Overall, in patients with PVE it may be beneficial to perform both TTE and TEE studies. In this way, a full evaluation of the infected area can be performed including: the annulus of the valve infected; the function of the valve; abscess formation; presence of a fistula tract; assessment for dehiscence; assessment for perivalvular regurgitation; and full assessment of overall regurgitation.

Right-Sided IE

Patients with right-sided IE may also represent a special population when it comes to the selection of imaging modalities. For instance, although the tricuspid valve is

usually well seen in the standard TTE views, patients with tricuspid valve IE are more likely to be infected with organisms such as *S. aureus*. It is well documented that in patients with *S. aureus* IE, TEE has superior test characteristics. In addition, the pulmonic valve may not be adequately seen from the standard TTE views. These issues must be taken into context with clinical outcomes data which show that injection drug uses with isolated right-sided IE may be adequately treated with 2 weeks of appropriate antibiotic therapy. Therefore, in this specific clinical scenario, the small risk of TEE may be outweighed by the small likelihood of diagnostic information that will change therapeutic management. In these patients collaboration between the care team and the echocardiography laboratory is a necessity to develop the appropriate imaging strategy.

Intracardiac-Device-Related Infections

Intracardiac devices (e.g., pacemaker and implantable cardioverter defibrillators) have become an integral part of modern cardiovascular medicine. Recently, a steady stream of randomized trials has provided definitive evidence that these devices improve symptoms, rehospitalization, or outcomes in selected patient populations. The growing number of evidence-based indications for cardiac devices coupled with an aging population in the western world ensures a continued increase in the implantation of cardiac devices in the foreseeable future. Recent evidence from a study of the US Medicare population has shown that the device implantation rate had a relative increase of 42% in the 1990s but that there was a 124% relative increase in patients with documented device infections during the same time period.

There are several important imaging considerations in patients with suspected intracardiac device infections. For instance, it is imperative to image the device throughout its course in the cardiac chambers. Special attention should be made at the point where the device crosses a valve, such as the tricuspid valve, in that there is likely high-velocity regurgitation at this point establishing the appropriate milieu for infection. In addition, devices that tract from the superior vena cava (SVC) should be imaged as far as possible into the SVC due to the fact that device-related infections in this area have been well documented.

Consideration for Multiple Echocardiographic Evaluations

Several studies have shown that multiple echocardiographic evaluations may be useful in determining the prognosis of patients with IE. For instance, Rohmann and colleagues performed serial TEE studies in 83 patients. They found that if a vegetation stayed static or enlarged then prognosis was much worse than if the vegetation shrank with therapy.

Serial examinations can be taken to extreme. For instance, Vieira and colleagues recently published data evaluating serial echocardiographic examinations. Over a 3-year period they evaluated 262 patients with suspected IE referred for echocardiography. They found that repeat echocardiography was frequent; TTEs were repeated at least once in 192 (72.2%) patients while TEEs were repeated in 49 (18.4%) of patients. The average number of TTE examinations was 2.4, but six patients had at least six TTEs. In a similar fashion, the mean number of TEE examinations was 1.7, although four patients had at least four TEEs and one patient had five TEEs. The authors found that while repeated echocardiograms were occasionally helpful, no additional diagnostic information was provided after the second or third echocardiogram (TTE or TEE).

Other Imaging Modalities in IE

Other types of imaging may be used to support the diagnosis of IE and/or evaluate for potential complications. For instance, chest radiography can be used to provide supporting evidence of IE such as nodular pulmonary infiltrates in a febrile injection drug user likely signifying right-sided IE with septic pulmonary emboli. In addition, cardiomegaly may indicate chamber enlargement due to significant valvular regurgitation, while enlarged pulmonary vessels provide evidence for congestive heart failure.

Computed tomography (CT) and magnetic resonance imaging (MRI) have long been used to assess for evidence of thromboembolic complications, such as stroke or visceral embolic events, in patients with IE but their role in imaging cardiac pathology is less established. For instance, there have only been isolated case reports of the use of CT imaging to diagnosis

complications of IE such as aortic root abscess. In a similar fashion, there have been multiple case reports of the use of MRI in patients with IE, but no large studies have been performed.

For both CT and MRI, the enhanced spatial resolution provided by the current imaging modalities and the likely improvements in this resolution over time, provide for the possibility of evaluating cardiac manifestations of the infective process in a more refined way. Enthusiasm for either of these modalities must be tempered by current limitations due to temporal resolution. For instance, the length of time currently required to acquire images, the difficulty in evaluating motion, and the presence of motion artifacts are important limitations in a disease such as IE.

Conclusions

Prior to the availability of echocardiography, the diagnosis and management of patients with IE was based almost entirely on clinical findings. In the 1970s and 1980s echocardiography revolutionized our ability to not only make the appropriate diagnosis in patients suspected of having IE but also allowed for an understanding of complications and risk of complications. Based on this knowledge, echocardiography is not only essential in the diagnostic strategy in patients with suspected IE, but has become indispensable as a tool to detect serious complications and guide therapeutic decision making.

Acknowledgment This work was supported in part by National Institutes of Health grant HL70861 (CHC).

References

1. Sanfilippo AJ, Picard MH, Newell JB, et al. Echocardiographic assessment of patients with infectious endocarditis: prediction of risk for complications. *J Am Coll Cardiol*. 1991;18(5):1191–1199.
2. Durack DT, Lukes AS, Bright DK. New criteria for diagnosis of infective endocarditis: utilization of specific echocardiographic findings. *Am J Med* 1994;96:200–209.
3. Li JS, Sexton DJ, Mick N, et al. Proposed modifications to the Duke criteria for the diagnosis of infective endocarditis. *Clin Infect Dis* 2000;30:633–638.
4. Sachdev M, Peterson GE, Jollis JG. Imaging techniques for diagnosis of infective endocarditis. *Infect Dis Clin North Am*. 2002;16(2):319 337.
5. Greaves K, Mou D, Patel A, Celermajer DS. Clinical criteria and the appropriate use of transthoracic echocardiography for the exclusion of infective endocarditis. *Heart*. 2003;89(3):273–275.

Section 3
Pericardial Disease

Chapter 14
Pericardial Effusion, Tamponade, and Constriction

Teresa S.M. Tsang, Larry J. Sinak, and Jae K. Oh

Anatomy, Function, and Physiology of the Pericardium

The pericardium has two membranous layers, an outer parietal fibrous layer and an inner visceral serous layer (Fig. 14.1). The serous pericardium covers the heart and proximal great vessels. It is reflected to form the parietal pericardium. Normally, the intrapericardial space between the two pericardial layers contains 25–50mL serous fluid secreted by the visceral pericardium and the intrapericardial pressure is equal to the intrapleural pressure. The pericardium provides mechanical protection for the heart and lubrication to reduce friction between the heart and contiguous structures. Because of the relative lack of distensibility, the pericardium also exerts hemodynamic impact on cardiac function. It limits acute distention of the heart and contributes to diastolic interaction between the two ventricles (the distention of one ventricle affects the filling dynamics of the other). This ventricular interdependence is important to the pathophysiology leading to pericardial tamponade and constriction.

Diseases of the Pericardium

In this chapter, we will focus on pericardial effusion, tamponade, and constriction. Less common entities, such as congenital absence (partial or complete) of the pericardium, pericardial cyst, and pericardial tumors, can be encountered.

T.S.M. Tsang (✉), L.J. Sinak, and J.K. Oh
Division of Cardiovascular Diseases, Department of Medicine, Mayo Clinic, Rochester, MN, USA
e-mail: tsang.teresa@mayo.edu

Congenital Absence of the Pericardium

Congenital absence of the pericardium can be complete or partial (Fig. 14.2). It can be asymptomatic, or associated with atypical chest pain. Sudden cardiac death can occur with herniation of cardiac chambers through a partial defect. Echocardiographic windows in these patients appear different. Because the cardiac structures are shifted leftward, the right ventricle appears prominent, simulating right ventricular volume overload. There is both exaggerated cardiac motion and abnormal ventricular septal motion. Associations of congenital absence of pericardium include bicuspid aortic valve, atrial septal defect, and bronchogenic cysts. Surgical treatment may be necessary if symptomatic.

Pericardial Cyst

Pericardial cyst is usually discovered incidentally and is a benign condition. It is most commonly, but not invariably, found at the right costophrenic angle (Fig. 14.3). It needs to be differentiated from other masses, such as malignant tumors, diaphragmatic hernia, and cardiac chamber enlargement.

Pericardial Tumors

The leading cause of pericardial tumor is metastatic in nature, most commonly from lung or breast cancer, melanoma, lymphoma, and acute leukemia. Many cases are asymptomatic and are found only incidentally,

P. Nihoyannopoulos and J. Kisslo (eds.), *Echocardiography*,
DOI: 10.1007/978-1-84882-293-1_14,

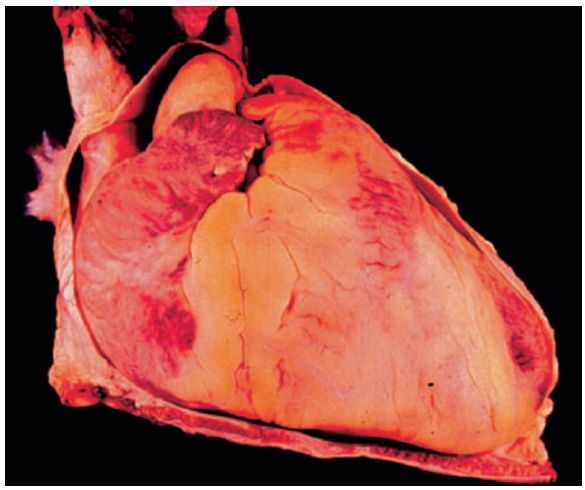

Fig. 14.1 Parietal and visceral pericardium. The outer layer is the parietal pericardium, and the inner layer, the visceral pericardium. There is normally a small amount of fluid in the pericardial space between these two layers

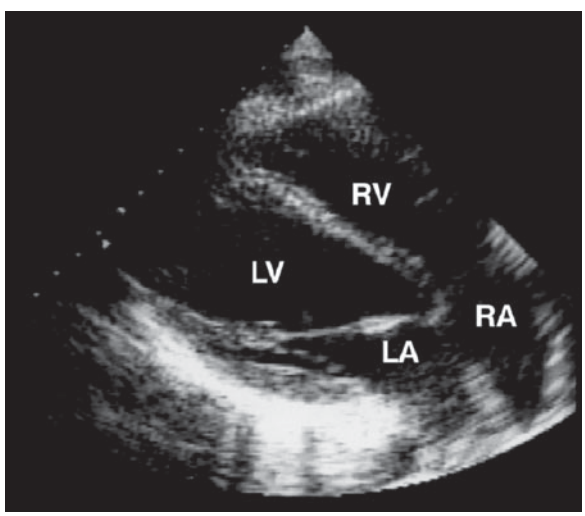

Fig. 14.2 Congenital absence of pericardium. With leftward shift of the heart, the right ventricle (RV) is at the center of the apical image rather than the left ventricular apex with an appearance of RV overload (From Oh JK, Seward JB, Tajik AJ. *The Echo Manual*. 2nd ed. PA: Lippincott-Raven, 1999, p 188. With permission of Mayo Foundation.)

but others cause symptoms and may progress to cardiac tamponade. Primary cardiac tumors may also invade the pericardium directly.

Primary mesothelioma of the pericardium is rare but highly lethal. Other primary tumors of the pericardium, such as teratomas, are quite rare.

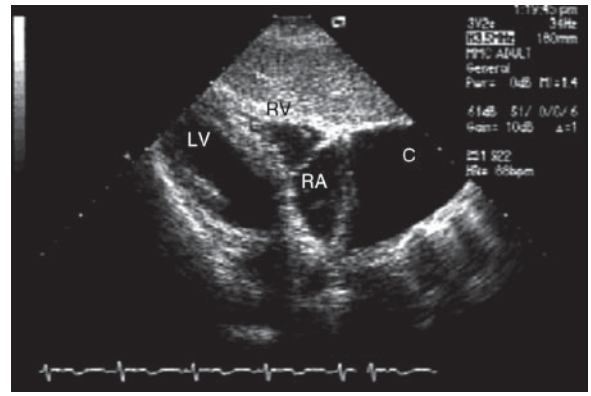

Fig. 14.3 Pericardial cyst. Subcostal view showing large pericardial cyst (C) adjacent to the right atrium. *RV* right ventricle, *LV* left ventricle, *RA* right atrium, *LA* left atrium

Pericardial Effusion and Tamponade

When the amount of fluid or blood in the pericardial space exceeds 25mL, an echo-free space persists throughout the cardiac cycle. Most commonly, pericardial fluid is circumferential. However, it can be loculated in the anterior, or more likely, posterior location. Posteriorly loculated pericardial effusion occurs not uncommonly following cardiac surgery.

Etiologies

The most common causes of pericardial effusion are malignancy, postpericardiotomy syndrome following cardiothoracic surgery, and secondary to perforation of the heart from invasive procedures. Other causes of pericardial effusions are listed in Table 14.1. Many remain "idiopathic" after careful investigations.

Clinical Features

Acute pericarditis is often associated fever and chest pain. Most commonly, it is attributed to viral illness, but can occur in the context of other conditions, including myocardial infarction. The constitutional symptoms are usually mild to moderate. A pericardial friction rub may be present. The disease ordinarily runs its course in 1–4 weeks, but recurrences may occur and relapsing cases can be debilitating. Accumulation of pericardial fluid is common, although

Table 14.1 Etiologies of pericardial effusion

Malignancy
Postoperative (postpericardiotomy)
Cardiac puncture from invasive procedures (electrophysiology studies, cardiac catheterization, pacemaker/ICD implantation)
Ischemic heart disease related (postinfarct as in Dressler's Syndrome; myocardial rupture)
Infectious
Immune/connective tissue diseases (lupus; rheumatoid arthritis; vasculitides)
Idiopathic
Renal failure
Drug-related and anticoagulants
Postradiation
Chest trauma
Hypothyroidism
Amyloidosis

tamponade is unusual. Residual sequelae can include constrictive pericarditis. The ST-segment alterations in the ECG usually disappear over weeks, but abnormal T waves may persist for years. Pleuritis and pneumonitis frequently accompany pericarditis.

Echocardiographic Features

- Two-dimensional echocardiography allows evaluation of the fluid amount, location, and distribution. Qualitatively, the size of the pericardial effusion can be described as small, moderate, or large. To facilitate comparison between studies, it is best to provide quantitative description. Simplistically, the size of the pericardial effusion would be considered as:
  - Small if maximal dimension of the effusion measures 1.0 cm or less
  - Small to moderate if 1.0–1.5 cm
  - Moderate sized if 1.5–2.5 cm
  - Large if exceeding 2.5 cm

When the amount of pericardial effusion is massive, the heart may have a "swinging" motion in the pericardial cavity (Fig. 14.4), which is responsible for the electrocardiographic finding of "electrical alternans." Cardiac tamponade can occur with a small amount of effusion, if the fluid accumulation is rapid, such as in the case of myocardial rupture following acute infarction or cardiac perforation from electrophysiology study or pacemaker implantation. In these situations, the small amount of rapid fluid accumulation in the relatively nondistensible pericardial sac leads to hemodynamic collapse, which can be life threatening if not promptly treated.

- M-mode and 2D echocardiographic features are usually characteristic in this life-threatening condition: early diastolic collapse of the right ventricle (Fig. 14.5), late diastolic right atrial inversion (Fig. 14.6), abnormal ventricular septal motion, respiratory variation in ventricle chamber size, and dilated inferior vena cava with blunted respiratory changes. However, these features may not be all present. For example, in the case of pulmonary hypertension, the pressures within the right-sided chambers are high, and collapse of the right ventricle and atrium may not occur even though significantly elevated intrapericardial pressure and cardiac tamponade may be present.

Blood clots, which may appear congealed or partially liquefied, can be found in the pericardial space (hemopericardium) in the case of acute myocardial rupture from infarction or trauma, and in proximal aortic dissection. The blood clots can cause compression of the cardiac chambers leading to tamponade (Fig. 14.7).

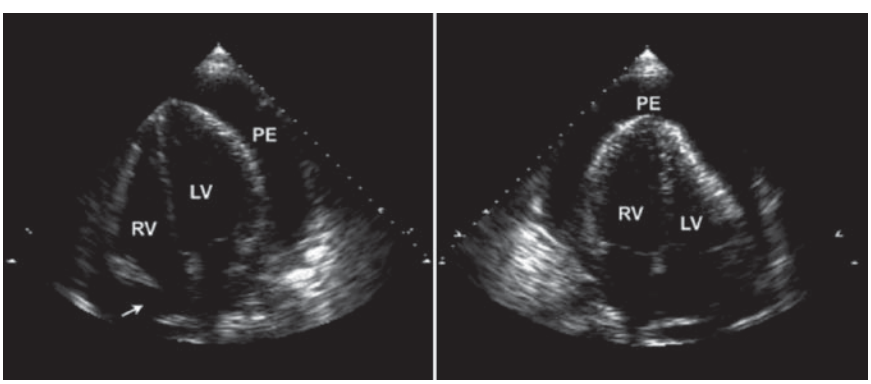

Fig. 14.4 "Swinging heart" in cardiac tamponade. With large amount of fluid, the position of the heart changes over the cardiac cycle (*left*, during diastole with right atrial inversion (*arrows*); *right*, during systole); *RV* right ventricle, *LV* left ventricle, *PE* pericardial effusion

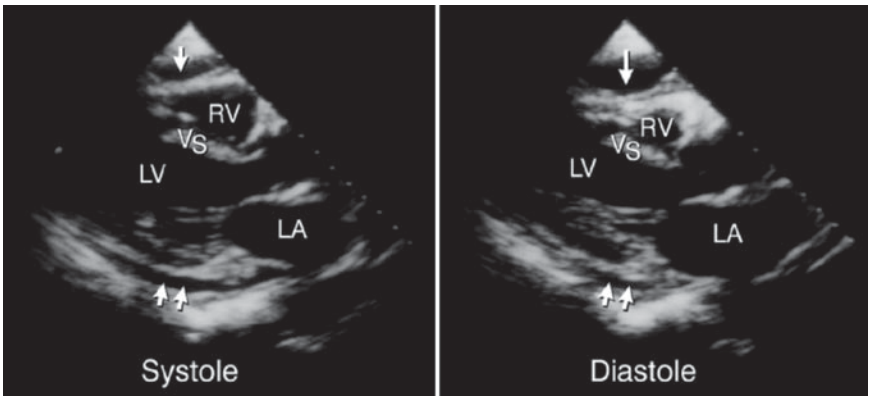

Fig. 14.5 Diastolic collapse of right ventricle in cardiac tamponade. Parasternal long-axis view of a patient with tamponade during systole (*left*) and diastole (*right*). The right ventricle (RV) collapses during diastole. *RV* right ventricle, *LV* left ventricle, *LA* left atrium, *VS* ventricular septum, *PE* pericardial effusion (From Oh JK, Seward JB, Tajik AJ. *The Echo Manual*. 2nd ed. PA: Lippincott-Raven, 1999, p 183. With permission of Mayo Foundation.)

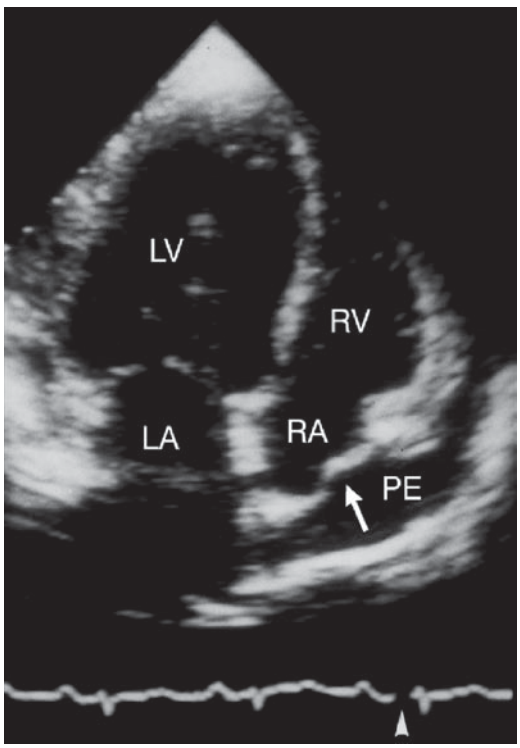

Fig. 14.6 Late diastolic right atrial inversion in cardiac tamponade. Apical four-chamber view showing late diastolic collapse of the right atrium (*arrow*). *LV* left ventricle, *RV* right ventricle, *LA* left atrium, *RA* right atrium, *PE* pericardial effusion (From Oh JK, Seward JB, Tajik AJ. *The Echo Manual*. 2nd ed. PA: Lippincott-Raven, 1999, p 183. With permission of Mayo Foundation.)

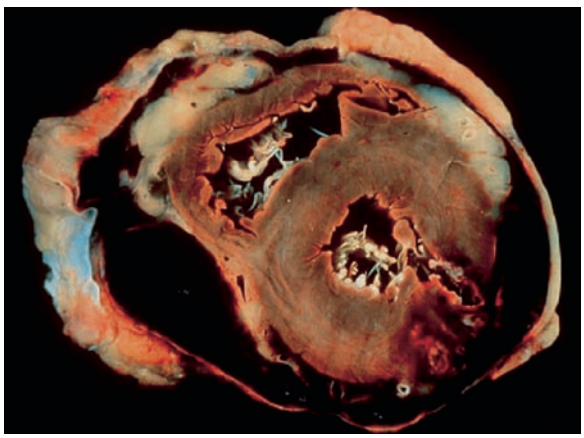

Fig. 14.7 Hemopericardium causing cardiac tamponade. Left ventricular rupture causing hemopericardium and tamponade

- Doppler echocardiographic findings are more sensitive for hemodynamic compromise due to pericardial effusion than the M-mode/2-D echocardiographic features. In normal circumstances, intrapericardial pressure and intrathoracic pressure fall by the same magnitude on inspiration. In cardiac tamponade, intrapericardial and intracardiac pressures fall less than intrathoracic pressure during inspiration. Therefore, the left ventricular filling pressure gradient (difference between pulmonary wedge pressure and left ventricular diastolic pressure) decreases. As a consequence, mitral valve opening is delayed, isovolumic relaxation time lengthens, and mitral *E* velocity decreases. As well, the filling hemodynamics in one ventricle are affected by those in the other ventricle (ventricular interdependence).

Thus, *during inspiration*, increased venous return to the right heart chambers is associated with decrease

in left ventricular filling, which is markedly exaggerated in cardiac tamponade. Clinically, this is manifested as pulsus paradoxus (drop of systolic blood pressure by more than 10mm Hg on inspiration), a classic sign of tamponade. Echocardiographically, on the left side, mitral *E* velocity drops (typically greater than 25% when compared to the expiratory *E* velocity, but this does not have to be evident in all cases of tamponade). Reciprocal changes occur in the right heart chambers (Fig. 14.8).

The respiratory flow velocity changes across the mitral and tricuspid valves are also reflected in the pulmonary and hepatic venous flow profile:

Inspiratory decrease and expiratory increase in pulmonary vein diastolic forward flow and expiratory decrease in hepatic vein forward flow with increase in expiratory reversal flow (Fig. 14.9).

- Not all classic 2D and Doppler features have to be present for the diagnosis of cardiac tamponade to be made. More importantly, it is the constellation of clinical and echocardiographic findings in the appropriate clinical context that clinches the diagnosis. It is important to recognize that certain features can be "masked" as a result of the concurrent presence of other pathologies (for instance, the lack of right-sided chamber collapse in cardiac tamponade in the presence of severe pulmonary hypertension).

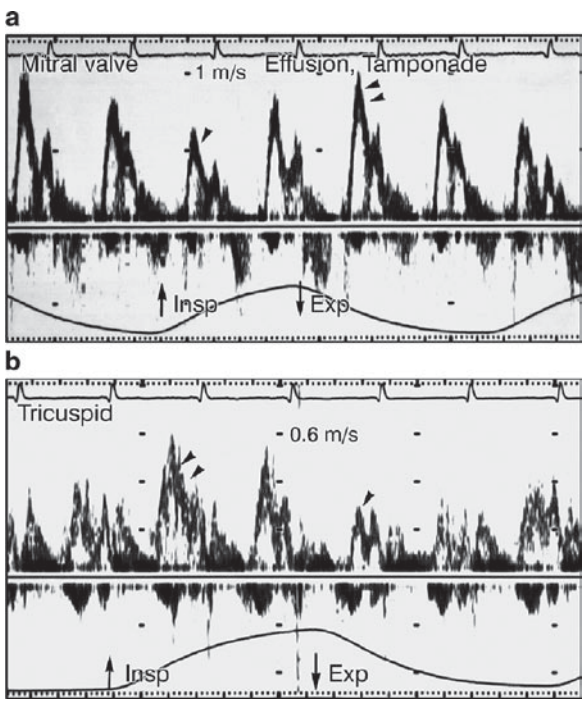

Fig. 14.8 Mitral and tricuspid inflow velocity profile of a patient with cardiac tamponade: mitral *E* decreases significantly with inspiration (*arrowhead*) and increases with expiration (*double arrowhead*), while tricuspid *E* increases with inspiration (*double arrowhead*) and decreases with expiration (*arrowhead*) (From Oh JK, Seward JB, Tajik AJ. *The Echo Manual*. 2nd ed. PA: Lippincott-Raven, 1999, p 185. With permission of Mayo Foundation.)

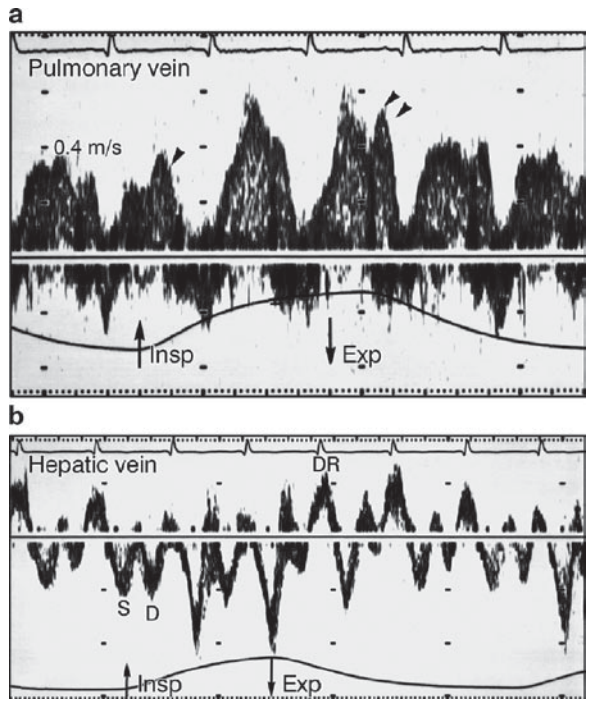

Fig. 14.9 Pulmonary and hepatic venous flow velocities in a patient with cardiac tamponade. On expiration, there is significant increase in diastolic forward flow (double arrowhead) in the pulmonary veins, and blunting of diastolic forward flow with increased diastolic reversals (DR) in the hepatic veins. *S* systolic forward flow, *D* diastolic forward flow, *DR* diastolic reversals (From Oh JK, Seward JB, Tajik AJ. *The Echo Manual*. 2nd ed. PA: Lippincott-Raven; 1999, p 185. With permission of Mayo Foundation.)

Echo-Guided Pericardiocentesis

The most effective, and potentially life-saving, treatment for cardiac tamponade is removal of the pericardial fluid. A blind percutaneous pericardiocentesis is associated with a high rate of complications, including death. Two-dimensional echocardiography can guide pericardiocentesis by locating the optimal site for needle

entry (Fig. 14.10). The position of the Teflon-sheathed needle can be evaluated by administration of agitated saline contrast while imaging (Fig. 14.11). Under most circumstances, a pig-tail (6 or 7 French) catheter is introduced and left in the pericardial sac for several days with intermittent drainage (every 4–6h). This practice has reduced the rate of recurrent effusion, and sclerosing agents are no longer used. The need for surgical management has also decreased considerably over the years.

At the Mayo Clinic, most pericardiocentesis procedures are performed by an echocardiographer with the guidance of 2D echocardiography. Based on our consecutive series consisting of 1,127 echo-guided pericardiocentesis procedures performed during a 21-year period, the most commonly selected location for needle entry is the para-apical area. Malignant effusion was most common (34%), followed by postoperative effusions (25%), and effusions occurring as complications of catheter-bases procedures (10%). In the recent years,

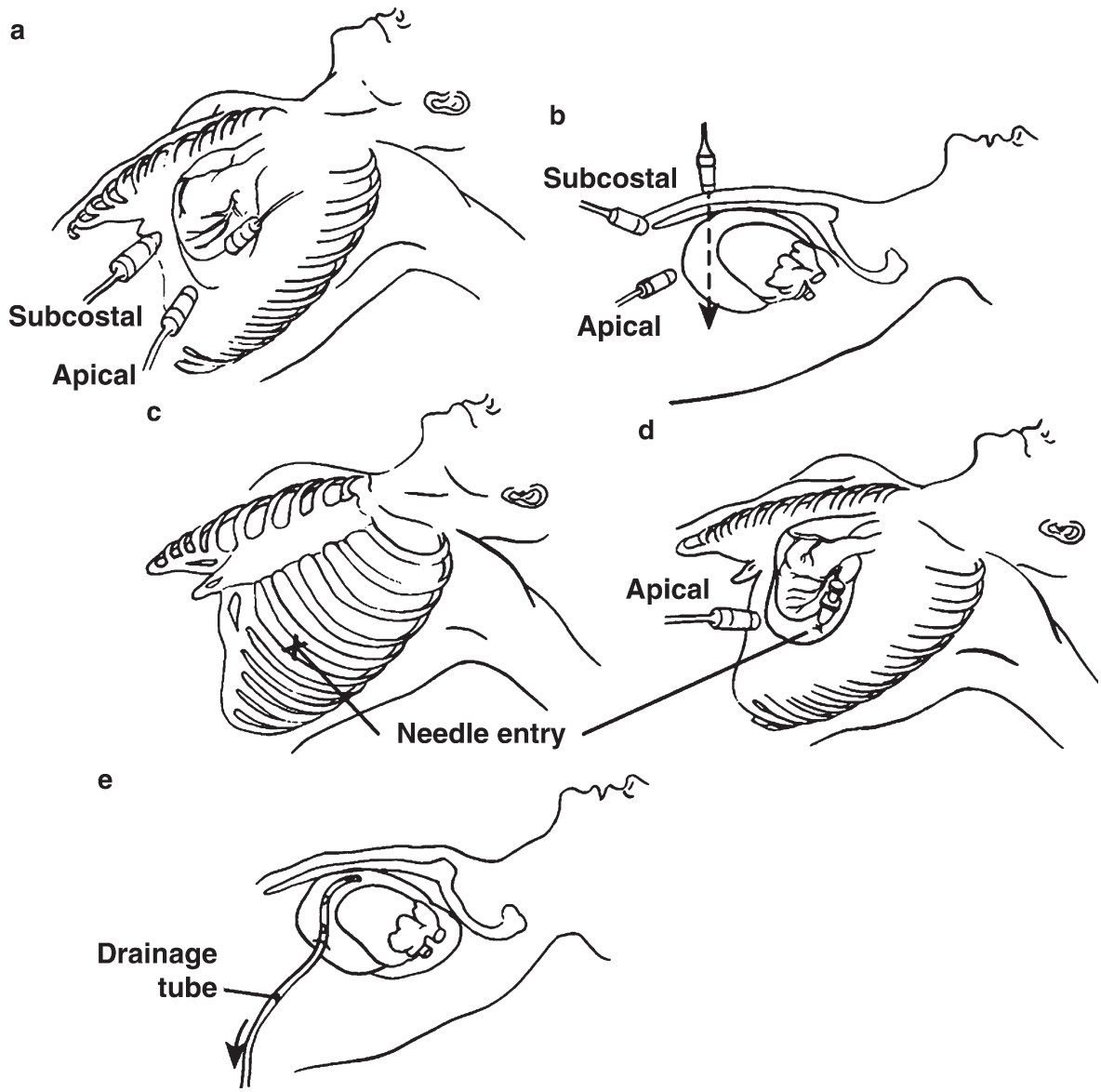

Fig. 14.10 Ideal site for needle entry by echocardiographic guidance. (From Oh JK, Seward JB, Tajik AJ. *The Echo Manual*. 2nd ed. PA: Lippincott-Raven, 1999, p 185. With permission of Mayo Foundation.)

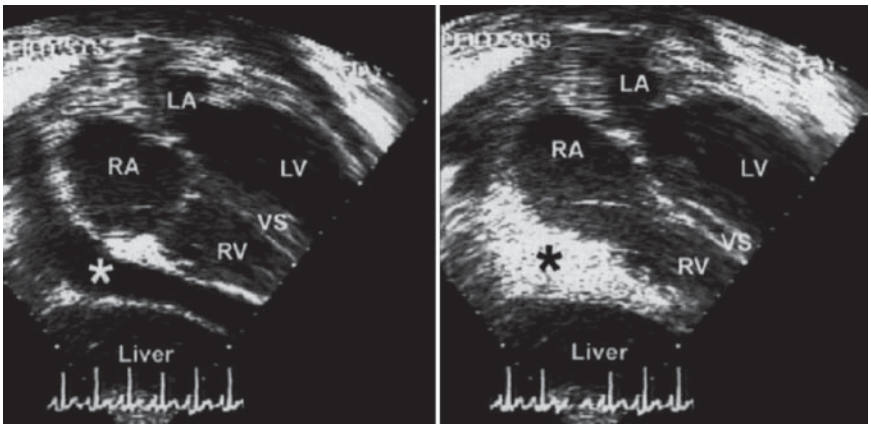

Fig. 14.11 Agitated saline contrast injection for assessment of position of Teflon-sheathed needle during pericardiocentesis with opacification of the pericardial space (*) after saline contrast injection. *RV* right ventricle, *LV* left ventricle, *RA* right atrium, *LA* left atrium, *VS* ventricular septum

postoperative effusion has surpassed malignancy as the leading cause of pericardial fluid accumulation requiring intervention. Echo-guided pericardiocentesis was successful in 97% of the cases.

There were a total of 14 major complications (1.2%). These included the death of a 50-year-old woman with severe primary pulmonary hypertension, who did not survive an attempted surgical rescue following a right ventricular puncture that led to hemorrhagic tamponade. Nonfatal complications included chamber lacerations requiring surgery (5), injury to an intercostal vessel necessitating surgery (1), pneumothoraces requiring chest tube placement (5), ventricular tachycardia (1), and bacteremia possible related to pericardial catheter placement (1).

There were 40 minor complications (3.5%), that did not require specific interventions, except for monitoring and appropriate follow up. These included transient chamber entries (11), small pneumothorax noted on radiographs (8), vasovagal response with transient fall in blood pressure (2), nonsustained supraventricular tachycardia (2), pericardial catheter occlusion (8), and probable pleuropericardial fistulas (9).

Differentiating Pericardial Effusion from Pleural Effusion

Occasionally, pericardial effusion can be confused with pleural effusion. Several features may help to differentiate pericardial from pleural effusion. Pericardial effusion is most often circumferential (although it can be loculated anteriorly or posteriorly). If there is an echo-free space anteriorly only, it may be difficult to distinguish an epicardial fat pad from pericardial effusion. Posteriorly, pericardial effusion is located anterior to the descending thoracic aorta, whereas pleural effusion is present posterior to the aorta (Fig. 14.12).

Pericardial Constriction

Pathophysiology and Etiologies

Constrictive pericarditis is characterized by restrictive ventricular filling due to a stiffened or noncompliant pericardium. The pericardium may be thickened and calcified, although there have been documented cases of constriction where stiffened pericardium accompanied by constrictive physiology occurs in the absence of persistent pericardial thickening. In the classic scenario of advanced constriction, the pericardium usually contains calcified fibrous scar tissue from an inflammatory process, and the scarring may involve the epicardium. There are multiple causes of constriction. These include acute pericarditis, collagen vascular disease, coronary artery bypass surgery, and tuberculosis (Table 14.2). However, it may be idiopathic. In modern era, cardiac surgery has become the most common etiology (about 30%) for constrictive pericarditis.

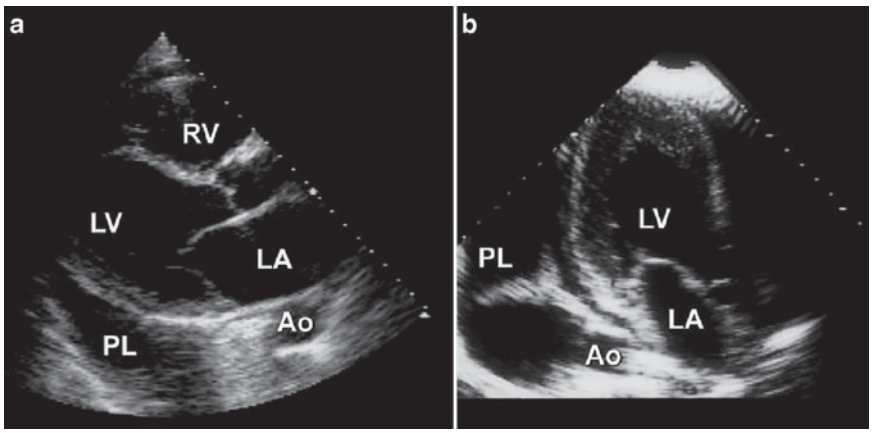

Fig. 14.12 Differentiating between posterior pericardial effusion and left pleural effusion from the parasternal long-axis view. Pericardial effusion can be seen between the posterior left ventricular (LV) wall and descending thoracic aorta (AO), while pleural effusion (PL) is seen behind the aorta. *LV* left ventricle, *LA* left atrium, *RV* right ventricle; PL, pleural effusion; AO, descending thoracic aorta (From Oh JK, Seward JB, Tajik AJ. *The Echo Manual*. 2nd ed. PA: Lippincott-Raven; 1999, p 186. With permission of Mayo Foundation.)

Table 14.2 Causes of constrictive pericarditis

Postoperative
Idiopathic
Postacute pericarditis of any cause
Radiation induced
Uremia
Connective tissue disease (systemic lupus erythematosus, scleroderma, rheumatoid arthritis)
Post-trauma
Drugs (procainamide, hydralazine, methysergide)
Neoplastic pericardial disease (melanoma, mesothelioma)
Tuberculosis, fungal infections (histoplasmosis, coccidioidomycosis), parasitic infections
Postmyocardial infarct
Post-Dressler syndrome
Postpurulent pericarditis
Pulmonary asbestosis

Clinical Features

Clinical features at presentation may include dyspnea, systemic venous congestion with hepatomegaly, ascites, and leg edema. The most prominent findings on physical examination are related to systemic venous congestion, such as distention of the jugular vein. Venous pressure often increases with inspiration (Kussmaul's sign) because of the inability of the right side of the heart to accommodate the increased cardiac input with inspiration. Unlike the patients with cardiac tamponade in whom a prominent "x" descent is observed, patients with constrictive pericarditis characteristically have rapid "y" descent, which reflects the early diastolic decrease in right ventricular pressure.

With high atrial pressure, rapid filling of the ventricle is accelerated with generation of a third heart sound, described as "pericardial knock," which usually occurs 80–120ms after aortic valve closure.

Most of the symptoms associated with constriction may resolve with pericardiectomy. However, the symptoms and clinical findings mimic those of restrictive cardiomyopathy, which is a progressive disease with no long-term effective treatment.

Echocardiographic Findings

Echocardiography is most helpful and may be the initial test in diagnosing constrictive pericarditis.

- *The characteristic M-mode/two-dimensional echocardiographic findings include*:
  - Abnormal ventricular septal motion ("septal bounce") (Fig. 14.13)
  - Increased pericardial thickness or calcification
  - Dilated inferior vena cava with no significant changes with inspiration, and – flattening of the left ventricular posterior wall during diastole
- *However, these findings are neither sensitive nor specific*. Although the underlying pathologic

mechanism of constriction is different from that of cardiac tamponade, the hemodynamic events of respiratory variation during left and right ventricular filling are similar in the two conditions.

- *The thickened pericardial layer prevents full transmission of intrapleural pressure* changes with respiration to the pericardial and intracardiac cavity, creating respiratory variation in the left-side filling pressure gradient (pressure difference between the pulmonary vein and the left atrium).
- *Therefore, the mitral inflow and the pulmonary venous diastolic flow velocities decrease immediately after the onset of inspiration and increase with expiration* (Fig. 14.14).
- *Reciprocal changes occur in tricuspid inflow and hepatic venous flow profile* because of the relatively

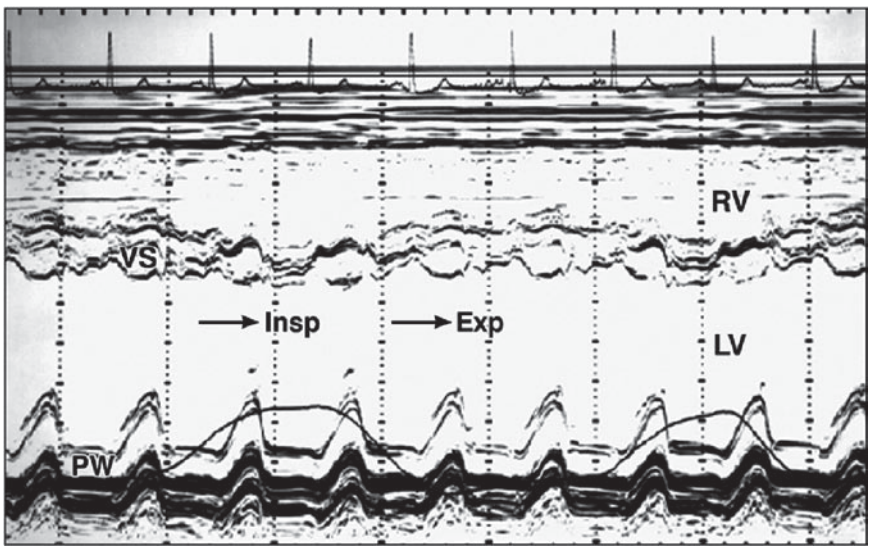

Fig. 14.13 M-mode echocardiogram with respirometry showing abnormal ventricular septal motion ("septal bounce") in a patient with constrictive pericarditis. There was septal shift of the ventricular septum (VS) toward the left ventricle (LV) during inspiration and toward the right ventricle (RV) on expiration, and flattening of the posterior wall (PW) due to limited diastolic filling (From Oh JK, Seward JB, Tajik AJ. *The Echo Manual*. 2nd ed. PA: Lippincott-Raven, 1999, p 186. With permission of Mayo Foundation.)

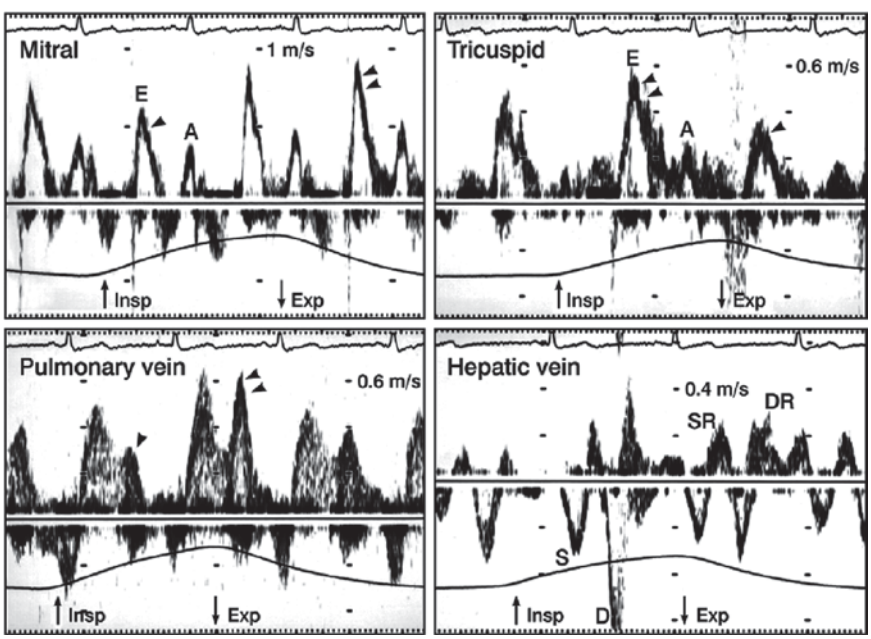

Fig. 14.14 Composite of mitral valve, tricuspid valve, pulmonary vein, and hepatic venous flow velocities typically seen in constrictive pericarditis. *D* diastolic flow, *DR* diastolic flow reversal, *Exp* expiration, *Insp* inspiration, *S* systolic flow, *SR* systolic flow reversal. (From Oh JK, Seward JB, Tajik AJ. *The Echo Manual*. 2nd ed. PA: Lippincott-Raven; 1999, p 188. With permission of Mayo Foundation.)

fixed cardiac volume. With decreased filling of the right cardiac chambers on expiration, there are exaggerated diastolic flow reversals and decreased diastolic forward flow in the hepatic vein with the onset of expiration (Fig. 14.14). In contrast, hepatic vein flow reversals are more prominent with inspiration in restrictive cardiomyopathy. It is not unusual to see significant diastolic flow reversals in the hepatic veins during both inspiration and expiration in patients with advanced constriction or combined constriction and restriction.

- *Exceptions:* A subgroup of patients with constrictive pericarditis may not have the characteristic respiratory variation of Doppler velocities. Mitral inflow velocities may not show respiratory variation in up to 50% patients with constrictive pericarditis, but expiratory diastolic flow reversal in hepatic vein is present in almost all patients with constrictive pericarditis. Therefore, the absence of respiratory variation of mitral inflow in patients with clinical evidence of significant systemic venous congestion does not exclude the diagnosis of constrictive pericarditis, and additional studies should be performed.
- *The typical respiratory variation and Doppler velocities also can occur in other conditions* such as chronic obstructive lung disease, right ventricular infarct, sleep apnea, asthma, and pulmonary embolism. This is due to increased respiratory efforts so that intrapleural pressure drop with inspiration is pronounced and not all of which can be transmitted to the heart.
- *Tissue Doppler:* Mitral annulus velocity by tissue Doppler imaging has become an important component of the echocardiographic examination for assessment of constriction and differentiation from restriction. The presence of preserved or even high mitral septal annulus velocity of ≥8 cm/s (Fig. 14.15a), especially in the context of restrictive left ventricular filling or high filling pressures (*E/A* ratio of >1.5 and

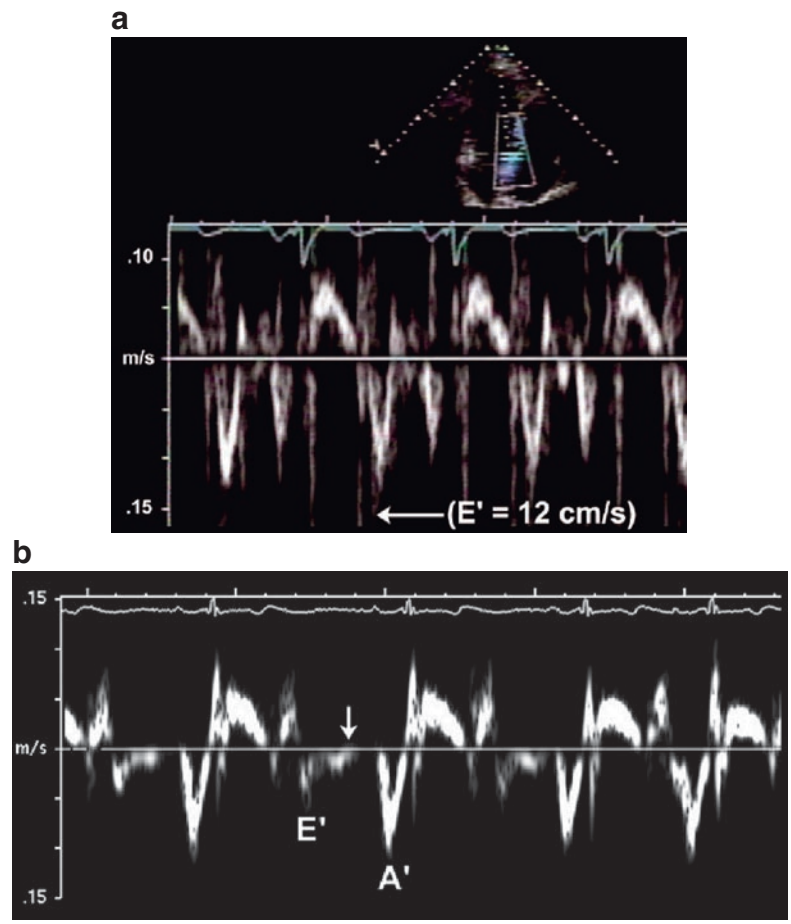

Fig. 14.15 Mitral annulus velocity profile in constriction (**a**) and restriction (**b**). *E′* is well preserved in constriction but blunted in restriction

deceleration time of <160ms), is suggestive of constriction. In restriction, the mitral annulus velocity is typically decreased (<8 cm/s) (Fig. 14.15b). In constrictive pericarditis, myocardial relaxation is relatively well preserved unless the myocardium is also involved as seen in radiation heart injury. The longitudinal motion, assessed by mitral septal annulus velocity, becomes exaggerated as the constriction gets worse with higher filling pressure, paradoxical to its change in myocardial disease. The phenomenon has been termed "Annulus Paradoxus". *E*/*E*′ is, therefore, inversely proportional to pulmonary capillary wedge pressure in constriction, whereas it is positively related to pulmonary capillary wedge pressure in myocardial disease. More recently, Sohn and his colleagues reported that *E*′ also varies with respiration, but usually in the opposite direction compared to mitral inflow.

Differentiating Constriction from Restriction

The clinical and hemodynamic profiles of restriction and constriction are similar, despite these conditions having distinctly different pathophysiologic mechanisms. Both are caused primarily by diastolic filling abnormalities, and systolic function is generally preserved. The diastolic dysfunction in restrictive cardiomyopathy results from noncompliant ventricular myocardium; whereas in constrictive pericarditis, from noncompliant pericardium.

- *Electrocardiographically,* voltage may be decreased in restrictive cardiomyopathy in cases of infiltrative disease, such as amyloid heart disease.
- *Echocardiographically,* restriction and constriction may have similar morphology.
  - The ventricles are usually normal size with enlarged atria (in restriction atrial size is usually greater)
  - The pericardium is often thickened in constriction (although this may not be obvious, and is not present in transient constriction)
  - Left ventricular wall thickness is increased in infiltrative disease associated with restriction. Left ventricular systolic function is generally normal and inferior vena cava is dilated

In constrictive pericarditis, the most striking finding is ventricular septal motion abnormalities, which can be explained on the basis of respiratory variation in ventricular filling. There are typical respiratory variations in ventricular filling (decreased filling of the left ventricle with inspiration and increased filling with expiration and significant hepatic venous flow reversal with expiration because of decreased filling on the right side).

Restrictive cardiomyopathy is characterized by the restrictive Doppler physiology, with increased *E* velocity, decreased *A* velocity, *E*/*A* ratio greater than 2, and shortened deceleration time of *E* velocity. Hepatic vein diastolic flow reversals occur with inspiration instead of expiration. A subgroup of patients with constrictive pericarditis may have similar Doppler findings without respiratory variation. In such cases, the Doppler examination should be repeated after an attempt has been made to reduce preload (head-up tilt position or diuretic therapy).

- *Tissue Doppler* recording of mitral annulus has become an important means to differentiate myocardial restrictive from pericardial constrictive heart disease. Typically, mitral annular *E*′ velocity is well preserved in constriction (often greater than 8cm/s) but significantly diminished in restriction. Mitral inflow propagation velocity (PFV) measured by color M-mode is also helpful in distinguishing restriction (PFV < 45cm/s) from constriction (PFV >45cm/s). However, it is more difficult to perform than TDI.
- *If the diagnosis remains uncertain* after a careful clinical examination, review of laboratory data, and 2D and Doppler echocardiographic evaluation, additional studies including CT or MRI can be helpful. Cardiac catheterization for assessment of characteristic discordant respiratory changes in the left and right ventricular pressure tracings can also be considered.

Differentiating Constriction from Chronic Obstructive Lung Disease

The most important Doppler finding that reliably distinguishes between these two entities is superior vena cava flow velocities. In chronic obstructive lung disease, superior vena cava flow is markedly increased with inspiration (Fig. 14.16). The underlying mechanism for respiratory variation in chronic obstructive

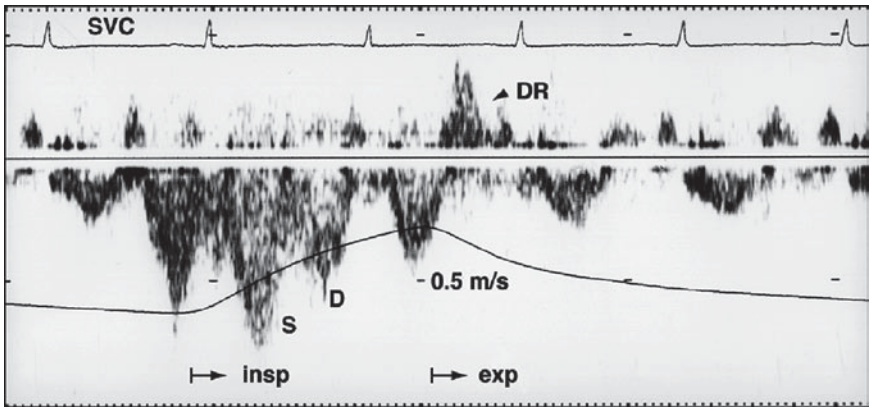

Fig. 14.16 Characteristic superior vena cava Doppler profile in chronic obstructive lung disease. The systolic forward flow is markedly accentuated on inspiration. *S* systolic forward flow, *D* diastolic forward flow, *DR* diastolic reversals. (From Oh JK, Seward JB, Tajik AJ: The Echo Manual. Second edition. Lippincott-Raven; 1999, p 190. With permission of Mayo Foundation.)

lung disease is a greater decrease in intrathoracic pressure with inspiration, which generates greater negative pressure changes in the thorax. This enhances flow to the right atrium from the superior vena cava with inspiration producing marked systolic forward flow accentuation on inspiration. In constrictive pericarditis, superior vena cava systolic flow velocities do not change significantly with respiration (Fig. 14.17). Generally, the difference in systolic forward flow velocity between inspiration and expiration is less than 20cm/s in constrictive pericarditis. Together with prominent diastolic reversals in the hepatic veins on expiration, and well preserved mitral annular E' velocity, the diagnosis of constriction can readily be made.

Diagnosing Constriction in Atrial Fibrillation

It is more challenging to diagnose constriction by echocardiography in patients with atrial fibrillation. Patients with constrictive pericarditis and atrial fibrillation should still have typical 2D features. Longer observation of Doppler velocities to detect velocity variation with respiration is necessary. Hepatic vein diastolic flow reversal with expiration is an important Doppler finding to suggest constrictive pericarditis, even when mitral inflow velocity pattern is not diagnostic. Respirometer recording may have a phase delay up to 1,000 ms, which makes the timing of velocity variation difficult. It is useful to remember that the lowest mitral inflow velocity usually occurs during inspiration. It is important that the patient tries to breathe smoothly during Doppler recording for timing of the Doppler profile. Ultimately, further studies with CT, MRI and/or cardiac catheterization are often necessary to confirm the diagnosis.

Effusive-Constrictive Disease

Effusive-constrictive pericarditis occurs when pericardial fluid accumulates between the thickened, fibrotic parietal pericardium and visceral pericardium. Radiation, malignancy, infection, connective tissue diseases, and idiopathic relapsing pericarditis are common anteceding conditions. Transient effusive-constrictive pericarditis has occurred with chemotherapy. The hemodynamic features of this condition include those of tamponade and constriction, and are often evident when constrictive physiology is present even after removal of pericardial fluid.

Role of CT and MR Imaging in Pericardial Disease

Echocardiography is generally the first test of choice in the evaluation of pericardial disease, but is occasionally limited or indeterminate. CT or MR imaging is often

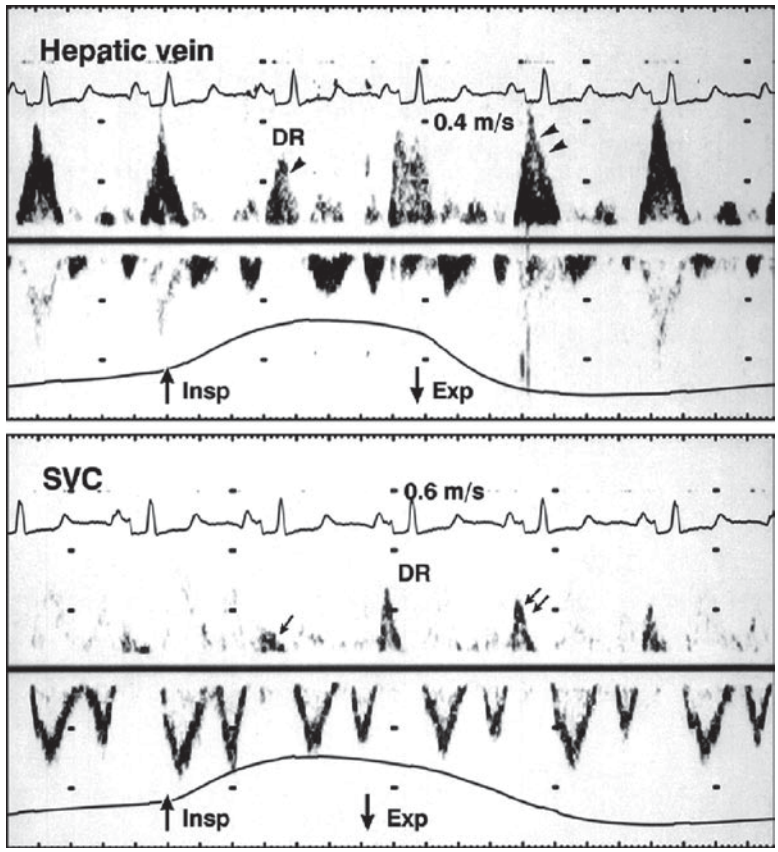

Fig. 14.17 Pulsed-wave Doppler recording from hepatic vein and superior vena cava (SVC) in constriction. The diastolic reversal (DR) in hepatic vein during expiration (double arrowhead) is significantly increased when compared to that during inspiration. There was little augmentation of SVC systolic forward flow on inspiration

helpful in these cases, offering superior soft tissue contrast and the ability to image the entire pericardium and its relationship to cardiac structure and function. Echocardiography is useful in evaluating the thickness of the pericardium, but is generally less sensitive than CT or MR imaging. CT and MR are often helpful in confirming, or diagnosing constriction when echocardiographic findings are indeterminate. Even in the case of pericardial effusion when the amount and location of the fluid is easily determined by echocardiography, and CT and MR imaging are generally unnecessary, the attenuation coefficients for blood, exudate, serous, and chylous fluid from CT are generally characteristic. MR imaging can identify inflamed pericardium and adhesions which have a high-signal intensity relative to pericardial fluid and myocardium, providing useful information regarding the nature of the effusion. MR imaging allows tissue characterization and is particularly helpful in the evaluation of pericardial mass.

Conclusion and Practical Tips

Echocardiography is the primary diagnostic modality of choice for pericardial disease. It is noninvasive, portable, and can easily identify the amount, location, and distribution of pericardial fluid. It provides accurate assessment of the hemodynamic impact of the effusion. With few exceptions, echo-guided pericardiocentesis is the primary treatment of choice for large symptomatic, or hemodynamically significant pericardial effusion. Echocardiography is generally also the first modality for assessing constrictive pericarditis.

CT or MR imaging may be necessary for confirmation or for diagnosis if echocardiographic findings are indeterminate. For other pericardial pathologies, such as partial or complete absence of pericardium, pericardial cyst, or tumors involving the pericardium, echocardiography is useful in making the diagnosis in most situations. However, CT or MR imaging can be highly complementary, especially since these imaging modalities are capable of tissue characterization, providing important information regarding the nature of some of these pathologies.

Bibliography

Ha JW, Oh JK, Ling LH, Nishimura RA, Seward JB, Tajik AJ. Annulus paradoxus: transmitral flow velocity to mitral annular velocity ratio is inversely proportional to pulmonary capillary wedge pressure in patients with constrictive pericarditis. *Circulation*. 2001;104:976–978.

Ha JW, Oh JK, Ommen SR, Ling LH, Tajik AJ. Diagnostic value of mitral annular velocity for constrictive pericarditis in the absence of respiratory variation in mitral inflow velocity. *J Am Soc Echocardiogr*. 2002;15:1468–1471.

Haley JH, Tajik AJ, Danielson GK, Schaff HV, Mulvagh SL, Oh JK. Transient constrictive pericarditis: Causes and natural history. *J Am Coll Cardiol*. 2004;43:271–275.

Hoit BD, Dalton N, Bhargava V, Shabetai R. Pericardial influences on right and left ventricular filling dynamics. *Circ Res*. 1991;68:197–208.

Ling LH, Oh JK, Breen JF, et al. Calcific constrictive pericarditis: is it still with us?. *Ann Intern Med*. 2000;132:444–450.

Ling LH, Oh JK, Schaff HV, et al. Constrictive pericarditis in the modern era: evolving clinical spectrum and impact on outcome after pericardiectomy. *Circulation*. 1999;100:1380–1386.

Oh JK, Hatle LK, Seward JB, et al. Diagnostic role of Doppler echocardiography in constrictive pericarditis. *J Am Coll Cardiol*. 1994;23:154–162.

Spodick DH. Acute cardiac tamponade. *N Engl J Med*. 2003;349:684–690.

Spodick DH. Acute pericarditis: current concepts and practice. *JAMA*. 2003;289:1150–1153.

Talreja DR, Edwards WD, Danielson GK, Schaff HV, Tajik AJ, Tazelaar HD, Breen JF, Oh JK. Constrictive pericarditis in 26 patients with histologically normal pericardial thickness. *Circulation*. 2003;108:1852–1857.

Tsang TSM, Enriquez-Sarano M, Freeman WK, et al. Consecutive 1127 therapeutic echocardiographically guided pericardiocenteses: Clinical profile, practice patterns, and outcomes spanning 21 years. *Mayo Clin Proc*. 2002;77:429–436.

Tsang TS, Oh JK, Seward JB. Diagnosis and management of cardiac tamponade in the era of echocardiography. *Clin Cardiol*. 1999;22:446–452.

Section 4
Ventricular Disorders and Ischemic Disease

Chapter 15
Clinical Echocardiography
Coronary Artery Disease: Assessing Regional Wall Motion

Paramjit Jeetley and Roxy Senior

Introduction

The assessment of left ventricular systolic function and particularly regional wall motion has become increasingly important in determining the severity and prognosis of coronary artery disease (CAD). Echocardiography, with its high spatial and temporal resolution, is an ideally suited noninvasive method of assessing such changes in wall motion. In the acute situation, the ability to detect these changes can be very useful in the early detection of myocardial ischemia, even preceding changes on ECG and symptoms. Equally in patients presenting acutely with chest pain, with inconclusive ECGs, normal regional wall motion may help exclude underlying ischemia.

In patients presenting with a prior history of CAD, the presence of regional wall motion abnormalities (RWMA) and extent of left ventricular wall thinning can give valuable information regarding the site and severity of damage together with the extent of remodeling. Re-evaluation of these patients can allow any change in left ventricular function and architecture due to therapy (revascularization or drug treatment) to be fully assessed.

The improved image quality on modern machines, particularly with harmonic imaging, has allowed regional wall motion assessment to be much more reliable. Newer techniques to improve endocardial definition, such as the use of contrast agents to improve left ventricular opacification (LVO), and automated endocardial border tracking software are also now making an impact into the reproducibility of this assessment.

P. Jeetley and R. Senior (✉)
Department of Cardiovascular Medicine, Northwick Park Hospital, Harrow, Middlesex, HA1 3UJ, UK
e-mail: roxy.senior@virgin.net

Regional Wall Motion Abnormality: How Does It Occur? The Mechanism for RWMA

There is a well-established relationship between regional coronary blood flow and contractile function in the corresponding territory. In patients with normal coronary arteries, coronary perfusion is maintained even when the oxygen demands of the tissue are increased. For example, during exercise there is an increase in myocardial blood flow, appropriate tissue oxygenation, and hence regional wall motion remains normal.

In patients with CAD, resting regional blood flow remains normal with adequate coronary perfusion, despite sometimes quite severe stenosis of the supplying artery. This is achieved by compensatory vasodilation of the arterioles which maintains resting myocardial blood flow (MBF) until the stenosis severity exceeds 90% (though collaterals may maintain normal MBF even in this situation). As a result resting wall motion may be entirely normal in patients with significant coronary disease. However, if the oxygen demand of the tissue is increased (e.g., during exercise), since the vasodilator response is nearly exhausted, there is an inability to increase coronary perfusion to that area. This leads to a reduction in the contractile function of that segment leading to a regional wall motion abnormality. When the oxygen demands of that tissue are reduced and return to normal, there is resolution of the ischemia and wall motion returns to normal.

Acute coronary artery occlusion as seen in acute myocardial infarction (AMI) leads to a rapid reduction in resting myocardial blood flow and hence cessation of muscular contraction in the area supplied, leading to a reduction in ventricular function. Relief of the occlusion,

P. Nihoyannopoulos and J. Kisslo (eds.), *Echocardiography*,
DOI: 10.1007/978-1-84882-293-1_15, © Springer-Verlag London Limited 2009

either spontaneously or by treatment (such as thrombolysis), can lead to recovery of regional wall motion, but this is dependant on the duration of the occlusion and the extent of myocardial necrosis that has occurred as a result. The duration and severity of myocardial ischemia determines the degree of wall motion abnormality, and indeed wall motion may not return to normal for several hours after the acute episode ("stunned myocardium").

In chronic CAD, progressive reduction in myocardial blood flow due to the progression of CAD may result in down regulation of myocardial contractile function with preserved metabolic activity ("hibernating myocardium"). When the myocardial blood flow is restored through revascularization of the stenotic artery, contractile function is restored gradually. Diminished contractile function in chronic CAD may also occur due to myocardial stunning due to repeated ischemic episodes. These ischemic episodes may either occur at rest (vasospasm) or during increased myocardial oxygen demand such as exercise.

The detection of such wall motion abnormalities is important as they occur early in the "ischemic cascade" preceding ECG changes and symptoms (Fig. 15.1).

Wall Motion vs. Systolic Wall Thickening for the Assessment of CAD

There are some limitations to using wall motion as the sole criterion for ischemic muscle. The movement of any given segment of the ventricle is influenced by the adjacent muscle to which it is attached. For example, in a chamber with a dyskinetic ischemic segment, some of the adjacent normal tissue may appear hypokinetic because its motion is influenced by the attached dyskinetic muscle. The reverse phenomenon can also occur. If vigorously contracting normal muscle is next to an ischemic area, the hyperdynamic segment may pull the ischemic muscle toward the cavity, which may mask the abnormally perfused area. In general, wall motion abnormalities alone overestimate the degree of ischemia seen in the myocardium.

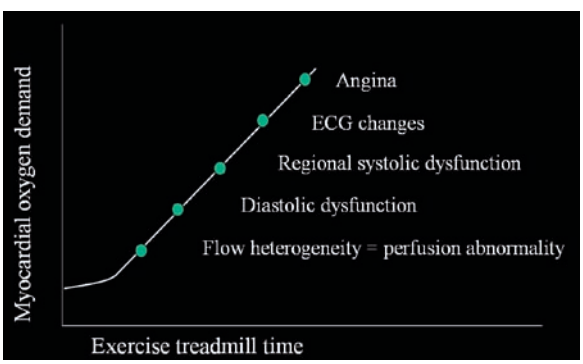

Fig. 15.1 Schematic representation of the sequence of changes in blood flow, EKG, and symptoms with increasing demand ischemia

A more specific finding for ischemic muscle is a deterioration of systolic wall thickening. Normal myocardial muscle increases in thickness during systole (Fig. 15.2). During ischemia there is a reduction or absence of systolic wall thickening. Indeed, there may also be systolic thinning during acute ischemia, i.e., wall thickening is greater in diastole compared to systole (Fig. 15.3). It has been shown that the extent and severity of wall thickening abnormality is superior to that of wall motion abnormality evaluation for predicting outcome after (AMI).[1]

Situations in which wall motion may be abnormal with preserved wall thickening include left bundle branch block (LBBB), Wolf–Parkinson–White syndrome, and when the patient has a paced rhythm. The presence of preserved systolic wall thickening in these conditions confirms that the wall motion abnormalities are not due to underlying CAD.

Basic Anatomy and Echocardiographic Findings

Three major epicardial arteries and their branches provide blood to different regions of the heart. Though there are small variations in between individuals, the pattern of this supply remains broadly the same. The left main coronary artery (or left main stem (LMS)) arises from the Aortic root (the left sinus of Valsalva) and divides into two branches: the left anterior descending artery (LAD) and the left circumflex artery (LCx). The LAD runs down the interventricular groove and supplies the anterior wall (via its diagonal branches), anterior septum, and apex of the heart. The left circumflex artery runs laterally down the atrioventricular groove where, together with its obtuse marginal branches, it supplies the lateral wall. The right coronary artery (RCA) originates from the right sinus of Valsalva, runs inferomedially down the atrioventricular groove.

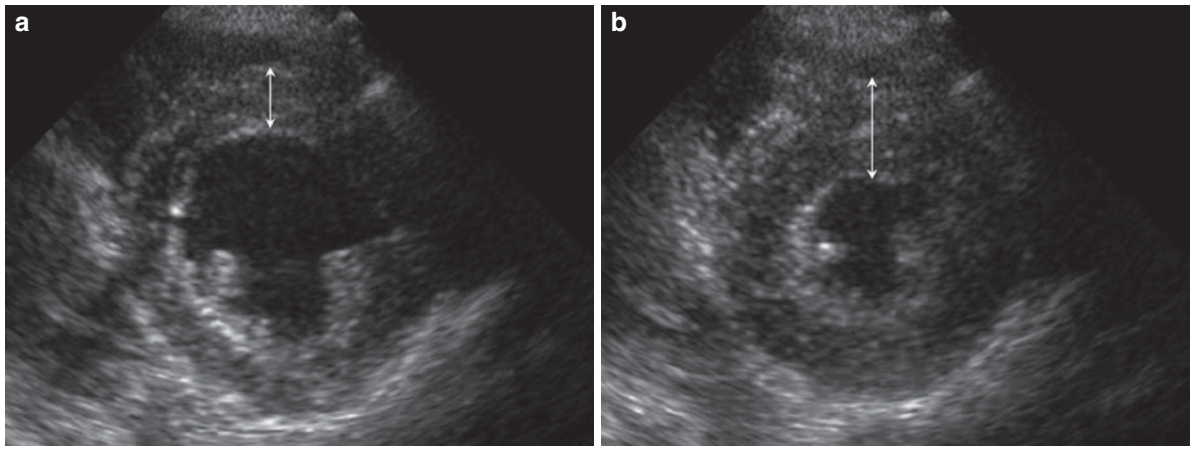

Fig. 15.2 Parasternal short axis views of the left ventricle during (**a**) diastole and (**b**) systole demonstrating normal systolic wall thickening

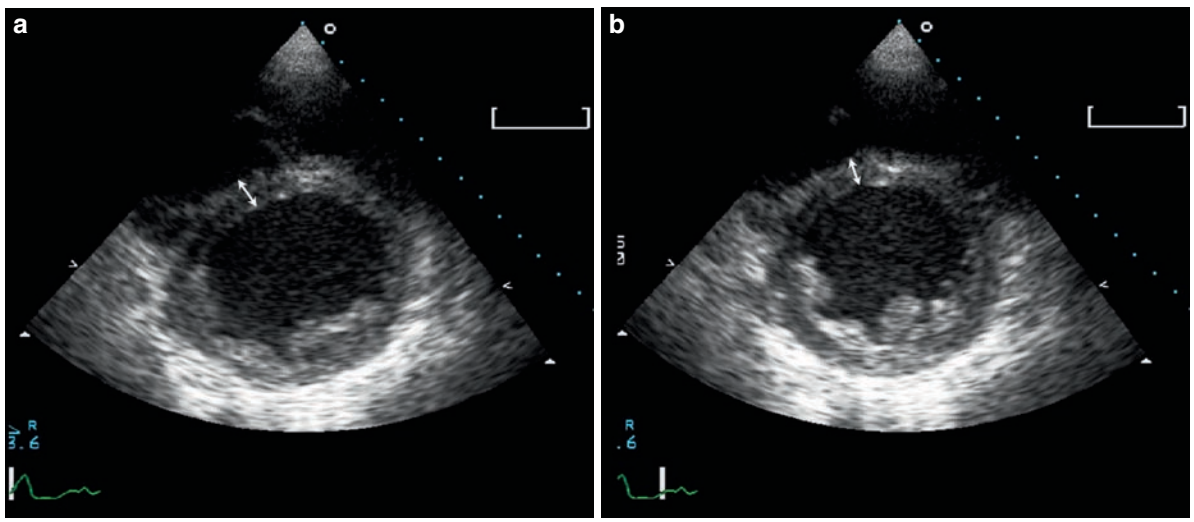

Fig. 15.3 Parasternal short axis views of (**a**) diastole and (**b**) systole of wall thickening of septum in a patient with AMI

Its branch, the posterior descending artery, supplies the inferior wall and the inferior septum. Eighty percent of patients have a dominant right coronary artery; the remaining 20% are left dominant with the posterior descending artery being a branch of the left circumflex artery (Figs. 15.4 and 15.5). The posterior wall can be supplied either by branches from the RCA or from obtuse marginal branches of the LCx. Equally, there is significant variation of the supply to the apex where both the LAD and the PDA may contribute to the others' territory.

The changes seen in regional wall motion correlate closely with the blood supply to that area of myocardium. Several methods have been described to describe left ventricle (LV) in order that regional wall motion can be accurately described, though the basic principles remain the same. The ventricle is divided into three sections: base, midventricular cavity, and the apex. Each section is then divided into segments that correspond to areas in the LV wall. The most recent recommendation from the American College of Cardiology (ACC) and the American Heart Association (AHA)[2] is to use a 17-segement model (Fig. 15.6). This divides the base and midventricular cavity into six segments each, with the apex section having four segments. A final segment is a very distal apical "cap"

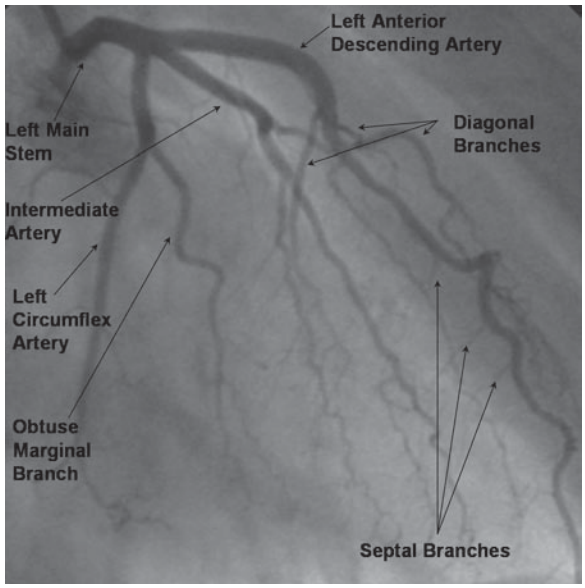

Fig. 15.4 Coronary angiogram demonstrating the left coronary system and its major branches

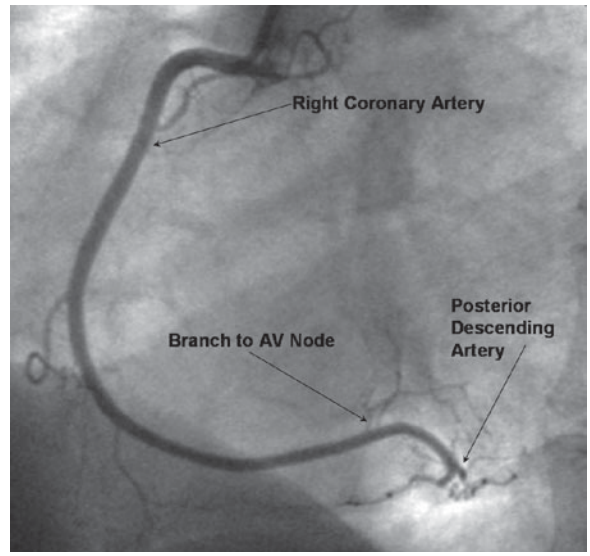

Fig. 15.5 Coronary angiogram demonstrating the right coronary system and its major branches

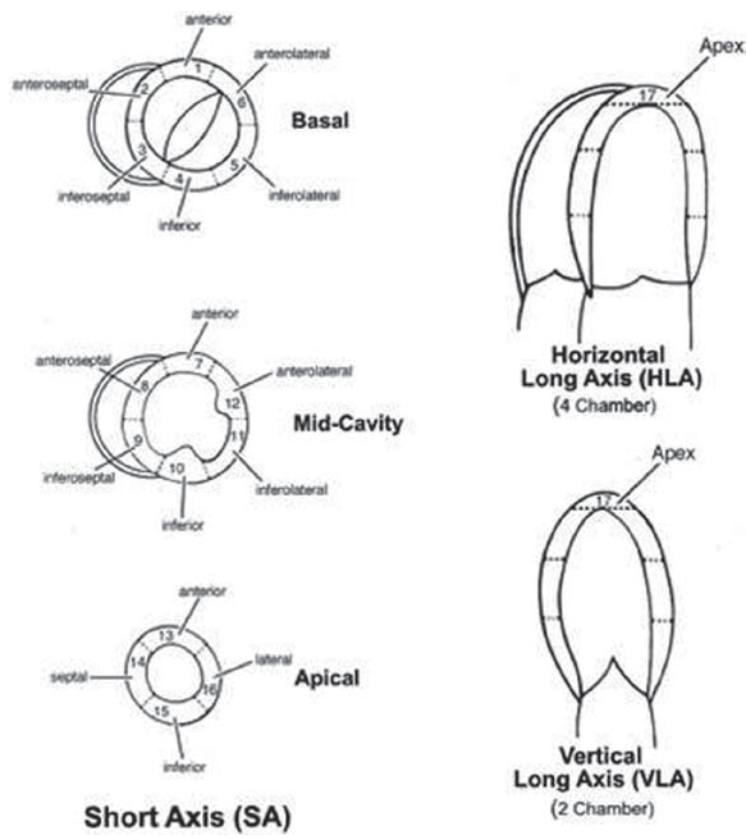

Fig. 15.6 Diagram representing the parasternal short axis, apical 4-chamber and apical 2-chamber views of the recommended 17-segment left ventricular model[2]

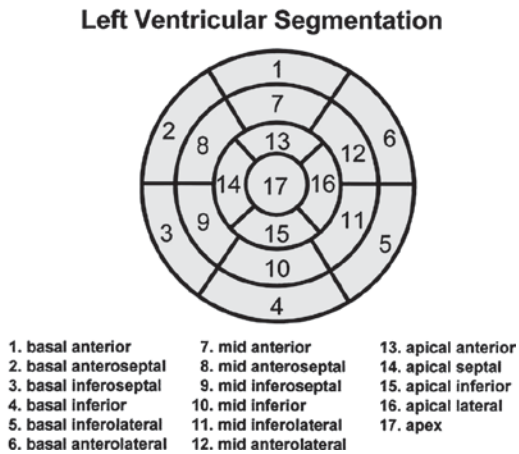

Fig. 15.7 Diagram of the "bulls-eye" plot representing the 17 left ventricular segments in the recommended model[2]

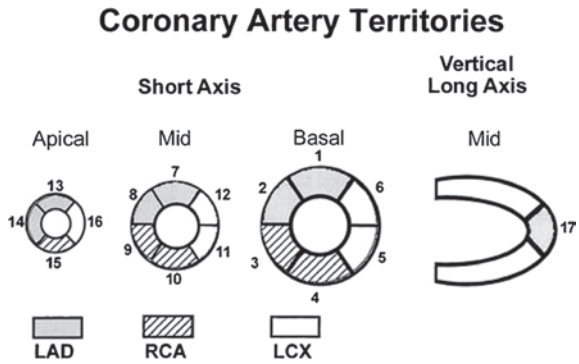

Fig. 15.8 Assignment of the 17 myocardial segments to the territories of the left anterior descending (LAD), right coronary artery (RCA), and left circumflex artery (LCx)[2]

which is best assessed in the apical 2- and 4-chamber views. Commonly a "bulls-eye" plot (Fig. 15.7) of all of these segments is used to note the individual segment scores, with the basal segments on the outside, followed by the midcavity, and then the apex. This allows clear localization of any defect on a single form with an indication of vascular supply (Fig. 15.8).

The regional wall motion abnormalities seen correspond to coronary arteries as follows:

LAD: Usually affects the anterior septum, anterior wall, and the anterior apex. Depending on the individual, the diagonal branches may also supply parts of the lateral wall. If the vessel is large, more of the apex (inferior and posterior aspects) may be supplied by the LAD.

Occlusion of the distal LAD commonly only affects apical segments; midvessel lesions affect both apex and midcavity segments, and proximal occlusion leads to reduction in wall motion along the whole of the anterior wall and septum. Occlusion of the first diagonal branch of the LAD commonly causes a specific anterolateral wall motion defect.

LCx: Disease in this artery tends to affect the lateral and posterior walls of the left ventricle. Individual variations in coronary anatomy do make precise localization of lesions in this territory difficult because of the overlap with the other arteries. Nevertheless, as posterior wall ischemia is difficult to identify by ECG, wall motion abnormality in this area does help in the identification of patients at risk of LCx disease.

RCA: The posterior descending branch of the right coronary artery supplies the inferior septum and inferior wall of the left ventricle. Wall motion abnormalities in these areas strongly suggest RCA involvement. Depending on the dominance of the vessel, inferior regions of the apex may also be affected.

Clearly individual differences in coronary anatomy affect the areas of wall motion abnormality caused by the occlusion of specific arteries. This is particularly true of the territories supplied by the right coronary artery and the left circumflex artery where there can be a considerable overlap in the areas of myocardium supplied. It can be helpful, therefore, to divide the regions of abnormality into the anterior circulation (comprising those affected by the left anterior descending artery and its branches) and posterior circulation (right coronary and circumflex lesions).

Collateral vessel formation in cases of chronic artery occlusion and ischemia as well as previous coronary artery bypass surgery also affects the localization of CAD by segmental analysis of the LV. However despite this, the areas of wall motion abnormality do correlate well to the location of disease in the coronary tree and can act as a guide for further management.

Assessment of Regional Wall Motion

The usual method of assessing left ventricular wall motion by echocardiography is the use of standard apical 4-, 2-, 3-chamber apical and parasternal long and short axis views. This allows complete visualization of all the left ventricular walls, and hence all three vascular territories, though care must be taken to ensure

clear endocardial border definition. Clear visualization of the endocardial border is crucial for the full assessment of wall motion. It is also important to remember that changes in the left ventricle are not uniform, and it is important to obtain different views of the same region to make an accurate assessment of segmental wall function. This is usually done by combining the use of the standard apical views with the parasternal views, particularly in the short axis, where different levels of function from base, through papillary muscle down to apex can be visualized.

The best way to assess wall motion in each of these views is to consider the endocardial border and the epicardium as a number of point targets. As normal contraction occurs, the endocardium moves inward (endocardial excursion) with left ventricular cavity shrinkage (area shrinkage). There is a reduction in the cavity perimeter (perimeter shrinkage), and the distance between the endocardium and epicardium increases (wall thickness). In patients with ischemia, there is a reduction in the degree of endocardial excursion together and a decrease in the amplitude of wall thickening. This can be seen clearly when compared to adjacent, normally contracting areas of myocardium. Of the two parameters, the degree of endocardial thickening is the most reproducible and reliable method of wall motion assessment. It is also important to emphasize at this point that one must be careful to take into account translatory and rotatory motion of the left ventricle which may give one a false impression of preserved wall motion. However, absence of endocardial excursion effectively rules out any significant wall thickening.

Once these changes have been established, wall motion can be scored according to a 4-point semiquantitative scale:

1. Normal
2. Hypokinetic – normally directed motion, but reduced endocardial excursion and wall thickening
3. Akinetic – absent wall motion/thickening
4. Dyskinetic – systolic bulging of the wall with no thickening

The sum of the individual segment scores gives a Wall Motion Score (WMS), which can be used give an indication of the severity of ischemia found; a wall motion score index (WMSI) can also be used (WMS divided by the number of segments assessed) and has been shown to be an important prognostic indicator in patients with CAD (Fig. 15.9).[3,4]

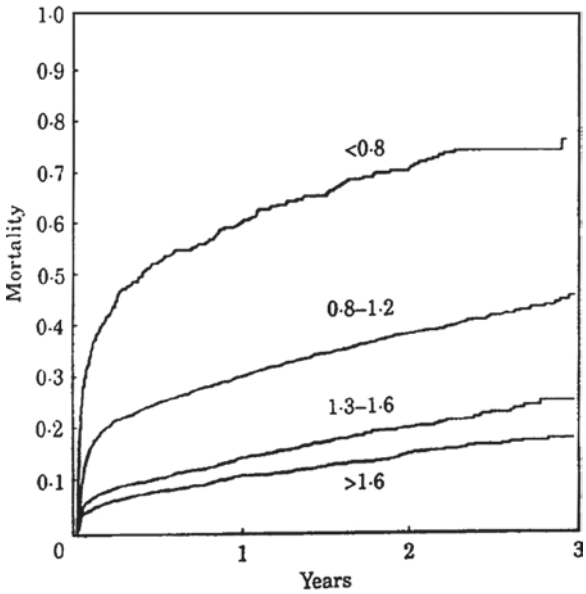

Fig. 15.9 Graph demonstrating relationship between mortality and varying Wall Motion Score Index (WMSI) over time[3]

Acute Myocardial Infarction

Acute myocardial infarction (AMI) occurs when there is acute occlusion of an epicardial coronary artery, leading to myocardial necrosis. The usual cause for this is rupture of an atherosclerotic plaque leading to thrombus formation. There is subsequent occlusion of the artery by the thrombus leading to a rapid decrease in perfusion to the region of myocardium supplied by that artery. Continued ischemia to that area leads to myocardial necrosis and permanent loss of contractile function.

Current treatments for AMI are designed to disperse the thrombus causing the obstruction (thrombolytic agents such as Streptokinase) or to mechanically open the vessel after occlusion (acute percutaneous coronary angioplasty). The purpose of both these treatments is to reduce the time of coronary occlusion, thereby reducing the degree of myocardial necrosis that occurs. It is well known that the degree of myocardial damage seen after infarction is directly related to the duration of artery occlusion supplying that area,

the extent of the myocardium at risk, and the degree of collateral circulation. It is also well recognized that the area of the myocardial segment that is affected first is the subendocardium, and that this has a strong influence on contractile function. Pathological studies have demonstrated that if 20% undergoes infarction, there is a reduction in wall thickening during systole of >50%[5] (Fig. 15.10). This area of necrosis can extend from the subendocardium and can traverse the full thickness of the affected left ventricular wall leading to severe abnormalities in wall structure and function.

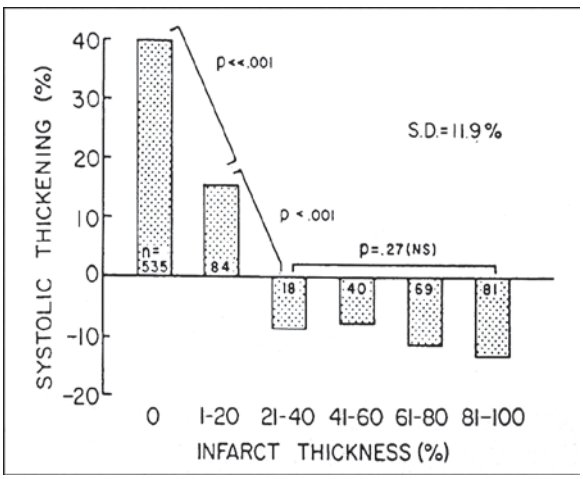

Fig. 15.10 Graph demonstrating the relationship between the transmural extent of infarction and regional wall thickening[5]

Echocardiographic Assessment in AMI

Since both myocardial ischemia and infarction produce regional wall motion abnormalities, it is not possible to differentiate between them in patients presenting acutely with chest pain. However as 90–100% of patients presenting with acute myocardial infarction have been shown to have regional wall motion abnormalities, echocardiography may be helpful in excluding ischemia in patients presenting with chest pain with equivocal ECGs.

After myocardial infarction, early assessment of patients can give useful information on the site and extent of wall motion abnormality, together with a response to any therapy given.

Assessment of regional wall motion allows localization of the infarct-related artery.

An occlusion of the LAD commonly leads to anterior septal, anterior ventricular wall, and apical akinesia. The anterior septum can be visualized in the parasternal long and short axis views, as well as the apical 3-chamber views. Anterior wall ischemia is best shown in the parasternal short axis and apical 2-chamber view, with the septum seen in 4-chamber view (Fig. 15.11).

Left circumflex stenosis often involves the lateral and posterior left ventricular walls. Identification of a posterior wall motion abnormality (using the apical 3-chamber and parasternal long axis view) may be helpful in the acute setting, as 12-lead ECG diagnosis of a posterior myocardial infarct is often missed.

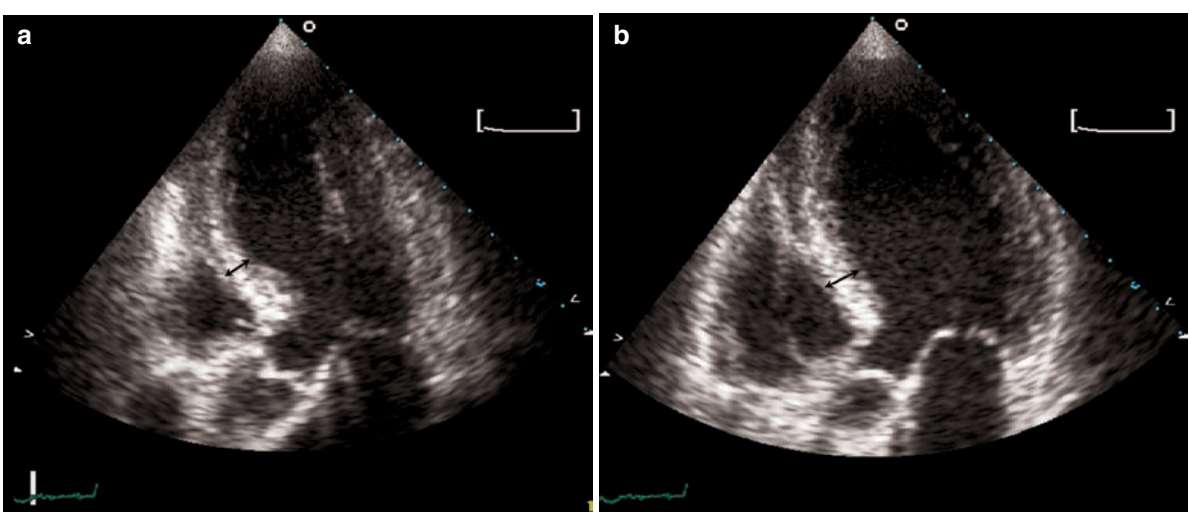

Fig. 15.11 Apical 4-chamber view of patient with septal myocardial infarction. There is lack of wall thickening in the septum in systole (**a**) comnpared to diastole (**b**)

Right coronary artery occlusion involves the inferior wall and inferior septum involvement. This is clearly seen in the apical 2-chamber view (Fig. 15.12). The right coronary artery also commonly supplies the right ventricle, the function of which may become impaired. This may be important in the acute management of patients, so assessment in the apical 4-chamber view may be important to assess the degree of right ventricular hypokinesia.

The presence of a wall motion abnormality following acute ischemia may be due to myocardial necrosis, stunned or hibernating myocardium, or more commonly combinations of these factors. Following an acute MI, the extent and severity of wall motion abnormality portends to unfavorable prognosis. Around 4–6 weeks after AMI, akinetic segments which have undergone significant damage become thinned and may even become dyskinetic. They also become more echogenic and brighter when visualized with ultrasound (Fig. 15.13). Due to the shear and pressure changes that occur in the LV, these areas can change the shape and size of the ventricle (remodeling), and can become anuerysmal, representing the final stages in the infarct process.

Areas that remain severely hypokinetic or akinetic, but do not demonstrate any other changes may be stunned or hibernating. Myocardial hibernation occurs when there is prolonged wall motion abnormality due to repetitive stunning. To distinguish necrotic from viable

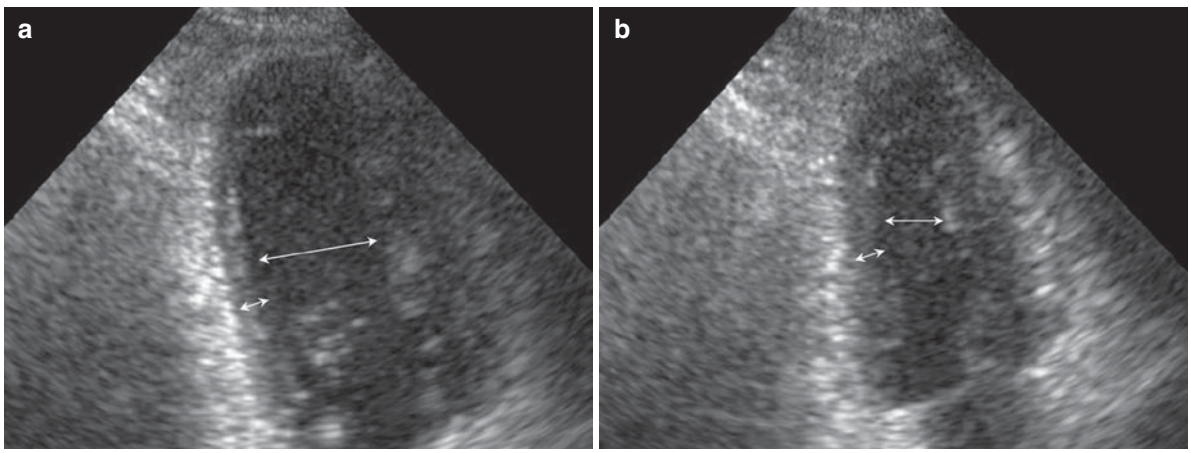

Fig. 15.12 Apical 2-chamber view of patient with an inferior myocardial infarction. There is normal anterior wall thickening with reduction in left ventricular cavity size. There is little thickening of the inferior wall from diastole (**a**) comnpared to diastole (**b**)

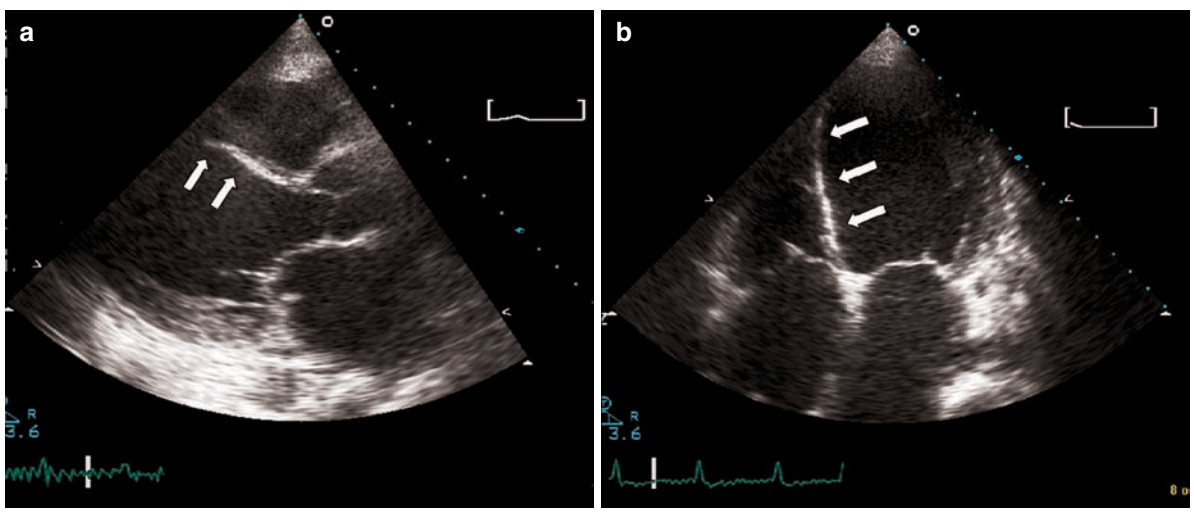

Fig. 15.13 Parasternal long axis (**a**) and apical 4-chamber (**b**) views of patient with an LAD infarction with and akinetic, thin, scarred septum

myocardium (i.e., stunned or hibernating), techniques assessing contractile reserve (dobutamine stress echocardiography), the microcirculation (myocardial contrast echocardiography), or metabolism (radionucleotide techniques) are useful. If these studies demonstrate lack of significant myocardial necrosis, these areas are considered viable and contractile function in these segments may improve if revascularization is undertaken.

Acute Coronary Syndromes

Acute Coronary Syndromes (ACS) encompass a spectrum of conditions ranging from unstable/crescendo angina to non-Q wave infarctions. The pathological process remains the same however. In a similar way to acute myocardial infarction, an atherosclerotic plaque in an epicardial artery undergoes rupture. Thrombus formation occurs and causes acute coronary occlusion. This occlusion is however only transient, and spontaneous dispersal of the thrombus follows. Small particles of thrombus may cause tiny areas of myocardial damage downstream, which can now be detected using highly sensitive serum assays (Troponin T and I).

The duration of ischemia and degree of myocardial damage is much less than in acute infarction. This leads to a reduction in the degree of segmental wall motion abnormality seen in patients with acute coronary syndromes. This is not to say the condition is any less serious; in many ways the patient must be assessed more urgently as significant myocardial damage has not occurred and the potential to prevent this still exists.

Echocardiography in Acute Coronary Syndromes

Similar to myocardial infarction, wall motion abnormalities are seen in patients with acute coronary syndromes. Unlike AMI, however, these abnormalities tend to be less marked and also may be transient in nature. As the duration of ischemia tends to be short, the wall motion may have time to recover between episodes of pain. This is why the assessment of wall motion abnormality in patients with ACS should be performed early after the onset of symptoms; normal wall motion in a patient who is pain free and a normal ECG does not exclude ACS. If the patient does complain of ischemic sounding symptoms, however, the ECG is equivocal, and there is no regional wall motion abnormality when assessed immediately after the acute episode, then the presence of acute ischemia is unlikely.

Once the diagnosis of an acute coronary syndrome has been made, echocardiographic assessment of wall motion becomes important in the assessment of site and severity. The site of the myocardial insult can be readily identified and the extent of the subendocardial damage determines the degree of wall thickening that takes place in the affected segments. Mild hypokinesia suggests only a small amount of myocardial damage which affects only a small part of the endocardium.

More severe hypokinesia is unusual in patients with small nontransmural infarctions though it may occur either reflecting significant myocardial damage, or a degree of myocardial stunning overlying a small infarction. Indeed it is not uncommon for adjacent segments to the ones affected to become hypokinetic due to variety of local factors (e.g., tissue tethering).

Improving Endocardial Definition

As already stated, clear visualization of the ventricular walls and in particular the endocardial border is vital to the assessment of regional wall motion. Around 15% of patients have poor endocardial definition on conventional echo. This may be due to a variety of reasons including large body habitus, lung disease, poor echo windows, or distorted architecture of the left ventricle.

A number of new methods have been developed to help overcome these limitations and improve left ventricular delineation.

Harmonic Imaging

Conventional (or fundamental) echocardiography uses a transducer to emit and receive ultrasound waves at one frequency. However, not all signals reflected back from myocardial tissue are of the original frequency; some may be twice or even three times the original. These are known as harmonic frequencies.

Harmonic imaging uses broad band transducers that are capable of receiving reflected signals of twice or three times the original frequency and thus improve image quality. The technique was originally developed for better visualization of microbubbles in contrast studies, but as myocardial tissue was also found to emit harmonic frequencies, its use is becoming more and more widespread. It reduces the number of spurious echoes detected within the LV cavity and allows clearer definition of the endocardial border (Fig. 15.14 a, b). It is, however, depth dependant, with fewer harmonics being produced in the near field, and attenuation being seen in the far field. There is also poorer lateral resolution than fundamental imaging. Despite this, harmonic imaging now well validated[6] and is being used routinely resulting in improved image quality and endocardial border definition.

Left Ventricular Opacification Using Contrast Agents

Despite harmonic imaging, there are still patients on whom endocardial definition remains a problem. This may be overcome by the use of intravenous contrast agents.

Contrast agents consist of gas-filled microbubbles in a protein shell, which reflect ultrasound, generate harmonic backscatter, and enhance ultrasound information. The development of microbubbles, that can be injected intravenously and remain stable through the pulmonary circulation into the LV cavity, has been a major advance in contrast technology.

Opacification of the left ventricle (Fig. 15.15) has been shown to significantly improve endocardial border delineation in a number of studies, and is now being used in patients with poor images in both resting and stress modalities. The use of intravenous contrast for LV opacification (LVO) has also improved the rate of inter- and intraobserver variability in the assessment of regional wall motion abnormalities.

Newer techniques such as power modulation and power pulse inversion are now being used to better detect microbubbles at lower powers and in real time, allowing clear visualization of the endocardial border.

Automated Endocardial Border Tracking

Analysis of two-dimensional gray scale images obtained during two-dimensional imaging tends to be subjective, qualitative, and dependant on the experience of the observer. Alternative methods of providing more objective methods of assessing wall motion have therefore been sought.

One of these methods is the automated detection of endocardial borders.[7] This was originally tried by manually tracing the borders, but was found to be time consuming, complicated, and could only be performed offline. Newer developments have been used to automate this procedure using the difference between the

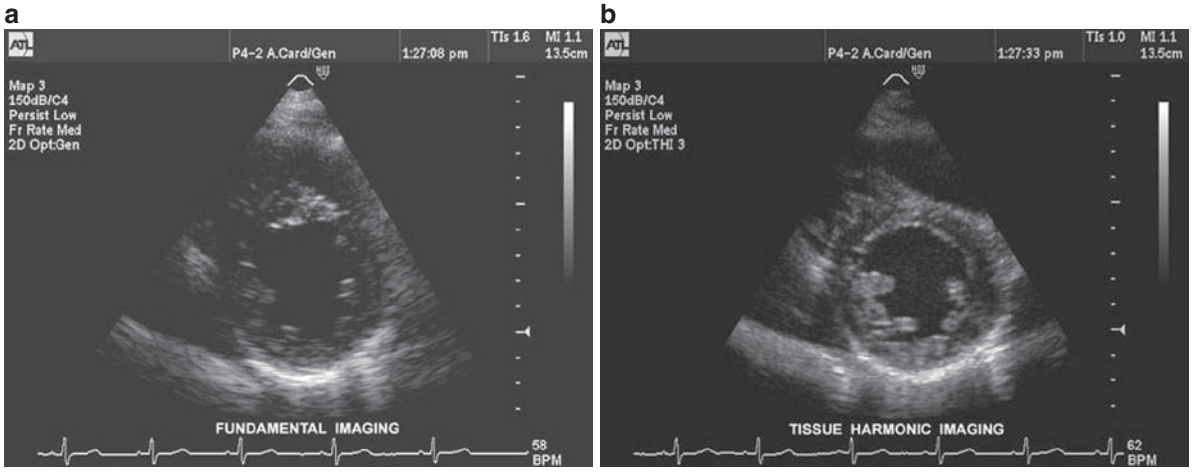

Fig. 15.14 Parasternal short axis views using (**a**) fundamental and (**b**) harmonic imaging demonstrating the improvement in endocardial definition

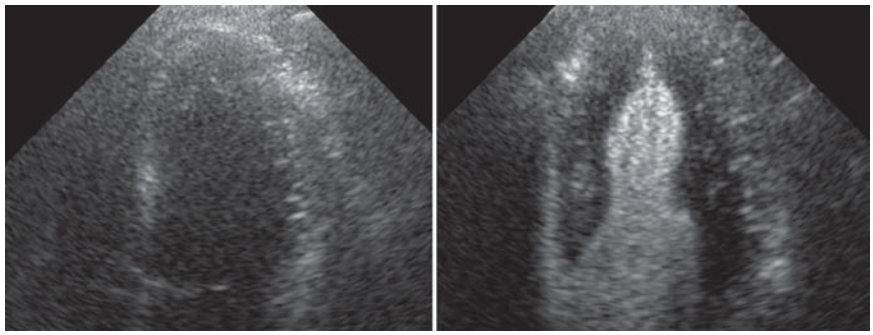

Fig. 15.15 Apical 4-chamber view in a technically difficult patient with poor endocardial definition which improved with intravenous contrast

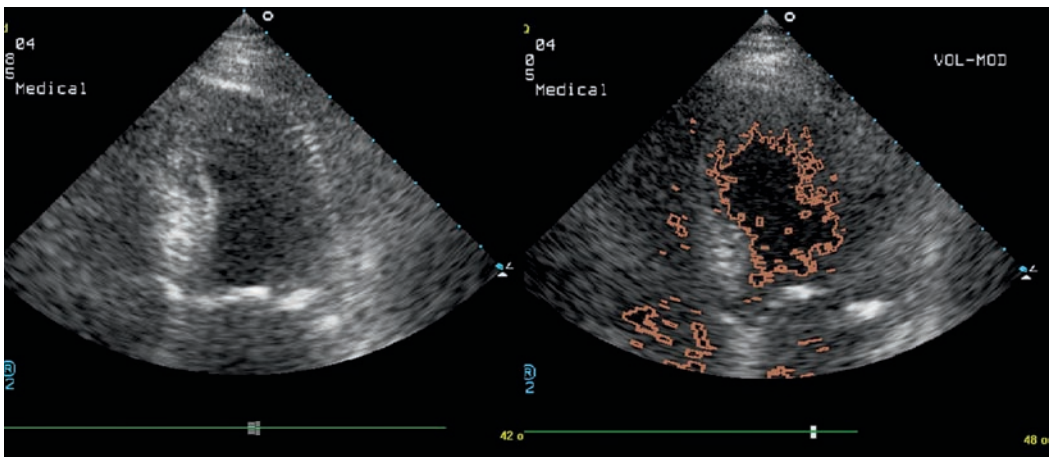

Fig. 15.16 Apical 4-chamber view with and without automated border tracking

ultrasound backscatter emitted from the endocardium and blood in the LV cavity.

When an image is acquired, there the backscatter information along the scan line is analyzed and each pixel classified as either blood or tissue. There is sufficient difference between the energy returned from the blood in the LV (low) and the endocardium (high) for this distinction to be made. Once this interface has been established along the whole of the endocardium, it can be tracked. Each pixel is color coded and is superimposed onto the two-dimensional image. The construction is then integrated with the original scan image and all can be performed online. This leads to real-time tracking of the endocardial border which is continually updated frame by frame (Fig. 15.16).

Color-coded endocardial tracking (Colour Kinesis and A-SMA) is an extension of this automated process. Once the endocardial border has been defined on the basis of the backscatter from the blood and tissue, the inward (systolic) and outward (diastolic) movement is color coded. Each pixel is given a specific color dependant on its movement which is compared to the previous frame so that an accurate measurement of systolic function and regional motion is possible.

The color overlays are superimposed onto the gray scale images which are updated on a frame-by-frame basis. This allows real-time assessment of systolic function and regional wall motion using a visual color scale (Fig. 15.17).

The problem with automated endocardial tracking is that its success depends on good image quality. The acquisition of poor images leads to poor tracking of the endocardial border which in turn leads to poor color-encoded tracking images. The use of contrast agents to

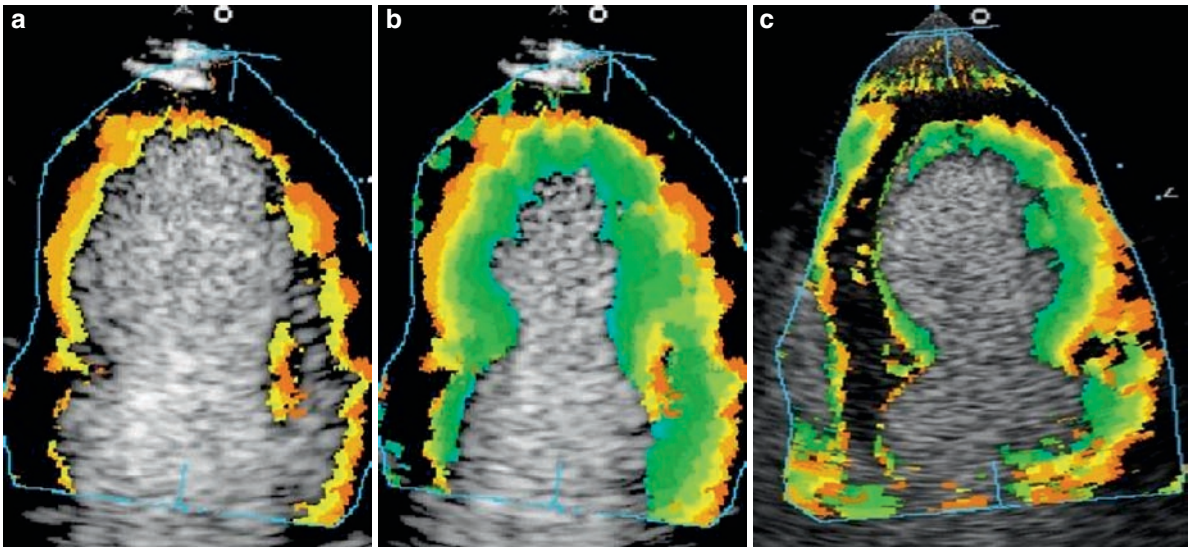

Fig. 15.17 Demonstration of automated endocardial tracking with color coding (Colour Kinesis™) in the apical 4-chamber view. At the beginning of systole (**a**), a thin rim of color delineates the endocardium. During systole (**b**) there is progressive change in color to demonstrate wall thickening. In a patient suffering acute myocardial infarction, there is failure of wall thickening in the septum and hence no change in color (**c**), whereas normal wall motion is represented in the lateral wall

improve the endocardial definition for automated tracking systems was previously not possible due to the imaging modalities available. Newer techniques such as Power modulation have improved this situation with improved contrast specific imaging modalities. The principle of detecting the energy difference between the blood-tissue interface remains, but the energy given out by the microbubbles causing LV opacification is far greater than that given out by the endocardium. The interface is therefore still well defined, and color-coded endocardial tracking can be achieved.

The benefits of such a technique are not only the clearer visualization of the endocardium, but also the potential for quantifying the degree of movement.

References

1. Senior R, Basu S, Khattar R, Lahiri A. Independent prognostic value of the extent and severity of systolic wall thickening abnormality at infarct site after thrombolytic therapy. *Am Heart J.* 1998;135:1093–1098.
2. Cerqueira MD, Weissman NJ, Dilsizian V, et al. Standardized myocardial segmentation and nomenclature for tomographic imaging of the heart: a statement for healthcare professionals from the Cardiac Imaging Committee of the Council on Clinical Cardiology of the American Heart Association. [Review] [11 refs]. *Circulation.* 2002;105:539–542.
3. Kober L, Torp-Pedersen C, Carlsen J, Videbaek R, Egeblad H. An echocardiographic method for selecting high risk patients shortly after acute myocardial infarction, for inclusion in multi-centre studies (as used in the TRACE study). TRAndolapril Cardiac Evaluation. *Eur Heart J.* 1994;15:1616–1620.
4. Kjoller E, Kober L, Jorgensen S, Torp-Pedersen C. Long-term prognostic importance of hyperkinesia following acute myocardial infarction. TRACE Study Group. TRAndolapril Cardiac Evaluation. *Am J Cardiol.* 1999;83:655–659.
5. Lieberman AN, Weiss JL, Jugdutt BI, et al. Two-dimensional echocardiography and infarct size: relationship of regional wall motion and thickening to the extent of myocardial infarction in the dog. *Circulation.* 1981;63:739–746.
6. Swinburn JM, Stubbs P, Soman P, Collinson P, Lahiri A, Senior R. Independent value of tissue harmonic echocardiography for risk stratification in patients with non-ST-segment elevation acute chest pain. *J Am Soc Echocardiogr.* 2002;15:1031–1037.
7. Platts DG, Monaghan MJ. Colour encoded endocardial tracking: the current state of play. [Review] [40 refs]. *Eur J Echocardiogr.* 2003;4:6–16.

Chapter 16
Stress Echocardiography

Thomas Marwick

Pathophysiology

The underlying principle of stress echocardiography is that ischemic tissue (and in nonischemic disease, other types of pathologic tissue) is unable to augment function during stress. Moreover, the extent of coronary disease determines the extent and severity of ischemia, which in turn determines the time course and spatial distribution of abnormal wall motion. Therefore, inducible wall motion abnormalities may be subtle (or even absent) if the stenosis is moderate, or distal, or if the level of stress is inadequate.

The implications of these pathophysiological considerations are that

(a) The nature of stress is selected to maximize the development of ischemia
(b) Acquisition needs to be optimized to pick up potentially transient wall motion abnormalities
(c) Diagnostic criteria should incorporate markers of subtle ischemic changes

Stress Testing

Preparations for stress testing are well known and should be little influenced by the addition of echocardiography, with the exception of leaving imaging windows clear of electrodes. Anti-ischemic therapy is usually stopped before diagnostic studies.

T. Marwick
University of Queensland School of Medcine,
Princess Alexandra Hospital, Brisbane, QLD, Australia
e-mail: t.marwick@uq.edu.au

Selection of Stress Method

Stress echocardiography may be performed with exercise and nonexercise stressors, although the use of echo contrast agents makes insertion of an intravenous line important for both techniques. The selection of either stress protocol should be tailored to each patient, and in the opinion of this author, an effective stress echo laboratory should offer both exercise and pharmacologic modalities.

Patients who are unable to exercise maximally (who account for up to 40% of patients requiring functional testing) require a nonexercise stress, of which there are four categories – exercise simulating agents (e.g., dobutamine), vasodilators (dipyridamole, adenosine), pacing stress and agents with specific indications such as ergonovine, cold pressor and mental stress. The latter two categories will not be discussed further.

In patients who are able to exercise maximally, either treadmill or bicycle exercise (upright or supine) may be used. The latter may not offer as potent a stress as does maximal exercise on the treadmill, but compensates for this by permitting peak imaging, which is sometimes of interest in identifying the time of onset of ischemia and avoiding the problem of rapid resolution of ischemia. The overall accuracies of treadmill and bicycle stress are similar, the bicycle being more sensitive and less specific.

The selection is driven by local preference and expertise. Finally, while exercise echo tests are equipment intensive (treadmill or ergometer, stress ECG computer, and echocardiography machine), they usually require only two persons (supervising physician or exercise physiologist and sonographer). In contrast, most sites involve three staff for pharmacologic stress – the additional person being a nurse to supervise the infusion.

P. Nihoyannopoulos and J. Kisslo (eds.), *Echocardiography*,
DOI: 10.1007/978-1-84882-293-1_16,

For both these reasons, and because of the duration of these protocols, pharmacologic stress is not performed in some laboratories.

Which Stressor?

1. *Exercise stress:* Exercise testing is preferable to pharmacologic stress if the patient is able to exercise, to allow symptoms to be better correlated with workload, obtain prognostically important hemodynamic and exercise capacity data, and stress the heart more vigorously, which optimizes test sensitivity.

   Imaging can be performed before and immediately after treadmill exercise, upright or supine bicycle ergometry. Careful consideration should be given to logistic details, especially regarding rapid acquisition of postexercise images, which should start within 10–20 s of the end of exercise and be finished within 60–90 s. The advantage of supine bicycle ergometry is that imaging can be performed throughout the stress test.

2. *Pharmacological stress:* The issue of which pharmacological stressor is most feasible and accurate has been hotly debated! Early animal work using quantitative two-dimensional echocardiography and microspheres showed that dobutamine was more effective in inducing myocardial dysfunction but produced smaller blood flow heterogeneity for similar coronary lesions. In contrast, dipyridamole induced large differences in regional subendocardial perfusion, but regional myocardial dysfunction was only observed when an absolute decrease in subendocardial blood flow was present. Subsequent clinical studies suggested that vasodilator stress echo was less sensitive, probably because the agents are not very potent stressors from the standpoint of inducing ischemia by increasing oxygen demand. As a consequence, "third-generation" protocols have been developed that incorporate an agent to increase cardiac workload (e.g., atropine and dobutamine), and these new protocols have analogous results to those obtained with dobutamine and atropine. Indeed, the development of myocardial contrast echocardiography is leading to new interest and application of vasodilator stress echocardiography because its intense coronary hyperemia allows detection of perfusion heterogeneity.[1]

   Specific indications for pharmacologic stress are listed in Table 16.1.

Dobutamine is by far the most widely used pharmacologic stress and is suitable for most patients, although it is contraindicated in patients with severe hypertension and serious arrhythmias. Dobutamine is usually administered incrementally in 3-min stages, starting at 5 μg/kg/min, and increasing to 40 μg/kg/min stages, with atropine being added (if not contraindicated) if the test is negative at peak dose.
The endpoints of the test are

Completion of the protocol
– Development of severe ischemia
– Intolerable symptoms

Development of side effects (Table 16.2), including arrhythmias, hypotension (symptomatic or to <100 mmHg), or hypertension (>220/120)

Over two-third of patients attain peak dose or achieve an ischemic endpoint. Usually, stopping the drug is sufficient for the treatment of side-effects, but sometimes beta blockers are required. Serious events (defined as those necessitating hospital admission) occur in 1 to 3:1,000 patients. Nonetheless, while side effects may concern the physician performing the test and compromising its sensitivity (see later), major complications are exceedingly rare.

One advantage of online echocardiographic imaging is that the extent and severity of ischemia may be better appreciated than they might with the electrocardiogram alone, or with pre- and poststress imaging alone. This may permit termination of the stress before severe left ventricular dysfunction develops or prevent a premature termination without any objective evidence of ischemia.

Table 16.1 Indications for pharmacologic rather than exercise stress

	Clinical situation
Inability to exercise maximally	Vascular disease
	Chronic lung disease
	Neurologic/orthopedic problems
	Poor functional capacity (advanced age)
Specific indications	Myocardial viability (dobutamine or dipyridamole)
	Detection of coronary spasm (ergonovine)
Interpretation	Resting wall motion abnormalities
Application of new technologies	Myocardial contrast echocardiography
	Myocardial tissue Doppler/strain

Table 16.2 Dose-limiting and serious side effects of pharmacologic stressors (reproduced with permission from ref. 13)

	Dobutamine	Dipyridamole	Dipyridamole	Adenosine
	Secknus	Ranhosky	Picano et al[4]	Cerquiera
Dose	40 mg/kg/min	0.54 mg/kg	0.81 mg/kg	Various
n	3,011	3,911	10,451	9,256
Total S/E	8% (dose-limit)	47%	–	81%
Major S/E	0.33%	0.26%	0.07%	0.10%
Fatal MI	0.00%	0.05%	0.01%	0.00%
Nonfatal MI	0.03%	0.05%	0.02%	0.01%
Bronchospasm	0.00%	0.15%	0.15%	0.07%
Anxiety/tremor	1.6%	–	–	–
Chest pain	3.5%	20%	–	35%
Dizziness	–	12%	–	9%
Dyspnea	–	3%	–	35%
Flushing	–	3%	–	37%
Headache	1.6%	12%	–	14%
Hypotension	3.8%	5%	1%	–
Hypertension	0.8%	–	–	–
Nausea	1.6%	5%	–	15%
Palpitations	1.6% (arrhythmias)	3%	–	7%
Paresthesia	–	1%	–	–

Coronary vasodilator stress is used as the stressor of choice in some parts of Europe.

The two vasodilator stressors used are dipyridamole and adenosine.

(a) *Dipyridamole* is the most widely used of the two. It exerts its effects indirectly, by increasing endogenous adenosine levels by reducing cellular reuptake and metabolism. Dipyridamole induces ischemia by causing coronary "steal" that effectively shunts blood from the territory of a stenosis by allowing it to run off into nonstenosed territories. The preparation of the test is similar to the other stressors, although an important difference is that coffee, tea, and cola drinks should be avoided for a day before the examination, because the xanthines contained in these agents antagonize the effects of dipyridamole on adenosine metabolism as well as competitively inhibiting adenosine activity. Dipyridamole is administered intravenously at a rate of 0.56 mg/kg/min over 4 min, followed 2 min later by an additional 0.28 mg/kg/min over 2-min infusion if the initial response is negative, and there have been no major side effects. Aminophylline 240 mg iv should be available for immediate use in case of an adverse dipyridamole-related event.

(b) *Adenosine* acts directly and rapidly on vascular smooth muscle, and is usually used with an incremental dose schedule; the most widely used dose for echocardiography is 140 μg/kg/min injected over a period of 6 min. Imaging is performed continuously throughout the infusion.

Side effects: Dipyridamole and adenosine have a similar side effect profile (Table 16.2). The high-dose dipyridamole protocol induces minor side effects in about two-third of patients, but these rarely prevent completion of the study. Aminophylline usually provides rapid relief. The side effects of adenosine are brief, but more intense and frequent than those of dipyridamole; side effects prevent about a third of patients from completion of high-dose protocols. The symptoms are similar to those with dipyridamole stress, although chest discomfort and dyspnea are more frequent. Cessation of the infusion is usually the only treatment required for side effects because of the very short duration of action. Serious side effects are very rare but include severe myocardial ischemia and infarction, bronchospasm, and complete heart block.

Dipyridamole and adenosine stress are contraindicated in patients with untreated atrioventricular block and bronchospastic disorders (asthma).

Acquisition

Equipment

Harmonic Imaging

The development of tissue harmonic imaging has had a major influence on image quality; its benefits on reproducibility and feasibility have made the technique indispensible for stress echocardiography. Lateral gain correction may also improve visualization of the lateral wall. Despite these developments, 2D image quality remains a problem in some patients, with failure to image >1 segment in 30% of patients (especially in the anterior and lateral walls), and some significant impairment in visualization in 10–15%. Unless severe, incomplete visualization may not jeopardize accuracy in experienced laboratories, but it does compromise the acquisition of clinically important information about the nature and extent of ischemia.

Contrast Imaging

The use of left heart contrast agents has become a practical solution for this problem, improving image quality, increasing the confidence level of readers, reducing downstream costs and improving accuracy for stress echocardiography (Fig. 16.1). However, we favor judicious and selective use of contrast in combination with stress echocardiography – potential problems include shadowing, emphasis of the endocardial border rather than thickening, and cost.

Image Acquisition

Digital Image Acquisition

Multiple views have to be recorded to ensure visualization of LV segments supplied by each of the three

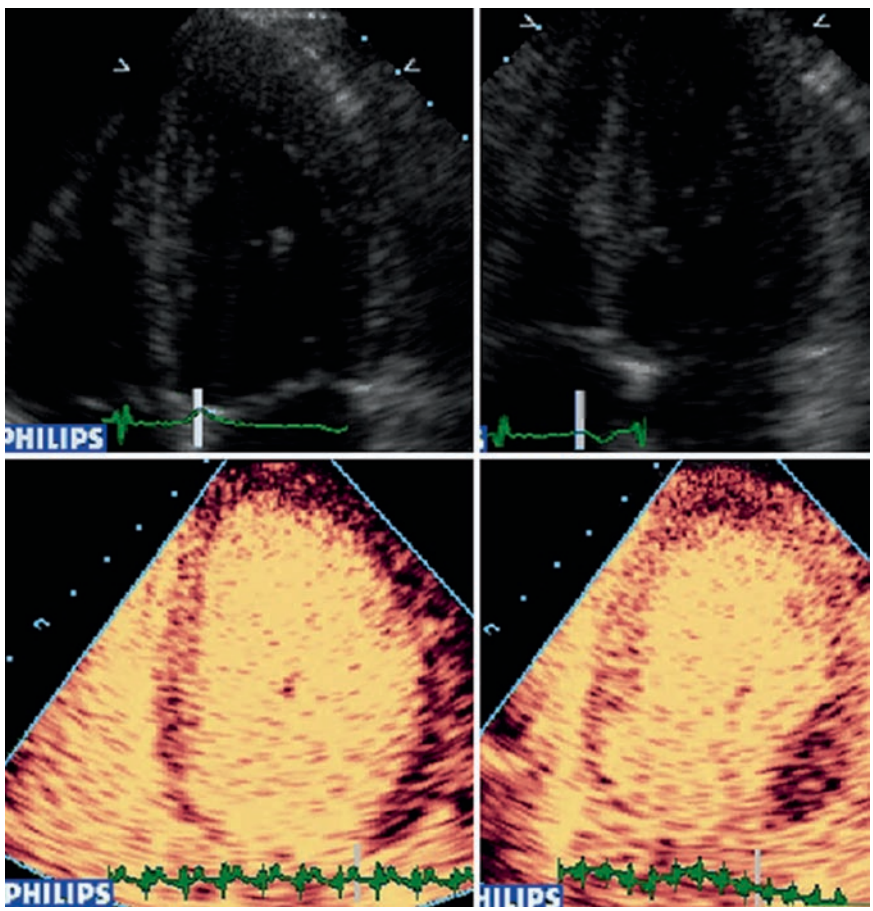

Fig. 16.1 Use of a left heart contrast agent to improve LV opacification. *Upper right* and *left images* show rest and stress images, respectively, illustrating poor visualization of the lateral wall. *Lower images* have been obtained after injection of Definity, including a flash for bubble destruction to facilitate assessment of myocardial perfusion. *Printed images* are end-systolic freeze frames

major coronary distributions. Typically, four views are sufficient: the parasternal long- and short-axis as well as apical four- and two-chamber views. Subcostal or additional short-axis views can be substituted when necessary or when more appropriate visualization of specific anatomy.

Video recording has significant disadvantages, including degradation of image quality, inability to freeze-frame images, and inability to postprocess images (including obtaining tissue Doppler data). Nonetheless, while stress echo studies should be reviewed in side-by-side digital format, back-up onto videotape remains essential, DVD or the principal benefits of tape review are the ability to examine off-axis images, the ability to see different walls in different parts of the respiratory cycle, and avoidance of sampling artifacts. A study from the Mayo Clinic showed an alteration of interpretation by review of videotape in 40% of segments from digital clips, and this altered the final diagnosis in 14% of patients.

Attention to detail: The successful performance of stress echocardiography is based upon meticulous attention to practical issues.

1. Avoid excessive gain settings (Fig. 16.2), as this may obscure endocardial detail. The depth and zoom window must be altered to optimize image size and definition.
2. Same myocardial regions: The acquired views must be of the same regions of myocardium throughout the test, so that the window and view must be the same (Fig. 16.3).
3. True two-chamber view: Particular attention should be paid to acquisition of a true apical two-chamber view (anterior and inferior walls) rather than an apical long-axis view (anteroseptal and posterior walls), as this may be the only view of the right coronary artery territory. Errors with ECG triggering may make the digital cine-loops useless, so care must be taken to optimize the ECG signal and avoid sampling extrasystolic cycles.

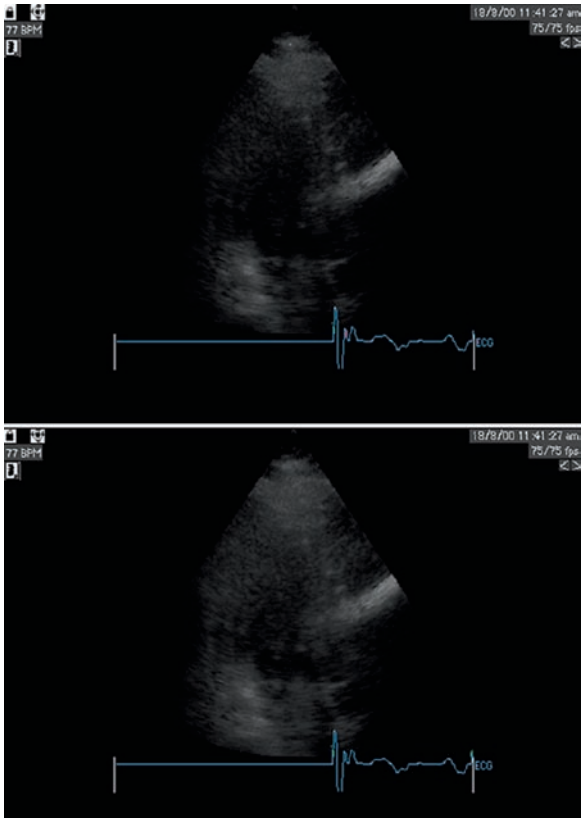

Fig. 16.2 Use of excessive gain settings. The response to suboptimal images is often to increase gain settings (*lower panel*). This is often counterproductive, increasing artifact and reducing endocardial resolution

The "Roadmap" for Good Acquisition

1. The initial imaging step in a stress echo exam should be a truncated standard echo-Doppler examination, including a brief M-mode, transmitral pulsed-wave Doppler, and color examination. A complete echocardiogram is often not possible for logistic reasons, so if an unexpected finding is identified, we reschedule the patient to return for a more complete study.
2. Images should comprise apical, parasternal, and/or subcostal views before, during, and after stress. The sequence for poststress images is best varied with the clinical setting. Because early poststress imaging time is particularly valuable, and the apex is the most common site of a wall motion abnormality, we perform apical views first. If resting dysfunction is already identified in one view, it is usually preferable to start with another view.
3. Optimizing endocardial definition and avoidance of foreshortening the left ventricular cavity are critical, but in other respects, the principles of 2D imaging for stress echocardiography are a little different

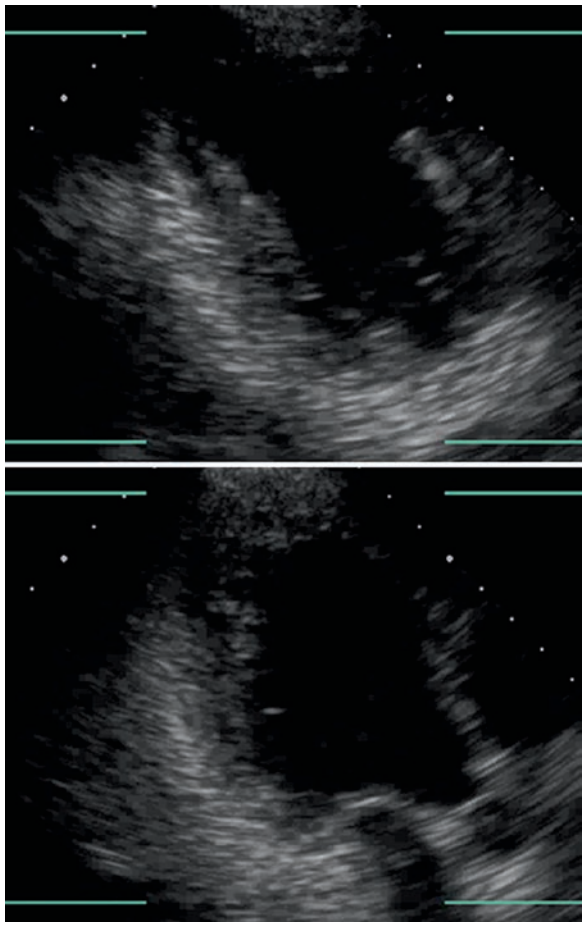

Fig. 16.3 Importance of maintaining the same imaging plane for comparison of pre- and poststress images. Failure to provide a true apical two-chamber view may preclude visualization of the right coronary territory

from normal. Images may be enhanced by asking the patient to exhale, although sometimes the window is improved by partial inspiration, especially in the apical two-chamber view. Contact between the heart and chest wall may be improved by lying as far as possible onto the left side (for supine imaging) or by leaning forward on the bicycle (for upright imaging). Views are modified to attend more to the myocardium than to the valves (e.g., long-axis parasternal images are often obtained through a lower window).

4. During exercise echo, image quality and speed of acquisition need to be balanced, because of the potentially rapid resolution of ischemia.
   Remember that a complete set of imperfect but "readable" images in the first minute may prove more useful than perfect views obtained over several minutes.
5. Use of Doppler: Although stress echocardiography is typically performed with 2D echocardiography, stress Doppler studies have been reported for the evaluation of both systolic and diastolic function. Their application to assessment of systolic function is constrained by measurement error in volumetric calculations. More favorable results have been obtained for evaluation of diastolic parameters, although these may be influenced by pathologies other than ischemia. Nonetheless, the evaluation of filling pressure with stress (calculated by transmitral flow and tissue velocity) may become an interesting application of stress echocardiography.
6. Color-flow Doppler may be used to identify stress-induced mitral regurgitation.

Table 16.3 "Do and don't" of stress echo

Do	Don't
Look at the left ventricle (not left atrium)	Overgain (especially in near-field)
Ensure pre- and postviews are same	Foreshorten the LV cavity
Acquire in inspiration or exhalation	Sacrifice speed for perfection
Optimize positioning	
Sample plenty of cycles	

In Table 16.3 we summarize what to do and what to avoid during a stress echo study.

Interpretation

Semiquantitative Interpretation

The qualitative comparison of regional function at rest and stress is the basis of the clinical interpretation of stress echocardiography. The left ventricle is typically divided into 16 segments (septal, lateral, anterior, and inferior at the apex, with these segments as well as anteroseptal, and posterior segments at the base and midpapillary muscle level), and each segment is scored as normal, hypokinetic, or dyskinetic (Fig. 16.4). By

averaging the scores of individual segments, a "score index" may be obtained, which gives a semiquantitative index of global systolic function.[2]

Structured Review

Use the digital side-by-side images as the primary data, supported by video images to examine nonstandard views, and to check M-mode and Doppler.

Technical review – check that images are triggered correctly and the pre-, peak, and poststress views are comparable.

Brief review of the whole study – checking if wall motion is normal at rest, then to see if there are obvious changes in cavity size (suggesting multivessel disease) or cavity shape.

Segmental analysis comparing regional function in each of the 16 segments at rest and stress. Function is compared both by examining the continuous cine-loop and then frame by frame, paying particular attention to contraction during the first part of systole (especially if there is excessive rotational or translational movement).

Regional scoring: For regional wall motion scoring, the distinction of severe hypokinesia from akinesia may be helped by assessment of endocardial excursion <5 and <2 mm, respectively. However, the timing of movement and thickening rather than excursion are important parameters; regions which fail to thicken or which move only in late systole (after movement of the adjacent myocardium) may be moving passively and should be considered as akinetic irrespective of endocardial excursion.

Resting Function

The schema for interpretation of rest and stress regional wall motion abnormalities is summarized in Table 16.4.

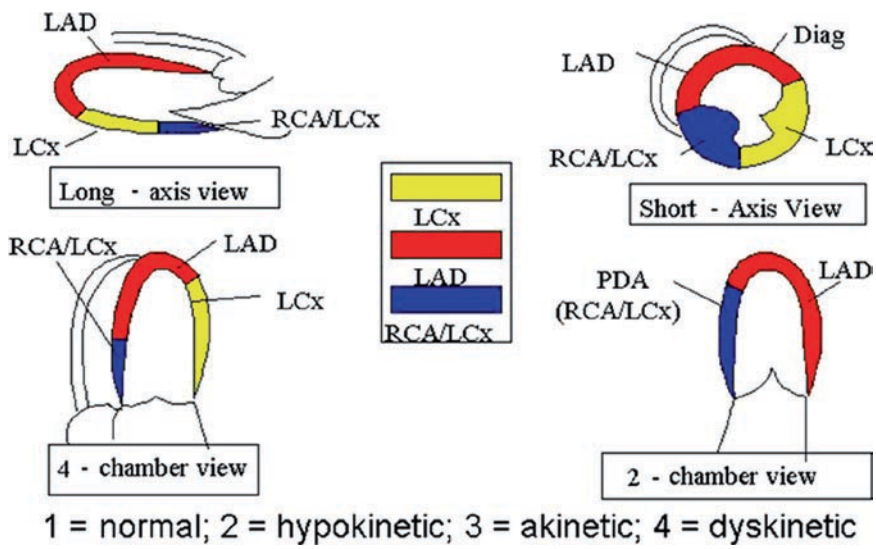

Fig. 16.4 Wall motion scoring and attribution to coronary vascular territories

Table 16.4 Interpretation of exercise and pharmacologic stress echocardiography

Nature of tissue	Resting function	Low dose	Peak/poststress function
Normal	Normal	Normal	Hyperkinetic
Ischemic	Normal	Normal (except with severe CAD)	Reduction versus rest Reduction versus adjacent Delayed contraction
Viable, nonischemic	Rest WMA	Improvement	Sustained improvement
Viable, ischemic	Rest WMA	Improvement	Reduction (compared with low dose)
Infarction	Rest WMA	No change	No change

1. Resting wall motion abnormalities are usually characterized as infarcted, but mild hypokinesis should be interpreted with caution, as it can be a normal variant.
2. Some segments considered to be infarcted using these criteria (maybe as much as 50%) are viable. The evaluation of wall thickness (Fig. 16.5) is a good resting marker of nonviable tissue (<6 mm), although myocardium of normal thickness does not exclude recent or nontransmural infarction.
3. Other resting markers of viability include preservation of cyclic variation of integrated backscatter, strain, and preservation of perfusion.
4. Augmentation of segmental function with low-dose dobutamine stress may also identify viable tissue (Fig. 16.6).

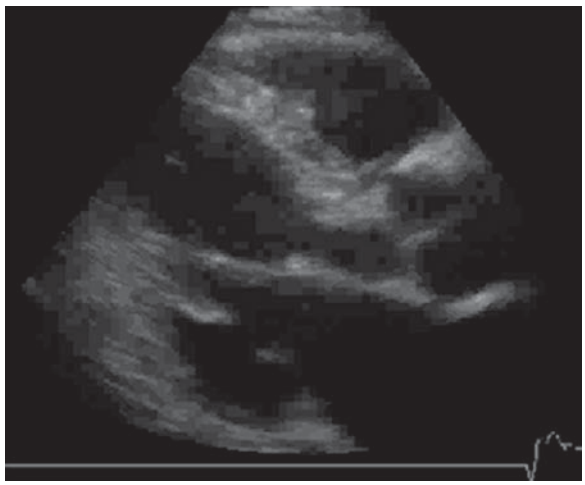

Fig. 16.5 Significance of wall thinning. The posterior wall is thinned, and would be very unlikely to show contractile reserve with dobutamine, or recover after revascularization

Defining an Ischemic Response

Myocardial ischemia is characterized by the development of

1. New or worsening regional dysfunction (Fig. 16.7). The normal response to either exercise or dobutamine stress is to increase myocardial thickening (the most reliable parameter). The speed of contraction (arguably the most sensitive parameter) and the endocardial excursion (probably the most widely used parameter).

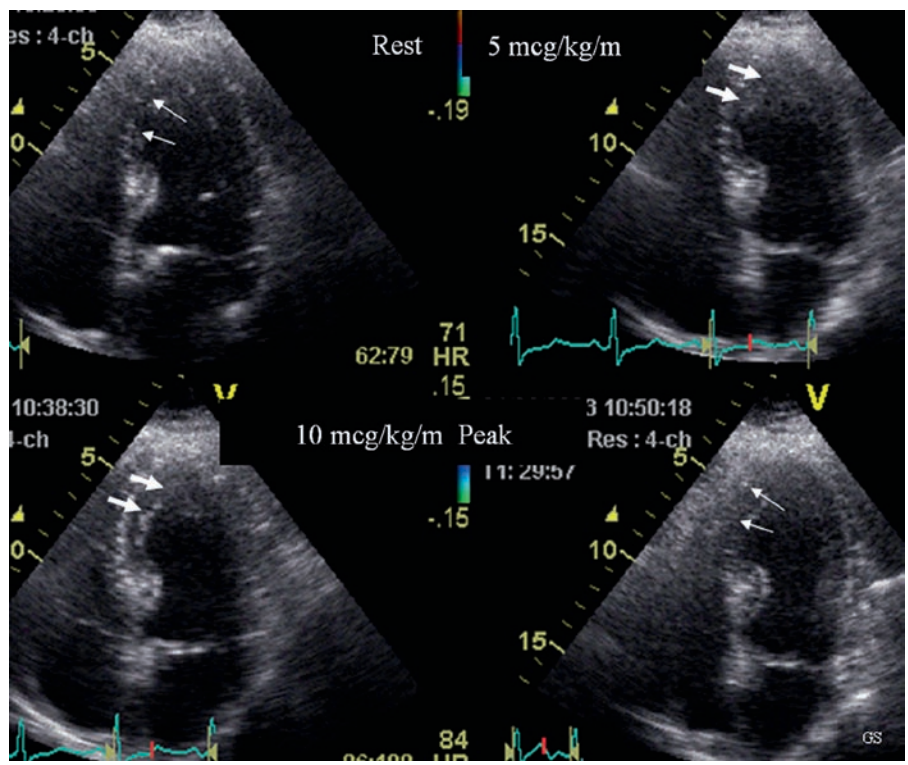

Fig. 16.6 Detection of myocardial viability with dobutamine stress echocardiography. The resting image shows an apical septal wall motion abnormality, which improves at 5 and 10 μg/kg/min of dobutamine and deteriorates at peak (a biphasic response). *Printed images* are end-systolic freeze frames and *arrows* identify new wall motion abnormalities

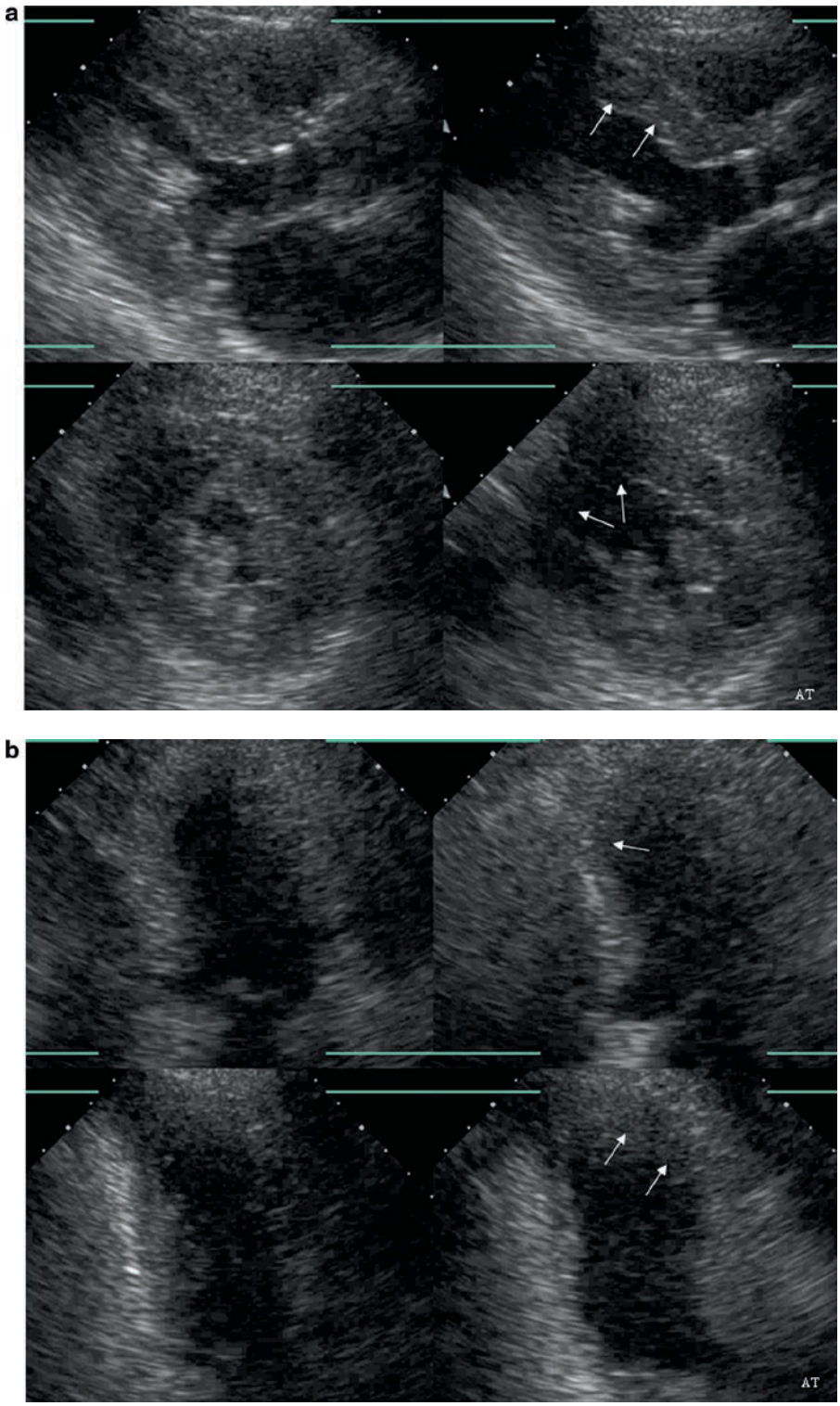

Fig. 16.7 (**a** and **b**). Detection of left anterior descending ischemia at exercise echo. This is a good case to emphasize the importance of putting the involved segments into a pattern – here involving anteroseptum, apex, and anterior wall. Resting images are shown on the *left* and postexercise images on the *right*. *Printed images* are end-systolic freeze frames and *arrows* identify new wall motion abnormalities

2. Failure to augment function has been reported in normal segments, so the previous characterization of this tissue as ischemic appears to be wrong. One exception to the use of worsening function as a marker of ischemia is the response of akinetic segments during bicycle or dobutamine echocardiography – we do not classify a further deterioration of function as ischemia, as increased loading may be responsible for such a response.
3. The changes in end-systolic ventricular shape are an often-neglected but quite accurate guide to the development of ischemia.

The Magnitude of Ischemia

The extent of coronary disease may be inferred from the site of abnormal wall motion, the number of abnormal segments, severity (segmental wall motion score), time of onset and offset of ischemia, and the effect of ischemia on global left ventricular function. Note that the most abnormal area always catches the eye, but be very careful to interpret function in all 16 segments, as this is vital for recognition of multivessel disease (Fig. 16.8).

The contents of a stress echo report are summarized in Table 16.5.

Rules for Qualitative Interpretation

The following rules for qualitative interpretation were devised by a group of expert centers.[3]

– *Rule 1:* Minor degrees of hypokinesia are not identified as ischemia (especially if only apparent at peak, and not postexercise)
– *Rule 2:* Abnormalities are corroborated whenever possible with another view
– *Rule 3:* Segments are not identified as abnormal if they do not make sense in terms of coronary territories (e.g., isolated midseptal abnormalities)
– *Rule 4:* Isolated basal inferior or basal septal segments are not identified as abnormal in the absence of an abnormal neighboring segment (Fig. 16.9)
– *Rule 5:* Read with multiple observers whenever possible, and to blind the interpretation to all other data

Pitfalls in the Standard Performance of Stress Echocardiography

Failure to recognize abnormal wall motion when angiographically significant coronary disease is present may be caused by

- Angiographic features,
- Patient characteristics,
- Inadequate stress, or
- Imaging and interpretation issues.

False-positive results: (i.e., an apparent wall motion abnormality without significant coronary stenosis) are most frequently due to interpretation errors.

- False-positive results may occur due to overinterpretation – especially of basal wall motion abnormalities.
- Sometimes, inducible dysfunction is apparent rather than real – for example, peri-infarct zones may be tethered by the akinetic infarcted segment and consequently fail to improve function with stress, or even appear dyskinetic if the infarct bulges during stress.
- False-positive scans may be induced by an abnormal activation sequence (pacing, left bundle branch block), abnormal septal motion (prior cardiac surgery or RV volume overload), and heterogeneity related to cardiomyopathy and aortic regurgitation.

While many of these false positives are avoidable with adequate training, some situations (e.g., patients with prior coronary bypass surgery, left bundle branch block, extensive wall motion abnormalities or in the presence of suboptimal images) are difficult even for experts.

- One important category that can be relied on to annoy angiographers is the "false-positive" angiogram, whereby coronary disease is identified on the basis of a moderate (e.g., 50 or 60%) stenosis that is actually not flow limiting, even during hyperemia. The arbitrary selection of >50% diameter stenosis to identify "significant" disease is because this approximates a level below which lesions do not limit flow under conditions of peak vasodilation, but it should be recognized that the 50–70% range includes many stenoses which are physiologically nonsignificant.
- Even allowing for discrepancies between anatomical stenosis severity and physiological sequelae, there are other fundamental problems in defining the

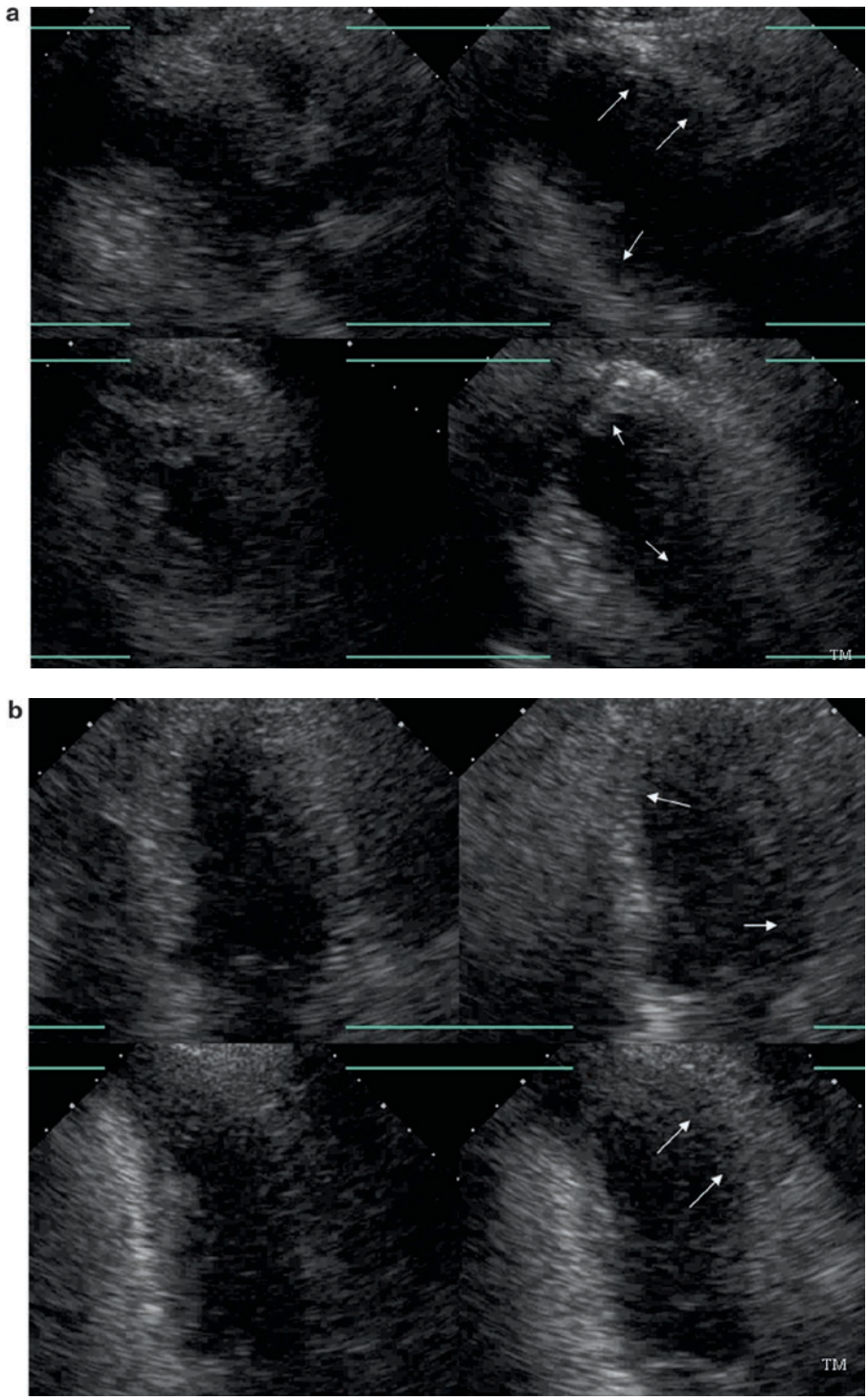

Fig. 16.8 (**a** and **b**). Detection of multivessel ischemia at exercise echo. In addition to left anterior descending wall motion abnormalities in the septum and anteroseptum, there is LV cavity enlargement, and posterolateral wall motion abnormalities are also detected. This is a good case to emphasize that every segment must be systematically compared – even when the test is clearly abnormal, and especially if there is LV cavity enlargement. Resting images are shown on the *left* and postexercise images on the *right*. *Printed images* are end-systolic freeze frames and *arrows* identify new wall motion abnormalities

Table 16.5 Contents of a stress echo report

Heading	Detail
Resting images	LV size and global function
	Resting wall motion abnormalities (including score)
	Other problems that may account for symptoms (e.g., valvular)
Stress response	Limiting symptoms, side effects
	Angina and ST segment responses
	Hemodynamic response (including adequacy of heart rate)
	Exercise capacity
Stress images	LV size and global function
	Segmental function – presence, site, extent and severity of abnormal function, time of onset, and duration after stress
	Wall motion score
Conclusion	Presence and extent of infarction and viability (if resting function is abnormal)
	Exercise/dobutamine stress response (nonecho aspects)
	Response based on subjective analysis, wall motion score, and/or ejection fraction

accuracy of noninvasive tests from the coronary arteriogram, including observer variability and problems posed by assessment of eccentric stenoses, and poor correlation between the anatomic severity of stenoses and their effects on flow.

- Newer invasive measures of coronary stenosis severity such as coronary flow reserve and myocardial fractional flow reserve offer both a physiologic index that addresses the anatomy versus physiology dichotomy and the problems of subjectivity. Patients with an FFR < 0.75 can be expected to have unequivocal evidence of reversible myocardial ischemia on noninvasive testing, and this approach is the best solution if there is concern about a negative stress echo in the setting of an apparently abnormal angiogram.
- Erroneous results may be due to inadequate equipment or insufficient training. Technically difficult studies due to poor image quality remain a problem, even in the era of harmonic imaging and echo contrast. The greatest potential pitfalls relate to the interpretation of studies.

False-negative results may occur due to failure to appreciate the subtle manifestations of ischemia (hypokinesis, tardokinesis).

- Patient factors may limit the ability to induce ischemia.
- Antianginal therapy may prevent the identification of ischemia, and therefore, diagnostic testing should be performed after interruption of therapy – especially beta blockers. The implications of ongoing therapy for prognostic testing are less clear – sometimes the assumption is made that events are less likely if the heart is protected from ischemia, but an important role of prognostic testing of patients with suspected disease is simply to allocate low risk to those without disease, and this process is compromised by testing on therapy.
- The use of an inappropriate stressor may contribute to false-negative results. A negative test due to inability to exercise maximally or tolerate maximal pharmacologic stress should be identified as nondiagnostic. Even if maximal, pharmacologic stress is less potent than exercise, and inadequate stress may fail to induce ischemia. A useful aphorism is that if the patient is able to exercise maximally, exercise stress is the better choice – because of the greater workload, the information derived from exercise capacity and the more reliable ST segment response.
- Extreme hemodynamic changes may influence wall motion. Severe stress-induced hypertension may magnify the development of regional wall motion abnormalities and actually cause wall motion abnormalities in the absence of coronary disease, and in contrast, reduction of LV volumes (e.g., "cavity obliteration" with peak doses of dobutamine) may hide wall motion abnormalities due to milder coronary disease.

Quantitative Interpretation

The problem: Subjectivity is the bane of stress echocardiography. Without special training, competent readers of transthoracic echo have an accuracy of approximately 60–70%. Picano et al[4] reported that 100 supervised studies were required to bring the accuracy of "novices" experienced in echocardiography to the level of "experts." As importantly, pattern recognition skills attenuate when they are not used, and limited data suggest that accuracy is related to reading volume.

- Subjective analysis leads groups of readers to have different reading styles, which leads to variations between expert centers. The first study of this topic[5] showed the major causes of discordant interpretation were milder degrees of coronary disease, and especially suboptimal image quality. A re-examination of the same topic over 7 years later showed improvement in concordance related to improved image quality

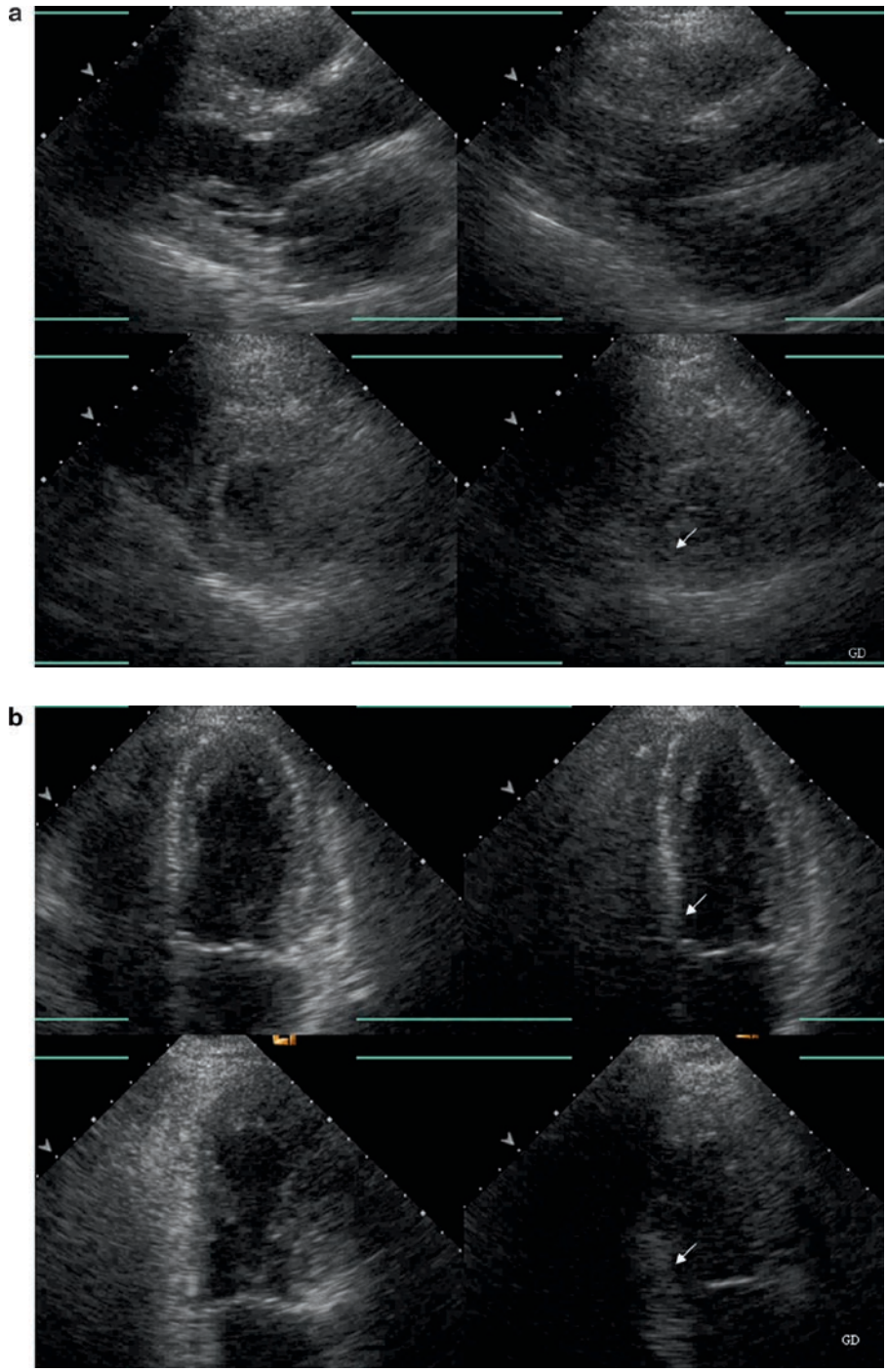

Fig. 16.9 (**a** and **b**). Difficulties posed by interpretation of the inferior wall. Apical two-chamber views show a shape change in the inferior wall. This is a good case to emphasize that the basal inferior should only be identified as abnormal in the presence of an adjacent abnormal segment – here both the basal septum and the mid-inferior are implicated. Resting images are shown on the *left* and postexercise images on the *right*. *Printed images* are end-systolic freeze frames and *arrows* identify new wall motion abnormalities

due to harmonic imaging, side-by-side review, and standard reading criteria.[6]

The solution to subjective interpretation may be the adoption of quantitative approaches to the evaluation of left ventricular wall motion – if not as a substitute, then as a guide to standard wall motion analysis.

1. Global systolic function may be quantified by tracing endocardial contours in systole and diastole in order to obtain ventricular volumes and ejection fraction. However, global indices are relatively insensitive to mild ischemia (because of compensation by nonischemic walls), and are nonspecific for coronary disease. Nonetheless, this approach is useful in some situations (e.g., assessment of contractile reserve in valvular disease and viability) and may be strengthened by the application of three-dimensional echocardiography.
2. The simplest approach to quantifying regional function is the application of a semiquantitative wall motion score, although these do not truly measure function independent of the observer.
3. True quantitation of regional function may be performed from M-mode, two-dimensional or Doppler methods, some of which are in the realm of "new technologies." Generally, these can be categorized into approaches that

   (a) Track endocardial radial motion and
   (b) Those that measure longitudinal shortening

   (a) The approach which is most analogous with standard visual assessment is the measurement of radial thickening or endocardial excursion. Although assessment of thickening is independent of tethering, translation, or rotation, its feasibility is limited by problems of not only tracking the endocardium but also the epicardial border.

   The most widely used approach was therefore the measurement of endocardial excursion using the centerline method, which involves tracing and superimposition of systolic and diastolic images, drawing of a centerline midway between these profiles, arrangements of chord perpendicular to the centerline, and measurement of chord lengths, normalized for body size and the diastolic perimeter length. Recent image processing advances have enabled automated contour detection and correction of translational movement by use of the apex and mitral valve plane as a frame of reference.

   An alternative approach tracks the myocardial border using the difference in backscatter between the myocardium and blood pool, with each frame being superimposed and the location of the endocardium in each frame being color coded. Normal ranges have been defined for this approach, and the technique is accurate for the diagnosis of coronary artery disease and may be especially valuable as a guide to less experienced readers. However, potential problems common to all endocardial tracking approaches include concerns about image quality (which limits the ability to trace the endocardial border), compensation for rotational or translational movement of the heart (both fixed and floating frames of reference have potential problems – failure to correct for such movement may cause false positives, but their correction may hinder the detection of milder abnormalities), and selection of appropriate systolic and diastolic frames.

   b. Tissue Doppler imaging measures the velocity of myocardial movement within a sample volume relative to the transducer, using the same principles as the use of Doppler for measurement of bloodflow, but with manipulation of the controls to include high-amplitude, low-velocity signals. This technique is especially valuable for quantification of longitudinal (base-apex) function. Supply-side ischemia has clearly been shown to alter myocardial velocity, strain and strain rate, and similar findings have been reported during exercise and dobutamine stress echocardiography. Indeed, recent designation of normal ranges (in isolation or using regression equations to correct for age and gender) has enabled tissue Doppler to provide a fully quantitative means of interpreting stress echocardiography, comparable to expert wall motion analysis. Tissue Doppler-based techniques are less dependent on image quality than the edge-detection methods, but these methods have important limitations – in particular, the apex cannot be assessed adequately as it is fixed and velocities are low. Problems posed by tethering and translation have been addressed by the development of strain rate and strain imaging, which examine a velocity gradient between adjacent sample volumes. Preliminary clinical studies with these techniques have also produced favorable results both for the assessment of viability (Fig. 16.10) and ischemia (Fig. 16.11), although the newer techniques have greater problems with signal quality than tissue velocity alone and are very susceptible to angulation issues.

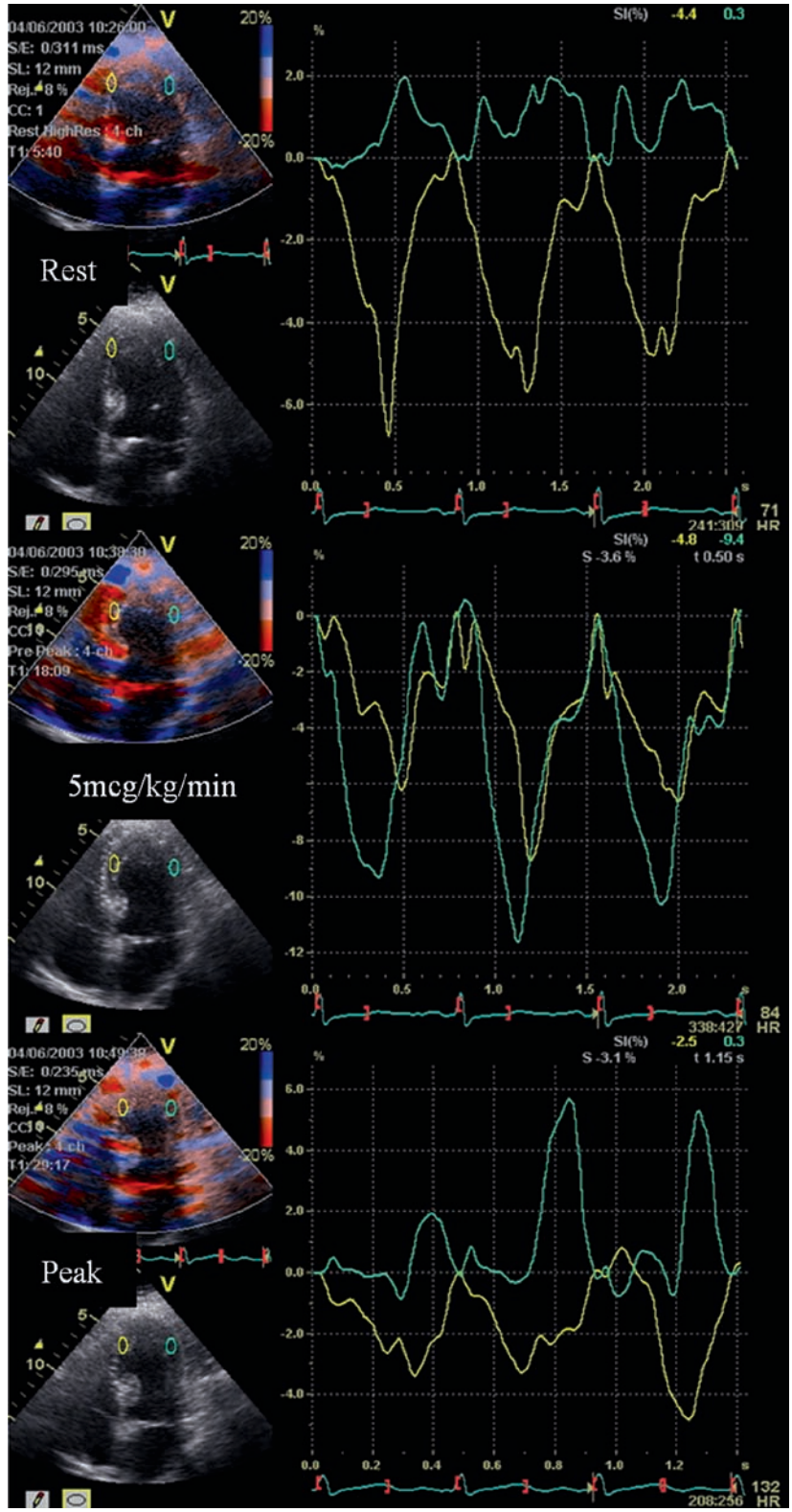

Fig. 16.10 Application of strain imaging to the identification of viability in a patient with resting apical wall motion abnormalities. The apical septal waveforms are shown in *yellow* and the apical lateral in *blue*. Strain is reduced in the septum at rest and the lateral is actually lengthening (positive wave). Low-dose dobutamine causes reversal of the lateral wall, which now shortens, compared to little change in the septum. At peak, the lateral deteriorates and again lengthens – signifying a biphasic response

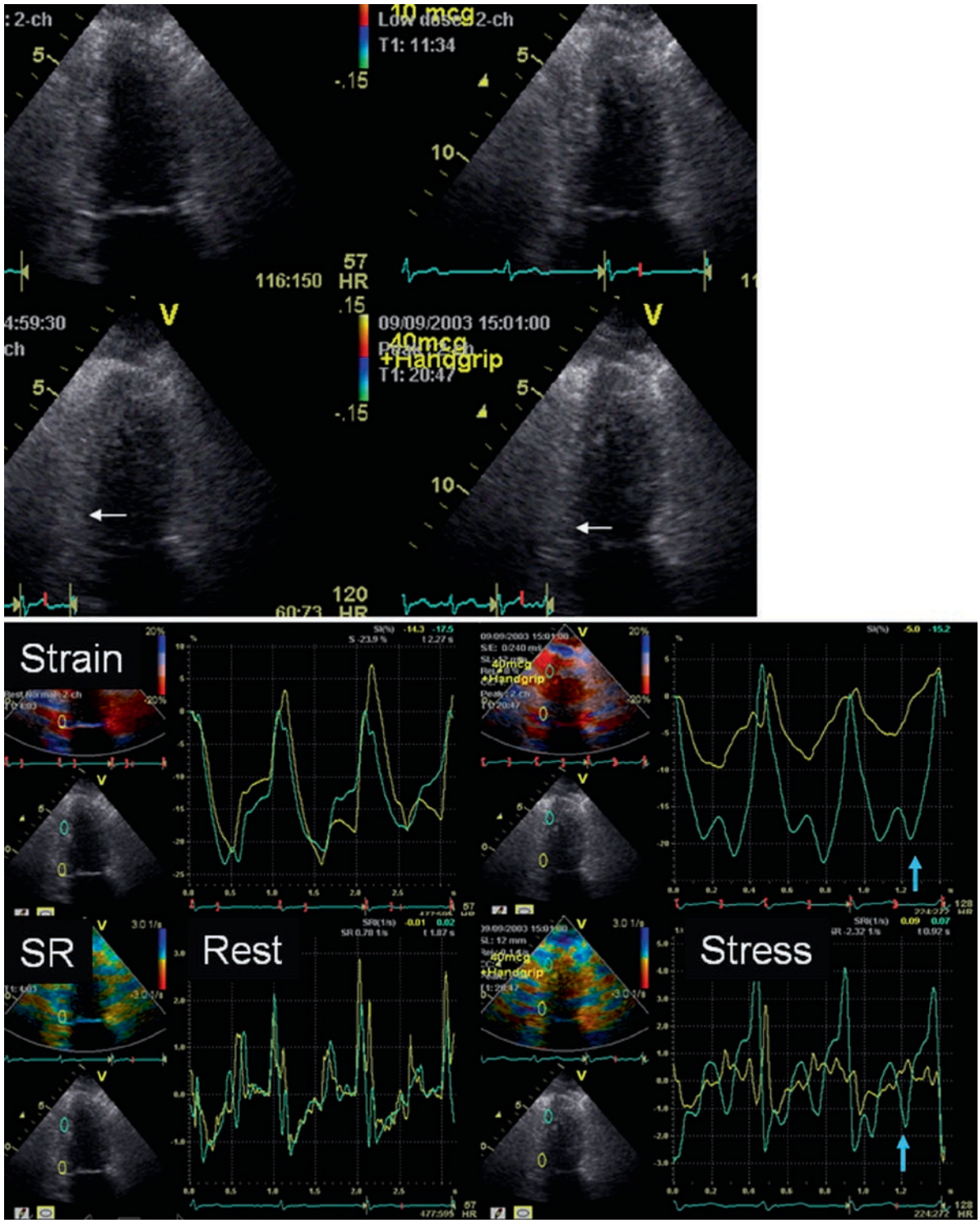

Fig. 16.11 Application of strain and strain-rate imaging to the identification of ischemia in the inferior wall. The basal inferior waveforms are shown in *yellow* and the apical in *blue*. Waveforms are normal in both at rest. At peak dobutamine, strain decreased and SR fails to increase in the basal inferior, and milder ischemia in the apex is evidenced by the development of postsystolic thickening (*blue arrows*)

Table 16.6 Application of new technology to stress echo interpretation

Category	Specific tests	Status
Radial motion	Color kinesis	Improves accuracy of novice readers
		Image quality dependent, best with contrast
	Centerline	Image quality dependent
	Strain, etc.	May be possible with speckle tracking
Longitudinal motion	Tissue Doppler	Improves accuracy of novice readers
		Limited by translational motion
	Strain rate and strain	Promising but still underdeveloped

The need for a reliable quantitative approach remains one of the greatest challenges of stress echocardiography. The reality is that quantitative stress echo is a research rather than a clinical tool at most centers (Table 16.6).

Accuracy

The calculation of sensitivity, specificity, and diagnostic accuracy is based on comparison of a noninvasive technique with a gold standard – generally coronary angiography. However, the measurement of sensitivity and specificity does not address the efficacy of stress echocardiography for addressing several important questions, including the ability to identify ischemia and viability in the postinfarction patient, the recognition of multivessel disease as such, and the ability to identify ischemia within a particular territory.

The reported accuracy of stress echocardiography is influenced by several technical and clinical aspects. The contributions of impaired image quality, submaximal stress, and the limitations of coronary angiography have been alluded to earlier.

Clinical Factors Influencing Accuracy

Referral bias may influence accuracy if a particular subgroup is over-represented and especially if a subgroup is referred preferentially to angiography (post-test referral bias). Studies showing the latter produce a characteristic pattern of high sensitivity (patients with a positive test proceed to angiography) and low specificity (the only patients with a normal angiogram are those with a false-positive result). Even when care is taken to avoid influencing the performance of angiography, study designs comparing the findings of stress echocardiography with coronary anatomy are necessarily biased toward a group with severe enough coronary disease to warrant angiography.

For similar reasons, over-representation of patients with more extensive CAD or prior infarction tends to inflate sensitivity. Patients with multivessel disease or tight stenoses are likely to have a more extensive area of abnormal wall motion and conversely, small risk areas in patients with mild or single-vessel disease may not be identified, leading to lower sensitivity in this situation. Indeed, single-vessel and mild coronary disease are the main angiographic predictors of false-negative results. Fortunately, the outcome of patients is more governed by functional evidence of ischemia than coronary anatomy, and patients with "false-negative" stress echocardiograms have a benign prognosis. In the postinfarct patient, the diagnosis of coronary disease is already established.

Accuracy of Stress Echocardiography

The accuracy of different stress echocardiography techniques is summarized in Fig. 16.12. Generally, sensitivities are in the 80–85% range, with specificities in the 85% range. Exercise echo is the more sensitive and dipyridamole echo the most specific – reflecting the more potent stress with exercise but the possibility of artifact due to image quality issues.

The ability to recognize multivessel disease, identify extent of disease, differentiate performance in each location, and discriminate ischemia from scar is an important parameter that is not expressed by sensitivity and specificity. The presence of multivessel disease makes it easier to identify that disease is present, but this high sensitivity for detection of disease hides quite limited ability to recognize that more than one vessel is involved, apart from in patients with previous myocardial infarction – where multivessel disease is implied by a new wall motion abnormality, separate from the infarct zone. Thus, the ability to recognize multivessel disease with prior infarction is >80%, while it is only 50% in those without prior infarction. Clues to the

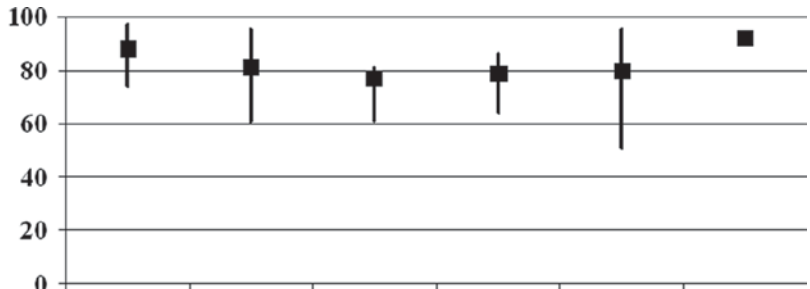

	ExE	DbE	DpyE	ExE	DbE	DpyE
Highest	97	95	81	86	95	94
Lowest	74	61	61	64	51	90
■Mean	88	81	77	79	80	92

Fig. 16.12 Accuracy of different approaches for diagnosis of CAD with stress echocardiography (reproduced with permission from ref. 8.)

presence of multivessel disease are left ventricular cavity enlargement and reduction of ejection fraction (but this is rare with dobutamine stress), the combination of a positive stress echo with ST segment changes of >0.2 mV, earlier onset of ischemia (i.e., at lower levels of exercise or lower dose of pharmacologic stress, or low heart rate and rate-pressure product).

Exercise Versus Pharmacologic Stress

There is no choice but to use pharmacologic stress in patients who can only exercise submaximally, but its use is more controversial in patients who could otherwise exercise. While this approach makes the acquisition easier, it makes the interpretation more difficult because the workload on the heart is less and therefore extent of ischemia is less. Comparative studies between dipyridamole and exercise stress (in patients able to exercise) have shown higher feasibility for the drug, with varying sensitivity and specificity, although the general consensus is that exercise is more sensitive and less specific. The same conclusions have been made with comparison of dobutamine and exercise stress.

Selection of the Optimal Pharmacologic Stress

The choice of stressor is simple in some subgroups of patients who cannot exercise, who have specific contraindications to one or other stressor. Patients with hypertension or arrhythmias should undergo a vasodilator rather than an inotropic stress, and patients with bronchospasm or conduction disorders should be submitted for dobutamine testing. In the majority of patients, who lack these contraindications, comparisons between dobutamine and dipyridamole have shown similar accuracy, although dobutamine is more sensitive for single-vessel disease and dipyridamole is more specific.

Comparison with Other Approaches

Comparison with the Exercise ECG

Although the exercise ECG is the simplest and most widely used test for noninvasive detection of coronary disease, its dependence upon adequate stress and an interpretable ECG limit its feasibility to <50% of patients warranting functional testing for CAD. The reported sensitivity and specificity of the exercise ECG varies widely, with mean values of 68 ± 16% and 77 ± 17%, respectively. Of course, the exercise test offers much more than just the ST segment response, and various scores that include not only the ST data, but also correction for heart rate, or a combination with exercise capacity and hemodynamics have improved the accuracy of the test.

In direct comparisons between exercise echo and conventional exercise ECG, the imaging test gave better sensitivity and specificity, as well obtaining otherwise inaccessible data such as the site of dis-

ease. Limited data with exercise scores show these to be better than the ST analysis alone, but still inferior to stress echo.

Difficult Subgroups for Standard Exercise Testing (LBBB, LVH, Women)

Circumflex artery: Imaging techniques certainly offer diagnostic information in the right coronary and left circumflex territories, and are therefore superior to the ECG, which may be nondiagnostic.

Left bundle branch block: The problems arise in the LAD territory, where left bundle branch block is a difficult situation for all noninvasive techniques, because this conduction disturbance may influence both perfusion and function in the absence of CAD. The sensitivity of stress echocardiography in the anterior circulation depends on the ability to interpret thickening rather than wall motion and to visualize the distal anterior wall in the two-chamber view. The specificity of stress echocardiography appears higher than SPECT.

LV hypertrophy is an important cause of false-positive ST segment responses at stress testing, even if the ST segment appears to be interpretable. While left ventricular hypertrophy has been associated with false-positive SPECT imaging, it has not been shown to influence the accuracy of stress echocardiography. The only exceptions are patients with concentric remodeling, in whom transmural wall stress is low and therefore ischemia may not be provoked, even in the presence of CAD.

Women: Although this is generally not acknowledged in stress testing guidelines, most clinicians accept that the accuracy of exercise ECG is less in women than in men. Myocardial perfusion imaging may be used to circumvent this problem, although it is not without problems, related to the smaller female heart and breast attenuation problems. The accuracy of stress echocardiography is not compromised in women, and the results are superior to those of the exercise ECG, even after correction for referral bias. Indeed, the use of exercise echo as an initial test incurred more initial expense but was ultimately less expensive, because of the avoidance of false-positive ECG provoking unnecessary angiograms.

Clinical Implications of Superiority of Exercise Echo Versus Exercise ECG

Stress echocardiography is the functional test of choice in patients who are unable to exercise and those with an uninterpretable ECG, or when management questions are poorly answered by the exercise ECG alone – for example, when the site of ischemia or the presence of multivessel disease requires definition. To this could be added subgroups of patients where the stress ECG has been shown to be inferior to stress echo – e.g., women, patients with LVH and hypertension. The unresolved question is whether stress ECG testing should be superceded by stress echo in patients with a moderate risk of coronary disease with an interpretable ECG, who are able to exercise. Although there are cost-effectiveness data that support this approach, at present there are insufficient data to justify it across the board, especially as patients undergo exercise testing for a variety of reasons – and in some, the ST segment data are of secondary importance to information pertaining to exercise capacity and hemodynamic responses to exercise.

Comparison with Other Stress-Imaging Approaches

The examination of myocardial function and perfusion at rest and after stress is now possible with both nuclear cardiology and magnetic resonance imaging, but still in its infancy with contrast stress echocardiography. Perfusion imaging identifies the presence of coronary disease on the basis of stress-induced perfusion heterogeneity – which may not necessarily parallel the presence of myocardial ischemia. This occurs earlier in the ischemic cascade, and therefore inherently more sensitive than awaiting the development of inducible wall motion abnormalities, as well as being less likely to be influenced by antianginal drug therapy, which prevents the development of ischemia.

The indications for perfusion scintigraphy, stress MRI, and stress echocardiography are similar

1. Diagnosis of coronary artery disease in patients unsuitable for routine exercise testing or in patients with an intermediate risk of disease
2. Assessment of the physiologic significance of known coronary stenosis

3. Assessment of prognosis, as determined from the quantity of infarcted tissue, and the amount of ischemic tissue
4. Follow-up after intervention

Despite the favorable record of the nuclear techniques and the benefit of more automated interpretation, they have disadvantages with respect to cost (of imaging equipment, isotopes, and disposables), patient convenience (particularly with thallium imaging), and availability. Stress echocardiography does not share these technical problems and can offer real-time imaging of the heart (possibly enhancing safety and enabling visualization of the time-course of ischemia), but is technically more difficult. The use of magnetic resonance imaging for the assessment of coronary disease is still under evaluation.

Accuracy of Stress Echocardiography Versus Perfusion Scintigraphy

The sensitivity and the specificity of SPECT are quoted as about 90 and 70%, respectively, comparing with 80 and 85% by stress echocardiography. The use of receiver operator characteristic curves to correct for the inevitable variations between studies showed similar levels of accuracy – with SPECT being more sensitive, but less specific than echocardiography.[7] These findings have been supported by head-to-head comparisons between the techniques using exercise or dobutamine stress. The results with vasodilator stress show less sensitivity for echocardiography.

As mentioned earlier, there are many clinical settings where the parameters of sensitivity and specificity are insufficient for comparison of the tests. Patients after myocardial infarction are one such example, as sensitivity and specificity do not discriminate between the diagnoses of scar and ischemia. However, differences between the tests certainly occur in this respect – the concordance between echocardiography and perfusion scintigraphy with respect to the identification of normal, ischemic, or infarcted myocardium is between 70 and 80%. In the situation that exercise echo identifies scar by within segments identified as ischemic by SPECT, the segments are often found to be viable. Generally, this may be avoided by the use of dobutamine (which permits recognition of a biphasic response).

When to Choose Stress Echocardiography Versus Scintigraphy (and Vice Versa)

Much has been written about the comparison between stress echocardiography and scintigraphy. However for both techniques, local expertise remains the most important issue. However, once this condition is fulfilled, we believe that the selection of one or other test should be tailored to the clinical circumstances as follows:[8]
Perfusion imaging may be more useful in

1. Postinfarction patients. Scintigraphy is more able to identify combinations of ischemia and infarction, is accurate for the detection of viable myocardium (although dobutamine echocardiography is useful in this respect), and lacks the problem of peri-infarct tethering seen with echocardiography.
2. Patients requiring vasodilator stress (those unable to exercise and also unable to undergo dobutamine testing). Perfusion imaging is recommended for diagnostic purposes, as vasodilator echocardiography is insensitive, particularly for single-vessel disease.
3. Patients with poor echocardiographic windows (though these individuals are difficult to predict without performing resting imaging, and the window may paradoxically improve with postexercise hyperventilation).

Echocardiography is more useful in

1. Those with left ventricular hypertrophy and left bundle branch block. Stress echocardiography appears to be more specific than perfusion scintigraphy in these situations (though these data await confirmation).
2. Patients in whom safety is a major concern (potentially unstable or severely ischemic). Using echocardiography, ischemia may be observed "online" and the appropriate action taken.
3. Studies being performed to assess the adequacy of therapy (as echocardiography visualizes ischemia) rather than perfusion heterogeneity.
4. Patients with a suspicion of significant valvular or pericardial components to their presentation.
5. Women. The use of nuclear perfusion imaging in women has some important limitations, including breast attenuation artifacts and ability to resolve ischemia in the small female heart. There have been no direct comparisons, but in a meta-analysis, both sensitivity and specificity were less with nuclear

than echo imaging.

6. Left ventricular hypertrophy. In contrast to the favorable results with echocardiography in LVH, perfusion scintigraphy in patients with LV hypertrophy often shows both false negatives (reduction of hyperemia in normal segments, suboptimal stress) and false positives (nonuniform reduction of perfusion reserve due to LVH). Direct comparison of stress echo with myocardial perfusion scintigraphy in hypertensive patients showed that the specificity of echocardiography was significantly greater than that of scintigraphy.

Stress Echocardiography Versus Magnetic Resonance Imaging

Magnetic resonance imaging may be used to assess wall motion at rest and stress, perfusion and viability. As the image quality is uniformly high, this technique may offer a quantitative solution to regional LV function assessment, and the first reports of such an approach are now 10 years old. Strain imaging is also feasible. To date, however, neither are part of the standard array of stress-imaging techniques that are routinely performed.

Most of the comparative studies between dobutamine MRI and dobutamine echocardiography have focused on the assessment of myocardial viability. In an original study of >200 patients, both tests were unable to evaluate 18 patients (9%) – due to poor image quality at echocardiography and due to claustrophobia and obesity with MRI. The sensitivity of dobutamine echocardiography and MRI were 74 and 86%, respectively, with specificities of 70 and 86%, but these differences were not significant when poor-quality echo studies were excluded.

Echocardiographic Determination of Myocardial Viability

Use of Echocardiographic Techniques to Predict Functional Recovery

The echocardiographic assessment of viability is often considered to relate to contractile reserve. However, a spectrum of information may be obtained from resting echocardiography (wall motion, wall thinning, and LV volumes), dobutamine or dipyridamole stress (ischemia and contractile reserve), contrast echocardiography (perfusion), and new technologies (myocardial backscatter, tissue Doppler, and strain imaging). These features are discussed in more detail by Vanoverschelde in Chap. 17.

Augmentation of regional function with low-dose dobutamine (5–10 μg/kg/min) or dipyridamole identifies the possibility of viability, but as discussed earlier, the reliability of this signal depends on what happens next. Continued augmentation up until peak dose may indicate a patent infarct-related artery or well collateralized tissue, but may also be seen in a nontransmural infarction. The development of ischemia at high heart rates (i.e., a "biphasic response") denotes a stenosed infarct-related artery and is a reliable predictor of functional recovery after revascularization. The determinants of the viability responses to stress include the amount of viable tissue, the degree of residual stenosis, the extent and magnitude of collaterals, the size of the risk area, tethering, and the presence of drug therapy. Impairment of coronary flow reserve is important in the development of ischemia, and therefore the biphasic response discussed earlier, but some preservation of flow reserve is critical to permit augmentation of function in response to low-dose dobutamine. These issues, as well as differences in populations and techniques, lead to some variation in the recorded accuracy of stress echocardiography for prediction of viability, but most studies are in the range from 76 to 87% for sensitivity and 82 to 92% for specificity.

The use of stress echo to predict functional recovery may be associated with some false-negative and false-positive results in addition to the usual causes mentioned in relation to predicting angiographic CAD. Viable tissue that has extensive ultrastructural damage may take time to recover both metabolism and function, so "false-positive" findings may relate to early performance of the postrevascularization scan. Similarly, revascularization that does not lead to functional recovery at rest may improve contractile reserve or function at peak stress.

Comparison with Other Approaches for the Detection of Myocardial Viability

There are four alternative techniques to contractile reserve for the assessment of myocardial viability;

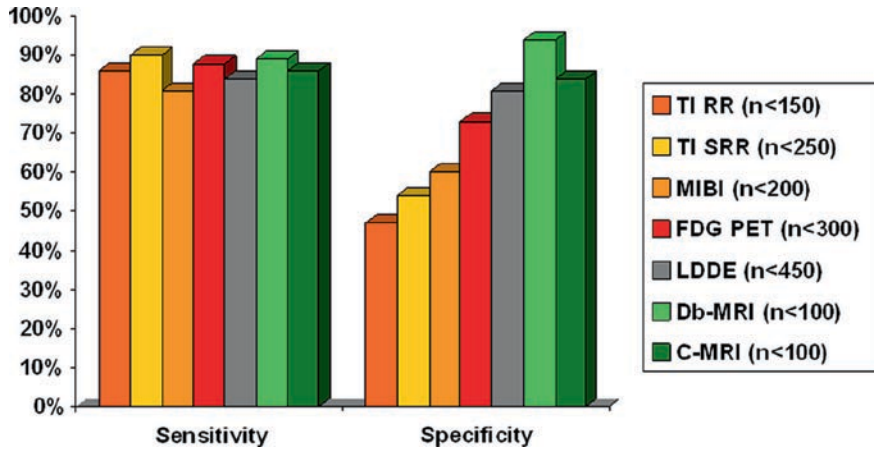

Fig. 16.13 Accuracy of different approaches for diagnosis of viability (modified from ref. 11)

metabolic approaches (SPECT or PET), cell membrane integrity (thallium) perfusion assessment (SPECT or contrast echo), and assessment of the extent of scar (contrast-enhanced MRI). The different modalities that assess these parameters have been compared in a meta-analysis, summarized in Fig. 16.13.

The number of possible tests for the identification of viability is bewildering. In general terms, the most appropriate test for patients after myocardial infarction is one that is able to detect heterozonal ischemia, peri-infarct ischemia, and viable myocardium. The following guidelines have previously been proposed[8]

1. The "local" best test should be chosen; both nuclear and echocardiographic techniques effectively identify regional and global functional recovery, as well as identifying patients at risk of major events
2. There may be some benefit in using resting thallium or sestamibi imaging to define viability in the unstable patient
3. Perfusion-based studies (SPECT or contrast echo) are sensitive and best used when the clinician has a high level of preparedness to proceed to revascularization

Perhaps the most important message, however, is to keep the presence and extent of viability in the context of a number of other clinical and angiographic parameters that determine the results of revascularization – including angina, ventricular size, infarct size, comorbid diseases of the LV, adequacy of adequate target vessels for bypass and collateral vessels.

Prognostic Value of Stress Echocardiography

The main determinants of risk in patients with coronary artery disease are the severity of LV dysfunction and the extent of myocardial ischemia. The standard approach to gathering these data for clinical decision making is based upon the extent of coronary disease and severity of LV dysfunction at coronary angiography and left ventriculography – the detection of three-vessel or left main coronary disease identifies subgroups with 5-year mortalities of 15 or 43%. Nonetheless, the reason why the number of stenosed coronary vessels carry prognostic significance is because of the extent of myocardial ischemia, which may be identified by stress echo or other noninvasive techniques. Especially in those who have limited symptoms or who are controlled on medical therapy, a valuable use of stress echo is therefore in the risk stratification of patients: intervention cannot be justified on prognostic grounds if the expected mortality is <1% per year.[9] For example, in chronic stable angina, the overall risk of a major event is 4%. Clinical data (pertaining to age, the severity of angina, a history of diabetes, hypertension or prior infarction, and resting ST segment depression) may be used to identify subgroups at higher and lower risk, and stress testing may be used to further substratify the groups.

Significance of a Negative Stress Echocardiogram

Patients with normal exercise or pharmacologic stress echocardiograms have a benign prognosis over several years of follow-up Table 16.7. The yearly mortality of these patients is <1%, confirming that their prognosis could not be improved by intervention. As always, no finding in isolation is reliable, and some patients with a negative stress echo have a higher risk of cardiac events. There are three major groups: first, those at higher risk on clinical grounds (older patients and those with diabetes mellitus or left ventricular hypertrophy), those in whom the negative test result is obtained at submaximal exercise (<85% age-predicted maximum heart-rate or <6 METS – reflecting that the heart was insufficiently stressed to become ischemic), and those in whom a wall motion abnormality may have been missed (e.g., patients having angina in the absence of identifiable wall motion abnormalities). A points score has been created to identify the likelihood of a stress echo result producing a misleading prognosis.

Significance of a Positive Stress Echocardiogram

Both death and cardiac events are predicted by the presence of ischemia, scar, or both at either exercise or dobutamine echocardiography. These echo data are both independent predictors of outcome and also incremental to other data. Nonetheless, the overall event rate in the presence of a positive test is <20%, and therefore positive results need to be substratified on the basis of clinical risk, extent and severity of ischemia and the extent of infarction, ischemic threshold, and the remainder of the stress testing data. Most important in this respect is the Duke treadmill score; the prognostic value of echo data is limited in patients with low-risk and high-risk scores, but intermediate-risk patients, who account for 40–50% of patients in most series, may be substratified by stress-imaging studies. In these patients, those with a negative or weakly positive test can be managed medically, while those with wall motion abnormalities in multiple vascular territories have an event rate similar to the high-risk patients and justify further investigation and intervention.

Prognostic Assessment After Myocardial Infarction

Although the interventional treatment of infarction has become progressively more aggressive in the acute stage or in patients with unstable coronary syndromes, there is currently no consensus regarding the superiority of an angiographic or a noninvasive approach in the stable post-Q wave infarction patient. Despite a frequent desire to define the coronary anatomy, this is not a powerful predictor of outcome (apart from in the highest-risk patients such as 3-vessel or left main disease) and provides only inferential information about the extent of ischemic burden or residual viable myocardium. The alternative is a stepwise approach, whereby the two goals of noninvasive testing are the identification of patients at low risk for recurrent events (a group in whom further testing is unnecessary), and the recognition of patients who are at high risk for recurrent cardiac events (in whom intervention should be focused with the goal of avoiding these events).[8]

This predictive process is based upon not just noninvasive but also demographic, clinical, and anatomic features:

1. Baseline demographic and clinical variables such as advanced age, female sex, prior medical history, including previous MI, and the presence of cardiovascular risk factors, particularly diabetes and hypertension
2. Clinical variables early in the course of the MI, such as tachycardia, hypotension, Killip class, site (anterior

Table 16.7 Meta-analysis of studies examining the prognostic implications of a negative stress echocardiogram[14]

Stress	*n*	F/U (m)	Death (%/year)	Hard events (%/year)	Total events (%/year)
Dipyridamole	1,109	33	0.2	0.9	2.5
Dobutamine	2,265	26	0.7	1.4	3.0
Exercise	3,425	26	0.2	0.5	1.3
Total	6,799	27	0.3	0.9	2.1

vs. other), type (Q wave vs. non-Q wave) and size of infarction, and ventricular arrhythmias
3. Functional indices including resting left ventricular function, exercise capacity, and the presence of spontaneous or inducible ischemia
4. Severity of coronary disease determined at contrast cineangiography

Both the extent of left ventricular damage (on the resting images) and the extent of jeopardized myocardium (on stress images) may be obtained by stress echocardiography. The selection of exercise echocardiography allows the detection of echocardiographic evidence of ischemia to complement prognostic information obtained from resting functional indices (e.g., ejection fraction), together with exercise capacity and ST segment analyses, and exercise testing is useful in reassuring patients about their ability to resume usual activities after myocardial infarction. However, pharmacologic stress techniques have been more extensively studied in the postinfarction population, because tests can be performed earlier and offer viability data. In the landmark Echo Persantine Italian Co-operative (EPIC) multicenter study of 925 patients, the mortality of patients with a negative study was only 2%, compared with only 7% of subjects with a positive test result at low dose. Likewise, the Echo Dobutamine International Co-operative (EDIC) study showed that cardiac death and major events were independently predicted by peak wall motion score index.

The relative roles of the stress echocardiogram and exercise ECG in the post-infarct patient are disputed. Some authors argue that because the negative predictive value of ExECG for mortality is comparable to that of a negative dipyridamole echo (2% vs. 1.6%), the standard stress test should be the initial step, with stress echocardiography used for risk stratification of positive stress tests. Others (including this author) favor replacing the exercise test because of its lower feasibility, limited prognostic power, and inability to identify the culprit vessel as well as viability.

Prediction of Perioperative Cardiac Risk in Patients Undergoing Major Noncardiac Surgery

The increasing prevalence of cardiac problems and the aging of the population have led cardiac complications of surgery to become a major cause of perioperative mortality and morbidity. As in other situations of risk evaluation, the first step should be a clinical evaluation of risk level – based on the nature of surgery and the cardiac history. Patients undergoing minor surgery or without clinical markers of risk (angina, past infarction, heart failure, diabetes, renal impairment, advanced age) are unlikely to have a cardiac complication and do not require stress echocardiography. In those that require stress echo, the predictive value of a negative test is >95%, implying that an at-risk patient with a negative test does not require further investigation. As in other situations, the degree of risk associated with a positive test should be substratified on the basis of clinical risk status and ischemic threshold (Fig. 16.14).

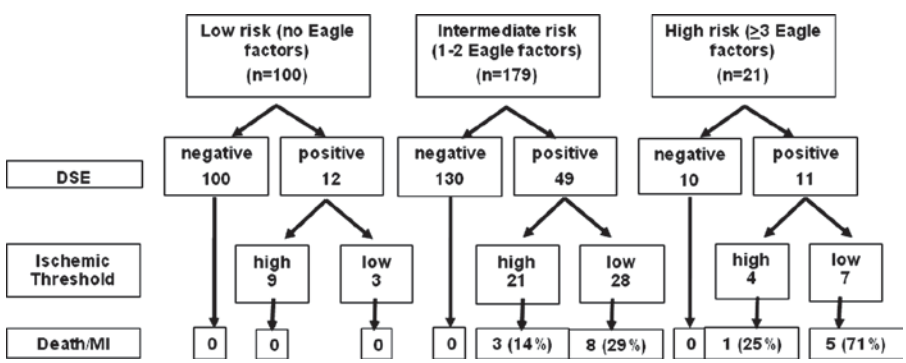

Fig. 16.14 Stepwise approach to risk stratification of patients undergoing vascular surgery (adapted from ref. 12). Patients with low clinical risk (i.e., no Eagle factors) have a low prevalence of ischemia, and none in this study had events. Those at intermediate and high risk with a negative scan have a low risk of events. Those with positive tests may be substratified based on the number of risk factors and ischemic threshold into groups having risks of from 14 to 71%

Use of Stress Echocardiography in Noncoronary Heart Disease

The findings of resting echocardiography may not explain the occurrence of exertional symptoms in patients with not only coronary but also noncoronary heart disease. In these situations, exercise echocardiography testing is the most physiologic means of gathering these data.

Stress Echo in Valvular Heart Disease

Assessment during stress may elucidate the cause of symptoms in patients with marked symptoms but only apparently moderate stenosis, or those with intermittent symptoms (e.g., ischemic mitral regurgitation or intermittent valve prolapse.

The principal indications for stress echo in aortic stenosis are asymptomatic individuals with severe stenosis and those with low gradients. The former may simply reflect inactivity, and a simple stress test (with careful monitoring) may be sufficient to quantify the real exercise capacity and symptom status. The second situation is perhaps more difficult – such patients have thickened aortic valves with severe left ventricular dysfunction, and it is unclear whether reduced valve excursion reflects reduced LV ejection or reduced function is due to severe aortic stenosis. The resting aortic valve area is of value; a valve area of <0.6 cm^2, typically associated with a mean gradient of >30 mmHg, usually signifies significant aortic stenosis.[10] However, if the distinction is unclear, the response to low doses of dobutamine may elucidate the mechanism. First, failure to improve LV function with dobutamine portends an adverse outcome. If the LV improves, an increment of gradient and fixed valve area suggests the underlying cause to be aortic stenosis. Improvement of valve area suggests that the valve is opening more because the ventricle is now pushing harder – although whether such individuals should forego surgery is debated, it is less likely to have a favorable effect than in the patients with a gradient response.

Exercise echocardiography may be of benefit in patients with apparently mild mitral stenosis at rest, who exhibit significant exertional symptoms. When this is performed, the most important parameter is tricuspid regurgitant severity and velocity, with some additional information from the increase in mitral gradient during exercise testing.

In healthy patients with mitral regurgitation and an obviously repairable mitral valve, early operation is probably the most reliable means of avoiding the development of LV dysfunction. Likewise, asymptomatic patients who are suitable for surgery should clearly proceed if the preoperative ejection fraction is <55%, as a delay will risk a further deterioration of postoperative function. However, in patients where the valve is nonrepairable or may not be repairable, or when there is concurrent disease that would increase the risk of surgery, further evaluation of risk and benefit may be of value. The rationale behind the use of stress echocardiography for assessment of regurgitant valve lesions is to examine LV contractile reserve. This may facilitate the early detection of LV decompensation and justify intervention before either symptoms or overt LV dysfunction are apparent. Indeed, the most accurate variables for prediction of postoperative LV dysfunction are exercise end-systolic volume index > 27 ml/m^2, ejection fraction <68%, or change of ejection fraction with exercise <5%. The identification of preserved contractile reserve has been associated with favorable outcome in both aortic and mitral regurgitation.

Conclusions

Stress echocardiography now has an established role as an accurate and cost-effective approach to the diagnosis and risk assessment of CAD, viability and noncoronary heart disease. Its biggest problem relates to lack of automation and the need for training, for which there may be a technical solution.

References

1. Porter TR, Kricsfeld A, Deligonul U, Xie F. Detection of regional perfusion abnormalities during adenosine stress echocardiography with intravenous perfluorocarbon-exposed sonicated dextrose albumin. *Am Heart J.* 1996;132:41–47.
2. Nishimura RA, Reeder GS, Miller FA, et al. Prognostic value of predischarge 2-dimensional echocardiogram after acute myocardial infarction. *Am J Cardiol.* 1984;53:429–432.

3. Hoffmann R, Lethen H, Marwick T, et al. Standardized guidelines for the interpretation of dobutamine echocardiography reduce interinstitutional variance in interpretation. *Am J Cardiol.* 1998;82:1520–5124.
4. Picano E, Lattanzi F, Orlandini A, Marini C, L'Abbate A. Stress echocardiography and the human factor: the importance of being expert. *J Am Coll Cardiol.* 1991;17:666–669.
5. Hoffmann R, Lethen H, Marwick T, et al. Analysis of interinstitutional observer agreement in interpretation of dobutamine stress echocardiograms. *J Am Coll Cardiol.* 1996;27:330–336.
6. Hoffmann R, Lethen H, Marwick T, et al. Standardized guidelines for the interpretation of dobutamine echocardiography reduce interinstitutional variance in interpretation. *Am J Cardiol.* 1998;82:1520–1524.
7. Fleischmann KE, Hunink MG, Kuntz KM, Douglas PS. Exercise echocardiography or exercise SPECT imaging? A meta-analysis of diagnostic test performance. *JAMA* 1998;280:913–920.
8. Marwick TH. Stress Echocardiography. Dordrecht: Kluwer, 2003.
9. Gibbons RJ, Chatterjee K, Daley J, et al. ACC/AHA/ACP-ASIM guidelines for the management of patients with chronic stable angina: a report of the American College of Cardiology/American Heart Association Task Force on Practice Guidelines (Committee on Management of Patients With Chronic Stable Angina). *J Am Coll Cardiol.* 1999;33:2092–2197.
10. Schwammenthal E, Vered Z, Rabinowitz B, Kaplinsky E, Feinberg MS. Stress echocardiography beyond coronary artery disease. *Eur Heart J.* 1997;18(suppl D):D130–D137.
11. Bax JJ. J Am Coll Cardiol. 1995
12. Poldermans, et al. *J Am Coll Cardiol.* 1995
13. Topol. *Textbook of Cardiovascular Medicine*. 2nd ed. Baltimore, MD: Lippincott Williams and Wilkins; 2002
14. Geleijnse M, AHA abstracts 2000

Chapter 17
Principles of Myocardial Viability Implications for Echocardiography

Jean-Louis J. Vanoverschelde, Agnès Pasquet, Bernhard Gerber, and Jacques A. Melin

Introduction

Each year, 400,000 new cases of congestive heart failure are diagnosed in the United States. Despite cardiac transplantation being the most efficacious treatment for end-stage heart failure, <1% of all heart failure patients eventually benefit from this procedure, mostly because of the limited donor heart availability. Cardiac transplantation is therefore not a realistic solution for the majority of patients with congestive heart failure, especially for the elderly. Coronary revascularization procedures, however, are commonly performed and not subject to similar limitations. As a result of improved anesthetic, surgical, and myocardial protection techniques, the surgical risks of performing coronary artery bypass graft (CABG) in these patients with heart failure have decreased significantly from 11 to16%, to <6%. Myocardial revascularization has subsequently become a valid treatment option in selected patients with observed survival benefits compared to medical therapy, and in some cases, improvement in symptoms and functional status.

Revascularization of chronically but reversibly dysfunctional myocardium, often referred to as "hibernating" or "viable," has emerged as an important alternative in the treatment of heart failure secondary to coronary artery disease. Obsevational studies have indeed suggested that, compared to patients with large areas of non viable myocardium, patients with ischemic left ventricular dysfunction and a significant amount of viable myocardium identified by various non-invasive imaging modalities have:

- Lower rates of perioperative mortality,
- Greater improvements in regional and global left ventricular function,
- Fewer heart failure symptoms, and
- Improved long-term survival after revascularization

It is the purpose of this chapter to review the more recent advances to the understanding of the pathophysiology of chronically dysfunctional but viable myocardium and its implications for detection of myocardial viability using echocardiography.

Historical Perspective

- The spectrum of left ventricular (LV) dysfunction caused by atherosclerotic coronary artery disease has expanded over the last quarter of the twentieth century. Traditionally, it was assumed that heart failure arose from either reversible ischemia (anginal equivalent) or irreversible myocardial infarction. Insights gained from more recent functional, metabolic, and morphological studies have led to the concept of dysfunctional but viable myocardium (stunned and hibernating) and to that of ventricular remodeling.
- The possible discordance between wall motion abnormalities and histopathological findings has been recognized clinically since the early 1970s.
  - Chatterjee et al were the first to report on improved regional myocardial wall motion abnormalities in the absence of myocardial scarring.
  - In 1974, Horn et al demonstrated improved regional wall motion with epinephrine infusion

J.-L.J. Vanoverschelde(✉), A. Pasquet, B. Gerber, and J.A. Melin
Division of Cardiology, Cliniques Universitaires St Luc, 1200, Brussels, Belgium
e-mail: vanoverschelde@card.ucl.ac.be

P. Nihoyannopoulos and J. Kisslo (eds.), *Echocardiography*,
DOI: 10.1007/978-1-84882-293-1_17,

in patients with coronary artery disease and chronic asynergy.
- In 1978, Diamond et al suggested that ischemic noninfarcted myocardium could exist in a state of functional hibernation.
- In the mid-1980s, Rahimtoola used the term "myocardial hibernation" to describe a state of diminished resting ventricular function in the setting of coronary artery disease, which occurs in at least a third of coronary patients. He proposed that myocardial hibernation develops as a protective mechanism wherein persistent myocardial hypoperfusion in the absence of myocardial necrosis leads to downregulation of myocardial contractility.
- The term "perfusion-contraction matching" was subsequently coined by John Ross to characterize the adaptive response of the hibernating myocardium to diminished perfusion.

- The concept of evaluating perfusion and contraction simultaneously to characterize the mechanisms underlying contractile dysfunction has fostered considerable research interests and stimulated the use of perfusion imaging, not only to address basic pathophysiological mechanisms but also to detect viable myocardium clinically in coronary patients.

Pathophysiology

Observations in Humans with Chronic Reversible Ischemic Dysfunction

- *Perfusion-contraction matching*. Assessment of perfusion-contraction matching in patients with chronic LV ischemic dysfunction requires the ability to measure regional myocardial blood flow in absolute terms and to correlate these findings with data on regional myocardial function, acquired simultaneously. In routine clinical practice, this has become possible with the advent of positron emission tomography (PET) and the use of either ^{13}N-ammonia or ^{15}O-water as flow tracers. PET is a truly quantitative method. It has a good spatial resolution; it allows for accurate correction of photon attenuation and, to some extent, of partial volume effects; and finally, when mathematically and physiologically appropriate models are used to describe the biological behavior of the radiotracers in blood and myocardium, it allows for computation of quantitative estimates of regional myocardial perfusion.

Resting PET flow measurements obtained in chronically dysfunctional but viable myocardium are summarized in Fig. 17.1. Transmural blood flow to dysfunctional but viable segments is remarkably variable; one half of the segments shows reduced perfusion, as predicted by Rahimtoola, whereas the other half displays only minor and often no reduction in transmural myocardial blood flow.

- *Myocardial flow reserve*. Irrespective of resting flow, perfusion reserve is always reduced in dysfunctional but viable myocardium, albeit more severely in segments with low rest perfusion than in those with normal rest perfusion. The severity of flow reserve reduction directly impacts on the ability of dysfunctional but viable myocardium to improve in contraction upon inotropic stimulation, as this requires increases myocardial blood flow and oxygen consumption (vide infra).

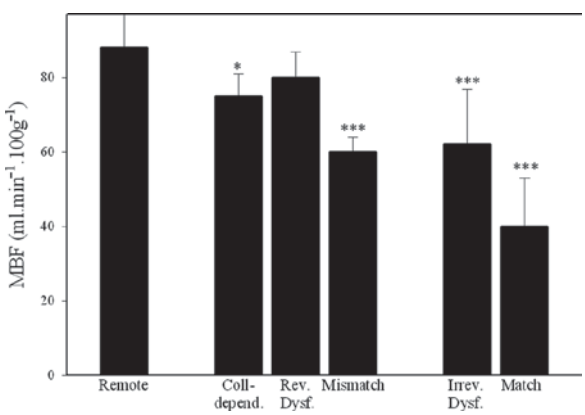

Fig. 17.1 Bar graph of rest myocardial blood flow (MBF) measured with ^{13}N-ammonia or ^{15}O-water in remote, noninfarcted collateral-dependent (Coll-dep.), reversibly dysfunctional (Rev. Dysf.), irreversibly dysfunctional (Irrev. Dysf.), PET flow-metabolism mismatch and PET flow-metabolism match segments of patients with chronic left ventricular ischemic dysfunction. *$p < 0.05$, ***$p < 0.001$ vs. remote segments. Reproduced with permission from Vanoverschelde J-L and Melin JA. The pathophysiology of myocardial hibernation. Current controversies and future directions. *Prog Cardiovasc Dis.* 2001;43:387-398

- *Inotropic reserve*. Dysfunctional but viable myocardium often has the capacity to improve function when challenged by an inotropic stimulus, such as postextrasystolic potentiation or the infusion of catecholamines. However, the response of viable segments to these stimuli greatly varies from segment to segment as well as with the intensity and the duration of stimulation.

Most viable segments exhibit a biphasic response when challenged by increasing levels of inotropic stimulation. At low levels and provided that sufficient residual flow reserve is present (vide infra), systolic wall thickening usually increases and starts earlier in systole. At higher levels, when the increased in demand cannot be matched anymore by a further increase in myocardial blood flow because of the underlying coronary disease, systolic function deteriorates back and can even become worse than at baseline. The observation of this peculiar biphasic pattern is extremely important to rule out other causes of regional dysfunction such as the presence of a subendocardial scar or the overall process of remodeling that accompanies left ventricular dilatation. In contrast to truly viable segments, segments affected by one of these two entities indeed usually display a sustained contractile response at both low and high levels of inotropic stimulation.

It is important to remember that not every viable segment improves during inotropic stimulation, and that about 25% of "metabolically" viable segments, i.e., those with preserved energy metabolism, exhibit no response to an inotropic challenge. Compared to viable segments with recruitable inotropic reserve, those lacking contractile reserve usually have a lower resting myocardial blood flow and take up more glucose under fasting conditions than normal segments or viable segments with recruitable inotropic reserve, a finding which is consistent with either ongoing or impending myocardial ischemia, and thus with a severely blunted myocardial flow reserve. This hypothesis is further supported by the results of several animal and human studies that have shown that improvements in mechanical function during inotropic stimulation are always attended by similar directional changes in myocardial blood flow and oxygen consumption. This implies that sufficient residual flow reserve must be present for the expression of a positive contractile response during inotropic stimulation

There certainly are other factors that contribute to the lack of inotropic reserve in otherwise viable myocardium. Preliminary data suggest that the severity of the structural changes affecting cardiomyocytes may also impact on the ability of viable myocardium to respond to an inotropic stimulus. In a recent study, the likelihood of a positive inotropic response to dobutamine was found to be inversely proportional to the mass of residual myocytes showing severe myofibrillar loss. There is also evidence that downregulation of β-adrenoreceptors in viable segments contributes to decrease to likelihood to unmask residual inotropic reserve.

- *Structural modifications*. Besides the changes in resting myocardial blood flow and flow reserve, several structural alterations that affect the microcirculation, the cardiomyocytes, and the extracellular matrix have described in dysfunctional but viable segments. Most of the available information on these structural changes has been gathered from studies in which human myocardial biopsy specimens were harvested at the time of bypass surgery.

1. *Microcirculation*. In general, histological analysis of human dysfunctional myocardium has demonstrated that the microvasculature was better preserved in the segments that will ultimately improve function after revascularization than in those that will not (Fig. 17.2). This is particularly true for the capillaries whose density and cross sectional area are usually within the normal range in reversibly dysfunctional segments. By contrast, there is a much greater heterogeneity among the segments that do not recover after revascularization; approximately half of them showing significant capillary rarefaction whereas the other half show no or minimal changes. As expected, the major determinant of capillary density appears to be the severity of interstitial fibrosis.
2. *Myocyte alterations*. The primary alterations include depletion of contractile elements. In some cells, this is limited to the vicinity of the nucleus, whereas in others it is very extended, leaving only few or no sarcomeres at the cell periphery. Myofibrillar loss is not accompanied by major cell volume changes, which is clearly different from atrophic degeneration. The space previously occupied by the myofilaments is filled with an amorphous, strongly PAS-positive material, typical of glycogen (Fig. 17.3). At the ultrastructural level, adaptive rather than degenerative ischemic changes are observed:

   – The number of mitochondria is increased and display alterations in size and shape. They are

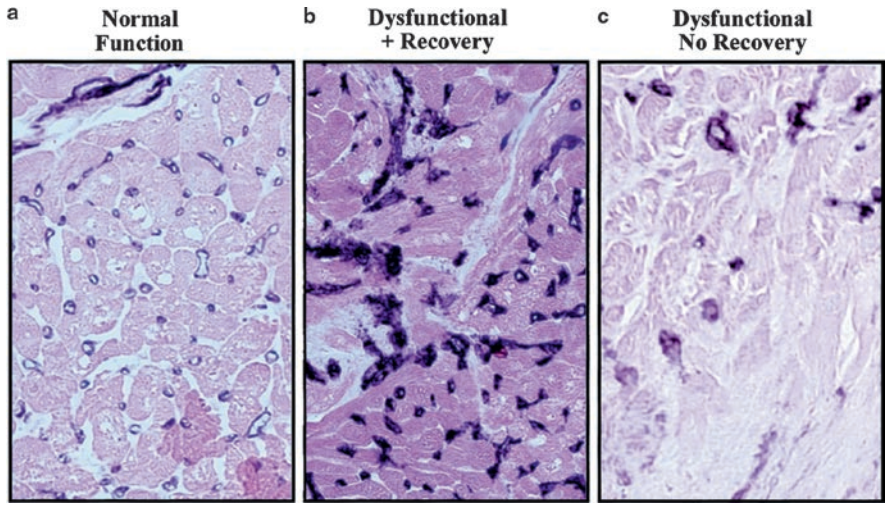

Fig. 17.2 Biopsy specimens from three different segments with CD31 staining. (**a**) In a segment with normal resting function, the microcirculation is preserved. (**b**) In a dysfunctional segment that improved after revascularization, the microvascular density is normal. (**c**) Low capillary density and significant fibrosis are seen in a dysfunctional segment that did not recover function. Reproduced with permission from Shimoni et al. Microvascular structural correlates of myocardial contrast echocardiography in patients with coronary artery disease and left ventricular dysfunction. Implications for the assessment of myocardial hibernation. *Circulation*. 2002; 106:950-956

unevenly distributed within the cytoplasm. Most appear doughnut shaped and show loss of contact sites between inner and outer mitochondrial membranes or decreased numbers of cristae.

- Nuclear alterations range from irregular tortuous nuclear outlines, with even distribution of heterochromatin over the nucleoplasm, to chromatin clumping near the nuclear membrane and throughout the whole nucleoplasm.
- Loss of sarcoplasmic reticulum, T-tubules, and sarcomeres but increased endoplasmic reticulum provides additional support for an adaptive phenomenon.
- The contractile protein myosin, the thin filament complex, titin, and a-actinin are reduced and the distribution of titin within the cardiomyocyte is altered.
- Cytoskeletal proteins such as desmin, tubulin, and vinculin are disorganized.
- The expression of connexin-43, a major gap junction protein, and that of nuclear A-type lamins is also reduced.
- From a biochemical point of view, tissue content of ATP, total adenine nucleotides, and phosphocreatine usual remain nearly normal, and mitochondrial function, as reflected by the ADP/ATP and PCr/ATP ratios, also remains nearly intact.

3. *Extracellular matrix*. The interstitial alterations consist in increased amounts of collagen deposition. Within the widened interstitium are variable numbers of fibroblasts and macrophages, and scant increased amounts of elastic fibers. Importantly, acute ischemic changes such as endothelial swelling of the microvasculature are absent. Given their severity, the structural changes that affect dysfunctional but viable myocardium impact on its ability to respond to an inotropic stimulus and on the speed at which it may or may not recover after revascularization. Segments with less fibrosis or with less severe cardiomyocyte alteration and remodeling are more likely to improve function following the administration of dobutamine or after revascularization.

It has been suggested that the structural changes occurring in hibernating myocardium are the consequence of a dedifferentiation process. The hibernating cardiomyocytes show many features of neonatal cardiomyocytes, including:

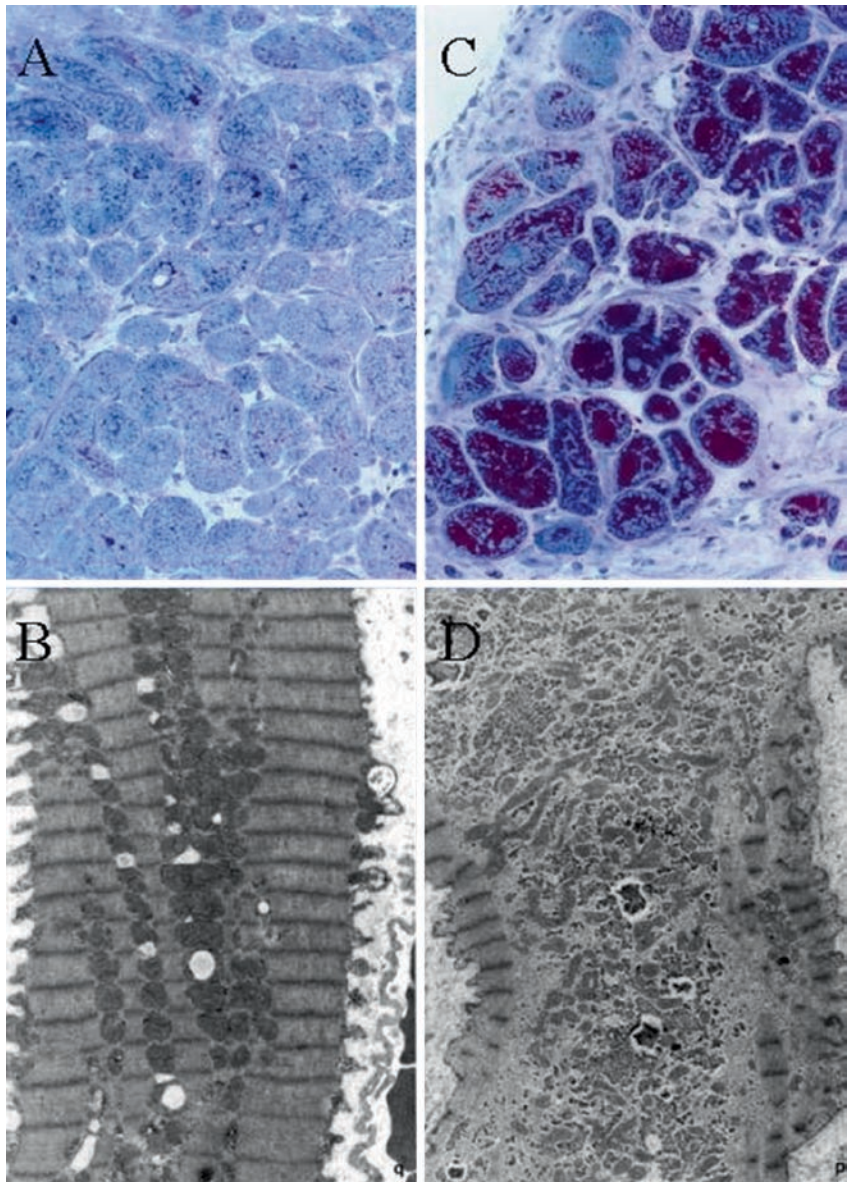

Fig. 17.3 (**a**) Light micrograph of myocardium showing normal cardiomyocytes with virtually no glycogen (PAS staining in *red*). (**b**) Transmission electron micrograph of a normal cardiac myocyte. (**c**) Representative light micrograph of a biopsy sample of human hibernating myocardium. Cardiac myocytes are depleted of their contractile material and filled with glycogen (PAS positive staining). (**d**) Representative transmission electron micrograph of a hibernating cardiomyocyte. The myolytic cytoplasm is devoid of sarcomeres and filled with glycogen. Magnification: (**a**, **c**) ×320; (**b**) ×7, 100; (**d**) ×7,500. Reproduced with permission from Vanoverschelde J-L et al. Chronic myocardial hibernation in humans. From bedside to bench. *Circulation.* 1997;95:1961-1971

1. Depletion of contractile filaments,
2. Presence of rough sarcoplasmic reticulum,
3. Accumulation of glycogen,
4. Occurrence of irregularly shaped nuclei with peculiar distribution of chromatin,
5. Loss of organized sarcoplasmic reticulum,
6. Lack of T-tubules, and
7. Vesiculization of the sarcolemma.

Not all the characteristics of the altered cardiomyocytes resemble those of embryonic cells, however. For instance, the remaining sarcomeres in the altered cells often retain their orderly arrangement at the cell periphery, while they are randomly distributed in embryonic cells. Also, the amount of glycogen seen in altered cardiomyocytes far exceeds that reported in the embryo.

The hypothesis of dedifferentiation is further substantiated by immunohistological studies showing that hibernating cardiomyocytes re-express contractile proteins that are specific to the fetal heart, such as the a-smooth muscle actin, while at the same time, they exhibit the same organization of structural proteins like titin as developing cardiomyocytes. In addition, cardiotin, a recently described high molecular weight protein absent in fetal cells, is also absent from the altered cells. These findings reinforce the thesis that hibernating cardiomyocytes undergo partial dedifferentiation.

Insights Gained from Animal Models of Chronic Reversible Ischemic Dysfunction

Chronic coronary stenosis and progressive ameroid occlusion models have shed a new light on both the mechanisms and the temporal progression of reversible ischemic dysfunction. During the first few weeks after the onset of dysfunction, endocardial blood flow has consistently been found to be either normal or only marginally decreased. At that time, chronic myocardial stunning is thus the most likely mechanism for the observed dysfunction, a hypothesis which is further supported by the strong relation between the reduction in subendocardial flow reserve and the severity of dysfunction. With time and probably also increases in the physiological significance of the underlying coronary narrowings, some of the dysfunctional segments, which appeared "chronically stunned" on early examination, eventually become underperfused. The transition from chronic stunning to chronic hibernation occurs for threshold reductions in myocardial flow reserve. The critical nature of coronary flow reserve reduction required to produce hibernating myocardium likely explains why not all studies have demonstrated a progression to hibernating myocardium distal to a chronic stenosis. For example, circumflex ameroid models (rapidly progressing stenoses) in dogs usually display normal resting perfusion, with a well-developed collateral circulation; yet hibernating myocardium can develop when source collateral flow is limited. The experimental data thus suggest that chronic reversible myocardial ischemic dysfunction is a complex, progressive, and dynamic phenomenon, that is initiated by repeated episodes of ischemia, and in which resting perfusion, although initially preserved, may subsequently become reduced, probably in response to the decrease in myocyte energy demand. Indeed, the persistence of some degree of flow reserve, even when resting myocardial blood flow is reduced, suggests that the reduction in rest flow is somehow secondary to that in resting contractile function and could serve as a way to increase residual myocardial perfusion reserve.

Animal models have also improved our understanding of the morphological alterations seen in reversible ischemic dysfunction. Myofibrillar disassembly, myofibrillar loss, and increased glycogen content develop rapidly after a critical limitation in flow reserve. These changes seem to take place similarly in dysfunctional and in normally perfused remote regions of the dysfunctional hearts. Thus, the pathological changes described in humans with chronic but reversible dysfunction do not appear to reflect the chronicity of LV dysfunction nor do they appear to arise as a direct consequence of ischemia. The fact that myolysis occurs globally in ischemic cardiomyopathy raises the possibility that these morphological changes reflect a response to chronic elevations in preload or stretch.

The Physiological Spectrum of Myocardial Viability

There is a spectrum of myocardial dysfunction existing in patients with coronary disease (Table 17.1). The initial stages of dysfunction may correspond to chronic stunning and are characterized by normal resting perfusion but reduced flow reserve, mild myocyte alterations, maintained membrane integrity (allowing the transport of cations and metabolic fuels), preserved capacity to respond to an inotropic stimulus, and no or little tissue fibrosis (Fig. 17.4). Following revasculari zation, functional recovery is likely to be rapid and complete.

Table 17.1 The patterns of chronic ischemic dysfunction

	Rest flow	Flow reserve	Inotropic reserve	Metabolism	Structural changes	Reversibility
Chronic stunning	↔	↓	Yes	↔	No	Yes
Transition phase	↔	↓	Yes	↔	Mild dedifferentiation	Yes
Chronic hibernation	↓	↓↓	May be absent	↔	More severe dedifferentiation/fibrosis	Delayed/ incomplete
Infarction	↓	↓↓	No	↓	Fibrosis	No
Remodeling	↔	↔	May be absent	↔	Fibrosis	No

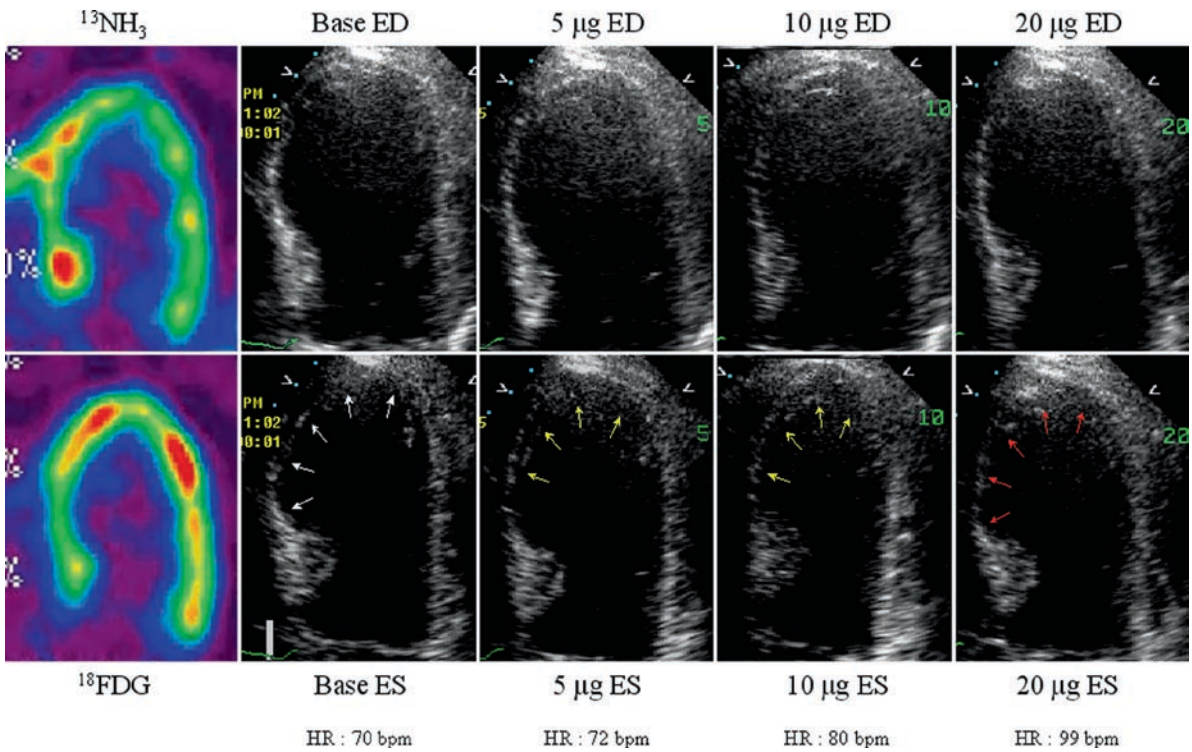

Fig. 17.4 Inotropic response to dobutamine in dysfunctional segments (*white arrows*) with normal rest flow ($^{13}NH_3$) and FDG uptake (^{18}FDG). The *upper row* shows images obtained from the apical four-chamber view in end-diastole at baseline and during the infusion of 5, 10, and 20 µg kg^{-1} min^{-1} of dobutamine. The *lower row* shows the corresponding end-systolic images. The *yellow arrows* indicate segments improving function, whereas *red arrows* indicate deteriorating segments. The sequence illustrates a typical biphasic response in the distal septum and the apex. Since blood flow and FDG uptake are normal in these segments, this is an example of chronically stunned myocardium

More advanced stages of dysfunction are probably associated with reduced rest perfusion, increased tissue fibrosis, perhaps more severe myocyte remodeling, and a decreased ability to respond to inotropic stimuli. Nonetheless, membrane function and energy metabolism long remain preserved (Figs. 17.5 and 17.6). Following revascularization, functional recovery, if any, is usually quite delayed and in the end mostly incomplete.

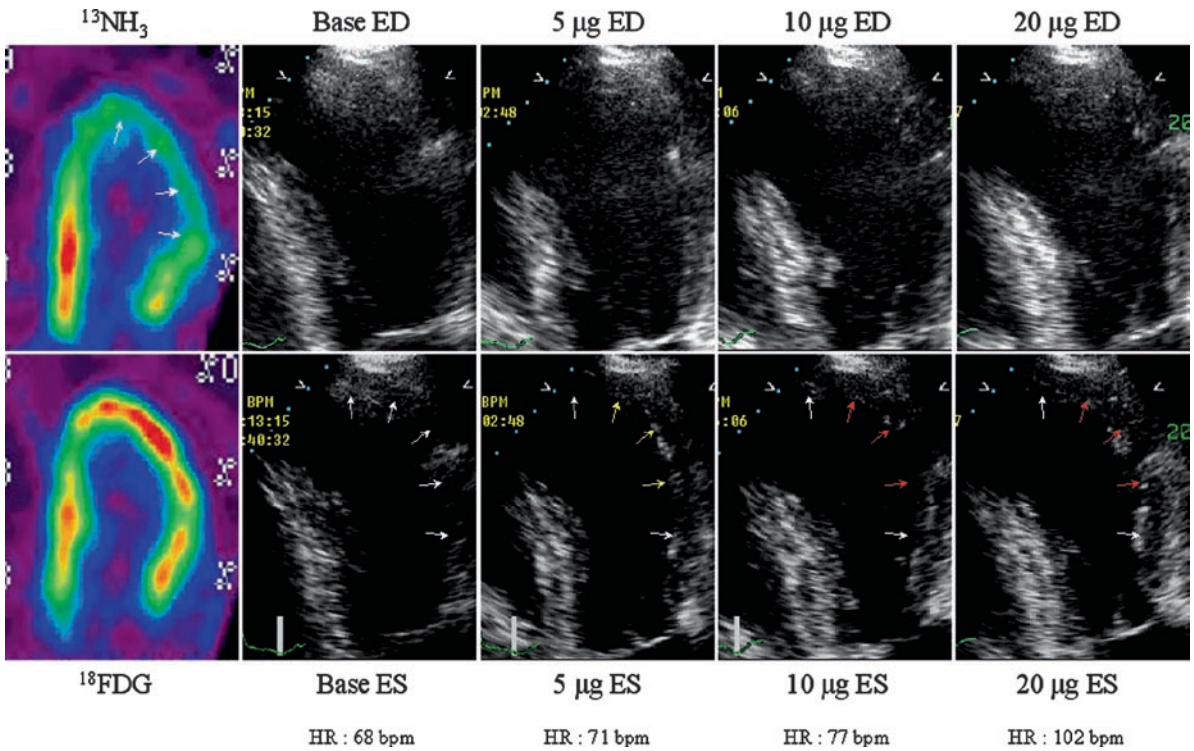

Fig. 17.5 Inotropic response to dobutamine in dysfunctional segments (*white arrows*) with mildly reduced rest flow ($^{13}NH_3$) and a normal FDG uptake (^{18}FDG). The *upper row* shows images obtained from the apical two-chamber view in end-diastole at baseline and during the infusion of 5, 10, and 20 µg kg^{-1} min^{-1} of dobutamine. The *lower row* shows the corresponding end-systolic images. The *yellow arrows* indicate segments improving function, whereas *red arrows* indicate deteriorating segments. The sequence illustrates a very transient biphasic response in the midanterior segment, followed by immediate deterioration at low heart rate. Since blood flow was slightly reduced and FDG uptake was normal in that segment, this is an example of mildly hibernating myocardium

Implications for the Clinical Identification of Viable Myocardium

Basic Principles for the Identification of Viable Myocardium (Table 17.2)

1. The most important determinant of the return of resting contractile function following revascularization is the severity of the underlying tissue fibrosis, whether interstitial or infarct related. Accordingly, methods that specifically assess the presence of tissue fibrosis, such as delayed enhancement Gadolinium magnetic resonance imaging, or its inverse, i.e., the mass of residual viable cardiomyocytes, such as thallium and metabolic imaging, should allow for a highly sensitive detection of myocardial viability.
2. The second most important determinant of functional recovery is the severity of the structural abnormalities affecting cardiomyocytes. When present, these structural alterations usually indicate a severe and long-lasting process. Reversibility, if any, will probably be incomplete and quite delayed. From an imaging point of view, the segments presenting with these alteration are quite easy to identify. Indeed, as any viable segment, they usually retain the ability to accumulate thallium or FDG. However, in contrast to viable segments lacking these alterations, they most often fail to respond to an inotropic stimulus.
3. Viable segments display a variety of perfusion patterns. During the early stages of the disease, rest flow is usually normal and perfusion reserve is reduced. The observation of a normal rest perfusion, by SPECT, PET, or myocardial contrast echocardiography, thus constitutes a strong argument in favor of myocardial

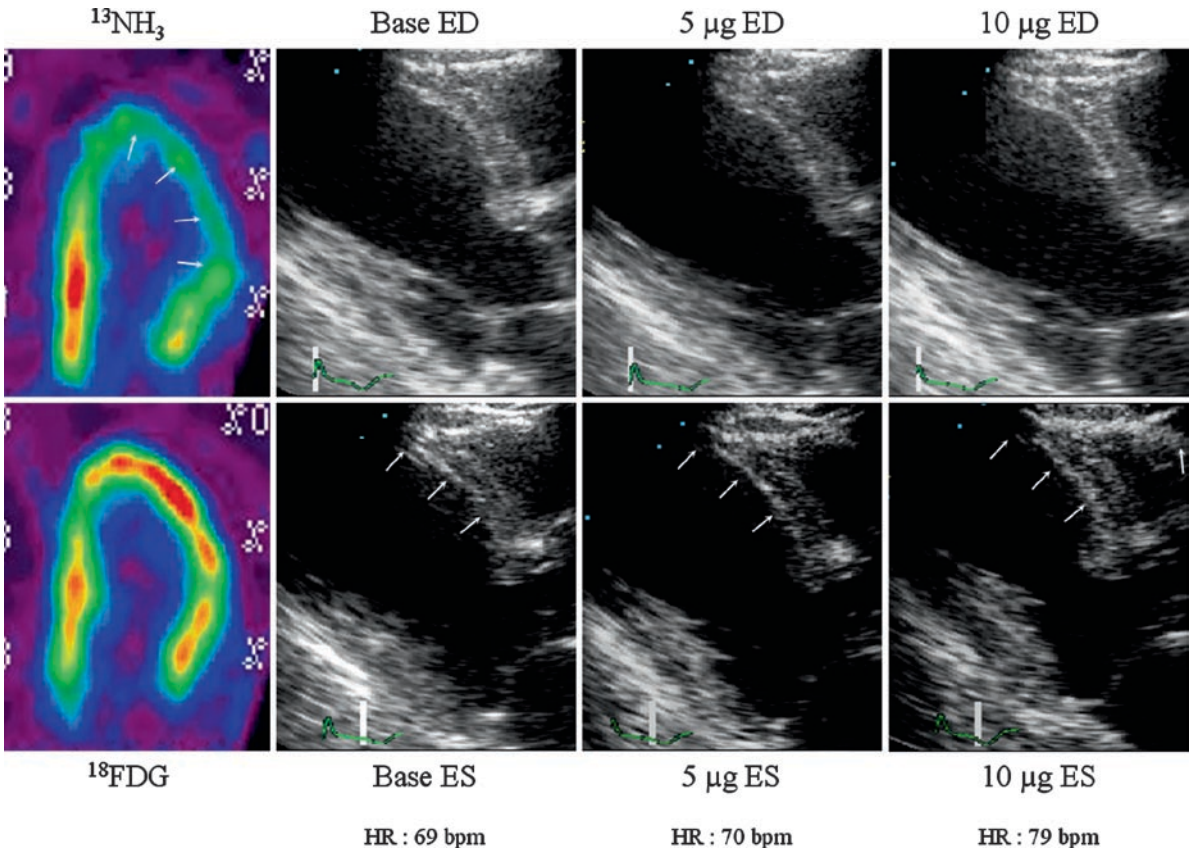

Fig. 17.6 Inotropic response to dobutamine in dysfunctional segments (*white arrows*) with moderately reduced rest flow ($^{13}NH_3$) and a normal FDG uptake (^{18}FDG). The *upper row* shows images obtained from the parasternal long-axis view in end-diastole at baseline and during the infusion of 5 and 10 µg kg^{-1} min^{-1} of dobutamine. The *lower row* shows the corresponding end-systolic images. The sequence illustrates the absence of inotropic reserve in the anteroseptal segment. Since blood flow was definitively reduced and FDG uptake was normal in that segment, this is an example of severely hibernating myocardium

Table 17.2 Main characteristics of viable myocardium

Mainly noninfarcted
Sufficient resting perfusion to
provide metabolic fuels
allow washout of metabolic byproducts
Maintained membrane integrity to
generate transmembrane ionic gradients
transport energy providing substrates
Preserved metabolic machinery for glucose, fatty acid, and O_2 consumption
Recruitable inotropic reserve

viability. However, in the absence of flow reserve measurements, it may be quite difficult to make the distinction between viable and remodeled myocardium. The mere presence of a normal rest flow is thus not sufficient to positively establish the diagnosis of myocardial viability. Similarly, a mildly reduced rest perfusion does not exclude the presence of residual viable myocardium. At the later stages of the disease, rest flow may indeed become slightly reduced. However, severe reductions in rest flow are not compatible with the presence of viable myocardium (Fig. 17.7). As viable segments with reduced rest flow rarely exhibit residual inotropic reserve, their identification probably requires some form of metabolic imaging.

The Working Hypothesis

– When flow, metabolic, and inotropic reserve imaging concur on the presence of residual viable myocardium, the likelihood of tissue fibrosis and myocyte

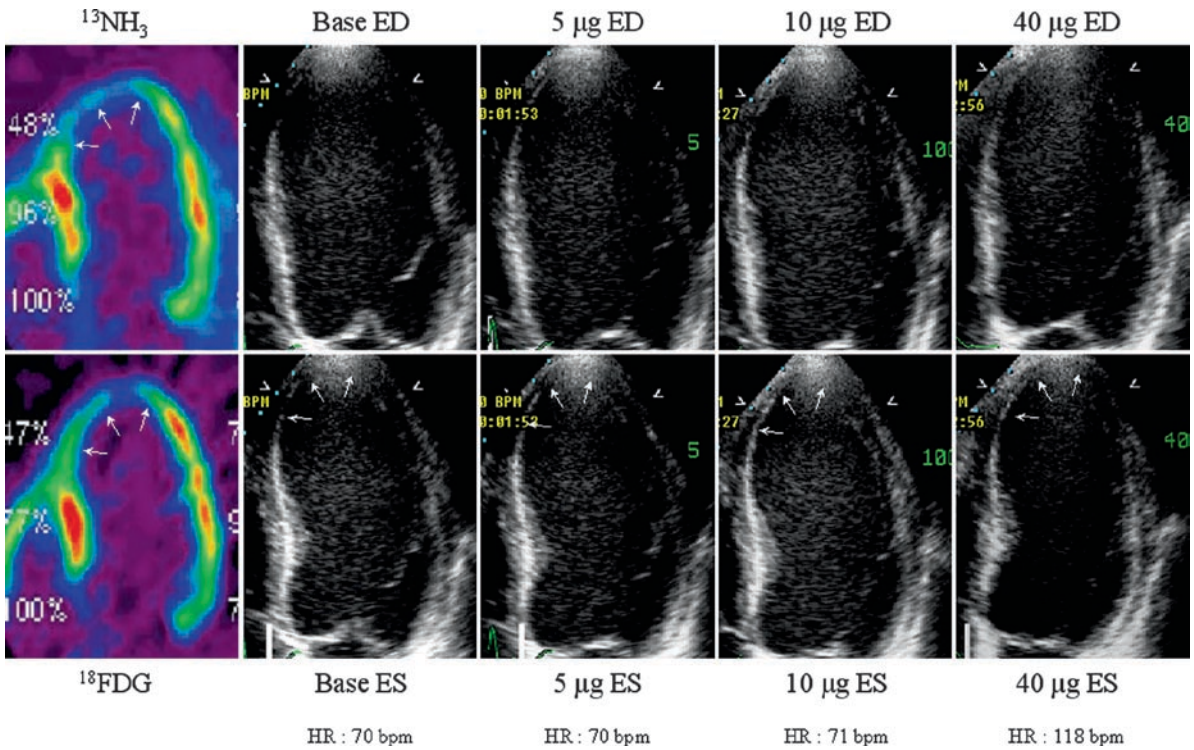

Fig. 17.7 Inotropic response to dobutamine in dysfunctional segments (*white arrows*) with severely reduced rest flow ($^{13}NH_3$) and FDG uptake (^{18}FDG). *The upper row* shows images obtained from the apical four-chamber view in end-diastole at baseline and during the infusion of 5, 10, and 40 μg kg^{-1} min^{-1} of dobutamine. The *lower row* shows the corresponding end-systolic images. The absence of inotropic reserve in the distal septum. Since both blood flow and FDG uptake were reduced in that segment, this is an example of irreversibly infarcted myocardium

structural alterations is small and the likelihood of functional recovery after successful revascularization is high;
- When flow, metabolic, and inotropic reserve imaging concur on the lack of residual viable myocardium, severe tissue fibrosis is probably present and revascularization is not likely to bring in any significant functional benefit or prognostic advantage;
- When metabolic imaging suggests the presence of viable myocardium but flow and/or inotropic reserve imaging does not, significant myocyte alterations, exhausted flow reserve or a combination of these factors are likely present. The recovery of resting contractile function following revascularization is uncertain, and, unfortunately, largely unpredictable. Based on previous studies, this particular viability pattern probably occurs in about 20–45% of "metabolically" viable segments and contribute to both the low specificity of the metabolic imaging approaches and the low sensitivity of the methods based on inotropic reserve.

Role of Echocardiography

How Echo Is Useful

Echocardiography is probably the most versatile cardiac imaging modality in our diagnostic armamentarium and is essential to the identification of myocardial viability:

- First, it readily identifies the core of the problem, i.e., the presence of regional wall motion abnormalities. It also allows to assess their extent and severity, both qualitatively and quantitatively.
- Second, it allows for the initial characterization of the dysfunctional segments, both in terms of residual wall thickness and tissue reflectivity. Segments thinner than 5 mm in diastole are frequently nonviable and those containing bright linear echoes, particularly in the subendocardium, are likely to be highly fibrotic.

– Third, when combined with the use of ultrasonic contrast agents, echocardiography permits the assessment and the quantification of myocardial blood flow, both at rest and during hyperhemia.
– Fourth, when performed during an inotropic challenge, such as the infusion of increasing doses of dobutamine, it allows for the evaluation of the presence of recruitable inotropic reserve.
– And last, it is the most frequently used technique to assess functional recovery after revascularization.

Echocardiography at Rest

- *Diastolic wall thickness* measured during resting echocardiography provides some information on the relative amounts of myocardial tissue versus fibrotic scar tissue within a particular myocardial segment. A diastolic wall thickness > 5 mm has a sensitivity of 100% but a specificity of only 28% for predicting recovery of contractility at 1 year following surgical revascularization. Reduced wall thickness, however, had a very high negative predictive value (97–100%), suggesting that if the diastolic wall thickness is <5 mm, additional testing and revascularization may not be indicated. The appeal of this method is obvious, as rest echocardiography is readily available and relatively inexpensive when compared with alternative techniques of assessing myocardial viability. However, it is limited by its poor specificity and the variability in the image quality which affects the accuracy and reproducibility of wall thickness measurements, as well as by the relatively small number of segments exhibiting reduced thickness (<15–20%). Yet, the high negative predictive value of a thinned segment confirms the long-standing clinical impression regarding the poor likelihood of recovery of contractility in scarred and thinned walls.
- *Ultrasonic tissue characterization* is another approach that can define the physical state of the myocardium and can therefore complement the assessment of LV function and chamber dimensions by rest 2-dimensional echocardiography. The baseline assumption underlying the use of ultrasonic tissue characterization is that pathological changes affecting the myocardium, including ischemia, result in alterations of its fundamental physical properties that can be detected using ultrasonic-integrated backscatter imaging. Experimental studies have indicated that physiologic myocardial contraction and relaxation were paralleled by a cardiac cycle-dependent variation of integrated backscatter that reflects regional, intramural contractile performance. Cyclic variations of the backscatter signal are blunted during experimental myocardial ischemia and recover more quickly than does systolic wall thickening with reperfusion. Studies in humans with reperfused myocardial infarction have shown that assessment of cardiac cycle-dependent variations of integrated backscatter allowed accurate delineation of reversible (stunning) from irreversible (infarction) tissue injury, thus providing a potentially useful adjunct for the noninvasive evaluation of regional contractile function and for the detection of potentially viable myocardium. Similar findings were recently made in patients with chronic left ventricular dysfunction (Fig. 17.8). In one study, the persistence of cardiac cycle-dependent variation of integrated backscatter was found to correlate with the presence of recruitable inotropic reserve. Assessment of ultrasonic tissue characterization may thus provide a simple measure

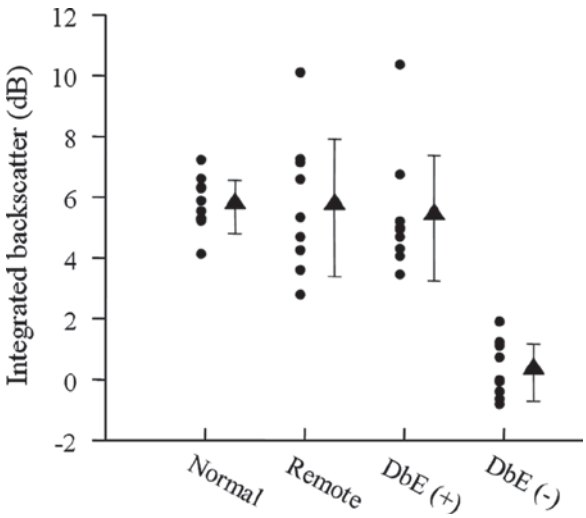

Fig. 17.8 Individual values of cardiac cycle-dependent variations of integrated backscatter among the control segments, the remote normally contracting segments, the dysfunctional segments showing improvement with inotropic stimulation (DbE+), and those with persistent dysfunction (DbE–). Reproduced with permission from Pasquet et al. Relation of ultrasonic tissue characterization with integrated backscatter to recruitable inotropic reserve in chronic left ventricular ischemic dysfunction. *Am J Cardiol.* 1998;81:68-74

of intramural contractile function which is relatively independent of resting wall motion or thickening and which parallels contractile reserve. The main disadvantage of this approach, however, is its dependence on fiber orientation and the need to acquire the data in segments that oriented perpendicular to the ultrasound beam.

Myocardial Contrast Echocardiography

Myocardial contrast echocardiography (MCE) allows for the evaluation of regional myocardial perfusion and segmental wall motion. The technique involves intracoronary or intravenous injection of an ultrasound contrast agent, which consists of microbubbles approximately the size of a red blood cell. These microbubbles are flow tracers and are able to pass into the microcirculation and be detected by echocardiography as opacification of myocardial tissue (Fig. 17.9).

The basic pathophysiological premise behind MCE is that viable myocardium has an intact microcirculation, whereas infarcted, nonviable tissue loses this microvasculature. Therefore, MCE provides a direct evaluation of microvascular integrity and an indirect estimate of cellular integrity. Earlier investigators used the intracoronary route for contrast administration. In both the immediate postinfraction setting or in patients with chronic dysfunction, MCE predicted recovery of LV function after revascularization with a high sensitivity (85–94%) and a lower specificity (43–65%). From these initial studies, MCE appeared to have similar test properties as other methods that assess myocardial perfusion, such as thallium scintigraphy. However, it has the added advantage of providing additional information regarding wall contractility and motion.

Thanks to the development of new ultrasonic contrast agents that can cross capillaries, and the introduction of newer contrast imaging modalities, such as power pulse inversion and power modulation, that greatly reduce the destruction of the microbubbles by ultrasound, interest in MCE to assess myocardial viability has grown even further. By allowing essential parameters of the microcirculatory function, such as myocardial blood flow and blood volume to be measured, MCE offers the unique opportunity to directly

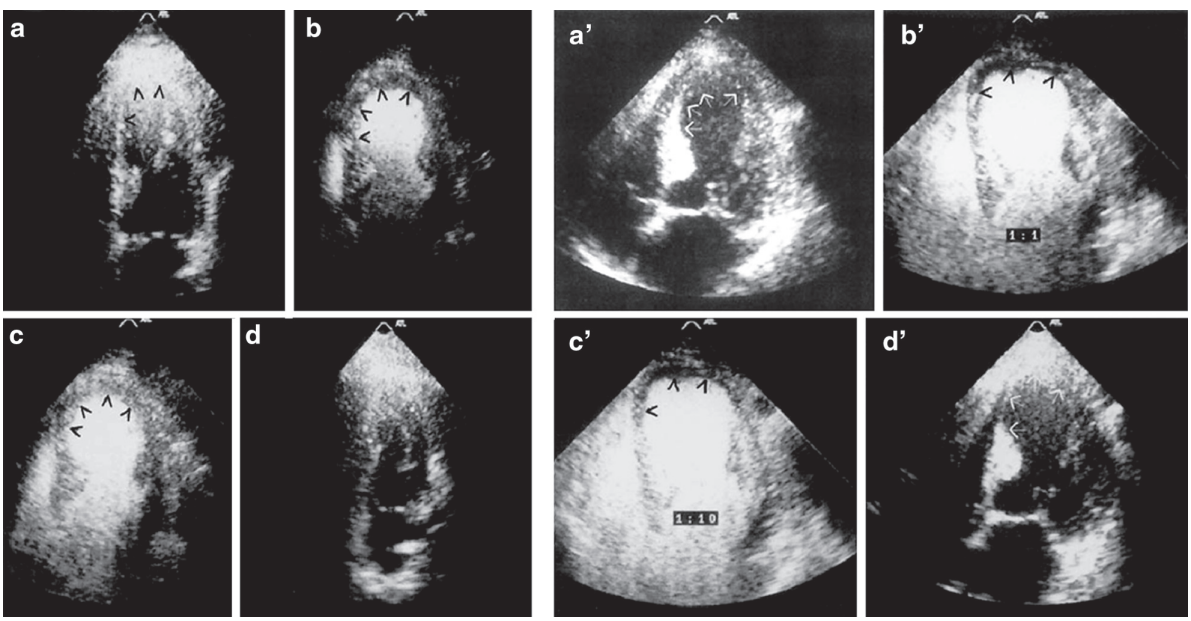

Fig. 17.9 *Left panel*. Four-chamber view showing an akinetic septum and apex (**a**) with absent contrast opacification in this region at short triggering intervals (**b**) but homogeneous opacification with delayed triggering (**c**), and normal resting function 6 months later (**d**). *Right panel*. Chamber view showing an akinetic septum and apex (**a**') with no contrast opacification in this area with early (**b**') or delayed (**c**') triggered imaging and failure of recovery of systolic function at follow-up (**d**'). Reproduced with permission from Swinburn et al. Intravenous myocardial contrast echocardiography predicts recovery of dysynergic myocardium early after acute myocardial infarction. *J Am Coll Cardiol.* 2001;38:19-25

assess the microcirculation of the dysfunctional segments and hence the likelihood of their recovery. As expected, measures of myocardial blood volume with MCE have been found to correlate with microvascular density and capillary area and inversely with collagen content. They can therefore be used to differentiate viable from nonviable segments. Measures of myocardial blood velocity and flow have also been shown to bear an inverse correlation with collagen content. Yet, their relationship with microvascular density appears to be somewhat more complex. When microvascular density is reduced, myocardial blood flow and velocity are also proportionally reduced. By contrast, when the microvascular density is preserved, myocardial blood flow and velocity can either be normal or reduced. Thus, in the presence of normal values for myocardial blood volume, MCE parameters of myocardial blood flow and velocity may help differentiate chronically stunned from truly hibernating myocardium. Accordingly, assessment of microcirculatory function with MCE allows to predict functional recovery with both a sensitivity and a high negative predictive value (>90%). Specificity is somewhat lower (±65%), but better than with thallium imaging.

Stress Echocardiography

The demonstration of contractile reserve using various provocative stimuli such as nitroglycerin, dipyridamole, postextrasystolic potentiation, catecholamine (e.g., isoprenaline, adrenaline, dopamine or dobutamine) infusion and exercise can be studied with echocardiography. Dobutamine stress echocardiography (DSE) is the most accepted and widely available of these techniques. Its diagnostic and prognostic value has been well documented in the detection of myocardial viability.

Dobutamine is a synthetic catecholamine that stimulates primarily β1-adrenergic receptors with minimal β2 and α1 effects. At low doses (<10 μg. kg^{-1}. min^{-1}), it demonstrates a relatively more potent inotropic effect than chronotropic effect, allowing stimulation of myocardial contractility before significant increases in heart rate, and presumably ischemia, occur. At higher doses, both inotropic and chronotropic stimulation occur, resulting in increased cardiac output, myocardial oxygen consumption, and ischemia in myocardial regions subtended by significantly stenosed coronary arteries.

- *The protocol* in most stress echocardiography laboratories uses dobutamine infusion at two low-dose stages (5 and 10 μg. kg^{-1}. min^{-1}), with each stage lasting 3 min. Some advocate utilizing an even lower starting dose of 2.5 μg. kg^{-1}. min^{-1} because in patients with critical coronary stenosis, myocardial ischemia may be precipitated even with doses as low as 5 μg. kg^{-1}. min^{-1}. Thereafter, the dose is increased in 10 μg. kg^{-1}. min^{-1} increments to a maximum dose of 50 μg. kg^{-1}. min^{-1}. Atropine may be given if the target heart rate is not achieved with standard dobutamine doses. The test is terminated when the patient achieves 85% of the age-predicted maximum heart rate or clinical or echocardiographic evidence of ischemia occurs.

Most viable segments will demonstrate improvement of contractility at doses of 10 μg. kg^{-1}. min^{-1} or less. The benefit of proceeding to higher doses of dobutamine, even if contractile reserve is demonstrated at lower doses, is to observe a "biphasic response." In the presence of significant coronary stenosis, an initial improvement in systolic wall thickening may occur at low doses of dobutamine, representing the region's contractile reserve as previously stated. However, as oxygen consumption increases as contractility and heart rate rise, the flow-limiting stenotic vessel is unable to keep up with the oxygen demand, and the ensuing ischemia leads to hypokinesis of the affected wall segment. This biphasic response demonstrates two critical components to the definition of myocardial viability, namely viability itself and flow limitation. It is therefore not surprising that the biphasic response has the best predictive value of all the possible responses to dobutamine in determining improvement in LV function following revascularization. In a recent study, <15% of myocardial segments demonstrating either no change or sustained improvement with low and high dose dobutamine had functional recovery with revascularization, while 72% of segments with a biphasic response recovered function. Accordingly, the combined low- and high-dose approach in all patients who do not have contraindications should be recommended.

- *Diagnostic accuracy:* The cumulative sensitivity, specificity, and predictive values of DSE based on a

recent meta-analysis were 81, 86, and 83%, respectively. Although generally good, these sensitivities and specificities imply that there were a significant number of false-positive findings (i.e., demonstration of contractile reserve without significant functional recovery on revascularization) as well as false-negative ones (i.e., functional recovery without evidence of contractile reserve). The former may be partially explained by tethering of nonviable segments to adjacent viable ones, leading to the illusion of improved function. Additionally, the presence of non-transmural infarction, where a segment of myocardium consists of an admixture of viable tissue and necrotic scar, can lead to this result. If the proportion of scar is relatively large, or the viable portion already has normal blood flow, then revascularization would not be expected to lead to functional improvement. Of course, if revascularization is incomplete, an otherwise viable segment may remain dysfunctional. Finally, functional recovery may occur more slowly than allowed for by the follow-up periods in these studies

The observation of improved LV function despite a "negative" DSE may be explained by the fact that the myocardial flow reserve in these regions may be so low that any increase in oxygen demand, even in viable segments, leads to ischemia. Additionally, the ultrastructural changes occurring in viable myocardium discussed earlier may be so profound that contraction is not possible until sustained restoration of blood flow has taken place.

- *Prediction of outcomes:* DSE also emerges as a tool to predict prognosis in patients with chronic left ventricular dysfunction. Several studies have now demonstrated that long-term survival is significantly better among patients with echocardiographic evidence of myocardial viability who had been revascularized than in those with either viable myocardium treated medically, nonviable myocardium undergoing revascularization, or nonviable myocardium treated medically. These data lend further support to the use of dobutamine echocardiography for assessment of myocardial viability, as this technique not only allows for accurate identification of which patient will improve regional and global left ventricular function after coronary revascularization, but also may indicate those most likely to benefit with respect to prognosis.
- *Limitations:* As with most imaging techniques, patient factors can limit image quality in DSE, which can adversely affect accuracy. Obesity and lung disease, for example, may lead to poor acoustic windows in approximately 10% of patients. Harmonic imaging and ultrasound contrast agents have been used to enhance endocardial border detection, as well as transesophageal imaging. Given that the interpretation of contractile function is subjective, improved image quality can reduce inter-reader variability.

Newer inotropic agents may also have advantages over dobutamine. Echocardiography during the infusion of enoximone, a selective inhibitor of cyclic AMP-specific phosphodiesterase, has been compared with DSE, and has shown a slightly higher sensitivity (88 vs. 79%) and a similar specificity (89 vs. 90%). These preliminary findings merit additional investigation into the use of this inotropic agent for viability testing.

- *Comparison with other modalities:* Finally, DSE has been compared with other methods for evaluating myocardial viability, such as single photon emission computed tomography (SPECT) and positron emission tomography (PET) in many studies and reviews. Bax et al pooled data from all published studies reporting the sensitivity or specificity of nuclear techniques and/or DSE in predicting functional recovery after revascularization. DSE had a slightly lower sensitivity (84%) compared with SPECT and PET (83–90%), but a significantly greater specificity (81% for DSE vs. 47–73% for SPECT and PET).

Conclusions

Over the past two decades, much has been learned about the mechanisms underlying myocardial viability in patients with coronary artery disease. Simultaneously, revascularization of chronically but reversibly dysfunctional myocardium has progressively emerged as a potential alternative in the treatment of heart failure secondary to coronary artery disease, as it seems to be able to improve regional and global left ventricular function, to decrease heart failure symptoms, and to improve long-term survival. Among the several techniques that are available for identifying viable myocardium, echocardiography appears to be particularly

well suited, as it allows to investigate two main features of myocardial viability, i.e., maintained resting perfusion and residual inotropic reserve.

Bibliography

Bax JJ, Wijns W, Cornel JH, Visser FC, Boersma E, Fioretti PM. Accuracy of currently available techniques for prediction of functional recovery after revascularization in patients with left ventricular dysfunction due to chronic coronary artery disease. *J Am Coll Cardiol*. 1997;30:1451–1460.

Borgers M, Thoné F, Wouters L, Ausma J, Shivalkar B, Flameng W. Structural correlates of regional myocardial dysfunction in patients with critical coronary artery stenosis: chronic hibernation? *Cardiovasc Pathol.* 1993;2:237–245.

Canty JR, Fallavollita JA. Resting myocardial flow in hibernating myocardium: validating animal models of human pathophysiology. *Am J Physiol*. 1999;277:H417–H422.

Ross J Jr. Myocardial perfusion-contraction matching. Implications for coronary heart disease and hibernation. *Circulation*. 1991;83:1076–1083.

Vanoverschelde J-L, Wijns W, Borgers M, Heyndrickx G, Depré C, Flameng W, Melin JA. Chronic myocardial hibernation in humans. From bedside to bench. *Circulation*. 1997;95:1961–1971.

Vanoverschelde J-LJ, Wijns W, Depré C, Essamri B, Heyndrickx G, Borgers M, Bol A, Melin JA. Mechanisms of chronic regional postischemic dysfunction in humans: new insights from the study of non-infarcted collateral dependent myocardium. *Circulation*. 1993;87:1513–1523.

Chapter 18
Echocardiography for Assessing Acute Myocardial Infarction

Otto Kamp and Cees A. Visser

Introduction

According to the sequence of the ischemic cascade, regional contractile dysfunction precedes both electrocardiographic changes and symptoms during myocardial ischemia (Fig. 18.1). Thus, due to the suboptimal performance of the electrocardiogram to reliably detect or exclude acute coronary syndromes, including myocardial infarction (MI), evaluation of regional contractile function using two-dimensional echocardiography in patients with acute chest pain is clinically relevant. Echocardiography is portable, noninvasive, easily repeatable, efficacious, low cost, and widely available, rendering it uniquely suited for emergency medicine use. The visual analysis of segmental wall motion is the hallmark for the diagnosis. Furthermore, transthoracic two-dimensional and Doppler echocardiography can be useful for assessing the location and extent of MI, in diagnosing left ventricular thrombus, left ventricular (pseudo) aneurysm, and also mechanical complications after MI. It also provides prognostic information that is important for risk stratification. Stress echocardiography can be applied in the emergency room for diagnosis of acute coronary syndromes and also for risk stratification after MI. Finally, three-dimensional echocardiography is now here and may be more sensitive than two-dimensional echocardiography for the evaluation of wall motion.

O. Kamp (✉) and C.A. Visser
Department of Cardiology, VU University Medical Center, P.O. Box 70571007MBAmsterdam, The Netherlands
e-mail: o.kamp@vumc.nl

Acute Chest Pain

The problem: Acute nontraumatic chest pain is one of the most common symptoms for which patients seek emergency medical consultation, comprising up to 15% of total patient volume in emergency departments. In the USA, an estimated 8 million annual visits for chest pain to the emergency department typically result in hospital admissions for further evaluation in approximately 70% of such patients at a cost of over $10 billion. It is among the more challenging and complex symptoms, as the diagnoses for patients with chest pain range from minor disease processes, such as costochondritis or esophageal spasm, to life-threatening conditions as acute MI, pulmonary embolism, or aortic dissection (Table 18.1). Furthermore, up to three-fourth of the admissions for presumed acute coronary syndromes prove to be incorrect, while anywhere between 2 and 8% of patients with acute cardiac ischemia or MI are erroneously discharged from the emergency department, with an increased associated short-term mortality rate ranging from 10 to 26%. Although relatively small, the incidence of failure to admit this patient category with a life-threatening condition is important as it may result in potentially serious and preventable morbidity and mortality in tens of thousands of patients.

Medicolegal implications: There are also medicolegal implications, as the failure to diagnose acute coronary syndromes or MI accounts for the single greatest cause of dollars lost in malpractice lawsuits in emergency medicine in the USA. Although currently mainly an issue in the United States, juridification of medicine is increasing rapidly elsewhere, and implications on the practice of emergency medicine may be equally profound. Consequently, focusing on patient welfare and medicolegal implications of failure to detect acute

P. Nihoyannopoulos and J. Kisslo (eds.), *Echocardiography,*
DOI: 10.1007/978-1-84882-293-1_18, © Springer-Verlag London Limited 2009

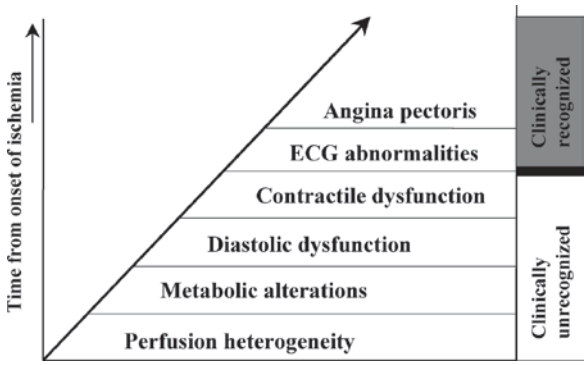

Fig. 18.1 The ischemic cascade: contractile dysfunction precedes electrocardiographic changes and symptoms as manifestation of myocardial ischemia

Table 18.1 Chest pain in the emergency room

Cardiac
Myocardial ischemia or infarction
Aortic dissection
Pericarditis
Pulmonary
Pulmonary embolism
Other causes of pulmonary hypertension
Chest wall trauma
Myocardial or pericardial contusion
Traumatic valve and aortic injury
Noncardiac chest pain
Gastrointestinal
Musculoskeletal

coronary syndromes alike results in the liberal admission policy as is traditionally applied in patients with chest pain syndromes. However, as the current era of managed care and health care reform requires cost containment, and as a result of the increasing awareness that an overly defensive medical system with its unnecessary admissions and procedures constitutes a form of iatrogeneous morbidity per se, impetus is added to the development of more efficient approaches to manage this particular group of patients.

Workup in Acute Chest Pain Syndromes

The aim of the initial triage of patients presenting with acute chest pain would be to differentiate acute coronary syndromes as the underlying cause from other potentially serious conditions, particularly aortic dissection and pulmonary embolism, or less serious conditions (Table 18.1). The short-term risk of death or life-threatening complications should be established readily in patients with suspected acute coronary syndromes in order to ensure rapid initiation of the most appropriate treatment while patients who are at very low likelihood of having an adverse outcome related to acute coronary syndromes may thus be safely discharged for outpatient follow-up.

Typically, history taking, the clinical examination, and ECG are important when performing the initial triage in acute chest pain patients. It is increasingly recognized that a number of specific patient groups typically present with atypical symptoms of myocardial ischemia, such as women, diabetics, and the elderly. Physical examination is often normal at presentation, while the initial 12-lead electrocardiogram is critically important. Patients with acute chest pain and ST-segment deviation of more than 0.1 mV in two or more contiguous leads or left bundle branch block not known to be old, are suspected to have myocardial ischemia or MI and are thus at very high risk for short-term major adverse cardiac events. Patients classified as having an acute coronary syndrome with ST elevation should undergo urgent revascularization unless contraindicated.

The presence of ST-segment depression of more than 0.1 mV raises the suspicion of myocardial ischemia and identifies patients suffering from an acute coronary syndrome with an associated intermediate-to-high risk. Emergency revascularization is generally considered not to be an option in these patients, while admission to hospital is indicated, preferably in cardiac care surroundings.

The majority of cases, however, present with normal electrocardiograms or nonspecific ECG changes, and it is these patients who pose the greatest diagnostic dilemma for triage.

As a second step to further stratify these low-to-intermediate risk patients, methods to detect biochemical evidence of irreversible myocardial injury are commonly applied. However, no single determination of any one serum biochemical marker of myocardial necrosis reliably identifies or excludes acute MI within 6 h after symptom onset, while no serum biochemical marker reliably identifies or excludes unstable angina at any time after symptom onset. Thus, the traditional "rule out acute MI" approach by serial enzyme testing alone may deprive many patients with acute coronary syndromes of early therapy to prevent progression to MI and death.

Although serial ECG or continuous ST-segment monitoring is of proven benefit, early noninvasive evaluation of myocardial ischemia by echocardiography may be of particular value.

Diagnosis of MI

The diagnosis of an acute MI is based upon history, 12-lead ECG, and serologic markers such as creatine kinase and cardiac troponines. Echocardiography has been used for early identification of acute coronary syndromes or MI patients whose presenting symptom is acute chest pain, as well as to evaluate prognosis in this population.

Myocardial ischemia produces regional wall motion abnormalities. The presence of regional asynergy can predict an acute MI/ischemia with a high sensitivity and moderate specificity. It is difficult however to distinguish between infarction (necrosis) and ischemia or stunning. Other conditions however may also produce regional wall motion abnormalities, such as prior MI, focal perimyocarditis, prior cardiac surgery, right ventricular volume overload, left bundle branch block, ventricular pre-excitation, and myocarditis. With transient coronary artery occlusion during percutaneous coronary interventions, within 20 s wall motion abnormalities are observed prior to onset of ECG changes or symptoms, the so-called ischemic cascade (Fig. 18.1).

In the setting of an acute MI, patients with multivessel coronary disease usually show more extensive regional asynergy than patients with single-vessel disease. Thus, there is a clear diagnostic yield of echocardiography over the use of conventional clinical and ECG criteria. The extent of regional asynergy is also predictive for in-hospital complications in patients with MI.

As summarized in Table 18.2, with the exception of two small-sized studies performed in a very low risk population, the large majority of studies indicate that echocardiography may indeed be of substantial benefit in the evaluation of patients with acute nontraumatic chest pain. Practically, in the absence of wall motion abnormality, an MI or an acute ischemic syndrome can be ruled out. Although the number of patients with false-negative studies may be of some concern, such patients typically have a low complication rate, while the accuracy of echocardiography may be significantly enhanced when imaging is performed during or shortly after resolution of symptoms.

Although clinically of less concern, the number of false-positive studies may be reduced when a simple comparison with an earlier echo study is possible.

In order for echocardiography to be most useful for diagnosis and early risk stratification of patients with acute coronary syndromes, it would need to be available immediately in the emergency department as the sensitivity to detect transient wall motion abnormalities is in its highest during or shortly after acute ischemia.

Technology to provide transtelephone interpretation of digital images is readily available and may significantly aid in realizing the optimal deployment of the technique. Although preliminary evidence suggests substantial cost-saving potential, a formal study of the economics of incorporating echocardiography into routine evaluation of chest pain patients in the emergency department, or of basing triage decision on its results, has yet to be materialized.

Extent of MI

Several investigators have addressed the ability of early echocardiography to provide prognostic information on intermediate or long-term follow-up in patients with acute coronary syndromes. Largely, these studies rely on the assessment of the number of affected segments or a wall motion score index, rather than on the presence of regional dysfunction alone. The number of affected myocardial segments may be more closely related to the degree of left ventricular dysfunction, a major determinant of mortality and morbidity in patients with acute coronary syndromes. Echocardiography may be of particular benefit to identify patients who are at high risk:

- In non-Q-wave MI, presence or absence of segmental contractile dysfunction in three or more segments on the first day of the event added significantly to the predictive power of routinely available parameters to identify patients at high risk for predicting in-hospital major adverse cardiac events.
- In patients with acute chest pain and a non-ST-segment elevation MI, echocardiography on admission could predict the risk of adverse events at 30 days (death, MI, revascularization), while the predictive power of wall motion abnormalities was better than that of clinical data, ECG, or baseline troponin I measurements.

In summary, echocardiography provides incremental prognostic information in patients presenting with acute chest pain syndromes. Specifically, the cardiac event rate does not only vary according to the presence or absence of left ventricular dysfunction but it also differs between the severities of contractile dysfunction.

Table 18.2 Studies evaluating the use of echocardiography to predict presence of acute myocardial infarction or acute coronary syndrome in patients with acute chest pain

Authors	Year	No. of adequate studies	Clinical criterion	Echocardiographic criterion	Sensitivity (%)	Specificity (%)	PPV (%)	NPV (%)	(+)LR	(−)LR
Horowitz et al	1982	65	AMI	RWMA	94	84	86	93	5.9	14
			CAD		94	93	94	93	13.4	15.5
Loh et al	1982	30	AMI	Severe hypokinesis	83	100	100	90	4	5.9
				Mild hypokinesis	83	72	67	90	3.0	4.2
Oh et al	1985	26	AMI	RWMA	71	100	100	90	4	3.4
Sasaki et al	1986	46	AMI	RWMA	93	87	78	96	7.2	12.4
			CAD		74	96	94	79	18.5	3.7
Peels et al	1990	43	AMI	RWMA	92	53	46	94	2.0	6.6
			ACS/CAD		88	78	85	82	4.0	6.5
Sabia et al	1991	169	AMI	RWMA	93	57	31	98	2.2	8.1
Gibler et al	1995	901	Cardiac disease	RWMA	47	99	32	99	47	1.9
Izumi et al	1995	74	AMI	RWMA	97	–	–	–	–	–
Kontos et al	1998	260	AMI	RWMA/EF < 40%	96	70	23	99	3.2	17.5
			AMI/PCI		91	75	44	98	3.6	8.3
Kontos et al	1998	185	AMI	RWMA/EF < 40%	100	82	16	100	5.6	4
			AMI/PCI/ CAD		85	85	32	99	5.7	5.7
Mohler et al	1998	92	AMI	nRWMA	83	84	56	95	5.2	4.9
			ACS		49	100	100	57	4	2.0
Luotolahti et al	1999	81	ACS	RWMA	97	50	95	67	1.9	16.7
Kontos et al	2002	149	AMI	RWMA/EF < 40%	91	–	–	–	–	–
Swinburn et al	2002	80	AMI	RWMA	92	47	23	97	1.7	5.8
Pooled data		996	AMI	RWMA	91	72	39	98	3.3	8.0
		726	ACS		83	81	70	90	4.4	4.8

The magnitude of the likelihood ratios represents the predictive rule-in (*positive* likelihood ratio) or rule-out (*negative* likelihood ratio) power of a test. Likelihood ratios are largely independent of the severity or the prevalence of disease in the index population, As opposed to sensitivity, specificity, and predictive values, and may thus represent predictive power more adequately

Stress Echocardiography in the Emergency Room

Stress echocardiography has been proposed for additional risk stratification of patients with normal early resting echocardiograms, or after an observation period during which myocardial injury markers prove negative. It may be of particular benefit in patients with acute coronary syndromes who do not show any resting wall motion abnormality as a result of the transient nature of ischemia-induced regional dysfunction, whose ischemic burden is below the detection threshold of echocardiography, or, in situations where there is pre-existing wall motion abnormalities.

- Using dobutamine stress echocardiography, 72% of patients without ischemic changes on the ECG who would otherwise have been admitted to the hospital could be discharged on average 5 h after presentation when the dobutamine stress is normal. In another study, patients with acute chest pain, nondiagnostic ECG and normal biochemical markers underwent simultaneous stress ECG and echocardiography. A normal echocardiographic study was associated with an event-free 12-month survival in 100% of patients, while prognostic power of stress echocardiography was superior than that of stress ECG.
- Dobutamine stress echocardiography was applied to risk stratify patients with similar clinical characteristics after a mean observation period of 3 h. In contrast to the earlier studies, patients were at relatively high risk, as evidenced by 45% of positive studies. At multivariate analysis, the only independent predictor of adverse cardiac events during 6-month follow-up was new or worsening wall motion abnormalities on the stress echocardiogram.
- A predischarge dobutamine stress echocardiogram has also important independent prognostic value in low-risk, troponin-negative, chest pain patients. It should be recognized that in this clinical setting the incremental yield of stress echocardiography over standard stress ECG remains yet to be determined.
- Although stress echocardiography provides an attractive alternative for functional testing in patients who are unable to perform physical exercise, who have abnormal baseline ECG, or who belong to a population where false-positive rates for stress electrocardiography testing is relatively high.
- *Pitfalls:* Stress echocardiography may not easily distinguish wall motion abnormalities due to reversible ischemia or acute MI from those that result from previous MI and scar. The observation that scarred segments may be characterized by increased echodensity in conjunction with a reduced diastolic thickness of 5 mm or less may be helpful to better discriminate acute ischemic dysfunction from scar. Also, a relatively small MI with only nontransmural involvement may not readily be detected by echocardiography.

A good echocardiographic window is critical for reliable and accurate evaluation of segmental contractile function. The transesophageal approach invariably conquers the poor image quality in patients with limited transthoracic echogenicity. Intravenous contrast echocardiography is also increasingly advocated as an attractive, realistic, and less invasive alternative to transesophageal echocardiography. Contrast echocardiography may be of particular benefit for use in patients with acute chest pain (Fig. 18.2). Reliable endocardial border detection is the conditio sine qua non for the evaluation of segmental contractile function, but may be impaired in up to 10–15% of investigations.

Both at rest and during stress, an intravenous injection of contrast improved endocardial border definition in up to 96% of cases, which translates to a significant increase in diagnostic accuracy, as intra- and interobserver variability are reduced, not merely between expert readers, but also between assessments by novices compared with those made by experts.

Myocardial contrast echocardiography is increasingly close to clinical application and permits real-time bedside evaluation of myocardial perfusion as well as contractile function following intravenous injection of microbubbles. Identifying absence of a perfusion defect in conjunction with normal ventricular function virtually excludes acute ischemia in a symptomatic patient evaluated for acute chest pain. However, finding a defect in a patient without a history of acute MI confirms its presence. In an established acute MI, the size of the defect reflects the myocardial area-at-risk and may help choosing the optimal therapeutic option.

Risk stratification: Following initial triage on basis of clinical and ECG parameters, there is increasing evidence of the ability of two-dimensional echocardiography to accurately diagnose and risk stratify patient with chest pain. Echocardiography can detect early, before biochemical marker analysis become

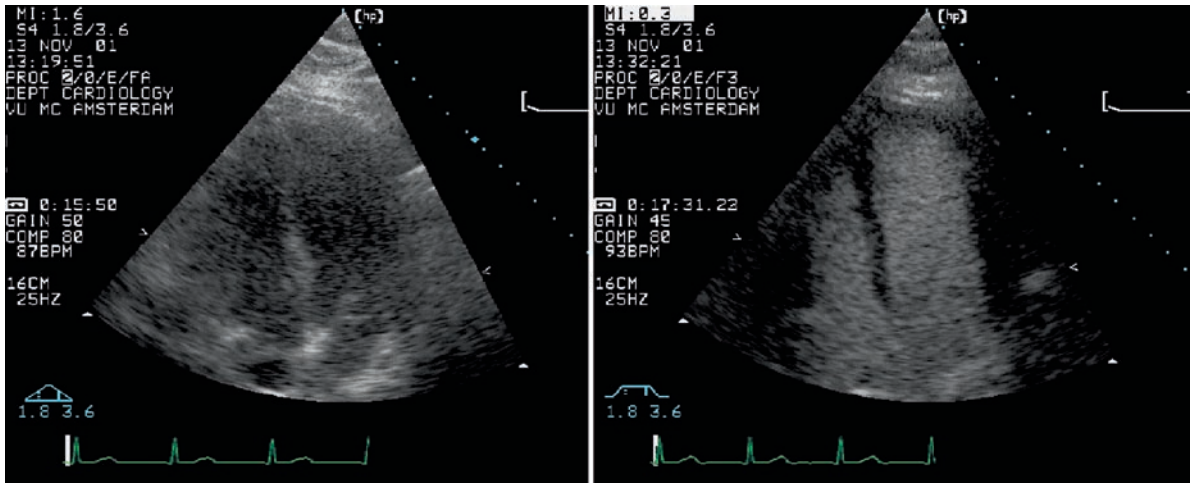

Fig. 18.2 Improved endocardial border detection using contrast agents

available, and more accurately patients with at low risk as the absence of segmental contractile dysfunction is a strong indicator against MI. It is likely that the accuracy of echocardiography in general and in the identification of acute coronary syndromes in particular improves significantly in the presence of symptoms.

As tertiary triage following exclusion of irreversible damage by biochemical marker analysis, stress echocardiography is a powerful tool offering significant additional diagnostic and prognostic information.

Apart from acute myocardial ischemia, echocardiography reliably identifies the presence or absence of most of the major nonischemic cardiovascular causes of acute chest pain, e.g., aortic dissection or pulmonary embolism.

Availability and trained staff: However, optimal use of the technique in the emergency department requires dedicated and trained sonographers, high-quality equipment, round-the-clock availability of both image acquisition and interpretation services, and, importantly, realistic and thorough knowledge on the performance of echocardiography in this specific setting. We would advocate the use of contrast to further enhance echocardiography's diagnostic accuracy and efficiency, both at rest and during stress.

Prognosis After MI

Outcome after acute MI is related to the severity of left ventricular dysfunction, the presence or absence of residual myocardial ischemia, and the occurrence of cardiac arrhythmias (Table 18.3). Using clinical characteristics and various noninvasive techniques, patients with acute MI can be stratified into low or high risk for subsequent morbidity and mortality. Two-dimensional and Doppler echocardiography has been shown to be useful and can easily be performed over time or during changes with treatment. It assists in the determination of prognosis based upon assessment of infarct size (regional left ventricular function), infarct expansion (global left ventricular function), and left ventricular diastolic function. Furthermore, inducible myocardial ischemia can be assessed by stress echocardiography, whereas low-dose dobutamine echocardiography can be used to detect myocardial viability.

Table 18.3 Factors influencing prognosis of patients after acute MI

Age	Myocardial viability
Sex	Residual/recurrent ischemia
Hypertension	Extent of CAD
Diabetes	Ventricular arrhythmias
Previous MI	Status of infarct-related artery
LV function	
LV size	

Regional Left Ventricular Function

In the acute phase, MI is a regional disease leading to segmental wall motion abnormalities in the region served by the occluded coronary artery, and this regional left ventricular dysfunction can be detected by two-dimensional echocardiography. Using the standard

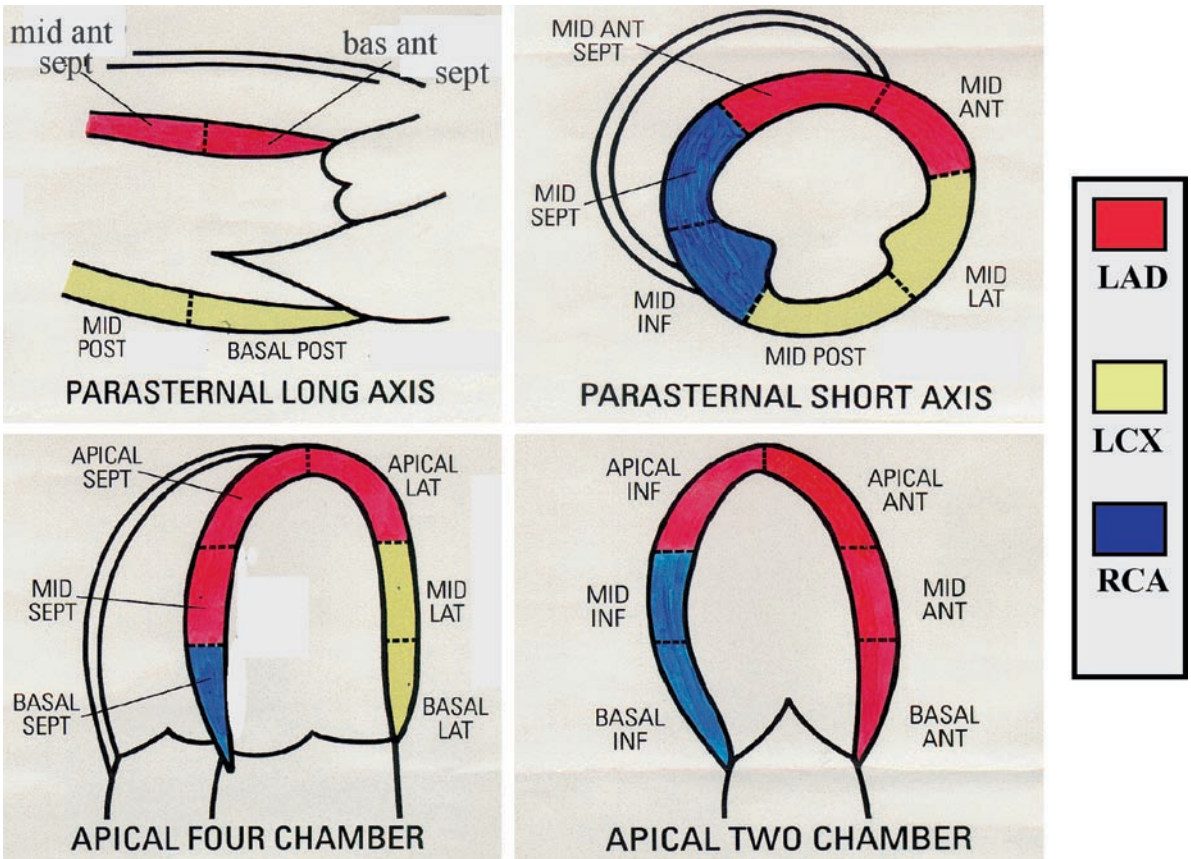

Fig. 18.3 The segmental division of the left ventricle as recommended by the American Society of Echocardiography

parasternal and apical windows, the left ventricular can be imaged and divided into multiple segments for wall motion analysis. The number of segments into which the ventricle can be divided differs between publications, but the American Society of Echocardiography has recommended 16 segments (Fig. 18.3). Recently, a 17-segment division has been proposed for all imaging modalities, identifying the top of the apex as a separate segment. Each segment is assigned a numerical value based on the degree of wall motion abnormality, e.g., normal contracting segment (=1); segment with hypokinesis (=2); akinesis (=3); dyskinesis (=4); or aneurysmatic deformed (=5). A compensatory hyperkinetic segment is frequently scored as 0 (Table 18.4). Analysis is not only performed by degree of endocardial motion but more specifically by degree of myocardial thickening: thickening of more than 5 mm is normal contraction, between 2 and 5 mm is hypokinesis, less than 2 mm thickening is akinesis, and no thickening and outward motion is dyskinesis. Frequently, the interface between contracting and noncontracting tissue forms a visually distinctive pattern, the so-called hinge point. A wall motion score (WMS) index is calculated by summing up the scores for each segment and dividing by the number of segments analyzed. This semiquantitative analysis has been shown to correlate well with clinical

Table 18.4 Regional wall motion score index

Each wall region (segment) is assigned a number, based upon its motion:
0 = Hyperkinetic
1 = Normal
2 = Hypokinetic
3 = Akinetic
4 = Dyskinetic
5 = Aneurysmatic
1½ = Mildly hypokinetic
2½ = Severely hypokinetic

$$\text{WMSI} = \frac{\text{sum of all segments}}{\text{no. of segments scored}}$$

Table 18.5 Regional wall motion score index and ejection fraction

WMSI: 1	Normal LV function (EF > 60%)
WMSI: 1–1.5	Mildly depressed LV function
WMSI: 1.5–2	Moderately depressed LV function (EF 30–45%)
WMSI: >2	Severely depressed LV function (EF < 30%)

status and ejection fraction and can identify high-risk patients (Table 18.5).

In the prethrombolytic period, patients with a high WMS (index) at admission had a higher rate of in-hospital mortality (27–40%) or serious in-hospital complications (death, shock, heart failure, and arrhythmias; 68–94%) than patients with limited dysfunction of the left ventricle (2–7% and 7–18%, respectively). Also, 1-year mortality was significantly higher in patients with a poor WMS at admission or predischarge compared with patients with a good WMS (44–63% vs. 0–13%). WMS index was an independent predictor of in-hospital and 1-year mortality, when compared with clinical variables.

In the thrombolytic era, WMS (index) remains predictive of mortality and other serious cardiac events. In 6,676 patients with acute MI it was shown that WMS index had prognostic importance for up to 5 years, both in patients treated with thrombolytic therapy and in patients not receiving this treatment (TRACE study). When compared with clinical variables or exercise test results, WMS index is the most powerful independent predictor. However, compared to WMS index during low- or peak-dose dobutamine stress echocardiography, resting WMS index has less predictive value.

Studies have shown that regional left ventricular function may change over time after acute MI. Again in the TRACE study, repeated echo examination of left ventricular function during the first year has independent prognostic value concerning death and worsening of heart failure. In that study, a decrease of 0.1 U of WMS index in patients with reduced systolic function was indicative of an increase in the risk of death of 24–37%, which stresses the importance of serial evaluations.

Compensatory Hyperkinesia and Remote Asynergy (Remodeling)

For the evaluation of the left ventricular remodeling after acute MI, attention also needs to be drawn to the noninfarcted area. Both compensatory hyperkinesia and remote asynergy, have important prognostic implications. Compensatory hyperkinesia, defined as increased contractility of the noninfarct zone, occurs in a significant proportion of patients with AMI. It is more common in the acute phase and reduced by the use of b-blockade. Compensatory hyperkinesia occurs more frequently in patients with one-vessel disease; absence of hyperkinesia is associated with a higher WMS and subsequent higher cardiac mortality. Hyperkinesia has been shown to have additional prognostic value to WMS index concerning long-term mortality in the TRACE study.

Remote asynergy, defined as asynergy not directly adjacent to the infarcted area, occurs in approximately 20% of patients with AMI. Whereas hyperkinesia is more common in patients with one-vessel disease, remote asynergy is predictive of multivessel disease. Remote asynergy is, like in multivessel disease, related to recurrent ischemic events and higher cardiac mortality.

Global left ventricular function: The WMS index is not only predictive of mortality and other serious cardiac events, but also related to infarct expansion and left ventricular remodeling (Fig. 18.4). Several investigations have shown that the extent of left ventricular dysfunction is independently associated with progressive left ventricular dilatation. In 233 patients with a first anterior MI, treated with thrombolysis and with an acute WMS index >2, an increase left ventricular volume indexes in the first 3 months was observed, whereas patients with a WMS index >2 did not have left ventricular remodeling.

Infarct expansion is an important and early complication of acute MI that can readily be detected by two-dimensional echocardiography. It refers to an alteration in regional ventricular topography due to lengthening and thinning of the infarcted segment and results in left ventricular dilatation with global distortion of left ventricular shape. Infarct expansion is generally seen in patients with large, transmural, anterior MI, and is accompanied by increased mortality independent of left ventricular function.

Global left ventricular shape is also important. Systematic quantitative assessment of left ventricular shape, apart from left ventricular volume and function, has been attempted only recently. Two methods used to assess left ventricular shape after AMI:

1. The length/width ratio: the ratio of the ventricular long-axis length to left ventricular diameter,
2. The sphericity index: volume observed/ volume of sphere using long axis as diameter.

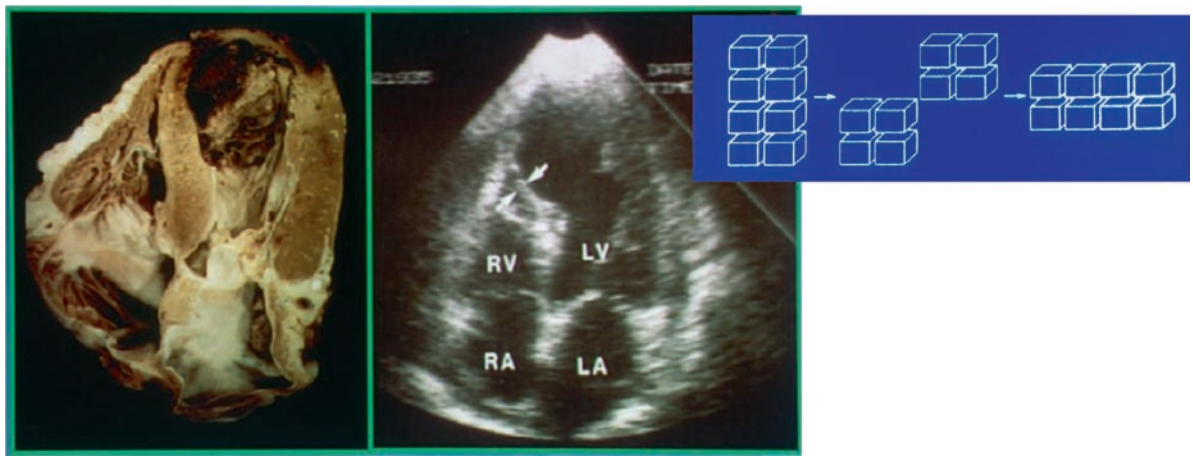

Fig. 18.4 Infarct expansion is caused by rearrangement of myocytes in the infarct zone

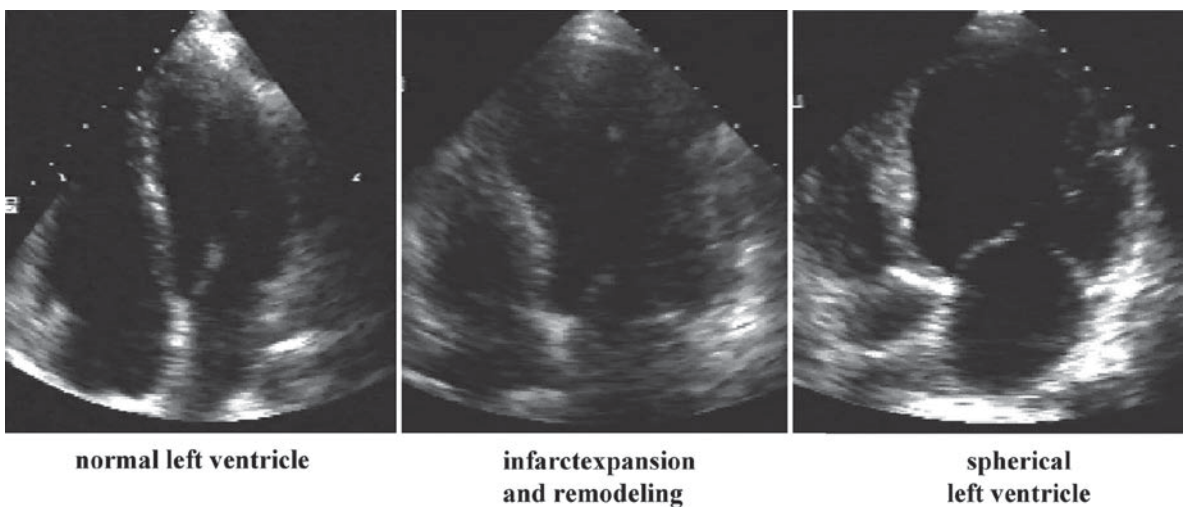

Fig. 18.5 Left ventricular shape changes in left ventricular dilatation

The shape of the normal left ventricle is referred to as ellipsoid. Left ventricular shape tends to become abnormally wide (spherical) in left ventricular dilatation (Fig. 18.5). A more pronounced shape distortion has been associated with increased left ventricular volumes, decreased ejection fraction, and more extensive wall motion abnormalities. After anterior MI, the degree of left ventricular sphericity correlates with exercise capacity: those with the highest sphericity index had the lowest exercise capacity and the highest heart failure score. In patients with idiopathic dilated cardiomyopathy, a more spherical left ventricular has been associated with poor survival. Finally, it has been shown that increased left ventricular sphericity is the primary factor in the etiology of mitral regurgitation rather than mitral annular dilatation or left ventricular enlargement.

Quantitating Left Ventricular Function

Left ventricular remodeling after AMI, resulting in dilatation of the left ventricle, is a progressive process beginning in the early phase and continuing for months and years. Our knowledge about the mechanisms and

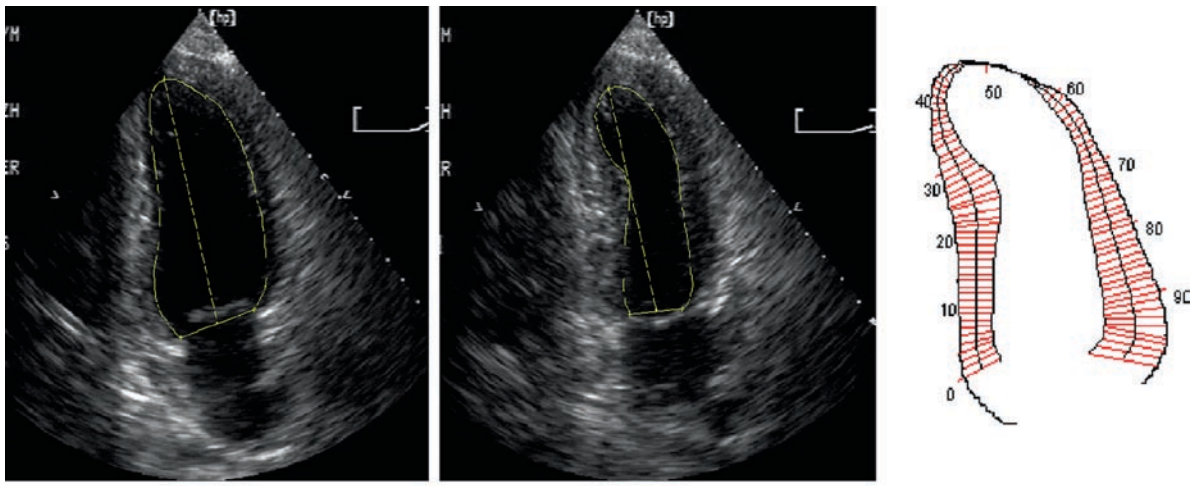

$$EF = \frac{EDV - ESV}{EDV} \times 100\%$$

Fig. 18.6 Quantitative 2-D echocardiographic evaluation of volumes and ejection fraction

temporal sequence of left ventricular remodeling has been mainly derived from quantitative two-dimensional echocardiographic evaluation (Fig. 18.6). Previous investigations have identified left ventricular function, anterior infarct location, and the patency status of the infarct-related artery as the most important independent predictors of remodeling. Furthermore, serial quantitative echocardiography has been used in several large, multicenter clinical trials (GISSI-1 to 3, SAVE, CONSENSUS-II) to demonstrate the beneficial effect of thrombolysis and angiotensin-converting enzyme inhibitors on left ventricular remodeling after AMI.

Progressive increase in left ventricular size is associated with deterioration in left ventricular function and increased mortality. It has been shown that left ventricular end-systolic volume is the primary predictor of mortality after AMI and the SAVE and GISSI-2 and 3 trials proved that quantitative echo measurements are the most powerful independent predictors of adverse cardiovascular events. Changes in left ventricular size and ejection fraction provide additional prognostic information, just like the additional value of changes in regional left ventricular function. In hospital survivors of acute MI treated with primary angioplasty for 5.3 years subsequent analysis showed that ejection fraction at 6 months and improvement in ejection fraction (from baseline to 6 months) were more important predictors of mortality than ejection fraction at the acute phase. Also in the V-HeFT trials, change in ejection fraction of >5% from baseline to 6 months and 1 year was the strongest predictor of mortality, even after adjustment for baseline ejection fraction. Regarding ejection fraction, the relation with mortality has been described as a hyperbolic curve with an upturn in mortality occurring at ejection fraction values of less than 40%. In the steep segment of the curve, a reduction of ten points in ejection fraction (from 30 to 20%) results in an upturn in mortality from 8 to 16%. In the flat part of the curve, the same reduction in ejection fraction (from 60 to 50%) leads to a nonsignificant increase in mortality from 1 to 1.5% (Fig. 18.7).

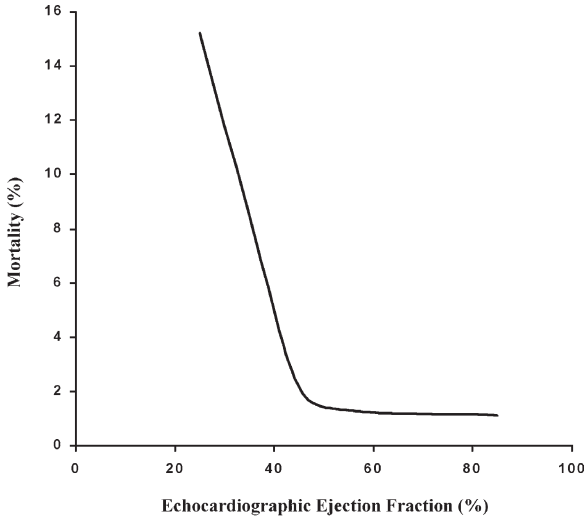

Fig. 18.7 Relation between mortality and ejection fraction (GISSI-2 trial)

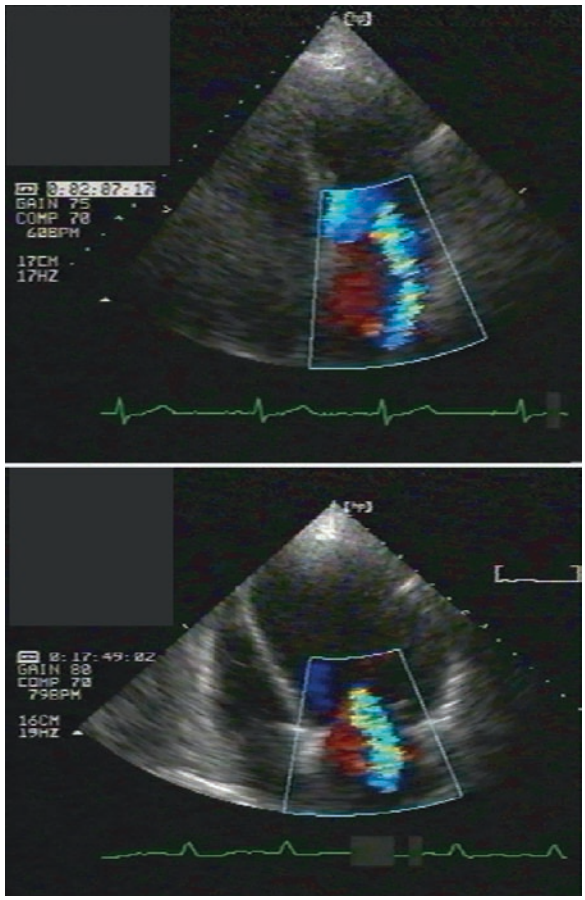

Fig. 18.8 Color Doppler evaluation of mitral regurgitation and mechanism of ischemic mitral regurgitation: papillary muscle rupture; papillary muscle dysfunction; mitral annular dilatation/ generalized dilatation

Ischemic Mitral Regurgitation

Color Doppler echocardiography can be used to assess the presence and severity of mitral regurgitation in patients with acute MI (Fig. 18.8). Significant mitral regurgitation – moderate (grade 2) or severe (grades 3 and 4), graded according to the method of Helmcke et al, – has been found in 3–21% of patients following acute MI. The incidence and severity of mitral regurgitation changes during follow-up, with the highest incidence on the seventh day. Most studies have demonstrated a relation between mitral regurgitation and inferoposterior infarct location, while others found either no influence of infarct location or an increased incidence in anterior infarctions. Significant mitral regurgitation has been correlated to female gender, older age, and previous MI. Furthermore, abnormalities of left ventricular shape – more spherical ventricles – and inferoposterolateral wall motion abnormalities have been found to be independent predictors of mitral regurgitation.

Mechanisms

- The most dramatic etiology results from frank rupture of a part or the entire papillary muscle. The incidence of this complication is reported to be only 1%. The infarction is usually posterior and is often small and localized; ejection fraction is frequently maintained. There is a high prevalence of one-vessel disease and occluded infarct-related arteries.
- Another form of ischemic mitral regurgitation results from papillary muscle dysfunction. The pathogenesis of this form of mitral regurgitation is unclear. Small changes in the spatial relation of the papillary muscles and the mitral valve leaflets and annulus (due to regional wall motion abnormalities and left ventricular shape changes) may produce incomplete mitral leaflet closure, resulting in eccentric mitral regurgitation. This mechanism is more common in inferoposterior MIs, possibly because the blood supply to the posterior papillary muscle is

provided by one rather than by two coronary vessels, as in the anterior papillary muscle.

- The third category consists of patients with multiple MIs or anterior aneurysms with low ejection fractions. The regurgitation results from the central area of the mitral leaflets and is secondary to generalized ventricular and initial annular dilatation. Presence of mitral regurgitation on catheterization or Doppler echocardiography has been related to higher cardiovascular mortality and severe congestive heart failure. In patients studied with Doppler echocardiography within 48 h after acute MI, the one-year mortality was 48% in patients with mitral regurgitation, and 11% in those without. In other studies, mitral regurgitation was found to be an independent predictor of cardiovascular mortality.

Left Ventricular Diastolic Function

Pulsed Doppler echocardiography is useful for assessment of left ventricular diastolic properties. Three distinct abnormal mitral inflow patterns have been described and correlated with hemodynamic findings.

- One pattern, characterized by a low E wave, a high A wave, a low E/A ratio, and a prolonged E deceleration time (Fig. 18.9b), is thought to be the consequence of impaired relaxation in the presence of normal left ventricular filling pressures. It has been described in normal aging, left ventricular hypertrophy, and acute ischemia.
- The opposite pattern, characterized by high E waves, low A waves, high E/A ratio, and short E deceleration time (Fig. 18.9c), is associated with high left ventricular filling pressure and increased chamber stiffness and is observed in advanced cardiac disease. The short deceleration time suggests an early equalization of pressures in the left atrium and the left ventricle.
- The third pattern is essentially a normal pattern that has been referred to as "pseudonormal." This pattern may represent a transitional state between impaired relaxation and restrictive patterns in patients with left ventricular systolic dysfunction.

Several investigators have studied the left ventricular filling patterns in patients with AMI. An abnormal relaxation pattern has been shown to be more common

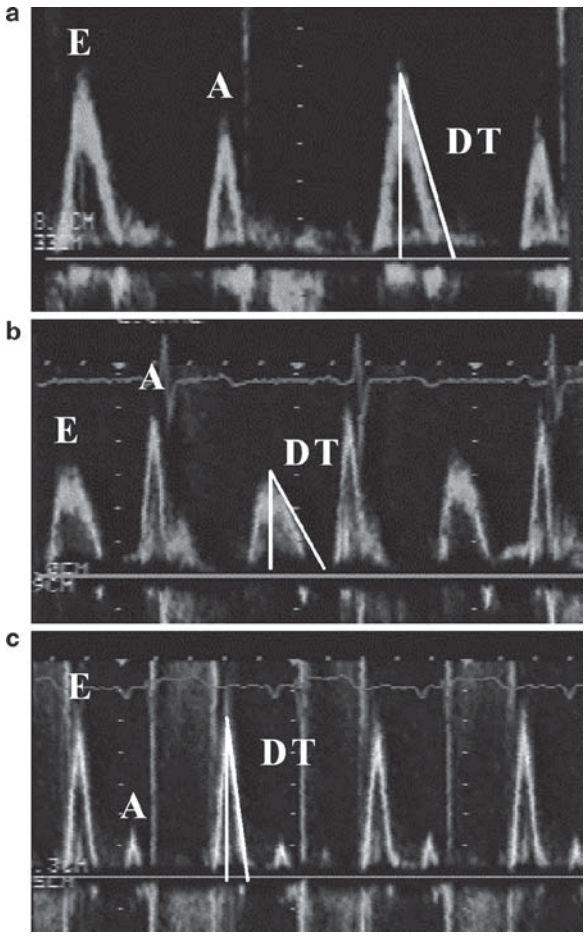

Fig. 18.9 Mitral inflow patterns after myocardial infarction

in patients with small infarctions. In contrast, patients with large infarctions often exhibit a "pseudonormalized" or even restrictive within the first week. It has been demonstrated that this frequently changes over time becoming less restrictive, maybe as result of left ventricular remodeling. Patients with anterior MI treated with primary angioplasty and a restrictive filling pattern at day 3 (defined as E deceleration time <130 ms) had progressive increases in left ventricular volume indexes at 6 months, in contrast to patients with nonrestrictive filling. E deceleration time was the most powerful predictor of left ventricular dilatation. Limited studies have assessed the relation between left ventricular filling patterns and prognosis after AMI. In patients examined with serial Doppler echocardiography on days 1.3, 7, and 3 months after AMI, left ventricular filling patterns were related to clinical follow-up for

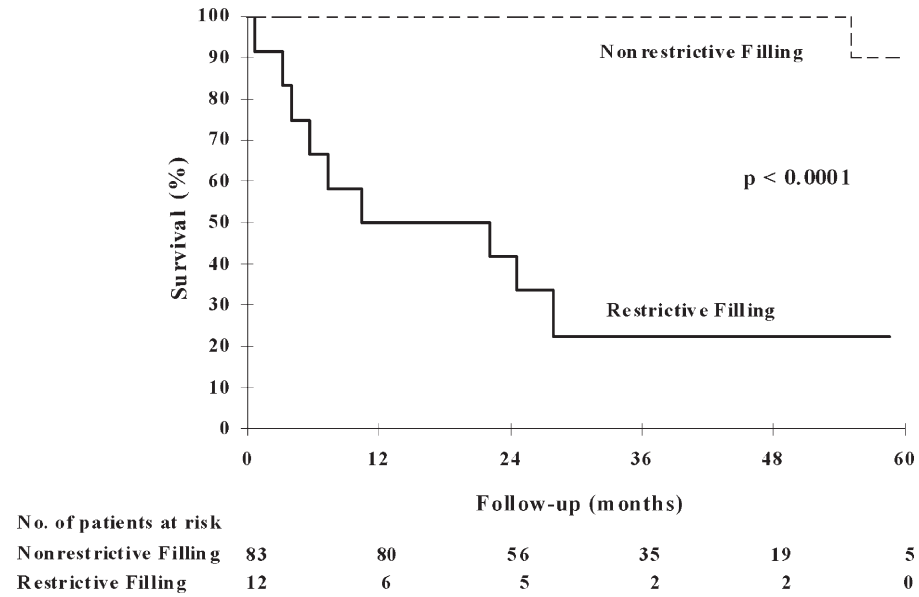

Fig. 18.10 Left ventricular filling and cardiac survival

32 ± 17 months. The survival rate at 1 year was 100% in patients without restrictive filling and 50% in those with restrictive filling (Fig. 18.10). Left ventricular filling pattern was the most powerful independent predictor of cardiac death and adds significant prognostic information to indicators of systolic dysfunction (ejection fraction and end-systolic volume). Other studies also found that restrictive filling was an independent predictor of cardiac death. Finally, it has been demonstrated that the presence of restrictive filling is an independent predictor of heart failure after AMI. An explanation for this observation may be the markedly elevated filling pressure often found in these patients. Also, a strong relation between restrictive filling and elevated pulmonary wedge pressure in post MI patients with left ventricular systolic dysfunction was observed. An E/A ratio >2 was associated with pulmonary capillary wedge pressure >20 mm Hg in 96% of patients, whereas E deceleration time provides an accurate estimate of left ventricular filling pressure in patients with a "normal" E/A ratio.

Recently, using Tissue Doppler of the LV annulus, E/Em has been shown to be a powerful predictor of survival after myocardial infarction and E/Em >15, an indicator of high LV filling pressures, is superior as predictor of prognosis to other clinical and echocardiographic variables.

Left Ventricular Spatial Flow Pattern

Color Doppler echocardiography and pulsed-wave Doppler flow mapping can be used to assess the flow patterns in the left ventricle.

Normal left ventricular flow is characterized by

1. Simultaneous onset of blood motion at the mitral valve leaflets and apical level
2. A discontinued Doppler signal along the lateral wall (a diastolic positive wave, followed by a negative wave during systole) and interventricular septum (an early diastolic positive wave, followed by a negative wave at late diastole and systole)

Abnormal flow patterns can be recognized:

1. Apical rotating flow and vortex ring formation characterized by systolic persistence of red near the lateral wall. On pulsed Doppler, there is a continuously positive flow signal near the lateral wall and a continuously negative signal near the septum.
2. Vortex ring formation is characterized by central red flanked on both sides by blue during diastole. On pulsed-wave Doppler this pattern is characterized by an apparent delay in onset of blood motion at the apical level compared with the mitral valve

left ventriculare; in addition, a higher flow velocity compared with normal is found at the apex.
- The presence of an abnormal flow pattern after AMI is highly associated with left ventricular thrombus formation. In patients with acute MI, flow patterns were examined within 24 h, after 6 weeks and 3 months. None of the patients with a normal left ventricular flow pattern at the first examination developed a thrombus, versus 40% of patients with an abnormal flow pattern. Furthermore, an abnormal left ventricular flow pattern has been shown to be an independent predictor of thrombus formation.

Left Ventricular Thrombi

A left ventricular thrombus is mostly found in the setting of a transmural MI with a clear akinetic or dyskinetic state of the infarcted wall segment. Disability or even mortality after acute MI may be the result of a left ventricular thrombus and subsequent embolization. In the GISSI-III study, the incidence was approximately 12% in anterior MIs, mostly observed in the left ventricular apex, and 2% in MI at other sites. Most thrombi occur within the first two weeks after acute MI and are easily detected by two-dimensional echocardiography with a sensitivity of almost 95% and a specificity of 90%. Oral anticoagulation (warfarin, coumarin) is the treatment of choice to prevent embolic events. Mobile and protruding thrombi and adjacent hyperkinesia are markers of high risk of systemic embolization. The disappearance or reduction in size of left ventricular thrombi during anticoagulation therapy can be observed by serial two-dimensional echocardiography in approximately half of the patients during one-year follow-up. Resolution was more likely to occur in patients without apical dyskinesis.

Myocardial Viability

Low-dose dobutamine echocardiography is one of the currently available techniques for determining the presence of viable myocardium (Fig. 18.11). The response of myocardial segments that are dysfunctional at rest to low-dose dobutamine predicts recovery of regional function after acute MI with sensitivities and specificities ranging from 66 to 100% and from 68 to 94%, respectively (Table 18.6). Several studies have evaluated the prognostic implications of myocardial viability in patients with AMI and in patients with recent or previous MI. The presence of myocardial viability in the Echo Dobutamine International Cooperative (EDIC) Study in 778 patients early after acute MI was associated with an increased incidence of unstable angina. Others also demonstrated that presence of viable myocardium independently predicts ischemic events. Myocardial viability was the single best predictor of cardiac events (mainly unstable angina and revascularization procedures) in patients with previous MI. The presence of myocardial viability independently predicted recurrent ischemia in patients early after acute MI.

The prognostic impact of viability on cardiac mortality remains unresolved. Myocardial viability did not predict cardiac death, which predominantly correlated with age and ejection fraction in some studies. Ejection fraction, but not myocardial viability, was significantly associated with the occurrence of cardiac death in some studies. Only in patients with an ejection fraction lower than 35%, cardiac death occurred less frequently in patients with viability who underwent revascularization. In these patients with reduced ejection fraction, absence of viability predicted a high mortality rate.

Similar conflicting results have been found *early* after acute MI. In patients with left ventricular systolic dysfunction and with myocardial viability, the presence of left ventricular dysfunction was predictive for hard cardiac events. In other studies, hard events were not predicted by the presence of myocardial viability and thus myocardial viability did not have independent prognostic value. Prospective studies on the impact of myocardial viability in patients' outcome however are lacking. Until that time, the presence of myocardial viability is currently a strong indicator for revascularization.

Residual Myocardial Ischemia

Stress echocardiography in patients after MI can be safely performed predischarge with use of exercise-related or pharmacologically induced stress, including dobutamine and dipyridamole. It is based on the principle that stress-induced ischemia results in new or worsening

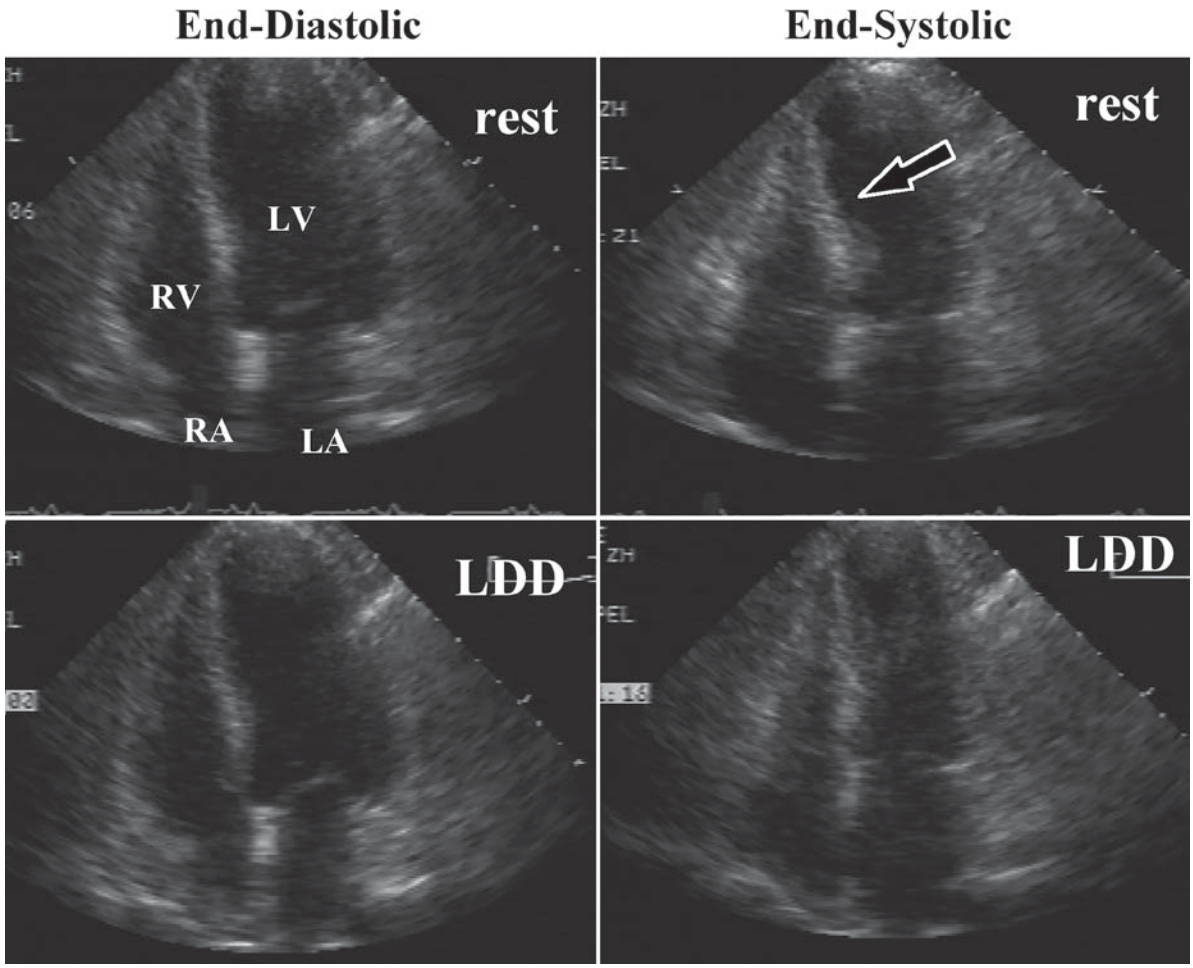

Fig. 18.11 Enddiastolic and endsystolic still frames of an apical four-chamber view at rest and during low-dose dobutamine infusion. Note the presence of myocardial viability in the middle and apical segment of the inferoseptal wall (*arrow*)

Table 18.6 Sensitivities and specificities of low-dose dobutamine echocardiography to detect functional recovery after acute MI

Authors	No. of patients	Follow-up echo (months)	Sensitivity (%)	Specificity (%)
Pierard	17	9	100	70
Smart	63	1	86	90
Previtali	59	2	79	68
Salustri	57	3	66	94
Watada	21	1	83	86
Leclerq	40	2	82	83
Smart	115	1–2	86	83

wall motion abnormalities that can be detected by two-dimensional echocardiography. During the last 10 years, digital technologies have rendered stress echocardiography more feasible. A single cardiac cycle can be stored before, during, and after stress, and replayed indefinitely. Each loop can be reviewed in synchrony, side by side with other loops, through which the comparison of different conditions is made easier.

Exercise echocardiography has been used to evaluate patients after acute MI. The occurrence of new or worsening wall motion abnormalities predicted the development of future cardiac events, with a sensitivity ranging from 63 to 80% and a specificity of 78 to 95%. However, major limitations of these studies are the relatively small sample size and the inclusion of soft and subjective endpoints, such as unstable angina and revascularization procedures, in order to document prognostic power.

High-dose dobutamine echocardiography has been found very useful for risk stratification after acute MI. Two-dimensional echocardiography is performed during infusion of dobutamine up to 40 mg/kg/min, and if necessary, with addition of atropine. The contractile response of stunned myocardium to high-dose dobutamine is variable, depending on the infarct-related artery stenosis. When there is a flow-limiting stenosis, a biphasic response can be found (improvement at low dose followed by worsening at high dose), while, when there is no flow-limiting stenosis, the improvement of stunned myocardium continues throughout the infusion. In this way, dobutamine echocardiography is able to predict the presence of a severe residual stenosis of the infarct-related artery and can identify high-risk patients who benefit most from revascularization procedures.

Moreover, dobutamine echocardiography is able to elucidate transient wall motion abnormalities in the remote area. The occurrence of remote asynergy during stress testing has shown to be correlated with multivessel coronary artery disease and is predictive of future ischemic events.

The prognostic impact of inducible ischemia by high-dose dobutamine after acute MI has been extensively studied. Several studies have evaluated the event rate of both hard and spontaneous cardiac events in patients with a negative versus a positive dobutamine stress echocardiogram. The risk of cardiac death doubles if the test is positive. Positivity of dobutamine stress echocardiography is an independent predictor of hard cardiac events (death and nonfatal reinfarction) and all cardiac events (death, nonfatal reinfarction, and unstable angina). Wall motion score index at peak-dose dobutamine, reflecting the extent of MI and ischemia, is found to be an independent predictor of cardiac death.

Dipyridamole echocardiography can also be used to evaluate myocardial viability, residual ischemia, and prognosis after AMI.

Future Developments

Three-dimensional echocardiography may become the ultimate diagnostic modality because it can display the left ventricle, its size, shape, and abnormalities in motion from any perspective. With the use of the real-time 3D modality with a matrix transducer, the echo examination will become more standardized and less operator dependent. Cardiac cross-sections that are difficult or impossible to obtain from the regular precordial studies can be computed from the data set in any desired plane (anyplane echocardiography). The images needed for diagnosis are only part of the total three-dimensional data set, and left ventricular function in patients with coronary artery disease can be visually assessed and quantified. Specifically, true volumes of aneursymal left ventricles can be assessed without geometric assumptions rather than using one or two orthogonal planes. The echo examination itself will be easier and quicker, although more time will be needed for subsequent wall motion analysis at a viewing station and for left ventricular volume calculations.

Clinical Recommendations and Implications

The goal of risk stratification after acute MI is to identify patients whose outcomes can be improved through specific medical interventions. Patients with the highest risk for cardiac death or recurrent ischemic events benefit most from aggressive medical therapy and/or revascularization procedures. In these times of evidence-based and cost-effective management, the selection of a test that provides the most useful diagnostic and prognostic information is of paramount importance. In this regard, echocardiography has proven its value. Patients who have nearly normal left ventricular function have a very low risk for death and may therefore be candidates for early discharge from the hospital.

Predischarge or early postdischarge stress testing should be used for further risk stratification within this group of patients. Only in patients who cannot exercise or whose baseline ECG precludes accurate interpretation of exercise-induced ischemia, pharmacologically induced stress echocardiography should be performed. The incremental value of additional echocardiography in all patients has not been shown to be worth the increased costs.

Routine re-evaluation by echocardiography in the absence of any change in clinical status is not recommended. In the evaluation of systemic hypotension and/or a suspected mechanical complication of MI, echocardiography is of utmost importance to differentiate between low output due to poor left ventricular function, decreased preload, peripheral vasodilation or cardiac tamponade, or mechanical complications such as ventricular septal rupture, papillary muscle rupture, and free wall rupture. This will be discussed in more detail in the next chapter.

Patients with moderate to severe systolic dysfunction are at higher risk for cardiac death, heart failure, and left ventricular dilatation. Pulsed-wave Doppler of left ventricular filling should be assessed, because presence of restrictive left ventricular filling identifies patients at very high risk of cardiac death. Assessment of myocardial viability and presence and extent of ischemia could be useful to define the potential efficacy of revascularization procedures.

Finally, serial echocardiography is recommended in patients with moderate to severe left ventricular dysfunction to assess changes in regional and global systolic function and left ventricular volumes, since these changes have independent prognostic value and can be used to guide therapy. Serial echocardiography is also recommended in patients with left ventricular thrombi.

Bibliography

Bholansingh R, Cornel JH, Kamp O, et al. Prognostic value of predischarge dobutamine stress echocardiography in patients with a negative cardiac troponin T. *J Am Coll Cardiol*. 2003;41:596–602.

Hillis GS, Moller JE, Pellikka PA, et al. Noninvasive estimation of left ventricular filling pressure by E/e' is a powerful predictor of survival after acute myocardial infarction. *J Am Coll Cardiol*. 2004;43:360–367.

Korup E, Kober L, Torp-Pedersen Ch, Toft E, Tranolapril Cardiac Evaluation (TRACE) Study Group. Prognostic usefulness of repeated echocardiographic evaluation after acute myocardial infarction. *Am J Cardiol.* 1999;83:1559–1562.

Nijland F, Kamp O, Karreman AJP, van Eenige MJ, Visser CA. Prognostic implications of restrictive left ventricular filling in acute myocardial infarction: a serial Doppler echocardiographic study. *J Am Coll Cardiol*. 1997;30:1618–1624.

Nijland F, Kamp O, Verheugt FWA, Veen G, Visser CA. Long-term implications of reocclusion on left ventricular size and function after successful thrombolysis for first anterior myocardial infarction. *Circulation*. 1997;95:111–117.

Nijland F, Kamp O, Verhorst PMJ, de Voogt WG, Visser CA. In-hospital and long term prognostic value of viable myocardium detected by dobutamine echocardiography early after acute myocardial infarction and its relation to indicators of left ventricular systolic dysfunction. *Am J Cardiol*. 2001;88:949–955.

Peels CH, Visser CA, Kupper AJ, Visser FC, Roos JP. Usefulness of two-dimensional echocardiography for immediate detection of myocardial ischemia in the emergency room. *Am J Cardiol*. 1990;65:687–691.

St John Sutton M, Pfeffer MA, Plappert T, et al, for the SAVE Investigators. Quantitative two-dimensional echocardiographic measurements are major predictors of adverse cardiovascular events after acute myocardial infarction. The protective effects of captopril. *Circulation*. 1994;89:68–75.

Van Dantzig JM, Delemarre BJ, Bot H, Koster RW, Visser CA. Doppler left ventricular flow pattern versus conventional predictors of left ventricular thrombus after acute myocardial infarction. *J Am Coll Cardiol*. 1995;25:1341–1346.

Visser CA, Kan G, Meltzer RS, Koolen JJ, Dunning AJ. Incidence, timing and prognostic value of left ventricular aneurysm formation after myocardial infarction: a prospective, serial echocardiographic study in 158 patients. *Am J Cardiol*. 1986;57:729–732.

Visser CA, Lie KI, Kan G, Meltzer R, Durrer D. Detection and quantification of acute, isolated myocardial infarction by two dimensional echocardiography. *Am J Cardiol*. 1981;47:1020–1025.

Chapter 19
Mechanical Complications of Myocardial Infarction

Daniel Monakier and Harry Rakowski

Echocardiography is the primary diagnostic tool for detection of potentially life-threatening complications of acute myocardial infarction (AMI). Its immediate availability and the detailed information it provides both on the heart's mechanical function and blood flow are critical in the management of patients with mechanical complications. The echocardiography-based decision of referring such patients for immediate surgery makes this diagnostic modality a life-saving procedure.

It is extremely important for the physician or sonographer performing the examination, not only to have knowledge of the echocardiographic characteristics of the different complications, but also of the patient's clinical history (Table 19.1). The time elapsed from the occurrence of infarction, the myocardial wall affected, and whether the patient was treated with direct angioplasty or thrombolytic therapy for AMI are all important data that can help in searching for a particular type of complication.

The role of echocardiography is not limited to diagnosis. It is an important tool in guiding the intraoperative management (usually with transesophageal echocardiography) and in assessing the outcome of high-risk and complicated surgeries. Newer echocardiographic modalities, such as real-time 3D echocardiography and contrast echocardiography, are playing a greater role in the diagnosis of these patients.

D. Monakier and H. Rakowski (✉)
Toronto General Hospital, 4N-Room 504,
200 Elizabeth Street, Toronto, ON, Canada, M5G2C4
e-mail: harry.rakowski@uhn.on.ca

Rupture of LV Free Wall

Free wall rupture (FWR) of the left ventricle (LV) is the most common form of myocardial rupture. It is the cause of death in approximately 10% of the patients who die of an acute myocardial infarction (AMI). It occurs within the first 24 h in 40% of the patients and within a week in 85%. Any wall – anterior, lateral, or posterior – can be involved (Fig. 19.1). Death usually occurs quickly unless an immediate diagnosis and surgery can be performed. However, in up to 40% of cases, ruptures have a subacute course with ongoing myocardial tearing and bleeding into the pericardial space. Pseudoaneurysm, which is discussed later, is a manifestation of a subacute tear that is spontaneously sealed. The usual presentation of FWR is with sudden hemodynamic collapse, electromechanical dissociation, and death occurring before an echocardiographic assessment can be performed. Symptoms and signs of recurrent chest pain, syncope, transient hypotension and bradycardia, nausea, agitation, restlessness, and unexpected alterations of T waves – especially directional changes, although nonspecific – are more frequently found in patients with a subacute FWR. Therefore, a high index of suspicion in such patients is the key for the echocardiographic detection of FWR. Several studies describe the incidence and risk factors of FWR in the current era of early direct coronary angioplasty and thrombolysis for treating AMI. In a recent series of 1,250 patients treated with direct coronary angioplasty for AMI, 12 patients (0.96%) had cardiac rupture (free wall rupture (9), septal rupture (3)). Old age, female gender, lower body mass index, and longer time to reperfusion were risk factors for cardiac rupture, while early successful direct coronary

P. Nihoyannopoulos and J. Kisslo (eds.), *Echocardiography*,
DOI: 10.1007/978-1-84882-293-1_19,

Table 19.1 Summarizes the principal clinical and echocardiographic findings in patients with mechanical complications of MI

	Clinical findings	Echo findings
Ventricular septal rupture	Risk factors: female, advanced age, extensive, anterior, transmural, RV infarction, and total occlusion of MI-related artery	Simple – Doppler color jet at the same level in LV and RV. Usually anteroapical. Complex – serpinginous tracts. Hemorrhage. More common in inferoposterior MI
Free wall rupture	Most common rupture. Dramatic presentation. Risk factors: female, advanced age, first MI, Ant. wall MI, prolonged time to reperfusion, no restriction of physical activity after MI. Early successful PCI is protective	Pericardial effusion (>5 cm), layered thrombus in pericardial space and tamponade. Site of rupture identified only in 50%
LV pseudoaneurysm	Subacute presentation (chest pain, nausea, hypotension) of rupture contained by pericardium. May evolve to FWR. Inf. Wall MI 2× common than anterior MI. "Mass" seen in CXR of 1/3 of patients	To-and-Fro color Doppler jet through a narrow neck (ratio < 0.5 with body of PA). May contain thrombus
LV aneurysm and thrombus	Common in anterior wall MI. Rarely ruptures. May present with CHF, Vent. Arrhythmias and systemic emboli	Bulging contour of an akinetic or dyskinetic LV segment, usually apex. Neck to body ratio: 0.9–1.0:1.0. May contain thrombus (acute-mobile, chronic-mural)
Rupture of papillary muscle	Rare. Severe pulmonary edema. Inferolateral MI. Can occur with NQMI. PM papillary muscle the most affected. DD-ischemic MR	Severe MR, flail mitral leaflet, head of PM may be seen in LA or as a mass with erratic motion (TEE) in LV. LV systolic function not significantly impaired

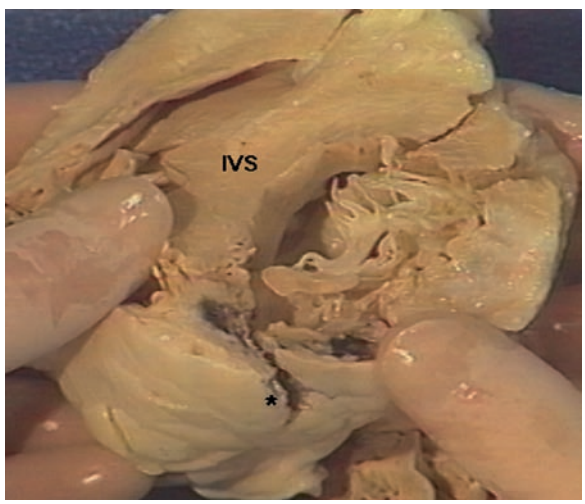

Fig. 19.1 Pathology specimen demonstrating slit-like LV free wall rupture (*asterisk*). Adjacent necrotic tissue of infarction is evident (*IVS* interventricular septum) (Courtesy of Dr. J. Kisslo)

angioplasty was the most powerful determinant for avoiding cardiac rupture. Thrombolysis has been reported to be an independent risk factor for the occurrence of FWR. In a study that evaluated the effect of primary angioplasty vs. thrombolytic therapy on the risk of FWR, 34 patients (2.5%) had FWR, of which 14 (1.8%) and 20 (3.3%) were treated with angioplasty and thrombolysis, respectively (difference was not statistically significant). In the multivariate analysis, age > 70 and anterior location were independent risk factors for FWR, whereas direct angioplasty was an independent protective factor. Other reported risk factors for FWR are: total occlusion of the LAD, mild pericardial effusion in the first 2 days post MI in patients >60 years with a first ST-segment elevation AMI, and pericardial rub associated with TIMI flow <3.

Echocardiographic Findings

Pericardial effusions secondary to hemopericardium, layered thrombus in the pericardial space, and cardiac tamponade are the most common findings in the hemodynamically unstable patient with FWR (Fig. 19.2). Post AMI pericardial effusion of 5 mm during diastole and layered thrombus within the pericardial space are highly sensitive (up to 100%) for the detection of FWR while specificity is 79%. The ruptured site is seldom detected with 2D echocardiography; however, this may be possible with color-flow Doppler (Fig. 19.3).

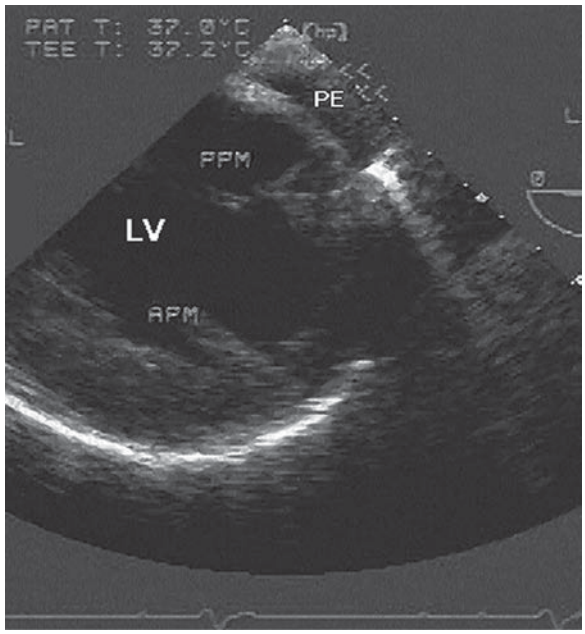

Fig. 19.2 Transgastric TEE view depicting the long-axis left ventricle (LV). A posterior, loculated pericardial effusion (PE) is evident. It is not uncommon that pericardial effusion is the only echocardiographic finding in free wall rupture. The site of rupture was not visualized in this patient (*PPM* posterior papillary muscle; *APM* anterior papillary muscle)

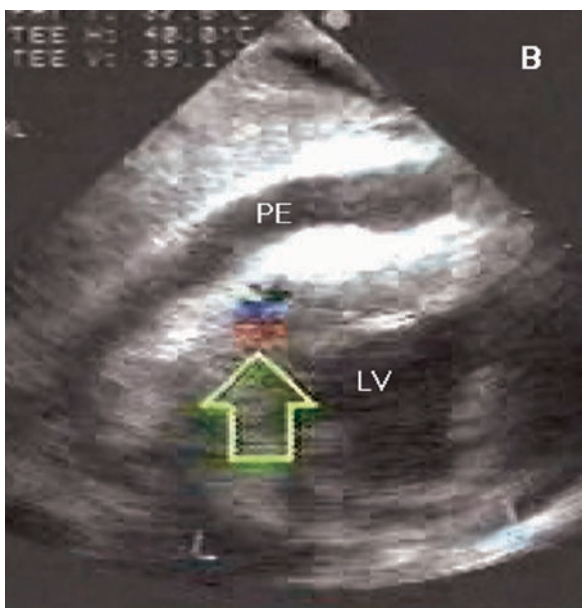

Fig. 19.3 Transgastric, short-axis view of the left ventricle. The posterior-inferior pericardial effusion (PE) was caused by rupture of the LV free wall. In addition, ventricular septal rupture was also present as shown by the turbulent jet in the ventricular septum (*arrow*)

The injection of IV contrast echocardiography may be helpful in confirming or excluding the diagnosis of FWR in patients with a subacute presentation. In a recent report, passage of an echo-contrast agent (optison) to the pericardial space after an IV injection helped to confirm rupture in one patient, while lack of staining of pericardial space with contrast helped in excluding FWR in a second patient.

The current surgical management for left ventricular FWR is patch-glue repair without extra corporeal circulation. The insertion of an intra-aortic balloon pump is advocated and access is obtained via median sternotomy. This approach is possible in patients with the subacute presentation of FWR and is an alternative to infarctectomy and ventricular reconstruction using cardiopulmonary bypass. In a series of 17 patients with FWR treated with the patch-glue repair, perioperative mortality was 23.5% and 30-day post-discharge survival was 85% at 2.2 years.

Transesophageal Echocardiography and AMI Complications

Transesophageal echocardiography (TEE) is a useful procedure for the detection of mechanical complications in post AMI patients. In a study of 55 patients who had TEE in a coronary care unit during the first week post AMI, the main reason for performing TEE (62% of cases) was to rule out the presence of mechanical complications. It helped in confirming the diagnosis in 2 of the 3 patients studied to rule out FWR and confirmed ventricular septal rupture in 12 of the 15 patients studied for that purpose. There were two deaths (3.6%) during and immediately following TEE. One was in a patient with cardiogenic shock due to partial rupture of the posteromedial papillary muscle resulting in severe mitral regurgitation and the other patient had acute rupture of the left ventricular free wall. None of the patients was intubated and both were sedated with IV benzodiazepines. The authors postulated that the Valsalva maneuver caused by esophageal intubation could have been the mechanism that triggered death in these patients, and therefore caution is advised in the usage of TEE in patients with mechanical complications of AMI. Our opinion is that tracheal intubation, mechanical ventilation, and appropriate sedation should be considered in hemodynamically

unstable post AMI patients in whom a TEE is required. Transesophageal studies should be considered whenever the surface study is inconclusive or if multiple abnormalities are suspected (Fig. 19.3).

LV Pseudoaneurysm

Left ventricular pseudoaneurysm (LVP) is formed when cardiac rupture is contained by adherent pericardium or scar tissue. No endocardial or myocardial elements are present in the external layer of the pseudoaneurysm, while in a true LV aneurysm the outer layer consists of thin areas of scarred myocardium. It is important to differentiate LVP from a true LV aneurysm, which rarely ruptures, because the treatment of the first condition usually requires surgical repair. This differentiation may be difficult, since the characteristics of these two entities overlap. Clinically, congestive heart failure and embolic events may occur, as with true LV aneurysm, and there may be similarities in findings of different imaging modalities. In a review of 290 case reports of LVP, the median age was 60 years and 68% of patients were male. Congestive heart failure, chest pain, and dyspnea were the most frequent conditions or symptoms reported (36, 30, 25%, respectively). Heart murmurs were found in two-third of patients. Electrocardiographic abnormalities were found in 95% of patients; however, most were nonspecific ST changes. Abnormal chest X-rays were reported in 97% of patients and the most common finding was "enlarged heart." Interestingly, almost one-third of patients had evidence of mass on chest X-ray. The most common diagnostic modality to be employed was angiography, revealing some abnormality in 98% of the patients and providing a definitive diagnosis in 87% of patients. Echocardiography was less frequently used in this series, and Doppler and TEE were performed only in a small proportion of the group. The most common location for LVP was the posterior wall, followed by lateral, apical, inferior, and anterior location. It is unclear why LVP is more common in the posterior wall, while the most common location of FWR is the anterior wall. A possible hypothesis raised by the authors was that with the recumbent position, post AMI patients have a greater inflammatory response to myocardial infarctions that involve the posterior wall. This may cause pericardial adhesions, which prevent hemopericardium and formation of tamponade. Of 140 patients who had follow up, 107 underwent surgery for the LVP. Twenty-three percent of patients died at a median of 3 days after operation, and all 82 patients who survived surgery were alive at a median of 46 weeks. Fifteen (48%) of the 31 patients who were treated conservatively, died at a median of less than 1 week. Recent case reports suggest that patients with LVP who have stable hemodynamic status can have long-term survival without surgery.

Echocardiographic Findings

The echocardiographic diagnosis of LVP is usually made when performing a routine post-MI study for LV function or evaluating a patient for congestive heart failure or embolic event. The 2D Echo characteristics of LVP are: a sharp discontinuity of the endocardial border at the communication site of the pseudoaneurysm with the LV cavity, a saccular or globular contour of the LVP chamber, and a relatively narrow orifice or "neck" comparing to the diameter of the fundus of the LVP (Fig. 19.4). A maximal ratio of 0.5 for the diagnosis of LVP has been reported in 82% of 92 patients with pseudoaneurysm. In contrast, true LV aneurysms

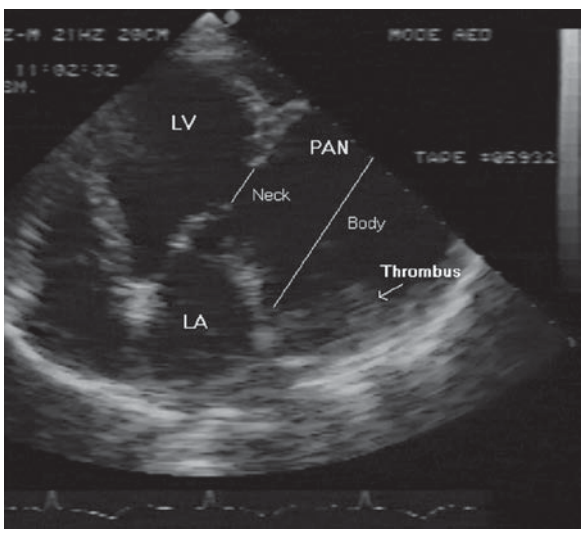

Fig. 19.4 A very large pseudoaneurysm (PAN) of the lateral wall is seen in this four-chamber apical view. Note that the diameter of the neck is significantly narrower than the diameter of the body. A thrombus layers the superior portion of the pseudoaneurysm. (*LA* left atrium; *LV* left ventricle)

have orifice-to-LVP diameter ratio of approximately 0.9–1.0. Careful examination and usage of unconventional planes may sometimes be required for the identification and characterization of the site of rupture. At times, a thrombus can be visualized (Fig. 19.4). Color-flow Doppler improves the probability for the detection of LVP and its typical feature is the bidirectional flow between the LV and pseudoaneurysm. This to-and-fro flow allows the distinction between LVP and pericardial effusion and the turbulence and size of jet differentiate LVP from true aneurysms. The use of contrast agents may aid in the diagnosis of LVP. Intravenous administration of contrast-echo agents has facilitated a definite diagnosis of LVP by showing the narrow neck and the blood flow communicating the LV and LVP cavity (Fig. 19.5). Three-dimensional reconstruction of TEE imaging has been reported to be useful in the assessment of a patient with LVP and severe mitral regurgitation: While 2D TEE failed to properly assess the anterolateral papillary muscle, 3D reconstruction clearly defined the rupture in LV free wall and the intact papillary muscle. Mitral regurgitation disappeared after LVP was repaired, obviating the need for mitral valve repair or replacement.

Intramyocardial rupture is another form of subacute rupture of the myocardium. In this rare entity rupture of the affected wall after an AMI causes a dissection plane within the myocardium. The rupture does not reach the pericardial surface, forming an intramyocardial hematoma. Echocardiography, especially TEE performed in the acute phase, typically shows a "cystic" formation seen as an echo-lucent mass containing blood that protrudes into the LV cavity. Echocardiography performed on subsequent days shows increasing echogenicity of the cavity, representing organization of the hematoma. Subsequently, the hematoma is reabsorbed and the echocardiographic appearance at 3 weeks is very similar to that of a chronic mural thrombus as shown by Vargas-Barron with 3D TEE reconstruction. Evidence of internal endocardial layer that contracts well can differentiate intramyocardial hematoma from a fixed mural thrombus.

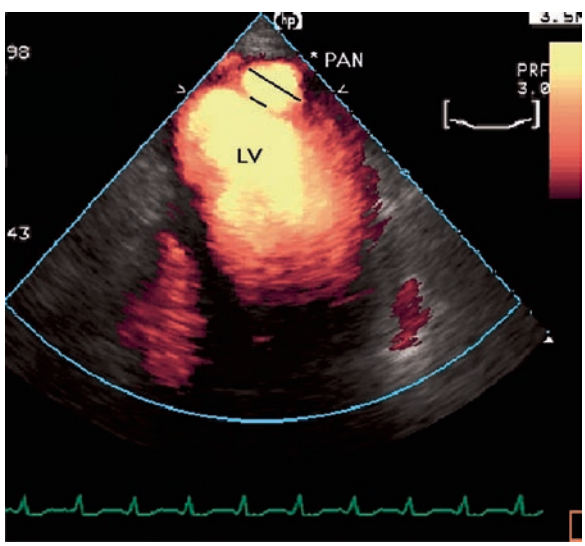

Fig. 19.5 Apical view of an apicolateral pseudoaneurysm (PAN) connected to the echo-contrast filled LV through its narrow neck (Courtesy of Dr. Roberto Lang, Chicago)

Ventricular Septal Rupture

The typical presentation for this complication is a patient with severe cardiac decompensation manifested by low cardiac output or shock, occurring usually within a week of an AMI. Often, it is associated with the appearance of a systolic murmur that has to be differentiated from that of acute mitral regurgitation secondary to rupture of a papillary muscle. It occurs in transmural MI and is more frequent in acute anterior infarction, extensive infarction, right ventricular infarction, and in total occlusion of the infarct-related artery. Other risk factors are female gender and advanced age. This complication of MI is rare, due to the dual blood supply of the ventricular septum, with the anterior two-third being supplied by branches of the left anterior descending coronary artery and the posterior third by the posterior descending artery of either the right or circumflex coronary arteries. In the prethrombolytic era, rupture of the interventricular septum occurred in 1–3% of all AMI. Thrombolytic therapy has largely reduced the rate of ventricular septal rupture (VSR) after AMI to only 0.2–0.3%. Hypertension and lack of history of angina or MI are risk factors for VSR in patients not treated with reperfusion therapy but not in those who received thrombolytic therapy. The timing of occurrence of VSR also varies. It occurs within the first week post MI in patients who did not receive reperfusion therapy, peaking on the first day and on days 3–5 post MI. In patients receiving thrombolytic therapy for AMI, most ruptures occur within the first 48 h.

Septal ruptures may be simple or complex. The first is a discrete defect with a direct through-and-through communication at the same level on both sides of the septum. The second is an irregular rupture with serpinginous tracts and extensive hemorrhage. While in anterior MI, septal rupture is usually apical and simple, the rupture in inferior MI occurs more commonly in the basal inferoposterior septum and is more often complex.

The treatment of VSR is surgical repair and patients should be operated on as soon as possible. The 30-day mortality rate is 70–80% in patients who are medically treated, 25% of them dying within 24 h, and 65% within 2 weeks of septal perforation. The 30-day mortality can be reduced to approximately 35% in patients who had surgical repair. Recently, a few case reports have described the feasibility of closing the ruptured septum with a percutaneous device closure (Fig. 19.6). It is unclear yet whether this could be an acceptable alternative to surgery.

Echocardiographic Findings

With 2D echocardiography, direct visualization of the ventricular-septal defect can be achieved in approximately 50% of patients (Fig. 19.7). Different acoustic windows should be used, including the parasternal short-axis, apical four-chamber, and the subcostal long-axis view to assess the size and location of rupture. The parasternal short-axis view is particularly helpful in the detection of rupture of the posterior septum. The search for the defect should be very meticulous with careful apical to basal and anterior to posterior sweeps of the transducer. However, even a thorough 2D examination may not detect small septal tears.

Color-flow Doppler is the most important modality for the detection of VSR, being up to 100% sensitive and specific. A turbulent trans-septal flow and systolic flow disturbance within the RV is typically observed, and it enables the visualization of complex defects such as multiple holes or serpinginous tracts from the LV to the RV (Fig. 19.8). Doppler color-flow imaging can rapidly detect the abnormal flow across the septum, accurately define its location, and assess the size of the defect or defects by measuring the width of the color jet. The latter was shown to correlate well with the size of septal defects found at surgery. The color flow left to right jet through the ruptured septum is pansystolic but can be diastolic when LV diastolic pressures exceed those of the right ventricle. A right to left shunt can occasionally be detected in early-mid diastole due to the existence of RV failure and RV end-diastolic pressure greater than the LV end-diastolic. Additional common findings include: (1) Aneurysm of the ventricular septum, defined by the appearance of a bulge of the apical or posterior septum protruding into the right ventricle, found in 40–50% of patients (Fig. 19.9). (2) Hyperkinetic segments opposite to the area

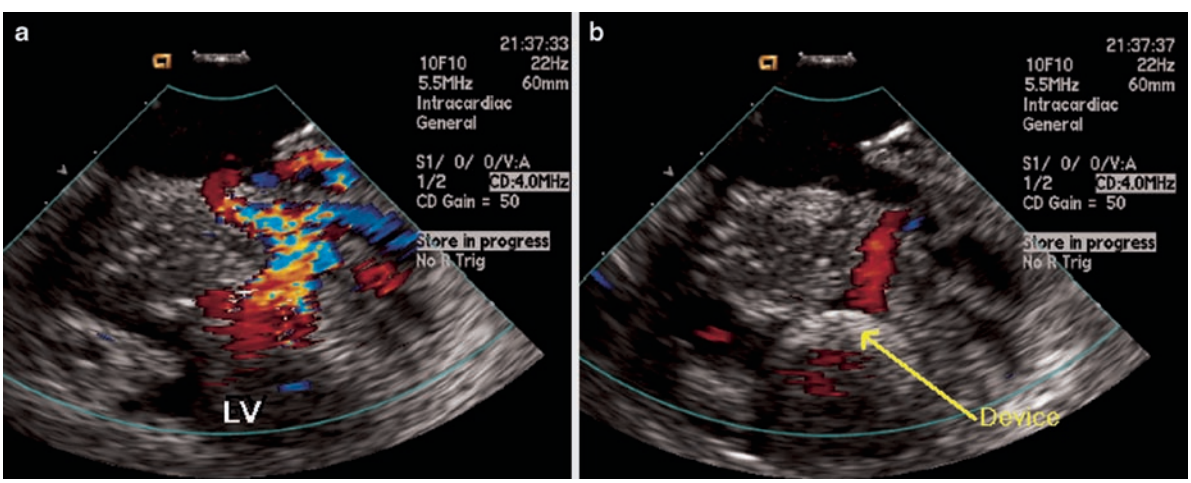

Fig. 19.6 Intracardiac echocardiography (ICE) of a complex rupture of the interventricular septum defined by the turbulent color-flow jet (**a**). A device closure to seal the rupture is being placed in the catheterization laboratory (**b**). Unfortunately, the benefit was transient in spite of a favorable procedural result (Courtesy of Dr. Peter McLaughlin, Toronto)

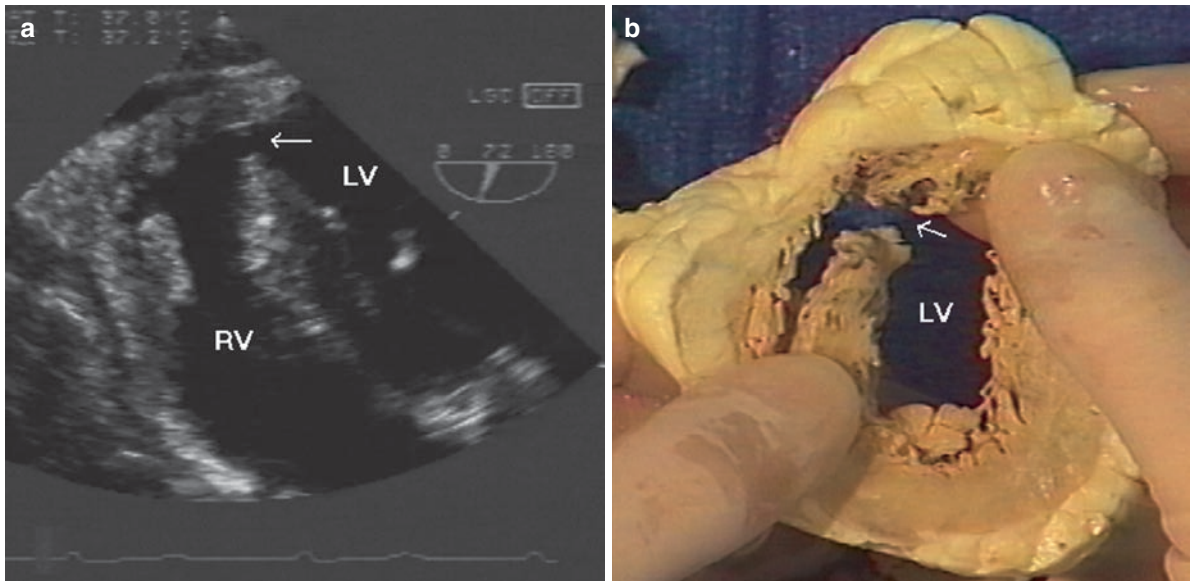

Fig. 19.7 Echocardiographic transgastric view (**a**) and a similarly oriented pathology specimen (**b**) of ruptured posterior interventricular septum (*arrows*) (Pathology courtesy of Dr. J. Kisslo)

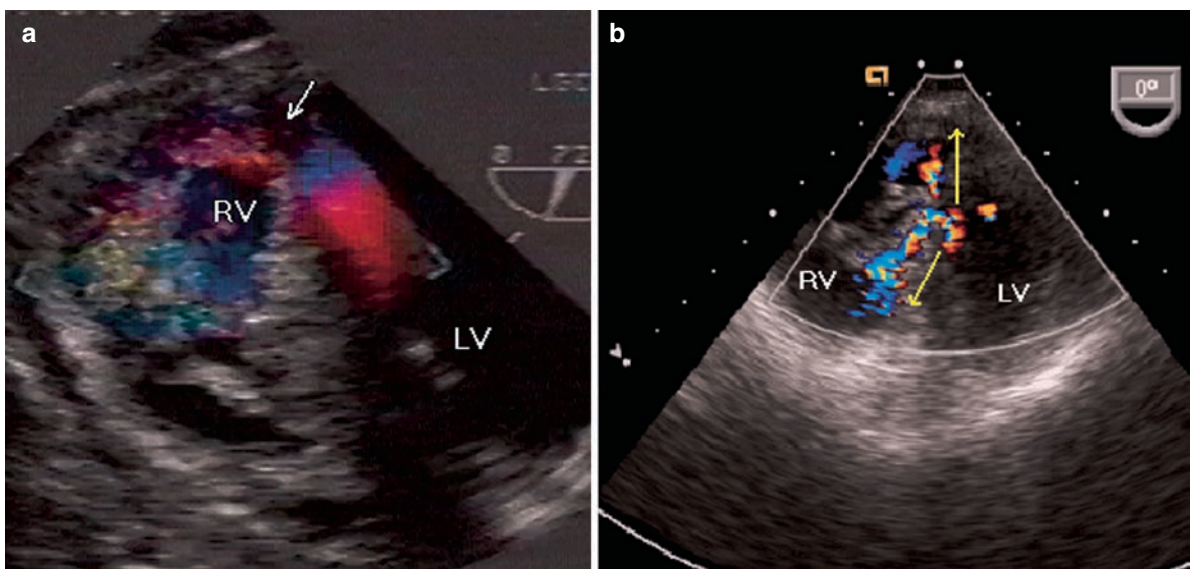

Fig. 19.8 (**a**) Transgastric view of the left and right ventricles (LV and RV) showing disruption of the interventricular septum (*arrow*). (**b**) A similarly oriented transgastric view in a different patient with a complex ventricular septal rupture. With color-flow Doppler, two long opposite directed rupture tracts are evident along the septum (*arrows*)

of infarction can be seen in almost half of the patients. (3) Tricuspid regurgitation is very frequent and is secondary to high right ventricular pressure or due to myocardial ischemia. (4) Poor right ventricular function is not uncommon when VSR complicates an inferior myocardial infarction and is associated with increased mortality.

Transesophageal echocardiography is frequently performed to assess the reason for decompensation of a cardiac patient when transthoracic echocardiography

is unclear. It may have the advantage of giving a better definition of the type of septal rupture compared to transthoracic echo, particularly in cases of poor image quality. It also has a major role in the perioperative assessment of a patient with VSR. There are two approaches for repairing the ruptured ventricular septum: One is infarctectomy and reconstruction of the septum and right and left ventricular walls with a single Dacron patch and another approach consists of excluding rather than excising the infarcted septum and ventricular walls. This is accomplished by performance of a left ventriculotomy through the infracted muscle and securing a bovine pericardium patch to the normal endocardium of the left ventricle excluding the infarcted myocardium. The latter approach is more physiologic in remodeling the acutely infracted left ventricle and enhances survival. As in many types of cardiac surgery, it is useful to use TEE to guide surgery, providing the surgeon with information about the exact location, size, and type of VSR and in assessing immediate operative results (Fig. 19.10).

Three-dimensional echocardiographic reconstruction has been reported to be helpful in the determination of diagnosis of VSR in challenging situations like

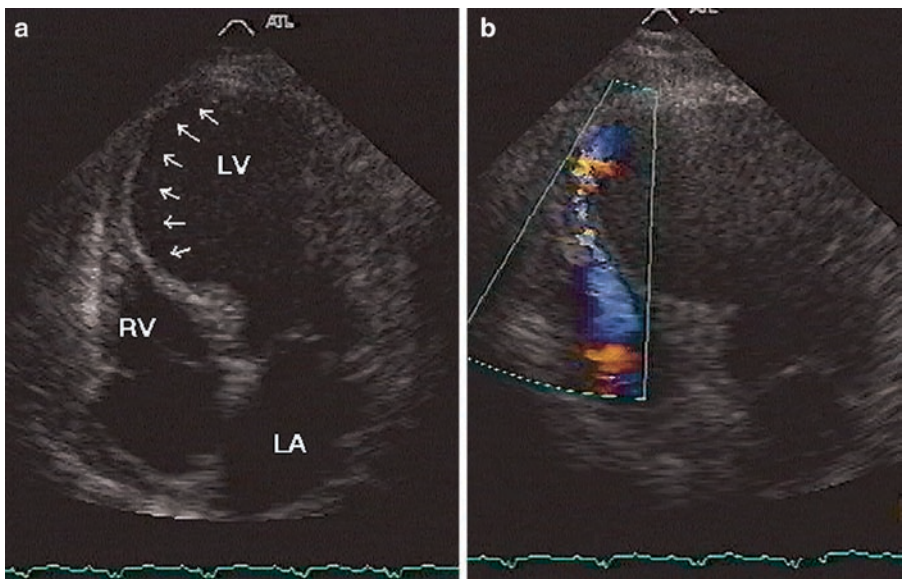

Fig. 19.9 (**a**) Transthoracic apical view in a post MI patient with a large aneurysm of the interventricular septum and apex (*arrows*). Color-flow Doppler shows a long ruptured tract from LV to RV through the septum (*LV* left ventricle; *RV* right ventricle; *LA* left atrium)

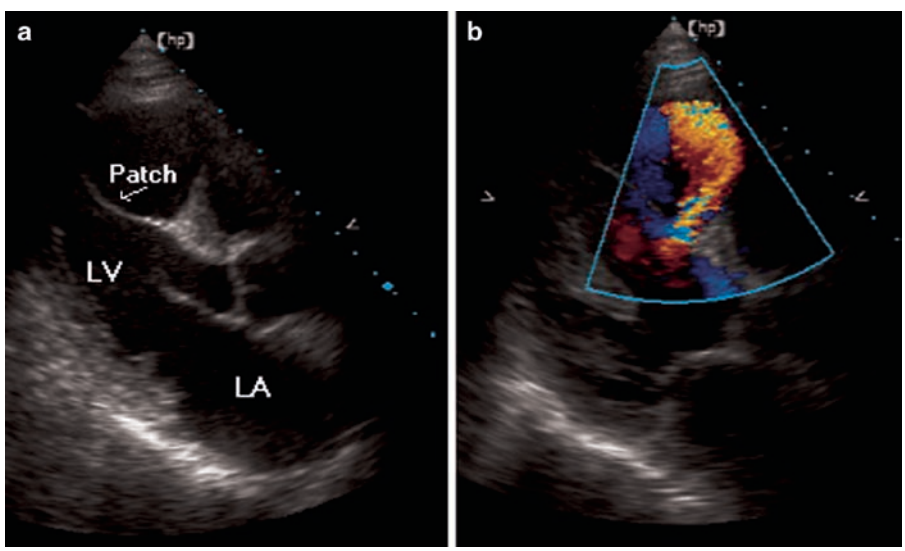

Fig. 19.10 A patch for the repair of a ventricular septal rupture is evident in this parasternal long-axis view (**a**). Color-flow Doppler revealed significant leakage of the patch requiring reoperation (**b**)

incomplete septal rupture or pseudoaneurysm coexisting with VSR. Very recently, live 3D echocardiography including 3D color Doppler has been commercially introduced. Three-dimensional images can be easily obtained and it appears that this modality has the potential to help in the assessment of complex forms of septal rupture providing the surgeon with valuable information.

Papillary Muscle Rupture

Papillary muscle rupture (PMR) is the rarest mechanical complications of AMI. This is probably due to protection by transencocardial diffusion and perfusion through thebesian sinusoids. The posteromedial papillary muscle is the most affected, having its blood supply solely from the posterior descending coronary artery as opposed to the anterolateral papillary muscle that has a dual blood supply, both from the diagonal branch and the left circumflex artery. The most frequent site of MI is, therefore, the inferolateral wall. Unlike other mechanical complications of AMI, even subencocardial (non-Q-MI) and relatively small infarctions can cause PMR. This complication usually occurs 2–7 days post MI and is responsible for almost 5% of deaths of AMI. The clinical presentation is that of hypotension and respiratory failure due to massive pulmonary edema. Findings may be less dramatic if only one head of papillary muscle is ruptured as opposed to rupture of the papillary muscle trunk, which may be rapidly fatal. Some characteristics that may distinguish patients with PMR as the cause for severe mitral regurgitation after acute MI are: first MI, older age, and decreased prevalence of: diabetes mellitus, previous angina, and multivessel disease. Systemic hypertension, delay in hospital admission with persistence of ambulatory activity since the onset of MI, and increased frequency of recurrent anginal pain preceding PMR also occurred more frequently in patients with PMR. Mortality is very high if left untreated. Fifty percent die within 24 h and 90% within a week without surgical therapy. Therefore, a rapid and early echocardiography diagnosis should be made. This complication may not be initially suspected since a murmur of mitral regurgitation may not be loud due to the large regurgitant orifice area and rapid increase in pressure in the left atrium in a hypotensive patient.

Echocardiographic Findings

The typical 2D echocardiographic findings include flail mitral valve leaflet and the mobile head of the ruptured papillary muscle, which is often seen as a mobile mass attached to the chordae and prolapsing into the left atrium during systole (Fig. 19.11a). LV function is hyperdynamic since the responsible MI is usually small and the ventricle contracts against the low impedance left atrium. Doppler color flow usually reveals severe mitral regurgitation, and the direction of the regurgitation jet points to the affected mitral leaflet: posteriorly directed regurgitation jet in flail anterior leaflet and anteriorly directed jet in posterior flail leaflet (Fig. 19.11b). If both leaflets are involved the jet is centrally directed. Severity of MR may be underestimated in the event of eccentric regurgitant jets, and whenever there are doubts regarding the severity or the mechanism of mitral regurgitation, TEE should then be performed. In that regard, TEE is very useful in differentiating PMR from ventricular septal rupture when searching for the etiology of a new murmur in the hemodynamic unstable patient with nondiagnostic 2D images. During the TEE examination, the LV should be examined carefully, and transgastric views should be obtained in search of a highly mobile papillary muscle, which may not prolapse into the left atrium. In a study of 20 consecutive patients with left ventricular PMR confirmed at surgery who underwent intraoperative TEE studies, the ruptured head was not seen to prolapse into the left atrium in 7 patients. However, a large echo density with large-amplitude erratic motion (1–5 cm in 17 patients and 0.5 cm in one patient) was seen in the LV of 18 of the 20 patients (specificity of 90%), including all seven patients without prolapse of the ruptured papillary muscle into the left atrium.

Medical treatment is limited and insertion of an intra-aortic balloon is often required. Coronary angiography, when possible, is performed prior to surgery. Early surgery, irrespective of whether stabilization by medical treatment can be achieved, is now the treatment of choice. This is based on the fact that many patients with PMR have limited extent of infarction; single vessel disease is seen in almost half and LV systolic function is usually not significantly affected. Early surgery changes the prognosis of these patients. In-hospital mortality is still relatively high (20–30%) however; intermediate and long-term survival is approximately

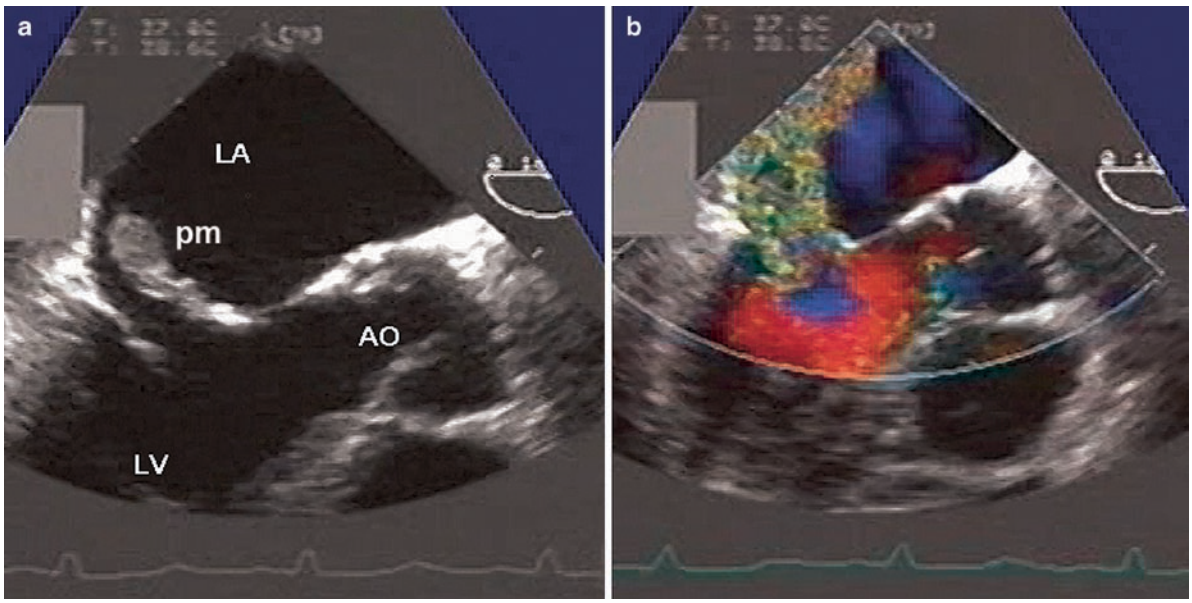

Fig. 19.11 (**a**) In this transesophageal view the trunk of the anterolateral papillary muscle is prolapsing into the left atrium during systole. The resultant turbulent jet of severe mitral regurgitation is eccentric and directed in a posterior direction (**b**). (*LA* left atrium; *LV* left ventricle)

80%. Papillary muscle repair is feasible and, recently, a modified papillary muscle repair with the use of pericardium for height/length adjustment of the papillary muscle and annuloplasty with a Carpentier-Edwards ring has been described in a small group of patients, with excellent results.

Left Ventricular Aneurysm and Thrombus Formation

A left ventricular aneurysm (LVA) can be defined as a demarcated bulge of the contour of the LV wall during systole and diastole, demonstrating dyskinetic or akinetic motion. It is a frequent complication of acute myocardial infarction and may be a cause of heart failure, thrombus formation predisposing to the risks of systemic embolization, and ventricular arrhythmias. Unlike the previous mechanical complications of MI mentioned earlier in this chapter, LVA is not secondary to myocardial rupture. Its occurrence is secondary to infarct expansion and remodeling of the involved segment, usually the LV apex, which is the thinnest segment of the LV wall. Early echocardiographic data reported sensitivity of 93% and specificity of 94% for the detection of LVA after MI. In a prospective echocardiographic study of 158 patients with a first acute Q-wave MI, 22% had an aneurysm detected within 3 months. In 77% of the patients, the location of the aneurysm was in the anterior wall, and in 17% it was located posteriorly. In that study, no thrombolysis or coronary angioplasty was performed, and 31% of all patients with anterior wall MI had an aneurysm. In almost half of the patients with an anterior aneurysm, the diagnosis was already made in the coronary care unit within 5 days of MI. Such early development of aneurysm was not seen with posterior MI. New aneurysms were not found 1 year after acute MI. The 1-year mortality rate was significantly higher in patients with an aneurysm (49 vs. 14% in those without aneurysm), and there was no difference between patients with and without LV aneurysm regarding age, previous hypertension, and peak CK. A recent study of 350 patients assessed the effect of thrombolytic therapy on the incidence of LV aneurysm after a first AMI. The overall incidence of LVA was 11.7%. There was no difference between the thrombolytic group (205 patients) and the control group (145 patients who presented >12 h after the onset of symptoms). However, patients receiving thrombolytic therapy with a resultant patent infarct-related artery had a significantly reduced incidence of LV aneurysm compared with those who did not have a patent artery (7.2 vs. 18.8%). Patients with total LAD

occlusion and proximal LAD stenosis were also found to have increased risk for LVA formation after AMI.

Echocardiographic determination of LV volume is challenging in the presence of an aneurysm due to its irregular geometry. Real-time 3D echocardiography may be preferable to 2D when assessing LV remodeling after MI since LV volume determination by 3D echo correlated better than 2D to LV volume determination by magnetic resonance imaging (MRI).

Indications for the surgical repair of LVA include congestive heart failure, VT originating from the aneurysm and asymptomatic patients with large aneurysm undergoing CABG. The original repair, performed by Cooley et al, consisted of scar excision with linear closure of the ventricular wall defect. This can be performed with or without placement of a felt. A different approach is the endoventricular repair (Dor's repair) consisting in placement of a Dacron patch lined with pericardium that is sutured circumferentially at the junction of the scar and normal muscle, in order to restore as much as possible the curvature of the myocardium (Fig. 19.12). Surgical results are good with relatively low operative mortality and significant improvement in symptoms, LV ejection fraction, and diastolic LV dimension.

LV thrombus occurs in one-third of patients with Q wave anterior wall MI. It is substantially less frequent in patients with non-Q wave or inferior wall MI (<5%). It is formed almost exclusively in the akinetic, dyskinetic apex with or without aneurysm formation (Fig. 19.13). Most thrombi are formed within 48 h to 1 week of infarction. Late formation of thrombus may be seen in patients with severe congestive heart failure and deteriorating LV systolic function. Systemic embolization may occur within 3 months in almost 30% of post acute anterior MI patients who have thrombus formation. Chronic LV thrombus, occurring 3 months or more after infarction, is associated with an LVA and

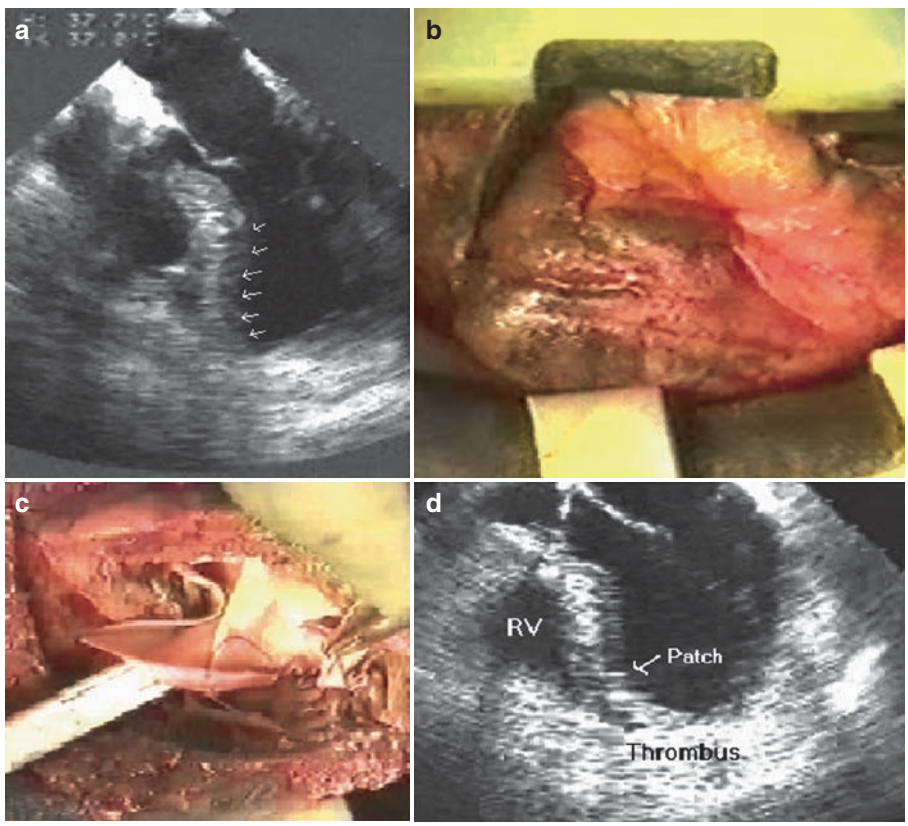

Fig. 19.12 Repair of anterior and septal wall aneurysm, ventricular septal and free wall rupture (same patient as Fig. 19.3). (**a**) Apical view depicting the large aneurysm (*arrows*). (**b**) Necrotic and aneurysmal tissue secondary to an extensive acute myocardial infarction. (**c**) Incision of the myocardium and placement of a patch by the exclusion technique. (**d**) Postsurgical echocardiography: The patch is evident as is thrombus formed between the patch and the pericardium. The LV is dramatically remodeled.

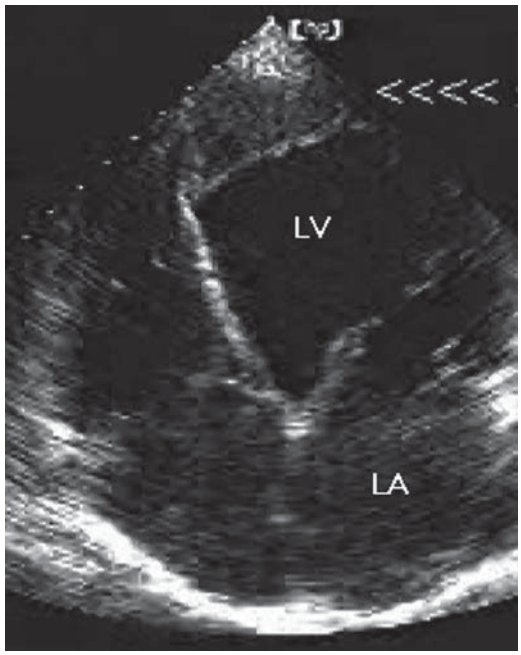

Fig. 19.13 Apical view of a large mural thrombus (*arrows*) in the typical apical location

fifty percent of all patients with an LVA have chronic LV thrombus. In spite of its high prevalence, chronic mural thrombi rarely embolize. Acute thrombi within an aneurysm have a greater risk of embolization. These two types of thrombi differ pathologically in that acute thrombi are likely to be mobile, fragile, and projecting into the lumen while chronic thrombi are organized and laminated.

Two-dimensional echocardiography is 86% sensitive and 95% specific in the detection of LV thrombi in patients with adequate studies. In 5–10% of patients studies are technically inadequate and the presence of a thrombus cannot be ruled out. False-positive results may occur when trabeculations, aberrant bands, papillary muscle, tumors, or ultrasonic noise and resolution problems are mistaken for LV thrombus. The use of harmonic imaging and beam focus near the apex improves visualization. The IV injection of an echocontrast agent may be very helpful in the determination of the presence of thrombus in such circumstances. Transesophageal echocardiography can be an additional helpful tool. The classic echocardiographic features that predict embolization in a patient with an LV thrombus are protrusion and mobility of the thrombus. Protruding thrombi are associated with embolization in more than 50% of patients; therefore, patients with these echocardiographic features should be treated with anticoagulation. There is no definite antithrombotic treatment strategy for LV thrombus and the time period of treatment is unclear. Patients with large anterior MI or anterior MI with heart failure should receive full-dose heparin followed by warfarin therapy for at least 3 months to prevent thrombus formation. Anticoagulation therapy is commonly administered to patients with an LVA and mural thrombi; however, there are insufficient data to routinely perform such practice unless echo characteristics of high risk for emboli are present. An LVA should be treated with anticoagulation if the patient had a previous embolus.

Summary

Reperfusion therapy has reduced the incidence of myocardial rupture secondary to an acute myocardial infarction. However, mechanical complications are still an important cause of death and stroke in post AMI patients, and clinical suspicion combined with proper echocardiographic assessment may save lives. Even the most fatal complication, that of free wall rupture, can potentially be prevented when a preceding subacute rupture is detected. A TEE study should be employed rapidly if the suspected diagnosis is not clear from the surface examination and should be used with caution. Contrast echocardiography has shown the ability to improve the sensitivity and specificity for detection and differentiation of mechanical complications of MI. Live 3D echocardiography is now clinically available and will probably play an important role in the rapid detection MI complications. Although surgical perioperative mortality is significant, long-term survival is good.

Bibliography

Birnbaum Y, Fishbein MC, Blanche C, Siegel RJ. Ventricular septal rupture after acute myocardial infarction. *N Engl J Med*. 2002;347:1426–1432.

Buda AJ. The role of echocardiography in the evaluation of mechanical complications of acute myocardial infarction. *Circulation*. 1991;84(suppl 1): I–109-I-121.

Figueras J, Cortadellas J, Calvo F, Soler-Soler J. Relevance of delayed hospital admission on development of cardiac rupture during acute myocardial infarction: study in 225 patients

with free wall, septal or papillary muscle rupture. *J Am Coll Cardiol*. 1992;32:135–139.

Fortin FD, Sheikh KH, Kisslo J. The utility of echocardiography in the diagnostic strategy of post-infarction ventricular septal rupture: a comparison of two-dimensional echocardiography versus Doppler color flow imaging. *Am Heart J*. 1991;121:25.

Frances C, Romero A, Grady D. Left ventricular pseudoaneurysm. *J Am Coll Cardiol*. 1998;32:557–561.

CA, Kan G, Meltzer RS, Koolen JJ, Dunning AJ. Incidence, timing and prognostic value of left ventricular aneurysm formation after myocardial infarction: a prospective, serial echocardiographic study of 158 patients. *Am J Cardiol*. 1986;57:729–732.

Chapter 20
Cardiomyopathies

Petros Nihoyannopoulos

Introduction

Cardiomyopathies are heart muscle diseases of no apparent cause. The term "cardiomyopathy" should therefore be restricted to diseases involving the heart muscle of unknown etiology, and other diseases affecting the myocardium should be termed specific heart muscle diseases. Cardiomyopathies are divided into four categories depending on morphologic and functional characteristics. These are: (1) Hypertrophic, (2) Dilated, (3) Restrictive, and (4) Arrhythmogenic right ventricular cardiomyopathy (Table 20.1). However, this classification is based on the morphologic and functional characterization of genetically defined disease and often may present with a combination of appearances. It is therefore possible that a patient with hypertrophic cardiomyopathy may deteriorate in the long run and become dilated or even restrictive.

Hypertrophic Cardiomyopathy

Definitions

HCM is currently defined as an inherited, primary disease of the heart muscle characterized by ventricular hypertrophy, impaired diastolic function, and vigorous ventricular contraction in the absence of a cardiac or systemic cause[1-4] (Table 20.2). There are several genes and hundreds of mutations that have been identified, involving primarily the sarcomeric proteins of the heart (Table 20.3). This makes the condition being genetically heterogeneous so that we may be talking about several disease entities. Echocardiographic screening of family members has shown a distinct genetic basis for the inheritance of HCM in 50–60% of cases. The transmission is autosomal dominant inheritance with variable penetrance.

Pathology

The gross pathology of HCM is characterized by ventricular hypertrophy involving predominantly the left ventricle, but also the right ventricle in a significant number of patients (Fig. 20.1). The hypertrophy can be either asymmetrical, that is, a significant difference in maximal thickness of ventricular septum and posterior wall, or concentric equally involving the entire left ventricle, or distal, affecting predominantly the cardiac apex. The hypertrophy frequently becomes manifest during puberty, although some cases of HCM are seen in infancy. Histologically, there is myocyte disarray (Fig. 20.2), whereby the normally parallel myocardial fibers are arranged in a disorganized fashion. However, fiber disarray may also occur in diseased hearts of other etiologies. When however myocardial disarray is found in more than 5% of the myocardium (of the entire heart), the diagnosis of hypertrophic cardiomyopathy can be made with 93% specificity and 89% sensitivity. Frequently, there is extensive fibrosis within the myocardium leading to reduced contraction and relaxation (Fig. 20.3).

Pathophysiology

The functional abnormalities include a forceful, overactive ventricular contraction often with complete

P. Nihoyannopoulos
Imperial College London, National Heart and Lung Institute, Hammersmith Hospital, London, UK
e-mail: p.nihoyannopoulos@imperial.ac.uk

P. Nihoyannopoulos and J. Kisslo (eds.), *Echocardiography*,
DOI: 10.1007/978-1-84882-293-1_20,

Table 20.1 Cardiomyopathies' classification

Hypertrophic
Dilated
Restrictive
ARVC

Table 20.2 Hypertrophic cardiomyopathy

Genetically transmitted
Idiopathic ventricular hypertrophy
Myocardial fiber disarray
Lack of ventricular dilatation
Normal/supernormal contractility
Diastolic function abnormalities

Table 20.3 Genetic heterogeneity of hypertrophic cardiomyopathy

β-Myosin
Troponin T
Troponin I
α Tropomyosin
Myosin-binding protein C
Essential myosin light chain
Regulatory myosin light chain

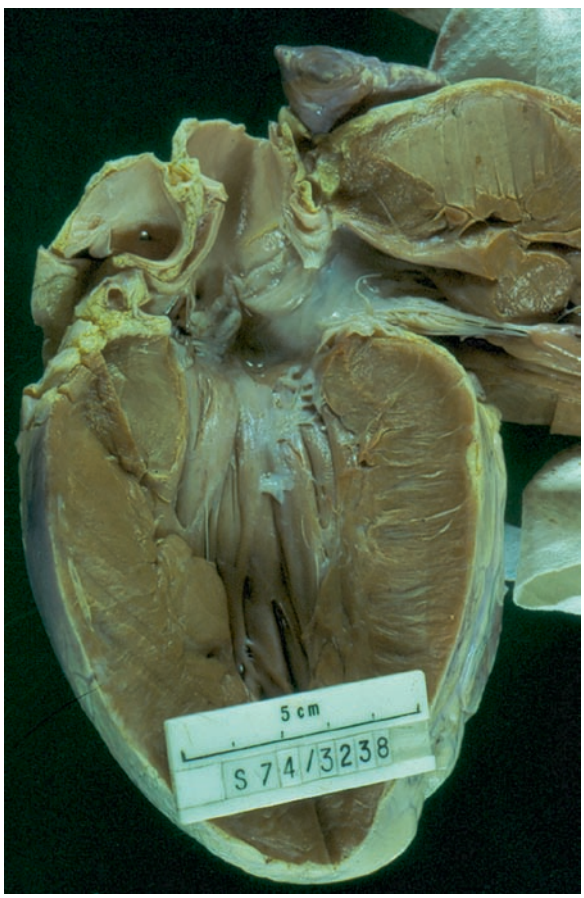

Fig. 20.1 Gross pathology of a patient with hypertrophic cardiomyopathy. Notice the marked amount of hypertrophy involving the entire heart

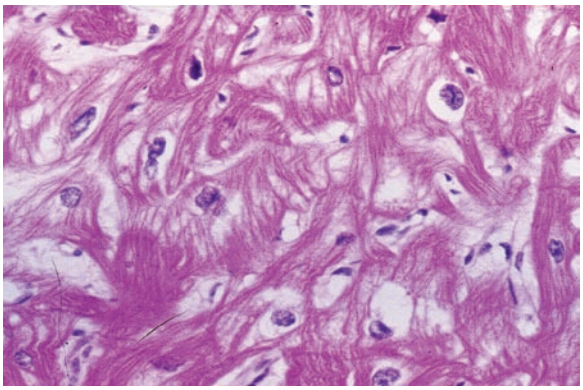

Fig. 20.2 Histology of the myocardium demonstrating the amount of abnormal fiber arrangement

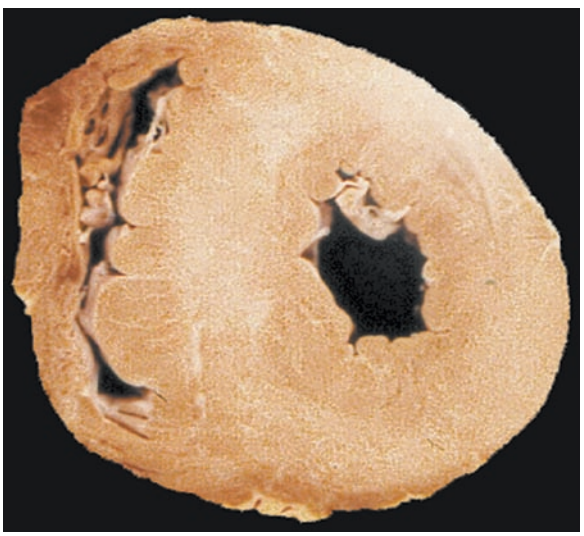

Fig. 20.3 Cross-sectional area from a patient with hypertrophic cardiomyopathy demonstrating the amount of fibrosis (*white areas* in the middle of the myocardium)

emptying achieving an ejection fraction of 80–100%. The powerful contraction and complete emptying of the ventricle often occurs in association with intraventricular pressure gradients. When the gradient is subaortic it occurs in association with a systolic anterior movement of the mitral valve. Gradients may be persistent (gradient at rest), labile (spontaneously variable), or appear only on provocation and do not correlate with prognosis. Although initially HCM was thought to be mainly a disorder of left ventricular systolic function, it is now widely appreciated that the main problem is in diastole with impaired relaxation and filling of the ventricles.

It has become progressively more difficult to define diagnostic limits of patients with "unexplained left

ventricular hypertrophy" mainly because of the inability to exclude the disease, unless a genetic screening is performed. The result has been that the clinical spectrum of HCM has widened with great heterogeneity of age, clinical presentation, and natural history and underscore the need to define the molecular basis of the condition. Until then, idiopathic hypertrophy represents the cornerstone of clinical diagnosis.

Diagnosis

The diagnosis of HCM is based upon the demonstration of unexplained left ventricular hypertrophy producing a small noncompliant, vigorously contracting left ventricle. The clinical findings of dyspnea, chest pain, dizziness, or syncope are the most frequent symptoms that lead to a discovery of HCM, but they are present in only half of the patients having the disease. In the remainder, particularly in children and adolescents, the diagnosis is made as a result of family screening or following the discovery of a murmur, or the electrocardiographic evidence of left ventricular hypertrophy. The indiscriminate use of echocardiography has brought to light many instances of HCM in patients thought to have had innocent murmurs, mitral valve prolapse, coronary artery disease, or normal hearts. The most dreaded symptom is sudden cardiac death. In a large study Maron[5] showed that 46% of patients who died suddenly were entirely asymptomatic and sudden death was the first manifestation of the disease. The annual mortality rate from sudden death is 2.5% in adults and at least 6–7% in children.

The electrocardiogram is often the first investigation that leads to a suspicion of HCM because it shows left ventricular hypertrophy (Fig. 20.4). Abnormal QRS axis and deep Q or inverted T waves in the setting of ventricular hypertrophy are strongly suggestive of HCM. In children, however, the electrocardiogram may be passed as normal but often may indicate nonspecific repolarization changes or the presence of old myocardial infarction.

The Role of Echocardiography

The diagnosis of HCM is made on the basis of the echocardiographic appearance of left ventricular hypertrophy in the absence of an underlying cause. Echocardiography however should play a supportive role to the clinical diagnosis of HCM, as the diagnosis of the condition is clinical and requires the exclusion of other causes of left ventricular hypertrophy.

The original M-mode recording techniques were invaluable in describing the early diagnostic criteria for HCM. Those were

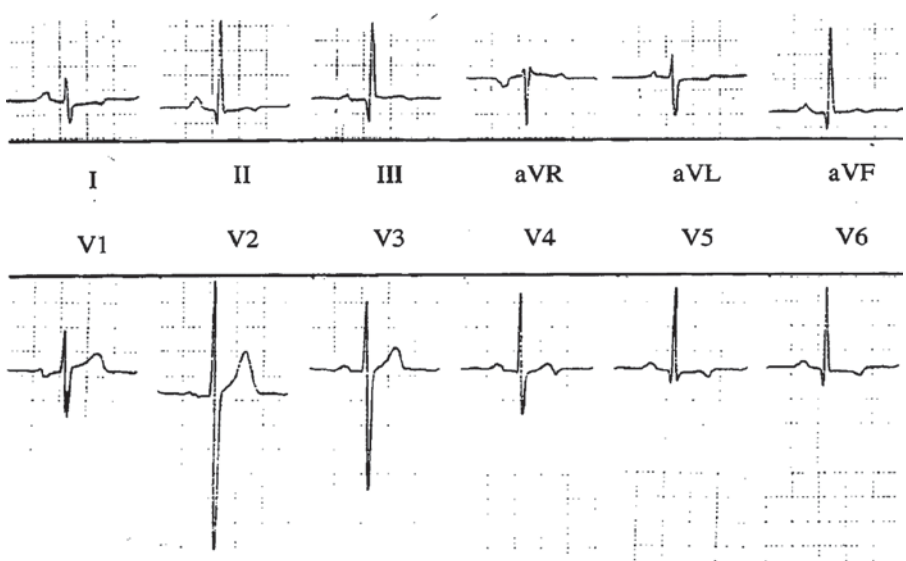

Fig. 20.4 A typical electrocardiogram from a hypertrophic cardiomyopathy patient demonstrating voltage criteria for ventricular hypertrophy, mainly in the septal leads, Q-waves inferiorly, as well as abnormal repolarization

1. The presence of asymmetric hypertrophy of the ventricular septum (ASH), defined as the ratio of septal and posterior left ventricular wall thickness at end-diastole been equal or greater than 1.3 cm
2. The systolic anterior motion of the mitral valve (SAM)
3. The premature, midsystolic closure of the aortic valve in the presence of a small and vigorously contracting left ventricle (Fig. 20.5)

An inherent disadvantage of M-mode echocardiography however is that only a small portion of the left ventricle can be examined at a time with a single ultrasound beam, usually passing through the anterior septum and posterior wall. Patients with HCM, however, may show a wide distribution of hypertrophy. Two-dimensional echocardiography shows anatomic sections of the heart so that the true size and shape of the valves and cavities can be appreciated. ASH, SAM, and midsystolic closure of the aortic valve are not pathognomonic of HCM, as each one can also occur in a variety of other conditions with no common pathophysiologic mechanism. The presence of ASH is no longer a prerequisite for the diagnosis of HCM. Conditions such as systemic hypertension, athlete's heart, or even aortic stenosis can cause the ventricular septum to appear thicker than the left ventricular free wall and conversely, in many patients with HCM the septum and the free wall may be of similar thickness (concentric hypertrophy). The recent recognition of a group of patients with HCM but without left ventricular hypertrophy[6] has demolished the last cornerstone of a firm echocardiographic diagnosis of HCM.

The parasternal long-axis view is important in the visualization of the ventricular septum, left ventricular outflow tract together with the mitral valve and its subvalvular apparatus (Fig. 20.6). It is the view of choice for the visualization of SAM. of the mitral valve and midsystolic closure of the aortic valve. It is important to obtain simultaneous M-mode and two-dimensional echocardiographic recordings of the mitral and aortic valve motion since M-mode provides a better temporal resolution and two-dimensional echocardiography better spatial resolution. High-frequency phenomena, such as SAM and midsystolic closure of the aortic valve, can then be better appreciated and analyzed. Left ventricular measurements can also be obtained from the parasternal long-axis view under simultaneous two-dimensional echocardiographic supervision to

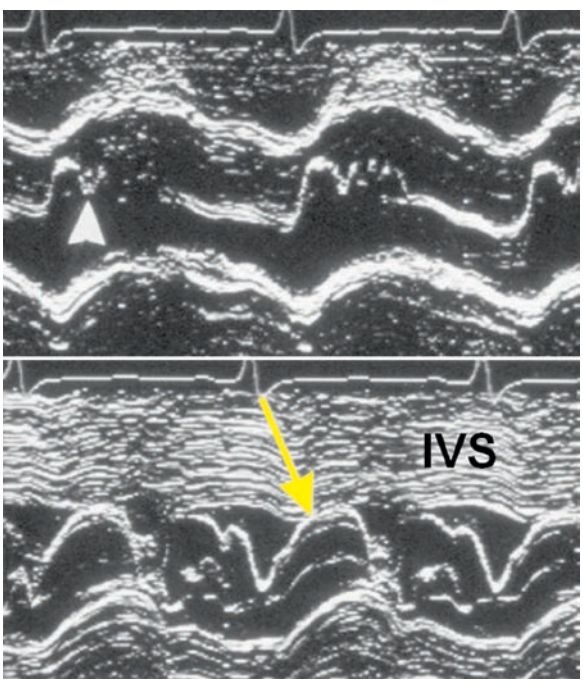

Fig. 20.5 A representative M-mode echocardiogram from a patient with hypertrophic cardiomyopathy highlighting the four main echocardiographic features of the condition. (**a**) Midsystolic closure of the aortic valve (*arrowhead*), (**b**) systolic anterior motion of the mitral valve (*arrow*), and asymmetric left ventricular hypertrophy together with a small, vigorously contracting left ventricle

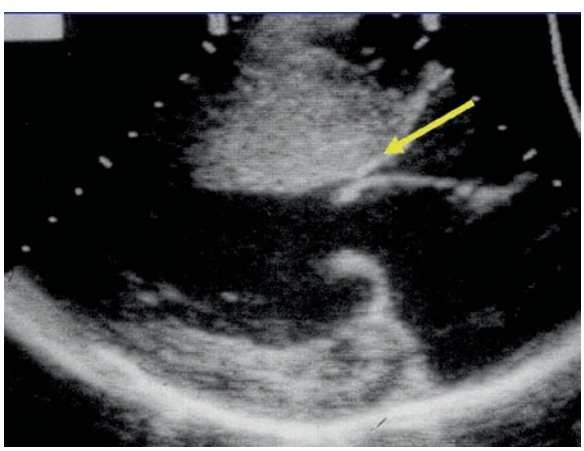

Fig. 20.6 Two-dimensional echocardiogram of the parasternal long-axis view of the left ventricle in diastole showing marked ventricular septal hypertrophy, small end-diastolic dimensions (41 mm). Note that the mitral valve is impinging the ventricular septum (*arrow*). At the point of contact with the ventricular septum the anterior mitral leaflet and the endocardial surface of the septum are more echogenic implying fibrosis

ensure that the M-mode beam line transects the left ventricle perpendicularly.

Parasternal short-axis view is useful to localize and describe the extent of ventricular hypertrophy (Fig. 20.7). Serial parasternal short-axis views are crucial for the definition of the extent and shape of left ventricular hypertrophy. They provide the opportunity to determine whether segmental hypertrophy exists in other areas of the left ventricle, such as the posterior septum, anterolateral free wall, and posterolateral free wall. The cross-sectional view at the left ventricular base shows the mitral valve in the left ventricular cavity. The midportion shows the two papillary muscles: the posteromedial to the left and the anterolateral to the right of the image. The cross-sectional view of the apex shows the left ventricle in circular orientation.

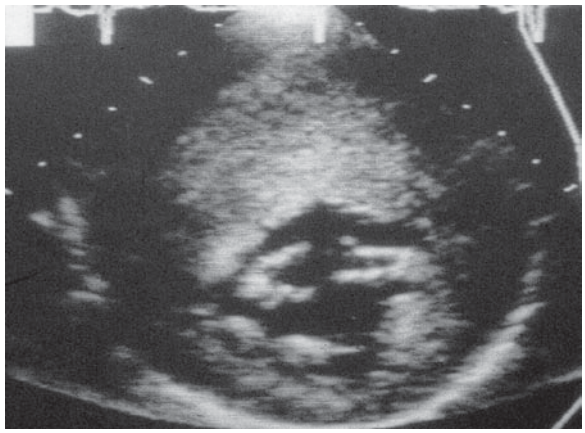

Fig. 20.7 Short-axis parasternal view of a HCM patient with marked septal hypertrophy and normal posterior wall at midventricular level

From these serial short-axis views the left ventricle can be divided into four segments at mitral and papillary muscle level and two at the apex, so that the anterior, lateral inferior and posterior septal walls can be measured (Fig. 20.8). Thus, by combining the parasternal long- and short-axis views, the left ventricular walls can be examined comprehensibly and the localization and extent of ventricular hypertrophy can be fully described. Occasionally, members of the same families with HCM may manifest a similar pattern of ventricular hypertrophy. Echocardiographic imaging of the right ventricle is also important, as approximately

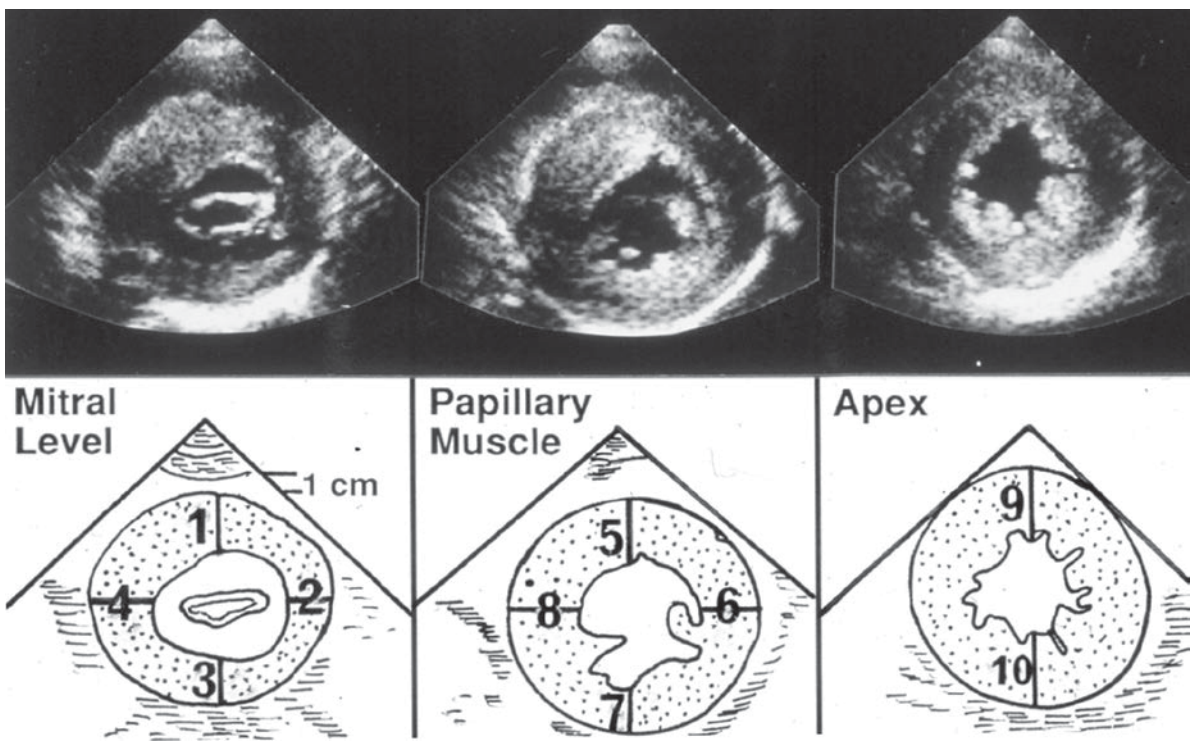

Fig. 20.8 Serial short-axis, cross-sectional views of the left ventricle at mitral valve, papillary muscles level and apex, demonstrating the segments of myocardial wall measured routinely in patients with hypertrophic cardiomyopathy

one-third of patients with HCM may also have right ventricular hypertrophy.

Echocardiographically, HCM is a condition characterized by

1. Hypertrophy of all (concentric) or portion of the walls of the left ventricle, that is, ventricular septum (asymmetric), or apex (distal)
2. Dilated left atrium
3. Small, nondilated ventricles
4. Absence of any other cardiac or systemic condition producing hypertrophy (aortic stenosis-valvular subvalvular, supravalvular, coarctation, systemic hypertension, renal failure, amyloidosis, metabolic disorders)
5. Normal or supernormal (vigorous) ventricular contraction in the absence of other hyperdynamic states (fever, pregnancy, hyperthyroidism)

Associated findings such as SAM or midsystolic closure of the aortic valve should not be considered diagnostic. When all the echocardiographic features are present, together with the suggestive clinical picture, a firm diagnosis of HCM can be made. When however only a number of these findings are present, the diagnosis can only be made after exclusion of other causes of ventricular hypertrophy.

Patterns of LV Hypertrophy

Two-dimensional echocardiography has demonstrated the existence of marked heterogeneity in left ventricular hypertrophy, indicating that HCM is not a discrete and well-circumscribed disease entity but, instead, it represents a spectrum of left and sometimes right ventricular abnormalities.

Asymmetric septal hypertrophy (ASH) is the most frequent form of left ventricular hypertrophy and has been regarded as the hallmark of HCM. Although this hypertrophy usually involves the basal anterior septum to a variable extent and severity, it may also involve the apical, mid, or posterior septum in isolation. ASH may be confined to the most proximal septum as a discrete "tumor-like" swelling in an otherwise normal ventricular septum. Variations in ventricular hypertrophy in HCM emphasize the need of obtaining serial parasternal short axis cuts at multiple levels along the left ventricle, so that the complete distribution of the ventricular hypertrophy can be ascertained. Using this, now well-standardized approach, Shapiro and McKenna[7] defined three patterns of left ventricular hypertrophy; asymmetric left ventricular hypertrophy encountered in 55% of their patients, symmetric in 31%, and distal in the remaining 14%. Although ASH has been commonly defined as a septum to posterior wall ratio of 1.3:1, the same authors proposed a ratio of 1.5:1 in defining ASH which increased the sensitivity and specificity of this echocardiographic finding for the diagnosis of patients with HCM.

Frequently, wall thickness is strikingly heterogeneous and contiguous segments of the left ventricle may differ greatly in thickness. Maron et al[8] described a large variability of distribution of left ventricular hypertrophy, grouped in four basic categories of ventricular hypertrophy.

- Type I was described as hypertrophy confined in the anterior portion of the ventricular septum and was encountered in 10% of their patients.
- Type II described as hypertrophy involving both the anterior and posterior segments of ventricular septum and was seen in 20% of their patients.
- Type III was the most frequently encountered distribution of ventricular hypertrophy seen in 52% of their patients, and it involved both the ventricular septum and the left ventricular free wall (Fig. 20.9).

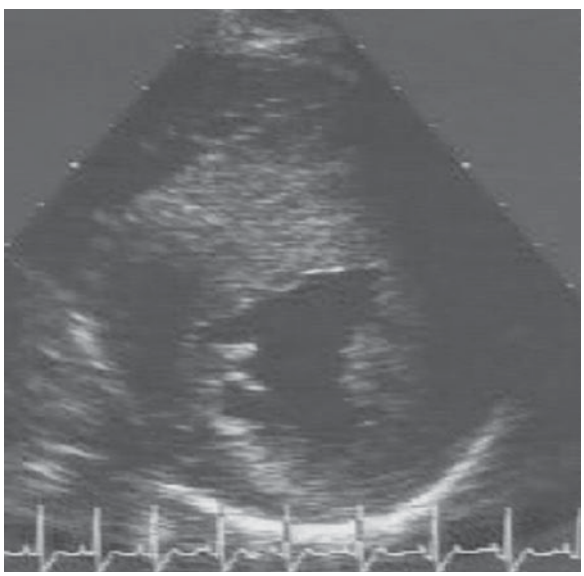

Fig. 20.9 Parasternal short-axis view from a patient with Type III distribution of ventricular hypertrophy. Note the extensive septal and anterior free wall hypertrophy

- Type IV left ventricular hypertrophy was encountered in 18% of their patients in whom it involved the posterior septum, lateral wall, or the apical regions, all inaccessible to the M mode echocardiographic beam (Fig. 20.10). Thus, in this type of hypertrophy, the anterior wall and ventricular septum and the inferior wall were free of hypertrophy, and the diagnosis of HCM would be missed should two-dimensional echocardiography not be performed with careful scrutiny of these areas.

Patients with widespread hypertrophy involving most of the ventricular septum as well as portions of the left ventricular free wall (Type III) had greater prevalence of functional limitations than did patients with the three other morphologic types combined.

Concentric or symmetrical left ventricular hypertrophy is also frequently seen in patients with HCM and when this occurs, the echocardiographic differentiation from secondary causes of left ventricular hypertrophy such as systemic hypertension, cardiac amyloidosis, or the "athlete's heart," may be difficult (Fig. 20.11).

Predominantly distal (apical) distribution of left ventricular hypertrophy is also found in a substantial number of patients (Fig. 20.12). This type was initially described in Japanese patients with giant negative T-waves on the ECG while ventricular hypertrophy was confined to the left ventricular apex. These patients were only mildly symptomatic and have a good prognosis. Based primarily on angiographic studies, as much as 25% of Japanese patients with HCM have been reported to have hypertrophy confined to the true left ventricular apex. This distribution of hypertrophy characteristically creates a spade-like deformity of the left ventricular cavity during diastole, and this is well seen by two-dimensional echocardiography from the apical four-chamber projection.

The right ventricle can also be involved in patients with HCM. Using standardized views across the right ventricular inflow tract, right ventricular outflow tract, and apical and subcostal views, the right ventricle can be imaged in its integrity. As much as 40% of patients with hypertrophic cardiomyopathy may also have right ventricular hypertrophy to a variable degree.

HCM can be seen with increasing frequency in the elderly. However, only a limited number of patients have the "classical" clinical and echocardiographic features with left ventricular outflow tract gradient. Most often such patients are discovered incidentally when undergoing investigations of coronary artery disease and yet others have been hypertensives. These elderly patients with septal hypertrophy often have mitral annular calcification (Fig. 20.13) and an angulated (sigmoid) septum (Fig. 20.14). The prognosis of these patients is good with no evidence of family history, and it can be argued whether this patient group really represents the same disease.

Many affected relatives of patients with HCM who are identified in echocardiographic surveys of pedigrees

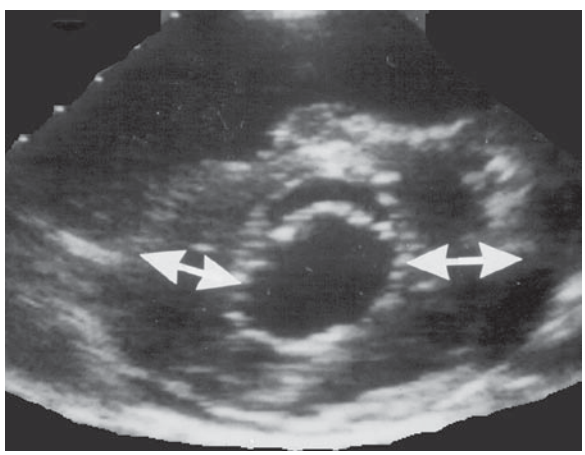

Fig. 20.10 Parasternal short-axis view of the left ventricle at mitral valve level demonstrating a very eccentric form of ventricular hypertrophy (Type IV). Here the lateral wall and posterior septum are markedly hypertrophied (25 and 20 mm, respectively), whereas the anterior and posterior walls are normal

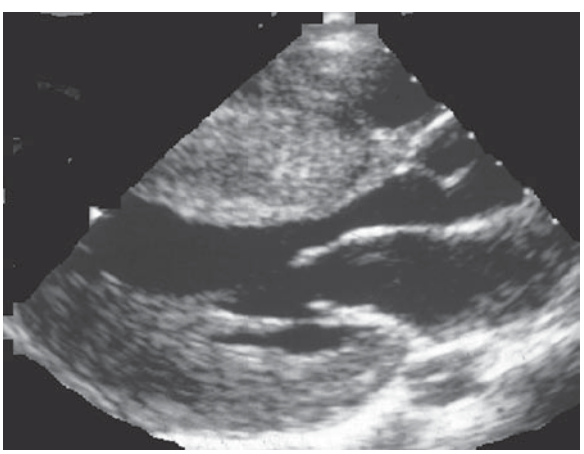

Fig. 20.11 Parasternal long-axis view from a patient with HCM of the concentric type. Note that both the septum and the posterior wall are of similar thickness

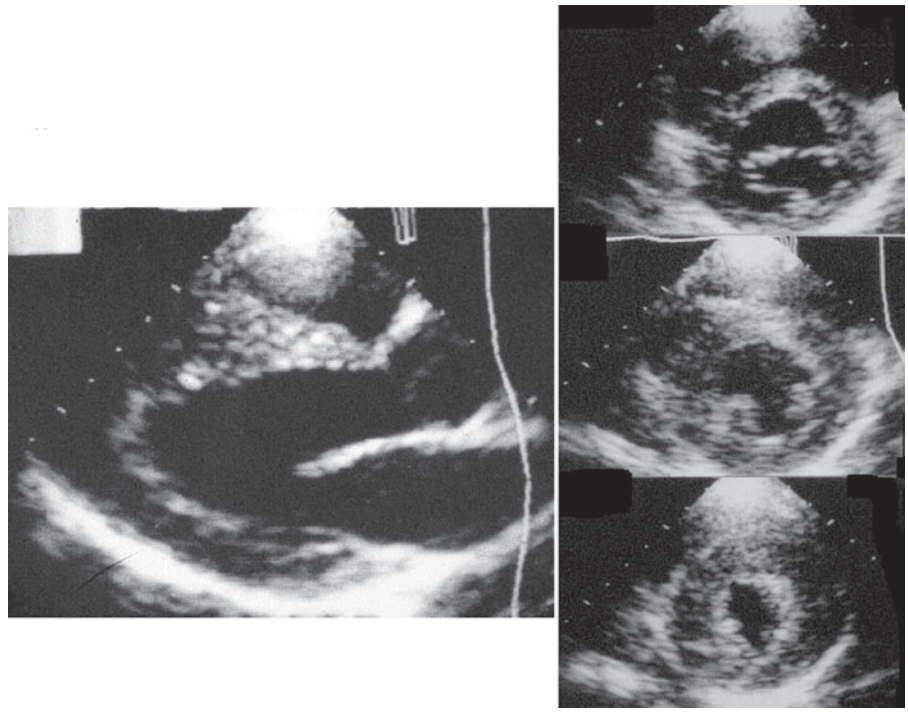

Fig. 20.12 Parasternal long-axis and serial parasternal short-axis views of the left ventricle from a patient with hypertrophic cardiomyopathy of the apical type. Note that the wall thickness is normal at the base (*upper panel*), marginally thickened (13 mm) at papillary muscle level (*middle panel*), and clearly hypertrophied (22 mm) at the apex

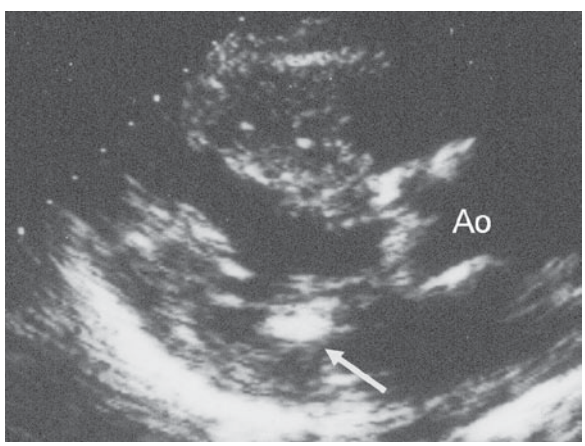

Fig. 20.13 Parasternal long-axis view from an 80-year old patient with chest pain. Notice the mild septal hypertrophy (13 mm) with normal LV cavity and normal size LA. There is extensive mitral annular calcification noted posteriorly (*arrow*)

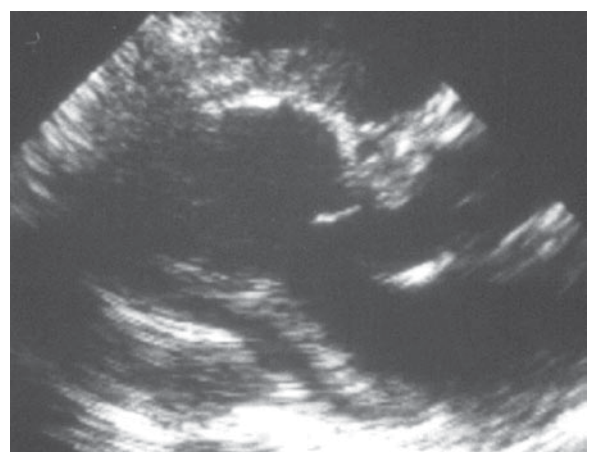

Fig. 20.14 Parasternal long-axis view from an 81-year old patient with a markedly angulated ventricular septum. Note that the very proximal portion of the septum is sharply angled toward the LV outflow which risks to be misinterpreted with HCM

prove to be asymptomatic, over 50 years of age, with or without intraventricular gradient, and usually with only a mild degree of concentric left ventricular hypertrophy. Such individuals may in fact be normal, or they may have a subclinical form of HCM in which the sole evidence of the disease is the morphologic expression detectable only by echocardiography.

Diagnostic Difficulties

It is becoming increasingly difficult to define the boundaries of HCM, with great phenotypic and genotypic heterogeneity. It is therefore reasonable to consider that no single diagnostic technique is currently sufficient to cover the entire spectrum of the

disease, and we need all the clinical, electrocardiographic, and echocardiographic skills to diagnose HCM. Table 20.4 lists some of the possible causes for misdiagnosing HCM.

1. *Mild or absent ventricular hypertrophy:* It is important to investigate suspected cases of HCM in order to exclude the diagnosis, particularly in high-risk families. Although the absence of ventricular hypertrophy can, in most instances, be sufficient to exclude the diagnosis of HCM, in some cases showing mild, perhaps localized hypertrophy and good ventricular function it may be very difficult to exclude the diagnosis. Some mutations in patients with hypertrophic cardiomyopathy present with mild hypertrophy, yet patients may be at high risk for sudden death. One such gene is troponin T. Fig. 20.15 is from a patient with normal echocardiogram yet the ECG is clearly abnormal. This patient had a troponin T mutation.
2. *Left ventricular false tendons* (Fig. 20.16): These are fibrous bands within the normal left ventricle running parallel to the ventricular septum. Echocardiographically, they appear as linear echoes within the LV cavity, which run parallel with the endocardial surface of the septum. When gray scale gain control is incorrectly set, they may give the impression of increased myocardial thickness. The differential diagnosis can be made from short-axis projections where the tendons are cut cross-sectionally, and therefore the septal thickness can better be appreciated.

Table 20.4 Possible causes of misdiagnosis of HCM

Tangential image (poor technique)
Left ventricular pseudotendons
Right ventricular moderator band
Sigmoid septum (angled septum)
ASH in the presence of aortic stenosis or systemic hypertension particularly in the presence of inferior myocardial infarction
High level of athletic training (?)
Specific heart muscle diseases

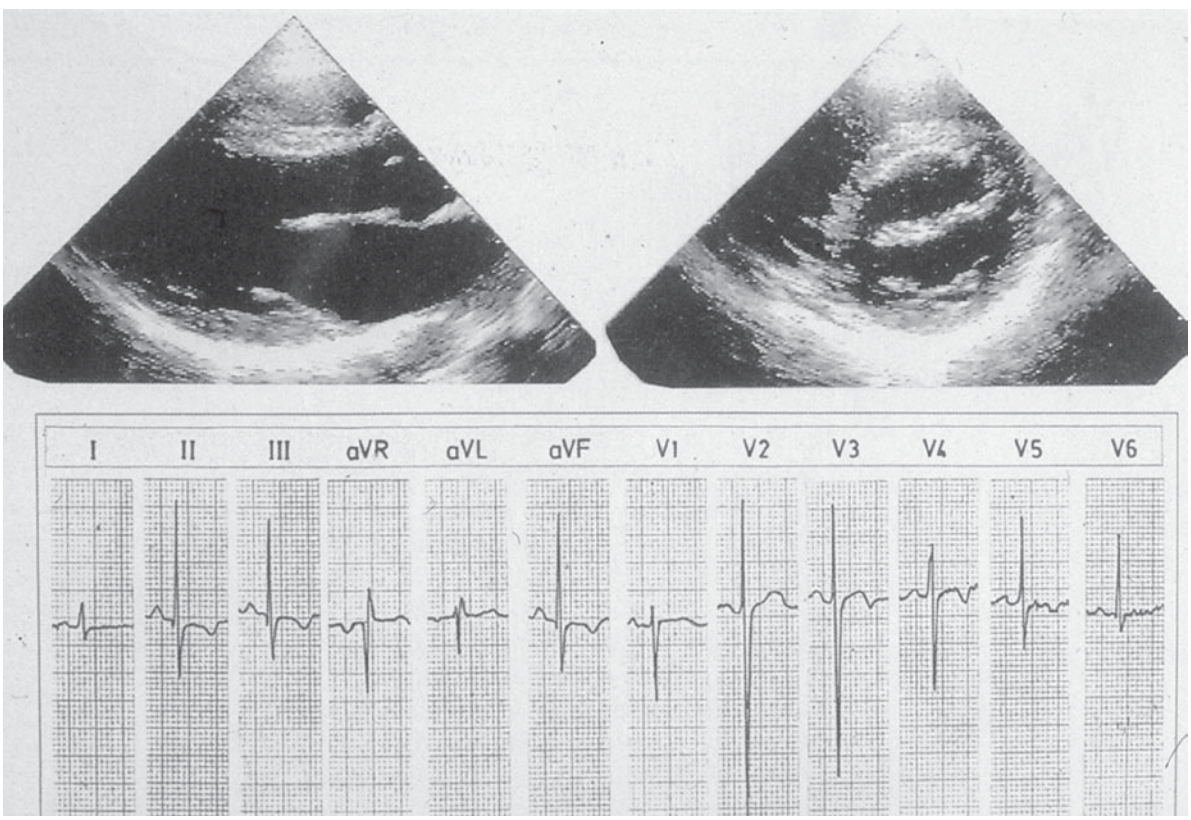

Fig. 20.15 Parasternal projections from a patient with Troponin T mutation. Notice the normal echocardiogram with a markedly abnormal ECG (produced with permission from *Heart*, Ref. 6)

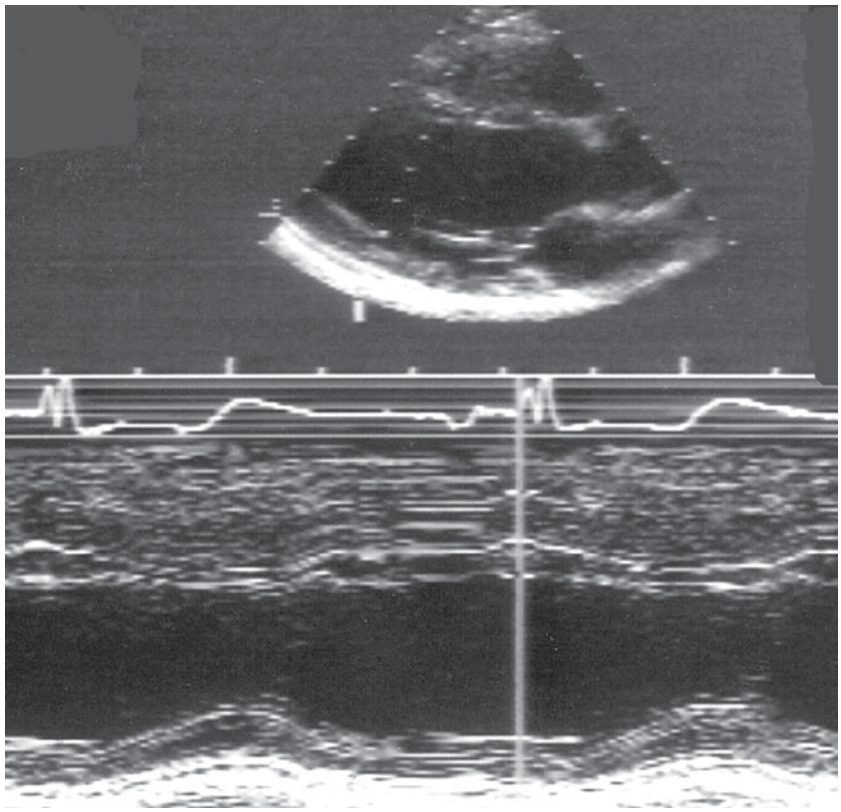

Fig. 20.16 Parasternal long-axis (*top*) and respective M-mode echocardiogram from a normal individual. Notice the bright linear echoes running in parallel to the ventricular septum that can potentially be included in the measurement of the septal wall thickness

3. *Right ventricular moderator band* (Fig. 20.17): This is a band of muscle that joins the right ventricular inflow to the outflow tract. It is a normal cardiac structure invariably present in all patients, and it is used to describe the right ventricle. As with the false tendons, when gain settings are inappropriately set, the space between moderator band and ventricular septum may not be apparent, thus including the moderator band with the septal wall measurements.
4. *Angulated (sigmoid) septum* (Fig. 20.14): One should be aware of the possible false diagnosis of asymmetrical septal hypertrophy, when acute angulations of the ventricular septum occurs (sigmoid septum). In the elderly population the ventricular septum tends to continue from the anterior aortic wall in an acute angle, so that it easily gives the false impression of a localized subaortic septal thickening viewed from left parasternal projections. Such angulation appears to form a localized septal thickening at the proximal portion of the anterior septum, particularly when the M-mode beam transects the septum at this level and can easily be misinterpreted as ASH and thus HCM. Left ventricular wall thickening, small outflow tract dimensions and a small incomplete SAM, may complete the illusion of HCM.
5. *Oblique (tangential) measurements*. These include misinterpretations of normal variants of left ventricular shape, or can be due to oblique longitudinal sections of the left ventricle (off-axis views) and the presence of other causes leading to ventricular hypertrophy. ASH may be a sensitive marker for HCM, but it is not specific for this condition.
6. *Congenital heart disease*: ASH is relatively common in infants with congenital heart disease. The overall prevalence of disproportionate septal hypertrophy in one study was 10% and was exceeding 20% in patients with pulmonary stenosis or pulmonary hypertension.
7. *Thinning of the posterior wall (myocardial infarction):* ASH may occur in conditions causing thinning or thickening of the left ventricular posterior wall relative to the septum. This abnormal septum to posterior wall thickness ratio is commonly

encountered in coronary artery disease patients either because of segmental hypertrophy of the septum, i.e., secondary to systemic hypertension or, more commonly, as a result of transmural myocardial infarction of the posterior wall, causing thinning which produces an abnormal ratio even in the presence of normal septal thickness.

8. *Concentric hypertrophy* is the predominant pattern in secondary left ventricular hypertrophy. Other entities that simulate HCM must be recognized (Table 20.5). Hypertensive heart disease, cardiac amyloidosis, and patients with chronic renal failure may show predominant concentric hypertrophy and may have an echocardiographic appearance mimicking that of HCM with or without a gradient. The vigorous left ventricular systolic contraction however seen in HCM together with an ECG, should, in the majority of cases, differentiate patients with HCM from those with cardiac infiltration where ventricular contraction is depressed. There is a subset of patients with small left ventricular cavity, moderate left ventricular hypertrophy, and hyperdynamic systolic function secondary to longstanding systemic hypertension. These patients are usually elderly and may exhibit a systolic anterior motion of the mitral valve, an outflow tract gradient, and impaired diastolic function. In practice, the diagnosis of HCM should not be made in these patients because the hypertrophy is secondary to a known etiology. It is conceivable, however, to have a common disease such as systemic hypertension in association with a rare cardiac condition such as hypertrophic cardiomyopathy, in which case the differential diagnosis is extremely difficult clinically and should be avoided. Perhaps genetic markers may be able to differentiate the two conditions. Finally, other conditions such as Fabry's disease (a-galactoctosidase deficiency) or Friedreich's ataxia may present ventricular hypertrophy indistinguishable from HCM where the definitive diagnosis must lie in the genetic markers or in the search of a-galactosidase deficiency.
9. *Cardiac amyloidosis* may occasionally prove difficult to differentiate from HCM patients with concentric hypertrophy, particularly at an early stage of the disease. Both may show a similar degree of concentric left and right ventricular hypertrophy, and the described "sparkling" myocardial texture lacks specificity for cardiac amyloidosis. The depressed systolic function in cardiac amyloidosis usually contrasts well with the usual vigorous ventricular contraction seen in HCM. The thickened valves and atrial septum (with amyloid infiltration) may on occasions be of some help in the differential diagnosis. A low-voltage electrocardiogram in patients with cardiac amyloidosis will add to the differential diagnosis, but cardiac biopsy will conclusively differentiate the two conditions.
10. *Hypertrophy in athletes:* Another major diagnostic difficulty occurs in some athletes who may present symmetric or even asymmetric left ventricular hypertrophy. Ventricular hypertrophy may represent either a physiologic adaptation with more hypertrophy than usual or abnormal hypertrophy because of underlying HCM, putting the patient at risk for sudden death. Regular intake of anabolic steroids, combined with intense isometric exercise, may lead to a further increase in left ventricular wall thickness in relation to internal ventricular dimensions overshadowing an underlying primary myocardial disorder.

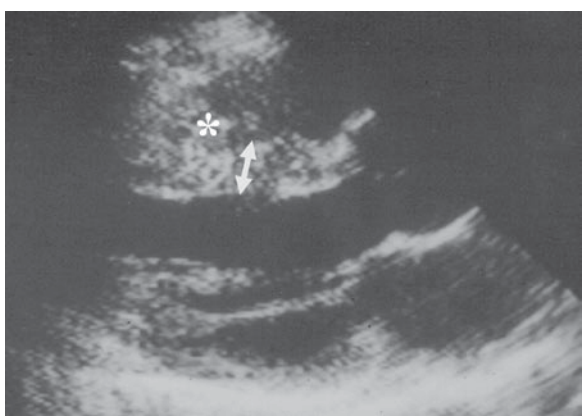

Fig. 20.17 Patients with mild right ventricular pressure overload demonstrating RV hypertrophy and a prominent moderator band (*asterisk*)

Table 20.5 Other cause of ventricular hypertrophy that can simulate HCM

Systemic pressure load, including renal disease
Glycogen storage disease (mainly in infancy)
Mucopolysaccharidoses (childhood)
X-linked lysosomal storage disorder
Anderson–Fabry disease
Freidreich's ataxia
Athlete (mainly isometric exercise)
Infiltrative disorders (amyloidosis)

The discrimination between HCM and physiologic adaptation may lie in cavity dimensions rather than in the wall thickness, whether asymmetric or not (Table 20.6). In HCM, the cavity dimensions tend to be at the lower end of the normal spectrum, whereas the athlete is vagotonic with resting bradycardia and the ventricular dimensions at the upper normal limits or above while LA size is increased. It is exceedingly rare for athletes of any sort to have a wall thickness greater that 13 mm. In practical terms, the combination of a wall thickness of >13 mm together with an LA size >41 mm should effectively rule out the diagnosis of athlete's heart.

The Mitral Apparatus

The mitral apparatus is visualized in its integrity from parasternal and apical long-axis as well as parasternal short-axis projections, and these represent the optimal views for the visualization and assessment of systolic anterior motion of the mitral valve (SAM) (Fig. 20.5b).

Controversy still exists as to the mechanisms of SAM. There are three dominant hypotheses evoking the mechanisms of SAM:

1. Venturi effect resulting in the mitral valve cusp to be aspirated into the relatively low-pressure chamber by the high velocity of blood flow through the left ventricular outflow tract
2. Abnormal mitral valve cusp apposition at the onset of systole in association with a small left ventricular cavity
3. Secondary to an abnormal positioning of the papillary muscles which are displaced forward and medially during systole in association with a small left ventricular cavity

Table 20.6 Differentiation between patients with HCM and athletes

Parameters	HCM	Athletes
Wall thickness (mm)	≥13	<13
LVEDd (mm)	≤50	>50
LA (mm)	≥41	<40
E (cm/s)	Reduced	Increased
A (cm/s)	Increased	Reduced
E/A	>1	<1
Deceleration time (ms)	Increased	Reduced
IVRT (ms)	Increased	Reduced

SAM is associated with the presence of left ventricular outflow tract gradient measured at cardiac catheterization. The presence of SAM is not pathognomonic of HCM. This systolic anterior motion of the mitral valve can also occur whenever there is a small, hypertrophied left ventricle in association with a hyperdynamic ejection as well as in patients who are hypovolemic and/or dehydrated. SAM is also common in elderly patients with an angled septum or hypertensive heart, especially when preload and afterload have been reduced by diuretics. Similarly, the absence of SAM does not necessarily preclude the diagnosis of HCM.

The Aortic Valve

Early closure of the aortic valve was one of the earliest echocardiographic features in HCM and usually concurs with the presence of SAM and a subaortic gradient (Fig. 20.5a). It has been thought to occur when the left ventricular outflow tract gradient peaks in mid-to-late systole, causing the aortic valve cusps to come together during this time, not because there is a significant amount of blood left in the ventricle unable to be ejected, but rather because there is not enough blood left in the ventricle to be ejected during the later part of systole. Like SAM, midsystolic closure of the aortic valve is nonspecific and may be seen in other conditions such as discrete subaortic stenosis as well as in any hyperdynamic left ventricle.

Rarely, patients with HCM have mild aortic incompetence. This may be the result of some degree of annular distortion without annular dilatation. This may arise from the asymmetrical septal hypertrophy, which causes the ejection flow to be directed eccentrically against the aortic valve. The constant impact of the high-velocity blood flow with the aortic valve would produce a wear and tear of the cusps leading to aortic regurgitation. The minor valvular degeneration may become the site of vegetations should bacteremia be produced and therefore prevention should be instituted.

Doppler Echocardiography

The addition of Doppler techniques to two-dimensional echocardiography has provided comprehensive hemodynamic assessment on HCM patients. Pulsed-wave

Doppler is particularly useful in the assessment of the left ventricular filling characteristics. Systolic events are predominantly characterized by the presence of increased intraventricular velocities and the presence or absence of gradient. Continuous-wave Doppler is a reliable method for measuring the peak systolic pressure drop (gradient) across the left ventricular outflow tract using the simplified Bernoulli equation ($P = 4V^2$). Color-flow imaging complements the anatomic information obtained by two-dimensional echocardiography and facilitates further the understanding of the underling pathophysiological changes occurring in HCM. It may demonstrate the pattern of progressive intraventricular flow systolic acceleration and the location of aliasing and/or the presence of outflow track turbulence at a glance.

Diastolic Events

The basic functional disorder in HCM occurs during diastole with impaired relaxation, filling and compliance of the ventricles. Far from being uniform, myocardial dysfunction is patchy and irregular depending upon the extent and distribution of the myofibrillar lesions.

Early studies using M-mode echocardiography have shown that the rates of filling and relaxation of the left ventricle were abnormal in patients with hypertrophic cardiomyopathy. Doppler echocardiographic recordings are easier to obtain in nearly all patients and provide a good overall estimate of diastolic filling abnormalities of the left ventricle.

Diastolic velocity waveforms are recorded with pulsed-wave Doppler by positioning the sample volume at the tips of the mitral valve during diastole. There are several patterns of left ventricular diastolic filling in a variety of different cardiac disease dependent upon the interrelation of left ventricular relaxation, left atrial pressure, and intrinsic left ventricular chamber stiffness. In HCM patients, the period during which the heart is isovolumic is often prolonged, left ventricular filling is slow and the proportion of filling volume resulting from atrial systole may be increased. These pathophysiologic changes are reflected in the pulsed Doppler recording of the transmitral waveform. Impaired ventricular relaxation results in prolonged isovolumic relaxation time, slower early ventricular filling ("E" wave), and a compensatory exaggerated atrial systolic filling ("A" wave), in patients who have kept normal left atrial pressure, so that the ratio E/A is reduced (Fig. 20.18). In more severe cases, with increased left atrial pressure (>15 mmHg), the extent of rapid filling is increased with a consequent reduction of the atrial contribution, giving the wrong impression of "normalization" of left ventricular filling (pseudonormalized). Normalization of the diastolic filling pattern in HCM can also happen in the presence of significant mitral regurgitation. More advanced still, with decreased compliance and high left ventricular filling pressures, there is accelerated rapid early filling and normal or reduced late filling similar to patients with restrictive physiology. It is therefore understandable that in a nonhomogeneous HCM population where patients exhibit different degrees of functional disability, they will be presenting with a spectrum of mitral inflow waveforms. It is, therefore, not surprising that often, no correlation can be found between patient's symptoms (predominantly breathlessness) and Doppler diastolic indices as a number of symptomatic patients may have "normalized" diastolic indices.[9] A much better correlation could be found between patient's professed symptomatic status and maximal oxygen consumption and anaerobic threshold during cardiopulmonary exercise testing.

While sensitive, these Doppler diastolic parameters lack specificity since they may be influenced by multiple factors, including the intrinsic properties of the cardiac

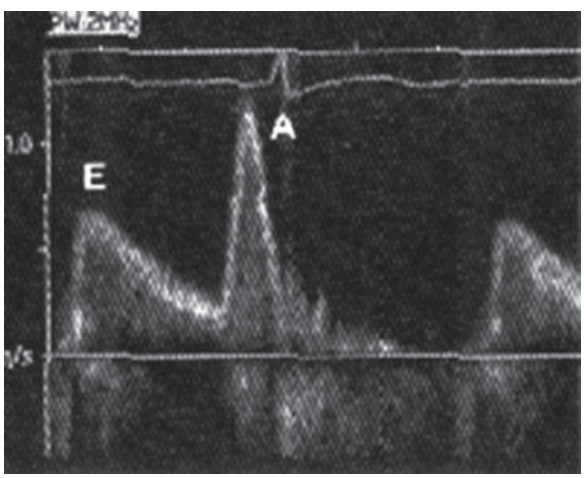

Fig. 20.18 A typical transmitral velocity profile from a patient with HCM. Note the reduced E-wave velocity with prolonged deceleration time and a compensatory increase of the A wave (impaired relaxation). This is the earliest diastolic abnormality that occurs in such patients and may not be associated with breathlessness

muscle and loading conditions of the heart as well as heart rate and the patient's age. Although heart rate and arterial pressure have important influences on left ventricular diastolic filling, it is the interplay between left atrial pressure at mitral valve opening, mitral regurgitation, left ventricular relaxation, chamber stiffness that determine the rate and extent of early and late diastolic filling.

Color-flow imaging can distinguish the high presystolic inflow velocity (A wave) from the lower velocity of the early diastolic filling flow (E wave) by the increased brightness of the red-orange color occurring in late diastole, which also often aliases. Since patients with HCM usually have small left ventricular cavity dimensions, the higher velocity in late diastole may be seen into the left ventricular cavity and even on occasions reaching the cardiac apex.

Systolic Events

The systolic events in patients with HCM may be categorized into two main groups. First, those occurring in the left ventricular cavity and outflow tract in which the highlight is the presence or absence of an intraventricular gradient and secondly the presence of mitral regurgitation.

1. *Intraventricular flow velocity:* Doppler echocardiography has been used to measure blood flow velocities within the heart, particularly for calculating pressure gradients across stenotic valves. This has also been proven to be valid for calculating the dynamic gradient across the left ventricular outflow tract in patients with HCM. In contrast with fixed obstruction, the flow velocity profile in patients with HCM, as obtained with continuous-wave Doppler, presents a slow and gradual increase which only reaches maximal velocity late in systole changing the overall shape of the flow velocity (Fig. 20.19). If there is no high velocity in the left ventricular outflow tract at rest, the late-peaking velocity contour may be brought out in some patients with provocative maneuvers following amyl nitrate inhalation, or during a Valsalva maneuver. The velocity contour reflects both the timing and the magnitude of the pressure drop across the left ventricular outflow tract.

Color-flow imaging can identify the uniformity or the nonuniformity of the intraventricular flow. In the normal individuals from the apical four-chamber and two-chamber projections, the ventricular flow coded in blue (blood flow directed away from the transducer) progressively becomes brighter as it moves from the apex toward the left ventricular outflow tract. At this position it will aliase and the flow map demonstrates a central red zone (color reversal) immediately below the aortic valve. In patients with HCM, the intraventricular color-flow map during systole is characterized by a nonhomogeneous blue color with a lighter hue compared with normals and typically aliases at midventricular

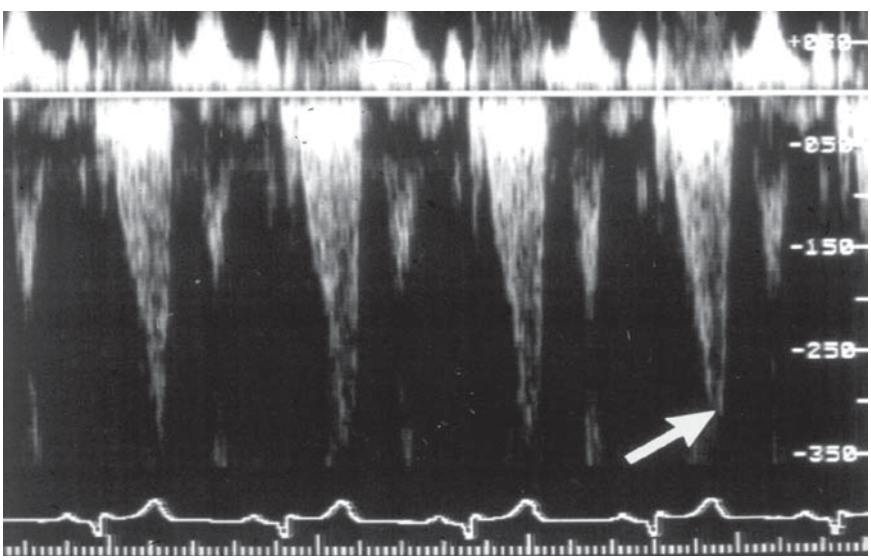

Fig. 20.19 Continuous-wave Doppler directed across the left ventricular outflow tract showing the characteristic delayed systolic peak (*arrow*) of the velocity waveform. In this patient the peak velocity was 3.2 m/s reflecting a pressure gradient of 42 mmHg

level, at the level of the hypertrophied papillary muscles or at the level of the mitral valve.

When SAM occurs, the systolic flow at this level becomes turbulent with a "mosaic" color pattern (Fig. 20.20). When the flow crosses the aortic valve into the ascending aorta it becomes laminar again with homogeneous red color, as seen from the suprasternal window (flow moving toward the transducer).

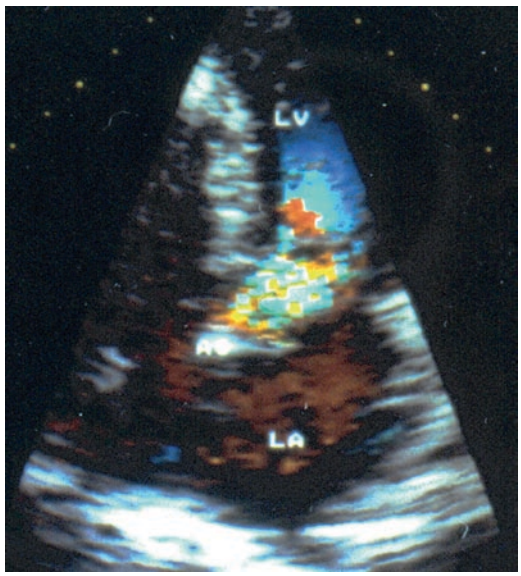

Fig. 20.20 Color-flow Doppler superimposed to M-mode echocardiography (*left*) and long-axis parasternal view from an HCM patient. Note that the mitral regurgitation on the M-mode begins before the SAM-septal contact, while the mitral regurgitation begins in midsystole. On the right, the mitral regurgitant jet is directed posteriorly into the left atrium while the left ventricular outflow gradient directed anteriorly toward the aorta

With the superimposition of color-coded blood flow on M-mode echocardiograms, an improved timing of the intraventricular systolic events can be obtained (Fig. 20.21). This provides higher temporal resolution and a wider range of velocities displayed in color so that an accurate analysis of timing and direction of the blood flow can be performed. High-velocity turbulent flow usually occurs at the time when the mitral valve leaflets impinge on the ventricular septum during systole. When it then reaches the outflow tract, it encounters the anteriorly positioned mitral leaflets (SAM) and loses its laminar characteristics to become turbulent with the typical mosaic pattern (green-yellow) on color-flow imaging. At this level further flow acceleration occurs reaching velocities as high as 5–6 m/s (Fig. 20.21).

Occasionally, in some patients with HCM, turbulent flow can be seen in the middle of the left ventricle or even at the apex. This would suggest that the gradient occurs distally at midventricular level (Fig. 20.22). It is this inhomogeneity of the intraventricular flow during systole that appear to be fairly specific in distinguishing most of the patients with HCM from secondary causes of left ventricular hypertrophy.

Gradients are usually associated with SAM and midsystolic closure of the aortic valve. When mitral leaflet-to-septal contact occurs during systole there is a pressure gradient but during this time, a large proportion of left ventricular stroke volume continuous to be

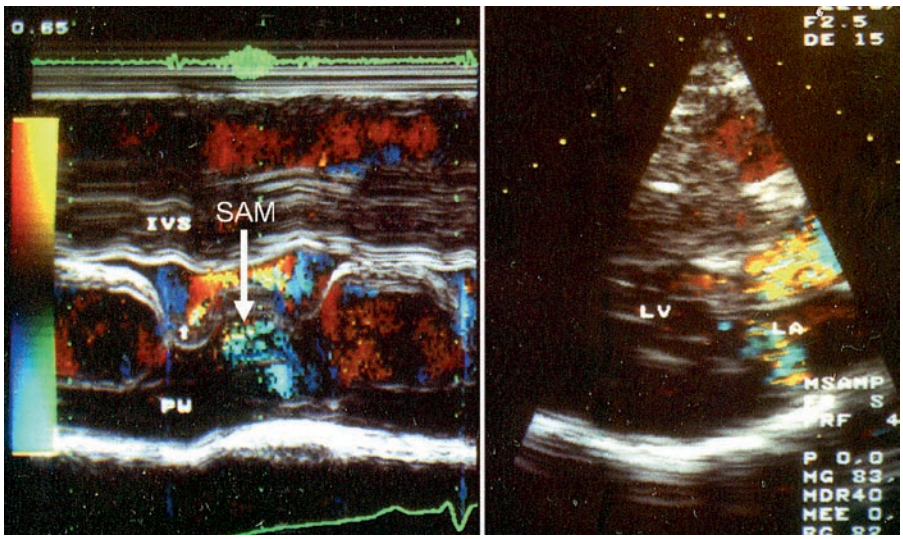

Fig. 20.21 Color-flow Doppler in a representative hypertrophic cardiomyopathy patient. From the apex, high-velocity systolic flow is apparent away from the transducer (*light blue*), passing from the middle of the left ventricle where in aliases into *red color*. When blood flow reaches the subaortic area, it becomes turbulent (*green-yellow color*) suggesting the presence of an outflow gradient

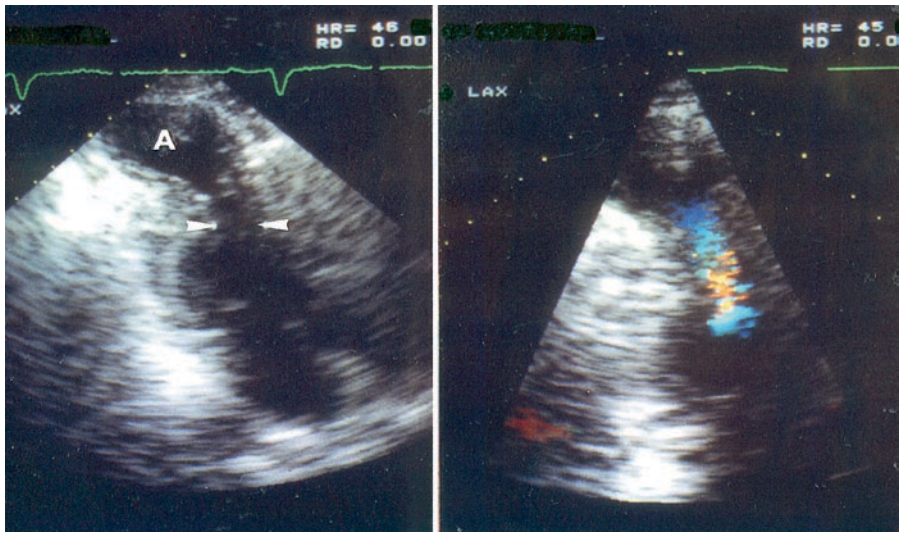

Fig. 20.22 Apical long-axis view with color-flow mapping in a hypertrophic cardiomyopathy patient with midventricular gradient. Note on the left the narrowing of the left ventricular cavity in its middle portion (*arrowheads*) and on the right, the turbulent flow originating at that level

ejected despite the presence of a gradient. If the term "obstruction" means a blocking of the passage of blood from the left ventricle to the aorta, then there is little evidence that this occurs. The left ventricle contracts rapidly and powerfully, expelling its contents in the first half of systole.

2. *Mitral regurgitation:* Mitral regurgitation is a well recognized component of the complex pathophysiology encountered in patients with HCM. Its association with the SAM of the mitral valve and the magnitude of the intraventricular gradient has also been well documented. Patients who do not present with SAM of the mitral valve rarely present with mitral regurgitation.

Color-flow imaging can detect the presence of mitral regurgitation with high sensitivity and specificity. The most useful transducer locations are generally the apical four-chamber and two-chamber projections, but also the parasternal long and short axis may be very useful in detecting jets directed posteriorly (Fig. 20.20). Mitral regurgitation in patients with HCM is noted as a mosaic pattern (turbulent flow) present in the left atrium during systole. When the jet is directed anteriorly it may easily be confused with the turbulent jet of the left ventricular outflow tract. With continuous-wave Doppler alone it can be very difficult to separate these two high-velocity jets and a great deal of expertise is required in both the recording and the interpretation. The shape of the two systolic flows is typically different. The left ventricular outflow tract velocity has the characteristic scimitar or dagger shape late peaking contour, as opposed to the more symmetrical velocity curve of mitral regurgitation.

With color-flow imaging the left ventricular outflow tract flow velocity and mitral regurgitant jet can readily be distinguished and allow for a better lining-up of the continuous-wave Doppler beam and outflow tract velocity.

The exact mechanism of mitral regurgitation in patients with HCM remains controversial and perhaps more than just one mechanism is involved. It is possible that an "eject, obstruct, leak" sequence occurs during which mitral regurgitation results from left ventricular outflow tract "obstruction." Mitral regurgitation however is usually the result of contortion of the mitral apparatus, which begins in early systole. This is supported by the Doppler studies showing that mitral regurgitation begins early, before the occurrence of systolic anterior motion to septal contact. The onset of mitral regurgitation occurs less than 100 ms after the electrocardiographic R wave, whereas the onset of systolic anterior motion of the mitral valve follows that. As systole progresses there is a further decrease in left ventricular systolic dimensions and mitral valve distortion following the anterior mitral leaflet-septal contact. This would therefore result in an increased amount of mitral regurgitation occurring later in systole.

A third cause of mitral regurgitation is secondary to the presence of mitral annular calcification. This pattern,

as mentioned earlier on, is particularly encountered in the older patients with HCM.

The Role of Tissue Doppler Imaging

Assessment of LV function in patients with cardiomyopathies is routinely performed by cross-sectional echocardiography. Being predominantly semiquantitative, relying on visual assessment of LV function, two-dimensional echocardiography poses a significant limitation to the assessment of both regional and global ventricular function. Volume changes such as ejection fraction, end-systolic, and end-diastolic volumes are also load dependent and insensible when it comes to quantify subtle ventricular changes over time. Tissue Doppler is now being introduced to the routine echocardiographic assessment of cardiomyopathy patients as a robust, objective method of assessing ventricular function. By inversing the amplitude and frequency filters, tissue Doppler can measure the lower velocities originating from myocardial motion and filter out the higher blood pool velocities in an inverse fashion of the traditional Doppler recordings.

The presence or absence of ventricular hypertrophy is not an infallible diagnostic criterion, and the phenotypic heterogeneity of hypertrophic cardiomyopathy patients renders the reliance of wall thickness measurements alone questionable. Mutations in myosin-binding protein C and cardiac troponin T are known to produce minimal amount of ventricular hypertrophy. Similarly, ventricular hypertrophy as a result of physiologic adaptation to exercise may in some cases render the differential diagnosis with hypertrophic cardiomyopathy difficult. While genetic testing may provide the ultimate diagnosis in mutation carriers, this may not be widely available for routine clinical practice for some years to come.

Tissue Doppler imaging may be used in three different ways:

1. Pulsed-wave recordings of the mitral annular velocities from up to six annular positions (four-chamber, two-chamber, and three-chamber projections)
2. Pulsed tissue Doppler imaging (TDI) from selected myocardial regions (basal, middle, and distal regions)
3. Color TDI from two-dimensional recordings of the myocardium

This latter recording of a wider myocardial region of interest may produce three types of measurement either longitudinally or radially. These include velocity differences between two selected myocardial points of interest, as well as myocardial deformation indices, such as myocardial strain and strain rate (Chap. 5). Myocardial strain reflects the deformation of tissue in response to an applied force. The first temporal derivative of strain is strain rate and represents the velocity change in myocardial fiber length over time. Recent software advances permit real-time strain and strain rate determination and regional strain rates between the epicardium and endocardium representing the myocardial velocity gradient, which correlates with regional ventricular contractility.

Because the pathophysiologic alteration in hypertrophic cardiomyopathy is myocardial disarray, this will lead to an impaired myocardial deformation during the cardiac cycle. When at an advanced stage myocardial fibrosis develops, this may further reduce myocardial deformation both along the longitudinal fibers and radial function, which may not be appreciated by routine two-dimensional echocardiography alone. TDI offers a unique modality that can monitor the presence and potential change of myocardial contractility over time.

TDI can be applied in five ways to assess the ventricle in hypertrophic cardiomyopathy patients:

1. Assess mitral annular velocities (systolic, diastolic, or both)
2. Assess longitudinal function of the proximal and mid-LV (velocities and strain and strain rate)
3. Assess radial LV function (myocardial velocity gradients or strain rate)
4. Assess diastolic function and filling LV pressures
5. Differentiation from athlete's heart

1. *Mitral annular velocities* (Fig. 20.23): A number of studies have now used TDI of mitral annular velocities for the early detection of mutation carriers, even when myocardial wall thickness was normal. Systolic (Sa) and early diastolic (Ea) PW velocities at the mitral annulus are lower in mutation carriers.[10]

    - A lateral Sa >13 cm/s had a sensitivity of 100% and a specificity of 93% for differentiating the mutation positives without hypertrophy from controls and a lateral Ea <14 cm/s had a 100% sensitivity and 90% specificity.

- A septal Sa <12 cm/s and Ea <13 cm/s both had a 100% sensitivity and 90% specificity.

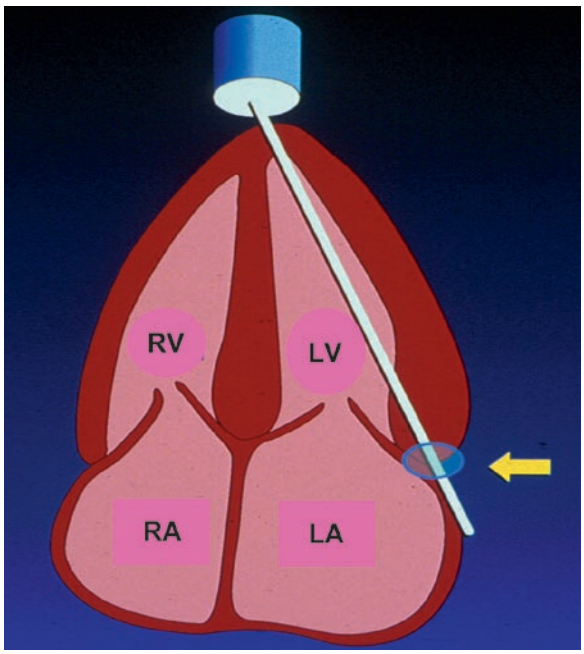

Fig. 20.23 Apical four-chamber projection demonstrating the Pulsed-Wave sample volume positioned at the lateral corner of the mitral annulus (*arrow*)

Although significant overlap exists between controls and cardiomyopathy patients, these studies indicate that TDI can provide an easy and complementary role in the diagnosis of hypertrophic cardiomyopathy patients. Importantly, it raises the possibility in identifying preclinical cases of cardiomyopathy patients.

2. *Assessing longitudinal function* (Fig. 20.24): From apical projections, longitudinal function of the LV can be assessed by specifically interrogating a myocardial region of interest (Fig. 20.24a). Three main parameters may be measured: tissue velocities (cm/s), strain rate (−1 s), and strain (%) (Fig. 20.24b). Tissue velocity measurements may not be able to differentiate tissue movement due to active contraction from passive motion that results either from translational motion of the whole heart or from a "tethering" of normal surrounding tissue on a segment of disease myocardium. Strain and strain rate in the other hand are minimally affected by passive motion and therefore are expected to be more sensitive readings of myocardial function. Very little data however are to date available to prove the value of longitudinal strain and strain rate in cardiomyopathy patients. One of the main limitations of strain rate is the usually very noisy signal that necessitates significant

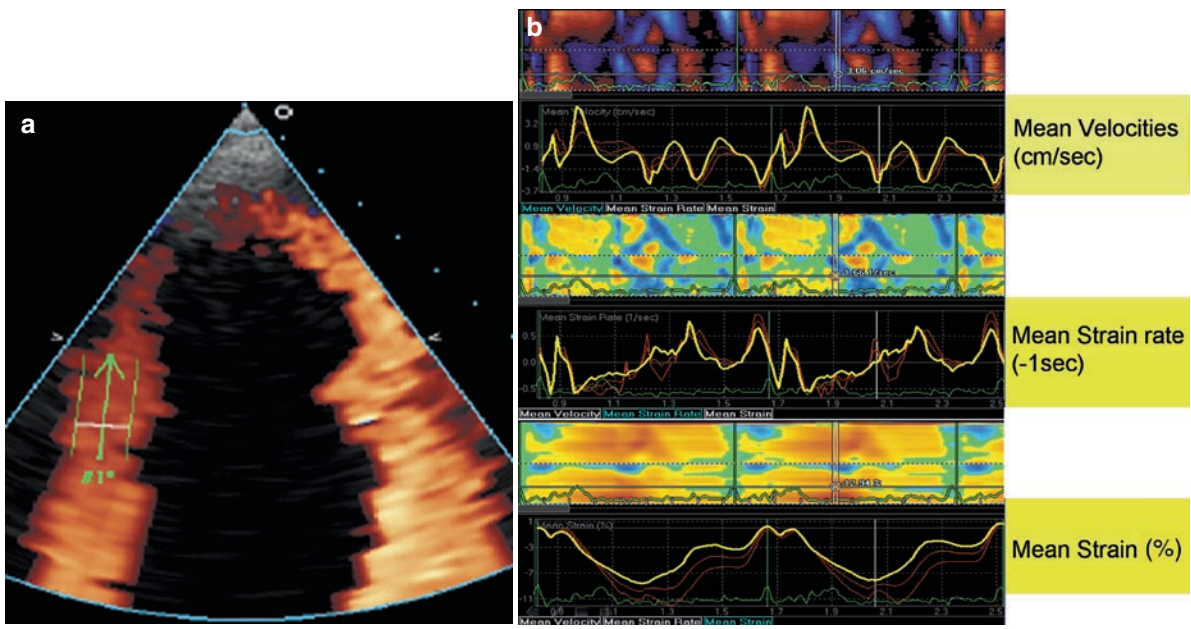

Fig. 20.24 (**a**) Apical four-chamber projection from a cardiomyopathy patient demonstrating the interrogation of the myocardial region of interest in the proximal (basal) septum. (**b**) Same patient with the three main tissue Doppler parameters of myocardial velocities and deformation. One systolic and two diastolic waveforms are identified each time and measured

postprocessing algorithms that may vary from one ultrasound system to another.

3. *Assessing radial LV function:* Left ventricular radial myocardial function may be assessed from parasternal long- or short-axis projections using color TDI. This is visually appealing and easily applicable technique, which discloses differential velocities between the subendocardium and subepicardium. Normally, a higher velocity of shortening and relaxation are observed in the endocardium compared to the epicardium, and this can be quantified as a myocardial velocity gradient (MVG). The myocardial velocity gradient across the septum or the posterior wall may be measured throughout the cardiac cycle. As with the longitudinal function, one systolic (S) and two diastolic (early and late) waveforms can be measured. MVG are typically reduced in HCM patient and this reduction is grater with a greater amount of hypertrophy. The amount of MVG reduction is also proportional to the degree of hypertrophy (Fig. 20.25).
4. *Assess diastolic function and filling LV pressures* (Fig. 20.26): The ratio between early transmitral diastolic velocity and mitral annular velocity (Em/Ea), either from the septal or lateral annular corners, often known as the Em/Ea index, has been used as a robust predictor of LV filling pressures.

In patients with a positive genotype for hypertrophic cardiomyopathy an Em/Ea >8 cm/s can be predictive of HCM even when filling pressures are normal.

5. *Differentiation from athlete's heart:* The distinction of physiologic versus pathologic LV hypertrophy is often difficult and may be crucial for the individual's career as a professional athlete. While two-dimensional echocardiography can offer some hints toward one versus the other (see earlier), these may be difficult to apply in all individuals. TDI can significantly add to the differential diagnosis. While in physiologic hypertrophy both systolic and diastolic

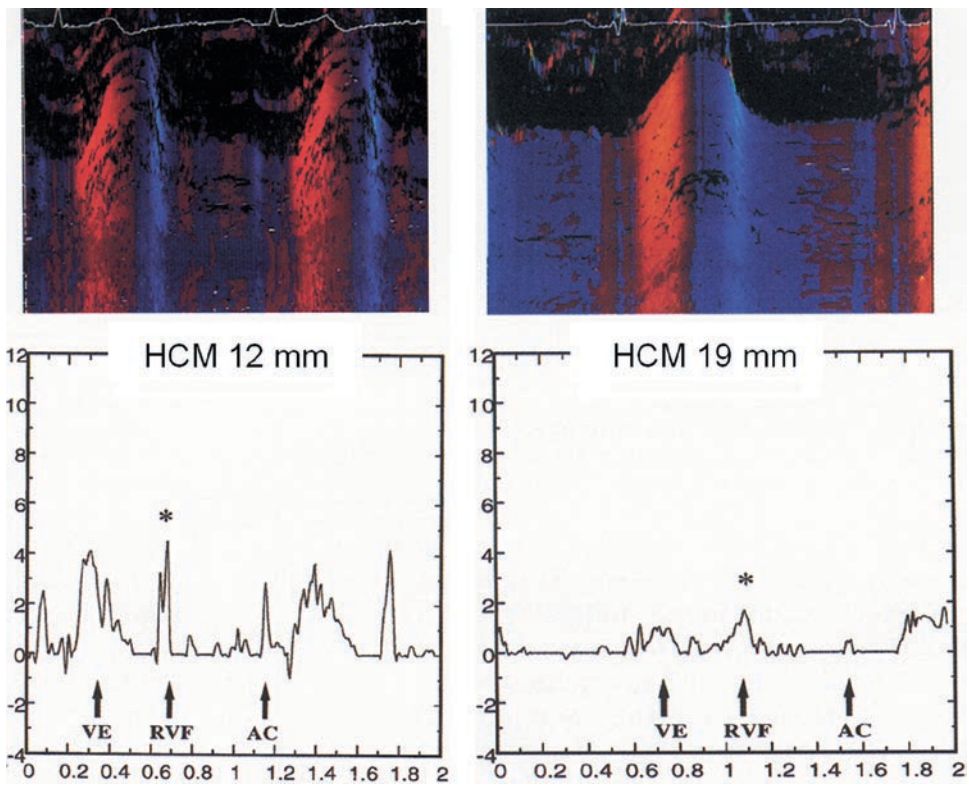

Fig. 20.25 Myocardial velocity gradient (MVG) in hypertrophic cardiomyopathy. From parasternal short-axis projections, the MVG of the posterior wall can be measured. Note that the greater the hypertrophy, the grater the reduction of MVG, particularly those of the systolic gradient (VE) and the early diastolic gradient corresponding to the rapid ventricular filling (RVF). AC atrial contraction

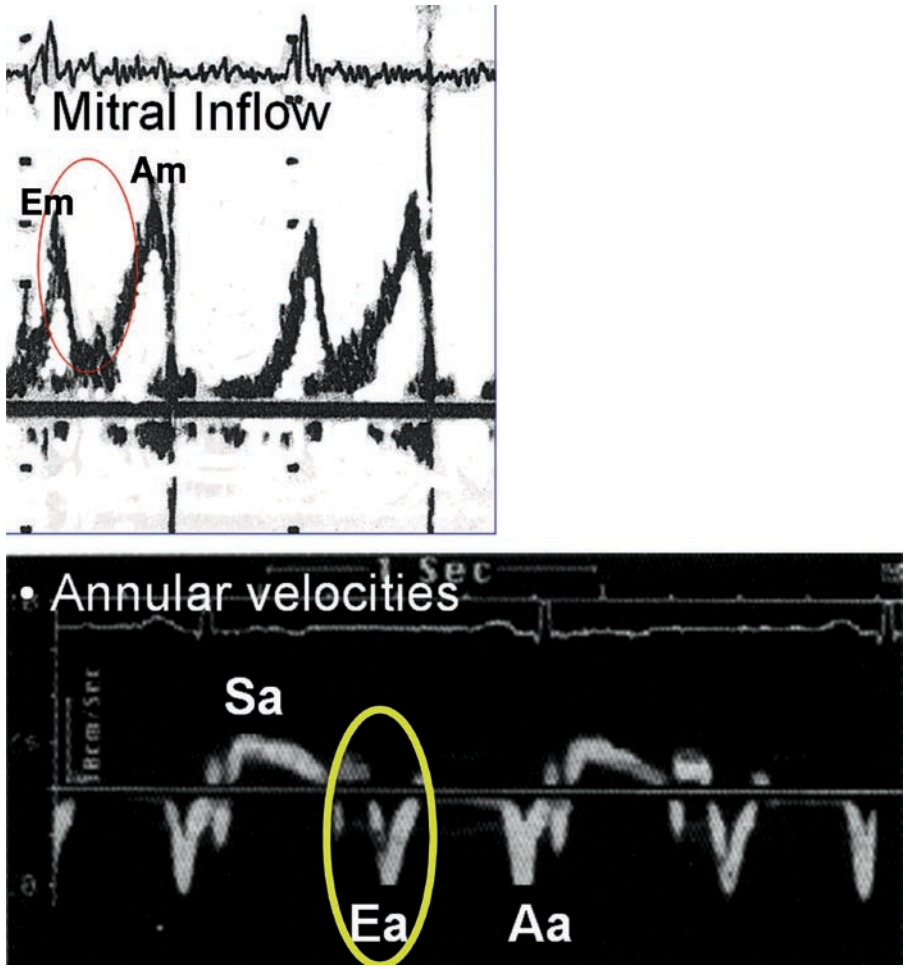

Fig. 20.26 The early mitral Em to annular Ea index of assessing diastolic filling pressures. Annular velocities may be measured from both lateral and septal annular positions

velocities and MVG are high, often higher than in normals, in pathologic hypertrophy (HCM), these velocities are reduced (Fig. 20.27).

The accuracy in separating HCM from athletes is high when the systolic MVG is ≤7 (sensitivity 96% and specificity 95%).[11]

Predictors of Prognosis

There is now evidence that the overall outcome of HCM is not that malignant, but predictors of a good versus a bad outcome are not clear. In Maron's study,[5] ventricular wall thickness was similar in patients who died suddenly and those who did not. Therefore, absolute ventricular wall thickness cannot be used as a predictor of sudden death. Similarly, the presence and the magnitude of outflow tract gradient are not predictive of sudden death.

Diastolic left ventricular dysfunction, as assessed by Doppler, is particularly common in HCM patients, but again these abnormalities are not related to patient's symptoms[9] nor are they related to the presence of intracardiac gradients. Perhaps one positive Echocardiographic finding in relation to severe breathlessness would be the detection of severe mitral regurgitation.

During longitudinal studies on same patients with HCM the development of progressive congestive heart failure can be associated with ventricular dilatation and impairment of a previously vigorous left ventricular contraction. This may also result in a progressive

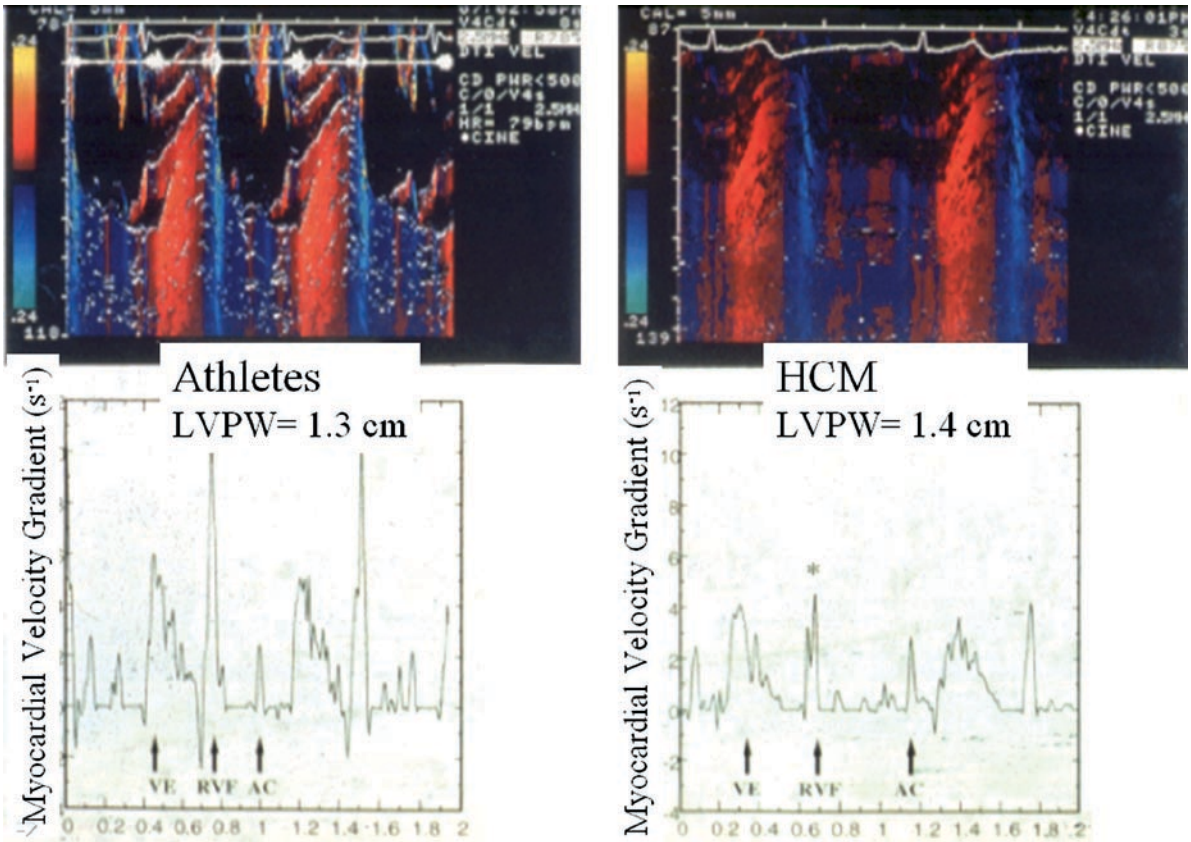

Fig. 20.27 Myocardial velocity gradients from an athlete (*left*) and a patient with hypertrophic cardiomyopathy (*right*). Notice that despite similar amounts of hypertrophy, the HCM patient presents with lower rapid filling (early diastolic) velocity gradient

decrease in the ventricular gradient. Serial echocardiographic and Doppler studies could illustrate the turning point toward progressive deterioration in this subgroup of patients by demonstrating a gradual decrease in intraventricular systolic flow velocity.

Dilated Cardiomyopathy

Idiopathic (Primary) Dilated Cardiomyopathy

Dilated (congestive) cardiomyopathy is primarily a disease of the systolic function of the heart and is traditionally a diagnosis of exclusion. Patients typically present with signs of heart failure and peripheral edema. The electrocardiogram is abnormal with repolarization changes, and it may show intraventricular conduction abnormalities and bundle branch block. Echocardiography will show evidence of ventricular dilatation with global ventricular dysfunction. For the diagnosis of dilated cardiomyopathy to be firmly established, the proof of normal coronary angiography should be demonstrated. According to the WHO definition, dilated cardiomyopathy is defined as cardiac dilatation and impaired contractility in the absence of a recognized etiology. Approximately one-third of all idiopathic dilated cardiomyopathies have a familiar substrate, 70% as an autosomal dominant transmission, while 15% are recessive (desmoplakin) and 10% X-linked (dystrophin) (Table 20.7).

While the cause of dilated cardiomyopathy is unknown, the condition may represent myocardial damage produced by familial, immunological, toxic, or infectious mechanisms. The natural history is not well established and a lot will depend on the underlying mechanism, which in some instances may be reversible.

Table 20.7 Conditions leading to dilated cardiomyopathy

	Gene encoding	Chromosome
Idiopathic DCM	–	–
Sporadic (predisposing factors?)		
Toxic (alcohol, doxyrubicin, etc.)		
Viral infections		
Familial DCM (11 genes)		
Autosomal dominant		
	ACT (actin)	15q14
	DES (desmin)	2q35
	TNNT (troponin T)	1q32
	MYH7 (b-myosin)	14q11
	VCL (metavinvulin)	10q22
	MLP (muscle LIM protein)	11p15
	PLN (phospholamban)	6q22
Muscular dystrophies		
X-linked		
Emery–Dreifuss	Emerin	Xq28
Autosomal dominant	Lamin A and lamin C	1Q21.2-q21.3
Laminopathy		
Limb-girdle	Sarcoglycan-sarcospan	
Autosomal dominant	SGCD (d-sarcoglycan)	5q33
Duchenne	Dystrophin	Xp21
Becker	Dystrophin	
Recessive	TAZ (tafazzin)	Xq28
Myotonic dystrophy		
Congenital	Fukutin-related protein	

An early diagnosis is often crucial to institute early management in an attempt to avoid ventricular remodeling and further dilatation.

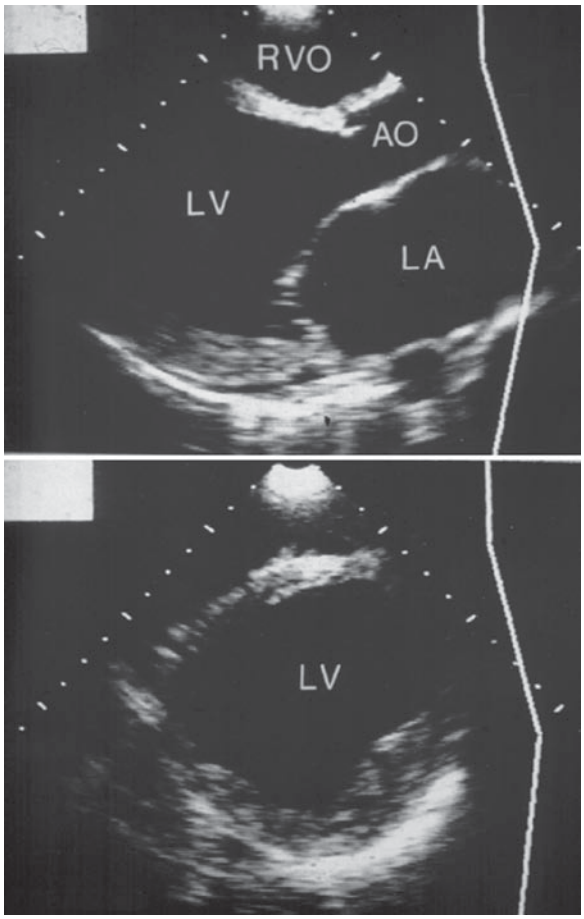

Fig. 20.28 Parasternal long axis (*top*) and short axis (*bottom*) from a patient with dilated cardiomyopathy. Note the marked dilatation of the left ventricle

The Role of Echocardiography

Echocardiography can quickly establish the diagnosis of left ventricular systolic dysfunction by demonstrating ventricular enlargement as well as ventricular systolic dysfunction (Fig. 20.28). This is typically diffuse and often it involves both the left and the right ventricles. The diagnosis of cardiomyopathy however is more of a diagnosis of exclusion and ruling out coronary artery disease is essential. Often, however, the left ventricular dimensions remain normal and the only abnormality may be diffuse ventricular dysfunction alone. This may well represent a milder form or an earlier stage of cardiomyopathy. Regular follow up with repeat echocardiographic examinations will be able to demonstrate changes of ventricular dimensions and echocardiography is ideally suited for such studies.

Particular attention should be made to measure the ventricular dimensions perpendicular to the ventricular walls as it is possible to overestimate the chamber dimensions when the ventricle is measured obliquely. In the author's experience, this oblique measurement is the single, most common etiology of false diagnoses of dilated cardiomyopathy (Fig. 20.29).

Patients with both coronary heart failure and dilated cardiomyopathy may present with similar symptoms of heart failure. It is obviously crucial to separate the two conditions as treatment is very different. This is difficult to achieve with echocardiography alone. There are however some clues that when present, could help to make a differential diagnosis. Typically, patients with coronary heart failure have dilated ventricles with regional wall motion abnormalities as opposed to DCM where the dilatation and the ventricular dysfunction

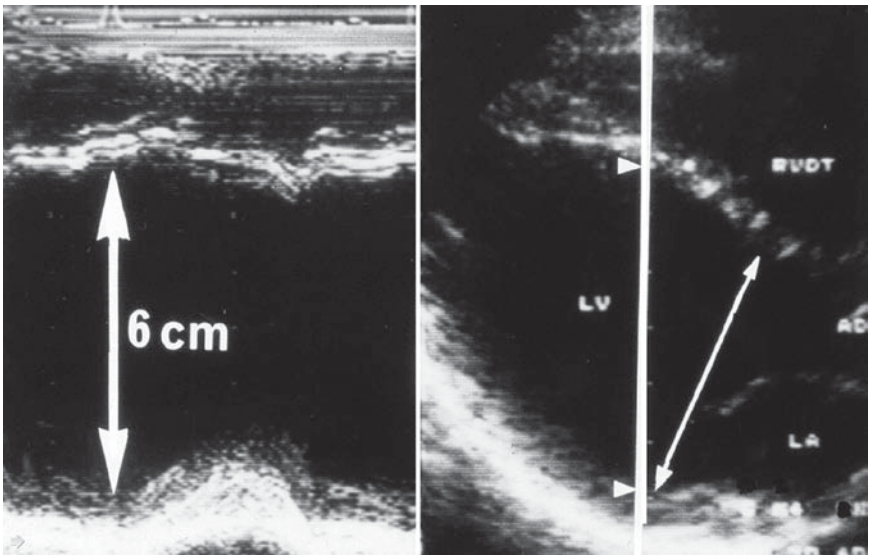

Fig. 20.29 Parasternal long-axis projection from a normal individual who was misdiagnosed as having dilated cardiomyopathy because of the oblique M-mode measurements of the ventricular cavity. Note that when the ventricle was measured perpendicularly, the size and function was normal

are more global. If there is an apical aneurysm this may be easily identified and suggest the diagnosis of coronary artery disease. Often, however, this is not the case. The right ventricle is not often involved in coronary artery disease, while in DCM it is frequently affected. Occasionally, the myocardium may be thin and echogenic in case of an old myocardial infarction which will imply scar tissue. Coronary artery disease patients tend to be older than 40 years of age while DCM patients are younger. Several studies however stressed the difficulties in ruling out an ischemic etiology when a dilated, globally hypokinetic LV has been identified.

Doppler Echocardiography

Mitral Regurgitation

The role of Doppler echocardiography is also very important. Left ventricular dilatation will lead to mitral annular enlargement, which will cause the mitral leaflets not to appose properly and consequently lead to functional mitral regurgitation. This can be visualized with color Doppler and quantified as necessary. While in some occasions the causal link between mitral regurgitation and dilated ventricle may be difficult to establish, the association of a globally hypokinetic LV with mitral regurgitation points to primary myocardial disease. Rarely is the mitral regurgitation severe in dilated cardiomyopathies and when this happens then it is more difficult to rule out mitral regurgitation as the prime culprit of LV dysfunction. When the mitral valve however is entirely structurally normal with normal leaflet texture and no prolapse, this should point out to a myocardial disease (or indeed ischemic) as the cause of mitral regurgitation.

Estimate of LV Pressures

With the use of continuous-wave Doppler, an estimate of intraventricular pressures could be ascertained and in particular the right ventricular pressures. In the presence of mild tricuspid regurgitation, the maximal velocity gradient will correspond to the pressure gradient between RV and RA. Adding the level of the jugular venous pressure to the pressure gradient would give us an estimate of RV pressure. When the JVP is not visible, then arbitrarily we add 10 mmHg to the pressure gradient assuming that this reflects the normal RA pressure.

With pulsed-wave Doppler the assessment of diastolic LV function can be ascertained and an estimation of LV filling pressures can be performed. As in patients with hypertrophic cardiomyopathy, transmitral velocities profiles may be used to obtain longitudinal follow-up data on disease progression. The mitral inflow velocity signals accurately reflect pressure differences between the left atrium and left ventricle. Abnormally

slow LV relaxation, with low LA pressure, gives rise to a pattern of slow acceleration of mitral flow in early diastole (E wave) with concomitant and probably compensatory increase in flow velocity with atrial contraction (A wave). At the opposite end of the spectrum are patients with stiff LV giving rise to a very high early velocity (E wave) across the mitral valve with rapid equalization of atrial and ventricular pressures, which represent the dip-and-plateau pressure contour at cardiac catheterization. This pattern usually is accompanied by a diminutive A wave during atrial filling. Between these two ends of the spectrum is the normal filling pattern with the early filling velocity somewhat larger than the atrial flow velocity.

Intracardiac Flow and Risk o.f Embolization

The reduced systolic ventricular function and chamber dilatation produce a fairly characteristic intracavitary flow pattern, commonly seen in patients with dilated, poorly contracting ventricles. Swirling of the intracardiac flow can often be spontaneously visualized at the cardiac apex reflecting the high intracavitary filling pressures and the decreased flow velocity profile, predisposing factors for thrombus formation. With color-flow imaging the pattern of intraventricular flow velocity profile can be characterized and predict those patients in which regional stasis occur. From apical four-chamber projections, a series of short boluses of flow can be visualized during diastole, giving the appearance of "puffs of smoke." Because of low output state, the velocity of flow is low so that the usual color-flow map of intraventricular inflow is shown by the darker shades of red. During systole, the left ventricular outflow tract will also exhibit low velocities with absence of aliasing indicative of low output.

Ventricular dilatation with diffuse hypokinesia in patients with dilated cardiomyopathy, together with the low intraventricular velocities, constitutes a major risk for the development of intraventricular thrombi with the risk of systemic embolization. Echocardiography can readily identify the presence of an intraventricular thrombus and lead to prompt anticoagulant treatment. Thrombi are usually attached at the apex (Fig. 20.30) and may be laminar or protruding with a narrow point of attachment on the endocardial surface.

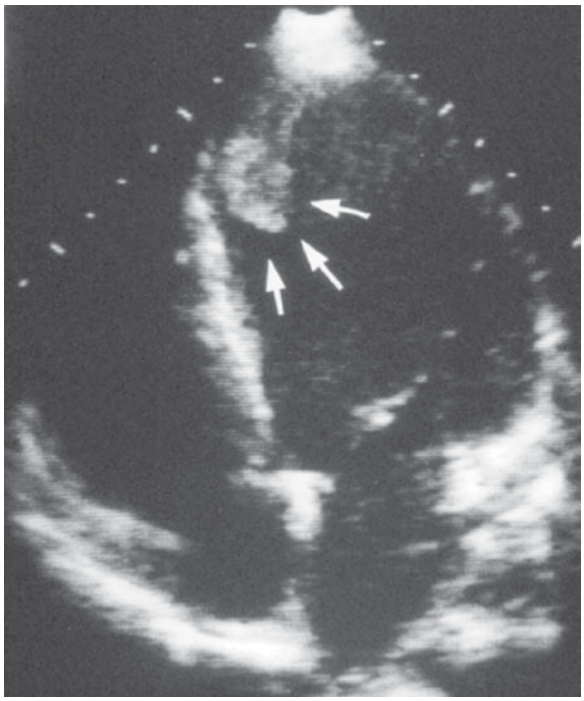

Fig. 20.30 Apical four-chamber view from a patient with dilated cardiomyopathy. Note the presence of an apical thrombus. The patient was not receiving anticoagulation

Tissue Doppler Imaging

Tissue Doppler may be used to detect regional or global myocardial dysfunction, particularly in patients with normal chamber dimensions. One particular application is in patients who have been identified suffering from a genetic condition, which may lead to left ventricular dysfunction and dilatation such as patients with Duchenne muscular dystrophy in whom it might be useful to detect early left ventricular dysfunction, prior to any clinical manifestation of heart failure. This may have therapeutic implications such that an early treatment might prevent left ventricular remodeling.

Tissue Doppler may be used by measuring mitral annular velocities as well as myocardial velocity gradients or left ventricular strain and strain rate. Mean tissue Doppler velocities and radial strain rate of the LV posterior wall at peak systole and early diastole may be reduced while conventional echocardiography may be normal.

The early diastolic mitral annular velocity (Em) is a good indicator of diastolic function.

At ≥10 cm/s, diastolic function is usually normal, but at ≤8 cm/s it will imply diastolic dysfunction.

Perhaps a more precise way to establish early ventricular dysfunction and predict elevation of LV filling pressures is by using the ratio of early transmitral diastolic velocity (E wave) over the early mitral annular velocity (Em).
A E/Em >10 will imply elevated filling pressures with high sensitivity and specificity.

Family Screening

Family screening is important and echocardiography is ideally suited for this. Large series of asymptomatic relatives have shown that 29% had abnormal echocardiograms. Among affected relatives, symptoms can be quite variable. The majority of affected relatives may be asymptomatic and cannot be identified by relying on history alone. Echocardiography therefore plays an important role for the early recognition of affected family members, which may promote the early institution of treatment in an attempt to prevent ventricular remodeling.

Myocarditis

Myocarditis is strongly suspected when a patient, previously normal, is suddenly in congestive cardiac failure, often as a result of a flu-like illness. Following standardization of the histopathological diagnosis of myocarditis by the Dallas criteria,[12] evidence of myocarditis in dilated cardiomyopathy varies between 18 and 55%. The therapeutic implications however are limited as the mere presence of inflammatory infiltrates does not necessarily signify active myocarditis. The possible link between viral infection and dilated cardiomyopathy has not yet affected the routine management of these patients. Steroid therapy has proven to be of no benefit when routinely administered to patients with dilated cardiomyopathy.

Echocardiographically, myocarditis is suspected when a patient is acutely ill and echocardiography demonstrated a nondilated LV with global hypokinesia. Often, however, there is only regional ventricular dysfunction involving the septum or even the right ventricle, which may be more difficult to detect. When this regional ventricular dysfunction is present, it is difficult to rule out an acute coronary syndrome. The patient's age and the clinical picture however should make the differential diagnosis.

Cardiac Toxins

A variety of substances can affect the heart leading to dilated cardiomyopathy. Perhaps the commonest toxin is alcohol. Macrocytosis is a useful indicator of chronically high alcohol consumption even in the absence of abnormal liver function. A raised gamma-glutamyltransferase (gamma-GT) may be an indicator of only recent rather than long-term alcohol intake, whereas raised levels of other liver enzymes may be due to a chronic alcohol hepatitis.

There is an individual susceptibility to the adverse effects of alcohol on the myocardium, which may well be genetically predisposed. The heart is typically markedly dilated with global ventricular dysfunction, but it may show dramatic improvement after a patient has stopped drinking. Figure 20.31 is from a patient with alcohol-induced dilated cardiomyopathy.

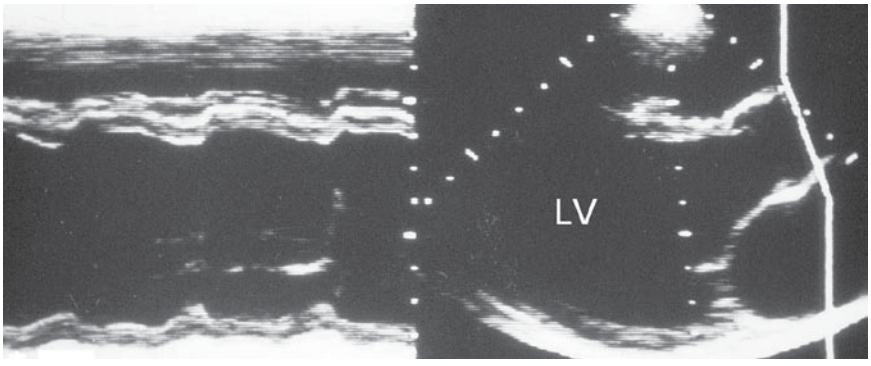

Fig. 20.31 M-mode echocardiogram (*left*) and parasternal long-axis view from a patient with marked alcohol consumption and heart failure. The echocardiographic pattern is that of dilated cardiomyopathy with reduced contraction

The heart is markedly dilated and shows diffuse hypokinesia as demonstrated by the simultaneous M-mode echocardiogram.

Anthracyclines given as doxorubicin have important toxic subcellular effects that can eventually lead to intracellular calcium overload and depressed cardiac function. The echocardiographic findings are again those similar to dilated cardiomyopathy with global ventricular dysfunction. As in all dilated cardiomyopathies, it is important to look for the presence in LV thrombus as those patients with dilated ventricles may be prone to thromboembolism.

Cardiomyopathy Associated with Pregnancy and Parturition

Peripartum cardiomyopathy typically occurs during the third trimester of pregnancy or during the first 6 months postpartum without obvious cause and without prior evidence of heart disease. Because it is rare, the literature is limited and filled with anecdotal cases and heterogeneous material. Heart failure with peripheral edema and ventricular dilatation may be sudden and catastrophic or more insidious. An immunological interaction between mother and fetus can be postulated. This may be responsible for "myocarditis" frequently found on biopsy with interstitial and perivascular lymphocytic infiltration in the presence of myocyte necrosis with or without fibrosis.

The echocardiographic findings are usually those of a nondilated left ventricle with global hypokinesia (increased end-systolic dimensions) similar to myocarditis (Fig. 20.32). Occasionally, the differential diagnosis with viral myocarditis is difficult and should rely mainly on clinical grounds. It is important to look for LV thrombus as this will carry a high risk for embolization and anticoagulation may be needed. When LV dysfunction is discovered in the context of arrhythmias and congestive cardiac failure during the third trimester or immediately post delivery, the diagnosis is straightforward. Careful follow-up is mandatory as the disease can deteriorate rapidly with ventricular dilatation and further ventricular dysfunction or can improve from severe hypokinesia to mild ventricular dysfunction and reduced ventricular size to complete recovery.

Typically, peripartum cardiomyopathy can evolve in three ways of approximately equal thirds: 30% of patients may return to normal in up to a year post delivery, 30% may deteriorate and evolve into dilated cardiomyopathy, and 30% may remain unchanged. The remaining 10% of patients may be in any intermediate stage. Persisting cardiomegaly at 6 months is usually associated with high mortality, and the women may be candidates for cardiac transplantation.

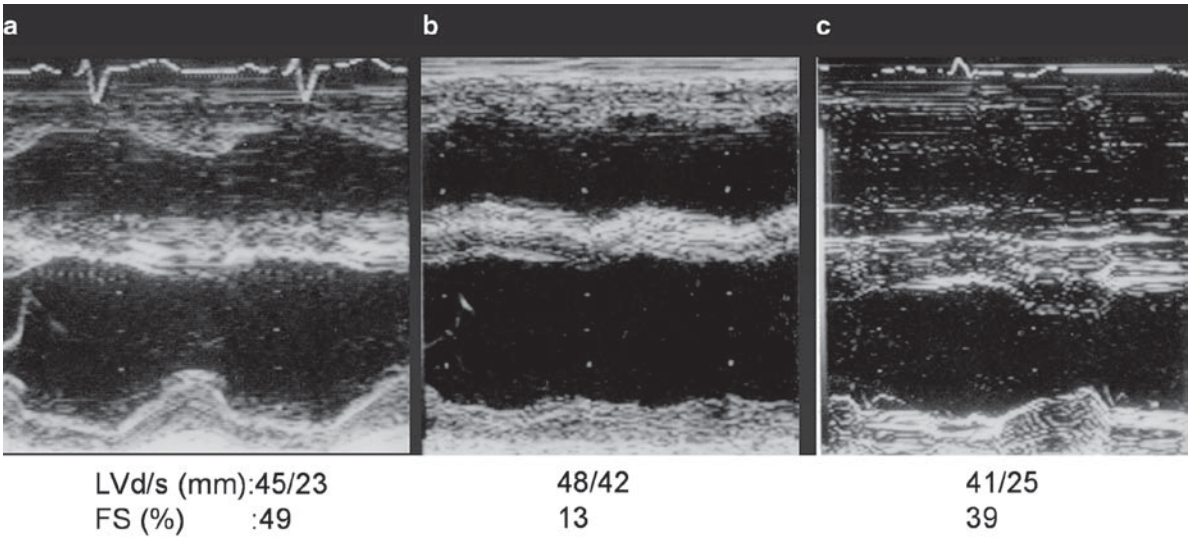

Fig. 20.32 Serial M-mode tracing from a patient with peripartum cardiomyopathy. (**a**) Before pregnancy, (**b**) three days after delivery of a healthy baby, and (**c**) one year later. At (**b**), the patient was extremely ill and was considered for cardiac transplantation. At (**c**) The patient had completely recovered

Isolated Left Ventricular Noncompaction

This is a rather recent description of a new form of cardiomyopathy. Its existence is still debated as to whether or not this is a true cardiomyopathy. It was described approximately a decade ago in patients presenting with symptoms of heart failure. It is characterized by prominent myocardial trabeculations with deep intertrabecular recesses which lie in continuity with the left ventricular cavity.

During early embryogenesis ventricular trabeculations develop in the distal left ventricle soon after looping and serves primarily as a means to increase myocardial oxygenation in the absence of effective coronary circulation. At the same time when ventricular septation occurs, the trabeculae start to condense (compact) in their portions adjacent to the outer myocardium adding to its overall ventricular thickness. At *6 weeks* of pregnancy, there are abandoned fine trabeculae that may be present. At *12 weeks*, the trabeculae begin to solidify at a time when ventricular septation is completed. In the early fetal period the compact layer forms most of the myocardial mass. Failure for the left ventricle to condense (become compacted) may result to the isolated left ventricular noncompaction.

The precise etiology for this remains unknown but it would appear that this is a nonspecific condition and can be presented in families with various forms of X-linked dilated cardiomyopathies but also associated with conditions that generate ventricular pressure overload. Whether or not isolated left ventricular noncompaction represents a distinct cardiomyopathy remains a matter of debate. As genetic evidence emerges, it appears that this is a heterogeneous and nonspecific disorder that may be associated with a variety of conditions such as dilated cardiomyopathies or hypertensive heart disease. Clinical presentation is often heart failure but also arrhythmia and thromboembolic events. Isolated left ventricular noncompaction may be presented in neonates and children, but also in young adults. It is rarely seen in mid or advanced ages.

The diagnosis is made by echocardiography in the vast majority of patients by the combination of the clinical picture of breathlessness or palpitations and the echocardiographic appearance of coarsely trabeculated left ventricle, often distally, presenting with a degree of subendocardial recesses (Fig. 20.33). The affected ventricle may present with two layers: a compact (solid) epicardial layer and an endocardial layer consisting of prominent trabecular meshwork and deep intertrabecular spaces/recesses. This is best visualized in apical four-chamber projections and parasternal short-axis views.

Accurate diagnosis is important as its clinical morbidity includes heart failure caused by progressive left ventricular dysfunction, arrhythmias, and systemic or pulmonary embolism.

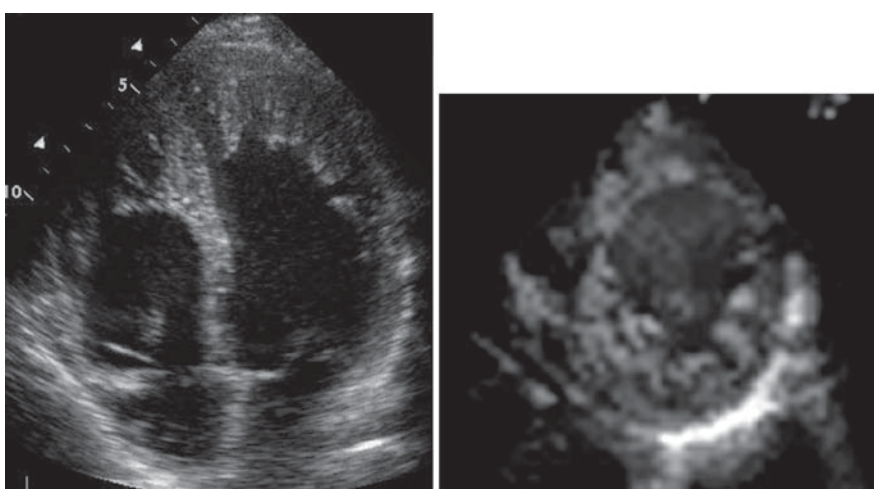

Fig. 20.33 Isolated left ventricular noncompaction. On the *left*, apical four-chamber view showing the unusually coarsely trabeculated LV. On the *right*, parasternal short-axis from the same patient clearly demonstrating the deep recesses seen at the apex. We are grateful to Dr. Perry Elliot for providing this picture

Restrictive Cardiomyopathy

Restrictive cardiomyopathy is the least common type of cardiomyopathy without uniformly accepted diagnostic criteria. Its classic anatomical features are those of a small left ventricle (not dilated) with marked atrial dilatation and normal systolic contraction, in the absence of pericardial disease. The typical pathophysiological features include normal systolic contraction with abnormal ventricular filling leading to rapid completion of LV filling with little or no late ventricular filling. This filling pattern represents the cornerstone of the diagnosis, often corresponds to the dip-and-plateau contour of early diastolic pressure.

Types of Restrictive Cardiomyopathies

The purest form of this category is the idiopathic restrictive cardiomyopathy in which the defined hemodynamic abnormalities occur without specific histological changes. Restrictive hemodynamics have been described in many additional conditions that affect the heart, giving rise to several disease entities that are grouped under the general title of restrictive cardiomyopathies. The archetype of these diseases is amyloid infiltration of the heart. While this is strictly speaking an infiltrative systemic disease that can also infiltrate the heart leading to increased myocardial stiffness and restricting filling, another type of restrictive cardiomyopathy is the eosinophilic endomyocardial disease. The fact that an etiologic factor and a specific pathological process have been documented in both cardiac amyloidosis and endomyocardial disease make their inclusion among primary cardiomyopathies controversial.

Cardiac Amyloidosis

The diagnostic criteria of restrictive cardiomyopathy depend a lot upon the underlying condition. In cardiac amyloidosis, interstitial infiltration of the atria and ventricles lends the cardiac chambers a firm rubbery consistency.

Systemic amyloidosis is a disorder of protein metabolism in which characteristic abnormal extracellular protein material is deposited in organs and tissues. It causes considerable morbidity and is usually fatal. The heart is often involved in light chain amyloid and congestive heart failure is one of the dominant clinical manifestations (Fig. 20.34). The advent of modern echocardiography has greatly contributed to the ante mortem recognition of amyloid infiltration of the heart.

Not every form of amyloidosis involves the heart. AL amyloidosis involves the heart in 90% of the cases and commonly presents as heart failure, while AA amyloidosis (reactive) only rarely affects the heart and when it does, it causes less functional impairment than in AL amyloidosis. Amyloid deposition begins in focal subendocardial accumulations and within the myocardium between the muscle fibers. Expansion of these myocardial deposits eventually causes pressure atrophy and separation of myocardial fibers. This mechanism is responsible for the marked thickening of the left and right ventricular walls, normal or decreased LV cavity size, reduced LV diastolic and systolic function. The walls of intramural coronary arteries as well as the conductive system are infiltrated, and this accounts for the electrocardiographic abnormalities seen in some patients. The endocardium is also involved and may be associated with overlying thrombus. It also causes focal or diffuse valvular thickening but clinical valvular dysfunction is uncommon. Finally, the small amyloid heart may be surrounded by a large pericardial effusion.

The echocardiographic findings suggestive of amyloid infiltration of the heart, which although nonspecific when taken individually, are highly suggestive in

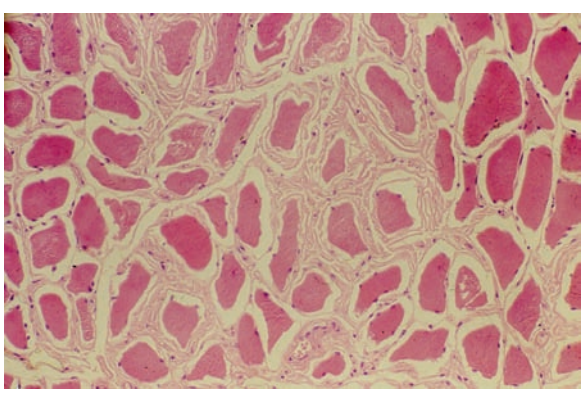

Fig. 20.34 Amyloid deposition among normal myocytes. Note that the myocardial fibers (here cut cross-sectionally) are normally arranged. The amyloid protein is infiltrated in the interstitial tissue among myocytes

combination, consisting of thickened RV and LV walls with granular sparkling (ground glass appearance), normal or small LV cavity, and enlarged atria (Fig. 20.35). Depressed myocardial contraction and relaxation is also characteristic of amyloid heart disease, and this finding may greatly facilitate the differential diagnosis with hypertrophic cardiomyopathy (Fig. 20.36). Figure 20.37 is from a patient with AL amyloidosis with marked wall thickening and an abnormal diastolic function. Note that the transmitral velocities exhibit a "restrictive filling pattern" with absent late diastolic filling suggestive of elevated filling pressures. Involvement of the heart valves and atrial septum which appear homogeneously thickened without altering the valves motion may also be present.

Eosinophilic Endomyocardial Disease

The diastolic filling abnormality in endomyocardial disease appears to be related to the presence of a thick endocardial fibrotic shell with finger-like penetrations into the myocardium. This develops through a well-defined pathological process after initial damage induced by toxic eosinophils. As in the case of cardiac amyloidosis, the fact that both have an etiologic factor and that a specific pathological process has been documented makes controversial their inclusion among primary cardiomyopathies.

Definitions: The definition of hypereosinophilic syndrome is when the eosinophilic count is greater than 1.5

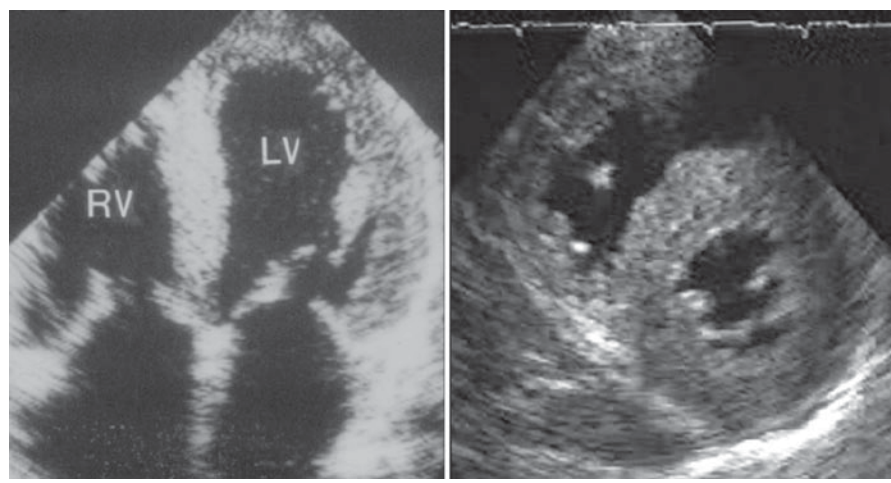

Fig. 20.35 Systemic amyloidosis. Apical four-chamber view (*left*) and short-axis (*right*) demonstrating marked wall thickness (15 mm) concentrically. Note the homogeneous texture of both ventricles and the thickening of the mitral and tricuspid leaflets. The right ventricle is also thickened

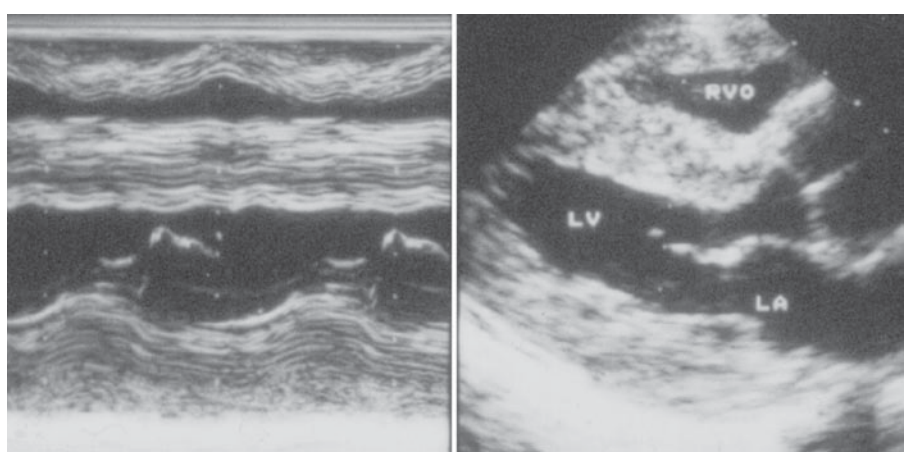

Fig. 20.36 Parasternal long axis from a patient with cardiac amyloidosis with the corresponding M-mode echocardiogram to demonstrate the reduced left ventricular function. Note again the markedly thickened RV free wall

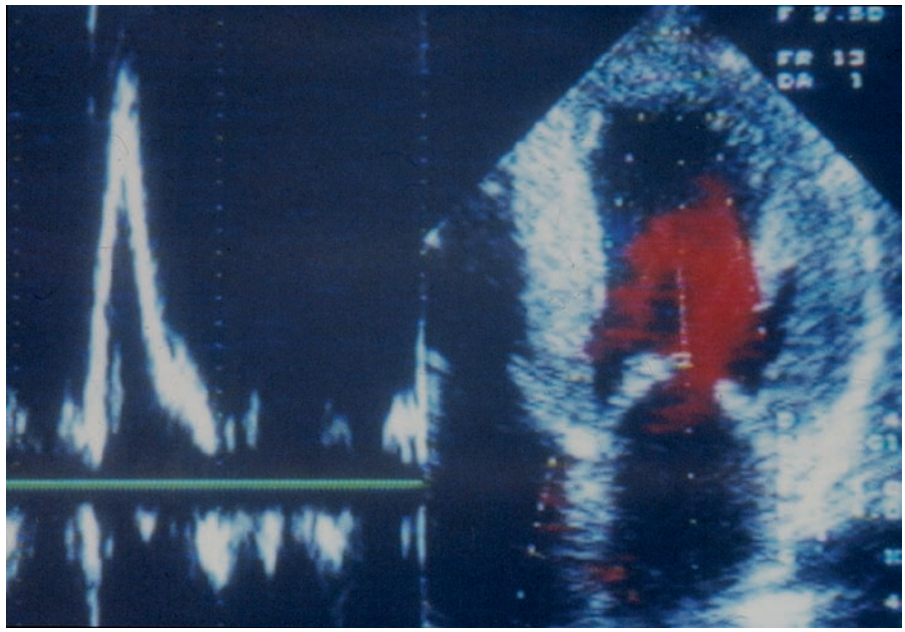

Fig. 20.37 Amyloid heart disease. Pulsed-wave Doppler from the mitral valve demonstrating a "restrictive pattern" with absent late diastolic filling of the transmitral velocity suggesting of markedly impaired left ventricular diastolic function with elevated filling pressures

× 10^9/l in the peripheral blood. There are two types of hypereosinophilic syndrome. The commonest is the secondary hypereosinophilia which occurs as the result of certain tumors, lymphoma, vasculitis or parasitic or infectious disease, as well as the hypereosinophilia that follows hypersensitivity reaction. The more rare form is the primary hypereosinophilic syndrome, which occurs with no apparent cause and has been described by Loffler in 1936. In certain African countries or the tropics hypereosinophilia is common leading to endomyocardial fibrosis, but this may be the result of parasitic infestation. In most European patients, there is no serological evidence for parasites, allergies, or inflammatory disease and the disease is clearly idiopathic.

Pathophysiology: Eosinophiles can damage the heart and induce endomyocardial disease. The pathogenesis follows the progressive degranulation of eosinophiles with granule dissolution and secretion of toxic products causing endomyocardial cell injury and fibrosis. Subsequently, there is thrombus formation and restricted LV and RV filling. It affects usually young men and can affect all organs, including the heart, lungs, nervous system leading to neurological deficits.

Echocardiography: The echocardiographic characteristics of hypereosinophilic syndrome are typical and pathognomonic. There is extensive LV and RV thrombus usually packing the ventricular apices (Fig. 20.38).

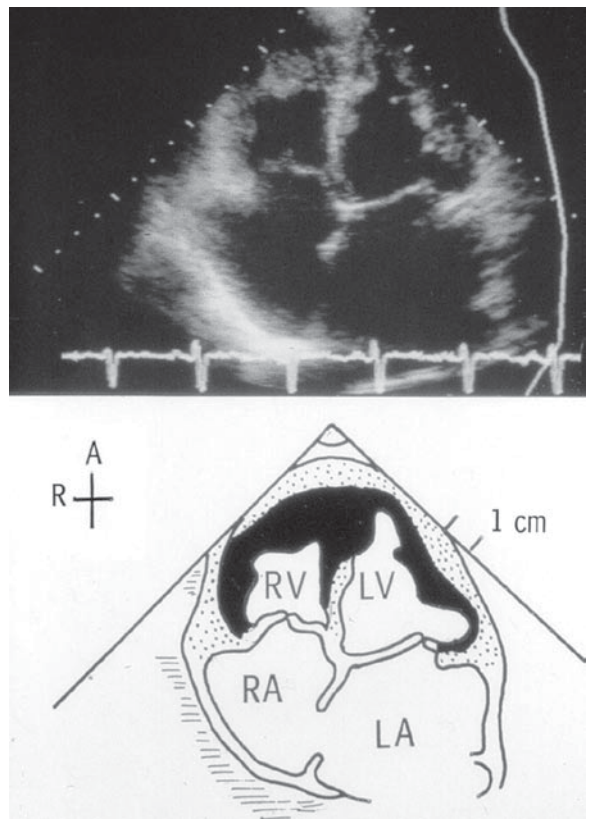

Fig. 20.38 Apical four-chamber view from a patient with endomyocardial fibrosis. Note the packing of the left and right ventricular apex and the marked dilatation of the atria

This is frequently called the "box-glove" sign because of the left ventricular resemblance of a box glove. The ventricular systolic function is usually preserved, but there is restriction to ventricular filling manifested by an early diastolic halt on the M-mode echocardiogram (Fig. 20.39). With high-resolution two-dimensional echocardiography, a distinct high intensity linear echo is identified covering the endocardial surface of the left and the right ventricles. This localized echo-dense area corresponds to areas of fibrosis extending from the apex to the basis of the ventricles and the papillary muscles (Fig. 20.40a). Cardiac Magnetic resonance imaging can also demonstrate the presence of intraventricular thrombus as well as the amount and extent of endocardial fibrosis (Fig. 20.40b). Often this material extends to the ventricular inflow track and involves the mitral or tricuspid chords and leaflets leading to significant valvular regurgitation (Fig. 20.41). Biatrial enlargement is also found in the majority of these patients as a result

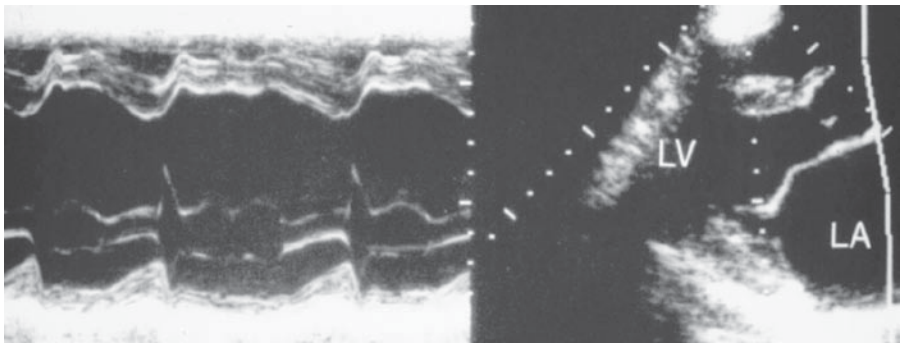

Fig. 20.39 M-mode and two-dimensional echocardiography from the same patient with endomyocardial fibrosis as in Fig. 20.38 demonstrating the abnormal diastolic left ventricular filling. During diastole, the left ventricle fills rapidly in early diastole and then remains unchanged during the rest of diastole. Note that the systolic function is preserved

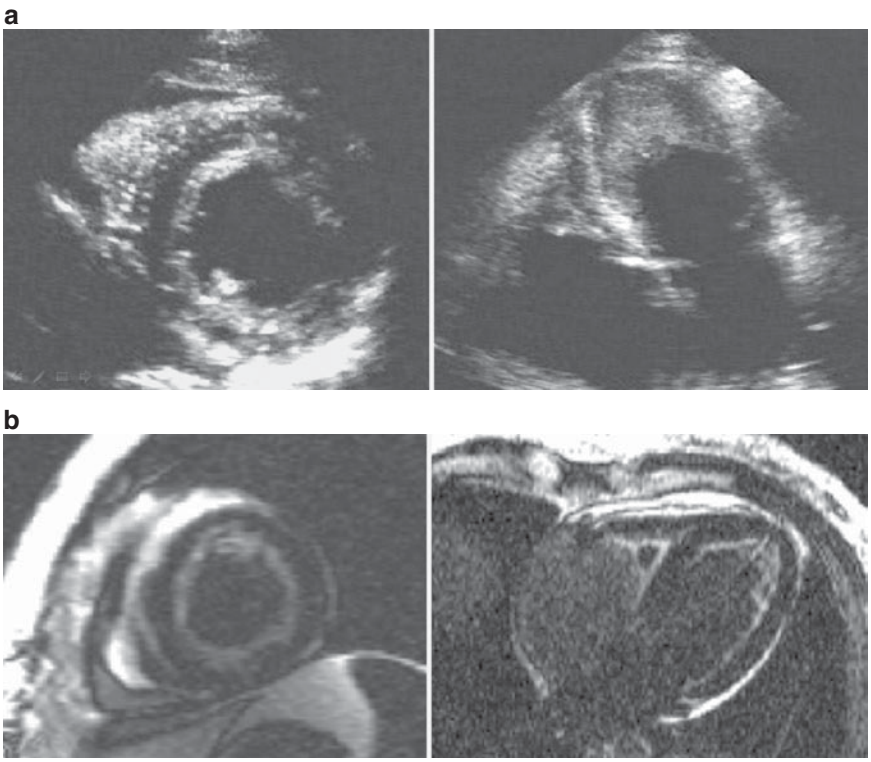

Fig. 20.40 (**a**) Parasternal short-axis (*left*) and four-chamber (*right*) views from a patient with hypereosinophilic syndrome. Notice the bright endocardial echoes surrounding the cavity suggestive of fibrosis. In the apical four-chamber view, a typical "boxing-glove" appearance of the left ventricle with the apical thrombus packing the apex of both the left and the right ventricles. (**b**) Cardiac magnetic resonance imaging with corresponding images from the same patient as in Fig. 20.33a showing again the extent of endocardial fibrosis (short axis and four chamber)

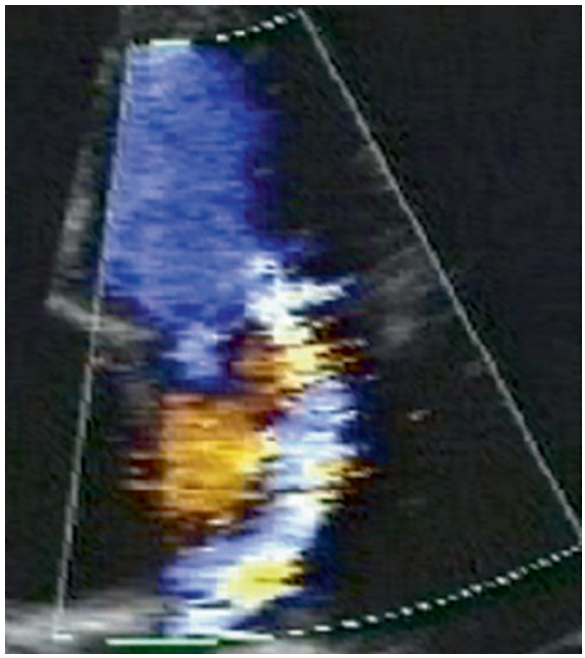

Fig. 20.41 Color Doppler imaging from the same patient as in Fig. 20.37 showing the extent of mitral regurgitation. Calculated regurgitant volume 35 ml (moderate)

of the restrictive ventricular filling imposed by the noncompliant ventricle. The extent of valvular involvement however can better be appreciated with echocardiography.

Idiopathic (Primary) Restrictive Cardiomyopathy

Using strict hemodynamic criteria the diagnosis of restrictive cardiomyopathy is supported by the absence of specific pathology on either endomyocardial biopsies or evaluation of whole heart specimens. Patients are typically in class III or IV of the NYHA classification for heart failure, the atria are usually disproportionate dilatated compared to the normal or near-normal ventricular size, the left ventricle has normal or near-normal contractility in the absence of hypertrophy. Histology is normally nondistinctive and can show normal findings or nonspecific degenerative changes, including myocyte hypertrophy and mild to severe interstitial fibrosis. Some myocardial disarray can also be present and when this occurs, some form of hypertrophic cardiomyopathy needs to be considered. Again, the role of genetic testing is of paramount importance.[6]

Restrictive Physiology

Increased ventricular filling pressures with the typical dip-and-plateau pattern are the hemodynamic hallmarks of restrictive cardiomyopathies, whatever the etiology. Atrial pressures usually exceed 15 mmHg, right atrial pressure is required to be more than 7 mmHg, and pulmonary capillary wedge pressure is required to be more than 12 mmHg.[13] In contrast with the equal left- and right-sided diastolic pressures in constrictive pericarditis, diastolic pressures are separable by more than 5 mmHg in restrictive cardiomyopathy due to unequal involvement and compliance of the two ventricles. However, this separation is not seen at baseline in restrictive cardiomyopathy, and it is often not demonstrable despite provocative tests such as volume loading, leg rising, exercise, or pharmacological interventions. Even the dip-and-plateau may be absent in restrictive cardiomyopathies.

Patients with restrictive cardiomyopathy either due to cardiac amyloidosis or endomyocardial fibrosis show ventricular filling abnormalities along the spectrum from a more advanced traditional restrictive pattern to a milder abnormal relaxation with long isovolumic relaxation time (IVRT), reduced rate of acceleration to the low early peak velocity (E wave), slow deceleration rate, and relatively high atrial wave.

Distinction Between Restrictive Cardiomyopathy and Constrictive Pericarditis

Restrictive cardiomyopathy presents a clinical and hemodynamic picture that is usually indistinguishable from constrictive pericarditis. The differential diagnosis is crucial as constrictive pericarditis is curable, whereas restrictive cardiomyopathy is not. Endomyocardial biopsy is useful in revealing the presence of myocardial disease. In addition to echocardiography, computed tomography and cardiac magnetic resonance imaging can be used to define pericardial thickness with or

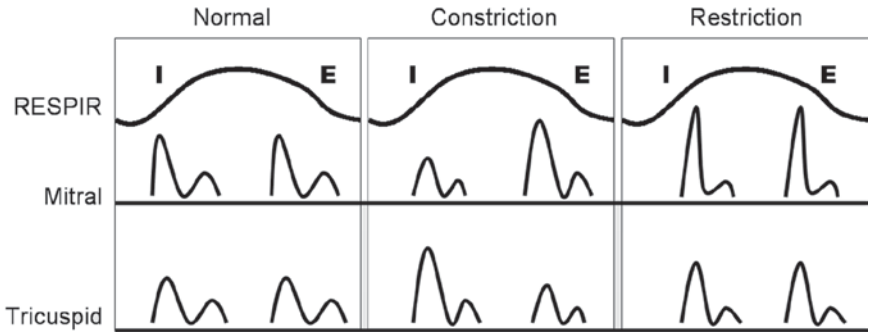

Fig. 20.42 Diagrammatic representation of the transmitral early (E wave) and late (A wave) velocities during diastole throughout the respiratory cycle. Note the dynamic differences between restrictive cardiomyopathy and constrictive pericarditis during inspiration and expiration. In constrictive pericarditis, the transmitral velocities are reduced while the tricuspid velocities are increased in deep inspiration, while the opposite happens during expiration. In restrictive cardiomyopathy there is little respiratory variation

without the presence of calcification. Most common causes of constrictive pericarditis used to be tuberculosis, followed by idiopathic (viral), and following open heart surgery, radiation therapy, and uremia. Now however the commonest cause is after open-heart surgery followed by radiation therapy and uremia, and these conditions rarely lead to calcification so that imaging techniques alone may not be sufficient to cover the entire spectrum of pericardial constriction. Consequently, when pericardial thickening is present, the diagnosis is relatively straight forward, but when this is not the case, dynamic Doppler echocardiography during the respiratory cycle will play a crucial role in the differential diagnosis.

Normally there is interdependence between the RV and LV during respiration as the pericardium transmits the intrathoracic pressures to the intrapericardial and intracardiac chambers. During inspiration, there is a drop in intrathoracic pressures which will be transmitted to the intracardiac chambers with a parallel reduction of pulmonary capillary and left ventricular diastolic pressures, keeping the transmitral and transtricuspid diastolic gradients virtually unchanged (<20%), an increase of venous return and a slight increase in RV size. In constrictive pericarditis because of the pericardial shell, the drop in intrathoracic pressures will not be transmitted to the intracardiac pressures so that the systemic venous and RA pressures do not fall during inspiration, and the transmitral gradient will be reduced as opposed to the transtricuspid gradient which will be increased. Consequently, during inspiration the transmitral velocities will be reduced (E wave) and tricuspid velocities increased (E wave) in constrictive pericarditis, while in restrictive cardiomyopathy they will remain unchanged[14] (Fig. 20.42).

Arrhythmogenic Right Ventricular Dysplasia/Cardiomyopathy

Definitions and Pathophysiology

This is a heterogeneous group of conditions characterized by right ventricular dysfunction and dilatation. While in the majority of cases the left ventricle is spared, it is also possible that this may become involved at a later stage of the disease progression. Most common presentation is patients complaining of arrhythmias, specifically with ventricular tachycardia originating from the right ventricle (LBBB morphology), which could be life threatening. Arrhythmogenic right ventricular dysplasia/cardiomyopathy (ARVD/C) is an important cause of sudden death in individuals <30 years of age and has been found in up to 20% of sudden deaths in young people.[15] ARVD/C is typically inherited as an autosomal dominant trait with variable penetrance and incomplete expression. It is characterized by adipose replacement of myocardial tissue in the right ventricular wall in a spotty or diffuse process that starts on the right ventricular subepicardium and progresses to the endocardium with fibrofatty replacement of myocytes and thinning of the wall. It affects men more frequently than women and is usually discovered between the second and fourth decades of life.

The regions of the right ventricle most frequently involved are the RV inflow area, the apex, and the infundibulum. These three areas form the "*triangle of dysplasia*." Histological diagnosis is often difficult as a small amount of fat is present in the epicardial layer and within the right ventricular myocardium in the

normal subjects and increases with the advancing age. When the left ventricle is also involved, the fibrofatty replacement can affect both the septum and left ventricular free wall.

Criteria for Diagnosis of ARVD/C

A definite diagnosis of ARVD/C requires the histological finding of transmural fibrofatty replacement of RV myocardium. Diagnosis by endomyocardial biopsy may be difficult in view of the patchy distribution of the fibrofatty replacement during the earlier stages of the disease. Because of these difficulties, a consensus group has proposed a number of major and minor diagnostic criteria,[15] Table 20.8. To qualify as ARVD/C, a patient must demonstrate either two major or one major plus two minor criteria or four minor criteria. Of the major criteria, the global or regional right ventricular dysfunction can best be appreciated by comprehensive echocardiography. Cardiac magnetic resonance imaging may be useful in characterizing myocardial tissue. More specifically, it may detect abnormal areas of fibrofatty replacement. The remaining diagnostic criteria are based on the electrical characteristics and depolarization/conduction abnormalities of these patients.

Table 20.8 Criteria for diagnosis of ARVC

1. Global or regional dysfunction and structural alterations

Major

(a) Severe dilatation and reduction of RV ejection fraction with no (only mild) LV impairment

(b) Localized RV aneurysms (akinetic or dyskinetic areas with diastolic bulging)

(c) Severe segmental dilatation of the RV

Minor

(a) Mild global RV dilatation or reduced ejection fraction with normal LV

(b) Mild segmental dilatation of the RV

(c) Regional RV hypokinesia

2. Tissue characterization of walls

Major

Fibrofatty replacement of myocardium on endomyocardial biopsy

3. Repolarization abnormalities

Minor

Inverted T waves in right precordial leads (V2 and V3) in 432 people aged more than 12 years in absence of RBBB)

4. Depolarization/conduction abnormalities

Major

Epsilon waves or localized prolongation (>110 ms) of the QRS complex in right precordial leads (V1–V3)

Minor

Late potentials (signal averaged ECG)

5. Arrhythmia

Minor

(a) LBBB type ventricular tachycardia (sustained and nonsustained)

(b) Frequent ventricular extrasystoles (more than 1,000/24 h) on Holter

6. Family history

Major

Familial disease confirmed at necropsy or surgery

Minor

(a) Familial history of premature sudden death (<35 years) due to suspected RV dysplasia

(b) Familial history (clinical diagnosis based on present criteria)

Echocardiographic Characteristics

Echocardiography is the diagnostic test of choice but this needs to be performed comprehensibly following standardized protocols for the detailed imaging of the right ventricle.[16] As ARVD/C affects primarily the right ventricle, it is important to perform all right ventricular views, which include the RV inflow and outflow views. The typical presentation will be that of a young patient with ventricular arrhythmias. This patient will be referred for an echocardiographic examination, which will have to be conducted in an expert department to look for subtle RV abnormalities.

The earliest abnormalities that can be detected may be focal areas of myocardial dysfunction, which may involve the RV inflow, apex and/or the RV outflow tract. These areas however may easily be missed or not interpreted as pathological as they may well be considered as normal variants of the RV function. Figure 20.43 shows a discrete aneurysm of the RV apex seen from the apical four-chamber view. Here, particular attention was made to visualize the entire right ventricle at the expense of the left, which is not always performed in routine echocardiography.

The more obvious and pathognomonic abnormalities are those of localized aneurismal regions of the *triangle of dysplasia* in the form of end-systolic bulges (Fig. 20.44). As long as the RV inflow and outflow tract projections are carefully recorded, missing those regional dyskinetic regions is difficult. It is possible that in one patient such abnormalities are seen in more than one region.

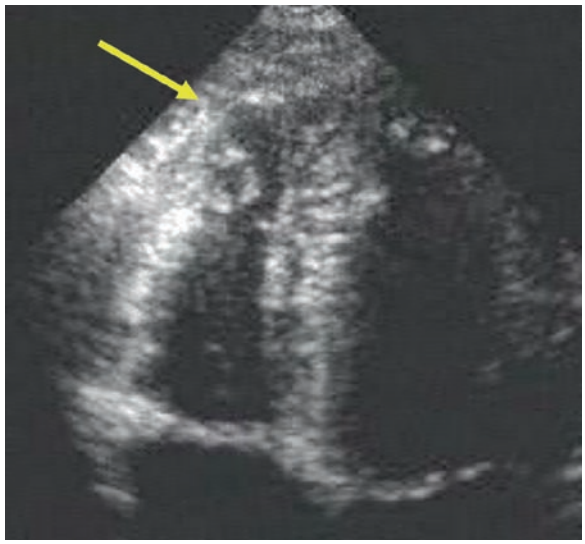

Fig. 20.43 Apical four-chamber view from a patient with ARVC. Notice that in this view, particular attention was made to visualize the entire RV. Only then, the discrete aneurysm at the apex was visualized (*arrow*)

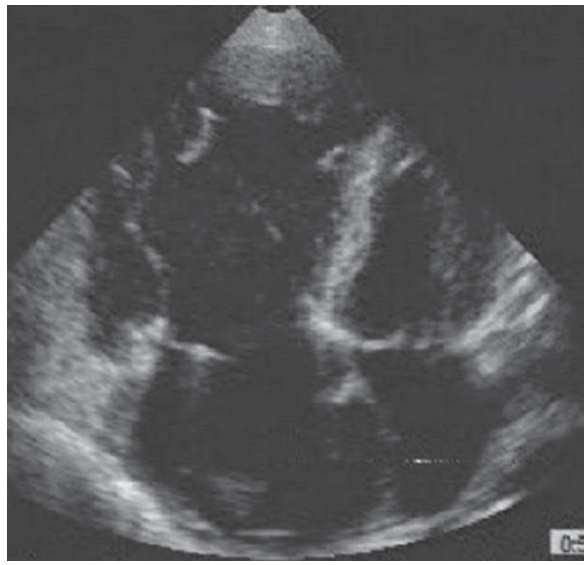

Fig. 20.45 Apical four-chamber view from a patient with a severe form of ARVC. In contrast with the patient in Fig. 20.42 where the aneurysm was very localized, here the entire RV is dilated and poorly contracting

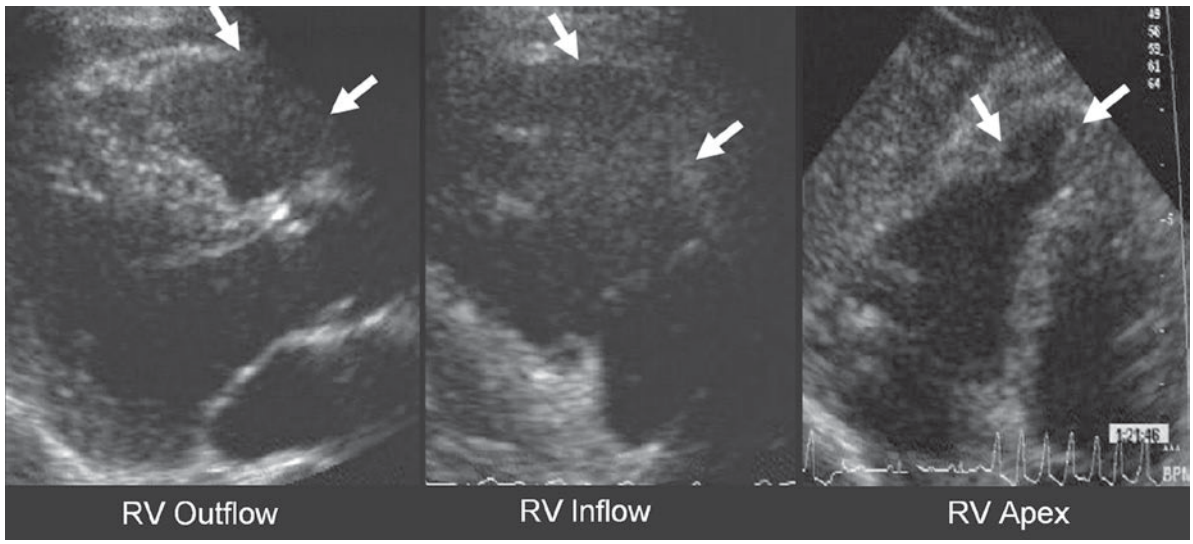

Fig. 20.44 Successive echocardiographic views from a patient with arrhythmogenic RV cardiomyopathy to illustrate the "*triangle of dysplasia*." On the *left panel*, there is a localized akinetic area in the outflow track seen from parasternal long-axis view (*arrows*). In the *middle panel*, the RV inflow track view with a localized akinetic region in the free wall (*arrows*). On the *right panel*, apical four-chamber projection demonstrating an apical aneurysm on the RV (*arrows*)

In a more advanced stage of ARVD/C, extended areas of RV free wall may become thin and akinetic which together with RV dilatation will form the typical pattern of ARVD/C (Fig. 20.45). The diagnosis here is difficult to miss. Ultimately, the whole of the RV will be dilated and hypokinetic.

Lastly, in the most severe and advanced cases, the LV will become involved and could mimic that of non-specific dilated cardiomyopathy. Global RV dysfunction is most common in patients with cardiac arrest, although this is not necessarily true in patients with first presentation. Functional and structural worsening

of RV performance may be the major risk factor for cardiac arrest in ARVD/C patients.

Conclusions

While it is convenient to classify cardiomyopathies in four major groups, there is an overlap between the anatomic and functional characteristics in many instances. As the genetic demystification of the cardiomyopathies continues, the boundaries of the various types of cardiomyopathies may better be determined. Until that time, we should continue to categorizing our patients in the four groups and echocardiography is currently the best imaging modality to do so. Cardiomyopathies have a familial nature and it is important to screen family members, as often the diagnosis may be more revealing once the family screening has been completed and again, the role of echocardiography here is pivotal. As the causes and pathophysiology of cardiomyopathies are better understood, it may be argued that in future, the term "idiopathic" may no longer be sustainable.

References

HCM

1. Goodwin JF, Oakley CM. The cardiomyopathies. *Br Heart J*. 1972;34:545.
2. Goodwin JF. The frontiers of cardiomyopathy. *Br Heart J*. 1982;48:1–18.
3. Maron BJ, Epstein SE. Hypertrophic cardiomyopathy: a discussion of the nomenclature. *Am J Cardiol.* 1979;43:1242–1244.
4 Report of the WHO/ISFC task force on the definition and classification of cardiomyopathies. Br Heart J. 1980;44:672-673.
5. Maron BJ, Roberts WC, Epstein SE. Sudden death in hypertrophic cardiomyopathy: a profile of 78 patients. *Circulation*. 1982;65:1388–1394.
6. McKenna WJ, Stewart JT, Nihoyannopoulos P, McGlnty F, Davies MJ. Hypertrophic cardiomyopathy without hypertrophy: a description of two families with premature cardiac death and myocardial disarray in the absence of increased muscle mass. *Br Heart J*. 1990;63:287–290.
7. Shapiro LM, McKenna WJ. Distribution of left ventricular hypertrophy in hypertrophic cardiomyopathy: a two-dimensional echocardiographic study. *J Am Coll Cardiol*. 1983;2:437.
8. Maron BJ, Gottdiener JS, Epstein SE. Patterns and significance of distribution of left ventricular hypertrophy in hypertrophic cardiomyopathy. A wide angle, two-dimensional echocardiographic study of 125 patients. *Am J Cardiol.* 1981;48:418–428.
9. Nihoyannopoulos P, Karatasakis G, Frenneaux M, McKenna WJ, Oakley CM. Diastolic function in hypertrophic cardiomyopathy; relation to exercise capacity. *J Am Coll Cardiol*. 1992;19:536–540.
10. Nagueh SF, Bachinski LL, Meyer D, et al. Tissue Doppler Imaging Consistently Detects Myocardial Abnormalities in Patients With Hypertrophic Cardiomyopathy and Provides a Novel Means for an Early Diagnosis Before and Independently of Hypertrophy. *Circulation*. 2001;104:128–130.
11. Palka P, et al., Differences in myocardial velocity gradient measured throughout the cardiac cycle in patients with hypertrophic cardiomyopathy, athletes and patients with left ventricular hypertrophy due to hypertension. J Am Coll Cardiol 1997; 30:760–768.

Dilated

12. Aretz HT, Billingham ME, Edwards WD, et al. Myocarditis: a histopathologic definition and classification. *Am J Cardiovasc Pathol*. 1987;1:3–14.

Restrictive

13. Shebatai R. Pathophysiology and differential diagnosis of restrictive cardiomyopathy. *Cardiovasc Clin*. 1988; 19:123–132.
14. Hatle LK, Appleton CP, Popp RL. Differentiation between constrictive pericarditis and restrictive cardiomyopathy by Doppler echocardiography. *Circulation*. 1989;79: 357–370.

ARVC

15. McKenna WJ, Thiene G, Nava A, et al. Diagnosis of arrhythmogenic right ventricular dysplasia/cardiomyopathy: task force of the working group myocardial and pericardial disease of the European Society of Cardiology and the Scientific Council on Cardiomyopathies of the International Society and Federation of Cardiology. *Br Heart J*. 1994;71:215–218.
16. Foale RA, Nihoyannopoulos P, McKenna WJ, et al. The echocardiographic measurements of the normal adult right ventricle. *Br Heart J*. 1986;56:33.

Chapter 21
Echocardiography in Heart Failure

Partho Sengupta and Bijoy K. Khandheria

Heart failure is referred to a constellation of clinical signs and symptoms that results from either an inadequate "forward" cardiac output (e.g., fatigue, cardiac cachexia, hypotension) or "backward" circulatory congestion (e.g., dyspnea, hepatomegaly, and ascites, dependent edema). It is estimated that nearly 5 million Americans suffer from heart failure, with an incidence approaching 10 per 1,000 population among persons older than 65 years of age. Heart failure accounts for nearly 20% of all hospital admissions among persons older than 65 years. The overall risk of death is approximately 5–10% per year, although an untreated patient with severe LV dysfunction has a 1-year survival of only 50%.[1,2] The term "left ventricular (LV) dysfunction" is used clinically in recognition of the fact that an abnormal myocardial function, either systolic, diastolic, or mixed, underlies the clinical syndrome of heart failure and determines the clinical pattern of presentation. Other factors playing vital roles include age, sex, underlying etiology, and the pattern of neurohormonal mechanisms that attempt to counterbalance the hemodynamic effects of a compromised heart muscle function. In absence of a reversible etiology, these homeostatic changes, however, initiate a vicious cycle in which the chamber progressively dilates, hypertrophies, and becomes spherical – a process referred to as "remodeling." Echocardiography, by virtue of its ability to provide simultaneous structural and functional assessment, plays a pivotal role for establishing the pattern and magnitude of myocardial dysfunction. Being user friendly, cost effective and readily available, its use has grown widely in recent years for risk stratification of heart failure in patients with either symptomatic or subclinical forms of left ventricular dysfunction and for serial tracking of responses following initiation of therapeutic strategies for halting or reversing cardiac remodeling.

P. Sengupta (✉) and B.K. Khandheria
Cardiovascular Division, Mayo Clinic Arizona, Scottsdale, AZ, USA
e-mail: sengupta.partho@mayo.edu

Clinical Staging and Etiology of Heart Failure: Role of Echocardiography

The current American College of Cardiology/American Heart Association (ACC/AHA) practice guidelines for CHF divides the disorder into four stages (Table 21.1), two of which (Stages A and B) are in asymptomatic individuals.[3] Echocardiography plays a key role in clinical staging of heart failure and differentiating reversible from nonreversible causes of left ventricular dysfunction. Coronary artery disease is the underlying cause of heart failure in approximately two-third of patients (Fig. 21.1). Systolic dysfunction results from myocardium that is either viable or irreversibly damaged. Identification of dysfunctional myocardium with preserved viability presents an excellent opportunity to ameliorate heart failure by revascularization. Dobutamine stress echocardiography or myocardial contrast echocardiography in such situations provides useful estimate of the extent of viable myocardial and coronary microcirculatory reserve. Similarly patients with nonischemic causes of systolic dysfunction have either an identifiable etiology (e.g., hypertension, valvular heart disease, myocardial infiltration, myocarditis, or pericardial diseases, Figs. 21.2–21.5) or may have no discernable cause (e.g., idiopathic dilated cardiomyopathy). Dobutamine stress echocardiography is also useful in these patients for identifying those who would benefit with beta blockade. Improvement in myocardial contractility with dobutamine has been

P. Nihoyannopoulos and J. Kisslo (eds.), *Echocardiography*,
DOI: 10.1007/978-1-84882-293-1_21, © Springer-Verlag London Limited 2009

Table 21.1 Stages of heart failure (ACC/AHA guidelines 2001)[3]

Stage A: Patients at a high risk for developing heart failure but has no structural disorder of the heart
Stage B: Patient with structural disorder of heart but who has never developed symptoms of heart failure
Stage C: Patient with past or current symptoms of heart failure with underlying structural heart disease
Stage D: Patient with end-stage disease requiring specialized treatment strategies as mechanical circulatory support, continuous inotropic infusions, cardiac transplantation, or hospice care

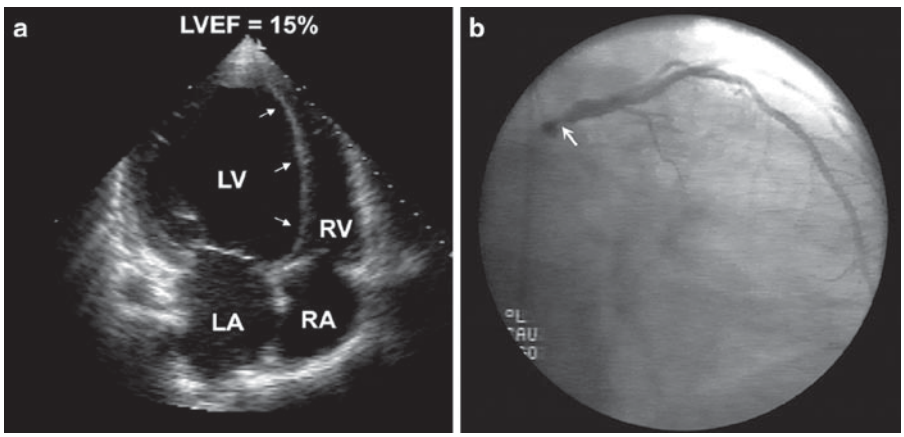

Fig. 21.1 Coronary artery disease is an underlying etiological factor in about two-third patients with heart failure. The picture shows echo in a patient with ischemic cardiomyopathy (**a**). Note the thinned out and scarred interventricular septum (*arrows*). Coronary angiogram (**b**) showed a tight stenosis of the left main coronary artery (*arrow*)

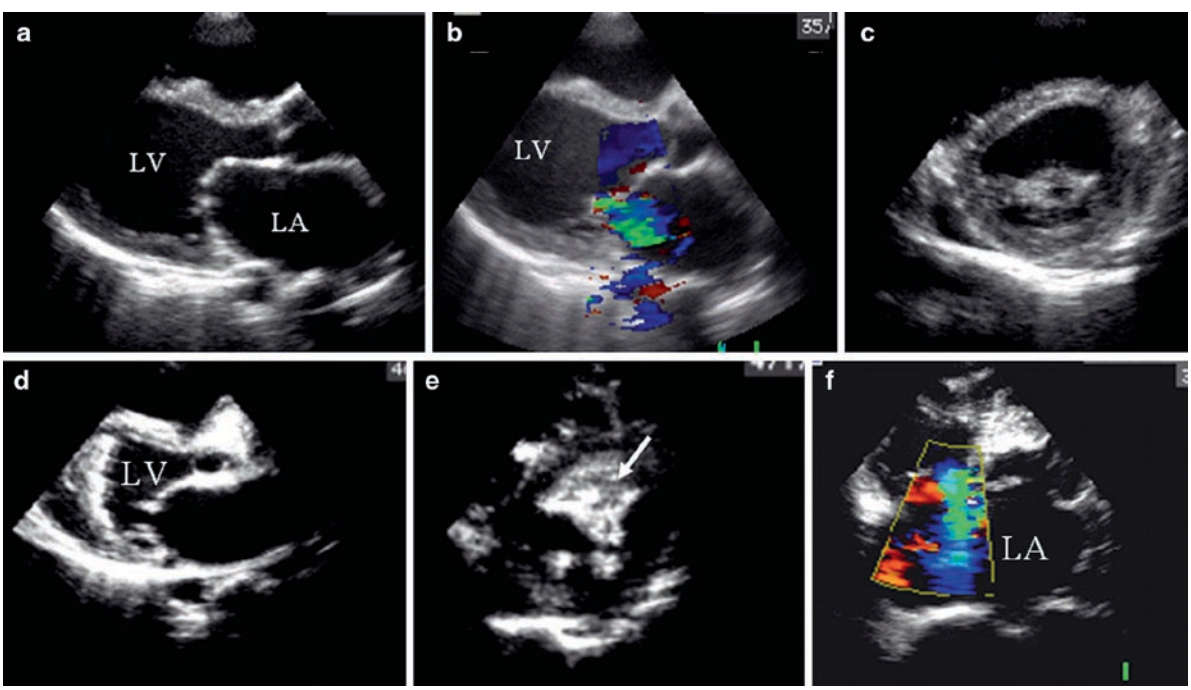

Fig. 21.2 Echocardiography is a versatile tool for identifying cardiac structural disorders in patients with heart failure. Panels (**a–c**) show echocardiographic findings in a patient with rheumatic mitral valve disease with severe left ventricular systolic dysfunction resulting from an underlying rheumatic carditis. Panels (**d–f**) show echocardiographic findings in a patient with heart failure resulting from a severe endomyocardial fibrosis. Note the obliterated left ventricular apex due to formation of mural thrombi (*arrow*; **d**, **e**) and tricuspid regurgitation due to severe pulmonary hypertension

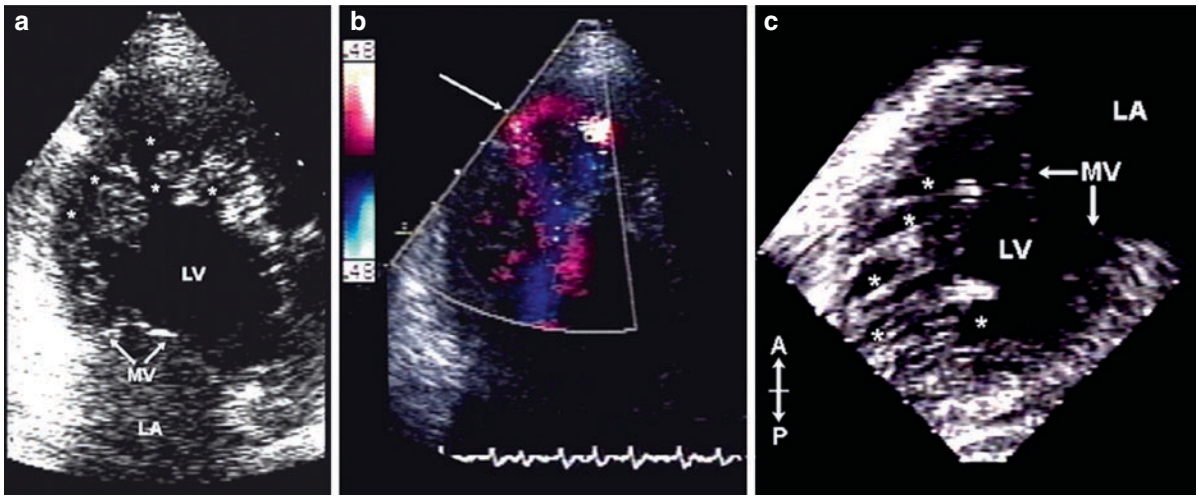

Fig. 21.3 Picture of an adult patient with noncompaction of left ventricle. Note the multiple intratrabecular sinusoids identified on transthoracic (**a**) and transesophageal echocardiography (**c**) which communicate with left ventricular cavity (free color flow, **b**). Noncompacted left ventricle is a relatively recent echocardiographic recognition of heart failure in children and adults

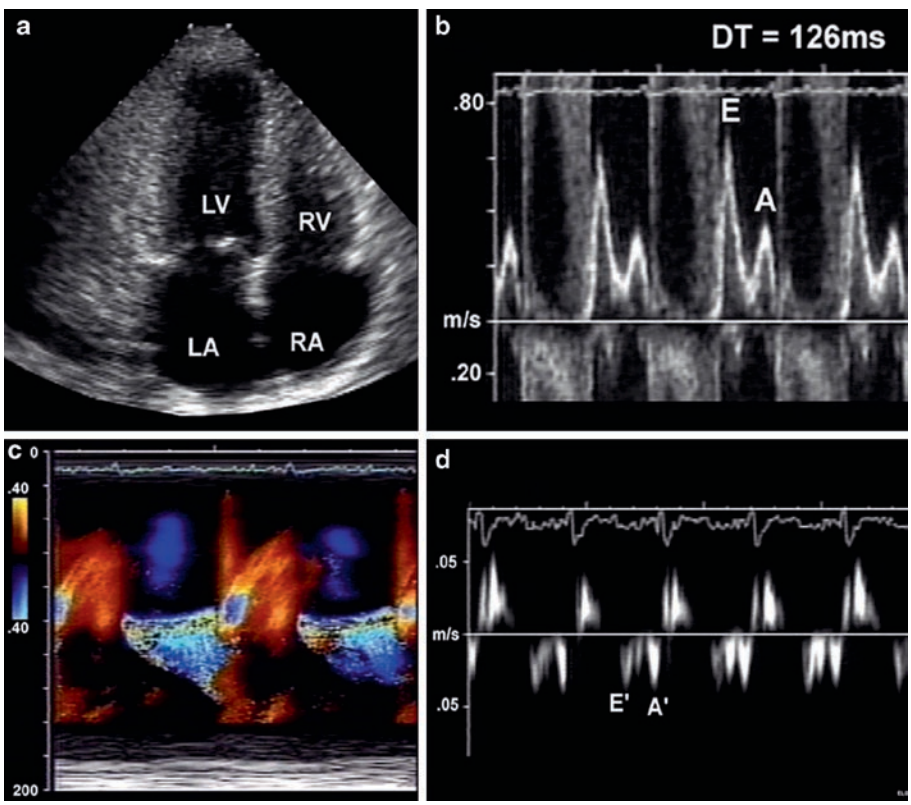

Fig. 21.4 Heart failure due to an advanced cardiac amyloid disease. Note the apical 4-chamber view with thickened myocardium (**a**). Mitral inflow velocities (**b**), Color M-mode of mitral flow (**c**), and tissue Doppler (**d**) indicate presence of a severe diastolic dysfunction (type IV)

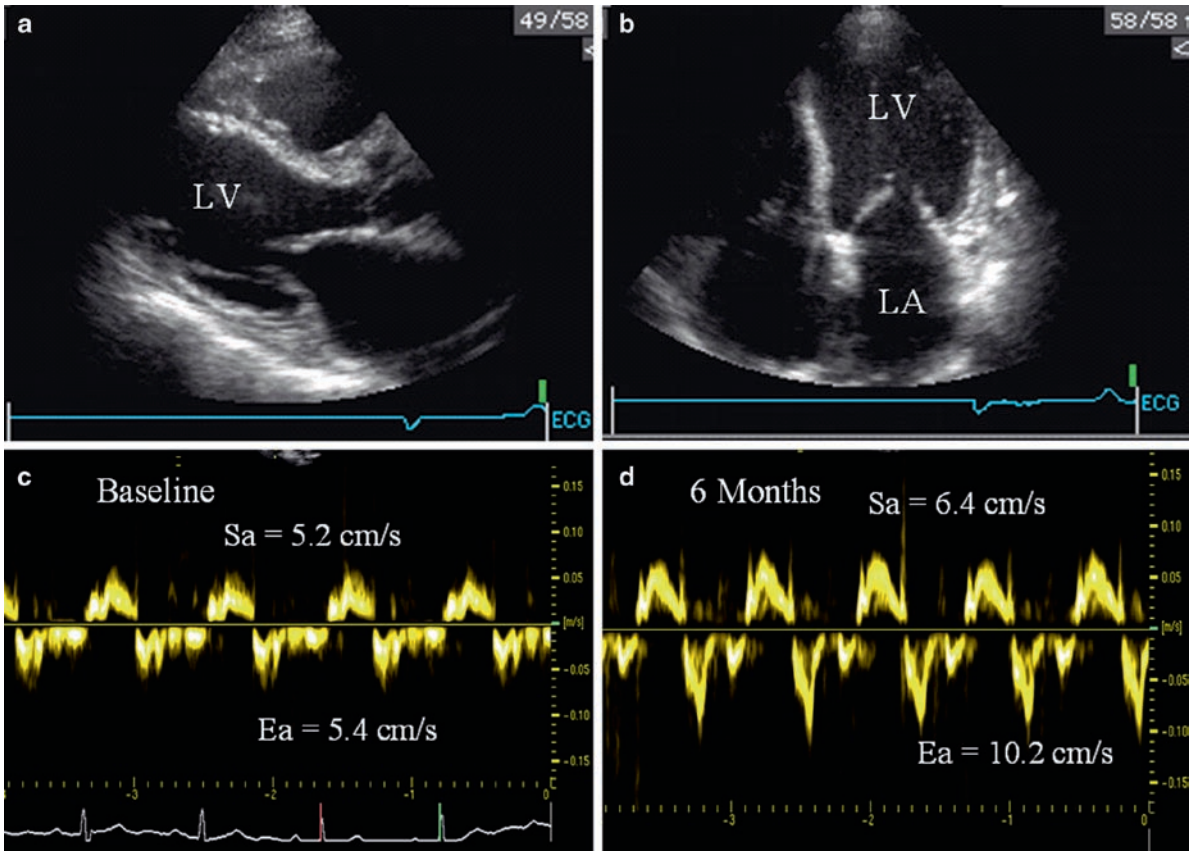

Fig. 21.5 Spontaneous improvement of left ventricular dysfunction in a patient with myocarditis. Mitral annular velocities from interventricular septum showed significant improvement within 6 months. Tissue Doppler imaging is a useful clinical technique for estimating the extent of myocardial dysfunction and its serial monitoring

shown to predict the extent of improvement in systolic ventricular function following use of beta-blockers.[4]

Quantification of Systolic Dysfunction

Left ventricular systolic dysfunction is generally defined as an ejection fraction less than 50% and occurs in 50–60% patients with heart failure. The differentiation of normal from reduced left ventricular systolic performance has therapeutic and prognostic implications.[5] In a recent population-based survey of middle aged to elderly adults without previous myocardial infarction or evidence of coronary artery disease, reduced ejection fraction by echocardiography (<40%) was associated with a 35% risk for cardiovascular death and 12% risk for all cause mortality. Segmental and global LV dysfunctions were associated with 3.3-fold and 3.8-fold higher rates of cardiovascular death.[5] Left ventricular ejection fraction is traditionally computed from echocardiography by using systolic and diastolic volumes obtained from biplane planimetry of paired orthogonal long-axis apical views. The threshold for qualifying left ventricular systolic dysfunction has however varied in various randomized controlled trials, ranging between 35 and 40%. While, in general, quantitative techniques provide more accurate thresholding, grading based on visual eyeballing has not been found to be inferior to other reference methods. In vast majority of centers, LV ejection fraction is usually mentioned as a descriptive grade of function, using subjective visual assessment by a single observer. Other echocardiographic variables that have been alternatively used for grading LV systolic function include fractional shortening and wall motion index or score. Doppler echocardiography provides useful noninvasive estimation of left ventricular stroke volume and cardiac output. Spectral velocity recordings in patients with

valvular regurgitation can also be used for estimating chamber pressures and d*p*/d*t* (rate of change of pressure over time). The current recommendation of the American society of echocardiography advocates routine measurement of left ventricular ejection fraction, diastolic volume, mass, and wall motion score using the 16-segment LV model. Assuming that the purpose of echocardiography is to establish whether or not left ventricular ejection fraction is in range of less than 40%, a value of <30% by Simpson's rule, or >1.7 by wall motion index, can be assumed to qualify as systolic dysfunction. Similarly a value of >50% or <1.0 can reliably be assumed to quantify a normal systolic function.[6]

Quantification of Diastolic Dysfunction

Although majority of patients with systolic dysfunction have some degree of diastolic dysfunction, population-based studies have highlighted that 40–50% of individuals with overt features of heart failure may have normal systolic function (ejection fraction more than 50%), also referred to as isolated diastolic dysfunction.[7] Recent reports highlight a high prevalence of preclinical isolated diastolic dysfunction in population who subsequently suffer a marked increase in all-cause mortality, independent of age, sex, and ejection fraction.[8] Thus quantification of an abnormal diastolic function is equally important in patients who exhibit symptoms of heart failure as well as those in whom diastolic dysfunction is clinically silent. Although clinical diagnosis of heart failure with normal ejection fraction correctly identifies those with abnormal diastolic function, an objective measurement of diastolic function is desirable for grading the pattern of dysfunction since it helps determining the underlying mechanisms and choice of therapeutic intervention.

Indices for Assessing Diastolic Dysfunction

Mitral Inflow Velocities

Left ventricular relaxation is an energy-dependent process that begins during the ejection phase of systole and continues through the isovolumic relaxation and the rapid filling phase. During exercise the rate and extent of LV relaxation increases proportionately and is crucial for continued normal pattern of LV filling despite shortening of diastolic filling period. This acceleration in LV relaxation during exercise is mediated by an enhanced sympathetic tone and is markedly blunted in heart failure. The left atrial to LV gradient and left atrial pressure during early diastolic filling therefore rises during exercise in patients with heart failure causing symptoms of shortness of breath. In a normal heart, a rapid flow velocity during early inflow occurs following mitral valve opening (E wave) followed by deceleration of flow during diastasis. Atrial contraction at the end diastole results in a second wave (A wave). The initial abnormality of diastolic function is characterized by a decrease in mitral *E* velocity and prolongation of deceleration time and a tall A wave causing a reduced *E*/*A* ratio (abnormal relaxation grade I or mild diastolic dysfunction). With progression of disease and further decline of active myocardial relaxation, filling of the left ventricle becomes increasingly dependent on the left atrial contraction and an increasing left atrial pressure. An increased mean left atrial pressure "pseudonormalizes" the flow from the left atrium to left ventricle, with increasing velocity of E wave and shortening of the deceleration time, resembling a normal state (pseudonormal or moderate or grade II diastolic dysfunction). In the latter stages, left ventricular chamber compliance is severely impaired so that a rising left atrial pressure causes rapid early mitral inflow (higher *E* velocity) with rapid equilibration of left atrial and left ventricular pressure causing early truncation of the E wave (very short deceleration time), with very little contribution to filling from atrial contraction (small A wave) (restrictive or severe or grade III–IV diastolic dysfunction).The filling pressures can be altered to reverse the restrictive pattern to lower grades of diastolic dysfunction in initial stages (grade III); however, the restrictive pattern persists later on despite manipulation of filling pressure indicating an irreversible stage of dysfunction (grade IV). Although mitral inflow velocities and *E*/*A* ratio have been shown to predict left ventricular filling pressures and determine prognosis, they have some limitations. The prediction of LV filling pressures is accurate only in patients with simultaneous systolic dysfunction, whereas patients with normal systolic function show a wide scatter. The distinction between normal versus pseudonormal filling is difficult, and other parameters are needed for differentiation. Preload modification, using glyceryl

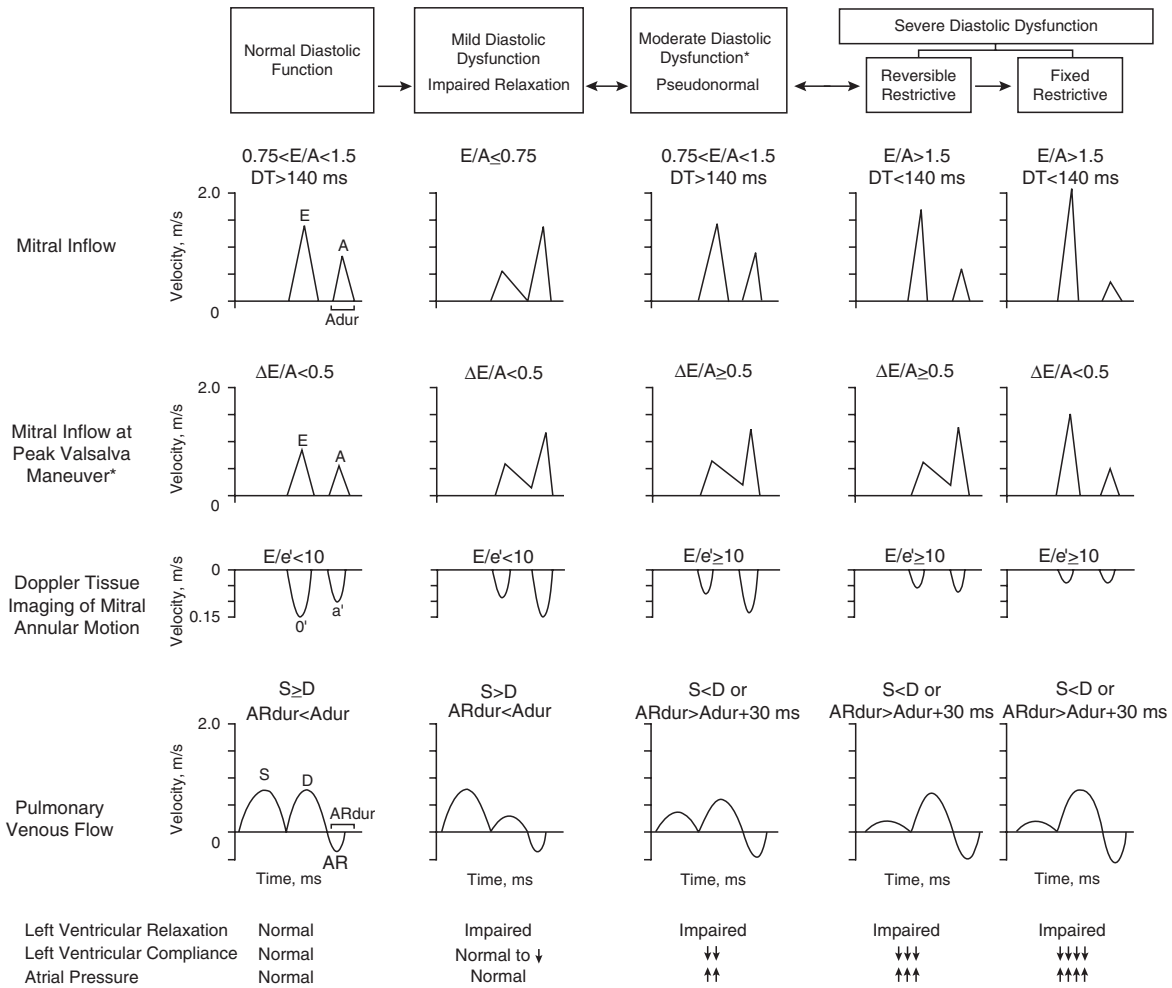

Fig 21.6 Echocardiographic evaluation of diastolic dysfunction (reproduced with permission from Redfield et al[8])

trinitrate or the Valsalva maneuver, is a useful means of unmasking patients with elevated filling pressures. However this may not be always practical in clinical practice, and some patients may not able to perform an adequate Valsalva maneuver[5,9,10] (Fig. 21.6).

Pulmonary Venous Doppler Velocities

Pulmonary venous flow (systolic versus diastolic predominance) has been used for predicting left atrial pressure in selected patients. The comparison of the duration of flow at atrial contraction across the mitral valve (mitral inflow) with the duration of flow reversal into the pulmonary veins can be used for estimating the left ventricular end diastolic pressure. In presence of normal left atrial pressure, systolic flow is dominant, and the systolic filling fraction is usually greater than 60%. There are small reverse components following the systolic and diastolic wave, reflecting atrial contraction. This back flow occurs because of lack of valves at the pulmonary vein–atrial junction. With rising filling pressures a worsening relative compliance of the left ventricle compared with the pulmonary venous circuit is observed. Transmitral flow at atrial contraction is shortened while retrograde flow at atrial contraction into low resistance pulmonary venous circuit continues for a longer duration. If the duration of atrial reversal flow in the pulmonary vein exceeds by more than 30 ms the duration of flow across the mitral valve, raised left ventricular end diastolic pressure can be

diagnosed with high specificity. Thus use of pulmonary venous flow is useful for distinguishing a normal transmitral filling pattern from pseudonormalization. However, the major limitations in the use of the pulmonary venous signals are that these signals are often difficult to obtain and interpret.

Mitral Annular Velocities

The velocity of the mitral annulus represents velocity of changes in left ventricular long-axis dimensions. In normal left ventricular relaxation after systole, the peak mitral annular velocity (E') recorded by tissue Doppler imaging precedes the peak early passive diastolic transmitral flow (E) recorded by conventional pulsed-wave Doppler ultrasound. In situations where this relaxation is impaired, E' follows E. The early diastolic velocity (E') has been proposed to represent the intrinsic speed of myocardial relaxation. This is used to determine the difference between the effect of "suction" versus "transmitral pushing" when left atrial pressure is high. The velocity of E' has a modest correlation with the time constant of relaxation. In the initial stages of diastolic dysfunction, the relaxation velocity (E') decreases and remains reduced throughout the remaining stages of impaired diastole. A combination of mitral inflow velocities with the mitral annular velocity into a ratio (E/E') has been shown to provide superior prediction of left ventricular filling pressure. This can be used for resolving normal from pseudonormal filling since patients with diastolic dysfunction and a normal mitral inflow pattern exhibit a reduced mitral annular velocity (E') and an elevated E/E' ratio. If E/E' is >15, left ventricular filling pressure is raised, and when E/E' is <8 filling pressure is low. However, between 8 and 15 there is considerable variability in filling pressure.[9,10]

Flow Propagation

Color Doppler M-mode provides a unique window into the fluid dynamics of flow across the mitral valve. The speed of propagation (slope of the black to red transition at the leading edge of the E-wave) is enhanced with rapid relaxation and LV suction. With normal LV diastolic filling, rapid relaxation generates a dynamic pressure gradient, from base toward apex. During early diastolic filling, peak LV filling therefore rapidly propagates sequentially from mitral orifice toward apex. In contrast, filling related to left atrial contraction does not pass the midportion of left ventricle. With onset of diastolic dysfunction, a blunting of flow propagation is seen; however, propagation velocity does not pseudonormalize. Color M mode flow propagation can be combined in a ratio with the mitral E velocity to provide a load-adjusted parameter (E/V_p) which strongly correlates with filling pressures. The chief limitations of this tool are lack of consensus on technique and theoretical concerns that this will be invalid in small left ventricular cavities.[11,12]

Other Doppler Variables in Hemodynamic Assessment

Doppler velocity tracings can also be used for calculating systolic and diastolic time intervals and have been shown to be closely linked with left ventricular performance. Combined Doppler myocardial performance index ((isovolumic contraction + isovolumic relaxation)/ejection time) has been shown to have significant correlation with left ventricular end-diastolic pressure and is a sensitive indicator of overall cardiac dysfunction in patients with mild-moderate congestive heart failure.[13] Other applications of Doppler in patients with heart failure include use of continuous-wave Doppler for estimating pulmonary artery pressures from spectral tracings of tricuspid and pulmonary regurgitation. Besides Doppler, a simple two-dimensional inspection of the inferior vena cava during subcostal imaging provides a useful estimate of the right atrial filling pressure.

Diastolic Function Assessment and Risk Stratification

In longstanding heart failure, the pulmonary artery wedge pressure has been shown to be a good predictor of survival, and aggressive therapy to reduce left ventricular filling pressures improves survival. Noninvasive indices described earlier can be combined together for

estimating left atrial and left ventricular filling pressures with fair accuracy. In patients with combined systolic and diastolic dysfunction, mitral deceleration time less than 150 ms and $E/A > 1.5$ provides an accurate estimation of filling pressures. Patients with a low E/A ratio (<0.75) and prolonged DT (>240 ms) have low to normal filling pressure (grade I). The E/E' ratio can also be applied in this group, with patients having grade I dysfunction showing a lower E/E' ratio, while those with grades II–IV having a raised E/E' ratio. Compared to pseudonormal or impaired relaxation, restrictive filling patterns are associated with higher mortality rates. In patients with preserved systolic function (LV EF > 50%), presence of $E/E' < 8$ is indicative of a normal filling pressure if they have a normal left atrial size. Those with $E/E' > 15$ have raised filling pressure. In the intermediate group (E/E' 8–15), abnormal filling pressure can be predicted only if other Doppler variables meet high specificity cut-off values. In such a patient left atrial pressure is elevated if the E/A ratio decreases by more than 0.5 during the Valsalva, or the pulmonary venous A wave duration exceeds the mitral a wave duration by at least 30 ms. If none of these is met and if the left atrial size is normal, filling pressures are likely to be normal.[9,10]

Echocardiography for Guiding Management Strategies in Heart Failure

Therapeutic and Surgical Interventions

Patients with exretional symptoms and an abnormal relaxation or pseudonormal relaxation pattern with preserved atrial filling benefit from agents that slow the heart rate and allow more time for diastolic filling. Patients with restrictive pattern benefit most with diuretic therapy. Patients with documented systolic dysfunction need treatment with angiotensin-converting enzyme inhibitors, beta blockade, digoxin, and diuretics.[14] End-stage ischemic heart disease is currently one of the primary indications for cardiac transplant. Accurate assessment of patients with ischemic cardiomyopathy who may benefit from coronary revascularization can be accomplished by combining hemodynamic parameters with results of stress echocardiography.

Echocardiography in Critical Care Units

In the evaluation of a patient who is in heart failure and hypotensive, it is often required to establish the volume status, especially if the patient is mechanically ventilated. A simple visual inspection for the left ventricular contractility by either transthoracic or transesophageal echo is immensely useful in these situations and a practical tool that allows rapid discrimination between depressed myocardial function and hypovolemia as the causative factor. Similarly diagnosing pulmonary embolism, extent of functional mitral regurgitation and presence of left ventricular clots, extent of right ventricular dysfunction is important for deciding management strategies in these patients and can be readily obtained from echocardiography.

Role of Echocardiography in Cardiac Resynchronization

Restoration of synchrony by cardiac pacing has been shown to improve ventricular contraction and reduce disease progression in heart failure. A left ventricular lead is positioned percutaneously either in the coronary vein or by thoracotomy over the epicardial surface, and synchronized activation of LV is used for enhancing left ventricular function. This reduces myocardial oxygen consumption, improves exercise capacity, functional class, and quality of life. Although prolonged electrical activation is used for identifying patients who maximally benefit with this therapy, it has been recently recognized that surface electrocardiogram remarkably underestimates the extent and pattern of left ventricular dyssynchrony. Temporal and spatial delays in regional myocardial function can be quantified more accurately by tissue Doppler and strain rate imaging. Tissue Doppler and flow Doppler indices are sensitive for evaluating the acute hemodynamic benefits of resynchronization and useful for optimizing the atrioventricular and interventricular delays. Regional velocity or displacement is studied by curved M-mode, which displays color data over time and provides a superior spatial and temporal assessment of regional function (Fig. 21.7). Strain rate imaging differentiates active contraction from passive motion and also is used for identifying delayed longitudinal contractions. These are identified as delayed waves of

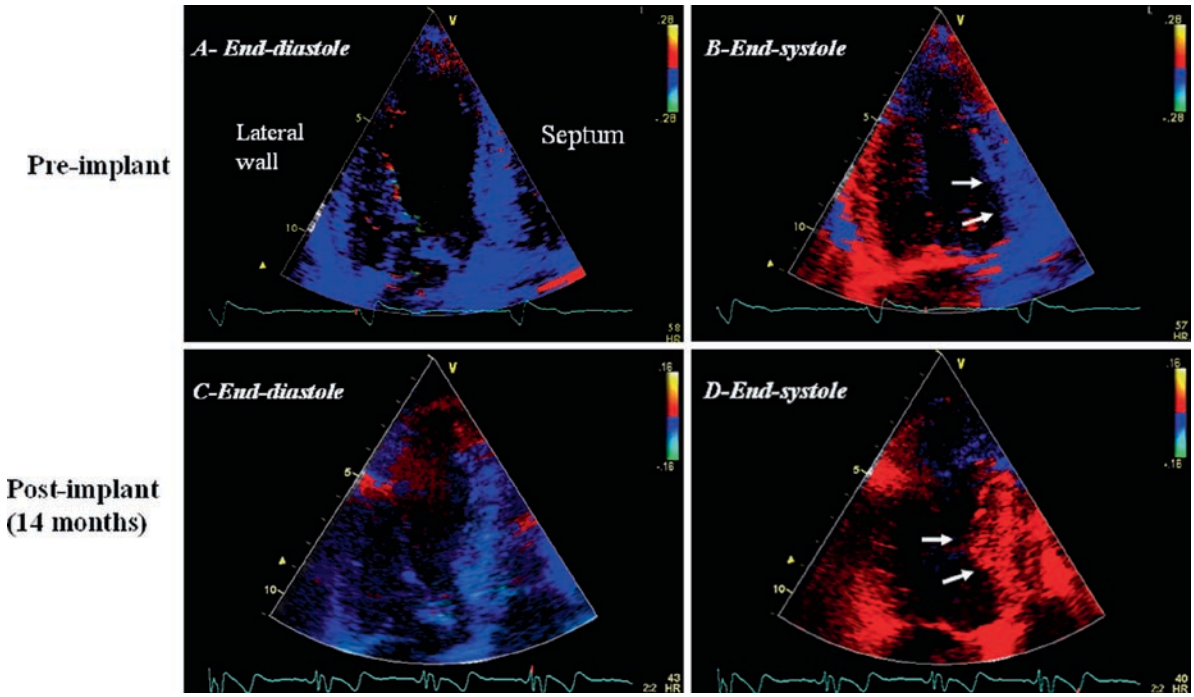

Fig. 21.7 Role of color Doppler myocardial imaging for demonstrating therapeutic response of biventricular pacing in a patient with ischemic cardiomyopathy. Simultaneous superimposition of color Doppler and gray-scale information provides improved assessment of regional synchrony during real-time two-dimensional imaging. The end-systolic frame at baseline (**b**) shows presence of a delayed longitudinal motion of the lateral wall toward the transducer (*red color*), while the septum has started relaxing (*blue color*). Note the improved synchrony and septal thickening (*arrows*, **d**) and smaller left ventricular end-systolic volume following biventricular pacing. Left ventricular systolic function improved significantly with ejection fraction increasing from 30 to 45% following biventricular pacing over a period of 14 months

shortening occurring following the closure of the aortic valve. The region with maximum delay in onset of contraction either on tissue Doppler or strain rate imaging also serves as a guide for lead placement. Pacing is performed at incremental intervals of 5–10 ms till maximum increase in duration and synchronicity of systolic waves is achieved. Changes in left ventricular size shape and function may be evident in some patients within one week however are more pronounced after 2–3 months of therapy, and indicate a favorable process of reversed LV remodeling[15,16] (Fig. 21.8).

Echocardiography and Heart Failure Screening

The progressive nature of heart failure has generated recent interests in its detection in early preclinical stages. In a recent large community-based study, 3% of overall population had asymptomatic left ventricular dysfunction (EF < 50%). During a mean follow up of 12 years, 26% of these patients developed congestive heart failure. Although the rates of heart failure and death in individuals with subclinical dysfunction were twofold to fourfold higher than those with normal LV function, the median survival free of heart failure was 10 years suggesting a window for early identification and intervention.[17] Randomized controlled clinical trials have established that therapy in these patients can delay or prevent onset of congestive heart failure. Echocardiography therefore is likely to play a vital role as a screening tool for primary and secondary prevention of heart failure in community-based interventions. However the major limitation in its use for mass screening is its cost. Recent advances in ultrasound technology have resulted in miniaturization of the echocardiography systems with development of portable ultrasound machines. Preliminary reports of its use for heart failure screening in community have found an acceptable

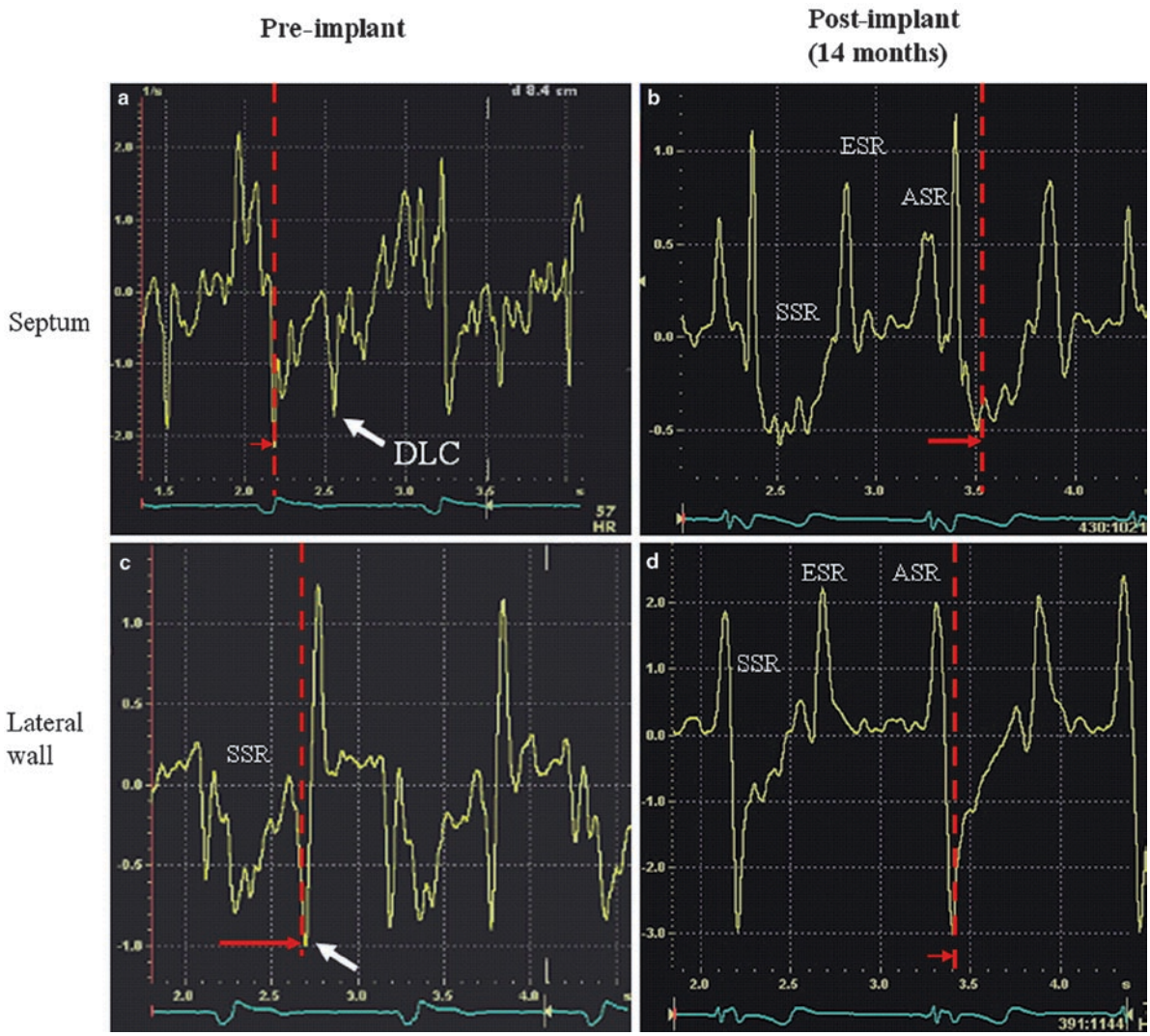

Fig. 21.8 Strain rate imaging for quantitative assessment of improvement in left ventricular function following biventricular pacing. At baseline both septum and lateral wall show asynchrony with presence of a delayed longitudinal wave of shortening (*arrow*). The onset peak systolic shortening (*red dotted line*) varies with lateral wall showing a significant delay in reaching peak strain rate (delayed longitudinal shortening, *arrow*). Note the remarkable improvement in regional strain rate and complete disappearance of delayed contraction following biventricular pacing

accuracy for detecting left ventricular systolic dysfunction, hypertrophy, and valvular regurgitation.[18]

Summary and Future Directions

During last two decades, two-dimensional echocardiography has emerged as an important clinical tool for providing reliable diagnostic and prognostic information in patients with heart failure. With recent emergence of quantitative parameters in Doppler ultrasound and development of novel strategies for halting or reversing cardiac remodeling, application of echocardiography as a noninvasive tool for identifying systolic and diastolic dysfunction has shown remarkable growth in clinical practice. However with wider utilization, standardization of variables and protocols for measuring left ventricular systolic and diastolic function would be needed. Ejection fraction has consistently been shown in clinical trials to predict risk of mortality, with patients with lower ejection fraction having higher

mortality. However a change in ejection fraction based on therapy has not been found to consistently correlate with clinical outcomes. The concept that any agent that reduces ejection fraction is harmful and any agent that increases ejection fraction is beneficial has also not been substantiated. With 40–50% of patients in recent heart failure trials having normal LV function, it may be required to develop a global parameter that would closely reflect the remodeling process and the functional aberrations in heart failure. Recent development of three-dimensional volumetric measures of left ventricular geometry and function appears particularly attractive in this regard, however, would need careful validation in larger trials. The current clinical utilization of Doppler for assessment of diastolic dysfunction is also highly variable between and within echocardiographic laboratories and merits standardization. Similarly an appropriate variable or a combination of variable whose recognition and modulation could prevent its progression of diastolic heart failure would be required to be identified. Recognition and treatment of asymptomatic left ventricular systolic dysfunction has been shown to halt progression of heart failure. However, benefits of identification of subclinical diastolic dysfunction by echocardiography and its intervention also remain to be addressed in future trials.

References

1. Jessup M, Brozena S. Heart failure. *N Engl J Med*. 2003;348:2007–2018.
2. Dhir M, Nagueh SF. Echocardiography and prognosis of heart failure. *Curr Opin Cardiol*. 2002;17:253–256
3. Hunt SA, Baker DW, Chin MH, et al.; American College of Cardiology/American Heart Association Task Force on Practice Guidelines (Committee to Revise the 1995 Guidelines for the Evaluation and Management of Heart Failure); International Society for Heart and Lung Transplantation; Heart Failure Society of America. ACC/AHA Guidelines for the Evaluation and Management of Chronic Heart Failure in the Adult: Executive Summary A Report of the American College of Cardiology/American Heart Association Task Force on Practice Guidelines (Committee to Revise the 1995 Guidelines for the Evaluation and Management of Heart Failure): Developed in Collaboration With the International Society for Heart and Lung Transplantation; Endorsed by the Heart Failure Society of America. *Circulation.* 2001;104:2996–3007.
4. Eichhorn EJ, Grayburn PA, Mayer SA, et al. Myocardial contractile reserve by dobutamine stress echocardiography predicts improvement in ejection fraction with beta-blockade in patients with h eart failure: the Beta-Blocker Evaluation of Survival Trial (BEST). *Circulation*. 2003;108:2336–2341
5. Devereux RB, Roman MJ, Palmieri V, et al. Prognostic implications of ejection fraction from linear echocardiographic dimensions: the Strong Heart Study. *Am Heart J*. 2003;146:527–534.
6. McGowan JH, Cleland JG. Reliability of reporting left ventricular systolic function by echocardiography: a systematic review of 3 methods. *Am Heart J*. 2003;146:388–397.
7. Vasan RS. Diastolic heart failure. *BMJ*. 2003;327:1181–1182.
8. Redfield MM, Jacobsen SJ, Burnett JC Jr, Mahoney DW, Bailey KR, Rodeheffer RJ. Burden of systolic and diastolic ventricular dysfunction in the community: appreciating the scope of the heart failure epidemic. *JAMA*. 2003 Jan 8;289(2):194–202.
9. Ommen SR, Nishimura RA. A clinical approach to the assessment of left ventricular diastolic function by Doppler echocardiography: update 2003. *Heart.* 2003;89 Suppl 3:iii18–iii23.
10. Naqvi TZ. Diastolic function assessment incorporating new techniques in Doppler echocardiography. *Rev Cardiovasc Med*. 2003;4:81–99.
11. Garcia MJ, Ares MA, Asher C, Rodriguez L, Vandervoort P, Thomas JD. An index of early left ventricular filling that combined with pulsed Doppler peak E velocity may estimate capillary wedge pressure. *J Am Coll Cardiol*. 1997;29:448–454.
12. Vitarelli A, Gheorghiade M. Transthoracic and transesophageal echocardiography in the hemodynamic assessment of patients with congestive heart failure. *Am J Cardiol*. 2000;86:36G–40G.
13. Bruch C, Schmermund A, Marin D, et al. Tei-index in patients with mild-to-moderate congestive heart failure. *Eur Heart J*. 2000;21:1888–1895
14. Lainchbury JG, Redfield MM. Doppler echocardiographic-guided diagnosis and therapy of heart failure. *Curr Cardiol Rep*. 1999;1:55–66
15. Kanzaki H, Jacques D, Sade LE, Severyn DA, Schwartzman D, Gorcsan J III. Regional correlation by color-coded tissue Doppler to quantify improvements in mechanical left ventricular synchrony after biventricular pacing therapy. *Am J Cardiol*. 2003;92:752–755
16. Sogaard P, Egeblad H, Kim WY, et al. Tissue Doppler imaging predicts improved systolic performance and reversed left ventricular remodeling during long-term cardiac resynchronization therapy. *J Am Coll Cardiol*. 2002;40:723–730.
17. Wang TJ, Evans JC, Benjamin EJ, Levy D, LeRoy EC, Vasan RS. Natural history of asymptomatic left ventricular systolic dysfunction in the community. *Circulation*. 2003;108:977–982.
18. Senior R, Galasko G, McMurray JV, Mayet J. Screening for left ventricular dysfunction in the community: role of hand held echocardiography and brain natriuretic peptides. *Heart*. 2003;89(Suppl 3):iii24–iii8.

Chapter 22
Cardiac Resynchronization Therapy

Petros Nihoyannopoulos

Introduction

The impact of echocardiography in patient assessment is such that it is almost inconceivable today for a patient with known or suspected heart disease not to have at least one Echocardiographic examination. The commonest request for an echocardiogram is without a doubt the assessment of ventricular function. Beyond its pivotal role in diagnosing heart disease, echocardiography is now essential in the management of patients with all forms of heart conditions. Heart failure is probably the biggest killer of all disease and treatment becomes ever more expensive.[1] There are tremendous therapeutic achievements ranging from drug treatment to expensive devise therapeutic strategies including transplantation, implantation of ventricular assist devices, intracardiac defibrillations, and biventricular pacing, the cost of which may not be sustainable by any health care system. It is therefore important to be able to better select patients based on their chances to benefit most from such treatment and echocardiography has the lion's share in this process.

Cardiac resynchronization therapy (CRT) has been proposed as an alternative treatment in patients with severe, drug-refractory heart failure.[2–4] The clinical results are very promising and improvement in symptoms, exercise capacity, and systolic left ventricular function have been demonstrated after CRT, accompanied by a reduction in hospitalization and a superior survival as compared to optimized medical therapy alone.

The role of echocardiography in Cardiac Resynchronization Therapy (CRT) is:

1. Describe the left ventricle, measure volumes, assess regional versus global dysfunction, and evaluate the presence and severity of mitral regurgitation.
2. Assess for myocardial viability (dobutamine stress)
3. Selecting patients who are going to benefit most prior to implantation (identifying responders)
4. Determining optimal lead placement during implantation
5. Optimizing the device after implantation (AV delay, VV delay)
6. Evaluating the reverse remodeling of the heart during follow-up

What Is Cardiac Dyssynchrony?

Ventricular dyssynchrony is a disruption of the collagen matrix of the heart, which impairs electrical conduction and weakens the overall pumping efficiency. This is manifested by the development of intre- or intraventricular conduction delays, most commonly in the form of left bundle branch block, and regional wall motion abnormalities whereby different myocardial regions contract at different times. The direct result of this dyssynchronous left ventricle will be an abnormal interventricular septal motion, a reduced dp/dt, reduced diastolic filling times, and a prolongation of mitral regurgitation if there is one. This cascade of events will lead to abnormal systolic and diastolic ventricular function and heart failure.

The aim of CRT is therefore to:

- Improve the LV contraction pattern
- Eliminate the paradoxical septal motion
- Increase diastolic filling duration
- Increase ejection fraction
- Reduce the amount of mitral regurgitation

P. Nihoyannopoulos
Imperial College London, National Heart and Lung Institute, Hammersmith Hospital, London, UK
e-mail: petros@imperial.ac.uk

P. Nihoyannopoulos and J. Kisslo (eds.), *Echocardiography*,
DOI: 10.1007/978-1-84882-293-1_22,

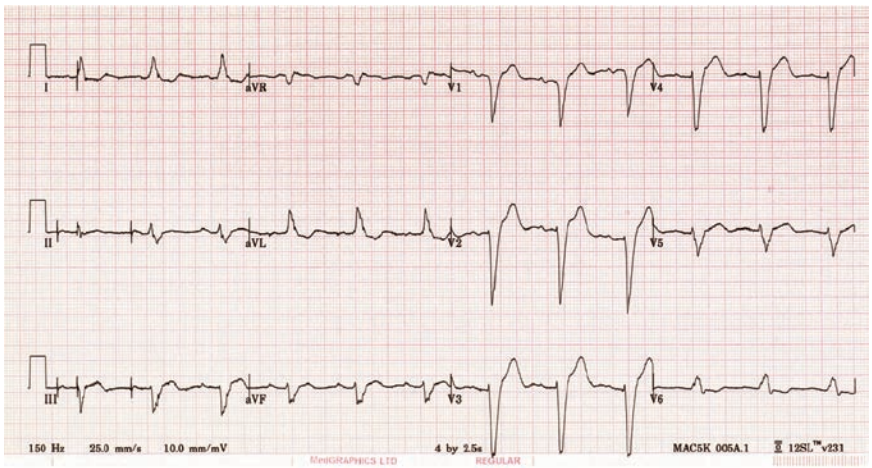

Fig. 22.1 A 12-lead ECG from a heart failure patient demonstrating the presence of left bundle branch block

The success of CRT is evaluated ultimately by an improved patients' quality of life in the form of NYHA functional class, improved exercise capacity and duration, and reduced amount of hospital admissions. Quantitatively, successful CRT is when patients' EF is increased and LSV reduced.

The classic method of assessing LV dyssynchrony is the ECG by demonstrating a QRS duration >120 ms in a patient with heart failure (NYHA classes III–IV), poor LV function (LV ejection fraction <35%) and this despite optimal medical therapy[3] (Fig. 22.1). However, the ECG alone has proven to be a poor predictor of CRT response. About 30% of patients who underwent this treatment failed to improve.[5,6]

Echocardiography may therefore improve the selection criteria by virtue of assessing the mechanical events over time.

Types of Mechanical Dyssynchrony

Left ventricular dyssynchrony may result from three levels of impaired ventricular interaction:

1. Between left atrium and left ventricle called atrioventricular dyssynchrony
2. Between right and left ventricles named interventricular dyssynchrony and
3. From within the left ventricle itself (intraventricular dyssynchrony.

AtrioVentricular Dyssynchrony

Atrioventricular dyssynchrony is related to the dysfunction of both the sinus node and the atrioventricular node. While sinus node dysfunction induces chronotropic incompetence, abnormal conduction of the atrioventricular node results in[7]:

- A delay between atrial and ventricular contraction time (AV dyssynchrony),
- Mitral valve incompetence with occurrence of late diastolic regurgitation,
- Shortened ventricular filling time, limiting diastolic stroke volume
- Atrial systole often occurs simultaneously with early passive filling, hence reducing LV filling.

Atrioventricular dyssynchrony may result by an inappropriate atrioventricular delay in case of a pacemaker implantation. The optimal AV delay (AV synchronization) may be assessed by the recording of simple transmitral velocities with pulsed-wave Doppler. An optimal AV delay is the temporal relation between LV and LA contraction that leads to an increase in LV pressure from LV contraction when starting after the peak of the increase in LA pressure from LA contraction but before atrial relaxation is complete. This will show a prominent A-wave on Doppler in end-diastole (Fig. 22.2a).

If the AV interval is too short, i.e., 60 ms, diastolic filling may be abbreviated when the LV pressure

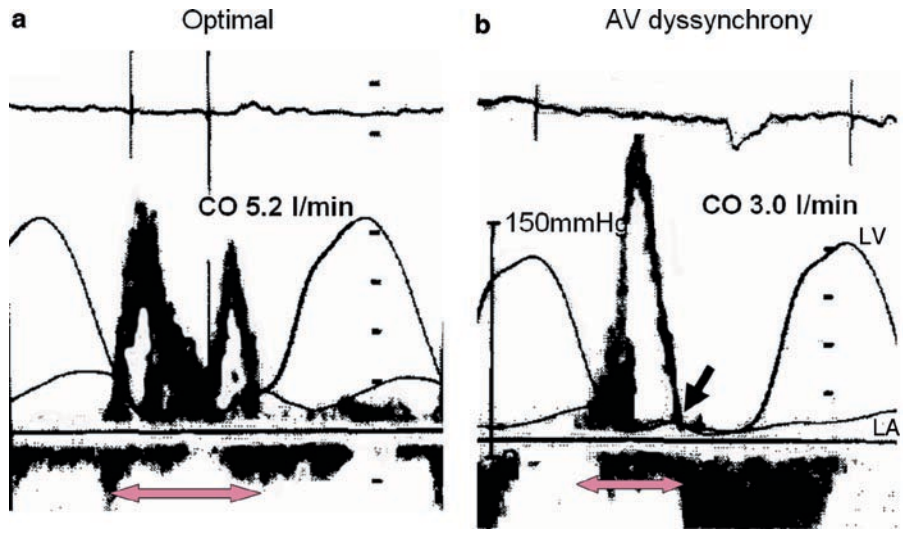

Fig. 22.2 Two distinct patterns of atrioventricular optimization. In (**a**), there is optimal AV delay with long LV filling time and the ventricular contraction (pressure wave) beginning after the end of atrial contraction. In (**b**), there is a truncated A-wave with reduced filling time and onset of diastolic mitral regurgitation. Note the cardiac output (CO) is reduced

increases above that of the LA pressure during atrial relaxation in mid-diastole (Fig. 22.2b). This will result in shortening of the diastolic filling time (restrictive pattern) and the onset of diastolic mitral regurgitation. Cardiac output will be inefficient.

Interventricular Dyssynchrony

In normal hearts, left and right ventricular contraction occurs almost simultaneously. Dyssynchronous ventricular electrical activation is associated with the right ventricular events preceding those of the left ventricle. This will lead to regional differences in contraction patterns, abnormal distribution of mechanical work in the LV, deficiencies in regional perfusion, and therefore decreased mechanical performance.

The delay in onset of LV contraction and relaxation produces interventricular dyssynchrony and affects mainly the interventricular septal motion and its contribution to LV ejection. Earlier onset of right ventricular contraction results in right ventricular ejection occurring during LV end-diastolic period. The higher pressure within the right ventricle reverses the trans-septal pressure gradient and therefore displaces the septum into the left.[8]

Interventricular dyssynchrony can be evaluated echocardiographically by assessing the extent of interventricular mechanical delay (IVMD) defined as the time difference between left and right ventricular pre-ejection intervals measured by pulsed-wave Doppler (Fig. 22.3). An IVMD >40 ms is considered indicative of interventricular dyssynchrony.[9,10]

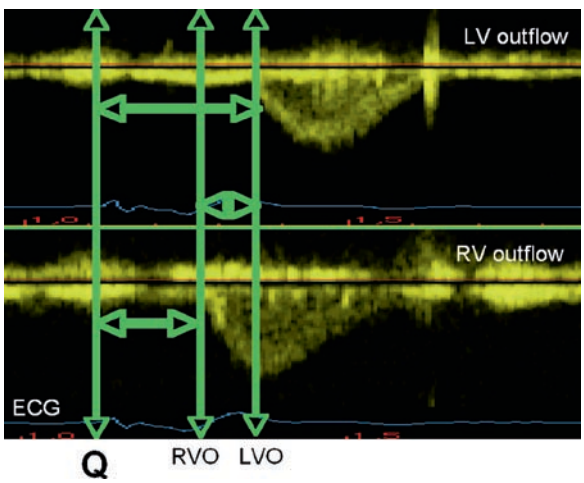

Fig. 22.3 Measurement of the interventricular mechanical delay by Doppler echocardiography: the right and left ventricular pre-ejection intervals are measured from the onset of the QRS on the ECG to the onset of pulmonary (RV outflow) and aortic (LV outflow) outflow. IVMD is calculated by subtracting the RVO from the LVO

This can be assessed using continuous-wave Doppler recordings by subtracting the time between Q-wave of the ECG and onset of the pulmonary velocity waveform at the RV outflow track from the time between Q-wave and onset of aortic velocity at the LV outflow track (Fig. 22.3):

Q-PV vs Q-AV (normally <40 ms)

Intraventricular Dyssynchrony

This is perhaps the most important aspect of the dyssynchronous ventricle because an electrophysiologist may be able to correct it by implanting a biventricular pacemaker. Echocardiography will need to assess the presence and perhaps the extent of intraventricular dysynchrony to better predict the patient's benefit from CRT. Coordinated LV contraction depends on normal ventricular activation. When a portion of the LV is activated prematurely, it generates regions of both early and delayed contraction that contribute to reduced LV performance. Loss of coordination within the Left Ventricle with regions of early and delayed activation leads to a decline in pump efficiency.

Early shortening or late ventricular shortening results in wasted work. The early contraction occurs when LV pressure is low and does not lead to ejection. The late contraction occurs at higher stress and results in paradoxical stretch of early contracting segments. The net result is a decline in systolic performance, an increase in end-systolic volume and wall stress, a delayed relaxation and again, a decline in efficiency.[9]

While it is unclear as to what extent each of these different forms of dyssynchrony contributes to the severity of heart failure, it remains crucial that all different forms of dyssynchrony are assessed to identify patients with the highest likelihood to responding to CRT.

In the next paragraphs the conventional and more advanced echocardiographic measurements are summarized.

How to Assess Intraventricular Dyssynchrony: Prediction of Responders

Echocardiographic Assessment and Quantification of Dyssynchrony

M-Mode Echocardiography

A simple echocardiographic technique for the detection of LV dyssynchrony has been developed by Pitzalis et al[11] The authors used an M-mode recording through the parasternal short-axis view (at the papillary muscle level) to measure the delay between the peak systolic excursion of the (anterior) septum and the posterior wall, the so-called septal to posterior wall motion delay (SPWMD) (Fig. 22.4). An optimal cut-off value in SPWMD of 130 ms was proposed, which yielded an accuracy of 85% (sensitivity 100%, specificity 63%) to predict response to CRT. This value was a strong predictor of cardiac events during long-term follow-up.

There are severe limitations however with the interpretation of M-mode recordings in more than 50% of patients (Fig. 22.5). These problems were generated from:

- Difficulties in identifying the maximal systolic thickening of the ventricular septum (either because it was akinetic or because it had a rounded shape making the clear identification of the peak difficult).
- Oblique sections of the left ventricle due to a deformed cavity
- Poor Echocardiographic windows leading to incomplete endocardial border detection

Summary

Advantages:

- No specific ultrasound equipment is needed
- Easy to perform
- High temporal resolution (>1000–3000 fps)

Disadvantages:

- Difficult to determine the timing of inward motion if the wall is akinetic or has plateau in motion
- Only can assess limited walls (anteroseptal and inferolateral wall)

Two-Dimensional Echocardiography

In patients with heart failure, severe LV dyssynchrony can sometimes be assessed visually from conventional 2D echocardiography. It is displayed as a counterclockwise rotation of the left ventricle in the apical 4-chamber view or a delayed activation of the posterolateral LV segments. However in the majority of cases, visual assessment alone is not precise enough to accurately characterize LV dyssynchrony. In addition, the presence of LV dyssynchrony will not be detected in patients with an intermediate extent of LV dyssynchrony, even in the hands of experienced sonographers.

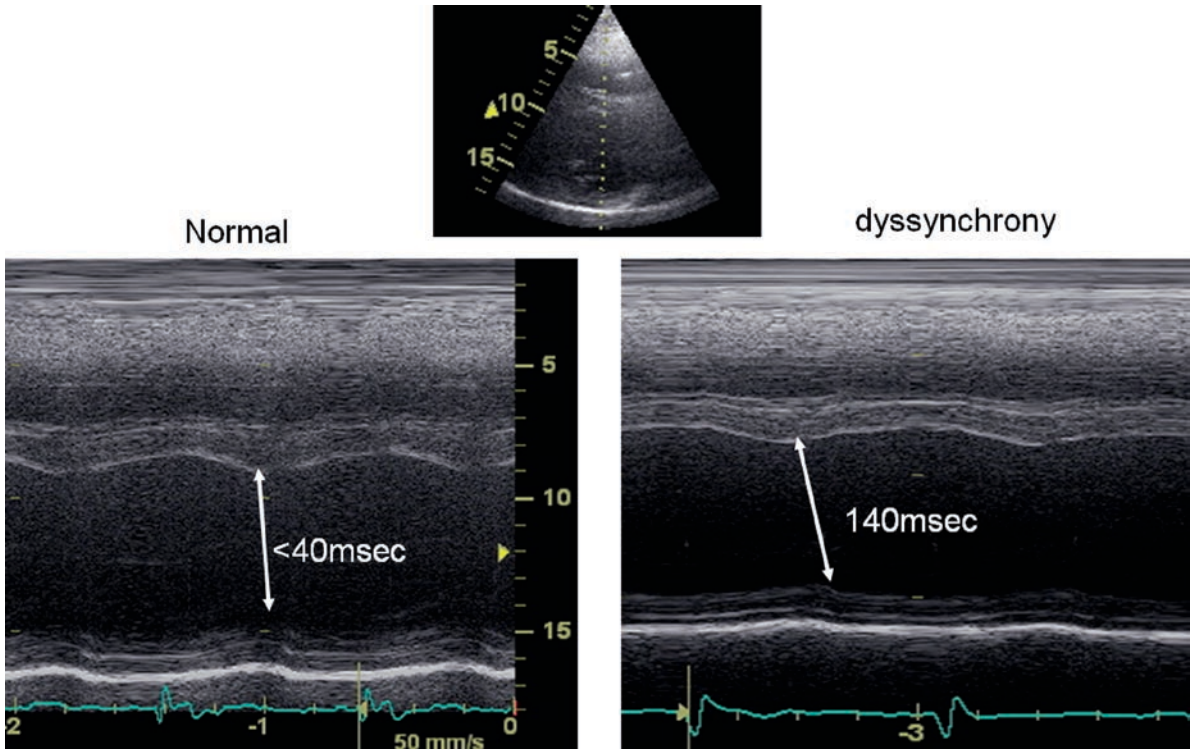

Fig. 22.4 Example of a normal SPWMD (<40 ms) and in a heart failure patient in whom the SPWMD is 140 ms indicating dyssynchrony

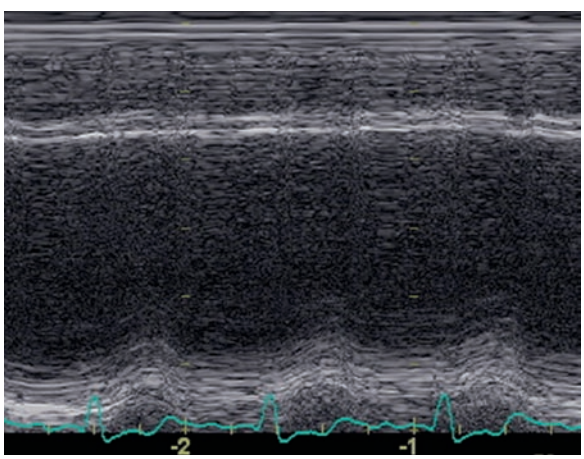

Fig. 22.5 M-mode recording from a heart failure patient secondary to anterior myocardial infarction. Note that it is impossible to assess dyssynchrony in this patient due to the absence of ventricular septal thickening

Real-Time 3D Echocardiography in the Assessment of Mechanical Dyssynchrony

The ability to provide an accurate evaluation of the dimensions and function of the left ventricle is essential for patient management, and echocardiography is the most widely used imaging modality used for this purpose. Conventional echo modalities (M-mode, 2D) rely heavily on geometrical assumptions and present with insufficient accuracy and inter- and intraobserver agreement, pointing to the need for more objective quantification techniques.

Early three-dimensional models of the left ventricle were using reconstructive methods, which were time consuming and copious. During the last 5 years, new transducer matrix technology and very fast computer software have succeeded in direct real-time three-dimensional acquisition. Real-Time Three-dimensional echocardiography allows a fast acquisition from a single apical acoustic window of four pyramidal subvolumes, which are then electronically reconstructed over 4–5 consecutive cardiac cycles. Several offline and online software packages offer extensive qualitative and quantities features.

The RT3DE LV volume dataset is then divided into several predetermined equi-angled longitudinal slices and after the identification of anatomical landmarks (Mitral and aortic valve and apex) and phases (end-systole,

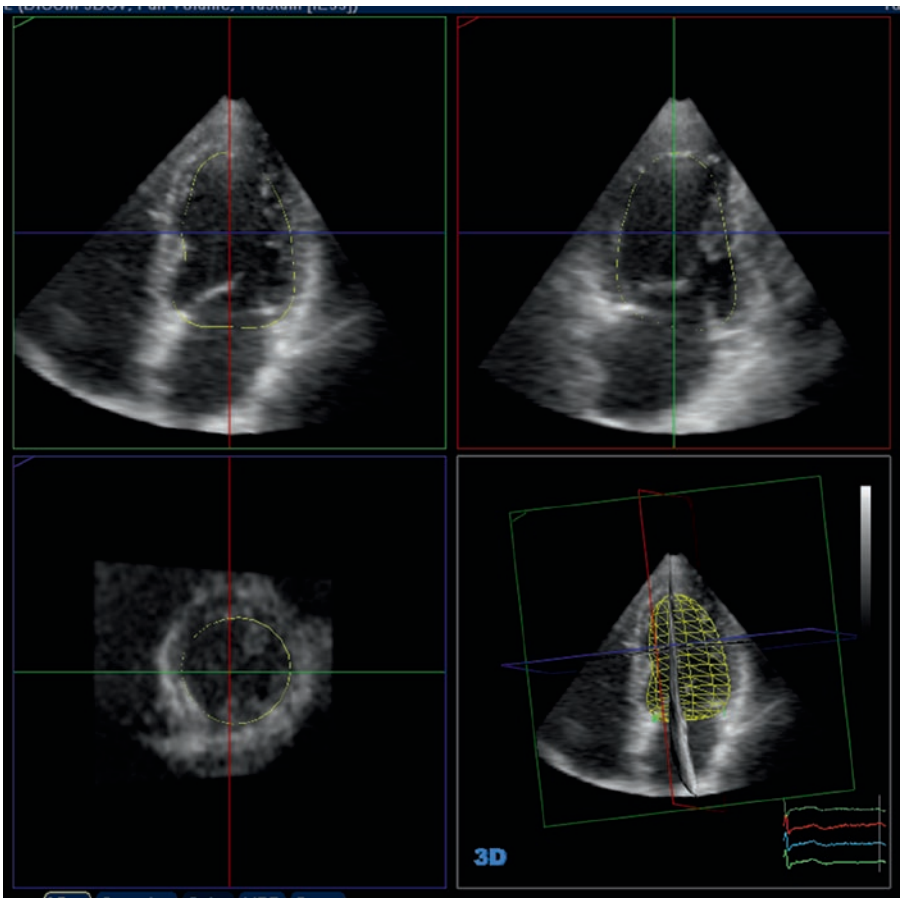

Fig. 22.6 Real-time three-dimensional datasets and subsequent model

end-diastole) by the operator in all the views, a semiautomated border detection algorithm is then used to trace the endocardial borders throughout the cardiac cycle (Fig. 22.6). The endocardial contours that are created with this process are then combined and a dynamic "cast" of the LV is obtained. This three-dimensional model simulates in real time the contraction and relaxation of the LV and with a detection of hundreds of points over the LV surface. Global and regional volumes as well as ejection fraction are calculated devoid of the geometrical assumptions found in two-dimensional techniques.

Evaluation of Global and Regional Volumes and Function

Many studies have demonstrated a high concordance between 3D echo LV volume and EF calculations and the considered "gold standard," Cardiac Magnetic Resonance.[12] The important role of RT3DE in the assessment of regional volumes and wall motion abnormalities has also been strongly supported by the results of more recent studies.[13]

Real-Time Three Dimensional Echocardiography provides:

- A robust and reproducible technique in assessing volumes
- All LV segments can be analyzed at once
- The apex can optimally be evaluated in relation to the rest of LV
- Imaging at lower frame rate but sampling is high enough for reliable volume/time curves
- More precise in evaluating volumes (global and regional)

RT3DE and Intraventricular Dyssynchrony Assessment

In the context of LV dyssynchrony the capability of analyzing regional volumes and function of the 16 or 17

segments according to the American Society of Echocardiography "bull's eye" model (Fig. 22.7) proves invaluable both for the qualitative and quantitative assessment of the synchronicity in the contraction of all LV segments. A series of plots representing the change in volume in each of the 16 segments throughout a cardiac cycle can be obtained. With synchronous contraction (Fig. 22.8 left), all regions reach their minimum volumes at approximately the same time. Conversely in the event of intraventricular LV dyssynchrony (Fig. 22.8 right) a scattering of the minimum volume points is observed. From these volume-time curves, qualitative information such as the identification of the most delayed walls can be obtained as well as a crude estimate of the degree of dispersion that exist between the timing of the minimum volume points of the LV segments.

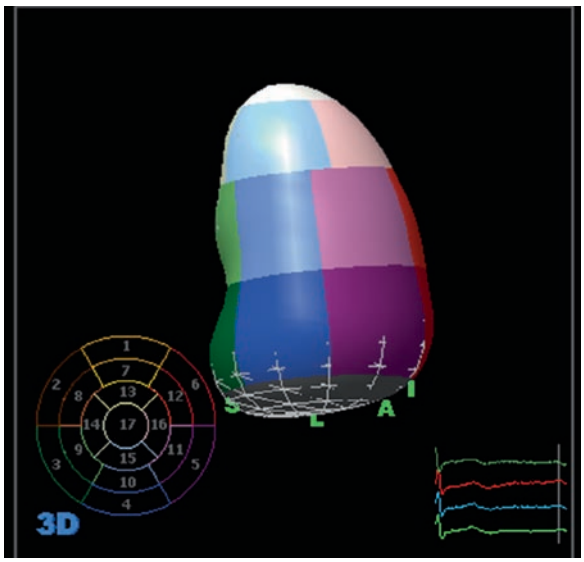

Fig. 22.7 Bull's eye model of the LV and color representations of the 17 segments on the 3D model

Dyssynchrony Index

These observations and the need to quantify accurately the degree of LV dyssynchrony have led to the derivation of the Systolic Dyssynchrony index which is defined as the standard deviation of the time it takes each of the segments of the LV to reach their minimum volume. This parameter provides a comparison of all segments simultaneously from the same view, eliminating any variability caused by differences in the R-R intervals, which are commonly found in heart failure patients. This index has been shown to be simple, intuitive, and highly reproducible when it was used in the selection and follow-up of patients eligible for CRT.[14]

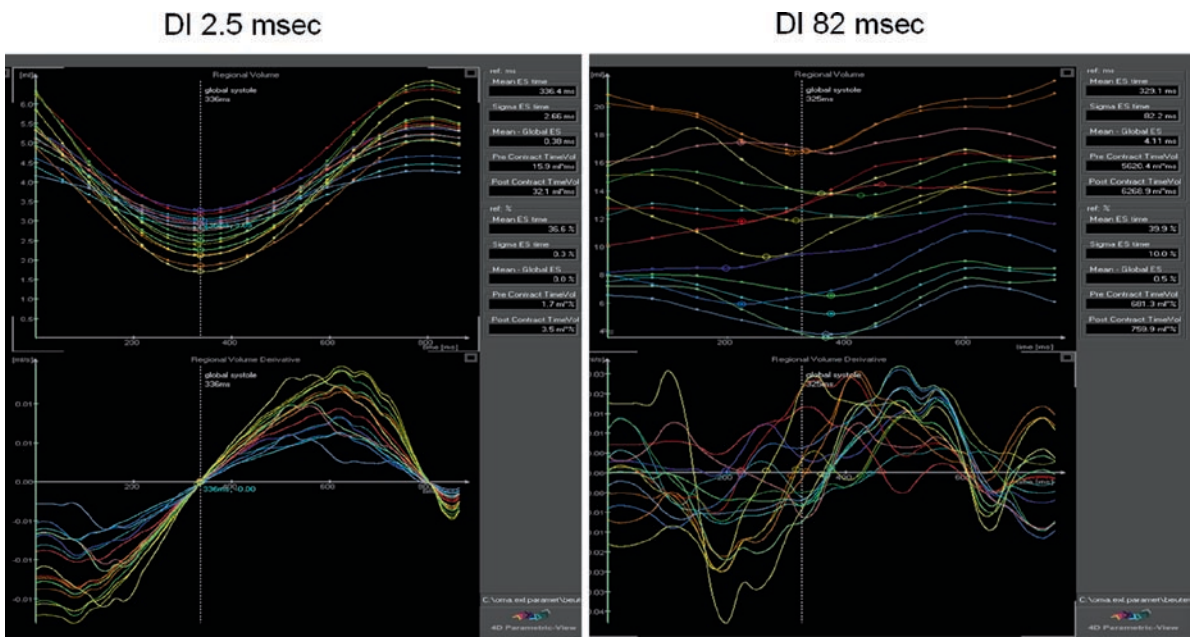

Fig. 22.8 Regional Volume-Time curves and assessment of regional dyssynchrony. Synchronous LV (*left panel*) and dyssynchronous LV (*right panel*). Note that the Dyssynchrony Index (DI) is below 10 (normal) on the right and markedly increased (82 ms) in the heart failure patient

In particular, a strong negative correlation has been found between ejection fraction and the SDI, demonstrating that a higher degree of intraventricular LV dyssynchrony is associated with a more severe impairment of the systolic function. Conversely, the relationship between SDI and the electrical dyssynchrony as expressed by the QRS width is much weaker. So in general, a dyssynchrony index greater than 10 would indicate intraventricular dyssynchrony while less than 10 would indicate its absence. The greater the value of dyssynchrony index, the more dyssynchronous the ventricle would be and the greater the benefit from resynchronization treatment with biventricular pacing.

Summary

Advantages:

- Enables the dyssynchrony assessment in one image
- Nearly automated analysis
- Option to display the temporal and spatial distribution of timing in bull's eye plot

Disadvantages:

- Low temporal (15–25 fps) and spatial resolution
- Requires specific high-end ultrasound equipment and probe
- Highly dependent on image quality
- Incomplete inclusion of dilated ventricle
- Requires several regular heart beats: cannot perform in atrial fibrillation or frequent ectopic beats

Tissue Velocity Imaging and Deformation Parameters

The use of TDI may be separated into four types:

1. Pulsed-wave TDI of the mitral annular velocities.
2. Tissue Doppler imaging derived from myocardial velocities (color-coded TDI) that necessitates complex postprocessing algorithms, at the base of the heart as well as midleft ventricular regions
3. Deformation parameters (strain and strain rate) based on velocities
4. Speckle tracking

1. Pulsed-wave TDI has the unique advantage that it is available to all modern machines and it does not require extensive expertise to use it routinely. It allows measurement of peak systolic velocity of different regions of the mitral annulus (apical four-, apical two-, and apical long-axis views), which may provide up to six measurements. The prevailing measurement is the "time-to-peak" of the systolic velocity in relation to the onset of electrical activity (QRS complex).

The disadvantage is that only one region can be interrogated at a time making the procedure time consuming and precludes simultaneous comparisons of regions. Because measurements are influenced by differences in heart rate, loading conditions, and respiration, measurements that are not simultaneous may be less meaningful. In addition, the timing of the peak systolic velocity is often difficult to identify resulting in imprecise information of LV dyssynchrony. As an alternative, the time to onset of systolic annular velocity has been proposed (Fig. 22.9), but this also suffers from the same limitations.

Summary

Advantages:

- High temporal resolution
- Does not require specific ultrasound equipment, software, or offline analysis

Disadvantages:

- Does not allow simultaneous sampling in multiple segments
- Requires multiple imaging to map the entire heart
- Susceptible to translational motion or tethering effect

2. Color-coded TDI is probably the most widely used method of assessing dyssynchrony and patient outcome.[15–20] This is based on Doppler information arising from specific myocardial regions at the base and midleft ventricle. TDI velocity tracings are obtained by postprocessing and the majority of studies have used the time-to-peak velocity to assess dyssynchrony. Figure 22.10 is from a patient with LBBB who has no dyssynchrony as assessed by color Doppler TDI. In contrast, Fig. 22.11 is from a patient with lateral wall delay compared to the septum. The advantage of this method is that the recordings have a very high frame rate (usually >100 Hz), simultaneous measurements can be obtained from paired walls, and the formation of the tracings is of the highest quality.

The commonest and perhaps the most practical measurement is using the apical four-chamber view to obtain velocity tracings from the basal septal and basal lateral segments. While in a normal ventricle

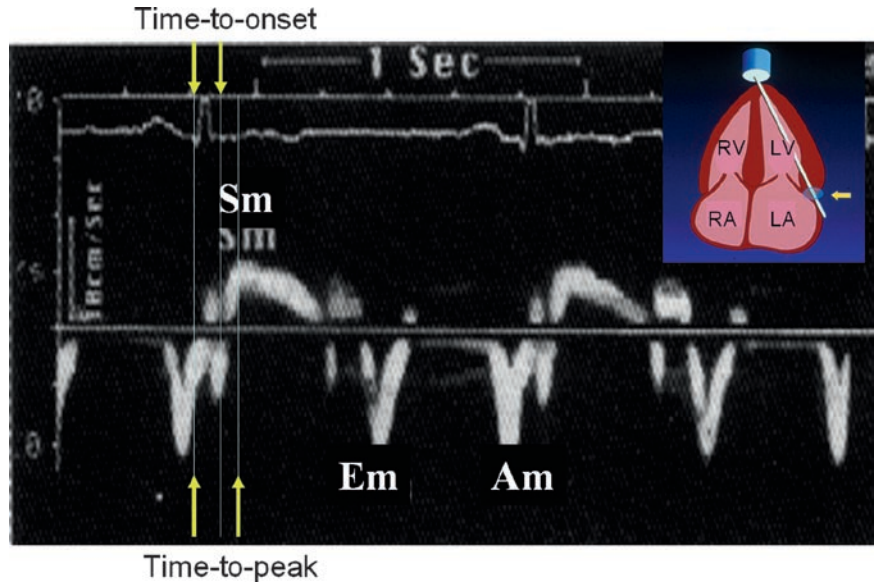

Fig. 22.9 Pulsed-wave Tissue Doppler Imaging with the sample volume located at the lateral wall. The time-to-peak and the time-to-onset intervals are demonstrated

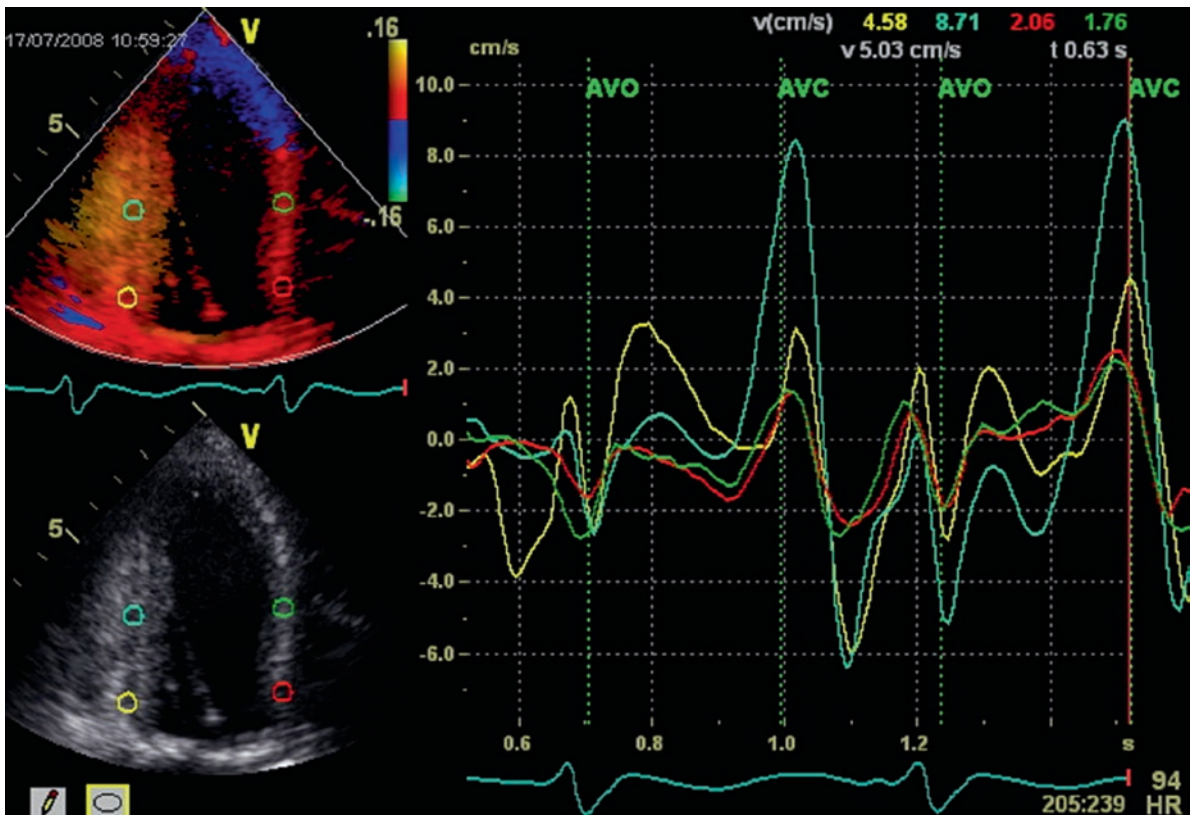

Fig. 22.10 Tissue velocity imaging from apical two-chamber projections from a patient with LBBB that demonstrates no dyssynchrony in the two opposing walls at proximal and midventricular levels

the paired tracing should be superimposed, when there is dyssynchrony, there will be a delay of the lateral wall by *≥60 ms*.[15]

Others have used a four-segment model (apical four- and two-chamber views) when a delay *≥65 ms* between any two walls would indicate dyssynchrony.

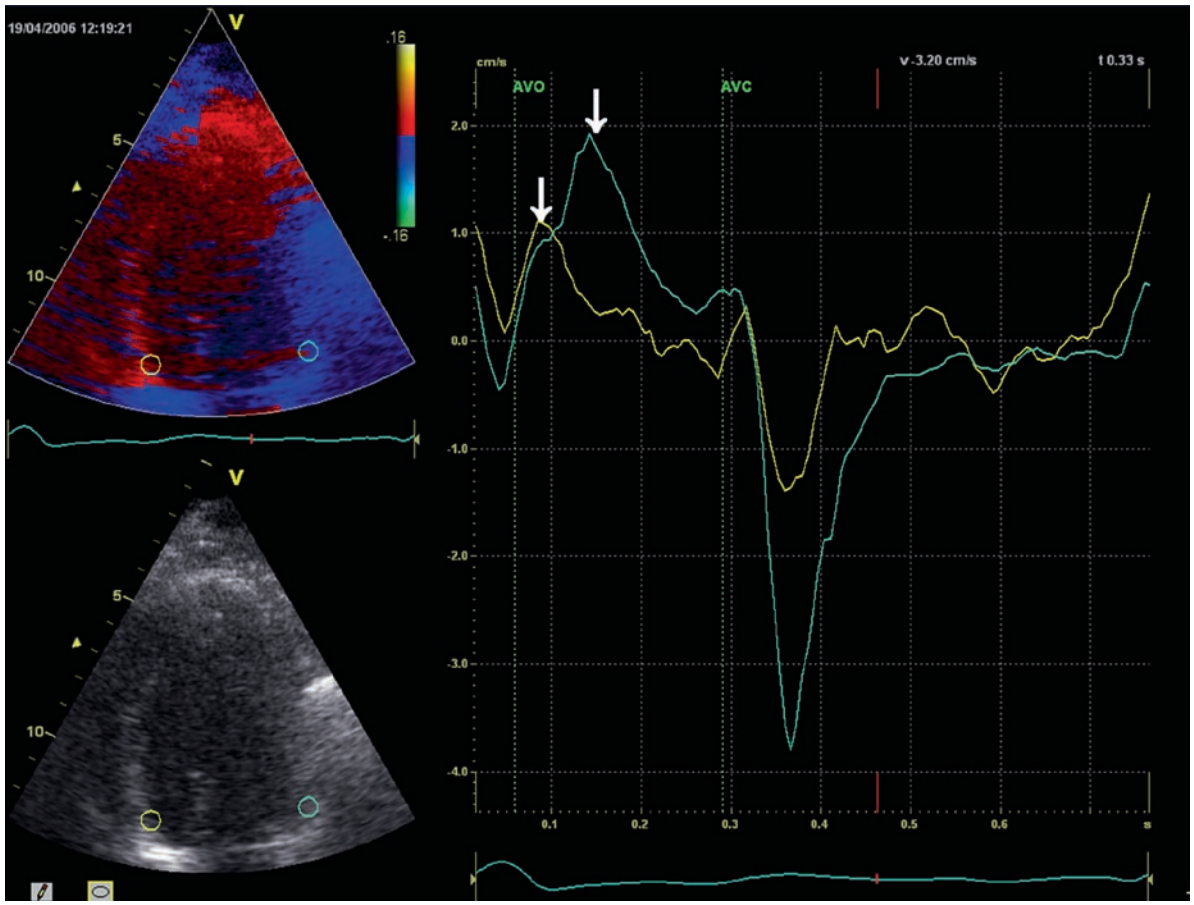

Fig. 22.11 LV dyssynchrony assessment using color-coded tissue Doppler imaging. The sample volumes are simultaneously placed in the basal parts of the septum and lateral wall with the corresponding traces. The delay in peak systolic velocity between the septum and the lateral wall is 70 ms (*yellow curve* septum; *green curve* lateral wall; *arrows* indicate peak systolic velocity; *AVO* aortic valve opening; *AVC* aortic valve closure)

Finally, Yu et al[16] used TDI to assess intraventricular dyssynchrony in 88 normal individuals, 67 patients with heart failure and a narrow QRS complex (>120 ms), as well as in 45 patients with a wide QRS complex (>120 ms). In this study, 12 sample volumes were placed in the myocardium and for each sample the time from onset-to-peak systolic velocity was measured. From these data, two parameters indicating intraventricular dyssynchrony were derived:

a. The maximal difference between peak systolic velocities of any two of the 12 segments. Intraventricular dyssynchrony defined as a difference *>100 ms* and
b. The standard deviation of all 12 time intervals measuring time-to-peak systolic velocity. Intraventricular dyssynchrony was defined as a standard deviation of *33 ms*, also referred to as dyssynchrony index.

They demonstrated absence of intraventricular dyssynchrony in normal individuals, whereas 73% of patients with a wide QRS had intraventricular dyssynchrony. Of interest, 51% of the patients with a narrow QRS complex also exhibited substantial intraventricular dyssynchrony suggesting that patients with heart failure and a narrow QRS may also exhibit dyssynchrony!

Summary

Advantages:

- High temporal resolution (>100 fps)
- Allows sampling of multiple segments simultaneously from one image

- Allows further parameter processing by offline analysis (displacement, strain rate, strain)

Disadvantages:

- Requires high-end ultrasound equipment
- Susceptible to translational motion or tethering effect

3. One limitation of TDI is that it does not distinguish between active and passive wall motion. Strain rate analysis helps in differentiating this and therefore provides more accurate information on regional myocardial contractile function. Using the digitally stored color-coded tissue Doppler images further extended offline analysis can be performed using deformation parameters. Strain analysis allows direct assessment of the degree of myocardial deformation during systole and is expressed as the percentage of segmental shortening or lengthening in relation to its original length.[17-19] it provides information on the timing of onset and peak of myocardial contraction, permitting measurement of (dys-) synchrony (Fig. 22.12). Compared to TDI, the main

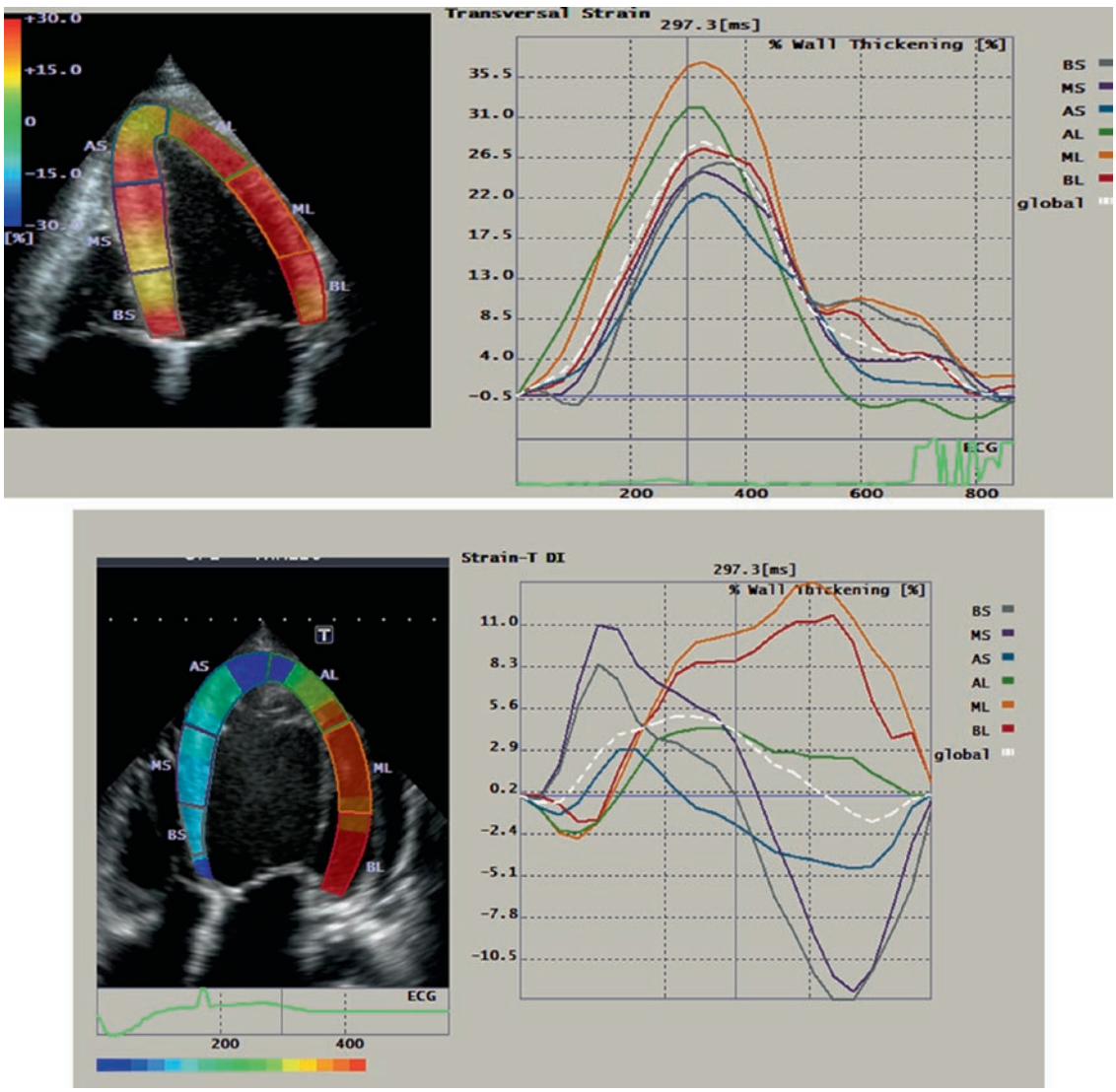

Fig. 22.12 Myocardial deformation as assessed by strain rate imaging. Negative strain indicates shortening and is expressed as the percentage from its initial end-diastolic length (%). On the *top*, strain curves obtained from six segments show synchronous onset and peak shortening in a normal individual. On the *bottom*, a delay in the onset and the peak of lateral wall shortening (*yellow curve*) is observed in a patient with heart failure and left bundle branch block

advantage of strain rate imaging resides in the better differentiation between active systolic contraction and passive displacement, which is of particular importance in ischemic patients with scar tissue. The disadvantage of these measurements is that they are hardly reproducible.

Summary

Strain imaging – TDI derived

Advantages:

- High temporal resolution (>200 fps for individual wall imaging, >100 for whole apical views)
- Less affected by translational and tethering motion

Disadvantages:

- Time-consuming image analysis
- High angle dependency: difficult in spherical heart
- Poor reproducibility
- Requires specific software
- Highly dependent on image quality: not feasible in all patients

4. Tissue or speckle tracking provides a color-coded display of myocardial displacement allowing for an easy and quick visualization of LV dyssynchrony and the region of the latest activation. It visualizes the longitudinal motion by frame-to-frame tracking of acoustic markers (speckle amplitude) in each myocardial segment during systole in a color-coded format and has been used to determine the extent of myocardium with delayed longitudinal contraction. Sogaard et al[20] pioneered this approach and demonstrated that the number of segments with delayed longitudinal contraction was related to the improvement of LV ejection fraction after CRT. Figure 22.13 is from a patient in sinus rhythm demonstrating a synchronous longitudinal strain from apical four-chamber view.

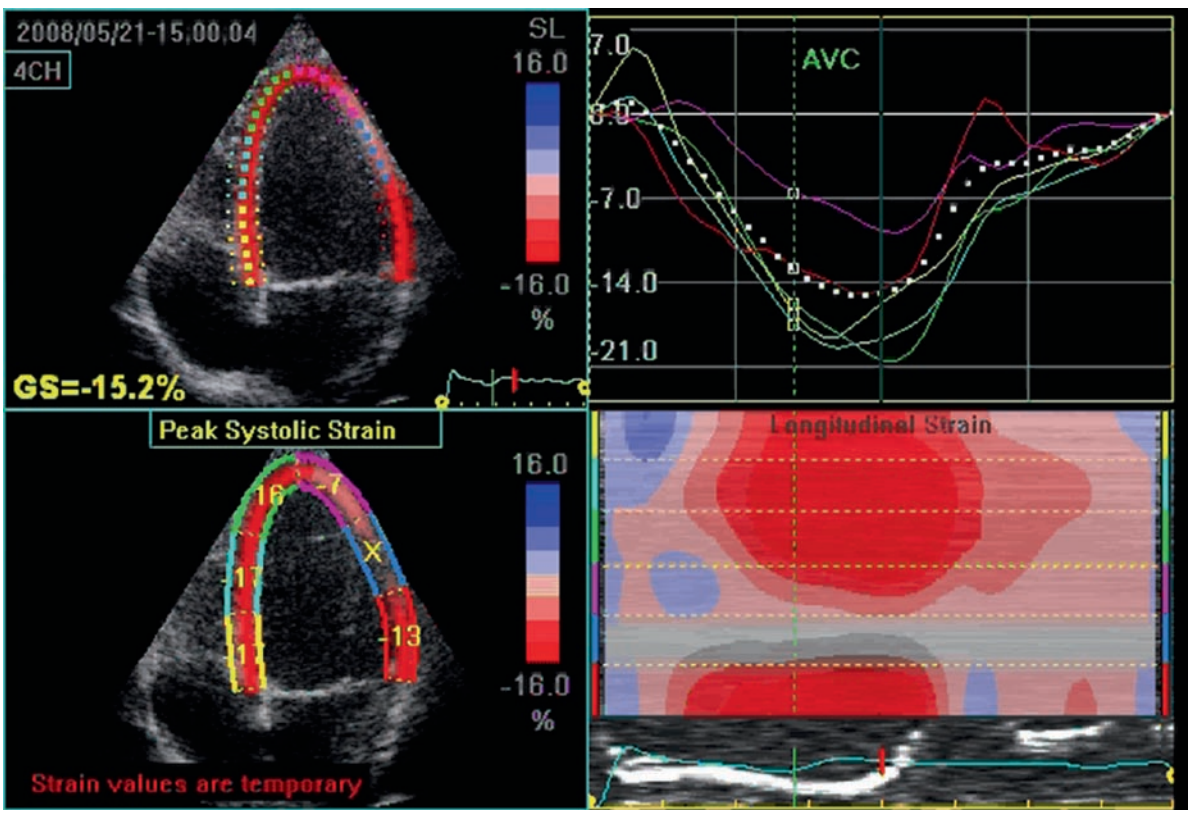

Fig. 22.13 Speckle tracking in cardiomyopathy patient. In this four-chamber view the six myocardial regions are displayed posteriorly (negative strain) in a synchronous manner but with increasing amplitudes from apex to base

Summary

Advantages:

- Less affected by translational and tethering motion
- Less time resolution (>40–80 fps)
- Nearly automated analysis: less variability

Disadvantages:

- Requires specific software
- Highly dependent on 2-D image quality: not feasible in all patients

Determining Optimal Lead Placement During Implantation

This primarily relates to the positioning of the left ventricular pacemaker lead by a transvenous approach via the coronary sinus and careful evaluation of the venous anatomy prior to lead placement. The role of echocardiography will be to identify the most delayed myocardial region by any of the previously described techniques. However, this implies having an ultrasound system in the catheter lab and may prolong the time of an already long procedure. It is therefore preferred to perform the patient's evaluation prior to pacemaker implantation. One major limitation of all TDI methods is that very often the most delayed region is the cardiac apex, which is not possible to be examined using tissue Doppler techniques. This may however may be ultimately very important as pacing strategy may need to be rethough and consider epicardial pacing of the apex.

Cardiac magnetic resonance imaging may also have an important complementary role by ruling out the presence of transmural scar in ischemic patients, particularly in the lateral wall as by pacing scar tissue it is unlikely that any benefit may be derived. Ultimately however, the electrophysiologist may be limited by choice of pulmonary venous anatomy for positioning of the pacing leads.

AtrioVentricular (AV) Optimization

Following successful implantation of the pacing device, it is important to optimize the AV delay so that the maximal ventricular performance may be obtained. Several acute pacing studies have demonstrated the importance of a short AV delay in providing hemodynamic benefit (Fig. 22.2a). The aim of AV optimization is to avoid LV systolic contraction occurring after incomplete LV filling.

The optimization of AV delay following pacemaker implantation can be achieved with pulsed Doppler echocardiography using the combination of the transmitral velocities and the LV outflow track velocity. Optimization should be performed at the patient's intrinsic heart rate when possible. Starting with a long AV delay, such that there is intrinsic conduction and no biventricular pacing. The transmitral pulsed-wave Doppler is then measured. The AV delay is then gradually reduced in 20-ms intervals and the LV filling time measured. This is done until the end of the A wave on transmitral flow (corresponding to LA contraction) occurs just prior to the onset of aortic systolic Doppler velocity or the closure of the mitral valve. There should be a progressive lengthening of LV filling time with clear separation of the E and A waves. As a general rule, the optimal AV delay should provide the longest LV filling time without premature truncation of the A-wave by mitral valve closure.

The mitral regurgitation time is reduced with eradication of the presystolic component. Too short an AV delay, seen by the truncation of the A wave by mitral valve closure, is also suboptimal and will again reduce the LV filling time (Fig. 22.2b).

Alternatively, the AV delay can be programmed guided by the aortic velocity time integral (VTI) with the maximum VTI recorded being defined as the optimal AV delay.

Evaluating the Reverse Remodeling of the Heart During Follow-Up

While the acute effects of CRT may be identified immediately after pacemaker implantation by documenting improved cardiac output and increased LV systolic pressure, the medium (3-months) to long-term (one-year) benefits may be evaluated by regular follow-up Echocardiographic evaluation.

Reversal of LV Dilatation (Reversed Remodeling)

This can be observed within three months following successful biventricular pacing. It is associated with a reduction of LV end-systolic and end-diastolic dimensions and volumes associated with an increase in ejection fraction. It is now well established that accurate assessment of LV volumes may be performed using the biplane Simpson's rule and have a low threshold in using contrast for optimal endocardial border detection. Alternatively, the use of three-dimensional echocardiography for volume calculations should be encouraged.

Improved Diastolic Function

Clinical data in the assessment of diastolic function are limited. Systolic and diastolic parameters can be obtained with conventional Doppler echocardiography and this includes: Diastolic filling time, myocardial performance index (Tei), E/A ratio, E-deceleration time, isovolumic relaxation time, and pulmonary vein flow. The most common change that one may be able to observe is the change of a "restrictive" E/A pattern becoming normalized or a "pseudonormal" pattern been normalized. In general, one would expect that diastolic dysfunction would improve by one grade within three months following successful resynchronization therapy. In the MUSTIC study,[21] Diastolic filling time increased between 13 and 27% and the deceleration time was prolonged in the VIGOR-CHF study.[22]

Effect of CRT on Mitral Regurgitation

Here it is expected to see a significant reduction of mitral regurgitation. In some patients this is seen immediately after CRT, while in others it occurs latter. Mitral regurgitation in heart failure and ventricular dilatation occurs secondary to mitral annulus dilatation leading to reduce mitral leaflet apposition and mitral regurgitation. In addition, regional wall motion abnormalities may result to leaflet tenting exaggerating mitral regurgitation. Finally, LV dyssynchrony itself may lead to mitral regurgitation. Prolongation of AV interval, may delay the onset of LV contraction predisposing to incomplete mitral valve closure with the occurrence of presystolic (diastolic) mitral regurgitation. This presystolic component of mitral regurgitation can effectively be eliminated by pacing with a short (optimized) AV delay as previously stated.

Conclusions

CRT is now considered an established therapy for patients with severe heart failure with good clinical results, although 20–30% of patients do not respond to CRT. At present, patient selection is mainly based on QRS duration.

There are several echocardiographic methods that one can use to evaluate responders to biventricular pacing. The only multicenter study that has evaluated all the parameters to assess which can best predict responders showed that these measurements were too variable with insufficient sensitivity to be used in everyday clinical practice.[23] Until more multicenter studies are performed, possibly using newer parameters such as real-time three-dimensional echocardiography or speckle tracking, it is important that one obtains a lot of experience using selected parameters in sufficient number of patients to obtain a good experience as these measurements are not easy to perform.

Finally, echocardiography can guide LV lead positioning and may be used to optimize AV delay and V-V delay as well as assessing patients' follow-up.

References

1. Cleland JGF. The heart failure epidemic: Exactly how big is it? *Eur Heart J*. 2001;22:623–626.
2. Abraham WT, Hayes DL. Cardiac resynchronization therapy for heart failure. *Circulation*. 2003;108:2596–2603.
3. Abraham WT, Fisher WG, Smith AL, et al. Cardiac resynchronization in chronic heart failure. *N Engl J Med*. 2002;346:1845–1853
4. ACC/AHA/NASPE 2002 guideline update for implantation of cardiac pacemakers and antiarrhythmia devices. *J Am Coll Cardiol*. 2002;40:1703–1719.
5. Leclercq C, Kass DA. Retiming the failing heart: principles and current clinical status of cardiac resynchronization. *J Am Coll Cardiol*. 2002;39:194–201.
6. Yu CM, Lin H, Zhang Q. High prevalence of left ventricular systolic and diastolic asynchrony in patients with congestive heart failure and normal QRS duration. *Heart*. 2003;89:54–60.

7. Kass DA. Ventricular dyssynchrony and mechanisms of resynchronization therapy. *Eur Heart J*. 2002;4: D23–D30.
8. Grines CL, Bashore TM, Boudoulas H, Olson S, Shafer P, Wooley CF. Functional abnormalities in isolated left bundle branch block. The effect of interventricular asynchrony. *Circulation*. 1989;79:845–853.
9. Park RC, Little WC, O'Rourke RA. Effect of alteration of left ventricular activation sequence on the left ventricular end-systolic pressure-volume relation in closed-chest dogs. *Circ Res*. 1985;57:706–717.
10. Rouleau F, Merheb M, Geffroy S, et al. Echocardiographic assessment of the interventricular delay of activation and correlation to the QRS width in dilated cardiomyopathy. *Pacing Clin Electrophysiol*. 2001;24:1500–1506.
11. Pitzalis MV, Iacoviello M, Romito R, et al. Cardiac resynchronization therapy tailored by echocardiographic evaluation of ventricular asynchrony. *J Am Coll Cardiol*. 2002;40:1615–1622.
12. Kuhl HP, et al. High-resolution transthoracic real-time three-dimensional echocardiography: quantitation of cardiac volumes and function using semi-automatic border detection and comparison with cardiac magnetic resonance imaging. *J Am Coll Cardiol*. 2004;43(11):2083–2090.
13. Jenkins C, et al. Reproducibility and accuracy of echocardiographic measurements of left ventricular parameters using real-time three-dimensional echocardiography. *J Am Coll Cardiol*. 2004;44(4):878–886.
14. Kapetanakis S, et al. Real-time three-dimensional echocardiography: a novel technique to quantify global left ventricular mechanical dyssynchrony. *Circulation*. 2005; 112(7):992–1000.
15. Bax JJ, Molhoek SG, van Erven L, et al. Usefulness of myocardial tissue Doppler echocardiography to evaluate left ventricular dyssynchrony before and after biventricular pacing in patients with idiopathic dilated cardiomyopathy. *Am J Cardiol*. 2003;91:94–97.
16. Yu CM, Chau E, Sanderson JE, et al. Tissue Doppler echocardiographic evidence of reverse remodeling and improved synchronicity by simultaneously delaying regional contraction after biventricular pacing therapy in heart failure. *Circulation*. 2002;105:438–445.
17. Bax JJ, Marwick TH, Molhoek SG, Bleeker GB, et al. Left ventricular dyssynchrony predicts benefit of cardiac resynchronization therapy in patients with end-stage heart failure before pacemaker implantation. *Am J Cardiol*. 2003;92:1238–1240.
18. Heimdal A, Stoylen A, Torp H, Skjaerpe T. Real-time strain rate imaging of the left ventricle by ultrasound. *J Am Soc Echocardiogr*. 1998;11:1013–1019.
19. D'hooge J, Heimdal A, Jamal F, et al. Regional strain and strain rate measurements by cardiac ultrasound: principles, implementation and limitations. *Eur J Echocardiogr*. 2000;1:154–170.
20. Sogaard P, Egeblad H, Pedersen AK, et al. Sequential versus simultaneous biventricular resynchronisation for severe heart failure: evaluation by tissue Doppler imaging. *Circulation*. 2002;106:2078–2084.
21. Linde C, Leclercq Ch, Rex S, et al. Long-term benefits of biventricular pacing in congestive heart failure: results from the MUltisite STimulation In Cardiomyopathy (MUSTIC) study. *J Am Coll Cardiol*. 2002;40:111–118.
22. Saxon LA, De Marco T, Schafer J, et al. Effects of long-term biventricular stimulation for resynchronization on echocardiographic measures of remodeling. *Circulation*. 2002;105:1304–1310.
23. Chung ES, Leon AR, Tavazzi L, et al. Results of the Predictors of Response to CRT (PROSPECT) trial. *Circulation*. 2008;117:2608–2616.

Section 5
Masses, Emboli and Trauma

Chapter 23
Intracardiac Masses

William Smith, David Adams, and Joseph Kisslo

Masses within the heart are most commonly due to thrombus formation or vegetations associated with endocarditis. Two-dimensional echocardiography is much better than M-mode for the detection and localization of any intracardiac mass. Thrombus formation is usually associated with an abnormally moving wall and may be very small and layered or in a case of dilated cardiomyopathies very large and pedunculated.

Most commonly a thrombus will occur in three clinical settings: recent myocardial infarctions, dilated (congestive) cardiomyopathies, and within chronic left ventricular aneurysms. The echocardiographic appearance of a thrombus can vary from a small, immobile mural thrombus (Fig. 23.1) to a large protruding mobile thrombus (Fig. 23.2) or in some instances multiple thrombi (Fig. 23.3). By far, the most difficult to diagnose is a small, immobile, apical mural thrombus. These small mural thrombi are often less echo dense and therefore more difficult to distinguish from underlying myocardium.

Left Ventricular Thrombi

A left ventricular (LV) thrombus is a common complication of acute myocardial infarction, chronic left ventricular aneurysm, or chronic dilated cardiomyopathy. The diagnosis of LV thrombus has important clinical ramifications, as stroke or peripheral embolism may occur, and anticoagulation or other therapeutic interventions need to be considered. The first M-mode ultrasound image of a left ventricular thrombus was published in 1976.[1] Today, transthoracic echocardiography is the *de facto* standard for the diagnosis of left ventricular thrombus. The diagnosis of left ventricular thrombus is usually based on the following criteria: underlying wall-motion abnormality and cardiac mass that can be distinguished from the surrounding myocardium through different acoustic characteristics.

In one recent year at Duke University Medical Center, nearly 15,000 echocardiograms were performed and interpreted. The overall incidence of definite or probable LV thrombus interpreted from those echoes was 1.16%. If only the ~2,000 echocardiograms in which there was significant LV systolic dysfunction (ejection fraction less than or equal to 35%) present are considered, however, the incidence was 8.6%. The prevalence of LV thrombus varies depending on the clinical correlate. In dilated cardiomyopathy, historical rates of thrombus range from 28 to 48%,[2] and one recent study reports a rate of 27%,[3] suggesting that the prevalence has not been dramatically altered in the new era of congestive heart failure management. In the setting of acute myocardial infarction (MI), LV thrombus occurs as a complication with a frequency of 7–20%, more often if the MI is anterior or apical. With chronic ventricular aneurysm, the prevalence of LV thrombus is up to 50%.[4]

As the prevalence of LV thrombus varies by the clinical scenario, so do the embolic complications. Despite the high incidence of LV thrombus in the presence of ventricular aneurysm, thromboembolic complications rarely occur. In contrast, the presence of LV thrombus by echo after an acute MI predicts over a fivefold greater risk for developing thromboembolism.[5] Recently, LV thrombus by echo has also been documented to be an independent predictor of stroke in the setting of dilated cardiomyopathy.[6] Due to the low incidence of complication from thrombus in the setting of chronic aneurysm,

W. Smith, D. Adams, and J. Kisslo (✉)
Division of Cardiovascular Medicine, Duke University Medical Center, Durham, NC, USA
e-mail: joseph.kisslo@duke.edu

P. Nihoyannopoulos and J. Kisslo (eds.), *Echocardiography*,
DOI: 10.1007/978-1-84882-293-1_23, © Springer-Verlag London Limited 2009

anticoagulation is rarely used in this population. Short-term anticoagulation is recommended at discharge in patients who have a thrombus complicating an anterior MI. The utility of warfarin in the setting of dilated cardiomyopathy and LV thrombus is still debated; clinical trials are ongoing.

Multiple authors have demonstrated the accuracy of echocardiography as a tool to identify LV thrombi. Reeder[7] identified LV thrombus by echo in 14 patients who ultimately underwent surgical evaluation of the left ventricle or autopsy. Thrombus was present at the gold standard examination in 11 of these patients (positive predictive value = 79%), a rate superior to that of angiography. In 67 patients at high risk for LV thrombus formation, Visser[8] demonstrated a sensitivity of echocardiography of 92% and specificity of 88%, compared to a gold standard of aneurysmectomy or autopsy. Stratton[9] compared echocardiography to the gold standard of autopsy, aneurysmectomy, or Indium scan and showed similar results (sensitivity and specificity of 86–95%). More recently, it was demonstrated that the addition of echocardiographic contrast agent to a nondiagnostic chest wall study resulted in a definitive scan in 90% of cases.[10]

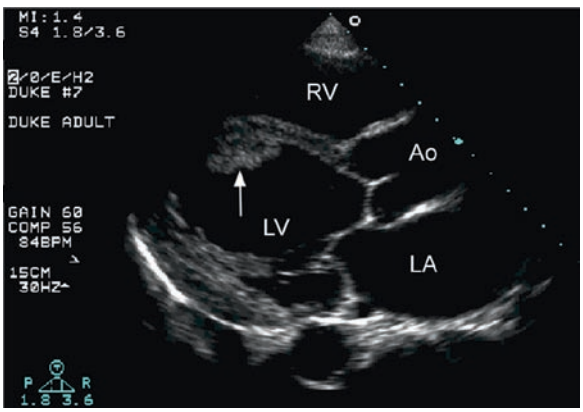

Fig. 23.1 An immobile thrombus is seen on the distal septal wall (*arrow*) in a patient with an ischemic cardiomyopathy. This is a left parasternal long-axis view

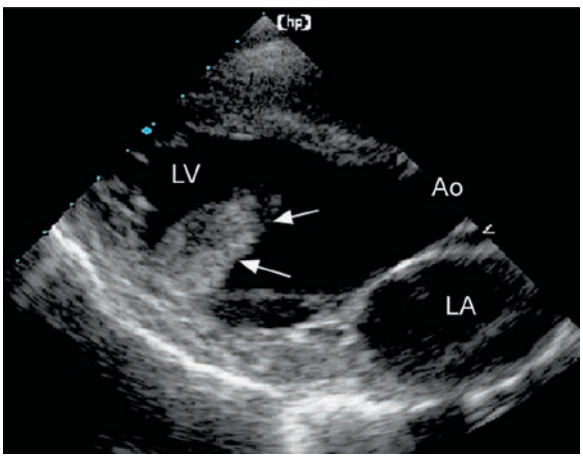

Fig. 23.2 A large, mobile left ventricular thrombus (*arrows*) in seen in this parasternal long-axis view

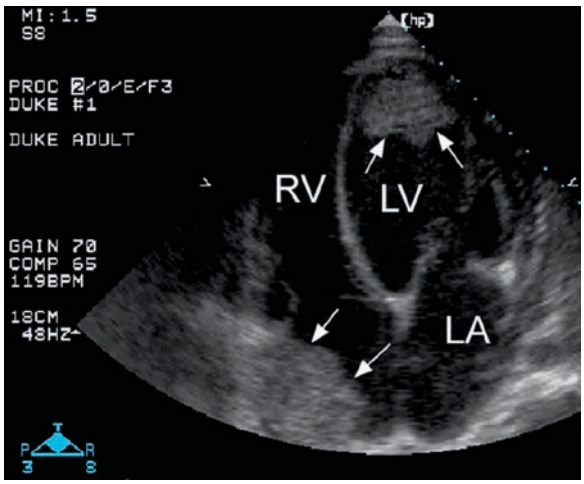

Fig. 23.3 Apical four-chamber view in a patient with both a left ventricular apical thrombus (*arrows*) and a right atrial thrombus (*arrows*)

Despite its documented utility, imaging of the left ventricular thrombus remains a challenge. A recent study documented a fourfold difference in the prevalence of interpreted left ventricular thrombi among different readers, even in the same population of patients![11] A recent evaluation of 300 patients in the Duke Heart Failure Clinic revealed apical echocardiographic abnormalities in over 70% of patients with severe left ventricular systolic dysfunction.[12] The abnormalities were not always thrombi, but the frequent presence of trabeculations, artifact, papillary muscles, and tendons complicates the interpretation of thrombus. Surprisingly high rates of visible trabeculations and bands (up to 15% or greater) are visible at the apex in populations at risk for ventricular thrombi. None of the currently available diagnostic criteria for LV thrombus (Table 23.1) is sufficient to definitely exclude some of the alternative apical findings when a thrombus is suspected.

Technical difficulties provide further barriers to imaging of a cardiac apex to exclude or confirm thrombus. Patients at risk for thrombus (cardiomyopathies,

prior myocardial infarctions) often have other comorbidities or body habitus which makes imaging difficult. The physical characteristics of the ultrasound must be optimized by an experienced sonographer to improve near-field visualization.

One recent advance for the detection of left-sided thrombi or masses is the use of contrast agents that can cross the pulmonary circulation. Figure 23.4 demonstrates the use of such a contrast agent to opacify the left atrium and ventricle and in doing so delineates a left ventricular apical thrombus that was not seen in the noncontrasted images.

The ability of transesophageal echocardiography (TEE) to detect clots in the left atrium and especially the left atrial appendage is well documented. Figure 23.5 shows a thrombus in the left atrial appendage of a patient who was to undergo electrical cardioversion for their atrial fibrillation.

Figure 23.6 is from a patient with a long history of severe mitral stenosis. He now has pulmonary hypertension and this apical four-chamber view demonstrates not only enlargement of the right and left atria but the presence of a large mass in the left atrium (arrows). Given this patient's history this mass is most likely a thrombus.

The left side of the heart is certainly not the only place that thrombi can occur. Figure 23.7 is an apical

Table 23.1 Characteristics used to describe the LV apex in patients with dilated cardiomyopathy

Well-defined border between abnormal echoes and myocardial cavity
Distinct delineation between abnormal echoes and endocardium
Different acoustic characteristics between echoes and myocardium
Apical wall motion abnormality (hypokinetic or worse)
Abnormal echoes seen in two or more views
Abnormal echoes seen throughout cardiac cycle
Abnormal echoes distinct from papillary muscle or trabeculation
Contrast filling defect at site of abnormal echoes

Stratton describes an LV thrombus as "contiguous with the endocardium"

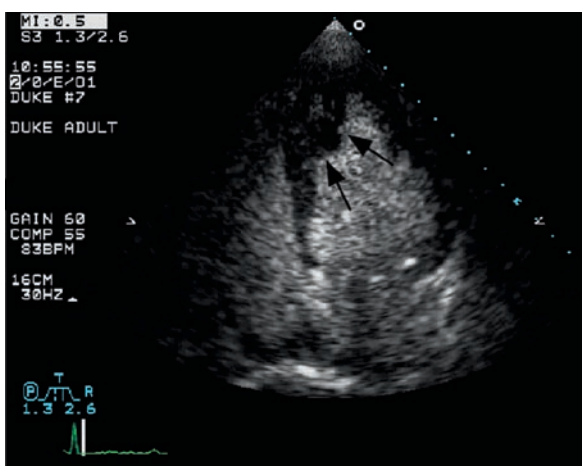

Fig. 23.4 A contrast study demonstrates a probable left ventricular apical thrombus (*arrows*)

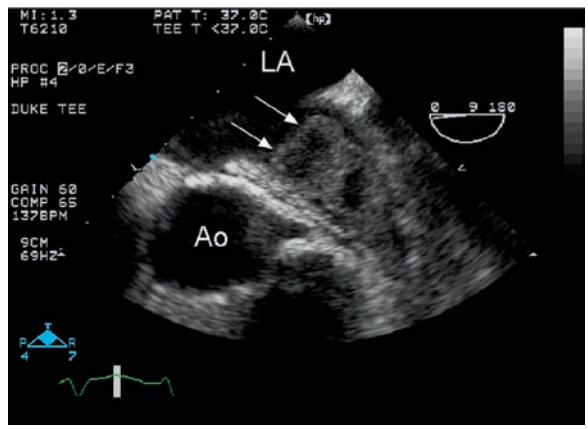

Fig. 23.5 A TEE was performed and the arrows point to a large thrombus in the left atrial appendage

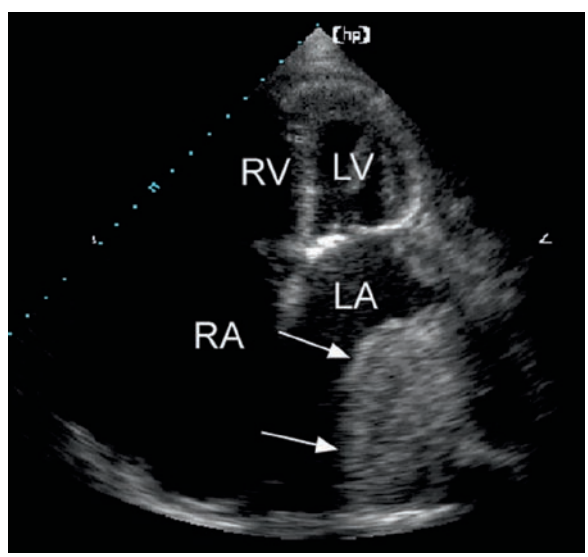

Fig. 23.6 This apical four-chamber view was obtained from a patient with mitral stenosis. There is a large left atrial mass (*arrows*) which probably is a thrombus

four-chamber view in a patient with a large multilobulated mass (arrows) in the right atrium. This mass is seen to be traversing the tricuspid valve during diastole.

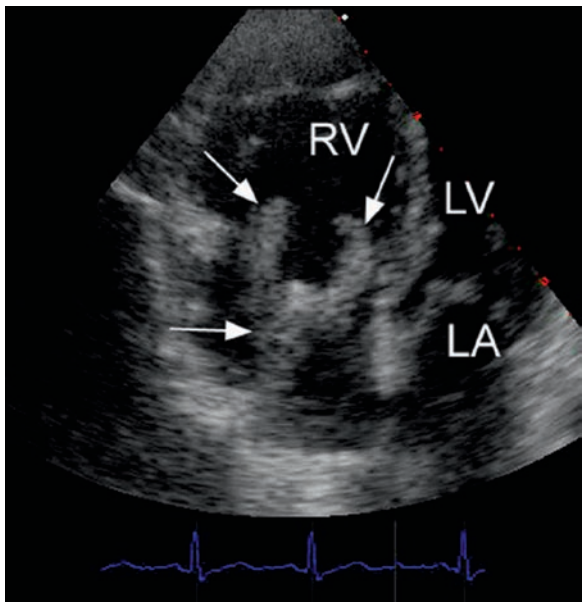

Fig. 23.7 A large multilobulated mass is seen in the apical four-chamber view. The mass is seen to move through the tricuspid valve during diastole

Myxomas

Of all the cardiac tumors myxomas are by far the most common. These are usually located in the left atrium and are pedunculated with their attachment to the atrial septum. A large left atrial myxoma is seen in the echocardiogram in Fig. 23.8. These images were obtained simultaneously using a transducer that can image in two planes at once. The myxoma is seen to prolapse through the mitral valve in diastole on the left in the long axis and is seen under the aorta in the short axis on the right.

In Fig 23.9 a large mass is seen in the left atrium occluding the mitral inflow during diastole. On the left this mass is seen by transthoracic and on the right by transesophageal echocardiography. Transesophageal echocardiography is particularly helpful in defining the point of attachment for patients with myxomas. Figure 23.10 shows a nonpedunculated left trial myxoma occupying the left atrium.

Myxomas may also be found in the right atrium (Fig. 23.11), the second most common site of occurrence after the left atrium. There are reported cases of biatrial myxomas where they may be found in both left and right atria. The length may range from 2 to 10 cm.

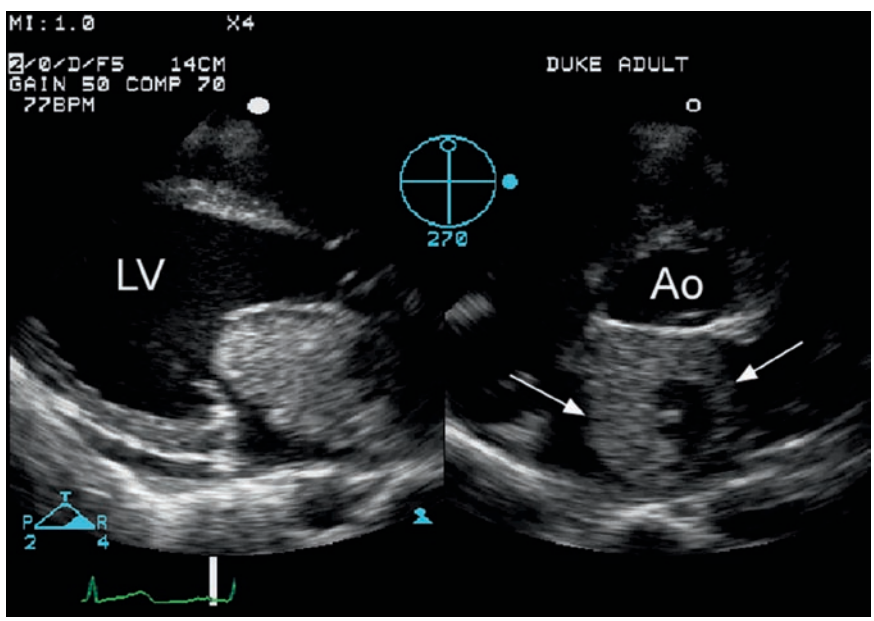

Fig. 23.8 A large left atrial myxoma is seen in the echocardiogram. These images were obtained simultaneously using a transducer that can image in two planes at once. The myxoma is seen to prolapse through the mitral valve in diastole on the left in the long axis and is seen under the aorta in the short axis on the right

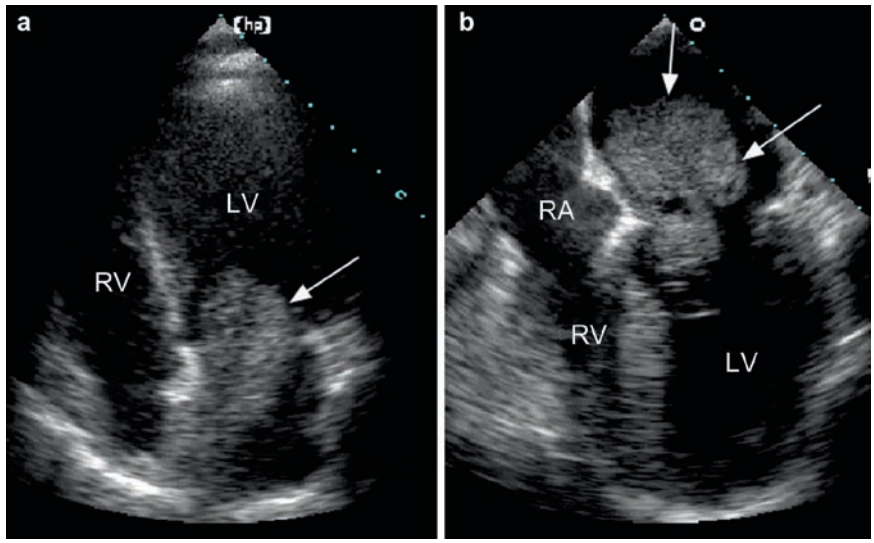

Fig. 23.9 A large mass is seen in the left atrium occluding the mitral inflow during diastole. On the left this mass is seen by transthoracic and on the right by transesophageal echocardiography

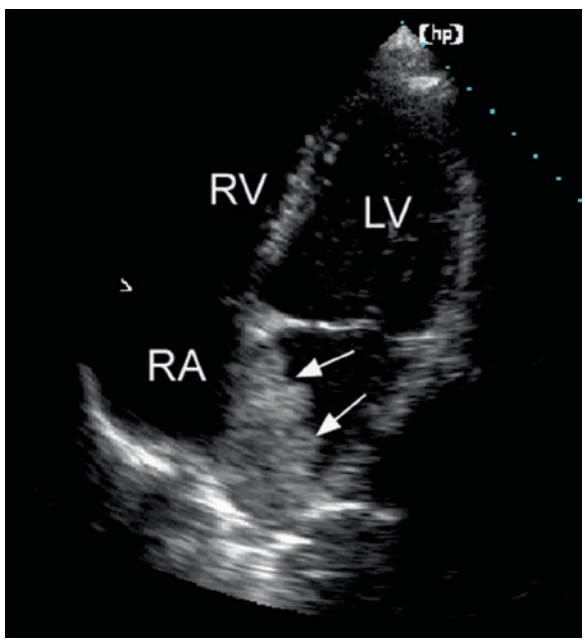

Fig. 23.10 A large left atrial mass is seen in the apical four-chamber view. This mass turned out to be a nonpedunculated left atrial myxoma by the pathology report

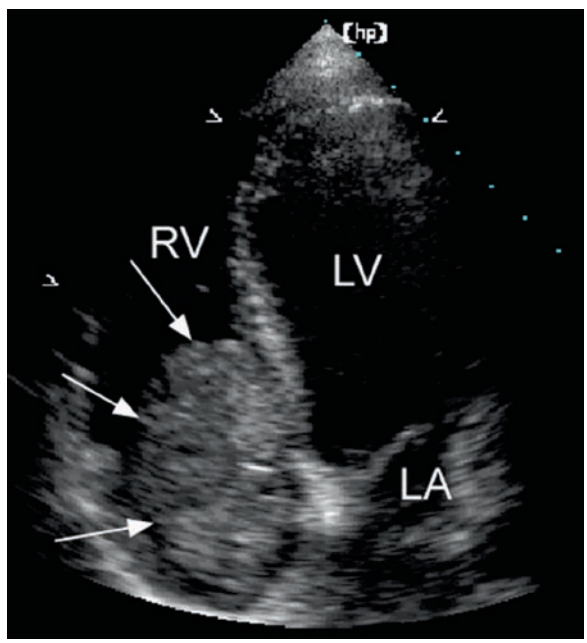

Fig. 23.11 This large right atrial mass (*arrows*) seen in the apical four-chamber view is an atrial myxoma

and occasionally they may show deformation from an impingement upon a valve orifice. Often the clinical signs of left atrium myxomas will mimic those of mitral stenosis.

Other Benign Tumors

Especially in children, rhabdomyomas are the most frequently appearing of the benign ventricular tumors.

Most often seen within the ventricular septum, they may appear in any wall of the chambers or even in the atrial septum. The second most common benign tumor found in the ventricles of children are fibromas followed by myxomas. Most tumors occurring in a ventricular wall or cavity do not produce any symptoms.

Malignant Tumors

Carcinoid syndrome sometimes results in cardiac involvement of valve thickening and stenosis. The most commonly infect valves are the tricuspid and pulmonic. Rhabdomyosarcomas and malignant teratomas are the most common primary malignant cardiac tumors and occur most frequently in the right side of the heart. Other tumors which commonly metastasize to the heart include carcinoma of the lung and breast, malignant melanoma, malignant lymphoma, and leukemia.

Scanning Techniques

Since the majority of left ventricular thrombus occurs at the cardiac apex the apical and subxiphiod windows are the most useful. It can also be helpful to obtain multiple views, often unconventional or foreshortened, with the transducer angled slightly to better visualize the apex. First, use as high a frequency probe as possible. A 5-MHz, short focus probe or even a 7 MHz is ideal. The higher frequency helps in giving better resolution for differentiating between a thrombus and the underlying myocardium. Often times apical thrombus can be obscured by noise artifact, and using a higher frequency transducer there will be less noise artifact introduced in most patients. Noise artifact can also be reduced by decreasing the focal zone to the depth of interest which can improve lateral resolution. Of course with a higher frequency probe there is less penetration, but that is not an issue since you are only looking at the left ventricular apex at a shallow depth (4–6 cm).

In general, always use the highest frequency possible with the lowest transmit power and overall gain settings in order to maximize resolution. Low gain settings will also decrease the occurrence of reverb or ring down artifacts as will sometimes changing scan depth or angle. Finally, document the presence of any mass from more than one echocardiographic view and remember to use nonstandard views in order to interrogate the entire left ventricular apex, left atrium, left atrial appendage or area in question.

Limitations

Many mural thrombi are small or layered, and difficult to differentiate from underlying myocardium. A new thrombus may not be very echogenic and could be missed without a thorough echocardiographic examination. Another problem is in patients with poor sound transmission in which the left ventricular apex is just not seen. Large left-sided trabeculae, anomalous bands, papillary muscles, and reverberations from strong, near-field apical echoes which ring down into the left ventricular cavity further confuse the diagnosis of a mural thrombus.

One further limitation with echocardiographic evaluation of apical thrombus is there is no absolute way to tell if a mass seen in the apex is a thrombus or another type of cardiac mass. Echocardiography can tell the location, size, shape, mobility, and point of attachment of masses, but not histologic evaluation. Patients exhibiting increased chamber size or an abnormally moving wall should be examined using a high-frequency two-dimensional transducer. Even with this technique, it is sometimes difficult to obtain diagnostic echoes in patients with laminated thrombus formation.

References

1. Horgan JH, Shiel FO, Goodman AC. Demonstration of left ventricular thrombus by conventional echocardiography. *J Clin Ultrasound* 1976;4:287–288.
2. Gottgiener JS, Gay JA, VanVoorhees L, DiBianco R, et al. Frequency and embolic potential of left ventricular thrombus in dilated cardiomyopathy: assessment by 2-dimensional echocardiography. *A. J Cardiol* 1983;52:1281–1285.
3. Crawford TC, Smith WT, Velazquez EJ, et al. Prognostic usefulness of left ventricular thrombus by echocardiography in dilated cardiomyopathy in predicting stroke, transient ischemic attack, and death. *Am J Cardiol* 2004;93:500–503.
4. Reeder GS, Lengyel M, Tajik AJ, et al. Mural thrombus in left ventricular aneurysm: incidence, role of angiography, and relation between anticoagulation and embolization. *Mayo Clin Proc* 1981;56:77–81.

5. Vaitkus PT, barnathan ES. Embolic potential, prevention and management of mural thrombus complicating anterior myocardial infarction: a meta-analysis. *J Am Coll Cardiol*. 1993;22:1004–1009.
6. Crawford TC, Smith WT, Velazquez EJ, et al. Prognostic usefulness of left ventricular thrombus by echocardiography in dilated cardiomyopathy in predicting stroke, transient ischemic attack, and death. *Am J Cardiol* 2004;93:500–503.
7. Reeder GS, Tajik AJ, Seward JB. Left ventricular mural thrombus: two-dimensional echocardiographic diagnosis. *Mayo Clin Proc* 1981;56:82–86.
8. Visser CA, Kan G, David GK, et al. Two dimensional echocardiography in the diagnosis of left ventricular thrombus. A prospective study of 67 patients with anatomic validation. *Chest* 1983;2:228–232.
9. Stratton JR, Lighty GW, Pearlman AS, et al. Detection of left ventricular thrombus by two-dimensional echocardiography: sensitivity, specificity, and causes of uncertainty. *Circulation* 1982; 66:156–166.
10. Thanigaraj S, Schechtman KB, Perez JE. Improved echocardiographic delineation of left ventricular thrombus with the use of intravenous second-generation contrast image enhancement. *J Am Soc Echocardiogr* 1999;12:1022–1026.
11. Berger AK, Gottdiener JS, Yohe MA, et al. Epidemiological approach to quality assessment in echocardiographic diagnosis. *J Am Coll Cardiol*. 1999;34:1831–1836.
12. Crawford TC, Smith WT, Velazquez EJ, et al. Prognostic usefulness of left ventricular thrombus by echocardiography in dilated cardiomyopathy in predicting stroke, transient ischemic attack, and death. *Am J Cardiol* 2004;93:500–503.

Chapter 24
Aortic Disorders

Ayan R. Patel, Stefano De Castro, and Natesa G. Pandian

Aortic Imaging

Introduction

With the advent of multiplane transesophageal imaging, echocardiography provides excellent visualization of the thoracic aorta in the majority of patients. Using a combination of right and left parasternal, suprasternal, and subcostal views, significant portions of the thoracic aorta may be visualized by transthoracic imaging. However, the sensitivity of transthoracic imaging for the detection of aortic dissection, intramural hematoma, and atheroma has been limited, making transesophageal imaging the optimal modality for patients in whom these conditions are suspected. Epicardial scanning may also be useful as an adjunct for imaging in the intraoperative setting.

Transthoracic Imaging

In patients with adequate transthoracic windows, transthoracic echocardiography can provide important diagnostic information in patients with suspected aortic disease.

- *Parasternal views*, From the right parasternal view, the aortic valve, aortic root, and ascending aorta can be visualized (Fig. 24.1a, b). In addition, a transverse view of the descending aorta can be obtained from the left parasternal view. Measurement of the aortic annulus, sinus of Valsalva, and ascending aortic diameters can be obtained from the transthoracic parasternal views in most patients. In patients with dissection of the ascending aorta, a dissection flap may be visualized from the parasternal views in patients with good transthoracic windows. The presence of other abnormalities such as aortic insufficiency or a pericardial effusion may provide indirect evidence of a possible dissection. Longitudinal views of the thoracic descending aorta may be obtained from the parasternal short-axis view and subcostal windows (Fig. 24.1c, d).
- *The suprasternal view* allows visualization of the aortic arch and proximal thoracic descending aorta. From this view, pathology such as aortic atheroma or dissection flaps may be seen in some patients (Fig. 24.2). The suprasternal view is also useful for evaluation of aortic coarctation, in which narrowing of the aorta may be visualized; complementary use of Doppler imaging provides evidence of a gradient across the area of stenosis.

Transesophageal Imaging

- *Ascending aorta.* Transesophageal imaging of the ascending aorta is predominantly obtained at the midesophageal level. The short-axis view of the aorta is usually obtained between 30 and 60°. Various levels of the aorta may then be imaged by withdrawing and advancing the probe. A long-axis view of the ascending aorta is obtained by rotating the angle to between 100 and 150°. From this view, the aortic annulus, sinuses of Valsalva, sinotubular junction, and proximal ascending aorta are visible. Further withdrawal of

A.R. Patel (✉), S. De Castro, and N.G. Pandian
Cardiovascular Imaging and Hemodynamic Laboratory, Tufts Medical Center, Tufts University School of Medicine, 800 Washington Street, Box 32Boston, MA, 02111, USA
e-mail: apatel@tufts-nemc.org

P. Nihoyannopoulos and J. Kisslo (eds.), *Echocardiography*,
DOI: 10.1007/978-1-84882-293-1_24,

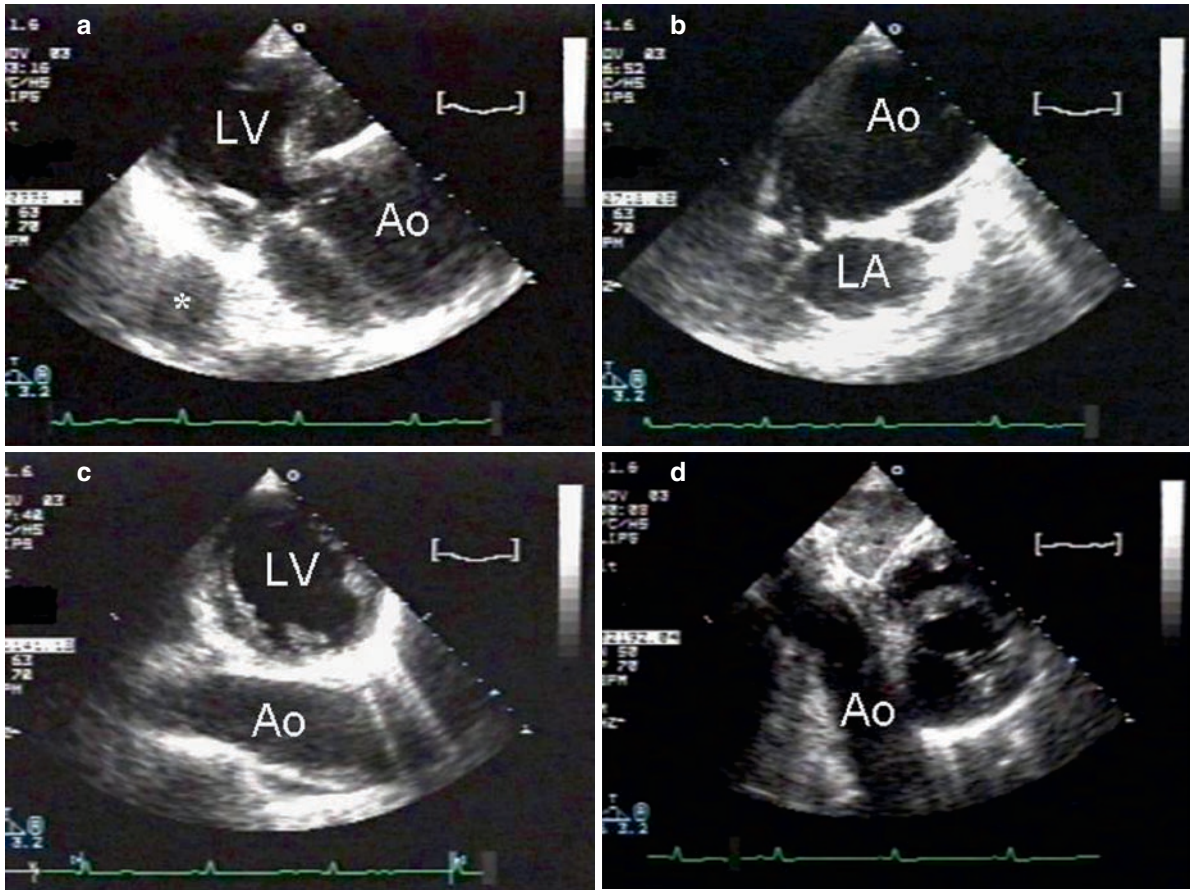

Fig. 24.1 Transthoracic imaging in a patient with an ascending aortic aneurysm and dilated descending aorta. (**a**) Left parasternal longitudinal view of the ascending aorta (transverse view of the descending aorta is marked with *asterisk*); (**b**) right parasternal view of the ascending aorta; (**c**) parasternal short-axis view of the descending aorta; (**d**) subcostal view of the descending aorta. *Ao* aorta; *LA* left atrium; *LV* left ventricle

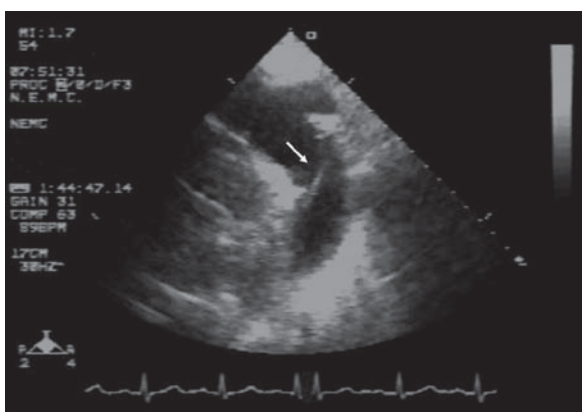

Fig. 24.2 Transthoracic imaging in the suprasternal view demonstrating a dissection flap (*arrow*) in the proximal descending thoracic aorta

the probe permits visualization of the more superior aspects of the ascending aorta in most patients. A portion of the distal ascending aorta is typically not visualized due to the intervening trachea.

- *The descending thoracic aorta*. It is visualized by rotating the probe counterclockwise, until a circular cross-sectional view of the aorta is obtained. Figure 24.3 demonstrates a transverse view of the descending aorta by transesophageal echo, in a patient with a mediastinal tumor. As the probe is withdrawn, more proximal aspects of the descending aorta are visualized. With further withdrawal of the probe, the aortic arch may be seen. Turning the probe clockwise allows visualization of the more proximal portion of the aortic arch. In some patients, the

origin of the left subclavian and left carotid arteries may also be seen by withdrawal of the probe from the aortic arch level.

Aortic Aneurysm

Definition

Aneurysms are defined as localized dilatation of the aorta (Fig. 24.1), typically at least 50% enlarged compared to normal diameter.[1] Normal aortic diameter values are shown in Table 24.1. Aortic diameter normally increases with age, usually expanding by 1–2 mm over a 10-year period.[2]

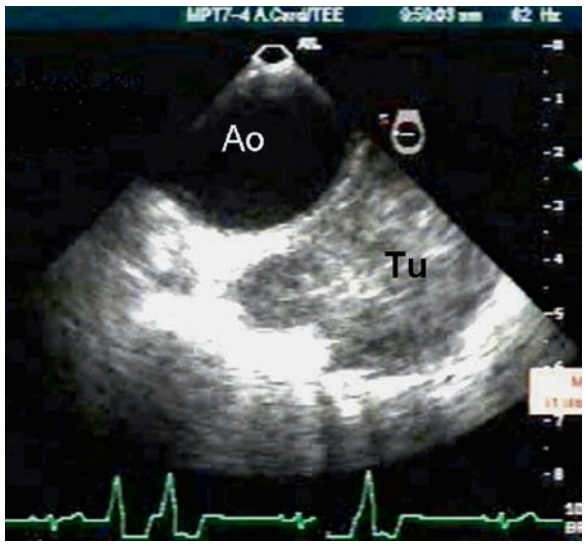

Fig. 24.3 Transesophageal echo transverse image of the descending aorta in a patient with an adjacent mediastinal tumor. *Ao* aorta; *Tu* tumor

Etiologies

Underlying conditions that cause degeneration of the medial layer of the aortic wall predispose to the development of aneurysms. The major causes of such degenerative changes include hypertension, atherosclerosis, poststenotic dilation, and inherited connective tissue disorders (such as Marfan's or Ehlers–Danlos syndrome). Bicuspid aortic valve and aortic coarctation are hereditary conditions that are associated with an increased prevalence of aortic aneurysm. Rarely, aortic dilatation may occur due to inflammatory vasculitis, such as Takayasu's disease, or infectious causes, such as syphilis. Localized forms of aneurysm include sinus of Valsalva aneurysms (Fig. 24.4), which may rupture into the right heart or interventricular septum, and annuloectasia, which involves dilatation of the aortic annulus and root.

Pseudoaneurysms

Pseudoaneurysms are characterized by partial disruption of the aortic wall and are contained by the adventitia and some of the medial layer. Pseudoaneurysms may occur due to hemorrhage of a penetrating aortic ulcer, infection, or trauma.

Aortic Rupture

Aortic Rupture is the most common cause of death associated with aortic aneurysms. It has been observed that aneurysms that are 6 cm or greater in diameter have a five-fold increase in risk of rupture, and that aneurysms that are 5–6 cm in diameter have a more rapid growth rate than smaller aneurysms.

Table 24.1 Mean and upper normal limits for aortic root dimensions

		Men		Women	
		Absolute (cm)	Indexed (cm/m^2)	Absolute (cm)	Index (cm/m^2)
Annulus	(upper limit)	3.1	1.6	2.6	1.6
	(mean ± SD)	2.6 ± 0.3	1.3 ± 0.1	2.3 ± 0.2	1.3 ± 0.1
Sinus of Valsalva	(upper limit)	4.0	2.1	3.6	2.1
	(mean ± SD)	3.4 ± 0.3	1.7 ± 0.2	3.0 ± 0.3	1.8 ± 0.2
Supraaortic ridge	(upper limit)	3.6	1.9	3.2	1.9
	(mean ± SD)	2.9 ± 0.3	1.5 ± 0.2	2.6 ± 0.3	1.5 ± 0.2
Proximal Ascending aorta	(upper limit)	3.7–3.8		3.7–3.8	
	(mean ± SD)	3.0 ± 0.4	1.5 ± 0.2	2.7 ± 0.4	1.6 ± 0.3

Adapted from Erbel et al.[8] and Roman et al.[22]

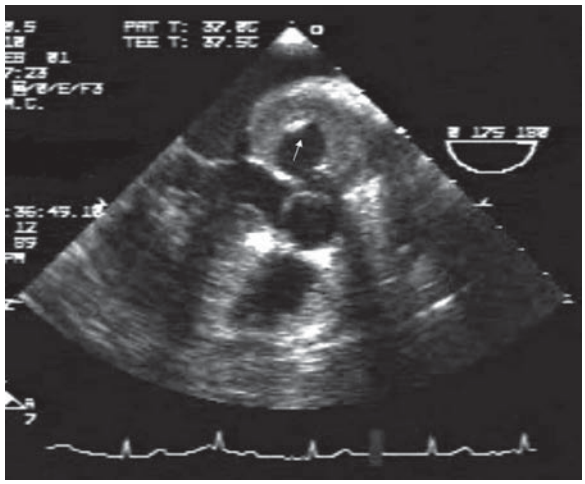

Fig. 24.4 Transesophageal echo image of a thrombosed Sinus of Valsalva aneurysm (*arrow*)

For this reason, aortic root replacement should be considered when aortic root diameter reaches 5.5–6 cm. In patients with Marfan's syndrome and a thoracic aortic aneurysm, elective root replacement is recommended when the aortic root diameter exceeds 5 cm.[1,2]

Imaging

In most cases, aneurysms can be adequately visualized with transthoracic echocardiography; in patients with known aneurysms, serial evaluation should be performed to assess for increase in aneurysmal size. Transesophageal echocardiography can help to define the shape and the extent of the aneurysm and visualize the descending thoracic aorta.

Aortic Dissection

Aortic dissection involving the ascending aorta is associated with an extremely high mortality, if untreated, and prompt diagnosis is therefore crucial. The reported incidence of aortic dissection is approximately 2,000 new cases annually in the United States. There is a 1–2% mortality associated with each passing hour after the development of an acute ascending aortic dissection, reaching up to 30% at 48 h.[3]

Imaging

The primary imaging modalities for diagnosing aortic dissection are transesophageal echocardiography, computed axial tomography (CT), and aortography. Magnetic resonance imaging can also provide high-resolution images, but is generally impractical in the acute setting. Transthoracic echocardiography may detect dissection in some patients, but has a lower sensitivity than transesophageal echocardiography. Transesophageal echocardiography has the advantage of being a versatile, relatively noninvasive technique that can be performed rapidly at the bedside. In addition, it avoids some of the risks associated with aortography, such as the use of contrast and introduction of intravascular catheters.

The reported sensitivities and specificities for detection of aortic dissection are 59–85% and 63–96%, respectively, for transthoracic echocardiography, and 94–100% and 87–100% for transesophageal echocardiography. CT scan has been reported to have a sensitivity ranging from 83 to 100%, and specificity of 87–100%. In ambiguous cases, use of more than one imaging modality may be necessary.

Pathophysiology

The aortic wall is composed of three layers: the outer tunica adventitia, the inner layer of the tunica intima, and the intervening tunica media. The tunica adventitia contains elastic tissue and the vasa vasorum, whereas the tunica media is composed of collagen, elastin, and extracellular matrix proteoglycans. A layer of vascular endothelium comprises the tunica intima. The presence of elastin provides the normal aorta with the ability to withstand pulsatile flow without rupturing. However, abnormalities in the structure of the aortic wall can result in an increased susceptibility to dissection or rupture. With increasing age, the amount of elastin in the aortic media decreases and the amount of collagen increases, thereby increasing vascular stiffness. In addition, dilation of the aorta can result in increased susceptibility to dissection. Increases in wall stress are primarily experienced by the media, and can result from increased aortic radius and increased radial pressure within the vessel. Conversely, wall stress is inversely related to vessel wall thickness. Subsequently, a dilated and thin-walled aorta is subject to increased stress forces. The aortic intimal layer is exposed to shear forces within the

vessel, which can also contribute to the development of dissection. An increase in these stress forces can result in separation of the intimal and medial layers of the aorta. The tear is propagated by shear forces further separating the layers of aortic wall.

Etiologies

Patients with connective tissue disorders, such as Marfan's Syndrome or Ehlers–Danlos Syndrome, are at increased risk for the development of aortic dissection.

1. *Marfan's Syndrome*. There is a deficiency of the glycoprotein fibrillin leading to a loss of elastic tissue and deposition of mucopolysaccharide substances in the aortic media.
2. *Ehlers–Danlos Syndrome* is associated with a collagen defect and subsequent structural abnormalities of the aortic wall.

Both these abnormalities are in the composition of the aortic media that result in an increased vulnerability to dissection. Factors associated with increased risk of dissection in patients with Marfan's Syndrome include advanced age, male gender, aortic root size greater than 60 mm, rate of increase of the aortic diameter, pregnancy, and family history of aortic dissection.[4-6]

3. *Systemic hypertension*. Other conditions which result in disruption of the aortic intima and media can also lead to aneurysmal dilation, increased wall stress, and increased susceptibility to dissection (Table 24.2). Hypertension is associated with degenerative changes in the aortic media. Increased blood pressure and these pathologic changes in the media can result in aortic dilatation and increased susceptibility to dissection in patients with hypertension.
4. *Vasculitis*. In patients with vasculitis, structural changes in the aortic media may weaken the aortic wall.
5. *Thoracic trauma* or iatrogenic injury is another potential cause of aortic dissection. Iatrogenic injury may occur during cardiac surgery, or due to percutaneous intravascular catheter procedures.
6. *Pregnancy*. The association between pregnancy and aortic dissection remains controversial. Some authors have reported an increased risk of aortic dissection in pregnant women; however, whether this association is independent of other risk factors (such as hypertension) is not well understood.

Classification

One of the key aspects in the evaluation of dissection is identification of the extent of dissection, which has critical implications for prognosis and management. Dissections involving the ascending aorta have an extremely high mortality rate and require immediate surgery. The Stanford and DeBakey classification systems are commonly used to describe the extent of dissection (Fig. 24.5). The Stanford system divides dissections into two forms: Type A, involving the ascending aorta; and Type B, which does not involve the ascending aorta. The DeBakey system of classification divides dissections into Type 1 (involvement of ascending aorta and extending distally to the arch or descending aorta), Type II (limited to ascending aorta), and Type III (descending aorta).

Table 24.2 Risk factors for aortic dissection

Hypertension
Connective tissue disorders
Marfan's syndrome
Ehlers–Danlos syndrome
Annuloaortic ectasia/ familial aortic dissection
Bicuspid aortic valve
Aortic coarctation
Vasculitis
Takayasu's arteritis
Giant cell arteritis
Behçet's disease
Syphilis
Blunt trauma
Rapid deceleration injury
Surgical manipulation
Cardiac surgery
Cardiac catheterization/intervention
Intra-aortic balloon pump
Cocaine use
Pregnancy (possible risk factor)

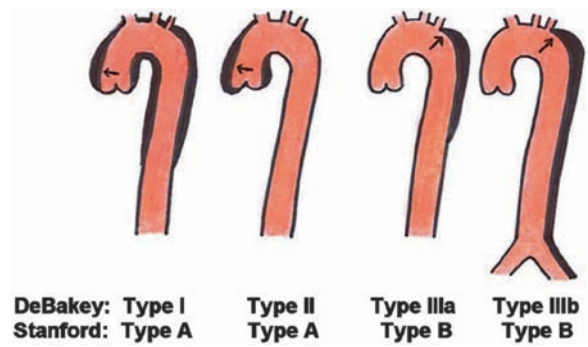

Fig. 24.5 Schematic of the commonly used DeBakey and Stanford classification systems

Clinical Presentation

Common presenting symptoms for patients with Type A dissections include chest pain, back pain, abdominal pain, syncope, and stroke.[3] Patients may also present with heart failure (due to aortic insufficiency or cardiac tamponade), pulse deficits, murmur of aortic insufficiency, cardiogenic shock, renal failure, or evidence of bowel or limb ischemia. The electrocardiogram is usually nonspecific, but may occasionally demonstrate ischemia, if the coronaries arteries are involved.

In patients with Type A dissection, medical therapy should be commenced immediately, and emergent surgery to replace the ascending aorta (with possible aortic valve replacement, if the aortic valve is involved) is indicated. Thoracic aortic dissections which do not involve the ascending aorta are generally managed medically, if the patient is asymptomatic. The mainstay of medical therapy is blood pressure control and reduction of arterial shear stress with intravenous beta-blockade. Nitroprusside is often also used to control blood pressure in the acute setting. Indications for surgical intervention in patients with Type B dissection include persistent pain, hypotension, limb or bowel ischemia, or paraplegia.

Echocardiographic Findings

Using multiple imaging planes, including parasternal and suprasternal imaging, transthoracic echocardiography can identify an aortic intimal flap in some cases. The finding of an otherwise unexplained pericardial effusion, dilated ascending aorta, or aortic insufficiency on transthoracic imaging should also heighten the suspicion for a possible dissection. However, the sensitivity of transthoracic echocardiography for the identification of aortic pathology is limited, and transesophageal imaging is required in many cases. Transesophageal echocardiography can be performed rapidly at the bedside and provides high-resolution images of the thoracic descending aorta, aortic arch, and most of the ascending aorta. The potential disadvantages of transesophageal echocardiography are that it is semi-invasive and often requires some sedation. In addition, some branch vessels may not be visualized. A small portion of the distal ascending aorta is not visualized by transesophageal echocardiography, due to the intervening air-filled trachea. However, dissection limited to only this portion of the distal ascending aorta is uncommon. Supplemental imaging with transthoracic echocardiography in the suprasternal view may be useful to further evaluate the distal ascending aorta and proximal arch.

The Intimal Flap

The classic finding in aortic dissection is an intimal flap, which may be visualized in the longitudinal and short-axis views (Fig. 24.6). Reverberations may occasionally create linear artifacts that resemble an intimal flap; imaging in multiple planes should therefore be employed to avoid making a false-positive diagnosis. The entry site of the dissection can often be identified. In patients with Type B dissections, the tear most often occurs at the aortic isthmus; in Type A dissections, the tear often begins in the right lateral aspect of the ascending aorta.[7] The dissection most commonly propagates distally, although it may occasionally extend proximally in the aorta. The dissection flap separates the lumen of the aorta into true and false lumens (Fig. 24.7).

False Lumen

Echocardiographic findings in patients with aortic dissection may include thrombus or spontaneous echocardiographic contrast in the false lumen of the aorta. In some cases, the false lumen may be completely thrombosed. Color-flow mapping is also helpful in identifying the true and false lumens (Figs. 24.8 and 24.9), as well for differentiating true dissection from artifact.

Coronary Arteries

Echocardiography is also useful in identifying the sequelae of aortic dissection. Extension of the dissection into the coronary arteries may be visualized, and

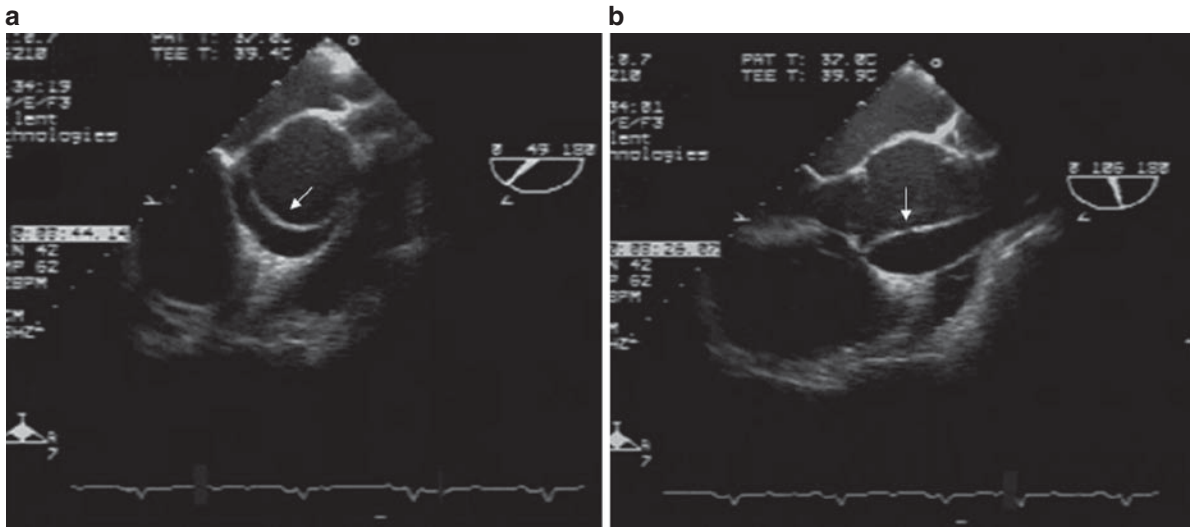

Fig. 24.6 Short-axis (**a**) and long-axis (**b**) transesophageal echo views of an ascending aortic dissection with intimal flap seen (*arrow*). *Ao* aorta

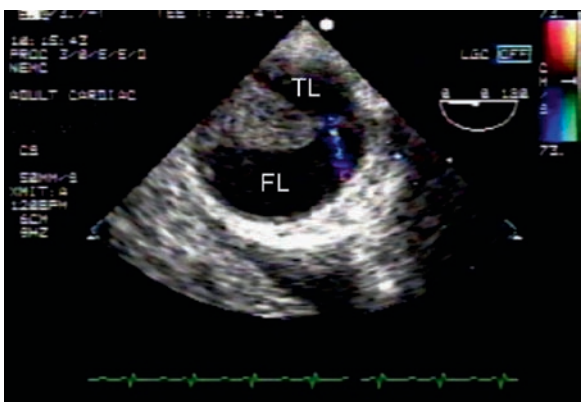

Fig. 24.7 Transverse-axis view of descending aorta, showing partially thrombosed false lumen (*arrow*). Color Doppler demonstrates communication between the true and false lumens. *FL* false lumen; *TL* true lumen

the presence of a wall motion abnormality may indicate possible ischemia and coronary involvement.

Aortic Regurgitation

Other cardiac complications which may be identified by echocardiography include aortic insufficiency (Fig. 24.10).

Pericardial Effusion

This is an important echocardiographic finding which may imply some partial aortic wall rupture and the development of cardiac tamponade.

Surgery

Even after surgical repair, patients with a history of aortic dissection may develop rupture of an aneurysm or dissection at a remote site. In view of the high mortality associated with rupture or dissection, these observations suggest that routine periodic follow-up of postoperative patients with imaging studies may be beneficial. It has been recommended that follow-up imaging be obtained at 1, 3, 6, and 12 months after the acute event, and yearly thereafter.[8]

Intramural Hematoma

Intramural hematoma is a variant of aortic dissection that has been increasingly recognized due to improvements in

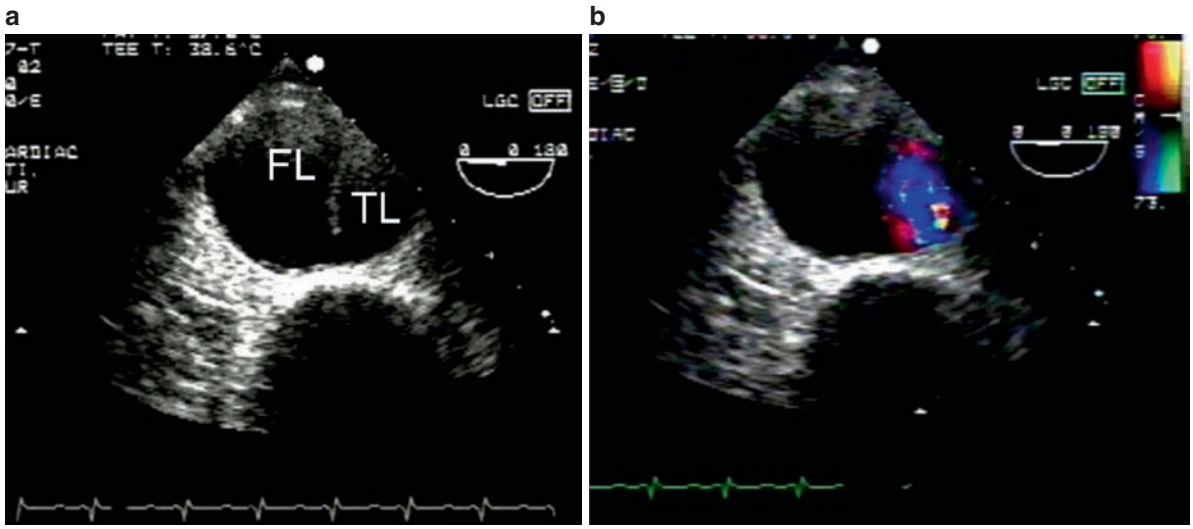

Fig. 24.8 Transesophageal echo image of a descending aortic dissection in a patient with Marfan's syndrome. (**a**) Two-dimensional imaging demonstrates the true lumen (TL), which is smaller than the false lumen (FL); (**b**) Color Doppler demonstrates flow in the true lumen

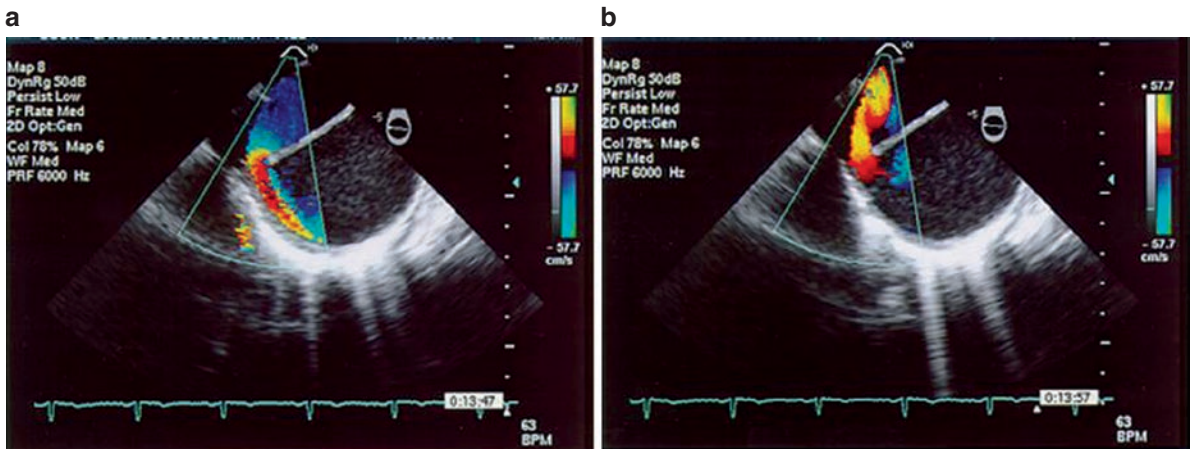

Fig. 24.9 Tranesophageal image of the descending aorta with a dissection flap. Color-flow imaging demonstrates to-and-fro flow between the true and false lumens. (**a**) Systole; (**b**) Diastole. Courtesy of Dr. Fernando Morcerf

aortic imaging. Its distinguishing feature is the lack of an intimal tear. Recent studies report that 13–29% of aortic dissections are intramural hematomas.[9] Intramural hematoma may occur via several mechanisms. Rupture of the vasa vasorum, with hemorrhage into the media of the aortic wall is one potential mechanism for the development of intramural hematoma. The presence of underlying medial degeneration may predispose to the development of hemorrhage. Another potential mechanism is rupture of atherosclerotic plaque or penetrating aortic ulcer, which can also lead to hemorrhage into the aortic media. Finally, blunt trauma to the aorta may be associated with the development of intramural hematoma.

Imaging

Since no intimal flap or false lumen is present, intramural hematoma may not be apparent on angiography. With echocardiography, the distinct features of intramural hematoma include the absence of an intimal flap, and crescentic or circular thickening of the aortic wall (>0.7 cm)[9] (Figs. 24.11 and 24.12). The major challenge in the diagnosis of intramural hematoma is distinguishing it from atherosclerotic plaque. The echocardiographic features of these two entities are summarized in Table 24.3. Central displacement of the intimal layer is seen in intramural hematoma. Compared to atherosclerotic plaque,

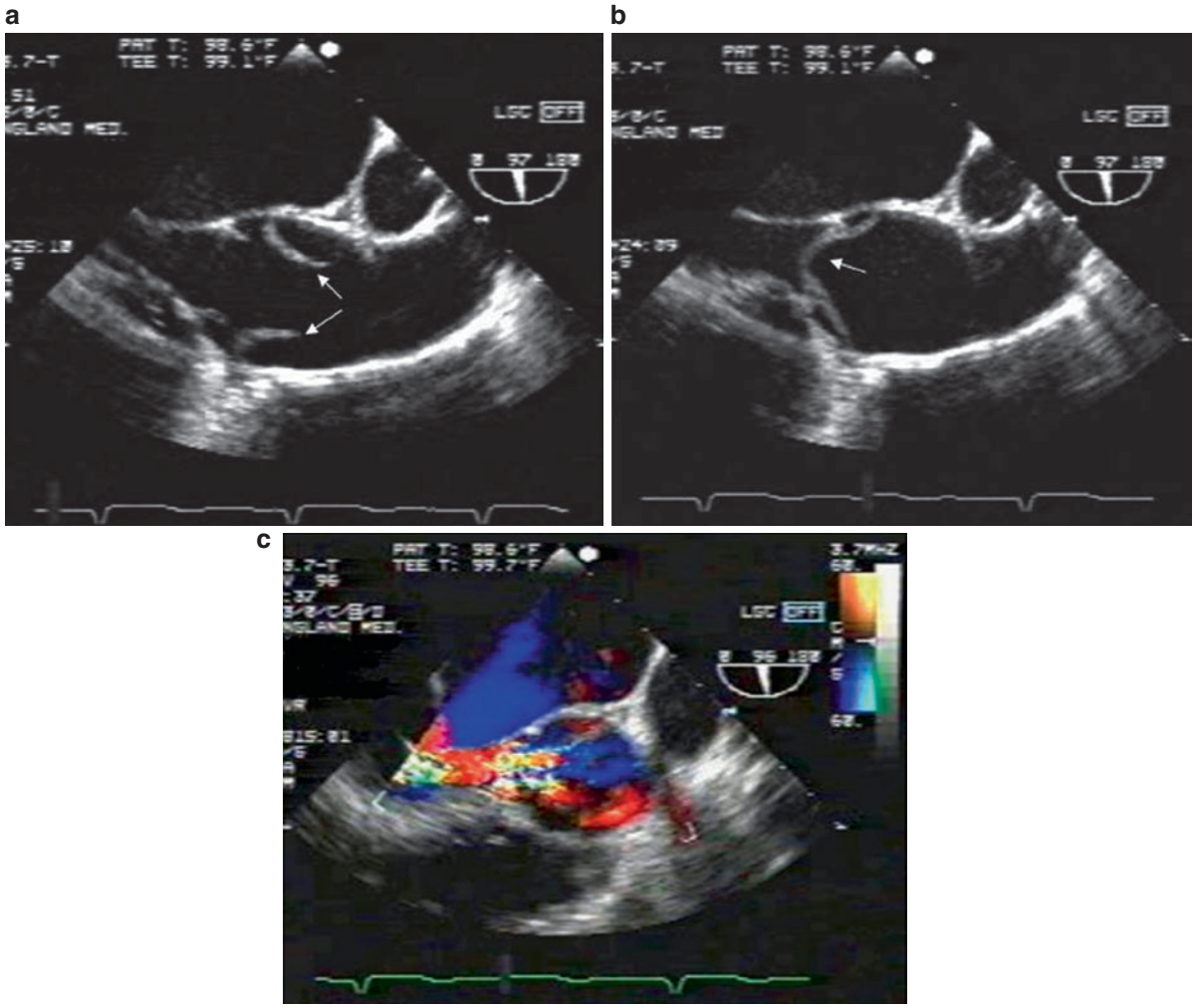

Fig. 24.10 Transesophageal echo long-axis image of an ascending aortic dissection, with intimal flap (*arrows*) prolapsing into the aortic valve; (**a**) systolic image; (**b**) diastolic image; (**c**) Color Doppler demonstrates severe aortic insufficiency

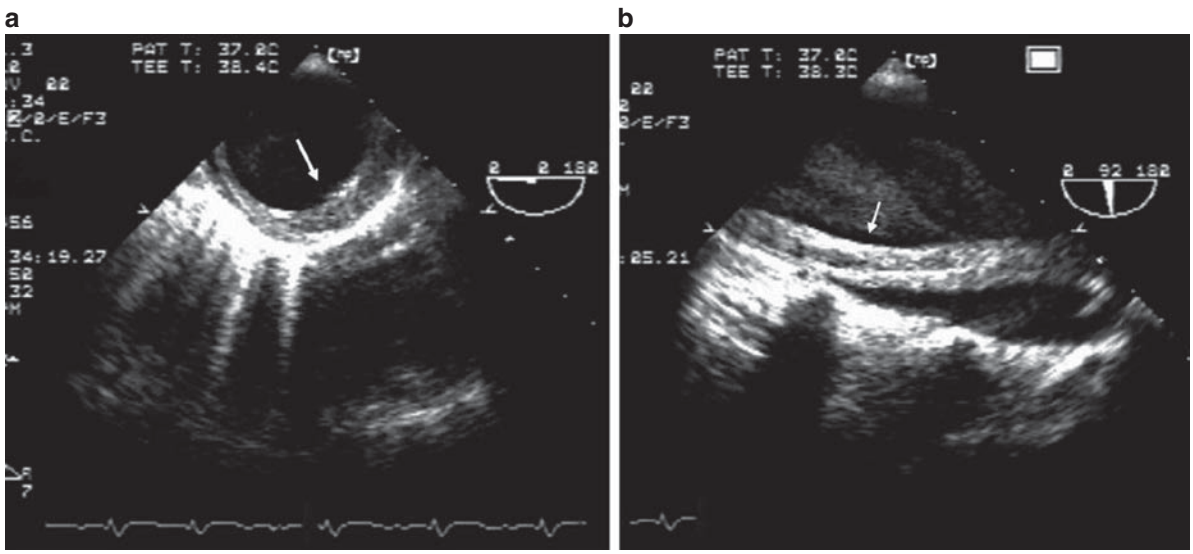

Fig. 24.11 Long-axis (**a**) and short-axis (**b**) transesophageal echo views of an intramural hematoma, showing central displacement of the intimal layer (*arrow*)

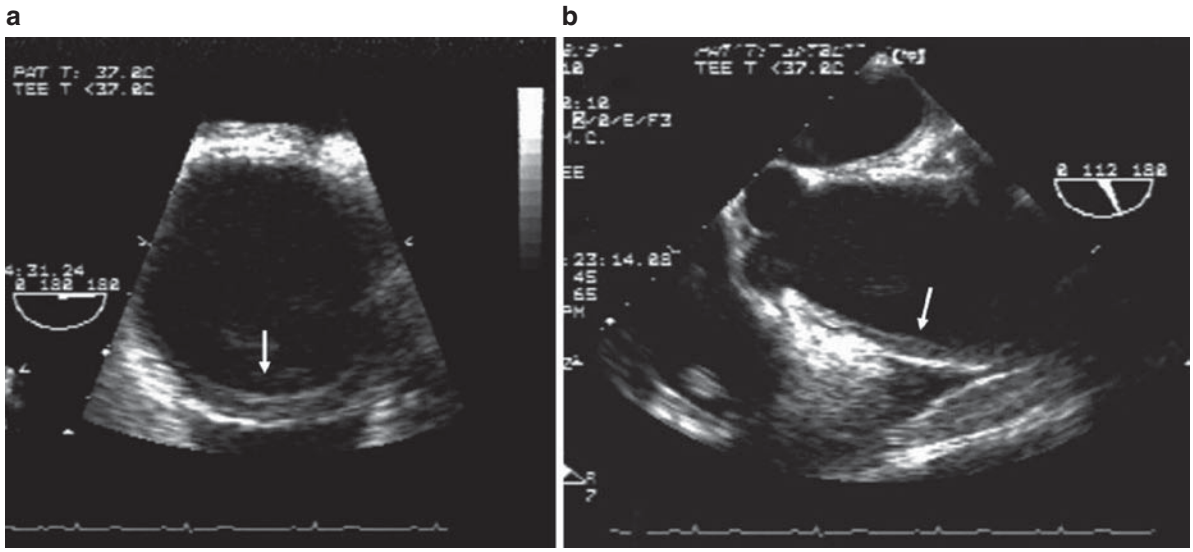

Fig. 24.12 Short-axis (**a**) and long-axis (**b**) transesophageal echo images of intramural hematoma (*arrow*) in the ascending aorta. The luminal surface has a smooth surface, and the area of hematoma appears relatively echolucent

Table 24.3 Echocardiographic characteristics of intramural hematoma vs. atherosclerotic plaque

	Intramural hematoma	Atherosclerotic plaque
Intraluminal surface	Usually smooth	Usually irregular
Echodensity	Hypoechoic	Hyperechoic
Intimal layer	Inwardly displaced	Nondisplaced
Extent of aortic Involvement	Usually localized	Usually diffuse
Pericardial effusion	May be present	–

the area of the hematoma frequently appears relatively homogenous and hypoechoic. In addition, the luminal wall in intramural hematoma is usually relatively smooth, compared with the irregular surface typically seen in patients with significant atherosclerotic plaque.[10]

Clinical Significance

Initial observations have reported that the prognosis and mortality rates for intramural hematoma are similar to those for classic aortic dissection. However, some more recent data suggest that intramural hematoma may have a more favorable prognosis than classic Type A dissection.[10] Patients with intramural hematoma may progress to dissection with an intimal tear or rupture, and the management of intramural hematoma remains similar to that of classic dissections (i.e., surgery for ascending aortic involvement, and medical therapy for stable patients without ascending aortic involvement).

Penetrating Aortic Ulcers

Pathophysiology

Penetrating atherosclerotic ulcer is a distinct pathologic entity that can lead to disruption of the aortic wall. Patients with atherosclerotic disease often have superficial ulcerations of atherosclerotic plaque (Fig. 24.13), which are usually confined to the intima.[11] However, in some cases, the ulcer may penetrate through the internal elastic lamina and into the media. Subsequent hemorrhage into and beyond the medial layer of the aorta can lead to intramural hematoma, pseudoaneurysm formation, or rupture. Occasionally, penetrating atherosclerotic ulcers may lead to a limited dissection. Penetrating ulcers are usually associated with extensive atherosclerotic disease, and unlike classic dissection, more commonly occur in the descending thoracic aorta.

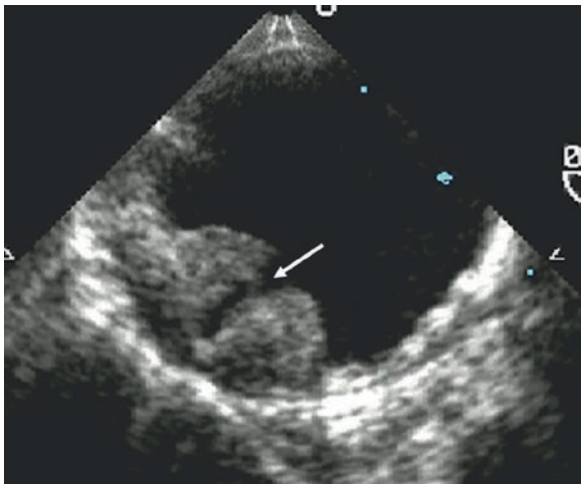

Fig. 24.13 Transesophageal echo image in a patient with an ulcerated atherosclerotic plaque in the descending aorta

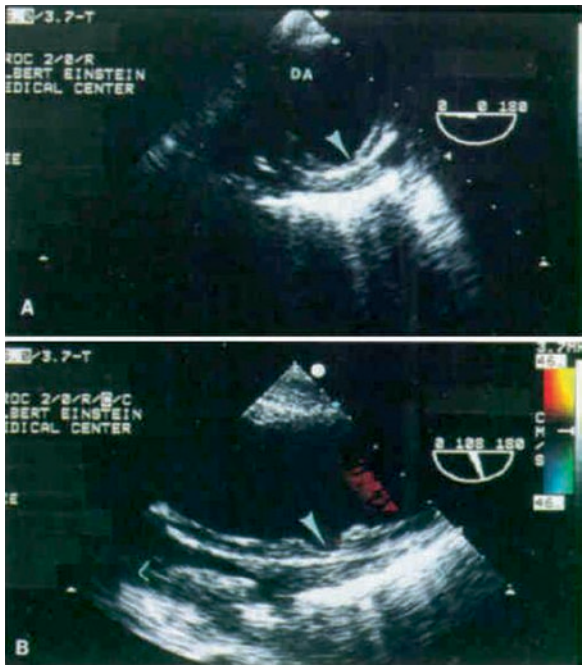

Fig. 24.14 Long-axis image of the aorta showing a penetrating aortic ulcer (*arrows*) in the descending aorta. There is a hypoechoic area in the aortic wall due to an associated intramural hematoma. From Joffe et al[21] Copyright 1996 with permission from Elsevier

Clinical Significance

Penetrating ulcers typically occur in elderly, hypertensive patients. The majority of patients present with symptoms of chest or back pain. Treatment with antihypertensive therapy should be begun immediately. Patients with symptomatic penetrating ulcers of the ascending aorta or arch are considered high risk for rupture, and early surgery has been recommended.[11] Penetrating ulcers of the descending aorta may be managed conservatively in stable patients. However, surgical intervention is indicated if complications such as persistent pain, hemodynamic instability, pseudoaneurysm, pericardial effusion, bloody pleural effusion, or expanding intramural hematoma ensue.[11]

Imaging

Penetrating aortic ulcers may be identified by transesophageal echocardiography, CT scan, magnetic resonance imaging, or aortography; however, the findings may be subtle. On transesophageal echocardiography, atherosclerotic plaque, crater-like ulcerations (Fig. 24.14), and asymmetric thickening of the aortic wall may be seen.[12] Patients who are managed conservatively should have serial follow-up imaging studies to identify the development of complications.

Aortic Trauma

Pathophysiology

Aortic trauma usually occurs as the result of a horizontal deceleration injury, such as in motor vehicle accidents, or vertical deceleration injury, such as falling from a height. The site most vulnerable to deceleration injury is the aortic isthmus, at the junction of the aortic arch and descending aorta, which is tethered by the ligamentum arteriosum. Other points which are susceptible to aortic trauma are the ascending aorta above the sinus of Valsalva, and the origin of the innominate artery.[13,14] Traumatic injury to the aorta is associated with a high mortality rate, with only 20% of patients surviving to reach the hospital.[15] Of patients who survive, many sustain an aortic rupture that is contained by the adventitial layer.

Imaging

Although angiography has been considered the standard imaging modality for detection of aortic trauma, it carries the risk of exacerbation of vascular trauma and requires transport of a potentially unstable patient. Transesophageal echocardiography has the advantage of providing rapid imaging at the bedside, but cannot be performed in patients with severe facial injury or cervical spine injury. In addition, injuries involving the distal ascending aorta or great vessels may not be detected, and other imaging modalities may be required in some cases.

A small series by Goarin et al reported several common transesophageal echo findings in patients with traumatic aortic injury. The most commonly reported finding was the presence of "thick stripes" in the lumen, due to deep laceration of the intimal and medial layers of the aorta (Fig. 24.15). In the case of less extensive lacerations, an intimal flap may occur; this may appear similar to a classic dissection, or may be a free flap without the presence of a false lumen. Other findings include pseudoaneursym, fusiform dilation of the aorta, intramural hematoma, or intraluminal thrombus. The presence of increased distance between the esophageal probe and the aorta (>1 cm) suggests the presence of a mediastinal hematoma, and may be indirect evidence of aortic trauma.[2,16]

Aortic Atheromatous Disease

Pathophysiology

Aortic atheromatous disease has been increasingly recognized as an important cause of stroke, particularly in elderly patients. In patients with stroke, the prevalence of aortic atheroma is as high as that of carotid artery disease or atrial fibrillation.[2] The prevalence of aortic atheroma in patients with an embolic event has ranged from 21 to 27%. Recognized risk factors for the development of atheromatous disease include advanced age, hypertension, hypercholesterolemia, and smoking. In addition, a correlation between fibrinogen and homocysteine levels and aortic atherosclerosis has been reported.[17]

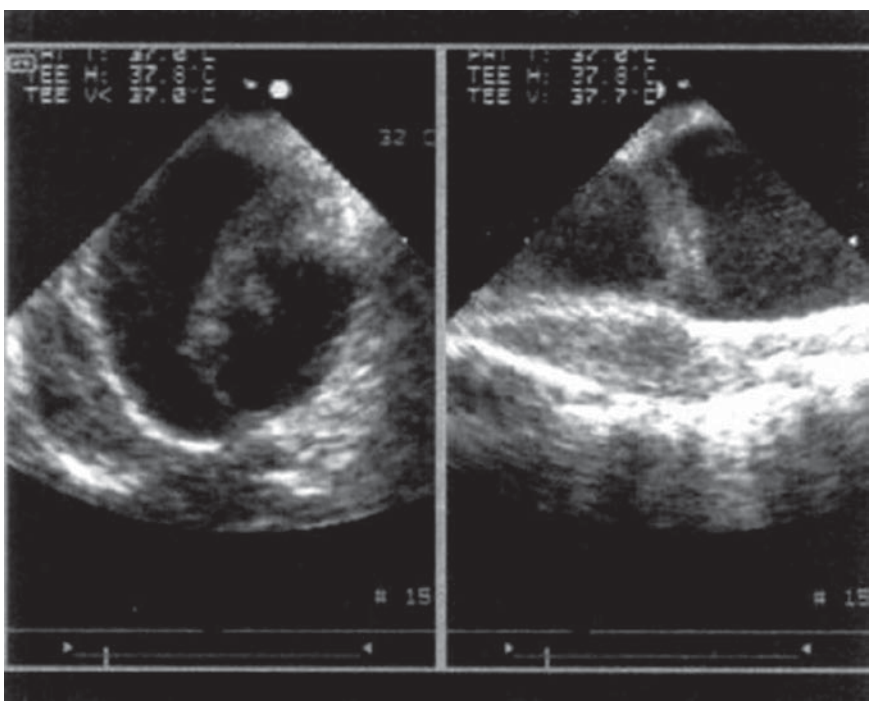

Fig. 24.15 Transesophageal short-axis (*left*) and long-axis (*right*) views showing a "thick stripe" due to intimal-medial laceration after a blunt thoracic injury[16]

Classification

Morphologic features of aortic plaque which are associated with an increased risk of embolization include increased plaque size, presence of ulcerations, and presence of mobile components. Accordingly, a staging system has been developed to grade severity of aortic atheroma (Table 24.4). Various degrees of aortic atheroma, as seen on transesophageal imaging, are shown in Fig. 24.16. Imaging from a patient with mobile Grade 5 atherosclerotic plaque is seen in Fig. 24.17. Most studies have defined significant atheroma as lesions having a thickness of ³5 mm. However, more recent data indicate that a plaque thickness of ³4 mm confers a significantly increased risk of an embolic event, compared to plaques <4 mm.[18]

Table 24.4 Classification of aortic atheroma

Grade I	Normal or minimal intimal thickening
Grade II	Non-protruding intimal thickening
Grade III	Atheroma <5 mm
Grade IV	Atheroma >5 mm
Grade V	Mobile atheroma

Clinical Significance

It has been observed that the mobile components seen on atherosclerotic plaque are usually thrombi. Embolic events due to aortic atheroma may occur spontaneously, or subsequent to procedures such as

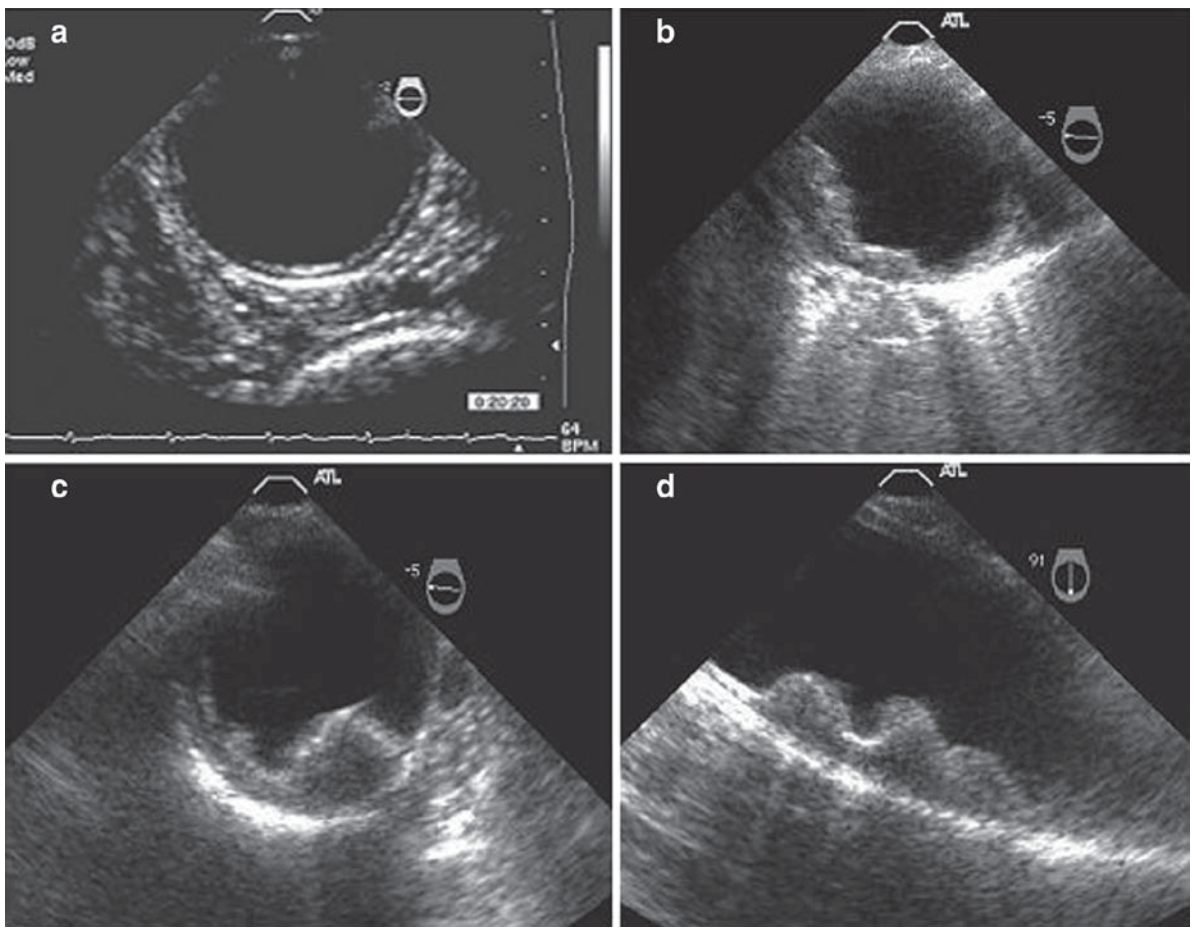

Fig. 24.16 Transesophageal imaging demonstrating varying morphologies of atherosclerotic plaque. (**a**) Mild layered plaque in the descending aorta; (**b**) Severe plaque in the descending aorta; (**c**) Longitudinal view of the descending aorta in a patient with severe protruding atheroma; (**d**) Transverse view in the same patient as shown in **c**. Courtesy of Dr. Fernando Morcerf

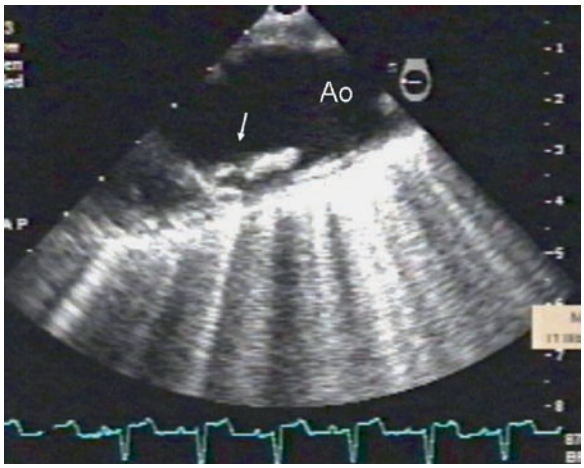

Fig. 24.17 Transesophageal echo image of the aortic arch in a patient with protruding and mobile atheroma (*arrow*). *Ao* aorta

cardiac catheterization, intra-aortic balloon pump, or cardiac surgery. In some cases, embolization may occur due to atheroembolic syndrome, but it is believed that thrombi are responsible for most embolic events. Despite this, the role of anticoagulation in these patients has not been clearly established. Several observational studies, however, have indicated that the incidence of embolic events is lower in patients treated with warfarin compared to those who are not. The use of hydroxyethyl glutaryl coenzyme A (HMG-CoA) reductase inhibitors in patients with aortic atheroma is supported by several randomized trials that have demonstrated a reduction in stroke with this therapy. HMG-CoA reductase inhibitors reduce low-density lipoprotein cholesterol levels and may thereby stabilize atherosclerotic plaque. In addition, antithrombotic actions of statins have also been described, which may have salutary effects on the development of plaque thrombosis.

Imaging

Transesophageal echocardiography is the primary modality used to detect aortic atheroma. There is some evidence that epicardial imaging may provide an even higher sensitivity for detection of atheromatous lesions and may be a useful adjunct in the intraoperative setting.[19] The clinical utility of aortic plaque imaging has primarily been in patients who have sustained an unexplained stroke and in patients who are undergoing cardiac surgery. Among patients undergoing cardiac surgery, elderly patients who have mobile lesions are at particularly high risk for embolic events. In a study of patients aged >65 years old who were undergoing cardiac surgery, 18% of subjects were found to have protruding atheroma on intraoperative transesophageal echo. Almost half of those with protruding atheroma also had mobile components, and there was a 25% incidence of stroke in these patients (compared with 2% in others). Intraoperative embolization may occur due to crossclamping of the aorta, "sand-blasting" effect from cannula flow, or manipulation of the aorta during surgery.

There is some evidence that modification of surgical techniques (such as alteration of the cannulation site) in high-risk patients may decrease the incidence of perioperative embolic strokes.[20] However, even with these measures, the stroke rate in high-risk patients appears to be higher than the general population. Studies of aortic endartectomy have not been promising, demonstrating a high risk of perioperative stroke. Graft replacement of the ascending aorta has been reported as an alternative therapeutic approach in patients with severe atheromatous disease who require cardiac surgery.[17]

Given the potentially devastating consequences of perioperative stroke, identification of the location and extent of athematous disease is important for planning the optimal surgical approach. Palpation of the aorta during surgery is a relatively insensitive technique[21] and fails to identify the majority of atheromatous lesions seen on transesophageal echo. Thus, use of aortic imaging is an important perioperative tool to identify patients at high risk.

References

1. Kouchoukos NT, Dougenis D. Medical progress: surgery of the thoracic aorta. *N Engl J Med*. 1997;336:1876–1888.
2. Erbel R. Diseases of the thoracic aorta. *Heart*. 2001;86: 227–234.
3. Nienaber CA, Eagle KA. Aortic dissection: new frontiers in diagnosis and management. *Circulation*. 2003;108: 628–635.
4. Roman MJ, Rosen SE, Kramer-Fox R, Devereux RB. Prognostic significance of the pattern of aortic root dilation in Marfan syndrome. *J Am Coll Cardiol*. 1993;22: 1470–1476.

5. Leggett ME, Unger TA, O'Sullivan CK, et al. Aortic root complications in Marfan's syndrome: identification of a lower risk group. *Heart*. 1996;75:389–395.
6. Gott VL, Pyeritz RE, Magovern GJ, Cameron DE, McKusick VA. Surgical treatment of aneurysms of the ascending aorta in the Marfan syndrome. *N Engl J Med*. 1986;314:1070–1074.
7. Vilacosta I, Aragoncillo P, San Román JA. Pathogenesis and morphological aspects. In: Vilacosta I, San Román, eds. Disección Aórtica. Madrid, Spain: Harcourt Brace de España; 1997:12.
8. Erbel R, Alfonso F, Boileau C, et al. European Society of Cardiology Task Force Report: Diagnosis and management of aortic dissection. *Eur Heart J*. 2001;22:1542–1681.
9. Mohr-Kahaly S. Aortic intramural hematoma: from observation to therapeutic strategies. *J Am Coll Cardiol*. 2001;37: 1611–1613.
10. Sawhney N, DeMaria AN, Blanchard DG. Aortic intramural hematoma: an increasingly recognized and potentially fatal entity. *Chest*. 2001;120:1340–1346.
11. Troxler M, Mavor AID, Homer-Vanniasinkam S. Penetrating atherosclerotic ulcers of the aorta. *Br J Surg*. 2001;88: 1169–1177.
12. Blanchard DG, Kimura BJ, Dittrich HC, DeMaria AN. Transesophageal echocardiography of the aorta. *JAMA*. 1994;272:546–551.
13. Vlahakes GJ, Warren RL. Traumatic rupture of the aorta. *New Engl J Med*. 1995;332:389–390.
14. Pretre R, Chilcott M. Current concepts: blunt trauma to the heart and great vessels. *New Engl J Med*. 1997;336:626–632.
15. Willens HJ, Kessler KM. Transesophageal echocardiography in the diagnosis of diseases of the thoracic aorta: Part II – atherosclerotic and traumatic diseases of the aorta. *Chest*. 2000;117:233–243.
16. Goarin JP, Catoire P, Jacquens Y, et al. Use of tranesophageal echocardiography for the diagnosis of traumatic aortic injury. *Chest*. 1997;112:71–80.
17. Tunick PA, Kronzon I. Atheromas of the thoracic aorta: clinical and therapeutic update. *J Am Coll Cardiol*. 2000;35:545–554.
18. Amarenco P, Cohen A, Tzourio C, et al. Atherosclerotic disease of the aortic arch and the risk of ischemic stroke. *N Engl J Med*. 1994;331:1474–1479.
19. Wilson MJ, Boyd SY, Lisagor PG, Rubal BJ, Cohen DJ. Ascending aortic atheroma assessed intraoperatively by epiaortic and transesophageal echocardiography. *Ann Thorac Surg*. 2000;70:25–30.
20. Katz ES, Tunick PA, Rusinek H, Ribakove G, Spencer FC, Kronzon I. Protruding aortic atheroma predict stroke in elderly patients undergoing cardiopulmonary bypass: experience with intraoperative transesophageal echocardiography. *J Am Coll Cardiol*. 1992;20:70–77.
21. Joffe II, Jacobs LE, Lampert C, Owen AA, Ioli AW, Kotler MN. Role of echocardiography in perioperative management of patients undergoing open heart surgery. *Am Heart J*. 1996;131:162–176.
22. Roman MJ, Devereux RB, Kramer-Fox R, O'Loughlin J. Two-dimensional echocardiographic aortic root dimensions in normal children and adults. *Am J Cardiol*. 1989;64:507–512

Chapter 25
Source of Embolus

Patrick J. Nash, Ronan J. Curtin, and Allan L. Klein

Introduction

Acute organ or limb ischemia due to arterial obstruction is typically due to one of two pathogenic processes: acute thrombotic occlusion on a substrate of significant local arterial disease or an embolism from the heart or proximal diseased large vessels (most commonly the thoracic aorta). The proportion of acute ischemic events that are embolic in etiology depend on a number of factors including the age of the subject, the likelihood of intrinsic vascular disease, and the vascular bed affected. Investigation after such an event is focused on defining the underlying process responsible for the event, with the primary aim being to prevent further potentially more devastating events. Echocardiography is the primary investigative tool for evaluating for a potential source of embolism. For the remainder of this discussion, intracardiac and thoracic aortic sources of emboli will be collectively labeled as "cardiovascular emboli," emphasizing that not all potential sources of emboli lie within the heart. This chapter initially focuses on defining the role of echocardiography in assessing for potential cardiovascular sources of embolus, including the indications for echocardiography, which is the optimal modality (transesophageal or transthoracic), and how to perform a comprehensive echocardiographic study. The remainder of the chapter discusses individual potential sources (both probable and possible sources), reviewing the evidence for the association between each potential source and embolic events, characteristic echocardiographic features, how to evaluate for it comprehensively with echocardiography, and current treatment strategies.

P.J. Nash (✉), R.J. Curtin, and A.L. Klein
Department of Cardiology, Galway University Hospital, Galway, Ireland
e-mail: patrick.nash@mailn.hse.ie

Epidemiology

Stroke is among the most common and devastating clinical sequelae of cardiovascular emboli. In 2001, it accounted for more than 1 in every 15 deaths in the U.S, ranking as the third most common cause of death. It is also a leading cause of long-term morbidity in the U.S. with more than 1,100,000 American adults in 1999 reporting functional difficulty following a stroke. Currently about 20% of acute neurological events are suggested to be attributable to cardiovascular emboli. A further 40% are classified as "cryptogenic," though there are increasing data suggesting associations with possible cardiovascular sources of emboli in these. For young people with acute ischemic strokes (≤45 years), the proportion that are due to cardiovascular emboli is significantly higher (>50%), as a potential embolic source is more likely to be the only identifiable cause. This is in contrast to older patients who are more likely to have identifiable coexisting intrinsic cerebrovascular disease. It is also possible that for some patients, the entire source of the embolus may have embolized, creating a false-negative echocardiographic study, underestimating the true proportion of patients who have a cardiovascular source of embolus.

Potential Cardiovascular Sources of Embolus

The literature documenting the relationships between potential cardiovascular embolic sources is limited by the fact that a large proportion of current evidence is based on nonrandomized case control series and

P. Nihoyannopoulos and J. Kisslo (eds.), *Echocardiography*,
DOI: 10.1007/978-1-84882-293-1_25, © Springer-Verlag London Limited 2009

not prospective studies. Potential sources of emboli within the cardiovascular system are best divided into two groups based on the level of current available evidence: probable or possible sources (Table 25.1). The majority are due to embolism of intracardiac thrombus, which in more than half of all cases is located within the left atrium (LA), primarily within the left atrial appendage (LAA). Atrial fibrillation and rheumatic mitral valve disease (primarily mitral stenosis) are the most common predisposing factors. Left ventricular (LV) thrombus, usually in the setting of a severe apical wall motion abnormality (akinesia or aneurysm), is the second most common potential source of embolism (25%). Large vegetations and left-sided tumors (myxoma or papillary fibroelastoma) are much rarer findings. Thoracic atheroma is increasingly being identified and linked to embolic events. The association is greatest for "complex" plaque (i.e. >4 mm thick, or pedunculated and mobile lesions). An acute ischemic event in a patient with a prosthetic mechanical valve is cardioembolic until proven otherwise.

Other echocardiographic findings are listed as possible sources as the level of evidence is less robust. A patent foramen ovale (PFO) has been associated with increased risk of ischemic stroke, especially in younger people, though it is such a common finding in the general population (20–25%) that determination of definite cause and effect is difficult. The combination of an atrial septal aneurysm (ASA) and a PFO is associated with a several fold increase in risk of stroke compared to a PFO alone. Other findings where possible associations with embolic events have been suggested include LA spontaneous echo contrast (SEC), valvular strands, mitral annular calcification, mitral valve prolapse, and smaller vegetations.

When to Use Echocardiography to Investigate for a Potential Cardiac Source of Embolus

A detailed history, examination, and electrocardiogram (ECG) are the core components to assessing any patient with an embolic event (Fig. 25.1). Clinical evidence to suggest cardiac disease increases the index of suspicion of a potential cardiovascular embolic source. Atrial fibrillation strongly suggests a cardiac source, though the coexistence of significant cerebrovascular disease especially in older subjects remains a possibility. In older patients, the next line of investigation is usually a carotid duplex scan. A negative scan should mandate more detailed cardiac assessment with echocardiography for a potential cardiovascular source of embolism. Younger patients are more likely to have a cardiovascular embolic source and an echocardiogram is generally performed, irrespective of a negative history, examination, and ECG. Acute occlusion of a large peripheral or visceral artery such as the femoral or renal artery is much more likely to be due to a large embolism than progression of intrinsic local vascular disease. Multiple ischemic events in different end-artery territories are also suggested to be more likely embolic in origin.

Table 25.1 Potential cardiovascular sources of embolus

Probable sources	Predisposing condition
Left atrial (appendage) thrombus	Atrial fibrillation; rheumatic mitral valve disease; severe LV dysfunction
Left ventricular thrombus	Previous MI (esp. anterior, with apical aneurysm); dilated cardiomyopathy
Vegetations ≥ 10 mm	Mitral and/or aortic valve
Cardiac tumors	Myxoma; papillary fibroelastoma
Complex aortic atheroma	
Prosthetic valves	Mitral or aortic
Possible sources	**Predisposing condition**
Patent foramen ovale	Atrial septal aneurysm
Spontaneous echo contrast	Atrial fibrillation; rheumatic mitral valve disease; severe LV dysfunction
Vegetations <10 mm	Mitral and/or aortic valve
Valvular strands/Lambl's excrescences	Mitral or aortic
Atrial septal defect	
Mitral annular calcification	

LV left ventricular; *MI* myocardial infarctionAdapted from Chen EW, Redberg RF. Echocardiographic evaluation of the patient with a systemic embolic event. In: Otto CM, ed. *The Practice of Clinical Echocardiography*. 2nd ed. Philadelphia. PA: WB Saunders, 2002, p 807

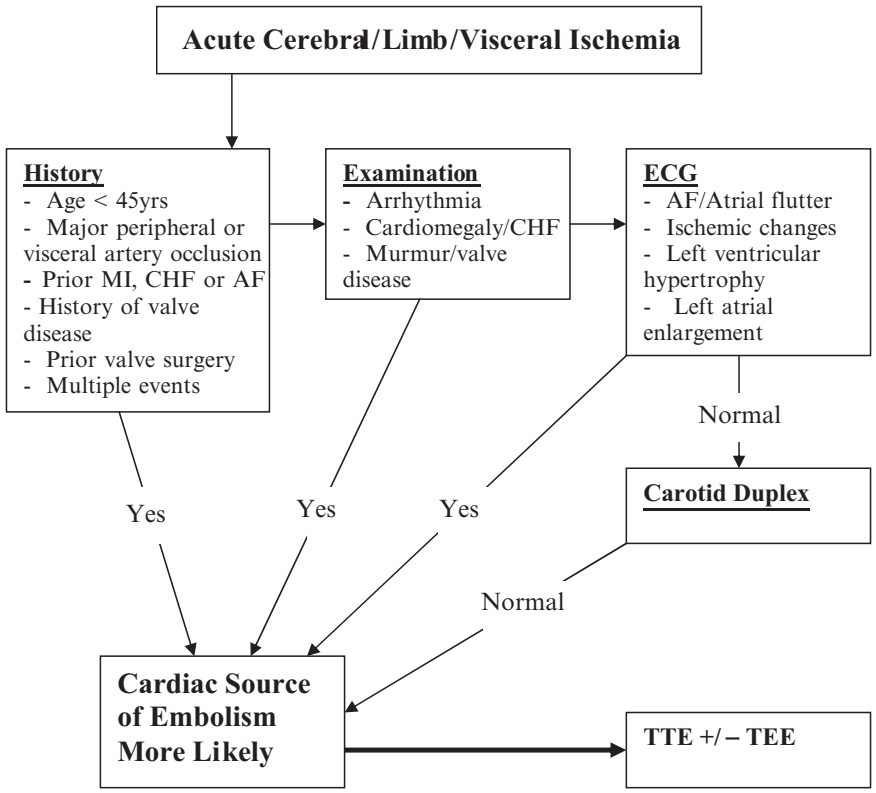

Fig. 25.1 Investigation Algorithm for a Potential Source of Embolus: (*MI* myocardial infarction, *CHF* congestive heart failure, *AF* atrial fibrillation, *ECG* electrocardiogram, *TTE* transthoracic echocardiography, *TEE* transesophageal echocardiography)

The 2003 ACC/AHA/ASE guidelines for echocardiography in patients with acute neurological events or other vascular occlusive events are outlined in (Table 25.2)

Transthoracic vs. Transesophageal Echocardiography

The sensitivity of transthoracic echocardiography (TTE) for detection of potential sources of embolus is low, as the most common potential causes are not well visualized by TTE. In the absence of clinical cardiac disease, the diagnostic yield is as low as 1%, increasing to 15% with clinical cardiac abnormalities. Its primary use is for assessing LV global and regional systolic function and apical LV thrombus.

Transesophageal echocardiography (TEE) is required to optimally visualize the LA and in particular the posterior-lying LAA (the most common location for intracardiac thrombus). It also permits optimal assessment of the interatrial septum and the thoracic aorta. Overall TEE identifies significantly more potential sources of embolus than TTE (39–57% vs. 15–19%). Evaluation for a potential source of embolus is now the leading clinical indication for TEE in most laboratories (26% in one registry series). However, it is probably best to consider the two modalities as complementary rather than mutually exclusive (Table 25.3). Thrombus in the LV is best visualized by TTE, while most other potential sources are better seen by TEE. A comprehensive approach to TEE for evaluation of possible sources of embolus is outlined in (Table 25.4).

Table 25.2 Recommendations for echocardiography in patients with neurological events or other vascular occlusive events (AHA/ACC/ASE 2003 guideline update for the clinical application of echocardiography)

Class I
Patients of any age with abrupt occlusion of a major peripheral or visceral artery
Younger patients (typically <45 years) with cerebrovascular events
Older patients (typically >45 years) with neurological events without evidence of cerebrovascular disease or other obvious cause
Patients for whom a clinical therapeutic decision (e.g., anticoagulation) will depend on the results of echocardiography
Class IIa
Patients with suspicion of embolic disease and with cerebrovascular disease of questionable significance
Class IIb
Patients with neurological events and intrinsic cerebrovascular disease of a nature sufficient to cause the clinical event
Class III
Patients for whom the results of echocardiography will not impact a decision to institute anticoagulant therapy or otherwise alter the approach to diagnosis or treatment

Adapted from: Cheitlin MD, Armstrong WF, Aurigemma GP, Beller GA, Bierman FZ, Davis JL, Douglas PS, Faxon DP, Gillam LD, Kimball TR, Kussmaul WG, Pearlman AS, Philbrick JT, Rakowski H, Thys DM. ACC/AHA/ASE 2003 guideline update for the clinical application of echocardiography: a report of the American College of Cardiology/American Heart Association Task Force on Practice Guidelines (ACC/AHA/ASE Committee to Update the 1997 Guidelines for the Clinical Applications of Echocardiography). 2003. American College of Cardiology Web Site. Available at <http://www.acc.org/qualityandscience/clinical/guidelines/echo/index.pdf>

Table 25.3 Role of transthoracic and transesophageal echocardiography for detection of potential sources of embolus

Possible source of embolus	Transthoracic echo	Transesophageal echo
LA mural thrombus/SEC	+	+++
LAA thrombus/SEC	–	+++
LAA filling velocity	–	+++
LA myxoma	++	+++
Mitral stenosis	++	+++
Valve strands	+	+++
Vegetations	+	+++
Papillary fibroelastoma	+	+++
LV aneurysm	+++	+
LV apical thrombus	++	+
Patent foramen ovale	–	+++
	++ (bubble)	
Atrial septal aneurysm	++	+++
Thoracic aortic atheroma	–	+++

– not seen; + poor; ++ intermediate; +++ excellent; *LA* left atrium; *LAA* left atrial appendage; *LV* left ventricle

Table 25.4 Comprehensive TEE examination for potential source of embolus

Midesophageal view at 0–15° rotation
Retroflex transducer to open a four-chamber view for initial assessment of the LA and mitral valve
Zoom in on the mitral valve and LA and examine in detail for any abnormalities
Slightly anteflex and/or withdraw the probe slightly to visualize the LAA (arises from anterolateral aspect of the LA near the lateral aspect of the mitral ring and left upper pulmonary vein)
Midesophageal 45–90°
Further views of the LA and LAA (usually best view to visualize the LAA)
Doppler LAA flow – 1 cm into the LAA from its junction with the main LA cavity
Clockwise rotation will give short-axis view of the aortic valve (strands, vegetations)
Visualize the interatrial septum in the near field – interrogate with color Doppler (decrease Nyquist <40 cm/s)
Midesophageal 120°
Further views of the LA and mitral valve and long-axis view of the aortic valve and aortic root
Slight clockwise rotation of the transducer will give a short-axis view of the LAA
Further clockwise rotation of transducer will give bicaval view–optimal view of the interatrial septum
Give agitated saline – to evaluate for right-to-left shunt at baseline and after Valsalva (ask patient to cough)
From the long-axis view of the aortic valve – bring angle back to ~100° and withdraw transducer to focus on the tubular ascending aorta
Transgastric view
Short- and long-axis views of the LV for LV function
Thoracic aorta
Begin in transgastric view at 0° (short axis of thoracic aorta) – decrease depth to maximize aorta
Withdraw transducer slowly – if any abnormality, visualize in long- and short-axis views (0° and 180°)
At ~20 cm from incisors the distal aortic arch will come into view – rotate 20° and turn clockwise to open the long-axis view of the aortic arch

Left Atrium

Anatomy

The LA is located posteriorly within the heart, in close proximity to the esophagus and therefore is best visualized by TEE. From an embolic perspective, most interest focuses on the LAA. This is a blind-ended sac located along the anterosuperior aspect of the LA and connected to the rest of the LA by a relatively narrow isthmus. It is a remnant of the original embryonic LA

and its exact physiologic role remains unclear. A number of anatomic features are important to be aware of when evaluating it by TEE (Figs. 25.2–25.5)

1. Its size varies widely (length between 16 and 51 mm, diameter: 5–40 mm). A very "small" appendage, often gives rise to concerns that a much larger appendage with laminated thrombus is being overlooked.
2. It typically has a twisted long axis, requiring multiple planes to visualize it comprehensively.
3. Typically it is multilobed (≥2 lobes in 80%). Therefore it is essential to comprehensively evaluate for any additional lobes that may not be immediately apparent (Fig. 25.2).
4. In contrast to the rest of the LA, its walls are trabeculated, with parallel ridges of muscle giving it a

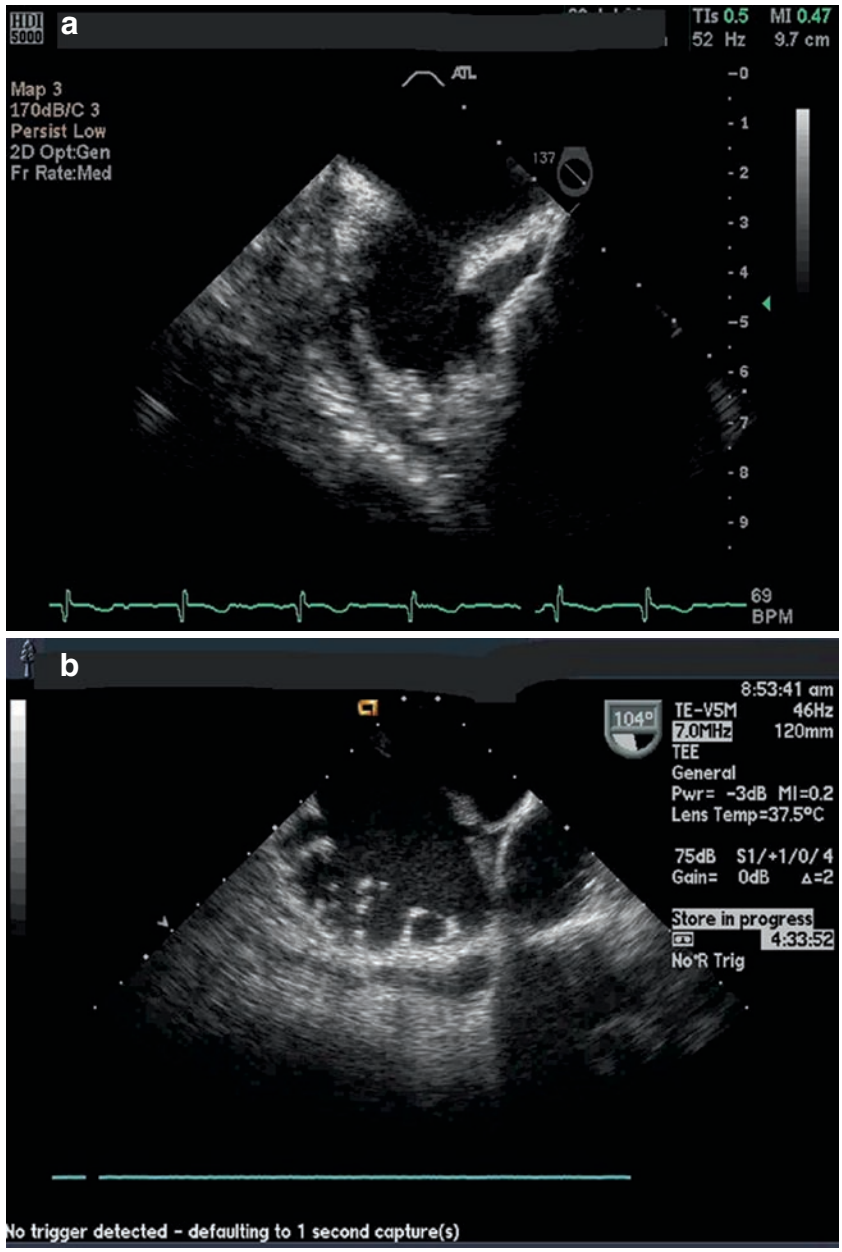

Fig. 25.2 TEE view (100–120°) of the LAA. The upper image shows a bilobed appendage. The lower image demonstrates prominent normal pectinate ridges (*arrow*), which may be confused for possible thrombus

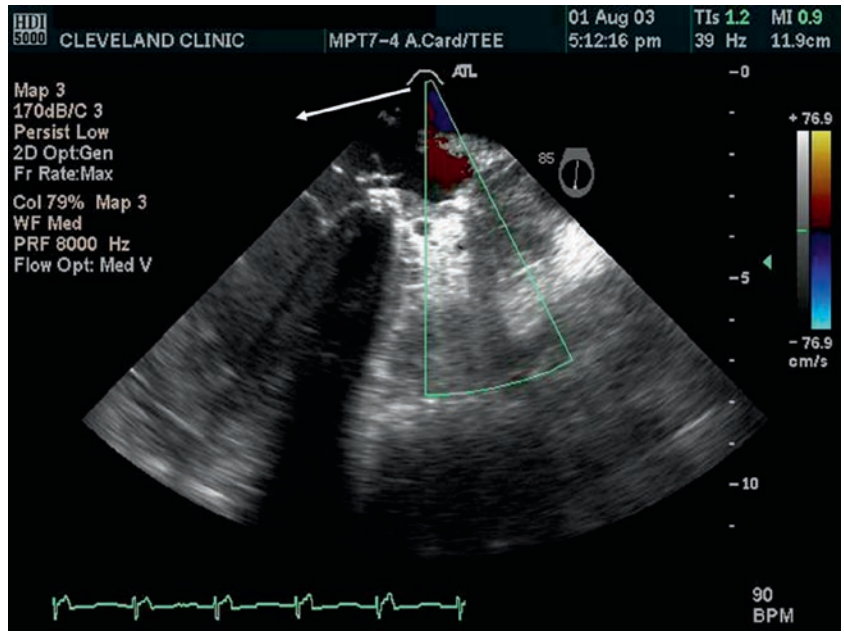

Fig. 25.3 TEE view at 85° showing that the LAA has been surgically removed

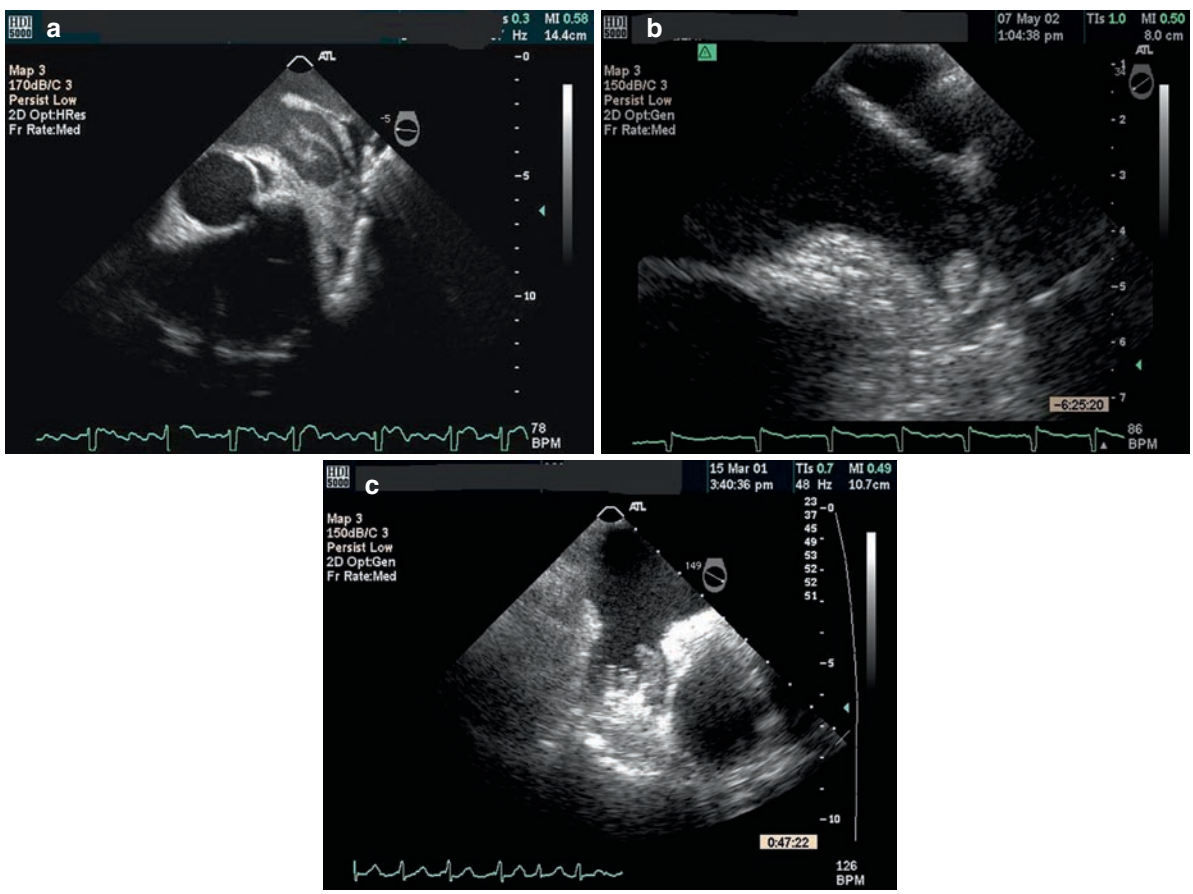

Fig. 25.4 LAA thrombus – the *upper left image* shows laminated thrombus in the LAA apex with spontaneous echo contrast in the rest of the LAA. The *upper right image* shows a small focal protuberant mass typical of thrombus. The *lower image* shows a LAA full of thrombus

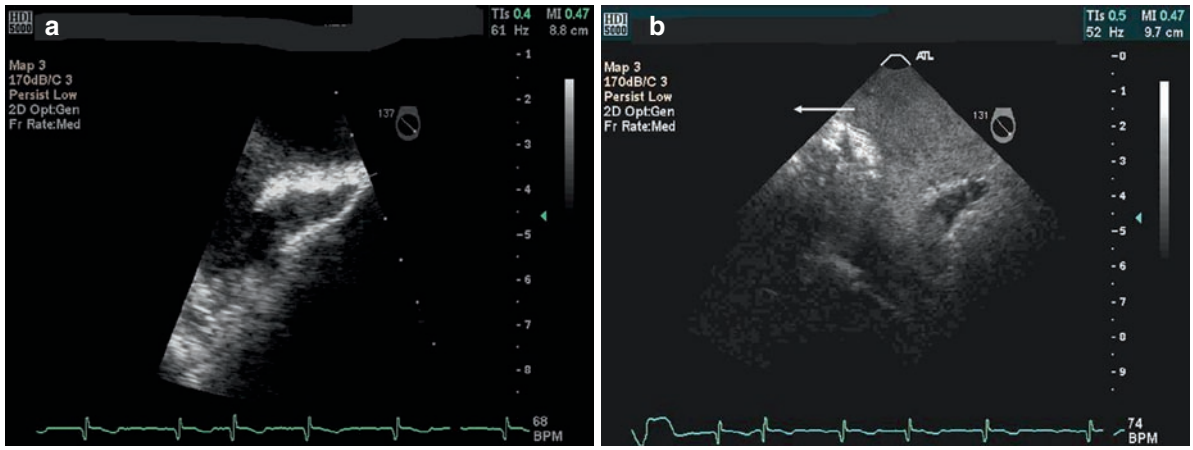

Fig. 25.5 Intravenous microbubble contrast clarifies possible LAA thrombus. The image on the left shows some haziness in the LAA, which raises a suspicion of possible thrombus. The image on the right was obtained after contrast demonstrating a filling defect, highly suggestive of thrombus

comb-like appearance (pectinate muscles) (Fig. 25.2). These may be mistaken for thrombus or conversely small thrombi between these ridges may be overlooked. A thrombus typically appears as a more solitary protrusion into the LAA cavity and may have independent motion (Fig. 25.4).

Left Atrial Appendage Doppler

Contractile function of the LAA is best assessed with pulsed-wave (PW) Doppler of flow into and out of the LAA by TEE. In sinus rhythm, a typical quadriphasic flow pattern is seen (Fig. 25.6). This begins with a late diastolic positive forward flow wave (out of the appendage – toward the TEE probe), associated with LA contraction, (after the electrocardiographic P wave, normal peak velocity >50 cm/s), and followed by an early negative systolic wave. The remaining Doppler pattern typically consists of at least two low-amplitude alternating waves with the final forward wave (positive wave) representing LAA outflow associated with early passive filling of the LV (correlated with the mitral inflow E wave). In atrial fibrillation the flow pattern changes, though active flow is still commonly seen with alternating positive and negative "fibrillatory" waves (Fig. 25.7), typically with lower flow velocities than those seen in sinus rhythm.

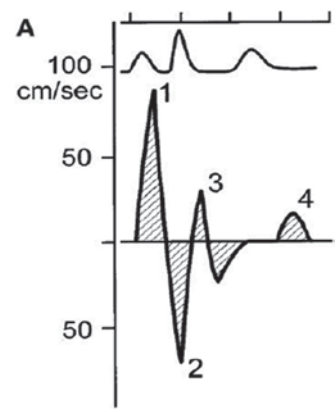

Fig. 25.6 Normal Doppler appearance of LAA flow. From: Agmon Y, Khandheria BK, Gentile F, Seward JB. *J Am Coll Card*. 1999;34:1867-77. Copyright 1999 with permission from Elsevier

Echocardiographic Assessment of the Left Atrium (Figs. 25.2–25.8)

Only limited information about the LA can be obtained by TTE. Left atrial size (either by internal dimension, area, or volume) can usually be satisfactorily obtained. The presence of left atrial enlargement (transverse diameter for the parasternal long-axis view >4.0 cm) or rheumatic mitral stenosis in a patient with a history of cerebral/systemic embolism, especially with atrial fibrillation, increases the likelihood of LAA thrombus.

Mural LA thrombus (if extensive enough) can be visualized by TTE (sensitivity of 25–57%, specificity of 63–83%). However most LA thrombus occurs in the LAA, and this is rarely satisfactorily seen by TTE (sensitivity of 0–16%). TEE is, therefore, the imaging modality of choice for accurate and comprehensive assessment of the LA for thrombus.

With TEE, the LA is in near field and the transducer should be adjusted to the highest frequency (typically 7 MHz) for optimal imaging, with the image depth adjusted to approximately 10 cm to maximize the LA size in the display. It is important to adjust all imaging parameters to avoid misinterpreting near-field artifacts. Starting at the midesophageal view (0° of rotation), the probe should be gently advanced and withdrawn a few centimeters to image the inferior and superior aspects of the LA and inspected in multiple angles of rotation, to prevent overlooking mural thrombus, especially along the posterior wall (Fig. 25.8). The LAA is located near the anterosuperior aspect of the mitral valve

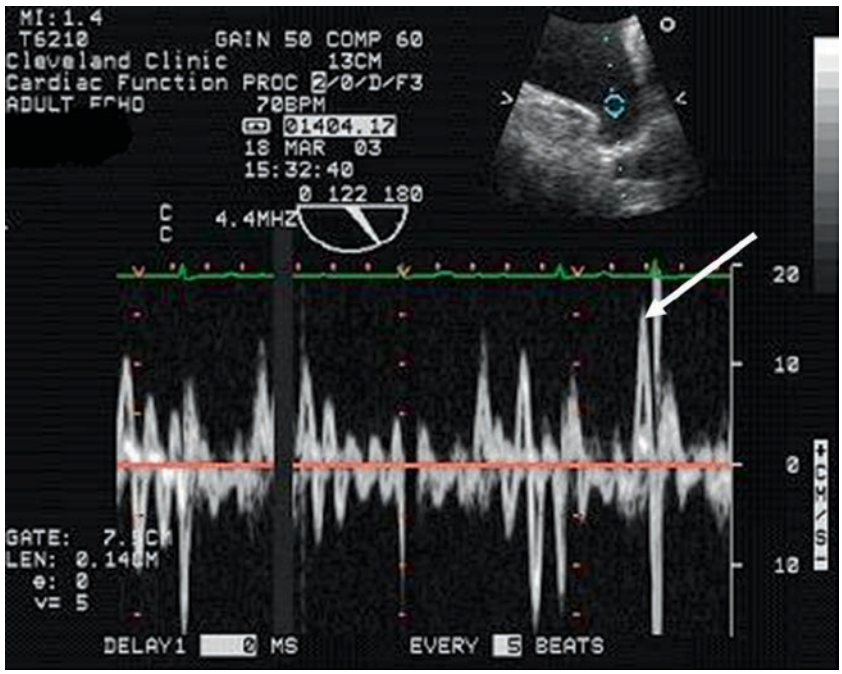

Fig. 25.7 LAA Doppler flow in a patient with atrial fibrillation. Peak emptying velocities (*highlighted*) are markedly reduced (<20 cm/s)

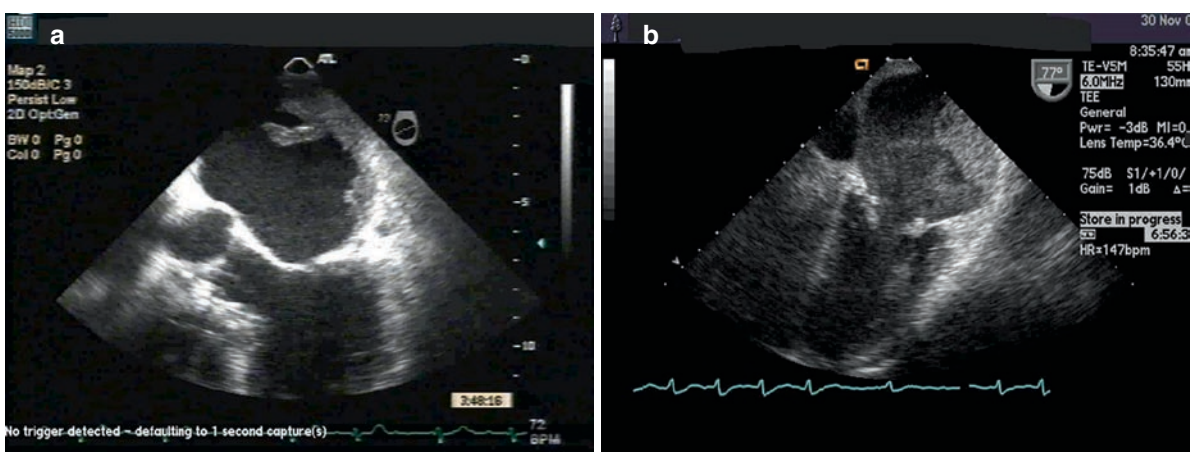

Fig. 25.8 Two examples of LA mural thrombus. The *image on the left* shows mobile pedunculated mural thrombus along the posterior wall of the LA. The *image on the right* shows thrombus along the lateral wall of the LA in a patient with mitral stenosis

annulus, and at 0° of rotation usually requires the probe to be withdrawn a little, where it typically has a triangular appearance, separated from the left upper pulmonary vein by a ridge of tissue called the limbus. Once located, it should be closely examined in multiple imaging planes, including 45°, 90°, and 120° views. Long-axis views of the LAA are obtained between 0° and 90°, with the orthogonal short-axis views typically best seen at ≥120° (Figs. 25.2–25.4). Pulsed-wave Doppler of LAA flow is often best obtained at 90–120° views, as it can usually be optimally aligned with LAA outflow in this view. Thrombi may be very small and any possible thrombus should be imaged in at least two orthogonal planes (Fig. 25.4). If there is persistent concern about possible thrombus in the LAA, use of a contrast agent (Optison™ or Definity™ – albumin or phospholipid coated microbubbles, that cross the pulmonary vasculature and opacify the left heart) can help to clarify its presence/absence (Fig. 25.5).

Increasingly the LAA is being ligated or stapled during cardiac surgery, especially if the patient has a history of atrial fibrillation (Fig. 25.3). Though still in its typical location, no flow should persist across its isthmus with the main LA cavity when interrogated with color-flow Doppler. Residual flow implies a residual channel and potential for LAA thrombus to embolize. With some surgical procedures it has been standard to remove the entire LAA (historical closed mitral valvotomy, Maze procedures), and confusion can arise about the presence or absence of the LAA if the exact operative procedure is unclear. Recently, a number of potential percutaneous devices to occlude the LAA have been developed. TEE is likely to have an important role in real-time guidance for their deployment.

Left Atrial Thrombus (Figs. 25.4, 25.5, 25.8)

Thrombus in the LA can be sessile or pedunculated, fixed or mobile, and typically appears as an irregularly shaped, gray, echodense intracavitary mass that is acoustically distinct from the LA endocardium. It is commonly associated with spontaneous echo contrast (SEC) (Fig. 25.4). Atrial fibrillation is the usual predisposing factor for LA thrombus and in particular LAA thrombus, though 5–10% of all thrombi occur in patients in sinus rhythm without significant mitral valve disease, often in the setting of severe LV dysfunction. The prevalence of LA thrombus in patients with atrial fibrillation of >48 h duration (who were not anticoagulated) has been reported as between 8 and 15%, almost all occurring within the LAA. A comprehensive TEE examination in experienced hands can usually detect LA thrombus with a sensitivity and specificity approaching 95–100%. Patients in atrial flutter, despite having more organized LA contraction compared to those with atrial fibrillation, can have evidence of LAA dysfunction (lower Doppler velocities) and LAA thrombus may still occur.

Factors Associated with Left Atrial Thromboembolism in Atrial Fibrillation

A number of significant independent clinical predictors of stroke in patients with AF have been identified, including increasing age, female sex, hypertension, prior cerebrovascular event, LV dysfunction, diabetes mellitus, and coronary artery disease with a protective effect from mitral regurgitation. In addition, a number of echocardiographic factors have been identified that are associated with LA thrombus formation and thromboembolism.

1. LAA Size:

The larger the LAA, the more likely it will contain thrombus

2. LAA Doppler flow pattern (Fig. 25.6):

Peak emptying LAA velocities represent LAA function and lower velocities are associated with more severe LAA dysfunction. Low velocities (≤20 cm/s) correlate strongly with the presence of LA thrombus and SEC. Low Doppler velocities can help with the evaluation of unclear LAA masses, increasing the likelihood that these represent LA thrombus. The risk of stroke for patients in atrial fibrillation is increased for those with reduced LAA velocities and is more than four times greater for patients with peak velocities <20 cm/s.

3. Presence of SEC (Fig. 25.9):

SEC or "smoke" representing local blood stasis is associated with an increased incidence of thrombus formation and thromboembolism. Increasingly severe qualitative

gradations of SEC (from mild intermittent SEC to a severe semiturbid appearance -"sludge") are associated with incremental increases in thromboembolic risk.

4. Size and mobility of LAA thrombus:

Larger (>1.5 cm), pedunculated and mobile thrombi are associated with a higher risk of systemic embolism.

5. Presence of complex aortic atheroma:

The coexistence of complex aortic atheroma (>4.0 mm thick, pedunculated, mobile) is associated with a greater risk of stroke in patients in atrial fibrillation. The exact mechanism underlying this relationship remains unclear as it applies also to plaque in the descending aorta and therefore is not entirely related to atheromatous emboli. It is suggested that it is a surrogate for a greater total vascular disease burden.

Evidence of either LAA thrombus, SEC, or a peak emptying velocity <20 cm/s are associated with an annual 7.5% risk of stroke. The combination of one of the above LAA findings and complex aortic atheroma increases the annual rate to ~20%. If neither of these TEE findings is present, the annual stroke risk is 1.2%. TEE also has an important role in evaluating patients prior to DC cardioversion. A TEE-guided approach as shown in the ACUTE multicenter trial (early cardioversion in the absence of LA clot) was associated with a quicker achievement of sinus rhythm, reduced major and minor bleeding rates, similar likelihood of maintaining sinus rhythm, and similar embolic rates when compared to the traditional conservative route of anticoagulation for 4 weeks prior to cardioversion.

Left Atrial Spontaneous Echo Contrast

The term "spontaneous echo contrast" (SEC) or "smoke" has been coined for the TEE appearance of swirling "smoke-like" echodensity within the heart, most commonly within the LA and in particular the LAA (Figs. 25.4 and 25.9). SEC can be appreciated by TTE but is much better seen by TEE. It is a marker of stasis, reflecting low flow states and probably reflecting aggregation of blood cells at low shear rates. SEC is also a likely precursor of thrombus. It is the most common TEE finding among patients referred for evaluation of a possible cardiac source of embolism, especially those with atrial fibrillation or left atrial enlargement. SEC is best appreciated with higher gain settings and can be differentiated from background "noise" by its swirling motion. Its dependence on transducer settings makes it difficult to quantify; however, it can be generally graded into mild or severe groups. The term "LAA sludge" has been coined for severe viscid SEC, without clear thrombus formation, though often differentiation between these is difficult. It is regarded as representing a stage further along the continuum toward thrombus formation and has been suggested to have greater prognostic significance than SEC.

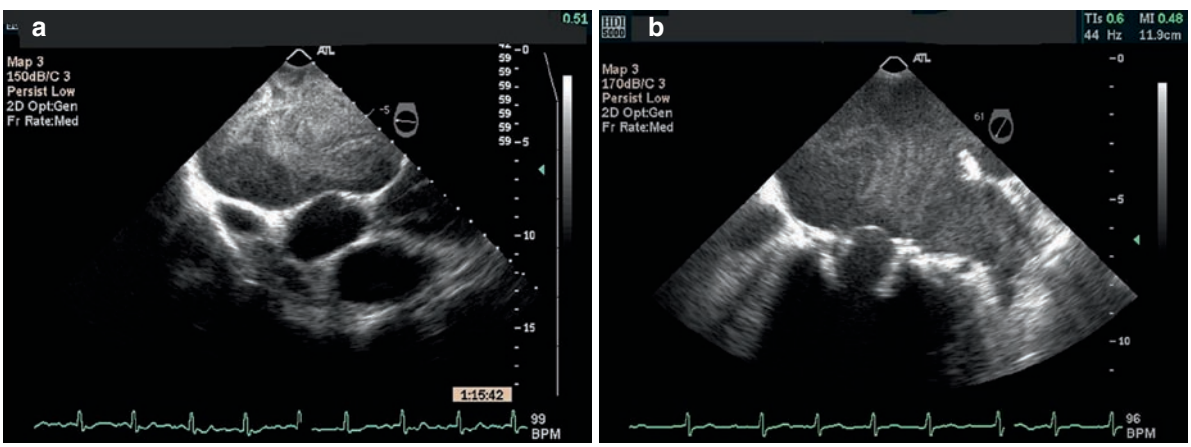

Fig. 25.9 Two examples typical of spontaneous echo contrast (SEC) or "smoke" in the LA

Spontaneous Echo Contrast and Thromboembolism

There is a strong association between SEC and LA thrombus. The presence of SEC is an independent predictor of thromboembolic risk; and in patients with atrial fibrillation, it is associated with an increase in the embolic rate from 3 to 12% per year. Mitral regurgitation is associated with reduced frequency of SEC, as presumably the regurgitation "washes" out the LA preventing stasis. It is much less commonly seen in patients in sinus rhythm (2% in one large series, all of whom had LA enlargement) than those with atrial fibrillation (20% prevalence in one series), but it is still associated with a higher incidence of stroke. Currently, there is no consensus on treatment of SEC in the absence of definite LA thrombus or atrial fibrillation, though its presence mandates a comprehensive examination of the LA for possible thrombus.

Left Atrial Tumors

Primary cardiac tumors are rare with a prevalence of 0.002–0.03% at autopsy, with myxomas accounting for up to 50% of all primary tumors and more than 80% of LA tumors. Metastatic tumors rarely extend into the LA and can simulate an atrial myxoma. LA myxomas are the usual tumors associated with embolic events though any left-sided tumor can cause embolic complications either due to embolism of tumor fragments itself or embolization of fragments of thrombus that form on the tumor surface.

Left Atrial Myxoma

These benign tumors occur more frequently in women, with a mean age of presentation of 56 years. Morphologically they appear as a gelatinous friable mass that most commonly arises on a stalk from the interatrial septum in the region of the fossa ovalis. They vary in size but are often not detected until they become very large, by which time they may prolapse through the mitral valve during diastole (Fig. 25.10). From an echocardiographic point of view, they typically appear as a mobile, well-circumscribed, nonhomogenous mass that may contain cyst-like structures and/or areas of calcification. Usually they can be identified by TTE; however, TEE is often required to comprehensively visualize the tumor and help plan the surgical approach. It is important to exclude the presence of multiple masses, confirm the point of attachment, and ensure that the mitral valve appears normal. This should be distinguished from a large LA thrombus, though these typically are attached to the posterior wall and produce a layered appearance. From a clinical perspective, an embolic event (often multiple territories) is the initial presentation in up to one-third of

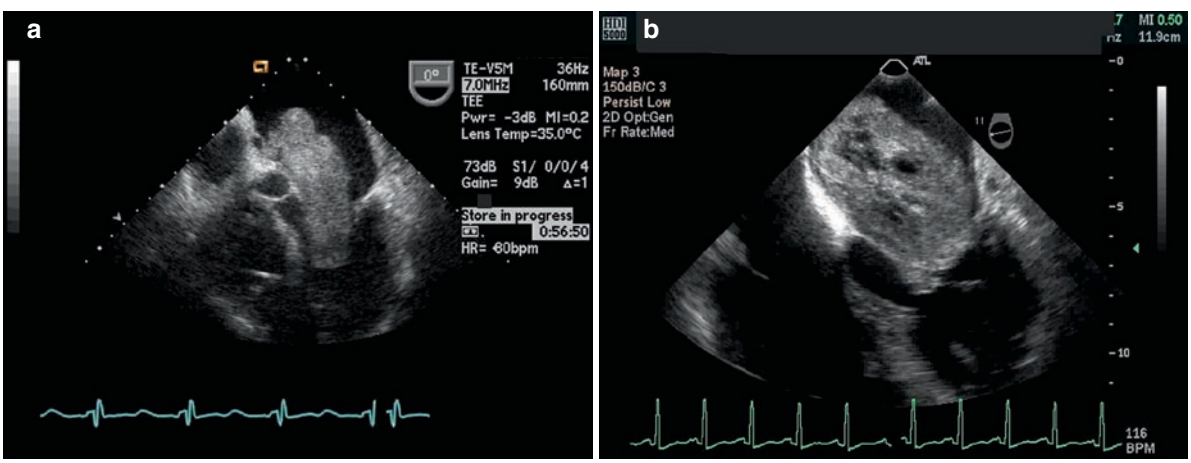

Fig. 25.10 LA myxoma – the image on the left shows a large tumor that appears to be attached to the interatrial septum, prolapsing through the mitral valve during diastole. The image on the right shows a large tumor with some cystic features prolapsing through the mitral valve

patients. Other presentations include symptoms associated with mitral valve obstruction or systemic constitutional symptoms (fever, weight loss). Once identified, a myxoma should be surgically removed. Long-term outlook is excellent, though 5% may recur, especially in those patients with the familial form.

Left Ventricular Thrombus

Thrombus in the LV usually occurs in the setting of marked regional systolic dysfunction post acute myocardial infarction (AMI), typically after large anteroapical infarcts, especially if there is evidence of LV aneurysm formation. Though less common, thrombus can also form (typically at the apex) in those with a dilated cardiomyopathy and severe global LV systolic dysfunction. Modern reports suggest that LV thrombus develops in about 5% of patients with AMI (~12% in those with anterior wall infarcts) who receive thrombolysis, an incidence that is significantly lower than in the prethrombolytic era (~20%). Most LV thrombi develop within the first 2 weeks post AMI (mean of 9.5 days). Those who develop thrombus early (within 48–72 h of infarction) have a very poor prognosis, dying from complications related to the size of their infarct and not embolic complications. Stasis in large areas of infarction and possibly endocardial inflammation during the acute phase of infarction providing a thrombogenic surface are suggested as the primary pathophysiologic factors.

Echocardiographic Identification

LV thrombus is better seen by TTE than TEE (Fig. 25.11). High sensitivity (95%) and specificity (90%) of TTE for LV thrombus have been reported in the past; however, more recent studies suggest a sensitivity of less than 50% when compared to contrast-enhanced MRI and/or surgical confirmation. TEE is not the test of choice as it is usually difficult to visualize the true apex, making exclusion of apical thrombus difficult. Typically LV thrombus appears as a distinct echodensity in the LV apex, which is seen throughout the cardiac cycle in at least two different echocardiographic views. It may have an irregular surface and may be sessile or pedunculated, mobile, or fixed. The thrombus is typically attached to the endocardium in an area of abnormal wall motion. It

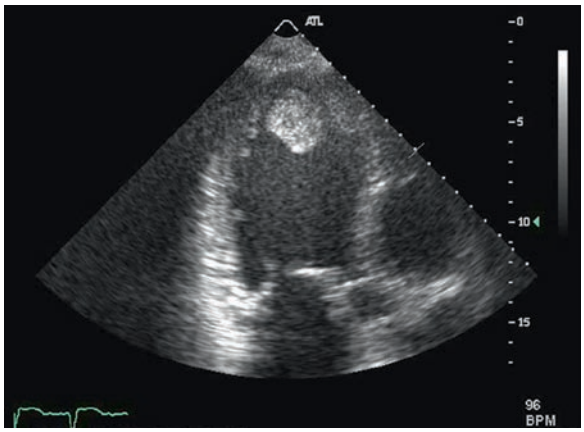

Fig. 25.11 Apical three-chamber view demonstrating a large left ventricular apical mass suggestive of thrombus

is mandatory to adequately visualize the LV apex in all patients with anteroapical LV dysfunction to prevent missing small thrombi that may not appear in all views. Using modern multifrequency transducers, the apical region should be magnified, the frequency maximized to optimize resolution in the near field, and the focus adjusted toward the LV apex. If there is uncertainty about an LV apical thrombus, filling the area with color-Doppler signals of low velocity (reduce the Nyquist limit) will enable color interrogation of the LV apex and can help to better define if there is an apical filling (flow) defect. Also, intravenous contrast agents can and should be utilized to opacify the LV apex and confirm any apical filling abnormality if there is uncertainty.

Risk of Embolization

The risk of systemic embolization from an LV thrombus is reportedly as high as 10%. The risk is greatest in the first 3 months post infarction, after which time the thrombus becomes organized and is less likely to embolize. Older age, lower ejection fraction, and absence of antithrombotic agents or anticoagulation are independently associated with increased embolic risk and stroke. Also larger, protruding, mobile thrombi are more likely to embolize. The presence of contiguous zones of akinesia and hyperkinesia is suggested to increase the risk of embolus. These patients with LV systolic dysfunction, irrespective of whether they are in sinus rhythm or atrial fibrillation, are also at increased risk for LAA thrombus formation. All

patients with LV thrombus should be anticoagulated for at least 3 months and up to 1 year. Currently both European and American consensus guidelines do not advocate routine anticoagulation for patients (whether ischemic or nonischemic) with severe LV dysfunction unless there is echocardiographic evidence of LV thrombus, a history of atrial fibrillation, or other indication for anticoagulation.

Valvular Vegetations

Vegetations due to infective endocarditis are potentially important sources of embolism. Typically the patient has a history of recurrent fever and constitutional symptoms and a possible precipitant (recent dental or other invasive procedure). The primary identification of vegetations during evaluation for a potential source of embolus is unusual, as clinically the diagnosis is usually suspected. Therefore, a large proportion of vegetations are identified before major embolic complications occur.

Echocardiographic Features

Vegetations have a number of typical echocardiographic features and the diagnosis can usually be made with a relatively high degree of certainty by echocardiography in combination with the clinical scenario (Fig. 25.12). They appear less reflective (gray) compared to normal valve tissue and are located upstream of the valve in the line of the jet of regurgitation (atrial surface of the mitral valve and ventricular surface of the aortic cusps). Typically they appear lobulated with irregular, poorly defined borders and have chaotic motion, in contrast to other valvular masses (fibroelastomas, etc.), which tend be more highly reflective, with well-defined borders and less chaotic motion. Thin stringy valvular attachments, with a narrow base, are more likely to be noninfectious fibrinous strands than vegetations. Features that help to discriminate vegetations from other masses include the presence of leaflet destruction, valve regurgitation, and abscess or fistula formation. The sensitivity of TTE for detecting features of endocarditis is reported to be between 44 and 60%, compared to a sensitivity of 88 and 100% for TEE. Small vegetations (<3.0 mm) are typically not seen by transthoracic imaging. Infection on prosthetic valves can be even more difficult to detect by TTE. Specificity for either modality is high (>90%), though with the superior resolution of TEE, the increased sensitivity may occur at the expense of a slightly reduced specificity (potential to label small benign fibrinous strands on native and prosthetic valves, or nonsignificant mobile suture material on prosthetic valves as small vegetations).

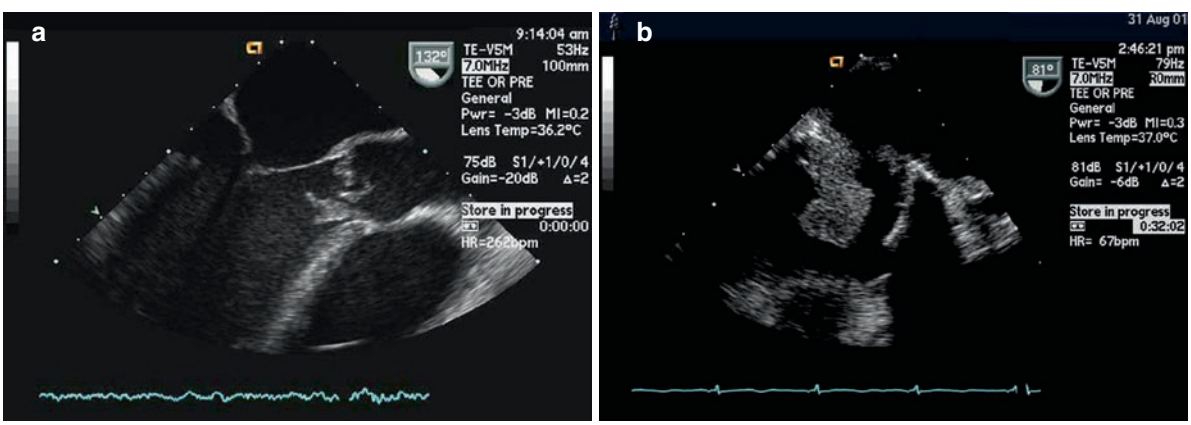

Fig. 25.12 The image on the left shows a vegetation on the right coronary cusp, prolapsing into the LV. The image on the right shows a large vegetation on the posterior leaflet of the mitral valve prolapsing into the LV during diastole

Factors Associated with Vegetation Embolism

The risk of embolization associated with vegetations varies widely (17–50%). Factors associated with embolic risk include vegetation size, mobility, and temporal changes in vegetation size. The most significant echocardiographic feature that is predictive of embolic risk is vegetation size. Vegetations >10 mm have a significantly higher incidence of embolic events compared to smaller vegetations (47% vs. 19%). Enlarging or unchanged vegetations after 4–8 weeks of therapy are associated with an increased incidence of embolic events (45% vs. 17%). Vegetations in the mitral position appear to have a greater embolic risk. Certain organisms are associated with larger vegetations including *Staphylococcus aureus* and the HACEK group of organisms. Despite adequate antibiotic therapy, vegetations may become organized and persist, and these residual lesions are much less likely to embolize.

No optimal treatment strategy for patients with large vegetations has been established. Vegetation size can change rapidly with treatment and in the absence of other indications for surgery (severe valvular destruction, abscess or fistula formation). A prudent strategy is to treat with appropriate antimicrobials and reassess with repeat TEE in 1–2 weeks.

Prosthetic Valves

An embolic event in a patient with a prosthetic valve is presumed related to the prosthesis until proven otherwise. The source of embolus can be valve thrombosis, valvular vegetations, or left atrial thrombus (with a mitral prosthesis). In one series of patients, with prosthetic valves undergoing TEE for investigation of a potential source of embolus, thrombus was detected on the valve in ~25%. For mechanical prostheses, the overall rate of thromboembolism is 0.7–1% per patient year for those treated with anticoagulation – a much lower rate (4% per patient year) than those without any anticoagulation. The relative risk of embolism is higher with mitral valve prostheses than aortic prostheses, most likely related to the lower flow velocities across the mitral valve. TEE is the investigation of choice for assessing prosthetic mechanical valves. Due to acoustic shadowing, the LA cannot be satisfactorily seen by TTE, and aortic prostheses are typically better seen with TEE. Vegetations or thrombus on these valves can appear similar, though vegetations are typically associated with constitutional symptoms and possible perivalvular regurgitation or partial valve dehiscence. Thrombus typically occurs in the scenario of inadequate anticoagulation. Typically thrombus is mobile, on the valve occluder and valve ring, is associated with SEC, and may cause valve obstruction with elevated Doppler gradients (Fig. 25.13). Treatment of mechanical valve thrombus depends on its severity and hemodynamic consequences. Those with evidence of valve obstruction are usually hemodynamically compromised and traditionally have required urgent surgery. Thrombolysis is now emerging as an effective alternative. For those without evidence of significant obstruction, aggressive and fastidious anticoagulation is warranted.

Fibrinous Strands/Lambl's Excrescences

The literature concerning these two terms is somewhat confusing and they are sometimes used interchangeably. Though the term "Lambl's excrescences" is usually only applied to those on the aortic valve, there is no evidence to suggest that mitral "fibrinous strands"

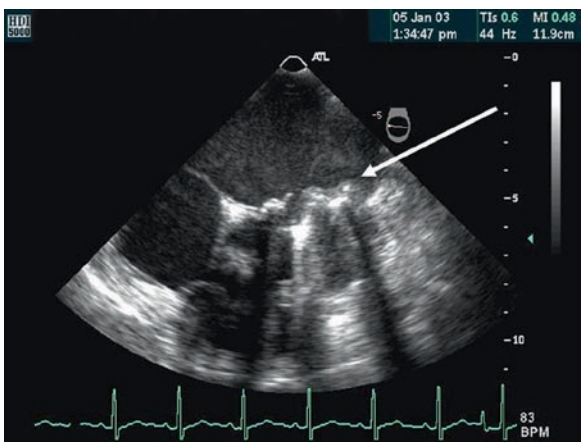

Fig. 25.13 Bileaflet mechanical mitral valve (St. Jude) with fixation of the lateral leaflet secondary to thrombus (*arrow*) and SEC in the LA cavity

are different. These strands are thin (up to 1.5 mm in width), elongated (up to 10 mm in length), frequently multiple, and located on the leaflet's line of closure, on the atrial side of the mitral valve, and on the ventricular side of the aortic valve (Fig. 25.14). Histologically they consist of a core of connective tissue with collagen and elastic fibrils or of an acellular hyaline material covered by endothelium. They have also been identified on prosthetic valves. They are equally frequent in both genders and all age groups, which negates against them being primarily a "degenerative" phenomenon. They are very common (~40% prevalence), with the mitral valve being a more common location than the aortic valve. The role of these valve strands in cardiac embolism is unclear. Initial retrospective studies suggested a relationship. However, more recent data have failed to show any association with embolic events and they do not appear to change over time. Therefore, based on current evidence, they are not thought to represent a significant embolic source and do not warrant treatment.

Papillary Fibroelastoma

These rare benign tumors are the most common type of valve tumor. They are more commonly seen on the aortic valve than the mitral valve but may arise from anywhere on the endocardium. From an echocardiographic perspective, they typically are small (<20 mm diameter), round, or oval in shape with well-demarcated borders, have a homogenous texture, and are more echodense than thrombus (Fig. 25.15). Typically they are single with more than half having a stalk and being mobile. They are most commonly seen on the aortic aspect of the aortic valve cusps or the atrial aspect of the mitral valve leaflets. Many are detected incidentally. Typically they do not cause valvular dysfunction. In the largest series reported, followed up for a mean of almost 2 years, there was a 6.6% incidence of neurologic events. The presence of a stalk (and hence tumor mobility) is reported to be a predictor of embolic risk. It is unclear whether embolic complications are due to thrombus forming on these tumors or embolization of fragments of the tumor itself. Current treatment of these tumors remains unclear. No data exist for the efficacy of anticoagulation or antiplatelet therapy, though treatment with aspirin appears sensible. Asymptomatic patients with small nonmobile tumors can be observed. It is unclear if large mobile tumors in asymptomatic people should be removed. In the setting of an embolic event, surgery is generally recommended.

Mitral Stenosis

Rheumatic mitral stenosis is typically associated with marked LA enlargement, atrial fibrillation, high risk of LA thrombus formation, and systemic embolization (20% lifetime incidence). These patients can have very large amounts of thrombus within the LA. Embolization

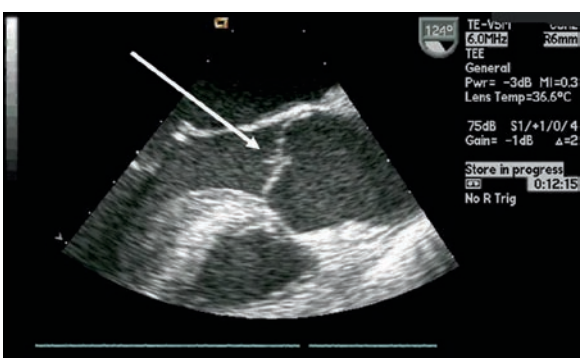

Fig. 25.14 Fibrinous strand on the right coronary cusp of the aortic valve (Lambl's excrescences)

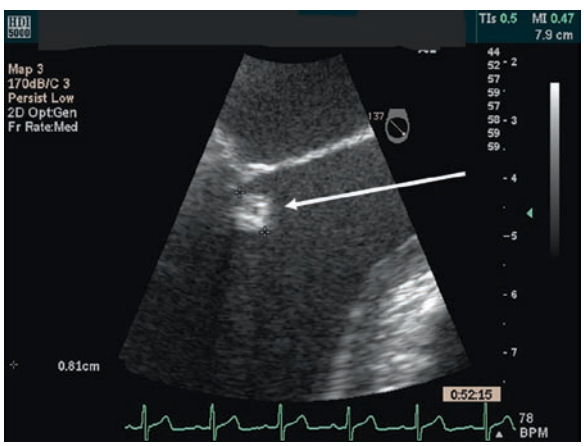

Fig. 25.15 Papillary fibroelastoma on the anterior leaflet of the mitral valve

can occur despite the presence of sinus rhythm and appears to be unrelated to the severity of the stenosis. The primary risk factors identified for thromboembolism are age and the presence of atrial fibrillation. Currently anticoagulation is indicated for all who have atrial fibrillation, a history of a systemic embolism, or echocardiographic evidence of LA thrombus (ACC/AHA Guidelines 2006). Anticoagulation of patients on the basis of severity of mitral stenosis, severe LA enlargement (LA diameter >5.5 cm), or the presence of spontaneous echo contrast remains controversial.

Mitral Annular Calcification

Mitral annular calcification (MAC) is one of the most common valve abnormalities detected by echocardiography in elderly patients who are referred for a cardiac source of embolism. It is easily seen by TTE (with TEE tending to underestimate the degree of calcification). MAC is defined by increased echodensity of the mitral annulus, most common posteriorly, but may extend around the entire annulus, giving the appearance of a calcified ring like at the base of the mitral valve. It is found predominantly in elderly women (48% prevalence in a series - mean age of 81 years) and is associated with obesity, systolic hypertension, aging, aortic stenosis, and renal failure. A number of retrospective studies have suggested that MAC is a risk factor for stroke, postulating that it may serve as a nidus for thrombus formation. However, in recent studies MAC was also found to be strongly associated with carotid and complex aortic atheroma. It therefore remains controversial whether MAC is an independent risk factor for stroke or just a marker of increased risk.

Mitral Valve Prolapse

It has been suggested that the redundant leaflets associated with myxomatous mitral valve prolapse (MVP) may act as a nidus for thrombus. Older studies showed a relationship between mitral valve prolapse and stroke, particularly in young patients. However the data from more recent studies have been conflicting. The largest prospective study of MVP and stroke (777 patients) demonstrated an overall twofold increased risk of ischemic stroke. Independent risk factors for ischemic stroke in this population of patients with MVP were older age, mitral leaflet thickening, subsequent development of atrial fibrillation, and need for cardiac surgery. Currently, guidelines (ACC/AHA 2006) advise that primary prevention of stroke with aspirin may be considered for patients in sinus rhythm with evidence of high-risk MVP (leaflet thickening >5 mm and/or leaflet redundancy). In addition, secondary prevention of stroke with warfarin may be considered for patients with evidence of high-risk MVP, but without standard indications for anticoagulation such as atrial fibrillation or LA thrombus.

Patent Foramen Ovale and Atrial Septal Aneurysm

Anatomy

During fetal development, the interatrial septum develops from the fusion of the residual septum primum (lower portion) and the septum secundum (upper portion). Normally the septum secundum overlies the septum primum on the left creating a flap, leaving a patent channel between both atria in utero. This serves as a conduit for the flow of oxygenated blood from the right atrium to the LA, bypassing the high-resistance unoxygenated lungs. After birth, with inflation of the lungs, right atrial pressure drops below LA pressure, causing the two layers of this flap to oppose each other and they typically fuse, closing over this connection (foramen ovale). However, in up to 25% of the population, these two flaps do not fuse completely resulting in a persistent PFO. Typically there is little flow across the residual PFO and any spontaneous flow is typically from left to right as the LA pressure is higher. However, if right atrial pressure exceeds LA pressure either transiently (with Valsalva or other such maneuvers) or more chronically (pulmonary thromboembolic disease), flow can be directed from right to left, with the potential that right-sided venous thromboembolism can cross into the arterial circulation and result in systemic emboli. An atrial septal aneurysm (ASA) is defined as a bulging of the interatrial septum in its midportion (fossa ovalis). The differentiation between a normal mobile septum and an ASA is arbitrary. The

most commonly used definition for an ASA is if the sum of the maximum excursions of the midpoint of the aneurysm in both directions from the midline is ≥15 mm. The prevalence of a PFO decreases with increasing age (34% in the first three decades, decreasing to 20% in the ninth decade). An ASA is much less frequent, occurring in 1–2% of the general population. Though when it is present, there is a very high prevalence of having an associated PFO (56–77%).

Echocardiography

Transesophageal echocardiography is the imaging modality of choice for evaluating for a PFO (Fig. 25.16). Its presence can often be suggested by TTE; however, the interatrial septum is in the "far field" and in the apical four-chamber view it lies parallel to the ultrasound beam. Therefore there is often "drop-out" of the echo signals giving a false impression of a defect. If optimal subcostal images are possible, a better alignment (the interatrial septum lies perpendicular to the imaging plane) provides for more optimal assessment. Often in this view with color Doppler, a PFO can be suggested by the appearance of a narrow jet of left-to-right flow. Assessment of right-to-left shunting is achieved by injecting agitated saline into an antecubital vein to opacify the right atrium and documenting the appearance of bubbles within the LA within 3–5 cardiac cycles, either spontaneously or during a Valsalva maneuver (transient increases in right atrial pressure). Late (>5 beats) appearance of bubbles within the LA may be due to intrapulmonary shunting and does not necessarily imply flow across the interatrial septum. Agitated saline is created by mixing 8–9 ml of sterile saline with 1 ml of air in a 10-ml syringe, followed by repeated rapid injection to and from another syringe connected via a three-way stopcock until the mixture appears cloudy. Addition of approximately 1 ml of

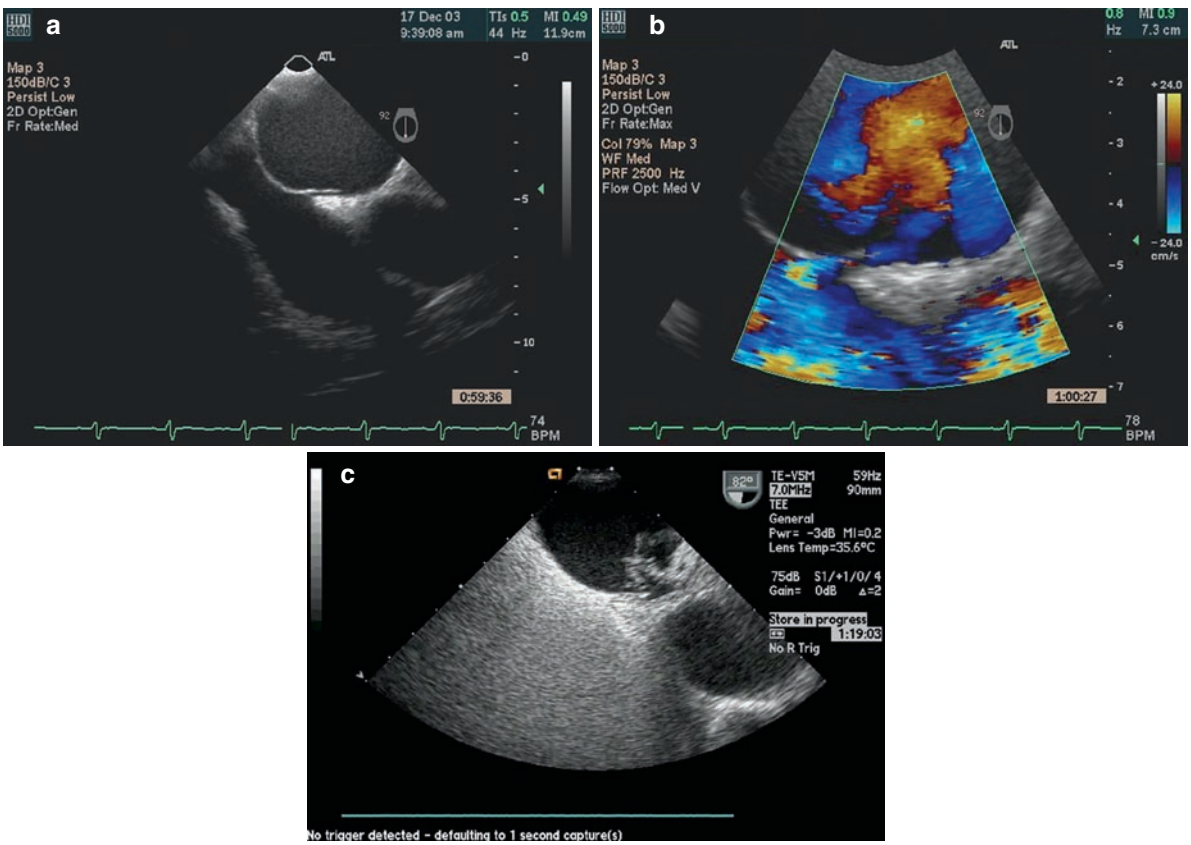

Fig. 25.16 Patent foramen ovale (PFO): the 2-D TEE image shows the typical appearance of a PFO, which was confirmed by color Doppler (left-to-right shunt) and bubble injection (right-to-left shunt)

blood (withdrawn prior to injection) improves its contrast potential.

TEE is more sensitive for the detection of a PFO than TTE (22% vs. 8%, in one series). By TEE, the interatrial septum lies in the "near field" and can be evaluated with superior resolution in multiple planes. Typically a PFO appears like a flap, near the inferior aspect of the interatrial septum, though color-Doppler interrogation of the septum is necessary to confirm its presence. Flow across a PFO is typically minimal and of low velocity; therefore, the color-aliasing velocity (Nyquist limit) should be reduced, to enable detection of lower velocity signals. Confirmation of right-to-left shunting (which is of most interest in the setting of its systemic embolic potential) requires right-sided contrast (agitated saline). Typically a PFO appears much smaller when measured by echocardiography than when it is sized with a balloon across it, emphasizing that it can stretch and potentially accommodate the passage of a much larger thrombus across it than would be appreciated visually. The size of right-to-left shunting across a PFO is graded arbitrarily based on the number of bubbles seen crossing, with <10 bubbles considered a trivial shunt, ≥10 bubbles a small shunt and intense opacification of the LA suggesting a large shunt.

An ASA can be seen by TEE or TTE but is more optimally seen by TEE (Fig. 25.17). In one series, 27% of ASA noted by TEE were not detected by TTE. By TTE, it is best appreciated in the four-chamber apical or subcostal views. By TEE, it can be seen in multiple views with the bicaval view (at ~90°) probably being best.

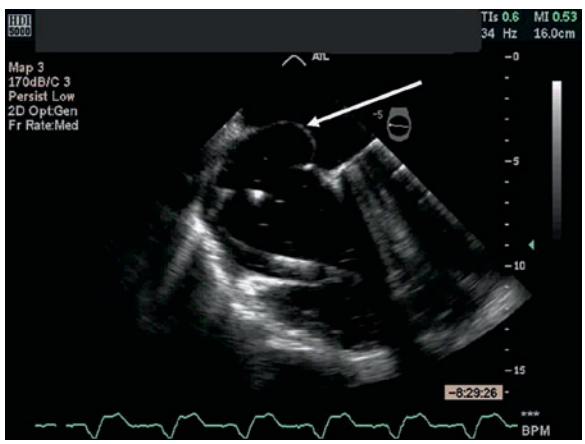

Fig. 25.17 An atrial septal aneurysm (*white arrow*) with bulging of the septum into the LA

Potential Mechanisms of Stroke

A number of potential mechanisms underlying stroke in patients with a PFO have been proposed, highlighting the persistent confusion surrounding this relationship.

1. Paradoxical embolism of a right-sided clot:

This remains the primary putative mechanism of stroke in these patients. There are anecdotal case reports of thrombus caught in transit across a PFO. In order for an embolism to cross the PFO, the embolism has to occur at the same time as there is increased right atrial pressures, either transiently (Valsalva) or more persistently (elevated right-sided pressures). One series of younger patients with stroke reported no difference in the frequency of a Valsalva provoking activity at the time of the stroke between those with and those without a PFO. Although one study found evidence of deep venous thrombosis (DVT) in 57% of patients with arterial embolism and a PFO, the rate in several other studies was much lower (4–10%). Overall, despite the appealing hypothesis of paradoxical embolism, evidence remains scanty.

2. Thrombosis in situ:

There are some anecdotal reports of small amounts of thrombus being identified in PFOs of patients with strokes and also within ASA, suggesting that local thrombus formation may be an alternative hypothesis.

3. Coexistence of atrial arrhythmias:

Some data suggest a potential role of transient atrial arrhythmias in thrombosis formation in patients with a PFO

Association of PFO with Embolic Events

A PFO is a common finding and confirming a cause and effect with embolic events has proven difficult. Most data have come from retrospective case control studies. The original study suggested that a PFO was present in 40% of young (<55 years) people with a stroke, and 54% of those with a cryptogenic stroke, compared to 10% in a control group. In a meta-analysis of nine studies in patients <55 years, the rate of stroke

was significantly associated with a PFO (odds ratio = 3.1) and an ASA (odds ratio = 6.1). The combination of a PFO plus ASA was associated with much higher rate of stroke (odds ratio = 15.6). These associations were not found in older patients. One recently published, prospective study followed up 585 randomly sampled community residents 45 years or older for a median of 5.1 years.140 (24.3%) had a PFO and 11 (1.9%) an ASA by TEE. There was no association between PFO and stroke (hazard ratio: 1.46, 95% confidence interval: 0.74–2.88, $p = 0.28$). However there was a trend toward a link between ASA and cerebrovascular events (hazard ratio: 3.72, 95% confidence interval: 0.88–15.71, $p = 0.074$). The risk of recurrent cerebrovascular events in patients with cryptogenic stroke and PFO ranges from 1.5 to 12% per year, depending on the study population. Although one study has shown a significantly higher risk of recurrent stroke in patients with PFO and ASA (4-year recurrence rate: 15.2% vs. 2.3% for PFO alone and 4.2% for neither), other studies have not replicated these findings.

Factors Associated with Increased Risk

A number of factors have been suggested to be associated with increased risk:

1. PFO size – the larger the PFO, the stronger the association
2. Right-to-left shunting – More shunting is associated with higher risk, especially right-to-left shunting without provocation.
3. Presence of an ASA/increased mobility of the septum - This may be due to the mechanical effect of it acting like a wind sail to direct flow from the inferior vena cava to the PFO.
4. PFO with a "tunnel" like appearance
5. Documented deep venous thrombosis

Treatment

There is no evidence to suggest that any treatment is warranted if a PFO or ASA is identified in an asymptomatic patient. There are limited data to guide therapy in patients who present with a cryptogenic stroke and an atrial septal abnormality. In a prospective study of aspirin therapy in 581 patients with cryptogenic stroke the risk of recurrent stroke at 4 years was 2.3% in patients with PFO alone, 15.2% in patients with both PFO and ASA, 0% in patients with ASA alone, and 4.2% among patients without an atrial septal abnormality. Only one study has prospectively compared therapy with aspirin to warfarin in patients with cryptogenic stroke and PFO. In the PICCS study (PFO in cryptogenic stroke), patients were randomized to warfarin (INR: 1.4–2.8) or aspirin 325 mg daily. In the subset of 98 patients with cryptogenic stroke and PFO there was no significant difference in the 2-year recurrent stroke and death rate between the two treatment arms (17.9% vs. 9.5%, respectively; $p = 0.28$).

Surgical closure of a PFO is achieved either by simple suture closure or patch occlusion. Several small series of surgical closure have been reported with varying rates of recurrent stroke (4–20%). Because of the morbidity and mortality of cardiac surgery, isolated surgical closure of a PFO has more or less been supplanted by percutaneous closure. Several devices have been developed for percutaneous PFO closure, and rates of recurrent stroke of 0–5% following device implantation have been reported in case series. Major complications appear to occur at a rate of 1–3% (device embolization, thrombosis, infection, fracture, CVA, pulmonary embolism, arrhythmia, transfusion). Only the Amplatzer™ and Cardioseal™ devices have received approval for the treatment of PFO through a Humanitarian Device Exemption from the U.S. Food and Drug Administration (FDA). The labeling of these devices restricts their use to patients with PFO and cryptogenic stroke who have failed conventional drug therapy. A number of prospective randomized trials are ongoing to comprehensively compare medical and percutaneous strategies. Recent consensus guidelines from the American Heart and American Stroke Associations for the treatment of patients with a cryptogenic stroke and PFO recommend initial antiplatelet therapy to prevent a recurrent event, or warfarin therapy for high-risk patients who have other indications for oral anticoagulation such as venous thrombosis or a hypercoagulable state. There are insufficient data to recommend surgical or percutaneous PFO closure. However, surgical or percutaneous intervention may be considered for recurrent cryptogenic stroke despite optimal medical management.

Therefore, current evidence appears to suggest that there is an increased prevalence of PFO in patients with cryptogenic strokes. Those with larger defects, more right-to-left shunting, and those associated with an ASA appear to be at higher risk. Current treatment strategies have not been clarified. Aspirin may be as efficacious as anticoagulation, though there may be a significant risk of recurrence. The low risk of recurrent stroke following percutaneous closure has led to the widespread adoption of this therapy. However, randomized trials are needed to determine if there is truly an improvement in outcome vs. medical management.

Thoracic Aortic Atheroma

Echocardiographic Assessment

Atherosclerotic changes in the thoracic aorta are increasingly being recognized as a potentially important source of embolus. It is common with a reported prevalence of 9–13% in asymptomatic adults. Atheroma in the thoracic aorta is not adequately visualized by TTE; thus, TEE is the imaging modality of choice (Fig. 25.18). It is usually divided into three portions: ascending portion, aortic arch, and descending aorta. From a cerebral embolic risk, it is the ascending thoracic aorta and the aortic arch proximal to the origin of the left common carotid that are of most interest. With TEE, the aortic root is best seen in the long-axis view of the aortic valve (~120°). Slight withdrawal of the transducer with a reduction in the angle of rotation (~90–100°) will give satisfactory long-axis visualization of the tubular ascending aorta. There is an echocardiographic blind spot at the junction of the upper ascending aorta and aortic arch due to the interposition of the left main bronchus. Visualization of the descending aorta begins in the transgastric view with posterior rotation of the probe shaft to bring the descending thoracic aorta into the imaging window. The descending aorta lies behind and very close to the upper portion of the stomach and the esophagus, and the depth of the imaging plane should be adjusted to magnify the aorta.

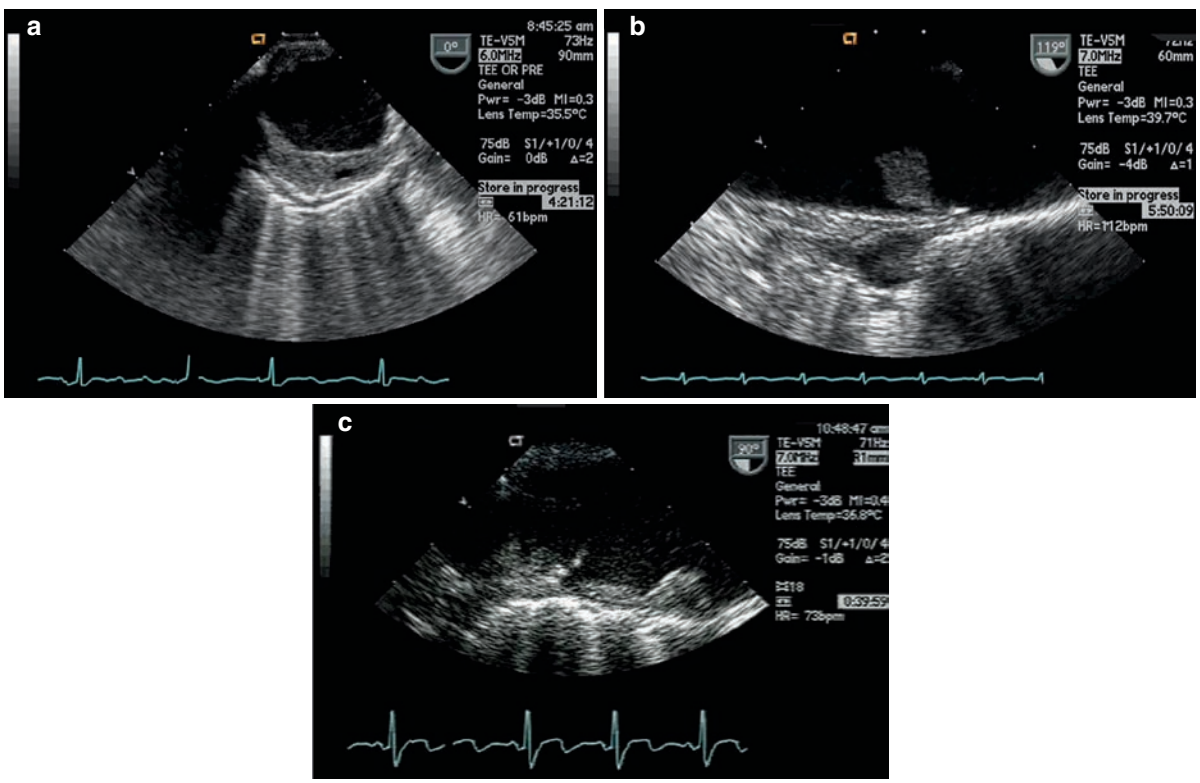

Fig. 25.18 Complex aortic atheroma: the *upper left image* demonstrates severe sessile atheroma in the descending aorta. The *upper right image* shows a focal pedunculated atheromatous lesion in the thoracic aorta. The *lower image* shows diffuse severe complex atheroma

The probe is gradually withdrawn to visualize the entire thoracic descending aorta, which at 0° of rotation appears in its short axis. Any abnormality should be evaluated in its short and long axes with imaging at 0° and 90° of rotation, respectively. As the probe is withdrawn to about 20 cm from the incisors, the aortic arch will begin to appear. This is best visualized by rotating the probe anteriorly to open out a long-axis view of the aorta and visualize the origin of the great vessels. Visualization of the aortic arch is generally kept until the end of the study as many patients experience reflex gagging with the probe in this position and find it the most uncomfortable part of the study necessitating its removal.

Ultrasound cannot differentiate the vessel intimal layer from the media but does detect a change between the media and the bright adventitia. Therefore, for quantification purposes, it is standard to measure the thickness to the level of the bright adventitia and label this as the "plaque" thickness. Traditionally aortic atheroma has been graded using a scoring system of I – IV, though it is probably better to measure the depth of the plaque and describe its characteristics (presence of areas of ulceration, calcification, sessile vs. pedunculated, and/or degree of plaque mobility). In histologic comparison, TEE showed good correlation in the separation of normal and minimal intimal thickening from more complex atheromas (93% agreement) with 100% agreement in the detection of mobile thrombus.

Association of Thoracic Aortic Atheroma and Stroke

Observational case-control series have shown a significantly higher prevalence of complex atheroma (mobile or ulcerated plaque and plaque >4 mm thick) in patients with a stroke (21–27%) compared to controls (4–13%). In prospective studies, the incidence of stroke at 1 year in patients with protruding atheroma was 12%, with an incidence for all embolic events of 33%. The combination of atrial fibrillation and complex aortic plaque is associated with a higher risk of stroke (12–20% at 1 year) compared to a stroke risk of 1–2% for those with atrial fibrillation without significant aortic plaque. Regardless of anticoagulation or aspirin, this is further evidence to suggest the independent significant embolic potential associated with aortic atheroma.

The prevalence of stroke or other embolic events appears to be influenced by plaque morphology. Plaque size (depth), plaque calcification, and plaque mobility are all important features. Increased plaque thickness is associated with a higher risk of stroke with a cut-off of ≥4 mm in particular associated with a significantly higher risk of stroke. The significance of visible plaque ulceration is unclear with the available data suggesting that ulceration in thinner plaques is associated with increased risk, while this relationship is not significant in thicker (>4 mm) plaques. The presence of calcification within plaques is associated with a reduced risk of embolic events, a feature likely explained by the fact that calcification most likely represents the presence of more chronic fibrotic, less lipid-laden plaques. Mobile components to aortic atheroma are also associated with increased embolic risk with echopathologic correlation suggesting that these mobile elements are thrombus. Based on current evidence, it appears that most embolic events related to aortic atherosclerosis are secondary to embolization of thrombus that formed on these atherosclerotic lesions.

Emboli During Aortic Manipulation

There is a risk of emboli with aortic manipulation during cardiac surgery or during left heart catheterization. Embolic complications are rare during cardiac catheterization (0.5% rate of stroke). However, when embolic complications do occur, aortic atheroma is a common association. Reported rates of embolic complications during cardiac surgery involving cardiopulmonary bypass are of the range of 2–7%. Those with aortic atheroma >5 mm on TEE have significantly higher risk of intraoperative stroke. Intraoperative TEE or epicardial echocardiography is used to assess the aorta to help risk stratify these patients and locate a safe point for cannula insertion and crossclamping. Epicardial echocardiography uses a high-frequency small-sized (transthoracic) transducer covered with a sterile sheath, placed directly on the aorta to visualize the ascending aorta and aortic arch with excellent resolution. A "stand-off" (a saline filled glove) can increase the distance between the transducer and the aorta enabling satisfactory visualization of the anterior wall that may be difficult to see (too close) with the transducer placed directly on the aorta.

Management of Patients with Aortic Atheroma

No consensus exists as to optimal management of patients with complex aortic atheroma. Use of antithrombotic agents and/or anticoagulants appears logical in view of the pivotal role of thrombus in embolic events. Aspirin therapy is generally given for all patients with significant atherosclerotic disease. HMG-Co-A reductase inhibitors (statins), with their documented benefits in people with atherosclerosis, are usually also considered. A reduction in the incidence of stroke has been documented for hyperlipidemic patients and also in those with more "normal" cholesterol levels. Despite the fact that anticoagulant therapy has not been prospectively assessed for patients with aortic atheroma, observational data suggest that it is probably beneficial. Thrombectomy and endarterectomy of complex aortic arch atheroma may be considered for good surgical candidates with recurrent embolic events despite optimal medical therapy. However this approach is associated with a high rate of neurological and vascular complications.

Overall Approach to Evaluation

A cardiovascular source of embolus is increasingly being identified when investigating patients with acute cerebral, peripheral, or visceral ischemia. Most reports have focused on sources of embolus in patients with a stroke. As outlined, the level of evidence demonstrating conclusive cause and effect is limited, and these potential sources are best described as "associations" rather than conclusive causes. It is important to thoroughly evaluate patients for all potential sources, and it is not exceptional to find more than one potential source in a patient, especially as the prevalence of many of these factors increases with advancing age. Additionally, both carotid disease and thoracic atheroma are manifestations of the same disease process, and it is not surprising that patients with significant carotid atherosclerosis have a higher prevalence of aortic arch atherosclerosis than those without carotid disease. Therefore, evaluation of the aorta may be warranted, especially if the neurologic event is contralateral to carotid stenosis or if carotid disease is associated with peripheral or visceral emboli.

Impact of Echocardiography on Patient Management

Once the acute phase of a neurological event has occurred, the primary aim is to identify any potentially treatable sources and prevent recurrent, potentially fatal events. Data suggest recurrence rates for all stroke subtypes of 9.4% per year and 10% for cryptogenic stroke. TEE has been reported as being useful in risk stratifying patients post stroke. One series of patients, who were followed for two years and stratified into low and high risk (based on the presence of at least one likely or possible risk factor for embolism at TEE), showed that those in the low-risk group had significantly better survival (92% vs. 63%, $p = 0.04$). In the STEPS study (242 patients followed after TEE for unexplained stroke) TEE, by demonstrating aortic atheroma and LV dilatation, identified subgroups at high risk of recurrent stroke if treated with aspirin alone, suggesting a potential role for TEE to help guide therapy and influence outcome after an index cerebral event. However, prospective studies are needed to determine whether identification of predictors of stroke recurrence can be translated into improved patient outcome.

Bibliography

Cheitlin MD, Armstrong WF, Aurigemma GP, et al. ACC/AHA/ASE 2003 guideline update for the clinical application of echocardiography–summary article: a report of the American College of Cardiology/American Heart Association Task Force on Practice Guidelines (ACC/AHA/ASE Committee to Update the 1997 Guidelines for the Clinical Application of Echocardiography). *J Am Coll Cardiol.* 2003; 42: 954–70.

Donal E, Yamada H, Leclercq C, Herpin D. The left atrial appendage, a small blind ended structure: a review of its echocardiographic evaluation and its clinical role. *Chest.* 2005; 128: 1853–1862.

Goldman ME, Croft LB. Echocardiography in search of a cardioembolic source. *Curr Probl Cardiol.* 2002; 27: 342–358.

Homma S, Sacco RL. Patent Foramen Ovale and Stroke. *Circulation* 2005; 112: 1063–1072.

Homma S, Sacco RL, Di Tullio MR, Sciacca RR, Mohn JP (PICSS Investigators). Effect of medical treatment in stroke patients with patent foramen ovale. *Circulation.* 2002; 105: 2625–2631.

Macleod MR, Amarenco P, Davis SM, Donnan GA. Atheroma of the aortic arch: an important and poorly recognized factor in the etiology of stroke. *Lancet Neurol.* 2004; 3: 408–414.

Section 6
Congenital Heart Disease

Chapter 26
Simple Congenital Heart Defects

George A. Pantely and Michael A. Gatzoulis

Introduction

The congenital heart defects discussed in this chapter are common, straightforward lesions with a structural abnormality causing a specific hemodynamic problem. Once identified, they can usually be repaired by well-established techniques, usually surgical.

Echocardiography plays a vital role in the diagnosis and management of these anomalies. This chapter focuses on the essentials of the echocardiographic evaluation of these lesions. It does not cover the infinite variations that occur.

Segmental Approach to Cardiac Anatomy

This section outlines an approach to determine the relationship of the cardiac chambers. This is important as cardiac malpositions are frequently present in congenital heart defects, especially the more complex anomalies. The steps of this approach include (Tables26.1–26.5):

- Apex position
- Cardiac situs
- Identification of chambers and vessels
- Atrioventricular relationships
- Ventriculoarterial relationships

G.A. Pantely (✉) and M.A. Gatzoulis
Adult Congenital Heart Disease Program, Oregon Health and Science University, Portland, OR, 97239, USA
e-mail: pantelyg@ohsu.edu

This is a brief summary of a systematic approach to determine the relationship of the various cardiac chambers. A variety of other complex relationships exist, however, which are not discussed here or may not adhere to the simplified scheme presented.

Shunts and Septal Defects

Atrial Septal Defect

Anatomy and Physiology

The three commonest atrial septal defects (ASDs) are named after their location in the interatrial septum (Fig. 26.1).

- Secundum (foramen ovale) defect (70–75% of cases) is a hole in the tissue that covers the fossa ovalis. It is usually an isolated lesion.
- Primum defect (15–20% of cases) involves the lower (primum) portion of the atrial septum. It may occur alone or in association with a small inlet ventricular septal defect (VSD) and a cleft mitral valve. This will be discussed further under AV septal defects.
- Sinus venosus defect (5–10% of cases) is located in the superior portion of the atrial septum near the SVC. It is associated with anomalous return of right pulmonary vein to RA/SVC junction.

These defects produce a left-to-right atrial shunt that causes right atrial and right ventricular enlargement. Pulmonary hypertension is rare. Individuals with small to moderate shunts are asymptomatic. Dyspnea, fatigue, and congestive heart failure occur in larger

P. Nihoyannopoulos and J. Kisslo (eds.), *Echocardiography*,
DOI: 10.1007/978-1-84882-293-1_26,

shunts. Most individuals with an ASD are identified and repaired in childhood.

Echocardiographic Evaluation

The goals for the examination are to:

- Determine the anatomic site of the septal defect
- Evaluate the hemodynamic significance of the shunt
- Determine RV systolic pressure
- Establish return of the four pulmonary veins
- Identify associated lesions

Table 26.1 Determination of apex position (subcostal view)

Term	Definition
Levocardia (normal position)	Apex points to the left side
Dextrocardia	Apex points to the right side

Table 26.2 Identification of chambers and vessels

Chamber/vessel	Characteristic
Aorta, abdominal	Round
	Thick walled
	Pulsatile
IVC	Ovoid
	Thin walled
	Nonpulsatile
	Collapses with inspiration
Right atrium	Receives IVC/SVC
	Broad, short appendage
	Eustachian valve
Left atrium	Receives pulmonary arteries
	Narrow, long appendage
Right ventricle	Trabeculated endocardial surface
	Moderator band
	Chordae attached to the septum
	Tricuspid valve remains part of RV
	Three-leaflet valve and more apically inserted than mitral valve
Left ventricle	Smooth endocardial surface
	Two papillary muscles without chordal attachments to the septum
	Mitral valve remains part of LV
	Two leaflet AV valve more basally displaced than the tricuspid valve
Aorta	Arching vessel
	Origin of coronary arteries
	Origin of great vessels
	Aortic valve remains with the aorta
Pulmonary artery	Bifurcation with branches running posteriorly
	Right branch passes behind the aortic arch
	Pulmonary valve remains with the pulmonary artery

Table 26.3 Determination of abdominal and cardiac situs from abdominal short-axis and subcostal views

Term	Definition
Atrial situs solitus (normal)	RA on right side and LA on left side
Abdominal situs solitus (normal)	Aorta to the left of the spine and IVC to the right
	Atrial situs follows abdominal situs 70–80% of cases
Atrial situs inversus	RA on left side and LA on right side
Abdominal situs inversus	Aorta to the right of the spine and IVC to the left
	High probability of atrial situs inversus when abdominal situs inversus is present
Left atrial isomerism	Two morphologic left atria
	Aorta and IVC on the same side of the spine with the IVC anterior to the aorta
Right atrial isomerism	Two morphologic right atria
	Aorta and IVC on the same side of the spine with the aorta anterior to the IVC

Table 26.4 Identification of atrioventricular relationships

Term	Definition
Atrioventricular concordance (normal)	Morphologic RA to morphologic RV Morphologic LA to morphologic LV
Atrioventricular discordance	Morphologic RA to morphologic LV Morphologic LA to morphologic RV
Double inlet (left or right) ventricle	Both atria enter into 1 ventricle (either left or right)

Table 26.5 Identification of ventriculoarterial relationships

Term	Definition
Ventriculoarterial concordance (normal)	Morphologic LV gives rise to aorta Morphologic RV gives rise to PA Pulmonary valve lies slightly anterior and to the left of the aortic valve
Ventricular-arterial discordance, D-type	Morphologic LV gives rise to PA Morphologic RV gives rise to aorta Ventricular positions are normal (RV to the right of LV)
Ventriculoarterial discordance, L-type	Morphologic LV gives rise to PA Morphologic RV gives rise to aorta Atrioventricular discordance is present and RV lies to the left of the LV
Double outlet (right or left) ventricle	Greater than 50% of both great arteries exit from one ventricle (either left or right)

The best views are the apical four chamber, subcostal four chamber (best for imaging the interatrial septum), and right parasternal (best for sinus venosus defects).[1] Echocardiography can usually establish the diagnosis by direct visualization of a secundum and primum ASD. Unexplained right heart enlargement should always prompt a search for an ASD. If a defect is not seen, agitated saline contrast or TEE is sensitive for detecting and localizing an interatrial shunt. A sinus venosus defect may require this level of scrutiny.

Color Doppler from the subcostal view will show flow across the interatrial septum. Since the pressure gradient between the atria is small, velocity is low (usually less than 1–1.5 m/s) and occurs in late ventricular systole and early diastole. Calculation of shunt ratio is usually not necessary. Right ventricular enlargement indicates a hemodynamically significant shunt, being present when the output of the right heart exceeds the left by 50% $Q_p/Q_s \geq 1.5$.

Right ventricular peak systolic pressure is essential information to obtain as part of the examination. The best tricuspid regurgitant Doppler signal should be sought from multiple views. By applying the modified Bernoulli equation to the peak velocity of the tricuspid regurgitation jet, the pressure gradient between the right ventricle and right atria is obtained. Adding on an assumed or measured mean right atrial pressure to this pressure gradient gives the estimate of right ventricular systolic pressure in mmHg. The modified Bernoulli equation is

$$\text{RV systolic pressure (mmHg)} = [(4) \times (\text{TRvelocity}\{\text{m/s}\})]^2 + \text{RA pressure (mmHg)}.$$

Cautions

- Normal anatomic variants are important to recognize to avoid confusion. These include atrial septal aneurysm, Eustachian valve (associated with the entrance of the IVC into the right atrium), and Chiari Network (a strand-like structure that extends from the orifices of the SVC and IVC).
- Dropout of echo signal from the foramen ovale occurs when the echo beam is parallel to the interatrial septum in the apical four-chamber view. This gives the false appearance of a septal defect. This is avoided by being certain a defect is present when the beam is perpendicular to the septum as in the subcostal view (Fig. 26.2).

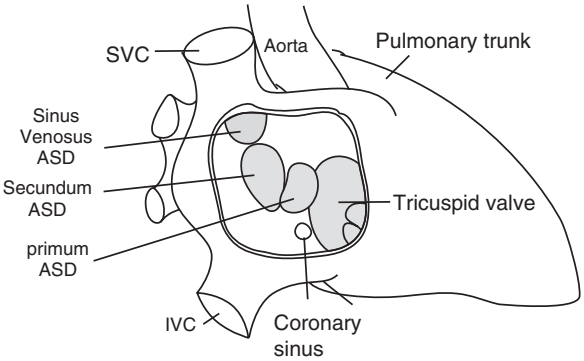

Fig. 26.1 Diagram illustrating the anatomic location of the three most common atrial septal defects. This is looking through the right atrium onto the interatrial septum. An ostium secundum defect is centrally located in the region of the foramen ovale. An ostium primum defect is in the septum inferior to the foramen ovale. A sinus venosus defect is located superior to the foramen ovale. It is adjacent to the right upper pulmonary vein that may drain anomalously into the superior vena cava/right atrial junction as part of the defect. *SVC* superior vena cava, *IVC* inferior vena cava

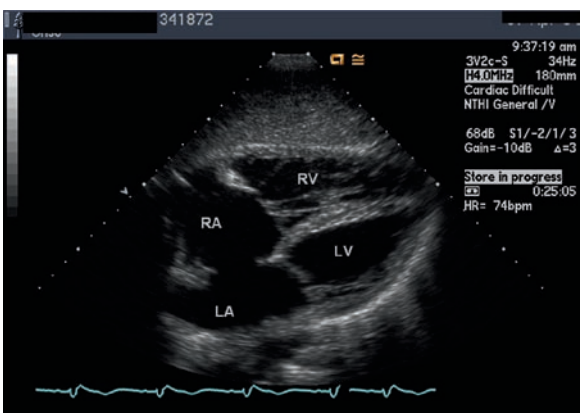

Fig. 26.2 Secundum atrial septal defect as seen in the subcostal view. The defect is located in the middle region of the septum. The right atrium and the right ventricle are enlarged indicating a hemodynamically significant left-to-right shunt. *RA* right atrium, *RV* right ventricle, *LA* left atrium, *LV* left ventricle

Atrioventricular Septal Defect

Anatomy and Physiology

Division of the common A–V canal occurs by fusion of the superior and inferior endocardial cushions. Failure of this affects the structures derived from endocardial cushion tissue to varying degree. A complete atrioventricular (AV) septal defect consists of

- Ostium primum ASD
- VSD of the inlet septum
- Common five-leaflet valve with an anterior bridging leaflet, a posterior bridging leaflet, a left mural leaflet, a right mural leaflet, and a right anterosuperior leaflet. This valve is all at the same level within the ASD and VSD (Fig. 26.3a, b). The AV valve is usually equally committed to both ventricles, but may be primarily committed to one ventricle. Further description of the AV valve is based on the extent and location of attachments of the anterior bridging leaflet
- Type A. Tethered by chordae to the crest of the ventricular septum
- Type B. Attached to an anomalous papillary muscle in the RV
- Type C. Free floating (no chordal attachments)

A partial AV septal defect (ostium primum ASD) consists of

- An AV valve divided into right- and left-sided orifices by a band of tissue connecting the superior and posterior bridging leaflets. In this case, the AV valve is displaced downward (but both sides still at the same level) into the ventricle and anchored to the crest of the septum eliminating the VSD component (Fig. 26.3c).
- A cleft in the anterior leaflet of the mitral valve
- A small, restrictive VSD may be present

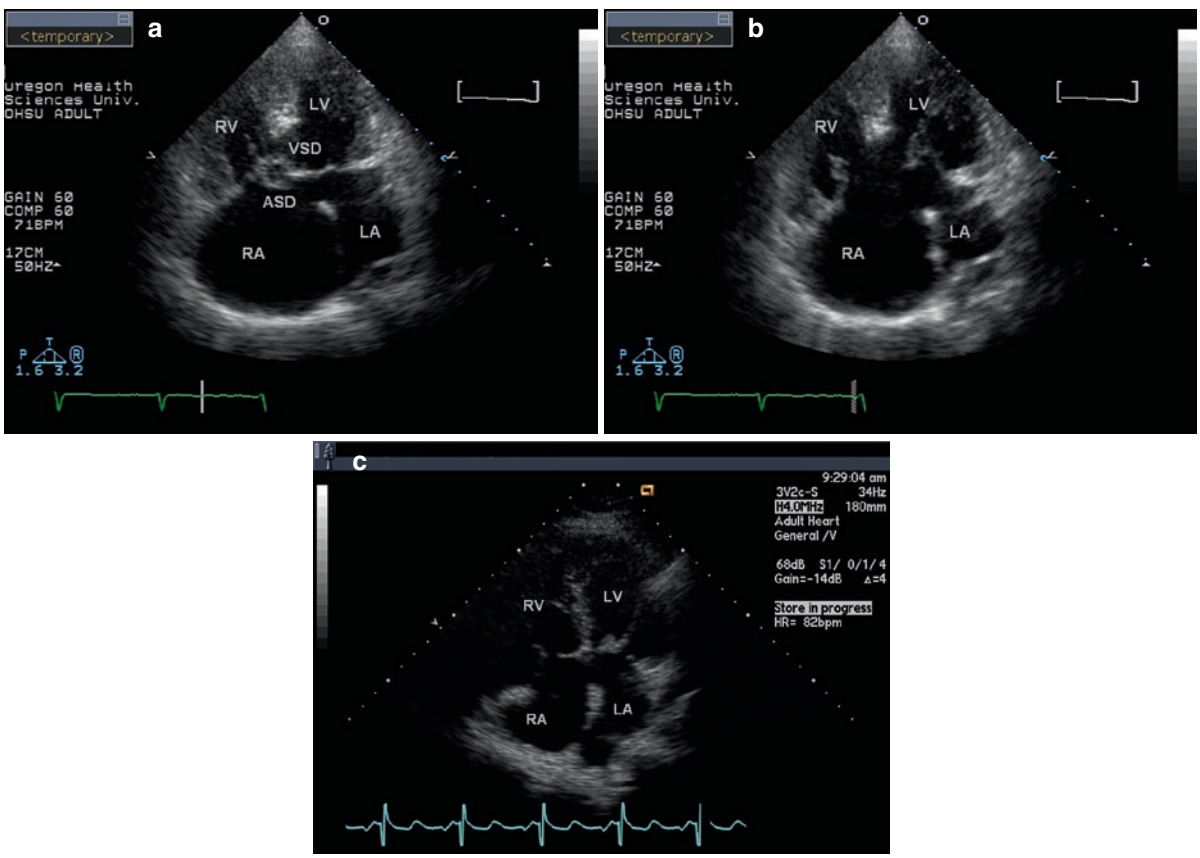

Fig. 26.3 (**a–c**) Apical four-chamber view of a complete AV septal defect with a common AV valve in systole (**a**) and diastole (**b**). In **a**, the common AV valve is displaced toward the apex of the heart due to the lack of the inlet ventricular septum. When closed, it appears to float in the middle of the large ventricular septal defect (VSD) and atrial septal defect (ASD). In **b**, the leaflets are open with chordal attachments to crest of the interventricular septum (not seen well). Shunting can occur at both ventricular and atrial levels. Panel C is an apical four-chamber view in systole with the AV valves attached to the top of the ventricular septum (no VSD present) with a primum ASD. *LA* left atrium, *RA* right atrium, *LV* left ventricle, *RV* right ventricle, *ASD* atrial septal defect, *VSD* ventricular septal defect

Echocardiographic Evaluation

The goals of the examination are to

- Define the components of the AV septal defect present
- Define the morphology (single orifice or two separate orifices) and chordal attachments of the leaflets of the AV valve
- Estimate size and function of the right and left ventricles
- Determine the extent of the ASD and VSD and the severity of shunting.

The best views are the apical (Fig. 26.3) and subcostal four chamber and the parasternal long- and short-axis views.[2] The apical and subcostal four-chamber views are best for evaluation of the inlet portion of the heart. They show the ASD and VSD well. In some instances, the VSD may be closed by chordal attachments or tricuspid valve tissue. The parasternal view at the mitral valve is helpful to determine whether one or two orifices are present and how well they line up with the ventricles. If two orifices are present, the mitral valve is cleft. This is seen best by watching the motion of the anterior leaflet that separates in the middle as the valve opens in diastole. Addition of color will show the location of the regurgitant jet where the cleft is located.

Doppler is helpful to define the types of intracardiac shunting present and the degree of AV valve regurgitation. The precise hemodynamics vary depending on the shunt.

- Predominate shunting at the atrial level produces the finding typical of an ASD.
- Shunting at both atrial and ventricular level occurs with complete AV septal defect. The risk of this physiology is early development of irreversible pulmonary vascular disease unless the pulmonary circulation is protected by RVOT obstruction.
- Significant AV valve regurgitation
- It is also important to evaluate both ventricular outflow tracts for obstruction. This can be due to a muscular obstruction or chordae crossing the outflow tract and inserting into the septum, especially on the left side.

Cautions

Because of the broad spectrum of anomalies that may be present, a thorough echocardiographic evaluation by a sonographer familiar with is defect is essential.

Ventricular Septal Defect

Anatomy and Physiology

The interventricular septum has a membranous and a muscular portion.

- The membranous septum is thin and relatively small, roughly 5 mm in diameter. It is bounded by the aortic valve superiorly at the junction of the right and noncoronary cusps and inferiorly by the muscular septum.
- The muscular component comprises the majority of the septum and is divided into three regions.
  - Inlet portion between the mitral and tricuspid valves
  - Outlet (infundibular) portion between the aortic and pulmonic valves
  - Trabecular portion, the largest, extending from the membranous septum to the apex

VSDs are commonly described by location; however, the hemodynamic disturbance depends on size rather than location. The common locations are

- Perimembranous defect (70–80% of cases)
- Outlet defect (5–8% of cases). This is also referred to as supracristal, conal, subarterial, subpulmonic, or doubly committed VSD. Part of the rim is formed by the annulus of the pulmonary and aortic valves. The right cusp of the aortic valve may herniate into the defect creating progressive aortic regurgitation.
- Inlet defect (5–8% of cases). It is located posterior and inferior to the perimembranous defect and may be part of an AV septal defect.
- Muscular defects occur anywhere within the trabecular portion of the septum and may be multiple.

VSDs are among the most prevalent congenital cardiac anomalies in children. A moderate to large VSD, in contrast to an ASD, causes symptoms leading to early identification and closure of the defects. It is importance to identify and treat these individuals as they are at risk for development of pulmonary vascular obstructive disease during the first 6–12 months of life.

Partial or complete spontaneous closure of a VSD may occur in 30–40% of cases. This closure is accomplished by adhesion of the septal leaflet of the tricuspid valve, proliferation of fibrous tissue, or prolapse of the aortic leaflet for membranous VSDs, and by hypertrophy

of septal muscle for muscular defects. Inlet and infundibular defects rarely become smaller or close by these mechanisms.

Echocardiographic Evaluation

The goals of the examination are to

- Determine the anatomic location and size of the defect within the septum
- Characterize the hemodynamic significance of the shunt
- Establish RV systolic pressure
- Identify associated lesions

The best views to do this are the parasternal long- and short-axis views, the apical and subcostal four chamber views.[3] The short-axis view at the aortic valve assesses the membranous and outlet septum. A defect between the 9 and 12 o'clock position is in the membranous septum (Fig. 26.4), and one between the 12 and 3 o'clock position is in the outlet septum. Prolapse of the right cusp of the aortic valve into the defect may occur with an outlet lesion. Defects in the trabecular septum are best seen using color Doppler in the apical four-chamber view (Fig. 26.5).

Color Doppler enhances the ability to detect and localized the shunt including defects that are too small to be seen on 2-D. Color Doppler flow oriented parallel to flow permits recording of the peak jet velocity (Fig. 26.4). The modified Bernoulli equation is used to calculate the transventricular pressure difference to obtain an estimate of RV and PA systolic pressure.[4] Jet velocity is high with restrictive defects, reflecting normal RV systolic pressure and normal pulmonary vascular resistance. Flow across the defect may continue into diastole as LV diastolic pressure usually exceeds RV diastolic pressure. With larger defects and elevated pulmonary artery systolic pressure, jet velocity is lower, but pulmonary vascular resistance may still be normal or only mildly elevated. With large defects and elevated RV systolic pressure and pulmonary vascular resistance, little flow may occur across the VSD indicating obstructive pulmonary vascular disease (Eisenmenger physiology).

As with an ASD, the significance of the shunt is inferred from the effects of volume overload. Left atrial and ventricular enlargement are usually present when the left-to-right shunt volume exceeds 50% of systemic flow $Q_p/Q_s \geq 1.5$.

Cautions

- Trabecular defects are more difficult to detect with 2-D. They are often serpiginous and right and left ventricular sites may not be in the same plane.
- Measurement of peak VSD velocity can be problematic if the jet is deflected by the tricuspid valve, septal

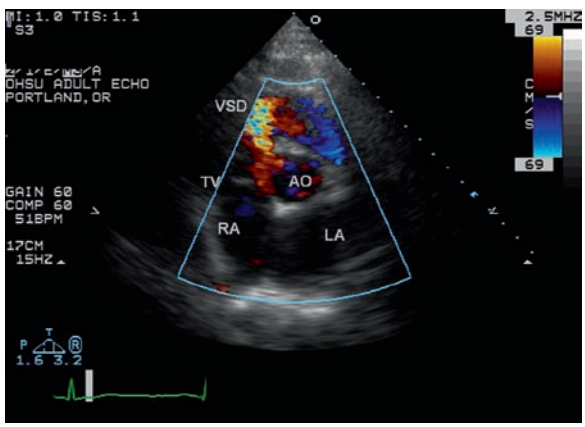

Fig. 26.4 Parasternal short-axis view just below the aortic valve showing the typical "9 o'clock to 12 o'clock" location of a perimembranous ventricular septal defect (VSD) with color Doppler. Flow is from left ventricle to right ventricle and the mosaic of colors indicates a turbulent high-velocity flow consistent with a restrictive VSD. *RA* right atrium, *LA* left atrium, *AO* aortic valve region, *VSD* ventricular septal defect, *TV* tricuspid valve

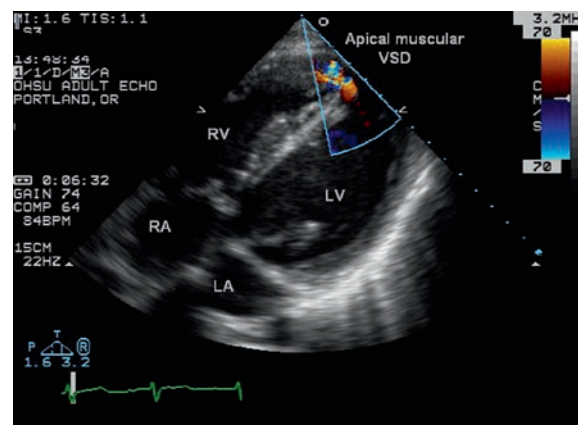

Fig. 26.5 Mosaic color pattern for a restrictive VSD in the apical portion of the muscular septum as seen in an "off-axis" apical four-chamber view. *LA* left atrium, *RA* right atrium, *RV* right ventricle, *LV* left ventricle

aneurysm, or muscle bundle. Underestimation of the pressure difference results if it is not possible to direct the continuous wave beam parallel to the VSD jet. Because of this, the TR velocity jet usually gives a more accurate estimate of peak RV systolic pressure.

- The estimate of the RV pressure from the VSD velocity must correlate with that determined by the TR velocity. Any significant disparity needs to be resolved.

Patent Ductus Arteriosus

Anatomy and Physiology

The duct arises at the origin of the left pulmonary artery and connects to the inner curvature of the aorta opposite the left subclavian artery. While essential in the fetus, the ductus normally closes once flow through the lungs is established shortly after birth. Failure to close results in a left-to-right shunt through the ductus. The consequences of the left-to-right shunt from a patent ductus arteriosus (PDA) depend upon its size and the pulmonary vascular resistance. Trivial shunts may be asymptomatic, detected only when a murmur is heard, or noted incidentally on echocardiography done for another indication. Medium and large shunts cause CHF due to increased pulmonary blood flow and volume overload of the left heart. If uncorrected, pulmonary hypertension develops and the shunt becomes bidirectional with cyanosis of the lower, but not the upper extremities (differential cyanosis).

Echocardiographic Examination

The goals of the examination are to

- Identify the presence and size of the ductus
- Quantify the hemodynamic significance
- Establish RV and PA systolic pressure

The best 2-D views are high left parasternal directed toward the PA bifurcation, suprasternal notch focusing on the descending aorta opposite the left subclavian and swinging toward the left PA (Fig. 26.6), and short axis at the base of the heart. A PDA is usually cone shaped with a smaller orifice at the pulmonary artery end. The shape, however, can be short, long, straight, or tortuous, making complete visualization difficult.

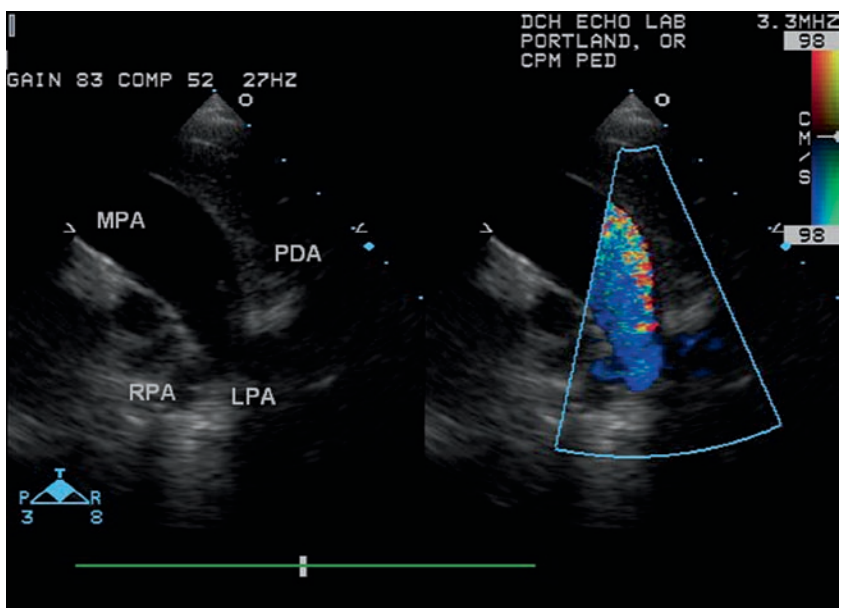

Fig. 26.6 High left parasternal view (between the suprasternal and parasternal views) showing the ductus arteriosus (PDA) connecting the main pulmonary artery to the descending aorta. The left side is the 2-D image showing the duct entering the pulmonary artery. The right side has color Doppler added showing the large duct with flow directed into the main pulmonary artery toward the pulmonary valve from the descending aorta. *MPA* main pulmonary artery, *RPA* right pulmonary artery, *LPA* left pulmonary artery, *PDA* patent ductus arteriosus

As with a VSD, the degree of enlargement of the left atrium and left ventricle is a useful marker of the magnitude of the shunt.

The diagnosis is made more easily with Doppler than 2-D imaging of the duct.[5] Turbulent flow in the main pulmonary artery that persists throughout the cardiac cycle is an important clue that a PDA is present. Flow within the duct can also be evaluated. Most commonly, a high-velocity flow from left to right reaching a peak in late systole is present. The Doppler velocity measurement provides information about RV and PA systolic pressure by the pressure gradient across the duct or by the tricuspid regurgitant velocity. As with a VSD, the TR velocity may provide a more accurate estimate of PA systolic pressure. In most instances, PA systolic pressure is normal or only slightly increased. Rarely, a bidirectional shunt is present, characterized by a right-to-left shunt in early diastole followed by left-to-right flow in late systole and diastole. This indicates significantly elevated pulmonary vascular resistance and probable Eisenmenger physiology.

Cautions

- Low-velocity retrograde flow in late systole secondary to swirling flow within an enlarged PA should not be mistaken for ductal flow.
- Continuous flow into the PA is also seen with a coronary artery fistula or an aortopulmonary window. These are rare congenital abnormalities that should not be confused with a PDA.

Valvular Abnormalities

Pulmonary Stenosis

Anatomy and Physiology

Pulmonary stenosis (PS) can be valvular, subvalvular (infundibular), or supravalvular. This section will focus on valvular stenosis.

In valvular stenosis,

- Three leaflets are present, but with thickened and fused commissures and a reduced orifice.
- Unicuspid or bicuspid valves are uncommon
- It is usually an isolate finding, but is associated with Noonan syndrome (dysplastic or myxomatous pulmonary valve with small annulus).

Echocardiographic Evaluation

The goals of the examination are to

- Characterize the anatomy of the valve
- Define the site and severity of the stenosis
- Determine consequences of stenosis on the RV

Best views include the parasternal short and long axis and subcostal of the RV.[6] The 2-D images show thickened pulmonary valve cusps, restricted systolic motion, and doming in systole. The main PA is often dilated, but the extent of dilation does not correlate with the severity of stenosis.

The severity of the obstruction is determined by measuring the peak Doppler velocity across the pulmonary valve. Multiple transducer positions should be checked to be certain to obtain the highest velocity. The pressure gradient is calculated using the modified Bernoulli equation. The instantaneous pressure gradient by Doppler echo correlates well with the peak-to-peak gradient obtained at catheterization. The degree of stenosis is judged mild when the peak instantaneous gradient is less than 40 mmHg, moderate with gradients between 40 and 70mmHg, and severe when >70 mmHg. Valvuloplasty or surgery is usually considered with gradients above 50 mmHg. With at least moderate obstruction, right ventricular hypertrophy, particularly of the infundibulum, may be present. When mild stenosis is present, progression is rare; however, moderate to severe stenosis usually progresses.

Cautions

- The pressure gradient is flow dependent and may not always be a reliable indicator of severity of stenosis. This is the case when flow across the valve is reduced secondary to poor RV systolic function or when flow is increased due to insufficiency of the pulmonary valve.
- A large left-to-right shunt can cause increased velocity across the pulmonary valve when no stenosis of the valve is present. If increased flow is due to a shunt, both RVOT and PA velocities are increased. In contrast, in pulmonary stenosis, the RVOT velocity should be normal while the PA velocity is increased.

Aortic Stenosis

Anatomy and Physiology

Sites of obstruction in the aortic valve region include the valve (71%), the subvalvular region (23%), and the supravalvular region (6%). This section will focus on valvular aortic stenosis.

Valvular abnormalities include

- Bicuspid valve (most common)
- Unicuspid valve
- Acommissural (diaphragmatic) valve
- Three-leaflet valve with fusion along the commissures (uncommon)
- Quadraleaflet valve (extremely rare).

Aortic stenosis may be present at birth (usually acommissural or unicuspid valves), or a congenitally abnormal valve becomes stenotic over time.

Echocardiographic Evaluation

The goals of the examination are to

- Characterize the anatomy of the valve
- Determine the severity of the stenosis
- Evaluate the effect of the stenosis on the LV
- Identify associated anomalies

Views to interrogate the aortic valve include the parasternal short and long and apical and subcostal 4-chamber. 2-D images easily define the abnormalities of the valve. The parasternal short axis is best for defining the leaflet morphology (Fig. 26.7), while the long axis is best for valve motion during systole.

- In the short-axis view, a bicuspid valve does not show the usual "Y" pattern of the normal three-leaflet valve, but has two leaflets of relatively equal size, a straight closure line in diastole, and a noncircular orifice in systole.
- A three-leaflet valve with fused commissures has the "Y" pattern, but the commissures are very much thickened with varying degrees of leaflet fusion.
- A unicommissural valve is seen in infants and children. It has a single commissure along half the diameter of the orifice and in systole a circular orifice that is eccentrically positioned.

To be certain to obtain the highest Doppler velocity, the valve is imaged in multiple views including the apical, suprasternal, right parasternal, and subcostal. Three methods are used to determine the severity of the stenosis and the need for intervention: peak instantaneous gradient, mean gradient, and valve area.[7] Inherent differences exist between the methods. Whichever one is used needs to be integrated with clinical information.

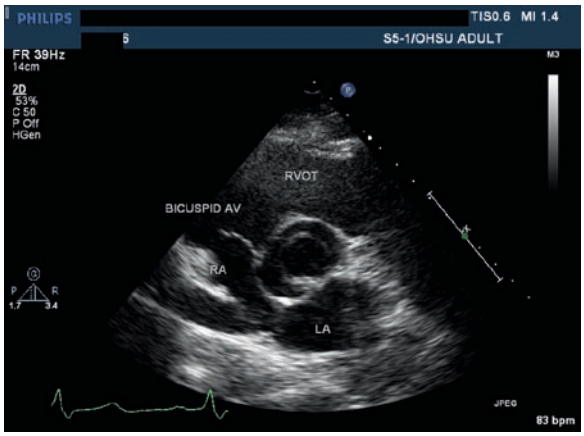

Fig. 26.7 Bicuspid aortic valve as seen from the parasternal short-axis view. In systole, the ovoid opening of the bicuspid valve is seen with orientation of the commissure from 10 o'clock to 4 o'clock. *RVOT* right ventricular outflow tract, *RA* right atrium, *LA* left atrium, *Bicuspid AV* bicuspid aortic valve

The peak instantaneous gradient is used widely to determine the need for intervention. Intervention is recommended

- When the gradient is >75 mmHg.
- When peak systolic gradient is between 50 and 75 mmHg, the decision for surgery is more variable and patient dependent.
- Close follow-up is considered if the gradient is <50 mmHg and no other clinical findings of concern are noted.

Mean gradient from echo correlates well with the mean gradient from cardiac catheterization. Guidelines for when an intervention is recommended based on the mean echo gradient include

- Mean gradient > 27 mmHg
- Mean gradient between 17 and 27 mmHg with symptoms or an abnormal exercise test
- No intervention is recommended if the mean gradient is <17 mmHg.

Aortic valve area can be calculated using the continuity equation. While this is the standard method used in adults with aortic valve disease, this method has not been well studied in infants and children.

Cautions

- In infants, critical aortic stenosis with severe LV dysfunction must be separated from a primary abnormality of LV function. A hypertrophied LV due to critical AS must be separated from a hypoplastic LV. A normal appearing aortic valve and normal Doppler velocity across the valve make these two alternatives more likely.
- Proper alignment with the jet is imperative to avoid underestimating the gradient.
- The gradient is affected by volume of flow so that LV dysfunction and low cardiac output give a lower gradient while aortic insufficiency increases the gradient.[8]

Coarctation of the Aorta

Anatomy and Physiology

A coarctation of the aorta is almost always opposite the ductus arteriosus or ligamentous arteriosum and appears as a shelf-like narrowing into the aorta just below the left subclavian artery. Associated defects other than bicuspid aortic valve (occurs in 85% of cases) are rare in these children. Aortic atresia or interrupted aortic arch is severe, but uncommon, variations of coarctation with the descending aorta supplied by blood from the right heart via the ductus arteriosus. This lesion is associated with other cardiac abnormalities including aortic hypoplasia, abnormal aortic valve, VSD, PDA, mitral valve anomalies, or as part of TGA and double outlet right ventricle (Taussig-Bing anomaly).

Echocardiographic Evaluation

The descending aorta is best seen from the suprasternal view. Particular attention must be paid to

- Identifying all the great vessels
- Size of the proximal aorta
- Site of narrowing in the descending aorta and its distance from the orifice of the left subclavian artery
- Degree of obstruction by the Doppler flow pattern
- Patency of the duct

Color Doppler is useful to locate the site of turbulence and the CW beam is directed to this region. The pattern for significant obstruction is increased systolic velocity with continuous forward flow throughout diastole (Fig. 26.8).[9] Doppler gradients from the peak systolic

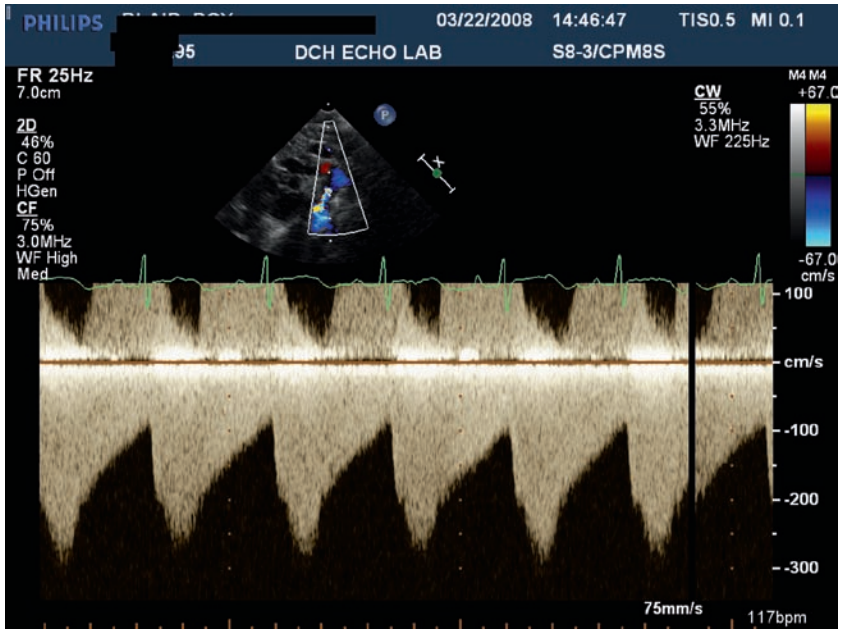

Fig. 26.8 Continuous-wave Doppler directed through the region of coarctation in the descending aorta from the suprasternal notch view in an infant. The peak velocity in systole of 2.7 m/s calculates to a peak gradient across the coarctation of 30 mmHg. Note that the flow signal continues throughout diastole indicating continuous antegrade flow (and pressure gradient) across the coarctation

velocity (V_2) alone tend to overestimate the catheter-measured gradient. A better correlation has been shown when the velocity proximal to the coarctation (V_1) is included in the expanded Bernoulli equation $P = 4 (V_2 - V_1)^2$. This may not be necessary if the proximal aortic flow is <1 m/s.

Cautions

- A long, narrowed segment of the aorta without discrete obstruction causes acceleration of flow, giving an increased peak velocity suggestive of obstruction. The lack of diastolic forward flow, however, helps distinguish this flow acceleration from true obstruction.
- Left-to-right runoff of flow through a patent ductus reduces the velocity through the coarctation, leading to an underestimation of the pressure gradient.
- With aortic atresia or interruption, the large duct supplying the descending aorta must not be mistaken as the aortic arch. This is avoided by identifying where the arch vessels originate.
- With a severe coarctation or interrupted aorta, no increase in velocity will be seen if the descending aorta is supplied by an unrestrictive patent ductus.

Ebstein Anomaly of the Tricuspid Valve

Anatomy and Physiology

This lesion is characterized by apical (downward) displacement of the septal and posterior leaflets of the tricuspid valve into the RV chamber. The anterior leaflet is tethered to the RV free wall and may have restricted movement or be a large sail-like leaflet that can obstruct the RV outflow tract. This abnormal tricuspid valve is invariably regurgitant and occasionally stenotic. A portion of the proximal right ventricle is incorporated into the RA (atrialized RV). The functional RV may be hypoplastic with impaired systolic function. A PFO or ASD is frequently present. WPW syndrome is associated with this anomaly (10–15% of cases), predisposing to tachyarrhythmias. Variation in the severity of the valvular abnormalities results in a wide spectrum of symptoms from critically ill to an incidental finding in an asymptomatic individual.

Echocardiographic Evaluation

Goals are to

- Define severity of apical displacement of the septal and posterior leaflets from the anatomic annulus and the size and tethering of the anterior leaflet
- Determine degree of regurgitation
- Quantify adequacy of RV size and systolic function
- Establish presence of ASD/PFO

The best views for evaluating the TV include the apical four-chamber view (Fig. 26.9) and the subcostal coronal view.[10] There is no uncertainty in making the diagnosis in moderate to severe cases, but milder forms can be problematic. Since the tricuspid valve is normally more apically positioned than the mitral valve, accepted criterion for abnormal apical displacement of the TV is more than 8 mm/m2 (or >20 mm in adults) from the mitral valve insertion in the apical four chamber view.

Doppler provides an estimate of the severity of regurgitation and whether stenosis of the valve is present. The subcostal view enables interrogation of the interatrial septum to look for a PFO or ASD. If unclear, the rapid IV injection of agitated saline can be used to determine if right-to-left shunting is present.

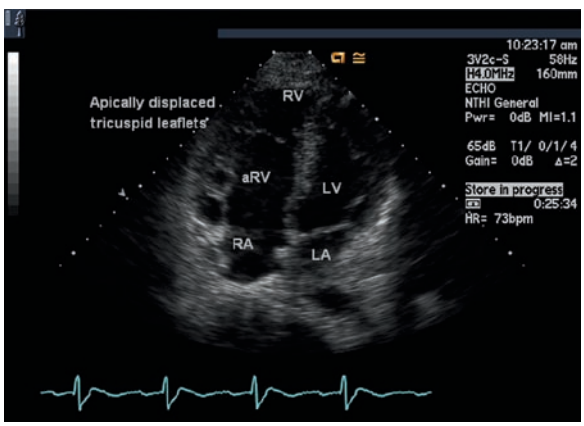

Fig. 26.9 Apical four-chamber image of Ebstein anomaly of the tricuspid valve in diastole. The annulus of the tricuspid valve is just above the RA label. The displaced septal leaflet that is adherent to the right side of the interventricular septum with the valve leaflets coapting near the apex of the right ventricle. The area between the tips of the tricuspid leaflets near the apex of the RV and the tricuspid annulus represents the atrialized portion of the right ventricle (aRV). The right heart is significantly enlarged. *RA* right atrium, *LA* left atrium, *RV* right ventricle, *LV* left ventricle, *ARV* atrialized portion of the right ventricle

In symptomatic individuals, surgical repair of the valve is possible if the anterior leaflet is of sufficient size and mobility to create a monocuspid valve and if the RV is of sufficient size and with adequate function after plication of the atrialized portion of the RV. If repair is not possible, the preferred replacement valve is a stented allograft or heterograft. A Fontan repair is done with severe RV dysfunction or hypoplasia.

Cautions

- The fibrous annulus of the tricuspid valve should not be mistaken for valve tissue
- RV tissue bands should be distinguished from displaced valve tissue
- Myxomatous disease of the TV should be distinguished from a large sail-like anterior leaflet

References

1. McDonald RW, Rice MJ, Reller MD, Marcella CP, Sahn DJ. Echocardiographic imaging techniques with subcostal and right parasternal longitudinal views in detecting sinus venosus atrial septal defects. *Am Soc Echocardiogr*. 1996;9:195–198.
2. Zellers TM, Zehr R, Weinstein E, Leonard S, Ring SW, Nikaidoh H. Two-dimensional and Doppler echocardiography alone can adequately define preoperative anatomy and hemodynamic status before repair of complete artioventricular septal defect in infants <1 year old. *J Am Coll Cardiol*. 1994;24:1565–1570.
3. Hagler DJ, Edwards WD, Seward JB, Tajik AJ. Standardized nomenclature of the ventricular septum and ventricular septal defects, with applications for two-dimensional echocardiography. *Mayo Clin Proc*. 1985;60:741–752.
4. Houston AB, Lim MK, Doig WB, Reid JM, Coleman EN. Doppler assessment of the interventricular pressure drop in VSD. *Br Heart J*. 1988;60:50–56.
5. Swensson RE, Valdes Cruz LM, et al. Real-time Doppler color flow mapping for detection of patent ductus arteriosus. *J Am Coll Cardiol*. 1986;8:1105–1112.
6. Mulhern KM, Skorton DJ. Echocardiographic evaluation of isolated pulmonary valve disease in adolescents and adults. *Echocardiography*. 1993;10:533–543.
7. Barker PC, Ensing G, Ludomirsky A, Bradley DJ, Lloyd TR, Rocchini AP. Comparison of simultaneous invasive and noninvasive measurements of pressure gradients in congenital aortic valve stenosis. *J Am Soc Echocardiogr*. 2002;15:1496–1502.
8. Beckman RH, Rocchini AP, Gillon JH, Mancini GB. Hemodynamic determinants of the peak systolic left ventricular-aortic pressure gradient in children with valvar aortic stenosis. *Am J Cardiol*. 1992;69:813–815.
9. Carvalho JS, Redington AN, Shinebourne EA, Rigby ML, Gibson D. Continuous wave Doppler echocardiography and coarctation of the aorta: gradients and flow patterns in the assessment of severity. *Br Heart J*. 1990;64:133–137.
10. Rusconi PG, Zuberbuhler JR, Anderson RH, Rigby ML. Morphologic-echocardiographic correlates of Ebstein's malformation. *Eur Heart J*. 1991;12:784–790.

Chapter 27
Echocardiographic Evaluation of Complex Congenital Heart Disease

Marcy L. Schwartz and Gerald R. Marx

Introduction

This chapter describes the application of echocardiography in the evaluation of complex congenital heart disease. The anatomy and the surgical repair, often performed during infancy, are explained for each diagnosis, providing the basis for evaluating these patients as they grow into adulthood. Each anatomic diagnosis actually represents a spectrum of disease severity. The specific variations, associated features, and severity of lesions may significantly affect the surgical repair strategy and resultant clinical status. Accordingly, serial postoperative echocardiographic assessments are based on knowledge of the anatomy and surgical repair.

Several specific yet representative complex congenital defects are presented. For each defect the underlying anatomy, pathophysiology, and preoperative echocardiographic findings are presented. Based on the type of surgery, the specific postoperative potential complications are described. Based on the initial anatomy and surgery, the postoperative serial echocardiographic evaluation of these patients is described in detail.

M.L. Schwartz
Department of Cariology, Cleveland Clinic, Cleveland, OH, USA

G.R. Marx (✉)
Department of Cardiology, Boston Children's Hospital, Boston, MA, USA
e-mail: Gerald.marx@cardio.chboston.org

Tetralogy of Fallot

Pathology

Tetralogy of Fallot (TOF), as the name suggests, has four main components: (1) ventricular septal defect, (2) overriding of the aorta, (3) right ventricular outflow tract obstruction (RVOTO), resulting in (4) right ventricular hypertrophy. For practical purposes, the surgical repair focuses on two of these components, relief of RVOTO and closure of the ventricular septal defect. The VSD in TOF is conoventricular with anterior, superior malalignment of the conal septum. This shift aligns the aorta more anterior and rightward over the crest of the ventricular septum (Fig. 27.1). RVOTO can occur at any or multiple levels. This includes subvalvar narrowing from the anteriorly deviated, hypertrophied conal septum; stenosis or hypoplasia of the pulmonary valve; and hypoplasia of the main pulmonary artery and/or branch pulmonary arteries. In the mildest form, minimal RVOTO can lead to unprotected pulmonary blood flow and congestive failure. With severe RVOTO, diminutive branch pulmonary arteries with aortopulmonary collateral arteries can be considered part of the spectrum of tetralogy of Fallot with pulmonary atresia (TOF/PA), discussed separately.

Preoperative Evaluation

Preoperative echocardiographic evaluation includes interrogation of the level(s) and severity of RVOTO and inspection for additional VSDs and other associated lesions. The coronary anatomy is also of particular importance. The typical coronary pattern for TOF involves clockwise rotation of the crux of the heart such that the

P. Nihoyannopoulos and J. Kisslo (eds.), *Echocardiography*,
DOI: 10.1007/978-1-84882-293-1_27,

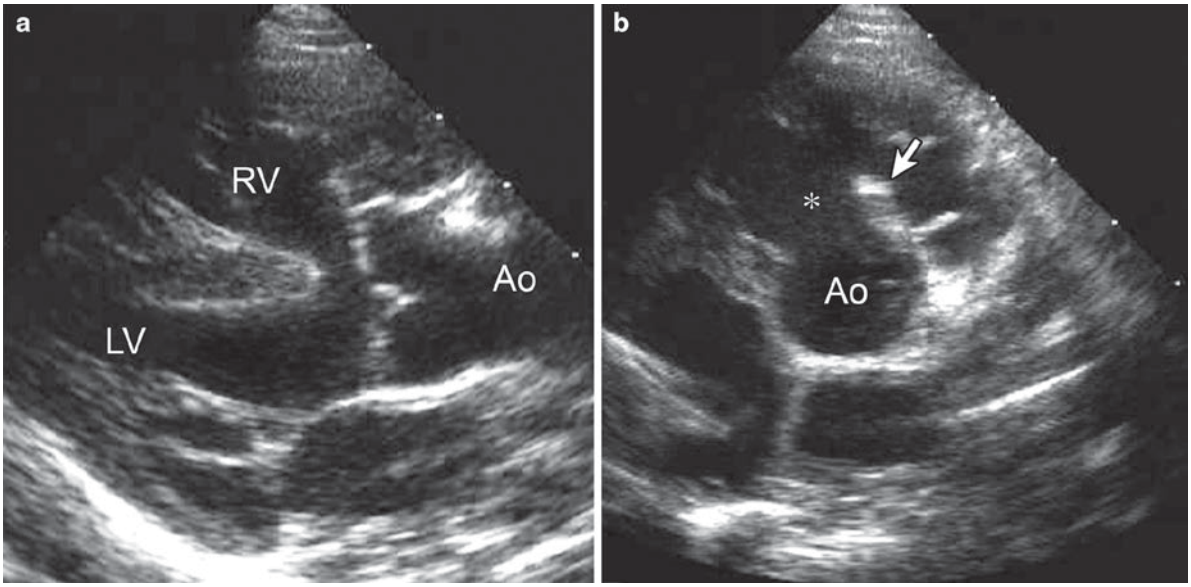

Fig. 27.1 Tetralogy of Fallot. (**a**) Parasternal long-axis view showing the aortic valve overriding the crest of the ventricular septum; (**b**) parasternal short-axis view showing anterior malalignment of the conal septum resulting in subpulmonary obstruction. *Arrow* indicates conal septum. *Asterisk* indicates the ventricular septal defect. *Ao* aortic valve; *RV* right ventricle; *LV* left ventricle

left coronary artery arises more posteriorly and the RCA more leftward than usual. Often a prominent conal branch from the RCA can be seen in the presence of right ventricular hypertrophy. This should be distinguished from a significant dual or a single left anterior descending coronary arising from the RCA and crossing the RVOT, especially if a right ventricular outflow tract patch is placed to expand this area. Incision across an unrecognized significant LAD would result in myocardial infarction.

Surgical Repair

The repair of TOF includes patch closure of the large conoventricular septal defect and closure of any additional VSDs which may be present. Relief of subvalvar pulmonary stenosis may involve muscle bundle resection and/or patch augmentation of the RVOT. If the pulmonary valve is very hypoplastic, a transannular RVOT patch may be required.

Postoperative Evaluation

Postoperative evaluation includes inspection for the presence and degree of residual RVOT obstruction, presence of significant pulmonary regurgitation, and presence of residual VSDs. Right ventricular systolic pressure should be estimated from the velocity of the tricuspid regurgitation jet. Ventricular septal position and/or gradient across a residual VSD can be misleading in the setting of a complete right bundle branch block, which is often present postoperatively, due to asynchronous ventricular contraction. In the older patient, significant pulmonary regurgitation can produce right ventricular volume overload with right ventricular dilation and tricuspid regurgitation. Elevated right ventricular pressure from residual pulmonary stenosis can exacerbate right ventricular dysfunction. Although degree of pulmonary regurgitation and right ventricular dilation/dysfunction can be roughly estimated by echocardiography, MRI is commonly used to assess pulmonary regurgitation fraction and right ventricular size and function. Optimal timing for pulmonary valve replacement has not been clearly established. Progressive aortic root dilation and significant aortic regurgitation have been observed in adult patients with TOF late after repair, requiring aortic valve replacement in some. Therefore, postoperative evaluations should include measurement of aortic root size and assessment of aortic regurgitation.[1]

Tetralogy of Fallot with Pulmonary Atresia

Pathology

TOF/PA, considered to have the severest degree of RVOTO, has no direct communication between the right ventricle and pulmonary arteries. The spectrum of severity for TOF/PA is based on the continuity and size of the branch pulmonary arteries, and associated aortopulmonary collateral arteries.

Preoperative Evaluation

Assessment of the pulmonary artery supply and size is relevant to the timing and type of repair. Delineation of aortopulmonary collaterals arteries has traditionally required angiography; however, echocardiographic evaluation of proximal branch pulmonary artery diameters may be used to predict the presence of important APC arteries.[2] Similar to TOF, echocardiographic assessment requires interrogation for multiple VSDs and imaging of the coronary anatomy.

Surgical Repair

If the branch pulmonary arteries are of good size, a right ventricle to pulmonary artery conduit is placed. These conduits may be dilated and stented for maximal longevity. Ultimately, the conduit is replaced as the child outgrows the initial conduit. Aortopulmonary collateral arteries without dual antegrade supply are recruited or unifocalized and incorporated into the antegrade pulmonary circulation. With adequate size pulmonary arteries, the conoventricular VSD is closed at the time of conduit placement. However, with severely diminutive branch pulmonary arteries, delayed closure of the ventricular septal defect or a fenestrated patch may be necessary.

Postoperative Evaluation

Often echocardiography is not the optimal modality for assessing growth of the branch pulmonary arteries; however, assessment of conduit obstruction and right ventricular pressure, size, and function may indicate the need for an intervention.

Truncus Arteriosus

Pathology

Truncus arteriosus is a conotruncal abnormality in which a single semilunar or truncal valve and trunk give rise to the coronary arteries, to the branch pulmonary arteries, and to the aorta. This is almost always associated with a large conoventricular septal defect with the truncal valve oriented over the crest of the ventricular septum. The pulmonary arteries may arise from a main pulmonary artery versus each branch directly from the trunk. The truncal valve is often abnormal with any number of leaflets, usually 2–4, and may exhibit varying degrees of regurgitation and/or stenosis. Truncus arteriosus may also be associated with an interrupted aortic arch with the descending aorta supplied by a patent ductus arteriosus.

Preoperative Evaluation

Presence of additional VSDs must be identified. The echocardiogram should examine the length of the main pulmonary artery, if present, and/or the size and degree of stenosis of the branch pulmonary arteries (Fig. 27.2). The distance of the main or branch pulmonary arteries from the orifice of the left coronary artery is also important to visualize since the coronary artery may be damaged at surgery when dividing the pulmonary arteries from the common trunk. The presence and degree of truncal valve regurgitation and/or stenosis should be assessed. The aortic arch should be examined for interruption.

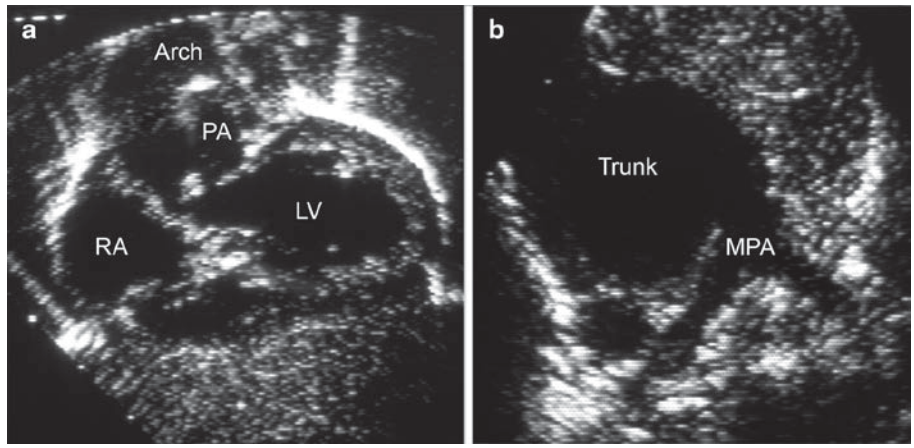

Fig. 27.2 Truncus arteriosus. (**a**) Subcostal long-axis view depicting the left pulmonary artery arising from the common trunk; (**b**) parasternal short-axis view showing the main pulmonary artery arising from the common trunk. *LV* left ventricle; *RA* right atrium; *LPA* left pulmonary artery; *MPA* main pulmonary artery

Surgical Repair

Surgical repair involves resection of the main pulmonary artery or individual branch pulmonary arteries from the trunk and connection to the right ventricle via a conduit. The conoventricular septal defect is closed with a patch directing flow from the left ventricle to the truncal valve. When present, arch interruption is repaired, usually by direct anastomosis.

Postoperative Evaluation

Postoperatively, the echocardiogram should focus on truncal valve function, detection of residual patch margin or other VSDs, and branch pulmonary artery stenosis. As with TOF/PA, conduit stenosis and right ventricular hypertension are assessed to detect need for reintervention or conduit replacement. The truncal (neoaortic) valve is assessed for progressive stenosis and regurgitation. If the aortic arch was repaired, recurrent arch obstruction is also assessed over time.

Common Atrioventricular Canal Defect

Pathology

Endocardial cushion defects are a spectrum of diseases ranging from a primum ASD with cleft mitral valve to complete common atrioventricular canal defect (CAVC) with absence of the endocardial cushion resulting in a large primum ASD, inlet VSD, and a common atrioventricular valve (AVV). The AVV may have dense attachments to the crest of the ventricular septum such that the actual ventricular shunt is small (transitional AVC) or even absent.

Preoperative Evaluation

Echocardiographic evaluation includes assessment of the presence and size of the endocardial atrial and ventricular septal defects, and inspection for additional atrial or ventricular septal defects. In addition, the relative right and left ventricular size and the alignment of the common AVV over the ventricles are important in determining the surgical repair. For example, with extreme size dominance of one ventricle, division of the AVV allowing adequate and unobstructed flow to both ventricles may not be possible, necessitating a single ventricle palliation, as will be described later (see Section “Hypoplastic Left Heart Syndrome”). The number of left ventricular papillary muscles is also important since the mitral valve may be parachute with a single papillary muscle. In this anatomic setting, surgical septation of the common A-V valve, and closure of the ASD and VSD could result in severe mitral stenosis. Subcostal imaging is best for assessing the relative balance of the AVV over the ventricular septum, often in a modified short-axis view rotated counterclockwise (Fig. 27.3a). From the apical view, one

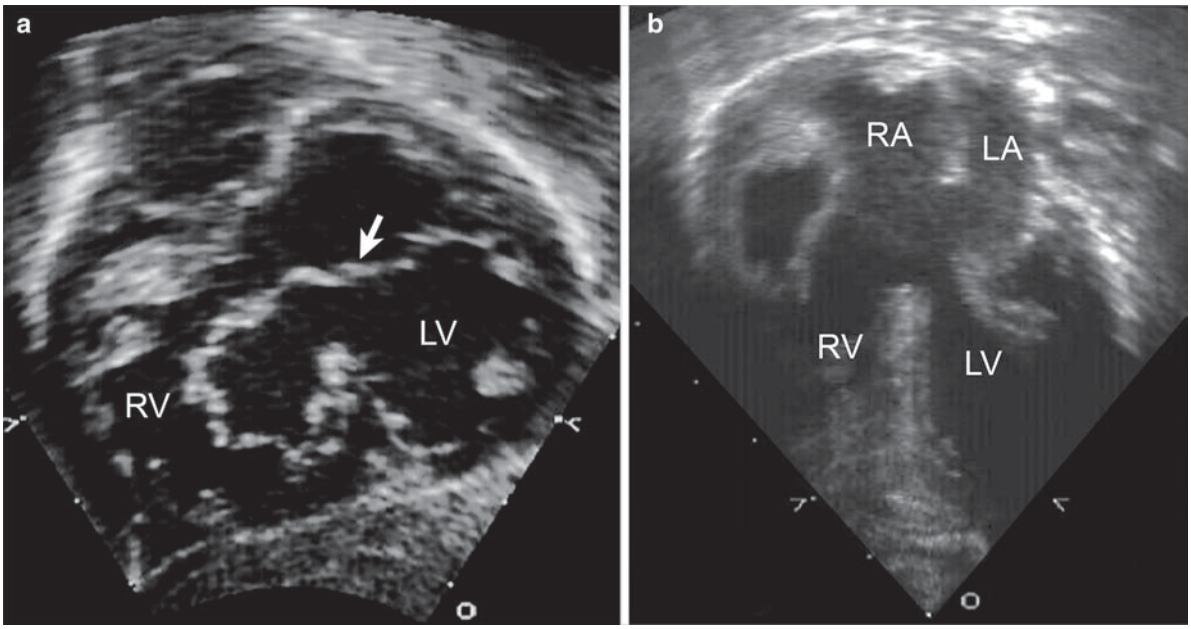

Fig. 27.3 Common atrioventricular canal. (**a**) Subcostal short-axis view; (**b**) apical four-chamber view, showing a common atrioventricular valve well balanced over both ventricles. *RA* right atrium; *LA* left atrium; *RV* right ventricle; *LV* left ventricle

can also assess attachments of the anterior bridging leaflet (Fig. 27.3b). Other variations of the morphology of the mitral aspect, such as double orifice MV, can be seen. The degree of AVV regurgitation and the presence of subaortic stenosis from AVV tissue crossing the left ventricular outflow tract are seen from apical and parasternal long-axis views.

Surgical Repair

Repair involves septation of the common AVV, closure of the defect components, and often suture closure of the mitral valve cleft.

Postoperative Evaluation

Postoperative issues may include residual atrial or ventricular septal defects, AVV regurgitation or stenosis, or development of subaortic stenosis. Degree of mitral and tricuspid regurgitation and /or stenosis should be examined echocardiographically over time. In addition, the mechanism of significant mitral regurgitation can be identified. Mitral regurgitation may emanate through a residual cleft or centrally from insufficient anterior leaflet tissue after suture closure of the cleft. Again, residual septal defects or a left ventricle to right atrial shunt should be identified. Left ventricular outflow tract obstruction may occur postoperatively from AVV tissue or a subaortic membrane.

d-Loop Transposition of the Great Arteries

Pathology

d-loop transposition of the great arteries (d-TGA) is a conotruncal abnormality in which the aorta arises from the right ventricle and the pulmonary artery from the left ventricle. In d-TGA, the aortic valve is usually anterior and rightward of the pulmonary valve. Since the systemic and pulmonary circulations are in parallel (rather than in series), the amount of effective blood flow is dependent on bidirectional shunting or mixing. Potential sites of mixing are at the patent ductus arteriosus and/or ASD or patent foramen ovale. Approximately 40% of cases of d-TGA have an associated VSD.

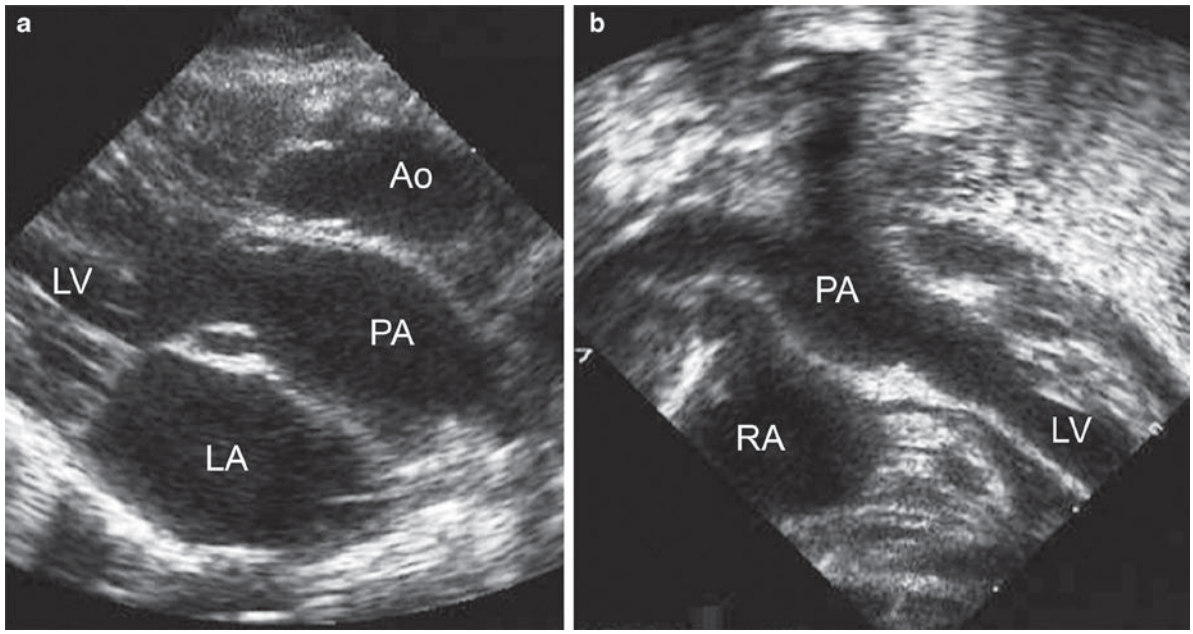

Fig. 27.4 d-Transposition of the great arteries. (**a**) Parasternal long-axis view showing the parallel orientation of the aorta and pulmonary artery; (**b**) subcostal long-axis view showing the pulmonary artery arising from the left ventricle. *Ao* aorta; *LV* left ventricle; *PA* pulmonary artery; *LA* left atrium; *RA* right atrium

Preoperative Evaluation

One of the first echocardiographic clues to the diagnosis of d-TGA in a cyanotic infant is the parallel orientation of the great arteries (Fig. 27.4a), as seen in the initial subcostal long-axis sweep. The pulmonary artery is identified by the bifurcation of the great artery arising from the posterior left-sided left ventricle (Fig. 27.4b). Continuation of the sweep anteriorly demonstrates the aorta from the right ventricle.

After assessing the patency of the ductus arteriosus, the echocardiographer must assess for restriction across the atrial septum, examining the size of the defect and mean Doppler gradient. In most cases, a balloon atrial septostomy is necessary for maximum atrial shunting. This is now commonly performed with echocardiographic guidance (Fig. 27.5). In addition to guiding the catheter course and assuring balloon inflation within the left atrium, this also allows evaluation of the effectiveness of the septostomy.

Posterior deviation of the conal septum or other etiologies of left ventricular outflow tract obstruction should be identified as postoperative subaortic stenosis may be poorly tolerated. Preoperatively, the diameters of the ascending aorta and main pulmonary artery are measured to anticipate size discrepancy with reanastomosis.

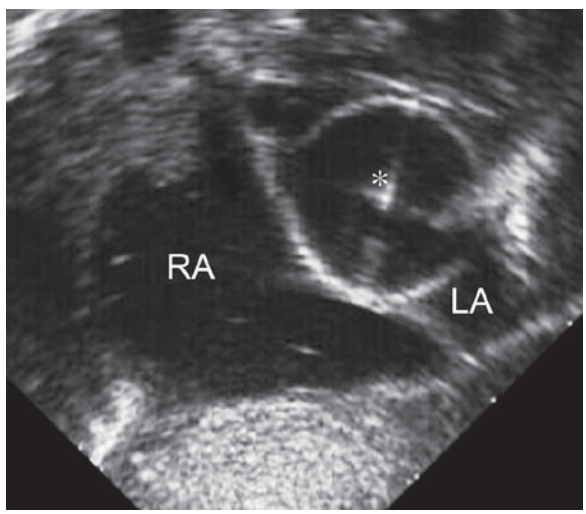

Fig. 27.5 Balloon atrial septostomy for transposition of the great arteries. Subcostal short-axis view demonstrating a balloon inflated in the left atrium, prior to the Rashkind procedure. *Asterisk* indicates balloon. *RA* right atrium; *LA* left atrium

Preoperatively, the coronary artery pattern is important to delineate. In the usual pattern for d-TGA,

the RCA arises from the rightward posterior facing sinus and the LCA from the leftward anterior facing sinus. However, several variations may be seen, including intramural courses with a coronary traveling between the aortic and pulmonary roots, which may add further challenge to the surgical repair.

Surgical Repair

Previous surgical repair of d-TGA included atrial switch techniques (Mustard and Senning) in which the systemic venous return is baffled to the mitral valve and left ventricle and the pulmonary venous return to the tricuspid valve and right ventricle. Since the right ventricle is systemic, many patients developed right ventricular failure. In the 1980s, the arterial switch operation started to replace the previous techniques and is now considered the operation of choice for most patients with d-TGA. This operation involves transaction of the aorta and pulmonary artery above their respective roots, switching, and reattachment. To reduce tension on the branch pulmonary arteries, the surgical technique usually includes the Lecompte maneuver wherein the distal pulmonary artery segment is brought anterior to the aorta prior to reanastomosis. The coronary arteries must be transferred to the neoaorta (native pulmonary root). With extreme left ventricular outflow tract obstruction or pulmonary atresia and a large VSD, a Rastelli operation may be surgically optimal. During this operation, a VSD patch is placed baffling the left ventricle to the anterior aorta and a right ventricle to pulmonary artery conduit is inserted.

Postoperative Evaluation

Following arterial switch operation, the echocardiographic evaluation includes assessment for development of supravalvar aortic and/ pulmonary stenosis at the reanastomosis sites. Following the Lecompte maneuver, the ascending aorta is seen between the branch pulmonary arteries (Fig. 27.6). Mild turbulence in the branch pulmonary arteries is not uncommon. The branch pulmonary arteries should be interrogated for significant stenosis. Residual atrial septal defects,

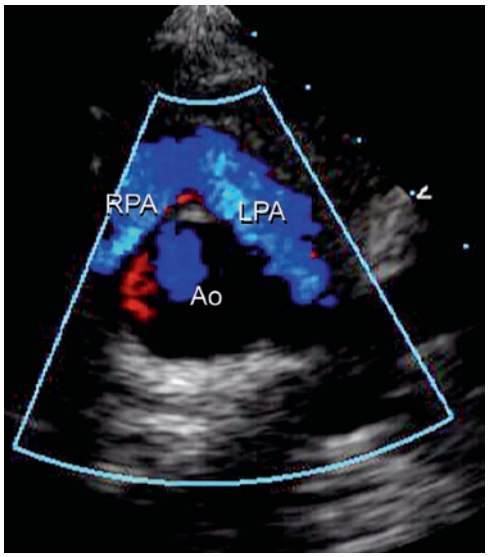

Fig. 27.6 d-Transposition of the great arteries after arterial switch operation with Lecompte maneuver. The ascending aorta is seen between the branch pulmonary arteries. *RPA* right pulmonary artery; *LPA* left pulmonary artery; *Ao* ascending aorta

patent ductus arteriosus, and, when applicable, ventricular septal defects should also be identified. Detection of global ventricular dysfunction or a regional wall motion abnormality may suggest a coronary perfusion defect. If the preoperative evaluation identified left ventricular outflow tract obstruction, residual subaortic stenosis may occur postoperatively. When a Rastelli operation is performed, the postoperative echocardiograms should interrogate for residual obstruction from the left ventricle to the aorta via the ventricular septal defect patch. Conduit obstruction may progress over time.

In addition, the aortic root may become dilated and/ or neoaortic regurgitation may develop. Serial echocardiograms over time should include measurement of the neoaortic root diameter and assessment of the degree of neoaortic regurgitation.

For patients in whom an atrial switch repair (Senning or Mustard operation) was performed, postoperative echocardiograms should assess for the development or progression of systemic and/or pulmonary venous pathway obstruction. The Senning and Mustard repairs appear echocardiographically similar. The pulmonary venous pathway may be visualized from standard apical four-chamber view with flow seen from left to right atrium over the systemic venous baffle. With anterior and clockwise rotation from this initial position, the

superior vena caval pathway can be elongated for optimal Doppler interrogation. The inferior vena caval pathway is best seen with posterior and counterclockwise rotation. Parasternal short- and long-axis views are also useful for evaluating these venous pathways. In addition, serial echocardiograms over time should evaluate the systemic right ventricular size and function and degree of tricuspid regurgitation.

Hypoplastic Left Heart Syndrome

Pathology

Hypoplastic left heart syndrome (HLHS) occurs when there is a failure of development of left heart structures, including the mitral valve, left ventricle, left ventricular outflow tract, aortic valve, and aortic arch. In the most severe form, the aortic and the mitral valve are atretic with a diminutive left ventricle and hypoplastic aortic arch (Fig. 27.7). However, each component of the left heart anatomy may be underdeveloped or hypoplastic to a variable degree. The term HLHS with its variants has come to suggest that the left heart is incapable of supporting systemic load or sustaining a full systemic cardiac output, which would necessitate a "single ventricle palliation" ultimately culminating in the Fontan operation. In the newborn, systemic perfusion is dependent on flow via a patent ductus arteriosus, with retrograde flow to the ascending aorta and antegrade flow to the descending aorta. An atrial communication is required to decompress the left atrium in the presence of mitral atresia or significant mitral hypoplasia.

Preoperative Evaluation

Careful measurement and Doppler interrogation of each left heart structure is necessary. The actual Doppler gradient across any structure may not reflect the degree of obstruction if there is minimal flow across that structure or the cardiac output is reduced. The right ventricular function and degree of tricuspid regurgitation should be assessed. The patency and size of the atrial septal communication and the ductus arteriosus must be evaluated.

Surgical Repair

HLHS is considered the paradigm for single ventricle palliation. The ultimate objective of repair is to channel systemic venous flow directly to the low resistance

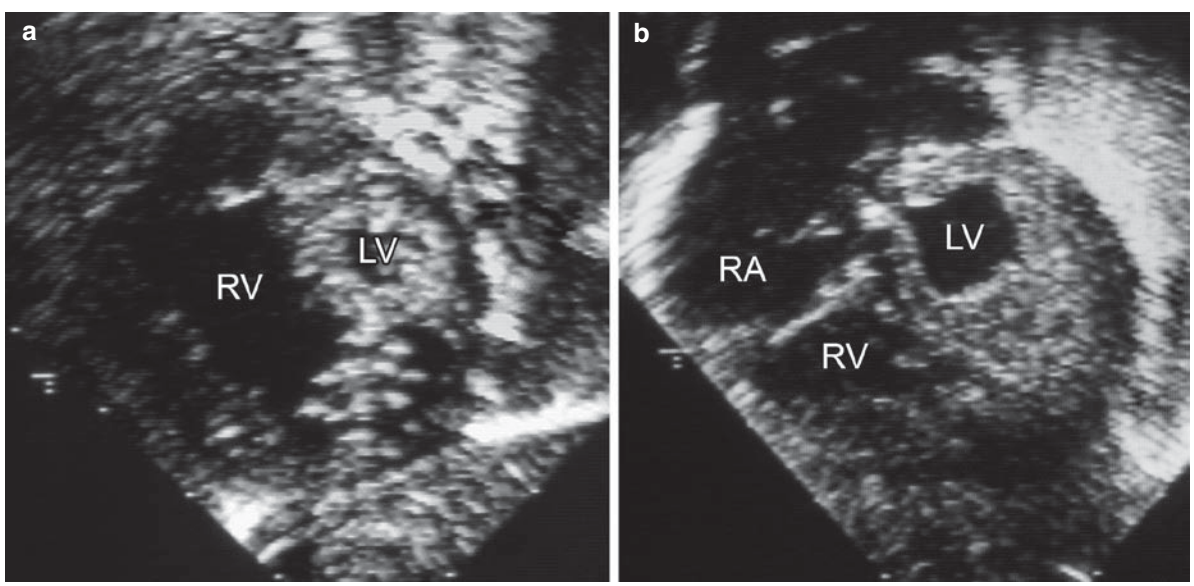

Fig. 27.7 Hypoplastic left heart syndrome. (**a**) Subcostal short-axis view; (**b**) apical four-chamber view, showing a severely hypoplastic left ventricle. *RA* right atrium; *RV* right ventricle; *LV* left ventricle

pulmonary bed, allowing the single ventricle to function as the systemic pump. Since the pulmonary resistance of the newborn is not sufficiently low to accept passive flow, the palliation is accomplished using a stage approach over time. As for other diseases with single ventricle physiology, surgery for HLHS includes a three-stage palliative surgical strategy.

Stage I or the Norwood operation includes an aortopulmonary anastomosis (Damus–Kaye–Stansel), aortic arch reconstruction, a Blalock–Taussig shunt (approximately 3.5-mm graft from the subclavian artery to the pulmonary artery), and creation of a large atrial septal communication. Recently a right ventricle to pulmonary artery conduit (Sano modification), has replaced the creation of a Blalock–Taussig shunt. Information is currently being gathered to determine if this modification has improved morbidity and mortality than the standard Blalock–Taussig shunt.

Stage II, or superior vena cavopulmonary connection, includes takedown of the shunt or conduit and anastomosis of the superior vena cava to the right pulmonary artery.

Finally, the third stage is the Fontan operation or total cavopulmonary anastomosis in which the IVC flow is directed to the pulmonary artery via a lateral tunnel through the atria, or occasional via extracardiac conduit. A fenestration may be placed in the baffle as a pop-off when the baffle pressure is elevated. This allows adequate systemic blood flow at the expense of lower systemic arterial saturation.

Postoperative Evaluation

Table 27.1 outlines the important postoperative factors to assess by two-dimensional Doppler echocardiography, following each stage of palliation (Figs. 27.8–27.11).

Shone Syndrome

The original constellation of findings described by Dr. Shone included ventricular septal defect, parachute mitral valve, supramitral ring, subaortic stenosis, and coarctation of the aorta.[3] The term has since been applied to patients with a combination of multiple left heart obstructive lesions. As with HLHS, each left heart structure should be evaluated by imaging and Doppler to help guide the surgical approach, one-ventricle palliation (as above) versus a two-ventricle repair.[4] Progressive or newly developed obstructions may occur after presentation, and therefore repeated evaluations of anatomy are required over time.

Table 27.1 Postoperative echocardiographic evaluation for three-stage single ventricle palliation

Stage of palliation	Anatomic considerations	Recommended views
Stage I – Norwood	ASD size	SC views
	Aortopulmonary anastomosis (Damus–Kaye–Stansel))	SC and PSL
	Aortic arch reconstruction and distal arch anastomosis	SSN (Fig. 27.8)
	Systemic ventricular function	
	Atrioventricular valve function	
	BTS and PA at insertion site	SSN and PSS
	Or with Sano modification	
	RV–PA conduit	SC and PSS
Stage II – Bidirectional Glenn (BDG)	Same as above, except with shunt or conduit takedown	
	Superior cavopulmonary anastomosis	SSN or high RSB for right CPA or high LSB for left CPA (Fig. 27.9)
	Branch Pas	
Stage III – fenestrated Fontan	Same as for Stage II	
	Lateral tunnel (intra-atrial baffle) obstruction and/or thrombus formation	SCS (Fig. 27.10)
	Fenestration patency and mean gradient	Apical or PSL (Fig. 27.11)

ASD atrial septal defect; *SC* subcostal; *PSL* parasternal long; *BTS* Blalock–Taussig shunt; *PA* pulmonary artery; *SSN* suprasternal notch; *PSS* parasternal short; *RSB* right sternal border; *LSB* left sternal border; *CPA* cavopulmonary anastomosis; *SCS* subcostal short

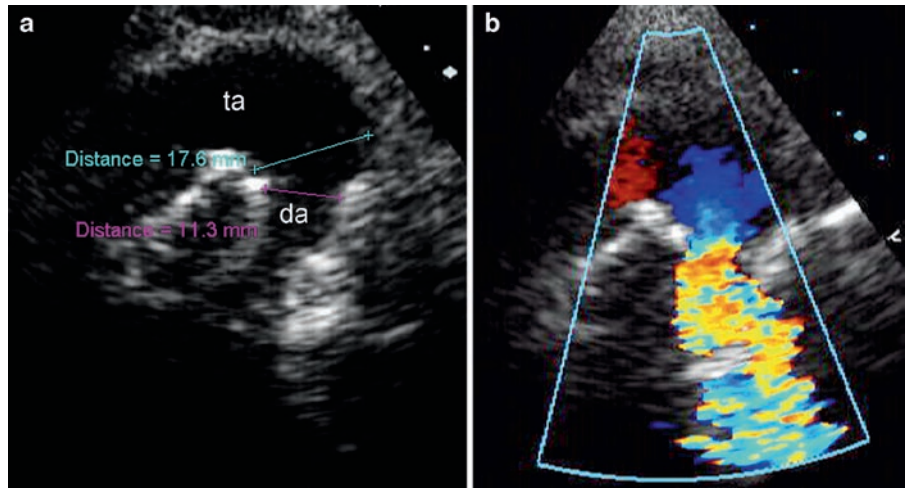

Fig. 27.8 Distal aortic arch after Stage I palliation for hypoplastic left heart syndrome. The size discrepancy between the large neotransverse aortic arch and the smaller native distal arch and descending aorta is seen from suprasternal notch view. There is mild arch obstruction at the distal anastomosis. *ta* transverse arch; *da* distal arch **(a)** suprasternal notch imaging aorta, **(b)** suprasternal notch imaging of descending aorta ta, trans seveare arch; da, decending aorta

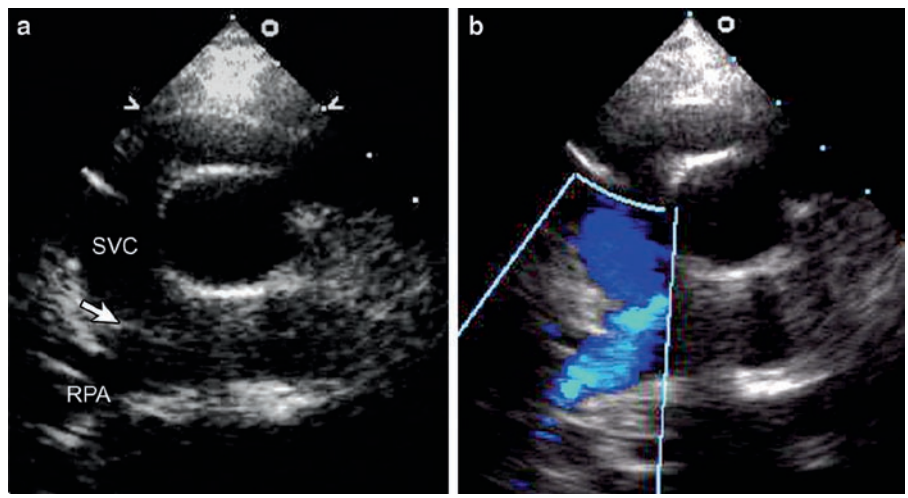

Fig. 27.9 Superior cavopulmonary anastomosis from suprasternal notch view. *Arrow* indicates the anastomosis at the superior vena cava to the right pulmonary artery. *SVC* superior vena cava; *RPA* right pulmonary artery **(a)** suprasternal notch imaging in coronal view **(b)** same view with color

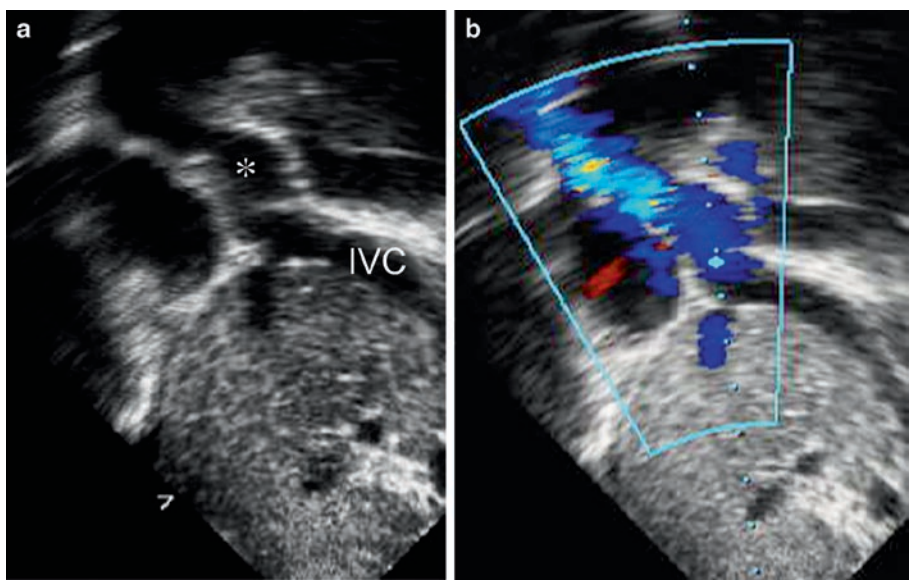

Fig. 27.10 Fontan pathway (total cavopulmonary anastomosis). Subcostal short-axis view showing a lateral tunnel baffle through the right atrium. *Asterisk* indicates lateral tunnel. *IVC* inferior vena cava **(a)** subcostal shad axis view. **(b)** same view with color

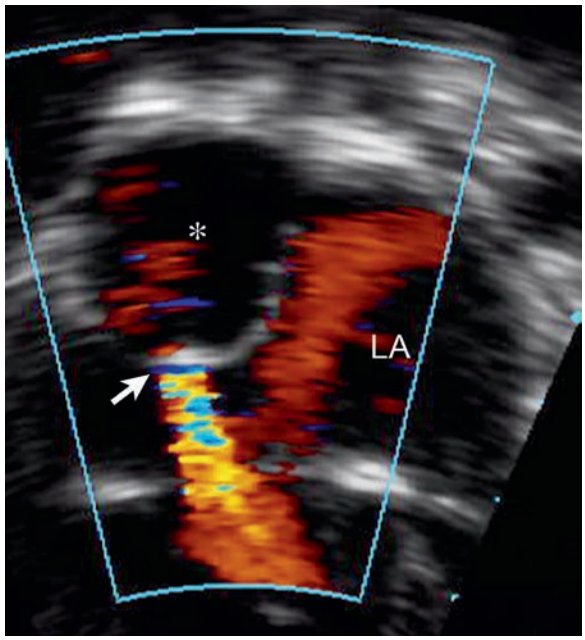

Fig. 27.11 Fenestrated Fontan. Apical four-chamber view showing a Fontan baffle in cross-section with fenestration flow. *Asterisk* indicates Fontan baffle; *arrow* indicates the fenestration. *LA* left atrium

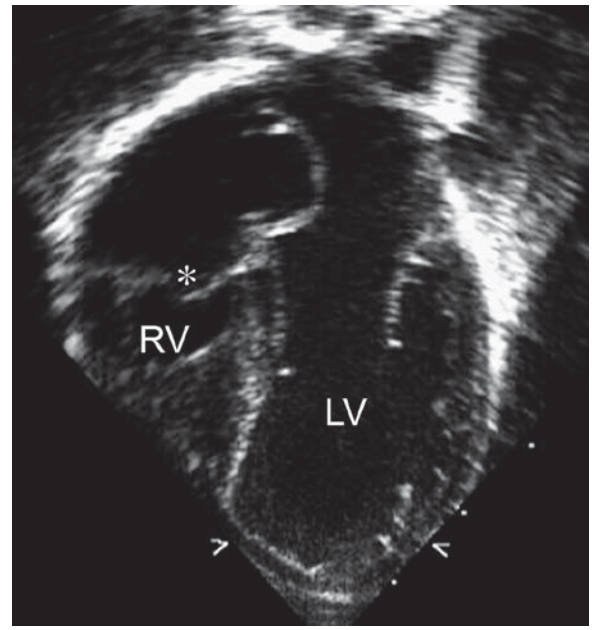

Fig. 27.12 Pulmonary atresia with intact ventricular septum. Apical four-chamber view showing a hypoplastic tricuspid valve and right ventricle. *Asterisk* indicates tricuspid valve. *RV* right ventricle; *LV* left ventricle

Pulmonary Atresia with Intact Ventricular Septum

Pathology

In pulmonary atresia with intact ventricular septum (PA/IVS) the pulmonary valve is atretic and usually associated with good sized branch pulmonary arteries in continuity with a smaller main pulmonary artery. The right ventricular size may vary from severe hypoplasia to adequate size. Pulmonary blood flow is supplied by a patent ductus arteriosus.

Right ventricular coronary sinusoids with connection to the coronary arteries may be present. When the coronary artery connections from the aorta are stenotic or atretic, the coronary circulation is dependent on the sinusoidal flow from a high-pressure right ventricle.

Preoperative Evaluation

The initial echocardiogram should focus on tricuspid valve and right ventricular size (Fig. 27.12), examination of the MPA length, size of the branch pulmonary arteries, and presence of RV coronary sinusoids. RV sinusoids can sometime be detected by close echocardiographic inspection of the RV myocardium using color Doppler enhanced by lowering the Doppler scale. Some authors have found a correlation of the tricuspid valve annulus size with the presence of right ventricular sinusoids and right ventricular coronary circulation[5]; however, coronary artery anatomy and supply is best evaluated by coronary angiography.

Surgical Repair

In the absence of right ventricular dependent coronary circulation, even when the tricuspid valve and right ventricle are hypoplastic, the initial neonatal repair is to open the RVOT with a patch. In addition, surgical repair includes ensuring an adequate ASD to decompress the right atrium and placement of a Blalock–Taussig shunt for adequate pulmonary blood flow. This allows time for right ventricular "growth." Occasionally, pulmonary valve atresia may be amenable to perforation using radiofrequency ablation in the cathelicatia

laboratory. When antegrade flow through the RV and RVOT is thought to be sufficient, the ASD and Blalock–Taussig shunt can be closed in the catheterization laboratory. Alternatively, if antegrade flow remains limited by a small, noncompliant right ventricle or stenotic tricuspid valve, a so-called one and a half ventricle repair could be undertaken. This includes an RVOT patch, superior cavopulmonary anastomosis, and closure of the atrial septal defect. In essence, the cavopulmonary anastomosis decompresses the right ventricular flow by approximately one-third, allowing flow from the inferior vena cava to be ejected to the pulmonary arteries by the right ventricle.

When a right ventricular-dependent coronary circulation is present, placement of an RVOT patch would decompress the right ventricle resulting in coronary insufficiency and myocardial ischemia or infarction. Therefore, a single ventricle palliation is performed instead.

Postoperative Evaluation

Following RVOT patch and shunt placement, the degree of antegrade flow through the RV should be assessed, as well as atrial septal defect size and direction of flow. Growth of the right ventricle can be evaluated. As with all pre- and postoperative echocardiographic examinations, evaluation of the systemic ventricular and atrioventricular valve function is of obvious importance.

Tricuspid Atresia

Pathology

In tricuspid atresia, no discernible patency of tricuspid valve leaflet tissue is present. A thick membrane overlies the right ventricular inlet, and this entity is associated with a hypoplastic right ventricular sinus (Fig. 27.13). Egress of blood from the right atrium necessitates an atrial septal defect or patent foramen ovale, resulting in complete mixing with pulmonary venous blood in the left atrium. The presence/size of the VSD regulates the amount of antegrade flow through the great artery arising from the right ventricle. With normally related great arteries, a large VSD allows significant flow to the pulmonary arteries. This may lead to congestive heart failure, possibly necessitating a pulmonary artery band. Conversely, if the VSD is restrictive or absent, severe subpulmonary stenosis or atresia results, and the infant will be duct- or shunt dependent. With transposed great arteries, a restrictive VSD will functionally result in subaortic stenosis, often associated with the aortic arch hypoplasia.

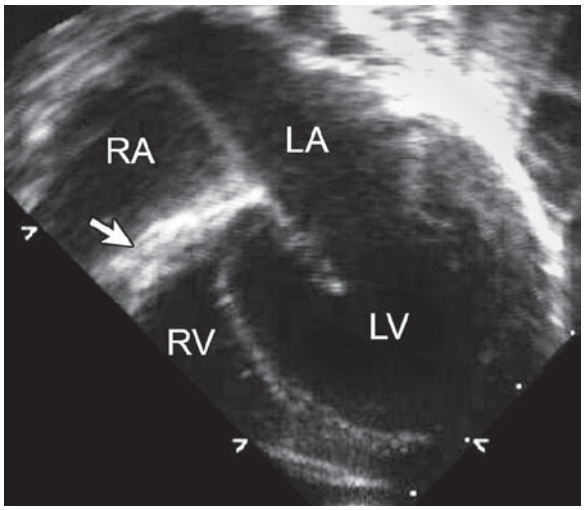

Fig. 27.13 Tricuspid atresia. This apical four-chamber view shows a thick membrane (*arrow*) overlying the right ventricular inlet and an associated hypoplastic right ventricular sinus. *RA* right atrium; *RV* right ventricle; *LA* left atrium; *LV* left ventricle

Preoperative Evaluation

The preoperative echocardiographic evaluation should focus on the relationship of the great arteries, and on the presence, size, and degree of restriction of the VSD. In addition, size and degree of obstruction at the semilunar valve and great artery arising from the right ventricle are assessed. Rarely, the atrial septal defect or patent foramen ovale is restrictive.

Surgical Repair

The surgical strategy for this form of congenital heart disease is a single ventricle palliation. The initial stage depends on the relationship of the great arteries and the presence and size of the ventricular septal defect (Table 27.2).

Table 27.2 Initial palliation for tricuspid atresia

Anatomy	Physiology	Initial palliation
NRGV		
Large VSD	Unrestrictive PBF	Pulmonary artery band
Restrictive VSD or sub-PS	Subpulmonary stenosis	Blalock–Taussig (aortopulmonary) shunt
TGA		
Large VSD	Unrestrictive PBF	Possible shunt
Restrictive VSD	Subaortic stenosis	Aortopulmonary anastomosis and/or aortic arch repair

NRGV normally related great vessels; *TGA* transposition of the great arteries; *VSD* ventricular septal defect; *PBF* pulmonary blood flow

Postoperative Evaluation

The postoperative echocardiogram should assess the initial palliation. In addition, the cavopulmonary anastomosis and Fontan pathway is evaluated following the second and third stages of repair (Table 27.1). The assessment of mitral valve and left ventricular function is important at all stages of repair.

Double Outlet Right Ventricle

Pathology

Double outlet right ventricle (DORV) occurs when both great arteries arise from the right ventricle. In some patients one great vessel may override the ventricular septum and appear to arise in part from the left ventricle. DORV is diagnosed by some anatomists when this overriding great vessel arises primarily over the right ventricle. Perhaps a more reliable determinant of DORV is when there is absence of continuity between the annulus of the overriding great vessel and the mitral valve, separated by an elongated intervalvar fibrosa.

The critical factors in DORV are the relationship of the great arteries to the VSD and the relative degree of pulmonary or aortic obstruction. The VSD may be subaortic, subpulmonary, relate equally to each ("doubly-committed"), or be uncommitted. When the VSD is subaortic with anterior malalignment of the conal septum, the pathophysiology is that of a large VSD. If there is subpulmonary stenosis, the pathophysiology is similar to TOF. If the pulmonary artery is posterior with a subpulmonary VSD, the pathophysiology is similar to d-TGA/VSD. In typical Taussig–Bing DORV there is bilateral conus beneath the aorta and the pulmonary artery with the possibility of subaortic or subpulmonary obstruction. Without subpulmonary obstruction, pulmonary blood flow will be increased and the patient may exhibit congestive heart failure, yet with relative cyanosis due to the streaming of desaturated blood to the ascending aorta. In such situations, subaortic obstruction will exacerbate heart failure. The presence of subaortic stenosis or aortic annular hypoplasia is a harbinger for aortic arch hypoplasia. Pulmonary or subpulmonary stenosis is associated with decreased pulmonary blood flow and more profound cyanosis.

When the aorta and pulmonary artery are anterior–posterior to each other, a large conoventricular septal defect may be "double committed." The pathophysiology would again be dependent on the presence of subpulmonary or subaortic or valvar obstruction. When the VSD is in the endocardial cushion region or inlet septum, the ventricular septal defect is "noncommitted." Such inlet VSDS may be associated with straddling or overriding of an atrioventricular valve, rendering VSD closure more difficult. Moreover, straddling tricuspid valves can be associated with corresponding ventricular hypoplasia, obviating the potential for biventricular repair.

Surgical Repair

The surgical repair depends on the anatomic type of DORV (Table 27.3). For example, the repair of DORV with subaortic VSD may consist of simple VSD patch closure baffling the aorta to the left ventricle. Associated right ventricular outflow tract obstruction is relieved similar to TOF repair with either a transannular, or nontransannular patch, or conduit. DORV with subpulmonary VSD is repaired similar to d-TGA/VSD with an arterial switch operation and VSD closure. Associated subpulmonary stenosis may consist of resection of the subpulmonary obstruction if the valve is normal or only minimally affected. Severe valvar or subpulmonary stenosis may necessitate a Rastelli operation with patching of the VSD to the aorta and placement of a right ventricle to pulmonary artery conduit. Patients with subaortic stenosis may undergo an arterial switch operation with resection of subaortic

Table 27.3 Double outlet right ventricle

Anatomy	Pathophysiology	Surgical repair
Subaortic VSD		
No pulmonary outflow obstruction	Increased PBF + CHF	Patch close VSD with LV to aorta
Pulmonary outflow obstruction	Decreased PBF + cyanosis	Patch close VSD + correct pulmonary outflow obstruction
Subpulmonary VSD		
No subaortic stenosis	Increased PBF + CHF	Arterial switch + VSD closure
Aortic outflow obstruction	CHF and LCO	Arterial switch + resect sub AS
Severe aortic outflow obstruction	CHF and LCO	DKS and shunt
Coarctation or interrupted aortic arch	CHF and LCO	Same as above and repair arch
Noncommitted VSD		
No pulmonary outflow obstruction	Increased PBF + CHF	PA band, subsequent Fontan or close VSD to aorta or close VSD to PA and arterial switch
Pulmonary outflow obstruction	Cyanosis	Initial shunt + then Fontan or close VSD to aorta and correct pulmonary outflow obstruction
Aortic outflow obstruction	CHF and LCO	DKS and shunt then Fontan, or DKS then close VSD to native PA and conduit RV to PA

VSD ventricular septal defect; *PBF* pulmonary blood flow; *CHF* congestive heart failure; *LCO* low cardiac output; *DKS* Damus–Kaye–Stansel; *PA* pulmonary artery; *RV* right ventricle

tissue. It the native aortic annulus and the ascending aorta are hypoplastic the patient may undergo a Stansel anastomosis (main pulmonary artery to the ascending aorta) and placement of a conduit from the right ventricle to the pulmonary arteries. The VSD is closed with a patch from the left ventricle to the pulmonary artery such that blood flows from left ventricle to pulmonary artery to ascending aorta.

When the VSD is uncommitted, it may difficult to baffle the aorta to the left ventricle without causing significant subaortic obstruction. In those patients in whom a two-ventricular repair is not feasible, the patient would undergo single ventricle palliation. This consists of three operations, as outlined for the hypoplastic left heart syndrome. However, the first operation depends on the aortic and pulmonary anatomy. If there is unrestrictive pulmonary blood flow, the patient will undergo placement of a pulmonary arterial band. Alternatively, if there is severe pulmonary outflow obstruction, the patient may require placement of a systemic to pulmonary arterial shunt, usually a modified Blalock–Taussig shunt. If the patient has significant subaortic stenosis, the repair will involve either resection of the subaortic stenosis or a Stansel anastomosis with a Blalock–Taussig shunt.

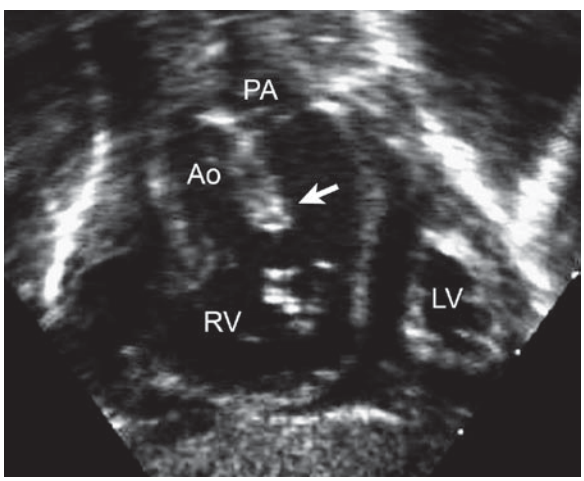

Fig. 27.14 Double outlet right ventricle. Subcostal long axis showing both great arteries arising from the right ventricle with subaortic conus, i.e., Taussig–Bing. *Arrow* indicates subaortic conus. *RV* right ventricle; *LV* left ventricle; *PA* pulmonary artery; *Ao* aorta

Preoperative Evaluation

Orientation and alignment of the great vessels and their relationship to the VSD are best seen from subcostal imaging sweeps (Fig. 27.14). Since the type of surgical intervention is based on delineation of the anatomy, careful attention must be applied to evaluate for subaortic or subpulmonic stenosis or annular hypoplasia. Short-axis transthoracic views provide the best imaging for the coronary arteries, especially if a patient is to be considered for an arterial switch operation. This plane is important to evaluate the anatomy of the semilunar valves and branching of the pulmonary arteries. A combination of short-axis and apical four-chamber views provides important additional detail as to the anatomy of the atrioventricular valves, including straddling or overriding, size of the corresponding ventricular chambers, and important

additional views of the ventricular septum. Suprasternal notch imaging is used to evaluate for coarctation of the aorta or aortic arch hypoplasia. This view is also useful for evaluating the branch pulmonary arteries.

Postoperative Evaluation

The follow-up echo evaluation is entirely dependent on the initial anatomy and subsequent surgical repairs. For example, the echocardiographic evaluation may be for a patient that had one of the following operations: (1) VSD closure, (2) arterial switch operation with VSD closure, (3) Rastelli operation, and (4) serial operations for single ventricle physiology. However, persistence of a specific problem may occur. The patient may undergo a second operation for subaortic stenosis, or reoperation for a stenotic conduit, or perhaps for evaluation of aortic arch recoarctation. The previous sections outline the postoperative evaluation for these specific problems.

Summary

Due to the significant recent advances in medical and surgical care, many patients with complex congenital heart disease are now reaching adolescence and adulthood. Many echocardiographers are requested to evaluate these patients, as part of the patient's clinical evaluation. The purpose of this chapter was to present the presenting anatomy and pathophysiology of specific complex congenital heart disease, which serves as the underpinnings for the understanding of the serial echocardiographic evaluation of these patients as they become adults.

References

1. Niwa K, Siu SC, Webb GD, Gatzoulis MA. Progressive aortic root dilation in adults late after repair of tetralogy of Fallot. Circulation. 2002;106:1374–1378.
2. Mackie AS, Gauvreau K, Perry SB, del Nido PJ, Geva T. Echocardiographic predictors of aortopulmonary collaterals in infants with tetralogy of Fallot and pulmonary atresia. J Amer Coll Cardiol. 2003;41:852–857.
3. Shone JD, Sellers RD, Anderson RC, Lillehei CW, Edwards JE. The developmental complex of 'parachute mitral valve,' supravalvular ring of the left atrium, subaortic stenosis, and coarctation of the aorta. Am J Cardiol. 1963;11:714–725.
4. Schwartz ML, Gauvreau K, Geva T. Predictors of outcome of biventricular repair in infants with multiple left heart obstructive lesions. Circulation. 2001;104:682–687.
5. Satou GM, Perry SB, Geva T. Echocardiographic predictors of coronary artery pathology in pulmonary atresia with intact ventricular septum. Am J Cardiol. 2000;85:1319–1324.

Chapter 28
Adult Congenital Heart Disease

Kate M. English and John L. Gibbs

General Principles

Obtaining high-quality echocardiographic images in adults with congenital heart disease is often challenging. Not only is cardiac anatomy abnormal, but the cardiac position within the chest may be abnormal, the patient may have undergone previous surgery distorting cardiac anatomy, and patients with underlying genetic or syndromic abnormalities frequently have spinal and other skeletal abnormalities. All these features can make standard echocardiographic views difficult to obtain with the patient in the regular positions. It is important to remember that an echocardiographic study in an adult with complex congenital heart disease is likely to be much more time consuming than one in an adult with a normally positioned and related heart. One must adopt an attitude of flexibility toward positioning of the subject and transducer position on the chest to obtain the maximal anatomic and functional information. The echocardiographer needs a basic understanding of congenital heart disease as well as its natural and unnatural history to help anticipate the changing echocardiographic features and the late complications of congenital heart disease in the adult.

It is of fundamental importance that those requesting echocardiography in patients with congenital heart disease have a sound understanding of the anatomy of congenital heart disease as well as its treatment, so that adequate details are given to the echocardiographer and it can be made clear what clinical questions are being asked. Adequate training is often difficult for echocardiographers and cardiologists alike to obtain because centers with large numbers of adults with congenital heart disease are few in number. It takes considerable experience to identify reliably the complications and consequences of congenital heart disease and its treatment.

K.M. English (✉) and J.L. Gibbs
Yorkshire Heart Centre, Leeds General Infirmary, Calverley Street, Leeds, LS1 3EX, UK
e-mail: kateenglish10@hotmail.com

Sequential Segmental Analysis and Normal Anatomy

When examining complex congenital heart disease it is easy to focus on particular abnormalities while missing parts of the "bigger picture." It is often helpful to adopt the traditional approach of sequential segmental analysis, treating the heart as a series of building blocks, each of which can have only a limited number of abnormalities. Thus, if one considers the visceroatrial situs (including the position of the heart and major organs), the anatomy and connections of the great veins, then the atriums, the atrioventricular connections, the ventricles, the ventriculoarterial connections and, finally, the great arteries it becomes relatively simple to build up a comprehensive picture of even the most complex congenital heart disease.

The inferior vena cava should normally be seen on the right-hand side of the spinal column and should connect directly with the right atrium. The right-sided superior vena cava can be identified in the majority of adults, along with its connection to the right atrium. Persistence of a left superior vena cava (coexisting with a right-sided superior caval vein) should be considered as a variant of normal anatomy, draining to the coronary sinus, which is usually enlarged. The degree of coronary sinus dilatation will depend upon the venous return to it, so it is most marked when there are bilateral caval veins without an innominate connection between the two (so venous return from the left arm and the left

P. Nihoyannopoulos and J. Kisslo (eds.), *Echocardiography*,
DOI: 10.1007/978-1-84882-293-1_28,

jugular vein must drain to the coronary sinus). Identification of a left superior caval vein is of particular relevance in patients who are candidates for permanent pacemaker implantation; the echocardiographer should alert the operator, recommending a right-, rather than left-, sided approach for electrode implantation.

The normal right atrium can often be identified in children by the appearance of its blunt, triangular appendage (in contrast to the elongated left atrial appendage), but it is rare in the adult to be able to identify detailed appendage anatomy without the aid of a transesophageal probe. The normal connection of the right atrium to the tricuspid valve and right ventricle is characterized by the morphology of the tricuspid valve apparatus, which inserts to both the ventricular septum and the free right ventricular wall (in contrast to the mitral valve apparatus, which inserts into the paired papillary muscles of the free left ventricular wall). In addition, the septal leaflet of the tricuspid valve is attached slightly more toward the apex than its mitral counterpart, producing the normal "offset" of the atrioventricular valves. The right ventricle is more coarsely trabeculated than the left and can also be identified by its moderator band (a muscular band seen toward the apex). Fortunately, even in complex disease these features persist; the tricuspid valve almost always retaining its normal commitment to the right ventricle (exceptions being rare anomalies such as double inlet left ventricle), so identification of the tricuspid valve almost always leads to identification of the right ventricle. The hallmarks of normal right ventriculoarterial connection are the bifurcating pulmonary artery, which arises almost at right angles to the aorta such that when the aorta is imaged in short axis, the pulmonary trunk appears in long axis, and vice versa. A parallel course of the ascending aorta and pulmonary trunk is never normal.

A similar approach can be applied to the left side of the heart. Identification of at least two pulmonary veins draining to the left atrium is possible in most adults, although transesophageal studies might be necessary to reliably identify all four in cases of doubt.

The lightly trabeculated left ventricle gives rise to the aorta, identified by its lack of bifurcation and its continuity into the aortic arch with its innominate, carotid, and subclavian branches.

Despite a painstaking transthoracic study, complete information may not always be obtainable and additional imaging modalities such as transesophageal echo, magnetic resonance imaging, and cardiac catheterization may need to be employed to define fine details of anatomy and function.

Transesophageal Echocardiography

Transesophageal echocardiography has an important role when inadequate precordial images are obtained. This might be for a variety of reasons such as abnormal position of the heart, skeletal abnormalities, or poor echo windows in patients with lung disease. Even in patients in whom transthoracic echo produces good quality images, transesophageal echo is particularly useful in defining the anatomy of certain areas which are not well seen on transthoracic echo. These include the superior vena cava, the pulmonary veins, the atriums and atrial septum (particularly after intra atrial surgery), the ascending and descending aorta, the proximal coronary arteries and aortopulmonary as well as cavopulmonary shunts.

Transesophageal echo is an invaluable adjunct to fluoroscopy during therapeutic catheterization, particularly during closure of septal defects.

Contrast Echocardiography

Simple agitated saline (9.5 ml of normal saline rapidly squeezed back and forth between two 10-ml syringes via a three-way tap) rapidly injected into a large upper limb peripheral vein will confirm the site of superior caval vein connection to the heart, and the presence of a left superior caval vein in cases where there is doubt about the venous connections. Similarly, contrast into a lower limb vein will delineate inferior caval drainage to the heart. When the atrial septum cannot be imaged clearly, contrast may be seen to appear in the left atrium directly after its appearance in the right atrium in patients with an atrial septal defect or patent foramen ovale (Fig. 28.1). The Valsalva maneuver performed simultaneous to the peripheral injection improves the ability to detect a right to left shunt through a PFO (it is rarely necessary to perform a transesophageal echo in this situation if a good precordial contrast study has been undertaken). Contrast agents are also useful in determining the presence of atrial shunts (defects in the intra-atrial baffles used to redirect venous return)

in patients who have had Mustards' or Sennings' operations for Transposition of the great vessels. "Designer" manufactured echo contrast agents have a limited role. They have the benefit of being more echogenic than simple agitated saline, but in our experience they may sometimes cross the pulmonary vascular bed rapidly in some patients, potentially leading to an erroneous diagnosis of an interatrial shunt. These agents are probably best restricted to the purposes they were designed for, such as enhancing endocardial wall detection and assessing myocardial perfusion.

Atriums and Great Veins

Anomalous Venous Drainage

If the right heart is volume loaded but the atrial septum appears intact, the patient may have partial anomalous pulmonary venous drainage. Particularly when detected in adult life, this condition most commonly occurs in association with a sinus venosus defect.

Anomalous systemic venous drainage is rare outside the context of complex disease associated with atrial isomerism. In cases where organ position is abnormal it becomes of particular relevance to assess the position and site of drainage of both the systemic and the pulmonary veins.

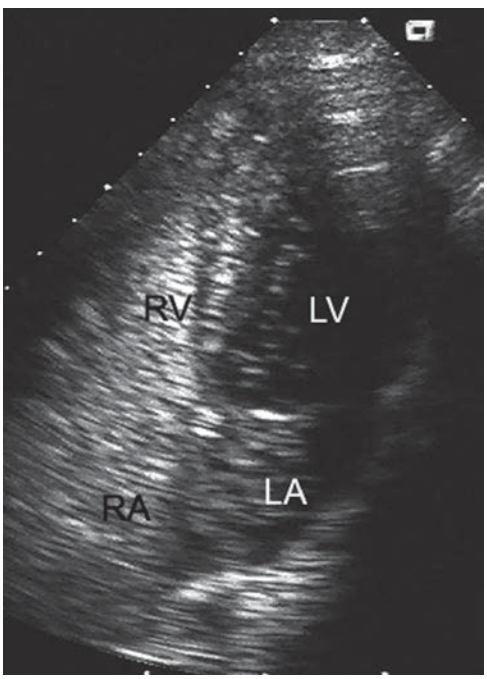

Fig. 28.1 PFO contrast study of apical four chamber. Apical four-chamber view showing the right atrium and right ventricle completely opacified by bubble contrast. A "whiff" of bubble contrast can be seen in the left atrium, and a few bubbles in the left ventricle, demonstrating flow across a patent foramen ovale. *LA* left atrium; *LV* left ventricle; *RA* right atrium; *RV* right ventricle

Cor Triatriatum

Subdivision of the left atrium (cor triatriatum) may present for the first time in adulthood. The finding can be made incidentally during echocardiography for other reasons, or the patient may present with breathlessness (due to elevated pulmonary venous pressure) or rarely with atrial arrhythmias. The membrane is well seen by transthoracic echocardiography in the parasternal long-axis, parasternal short-axis, and apical views (Fig. 28.2). The membrane is perforated in one or more places, and there is almost always restricted flow through it, resulting in a situation that is physiologically similar to mitral stenosis. There will be a

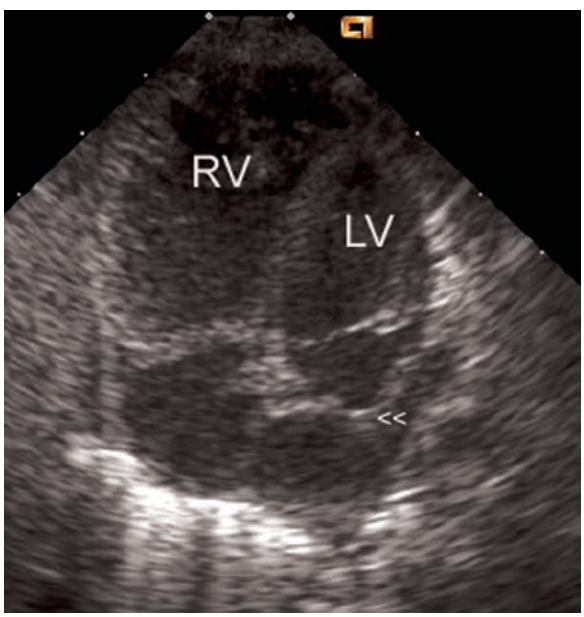

Fig. 28.2 Cor triatriatum apical four chamber. Apical four-chamber view demonstrating the cor triatriatum membrane (*arrowed*) dividing the left atrium into two chambers. *LV* left ventricle; *RV* right ventricle

continuous color jet of flow through the perforation(s) in the membrane (Fig. 28.3). TOE is rarely necessary, but will confirm the diagnosis in patients with inadequate transthoracic imaging.

Subdivision of the right atrium (cor triatriatum dexter) is exceedingly rare, particularly in adults. Eustachian and Thebesian valve remnants may be very prominent in normal adults (particularly on TOE); it is most important not to mistake these structures for a subdividing membrane in the right atrium (Fig. 28.4).

Atrial Septal Defects

Atrial septal defect commonly presents for the first time in adulthood. Patients often have few, if any, symptoms, and the defect is often picked up after an incidental finding of an abnormal chest radiograph or on an echocardiogram performed because of an asymptomatic murmur (or breathlessness, palpitations, or embolic events in symptomatic patients). Small atrial septal defects may occur with small left to right shunts which are of little consequence. The hallmark of an important left to right atrial shunt is volume loading of the right ventricle (dilatation of the ventricle and with larger shunts, paradoxical ventricular septal motion) (Figs. 28.5 and 28.6). The larger the left to right shunt, the higher the flow through the tricuspid and pulmonary valves, with corresponding increase in tricuspid inflow and pulmonary outflow velocities. Major elevation of pulmonary arterial pressure is not a feature of atrial septal defects, so in most cases peak velocity of tricuspid regurgitation will be near normal. Secundum atrial septal defects (i.e., within the confines of the foramen ovale) can almost always be visualized directly by 2-D transthoracic echocardiography using standard views, (Figs. 28.7) but sinus venosus defects (the more common superior variety adjacent to the orifice of the superior caval vein, and the rare inferior variety rarely adjacent to the orifice of the inferior caval vein) and coronary sinus defects (communications between the coronary sinus and the left atrium) can be easily missed on transthoracic echocardiography. Transesophageal echocardiography offers advantages in these situations and is particularly good for identifying the anomalous return of the right upper pulmonary vein associated with sinus venosus defects (Figs. 28.8a, b).

It is easy for the inexperienced echocardiographer to incorrectly diagnose a secundum atrial septal

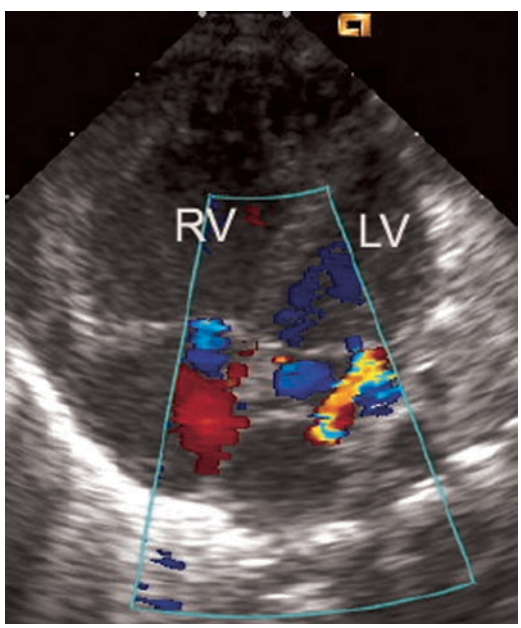

Fig. 28.3 Cor triatriatum color flow. Apical four-chamber view demonstrating high-velocity color flow at the site of perforation of the cor triatriatum membrane. *LV* left ventricle; *RV* right ventricle

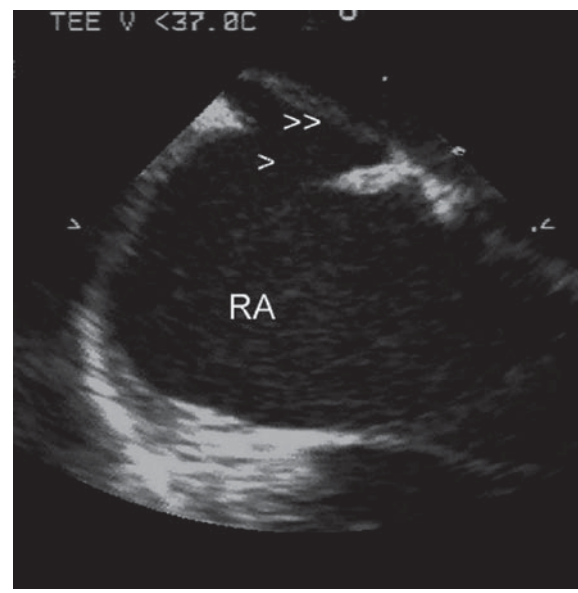

Fig. 28.4 TOE image of Eustachian valve. Transesophageal echo image of a prominent Eustachian valve (*single arrow*). This structure could easily be mistaken for the atrial septum with a secundum defect. The atrial septum is clearly seen (*double arrows*). *RA* right atrium

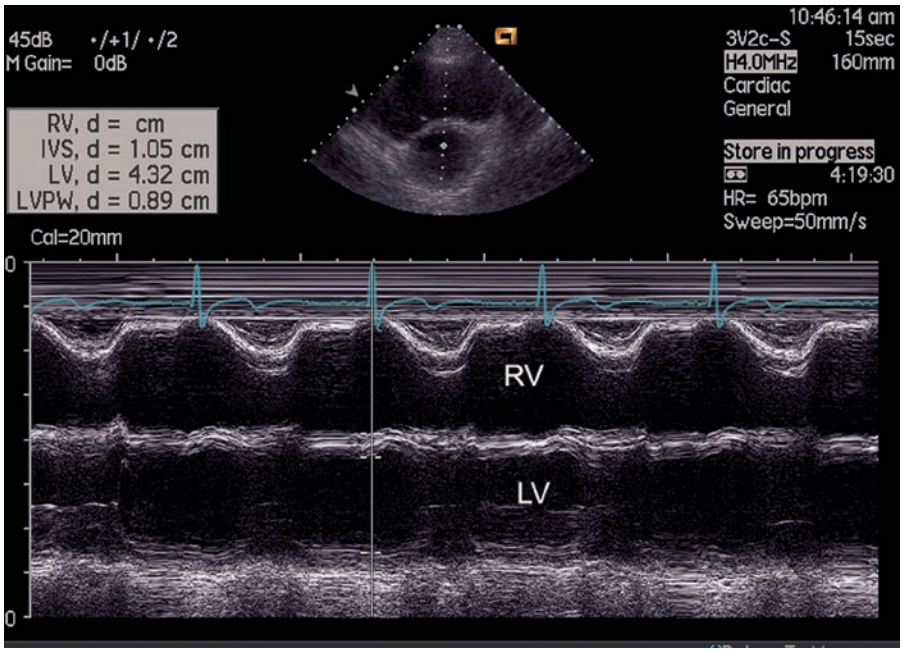

Fig. 28.5 Dilated right heart, M mode. M-Mode echocardiogram from parasternal short-axis view demonstrating significant right ventricular dilatation. *LV* left ventricle; *RV* right ventricle

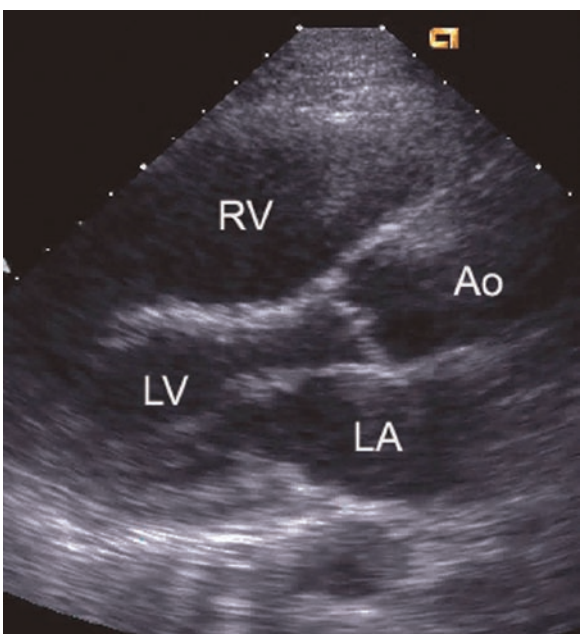

Fig. 28.6 Dilated right heart, parasternal long axis. Parasternal long-axis view demonstrating significant right ventricular dilatation. *Ao* aorta; *LA* left atrium; *LV* left ventricle; *RV* right ventricle

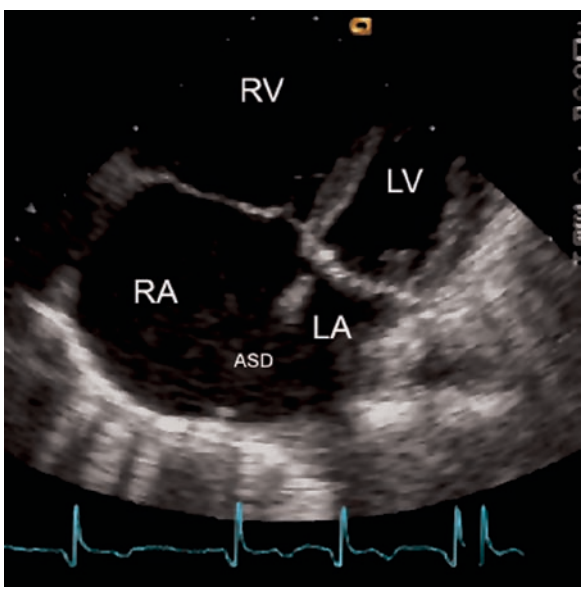

Fig. 28.7 Secundum ASD four-chamber view. Apical four-chamber view demonstrating a large secundum atrial septal defect and significant right heart dilatation. *LA* left atrium; *LV* left ventricle; *RA* right atrium; *RV* right ventricle; *ASD* atrioventricular septal defect

defect when the septum is thin but intact. There is often signal dropout in the region of the interatrial septum, particularly in the apical four-chamber view. If there is a genuine defect, color Doppler will confirm low-velocity flow from left to right (Fig. 28.9). Pulsed-wave Doppler also confirms left to

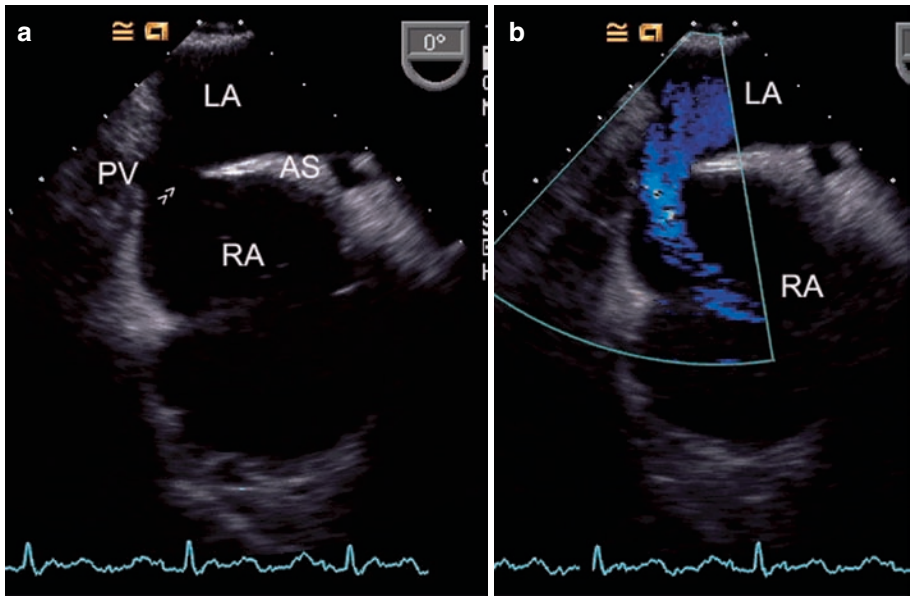

Fig. 28.8 (**a**) Supravalvar aortic stenosis clor flow. TOE image of a sinus venosus ASD. Transesophageal echo image of a sinus venosus ASD (*arrowed*). (**b**) TOE image of a sinus venosus ASD with color flow. Color-flow mapping of the sinus venosus defect seen in (**b**). Low-velocity flow can be seen passing from left atrium to right atrium. *AS* atrial septum; *LA* left atrium; *PV* pulmonary vein; *RA* right atrium

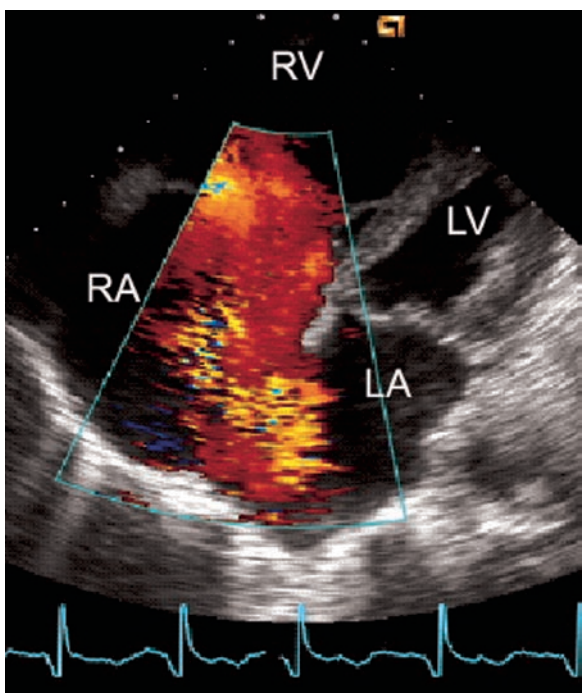

Fig. 28.9 Secundum ASD four-chamber view color flow. Color-flow imaging of the secundum atrial septal defect seen in Fig. 28.7, demonstrating low-velocity flow from left atrium to right atrium across the defect. *LA* left atrium; *LV* left ventricle; *RA* right atrium; *RV* right ventricle

right shunting with an increase in flow across the defect in expiration and decrease in flow during inspiration. This relationship helps to differentiate between flow through an atrial septal defect and caval flow (which has the opposite relationship to respiration). Care must be taken to avoid misinterpreting flow from the superior vena cava as flow across the atrial septum. A prominent Eustachian valve can be mistaken for the interatrial septum giving the appearance of an atrial septal defect, particularly in short-axis views.

An estimation of the degree of left to right shunting (Q_p:Q_s) can be made using a variety of techniques.

About 60% of atrial septal defects can be closed at cardiac catheterization. The important echo features to assess when deciding on the suitability for transcatheter closure are the number of defects in the septum, whether the foramen is aneurysmal, and the diameter of the defect in short-axis, four-chamber, and long-axis views. It is also important to measure the proximity of the margins of the defect to adjacent structures such as the septal leaflet of the mitral valve, the orifice of the coronary sinus, the orifices of the right pulmonary veins and the caval veins; normally a distance of at least 5 mm is required to anchor a

device securely (although, for some devices, the margin to the aorta does not seem to be important). In the vast majority of cases these measurements can be made with precordial echo alone, transesophageal echo only being required to assist at transcatheter closure (Fig. 28.10a–f).

When ASDs are closed in childhood right ventricular dilatation usually resolves rapidly and completely, but this is rarely the case in adults after many years of chronic volume overload, so some degree of persistent right heart dilatation and tricuspid regurgitation is to be expected even after successful ASD closure.

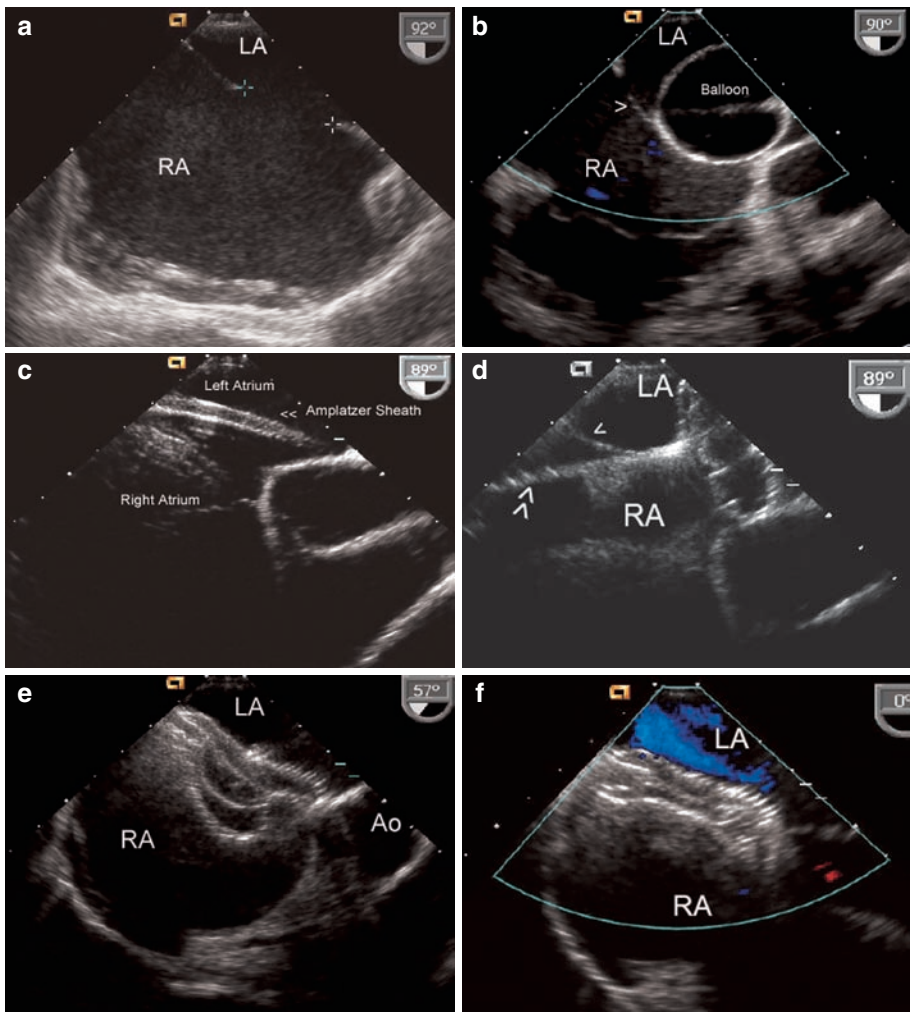

Fig. 28.10(a) Secundum ASD chosen for percutaneous closure. TOE image of a typical secundum ASD chosen for percutaneous closure. The defect can be seen between the two markers, measuring 2.4 cm. (**b**) Sizing balloon. A guide wire has been passed across the ASD; the sizing balloon has been passed over the wire into the left atrium and inflated. It is inflated incrementally until it will no longer pass across the ASD from left to right. The volume required to inflate the balloon to this degree is carefully noted. The sizing balloon is then taken out and ex vivo, inflated with the same volume of liquid as was previously noted. This balloon is then compared to a sizing plate to guide in the choice of device size. The atrial septum is arrowed. (**c**) Amplatzer sheath across ASD. An Amplatz delivery sheath has been passed over the guide wire. The delivery sheath can be clearly seen crossing the defect. (**d**) Left atrial disc deployed. The distal disc of the Amplatz atrial septal occluder has been deployed. This disc can be seen in the left atrium at the end of the delivery sheath. (**e**) Both discs deployed. The proximal disc of the device has now been deployed. The device is still attached to the delivery cable. (**f**) Final result. The device has been released from the delivery cable, taking up a more satisfactory position. There is no evidence of residual shunting either through or around the device. *Ao* aorta; *LA* left atrium; *RA* right atrium

Patent Foramen Ovale

Patent foramen ovale is a common normal finding in infants but often closes in the early years. Estimates of the incidence of probe patency of the foramen ovale in adults at autopsy range from 9 to 35%. Persistence of patency of the foramen ovale usually comes to light as an incidental finding during echocardiography, or during the investigation of cryptogenic stroke. It is thought that the etiology of stroke in some of these patients may be paradoxical embolization of thrombi across the PFO into the systemic circulation, particularly in the presence of an atrial septal aneurysm.

Patent foramen ovale can be detected in subcostal views using transthoracic echocardiography alone. A small jet of color flow may be seen passing from right to left atrium at the site of the fossa ovalis. Sensitivity is greatly increased by the use of agitated saline or specially designed echo contrast agents. The contrast is injected into a large peripheral (or central) vein and will be seen passing promptly from the right atrium to the left atrium in the presence of a patent foramen ovale. Sensitivity of detection of shunting right to left through a patent foramen ovale is further improved by increasing right atrial pressure by performing the Valsalva maneuver at the time of injection of chosen contrast agent, or pressing over the liver of patients undergoing transesophageal echocardiography, when it is difficult to perform the Valsalva maneuver adequately.

Almost all PFOs are technically closeable at cardiac catheterization. It is important to report on the anatomy of the foramen, not just the presence of shunting; when the septum is aneurysmal positioning of a device in the foramen can be more difficult and should be performed with transesophageal echo. Straightforward, nonaneurysmal PFOs can usually be closed quickly and safely without TOE (Figs. 28.11–28.13).

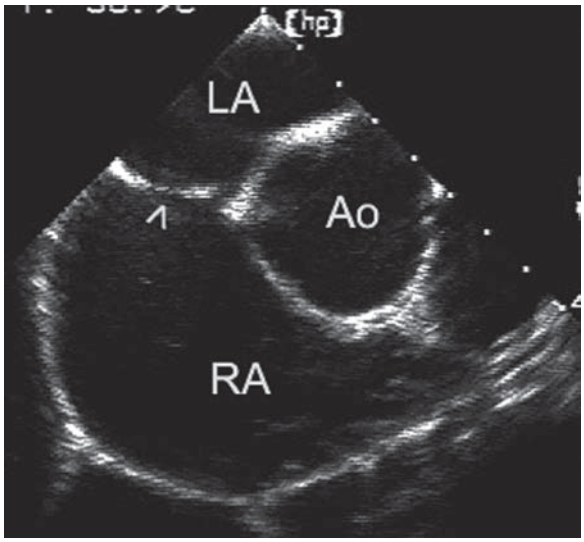

Fig. 28.11 PFO on TOE. Transesophageal echo picture of the typical "flap valve" appearance of a patent foramen ovale toward the aortic root. *Ao* aorta; *LA* left atrium; *RA* right atrium

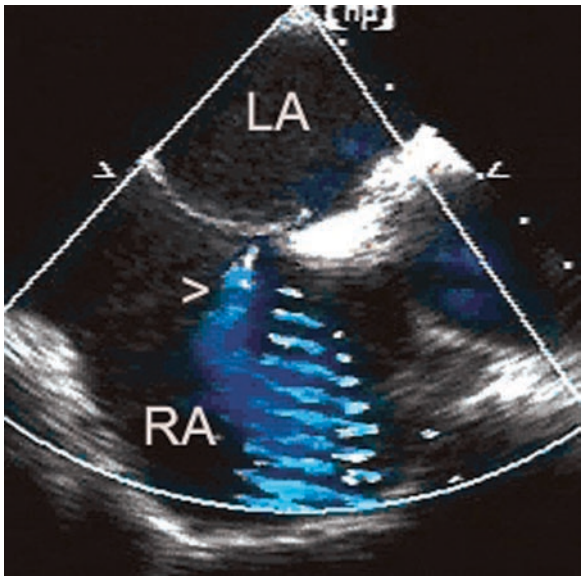

Fig. 28.12 PFO color flow on TOE. Transesophageal echo image demonstrating color flow from left atrium to right atrium across the PFO seen in Fig. 28.10. Shunting from right to left atrium is best seen when the right atrial pressure is increased, for example during the Valsalva maneuver. *LA* left atrium; *RA* right atrium

Partial Atrioventricular Septal Defect (Ostium Primum ASD)

Ostium primum atrial septal defects are part of the spectrum of atrioventricular septal defect, where there is a defect in the atrial septum immediately adjacent to the atrioventricular junction, the normal offset of the atrioventricular valves is absent and there are shared components (bridging leaflets) of the two atrioventricular valves (Fig. 28.14). Most primum defects are diagnosed in childhood because they are often associated with large shunts, but occasionally smaller defects may present de novo in adulthood. Similar echocardiographic criteria of right ventricular volume overload are used as for secundum defects to establish the need for treatment.

Some degree of mitral and/or tricuspid incompetence is common both pre- and postoperatively, so it is important to assess atrioventricular valve function in addition to the secondary effects of the atrial shunt. After repair the majority of patients will be left with some degree of mitral regurgitation (usually mild), which requires serial assessment in the standard manner.

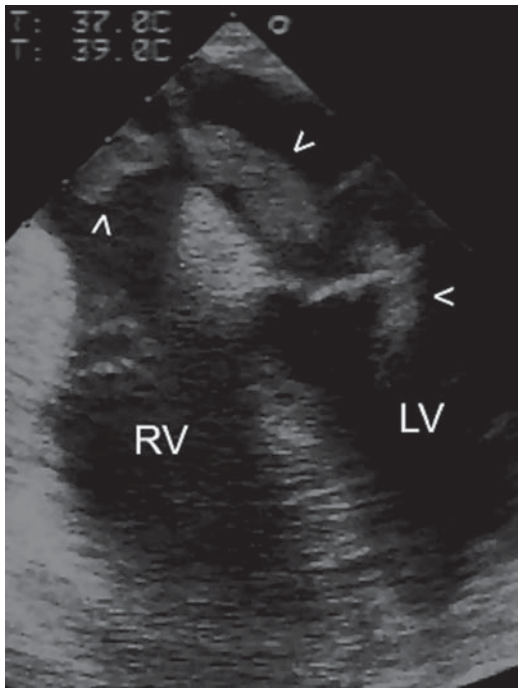

Fig. 28.13 PFO thrombus. Four-chamber transesophageal view showing a large thrombus lodged across a patent foramen ovale. Thrombus can be seen prolapsing through both mitral and tricuspid valves. *LV* left ventricle; *RV* right ventricle

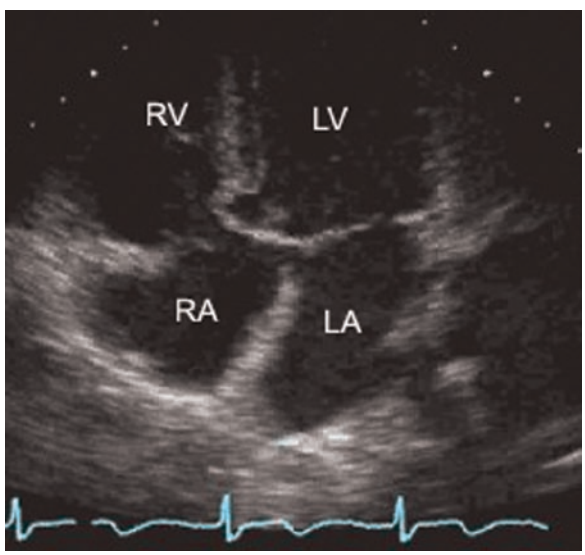

Fig. 28.14 Primum ASD. Apical four-chamber view demonstrating a small ostium primum defect. Also note the loss of normal offsetting of the mitral and tricuspid valve. *LA* left atrium; *LV* left ventricle; *RA* right atrium; *RV* right ventricle

Complete Atrioventricular Septal Defect

Adults with unoperated complete atrioventricular septal defect (CAVSD) will have pulmonary vascular disease, rendering the details of their cardiac anatomy largely academic (Fig. 28.15). In the presence of Eisenmenger's syndrome right to left shunting will be seen at ventricular level (Fig. 28.16), the atrial shunt is often bidirectional, and the pulmonary artery will be dilated with high-velocity pulmonary regurgitation (the modified Bernoulli equation can be used to estimate diastolic pulmonary artery pressure).

Adults with repaired complete AVSD require long-term follow-up and so will regularly present for serial echocardiography. As is the case with repaired partial AVSD, most will be left with some degree of tricuspid and mitral regurgitation, and on rare occasions either one or both valves may be rendered mildly stenotic by

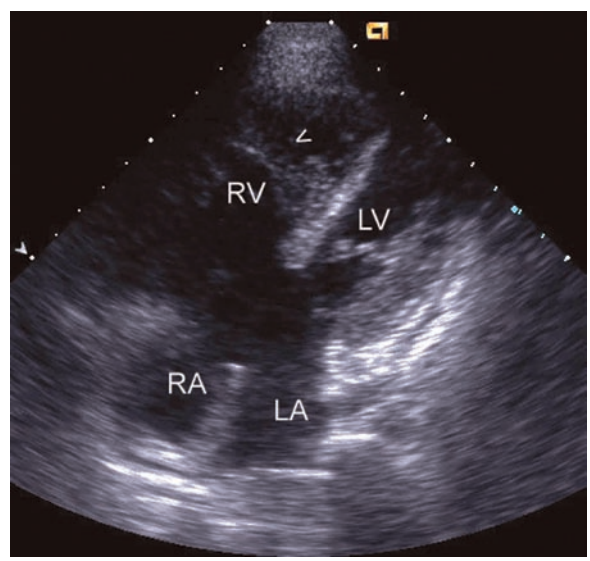

Fig. 28.15 Eisenmenger AVSD. Apical four-chamber view demonstrating a complete atrioventricular septal defect. Note that the right ventricle is dilated and hypertrophied with a prominent moderator band (*arrowed*), in keeping with high pressure in the pulmonary circulation. *LA* left atrium; *LV* left ventricle; *RA* right atrium; *RV* right ventricle

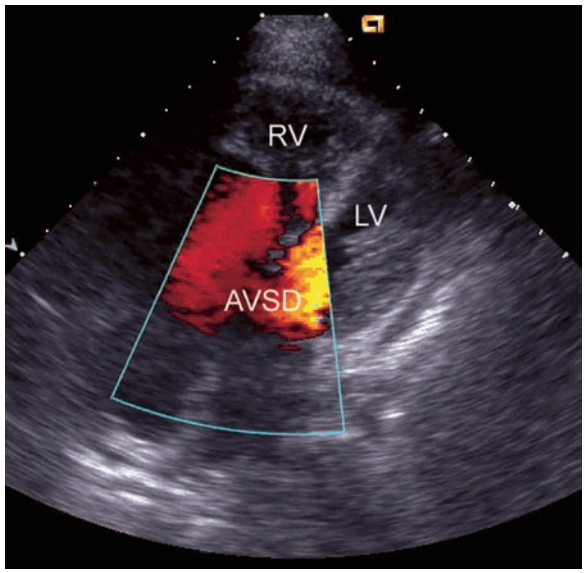

Fig. 28.16 Eisenmenger AVSD color flow. Color-flow imaging of the patient seen in fig above. Low-velocity flow is seen at the site of the defect indicating equalization of pressures in the two ventricles. *AVSD* atrioventricular septal defect; *LV* left ventricle; *RV* right ventricle

the repair. There may be residual shunts at ventricular or atrial level, and it is not uncommon to detect a small jet, arising from a small residual ventricular septal defect, directed through the tricuspid valve to the right atrium, coinciding with mild tricuspid regurgitation and giving an appearance of shunting from the left ventricle to the right atrium. This high-velocity jet can lead to misdiagnosis of elevated right ventricular pressure. The left ventricular outflow tract is always narrower than normal in atrioventricular septal defects, both before and after repair. This is rarely important, but discrete subaortic stenosis may occasionally develop after repair and may be progressive. Its severity should be assessed regularly in the same manner as acquired ventricular outflow obstruction.

Atrioventricular Valves

Mitral Valve

Congenital mitral stenosis is rare at any age. It may be due to obstruction above the valve annulus (a supravalvar ring), due to commissural fusion, due to subvalvar obstruction, or to a combination of any of these. Supravalvar stenosis may be very difficult to diagnose, easily being mistaken for valvar stenosis, because the obstructing membrane may be very closely applied to the valve leaflets; differentiation between the two is of great importance as the former is usually amenable to conservative surgery, while the latter usually requires valve replacement. Color Doppler is sometimes helpful, with aliasing and turbulence originating at the level of the annulus rather than at the leaflets tips. Subvalvar obstruction is usually part of the spectrum of "parachute" mitral valve when there is a single papillary muscle to which all the chordae tendinae attach. The chordae are also often fused to one another to some extent. If there is any doubt whatever relating to the level of obstruction transesophageal echocardiography is essential.

Congenital mitral regurgitation is most common due to leaflet prolapse. It may also occur with a cleft anterior mitral leaflet or more rarely in the context of double orifice mitral valve. Severity of regurgitation is assessed in the usual manner.

Tricuspid Valve

Tricuspid Regurgitation

Ebstein's anomaly of the tricuspid valve frequently presents for the first time in adult life when the development of atrial arrhythmias, limited exercise capacity, or cyanosis brings the patient to the attention of their physician. The septal attachment of the tricuspid valve is displaced a variable distance toward the apex of the right ventricle, along with a variable degree of tethering of the septal leaflet to the septum (Fig. 28.17). The abnormal position of the valve leads it to be incompetent. The tricuspid regurgitation is often severe, but at low velocity as the right ventricular pressure is normal unless there is associated pulmonary stenosis (Fig. 28.18). The right atrium is large, consisting of the "true" right atrium and the atrialized portion of the right ventricle. There is usually an associated interatrial connection, either a patent foramen ovale or a secundum atrial septal defect, with right to left shunting because of raised right atrial pressure. This is best detected by color-flow imaging or injection of agitated saline into a peripheral vein. Tricuspid regurgitation is the predominant hemodynamic abnormality in these patients, although occasionally the valve may also be

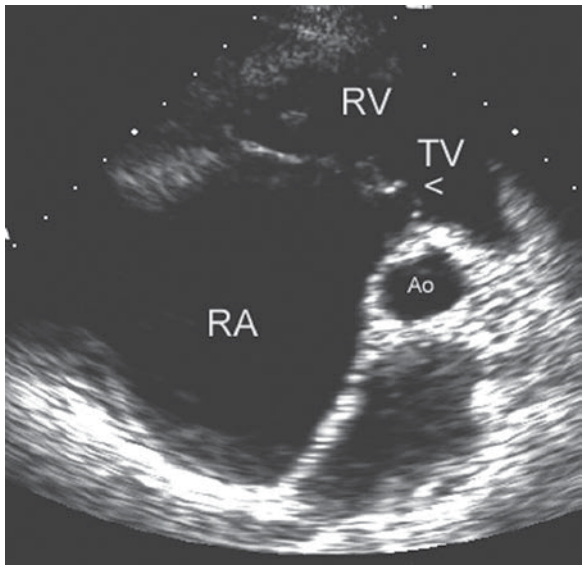

Fig. 28.17 Ebstein's anomaly in short axis. Short-axis view demonstrating marked apical displacement of the attachment of the septal leaflet of the tricuspid valve. *Ao* aorta; *RA* right atrium; *RV* right ventricle; *TV* tricuspid valve

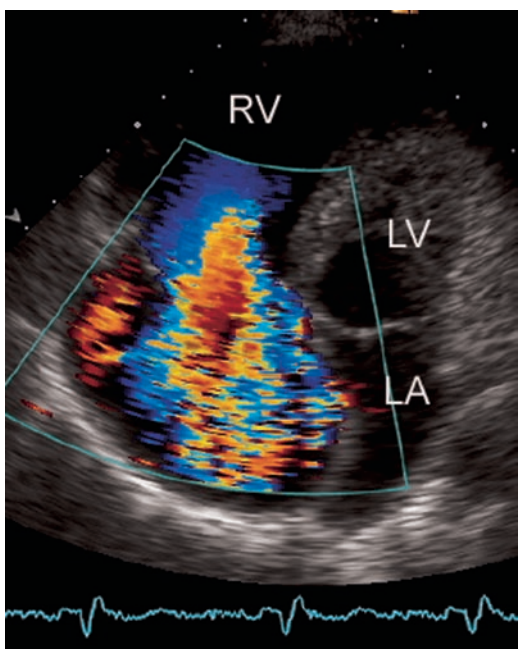

Fig. 28.18 Ebstein's anomaly, apical four-chamber color flow. Apical four-chamber color-flow view of Ebstein's anomaly. There is a broad jet of tricuspid regurgitation. It can be seen originating from the apically displaced tricuspid valve. *LA* left atrium; *LV* left ventricle; *RV* right ventricle

stenotic. Congenital tricuspid regurgitation may sometimes be due to leaflet dysplasia without displacement of the leaflet attachments.

Atrioventricular Connections

Discordant Atrioventricular Connections

Discordant atrioventricular connections (the left atrium connecting to the right ventricle and/or the right atrium connecting to the left ventricle) are most commonly seen in the context of "congenitally corrected transposition" (also known as double discordance) when there are also discordant ventriculoarterial connections (see later). Discordant atrioventricular connections are usually part of very complex disease often with numerous other abnormalities. The connections may almost always be established by using the criteria set out in the section on sequential analysis.

Tricuspid Atresia, Mitral Atresia, Double Inlet Left Ventricle

When an atrioventricular valve is atretic the respective ventricle is almost invariably hypoplastic, and when both atrioventricular valves are committed to the left ventricle the right ventricle is hypoplastic, such that there is effectively only one ventricle. The terms "univentricular heart" and "single ventricle," used in the past to describe these anomalies, have largely disappeared; it is very rare for only one ventricle to be present and the echocardiogram will almost always identify a second, rudimentary ventricle. The relevance of this group of unrepairable anomalies to the adult echocardiographer is that they are generally treated in a similar manner ("single-pump" surgery) and pose similar problems in their long-term echocardiographic follow-up. It is common with these anomalies to have additional abnormalities such as discordant ventriculoarterial connection, ventricular outflow obstruction, or coarctation which should all be borne in mind by the echocardiographer during long-term follow-up. Other complex anomalies may fall into the category of single-pump palliative surgery such as unbalanced

atrioventricular septal defect (one ventricle and/or AV valve being hypoplastic) or complex transposition of the great arteries unsuitable for "two-pump" repair.

Palliated "Single-Pump" Disease

Pulmonary Artery Banding

Surgical creation of pulmonary trunk stenosis (banding) is used to palliate young patients with complex disease and pulmonary hypertension related to large left to right shunts at ventricular level. Some patients reach adult life still banded (if they are not suitable for more definitive palliative surgery). The modified Bernoulli equation applied to the peak velocity across the band will give a good estimate of distal pressure just as it does in naturally occurring pulmonary stenosis.

Shunts and the Fontan Circulation

Patients with unrepairable disease associated with low pulmonary blood flow are palliated by surgery to increase pulmonary blood flow, in the very young usually with an aortopulmonary shunt. The most commonly used shunt is between the subclavian artery and the ipsilateral pulmonary artery (the Blalock shunt); the Waterston shunt is a direct side-to-side anastomosis between the ascending aorta and the right pulmonary artery, the Potts shunt between the descending aorta and the left pulmonary artery. Central shunts are fashioned using a short conduit between the ascending aorta and the pulmonary trunk. The best echo approach to all these shunts is from the suprasternal notch or supraclavicular window, but in cases of difficulty transesophageal echo can be helpful. Flow through the shunt should be continuous and at high velocity, much like the flow pattern through a naturally occurring restrictive arterial duct. The peak velocity will allow a rough estimate of pressure drop across the shunt.

In older children and adolescents pulmonary blood flow is increased by fashioning either a cavopulmonary shunt (connecting the superior caval vein directly, end to side, to the right pulmonary artery) or by redirecting both superior and inferior caval return to the pulmonary arteries. The latter is often referred to as the Fontan circulation, although there are a number of different ways of achieving it. The classical Fontan operation involves connecting the right atrium to the pulmonary arteries using the atrial appendage (the echocardiographic hallmark being marked right atrial dilatation) (Fig. 28.19). Newer techniques designed to reduce right atrial dilatation (and arrhythmias) involve a conduit or tunnel between the inferior caval vein (either inside or outside the right atrium) and the pulmonary artery. All these venous connections are very difficult to image clearly with precordial echo, and transesophageal echo may be required to establish their anatomy and to exclude thrombus in the venous pathways (a major complication of this type of surgery). When serially following these patients the echocardiographer should also look for residual interatrial shunts and obstruction at anastomotic sites; it may also be useful to image the hepatic veins, which are always dilated to some extent, particularly in the presence of obstruction in the systemic venous pathway. A rare complication of the Fontan circulation, if hepatic venous effluent has not also been redirected to

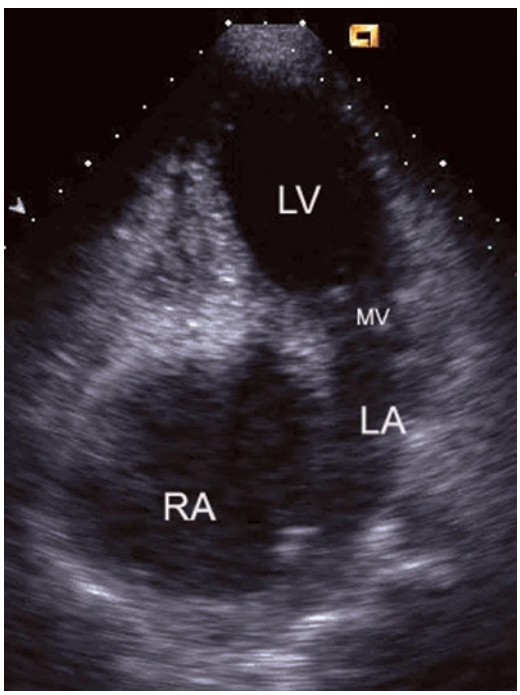

Fig. 28.19 Fontan for tricuspid atresia. Transthoracic image from the standard apical four-chamber position. The right atrium incorporating the Fontan circuit can be seen to be dilated. There is tricuspid atresia and a rudimentary right ventricle only. *LA* left atrium; *LV* left ventricle; *MV* mitral valve; *RA* right atrium

the pulmonary arteries, is the development of multiple pulmonary arteriovenous fistulae (these also occur after the classical Glenn shunt – end-to-end anastomosis of the superior caval vein with the right pulmonary artery). These fistulae cannot be directly seen on echocardiography, but intravenous injection of contrast will demonstrate very rapid transit of bubbles to the left atrium.

Ventricles

Ventricular Septal Defect

Ventricular Septal defects are usually detected in childhood, but the occasional adult will present de novo. Most ventricular septal defects diagnosed in adulthood will be small and hemodynamically unimportant (Fig. 28.20). Hemodynamics are assessed using the same methods as in children (outlined in previous chapters). Most ventricular septal defects can be imaged using transthoracic echocardiography. Transesophageal echocardiography is only required to assess fine detail when complications have arisen such as aortic regurgitation due to prolapse of the aortic valve cusp into the defect, development of subaortic stenosis or suspected endocarditis. Ventricular septal defects which have closed spontaneously during childhood may still be in evidence; adherence of tricuspid valve tissue to the defect may close it completely but leave an appearance of a ventricular septal "aneurysm" (Fig. 28.21). Occasionally an adult may still have an important left to right shunt through a modest sized VSD without having elevated pulmonary artery pressure, causing chronic left ventricular volume loading. Progressive left ventricular dilatation may occur, necessitating closure of the defect.

If a large ventricular septal defect is not closed in childhood, the excess pulmonary blood flow may lead to pulmonary vascular disease and eventually to full-blown Eisenmenger's syndrome, with high pulmonary artery pressures and reversal of the shunt direction at the level of the VSD (Figs. 28.22 and 28.23).

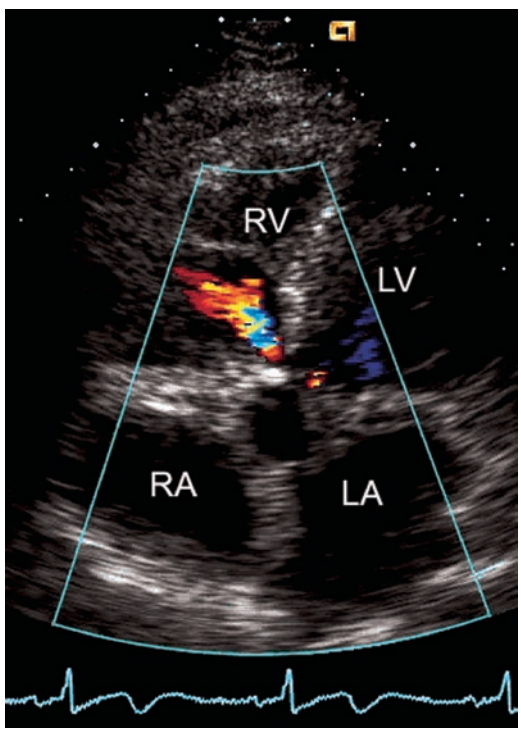

Fig. 28.20 Restrictive VSD color flow. Apical four-chamber view demonstrating a narrow high-velocity jet of flow across a restrictive ventricular septal defect from left ventricle to right ventricle. Both ventricles are normal size. *LA* left atrium; *LV* left ventricle; *RA* right atrium; *RV* right ventricle

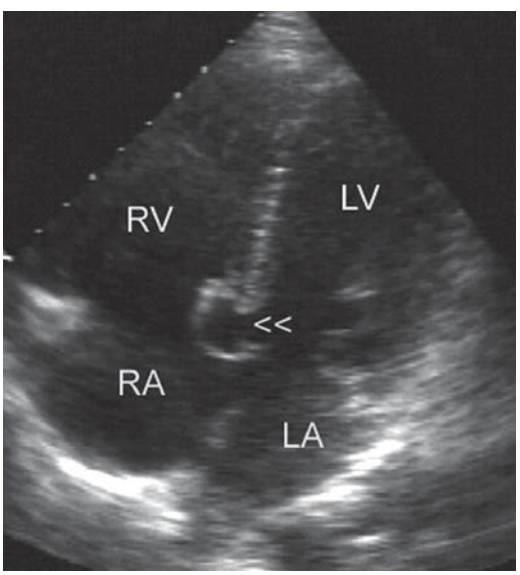

Fig. 28.21 VSD septal aneurysm. This patient originally had a CAVSD. Tissue from the tricuspid valve has formed an aneurysm of the ventricular septum (*arrowed*), closing the ventricular septal component. There is a residual primum ASD. *LA* left atrium; *LV* left ventricle; *RA* right atrium; *RV* right ventricle

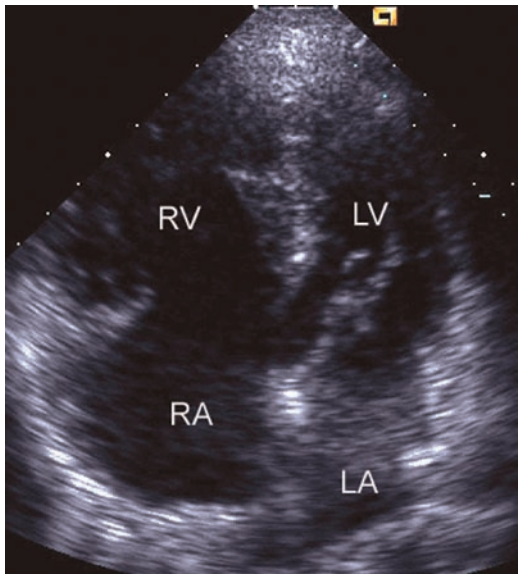

Fig. 28.22 Eisenmenger VSD. Apical four-chamber view demonstrating a large ventricular septal defect. There is associated dilatation and hypertrophy of the right ventricle indicating high pulmonary artery pressures. *LA* left atrium; *LV* left ventricle; *RA* right atrium; *RV* right ventricle

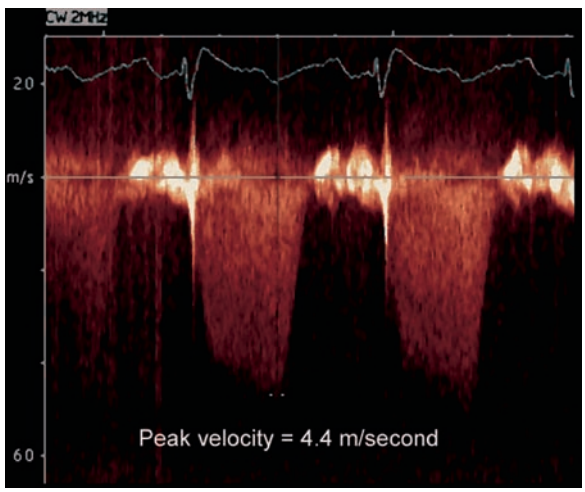

Fig. 28.23 Tricuspid regurgitation in Eisenmenger's syndrome. Continuous-wave Doppler recording through the tricuspid valve in the patient seen in Fig. 28.21. There is high-velocity tricuspid regurgitation; the maximum velocity is over 4 m/s, indicating that the estimated right ventricular systolic pressure is easily in excess of 80 mmHg

Left ventricular Outflow Obstruction

Congenital abnormalities of the aortic valve commonly present for the first time in adulthood, when the valve becomes sufficiently damaged to cause an audible murmur bringing it to the attention of the patient's physician. Congenitally abnormal aortic valves are likely to degenerate prematurely because of abnormal shear stresses in the presence of abnormal cusp morphology. Aortic valve disease is dealt with comprehensively in Chap. 7. However it is important to remember that not all stenosis is valvar – stenosis at supravalvar or subvalvar level may present in adulthood and may coincide with valvar stenosis or regurgitation.

Transesophageal echo is an important adjunct in patients with poor echo windows and is mandatory if there is any doubt as to the exact nature of left ventricular outflow obstruction. In some cases of discrete membranous subaortic stenosis the membrane may be so close to the valve that it may be missed unless the echocardiographer's index of suspicion is high. Misdiagnosis is disastrous as it may lead to valve replacement when a conservative operation might have been possible. Subvalvar stenosis may recur, even after a very satisfactory initial operation. It is often associated with some degree of aortic regurgitation due to leaflet damage caused by systolic turbulence. Subaortic stenosis may occasionally be caused by more diffuse fibromuscular obstruction rather than a membrane; this may sometimes be very difficult to differentiate from hypertrophic cardiomyopathy (Figs. 28.24 and 28.25).

It is worth bearing in mind that coarctation of the aorta is often associated with congenital aortic valve anomalies; a proper evaluation of any young adult with aortic valve disease should include examination of the descending aorta. It is also wise to assess the ascending aortic dimensions; post stenotic dilatation is commonly seen, but progressive ascending aortic dilatation may occur (particularly if the valve is bicuspid) along with a risk of dissection. Pulmonary valve assessment is also important because some patients (particularly young women) will be candidates for a Ross procedure (replacement of the aortic valve with the patient's own pulmonary valve and pulmonary valve replacement with a homograft), rather than traditional aortic valve replacement.

Supravalvar stenosis is often associated with Williams Syndrome; when it is not it may be familial and there may also be multiple peripheral pulmonary artery stenoses. When supravalvar stenosis is progressive it usually requires surgical treatment during childhood, so it is rare to find important obstruction at this level in adults (Figs. 28.26 and 28.27).

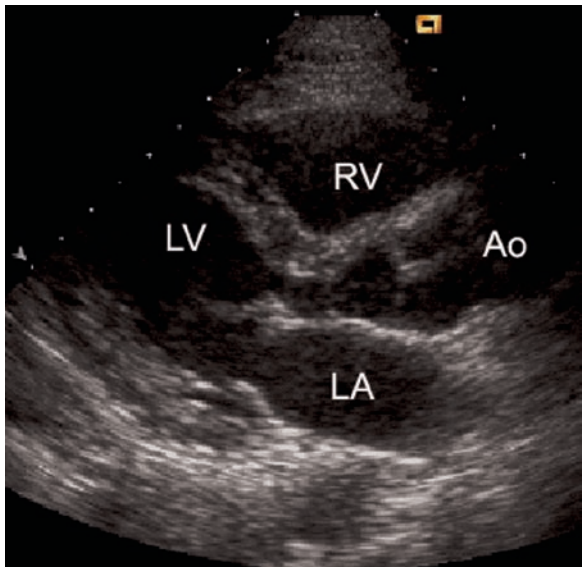

Fig. 28.24 Subaortic stenosis in parasternal long-axis view. Parsternal long-axis view demonstrating an area of narrowing of the left ventricular outflow tract well below the aortic valve itself. *Ao* aorta; *LA* left atrium; *LV* left ventricle; *RV* right ventricle

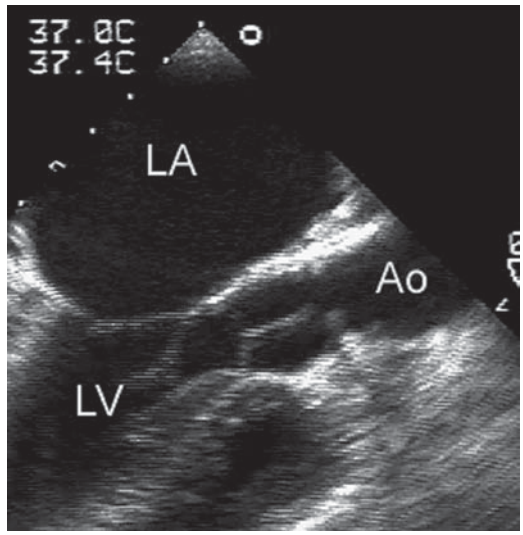

Fig. 28.26 Supravalvar aortic stenosis. Transesophageal image from a patient with severe supravalvar aortic stenosis. The fibrous ridge can be clearly seen well above the mobile aortic valve leaflets. *Ao* aorta; *LA* left atrium; *LV* left ventricle

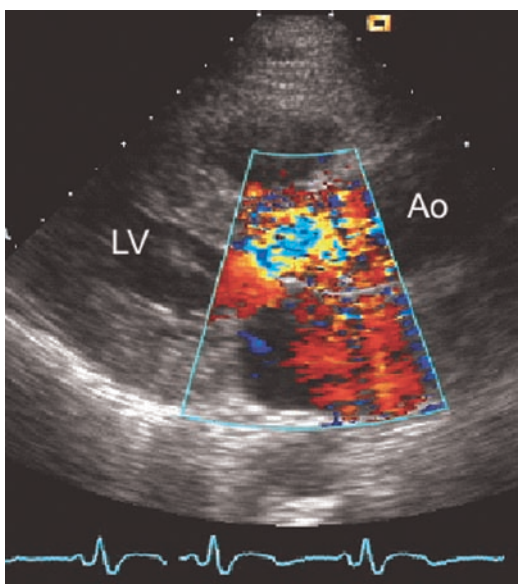

Fig. 28.25 Color-flow image of subaortic stenosis. Color-flow image of the patient seen in Fig. 28.23. Aliasing can be seen to start well below the level of the aortic valve leaflets indicating that the level of obstruction is subvalvar. *Ao* aorta; *LV* left ventricle

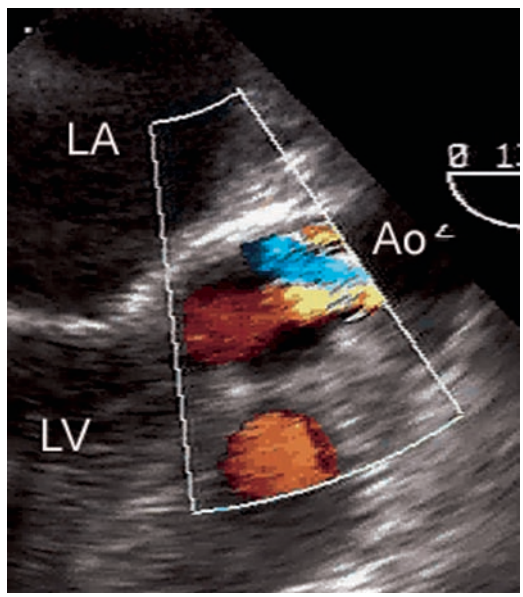

Fig. 28.27 Supravalvar aortic stenosis color flow. Color-flow image from the patient seen in Fig. 28.27. The aliasing can be clearly seen to originate at the level of the fibrous ridge and not at the level of the valve leaflets. *Ao* aorta; *LA* left atrium; *LV* left ventricle

Right Ventricular Outflow Obstruction

If valvar pulmonary stenosis has remained mild without treatment or after treatment during childhood it rarely becomes severe during adult life. Cross-sectional imaging of the valve itself is often unhelpful; even with severe stenosis, the valve leaflets may not appear

particularly abnormal (although calcification often occurs in middle age), but color Doppler will show turbulence in the proximal pulmonary trunk. The parasternal short-axis view is standard, although the subcostal approach is particularly useful in patients with poor precordial windows (Figs. 28.28 and 28.29).

Just as for left ventricular outflow obstruction, obstruction is not always at valve level. When it is subvalvar it is usually dynamic, due to hypertrophied infundibular muscle. In such cases there is often a typical dynamic pressure drop across the outflow tract, with a gradual increase in flow velocity as systole progresses (as seen in hypertrophic cardiomyopathy in the left side of the heart). Supravalvar stenosis is rare in isolation, but when there are multiple stenoses in the branches of the pulmonary arteries the heart itself usually is structurally normal. Multiple pulmonary artery stenoses may occur in association with supravalvar aortic stenosis (often familial, or in Williams syndrome).

The severity of obstruction is assessed in the usual way by continuous-wave Doppler (best with a dedicated transducer). The modified Bernoulli equation gives a good estimate of the pressure gradient in cases of discrete obstruction but becomes less reliable when there are multiple sites of obstruction or long segment stenosis. It is important to ensure that increased pulmonary flow velocity is indeed due to stenosis and not merely the consequence of increased pulmonary blood flow due to a left to right shunt (for example an atrial septal defect). This is particularly important in cases where the maximum forward flow velocity is only modestly increased. The peak velocity of tricuspid regurgitation will give an accurate estimate of right ventricular pressure, and simple imaging of the right ventricle is useful as a semiquantitative measure of the degree of right ventricular hypertrophy.

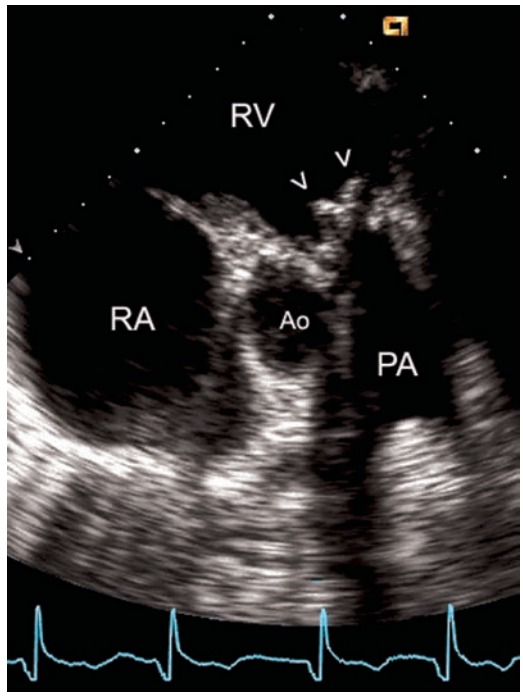

Fig. 28.28 Pulmonary stenosis in short axis. Parasternal short-axis view showing calcific degeneration of a congenitally abnormal pulmonary valve (*arrowed*). Note the acoustic shadows cast by the calcification in the valve. *Ao* aorta; *PA* pulmonary artery; *RA* right atrium; *RV* right ventricle

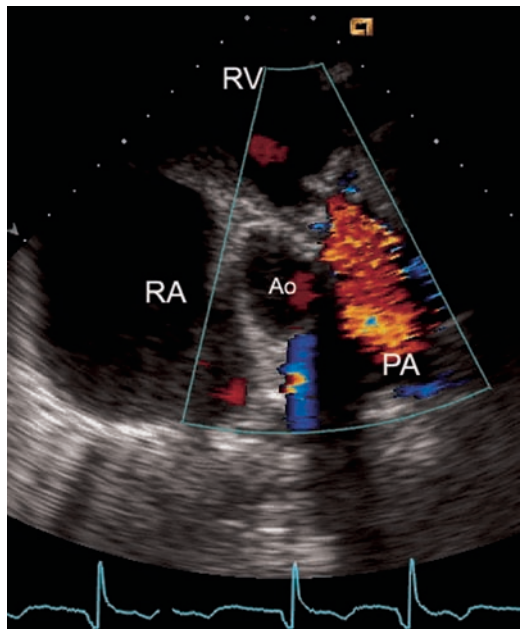

Fig. 28.29 Pulmonary stenosis color flow. Parasternal short-axis view showing high-velocity color flow through the stenosed pulmonary valve seen in Fig. 28.28. *Ao* aorta; *PA* pulmonary artery; *RA* right atrium; *RV* right ventricle

Tetralogy of Fallot and Pulmonary Atresia with Ventricular Septal Defect

Survival of a patient with unoperated tetralogy of Fallot well into adulthood is not unknown, but almost all adults under follow-up will have had surgical repair. The term "repair" is a misnomer as the heart is never normal postoperatively. Many adults with repaired tetralogy or with pulmonary atresia with ventricular septal defect (an extreme form of tetralogy) run into problems in later life, particularly related to chronic

pulmonary regurgitation, sometimes with residual stenosis or hypoplasia of the pulmonary arteries. It is rare for pulmonary stenosis to recur after a satisfactory repair, but where it has been necessary to implant a conduit between the right ventricle and pulmonary trunk late conduit stenosis and calcification is common. Conduits are, understandably, much more commonly employed in repair of pulmonary atresia with ventricular septal defect. Conduit obstruction is assessed in the usual way using continuous-wave Doppler; but assessment of severity of stenoses in the branch pulmonary arteries is less reliable due to difficulties aligning with flow. The tricuspid regurgitant jet will give the best overall assessment of the severity of outflow obstruction (Figs. 28.30 and 28.31).

Pulmonary regurgitation, if severe, will cause some increase in flow velocity not necessarily wholly attributable to true pulmonary stenosis (Fig. 28.32). Pulmonary

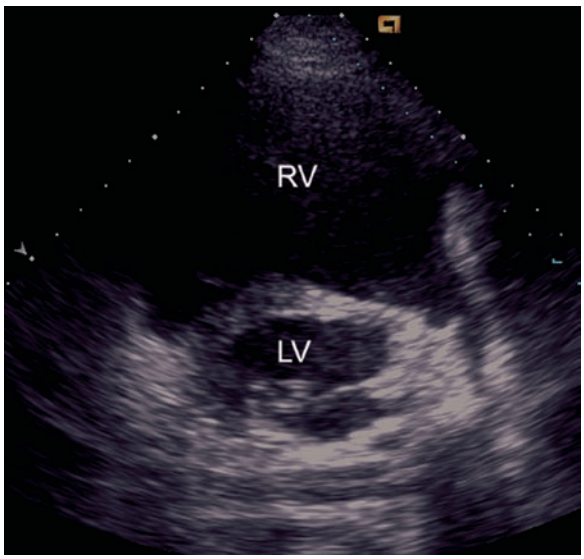

Fig. 28.30 Tetralogy dilated RV. Parasternal short-axis view from a patient with previously repaired tetralogy of Fallot, demonstrating marked dilatation of the right ventricle, compared to the left ventricle. *LV* left ventricle; *RV* right ventricle

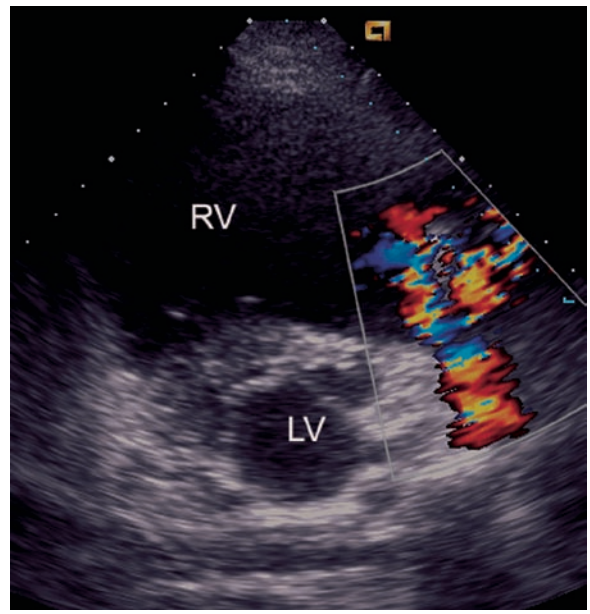

Fig. 28.31 Tetralogy dilated RV color. Color-flow imaging of the patient seen in Fig. 28.30, showing significant pulmonary regurgitation into the dilated RV. *LV* left ventricle; *RV* right ventricle

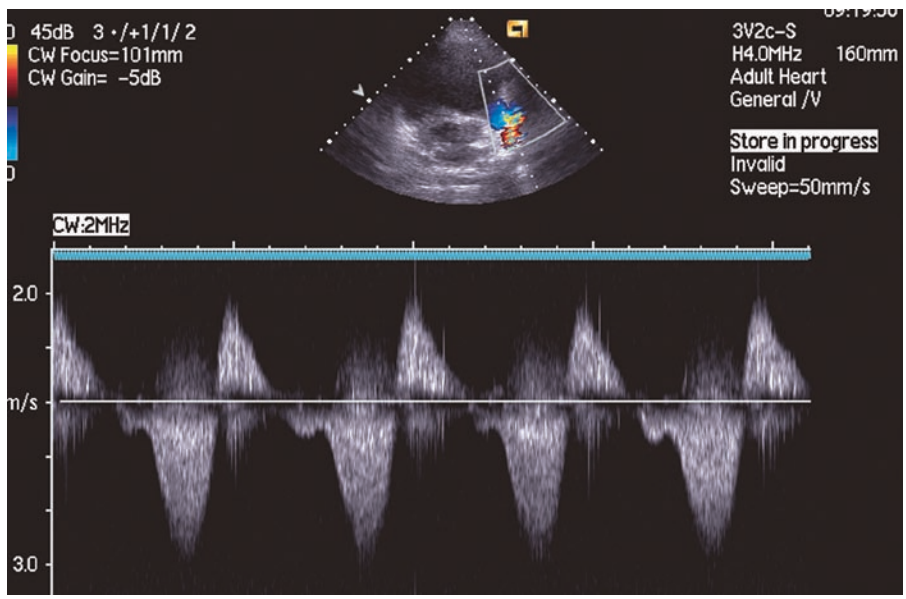

Fig. 28.32 Pulmonary stenosis/pulmonary regurgitation. Continuous-wave Doppler through the pulmonary valve of the patient seen in Figs. 28.30 and 28.31. Note the increased forward flow velocity of almost 3 m/s, and the steep deceleration slope of reverse flow in diastole indicating severe pulmonary regurgitation

regurgitation can be difficult to quantify accurately, but in severe pulmonary regurgitation the regurgitant jet will show rapid deceleration because of early equalization of the pulmonary artery and right ventricular diastolic pressures. Pulmonary regurgitation, even when severe, is often remarkably well tolerated for many years, but eventually may lead to progressive right ventricular dilatation and then to systolic dysfunction with progressive functional tricuspid regurgitation. When there has been extensive right ventricular outflow tract muscle resection, and/or a transannular patch, the right ventricular outflow tract can become aneurysmally dilated.

Residual ventricular septal defect around the margins of the patch used to close the original defect are common and are usually of no hemodynamic consequence. The jets are often in an unusual direction but can be picked up on color-flow imaging in parasternal long-axis, parasternal short-axis, and apical views. Continuous-wave Doppler across the ventricular septal defect demonstrates a high-velocity jet, unless the right ventricular pressure is elevated because of residual pulmonary stenosis.

Aortic Root Enlargement and Aortic Regurgitation

Some degree of aortic root dilatation is usually present both before and after repair of tetralogy (along with secondary aortic regurgitation) which requires serial echocardiographic follow-up. Fortunately it is rare for either to become sufficiently severe to require surgery. The aortic regurgitation is assessed in the usual ways.

Pulmonary Atresia with Multifocal Aortopulmonary Collaterals

The majority of patients with pulmonary atresia with ventricular septal defect are extreme forms of tetralogy, the outflow tract (and sometimes the pulmonary trunk) being atretic rather than stenosed. In a small proportion of cases, however, the pulmonary arteries fail to develop or are severely hypoplastic, and the pulmonary blood supply is derived from major aortopulmonary collateral vessels (MAPCAs). The echo will usually fail to identify any central pulmonary arteries, although some collateral vessels may be visible arising from the thoracic aorta (particularly with color Doppler). These patients may not be amenable to repair and therefore retain the intracardiac features of tetralogy (a large ventricular septal defect with overriding aorta and dilated aortic root) into their adult lives.

Ventriculoarterial Connections

Transposition of the Great Arteries

Most patients born within the last two decades with transposition of the great arteries have undergone the arterial switch operation (Jatene procedure). Adult survivors of the arterial switch operation are beginning to appear, but the majority of current adult survivors are of an earlier generation treated with an “atrial switch” procedure, either Mustard’s or Senning’s operations. The Mustard operation involves removal of the atrial septum and redirection of systemic venous inflow from the vena cava to the mitral valve orifice by a surgically created baffle formed from pericardium or synthetic material. Senning’s procedure produces a similar effect without the use of extraneous tissue, using the tissue of the atrial septum and the atrial appendage to redirect systemic venous return to the mitral valve and pulmonary venous return to the tricuspid valve. The right ventricle therefore remains at systemic pressure, while the left ventricle remains at low pressure (unless there is coincident left ventricular outflow obstruction). This produces a typical appearance of a “squashed,” left ventricle with a dilated and hypertrophied right ventricle. The posterior displacement of the ventricular septum by this reversal of the normal ventricular pressure relationship sometimes produces subpulmonary obstruction, detectable by turbulence in the left ventricular outflow tract. Late complications of inflow redirection include systemic (right) ventricular dysfunction, systemic atrioventricular (tricuspid) valve regurgitation, residual shunts through the intra atrial baffles, stenoses of the venous pathways within the heart and conducting system abnormalities (Figs. 28.33–28.35).

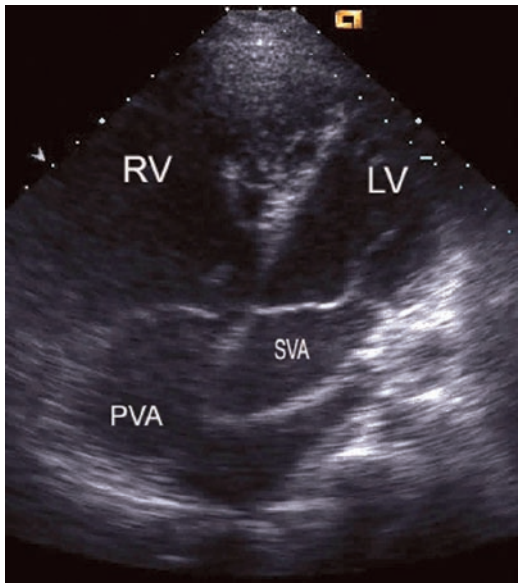

Fig. 28.33 Mustard operation for TGA. Apical four-chamber view delineating the systemic venous atrium in continuity with the mitral valve and left ventricle, and the systemic venous atrium in continuity with the tricuspid valve and right ventricle. *LV* left ventricle; *RV* right ventricle; *PVA* pulmonary venous atrium; *SVA* systemic venous atrium

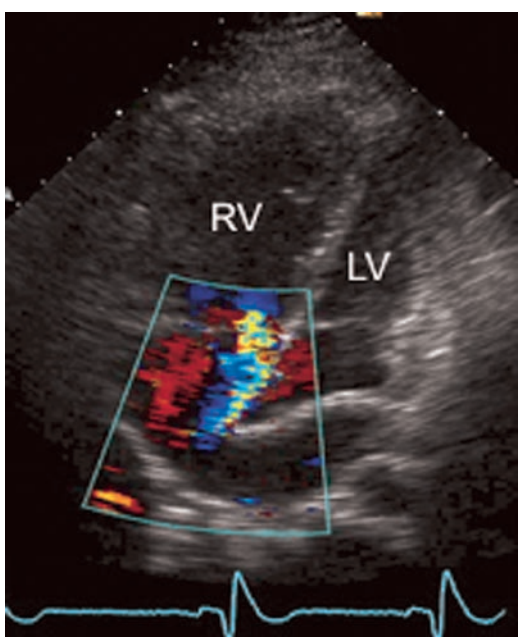

Fig. 28.34 Mustard operation for TGA, color flow. Apical four-chamber view showing mild regurgitation through the tricuspid (systemic AV) valve. *LV* left ventricle; *RV* right ventricle

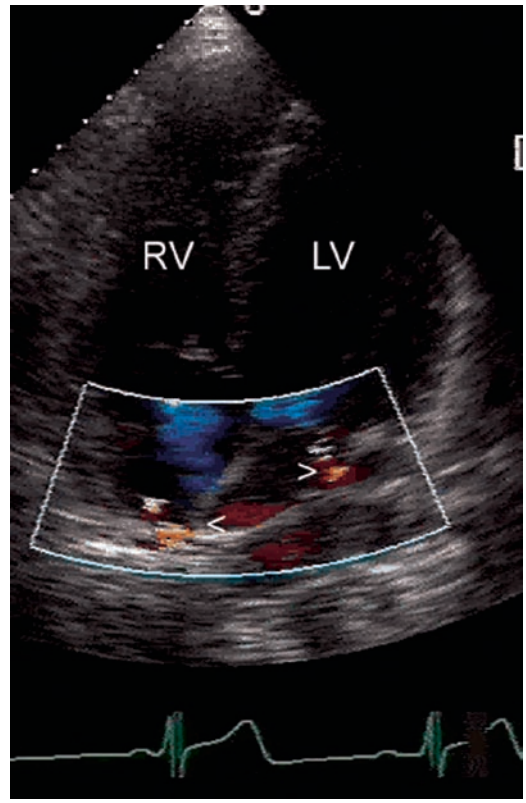

Fig. 28.35 Mustard operation for TGA showing baffle leaks. Apical four-chamber view demonstrating baffle leaks at two positions within the venous baffles (*arrowed*). *LV* left ventricle; *RV* right ventricle

One of the tasks of the echocardiographer in any situation is to assess ventricular function. While there are various methods of assessing left ventricular function, reproducible measurement of right ventricle function is very difficult and most assessments tend to be made by "eyeballing" on long-axis and four-chamber views. Serial measurements of the right ventricular diameter at the level of the tricuspid valve may show serial increases, but this is a very crude surrogate for function; there are no validated standard methods to estimate ejection fraction or fractional shortening. Recently there has been research interest in assessment of long-axis right ventricular function, but these methods have not come into everyday use. The severity of tricuspid regurgitation is assessed in the same manner as mitral regurgitation in the normally connected heart.

Small residual shunts through the intra-atrial baffles can be seen in some patients. The direction of the shunt will depend upon the relative patency of the intracar-

diac systemic and pulmonary venous channels. When systemic to pulmonary venous shunts are detected it should prompt the echocardiographer to look for systemic venous pathway obstruction. Baffles formed with synthetic materials (rather than autologous tissue) are particularly prone to develop calcification and narrowing. The best images of the venous channels are usually obtained from the apical four-chamber and subcostal views. Patency of the venous pathways is assessed by examining their caliber, and color-flow imaging will identify areas of turbulence. These areas can then be interrogated using pulsed-wave or continuous-wave Doppler which will show increases in peak flow velocity at the site of stenosis, although severe stenosis may be associated with only modest increases in velocity (analogous to the small changes in peak mitral flow velocity in mitral stenosis). It is useful to be specific about the site of stenoses or residual shunts as both may be amenable to transcatheter treatment (when transesophageal guidance of intervention can be invaluable).

In contrast to the Mustard or Senning operations, late complications after the arterial switch operation are few. Stenosis at the pulmonary artery anastomosis or at the pulmonary artery bifurcation was relatively common in early surgical series, but aortic anastomotic stenosis is exceedingly rare. The pulmonary anastomosis may be very difficult to image (due to the pulmonary artery being positioned more anteriorly than normal). The suprasternal approach may be useful for imaging and Doppler of the proximal right and left pulmonary arteries, with the tricuspid regurgitant jet being the best indicator of overall increase in right ventricular pressure. Dilatation of the aortic root and aortic regurgitation may also occur but fortunately it is rare for either to become important. The theoretical risk of coronary artery anastomotic stenosis has not proved important in practice (yet!). Transesophageal echo will allow inspection of the proximal coronary arteries as well as their sites of anastomosis to the aorta.

Congenitally Corrected Transposition of the Great Arteries

In congenitally corrected transposition there is both atrioventricular and ventriculoarterial discordance. Thus systemic venous return enters the right atrium through the superior and inferior caval veins, passes through the mitral valve to the left ventricle, and then through the pulmonary valve to the main pulmonary artery. Pulmonary venous return enters the left atrium, passes to the right ventricle via the tricuspid valve, and then through the aortic valve to the aorta. Because blood flow is physiologically normal this condition can lie undiagnosed until adult life when the patient may present with heart block, an incidental finding of dextrocardia or, rarely, right ventricular failure. Pulmonary and subpulmonary stenosis, ventricular septal defect, and dextrocardia are common related features.

The diagnosis is often first considered if there is difficulty obtaining a standard parasternal long-axis view. This is because the interventricular septum lies in a more anteroposterior plane than normal, resulting in the ventricles appearing to lie side by side. Sequential analysis will establish the ventricular morphology, the right ventricle being identified by its trabeculation, its moderator band, by the septal attachment of the tricuspid chordae, and by the more apical attachment of the septal leaflet of the tricuspid valve. The aorta arises from the morphologic right ventricle and lies anterior and to the left of the pulmonary artery which arises from the morphologic left ventricle, the two valves lie in the same plane and orientation in short axis, and the proximal great arteries run with parallel courses (Fig. 28.36).

Dysfunction of the systemic (morphologic right) ventricle and regurgitation of the systemic AV (tricuspid) valve are common in these patients in adult life. As for patients who have undergone the Mustard or Senning operations, standard methods of echo assessment of left ventricular function cannot be applied to the morphologic right ventricle. The degree of regurgitation of the systemic atrioventricular valve is assessed in the usual ways using color-flow imaging and continuous-wave Doppler.

The Great Arteries

Patent Ductus Arteriosus

The occasional adult will have a patent ductus arteriosus diagnosed for the first time either when a typical machinery murmur is noted, or as an incidental finding on echocardiography. The parasternal short-

axis view of the pulmonary artery will demonstrate a continuous jet into the distal main pulmonary artery near the junction with the left pulmonary artery, but it is rare to be able to image the duct itself clearly. The jet usually hugs the wall of the pulmonary artery and is directed toward the pulmonary valve (Fig. 28.37). The jet may also be seen in suprasternal views of the aortic arch. If there is a substantial shunt the pulmonary arteries and left-sided chambers may be dilated. Pulmonary artery pressure may be estimated from the peak velocity of the ductal jet (Fig. 28.38). In the presence of pulmonary vascular disease flow

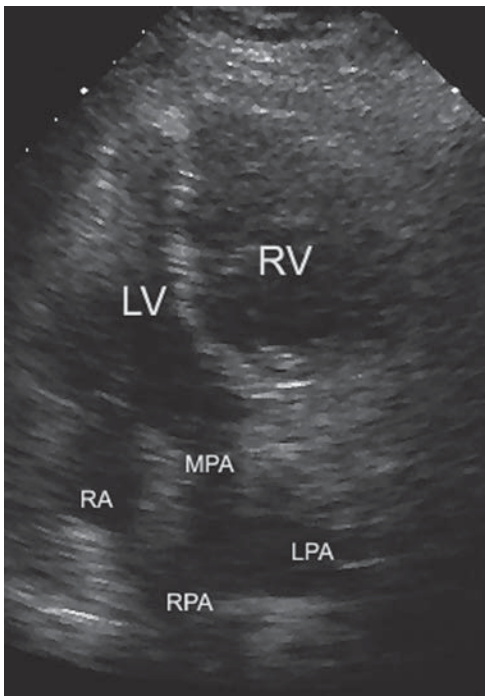

Fig. 28.36 Congenitally corrected transposition of the great vessels. Apical four-chamber view in a patient with congenitally corrected transposition. The main pulmonary artery can be seen arising from the morphologic left ventricle, which itself arises from the right atrium. A moderator band can be seen in the right ventricle. *LV* left ventricle; *RV* right ventricle; *RA* right atrium; *MPA* main pulmonary artery; *LPA* left pulmonary artery; *RPA* right pulmonary artery

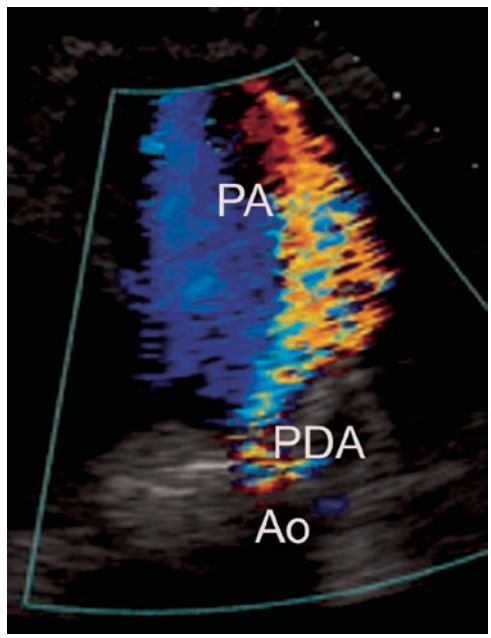

Fig. 28.37 Adult duct. Parasternal short-axis view at the level of the pulmonary artery showing a jet of color flow into the main pulmonary artery. *Ao* aorta; *PA* pulmonary artery; *PDA* patent ductus arteriosus

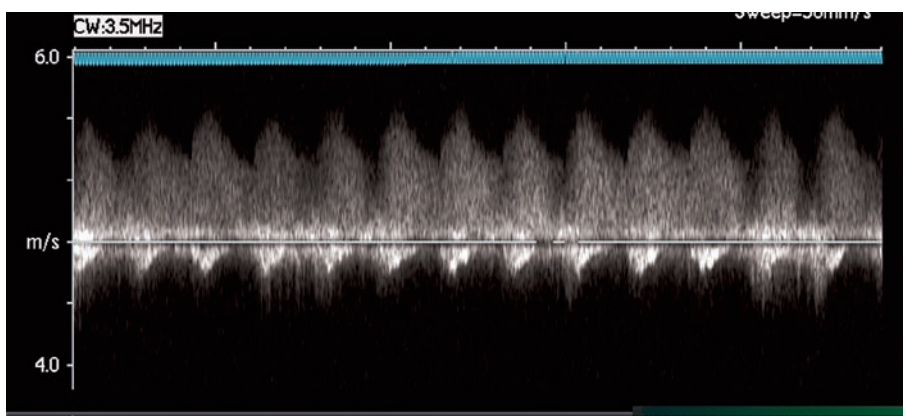

Fig. 28.38 Duct continuous wave. Continuous-wave Doppler showing high-velocity continuous flow from the high-pressure aorta to low-pressure pulmonary artery through the patent ductus arteriosus seen in Fig. 28.36

will often be bidirectional, from pulmonary artery to aorta in systole and from aorta to pulmonary artery in diastole. Sometimes a very small, unsuspected duct will be detected on echocardiography when there is no murmur. These are often referred to as "silent" ducts. The general consensus view is that these do not pose a risk for endocarditis and do not require closure. Ducts in adults do not require surgical treatment; they can invariably be closed at cardiac catheterization, when precordial echocardiography is useful to confirm the occlusion device position and will demonstrate any residual shunt. Transesophageal echo is of little use in the diagnosis or closure of the arterial duct.

Coronary Arteries

Congenital coronary artery anomalies are rare but may present in adults. Children born with anomalous origin of the left coronary artery from the pulmonary artery may go undiagnosed during childhood because of the development of extensive collateral flow from the right coronary arterial system. Collateral flow does not, however, prevent myocardial ischemia in the long term as there is usually a steal phenomenon due to the left coronary artery emptying retrogradely into the pulmonary artery in diastole. Patients may present with functional mitral regurgitation (despite well-preserved global left ventricular function), or with poor left ventricular function. When there are extensive collaterals the proximal right coronary artery is usually visibly dilated on the echocardiogram, and the diagnosis is confirmed by the finding of diastolic flow into the pulmonary trunk from the left main coronary artery (Figs. 28.39 and 28.40).

Congenital coronary artery fistulae are usually detected in childhood (presenting with a continuous murmur) and may become important in adulthood as the fistula enlarges, the shunt increases, and a coronary steal syndrome may develop. The fistulae may arise from any branch of either coronary system and may drain to any intracardiac site (the right atrium most commonly) or even to the pulmonary artery. They may be multiple. On echocardiography the affected vessel is seen to be dilated and color Doppler will usually identify the site of drainage.

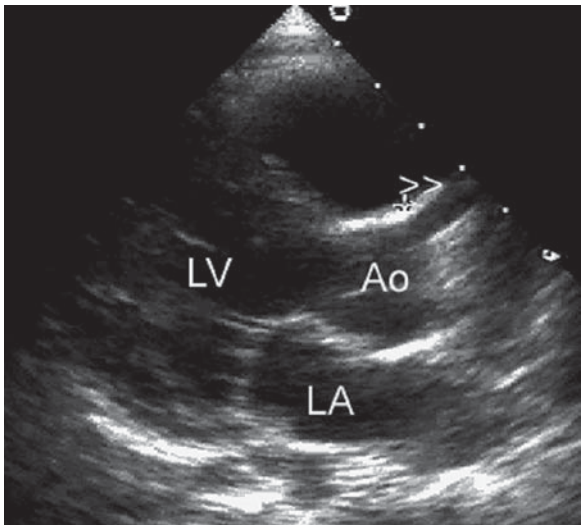

Fig. 28.39 Anomalous LCA parasternal long axis. Parasternal long-axis view showing the marked dilatation of the proximal right coronary artery in a patient with an anomalous left coronary artery arising from the pulmonary artery. *Ao* aorta; *LA* left atrium; *LV* left ventricle

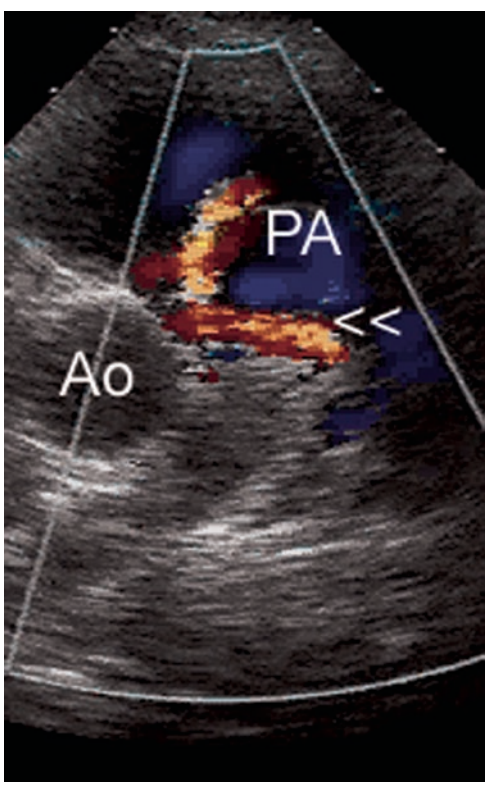

Fig. 28.40 Anomalous LCA color flow in the PA. Short-axis view at the level of the pulmonary artery demonstrating reverse flow in the tortuous left coronary artery where it empties into the pulmonary artery. *Ao* aorta; *PA* pulmonary artery

Coarctation of the Aorta

Coarctation of the aorta may present for the first time in adult life with hypertension, with or without an associated murmur. Echocardiography in hypertensive patients must include suprasternal views of the aortic arch as well as continuous-wave Doppler recording of flow velocity in the descending aorta. Imaging of the aortic arch in adults is often not sufficiently clear to identify the precise anatomy of coarctation, but color Doppler will show turbulence at its site (Figs. 28.41 and 28.42); continuous-wave Doppler will show high-velocity flow with delayed flow deceleration when the obstruction is important (Fig. 28.43a, b). Severity of obstruction is more reliably assessed by the degree of delay in flow deceleration rather than the peak flow velocity alone. Doppler parameters of obstruction may be misleading if there is a well-established collateral circulation. The degree of left ventricular hypertrophy is also a useful indicator of need for treatment. Transesophageal echo is rarely helpful as image quality of the distal aortic arch is usually poor.

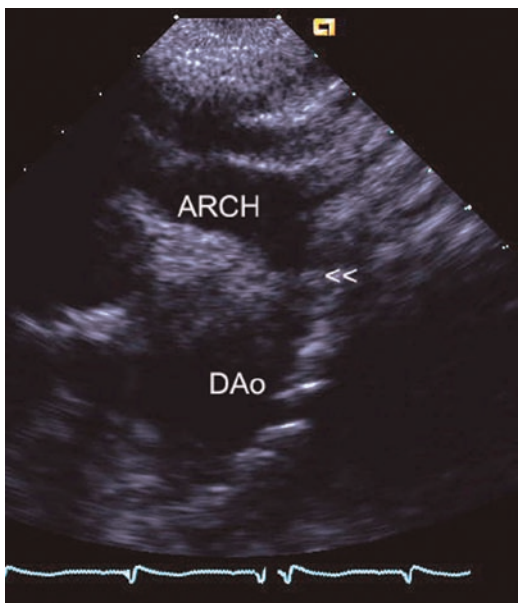

Fig. 28.41 Aortic coarctation. 2-D image of coarctation from the suprasternal notch. The site of coarctation can be seen distal to the origin of the left subclavian artery. ARCH; *DAo* descending aorta

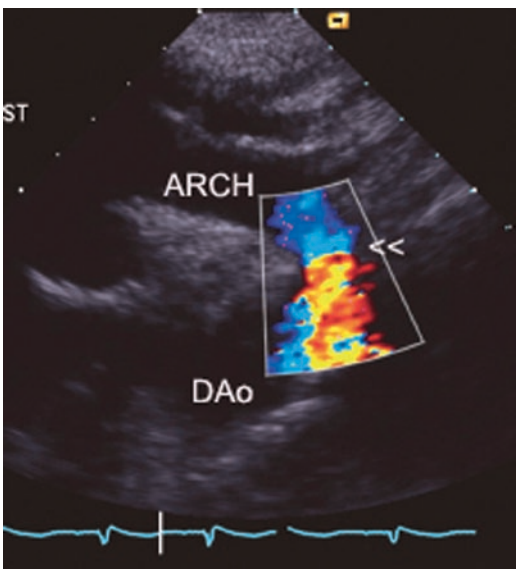

Fig. 28.42 Aortic coarctation color flow. Color-flow imaging of the coarctation seen in Fig. 28.40. Aliasing can be seen arising from the site of the coarctation. ARCH; *DAo* descending aorta

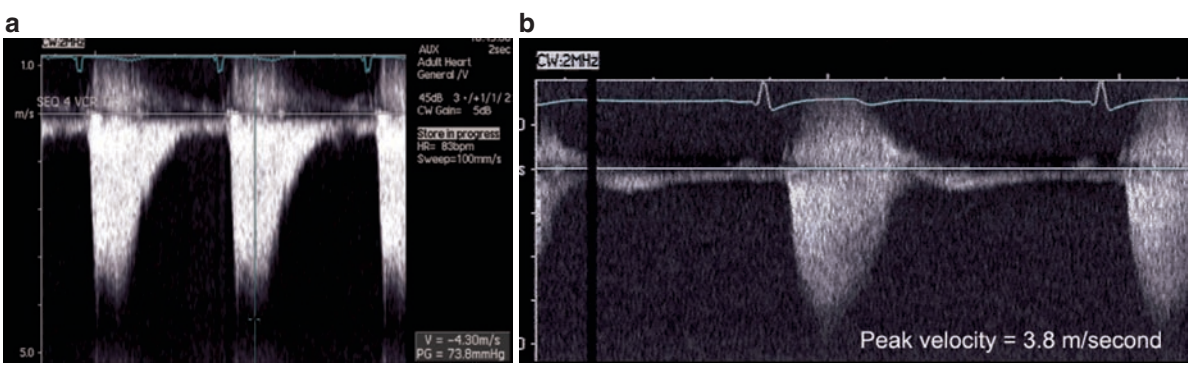

Fig. 28.43(a, b) Continuous-wave Doppler aortic coarctation. Continuous-wave Doppler through the coarctation seen in Fig. 28.40 demonstrates an increase in maximum flow velocity to 4.3 m/s. Note there is continuous flow well into diastole in this patient indicating significant coarctation. Compare this with the CW Doppler in (**b**). Although the maximum flow velocity is increased at 3.8 m/s, there is no diastolic tailing in this patient indicating a relatively mild coarctation

Even after satisfactory repair of coarctation, Doppler will usually reveal mildly elevated flow velocity in the descending aorta. A peak velocity of, say, up to 3 m/s is acceptable if there is no delay in deceleration and there are no other indicators of obstruction. When recoarctation occurs the same techniques are used for assessing severity as for unoperated coarctation. Late aneurysm formation at the site of the repair is a rare but well-described complication of treatment and can be difficult to detect or exclude with echo alone. The association of coarctation with aortic valve anomalies and progressive ascending aortic dilatation dictates that these structures should be also assessed as part of routine, serial, follow-up echocardiograms. Careful, regular follow-up of these patients is particularly important during pregnancy (and before embarking on it), because of the increased risk of dissection during pregnancy. Magnetic resonance imaging is superior to echocardiography for imaging the site of coarctation repair itself.

Common Arterial Trunk

Truncus arteriosus (a single great artery arising from the heart, usually overriding the ventricular septum and giving rise to both the aorta and the pulmonary artery) is normally repaired in infancy. The aortic (originally truncal) valve is invariably abnormal, often with four or more cusps and is often stenotic and incompetent to some degree. The aortic root (the proximal part of the original common trunk) is inherently abnormal, and root dilatation is common, but not necessarily progressive. A conduit is used to connect the right ventricle to the pulmonary arteries when they have been disconnected from the common trunk; the conduit always becomes stenotic with age (but at very variable age; some last for many years), and either direct measurement of peak flow velocity or estimation of right ventricular pressure from the tricuspid regurgitation jet will give a good guide to the severity of obstruction.

Double Outlet Right Ventricle

Double outlet right ventricle is deemed to be present when more than 50% of the origins of both great arteries arise from the right ventricle. It is commonly associated with tetralogy of Fallot, when it is usually repaired by appropriate positioning of the patch used to close the ventricular septal defect, with similar post-operative echo appearances to "ordinary" tetralogy. When an isolated phenomenon it is treated in the same manner as a large ventricular septal defect, but the relative positions of the great vessels in relationship to the ventricular septal defect will govern what form surgical intervention will have taken. In some cases repair is not possible, when "single-pump" surgical palliation is undertaken (see above) (Figs. 28.44 and 28.45).

Endocarditis

The typical echo findings of vegetations and associated progressive valvar dysfunction are the same as those seen in cases of endocarditis in structurally normal hearts. Vegetations may form at the site of a restrictive ventricular septal defect, on the tricuspid valve because of a jet through a ventricular septal defect, at the pulmonary artery end of a patent ductus

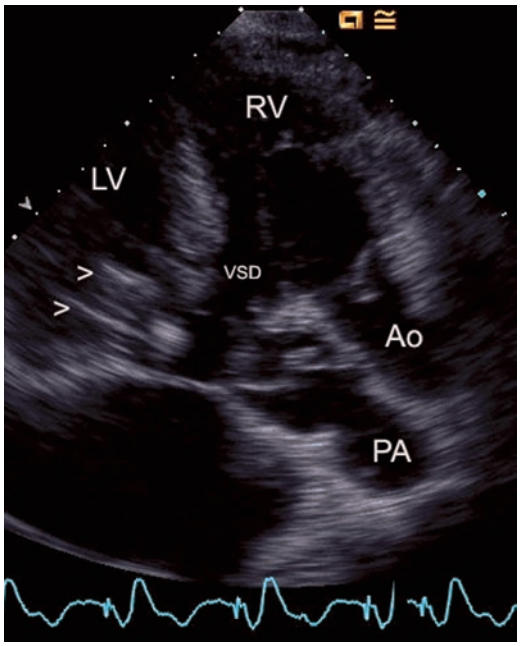

Fig. 28.44 Double outlet right ventricle. Transthoracic echo image demonstrating the large VSD, transposed and parallel great vessels. Pacing wires can be seen (*arrowed*). *Ao* aorta; *LV* left ventricle; *PA* pulmonary artery; *RV* right ventricle; *VSD* ventricular septal defect

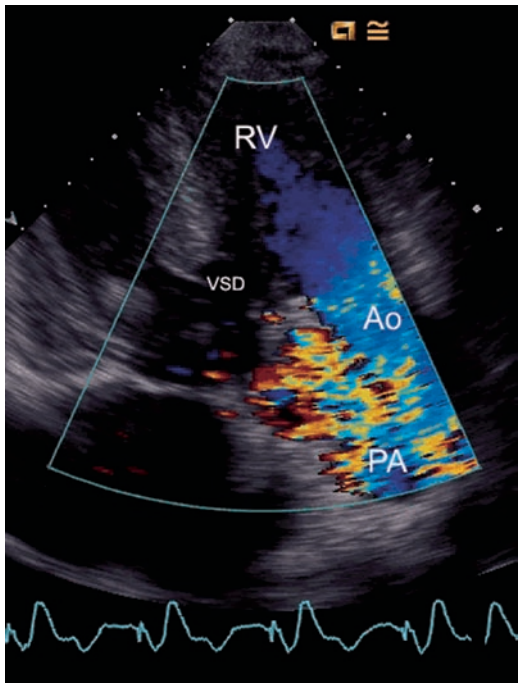

Fig. 28.45 Double outlet right ventricle color flow. Turbulent flow can be seen in the proximal PA because of subpulmonary stenosis. Above the pulmonary valve, the site of a PA band placed in infancy can be clearly seen. *Ao* aorta; *PA* pulmonary artery; *RV* right ventricle; *VSD* ventricular septal defect

arteriosus, or within an aortopulmonary shunt, or an implanted conduit. In those whose congenital heart disease has led to impairment of systemic ventricular function, a further decline in this function is often seen because of the effects of generalized sepsis. Patients with right to left shunting have a risk of systemic embolization of right-sided vegetations. Any prosthetic material used in previous cardiac surgery is liable to infection in the event of bacteremia, particularly shortly after surgery, likewise intra-aortic stents used in the balloon dilatation of recoarctation, and percutaneous closure devices for atrial septal defects, patent foramen ovale, and patent ductus arteriosus.

Pregnancy

Echocardiography aids the assessment of the female adult congenital heart disease patient who wishes to embark upon a pregnancy. Certain conditions, for example pulmonary hypertension and other cyanotic heart disease, carry such a high maternal and/or fetal risk that pregnancy in these patients is mostly actively discouraged regardless of parameters of ventricular function. For the remainder the assessment which must be made prior to a pregnancy includes cardiac function and ventricular dimensions to aid in assessment of how the heart is likely to cope with the hemodynamic changes of pregnancy, bearing in mind that the heart will be expected to deliver a 30–50% rise in cardiac output, a 20% rise in heart rate, to cope with a 40–50% rise in plasma volume, and a reduction in both systemic and pulmonary vascular resistance. At delivery there is a sudden fall in systemic vascular resistance and often significant blood loss, both leading to significant hypotension. Stress echocardiography to examine the response of the heart to increased loading conditions in a controlled situation prior to them embarking upon a pregnancy in women with doubtful cardiac reserve can be very helpful. A heart which has good biventricular function, only mild to moderate valvar dysfunction, normal pulmonary artery pressure, normal chamber sizes, and modest degrees of left to right shunting is likely to tolerate an uncomplicated pregnancy with little difficulty. These features can all be assessed by standard echocardiographic examination. Once any patient with congenital heart disease becomes pregnant regular clinical and echocardiographic review is mandatory.

Bibliography

Gatzoulis MS, Webb GD, Daubeney PEF. *Diagnosis and Management of Adult Congenital Heart Disease*. Philadelphia: Churchill Livingstone; 2003.

Houston A, Hillis S, Lilley S, Richens T, Swan L. Echocardiography in adult congenital heart disease. *Heart*. 1998;80 (Suppl 1):S12–S26.

Linker DT. *Practical Echocardiography of Congenital Heart Disease*. Philadelphia: Churchill Livingstone; 2001.

Perloff JK, Child JS. *Congenital Heart Disease in Adults*. 2nd ed. Philadelphia: Saunders; 1998.

Ueti OM, Camargo EE, de A Ueti A, de Lima-Filho EC, Nogueira EA. Assessment of right ventricular function with Doppler echocardiographic indices derived from tricuspid annular motion: comparison with radionuclide angiography. *Heart*. 2002;88:244–248.

Section 7
Special Methods

Chapter 29
Intraoperative Echocardiography

William J. Stewart and Robert M. Savage

Intraoperative echocardiography (IOE) is an important component in the management of patients undergoing cardiac surgery. It provides information about valve structure and function, ventricular size and function, and hemodynamics that is crucial to contemporary management decisions in modern heart surgery. Although IOE is used to monitor cardiac patients in the setting of noncardiac surgery, that topic is outside the scope of this chapter. Intraoperative echo is an essential element in basic procedures such as valve repair, and also contributes substantially in cases where the surgical mission is more challenging or the patient's perioperative risk is higher.

Epicardial vs. Transesophageal Echocardiography

Transesophageal echo (TEE) is the chosen modality for IOE because it does not interrupt cardiac surgery, and is performed by someone other than the surgeon, usually a cardiologist or anesthesiologist. Epicardial echocardiography can be performed using a standard transthoracic transducer placed directly on the heart. Sterility is maintained by placing the probe within a sterile sheath, with ultrasonic gel to eliminate the air. This method was the primary mode of IOE in the mid 1980s, but was displaced in the last 20 years by transesophageal echocardiography (TEE). Epicardial echo is still a useful option in instances when TEE is unable to provide adequate imaging, more common for anterior structures, ascending aortic atheroma, and left ventricular (LV) outflow tract obstruction. Epicardial echo is also the procedure of choice in a situation where the surgeon prefers to do the transducer work, or esophageal abnormalities abriate TEE.

Essentials of the IOE Exam

It is essential that the echocardiographer be well versed in the process of cardiac surgery, the hemodynamic effects of anesthesia and the heart–lung machine, as well as the diagnostic elements of echocardiography and Doppler echocardiography. It is important to have equipment available which is of sufficient quality to achieve the diagnostic agenda. In addition, the best method of image storage is digital format, which is easier to retrieve for later comparison. It is essential to generate a report from the diagnostic IOE study, so that the results can be factored into the patient's subsequent clinical management.

In most cases, cardiac surgery utilizes cardiopulmonary bypass. Exceptions include off-pump coronary bypass and pericardial stripping. Therefore, most IOE is done in two portions, the *prepump* and the *postpump* examinations. Each has its purposes (Table 29.1).

Prepump IOE

It is important to have the patient fully evaluated prior to entering the operating room. IOE should not be a substitute for good preoperative clinical and imaging evaluation. An exception to this is extremely emergent surgery, where death hangs in the balance of minutes,

W.J. Stewart (✉) and R.M. Savage
Department of Cardiovascular Disease, The Cleveland Clinic, Cleveland, OH, USA
e-mail: Stewarw@ccf.org

P. Nihoyannopoulos and J. Kisslo (eds.), *Echocardiography*,
DOI: 10.1007/978-1-84882-293-1_29, © Springer-Verlag London Limited 2009

Table 29.1 Objectives of intraoperative echocardiography

Prepump TEE
Redefine primary surgical target(s)
Severity, mechanism of valve dysfunction
Evaluation of other valves, unexpected lesions
Define ventricular function
Baseline under anesthesia
Global and segmental wall motion
Assist with cannulation, instrumentation
Atheroma, thrombi, anatomic variants
PostPump TEE
Safety net on results
Define success of primary surgery
Evaluation for residual regurgitation or stenosis
Assess complications of surgery
Assess intraoperative myocardial ischemia/infarction
Assess residual intracardiac shunting

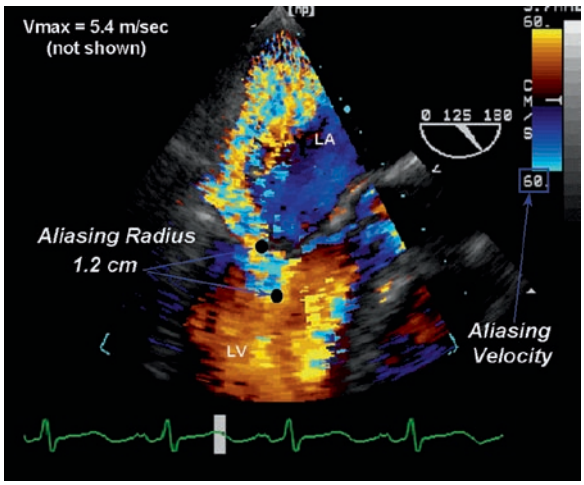

Fig. 29.1 Midesophageal long-axis view at 125° multiplane angle of a patient with severe mitral regurgitation (MR) from anterior leaflet prolapse, with the jet deflected posteriorly, showing the measurement of a 1.2-cm aliasing radius (R) within the flow convergence zone (measured between the *black dots*). Note that the aliasing velocity (V_a), is 60 cm/s. Using the formula to calculate regurgitant orifice area (ROA) of $2\pi R^2 V_a / V_{max}$, and knowing that the maximum MR velocity (V_{max}) by continuous-wave Doppler was 5.4 m/s, the calculated ROA is 1.0 cm^2. An ROA over 0.4 cm^2 is considered severe for MR

such as aortic dissection with impending tamponade or acute aortic or ventricular rupture. Therefore, it should be a rare circumstance where the prepump IOE is relied upon as the sole determinant of the cardiac operation. However, IOE does provide a last-minute update on the status of the heart and cardiovascular hemodynamics in the operating room. It can provide a substantial "quality control," especially in cases where some of the patient's pathology was not understood fully preoperatively.

Many patients come to the operating room without transesophageal echo done preoperatively, and TEE is a more sensitive tool for defining many intracardiac abnormalities. Additional diagnostic features leading to changes in the operative mission are found from 6 to 19% of the time.

Particular care should be paid to the difference between ambulatory hemodynamic conditions and the anesthetic state. Compared to "street conditions," the anesthetized patient may have less sympathetic tone, altered intravascular volume status, interval treatment, or different heart rate and rhythm. Many patients have less mitral or tricuspid regurgitation on the prepump TEE than was found in the echo lab or the cath lab. Quantitative Doppler techniques to accurately measure the severity of the regurgitation are very feasible with high-quality TEE images (Fig. 29.1).

Whenever the prepump IOE makes a substantive change in the surgical plan, the patient's clinical physicians should be contacted to discuss the proposed changes in light of preoperative impressions. Tricuspid regurgitation, dynamic LV outflow tract obstruction, and myocardial ischemia are the most common examples where loading conditions can erroneously suggest that certain goals of surgery need to be altered.

Postpump IOE

The TEE study after cardiopulmonary bypass is a golden opportunity to evaluate the success of the surgical missions and provide a "safety net" for its objectives. It allows the surgical team to determine if the elimination of valve dysfunction is complete and if new valvular or other complications have developed. It also provides an immediate evaluation of both overall and segmental myocardial function, and to check for intraoperative ischemia or infarction at a time when additional bypass surgery can be done. New or residual intracardiac shunts can be identified and defined.

It is unwise to ignore the information defined by postpump intraoperative echo. Residual valve dysfunction on postpump echo has been associated with substantially higher early post op complications (86 vs. 15%) and higher mortality rate (43 vs. 5%) when these findings are not corrected.

Our guidelines for doing further surgery during a second run of cardiopulmonary bypass, a *second pump run*, are as follows: When there is no residual valve regurgitation or stenosis or it is mild (1+ on a scale of 4+), no further surgery is done. When there is moderately severe to severe (3+ to 4) residual valve regurgitation or stenosis after attempted repair, then further repair or replacement during a second pump run is done. When there is moderate (2+) residual valve dysfunction, further surgery should be done if there is no contraindication. In this latter case, we often try to observe the situation for a few minutes without decannulating or giving protamine. In many circumstances, this time provides the opportunity to observe the amount of valve dysfunction further, while allowing transient myocardial problems to resolve. In this circumstance, we often challenge the patient to unmask latent regurgitation, increasing blood pressure to a mean pressure of 100–110 mmHg, using 100 mcg boluses of intravenous phenylephrine, and using volume loading.

Process and Completeness of the IOE Study

It is important to approach the echo examination with efficiency and completeness. In evaluating a patient with a single abnormality, we first look at the valve or structure in question, the one that will be addressed by the operation. This has been called "Willie Sutton's law, *going for the money.*" If the patient suddenly becomes unstable thereafter, at least the most important questions have been answered. Both structural imaging (black and white) and color Doppler images of that structure are recorded from multiple long-and short-axis views. Because each structure has three-dimensional anatomy, a single plane with often miss important structural or flow patterns that will be covered by using numerous orthogonal planes. After addressing the most important questions for that case, a complete echo survey is done, looking at all four chambers, all four valves, pulmonary and systemic veins and arteries. A digital or video tape record is made of each structure, for later side-by-side comparison with the postpump images, useful particularly if there are new abnormalities.

Indications for Intraoperative Echo

The most common uses of IOE are listed in Table 29.2. The most important patients to use intraoperative echo are those in whom the study leads more commonly to changes in the surgical or anesthetic management. In *valve repair*, the most common prepump contribution of the IOE is the detailed understanding of the *mechanism* of the valve dysfunction, based on the echo (Fig. 29.2), which is key to knowing what specific surgical maneuvers are needed to correct the problem.

IOE in Mitral Valve Repair

The most common indication for IOE is valve repair for mitral regurgitation (MR). The prepump echo evaluates the structure and flow abnormalities of each component of the mitral valve (annulus, leaflets, chordae, papillary muscles, left ventricle, and left atrium) in multiple midesophageal planes, and a short-axis view from a transgastric probe position. Each plane is imaged in color and 2D echo (Fig. 29.3a, b). Pulsed- and continuous-wave Doppler is used to characterize the antegrade velocity profile. Pulsed Doppler of pulmonary vein velocity is also useful to assess for velocity waveforms, especially systolic reversal, a common finding in severe MR (Fig. 29.4).

Table 29.2 Indications for intraoperative echo

Repair of any valve
Mitral, aortic, or tricuspid valve repair
Left ventricular function; global and segmental
Location and persistence of ischemia
Complex congenital heart surgery
Complex infection - abscess, prosthetic endocarditis
Periprosthetic regurgitation
Dissection, aortic root surgery
especially with aortic valve resuspension
Myectomy-hypertrophic cardiomyopathy
Ongoing
Cardiac tumor
Minimally invasive procedures (MIP)
Hemisternotomy, port access,
Offpump coronary bypass (OPCABG)
Alternative valve replacements (stentless and transcathetor)
Homograft, Ross procedure, stentless bioprosthesis
Implantable LV assist devices
High-risk coronary bypass
Guidance in cannulation (atheroma)

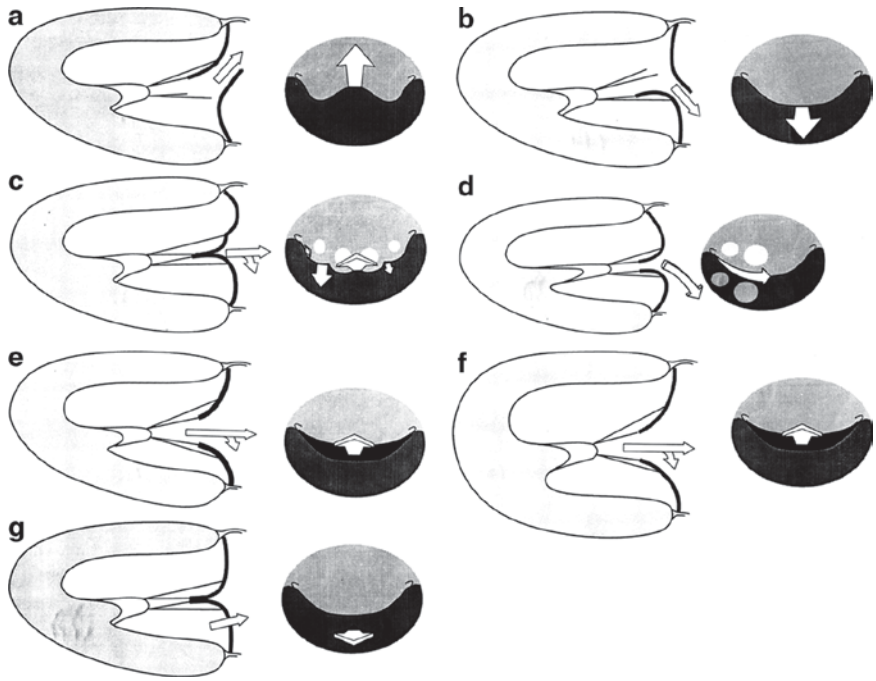

Fig. 29.2 Composite diagram of seven types of mitral regurgitation (MR) mechanisms based on mitral leaflet motion and jet direction (see *arrows*), determined by echo imaging and color Doppler imaging, respectively. Each pair indicates leaflet and jet characteristics in long-axis (*left*) and short-axis (*right*) images. (**a**) Posterior prolapse or flail. (**b**) Anterior prolapse or flail. (**c**) Bileaflet prolapse of flail. (**d**) Commissural chordal elongation or papillary muscle disruption. (**e**) Restricted leaflet motion. (**f**) Relative restriction and apical tethering of normal leaflets caused by left ventricular enlargement and dysfunction. (**g**) Leaflet perforation or congenital cleft

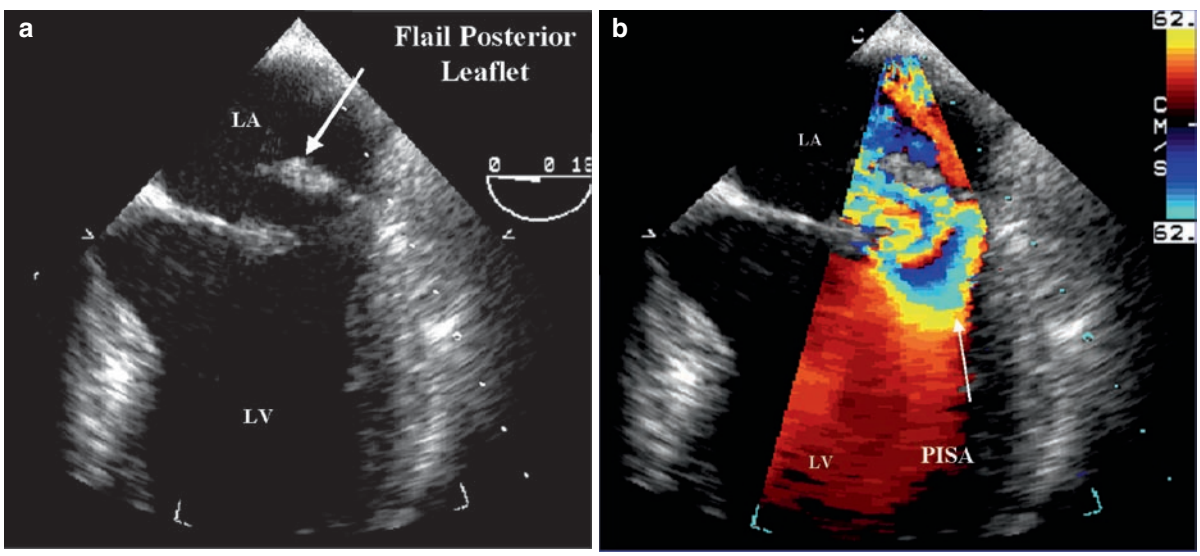

Fig. 29.3 Mid-esophageal long-axis view at 0° multiplane angle of a patient with severe mitral regurgitation (MR). *Left*: posterior leaflet flail (*arrow*), within the left atrium (LA). *Right*: the jet is deflected posteriorly and there is a large flow convergence (*arrow*), also called the proximal isovelocity surface area (PISA)

In particular, which leaflet is abnormal is determined in various long-axis views, such as the midesophageal transverse view of the mitral valve at 0° multiplane angle, and the midesophageal long-axis view of the mitral valve at 120–150°. The midesophageal intercommissural view of the mitral valve at about 60°, aligned parallel to the line between the medial and lateral commissures, is particularly helpful in learning

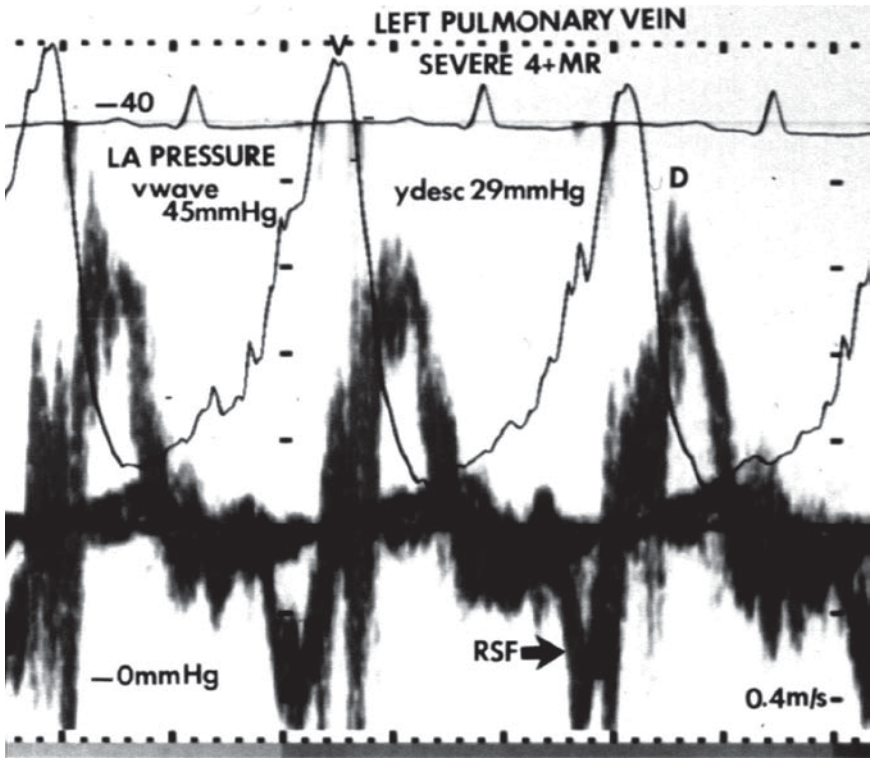

Fig. 29.4 Pulsed-wave Doppler spectrum (*gray-scale contours*) recorded by TEE from the left upper pulmonary vein in a patient with MR, showing reversal of systolic flow (RSF), indicating that the MR is severe. Superimposed is a directly measure left atrial pressure (*thin line waveforms*), illustrating, on a scale of 0–40 mmHg large 45 mm "V" waves during each ventricular systole, which transiently exceed pulmonary parenchymal pressure, causing the flow reversal

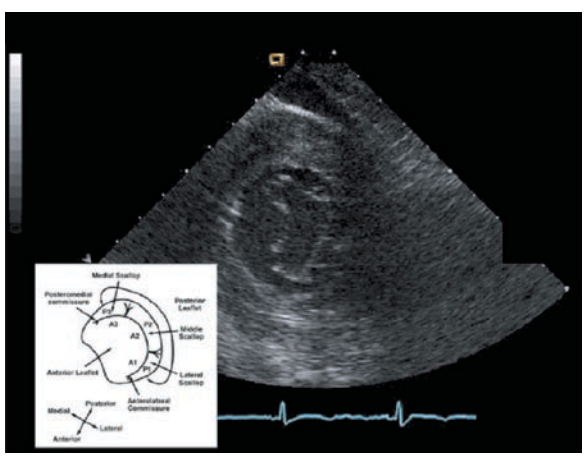

Fig. 29.5 Transgastric short-axis view of the mitral valve at 0° multiplane TEE angle, showing the various parts of mitral leaflet anatomy, corresponding to those labeled in the inset diagram

the medial-versus-lateral locations of the structural and flow abnormalities of the most involved leaflet. In addition, three dimensional echo imaging during surgery this helps to distinguish which scallop of the posterior leaflet is abnormal. The transgastric short-axis view of the mitral valve also helps to determine the medial versus lateral aspects of mitral valve pathology and flow (Fig. 29.5).

IOE in Left Ventricular Outflow Tract Surgery

In aortic valve disease and dynamic LV outflow tract obstruction, a similar approach is made using imaging and color Doppler views from multiple imaging planes. The short axis of the aortic valve is best viewed from a midesophageal view at about 35–60°. The long-axis view of the aortic valve and LV outflow tract should be evaluated at an angle of about 125–140°, approximately 90° from where the short-axis view was ideal. Antegrade aortic valve velocity is recorded using the deep transgastric views, aligning the cursor through the

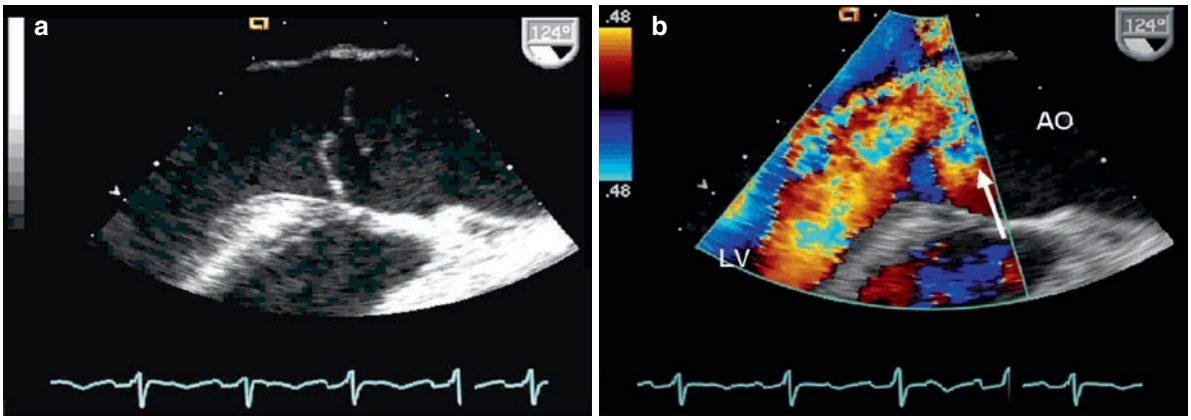

Fig. 29.6 Midesophageal long-axis view of the aorta (AO) at 124° multiplane angle, in a patient with severe aortic regurgitation (AR). *Left*: prolapse of the conjoined right–left cusp of a noncalcified bicuspid valve. *Right*: color Doppler image, showing that the AR jet is deflected posteriorly within the left ventricular (LV) outflow tract. Note the large flow convergence (*arrow*), allowing calculation of regurgitant orifice area by the proximal isovelocity surface area method. An ROA over 0.3 cm^2 is considered severe for AR

flow convergence in the LV outflow tract seen on the color image. Most patients with aortic valve disease undergo aortic valve replacement, for which IOE is less essential because the likelihood of changes in operative management based on IOE is low. For the patient with severe aortic regurgitation (AR), valve repair is feasible if the mechanism of dysfunction (definable by IOE) is a prolapsing noncalcified bicuspid aortic valve (Fig. 29.6a, b). The maneuver needed to correct the AR is triangular exclusion of a portion of the conjoined leaflet edge. This reduces the length of its edge to the length equal to that of the nonconjoined leaflet. The pledgetted commissural sutures at the commissures bring the suspension points of the valve inward to enhance coaptation. After repair, detecting residual regurgitation is the most common abnormality.

Myectomy for hypertrophic cardiomyopathy is an important role for IOE. On the prepump TEE we define the thickness of the septum in the location of the myectomy, and the farthest point of contact of the mitral systolic anterior motion (SAM) with the septum. This helps the surgeon to know the location and extent of resection, as the thickness of the septum cannot be determined by the surgeon through the aortotomy. In addition, it is important to distinguish mitral regurgitation resulting from SAM, versus MR resulting from intrinsic disease of the mitral valve such as prolapse or flail. The LV outflow gradient can often be recorded by TEE using a deep transgastric view for continuous-wave Doppler. If not, epicardial echo (Fig. 29.7) may

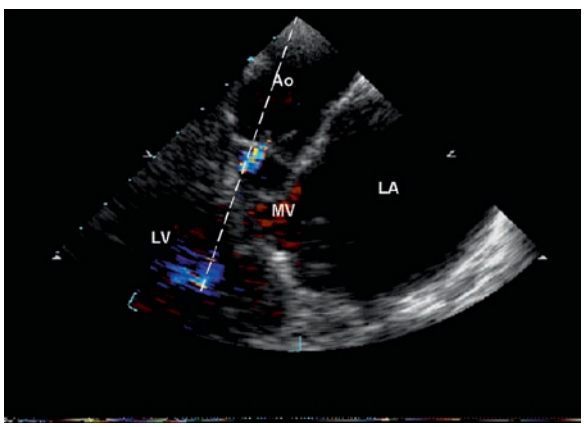

Fig. 29.7 Color flow image recorded by epicardial imaging in a patient with hypertrophic cardiomyopathy undergoing myectomy to relieve dynamic subaortic obstruction. A transthoracic transducer within a sterile sheath is used to place a continuous-wave Doppler cursor (*dashed line*) directly through, and parallel to, the high-velocity flow located at the point of apposition of the mitral valve (MV) leaflets against the hypertrophied interventricular septum

be useful to record the highest velocity at the point of SAM-septal contact. After myectomy, we look for persistent SAM and MR, or a persistent gradient of over 40 mmHg at rest or with Isoproterenol infusion, which is the most common reason mandating a second run of cardiopulmonary bypass. Although unusual, we also look for a new ventricular septal defect at the location of the myectomy.

IOE in Coronary Atherosclerosis

In any patient undergoing cardiac surgery, but especially in those with significant coronary disease, we look for segmental abnormalities of the left (and right) ventricles. Prior to surgery, we store a digital clip of each standard view of the left ventricle, including midesophageal views from multiplane angles of 0, 60, and 120° (Fig. 29.8), and transgastric short- and long-axis views, at 0 and 90°, respectively. After surgery these same views can be obtained and juxtaposed with the prepump images to accurately diagnose new ischemia or infarction.

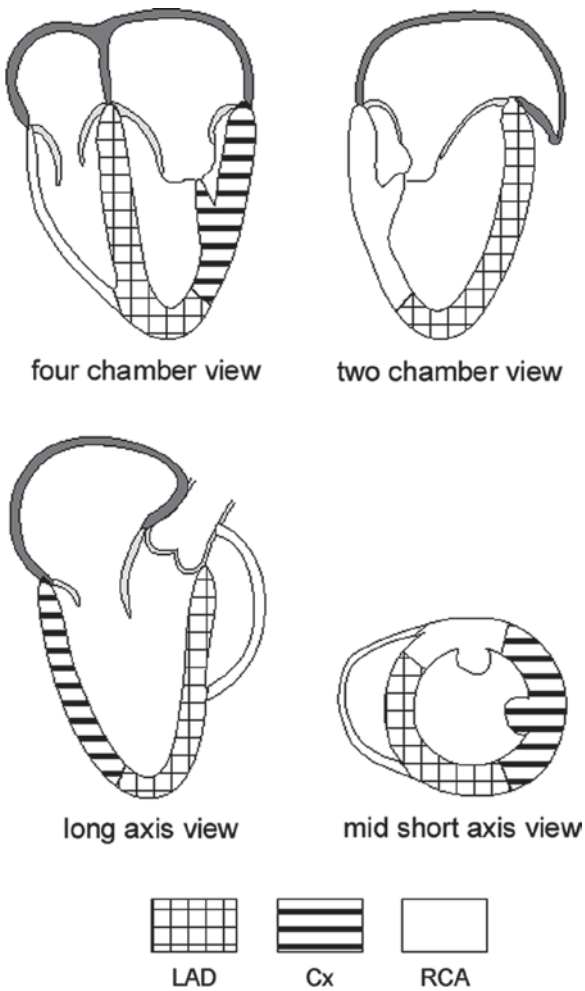

Fig. 29.8 Diagrams of typical coronary artery perfusion beds as they are distributed in standard TEE image planes, midesophageal images at zero (four chamber), 60 (two chamber), and 120 (long axis) degrees multiplane angle, and the transgastric image plane at 0° multiplane angle. The shadings depict the left anterior descending (LAD) territory with a checkered pattern, the circumflex (Cx) territory in a striped pattern, and the right coronary artery territory in a plain white pattern. Individual patients' coronary distributions vary substantially

One of the most common and devastating complications of coronary bypass surgery is atherosclerotic embolization to the brain, kidneys, liver, etc. This occurs more commonly in patients with *atheroma of the thoracic aorta* (Fig. 29.9). Because it is very sensitive to detection of atheroma, it would be ideal to do epicardial echo on all at risk patients undergoing cardiopulmonary bypass, to help define the location and method of arterial cannulation. Transesophageal echocardiography is not as good for imaging atheroma in the ascending aorta because it is in the far field, and partly hidden in the blind spot for TEE, where the tracheal bifurcation blocks the imaging access. However, in practice epicardial echo is used more selectively for this purpose, favoring cases when there are clinical suspicions of severe ascending atheroma, known severe carotid disease, or heavy aortic knob calcification by chest X-ray. When a TEE is done for another purpose prior to cannulation for cardiopulmonary bypass, information about the presence and severity of atheroma of the thoracic aorta may be the reason for deciding to do epicardial echo for ascending atheroma. It is known that atheroma typically get worse as one proceeds distally, so severe mobile atheroma are unlikely in the ascending aorta if they are not found distally.

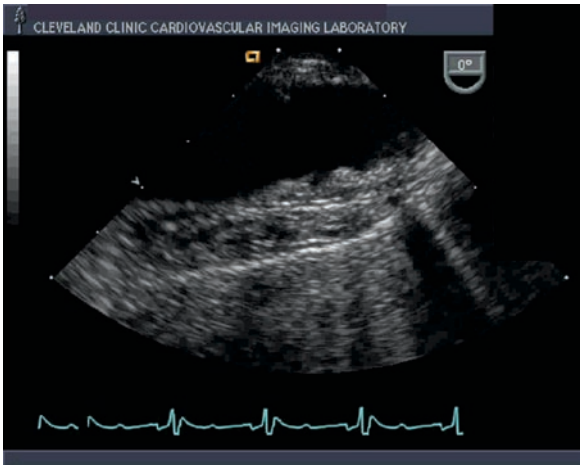

Fig. 29.9 Transesophageal echo image at 0° multiplane angle of the aortic arch in a patient with severe protruding atheroma. When these are large and/or mobile, the likelihood of embolization increases, especially with more manipulation of the aorta during heart surgery

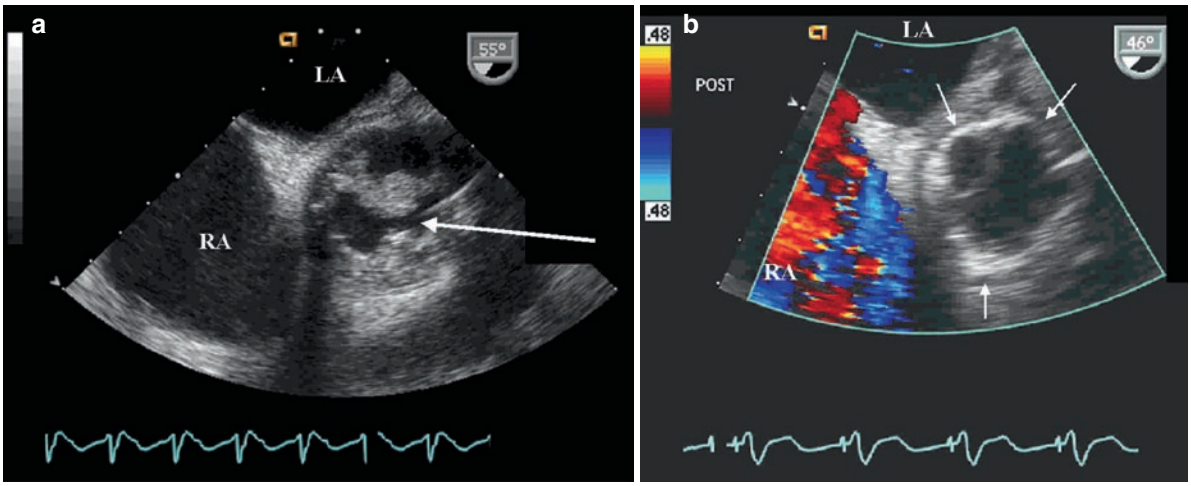

Fig. 29.10 Midesophageal short-axis views of the aortic valve in endocarditis. *Left*: Prepump TEE image showing a periaortic abscess, causing regurgitation adjacent to an aortic prosthesis. *Right*: Post-pump TEE image shows a normal aortic homograft, with a concentric double density with a thin clear space (*arrows*) between the donor aortic annulus (homograft inclusion cylinder) and the recipient's aortic annulus. *RA* right atrium

IOE in Other Cardiac Conditions

In *congenital heart disease*, the primary goal is to define the location and size of septal defects and exclude additional abnormalities. The challenge of very little babies is the unavailability of TEE probes that are small enough. One solution is to use intracardiac echo (ICE) probes either in the esophagus or on the surface of the heart. We utilize intravenous contrast echo frequently after shunt surgery to verify the elimination of the septal defect. Continuous-wave Doppler from the epicardial window is useful for determination of LV and RV outflow tract obstruction.

In *endocarditis*, and especially periprosthetic regurgitation and perivalvular abscesses, IOE is an essential element for planning the degree of resection as well as the location of infection-related fistulas. After surgery, excluding periprosthetic leakage is similar to other valvular lesions, but there is the additional issue of determining the exclusion of persistent fistula. The use of the aortic homograft is an essential surgical tool in periaortic infection. After implantation of a *homograft* (Fig. 29.10a, b), *Ross procedure*, or *stentless valve*, the postpump echo is important in verifying competency and determining that the leaflets are suspended well without prolapse.

A similar set of statements can be made about patients undergoing aortic valve surgery together with surgery for an ascending *aortic aneurysm*. The prepump IOE is helpful in defining if the aortic valve leaflets are inherently abnormal, and the diameters of the aortic annulus, sinuses, and sinotubular junction. If the valve is resuspended using a supracoronary conduit, or with a David procedure, the post-pump TEE is used to look for residual aortic regurgitation.

Lastly, with the advent of *minimally invasive and robotic surgery* done through a limited thoracotomy, IOE is important to make up for some limitations caused by a less optimum access to the heart by the surgeon. Most patient who undergo repair or replacement of a single valve (aortic or mitral) are operated via a hemisternotomy. However, this smaller incision induces some limitations on the operative team. It is harder to follow heart size and therefore to judge the adequacy of volume filling from the pump. In addition, intracardiac air is more difficult to remove, because the LV apex cannot be lifted up for needle deairing. IOE helps to optimize management of these issues.

Complications of Heart Surgery Definable by IOE

Persistence of valvular regurgitation is the most common problem encountered on the postpump intraoperative echocardiogram. However new valvular regurgitation of

a valve not previously abnormal is a problem that occurs occasionally. The most common surprise is new MR resulting from worsened LV enlargement. Periprosthetic regurgitation (Fig. 29.11), after a new prosthesis is implanted, is not uncommon, particularly in patients with perivalvular infection or a calcified mitral annulus. A stitch from the mitral prosthesis placed all the way through to the aortic valve is a rare complication of which to be aware. A new atrial septal defect has been found on some postpump IOE studies, especially when the mitral valve is approached via the right atrium and the interatrial septum. Iatrogenic aortic dissection is a rare result of aortic cannulation, the aortic vent, or a proximal vein graft anastomosis.

Pitfalls of IOE

The most important problem encountered in the practice of intraoperative echo is inexperience, see Table 29.3. It is a daunting task to apply all the diagnostic acumen needed for accurate outpatient TEE to the operating room environment. It is challenging to have persons on hand who have sufficient echo experience who also are familiar with and available in the operative environment. It is recommended that the practitioner of IOE have at least level 2 training in TEE as defined by the American Society of Echocardiography. This includes training under supervision for at least 300 echo studies. This educational agenda is therefore long and difficult to accomplish without a concentrated period of fellowship in a formal training environment.

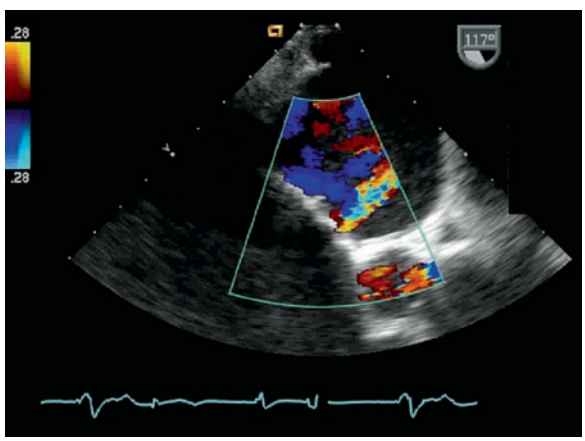

Fig. 29.11 Midesophageal view of the left atrium and left ventricle at 117° multiplane angle, early after mitral valve replacement showing very mild 1+ periprosthetic mitral regurgitation, with the color jet located anterior and superior to the mitral sewing ring. Note that the Nyquist (color aliasing limit) was purposely set to 28 cm/s, to create a larger spatial distribution of the periprosthetic MR, to localize it better. This Nyquist is lower than our usual practice of setting it at 50–60 cm/s for most spatial mapping of color jets. The amount of periprosthetic MR often improves after giving protamine. This patient did not have a second pump run, and had no MR murmur after surgery, with no periprosthetic MR by transthoracic echo

Table 29.3 Intraoperative echo pitfalls

Inexperience
Inadequate study
Imaging time too short
Imaging planes too few
Coupling (sleeving, contact)
Hemodynamic instability: hypotension, hypovolemia
Interference to imaging
Electronic (electrocautery, environment)
Room lights on

The persons doing intraoperative TEE studies are often cardiology or cardiothoracic anesthesiology physicians. Each has a substantial learning curve, that is often not facilitated in a standard fellowship without personal initiative. For example, a cardiology fellow may lack experience with the process of cardiac surgery, or be uncomfortable engaging in diagnostic studies in the operative environment, with changing hemodynamic conditions. The anesthesiology fellow often has inadequate exposure to ultrasound technology, intracardiac anatomy, and the diagnostic process inherent in imaging and flow analysis.

In many hospitals, the ideal IOE team includes both cardiologists and anesthesiologists, working together to provide coverage of the various patients presenting for cardiac surgery. The team also involves the echo competence of the cardiac surgeon(s). Even if the surgeon does not *perform* the study, understanding the flavor of the information of the imaging and flow analysis takes a substantial learning curve, which should be included in the agenda of cardiac surgical training.

Summary

Care of the patient undergoing cardiac surgery is enhanced substantially by a careful and selective program of intraoperative echocardiography. This enhances patient outcomes by giving up to the minute information about the patient's cardiac performance before and after the corrective procedure.

Bibliography

Amarenco P, Cohen A, Tzourio C, et al. Atherosclerotic disease of the aortic arch and the risk of ischemic stroke. *N Engl J Med*. 1994;331:1474–1479.

Blauth CI, Cosgrove DM, Webb BW. Atheroembolism from the ascending aorta: an emerging problem in cardiac surgery. *J Thorac Cardiovasc Surg*. 1992;103:1104–1112.

Click RL, Abel MD, Schaff HV. Intraoperative transesophageal echocardiography: 5-year prospective review of impact on surgical management. *Mayo Clin Proc*. 2000;75(3):241–247.

Cosgrove DM, Rosenkranz ER, Hendren WG, Bartlett JC, Stewart WJ. Valvuloplasty for aortic insufficiency. *J Thorac Cardiovasc Surg*. 1991;102:571–576.

Cosgrove DM, Stewart WJ. Mitral valvuloplasty. *Curr Probl Cardiol*. 1989;14:359–415.

Cosgrove DR, Sabik JF. Minimally invasive approach for aortic valve operations. *Ann Thorac Surg*. 1996;62:596–597.

Currie PJ, Stewart WJ. Intraoperative echocardiography for surgical repair of the aortic valve and left ventricular outflow tract. *Echocardiography*. 1990;7:273–288.

Daniel WG. Improvement in the diagnosis of abscesses associated with endocarditis by transesophageal echocardiography. *N Engl J Med*. 1991;324:795–800.

Davila-Roman VG, Phillips KJ, Daily BB, Dávila RM, Kouchoukos NT, Barsilai B. Intraoperative transesophageal echocardiography and epiaortic ultrasound for assessment of atherosclerosis of the thoracic aorta. *J Am Coll Cardiol*. 1996;28(4):942–947.

DeBruijn NP, Clements FM, Kisslo JA. Intraoperative transesophageal color flow mapping: initial experience. *Anesth Analg*. 1987;66:386–390.

Erbel R, Oelert H, Meyer J, et al. Effect of medical and surgical therapy on aortic dissection evaluated by transesophageal echocardiography. Implications for prognosis and therapy. The European Cooperative Study Group on Echocardiography. *Circulation.* 1993;87:1604–1615.

Fraser C Jr, Wang N, Mee RB, et al. Repair of insufficient bicuspid aortic valves. *Ann Thorac Surg*. 1994;58:386–390.

Freeman WK, Schaff HV, Khandheria BK, et al. Intraoperative evaluation of mitral valve regurgitation and repair by transesophageal echocardiography: incidence and significance of systolic anterior motion. *J Am Coll Cardiol*. 1992;20:599–609.

Gillinov AM, Cosgrove DM, Blackstone EH, et al. Durability of mitral valve repair for degenerative disease. *J Thorac Cardiovasc Surg*. 1998;116(5):734–743.

Grigg LE, Wigle ED, Williams WG, Daniel LB, Rakowski H. Transesophageal Doppler echocardiography in obstructive hypertrophic cardiomyopathy: clarification of pathophysiology and importance in intraoperative decision making. *J Am Coll Cardiol*. 1992;20:42–52.

Grimm RA, Stewart WJ. The role of intraoperative echocardiography in valve surgery. *Cardiol Clin*. 1998;16(3):477–489.

Kouchoukos NT, Wareing TH, Daily BB, Murphy SF. Management of the severely atherosclerotic aorta during cardiac operations. *J Cardiac Surg*. 1994;9:490–494.

Marwick TH, Stewart WJ, Lever HM, et al. Benefits of intraoperative echocardiography in the surgical management of hypertrophic cardiomyopathy. *J Am Coll Cardiol*. 1992;20:1066–1072.

Muhiudeen IA, Roberson DA, Silverman NH, Haas GS, Turley K, Cahalan MK. Intraoperative echocardiography for evaluation of congenital heart defects in infants and children. *Anesthesiology*. 1992;76:165–172.

Scalia GM, McCarthy PM, Savage RM, Smedira NG, Thomas JD. Clinical utility of echocardiography in the management of implantable ventricular assist devices. *J Am Soc Echocardiogr*. 2000;13(8):754–763.

Secknus MA, Asher CR, Scalia GM, Cosgrove DM III, Stewart WJ. Intraoperative transesophageal echocardiography in minimally invasive cardiac valve surgery. *J Am Soc Echocardiogr*. 1999;12(4):231–236.

Secknus MA, Klein AL, Smedira NG, Cosgrove DM, Stewart WJ. Does prepump intraoperative echocardiography change operative plans in mitral valve repair? *J Am Soc Echocardiogr.* 1996;9:374.

Secknus MA, Scalia GM, Asher CR, Savage RM, Cosgrove DM, Stewart WJ. Intraoperative transesophageal echocardiography in minimally invasive cardiac valve surgery. *Circulation*. 1996;94:1442.

Shah PM, Raney AA, Duran CM, Oury JH, Multiplane transesophageal echocardiography: a roadmap for mitral valve repair. *J Heart Valve Dis.* 1999;8(6):625–629.

Shah PM, Stewart SD, Calalang CC, Alexson C. Transesophageal echocardiography and the intraoperative management of pediatric congenital heart disease: initial experience with a pediatric esophageal 2D color flow echocardiographic probe. *J Cardiothorac Vasc Anesth*. 1992;6:814.

Shanewise JS, Cheung AT, Aronson S, et al. ASE/SCA guidelines for performing a comprehensive intraoperative multiplane transesophageal echocardiography examination: recommendations of the American Society of Echocardiography Council for Intraoperative Echocardiography and the Society of Cardiovascular Anesthesiologists Task Force for Certification in Perioperative Transesophageal Echocardiography. *J Am Soc Echocardiogr*. 1999;12(10):884–900.

Sheikh KH, Bengtson JR, Rankin JS, de Bruijn NP, Kisslo J. Intraoperative transesophageal Doppler color flow imaging used to guide patient selection and operative treatment of ischemic mitral regurgitation. *Circulation*. 1991;84:594–604.

Sheikh KH, de Bruijn NP, Rankin JS, et al. The utility of transesophageal echocardiography and Doppler color flow imaging in patients undergoing cardiac valve surgery. *J Am Coll Cardiol*. 1990;15:363–372.

Simon P, Owen AN, Havel M, et al. Transesophageal echocardiography in the emergency surgical management of patients with aortic dissection. *J Thorac Cardiovasc Surg*. 1992;103:1113–1117.

Stewart WJ, Currie PJ, Salcedo EE, et al. Intraoperative Doppler color flow mapping for decision-making in valve repair for mitral regurgitation. Technique and results in 100 patients. *Circulation.* 1990;81:556–566.

Stewart WJ, Currie PJ, Salcedo EE, et al. Evaluation of mitral leaflet motion by echocardiography and jet direction by

Doppler color flow mapping to determine the mechanisms of mitral regurgitation. *J Am Coll Cardiol*. 1992;20: 1353–1361.

Thys DM, Abel M, Bollen BA, Stewart WJ, Pearlman, et al. American Society of Anesthesiologists and the Society of Cardiovascular Anesthesiologists Tack Force on Transesophageal Echocardiography. Practice guidelines for perioperative transesophageal echocardiography. *Anesthesiology*. 1996;84: 986–1006.

Tunick PA, Rosenzweig BP, Katz ES, Freedberg RS, Perez JL, Kronzon I. High risk for vascular events in patients with protruding aortic atheromas: a prospective study. *J Am Coll Cardiol*. 1994;23:1085–1090.

Wareing TH, Davila-Roman VG, Barzilai B, Murphy SF, Kouchoukos NT. Management of the severely atherosclerotic ascending aorta during cardiac operations. A strategy for detection and treatment. *J Thorac Cardiovasc Surg*. 1992;103:453–462.

Yoshida K, Yoshikawa J, Yamaura Y, Hozumi T, Akasaka T, Fukaya T. Assessment of mitral regurgitation by biplane transesophageal color Doppler flow mapping. *Circulation*. 1990;82:1121–1116.

Chapter 30
Contrast Echocardiography

Mark J. Monaghan

Introduction

The use of contrast in echocardiography is not new. In 1968 Gramiak and Shah first described the utilization of hand-agitated saline as an ultrasound contrast agent. The technique of injecting agitated saline containing very small air bubbles is still used regularly today and has become a standard technique for identifying shunts through a patent foramen ovale or small atrial septal defects. Furthermore, contrast agents are used in almost every medical imaging technology to enhance image quality and provide new information. Therefore, it is not surprising that they should have found an emerging and important role in ultrasound imaging of the heart and other organs in the body.

This chapter describes the important interaction between contrast microbubbles and ultrasound. It explains how that interaction can be utilized to provide sensitive contrast detection so that the technique can be utilized in a variety of different clinical settings.

Basic Principles

Types of Contrast Agent

In order to provide efficient ultrasound backscatter, ultrasound contrast agents must contain microbubbles which have a very different acoustic density to the surrounding blood. Therefore, these contrast agents contain a gas, which has a much lower density than blood. Hand-agitated saline contains small bubbles of air, suspended in saline, which are not designed to cross the pulmonary capillary bed. Indeed, the presence of contrast bubbles within the left heart, following an intravenous injection, suggests an intra-cardiac shunt with a right to left component. However, commercially produced agents are specifically designed to cross the cross the lungs, opacify the left heart and, more recently, the myocardium.

To do this, they require a number of specific characteristics. These include the ability to survive transpulmonary passage and the ability to behave physiologically within the circulation. This means that they must have a shell and contain gas which is physiologically inert and a size comparable to that of red blood cells.

These demands place a number of constraints upon the design of ultrasound contrast agents. In order to survive transpulmonary passage, the contained gas within the contrast microspheres must be prevented from dissolving in blood. This objective can be achieved by either using a thick microbubble shell to prevent diffusion, or a high molecular weight gas, which is not soluble in blood. Contrast agents containing air or nitrogen, which are highly soluble in blood, require a thick, impermeable shell. However, agents with a thin shell require a high molecular weight gas such as sulfur hexafluoride or perfluorocarbon. Figure 30.1 illustrates the basic principles involved in the design of microbubbles for ultrasound contrast agents.

Contrast Microbubble Response to Ultrasound

Figure 30.2 demonstrates the very important ratio between the incident or transmitted ultrasound energy and the backscattered or reflected energy.

M.J. Monaghan
Department of Cardiology, King's College Hospital, London, UK
e-mail: mark.monaghan@kch.nhs.uk

P. Nihoyannopoulos and J. Kisslo (eds.), *Echocardiography*,
DOI: 10.1007/978-1-84882-293-1_30,

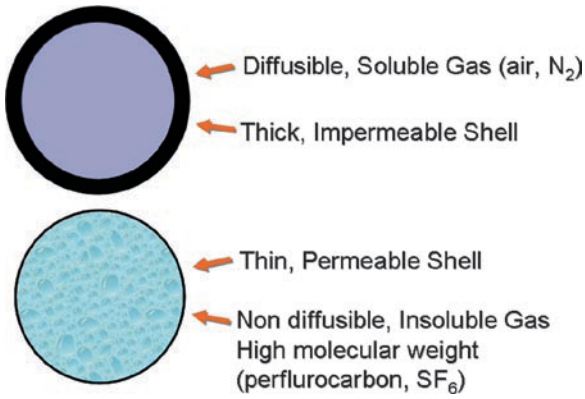

Fig. 30.1 In order to survive transpulmonary passage and persist in the circulation, the gas within contrast agents must be prevented from diffusing into blood. This is achieved either by using a thick, impermeable shell or by using a high molecular weight, insoluble gas

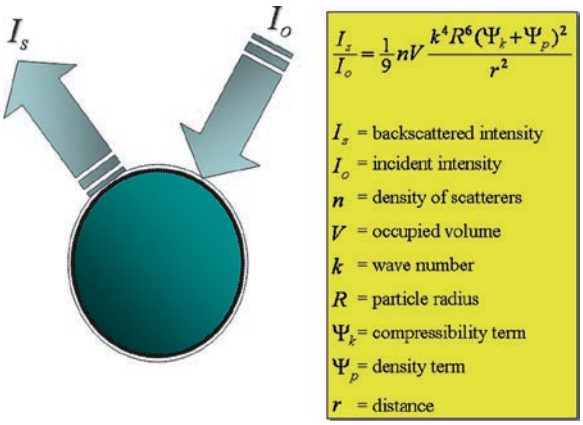

Fig. 30.2 Formula describing the ratio between incident and backscattered ultrasound intensity from a free gas bubble. One of the most important components is the bubble size. The magnitude of the backscattered signal intensity is proportional to the 6th power of the radius

Although this ratio is described by a very complex formula, with a number of important components, the most important factor determining the magnitude of the backscattered signal is the bubble size. As previously stated, the contrast microbubbles must have a size not greater than red blood cells so that they behave physiologically within the microcirculation. In practice, this means that the modal diameter is approximately 4 microns (4u). Using a diameter of 4u and standard values for the other parameters described in Fig. 30.2, the difference in backscattered ultrasound intensity between a typical ultrasound contrast agent and blood is approximately 100 million.

Although this difference is extremely large and therefore contrast microbubbles are very powerful scatterers of ultrasound, in practice there are a number of important factors which limit the ability of an ultrasound scanner to image contrast microbubbles efficiently. As shown in Fig. 30.3, the behavior of a gas microbubble in an ultrasound field varies with the changing intensity of the incident ultrasound. At normal diagnostic ultrasound intensities, most contrast microspheres will fracture, implode, and be destroyed. This gives rise to a swirling appearance of contrast within the cardiac chambers as blood containing destroyed contrast mixes with undestroyed contrast. This is most apparent near the left ventricular apex, when an apical imaging window is used, because the ultrasound intensity is at its greatest in the near field.

The proportional blood volume within the myocardium is significantly lower than within the ventricular cavities. The blood also moves much slower within the myocardium; therefore, a lower concentration of contrast microbubbles is exposed to ultrasound for a longer time than within the ventricles, and consequently it is more likely to be destroyed. Furthermore, the backscattered signal from myocardial tissue is significantly higher than that from blood. All these factors mean that it is much more difficult to detect and image contrast microbubbles within the myocardium than within the blood-filled cavities. Therefore, with conventional ultrasound imaging techniques, evaluation of myocardial perfusion is not possible. One potential solution to this problem may be to administer a larger volume of contrast so that the concentration of microbubbles within the blood, and hence the myocardium, is increased. However, if the microbubble concentration

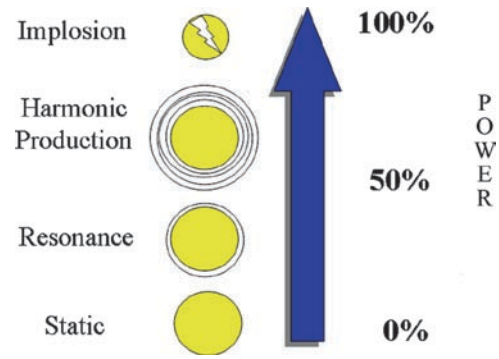

Fig. 30.3 As incident ultrasound power increases, the microbubble will resonate, generate harmonics and finally implode, releasing the encapsulated gas which quickly dissolves

is increased, this results in attenuation of the ultrasound signal as the microbubbles form an impenetrable barrier to ultrasound transmission. This phenomenon is frequently seen within the right ventricular cavity where the microbubble concentration is higher before transpulmonary passage. However, it can also be visualized in the left ventricle as the delivered contrast volume is increased.

Although conventional ultrasound imaging modalities can demonstrate contrast opacification of the cardiac cavities, to reliably detect contrast microbubbles within the myocardium, and therefore evaluate myocardial perfusion, it is clear that alternative ultrasound imaging techniques need to be utilized. Fortunately, gas microbubbles have very different acoustic properties to those of myocardial tissue. Therefore, it is possible to use a range of imaging techniques which are very sensitive to contrast microbubbles, but not sensitive to tissue. So the backscattered contrast signal is enhanced and the tissue signal suppressed, significantly increasing the contrast signal-to-tissue ratio. This is not just important for evaluating myocardial perfusion, but is also useful for enhancing endocardial border detection during left ventricular opacification studies.

The main difference in acoustic property between contrast microbubbles and tissue is that, as shown in Fig. 30.3, microbubbles will resonate and behave in a nonlinear fashion within an ultrasound field. Figure 30.4 illustrates the formula that describes the resonant frequency of a free gas bubble. If we use a microbubble diameter of 4u (the modal diameter of most contrast agents) and standard values for the other parameters in the equation, the resonant frequency is approximately 2 MHz. This frequency very conveniently falls within the bandwidth of ultrasound frequencies used in echocardiography and essentially means that contrast microbubbles, unlike tissue, will resonate within the ultrasound field. They resonate in a nonlinear fashion and generate harmonics. As previously mentioned, contrast specific imaging techniques utilize these nonlinear, resonant properties of microbubbles to significantly increase the detection sensitivity for contrast and suppress the tissue signal.

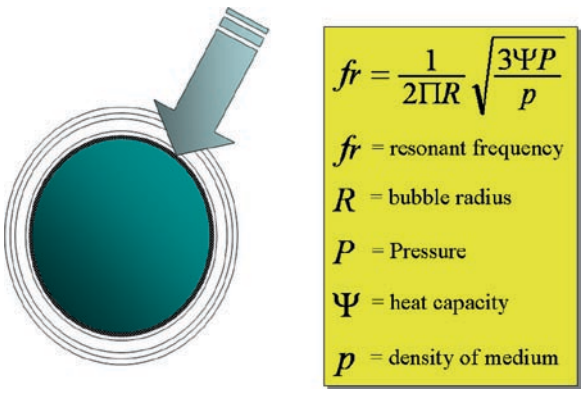

Fig. 30.4 Formula describing the resonant frequency of a free gas bubble. Using standard parameters and a bubble radius of 2μ, the resonant frequency is approximately 2MHz. This conveniently falls within the bandwidth of diagnostic ultrasound

Destructive Imaging Techniques

Contrast-specific imaging technologies conveniently separate themselves into methods that rely on or cause microbubble destruction and those techniques that aim to preserve the microbubbles – nondestructive imaging. Table 30.1 illustrates some of the currently available contrast-specific imaging techniques.

As a general rule, destructive imaging techniques use an MI (mechanical index or output power) >1.0, whereas nondestructive techniques need to use an MI < 0.3 in order to limit contrast destruction.

At higher MIs the nonlinear resonance of contrast microbubbles within the ultrasound field results in the generation of harmonic signals and then destruction of the microbubble. Typically these harmonics will occur at multiples of the transmitted (fundamental) frequency, with the strongest response occurring at the second harmonic.

Although there is also a tissue signal at the second harmonic frequency, it is lower in amplitude than the

Table 30.1 Destructive and nondestructive contrast-specific imaging modalities

Destructive contrast imaging techniques
Second harmonic imaging
Ultraharmonics
Pulse Inversion
Harmonic power doppler (Angio)
Nondestructive contrast imaging techniques
Low MI real-time methods
Power modulation
Power pulse inversion
Cadence contrast imaging
Contrast pulse sequencing

contrast signal. So if the frequency receive filters on the scanner are set to only receive the second harmonic frequency (twice the transmitted fundamental frequency) then the contrast signal amplitude will be greater than that of the tissue. Therefore, the all-important contrast to tissue signal ratio is increased. At even higher harmonics, the tissue signal will be negligible but there will still be a contrast signal. These techniques are called ultraharmonics and essentially rely upon receiving selected higher frequencies. However, the received contrast signal amplitude is still very small at these higher harmonics – making them susceptible to noise and artifacts. In addition, specially constructed broad-bandwidth transducers have to be utilized to detect these higher harmonics. In summary, these high MI destructive techniques cause high-amplitude resonance of the microbubbles, generation of harmonics and, of course, bubble destruction. Although these techniques are sensitive for microbubble detection, they have to be used in an intermittent imaging mode. This is to allow time for contrast microbubbles to replenish the myocardium following each destructive frame. In practice, this means that a frame is acquired every 1, 2, 3, or up to 10 cardiac cycles. Intermittent imaging is more difficult to use and this is considered a significant disadvantage by many.

Pulse inversion and harmonic power Doppler are considered to be high MI Doppler techniques in that they cause microbubble destruction, but they actually measure the change in backscattered signal from one pulse to another. Using these techniques, one pulse is sent down a scan line and a reflected signal is derived from both microbubbles and myocardium. However, this same pulse causes microbubble destruction so that when a second pulse is transmitted down the same scan line, shortly after the first, the reflected signal is generated from myocardium alone. The ultrasound scanner analyzes the difference between the backscattered/reflected signal from these two pulses. A significant difference is taken to indicate the presence of contrast microbubble destruction, and a corresponding signal is displayed upon the image. This technique is very similar to that utilized in color-flow Doppler – essentially a moving target indicator. It is extremely sensitive for contrast destruction. However, it has a limited dynamic range meaning that it is effectively an all-or-nothing technique.

Pulse inversion Doppler is again very similar but utilizes two pulses which are 180° out of phase with each other. The contrast microbubbles respond differently depending on the phase of the pulse; this difference in the backscattered signal again indicates the presence of contrast. However, the relative high MI at which this technique works also causes microbubble destruction and intermittent imaging is again needed.

Nondestructive Imaging Techniques

As previously mentioned, the need to utilize intermittent imaging does make destructive imaging techniques more difficult to use. Also the absence of any wall motion information is considered by many to be an important disadvantage. In order to provide wall motion information, the frame rate needs to be increased from one frame every few cardiac cycles to a minimum of 20 frames a second. If the frame rate is to be increased without causing bubble destruction then the MI needs to be decreased significantly and usually needs to be <0.3.

A low MI will minimize microbubble destruction, but will generate only a very weak backscattered signal. Therefore, more sensitive contrast detection methods have to be used, which at the same time will suppress the tissue signal. These low MI methods are called real time because the higher frame rates allow evaluation of wall motion and perfusion simultaneously.

Essentially these techniques work on similar principles. They all send multiple, low-amplitude pulses down each scan line. Each pulse varies from the preceding one in either amplitude, phase, or a combination of both. Different manufacturers use one or more of these methods for their low MI real-time methods, and some of the proprietary names for these techniques are listed in Table 30.1.

Figures 30.5 and 30.6 illustrate the basic principles utilized in Power Modulation, which is one of the low MI real-time methods. With this methodology, multiple pulses are transmitted down each scan line; however, each alternate pulse is of 50% amplitude. The ultrasound scanner receive circuitry doubles the received signals from the 50% amplitude pulses and then subtracts that from the received signal from the 100% amplitude pulses. This means that in theory backscattered signals from a linear reflector such as myocardial tissue should cancel each other out, thereby suppressing the myocardial signal. However, contrast microbubbles are nonlinear reflectors and so the doubled backscatter signal from the 50% amplitude pulse does not cancel the signal created by the 100% amplitude

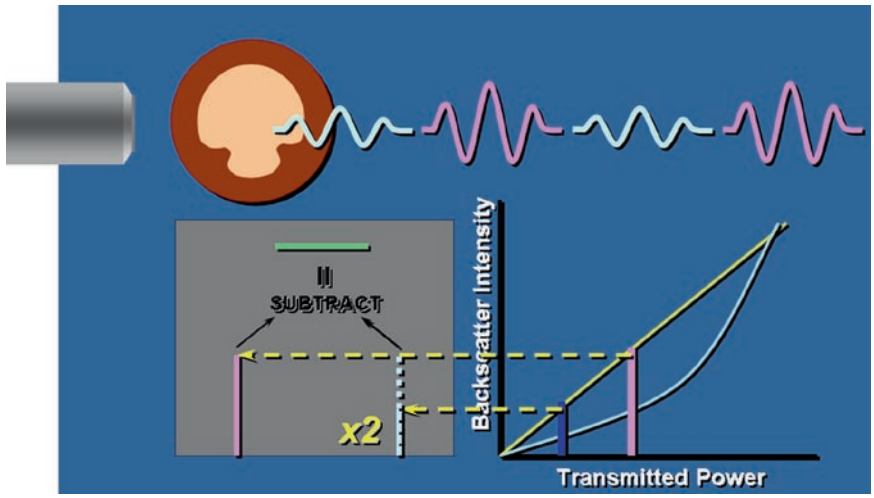

Fig. 30.5 Power modulation uses varying amplitude ultrasound pulses where alternate pulses are 50% in amplitude of the preceding one. When scattering occurs from a linear tissue reflector, the 50% amplitude pulse creates a 50% amplitude backscattered signal. This received signal is doubled in amplitude and then subtracted from the signal received from a full amplitude pulse. This effectively means that the backscattered signals from linear reflectors such as myocardial tissue cancel each other out, suppressing the tissue signal

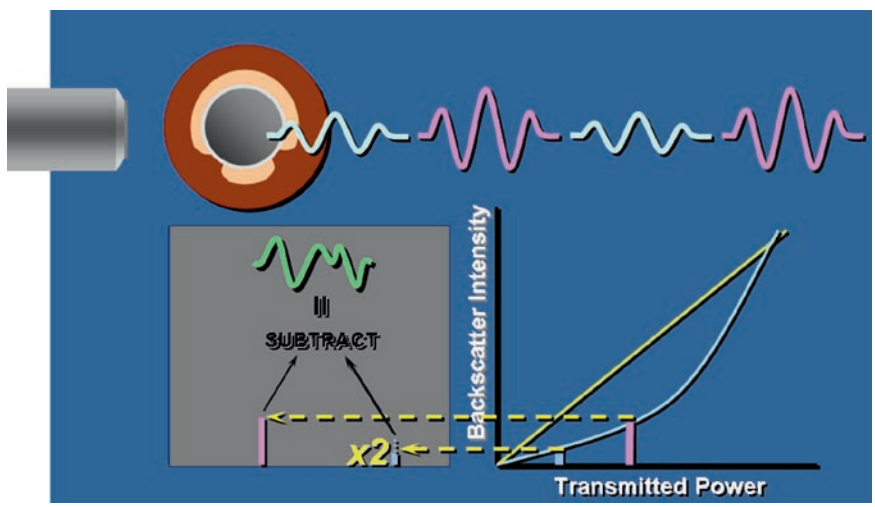

Fig. 30.6 Contrast microbubbles are non-linear scatterers, therefore the backscattered signals from the doubled 50% amplitude pulses and the full amplitude pulses do not cancel each other out when subtracted. This leaves a signal representing the presence of contrast

pulse. The remaining signal indicates the presence of contrast within the scan plane.

In theory and usually also in practice, the only image signals seen when utilizing low MI nondestructive real-time imaging are those derived from contrast microbubbles and tissue signals are completely suppressed. At low contrast microbubble concentrations, there may be insufficient contrast within the myocardium to cause any enhancement, and the only contrast that can be seen is within the LV cavity. Since the myocardium will be black and the cavity bright, this results in excellent endocardial definition. Frame rates of >25 Hz can be achieved and this is quite satisfactory for use during stress echocardiography. Furthermore, the absence of contrast destruction allows much better visualization of the left ventricular apex than when conventional high MI second harmonic imaging is used with contrast. High MI second harmonic imaging also creates a significant tissue signal, and this can make it more difficult to determine the endocardial boundary. If second

harmonic imaging is to be used with contrast for left ventricular opacification then it is sensible to reduce the MI < 0.4 to limit the tissue signal and contrast destruction.

As the contrast microbubble concentration is increased in the blood, either by increasing the bolus volume or infusion rate, then sufficient microbubbles will appear within the myocardium to cause myocardial enhancement. The myocardial contrast signal intensity is directly proportional to the number of microbubbles within a unit volume of myocardium and this equates to the myocardial blood volume. As previously mentioned, the great advantage of this type of contrast imaging technique is that it potentially permits evaluation of both left ventricular wall motion with excellent endocardial definition and myocardial perfusion through evaluation of myocardial blood volume.

Enhancement of Doppler Signals

Modern echocardiographic imaging systems have extremely sensitive Doppler processing and the need for enhancement is limited. However, enhancement can be performed using contrast microbubbles. Even after the microbubbles have collapsed and only shell fragments are left in the circulation, considerable spectral Doppler enhancement occurs. This means that contrast-enhanced Doppler recordings can be performed at the end of a conventional contrast LV opacification or perfusion study, when there is no visible contrast left in the cavities. Shell fragments will still be circulating and these act as excellent Doppler scatterers.

An example of spectral Doppler enhancement using contrast is seen in Fig. 30.7. In this case, considerable enhancement of the continuous-wave Doppler

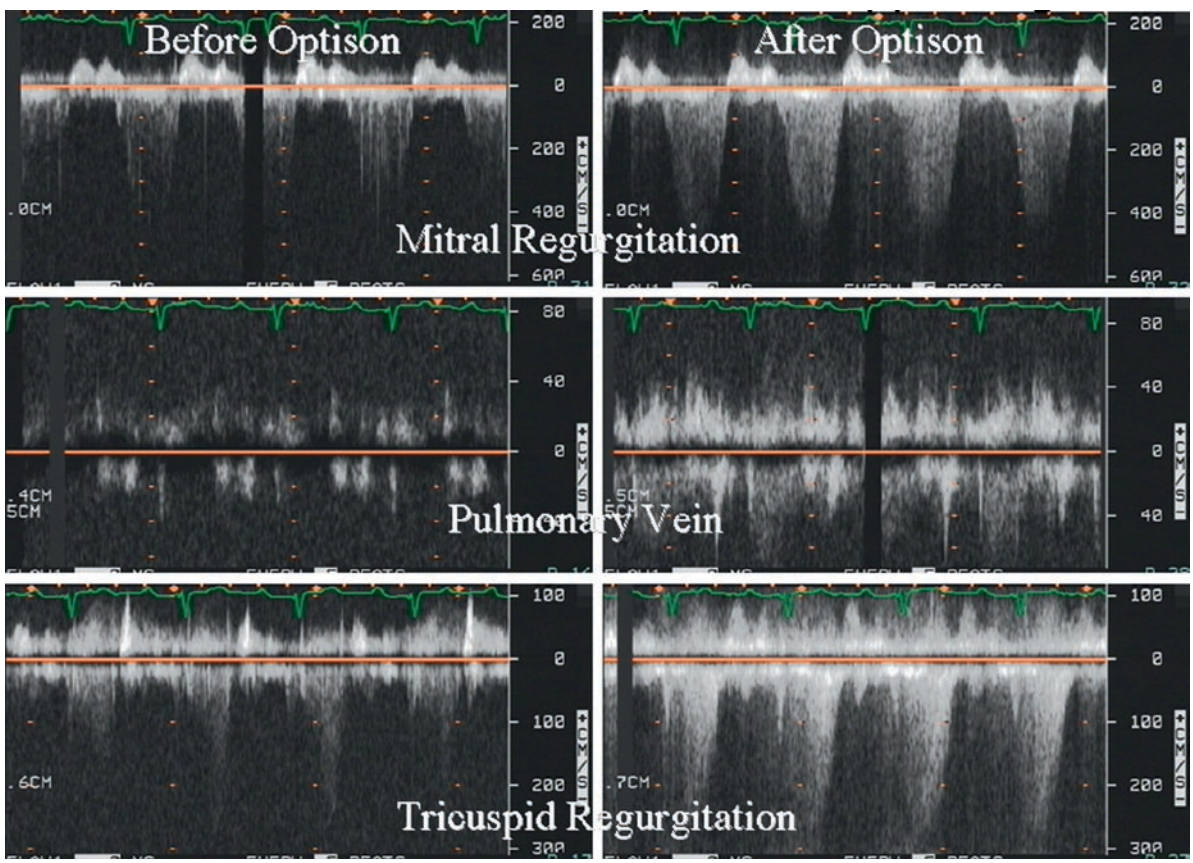

Fig. 30.7 Enhancement of spectral Doppler recordings using the Contrast agent Optison. This was obtained at the end of a conventional LVO contrast study when very little contrast was visible, however the Contrast shell fragments still generate a strong Doppler signal and show enhanced visualisation of mitral, tricuspid and pulmonary vein flow

signal from mitral and tricuspid regurgitation is seen. In addition, pulsed-wave analysis of pulmonary vein flow is also improved.

Contrast Administration: Bolus or Infusion?

Generally speaking, most commercially available contrast agents can be administered using either using bolus or infusion administration methods.

Bolus injections are usually considered satisfactory for left ventricular opacification studies. They have the advantage of being easy and quick to set up and they usually result in less contrast usage. However, as shown in Fig. 30.8, bolus injections result in a shorter time period during which the contrast signal intensity is at an appropriate level without significant attenuation. Since the contrast concentration is constantly changing during a bolus injection it is not possible to quantify myocardial blood flow as described later. However, relatively underperfused myocardial segments can often be appreciated for a transient period during the decay phase of the bolus.

The microbubbles used in most commercial contrast agents usually settle out quite rapidly and rise to the top of the solution in which they are suspended. This means that it is necessary to constantly agitate the syringe containing the contrast to keep the microbubbles suspended. During an infusion this may be even more difficult. Some infusion pumps have been developed which help to keep the contrast suspended by constantly rotating the syringe containing the microbubbles. With some agents, settling out of the contrast microbubbles is less of an issue, and they can be effectively administered by dilution with saline and using a conventional intravenous drip.

The main advantage of contrast infusion is that the infusion rate can be precisely adjusted so that the contrast concentration falls between the detection threshold and attenuation zones, allowing for a long useful imaging time window, as illustrated in Fig. 30.9. Once set up, an infusion requires less operator intervention and could reduce the number of operators required for a contrast study. Infusions can be used for both LV opacification and perfusion studies. If quantification of myocardial blood flow is to be performed (as described later) then a constant contrast infusion is mandatory. However, an infusion inevitably results in use of increased volumes of contrast, and this of course adds to the cost of the study. Nevertheless, contrast delivery via an infusion confers so many advantages that it has become the most common method of administration for cardiac applications.

Left Ventricular Opacification

The American Society of Echocardiography and European Association of Echocardiography position papers on Contrast Echocardiography have recom-

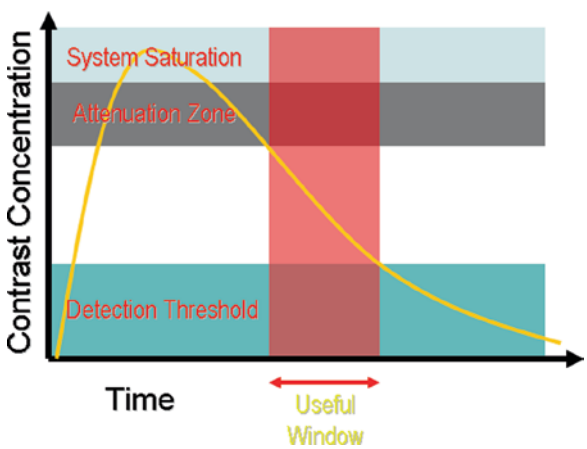

Fig. 30.8 During a bolus contrast injection, there is a limited time window on the decay part of the concentration curve where the contrast concentration is below the attenuation level but above the detection threshold

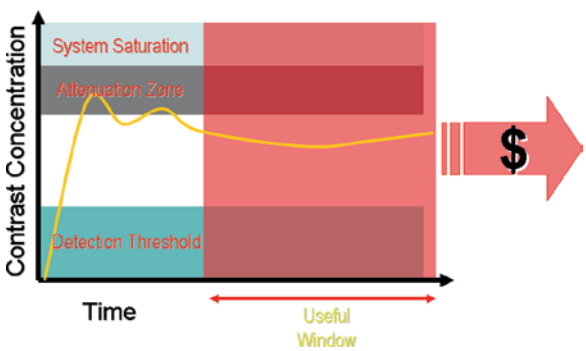

Fig. 30.9 With a constant infusion of contrast, the infusion rate can be adjusted so that contrast concentration is at a level which is above the detection threshold but below the attenuation level. This results in a prolonged imaging window but results in higher contrast usage and increased associated costs

mended the use of a contrast agent to improve endocardial definition when two or more segments are not visualized adequately. This situation can arise in patients who have a poor imaging window because of lung/rib artifacts or obesity. Patients who are ventilated also frequently have very poor quality echo images, and the use of contrast may make a transesophageal echo to evaluate left ventricular function unnecessary. Stress echocardiography requires excellent endocardial definition on a segmental basis, often under difficult imaging conditions. Contrast echo has become a vital tool during stress, as described later.

As previously mentioned, conventional second harmonic imaging can be used for left ventricular opacification studies. However, this requires a relatively low MI setting to avoid contrast destruction and minimize tissue harmonics. In addition, the receive filters on the ultrasound system need to be adjusted to endure exclusion of the tissue fundamental signal. Most modern echo systems have a manufacturer's preset which will optimize the machine settings for this type of study and use of this, if it is available, is recommended.

Low MI nondestructive real-time imaging methods, as described previously, are considered optimal for left ventricular opacification studies. Again, these can usually be accessed through a preset and if available, should always be used.

LV Thrombus and Masses

In patients with suboptimal echo windows, identification of left ventricular thrombi or masses can be challenging. The left ventricular apex is the most common site for thrombus formation, and it can be the most difficult area to visualize because of near-field artifacts on conventional fundamental or harmonic imaging. Standard echo techniques to help clarify the diagnosis include identification of associated wall motion abnormality, use of higher imaging frequencies with harmonics, adjustment of the focal point to the depth of interest, and use of color-flow Doppler with a low velocity scale (low PRF) to see if there is flow across the area of the image where thrombus is being questioned.

In a substantial number of patients, these techniques will still leave the question of possible LV thrombus unresolved and contrast can be extremely useful. Again, we would advocate the use of low MI real-time imaging, if available. Thrombus will appear as a dark filling defect adjacent to the akinetic myocardium. In many patients with scar or with reasonable myocardial perfusion, the myocardial intensity may be greater than that of the thrombus. An example of an apical LV thrombus that could not be satisfactorily delineated using conventional echo techniques is shown in Fig. 30.10.

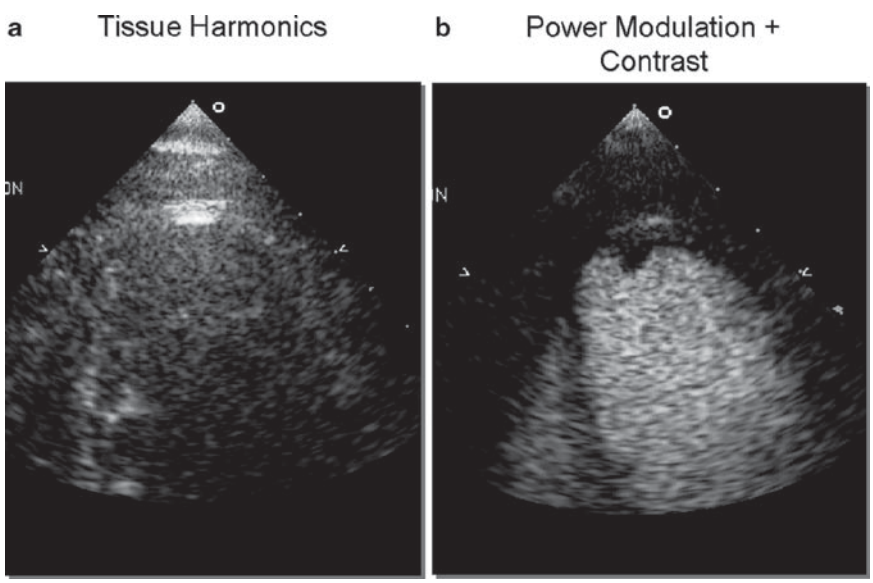

Fig. 30.10 Zoomed apical 4 chamber views in a patient who had an anterior infarct and a conventional echocardiogram (left) suggestive of a large apical thrombus. A contrast study using Power Modulation demonstrates that the structure previously thought to represent a thrombus is probably a false tendon. However, there is a small filling defect at the apex which was subsequently confirmed at surgery to represent a small thrombus

More rarely, intracardiac masses may represent tumors. Here contrast echo, using low MI real-time imaging, can demonstrate vascularized or malignant tumors and differentiate them from thrombus or stromal tumors. A thrombus or stromal tumor will not opacify with contrast, whereas a vascularized or malignant tumor will. The use of flash destruction/reperfusion low MI imaging, as described later, may also help verify the degree of vascularization, although there have been very limited data published on this.

Other pathologies where contrast left ventricular opacification has helped with the diagnosis include noncompaction cardiomyopathy where visualization of the deep myocardial recesses and trabecullation is essential and apical hypertrophic cardiomyopathy. In the latter condition, the small and almost obliterated apical left ventricular cavity can be difficult to see without contrast enhancement.

Global and Regional LV Function

Assessment of left ventricular function is the most common reason for performing an echocardiogram in the adult patient population. Yet, as we know, image quality is frequently suboptimal, and the accuracy and reproducibility of echo measurements of left ventricular volumes and ejection fraction can be poor.

When performing a resting contrast study for evaluating LV function we would again advocate the use of low MI real-time imaging. Alternatively, use the contrast harmonic preset on the scanner which will automatically select a relatively low MI and optimize the receive filters to improve contrast enhancement.

Use conventional tissue harmonic imaging to adjust the scanplanes, starting with apical views to minimize the effects of contrast attenuation. Activate the contrast preset as previously discussed. Adjust the gain to obtain very low background noise, move the focal position to mitral valve level, and reduce the sector width until a frame rate >25 Hz is obtained. Bolus injections of contrast (followed by saline flush) or an infusion may be used for this type of study. Images may be stored on video tape, although digital acquisition will provide best quality and single beat loops will usually suffice.

If inadequate contrast opacification is obtained then a larger bolus volume or higher infusion rate should be tried. If attenuation occurs and far-field objects are obscured, then reduce the bolus volume or infusion rate. Alternatively, or in addition, a few frames (5–10) at high power (impulse or flash function) will destroy contrast within the LV cavity and myocardium, reducing attenuation and improving endocardial definition.

An example of a contrast LV opacification study is shown in Fig. 30.11. This study was performed in an ITU patient where the only other way of assessing left ventricular function satisfactorily would have been to perform a transesophageal echo.

In the case shown in Fig. 30.11 a qualitative, visual assessment of LV function was deemed adequate for further clinical management. However, quantitative information such as LV volumes or ejection fraction is often needed, and the improved endocardial definition afforded by contrast allows more precise tracing of the endocardial border for calculation of volumes etc. Although contrast undoubtedly increases the accuracy and reproducibility of these types of measurements, it should go without saying that the basic rules of ensuring precisely defined scan planes, avoiding foreshortened views and careful tracing of the endocardial border, still apply as they do in noncontrast studies.

Automatic endocardial border detection systems have the potential to improve quantitative analysis by removing the need for manual tracing of the LV border. However, these systems are also limited by poor image quality. If the endocardium is poorly defined, then the software will have as much difficulty following the endocardial boundary as will the human eye. Some ultrasound system manufacturers have adapted their automatic endocardial border detection systems to work with contrast, so that the LV cavity is recognized as having a bright, high intensity signal from contrast, whereas the myocardium is recognized as being dark. The high contrast change from the bright cavity to dark myocardium provides an easy boundary for the software to follow and LV volumes can be calculated on a frame-by-frame basis, which is impractical during manual tracing. This allows calculation of more sophisticated parameters of LV function and application to a wider patient population, including those with suboptimal windows. An example of this technology is shown in Fig. 30.12.

Similar technology can also be used to study regional left ventricular function as shown in Fig. 30.13. Here, the automatic boundary detection system again detects the border between the contrast-filled cavity and the dark myocardium. As the border moves in during systole, a colored band is overlaid on the image every 35 or 40 ms. Thicker bands represent more excursion of the endocardium, whereas very thin bands represent

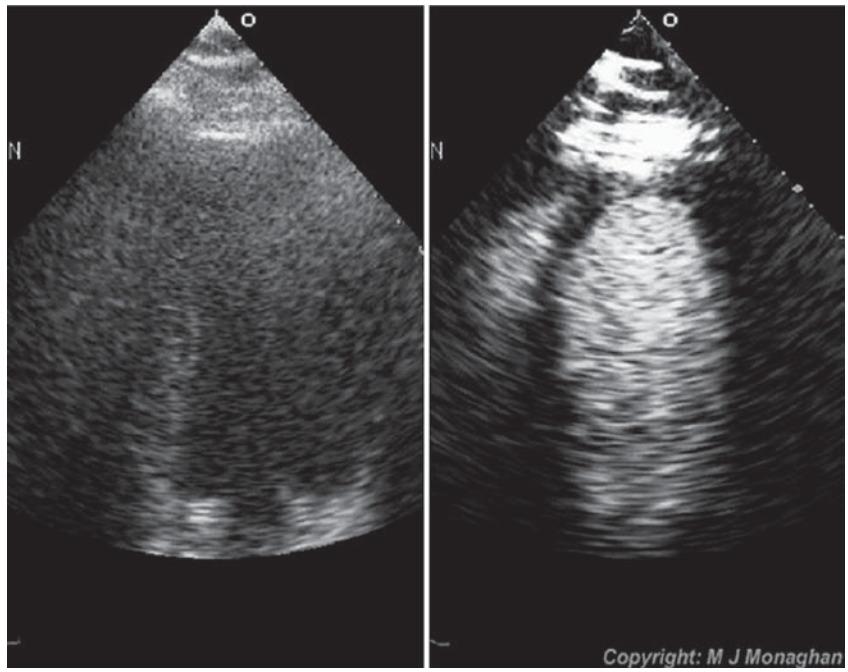

Fig. 30.11 Apical 4 chamber view using tissue harmonic imaging (on left) in an ITU patient with very poor imaging windows. The patient had been recovering slowly post cardiac surgery and the request was to assess LV function. Image quality was so poor that no comment could be confidently made about LV function. Before proceeding to perform a transesophageal echo a contrast study was performed using a 0.3 ml injection of Optison through an existing IV line and Power Modulation low MI contrast imaging (right frame). Evaluation of the LV endocardial border was significantly enhanced, especially at the apex and the lateral wall, allowing an accurate assessment of LV function without needing to proceed to a transesophageal echo. The improvement in image quality was even more evident on real-time images than on these still frames

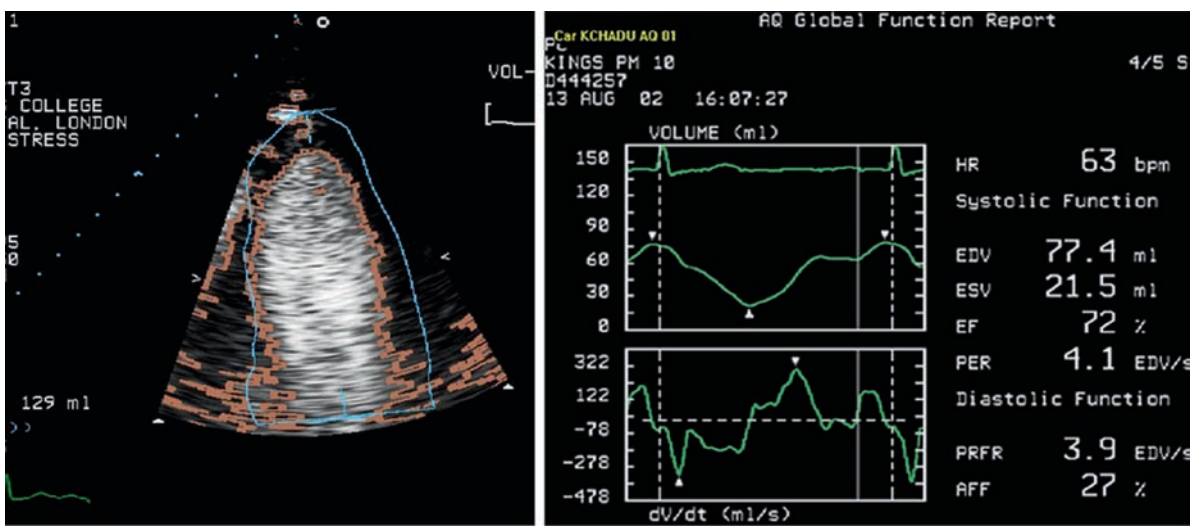

Fig. 30.12 Evaluation of global left ventricular function during a continuous contrast infusion of Sonovue and using the Contrast CK software from Philips Medical Systems. The left frame shows a bright contrast filled LV cavity and a dark myocardium. The LV endocardium is tracked (orange) on a frame by frame basis and LV volume within the blue region of interest is calculated using the method of discs. In the right hand frame a graph displaying LV volume changes during one cardiac cycle and the first derivative (dV/dt) is seen. Automatically generated calculations such as end-diastolic and end-systolic volumes together with ejection fraction etc are also displayed

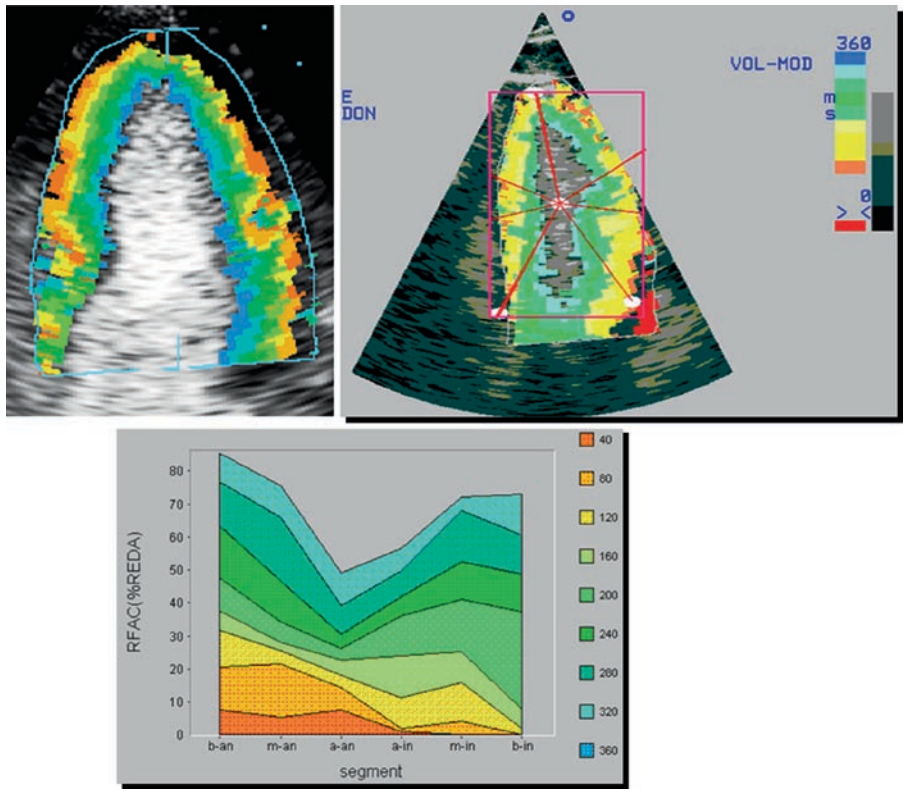

Fig. 30.13 Quantitative Contrast Colour Kinesis (Philips Medical Systems) images showing an apical 4 chamber view at the top left with contrast in the LV cavity and coloured bands overlaid on the image representing systolic excursion of the endocardium. Thicker colour bands represent more systolic excursion of the corresponding segments. The scan plane has been semi-automatically segmented into six segments (top right) and the fractional area change calculated in each segment. The fractional area changes for all six segments are plotted in the bottom diagram and allow comparison of contraction between segments. In this example, the apical segments show reduced fractional area change

akinetic or hypokinetic segments. These images can be segmented, as shown in Fig. 30.13, and the regional contraction (fractional area change) calculated and compared for all segments. It is really only the advent of contrast that has made it possible to quantify regional LV function in a wide variety of patients, including those with poor echo windows.

Stress Echocardiography

Although stress echocardiography has a high sensitivity and specificity for the detection of coronary disease and evaluating myocardial viability it is the most demanding and difficult echo technique to perform and interpret. This is because image quality can often be very poor at peak stress, irrespective of whether pharmacological or exercise stress has been performed. High image quality with excellent endocardial definition is essential for the performance and analysis of stress echo studies. It is important to be able to visualize all myocardial segments and detect subtle wall motion or thickening abnormalities. For these reasons, contrast agents have become an almost mandatory component of most stress echo laboratories. In our own department, contrast is used in virtually every stress echo study because it is difficult to predict, based upon the baseline images, how much image quality will deteriorate by the time peak stress is reached, and it can be very difficult to compare noncontrast baseline images with contrast-enhanced peak stress images. Therefore, this author advocates the use of contrast in most stress echo cases.

Contrast can be administered via bolus injections if necessary. However, as described previously, contrast infusions do confer several advantages and can reduce the number of personnel required in the stress

lab. For the reasons previously mentioned, low MI real-time imaging is the preferred contrast specific imaging modality to use. Apical destruction of contrast at high MI can really limit the detection of localized apical wall motion abnormalities, limiting the sensitivity of the test. Since low MI real-time techniques often have lower frame rates, it may be necessary to reduce the sector width by 20–30° in order to ensure that the frame rate is greater than 25 Hz. It is obviously very important at high heart rates to maintain a reasonable imaging frame rate, and this is one of the limitations of many of the low MI techniques. Nevertheless, unless the LV cavity is very large it is usually possible to reduce the sector width enough to get an adequate frame rate.

It is very easy to incorporate contrast into a standard stress protocol, especially when pharmacological stress is being performed and an IV line is already in place. If a three-way tap is connected to the end of venous cannula then the contrast should not be administered through the side arm or the top port of the cannula. This is to minimize contrast destruction by avoiding the shear forces associated with a 90° turn. We prefer to use a Y connector with a narrow bore connection for the contrast to avoid microbubbles settling out, which can happen in a three-way tap. Contrast infusion pumps usually have narrow bore connection tubing for the same reason, and this should always be used.

Figure 30.14 illustrates a suggested protocol for using contrast during dobutamine stress echo. This can be adapted for either bolus injections or infusions. Bolus injections are usually performed approximately 20–30 s before images are acquired. On the other hand, infusions take a little longer to reach a steady state and 45-s lead-in is usually necessary. The infusion can and should be discontinued between imaging stages; in fact, once the apical views have been obtained there will be sufficient contrast left in the circulation to allow parasternal images to be obtained. As shown in the protocol, it is preferable to collect apical images first and then the parasternal images so that the contrast level has fallen and the chances of attenuation minimized. Contrast attenuation is less of a problem with low MI imaging techniques, and Fig. 30.15 illustrates contrast-enhanced parasternal short-axis images with minimal attenuation. However, it is prudent to try and modify the imaging window to avoid the right ventricle as much as possible. The high contrast concentration in the RV may result in attenuation. If parasternal windows are unobtainable because of attenuation or some other reason, then the apical three chamber view may be substituted for the parasternal long axis and the short axis omitted since all segments will be seen in other views.

As previously described for resting LV opacification studies, the contrast bolus dose or infusion rate should be adjusted so that attenuation is minimized and far-field structures are clearly seen. During the peak of a bolus, some attenuation is inevitable and it is important to wait until the optimal part of the decay curve before acquiring images. A transient reduction in contrast concentration can be achieved by using the "flash" or "impulse" function which will destroy

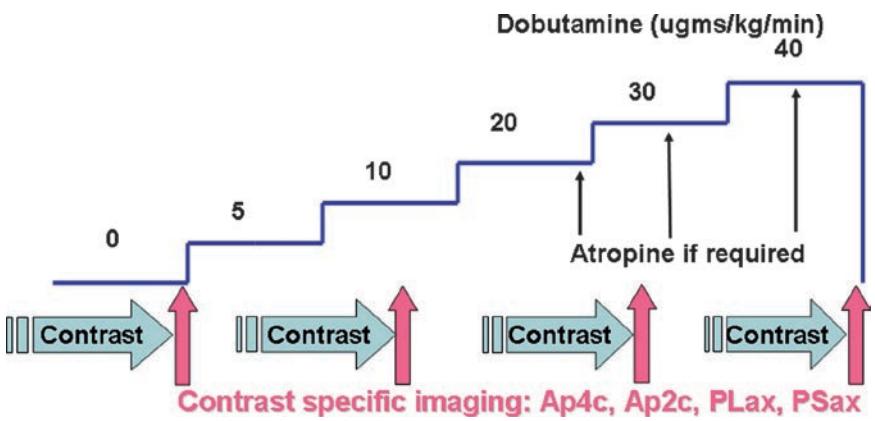

Fig. 30.14 Suggested protocol for combining contrast with a dobutamine stress echo protocol. Imaging is performed at baseline, low dose, intermediate dose and at peak. Imaging sequence commences with apical views to minimise the effects of attenuation. Contrast bolus injections are administered approximately 30 seconds before each imaging acquisition sequence and repeated if necessary. Infusions would need to be re-started approximately 45 seconds before imaging and can be stopped after apical views have been obtained

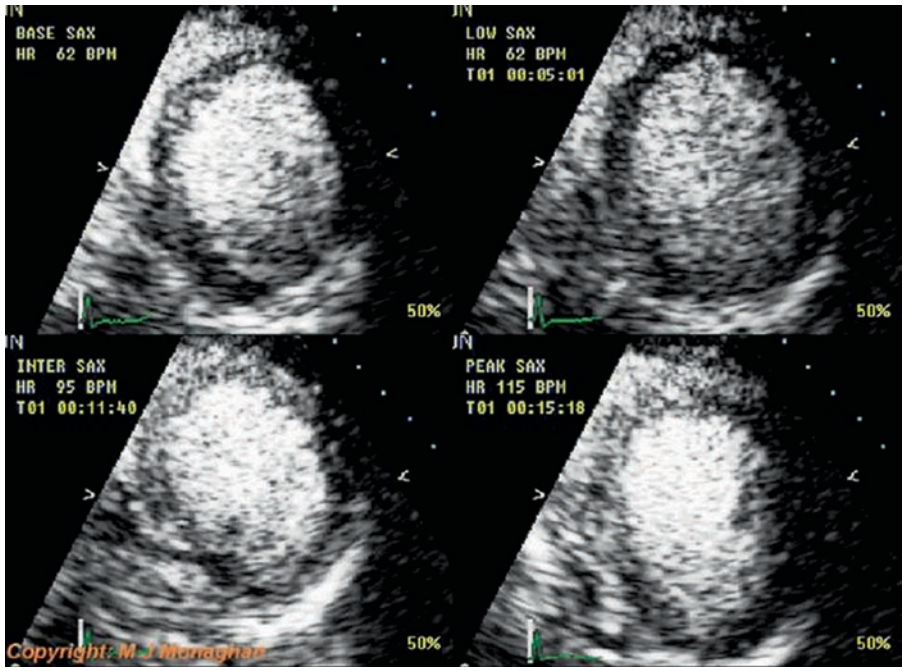

Fig. 30.15 Using low MI imaging, contrast attenuation is minimised and so parasternal views (as shown here) can usually be used. Good endocardial definition is seen at all stages of dobutamine stress and some myocardial enhancement is also evident, allowing appreciation of myocardial thickness

contrast, especially in the myocardium, and usually creates excellent endocardial definition in the few beats following destruction.

This section has concentrated on the use of contrast for improving endocardial definition during stress echo studies. This currently represents the major licensed application for contrast agents and is undoubtedly the appropriate starting point for introducing contrast into the echo lab. In the next section, the use of contrast is extended into the evaluation of myocardial perfusion. In the future, this role will become as important as improving endocardial definition.

Myocardial Perfusion

Stress Myocardial Perfusion

The classical ischemic cascade, as illustrated in Fig. 30.16, demonstrates that one of the first indicators of an imbalance between myocardial oxygen demand and supply is a reduction in myocardial perfusion. MCE has the ability to demonstrate both myocardial blood volume and velocity on a regional basis. The combination of these two parameters has been shown to represent myocardial blood flow, and we can assume that this is directly proportional to myocardial perfusion. Therefore, stress MCE has the potential to facilitate evaluation of stress-induced changes in myocardial perfusion. Since we know that these occur early in the ischemic cascade, they should be more sensitive markers than chest pain, ECG changes, or regional wall motion/thickening abnormalities. In addition, the excellent spatial resolution of MCE affords significant advantages over nuclear techniques. Cost, availability, and patient preference also means that stress MCE has the potential to be a more appropriate investigation than Stress CMR in the evaluation of reversible ischemia.

The intensity of backscattered ultrasound (i.e., video intensity) from a unit volume of myocardium is directly proportional to the number of scattering interfaces within that volume of myocardium. During MCE studies, those interfaces will consist of tissue structures and contrast microbubbles. Most contrast-specific imaging modalities suppress tissue signals so that the backscattered ultrasound signal intensity is mainly due, and proportional, to the number of contrast microbubbles within the unit volume of myocardium.

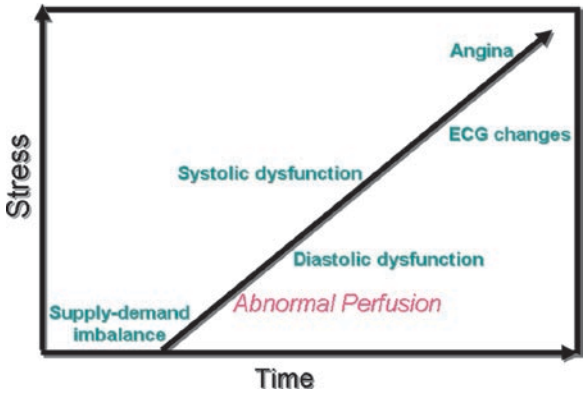

Fig. 30.16 The classical ischemic cascade demonstrating the sequence of events that occur during stress induced ischemia. Abnormalities in myocardial perfusion occur earlier than mechanical or ECG changes. Therefore, methods which are able to detect stress induced perfusion abnormalities should have good sensitivity for diagnosing reversible ischemia

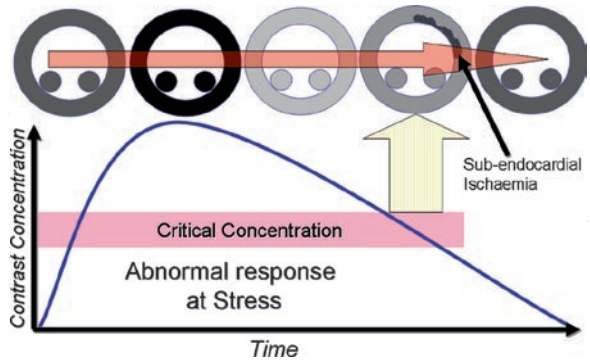

Fig. 30.17 Diagram illustrating the principle of using bolus injections during stress MCE studies. During the wash-out phase of the bolus, the contrast concentration falls through a critical level where it is possible to visualise spatial differences in myocardial blood volume secondary to ischemia. During the peak of the bolus, the myocardium is saturated with contrast and during the tail, the contrast concentration is insufficient to cause myocardial opacification. The available imaging time window, during which the critical concentration occurs, is fairly short

Since the contrast microbubbles are entirely contained within the vascular volume, the number of microbubbles, and hence backscattered signal intensity, is proportional to the blood volume within the myocardium being imaged. Hence the video intensity of the contrast signal we measure or see on the screen is directly proportional to myocardial blood volume.

Ischemia, as generated during stress in myocardial segments subtended by epicardial coronary vessels with flow-limiting lesions, results in a relative reduction in myocardial blood flow. Myocardial blood flow is directly proportional to the product of blood volume and velocity. Both these parameters can be readily evaluated and appreciated during stress MCE, using a variety of techniques, as described later.

An important variable in the methodology for stress MCE is the choice of stress agent. The choice is really between a positive inotrope such as Dobutamine, or a coronary vasodilator such as Dipyridamole or Adenosine.

These two classes of drugs work in different ways, and they have their own advantages and disadvantages. The inotropes work by increasing myocardial oxygen demand, and this in turn causes an increase in myocardial blood flow. However, in myocardial segments supplied by vessels with poor coronary flow reserve, flow is unable to increase and, in order to maintain adequate coronary perfusion pressure, capillary derecruitment occurs. This autoregulation mechanism means that myocardial blood volume effectively decreases in these segments and, therefore, the backscatter contrast signal intensity decreases as explained previously.

ume and reduced reperfusion rates following destruction. As previously explained, both these parameters can be evaluated from the myocardial contrast signal.

As previously discussed, real-time low MI imaging techniques provide excellent endocardial definition at adequate frame rates. Myocardial perfusion information can also be simultaneously obtained and is therefore incremental to the wall motion data. This methodology provides an excellent starting point for performing stress MCE studies.

The principle of performing stress perfusion imaging with a contrast bolus is illustrated in Fig. 30.17. During the decay portion of the contrast bolus, the contrast concentration in the myocardium falls through a critical level, where it is possible to differentiate ischemia-induced differences in myocardial blood volume. This is usually visualized initially in the subendocardium as a dark rim, while the subepicardium remains bright. As the contrast concentration decays further, the entire transmural extent of the myocardium becomes dark. Spatial variations in contrast enhancement during the bolus decay phase are critical aids to recognizing ischemic segments. A homogeneous, transmural decay in contrast intensity (mirrored in other segments at the same image depth) simply represents contrast decay, while heterogeneous opacification and especially a dark subendocardium is highly suggestive of stress-induced ischemia.

Myocardial segments that remain unopacified during the entire contrast administration usually represent

infarcted and irreversibly ischemic tissue. This is especially the case if a significant resting wall motion abnormality is present.

Although it is sometimes useful to record baseline myocardial contrast studies at rest, we know that even in the presence of an epicardial coronary stenosis <80%, resting myocardial blood flow will be normal. Therefore, if resting wall motion and thickening is normal in an individual segment, one can usually assume that perfusion will be normal and a contrast study at this point may be superfluous. If myocardial contrast opacification is absent in a normally contracting segment at rest then this represents an artifact due to attenuation or inadequate gain/ultrasound penetration. During stress, we would expect changes in perfusion to be evident before wall motion abnormalities. Therefore, the stress MCE images can be taken, if required, at a submaximal stage.

This technique can be utilized successfully during conventional dobutamine stress echo, since at low doses, dobutamine does act as a coronary vasodilator and during stress ischemia, changes in myocardial blood volume will occur, as described previously. The fact that this methodology can be used during dobutamine stress further underlines its suitability as a starting point for performing these types of studies.

If a contrast infusion is used in combination with low MI real-time imaging it is best to use a destruction-reperfusion technique for evaluating perfusion. The contrast infusion rate is set at a level which provides adequate myocardial opacification without contrast attenuation. Again, good endocardial definition is nearly always obtained, although if the myocardium is very bright, it can be difficult to differentiate it from the left ventricular cavity.

The low MI imaging methodology typically uses an output MI of <0.3, and often <0.1 (depending on the contrast agent characteristics). If a few frames (usually 5–10) of high output power (MI > 1.0) are fired using the "impulse," "burst," or "flash" function, then contrast microspheres will be destroyed. This usually results in the myocardial contrast effect disappearing, whereas the left ventricular cavity remains bright because the contrast concentration is significantly greater in the cavity. The wash-in of contrast into the myocardium, following destruction, can then be observed.

Careful adjustment of contrast infusion rate and machine settings is critical to ensure that complete contrast destruction in the myocardium occurs, without significant cavity destruction. Offline analysis of the images allows for a region of interest to be positioned within individual myocardial segments. The contrast signal intensity can then be plotted as a reperfusion curve, as illustrated in Fig. 30.18. As previously described, the slope of the curve is proportional to blood flow velocity

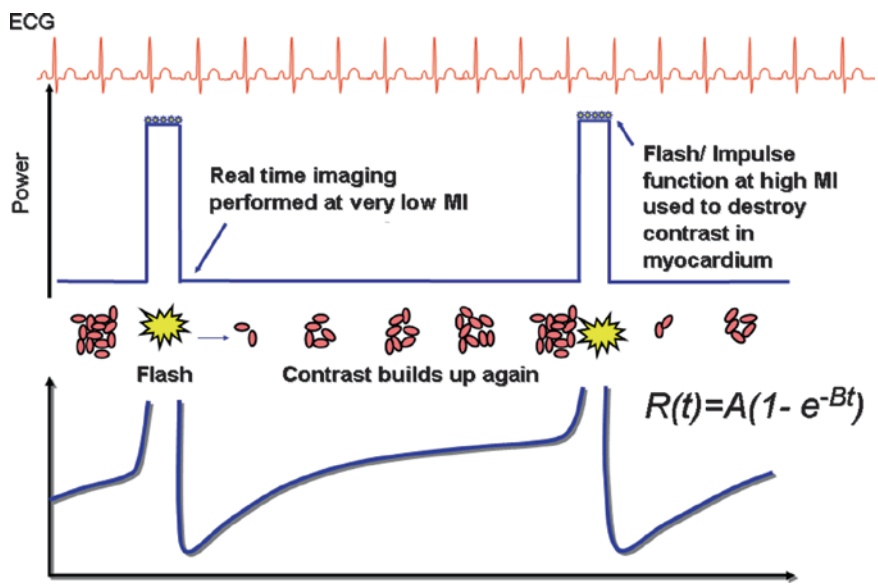

Fig. 30.18 Diagram illustrating the basic principles of low MI real-time perfusion imaging with flash/impulse contrast destruction. Following the destruction frames, contrast re-perfuses into the myocardium. A = the plateau portion of the re-perfusion curve and is proportional to myocardial blood volume. B = the initial slope of the curve and is proportional to blood flow velocity. R(t) is proportional to myocardial blood flow

and the plateau to blood volume. The product of both parameters is proportional to absolute blood flow, which will be reduced in ischemic zones. A comparison before and after stress (especially vasodilator) will permit an assessment of coronary blood flow reserve.

However, a semiquantitative approach can also be taken by direct observation of the number of cardiac cycles taken for an individual segment to reperfuse. Delayed reperfusion (>3–4 cycles at rest), especially in the subendocardium, is highly suggestive of ischemia. During stress, increased myocardial blood flow should mean that an individual segment will reperfuse more quickly than at rest, and this should occur in one cardiac cycle post destruction.

There is a naturally occurring cyclic variation in the myocardial contrast effect and this, together with segmental motion, can make interpretation of these images in a real-time mode difficult. Therefore, it is often easier to use a triggered capture mode on the ultrasound system, so that only end-systolic or end-diastolic frames are stored. Subsequent analysis of these frames, without the confounding effects of cyclic intensity variations and wall motion, is often easier.

Again this methodology can be used with both inotropic or vasodilator stress, as previously outlined. In practice, it is most commonly utilized with vasodilator stress since it is perfusion alone, rather than perfusion and wall motion data that are being analyzed. However, in Fig. 30.19 the use of this technique during dobutamine stress, demonstrating both perfusion and wall motion abnormalities, is seen.

As previously mentioned, high MI imaging causes destruction of contrast microspheres within the myocardium (second harmonic imaging, pulse inversion imaging). In addition, the destruction and subsequent disappearance of the microspheres paradoxically

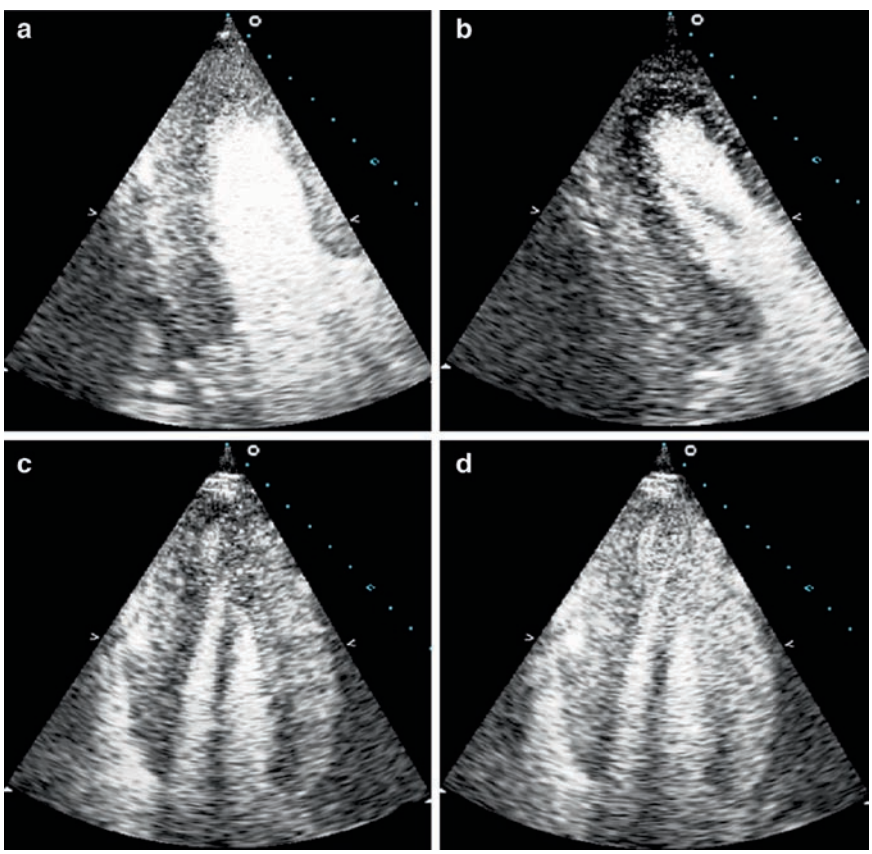

Fig. 30.19 Contrast destruction-reperfusion study during dobutamine stress echo in a patient with 70% mid LAD lesion and severely diseased RCA with a 90% lesion. Panels A and B are end-systolic apical 2 chamber views at rest (**a**) 3 beats post destruction and at peak stress (**b**) 1 beat post destruction. A significant subendocardial defect is seen in the anterior, apical and inferior walls. Panels C and D are both apical 4 chamber views at peak stress. Panel C is 1 beat post destruction and shows an apical and septal subendocardial defect. It also demonstrates and aneurysmal "pouching" of the apex which was even more evident on real-time images. Panel D is 3 beats post destruction and the subendocardial defects have filled in although the apical shape distortion is still evident

enables their detection with harmonic power Doppler methodology. Due to contrast destruction, these methods are utilized with intermittent imaging, and therefore no wall motion data are available.

By varying the triggering interval from one frame every cardiac cycle to up to one frame every ten cycles it is possible to obtain data on myocardial blood flow. It is important to step through an acquisition sequence where the triggering interval is varied and increased in a stepwise fashion. Software on some ultrasound systems permits the creation of a triggering sequence which simplifies and standardizes image acquisition.

During long triggering intervals it can be difficult to maintain a constant scan plane, since the echocardiographer has no moving landmarks. It is possible on some ultrasound systems to utilize low MI real-time imaging ("monitoring mode") between the high MI destructive frames, and this certainly makes performing intermittent imaging much easier.

The other important issue during this type of stress MCE imaging is to decide which part of the cardiac cycle should be used for the trigger acquisition point. Although there is no absolute rule, end-systole is most commonly utilized because the myocardium is thicker, the left ventricular cavity is small, and contrast attenuation is limited. Setting up the instrument controls for this type of imaging requires considerable experience in order to avoid artifacts caused by wall motion, contrast attenuation, or incomplete contrast destruction.

Since myocardial blood flow increases during stress we would expect that reperfusion will occur with shorter trigger intervals than at baseline. For example, during vasodilator stress using either dipyridamole or adenosine, the normal coronary flow reserve response results in blood flow increasing by a factor of four. Therefore, at rest it may take a trigger interval of four cardiac cycles for an individual segment to reperfuse. However, under maximum coronary vasodilation, reperfusion should occur in one cycle. So we can compare baseline images with a trigger interval of four cycles to stress images acquired with a one-cycle interval.

An example of this technique is shown in Fig. 30.20. This study was performed using intermittent harmonic power Doppler imaging and a continuous

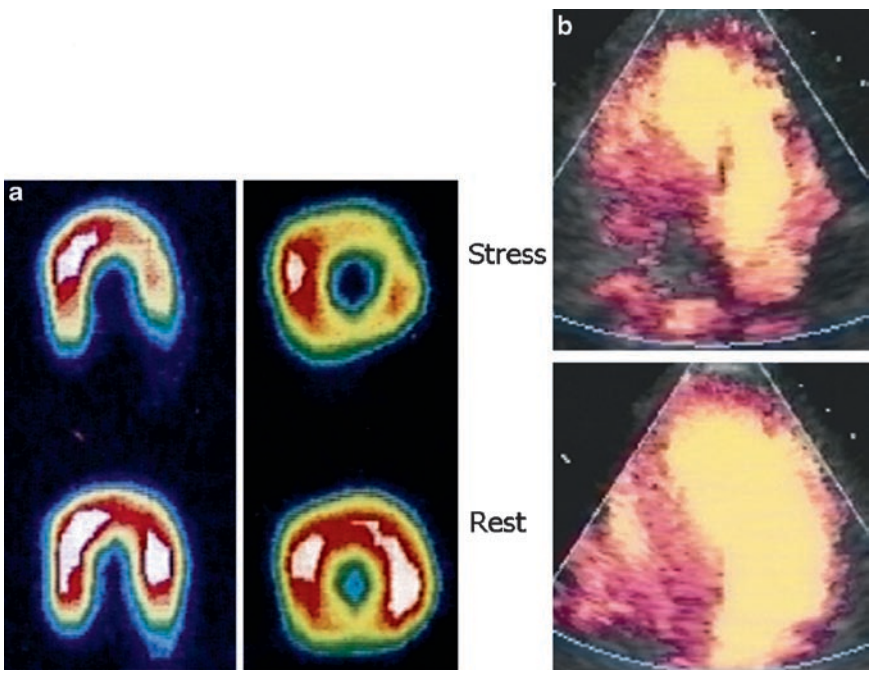

Fig. 30.20 (**a**) Sestamibi and MCE (Ap4c) scans obtained at rest and during dipyridamole stress. End-systolic contrast MCE images were obtained using a contrast infusion and intermittent harmonic power Doppler imaging. Resting MCE images were acquired with a 4 beat trigger interval whereas a 1 beat trigger interval was used at peak stress to compensate for increased myocardial blood flow. A reversible defect is seen in the basal septum, apex and apical lateral wall. This correlates well with the Sestamibi scans and the coronary anatomy demonstrated in figure 20b. (**b**) Coronary angiograms from the patient shown in figure 20a. The LCX is occluded but has collaterals. Previous angioplasty has been performed in the LAD and RCA. In addition, the postero-basal LV segments were hypokinetic on the resting echocardiogram.

infusion of a contrast. The baseline images are acquired using a four-beat triggering interval and demonstrate relatively homogeneous perfusion in all segments. However, during dipyridamole stress, the images acquired at a one-beat interval demonstrate a reversible perfusion defect in the basal septal, apex, and apical lateral segments. These defects correlate well with the coronary anatomy and the stress Sestamibi scan obtained at the same time.

Although this form of stress MCE is usually performed with vasodilator stress, it can also be utilized with inotropic stress. As previously mentioned, coronary physiology dictates that during stress-induced ischemia, relative reductions in myocardial blood volume, secondary to capillary derecruitment, will result in slower reperfusion into ischemic territories. Therefore, at short triggering intervals during stress, a perfusion defect may be visualized. Increased wall motion, due to the inotropic effect, may result in more wall motion artifacts when this type of stress is used. Consequently, harmonic power Doppler is more commonly used in combination with vasodilator stress.

A relative reduction in myocardial perfusion is one of the earliest consequences of reversible myocardial ischemia. MCE can detect myocardial contrast parameters which are directly related to perfusion at both rest and stress. This technology therefore has the potential to increase the diagnostic sensitivity for the detection of reversible ischemia over and above that already established for conventional stress echo. Since stress MCE can be used in combination with conventional stress echo techniques and can provide enhanced wall motion plus perfusion data, it should also increase our diagnostic confidence.

Acute Coronary Syndromes

Following acute myocardial infarction, the aim of treatment must be to salvage as much myocardium as possible using some form of reperfusion therapy. It is important to know if patency has been restored to the infarct-related artery and if microvascular perfusion has been achieved. The demonstration of microvascular perfusion implies microvascular integrity and therefore myocardial viability. As discussed in the forthcoming section, demonstration of microvascular integrity is correlated with a reduction in infarct size, prevention of remodeling, and is a predictor of reduction in major cardiac events.

As previously discussed, contrast microbubbles remain entirely within the intravascular space and provide important information on regional myocardial perfusion. Despite restoration of coronary artery patency, prolonged ischemia may cause sustained microvascular damage and absence of microvascular perfusion. This is known as the low-reflow or no-reflow syndrome. Therefore, in the setting of acute myocardial infarction, contrast echo should be able to provide information on infarct size, patency of the infarct-related artery, and myocardial viability.

In Fig. 30.21 an apical 4-chamber power modulation contrast perfusion image is seen in a patient with an acute anterior myocardial infarction treated with thrombolysis. At the apex a perfusion defect is seen

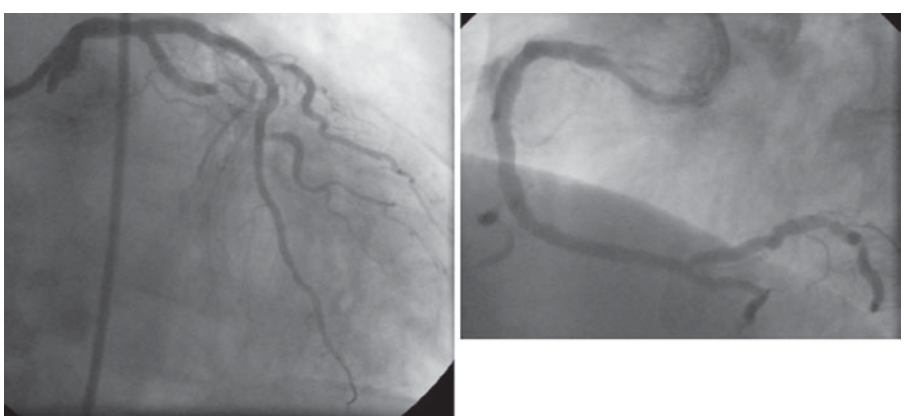

Fig. 30.21 Ap4c power modulation contrast perfusion image in a patient with an acute anterior myocardial infarction treated with thrombolysis. At the apex a perfusion defect is seen which is almost completely transmural (no-reflow). Whereas the septum demonstrates patchy perfusion and a subendocardial rim of poor perfusion (low-reflow). The patient proceeded acutely to angiography and stenting of a 99% LAD lesion

which is almost completely transmural (no-reflow), while the septum demonstrates patchy perfusion and a subendocardial rim of poor perfusion (low-reflow). The patient proceeded acutely to angiography and stenting of a 99% LAD lesion.

We know that the size of a perfusion defect late after a destruction-reperfusion sequence corresponds to the ultimate infarct size and that the rate of replenishment predicts collateral flow. The image seen in Fig. 30.21 was obtained >10 beats following destruction, and we can see a fairly large perfusion defect that has clearly failed to replenish. We know therefore that there is a fairly extensive area of myocardium at jeopardy which is unsupported by collaterals. Furthermore, the near transmural extent of the apical defect implies failure of thrombolysis to achieve infarct-related artery patency. Hence the decision in this case to proceed to urgent percutaneous intervention. Post restoration of patency, it is probably sensible to wait >3 h before repeating contrast perfusion studies because the presence of postischemic hyperemia may cause an underestimation of ultimate infarct size.

Contrast echo is well placed to evaluate myocardial status post acute infarction at the bedside. Perfusion parameters in the infarct zone have been shown to correlate with important clinical and angiographic data. They may be used to guide acute management and help achieve the ultimate goal of myocardial salvage.

Myocardial Viability Studies

As previously mentioned, the presence of contrast opacification of the myocardium implies an intact coronary microvasculature. Intact coronary microvasculature is a prerequisite for maintaining myocardial viability. When viable myocardium is not present, the microcirculation collapses and therefore contrast opacification will be reduced, patchy, or absent.

Ito demonstrated in 1992 that in 25% of their patients with myocardial infarction and no myocardial contrast opacification, despite a patent infarct-related artery, regional and global LV function were worse at 1-month follow-up, compared to those showing opacification in the infarct bed.

An example of a patient with no opacification in the infarct bed is shown in Fig. 30.22. The lack of microvascular integrity in this thin infarct bed implies no myocardial viability. A low-dose dobutamine study confirmed lack of contractile reserve in the same area,

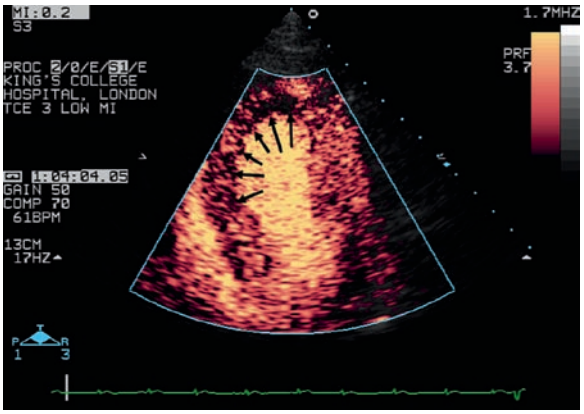

Fig. 30.22 Apical 4 chamber views at rest (left) and during low dose (20 μg/kg/min) dobutamine stress (right) in a patient with extensive anterior myocardial infarction. Simultaneous low-MI contrast perfusion imaging has been performed and demonstrates no contrast opacification in the apical segments but relatively good opacification of the septum and lateral wall. This implies lack of microvascular integrity in the apical myocardium and this same territory also failed to demonstrate any contractile reserve during low dose dobutamine

and revascularization of an occluded LAD lesion was not attempted. It appears that contrast echo may have a higher sensitivity but lower specificity than dobutamine stress echo for predicting recovery of function in this setting. Therefore it may be reasonable to also perform a dobutamine stress if contrast opacification is not seen. However, there are a number of technical factors that may contribute toward this apparent lack of specificity, especially early after acute myocardial infarction. These include dynamic changes in the myocardium, reactive hyperemia, and the fact that subendocardial infarction can render the myocardium akinetic, despite viable myocardium existing in the epicardial layers. Furthermore, if improvement in function post revascularization is taken as the "gold standard" for viability, then we may be missing an important group of patients, where prevention of remodeling would be just as important.

Myocardial blood flow velocities may be very low in akinetic but viable myocardial segments; therefore, it may take >10 beats post destruction for a segment to reopacify with contrast following destruction. So it is important to wait for between 10 and 15 beats before making a judgment on microvascular integrity. In Fig. 30.23, late opacification of the distal akinetic septum was seen in this patient with previous anteroseptal infarction. Follow-up echo studies post revascularization demonstrated a significant improvement in wall

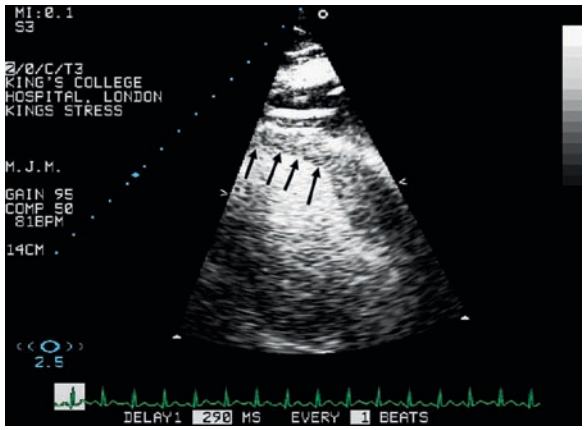

Fig. 30.23 End-systolic parasternal long axis view during low-MI contrast perfusion imaging in a patient with an anteroseptal infarct. The distal septum is thin compared to the basal septum and it was akinetic however it did opacify late with contrast, implying microvascular integrity. Furthermore, subsequent low dose dobutamine stress study demonstrated contractile reserve in this territory. PTCA was performed to a high grade proximal LAD lesion and a follow-up echocardiogram at 2 months demonstrated only minor antero-apical hypokinesia

motion. Although this patient also had a low-dose dobutamine stress echo to demonstrate contractile reserve, the demonstration of viability by contrast really made this superfluous. It may be that contrast studies will replace dobutamine stress echo and other techniques for assessment of myocardial viability in the future. Certainly, cost, accessibility, spatial resolution, lack of ionizing radiation, and the fact that it is a bedside technique confers many advantages over more traditional methods of assessing this phenomenon.

Future of Contrast Echo

Drug Delivery

An interesting and very promising use of contrast appears to be in the area of drug delivery or gene therapy. When a contrast microbubble is destroyed by ultrasound it appears that extreme shear forces are created around the bubble. These shear forces may open up pores in the vessel endothelium and/or cell membrane. If a drug or relevant DNA is attached to the bubble by binding, electrostatic charge, or by incorporating it within the bubble structure then it has been shown bubble disruption significantly enhances transfection of the carried material into the vessel wall or cell matrix.

This has the potential of allowing high concentration local delivery of drugs or genes to a specific area of interest in an organ, without exposing the whole body to potentially toxic levels of the material. Contrast microbubbles can be designed to have a critical fragility so that they can be visualized in the circulation at a low MI or certain imaging frequency without destruction. Then they can be destroyed/disrupted at a desired location by applying one or more focused ultrasound beams which have a power or frequency designed to exceed the bubble fragility limit. Potential applications of this technology include treating thrombus, ischemia/infarct, infection, neoplasm, gene delivery, and angiogenesis. In addition contrast agents have also been shown in the experimental setting to enhance thrombus lysis and also to enhance the detection of endothelial dysfunction by adhering to inflammatory endothelial extracellular matrix.

While these techniques have yet to be applied clinically, experimental studies are extremely promising and the applications of contrast echo will undoubtedly be further expanded in the future.

3D Contrast Studies

Real-time 3D echocardiography offers significant advantages in the analysis of left ventricular volumes, ejection fraction, regional wall motion, and shape over conventional 2D echo techniques. However, 3D suffers from the same degradations in image quality that beset 2D echo. In particular, lung and rib artifacts can significantly degrade endocardial definition on 3D studies. Contrast agents can improve 3D image quality and endocardial definition to the same extent that they improve 2D images. However, since "whole volume" 3D images are usually acquired over several cardiac cycles, it is preferable to use a contrast infusion rather than a bolus.

Real-time 3D echo is emerging as a useful technique during stress echocardiography, and again contrast is proving to be an invaluable tool to enhance analysis of wall motion and thickening during these studies.

Preliminary attempts to demonstrate myocardial perfusion using real-time 3D echo have been extremely

encouraging, although this is a research technique at the time of writing. The potential of being able to calculate precisely, in 3D, infarct size of volume of ischemic myocardium, etc. is very exciting.

Conclusion

Contrast echo has proved itself an invaluable technique for the enhancement of endocardial borders in patients with suboptimal images and during stress studies. In addition, the delineation of intracardiac masses and the enhancement of cardiac Doppler signals is also proving an important application, although not as widely used. However, the major clinical utility of ultrasound contrast agents in the heart is in the evaluation of myocardial perfusion. Whether used for demonstrating reversible ischemia, myocardial viability or following acute myocardial infarction, contrast agents can significantly enhance diagnosis at the bedside and positively influence patient management. They have also been shown in several studies to reduce the need for further investigations in patients with poor echo windows and therefore are highly cost effective.

Chapter 31
Three-Dimensional Echocardiography

J.R.T.C. Roelandt

Although two-dimensional echocardiography (2DE) was a major step forward for the noninvasive assessment of cardiac structure and function, the diagnosis of complex disorders remained a difficult mental conceptualization process. In addition, the measurement of left ventricular volume and function, the most common referral reason for echocardiography, required important geometric assumptions about its shape causing inaccuracy and significant variability. Also, quantitative assessment of the right ventricle and left atrium with their peculiar shape continued to be elusive. Consequently, imaging methods to display cardiac structures in relationship to each other in the three spatial dimensions were investigated soon after the introduction of 2DE in the 1970s.

Three-Dimensional Imaging Techniques (Table 31.1)

The initial approach to three-dimensional echocardiography (3DE) was the offline reconstruction of a volumetric dataset using an external positional locator (mechanical, acoustic, optical, or electromagnetic) linked to the transducer for recording the spatial coordinates of each individual image.[1-4] This method allowed free hand transthoracic scanning from one or multiple acoustic windows (Table 31.1). An intersectional line or an image plane (usual a long-axis view) is used as a reference for the position and orientation of all other recorded imaging planes.[5] Gated end-respiratory end-diastolic and end-systolic LV contours were obtained and manually traced to produce a wire-frame or surface-rendered reconstruction of the LV cavity. The whole procedure was tedious and time consuming, the images static, and there was no tissue information. Consequently, this approach has not been clinically successful. However, the LV volume and mass quantification from these LV reconstructions in both symmetrical and aneurysmatic ventricles proved to be more accurate and reproducible than from 2DE.[6,7]

The next generation of 3DE techniques was based on an internal coordinate system in which a continuum of 2D images is captured by a stepwise computer-controlled transducer motion (linear, fan-like, or rotational).[8-11] To realize dynamic imaging, a steering logic algorithm, which considers the heart cycle and respiration phase, controls the stepwise image acquisition. A workstation is used to input the images for Cartesian coordinate conversion and the reconstruction of a volumetric dataset. Rendering algorithms provide cavity and tissue information with the aid of computer interpolation. Paraplane analytic methods provide multiple equidistant parallel short-axis planes allowing a systematic cross-sectional review of the 3D dataset. The transthoracic reconstruction approaches have not been widely accepted because of the frequent artifacts and the marginal image quality for making diagnostic decisions. The method has been used mainly in combination with transesophageal echocardiography using rotational transducer motion.

Rotational techniques to shorten the acquisition time have been proposed. Fast continuous rather than stepwise rotational scanning allows scanning of the LV and rapidly provides the basic 2D images for 3D reconstruction and LV volume calculation.[12,13] Acquisition can only be performed from an apical transducer position.

J.R.T.C. Roelandt
Department of Cardiology-BD-589, Erasmus MC,
Dr. Molewaterplein 40, 3015 GD Rotterdam,
The Netherlands
e-mail: j.r.t.c.roelandt@erasmusmc.nl

P. Nihoyannopoulos and J. Kisslo (eds.), *Echocardiography*,
DOI: 10.1007/978-1-84882-293-1_31,

Table 31.1 Three-dimensional echocardiography: approaches

Reconstruction techniques
External reference system (nonsystematic image acquisition or free-hand scanning)
Mechanical arm[1]
Acoustic (spark gap) locator[2]
Optical sensor[3]
Electromagnetic sensor[4]
Internal reference system (systematic image acquisition by predetermined transducer motion)
Linear transducer motion[8]
Fan-like transducer motion[9]
Rotational transducer motion (stepwise or continuous)[10-13]
Real-time three-dimensional acquisition

The transesophageal rotational approach has made major contributions. The advantages of dynamic 3D imaging for analyzing complex pathomorphology and sectioning structures at various levels (paraplane) and angulations (anyplane), together with the "en face" visualization of pathology from any perspective, were amply documented (Fig. 31.1). It was also shown that the quantification of LV and RV volumes and function is more accurate and more reproducible than with 2DE by overcoming the problem of cavity foreshortening and avoiding the need of geometric assumptions (Table 31.2).[14-22]

A quantum leap forward in 3DE was the development of matrix-array transducers which with more powerful microelectronics allows the real-time acquisition and rendering of pyramidal volumetric datasets from a transthoracic fixed transducer position. ECG and respiratory cycle gating as well as motion artifacts resulting from misregistration of images due to transducer or patient movement during the long acquisition time of the reconstructive techniques are now avoided.

In an earlier RT3DE system developed at Duke University, a sparse matrix phased-array transducer of 512 elements to scan 60° × 60° pyramidal volume was used.[23] Parallel processing was applied to permit the reception of 16 lines for each transmitted signal, which allows an imaging rate of 17 pyramidal volumes/s with a depth of 16 cm. This system was mainly used for the simultaneous display of two perpendicular long-axis views or three views orthogonal to the long axis in selected orientations (C-scans).[24] However, the image quality was rather poor which has limited its widespread application.

Another approach was used in real-time triplane 3DE. In this system, three equally spaced long-axis views are simultaneously acquired with the matrix-array transducer from the same heart beat. Surface-rendered

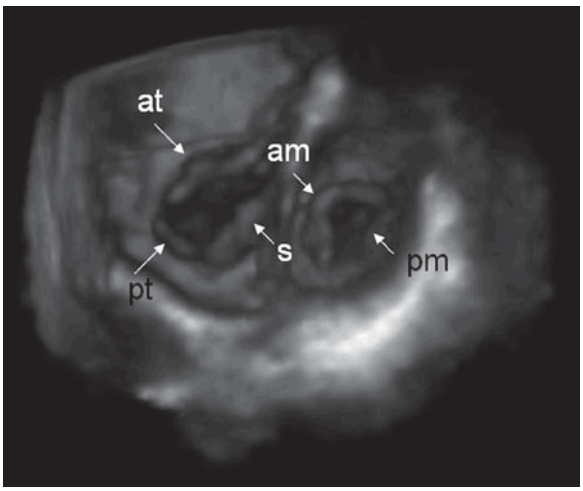

Fig. 31.1 "En face" image of the tricuspid and mitral valves seen from an apical perspective. *Am* anterior mitral valve leaflet; *at* anterior tricuspid leaflet; *pm* posterior mitral leaftlet; *pt* posterior tricuspid leaflet; *s* septal tricuspid leaflet

LV cavities are reconstructed after tracing the endocardial contours.

The second generation RT3DE systems is based on a complex matrix array, which contains around 3,000 miniature elements. Each of these elements is electronically controlled by a microbeam former incorporated in the transducer head to achieve multidirectional beam steering through a pyramidal volume of 30° × 60°. To capture a dataset large enough to encompass the whole (dilated) LV from the apical transducer position, four or seven consecutive ECG triggered real-time volumes of 20° × 93° are acquired during held respiration and electronically "stitched" together in a composite pyramidal dataset of 80° × 90°.

Powerful microelectronics process multiple data streams in the transducer and the cardiac structures are reconstructed and rendered in the ultrasound system memory. This process is extremely fast and allows the real-time display of the rendered images (Fig. 31.2). Real-time 3D color Doppler flow has been integrated in the volumetric images and allows the combined display of blood flow and tissue data (Fig. 31.2). This provides hemodynamic information from RT3DE studies. The origin, direction, and size (volume) of the jet can be directly appreciated. Quantification of jets is currently being investigated.[25]

Anyplane and paraplane sectioning of the dataset and cropping away parts of the pyramidal dataset allow online assessment of the relationship, orientation, and

Table 31.2 Left ventricular volume and function measurement by reconstruction 3DE in comparison with magnetic resonance imaging

Author/reference	Object	*n*	*r*	SEE	Mean diff. ± SD
Stepwise acquisition					
Gopal et al[7]	EDV	15	0.92	7 ml	
	ESV	–	0.81	4 ml	
Iwase et al[16]	EDV	30	0.93		−17 ± 23 ml
	ESV	–	0.96		−4 ± 18 ml
	EF	–	0.85		−2 ± 6%
Buck et al[17]	EDV	23	0.97	14.7 ml	−10.7 ± 14.5 ml
	ESV	–	0.97	12.4 ml	−3.4 ± 12.9 ml
	EF	–	0.74	5.6%	−2.5 ± 6.7%
Altmann et al[18]	EDV	12	0.98	8.7 ml	−14.2 ± 8.3 ml
	ESV	–	0.98	5.6 ml	−3.4 ± 5.5 ml
	EF	–		5.3%	−4.4 ± 5.3 ml
Nosir et al[19]	EDV	46	0.98		−1.4 ± 13.5 ml
	ESV	–	0.98		−1.5 ± 10.5 ml
	EF	–	0.98		0.2 ± 2.5%
Kim et al[20]	EDV	18			6.4 ± 20 ml
(patients)	ESV	–			
	EF	–			0.0 ± 13.3 ml
					1.4 ± 3.5 %
(volunteers)	EDV	10			−3.1 ± 4.9 ml
	ESV	–			−1.4 ± 2.2 ml
	EF	–			0.5 ± 1.8%
Poutanen et al[21] (children)	EDV	21	0.80		4.0 ± 19.6 ml
	ESV	–	0.88		0.4 ± 13.0 ml
	EF	–	0.20		1.7 ± 15.1%
Mannaerts et al[22]	EDV	17	0.74		−13.5 ± 13.5%
	ESV	–	0.88		−17.7 ± 23.9%
	EF	–	0.89		−1.8 ± 5.8%
Krenning et al[13]	EDV	15	0.98	13.4 ml	−22.7 ± 27.2 ml
	ESV	–	0.99	8.7 ml	−12.6 ± 19.8 ml
	EF	–	0.97		

3DE three-dimensional echocardiography; *n* number of subjects; *r* correlation coefficient; *SEE* standard error of estimate; *diff*. difference; *SD* standard deviation; *EDV* end-diastolic volume; *ESV* end-systolic volume; *EF* ejection fraction

motion of any structure and blood flow from different perspectives in a fashion similar to magnetic resonance imaging. Optimal cross-sectional planes can be reconstructed for accurate measurement of various dimensions and surface areas of cavities, defects, and diseased valves. The "en face" views uniquely allow to understand the morphology of these surface areas. A zoom mode permits focusing in on a specific structure.

Image quality is the most important aspect of any imaging system and is crucial for quantitative analysis of RT3DE. The rapid developments in microelectronics have increasingly contributed to improved image quality and the method continues to evolve rapidly.

A major step forward has recently been made with the introduction of broadband (1–5 MHz) monocrystal transducer technology. The electromechanical efficiency of these monocrystals is 80–100% better than that of the currently used piezoelectric crystals making them twice as sensitive. This results in better penetration, resolution, and a better signal-to-noise ratio. These transducers allow high-resolution harmonic imaging with improved cavity delineation. They also offer advantages when left heart contrast agents are needed in patients with less than optimal image quality as the tissue/contrast echo separation is better handled. However, continuous contrast infusion or contrast agents, which are more resistant to ultrasound pressure, must be used since acquisition of LV full-volume data requires several heart cycles.

The first clinical results with a transthoracic phased-array monocrystal transducer for 2DE and a pediatric matrix-array monocrystal transducer for RT3DE are

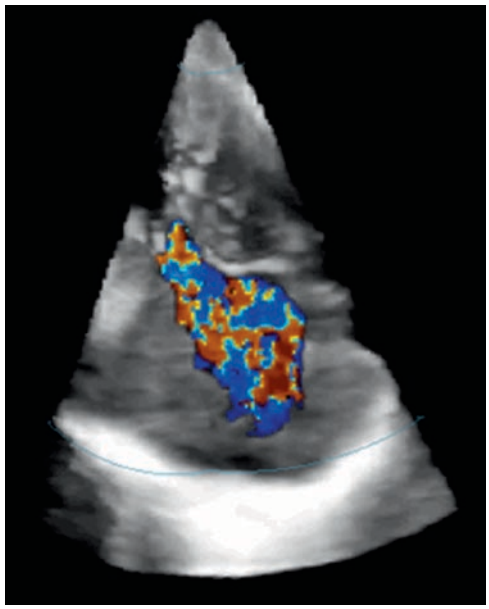

Fig. 31.2 Image obtained from a real-time 3DE study of a patient with tricuspid regurgitation. The dilated right atrium with the color Doppler regurgitant jet is seen

already available (Fig. 31.3). The image quality and the resolution are excellent and competitive with MRI. The advantages over MRI in babies and small children is that no sedation is needed during the examination. Transesophageal monocrystal matrix transducers for RT3DE will become available since the higher efficiency allows the construction of a much smaller matrix transducer with good imaging performance. Clearly, the improved image quality will have a major impact on the diagnostic performance and automated quantitative analysis for global and segmental function.

Clinical Uses (Table 31.3)

An examination protocol for a systematic 3DE examination has been proposed.[26] The real-time "en face" display of structures in relation to each other has significant advantages for the assessment of *valvular disease*.

However, most of the advantages of 3DE for valvular assessment and management have already been documented with reconstruction 3DE and are now further confirmed with RT3DE[27-31] (Figs. 31.4–31.8). The major advantage is that the data are now obtained from

Table 31.3 Three-dimensional echocardiography: clinical uses

Current applications
Analysis of complex (patho) morphology
Valvular heart disease
Congenital heart disease
Quantification of cavity volumes and function (LV, RV, and LA)
Planning and guiding interventions
Future applications
Multiparametric imaging
Virtual reality, holographic display
Innovative research

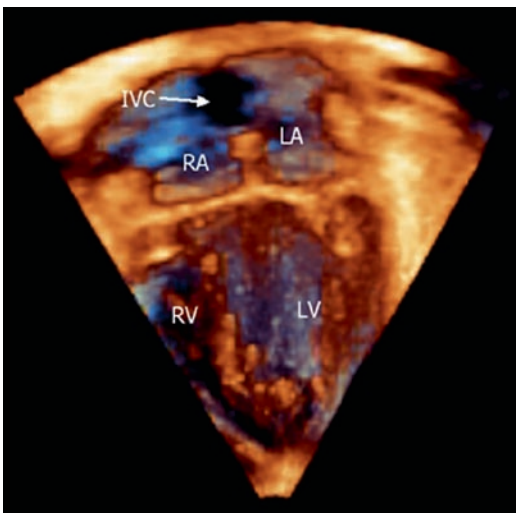

Fig. 31.3 An image from a real-time 3D study with a monocrystal matrix-array transducer of a newborn infant (3 kg) with a double inlet left ventricle. *IVC* inferior vena cava; *LA* left atrium; *LV* left ventricle; *RA* right atrium; *RV* right ventricle. (Courtesy: J. Simpson, Guy's Hospital, London)

a precordial rather than transesophageal approach, but the success rate of adequate images is less.[32]

RT3DE provides a dynamic view from any perspective of the surgical anatomy of the diseased valve giving the surgeon an advanced look on what he will encounter intraoperatively (Figs. 31.9 and 31.10). This is crucial for the decision to repair or replace the valve. Anyplane and paraplane analysis of the stenotic valve helps to find the cutplane through the smallest area for accurate planimetry (Fig. 31.10). Zamorano et al[33] showed in a series of 29 patients that the planimetered orifice area from RT3DE had the highest accuracy when compared to invasive methods.

Xie et al[34] showed in their study a good correlation between RT3DE valve area and pressure half-time. In mitral valve prolapse the exact location and the extension

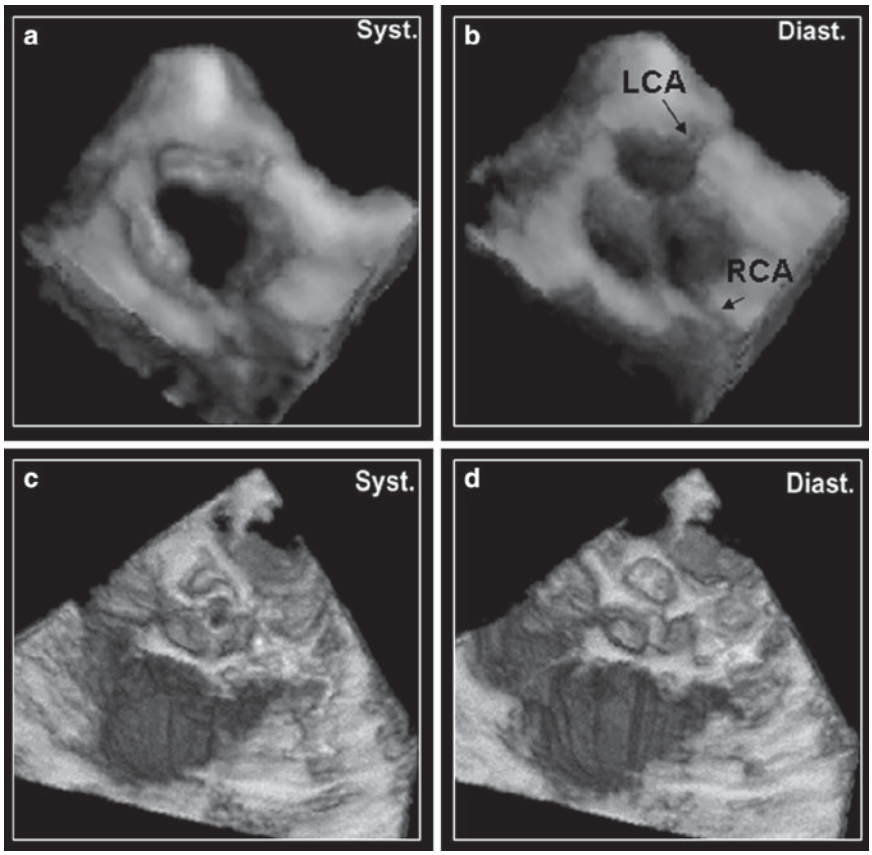

Fig. 31.4 Reconstruction 3DE systolic and diastolic images of a normal aortic valve (**a**, **b**) and of a patient with severe aortic stenosis (**c**, **d**). Note the small stenotic orifice. *LCA* and *RCA* left and right coronary arteries

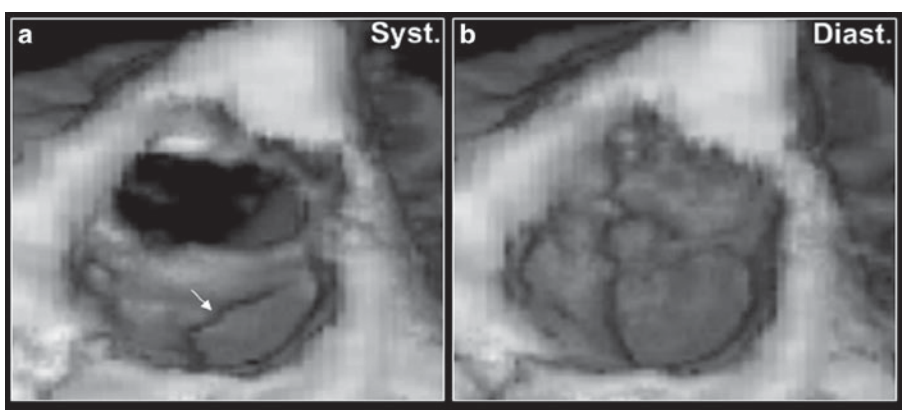

Fig. 31.5 Reconstruction 3DE images of a bicuspid aortic valve in systole (**a**) and in diastole (**b**) seen from above (surgical view). The mouth-like orifice and the raphe (*arrow*) are visualized

of the bulging leaflet(s) are clearly visualized which is most useful when the pathology is complex.[32,35,36] Pseudoprolaps are also more easily recognized[37] and the origin, direction, and distribution of the regurgitant jet(s) are now better evaluated with the dynamic color flow volumetric display.

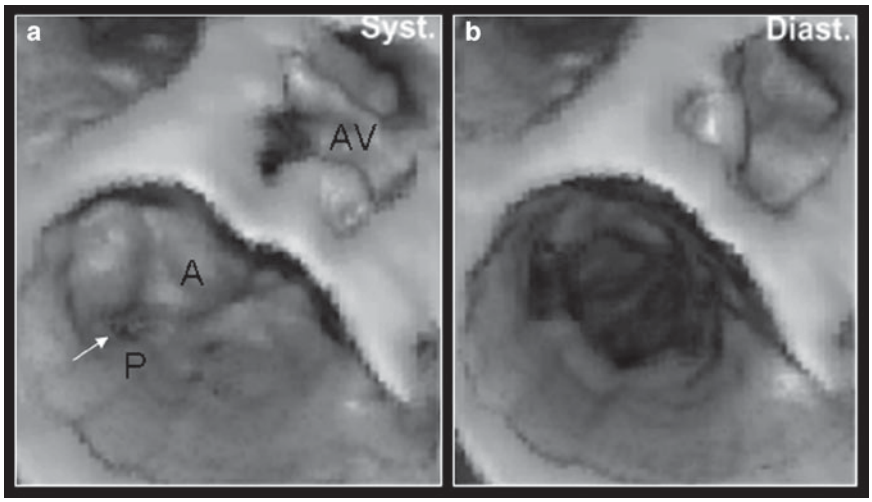

Fig. 31.6 Reconstruction 3DE images of a mitral valve prolaps seen from an atrial perspective (surgical view). The prolapsing scallops of the anterior (aortic) leaflet and lateral commissural leaflets are bulging into left atrium in systole (**a**). Note lack of cooptation between the mitral leaflets (*arrow*). The aortic valve (AV) is open in systole and closed in diastole (**b**). *A* anterior (aortic) mitral leaflet; *P* posterior mitral leaflet

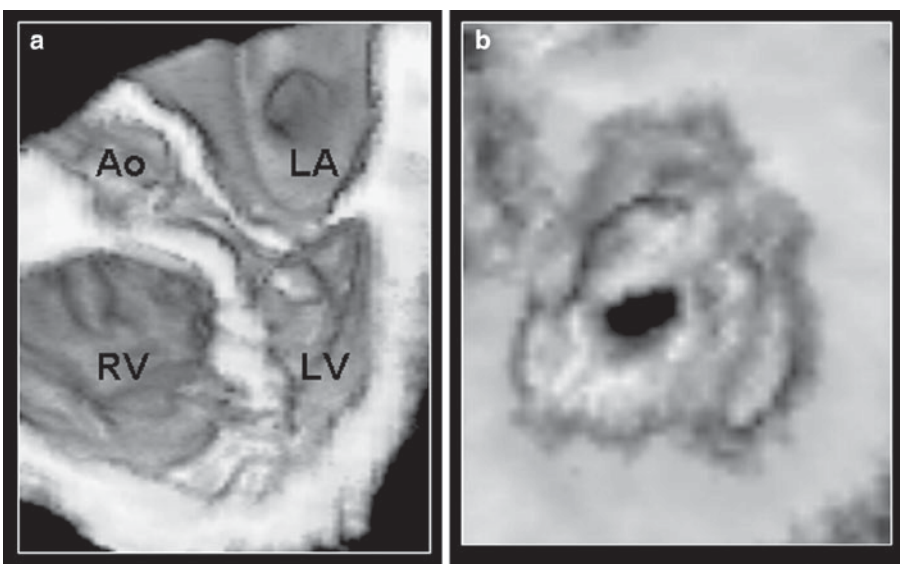

Fig. 31.7 Mitral stenosis. (**a**) The 3D dataset is sliced in a long-axis view and shows the dilated right ventricle (RV) and left atrium (LA). The bulging stenotic mitral valve is seen. (**b**) Short-axis view on the stenotic mitral valve from an apical perspective. The orifice size and the shape are visualized

In *congenital heart disease*, RT3DE is particularly useful by better visualization of complex spatial relationships. Valvular abnormalities, location of defects as well as their size, shape, and neighboring structures are readily appreciated (Figs. 31.11 and 31.12). "En face" views are particularly useful and allow accurate measurement of the dimensions of a defect and the surrounding tissues which is crucial for planning interventional procedures.[38-41] Most children and young adults have good image quality. In newborns and babies, the new high-frequency transducers allow excellent imaging which makes it the superior imaging modality in that age group (Figs. 31.3 and 31.13). The real-time 3D display also offers significant advantages

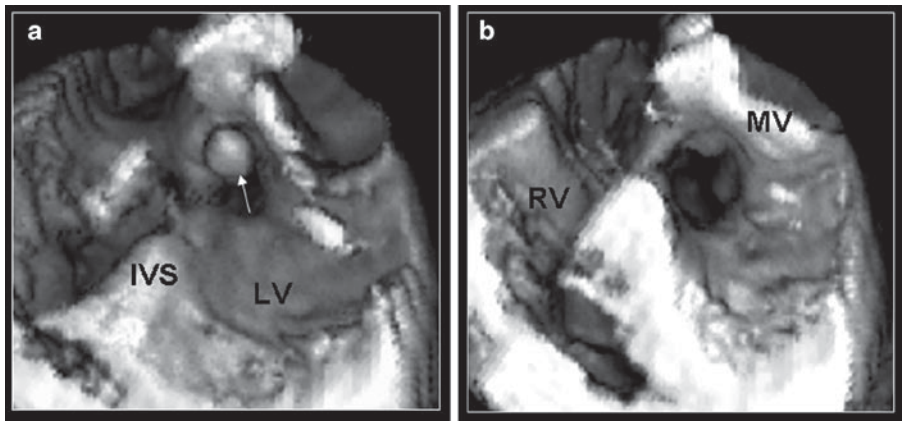

Fig. 31.8 Diastolic 3DE reconstruction images from a study of a patient with an aortic valvular vegetation (*arrow*) seen in the left ventricular outflow tract from an apical perspective. *IVS* interventricular septum; *LA* left atrium; *LV* left ventricle; *RV* right ventricle

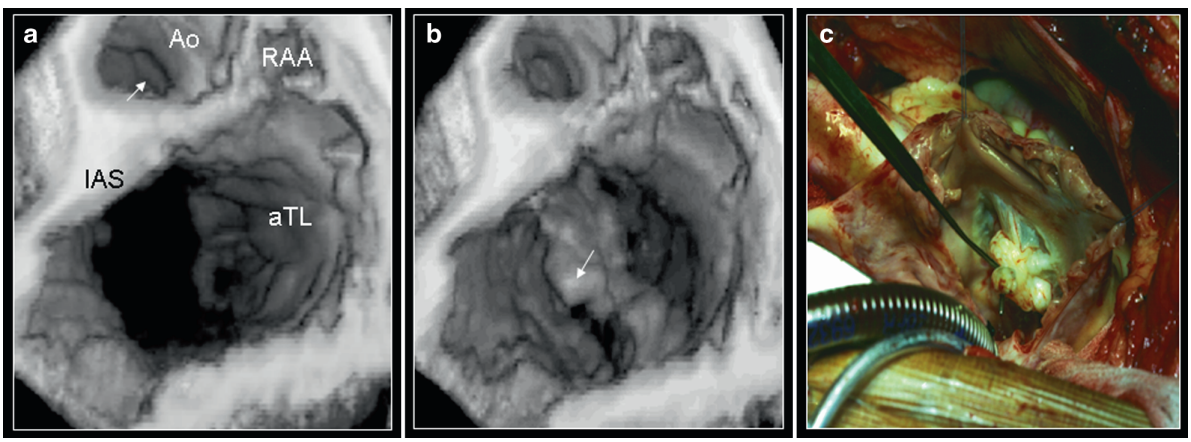

Fig. 31.9 Reconstruction 3DE surgical view from a right atrial perspective of a patient with a flail anterior tricuspid valve leaflet (aTL) due to a ruptured papillary muscle. (**a**) The open tricuspid valve in diastole and (**b**) the flailing aTL and part of the papillary muscle in the right atrium in systole (*arrow*) are seen. The intraoperative photo (**c**) shows the ruptured papillary muscle and confirms the three-dimensional echo findings. Note the closed aortic valve cusps in diastole (**a**) and open in systole (**b**). *IAS* interatrial septum, *RAA* right atrial appendage

for guiding intracardiac interventions (e.g., endocardial biopsy).[42]

Sophisticated software is available for quantitative analysis of *LV ventricular function* from 3D echo data. The 3D dataset is automatically sliced into several equiangular 2D planes after indicating a few anatomical landmarks. A semiautomated blood-endocardial interface detection algorithm allows the instantaneous calculation of cavity contours and a display of their changes during the cardiac contraction cycle. A surface-rendered cavity cast of the LV, RV, or LA is then constructed of which the volume is computed without geometric assumptions directly from the voxel counts (Fig. 31.14). This process is automatically repeated every 40 ms (imaging rate 25 datasets/s) throughout the cardiac cycle and is presented in a volume vs. time plot (Figs. 31.15a and 31.16). The calculation of *LV volume and function* is rapid, more accurate, and reproducible than with 2D. Accuracy is similar to MRI, although the variability may be higher as a result of varying image quality[43-54] (Table 31.4). The availability of the cavity shape

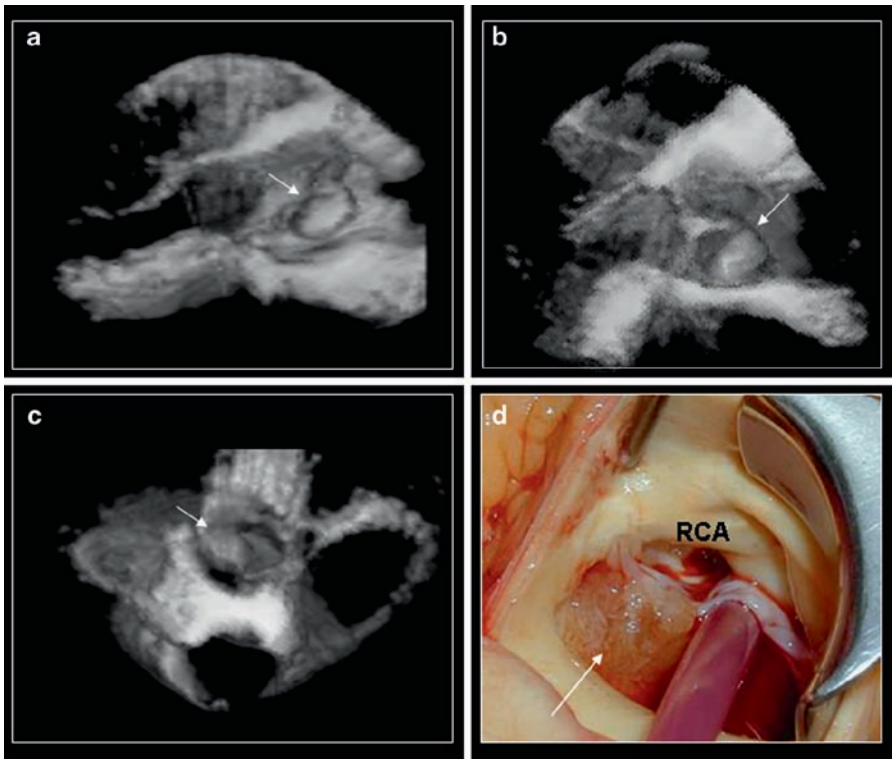

Fig. 31.10 Reconstruction 3DE of a fibroelastoma (*arrows*) of the aortic valve seen in systole (**a**) and diastole (**b**). (**c**) It also shows the mass lesion from above (surgical view) and (**d**) the intraoperative photo. *RCA* right coronary artery (Courtesy: R. Erbel)

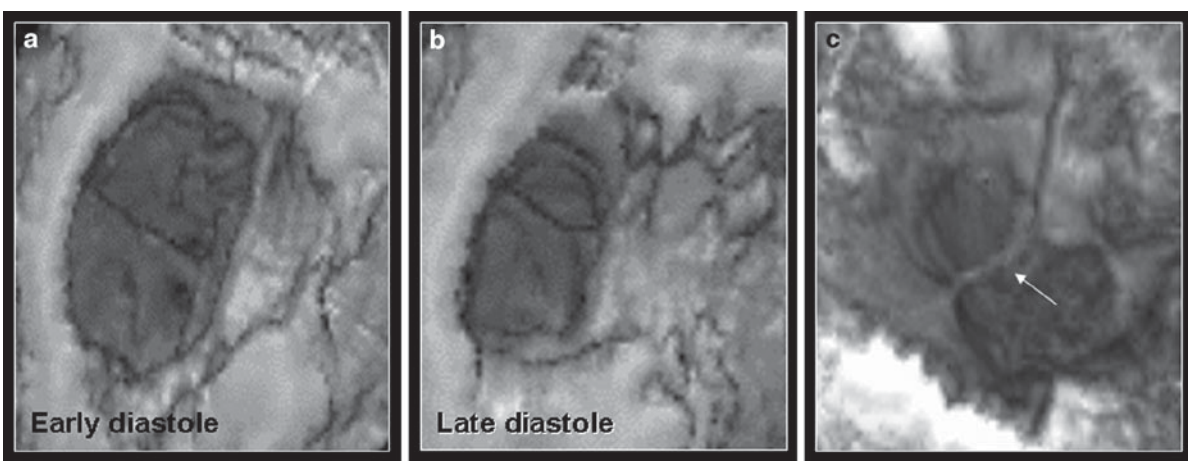

Fig. 31.11 "En face" visualization of atrial septal defects of the secundum type. The early diastolic image before opening of the tricuspid valve (TV) (**a**) and late diastolic image after atrial emptying (**b**) illustrate the dynamic change in size of the defect during the cardiac cycle. (**c**) An atrial septal defect with a muscular bridge (*arrow*)

allows to extract additional quantitative information in patients with LV dysfunction (3D sphericity index) and to study the LV remodeling process after myocardial infarction.

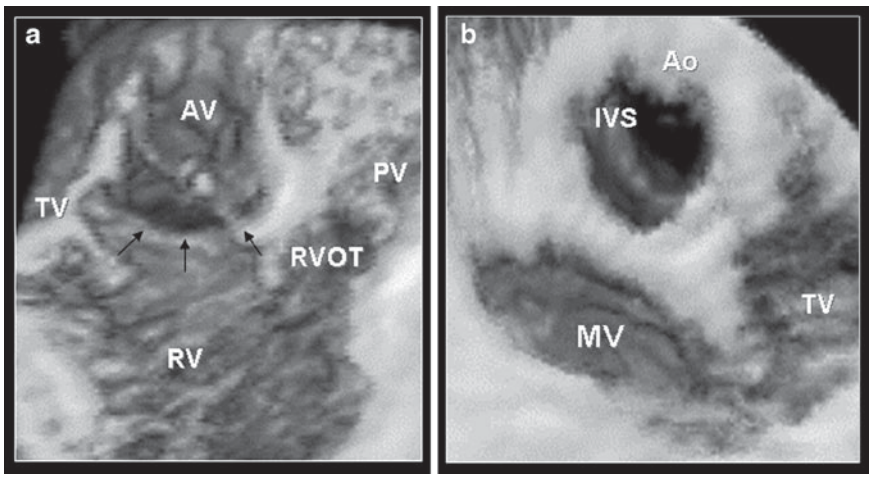

Fig. 31.12 Images of a patient with tetralogy of Fallot. (**a**) is a view from the right ventricle and shows the aortic valve (AV) through the ventricular septal defect. The *arrows* indicate the rim of the interventricular septum. (**b**) A systolic image from above through the aortic valve in which overrides the interventricular septum (IVS) by approx. 50%. *Ao* aorta; mitral valve; *PV* pulmonary valve; *RV* right ventricle; *RVOT* right ventricular outflow tract; *TV* tricuspid valve

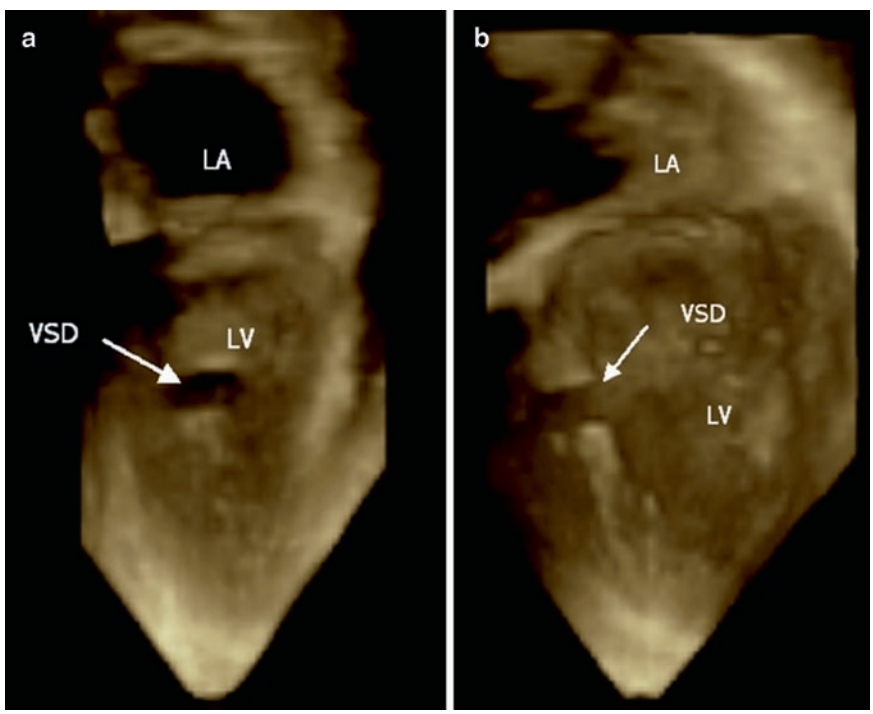

Fig. 31.13 (**a**) An "en face" view from the left ventricle (LV) on the muscular ventricular septal defect (VSD) in a 5-kg infant (4 months old) with a tricuspid atresia studied with a monocrystal matrix transducer. (**b**). Sagittal view on the VSD which is sliced in the middle. *LA* left atrium; *LV* left ventricle. (Courtesy: J. Simpson)

The feasibility and accuracy of 3DE for RV volume calculation has been demonstrated both in experimental studies and in humans.[55-57]

Because the left atrium is an asymmetrical cavity and its enlargement is not evenly distributed in all planes, 3DE is the best reproducible method to measure left atrial volume and function and is more sensitive to detect small volume changes than other echocardiographic approaches for serial follow-up studies.[58-61] Left atrial size is an important predictor of cardiovascular

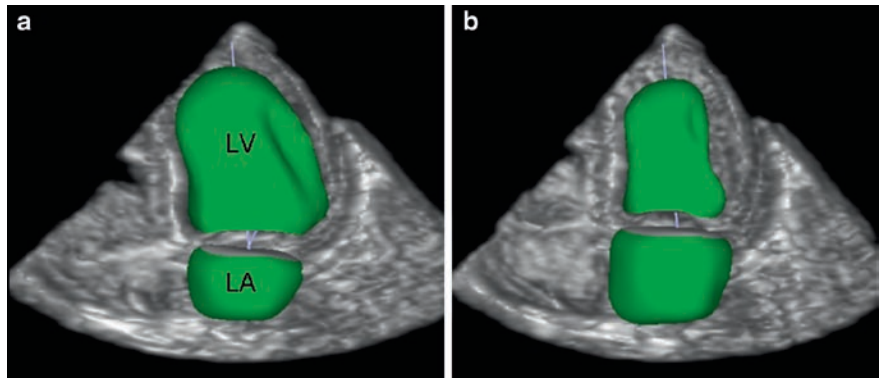

Fig. 31.14 Surface-rendered casts of the left ventricle (LV) and left atrium (LA) in diastole (**a**) en systole (**b**). Cavity volumes are calculated from the voxel counts every 40 ms and provide a volume vs. time curve of the LV or LA during a cardiac cycle. Ejection fraction is calculated from the end-diastolic and end-systolic volumes. (Data for Figs. 31.14–31.17 are kindly provided by TomTec Imaging GmbH)

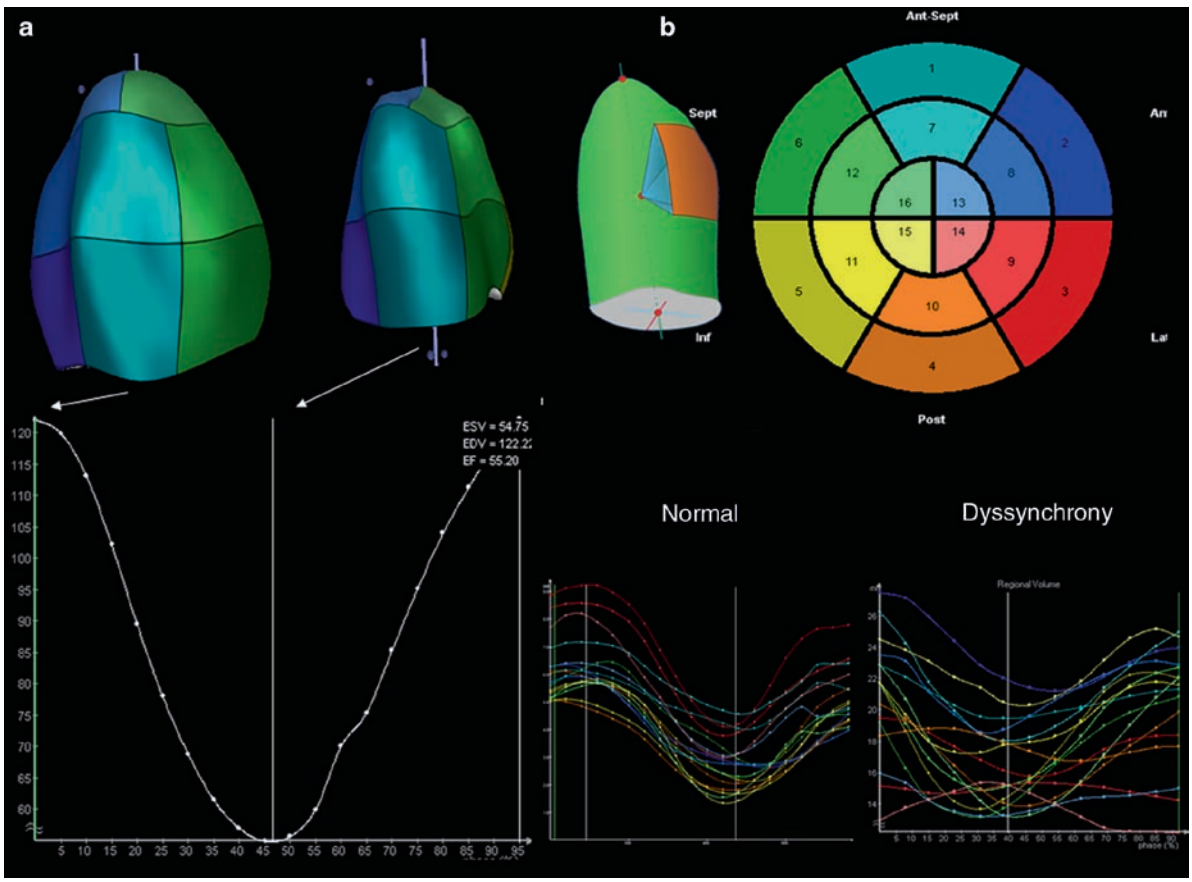

Fig. 31.15 Principles of quantitative global and segmental left ventricular function assessment. (**a**) An end-diastolic and end-systolic cavity (smallest volume) cast of the left ventricle rendered from semiautomated calculated cavity contours of a 3D dataset are shown. The cast volumes of all 3D datasets acquired during a cardiac cycle are calculated from the voxel counts and plotted against time yielding a volume vs time curve. (**b**) The casts are automatically segmented into 16 segments and their volume relative to the center of gravity (or centerline in the 17 segment model) is calculated. This is done for all 3D datasets recorded in the cardiac cycle. The volume vs. time curve of each color-coded segment indicated in the "bull's eye" view is represented in the *lower left panel*. The minimal volumes of all segments occur at about the same moment in the cardiac cycle indicating normal synchronous contraction. The *right panel* shows dispersion of the timing of the minimal volumes indicating dyssynchrony in a patient with diseased LV.

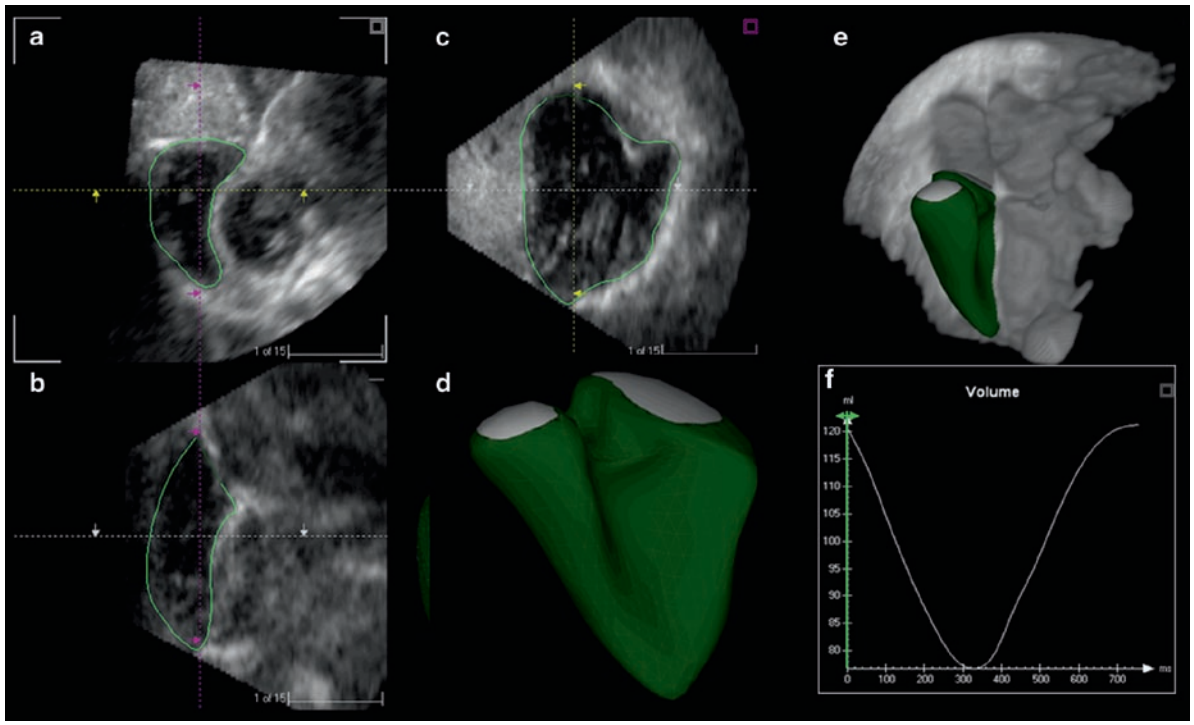

Fig. 31.16 Quantitative analysis of the right ventricle. Three planes are selected from the dataset and semiautomatically contoured over a complete cardiac cycle: a coronal plane (**a**), a four-chamber plane (**b**), a sagittal plane through the apex and right ventricular outflow tract. An RV cavity cast in reconstructed (**d** and **e**) and their volume is calculated every 40 ms represented as a volume vs. time plot (**f**) ejection fraction is calculated from end-diastolic and end-systolic volumes

risk and is more sensitive than left atrial diameter and surface area.

More user interaction is required to identify the epicardial (and right ventricular septal) contours for the *calculation of LV mass*.[62-66] However, 3DE has accuracy similar to MRI in most patients but is less expensive and more practical (Table 31.5).

For the analysis of *segmental wall function* the surface-rendered LV cavity casts are automatically subdivided into 16 segments after indicating a few anatomical landmarks. Then the volume of each individual segment relative to the LV center of gravity is calculated (some programs use a 17-segment model and calculate the individual segment volume relative to the LV center line). This is done for all the datasets and a volume vs. time curve of each segment is then plotted throughout the cardiac cycle (Fig. 31.15b). It is assumed that the segmental volume change reflects segmental wall function. Theoretically, RT3DE stress echocardiography has advantages over 2D stress echocardiography since the four standard views used for segmental analysis are obtained from the same full-volume dataset (four or seven consecutive heartbeats) rather than from multiple sequential transducer positions. This is currently being investigated, but the temporal resolution remains a serious limitation with the current generation of systems.[67,68]

The segmental volume vs. time plots allow the measurement of temporal differences in segmental wall contraction or *LV dyssynchrony*. This technique has promise for identifying patients who are suitable for cardiac resynchronization therapy (CRT) and for the immediate evaluation of procedural results and follow-up.[69] Minimal volume (maximal contraction) normally occurs at about the same moment in systole for all segments. In dyssynchrony, there is dispersion in the timing of reaching the minimal volume as the diseased segments achieve their contraction later (Fig. 31.15b). This can be expressed as a systolic dyssynchrony index.[70] The value of RT3DE for assessment of intraventricular dyssynchrony is currently being investigated.

Table 31.4 Left ventricular volume and function measurement by real-time 3DE in comparison with magnetic resonance imaging

Author/reference	Object	*n*	*R*	SEE	Mean diff. ± SD
Shiota et al[43]	EDV	28	0.97	27 ml	−43 ± 65 ml
	ESV	–	0.94	29 ml	−37 ± 67 ml
	EF	–	0.98	0.04%	1 ± 4%
Schmidt et al[44]	EDV	25	0.88		
	ESV	–	0.82		
	EF	–	0.72		
	Vol.	–	0.91	28.0 ml	−16 ± 36 ml
Qin et al[45] (controls)	Vol.	13			−13 ± 18 ml
(aneurysms)	Vol.	16			
Lee et al[46]	EDV	25	0.99	11.28 ml	−28 ± 25 ml
	ESV	–	0.99	10.21 ml	
	EF	–	0.92	0.06	
Zeidan et al[47]	EDV	15			−6 ± 11 ml
	ESV	–			−4 ± 9 ml
	EF	–			2 ± 5%
Jenkins et al[48]	EDV	50			−4 ± 29 ml
	ESV	–			−3 ± 18 ml
	EF	–			−0 ± 7%
Kuhl et al[49]	EDV	24	0.98		−13.6 ± 18.9 ml
	ESV	–	0.98		−12.8 ± 20.5 ml
	EF	–	0.98		0.9 ± 4.4%
Caiani et al[50]	EDV	14	0.97	17 ml	−4.1 ± 29 ml
	ESV	–	0.97	16 ml	−3.5 ± 33 ml
	EF	–	0.93	6%	−8 ± 14%
Chan et al[51]	EDV	30	0.90	26.9 ml	−10.4 ± 26.4 ml
	ESV	–	0.94	16.9 ml	−0.9 ± 18.8 ml
Sugeng et al[52]	EDV	31	0.94		
	ESV	–	0.93		
	EF	–	0.93		
Nikitin et al[53]	EDV	64	0.96		1 ± 28 ml
	ESV	–	0.97		3 ± 22 ml
	EF	–	0.93		−1 ± 10%
Jacobs et al[54]	EDV	50	0.96		−14 ± 17 ml
	ESV	–	0.97		−6.5 ± 16 ml
	EF	–	0.93		−1 ± 6%

3DE three-dimensional echocardiography; *n* number of subjects; *r* correlation coefficient; *SEE* standard error of estimate; *diff.* difference; *SD* standard deviation; *EDV* end-diastolic volume; *ESV* end-systolic volume; *EF* ejection fraction

Table 31.5 Left ventricular mass measurement by real-time 3DE in comparison with magnetic resonance imaging

Author/reference	*n*	*r*	SEE (g)	Mean diff. ± SD
Qin et al[62]	27	0.92	29	−9 ± 33 ml
Mor-Avi et al[63]	19	0.90	–	−4 ± 17 ml
Oe et al[64]	20	0.95	20	−14.1 ± 29.1 ml
Van den Bosch et al[65]	20	0.98	9.8	2 ± 20 ml
Caiani et al[66]	19	0.96	10.5	−2.1 ± 11.5 ml

3DE three-dimensional echocardiography; *n* number of subjects; *r* correlation coefficient; *SEE* standard error of estimate; *diff.* difference; *SD* standard deviation; *EDV* end-diastolic volume; *ESV* end-systolic volume; *EF* ejection fraction; *g* grams

Parametric images using a color scheme representing timing differences in segmental contraction can be generated in a "bull's eye" display, which is a practical tool for online identifying and localizing LV dyssynchrony (Fig. 31.17).

Conclusion

Proven benefits of RT3DE compared with 2DE are the more accurate and reproducible calculation of cavity volumes, LV ejection fraction, and mass. The results are comparable to MRI. Since RT3DE is more widely available and less expensive it will become the technique of choice for these applications in many clinical scenarios. When images are suboptimal in quality one should move to MRI for clinical decision making, but this is not possible in several clinical settings. Its use in stress procedures for detecting ischemia and for diagnosing LV dyssynchrony and testing CRT results remains investigational. However, with the availability of newer sensitive transducers and the next generation of high-speed processors, the spatial and temporal resolution will continually increase and RT3DE is likely to become the most practical test to detect ischemia, LV dyssynchrony and to monitor CRT procedures.

The direct visualization of structure relationships and direct views of dynamic pathomorphology make RT3DE unique for the assessment of valvular and congenital heart disease. The advantages of RT3DE for guiding interventional procedures are increasingly reported.

Virtual reality, the immersive environment created by ultrafast computers, is another important frontier which will be opened by RT3DE. Virtual reality allows the cardiologist to interact with cardiac data and heralds a revolution for medical diagnosis, internet-based distance learning and treatment (e.g., remote robotic interventions).

RT3DE will not replace 2DE but will become an integral part of a complete echo examination, including M-mode (high time resolution for intervals and specific motion patterns), 2D imaging (accurate dimensional measurements), and quantitative Doppler hemodynamics.

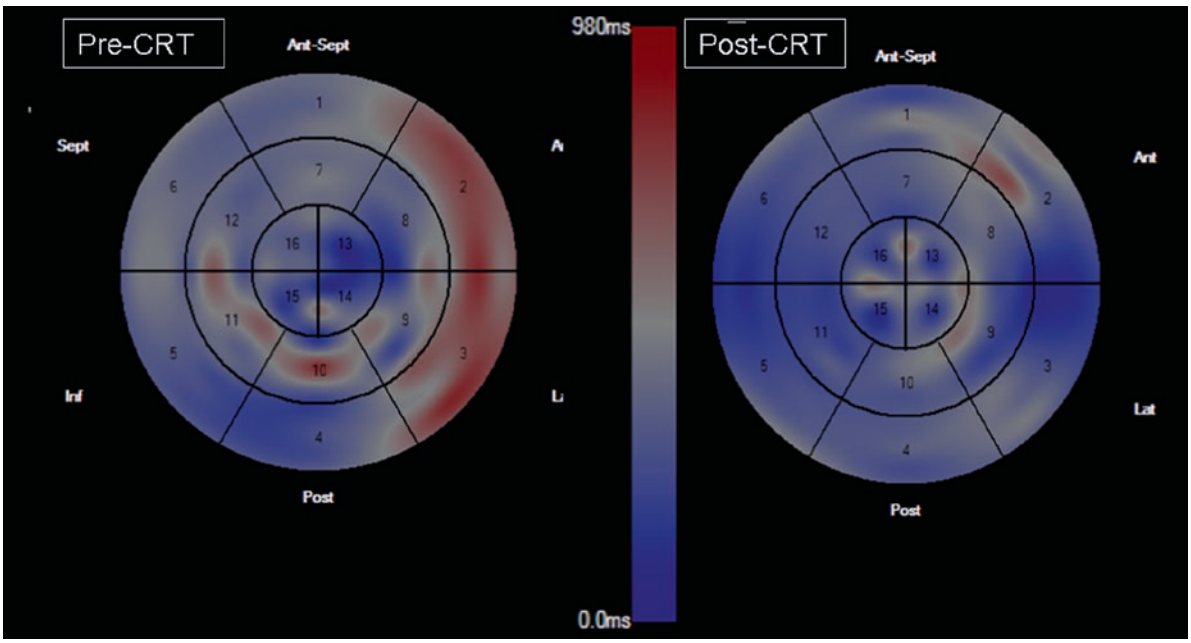

Fig. 31.17 Time to peak contraction of a segment can be measured and represented using a color scheme on a "bull's eye" display. Peak contraction is the moment of reaching minimal volume. *Blue color* indicates early/normal contraction while *red color* indicates delayed contraction or asynchrony. This is present in segments 11, 14, and 15 before cardiac resynchronization therapy (Pre-CRT). Post-CRT, the *blue color* becomes more homogeneous which means that the dyssynergic segments are normalized

Keypoints

- 3DE provides a realistic portrayal of cardiac (patho) morphology.
- Unique "en face" views give incremental qualitative and quantitative information for assessment.
- 3DE allows accurate and reproducible quantification of all cardiac chambers volumes, function, and LV mass.
- 3DE offers new directions for clinical research (new parameters and multiparametric imaging).

References

1. Dekker DL, Piziali RL, Dong E Jr. A system for ultrasonically imaging the human heart in three dimensions. *Comput Biomed Res.* 1974;7:544-553.
2. Moritz WE, Shreve PL. A microprocessor based spatial locating system for use with diagnostic ultrasound. *Proc IEEE.* 1976;64:966-974.
3. Frangi AF, Niessen WJ, Viergever MA. Three-dimensional modeling for functional analysis of cardiac images: a review. *IEEE Trans Med Imaging.* 2001;20:2-25.
4. Raab FH, Blood EB, Steiner TO, Jones HR. Magnetic position and orientation tracking system. *IEEE Trans Aerosp Electron Syst.* 1979;AES-15:709-718.
5. King DL, King DL Jr, Shao MYC. Three-dimensional spatial registration and interactive display of position and orientation of real-time ultrasound images. *J Ultrasound Med.* 1990;9:525-532.
6. King DL, Harrison MR, King DL Jr, et al. Improved reproducibility of left atrial and left ventricular measurements by guided three-dimensional echocardiography. *J Am Coll Cardiol.* 1992;20:1238-1245.
7. Gopal AS, Keller AM, Rigling R, et al. Left ventricular volume and endocardial surface area by three-dimensional echocardiography: comparison with two-dimensional echocardiography and nuclear magnetic resonance imaging in normal subjects. *J Am Coll Cardiol.* 1993;22:258-270.
8. Wollschläger H, Zeihet AM, Klein HP, et al. Transesophageal echo computer tomography (ECHO-CT): a new method for perspective views of the beating heart. *Circulation.* 1990;82(Suppl.3):III-670 (abstract).
9. Kuroda T, Kinter TM, Seward JB, et al. Accuracy of three-dimensional volume measurement using biplane transesophageal echocardiographc probe: in vitro experiment. *J Am Soc Echocardiogr.* 1991;4:475-484.
10. Roelandt JRTC, Ten Cate FJ, Vletter WB, et al. Ultrasonic dynamic three-dimensional visualization of the heart with a multiplane transesophageal imaging transducer. *J Am Soc Echocardiogr.* 1994;7:217-229.
11. Roelandt JRTC, Salustri A, Vletter WB, et al. Precordial three-dimensional echocardiography with a rotational imaging probe: methods and initial clinical experience. *Echocardiography.* 1995;12:243-252.
12. Nguyen LD, Leger C. Four-dimensional reconstruction of the left ventricle using a fast rotating classical phased array scan head; preliminary results. *J Am Soc Echocardiogr.* 2002;15:593-600.
13. Krenning BJ, Voormolen MM, Van Geuns RJ, et al. Rapid and accurate measurement of left ventricular function with a new second-harmonic fast rotating transducer and semi-automated border detection. *Echocardiography.* 2006;23:447-454.
14. Roelandt JRTC. Three-dimensional echocardiography: the future today! *Comput Graph.* 2000; 24: 715-729
15. Nosir YFM, Fioretti PM, Vletter WB, et al. Accurate measurement of left ventricular ejection fraction by three-dimensional echocardiography. *Circulation.* 1996;94:460-466.
16. Iwase M, Kondo T, Hasegawa K, et al. Three-dimensional echocardiography by semi-automatic border detection in assessment of left ventricular volume and ejection fraction: comparison with magnetic resonance imaging. *J Cardiol.* 1997;30:97-105.
17. Buck T, Hunold P, Wentz KU, et al. Tomographic three-dimensional echocardiographic determination of chamber size and systolic function in patients with left ventricular aneurysm: comparison to magnetic resonance imaging, cineventriculography, and two-dimensional echocardiography. *Circulation.* 1997;96:4286-4297.
18. Altmann K, Shen Z, Boxt LM, et al. Comparison of three-dimensional echocardiographic assessment of volume, mass, and function in children with functionally single left ventricles with two-dimensional echocardiography and magnetic resonance imaging. *Am J Cardiol.* 1997;80:1060-1065.
19. Nosir YF, Lequin MH, Kasprzak JD, et al. Measurements and day-to-day variabilities of left ventricular volumes and ejection fraction by three-dimensional echocardiography and comparison with magnetic resonance imaging. *Am J Cardiol.* 1998;82:209-214.
20. Kim WY, Sogaard P, Kristensen BO, et al. Measurement of left ventricular volumes by 3-dimensional echocardiography with tissue harmonic imaging: a comparison with magnetic resonance imaging. *J Am Soc Echocardiogr.* 2001; 14:169-179.
21. Poutanen T, Ikonen A, Jokinen E, et al. Transthoracic three-dimensional echocardiography is as good as magnetic resonance imaging in measuring dynamic changes in left ventricular volume during the heart cycle in children. *Eur J Echocardiogr.* 2001;2:31-39.
22. Mannaerts HF, Van Der Heide JA, Kamp O, et al. Quantification of left ventricular volumes and ejection fraction using freehand transthoracic three-dimensional echocardiography: comparison with magnetic resonance imaging. *J Am Soc Echocardiogr.* 2003;16:101-109.
23. Von Ramm OT, Smith SW. Real time volumetric ultrasound imaging system. *J Digit Imaging.* 1990;3:261-266.
24. Kisslo J, Firek B, Ota T, et al. Real-time volumetric echocardiography: the technology and the possibilities. *Echocardiography.* 2000;17:773-779.
25. Iwakura K, Ito H, Kawano S, et al. Comparison of orifice area by transthoracic three-dimensional Doppler echocardiography versus proximal isovelocity surface area (PISA) method for assessment of mitral regurgitation. *Am J Cardiol.* 2006;97:1630-1637.
26. Nanda NC, Thalec W, Niel J, et al. Examination protocol for three-dimensional echocardiography. *Echocardiography.* 2004;21:763-768.

27. Cheng TO, Xie MX, Wang XF, et al. Evaluation of mitral valve prolapse by four-dimensional echocardiography. *Am Heart J.* 1997;133:120-129.
28. Salustri A, Becker AE, Van Herwerden LA, et al. Three-dimensional echocardiography of normal and pathologic mitral valve: a comparison with two-dimensional transesophageal echocardiography. *J Am Coll Cardiol.* 1996;27:1502-1510.
29. Kupferwasser I, Mohr-Kahaly S, Menzel T, et al. Quantification of mitral valve stenosis by three-dimensional transesophageal echocardiography. *Int J Card Imaging.* 1996;12:241-247.
30. Hozumi T, Yoshikawa J, Yoshida K, et al. Assessment of flail mitral leaflets by dynamic three-dimensional echocardiographic imaging. *Am J Cardiol.* 1997;79:223-225.
31. Kasprzak JD, Salustri A, Roelandt JRTC, et al. Three-dimensional echocardiography of the aortic valve: feasibility, clinical utility and limitations. *Echocardiography.* 1998;15:127-138.
32. Sugeng L, Coon P, Weinert L, et al. Use of real-time three-dimensional transthoracic echocardiography in the evaluation of mitral valve disease. *J Am Soc Echocardiogr.* 2006;19:413-421.
33. Zamorano JL, Cordeiro P, Sugeng L, et al. Real-time three-dimensional echocardiography for rheumatic mitral valve stenosis evaluation: an accurate and novel approach. *J Am Coll Cardiol.* 2004;43:2091-2096.
34. Xie MX, Wang XF, Cheng TO, et al. Comparison of accuracy of mitral valve area in mitral stenosis by real-time three-dimensional echocardiography versus two-dimensional echocardiography versus Doppler pressure half-time. *Am J Cardiol.* 2005;95:1496-1499.
35. Pepi M, Tamborini G, Maltagliati A, et al. Head-to-head comparison of two-and three-dimensional transthoracic and transesophageal echocardiography in the localization of mitral valve prolapse. *J Am Coll Cardiol.* 2006;48:2524-2530.
36. Goktekin O, Matsumura M, Omoto R, et al. Evaluation of mitral valve prolapse using newly developed real-time three-dimensional echocardiographic system with real-time volume rendering. *Int J Cardiovasc Imaging.* 2003;19:43-49.
37. Gutierrez JL, Zamorano JL, Gomez, et al. Clinical meaning of a new echocardiographic sign in the study of mitral prolapse with 3D echo: the pseudo-clift (abstr.). *Eur Heart J.* 2004;25 (suppl): 259.
38. Xie MX, Fang LY, Wang XF, et al. Assessment of atrial septal defect area changes during cardiac cycle by live three-dimensional echocardiography. *J Cardiol.* 2006;47:181-187.
39. Van den Bosch AE, Ten Harkel DJ, McGhie JS, et al. Characterization of atrial septal defect assessed by real-time 3-dimensional echocardiography. *J Am Soc Echocardiogr.* 2006;19:815-821.
40. Van den Bosch AE, Ten Harkel DJ, McGhie JS, et al. Feasibility and accuracy of real-time three-dimensional echocardiographic assessment of ventricular septal defects. *J Am Soc Cardiogr.* 2006;19:7-13.
41. Sinha A, Nanda NC, Misra V, et al. Live three-dimensional transthoracic echocardiography assessment of transcatheter closure of atrial septal defect and patent foramen ovale. *Echocardiography.* 2004;21:749-753.
42. Amitai ME, Schnittger I, Popp RL, et al. Comparison of three-dimensional echocardiography to two-dimensional echocardiography and fluoroscopy for monitoring of endomyocardial biopsy. *Am J Cardiol.* 2007;99:864-866.
43. Shiota T, McCarthy PM, White RD, et al. Initial clinical experience of real-time three-dimensional echocardiography in patients with ischemic and idiopathic dilated cardiomyopathy. *Am J Cardiol.* 1999;84:1068-1073.
44. Schmidt MA, Ohazama CJ, Agyeman KO, et al. Real-time three-dimensional echocardiography for measurement of left ventricular volumes. *Am J Cardiol.* 1999;84: 1434-1439.
45. Qin JX, Jones M, Shiota T, et al. Validation of real-time three-dimensional echocardiography for quantifying left ventricular volumes in the presence of a left ventricular aneurysm: in vitro and in vivo studies. *J Am Coll Cardiol.* 2000;36:900-907.
46. Lee D, Fuisz AR, Fan PH, et al. Real-time 3-dimensional echocardiographic evaluation of left ventricular volume: correlation with magnetic resonance imaging--a validation study. *J Am Soc Echocardiogr.* 2001;14:1001-1009.
47. Zeidan Z, Erbel R, Barkhausen J, et al. Analysis of global systolic and diastolic left ventricular performance using volume-time curves by real-time three-dimensional echocardiography. *J Am Soc Echocardiogr.* 2003;16:29-37.
48. Jenkins C, Bricknell K, Hanekom L, et al. Reproducibility and accuracy of echocardiographic measurements of left ventricular parameters using real-time three-dimensional echocardiography. *J Am Coll Cardiol.* 2004;44:878-886.
49. Kuhl HP, Schreckenberg M, Rulands D, et al. High-resolution transthoracic real-time three-dimensional echocardiography: quantitation of cardiac volumes and function using semi-automatic border detection and comparison with cardiac magnetic resonance imaging. *J Am Coll Cardiol.* 2004;43:2083-2090.
50. Caiani EG, Corsi C, Zamorano J, et al. Improved semiautomated quantification of left ventricular volumes and ejection fraction using 3-dimensional echocardiography with a full matrix-array transducer: comparison with magnetic resonance imaging. *J Am Soc Echocardiogr.* 2005;18:779-788.
51. Chan J, Jenkins C, Khafagi F, et al. What is the optimal clinical technique for measurement of left ventricular volume after myocardial infarction? A comparative study of 3-dimensional echocardiography, single photon emission computed tomography and cardiac magnetic resonance imaging. *J Am Soc Echocardiogr.* 2006;19:192-201.
52. Sugeng L, Mor-Avi V, Weinert L, et al. Quantitative assessment of left ventricular size and function: side-by-side comparison of real-time three-dimensional echocardiography and computed tomography with magnetic resonance reference. *Circulation.* 2006;114:654-661.
53. Nikitin NP, Constantin C, Loh PH, et al. New generation 3-dimensional echocardiography for left ventricular volumetric and functional measurements: comparison with cardiac magnetic resonance. *Eur J Echocardiogr.* 2006;7: 365-372.
54. Jabobs LD, Salgo IS, Goonewardena S, et al. Rapid online quantification of left ventricular volume from real-time three-dimensional echocardiographic data. *Eur Heart J.* 2006;27:460-468.
55. Shiota T, Jones M, Chikada M, et al. Real time three-dimensional echocardiography for determining right ventricular stroke volume in an animal model of chronic right ventricular volume overload. *Circulation.* 1998;97:1897-1900.
56. Vogel M, Gutberlet M, Dittrich S, et al. Comparison of transthoracic three dimensional echocardiography with magnetic

resonance imaging in the assessment of right ventricular volume and mass. *Heart.* 1997;78:127-130.
57. Schindera ST, Mehwald PS, Sahn DJ, et al. Accuracy of real-time three-dimensional echocardiography for quantifying right ventricular volume: static and pulsatile flow studies in an anatomic in vitro model. *J Ultrasoun Med.* 2002;21:1069-1075.
58. Keller AM, Gopal AS, King DL. Left and right atrial volume by freehand three-dimensional echocardiography: in vivo validation using magnetic resonance imaging. *Eur J Echocardiogr.* 2000;1:55-65.
59. Anwar AM, Soliman OI, Geleijnse ML, et al. Assessment of left atrial volume and function by real-time three-dimensional echocardiography. *Int J Cardiol.* 2008;123:155-161.
60. Maddukiri PV, Viera ML, De Castro S, et al. What is the best approach for the assessment of left atrial size? Comparison of various unidimensional and two-dimensional parameters with three-dimensional echocardiographically determined left atrial volume. *J Am Soc Echocardiogr.* 2006;19:1026-1032.
61. Jenkins C, Brickwell K, Marwick TH. Use of real-time three-dimensional echocardiography to measure left atrial volume: comparison with other echocardiographic techniques. *J Am Soc Echocardiogr.* 2005;18:991-997.
62. Qin JX, Shiota T, Thomas JD. Determination of left ventricular volume, ejection fraction, and myocardial mass by real-time three-dimensional echocardiography. *Echocardiography.* 2000;17:781-786.
63. Mor-Avi V, Sugeng L, Weinert L, et al. Fast measurement of left ventricular mass with real-time three-dimensional echocardiography: comparison with magnetic resonance imaging. *Circulation.* 2004;110:1814-1818.
64. Oe H, Hozumi T, Arai K, et al. Comparison of accurate measurement of left ventricular mass in patients with hypertrophied hearts by real-time three-dimensional echocardiography versus magnetic resonance imaging. *Am J Cardiol.* 2005;95: 1263-1267.
65. Van den Bosch AE, Robbers-Vissers D, Krenning BJ, et al. Comparison of real-time three-dimensional echocardiography to magnetic resonance for assessment of left ventricular mass. *Am J Cardiol.* 2006;97:113-117.
66. Caiani EG, Corsi C, Sugeng L, et al. Improved quantification of left ventricular mass based on endocardial and epicardial surface detection with real-time three-dimensional echocardiography. *Heart.* 2006;92:213-219.
67. Takuchi M, Otoni S, Weinert L, et al. Comparison of contrast-enhanced real-time live 3-dimensional dobutamine stress echocardiography with 2-dimensional echocardiography for detecting stress-induced wall motion abnormalities. *J Am Soc Echocardiogr.* 2006;19:249-249.
68. Krenning BJ, Vletter WB, Nemes A, et al. Real-time three-dimensional contrast stress echocardiography: a bridge too far? *J Am Soc Echocardiogr.* 2007;20:1224-1225.
69. Monoghan MJ. Role of real-time 3D Echocardiography in evaluating the left ventricle. *Heart.* 2006:92:131-136.
70. Kapetanakis S, Kearney MT, Siva A, et al. Real-time three-dimensional echocardiography: a novel technique to quantify global left ventricular mechanical dyssynchrony. *Circulation.* 2005;112:992-1000.
71. Salustri A, Spitaels S, McGhie J, et al. Transthoracic three-dimensional echocardiography in adult patients with congenital heart disease. *J Am Coll Cardiol.* 1995;26:759-767.
72. Acar P. Three-dimensional echocardiography in congenital heart disease. *Arch Pediatr.* 2006;13:51-56.

Chapter 32
Ultrasound Stethoscopy

Eleni C. Vourvouri, and Jos R.T.C. Roelandt

Introduction

Cardiac ultrasound has been one of the most important advances in noninvasive cardiac imaging and is currently the most widely used and cost-effective diagnostic imaging tool in cardiology.[1] Since it is often the best or even the only applicable method, it has largely supplanted other imaging modalities in a wide variety of health care environments. Miniaturization and digital techniques recently resulted in the development of high-resolution battery-powered small hand-held ultrasound devices with excellent gray-scale and color blood-flow imaging capabilities.

These devices are referred to in the literature with various names: hand-held ultrasound or hand-carried cardiac ultrasound devices (HCU), personal ultrasound imagers (PUI), small personal ultrasound devices (SPUD), point-of-care echocardiography, ultrasound cardioscopes or ultrasound stethoscopes, and hand-held scanners. These instruments can be used anytime anywhere just like a conventional stethoscope and augment significantly the yield of the physical examination. Since stethoscopy stands for "seeing the heart," the term ultrasound stethoscope (from the Greek words stethos = chest and skopein = see) seems to be the most appropriate term describing these instruments in Cardiology, while the standard stethoscope should be named a "stethophone" (phone = sound).

Seeing the invisible pathology strengthens its diagnostic accuracy and provides valuable quantitative information for patient management. These devices will be useful in the emergency room and critical care environment where the diagnosis or exclusion of some life-threatening conditions will shorten delays in therapy. Better indications and more targeted referrals for expensive imaging technologies will lead to significant cost savings. "Focused" or goal-oriented echocardiographic examinations with these devices allow to answer specific questions, to follow-up common conditions, and to test the effect of therapy at the bedside or in office practice.

A Historical Perspective

In 1904, W. Rollins described the "Seehear," a device combining a fluoroscope with a standard stethoscope extending the clinical perception of the auscultation with seeing. In 1978 an ultrasound stethoscope (Minivisor™, Organon Teknica) was developed by the Thoraxcenter group[2] and in 1988, a hand-held sector scanner (ScanMate™, Damon Corp) was introduced by the Rochester group. However limited imaging performance and reimbursement issues did not stir the enthusiasm of cardiologists who were confronted in those days with the rapidly expanding capabilities and applications of the high-end ultrasound systems. Now, technology allows to construct small hand-held ultrasound systems with excellent structure and blood-flow imaging.

The Equipment

In 1978, the first small hand-held ultrasound device was constructed by Ligtvoet et al and introduced as part of the physical examination by Roelandt et al in

E.C. Vourvouri (✉) and J.R.T.C. Roelandt
Thoraxcenter-Room Ba302, Erasmus MC, Dr. Molewaterplein 40, 3015 GD, Rotterdam, The Netherlands
e-mail: e.vourvouri@erasmusmc.nl

P. Nihoyannopoulos and J. Kisslo (eds.), *Echocardiography*,
DOI: 10.1007/978-1-84882-293-1_32,

Rotterdam (Fig. 32.1).[2,3] However, the concept was ahead of its time and the combination of poor image quality, practical limitations, and reimbursement issues discontinued its further development.

Today, miniaturization and digital technology has led to the development of the following ultrasound stethoscopes (Fig. 32.2):

- The SonoHeart SonoSite™ (Plus, Elite and *ilook*) (SonoSite Inc., Bothell, WA, USA) and the OptiGo™ (Philips Medical Systems, Eindhoven, NL). They make use of phased-array transducers providing high-resolution two-dimensional dynamic grey-scale tissue imaging combined with color Doppler flow imaging (directional for the SonoHeart™ system).
- The upgraded SonoHeart Plus™ device features second harmonic imaging and has integrated M-mode and pulsed-wave Doppler capabilities as well as an electrocardiographic reference lead. SonoHeart Elite™ has the additional feature of continuous-wave Doppler.
- The SonoSite™ *ilook* which is presently the smallest all-digital ultrasound platform in the world.
- The latest development is the SonoSite Titan™ (Fig. 32.3) which has the same features as SonoHeart Elite™ but has a laptop screen.
- The ultrasound stethoscopes operate on a rechargeable battery or AC current and have linear measurement calipers. The internal memory of the SonoHeart™ allows storage up to 120 images (up to 75 for the SonoSite™ *ilook*), which can be downloaded into a PC, and there is a video output, which can be connected

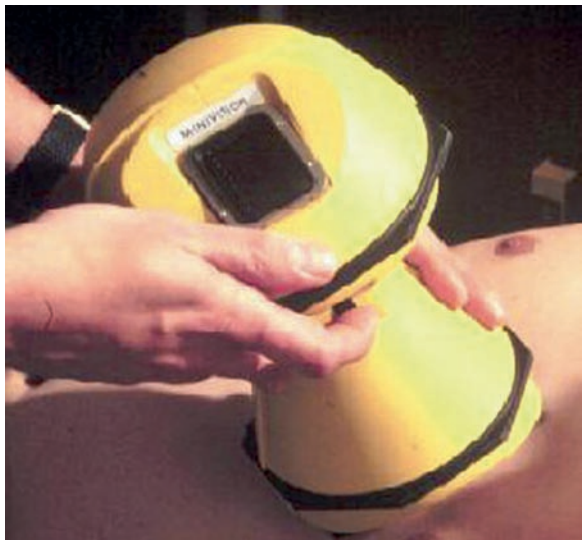

Fig. 32.1 Photograph of the Minivisor™ developed in 1978

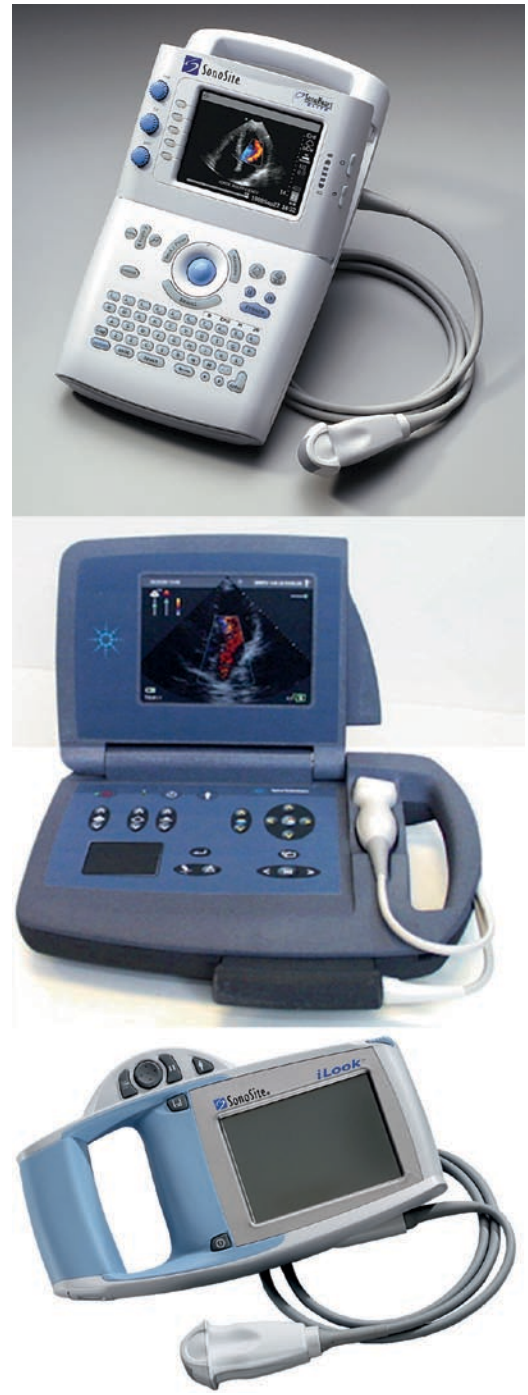

Fig. 32.2 Photographs of the (*from the top to the bottom*) handheld ultrasound devices SonoHeart™ Elite, OptiGo™ (Philips), and SonoHeart *i* look™

to a monitor or to a VCR for permanent recording.

- The OptiGo™ allows images to be documented on a CompactFlash card. Table 32.1 gives an overview of the available ultrasound stethoscopes and their technical characteristics.
- The Micromaxx™ (SonoSite) (Fig. 32.4) and the Vivid *i* ™ (General Electric) (Fig. 32.5) are the latest most complete laptop-like ultrasound stethoscopes that provide additional the possibility for contrast imaging, Tissue Doppler Imaging and transesophageal studies.

A variety of high-quality broadband transducers designed for hand-held ultrasound devices have been produced (SonoSite Inc) enabling their use practically in every medical field where ultrasound is used as a diagnostic imaging tool. Thus, they are used in obstetrics/

Fig. 32.3 Photographs of the newer hand-held ultrasound device TitanTM (SonoSite)

Fig. 32.4 Photographs of one of the latest hand-held ultrasound devices MicromaxxTM (SonoHeart)

Table 32.1 Overview of the characteristics of the available ultrasound stethoscopes

Devices	Weight (kg)	2-D	Second harmonic	Color-flow Doppler	Pulsed Doppler	Continuous Doppler	M-Mode	Archiving/ saving images	Video output	Contrast imaging	Tissue Doppler Imaging	Transeso Phageal
SonoHeart™-Plus	2.6	Yes	Yes	Directional Color power Doppler	Yes	No	Yes	Yes	Yes	No	No	No
SonoHeart™-Elite	2.6	Yes	Yes	Directional Color power Doppler	Yes	Yes	Yes	Yes	Yes	No	No	No
SonoSite-*ilook 15*	1.4	Yes	Yes	Yes	No	No	Yes	Yes	Yes	No	No	No
OptiGo™	<3.36	Yes	No	Yes	No	No	No	Yes	No	No	No	No
SonoSite Titan		Yes	Yes	Yes	Yes	Yes	Yes	Yes	Yes	No	No	No
SonoSite Micro-maxx		Yes	Yes	Yes	Yes	Yes	Yes	Yes	Yes	Yes	Yes	Yes
Vivid*i*		Yes	Yes	Yes	Yes	Yes	Yes	Yes	Yes	Yes	Yes	Yes

Fig. 32.5 Photographs of one of the latest hand-held ultrasound devices and Vivid *i*™ (GE)

gynecology, neonatal and pediatrics, emergency medicine, surgery, orthopedics, radiology, and vascular medicine.

The small ultrasound devices should not be confused with the portable desktop systems which are full-featured systems. Ultrasound stethoscopy is a fast developing field. Pocket-sized ultrasound stethoscopes are already being developed and will soon emerge into the market of hand-held ultrasound devices.

Clinical Uses

More Reliable Examination

The physical examination remains the cornerstone of the initial evaluation of a patient with suspected cardiovascular disease. One could argue that the introduction of echocardiography at the bedside could weaken the importance of the physical examination and auscultation in particular. However, it was echocardiography that brought out the limitations of physical examination in many cardiac conditions and also exposed human auditory limitations.[4] Although auscultation entered a modern era with the introduction of electronic stethoscopes, physicians rely on more sophisticated technology. Inadequate training and time pressure due to increasing work load of patients in combination with the availability of advanced technologies are the reasons of poor auscultatory proficiency seen in recently trained physicians particularly in developed countries. Nevertheless, direct observation such as seeing is more accurate for cardiac diagnosis than indirect observation such as hearing. "Visualizing the heart" with the ultrasound stethoscope as part of the physical examination provides additional qualitative and quantitative information beyond what we can perceive with inspection, palpation, and auscultation. Sounds or abnormal movements can be directly related to anatomic or flow abnormalities, and a definitive diagnosis can be made (valve disease, shunt, cavity dilatation, hypertrophy, pericardial effusion, mass lesion, wall motion abnormality, valvular vegetation) in a variety of clinical settings (Fig. 32.6), (Tables 32.2 and 32.3).[5,6] "Seeing" enables the detection of "presymptomatic" disease and pathologies that are beyond the perception of physical signs, e.g., small mass lesions (Fig. 32.7, Table 32.4). It has been shown that the use of ultrasound stethoscopy at the point of care leads to the diagnosis of unanticipated clinically significant abnormalities in approximately 20% of patients (Figs. 32.8 and 32.9) and enhances significantly the diagnostic accuracy of expert physical examination.[7-10] Furthermore is shown that the incorporation of ultrasound stethoscopy in the physical examination during cardiac consultation rounds in noncardiac departments provides with efficient instant information resulting in immediate management of patients and leading to cost savings (Fig. 32.10).[11,12]

The routine physical cardiovascular examination can be extended by imaging and by obtaining limited quantitative measurements of the inferior vena cava, liver, spleen, and abdominal aorta. The loss of inspiration narrowing of the inferior vena cava is a reliable and sensitive marker of elevated central venous pressure and right heart failure (Fig. 32.11).

On the basis of normal structure and functional findings, in the absence of blood-flow turbulence, all of which can be tested in a limited number of imaging views, a cardiac disorder can be excluded with a high degree of certainty. This high negative predictive value is ideal for rapid screening to avoid referral of normals and for a more cost-effective use of our expensive diagnostic imaging facilities

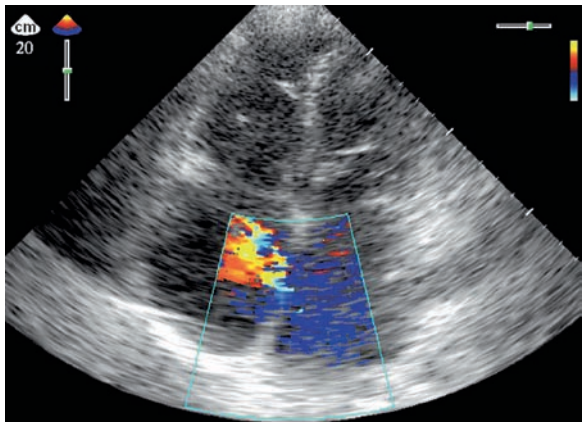

Fig. 32.6 Apical four-chamber view of a patient with an atrial septum defect of the secundum type. Both atria are dilated and the left-to-right shunting blood flow through the defect is visualized (OptiGo™)

Table 32.2 Additional information with the ultrasound stethoscope as part of the physical examination

Higher diagnostic specificity and sensitivity
Early (preclinical) diagnosis
Functional assessment
Blood-flow information
Inferior vena cava collapse
Quantitative information
Abdominal aorta measurement

Table 32.3 Clinical settings where the ultrasound stethoscope can be used

Emergency department, CCU, and ICU
Hospital ward rounds
Outpatient clinic
Surgical theatre
Cardiac catheter lab
Private office practice

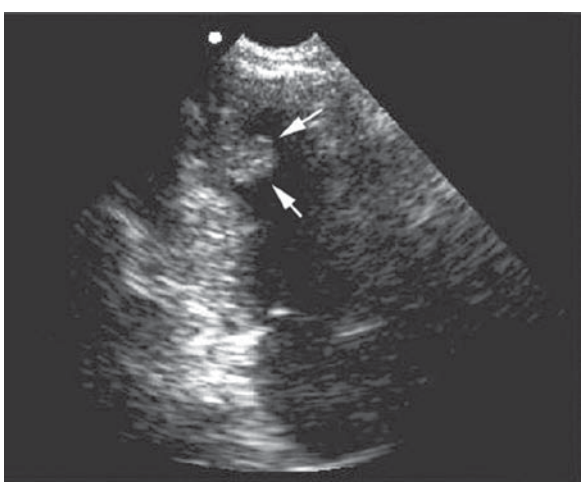

Fig. 32.7 Apical four-chamber view of a patient with a mass in the left ventricular apex (SonoHeart™)

Table 32.4 Cardiac abnormalities diagnosed with the use of the ultrasound stethoscope

Source of murmurs
Dilated heart
Pericardial effusion, emergent tamponade
Pulmonary embolus
Valvular disease
Mass lesion
Wall function
Dilatation abdominal aorta/aneurysm

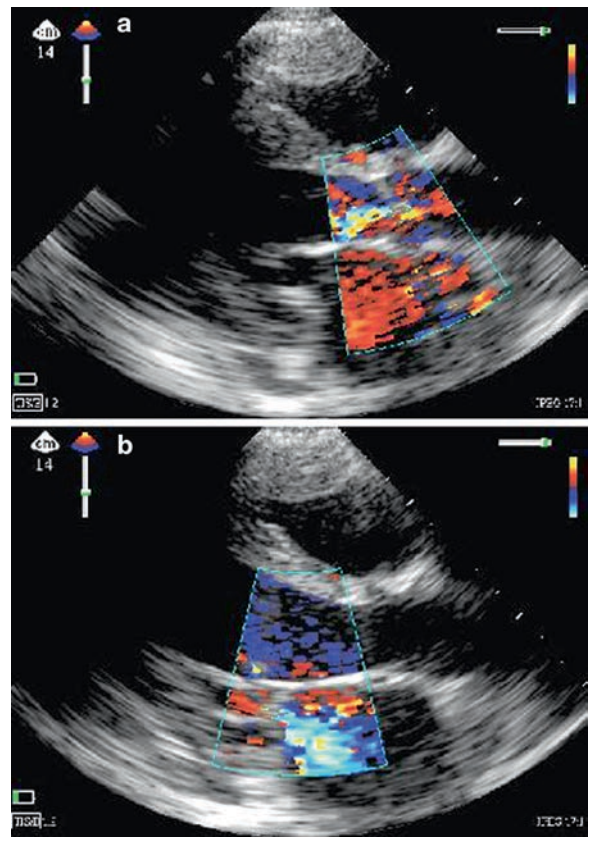

Fig. 32.8 Apical four-chamber view of a 25-year-old female with systemic lupus erythematosus and shortness of breath. The referral diagnosis was: pericarditis? The patient has regurgitant jets of aortic regurgitant (**a**) and mitral regurgitation (**b**), but no pericarditis (OptiGo™)

Point of Care for Faster Decisions

Standard echocardiography involves a comprehensive examination with complex equipment by an operator with considerable training and experience. However, the diagnosis and follow-up of many cardiac conditions requires only a fraction of the potential of these expensive facilities, and a specific clinical question can often be answered FASTER by limited examination

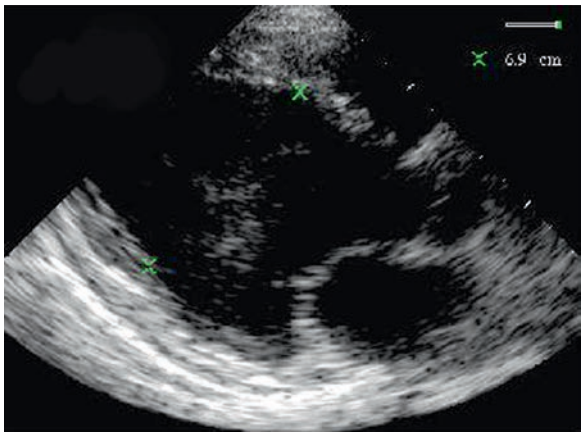

Fig. 32.9 Parasternal long-axis view of a 46-year-old woman with a history of cancer. She was referred for preoperative evaluation. The left ventricular end-diastolic dimension is 69 mm. The EF was visually estimated to be<35%. The patient has dilated cardiomyopathy

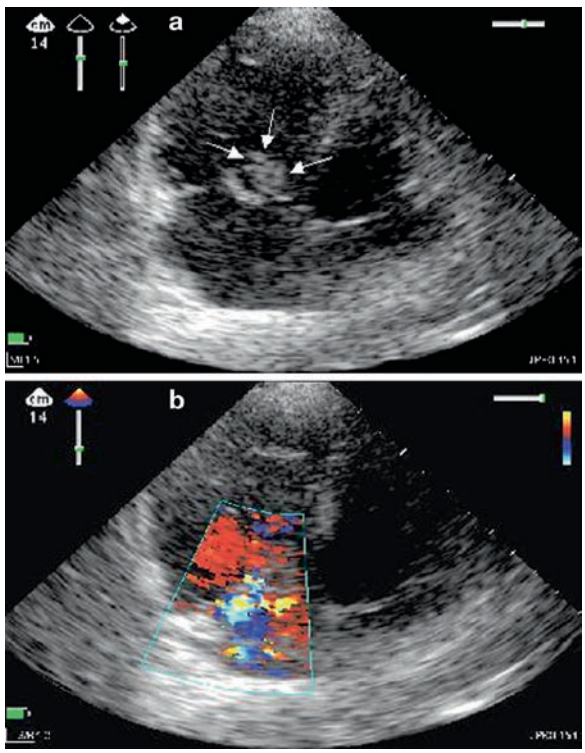

Fig. 32.10 (**a**) Imaging of a vegetation on the tricuspid valve (*arrows*) in the apical four-chamber view (OptiGo™).(**b**) A severe tricuspid regurgitation is visualized

protocols. The ultrasound stethoscope is suitable for a *"focused"* or *"goal-oriented"* examination.

- The resolution of a pericardial effusion after a pericardiocentesis (Fig. 32.12),

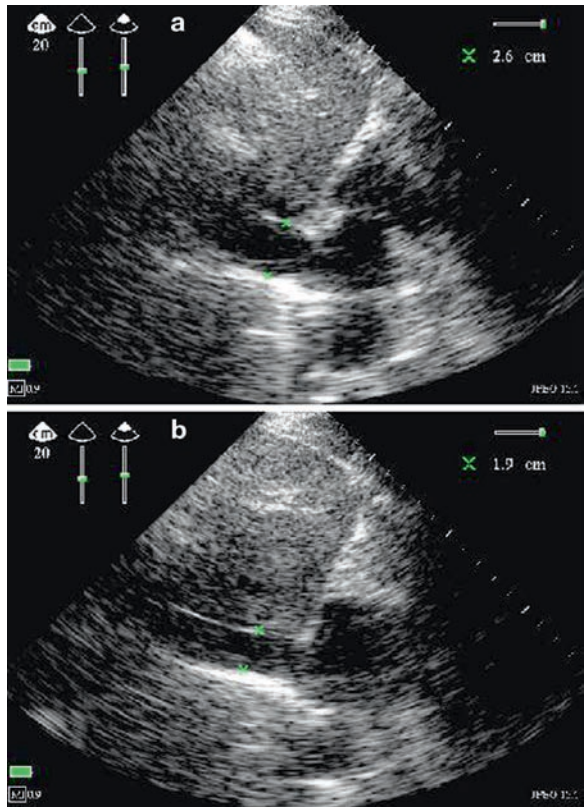

Fig. 32.11 Imaging of the inferior vena cava (IVC) through the liver during expiration (**a**) and inspiration (**b**). The caliper function allows measurement of the IVC dimension during expiration (2.6 cm) and during inspiration (1.9 cm). A collapse of less than 50% indicates an elevated right-sided filling pressure[37] (OptiGo™)

- Cardiac dimensions and left ventricular (LV) function, which are important parameters in the follow-up of many patients, are rapidly assessed at the bedside.
- LV hypertrophy is considered an independent potent marker of cardiovascular risk in arterial hypertension. Early detection can initiate therapy and improve outcome. Physical examination and electrocardiography can easily miss this pathology, whereas it can be instantly and reliably detected with the use of echocardiography. However, echocardiography is not considered cost effective, and the World Health Organisation-International Society of Hypertension (WHO-ISH) does not recommend echocardiography in all hypertensive patients. Ultrasound stethoscopy may broaden the indication of echocardiography allowing focused examinations in all hypertensive patients. A very good agreement between standard echocardiography and ultrasound stethoscopy in

diagnosing LV hypertrophy is reported (of 93% for left ventricular mass/body surface area and 90% for left ventricular mass/height) (Fig. 32.13).[13] The incorporation of ultrasound stethoscopy to the physical examination will provide the clinician with immediate, valuable information about prognosis and risk classification, assisting him in his decision of therapy. Thus, in patients with borderline hypertension, the presence of LV hypertrophy could mark the initiation of antihypertensive drug therapy (Fig. 32.14). Furthermore, the success or failure of the antihypertensive treatment can be assessed by repeated wall thickness and left ventricular mass measurements in office practice.

Critical Care Environment

The ultrasound stethoscope can effectively assist in the initial evaluation and rapid diagnosis of potentially life-threatening conditions in the intensive care environment or in situations where quick decision making is essential. It is a fact that physical examination in an emergency department is further limited due to the

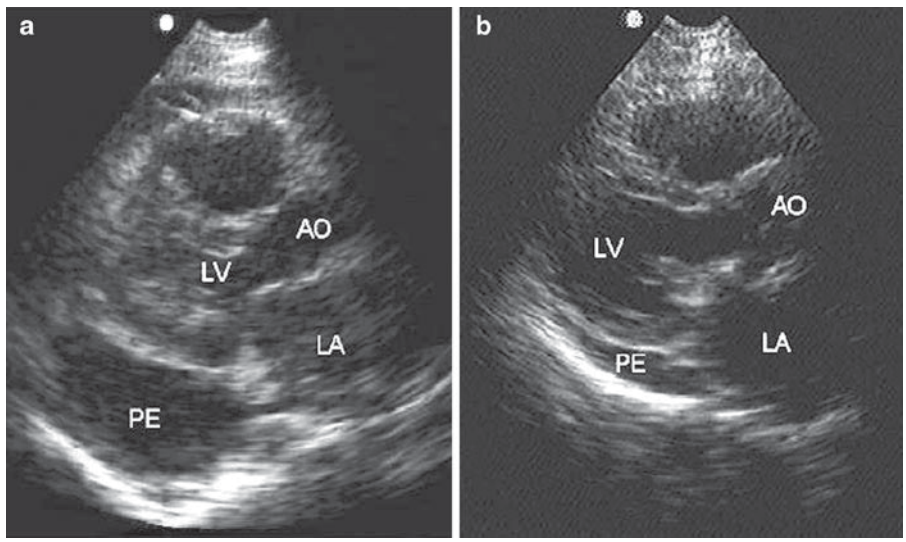

Fig. 32.12 Long-axis views of patients with pericardial effusion (PE). (**a**) A small PE postoperatively and (**b**) a large PE of a patient with clinical signs of tamponade (SonoHeart™)

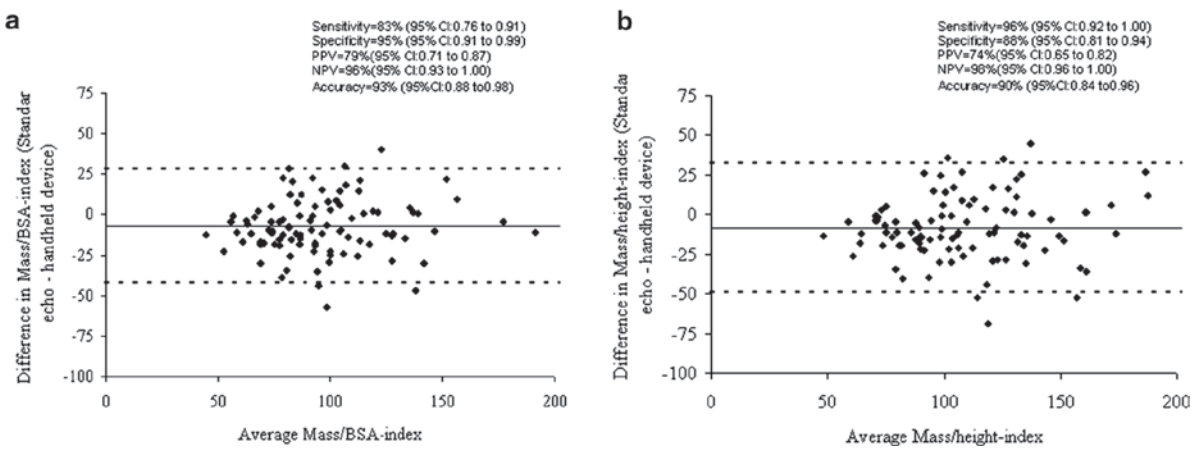

Fig. 32.13 Agreement of the LV mass (LVM) indexed by BSA (**a**) and by height (**b**), measured by the hand-held device and the standard echocardiographic system

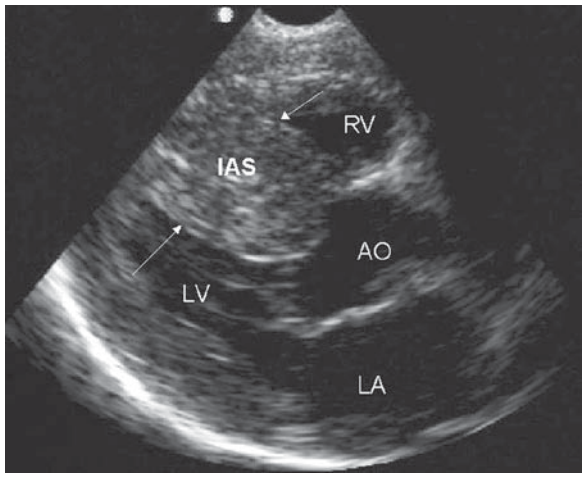

Fig. 32.14 Long-axis views of patient with hypertrophic cardiomyopathy (SonoHeart™). The *arrow* indicates the increased septal thickness

existing pressure, time constraints, and due to extraneous noise. It has been shown that even after limited training, a single echocardiographic view (parasternal long-axis view) has better diagnostic accuracy in identifying cardiac abnormalities than physical examination. However, standard echocardiography or other imaging methods are not rapidly available. The ultrasound stethoscope due to its ultraportability enables an echocardiographic evaluation anywhere, anytime and provides data inaccessible by clinical examination allowing to immediately diagnose or exclude an emergent tamponade, a dilated heart, or a valvular pathology (e.g., calcific aortic stenosis in low output state) (Figs. 32.15 and 32.16).

Studies using a prototype ultrasound stethoscope in critically ill patients reported that although it provided important anatomic information, it missed clinical findings in half of the patients.[14] The main reason was the lack of sensitivity of the color power Doppler feature, the lack of spectral Doppler, and image-quality problems. However, Table 32.5 shows the results of a more recent study using a newer generation devices in the critical care overcoming the earlier-mentioned limitations.[15] The bedside ultrasound examination led to changes in the diagnosis in 39.8% of patients and to changes in the management in 20.8% of patients. This is an example of the fact that ultrasound stethoscopes are continuously evolving and improving their technical capabilities resulting in better performance results.

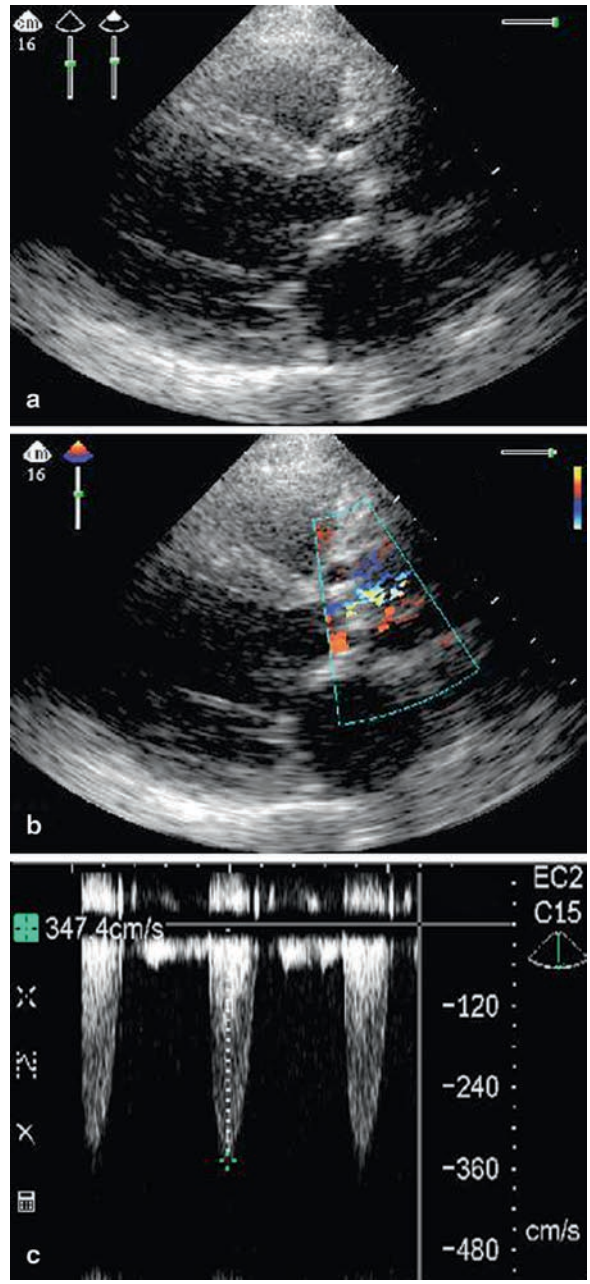

Fig. 32.15 Parasternal long-axis view of a 54-year-old patient with a calcified aortic valve (**a**) and turbulent flow (**b**) in the outflow tract in systole. The high flow velocity through the valve can be appreciated (**c**). The patient had no history of cardiac disease and was referred for progressive dyspnea to the outpatient cardiology clinic

Newer studies with the use of ultrasound stethoscope from critical care physicians have shown the real value in the critical care environment.[16,17]

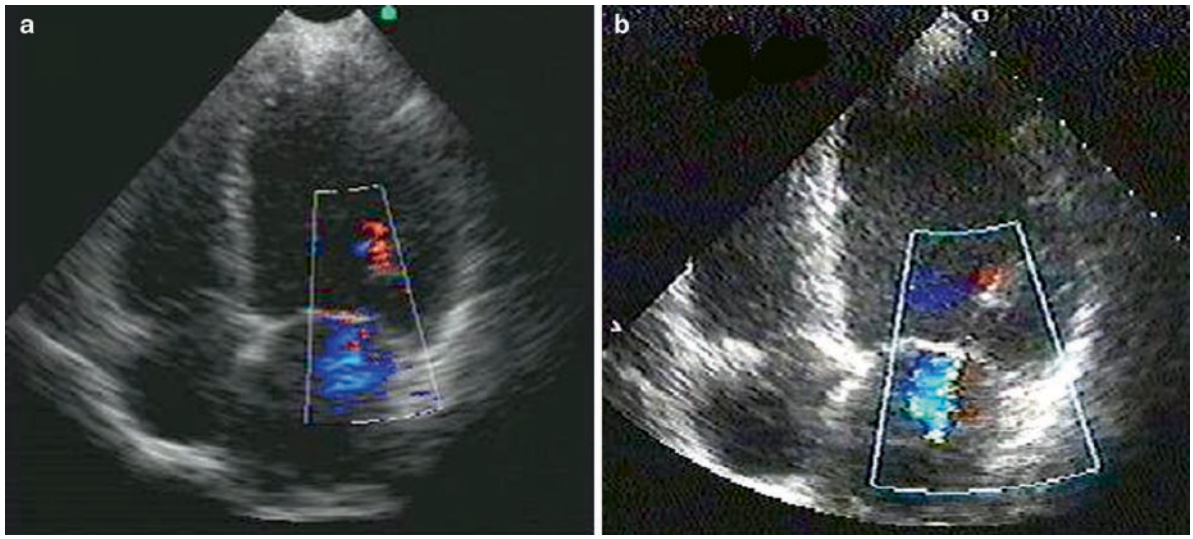

Fig. 32.16 Apical four-chamber view of a 45-year-old male with dilated cardiomyopathy. (**a**) A mitral regurgitant jet is visualized (SonoHeart™). The imaging quality of the hand-held device can be appreciated against that of a standard echocardiographic system (HP, Sonos 5000™)

Table 32.5 Ultrasound stethoscopes in the critical care environment

Number of changes in principal diagnosis out of 133 after initial evaluation (%)									
Shift of likelihood									
			Positive		Negative			Secondary Diagnosis	
	Total changes (%)	New DX	Minor	Major	Minor	Major	Total	New	Excluded
Heart failure	28(21.1)	1	9	4	10	4	27	–	–
Pericardia effusion	11(8.3)	1	1	–	6	3	10	–	–
RV dysfunction	5(3.8)	1	–	–	3	1	4	–	–
Drug toxicity	1(0.8)	–	–	–	–	1	1	–	–
Aortic stenosis	5(3.8)	1	–	1	1	2	4	–	1
Myocardia infarction	1(0.8)	–	–	–	1	–	1	–	–
Mitral regurgitation	1(0.8)	–	–	–	1	–	1	5	1
Tricuspid regurgitation	1(0.8)	–	–	1	–	–	1	7	–
Thrombus	–	–	–	–	–			1	–
Aortic regurgitation	–	–	–	–		–		8	2
LV Hypertrophy	–	–	–	–	–			1	–
Total	53(39.8)	4(3.0)	10(7.5)	6(4.5)	22(16.5)	11(8.3)	49(36.8)	22	4

LV left ventricular, *RV* right ventricular, *DX* diagnosis

- Pericardiocentesis can be guided and the effects of acute interventions (e.g., fluid challenge in hemodynamically compromised patients, inotropic drugs) monitored through estimation of cavity dimensions (Fig. 32.17), ejection fraction, and wall dynamics.
- Right ventricular involvement in acute myocardial infarction and the mechanical complications of a myocardial infarction are readily diagnosed in the coronary care unit (Fig. 32.18). Moreover, echocardiography of the right heart is of great value in patients with acute pulmonary embolism. The demonstration of right ventricular dilatation and paradoxical septal motion in patients clinically suspected raises the level of suspicion significantly while their absence does not exclude pulmonary embolism. On the other hand, many conditions that clinically mimic pulmonary embolism are rapidly identified.

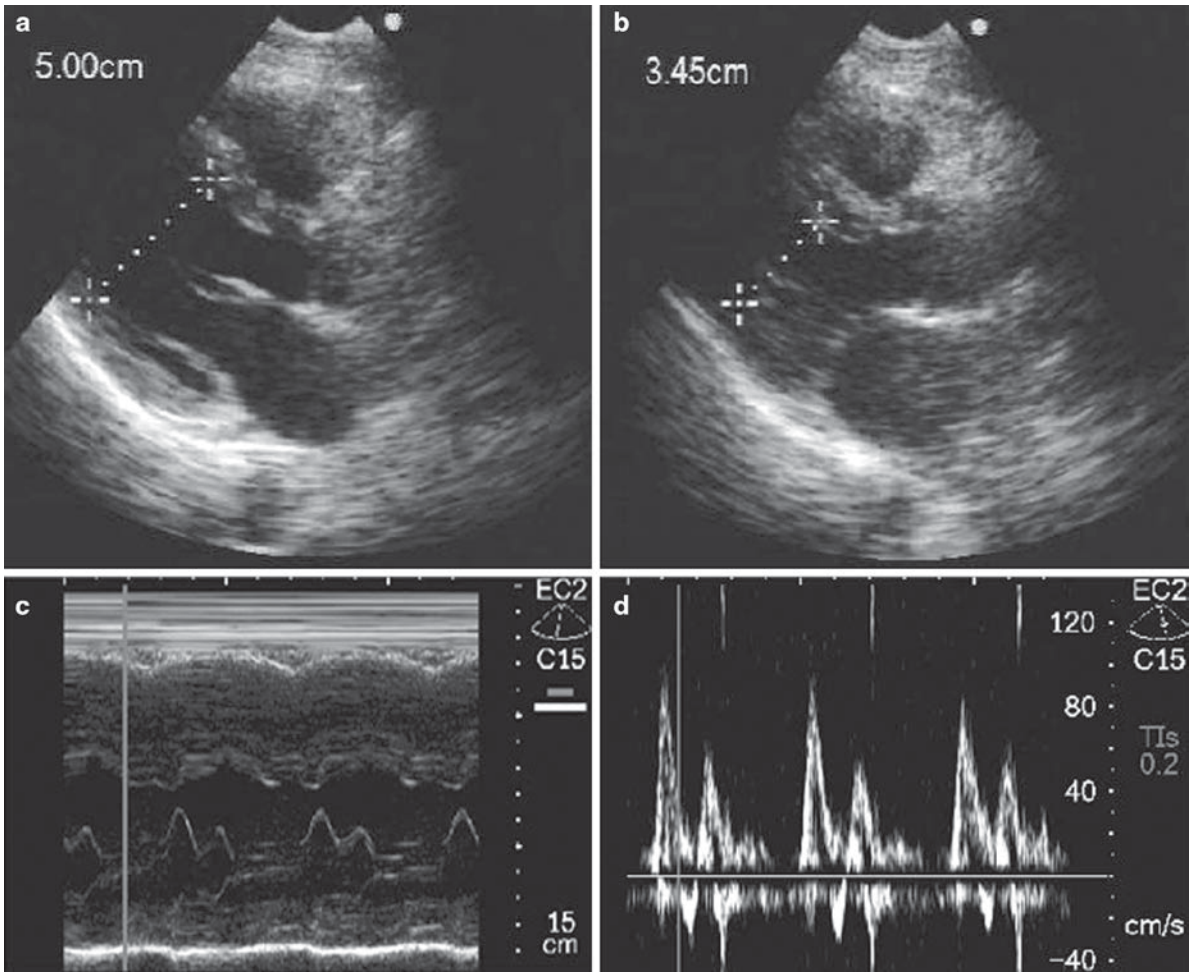

Fig. 32.17 Principle of systolic (**a**) and diastolic (**b**) measurements of the left ventricle in the parasternal long-axis view. A caliper function allows to measure the left ventricular dimensions in end-diastole (5 cm) and end-systole (3.45 cm) (**c**) M-Mode and Pulsed Doppler features (SonoHeart™)

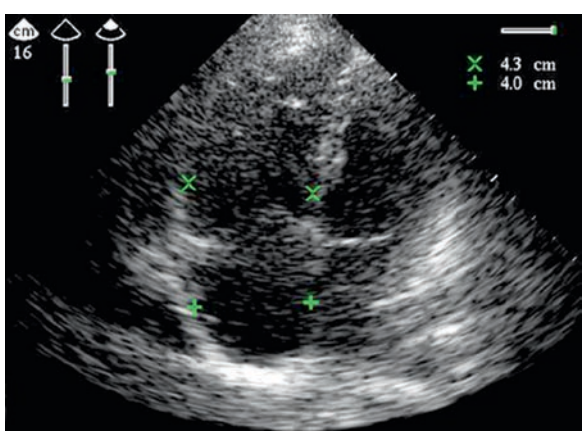

Fig. 32.18 Measurement of right ventricular and right atrial end-diastolic dimension in a four-chamber view (SonoHeart™)

- In the trauma emergency care, immediate echocardiographic assessment in the emergency room has proven to considerably shorten the time to diagnosis of penetrating cardiac injury and to improve the chances of survival. Furthermore, hand-held ultrasound devices enable reliably focused assessment with sonography for trauma (FAST) in patients with penetrating abdominal trauma in level-I urban trauma centers and during helicopter transports of casualties.
- Hand-held ultrasound devices can be used in the neonatal intensive care nursery allowing the rapid diagnosis of common neonatal problems and enabling the continuous evaluation of critically ill neonates.

Screening

The ultrasound stethoscope can be used for screening and identifying cardiac disorders in selected risk groups or in the general population.

Abdominal Aortic Aneurysm Screening

Patients with abdominal aortic aneurysm rupture experience high perioperative mortality rate (50%) in contrast to patients undergoing elective aortic surgery (2–3%). It is therefore recommended that patients at risk are screened by ultrasound and undergo prophylactic surgery if the diameter exceeds 55 mm (UK small aneurysm trial). Male gender, smoking, elderly age (>65 years), hypertension, coronary artery disease, and family history are high-risk parameters. Physical examination is notably insensitive in moderately enlarged aneurysmata and obese patients. Recently, the multicenter aneurysm screening study (MASS) provided evidence of benefit from a population-based screening program for abdominal aortic aneurysm in men aged 65–74. Furthermore, results from a "quick-screen" ultrasound program for abdominal aortic aneurysm suggest screening in all males above the age of 60 as essential and cost effective. Such screening programs could be most effectively applied with the ultrasound stethoscope. Abdominal aortic diameter measurements with ultrasound stethoscopy compare well to those obtained with standard equipment and are obtained in a few minutes during a routine physical examination (Figs. 32.19 and 32.20).[18-20]

LV Dysfunction Screening

Ischemic LV dysfunction is the main cause of congestive heart failure, which is associated with high morbidity and mortality and high health care costs. However, clinical diagnosis of LV dysfunction with the existing conventional criteria is often difficult and inaccurate. Appropriate management of these patients can delay if not prevent the development of chronic heart failure. Echocardiography is known to be the screening method of choice for LV dysfunction assessment but is considered not cost effective as a screening tool, especially in the community with a low probability of cardiac dysfunction. Furthermore its availability is often limited in the different clinical settings. Brain natriuretic peptide is a sensitive marker of increased intracardiac pressure of any cause and has been introduced as a new simple and cost-effective screening tool for LV dysfunction by the European Society of Cardiology. However, the major advantage of echocardiography is that it allows etiologic diagnosis of LV dysfunction and follow-up examinations. Today, ultrasound stethoscopy brings echocardiography into the community setting for the first time. Studies have shown that ultrasound stethoscopes compare well with standard echocardiographic devices in identifying LV dysfunction (Table 32.6)[21,22] and that the combination with physical examination improves the diagnostic evaluation of this disorder. However, a discordance rate of 10% for ultrasound stethoscopy versus SE LV function evaluation has been reported when using a broad range of LV function classification (EF <40%, 40–54%, 55–70%).[23] Borderline EFs can be misclassified even by experienced echocardiographers. It is obvious that this limitation does not only apply to the ultrasound stethoscopes but also to the standard echocardiographic systems and proves that echocardiography is operator dependent.

Ultrasound stethoscopes can be potentially utilized in chest pain clinics for rapid screening to exclude wall motion abnormalities in the context of acute chest pain and a nondiagnostic electrocardiogram.

Mitral Valve Prolapse Screening

Diagnosis of mitral valve prolapse may be difficult with auscultation and is often suspected in otherwise asymptomatic individuals. Echocardiography can accurately conform or exclude this disorder by a single parasternal long-axis view. Ultrasound stethoscopy has proven reliable in detecting this abnormality (Fig. 32.21) and may allow screening programs in primary care with little time and cost.

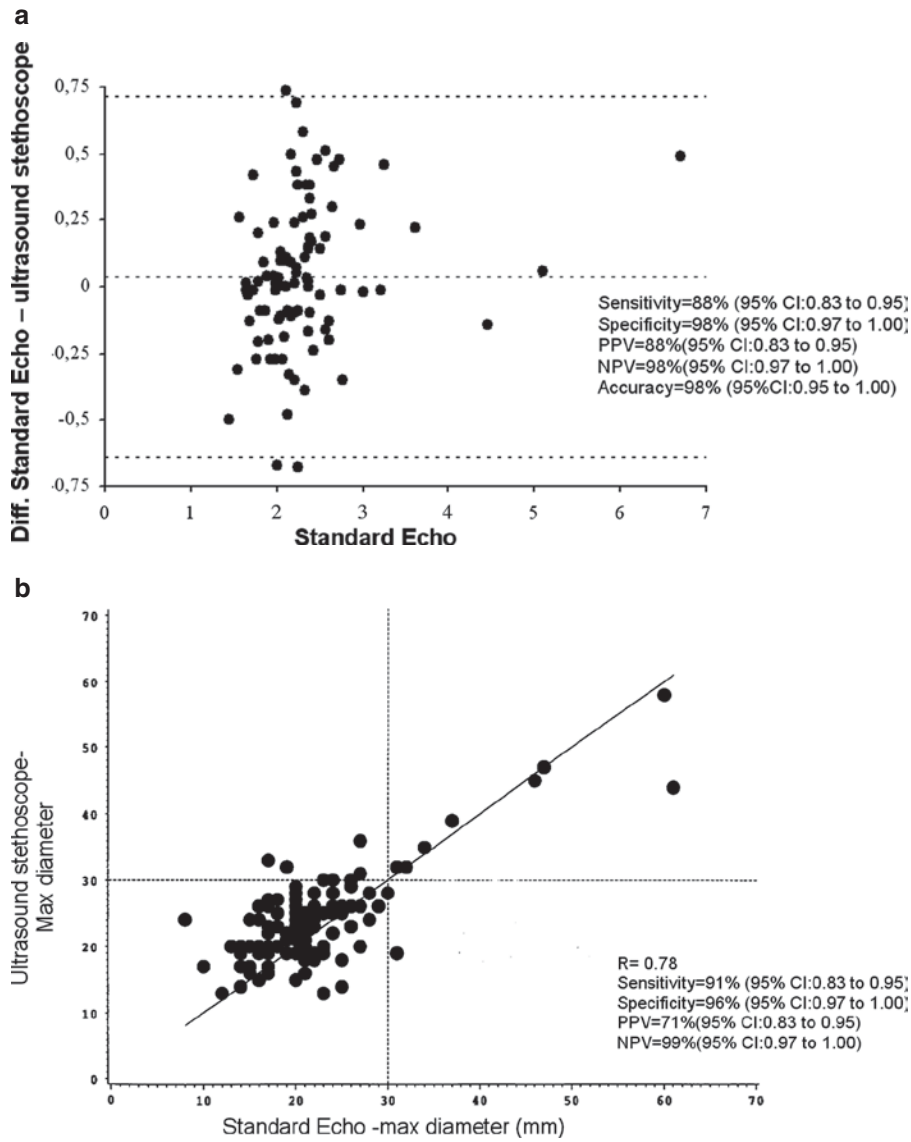

Fig. 32.19 (**a**) Bland-Altman plot, demonstrating the magnitude of the difference between the measurements of the abdominal aorta with the two techniques (differences plotted against their mean average). 2 SD = 2 standard deviations of the mean difference in the measurements of the two devices.[18] (**b**) Correlation between ultrasound stethoscope versus standard echocardiography for measurements of the abdominal aorta[20] In both studies using the standard echo as the gold standard, the sensitivity and the specificity of the ultrasound stethoscope for screening of the presence of Aortic abdominal aneurysm were calculated as well as the positive predictive value (PPV), negative predictive value (NPV), and accuracy

Screening of Athletes

Potentially dangerous conditions can be identified in preparticipation screening of athletes. Hypertrophic cardiomyopathy, a dilated ascending aorta (Marfan's disease) (Fig. 32.22), and valvular abnormalities (bicuspid valve, mitral valve prolapse) are the most common disorders and are reliably detected by experienced examiners.

Studies have shown that abnormal findings are detected during such preparticipation screening strategies in otherwise asymptomatic individuals. A limited echocardiographic screening program reported that in 10.4% of the screened athletes, prophylaxis for endocarditis

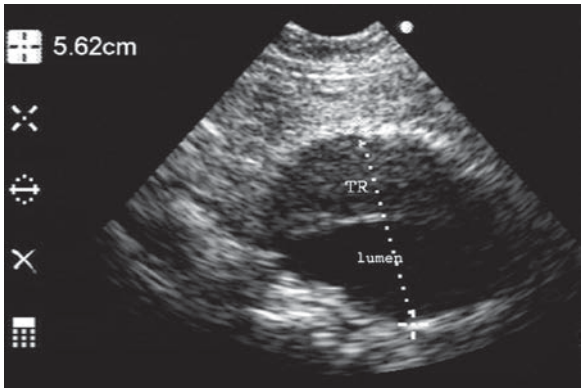

Fig. 32.20 Transverse image of the aneurysm of the abdominal aorta (56 mm in diameter) which contains a large thrombus (TR). *Dotted line* represents the caliper used for measurements of the diameter of the aneurysm

was recommended after the echocardiographic examination proving the importance of such programs.

However, screening for cardiac disorders in young athletes and asymptomatic individuals involves a high risk of a false-positive diagnosis and should be performed by well-trained and experienced clinicians.

Screening for LV Hypertrophy

Ultrasound stethoscope allows to screen for LV hypertrophy and to follow the effect of antihypertensive treatment in office practice.

Discrepancies between study results may, however, be due to the use of earlier versions of ultrasound

Table 32.6 Agreement of regional of regional wall motion analysis (RWMA) between an ultrasound Stethoscope and a standard echocardiographic device

(A) RWMA (SE)				
		Abnormal	Normal	
RWMA (Ultrasound stethoscope)	Abnormal	16	8	
RWMA (Ultrasound stethoscope)	Normal	1	57	
(B)	Standard examination (no RWMA)	Standard examination (single territory)	Standard examination (multiple territories)	Total
HCU (no RWMA)	22	5	7	34
HCU (single territory)	5	20	27	52
HCU (multiple territories)	0	7	31	38
Total	27	32	65	124

(C) Agreement of global left ventricular function between an ultrasound stethoscope and a standard echocardiographic device

LVEF (SE)		Abnormal	Normal
LVEF-(Ultrasound stethoscope)	Abnormal	17	1
LVEF-(Ultrasound stethoscope)	Normal	2	62

Agreement = 90%, kappa = 0.80
No. of patients: 34
No. of segments: 204. The numbers inside the table express the number of segments
SE = Standard echocardiographic device
Vourvouri et al. J Am Soc Echocardiogr. 2002
Number of patients = 394
Agreement for presence or absence of RWME between HCU and SE = 86.3%
Agreements for the assessment of the mumber of coronary artery territories involved and their location = 60%
HCU = Hand-carried ultrasound device
Burce et al. Am J Cardiol 2002
Number of patients = 82
Agreement = 96%, Kappa = 0.89
Sensitivity = 89% (95% Cl:0.72 1/N 0.94)
Specificity = 98% (95% Cl:0.93 1/N 0.99)
PPV = 94% (95% Cl:0.76 1/N 1.0)
NPV = 97% (95% Cl:0.92 1/N 0.98)
LVEF = left ventricular ejection fraction.
The LVEF was estimated visually with the ulrasound stethoscope.
The SE 1/N LVEF derived by the Simpson's biplane method.
A LVEF <40% represented LV dysfunction
SE = standard echocardiographic device
Vourvouri et al. Eur J Heart Faill. 2003.

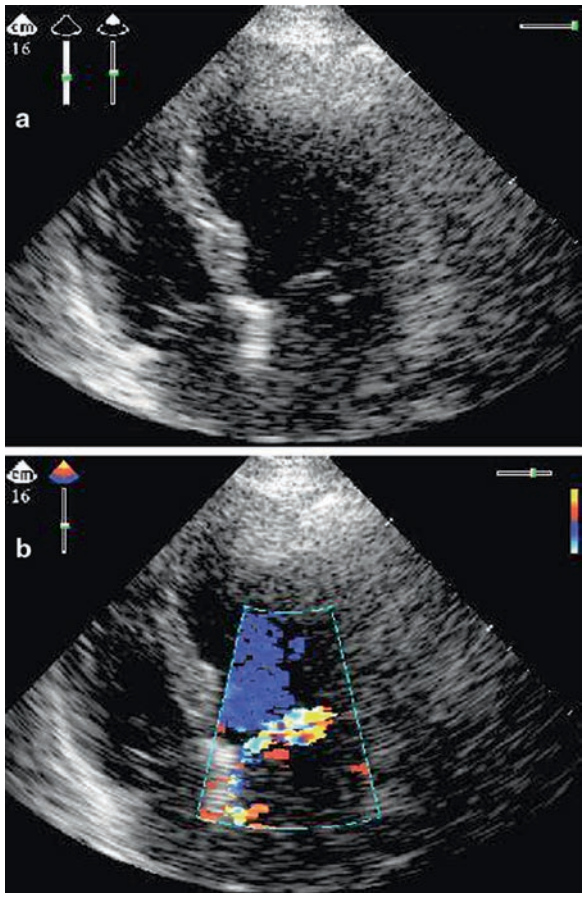

Fig. 32.21 Apical four-chamber view of a 45-year-old patient with prolapse of the posterior mitral leaflet and eccentric jet toward the interatrial septum. The patient was referred for the evaluation of palpitations and was known to have a systolic murmur

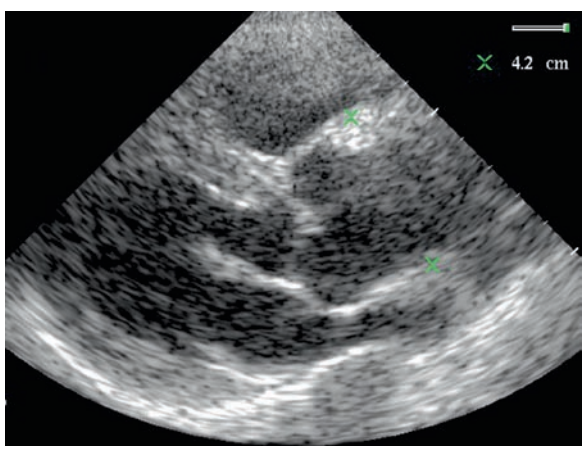

Fig. 32.22 Long-axis view of an 18-year-old female with the phenotype of Marfan. A dilatation of the ascending aorta measuring 4.2 cm is seen (OptiGo™)

stethoscopes that do not reflect their current or future technical performance. Furthermore, it is important to consider not only the sensitivity of a hand-held device for identifying or excluding a specific condition but also the competence of the examiner.

Cost Effectiveness

Since most of the patients are referred for echocardiography to answer a single clinical question, a new strategy of limiting echo services has been introduced in daily clinical practice. It is shown that a limited echocardiographic imaging protocol can reduce the time of examination and lead to cost savings. A full SE is suggested only when an abnormality is discovered. However, it is documented that a limited echocardiographic protocol is cost effective in young outpatients rather than in older patients since the prevalence of cardiovascular abnormalities in the latter group is higher. Ultrasound stethoscopy, being ultraportable and easy to use, is a perfect candidate for a limited, goal-oriented echo examination. In addition, many of these devices have the potential to proceed to a more complete examination whenever this is considered necessary.

Like all technological breakthroughs, ultrasound stethoscopy had to be evaluated in financial terms as well as by clinical effectiveness in order to gain wide acceptance. The capital investment of such a device is economical (~1/12th of the cost of a SE) and the maintenance costs are low.

It is demonstrated that the ultrasound stethoscope provides the physician in 78.5% of patients with efficient instant information making a further SE or other imaging examination redundant and leading to a cost reduction of 33.4%. Furthermore, it is reported that the presence of an abnormal initial limited echocardiographic examination at the emergency department has the consequence of a significant hospital stay length (i.e., >2 days). This stresses the importance of such an initial examination at the point of care.

Ultrasound stethoscopy leads to cost savings not only by reducing the number of referrals for SE but also by reducing the time required for performing an ultrasound examination at the bedside. It is demonstrated that the time saved for acute ultrasound assessment at the bedside using an ultrasound stethoscope

compared to a mobile system is considerable.[24] Saving time translates into cost savings, more time for other patients, and potentially into the saving of lives.

Ultrasound stethoscopy has been proven to be suitable for screening for various cardiac pathologies. However, unlike a diagnostic test, a screening test is performed in apparently healthy people, which raises unique ethical and reimbursement issues. The following factors are therefore important regarding the initiation of a screening test (1) the effectiveness of the test in detecting the screened abnormality, (2) the cost of a test, (3) the prevalence of disease, and (4) the potential therapeutic or survival benefit of an early detection and treatment.

The prevalence of disorders like abdominal aortic aneurysm, LV dysfunction, and LV hypertrophy in high-risk patients is high and screening for these disorders is worthwhile and cost effective in terms of therapeutic benefit to the patients and in terms of reducing the cost of lifetime management. Ultrasound stethoscopes, having proven reliable in detecting these disorders and being of low cost, seem to be the perfect screening tool bringing furthermore echocardiography to the patient and into the community.

Training Requirements Using Ultrasound Stethoscopy

No doubt that training is required to use an imaging device. Recently the American Society of Cardiology[25] published guidelines regarding the use of ultrasound stethoscopes recommending Level I of training (Table 32.7) as an absolute minimal level required. However, recent studies have shown that it is possible to train physicians and students for the detection of significant pathologies in a short period of time (Table 32.8). It seems that identifying the basic major cardiac disorders limited training may be sufficient.

Future Directions

The idea of a "personal" ultrasound stethoscope (Table 32.9) is certainly appealing and in combination with its low cost it is clear that in future larger number of physicians and not just cardiologists will have access to these devices. Training of non-echocardiographers may become an important issue and should focus on criteria of normalcy and identifying both major and acute cardiac disorders. In fact, the device should be used in a way comparable to auscultation; whenever there is doubt, further echo/Doppler examination should follow. Training programs and continuing medical education including performance testing can be organized with modern electronic means. Moreover, introducing the ultrasound stethoscope into the medical school curriculum like the stethoscope will result in physicians capable of using these devices as an extension to physical examination. The use of ultrasound stethoscopes by general practitioners can lead to early diagnosis and management of patients and hospitals will benefit from the lower rate of inappropriate referrals.

In the future, advances in telecommunications and software will allow for diagnostic support from experienced laboratories or intensive care units. In pediatrics, telemedicine consultations have already successfully started in terms of remote assessment of heart murmurs sent as e-mail attachments to cardiologists in specialized centers.

Furthermore, immediate feedback from the echocardiographic examination leads to improvement of our clinical skills and especially of our auscultation skills. It should be remembered that the real value of any imaging technology is intimately dependent on our intellectual contribution and individual responsibility.

With the impressive progress in other imaging modalities such as computed tomography (CT) and magnetic resonance imaging (MRI) it is likely that the more complicated clinical questions and scenarios will be directed to such, giving to the ultrasound stethoscope the role of the everyday available imaging tool in our pocket.

Conclusion

Ultrasound stethoscopy is a fast developing field in cardiology. Physicians should embrace this innovation and add it to their physical examination. This will result in better patient care and cost savings since a definitive diagnosis is made in the majority of patients leading to their instant management.

Table 32.7 Core Cardiology Training in adult cardiovascular medicine (COCATS). Task Force 4: training in echocardiography

Duration of training		Cumulative duration of training	Minimal additional No. of examinations	Cumulative No. of examinations	TEE and special procedures
Level 1	3 months	3 months	150[a]	150a	No
Level 2	3 months	6 months	150[a]	300	No
Level 3	6 months	12 months	450[a]	750	Yes

*TEE*transesophageal echocardiography

From Ryan et al[26]

[a]Performance and interpretation of the study

Table 32.8 Overview over published clinical studies/reviews in cardiology regarding the training for the use of ultrasound stethoscopy

Author	Title of study	Journal published
Alexander et al	Training and accuracy of noncardiologists in simple use of point care echo: a preliminary report from the Duke limited echo assessment project (LEAP)	*Thoraxcenter J*. 2001;13:105-110
Bruce et al	Utility of hand-carried ultrasound devices used by cardiologists with and without significant echocardiographic experience in the cardiology inpatient and outpatient settings	*Am J Cardiol*. 2002;90:1273-1275
Zamorano et al	Echocardiography performed by physicians outside echo labs: Is it possible?	*Eur Heart J*. 2002;23:908-909
DeCara et al	The use of small personal ultrasound device by internists without training in echocardiography	*J Am Soc Echocardiogr*. 2001;14: P3-P40 (abstr)
Croft et al	The echo stethoscope: is it ready for prime time for medical students?	*J Am Coll Cardiol*. 2002 (Suppl A);39:448A (abstr)
Harish et al	Is it possible to train medical students to perform and interpret diagnostic limited echocardiograms performed with a minimachine?	*J Am Soc Echocardiogr*. 2001;14;P3-42 (abstr)
Kimura et al	Usefulness of a hand-held ultrasound device for bedside examination of left ventricular function	*Am J Cardiol*. 2002;90:1038-1039
Wittich et al	Teaching cardiovascular anatomy to medical students by using a hand-held ultrasound device	*JAMA*. 2002;288:1062-1063
Seward et al	Hand-carried cardiac ultrasound (HCU) device: recommendations regarding new technology. A report from the echocardiography task force on new technology of the nomenclature and standards committee of the American Society of Echocardiography	*J Am Soc Echocardiogr*. 2002;15: 369-373

Table 32.9 Overview over peer-reviewed published clinical studies/reviews in cardiology performed with ultrasound stethoscopy stressing it's widely acceptance and future perspectives

Author	Title of study	Journal published
Roelandt et al	The ultrasound cardioscope: a hand-held scanner for real-time cardiac imaging	*J Clin Ultrasound*. 1980;8:221-225
Schwarz et al	Experience rounding with a hand-held two-dimensional cardiac ultrasound device	*Am J Cardiol*. 1988;62:157-159
Bruce et al	Personal ultrasound imager: abdominal aortic aneurysm screening	*J Am Soc Echocardiogr*. 2000;13:674-79
Vourvouri et al	Abdominal aortic aneurysm screening using a hand-held ultrasound device	*Eur J Vasc Endovasc Surg*. 2001;22:352–354
Spencer et al	Physician performed point-of-care echocardiography using a laptop platform compared with physical examination in the cardiovascular patient	*J Am Coll Cardiol*. 2001;37:2013-2018
Goodkin et al	How useful is a hand-carried bedside echocardiography in critically ill patients?	*J Am Coll Cardiol*. 2001;37:2019-2022
Rugolotto et al	Rapid assessment of cardiac anatomy and function with a new hand-carried ultrasound device (OptiGo): a comparison with standard echocardiography	*Eur J Echocardiogr*. 2001;2:262-269

(continued)

Table 32.9 (continued)

Author	Title of study	Journal published
Sianos et al	Aneurysm of the abdominal aorta	*Circulation*. 2001;104:e10–e11
Vourvouri et al	Experience with an ultrasound stethoscope	*J Am Soc Echocardiogr*. 2002;15:80-85
Vourvouri et al	Clinical utility and cost effectiveness of a personal ultrasound imager in the cardiac evaluation during consultation rounds in patients with suspected cardiac disease	*Heart*. 2003;89:727–730
Vourvouri et al	Left ventricular hypertrophy screening using a hand-held ultrasound device	*Eur Heart J*. 2002, 26:1516-1521
Vourvouri et al	Screening for left ventricular dysfunction using a hand-carried cardiac ultrasound device	*Eur J Heart Failure*. 2003;5:767–774
Rugolotto et al	Clinical use of cardiac ultrasound performed with a hand-carried device in patients admitted for acute cardiac care	*Am J Cardiol*. 2002;90:1040-1042
Fischer et al	Ultrasound at the bedside:does a portable ultrasound device save time?	*Ultraschalll in Med*. 2002;81:311-314
Bruce et al	Utility of hand-carried ultrasound devices used by cardiologists with and without significant echocardiographic experience in the cardiology inpatient and outpatient settings	*Am J Cardiol*. 2002;90:1273-1275
Roelandt	A personal ultrasound imager (ultrasound stethoscope) in the physical cardiac diagnosis!	*Eur Heart J*. 2002; 23:523-527
Solomon and Braunwald	Point-of-care echocardiography: asking the right questions	*Eur J Echocardiogr*. 2001;2:216-218
Schiller	Hand-held echocardiography: revolution or hassle?	*J Am Coll Cardiol*. 2001;37:2023-2024
Salustri and Trambaiolo	Point-of-care echocardiography: small, smart, and quick	*Eur Heart J*. 2002;23:1484–1487

As it is ultraportable it can go into the community and be used in larger populations for screening purposes of pathologies like abdominal aortic aneurysm and LV dysfunction. Their early detection can play a live saving role and is long term cost effective.

References

1. Roelandt JRTC. Seeing the heart; the success story of cardiac imaging. *Eur Heart J.* 2000;21:1281-1288.
2. Ligtvoet CM, Rijsterborgh H, Kappen L, Bom N. Real time ultrasound imaging with a hand-held scanner. Part I-technical description. *Ultrasound Med Biol.* 1978;4: 91-92.
3. Roelandt J, Bom N, Hugenholtz PG. The ultrasound cardioscope. A hand-held scanner for real-time cardiac imaging. *J Clin Ultrasound.* 1980;8:221-225.
4. Popp RL. The physical examination of the future: echocardiography as part of the assessment. *ACC Current Rev.* 1998;7:79-81.
5. Vourvouri EC, Poldermans D, de Sutter J, Sozzi FB, Izzo P, Roelandt JRTC. Experience with an ultrasound stethoscope. *J Am Soc Echocardiogr.* 2002;15:80-85.
6. Rugolotto M, Hu BS, Liang DH, Schnittger I. Rapid assessment of cardiac anatomy and function with a new hand-carried ultrasound device (OptiGo): a comparison with standard echocardiography. *Eur J Echocardiogr.* 2001;2: 262-269.
7. Vourvouri EC, Poldermans D, Deckers JW, Roelandt JRTC. Evaluation of a hand-carried cardiac ultrasound device in an outpatient cardiology clinic. *Circulation.* 2002; 106(Suppl II):506.
8. Spencer KT, Anderson AS, Bhargava A, Bales AC, Sorrentino M, Furlong K, Lang RM. Physician-performed point-of-care echocardiography using a laptop platform compared with physical examination in the cardiovascular patient. *J Am Coll Cardiol.* 2001;37:2013-2018.
9. Trambaiolo P, Papetti F, Posteraro A, Amici E, Piccoli M, Cerquetani E, Pastena G, Gambelli G, Salustri A. A hand-carried ultrasound device in the outpatient cardiology clinic reduces the need for standard echocardiography. Heart 2007;93:470-475.
10. Kobal SL, Trento L, Baharami S, Tolstrup K, Naqvi TZ, Cercek B, Neuman Y, Mirocha J, Kar S, Forrester JS, Siegel RJ. Comparison of effectiveness of hand-carried ultrasound to bedside cardiovascular physical examination. *Am J Cardiol.* 2005;96:1002-1006.
11. Vourvouri EC, LY Koroleva, FJ ten Cate, D Poldermans, AFL Schinkel, RT van Domburg, WB Vletter, JRTC Roelandt. Clinical utility and cost-effectiveness of a personal ultrasound imager for cardiac evaluation during consultation

rounds in patients with suspected cardiac disease. *Heart.* 2003;89:727-730.
12. Greaves K, Jeetley P, Hickman M, Dwivedi G, Sabharwal N, Lim T, Janardhanan R, Senior R. The use of hand-carried ultrasound in the hospital setting- a cost-effective analysis. *J Am Soc Echocardiogr.* 2005;18:620-625.
13. Vourvouri EC, Poldermans D, Schinkel AFL, Koroleva L, Sozzi FB, Bax JJ, Roelandt JRTC. Left ventricular hypertrophy screening using a hand-held ultrasound device. *Eur Heart J.* 2002;26:1516-1521.
14. Goodkin GM, Spevack DM, Tunick PA, Kronzon I. How useful is hand-carried bedside echocardiography in critically ill patients?. *J Am Coll Cardiol.* 2001;37:2019-2022.
15. Rugolotto M, Chang CP, Hu B, Schnittger I, Liang DH. Clinical use of cardiac ultrasound performed with a hand-carried device in patients admitted for acute cardiac care. *Am J Cardiol.* 2002;90:1040-1042.
16. Spurney CF, Sable CA, Berger JT, Martin GR. Use of a hand-carried ultrasound device by critical care physicians for the diagnosis of pericardial effusions, decreased cardiac function, and left ventricular enlargement in pediatric patients. *J Am Soc Echocardiogr.* 2005;18:313-319.
17. Manasia AR, Nagaraj HM, Kodali RB, Croft LB, Oropello JM, Kohli-Seth R, Leibowitz AB, DelGiudice R, Hufanda JF, Benjamin E, Goldman ME. Feasibility and potential clinical utility of goal-directed transthoracic echocardiography performed by noncardiologist intensivists using hand-carried device (SonoHeart) in critically ill patients. *J Cardiothorac Vasc Anesth.* 2005;19:155-159.
18. Vourvouri EC, Poldermans D, Schinkel AFL, Sozzi FB, Bax JJ, van Urk H, Roelandt JRTC. Abdominal aortic aneurysm screening using a hand-held ultrasound device. A pilot study. *Eur J Vasc Endovasc Surg.* 2001;22:352-354.
19. Sianos G, Vourvouri E, Nieman K, Ligthart JM, Thuri A, de Feyter PJ, Serruys PW, Roelandt JR. Aneurysm of the abdominal aorta. *Circulation.* 2001;104:E10-E11.
20. Bruce CJ, Spittell PC, Montgomery SC, Bailey KR, Tajik AJ, Seward JB. Personal Ultrasound Imager: Abdominal aortic aneurysm screening. *J Am Soc Echocardiogr.* 2000;13:674-679.
21. Vourvouri EC, Schinkel AFL, Roelandt JRTC, Boomsma F, Sianos G, Bountioukos M, Sozzi FB, Rizzello V, Bax JJ, Karvounis HI, Poldermans D. Screening for left ventricular dysfunction using a hand-carried cardiac ultrasound device. *Eur J Heart Fail.* 2003;5:767-774.
22. Kimura BJ, Amundson SA, Willis CL, Gilpin EA, DeMaria AN. Usefulness of a hand-held ultrasound device for bedside examination of left ventricular function. *Am J Cardiol.* 2002;90:1038-1039.
23. Bruce CJ, Montgomery SC, Bailey KR, Tajik J, Seward JB. Utility of hand-carried ultrasound devices used by cardiologists with and without significant echocardiographic experience in the cardiology inpatient and outpatient settings. *Am J Cardiol.* 2002;90:1273-1275.
24. Fischer T, Filimonow S, Petersein J, Beyersdorff D, Muehler M, Bollow M, Badakhshi HR, Hamm B. Ultrasound at the bedside: does a portable ultrasound device save time?. *Ultraschalll in Med.* 2002;81:311-314.
25. Seward JB, Douglas PS, Erbel R, Kerber RE, Kronzon I, Rakowski H, Sahn DJ, Sisk EF, Tajik AJ, Wann S. Hand-carried cardiac ultrasound (HCU) device: recommendations regarding new technology. A report from the echocardiography task force on new technology of the nomenclature and standards committee of the American Society of Echocardiography. *J Am Soc Echocardiogr.* 2002;15:369-373.
26. Ryan T, Armstrong WF, Khanderia BK. Task Force 4: Training in echocardiography endorsed by the American Society of Echocardiography. *J Am Coll Cardiol.* 2008;51:361-367.

Chapter 33
Echo-Guided Interventions

Frank E. Silvestry

Introduction

The performance of complex percutaneous noncoronary interventional procedures has increased dramatically over the past several decades, with numerous devices and procedures designed to close atrial septal defects and patent foramen ovale, perform complex mitral valve repair, and implant percutaneous aortic valves. As these procedures evolve toward an increasingly complex, anatomically based approach, the use of real-time echocardiography for guidance has become essential to their success. Traditionally fluoroscopy and angiography have been utilized for procedural guidance in the catheterization and electrophysiology laboratory, but significant limitations exist. Fluoroscopy is unable to identify important anatomic structures such as the cardiac valves and annular structures, as well as the atrial septum, coronary sinus ostium, vena cava, and pulmonary veins. Angiography offers some improvement over fluoroscopy, but cannot delineate complex anatomical structures, and the relationship between two structures that do not share a common cardiac chamber, requires the use of radiographic contrast agents, and cannot be performed continuously in real time during the procedure. Furthermore targets of therapy such as the mitral and aortic valves, and the fossa ovalis are complex three-dimensional structures, and therapeutic devices must be deployed in a precise anatomic fashion for proper function. During percutaneous noncoronary interventions, echocardiographic guidance assists the interventional cardiologist in the performance of transseptal catheterization, in monitoring guide wire, delivery sheath, and balloon or device position, as well as in the evaluation for thrombus, pericardial effusion, and other procedural complications. This chapter will review the echocardiographic modalities (transthoracic echocardiography, transesophageal echocardiography, real-time 3D echocardiography, and intracardiac echocardiography) used to guide these procedures in the catheterization laboratory.

ACC/AHA/ASE Guidelines for the Clinical Application of Echocardiography

In 2003 the American College of Cardiology, American Heart Association, and American Society of Echocardiography Practice Guidelines were updated, and these guidelines are designed to provide a framework for the use of echocardiography in a wide variety of clinical settings.[1] The routine use of transthoracic echocardiography (TTE) and transesophageal echocardiography (TEE) is covered extensively in these guidelines; however to date, they do not specifically address real-time 3D echocardiography or intracardiac echocardiography (ICE). Recommendations for use of TTE and TEE in specific clinical settings are based on the strength of evidence in the medical literature. Wherever applicable, this chapter will note the task force recommendations in the sections that follow. An American Society of Echocardiography writing group publication designed to specifically address echocardiographic guidance of percutaneous noncoronary procedures is in press and includes ICE.

F.E. Silvestry
Department of Medicine, Cardiovascular Division, Hospital of the University of Pennsylvania, Philadelphia, PA, USA
e-mail: Fsilvest@mail.med.upenn.edu

P. Nihoyannopoulos and J. Kisslo (eds.), *Echocardiography*,
DOI: 10.1007/978-1-84882-293-1_33,

Echocardiographic Modalities Used to Guide Interventional Procedures

Echocardiographic guidance of interventional procedures can be accomplished with a variety of echocardiographic modalities, each with unique advantages and disadvantages (see Table 33.1). TTE is widely available, inexpensive, and can be easily performed in the catheterization laboratory by a sonographer or echocardiographer, and as such it has been described to guide a wide variety of interventional procedures. Common procedural uses of TTE include echo-guided pericardiocentesis, percutaneous balloon mitral valvuloplasty for mitral stenosis, and alcohol septal ablation in patients with hypertrophic obstructive cardiomyopathy. TTE has also been described as an adjunctive imaging modality, to supplement ICE during percutaneous ASD closure in patients with deficient atrial septal rims,[2] or to supplement TEE during percutaneous mitral valve repair with the edge-to-edge clip repair system.[3] TTE is limited by its image resolution, which can be problematic in patients who are obese, have underlying lung disease, or who are being mechanically ventilated, and in patients who are supine for the procedure and cannot be positioned appropriately. TEE and ICE offer improved image resolution; however, they are more invasive and expensive, require additional expertise, and have been described to facilitate the deployment of percutaneous ASD and PFO closure devices, perform percutaneous valvuloplasty, as well as to guide more complex, noncoronary interventions such as transseptal catheterization, percutaneous mitral repair, placement of LAA occlusion devices, and placement of stented aortic valves. TEE requires additional sedation (either conscious sedation or general anesthesia) and the presence of an expert echocardiographer, whereas ICE does not require any additional sedation and can be performed by the interventional operator when suitable expertise exists. ICE has additional vascular risk as does any intracardiac catheter, and the single-use catheters are expensive. ICE requires additional operator expertise and training as well. Risks of TEE include aspiration, and esophageal trauma, and risks of ICE are low (<1–2%) but include vascular trauma, hematoma, retroperitoneal bleed, cardiac perforation, and arrhythmia.

Table 33.1 Procedures guided by echocardiography

Pericardiocentesis
Transseptal catheterization
Percutaneous balloon valvuloplasty
Percutaneous transcatheter closure of septal defects
Alcohol septal ablation in hypertrophic obstructive cardiomyopathy
Placement of percutaneous left ventricular support devices
Percutaneous repair of mitral regurgitation with the edge to edge repair system (evalve)
Percutaneous repair of mitral regurgitation with the coronary sinus devices
Placement of LAA occlusion devices
Placement of stented valve replacement
Echocardiographically guided RV and LV biopsies
Laser lead extraction of pacemaker and defibrillator leads
Congenital heart disease applications such as completion of Fontan, coarctation repair
Electrophysiologic procedures such as pulmonary vein isolation for atrial fibrillation, sinoatrial node modification for inappropriate sinus tachycardia, and ablation of LV ventricular tachycardia

TTE-Guided Pericardiocentesis

In the early 1980s, TTE-guided percutaneous pericardiocentesis was described by Seward et al, and 20 years later they described the outcome of this procedure performed in 1,127 patients since their initial report.[4,5] Echo-guided pericardiocentesis has been listed as a Class IIa indication in the ACC/AHA/ASE task force guidelines on the use of echocardiography.

Prior to the procedure, TTE allows an assessment of the size and location of the pericardial effusion, can determine whether the effusion is free flowing, loculated, or organized; and transvalvular Doppler assessment provides physiologic evidence for increased intrapericardial pressure and tamponade physiology.[6-10] With increasing intrapericardial pressure, exaggerated respirophasic variation in right- and left-sided inflow and outflow velocities develops as a result of abnormal ventricular interdependence.[7] Increased intrapericardial pressure is present when mitral and aortic velocities vary by more than 30% with respiration, and tricuspid and pulmonic velocities vary by more than 50%. With frank tamponade diastolic collapse of the right ventricle is typically seen, and this finding has a greater than 80% specificity for tamponade physiology. Clearance for traditional subxiphoid pericardiocentesis is assessed by determining the distance between the epicardial and parietal pericardial surfaces

at the apex of the heart, traditionally assessed in the subcostal views.

Some centers use echocardiography to select the optimal entry point for the needle (parasternal vs. apical vs. subcostal), while others use traditional anatomical landmarks and perform pericardiocentesis via a standard subcostal approach, using echocardiography to confirm that the pericardium has been appropriately cannulated.[11] With either approach, care must be taken to avoid contamination of the sterile field. As the needle tip (or sheath) used for cannulation may not be easily visualized on TTE, after a small amount of fluid (i.e., 10 cc) is withdrawn, confirmation that the needle or sheath is in the pericardial space is achieved by the injection of a small amount of agitated saline mixed with air to form contrast bubbles that are easily imaged by TTE.[12-15] If a nonpericardial space has been cannulated, the needle or smaller sheath is removed prior to placing any additional catheters, thus avoiding the risk of perforation. Once confirmation by contrast injection that the pericardial space has been appropriately cannulated, a larger drainage catheter is placed to evacuate the pericardial fluid. TTE also allows confirmation of the adequacy of drainage, as well as changes in the hemodynamic effect of the effusion may be obtained to guide further therapy.

TTE-guided pericardiocentesis can be performed portably and rapidly, and as such it can be performed at the bedside in unstable patients. The necessary equipment is widely available, and the technique is applicable to a wide variety of clinical conditions including malignancy and inflammatory effusions. When combined with extended catheter drainage and intermittent aspiration to drain the effusion "dry," it offers distinct advantages over traditional fluoroscopic guidance when performed by experienced operators.

Transseptal Catheterization

Transseptal catheterization is performed whenever diagnostic or therapeutic access to the left atrium is required. Its use is increasing with the performance of percutaneous mitral valve repair, as well as ablation of atrial fibrillation and other left atrial arrhythmia. Although imaging is not invariably required for transseptal catheterization, it offers advantages over traditional fluoroscopic approaches.[16-20] Anatomic variation in the position and orientation of the fossa ovalis and its surrounding structures may present specific challenges to even the most experienced interventionalists, and imaging with echocardiography offers increased safety, with lower risk of cannulating other spaces adjacent to the fossa. Similarly, imaging can decrease the time required for the transseptal to be performed, as well as minimizing the amount of fluoroscopy required, reducing radiation exposure.[21-24] Imaging may also assist in shortening the "learning curve" for those operators without significant transseptal experience.[17,25]

TTE does not offer sufficient imaging resolution to guide transseptal catheterization, and as such is rarely used solely for this purpose. Typically TEE and more recently ICE have been used. As ICE imaging can be performed without additional sedation or general anesthesia, as well as with minimal additional patient risk and discomfort, ICE is becoming the preferred modality if imaging is required.[21-24]

Percutaneous Balloon Valvuloplasty

Echocardiography can be used in the guidance of percutaneous balloon valvuloplasty of stenotic valves, to assess the adequacy of the result, and monitor for complications during the procedure.[26,27] The greatest experience with echocardiographic guidance of valvuloplasty has been in percutaneous balloon mitral valvuloplasty. In the updated ACC/AHA/ASE guidelines, echocardiography has been given a Class I indication for use in guiding percutaneous mitral balloon valvuloplasty. Both TTE and TEE are typically used to evaluate the anatomic suitability for PBV and exclude LAA thrombus. TTE often provides acceptable image quality for assessment of the mitral valvuloplasty score (see Table 33.2), and may provide suitable information

Table 33.2 Mitral valve scoring by echocardiography prior to PBV[a]

The extent and severity of valvular and subvalvular deformity can be assessed by assigning a score of 0–4 for each of the following
Degree of leaflet rigidity
Amount of leaflet calcification
Severity of leaflet thickening
Extent of subvalvular thickening and calcification

[a]The maximum score is 16; higher scores indicate more severe anatomic disease and reduced likelihood of success

for procedural guidance, but cannot exclude atrial thrombus. TEE can also be used to calculate the mitral valvuloplasty score if TTE images are not of diagnostic quality, assess for significant preprocedural mitral regurgitation, and most importantly is required to exclude left atrial or left atrial appendage (LAA) thrombus that may preclude the procedure,[28-30] as LA or LAA thrombus is a relative contraindication due to the risk of embolic stroke. The mitral valvuloplasty score is used both to identify appropriate anatomical candidates for the procedure, as well as to identify those at risk for development of severe mitral regurgitation after valvuloplasty.[31]

Interventionalists performing PBV who are highly expert in transseptal catheterization may not require any additional echo imaging to perform this part of the procedure. Early on, real-time TTE was attempted to assist the transseptal puncture, although the resolution of TTE limits its utility in many cases. More often TEE and ICE are used when imaging is required for transseptal catheterization during mitral PBV[16,20,25,32,33] (see Fig. 33.1).

Once left atrial access is achieved, both TTE and TEE can be used to assess balloon position, estimate mitral valve gradients and mitral valve area after balloon inflation, as well to monitor for an increased mitral regurgitation that may preclude subsequent balloon inflation[27,34-42] (see Figs. 33.2–33.5). Typically long-axis or 4-chamber views are used to measure Doppler gradients and to assess for mitral regurgitation. The pressure half-time method for mitral valve area estimation may not correlate with the hemodynamically derived mitral valve area estimate using the Gorlin formula immediately following balloon valvuloplasty if a transseptal approach is used due to the creation of an ASD with left to right shunting,[43-45] and our practice is to measure the pressure half-time MVA

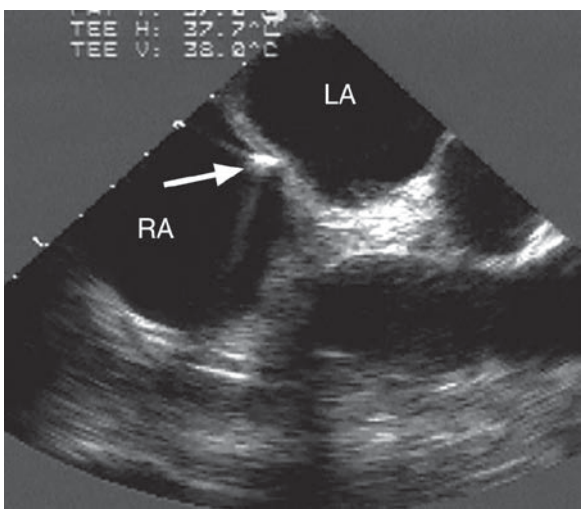

Fig. 33.1 Transesophageal echocardiogram from the midesophagus demonstrating the Brockenbrough needle position in the right atrium (RA) at the fossa ovalis, prior to entry into the left atrium (LA)

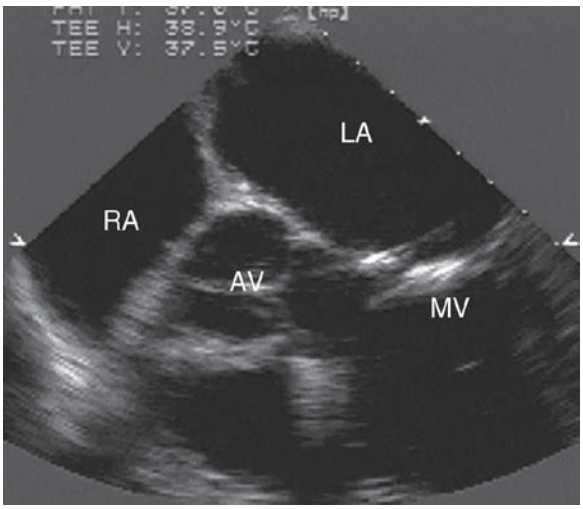

Fig. 33.2 Transesophageal echocardiogram from the midesophagus demonstrating a calcified and rheumatically deformed mitral valve (MV) prior to balloon valvuloplasty. *LA* left atrium; *RA* right atrium; *AV* aortic valve

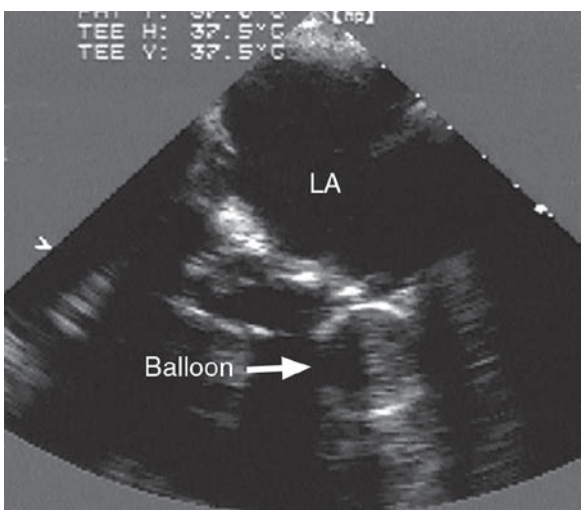

Fig. 33.3 Transesophageal echocardiogram from the midesophagus demonstrating the valvuloplasty balloon beginning to inflate, initially distally in the left ventricle. *LA* left atrium

prior to removal of the system from the atrium (while the shunt flow is blocked by the catheters), and also to rely upon peak and mean gradients to assess the adequacy of the result. If a retrograde (nontransseptal) approach is used, the Doppler-derived pressure half-time method is accurate. Planimetry of the mitral valve in short-axis views can also be used to estimate mitral valve area as well. Short-axis views of the mitral valve at the commissural level may also provide information as to the mechanism of improvement in stenosis immediately after valvuloplasty, as well as determining whether additional commissural separation is required for an adequate result. TTE and TEE can also be used to monitor for complications such as left atrial or catheter-associated thrombus, pericardial effusion and tamponade, left ventricular or left atrial perforation, and severe mitral regurgitation. Similarly TEE can assess the hemodynamic impact of the residual atrial septal defect resulting from the transseptal puncture. TEE may be of particular benefit when attempting to minimize the fluoroscopic exposure during the entire procedure (i.e., in pregnancy), or when initial attempts at fluoroscopically guided transseptal puncture are unsuccessful. As of this writing, there are no studies to suggest that TEE or ICE can reduce overall complications associated with PBV.

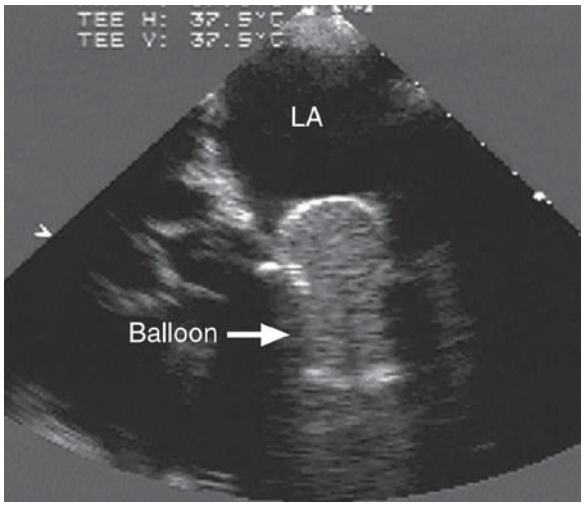

Fig. 33.4 Transesophageal echocardiogram from the midesophagus demonstrating the valvuloplasty balloon inflation, both distally in the left ventricle and proximally in the left atrium (LA)

ICE has recently been used to guide mitral valve PBV.[46-48] ICE offers advantages over TEE in that it does not require any additional sedation (or general anesthesia) and thereby improves patient comfort. With ICE, the transseptal catheterization can be monitored in real time, thereby potentially reducing the risk of complications. With ICE assessment of balloon position, mitral gradients, and severity of MR is feasible, and as such some operators have begun using this imaging modality during PBV (see Figs. 33.6–33.9). Direct comparison to TTE or TEE is lacking and requires further study to determine whether it provides sufficient advantage to justify its additional cost.

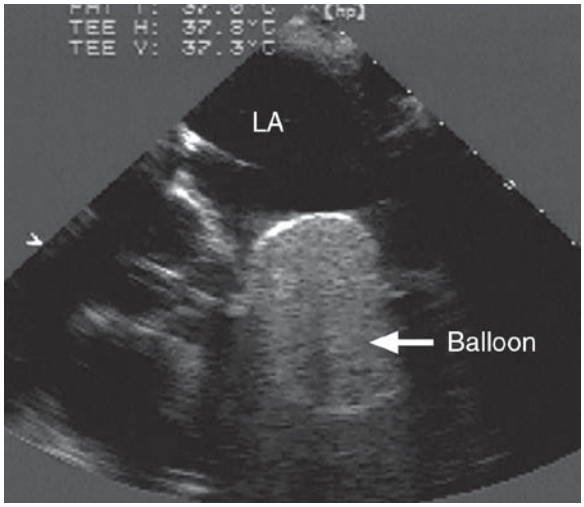

Fig. 33.5 Transesophageal echocardiogram from the midesophagus demonstrating full inflation of the valvuloplasty balloon

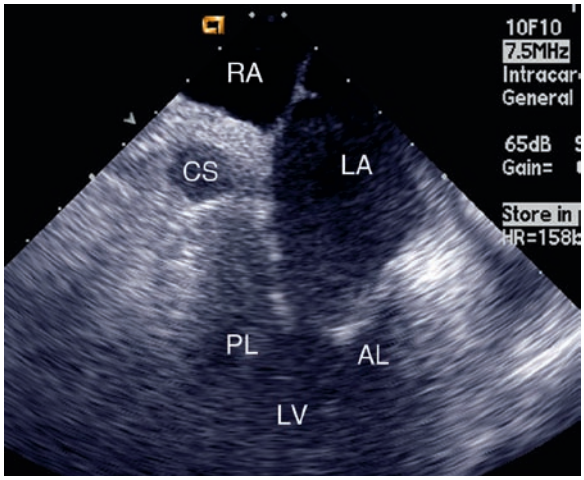

Fig. 33.6 Intracardiac echocardiographic view from the high right atrium (RA), with slight anterior flexion, demonstrating rheumatically deformed posterior and anterior MV leaflets (PL, AL), prior to percutaneous balloon valvuloplasty. *CS* coronary sinus; *LV* left ventricle

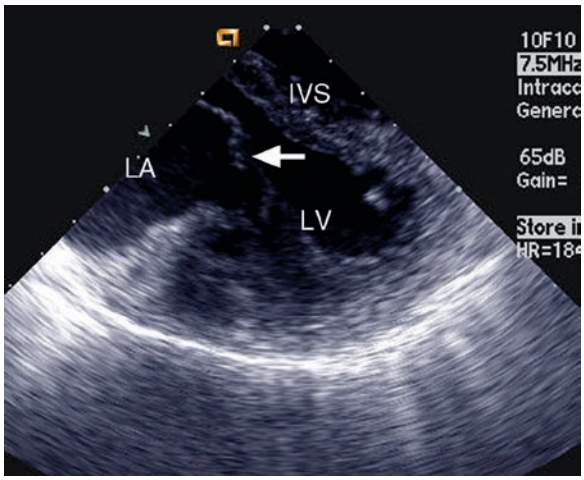

Fig. 33.7 Intracardiac echocardiographic view from the RV imaging through the interventricular septum (IVS), demonstrating the left ventricle (LV) as well as rheumatically deformed anterior mitral valve leaflet (*arrow*) with the classic "hockey stick deformity" typical of rheumatic mitral stenosis

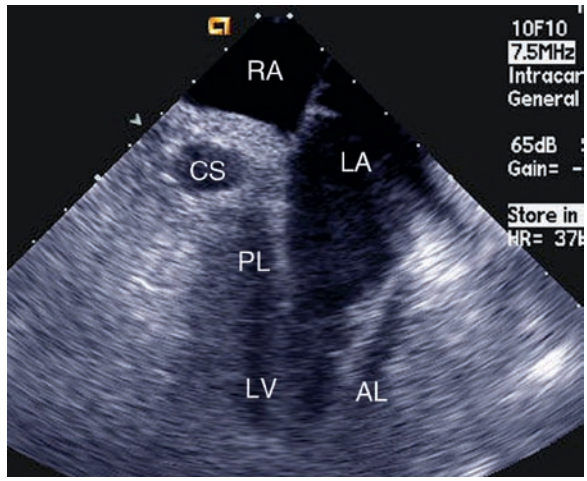

Fig. 33.9 Intracardiac echocardiographic view from the high right atrium (RA), with slight anterior flexion, demonstrating improved posterior and anterior MV leaflet mobility (PL, AL), immediately following percutaneous balloon valvuloplasty. *CS* coronary sinus; *LV* left ventricle

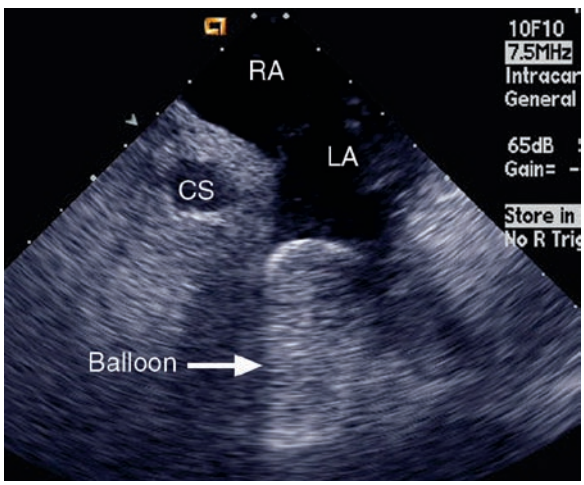

Fig. 33.8 Intracardiac echocardiographic view from the high right atrium (RA), with slight anterior flexion, demonstrating full inflation of the valvuloplasty balloon across the mitral valve. *CS* coronary sinus; *LA* left atrium

Alcohol Septal Ablation in Hypertrophic Obstructive Cardiomyopathy

In the management of hypertrophic obstructive cardiomyopathy (HOCM), surgical myomectomy is indicated to relieve symptoms of severe mechanical outflow obstruction. As an alternative nonsurgical procedure for reducing the left ventricular outflow tract gradients, percutaneous transluminal septal myocardial ablation by alcohol-induced septal branch occlusion has been described.[49-53] TTE and TEE can be used in alcohol septal ablation for patients with hypertrophic obstructive cardiomyopathy, to confirm that the selected septal perforator is an optimal site for ablation, as well as assess the adequacy of the hemodynamic result with Doppler (see Figs. 33.10–33.14). Echocardiographic views typically used include the long-axis views, which is used to determine the maximum region of septal hypertrophy, as well as the contact point between the interventricular septum and the systolic anterior motion of the anterior mitral valve leaflet (SAM contact point). Similarly, 3- and 5-chamber views offer similar anatomic delineation of the left ventricular outflow tract, as well as offering the ability to measure left ventricular outflow tract gradients by continuous-wave Doppler interrogation. Caution must be used to avoid measuring the signal from any associated mitral regurgitation, as this may result in an overestimation of the LVOT gradients. As with pericardiocentesis, the injection of a small amount of agitated saline mixed with saline-air microbubbles or other echocardiographic contrast agent or radiographic contrast agent, into the septal perforator vessel with balloon occlusion, allows confirmation that the ablation site will incorporate the region of maximum septal hypertrophy and involve the SAM contact point. In rare cases opacification of the medial papillary muscle or the left ventricular posterolateral free wall may be

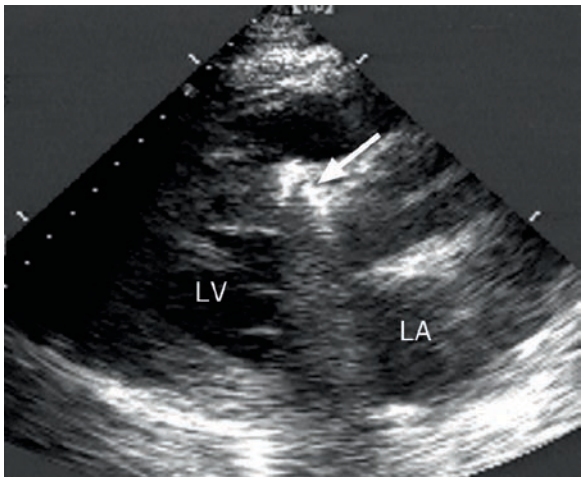

Fig. 33.10 Transthoracic echocardiographic view from the parasternal long axis demonstrating inflation of an occluder balloon in the first septal perforator to confirm position prior to alcohol septal ablation for hypertrophic obstructive cardiomyopathy. *LV* left ventricle; *LA* left atrium

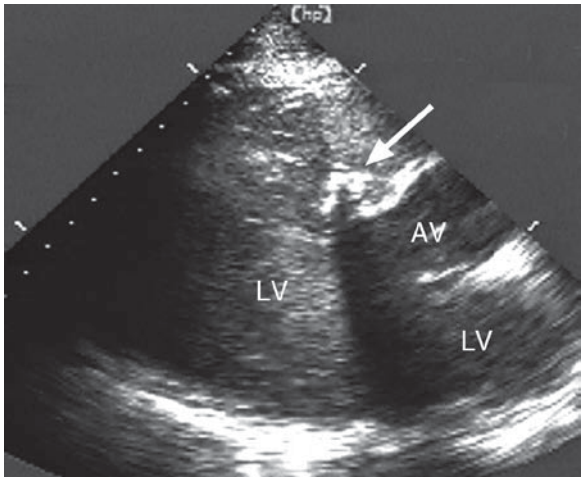

Fig. 33.12 Transthoracic echocardiographic view from the parasternal long axis demonstrating inflation of an occluder balloon in the first septal perforator as well as injection of left ventricular contrast (Optison) to confirm position prior to alcohol septal ablation for hypertrophic obstructive cardiomyopathy. *LV* left ventricle; *LA* left atrium; *AV* aortic valve

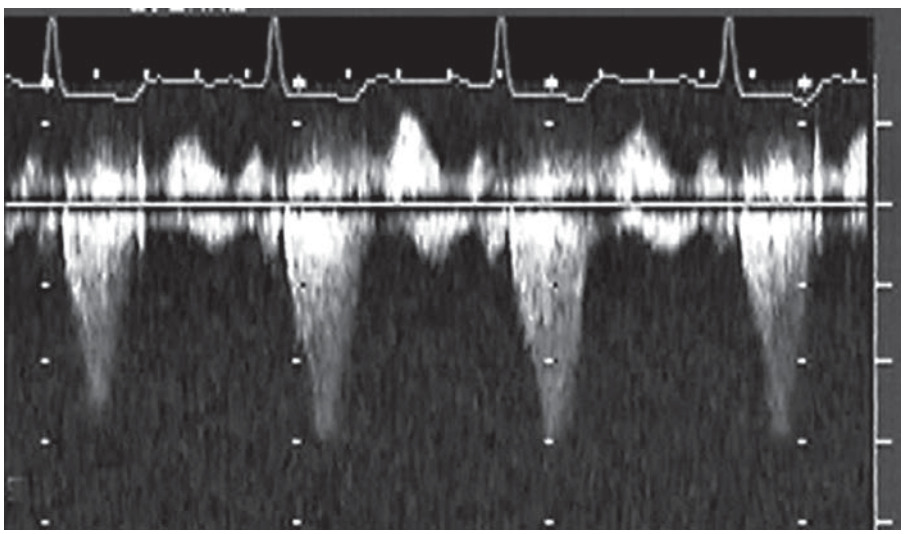

Fig. 33.11 Continuous-wave Doppler velocity profile prior to alcohol septal ablation for hypertrophic cardiomyopathy confirming left ventricular outflow tract obstruction, with a resting 36-mmHg predicted gradient (each of the vertical markers represents 1 m/s velocity)

seen, suggesting that an alternate ablation target vessel should be sought,[50] thus avoiding potentially fatal complications due to induction of a necrosis of myocardium distant from the septal target area. Post ablation, gradients may be remeasured, although post ablation edema may result in an elevated gradient for several weeks following ablation. As harmonic imaging can be used for detection of ultrasound contrast agents in myocardial perfusion studies, superharmonic imaging has been recently used to differentiate treated and nontreated myocardium in HOCM ethanol ablation.[54] This technique detects the third, fourth, and fifth harmonics which are not created in tissue, resulting, hence, in a high contrast-to-tissue ratio. Whether this technique offers advantages in the real-time guidance of these procedures is not known.

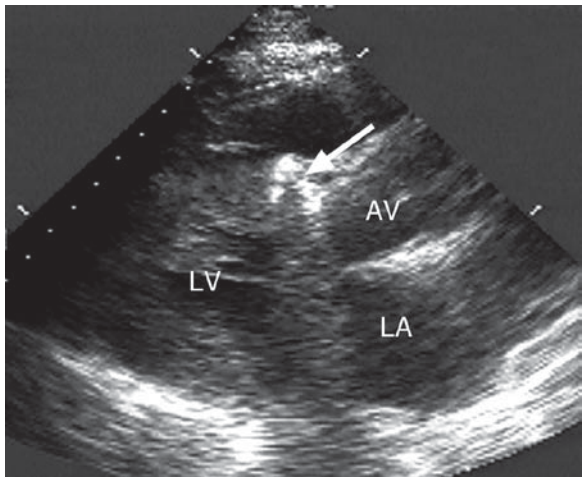

Fig. 33.13 With injection of contrast the region to be ablated becomes increasingly echogenic, with prominent shadowing noted over the mitral valve

As with MV PBV, procedural complications can also be monitored for, including pericardial effusion and tamponade. Some centers prefer TEE for performance of septal ablation over TTE, although measurement of the LVOT gradients is more challenging due to differences in alignment in the transducer with the direction of flow in the LVOT.[55] Limited studies exist examining the role of TEE in guiding alcohol septal ablation in HOCM. Although ICE guidance of septal ablation is possible as well, this has not been systematically evaluated and compared with other modalities directly.

Transesophageal Echocardiography in ASD and PFO Closure

Preprocedural transesophageal echocardiographic (TEE) measurement of the size and location of ASD and PFO has been helpful in the selection of the appropriate patients for PTC as well as selecting the appropriate device to use. In addition, TEE can be used to guide the procedure in real time, an approach that may eliminate the need for fluoroscopy.[46,47] The insertion of more than one device to close multiple ASDs is safe and effective; and both two- and three-dimensional TEE has been shown to be particularly helpful when multiple devices are used.[4] TEE provides an accurate assessment of atrial septal anatomy and assists in guidewire placement, transseptal puncture (if necessary),

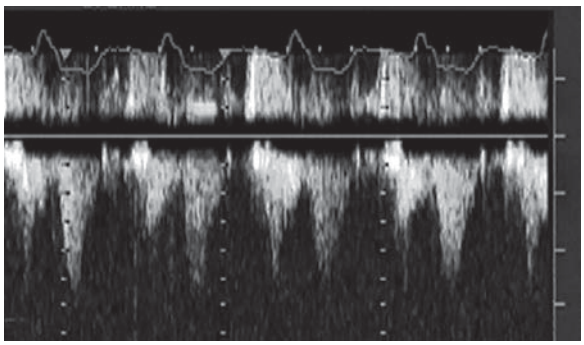

Fig. 33.14 Post ablation gradients are now normal, with each of the small vertical markers representing 20 cm/s velocity

closure device sizing and deployment. Furthermore, it gives immediate information regarding the adequacy of closure.[4,46-49] Drawbacks of TEE are potential patient discomfort and the risk of aspiration in the supine patient with prolonged esophageal intubation. As a result, TEE-guided PTC is often performed under general anesthesia with endotracheal intubation, which requires the expertise of an anesthesiologist and adds to the time and cost of the procedure.[50]

TEE may be supplemented by TTE in patients with attenuated or deficient anterior septal rims and unusual septal morphology as was shown in a small number of patients undergoing PTC.[51]

TEE in Complex MV Procedures

A percutaneous mitral valve repair system has been developed as an alternative to surgical repair, using the concepts of the edge-to-edge technique developed by Alfieri, but performed with a percutaneous endovascular repair system. The endovascular mitral repair system (Evalve™ Menlo Park, CA) uses a steerable guide catheter to position a two-armed V-shaped clip to approximate the leaflet tissue near the midline of the valve, thus reducing or eliminating mitral regurgitation. This system is currently being evaluated in phase II randomized trial. Patients with either functional or degenerative MR are under investigation, when the MR originates from the central portion of the valve, at the A2 and P2 segments. Patient selection is critically important to the success of this procedure, and TEE plays a critical role in identifying patients who may be treated. TTE is used to assist in evaluating MR severity prior to entry into the trial.

The delivery of this clip has five major steps that require echocardiographic guidance: transseptal catheterization, alignment of the clip delivery system perpendicular to the plane of the mitral valve and centered with reference to the line of coaptation, alignment of the approximation implant device with the open arms perpendicular to the coaptation line of the mitral valve, closing of the arms and approximation of the tips of the mitral valve, and release of the implant device. Transesophageal echo (TEE) and supplemental transthoracic echo (TTE) have been used to guide the entire procedure, and most recently real-time 3D TEE has been used. TEE monitoring also allows an assessment of the degree of mitral regurgitation (MR) and the assessment of transmitral gradients before the procedure, prior to clip removal, and immediately after the device was deployed.[3]

Newer percutaneous mitral annuloplasty and ventricular remodeling devices are also being developed to perform a percutaneous mitral repair, thereby reducing mitral regurgitation by enhancing mitral coaptation.[56] Echocardiography will play a crucial role in patient selection, procedure guidance, and in assessing results after the procedure has been performed.

Intracardiac Echocardiography

ICE is a newer modality that can also provide excellent imaging of the atrial septum and associated structures.[50] It utilizes a single-use ICE catheter and requires additional 8–11 French venous access. Benefits in using ICE for radiofrequency ablation of atrial fibrillation and more recently for transcatheter septal closure procedures have been demonstrated.[53,54] An advantage over TEE is that ICE obviates the need for additional sedation or general anesthesia, as well as additional echocardiography support, since the operator performing the percutaneous closure can also perform the ICE imaging. In some centers, however, additional echocardiography expertise is employed to assist in the ICE examination during the procedure.

There are three currently available ICE systems for the guidance of PTC. Each has unique features. The Boston Scientific UltraICE utilizes mechanically rotating radial ICE imaging, is not steerable, and is presently limited to 2D imaging. Both Siemens AcuNav and the newer Philips EP Medsystems ImageMate are steerable and deflectable, and have 2D, Color, and spectral Doppler capabilities.

Other advantages of ICE in the guidance of PTC when compared to TEE include shorter procedure and fluoroscopy times, and as such it is emerging as the standard imaging modality for guiding PTC.[55-58] ICE can be used as the primary imaging modality, without supplemental TTE or TEE. Recently, ICE has been shown to offer comparable cost to TEE-guided PTC, when general anesthesia is used for TEE-guided procedures.[57]

In guiding PTC of ASD and PFO, images are typically obtained from the midright atrium (See Figs. 33.15–33.31). In the case of the steerable and deflectable catheters, posterior and rightward tilting of the transducer away from the IAS provides excellent imaging of the septum and surrounding structures. The devices currently in use are typically double-disc devices with or without a self-centering mechanism. The method of implantation is variable and unique to each device. The mechanism of closure of all devices ultimately involves stenting the defect, with subsequent thrombus formation and neoendothelialization.

The preprocedural assessment of the interatrial septum by ICE includes evaluation of the entire interatrial septum. PFO is defined as a right to left communication through the fossa ovalis, and a stretched PFO is defined as the same anatomical defect with resting or intermittent left to right flow by color Doppler imaging. Right to left shunting is typically demonstrated by the injection of agitated saline at rest and with provocative maneuvers such as Valsalva. An atrial septal aneurysm

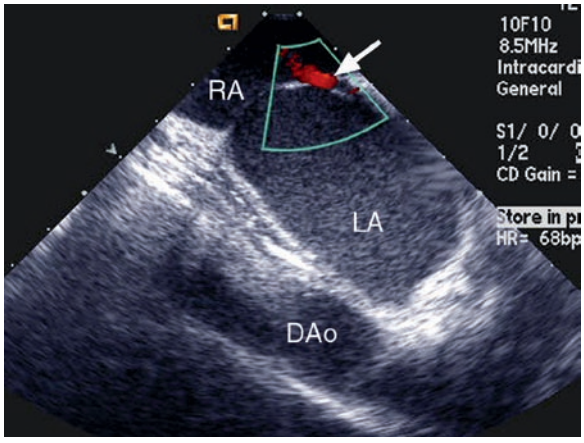

Fig. 33.15 Intracardiac echo image from the midright atrium (RA) with posterior and rightward tilting demonstrating *left* to *right* color Doppler flow (*arrow*) through a stretched patent foramen ovale. *LA* left atrium; *Dao* descending thoracic aorta

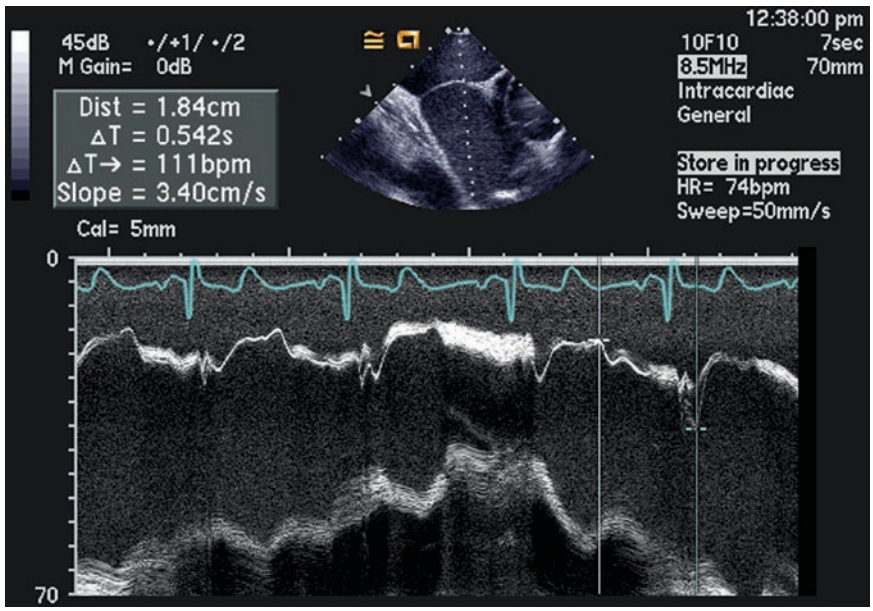

Fig. 33.16 M-mode recording through the interatrial septum demonstrating increased mobility (greater than 1.5 cm) consistent with atrial septal aneurysm

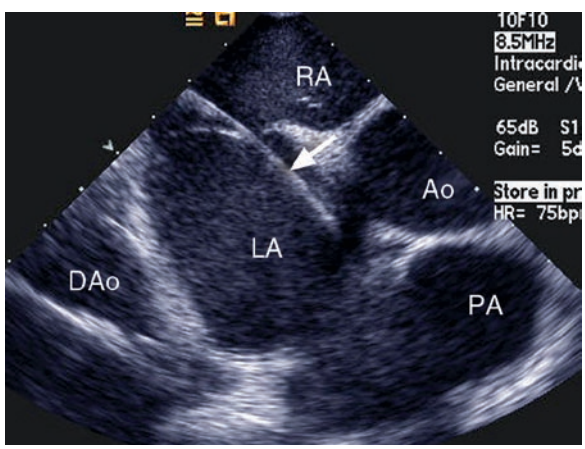

Fig. 33.17 Intracardiac echo image from the midright atrium (RA) with posterior and rightward tilting demonstrating guide wire (*arrow*) crossing through a patent foramen ovale into the left atrium (LA). *Ao* aorta; *PA* pulmonary artery; *Dao* descending thoracic aorta

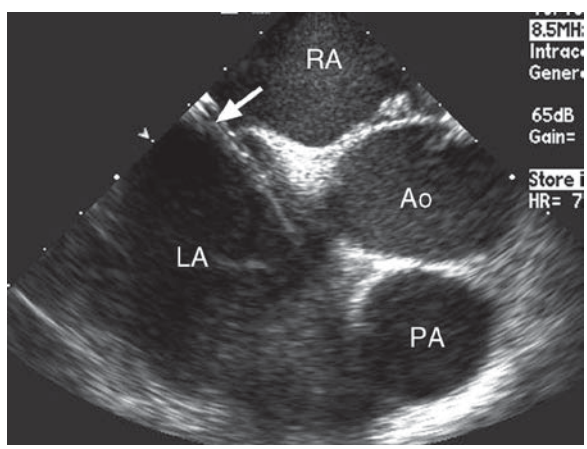

Fig. 33.18 Intracardiac echo image from the midright atrium (RA) with posterior and rightward tilting demonstrating the delivery sheath (*arrow*) crossing through a patent foramen ovale into the left atrium (LA). *Ao* aorta; *PA* pulmonary artery; *Dao* descending thoracic aorta

is defined as 15 mm of total movement of a 15-mm base of atrial septal tissue.

ASD type (ostium secundum, ostium primum, sinus venosus, coronary sinus), maximum ASD diameter, and defect number if multiple defects are present. Presently only ostium secundum atrial septal defects are amenable to PTC. Defects up to 38 mm in diameter have been closed successfully via PTC, as well as multiple atrial septal defects, and those associated with atrial septal aneurysm. Associated abnormalities of the pulmonary veins, IVC, SVC, coronary sinus, and AV valves should be excluded. Consideration of the size of the atrial septal rim of tissue surrounding the defect is important in evaluating patients for successful PTC,

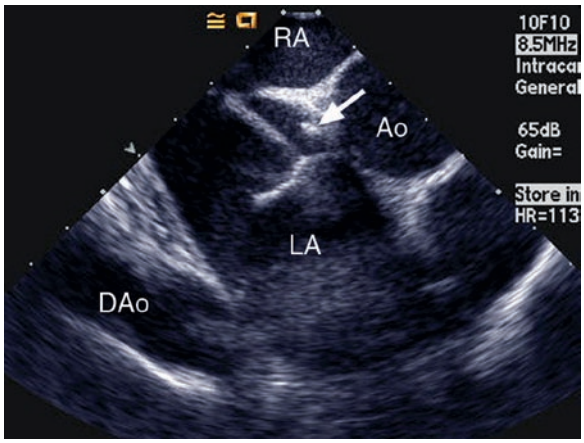

Fig. 33.19 Intracardiac echo image from the midright atrium (RA) with posterior and rightward tilting demonstrating a CardioSeal closure device with its upper arms malpositioned such that they are folding within the PFO tunnel (*arrow*). *LA* left atrium; *Ao* aorta; *Dao* descending thoracic aorta

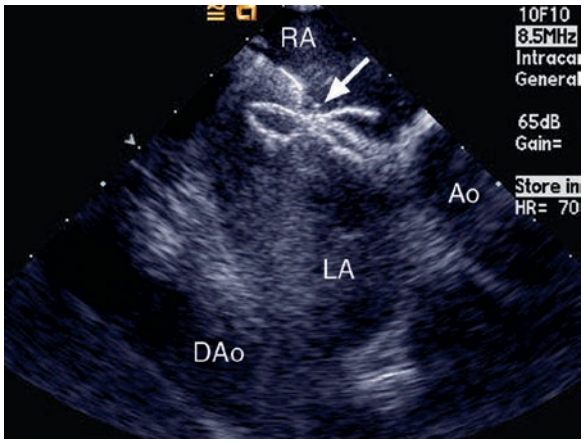

Fig. 33.21 Intracardiac echo image from the midright atrium (RA) with posterior and rightward tilting demonstrating a CardioSeal closure (*arrow*) with both sides of the disc fully deployed. The device is still attached to the guiding cable. *LA* left atrium; *Ao* aorta; *Dao* descending thoracic aorta

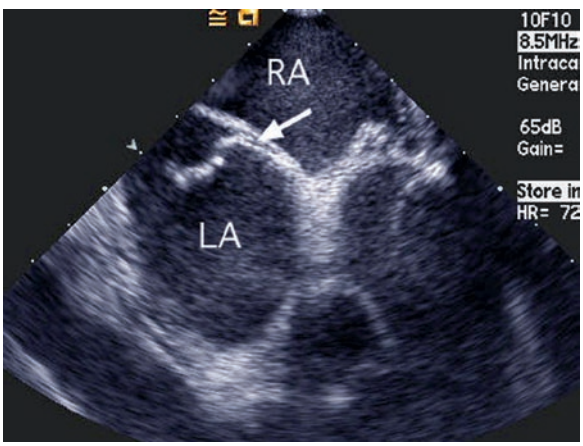

Fig. 33.20 Intracardiac echo image from the midright atrium (RA) with posterior and rightward tilting demonstrating a CardioSeal closure device with its upper arms now appropriately positioned such that they are compressing against the PFO tunnel (*arrow*) in the left atrium (LA)

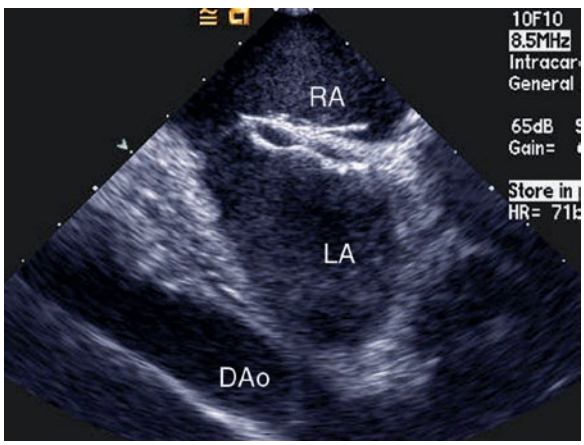

Fig. 33.22 Intracardiac echo image from the midright atrium (RA) with posterior and rightward tilting demonstrating a CardioSeal closure after release from the guiding cable. *LA* left atrium; *Dao* descending thoracic aorta

and a rim of 5 mm is generally considered adequate. The inferior and superior rims may be particularly important for successful PTC, although small series have reported success in patients with deficient rims. Balloon sizing of the ASD can be achieved with a balloon by one of two methods:

A "pulling technique" where a sizing balloon is inflated in the left atrium to a size larger than the ASD and pulled toward the defect until it occludes it (documented by color Doppler on either TEE or ICE). The balloon is then deflated until it moves from the left atrium to the right atrium. The amount of fluid inside the balloon at the time the balloon crosses the defect is measured, and once removed compared with a sizing plate that corresponds to the diameter of the defect.

Alternatively, the simpler "stationary balloon dilation," involves the use of a low-pressure balloon that is placed across the ASD and inflated. Imaging with TEE or ICE, as well as fluoroscopy monitor the inflation, and when the defect is completely occluded there will

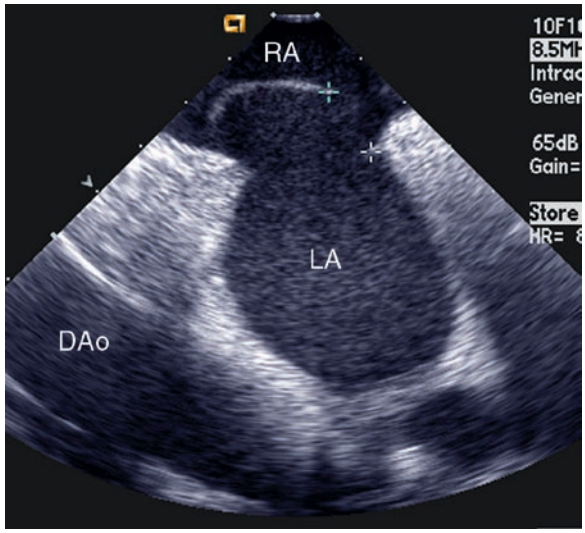

Fig. 33.23 Intracardiac echo image from the midright atrium (RA) with posterior and rightward tilting demonstrating a moderate size ostium secundum atrial septal defect. *LA* left atrium; *Dao* descending thoracic aorta

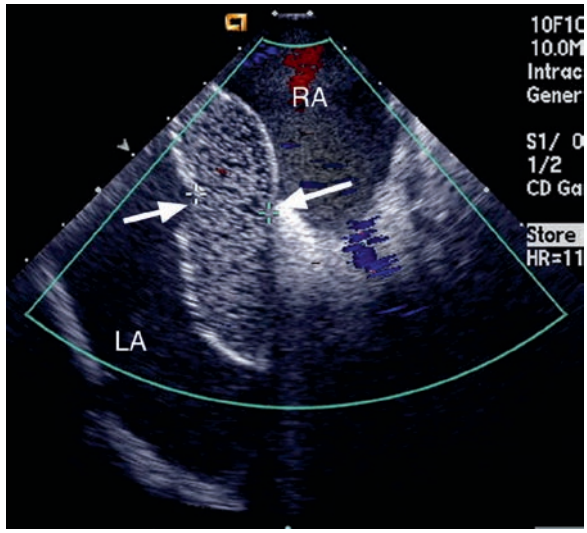

Fig. 33.25 Intracardiac echo image from the midright atrium (RA) with posterior and rightward tilting demonstrating a sizing balloon (*arrows* at balloon waist) across the atrial septal defect. Color Doppler is used to ensure stoppage of flow, thus confirming that the balloon fully occludes the defect

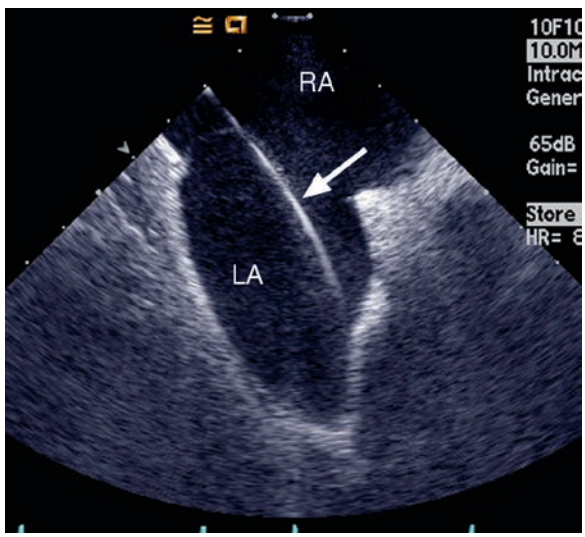

Fig. 33.24 Intracardiac echo image from the mid right atrium (RA) with posterior and rightward tilting demonstrating the guide wire crossing the atrial septal defect into the left atrium (LA)

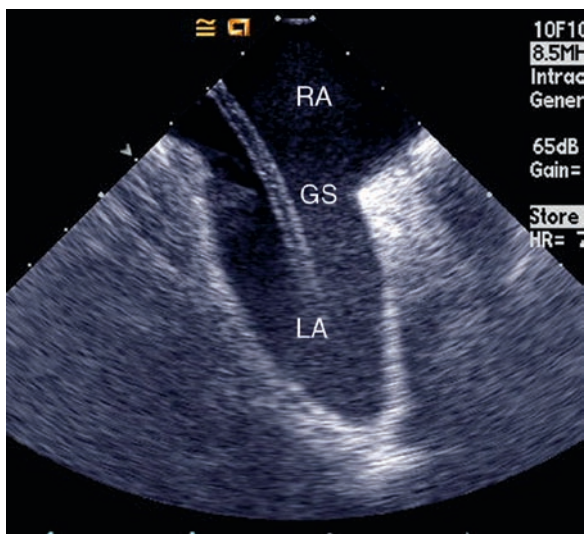

Fig. 33.26 Intracardiac echo image from the midright atrium (RA) with posterior and rightward tilting demonstrating the guiding sheath (GS) crossing the defect into the left atrium (LA)

be no color Doppler flow shunting seen, and a waist appears in the balloon contour. The balloon waist diameter is measured by echocardiography or fluoroscopy, and this size corresponds to the stretched diameter of the atrial septal defect.

The balloon is then removed leaving the guide wire in place, and the proper-sized device delivery sheath is passed over the wire into the left upper pulmonary vein (for stability) under echocardiographic guidance. The closure device is then delivered through the sheath into

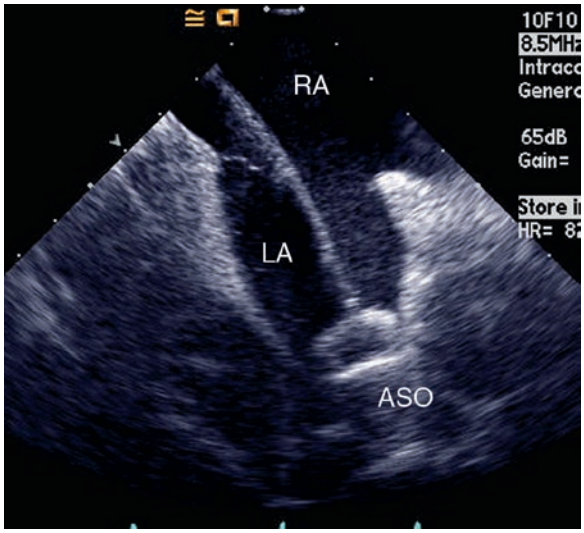

Fig. 33.27 Intracardiac echo image from the midright atrium (RA) with posterior and rightward tilting demonstrating the left atrial disc of an Amplatzer septal occluder opening

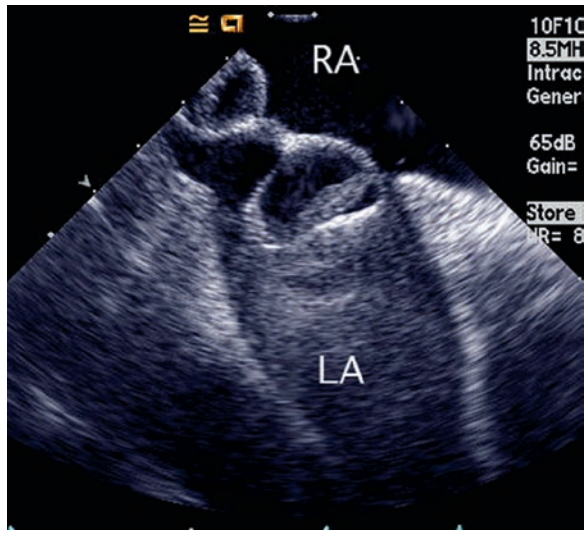

Fig. 33.29 After both discs are deployed a push pull maneuver is performed to confirm a stable position without risk of dislodgment prior to release. The device is being pulled on in this image

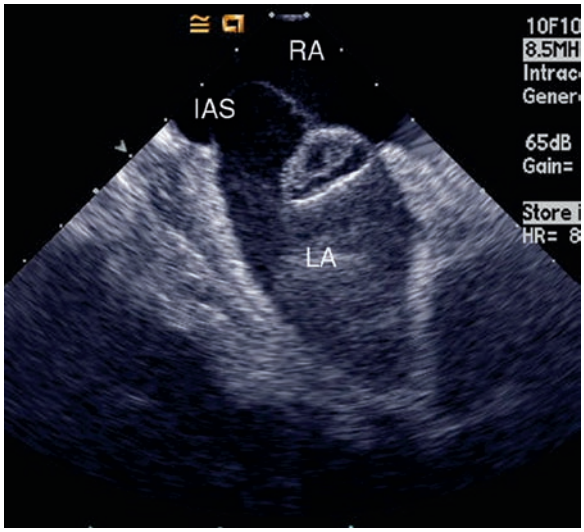

Fig. 33.28 The Amplatzer septal occluder is pulled back to the interatrial septum (IAS) in the left atrium (LA), prior to opening the right atrial (RA) disc

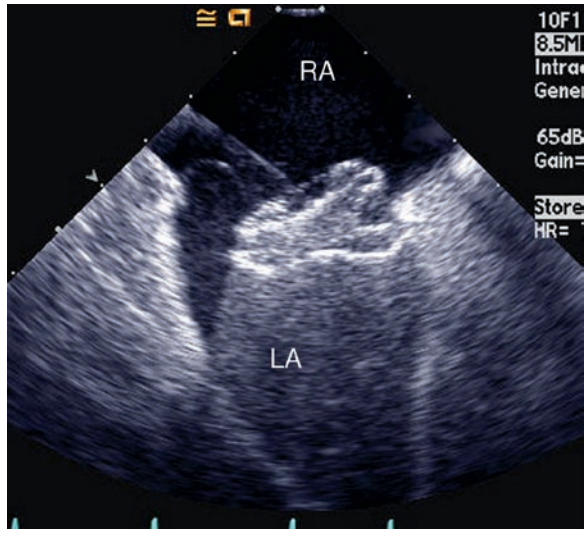

Fig. 33.30 Prior to release, the device is shown appropriately positioned

the left atrium. The individual insertion technique varies at this point, but typically employs opening the left atrial disc or arms, and pulling them back to the interatrial septum. Once the LA aspect of the device is in position, the RA aspect is opened thereby "sandwiching" the septum. The arms of the device rest on the rims of atrial tissue surrounding the defect, and as such in ASDs associated with deficiencies in these rims, a stable position can be more difficult to achieve. A stable device position for certain devices (i.e., Amplatzer Septal Occluder) is confirmed by moving the connecting cable (and thus the device attached to it) forward and backward.

When the device is confirmed to be in a satisfactory position, surrounding structures are evaluated. Large devices may threaten the patency of the right upper

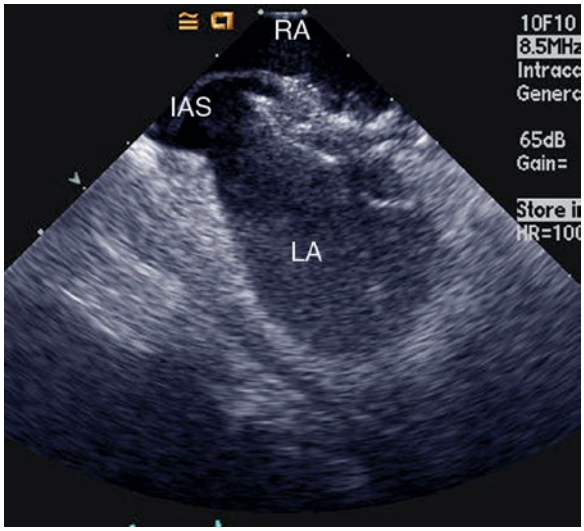

Fig. 33.31 Following release of the guiding cable, the device typically migrates as it is no longer under tension from the guiding cable. *RA* right atrium; *LA* left atrium; *IAS* interatrial septum

pulmonary vein, superior vena cava, inferior vena cava, coronary sinus, and occasionally the function of the tricuspid and mitral valves. The device is then released, and reimaged with echocardiography to assess for immediate ASD closure, as its position often changes once the traction of the connecting cable is no longer present.

Percutaneous Transcatheter Aortic Valve Replacement

Recently, percutaneous transcatheter aortic valve replacement (TAVR) has been described and initial studies are presently being performed with two distinct biologic valves mounted on stents, which are crimped onto a balloon and delivered via a valvuloplasty technique.[58-61] TAVR can be performed via a retrograde transaortic approach, or via a direct surgical transapical approach.[62] Echocardiography plays a critical role in patient selection, and in particular in choosing the appropriate size of the prosthesis to be implanted. Measurement of the aortic annular diameter is important in determining correct prosthesis size.[63] Small differences in aortic annular diameter and geometry have been recently demonstrated between TTE and TEE.[63] During the procedure, TEE has been used to ensure appropriate positioning of the prosthesis and to assess for paravalvular regurgitation after the valve has been implanted. Real-time 3D TEE has also been described during this procedure, but its exact role and incremental value when compared with standard 2D TEE is not fully known at this time.

Real-Time 3D Echocardiography

Newer imaging modalities that are either available commercially or in development include on line real-time three-dimensional TTE and TEE (RT3D) and real-time 3D ICE, which offers the potential for additional advantages in the guidance of percutaneous noncoronary interventions. Real-time 3D ICE is presently not commercially available. These modalities offer the advantage of being able to delineate the complex relationships between intracardiac anatomy, physiology, and device function, although have not been systematically evaluated in these settings.[64-78] Initial experience with RT3D TEE has been favorable in its ability to identify anatomic issues in procedural and device selection in patients undergoing ASD and PFO closure, as well as percutaneous repair of mitral regurgitation.

Interventional Echocardiographic Collaboration

As echocardiographically guided percutaneous interventions become increasingly complex, collaboration between the interventional cardiologist and echocardiographer becomes even more vital to the success of these procedures. Communication must be facilitated to ensure both operators are speaking "the same language" and referring to the same anatomic landmarks. The time required for performing complex procedures such as percutaneous mitral valve repair is significant and requires commitment on the part of the echocardiographer to be present for the duration of the procedure, unlike prior experience in the operating room where the echocardiographer performs two discrete examinations (before and after interventions). Echo-guided interventions are truly iterative and require real time moment-by-moment, movement-by-movement imaging. Finally, future goals for advanced echocardiography training

should include an interventional echocardiographic subspecialty, with training in all modalities used to guide procedures, including ICE. Currently training in ICE is available only as part of interventional and electrophysiology training in centers that have suitable expertise, as well as commercially by vendors that market and sell ICE systems.

References

1. Cheitlin MD, et al. ACC/AHA/ASE 2003 guideline update for the clinical application of echocardiography: summary article: a report of the American College of Cardiology/American Heart Association Task Force on Practice Guidelines (ACC/AHA/ASE Committee to Update the 1997 Guidelines for the Clinical Application of Echocardiography). *Circulation.* 2003;108(9):1146–1162.
2. Du ZD, et al. Comparison of transcatheter closure of secundum atrial septal defect using the Amplatzer septal occluder associated with deficient versus sufficient rims. *Am J Cardiol.* 2002;90(8):865–869.
3. Silvestry FE, Rodriguez LL, Herrmann HC, et al. Echocardiographic guidance and assessment of percutaneous repair for mitral regurgitation with the Evalve MitraClip: lessons learned from EVEREST I. *J Am Soc Echocardiogr.* 2007;20(10):1131–1140.
4. Callahan JA, et al. Pericardiocentesis assisted by two-dimensional echocardiography. *J Thorac Cardiovasc Surg.* 1983;85(6):877–879.
5. Callahan JA, Seward JB, Tajik AJ. Two-dimensional echocardiography during pericardiocentesis. *Am J Cardiol.* 1984;54(1):246.
6. Shah PM, Nanda NC. Echocardiography in the diagnosis of pericardial effusion. *Cardiovasc Clin.* 1976;7(3):125–130.
7. Singh S, et al. Right ventricular and right atrial collapse in patients with cardiac tamponade – a combined echocardiographic and hemodynamic study. *Circulation.* 1984;70(6):966–971.
8. Appleton CP, Hatle LK, Popp RL. Cardiac tamponade and pericardial effusion: respiratory variation in transvalvular flow velocities studied by Doppler echocardiography. *J Am Coll Cardiol.* 1988;11(5):1020–1030.
9. Leeman DE, Levine MJ, Come PC. Doppler echocardiography in cardiac tamponade: exaggerated respiratory variation in transvalvular blood flow velocity integrals. *J Am Coll Cardiol.* 1988;11(3):572–578.
10. Chandraratna PA. Echocardiography and Doppler ultrasound in the evaluation of pericardial disease. *Circulation.* 1991;84(3 Suppl):I303–I310.
11. Tsang TS, et al. Consecutive 1127 therapeutic echocardiographically guided pericardiocenteses: clinical profile, practice patterns, and outcomes spanning 21 years. *Mayo Clin Proc.* 2002;77(5):429–436.
12. Chabdraratna PA, et al. Echocardiographic contrast studies during pericardiocentesis. *Ann Intern Med.* 1977;87(2):199–200.
13. O'Sullivan J, Heads A, Hunter S. Microbubble image enhancement and pericardiocentesis. *Int J Cardiol.* 1993;42(1):95–96.
14. Weisse AB, et al. Contrast echocardiography as an adjunct in hemorrhagic or complicated pericardiocentesis. *Am Heart J.* 1996;131(4):822–825.
15. Betts TR, Radvan JR. Contrast echocardiography during pericardiocentesis [see comment]. *Heart.* 1999;81(3):329.
16. Kronzon I, et al. Use of two-dimensional echocardiography during transseptal cardiac catheterization. *J Am Coll Cardiol.* 1984;4(2):425–428.
17. Doorey AJ, Goldenberg EM. Transseptal catheterization in adults: enhanced efficacy and safety by low-volume operators using a 'non-standard' technique. *Cathet Cardiovasc Diagn.* 1991;22(4):239–243.
18. Goldstein SA, et al. Feasibility of on-line transesophageal echocardiography during balloon mitral valvulotomy: experience with 93 patients. *J Heart Valve Dis.* 1994;3(2):136–148.
19. Harrison JK, et al. Complications related to percutaneous transvenous mitral commissurotomy. Cathet Cardiovasc Diagn. 1994;(Suppl 2):52-60.
20. Hahn K, et al. Transesophageal echocardiographically guided atrial transseptal catheterization in patients with normal-sized atria: incidence of complications. *Clin Cardiol.* 1995;18(4):217–220.
21. Ben Farhat M, et al. Percutaneous balloon mitral valvuloplasty in eight pregnant women with severe mitral stenosis. *Eur Heart J.* 1992;13(12):1658–1664.
22. Mangione JA, et al. Percutaneous double balloon mitral valvuloplasty in pregnant women. *Am J Cardiol.* 1989;64(1):99–102.
23. Uygur D, Beksac MS. Mitral balloon valvuloplasty during pregnancy in developing countries. *Eur J Obstet Gynecol Reprod Biol.* 2001;96(2):226–228.
24. Nercolini DC, et al. Percutaneous mitral balloon valvuloplasty in pregnant women with mitral stenosis [see comment]. *Cathet Cardiovasc Interv.* 2002;57(3):318–322.
25. Hurrell DG, et al. Echocardiography in the invasive laboratory: utility of two-dimensional echocardiography in performing transseptal catheterization. *Mayo Clin Proc.* 1998;73(2):126–131.
26. Kultursay H, et al. Mitral balloon valvuloplasty with transesophageal echocardiography without using fluoroscopy. *Cathet Cardiovasc Diagn.* 1992;27(4):317–321.
27. Kronzon I, et al. Transesophageal echocardiography during percutaneous mitral valvuloplasty. *J Am Soc Echocardiogr.* 1989;2(6):380–385.
28. Olson JD, et al. Exclusion of atrial thrombus by transesophageal echocardiography. *J Am Soc Echocardiogr.* 1992;5(1):52–56.
29. Kamalesh M, Burger AJ, Shubrooks SJ Jr. The use of transesophageal echocardiography to avoid left atrial thrombus during percutaneous mitral valvuloplasty [see comment]. *Cathet Cardiovasc Diagn.* 1993;28(4):320–322.
30. Krishnamoorthy KM, et al. Usefulness of transthoracic echocardiography for identification of left atrial thrombus before balloon mitral valvuloplasty. *Am J Cardiol.* 2003;92(9):1132–1134.
31. Padial LR, et al. Echocardiography can predict the development of severe mitral regurgitation after percutaneous mitral valvuloplasty by the Inoue technique. *Am J Cardiol.* 1999;83(8):1210–1213.

32. Hung JS, et al. Usefulness of intracardiac echocardiography in complex transseptal catheterization during percutaneous transvenous mitral commissurotomy. *Mayo Clin Proc.* 1996;71(2):134–140.
33. Daoud EG, Kalbfleisch SJ, Hummel JD. Intracardiac echocardiography to guide transseptal left heart catheterization for radiofrequency catheter ablation. *J Cardiovasc Electrophysiol.* 1999;10(3):358–363.
34. Casale PN, et al. Transesophageal echocardiography in percutaneous balloon valvuloplasty for mitral stenosis. *Cleve Clin J Med.* 1989;56(6):597–600.
35. Chen CG, et al. Value of two-dimensional echocardiography in selecting patients and balloon sizes for percutaneous balloon mitral valvuloplasty. *J Am Coll Cardiol.* 1989;14(7): 1651–1658.
36. Chan K, et al. Role of transesophageal echocardiography in percutaneous balloon mitral valvuloplasty. *Echocardiography.* 1990;7(2):115–1123.
37. Jaarsma W, et al. Transesophageal echocardiography during percutaneous balloon mitral valvuloplasty. *J Am Soc Echocardiogr.* 1990;3(5):384–391.
38. Parro A Jr, et al. Value and limitations of color Doppler echocardiography in the evaluation of percutaneous balloon mitral valvuloplasty for isolated mitral stenosis. *Am J Cardiol.* 1991;67(15):1261–1267.
39. Arora R, et al. Role of transesophageal echocardiography during balloon mitral valvuloplasty. *Indian Heart J.* 1992; 44(6):391–394.
40. Pavlides GS, et al. The value of transesophageal echocardiography in predicting immediate and long-term outcome of balloon mitral valvuloplasty: comparison with transthoracic echocardiography. *J Interv Cardiol.* 1994;7(5):401–408.
41. Robinson NM, et al. The value of transthoracic echocardiography during percutaneous balloon mitral valvuloplasty. *J Am Soc Echocardiogr.* 1995;8(1):79–86.
42. Park SH, Kim MA, Hyon MS. The advantages of on-line transesophageal echocardiography guide during percutaneous balloon mitral valvuloplasty. *J Am Soc Echocardiogr.* 2000;13(1):26–34.
43. Shiran A, et al. Accuracy of two-dimensional echocardiographic planimetry of the mitral valve area before and after balloon valvuloplasty. *Cardiology.* 1998;90(3):227–230.
44. Pitsavos CE, et al. Assessment of accuracy of the Doppler pressure half-time method in the estimation of the mitral valve area immediately after balloon mitral valvuloplasty. *Eur Heart J.* 1997;18(3):455–463.
45. Fredman CS, et al. Comparison of hemodynamic pressure half-time method and Gorlin formula with Doppler and echocardiographic determinations of mitral valve area in patients with combined mitral stenosis and regurgitation. *Am Heart J.* 1990;119(1):121–129.
46. Schwartz SL, et al. Intracardiac echocardiography during simulated aortic and mitral balloon valvuloplasty: in vivo experimental studies. *Am Heart J.* 1992;123(3):665–674.
47. Salem MI, et al. Intracardiac echocardiography using the AcuNav ultrasound catheter during percutaneous balloon mitral valvuloplasty. *J Am Soc Echocardiogr.* 2002;15(12): 1533–1537.
48. Bruce CJ, Friedman PA. Intracardiac echocardiography. *Eur J Echocardiogr.* 2001;2(4):234–244.
49. Faber L, et al. [Percutaneous transluminal septal myocardial ablation in hypertrophic obstructive cardiomyopathy: acute results in 66 patients with reference to myocardial contrast echocardiography]. *Zeitschrift fur Kardiologie.* 1998;87(3): 191–201.
50. Faber L, et al. Intraprocedural myocardial contrast echocardiography as a routine procedure in percutaneous transluminal septal myocardial ablation: detection of threatening myocardial necrosis distant from the septal target area. *Cathet Cardiovasc Interv.* 1999;47(4):462–466.
51. Mutlak D, et al. Non-surgical myocardial reduction in hypertrophic obstructive cardiomyopathy [see comment]. *IMAJ.* 2002;4(2):86–90.
52. Nielsen CD, Spencer WH III. Role of controlled septal infarct in hypertrophic obstructive cardiomyopathy. *Cardiol Rev.* 2002;10(2):108–118.
53. Sakakibara M, et al. [Percutaneous transluminal septal ablation with ethanol in hypertrophic obstructive cardiomyopathy: a case report]. *J Cardiol.* 1999;34(1):35–40.
54. Ten Cate FJ, et al. Visualization of myocardial perfusion after percutaneous myocardial septal ablation for hypertrophic cardiomyopathy using superharmonic imaging. *J Am Soc Echocardiogr.* 2003;16(4):370–372.
55. Widimsky P, et al. Potential applications for transesophageal echocardiography in hypertrophic cardiomyopathies. *J Am Soc Echocardiogr.* 1992;5(2):163–167.
56. Condado JA, Velez-Gimon M. Catheter-based approach to mitral regurgitation. *J Interv Cardiol.* 2003;16(6):523–534.
57. Koenig P, et al. Role of intracardiac echocardiographic guidance in transcatheter closure of atrial septal defects and patent foramen ovale using the Amplatzer device. *J Interv Cardiol.* 2003;16(1):51–62.
58. Cribier A, Eltchaninoff H, Bash A, et al. Percutaneous transcatheter implantation of an aortic valve prosthesis for calcific aortic stenosis: first human case description. *Circulation.* 2002;106(24):3006–3008.
59. Cribier A, Eltchaninoff H, Tron C, et al. Early experience with percutaneous transcatheter implantation of heart valve prosthesis for the treatment of end-stage inoperable patients with calcific aortic stenosis. *J Am Coll Cardiol.* 2004;43(4): 698–703.
60. Lichtenstein SV, Cheung A, Ye J, et al. Transapical transcatheter aortic valve implantation in humans: initial clinical experience. *Circulation.* 2006;114(6):591–596.
61. Webb JG, Pasupati S, Humphries K, et al. Percutaneous transarterial aortic valve replacement in selected high-risk patients with aortic stenosis. *Circulation.* 2007;116(7): 755–763.
62. Ye J, Cheung A, Lichtenstein SV, et al. Six-month outcome of transapical transcatheter aortic valve implantation in the initial seven patients. *Eur J Cardiothorac Surg.* 2007;31(1): 16–21.
63. Moss RG, Ivens E, Pasupati S, Humphries K, Thompson C, Munt B. Role of echocardiography in percutaneous aortic valve implantation. *J Am Coll Cardiol Imaging* 2008;1: 15–24.
64. De Castro S, et al. Qualitative and quantitative evaluation of mitral valve morphology by intraoperative volume-rendered three-dimensional echocardiography. *J Heart Valve Dis.* 2002;11(2):173–180.

65. Gunasegaran K, et al. Three-dimensional transesophageal echocardiography (TEE) and other future directions. *Cardiol Clin.* 2000;18(4):893–910.
66. Hozumi T, Yoshikawa J. Three-dimensional echocardiography using a multiplane transesophageal probe: the clinical applications. *Echocardiography.* 2000;17(8):757–764.
67. Yu TH, Fu M, Chua S. Three-dimensional echocardiographic image of atrial septal aneurysm: report of two cases. *Changgeng Yi Xue Za Zhi.* 2000;23(11):701–705.
68. Chauvel C, et al. Usefulness of three-dimensional echocardiography for the evaluation of mitral valve prolapse: an intraoperative study. *J Heart Valve Dis.* 2000;9(3):341–349.
69. Applebaum RM, et al. Utility of three-dimensional echocardiography during balloon mitral valvuloplasty. *J Am Coll Cardiol.* 1998;32(5):1405–1409.
70. Magni G, et al. Two- and three-dimensional transesophageal echocardiography in patient selection and assessment of atrial septal defect closure by the new DAS-Angel Wings device: initial clinical experience. *Circulation.* 1997;96(6): 1722–1728.
71. Binder T, et al. Value of three-dimensional echocardiography as an adjunct to conventional transesophageal echocardiography. *Cardiology.* 1996;87(4):335–342.
72. Salustri A, et al. Three-dimensional echocardiography of normal and pathologic mitral valve: a comparison with two-dimensional transesophageal echocardiography. *J Am Coll Cardiol.* 1996;27(6):1502–1510.
73. Szili-Torok T, et al. Interatrial septum pacing guided by three-dimensional intracardiac echocardiography. *J Am Coll Cardiol.* 2002;40(12):2139–2143.
74. Light ED, et al. Feasibility study for real time three-dimensional Doppler intracardiac echocardiography. *Ultrasonic Imaging.* 2002;24(1):36–46.
75. Smith SW, et al. Feasibility study of real-time three-dimensional intracardiac echocardiography for guidance of interventional electrophysiology. *Pacing Clin Electrophysiol.* 2002;25(3):351–357.
76. Szili-Torok T, Roelandt JR, Jordaens LJ. Bachmann's bundle pacing: a role for three-dimensional intracardiac echocardiography?[comment]. *J Cardiovasc Electrophysiol.* 2002; 13(1):97–98.
77. Light ED, et al. Real-time three-dimensional intracardiac echocardiography. *Ultrasound Med Biol.* 2001;27(9): 1177–1183.
78. Foster GP, Picard MH. Intracardiac echocardiography: current uses and future directions. *Echocardiography.* 2001;18(1):43–48.

Index

B

D

T

U